



**MASARYKOVA
UNIVERZITA
PŘÍRODOVĚDECKÁ FAKULTA
ÚSTAV BIOCHEMIE**



Liposomy pro konstrukci cílených terapeutik a vakcín

Habilitační práce

RNDr. Jaroslav Turánek, CSc.

Brno 2016

Bibliografický záznam

Autor: RNDr. Jaroslav Turánek, CSc.
Přírodovědecká fakulta, Masarykova univerzita
Ústav biochemie

Název práce: Liposomy pro konstrukci cílených terapeutik a vakcín

Akademický rok: 2015/2016

Počet stran: 409

Klíčová slova: Liposom; vakcíny; imunoterapie; nanotechnologie; farmakologie; adjuvans; nosiče léčiv; protinádorové látky; antivirotika;

Bibliographic Entry

Author: RNDr. Jaroslav Turánek, CSc.
Faculty of Science, Masaryk University
Department of Biochemistry

Title of Thesis: Liposomes for construction of drug delivery systems and vaccines

Academic Year: 2015/2016

Number of Pages: 409

Keywords: Liposomes; vaccines; immunotherapy, nanotechnology; pharmacology; adjuvants; drug delivery; anticancer drugs; antiviral drugs;

PŘEDMLUVA

Předložená práce je souborem patnácti publikací, které jsou zaměřeny na hydrofobní látky s protinádorovým účinkem a na liposomy, které představují biokompatibilní nanočásticové systémy pro přípravu cílených terapeutik a konstrukci nosičů pro rekombinantní vakcíny.

Oblast liposomů je úspěšným odvětvím moderní farmakologie. Liposomy byly poprvé připraveny a popsány v šedesátých letech dvacátého století a stojí u počátku biomedicínckého využití nanočástic. Liposomy ovlivnily naše poznání struktury a funkce biomembrán, byly modelem pro pochopení osudu nanočástic v organismu, otevřely oblast pro výzkum a využití nanočástic pro cílení farmak a omezení jejich vedlejších účinků. Liposomy představují také jeden z nejlepších nevirových vektorů pro transfekci buněk *in vitro* a *in vivo* různými konstrukty DNA nebo RNA, které jsou využívány pro genovou terapii. Zcela samostatnou kapitolou je využití liposomů pro konstrukci bezpečných a biokompatibilních vakcín. Praktické výsledky „liposomologie“ lze nalézt především ve farmaceutickém průmyslu. Na trhu jsou protinádorové a antiinfekční preparáty renomovaných farmaceutických firem (například liposomální formulace doxorubicinu, amfotericinu B, paclitaxelu), existují liposomální vakcíny (například firma Epaxal-Berna) a liposomální imunoterapeutika (liposomální muramyltripeptid pro léčbu osteosarkomu – Novartis) dermatologické a kosmetické preparáty. Celá řada dalších liposomálních léčiv je ve fázi klinického zkoušení.

Publikace uvedené v této práci jsou uspořádány do čtyř sekcí, které jsou zaměřeny na určitou oblast výzkumu, který jsem vedl na Výzkumném ústavu veterinárního lékařství v Brně na oddělení Imunologie a později oddělení Imunofarmakologie.

Zcela nové téma biomedicínckého výzkumu na bázi biokompatibilních nanomateriálů a syntetických farmak jsem založil na VÚVeL v polovině devadesátých let. Pro tento typ výzkumu byly také vybudovány speciální laboratoře vybavené potřebným zařízením. Během svého pedagogického působení na Masarykově Univerzitě jsem vychoval celou řadu studentů v rámci magisterského a doktorandského studia. Současný tým, který vedu na oddělení Farmakologie a Imunoterapie je sestaven z mých současných studentů nebo spolupracovníků, které jsem vedl jako školitel nebo školitel – specialista.

Tento tým má navázanu dlouholetou spolupráci s kvalitními pracovišti v České republice a také v zahraničí. Z domácích institucí lze jmenovat ústavy Akademie věd ČR (Ústav organické chemie a biochemie, Biofyzikální ústav, Fyzikální ústav, Biotechnologický ústav, Ústav molekulární genetiky), universitami jako je Masarykova universita, Universita Palackého a Jihočeská Universita, biotechnologickými firmami (např. Bioveta, Contipro, Favea). Tyto spolupráce jsou doloženy společnými granty, publikacemi a patenty.

Dlouhodobá zahraniční spolupráce probíhá s Imperial Colledge a King's Colledge v oblasti cílených terapeutik. Tato spolupráce je opět doložena celou řadou publikací a společným patentem. Vedle této zásadní spolupráce existují krátkodobé spolupráce s universitami v EU, USA a Austrálii, které jsou opět doloženy společnými publikacemi, patenty a projekty.

V průběhu své práce na VÚVeL jsem řešil a řeším celou řadu komplexních grantů jako koordinátor nebo spoluřešitel (GAČR, TAČR, MPO, GAAV).

PODĚKOVÁNÍ

Především chci poděkovat všem svým učitelům, zejména pak RNDr. Janu Kovářovi, CSc., RNDr. Vladislavu Kahlemu, CSc., Doc. Ladislavu Skurskému, Dr.Sc. a Doc. Marii Studničkové, CSc., kteří mě vedli na počátku mé vědecké kariéry a jsou mi doposud vzorem svými lidskými kvalitami. Věřím, že jsem jim všem splatil svůj dluh výukou na své alma mater a výchovou studentů v rámci magisterského a postgraduálního studia.

Poděkování patří mým kolegům, se kterými jsem spolupracoval na zajímavých tématech a se kterými mě pojí přátelství. Tato přátelství považuji za jednu z velkých hodnot, které mi život dal.

Chci poděkovat i všem svým studentům, které jsem vedl a učil s nadějí, že předají štafetu dál. Oni mě na oplátku učí, jak i v raném podzimku dál oblékat lehký kabát mladosti.

Celé své rodině děkuji za podporu od dob studií až po tyto dny, kdy jsme zde pro jiné.

„Život je jen sen a jedinou skutečností v něm je láska“ (F. Bilek).

PROHLÁŠENÍ

Prohlašuji, že jsem svoji habilitační práci vypracoval samostatně s využitím informačních zdrojů, které jsou v práci citovány.

Brno, 8. března 2016

OBSAH

1.	LIPOSOMY	10
1.1.	CHARAKTERIZACE A TECHNOLOGIE PŘÍPRAVY LIPOSOMŮ	10
1.1.1.	Velikost a morfologie liposomů	10
1.1.2.	Dělení liposomů podle funkce a charakteru lipidní membrány	11
1.2.	METODY PŘÍPRAVY LIPOSOMŮ	12
1.2.1.	Metoda hydratace lipidního filmu	13
1.2.2.	Metoda odstranění detergentu	14
1.2.3.	Sekundární procesní metody	15
1.3.	LIPOSOMÁLNÍ NOSIČE	19
1.3.1.	Průmyslová technologie přípravy liposomů	21
1.4.	ZÁVĚR	23
1.4.1.	Publikace k tématu kapitoly	24
2.	HYDROFILNÍ A HYDROFOBNÍ LÁTKY, SURFAKTANTY: FORMULACE A INTERAKCE S MEMBRÁNAMI	73
2.1.	LÁTKY ROZPUSTNÉ VE VODĚ (HYDROFILNÍ LÁTKY)	73
2.1.1.	Podané patentové přihlášky k tématu kapitoly	76
2.1.2.	Publikace k tématu kapitoly	77
2.2.	LÁTKY ROZPUSTNÉ V NEPOLÁRNÍCH ROZPOUŠTĚDLECH (HYDROFOBNÍ, LIPOFILNÍ LÁTKY)	96
2.2.1.	Hydrofobní komplexy cis platiny	96
2.2.1.1.	Podané patentové přihlášky k tématu kapitoly	98
2.2.1.2.	Publikace k tématu kapitoly	99
2.2.2.	Paclitaxel	128
2.2.2.1.	Publikace k tématu kapitoly	131
2.2.3.	Deriváty vitamínu E s protinádorovým účinkem	156
2.2.3.1.	Publikace k tématu kapitoly	159
2.2.4.	Surfaktanty na bázi fluorovaných uhlovodíků se sacharidovou doménou	270
2.2.4.1.	Publikace k tématu kapitoly	271
2.2.5.	Senzory pro testování cytotoxického účinku farmak v modelech in vitro	300

2.2.5.1.	Publikace k tématu kapitoly	301
2.3.	ZÁVĚR	312
3.	LIPOSOMY PRO KONSTRUKCI REKOMBINANTNÍCH VAKCÍN	312
3.1.	NOVÝ SMĚR VÝZKUMU REKOMBINANTNÍCH VAKCÍN	318
3.2.	ZÁVĚR	323
3.2.1.	Publikace k tématu kapitoly	324
4.	SOUHRN LIPOSOMÁLNÍ PROBLEMATIKY	409

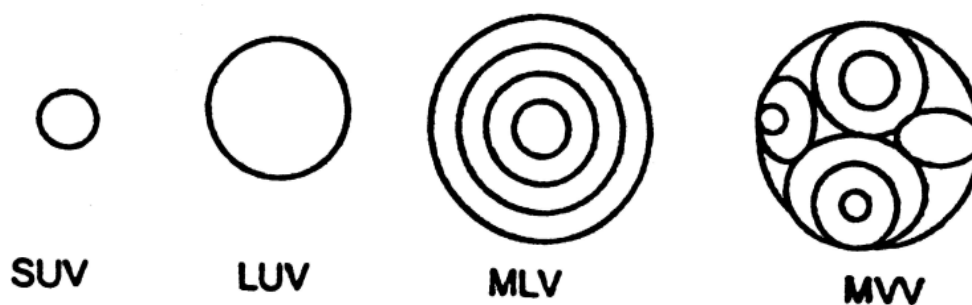
1. LIPOSOMY

Liposomy představují jedny z neúčinnějších struktur pro transport biologicky aktivních látek přímo do buněk a také patří k významným nosičům řady adjuvantních látek. Díky biologické podobnosti s biomembránami a možnosti cílené distribuce enkapsulovaných látek, jsou liposomy atraktivní pro celou řadu vědních oborů (farmakologie, imunofarmakologie, imunologie nebo genové inženýrství).

1.1. CHARAKTERIZACE A TECHNOLOGIE PŘÍPRAVY LIPOSOMŮ

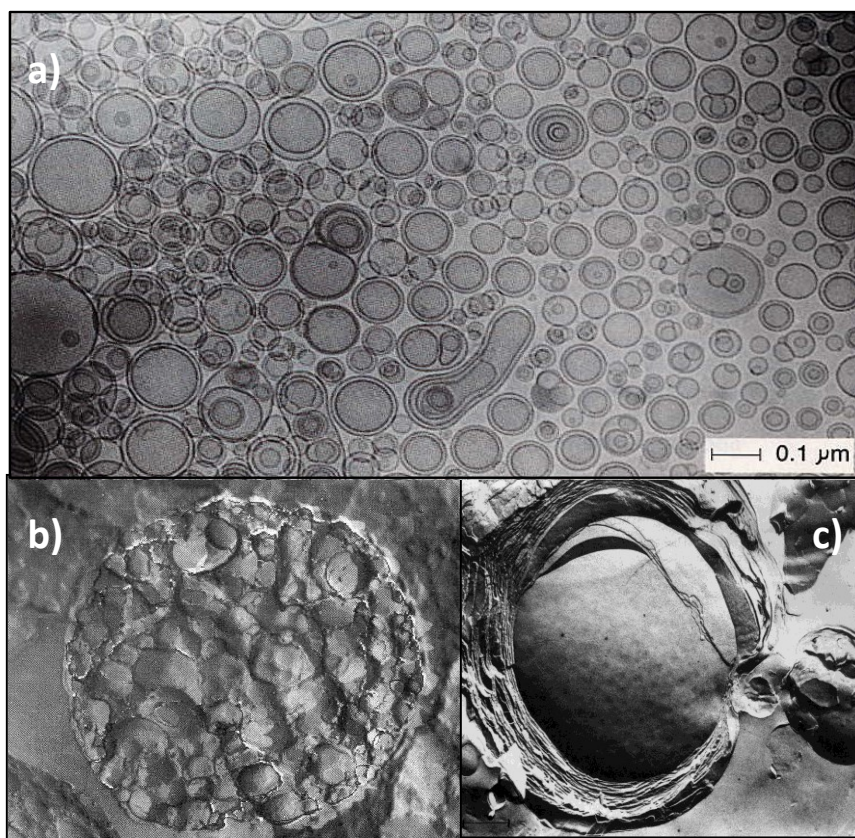
1.1.1. Velikost a morfologie liposomů

Nejběžněji používaný parametr pro rozdělení liposomů je klasifikace podle jejich velikosti a počtu lamel. Liposomy mohou mít různou velikost v rozmezí od 20 nm do 100 μm s lipidovou dvojvrstvou tenkou přibližně 4 nm. Lze je rozdělit na malé SUV (10–100 nm) a velké LUV (100–1000 nm) unilamelární vesikuly, které mají řádově pouze několik jednotek lamel, a dále velké multilamelární vesikuly MLV (100 nm – 20 μm) obsahující desítky koncentricky uspořádaných dvojvrstev stejně jako multivesikulární vesikuly MVV (100 nm – 20 μm), u nichž jsou lamely uspořádány nekonzentricky.



Obr.1 Liposomální vesikuly podle velikosti a počtu lamel.

SUV – small unilamellar vesicles, LUV – large unilamellar vesicles, MLV – multilamellar vesicles, MVV – multivesicular vesicles.



Obr. 2 Morfologie liposomů. (a) Morfologie liposomů pod kryoelektronovým mikroskopem. Multilamelární a oligolamelární liposomální vesikuly různých velikostí a tvarů. (b) „Freeze fracture“ multivesikulární liposom složený z mnoha fragmentů fosfolipidových dvojvrstev ohraničující vnitřní vesikuly, (c) MLV liposom připravený hydratací fosfolipidového filmu.

1.1.2. Dělení liposomů podle funkce a charakteru lipidní membrány

Liposomy můžeme rozdělit podle struktury membrány a její povrchové modifikace na několik základních typů, které mají různé využití při návrhu a přípravě systémů pro cílení různých molekul k buňkám.

Konvenční liposomy (conventional liposomes) - nespecifické interakce s prostředím, nestabilita v séru

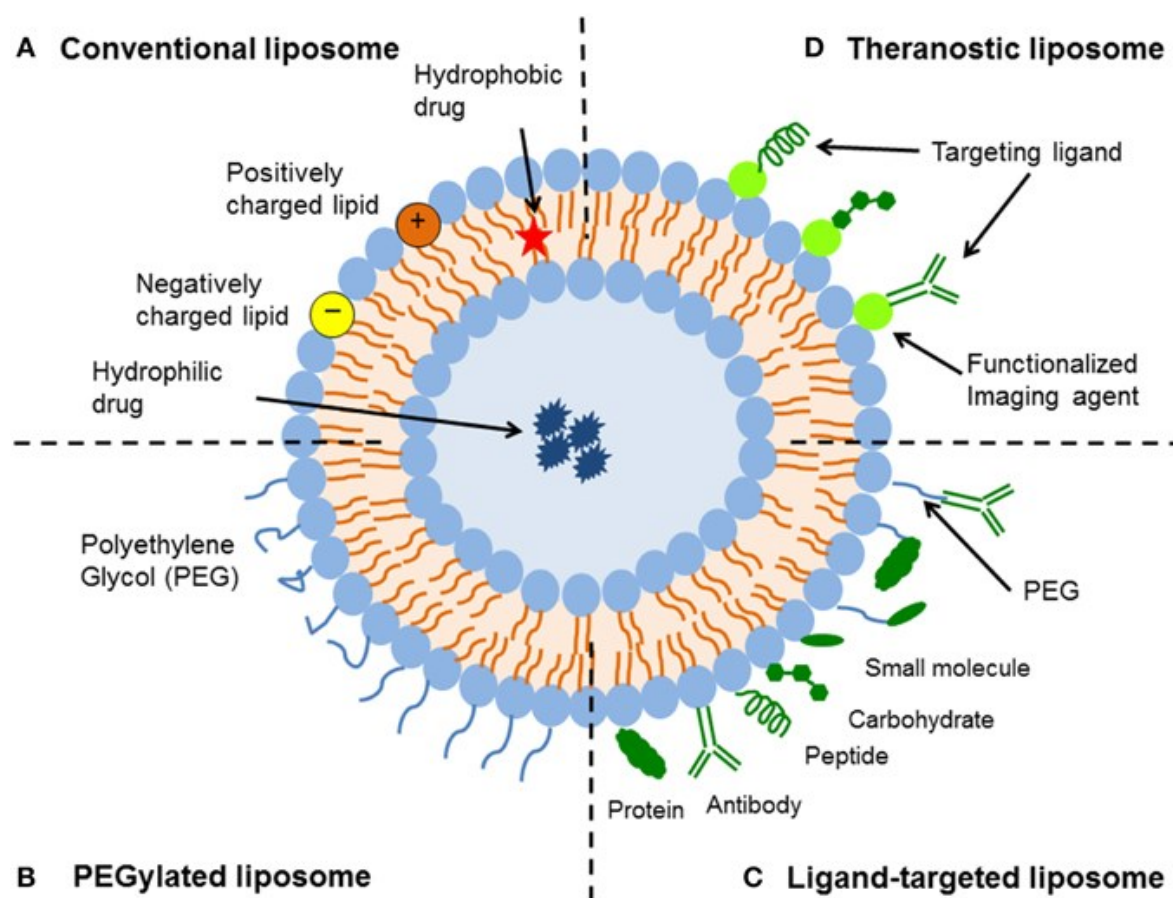
Stéricky chráněné liposomy (Stealth liposomes) - dlouhodobá cirkulace v krevním řečišti

Cílené liposomy (targeted liposomes) - specifické interakce přes navázaný ligand s povrchovými strukturama buněk (interakce ligand-receptor, protilátka – epitop)

Kationické liposomy (cationic liposomes) - schopnost interakce s negativně nabitou DNA a její kondenzace, elektrostaticky interagují s negativně nabitou DNA za tvorby

komplexů (lipoplexy), ochrana DNA před degradací nukleázami, interakce komplexů s povrchovými proteoglykany buňky, vstup do buněk pomocí endocytózy nebo fagocytózy, po injekci mohou být přijímány APC buňkami infiltrujícími místo injekce

Membrána liposomů může být modifikována tak, aby měnila svoji strukturu v závislosti na teplotě nebo pH prostředí. Tímto lze umožnit uvolnění enkapsulovaných látek např. v nádoru, kde je mírně zvýšená teplota a nižší pH v důsledku omezené cirkulace krve.



Obr. 3 Liposomy podle struktury membrány a její povrchové modifikace.

1.2. METODY PŘÍPRAVY LIPOSOMŮ

Při přípravě liposomů je využito přirozených vlastností fosfolipidů samovolně tvořit ve vodném prostředí lipidní dvojvrstvy. Při interakci vody s fosfolipidovým filmem se nejprve formují primární útvary zvané fragmenty fosfolipidové dvojvrstvy. Tyto intermediáty jsou následně přeměňovány na různě stabilní vesikulární struktury. Vesikulace vytvořených membránových fragmentů je důsledkem minimalizace interakcí

mezi molekulami vody a hydrofobních částí fosfolipidů. Vzdálenost mezi jednotlivými lamelami u vytvořených multilamelárních vesikulů je výsledkem působení repulsivních stérických a přitažlivých van der Waalsových sil.

Obecné postupy přípravy liposomů zahrnují přípravu lipidní a vodné fáze, po které následuje hydratace lipidů ve vodném médiu a v konečné fázi dochází k požadovaným finálním úpravám liposomů.

Základní etapy přípravy liposomů:

1. fyzikální nebo dvoufázová disperze lipidů do vodné fáze za vzniku emulze (proliposomů), solubilizace lipidů v detergentu za vzniku micel
2. odstranění organického rozpouštědla nebo detergentu za vzniku liposomálních vesikulů
3. sekundární procesy za účelem změnit morfologii, velikost a stabilitu primárně vytvořených liposomů (extruze přes membránové filtry, proces zmrazování a rozmrazování, lyofilizace s kryoprotektivy)
4. chemická modifikace liposomů (navázání ligandů)

Podle způsobu přípravy liposomů byly metody rozděleny do tří základních kategorií:

- a) mechanické dispersní metody (třepání na vortexu, sonikace, vysokotlaká homogenizace)
- b) detergentové dispersní metody (disperse solubilizovaného fosfatidylcholinu s detergentem za vzniku micel)
- c) dvoufázové dispersní metody (etanolová a etherová injektáž, reverzně-fázová evaporace)

1.2.1. Metoda hydratace lipidního filmu

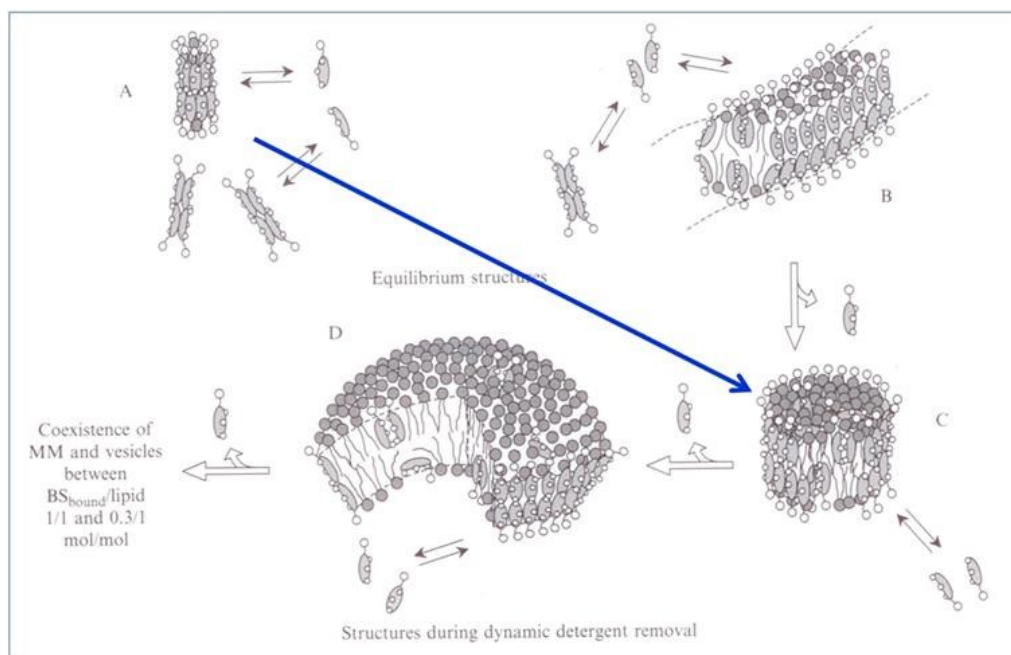
Nejběžnější metodou v laboratoři je příprava liposomů hydratací lipidního filmu, který se připraví odpařením organického rozpouštědla, ve kterém jsou rozpuštěny lipidy. Lipidní film připravíme na vakuové odparce a film hydratujeme při požadované teplotě vodným roztokem látek, které mají být enkapsulovány. Metodu lze doplnit krokem mražení a rozmražení, kdy vznikají liposomy o menší velikosti a s větším objemem enkapsulované vodné fáze. Následně lze použít další procesní metody (vysokotlaká extruze a homogenizace, mikrofluidizace a sonikace) na zmenšení velikosti a unifikaci distribuce velikosti.



Obr. 4 Vakuová rotační odparka pro přípravu lipidního filmu.

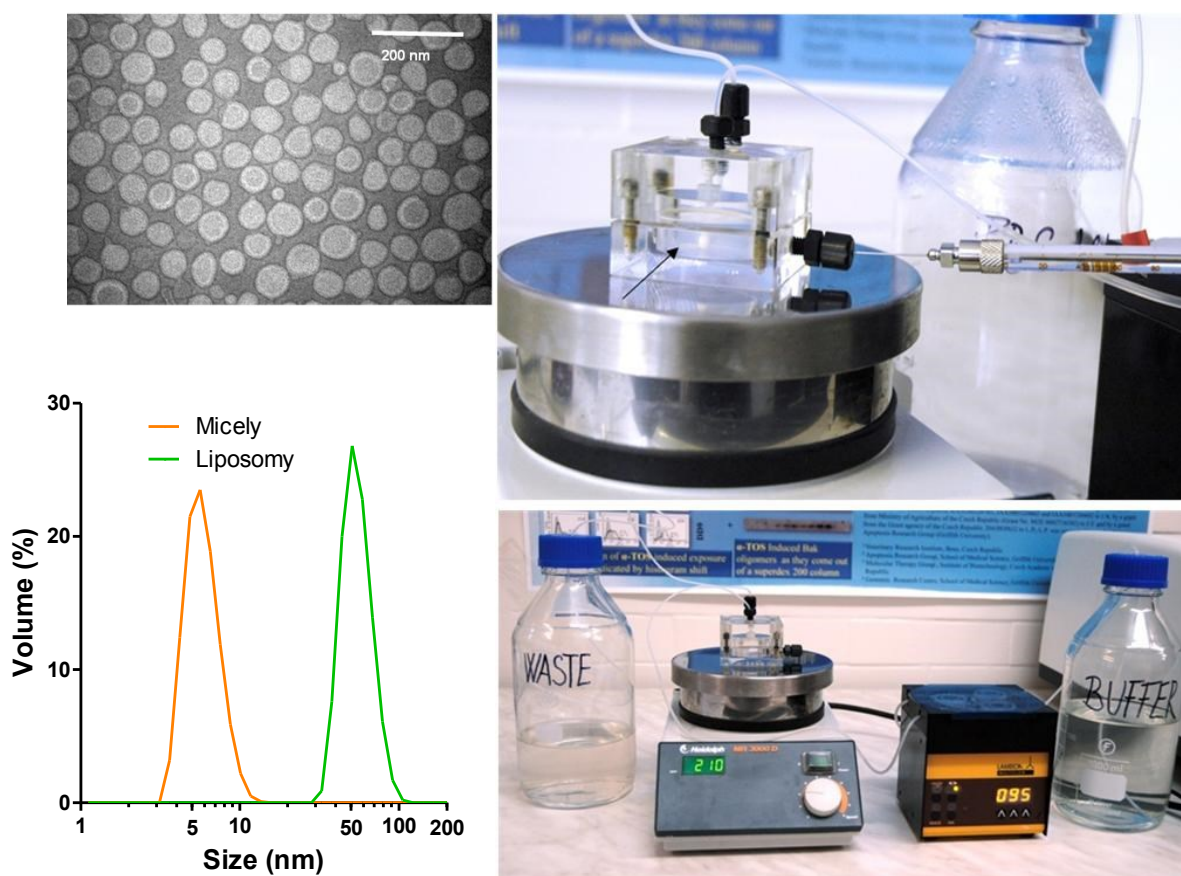
1.2.2. Metoda odstranění detergentu

Další primární metodou je tvorba liposomů z lipidních micel při odstranění detergentu. Toho lze dosáhnout například dialýzou s využitím různých zařízení (průtokový dialyzér, ultrafiltrace, využití sorbentů, zředění roztoku). Pro kontrolovaný proces jsou navrženy laboratorní a průmyslová zařízení. Liposomy připravené touto metodou jsou velmi unilamelární a homogenní. Příprava je vhodná zejména pro rekonstituci membránových proteinů. Princip metody spočívá v přeměně malých směsných micel fosfolipidu a vhodného detergentu (např. oktylglukosidu, deoxycholátu) na diskovité micely a dále jejich splýváním a vesikulací na liposomy. Tento proces je poháněn snižováním koncentrace detergentu jeho odstraňováním dialýzou.



Obr. 5 Princip metody odstranění detergentu a tvorba lipidních supramolekulárních struktur (micel různého typu a liposomů).

Na následujícím obrázku je ukázka homogenních liposomů (snímek z elektronového mikroskopu) a srovnání velikosti micel a liposomu (stanoveno metodou dynamického rozptylu světla). Laboratorní zařízení vlastní konstrukce pro kontrolovanou dialýzu je uvedeno jako příklad provedení metody. Takto lze připravit 10 ml liposomální suspenze o koncentraci lipidů 10 – 100 mg/ml.



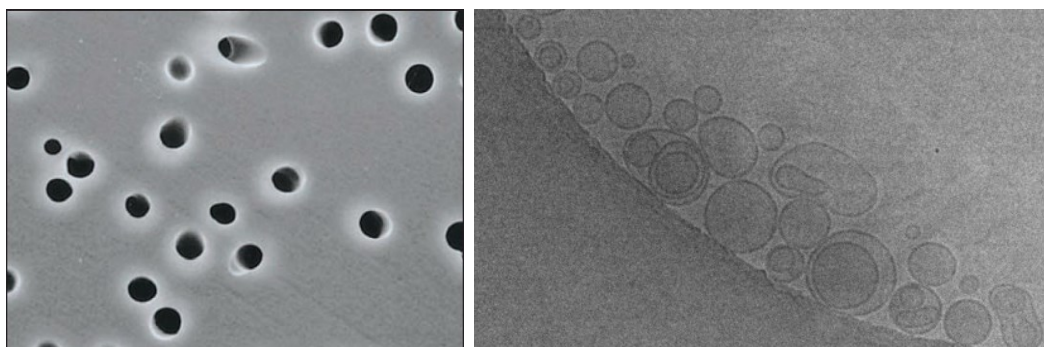
Obr. 6 Zařízení pro přípravu liposomů.

Zařízení vyvinuté v naší laboratoři pro přípravu liposomů metodou odstranění detergentu. Pro názornost jsou uvedeny distribuce velikosti micel a liposomů změřené pomocí dynamického rozptylu světla a elektronovou mikroskopií.

1.2.3. Sekundární procesní metody

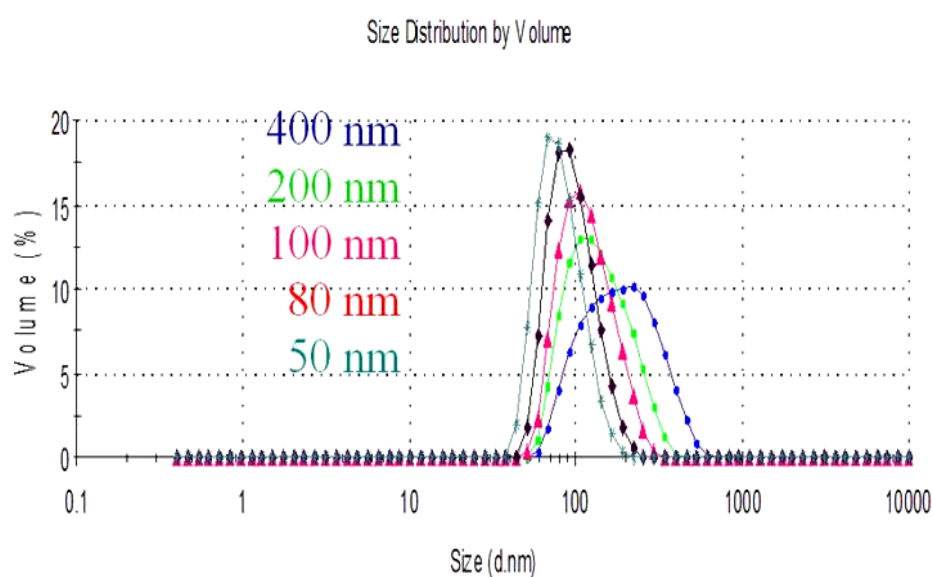
Nejběžnější sekundární procesní metodou je extruze liposomů přes polykarbonátové filtry. Princip metody je ukázán na následujícím obrázku stejně tak, jako dostupná instrumentace. Protlačování liposomů (je třeba pracovat při teplotě nad tranzitní

teplotou lipidů 30-60 °C) přes póry polykarbonátového filtru dochází k jejich deformaci a strhávání vnějších vrstev, což vede k snížení velikosti.



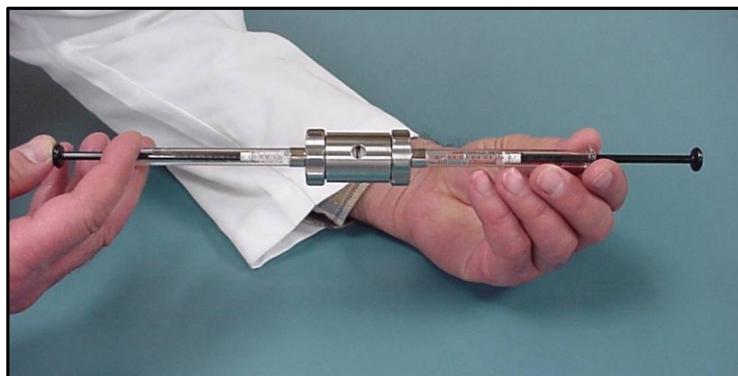
Obr. 7 Struktura polykarbonátového filtru.

Struktura polykarbonátového filtru (TEM) s definovanými póry a snímek liposomů (Cryo-TEM) připravených extruzí přes polykarbonátové filtry o velikosti pórů 100 nm.



Obr. 8 Distribuce velikosti liposomů.

Distribuce velikosti liposomů připravených extruzí přes polykarbonátové filtry o různé velikosti pórů. Jasně je patrné snížení velikosti liposomů a jejich polydisperzity (měření velikosti provedeno pomocí metody dynamického rozptylu světla).



Obr. 9 Zařízení pro ruční extruzi liposomů (0,1 – 2 ml suspenze liposomů).



Obr. 10 Zařízení pro preparativní extruzi liposomů.

Zařízení pro preparativní extruzi liposomů s využitím FPLC systému a vysokotlaké extruzní cely. Systém lze automatizovat s využitím automatických dávkovacích ventilů a použití dvou 50 ml „superloopů“. Detail vysokotlaké extruzní cely (vyrobena v dílnách VÚVeL).



Obr. 11 Laboratorní zařízení Lipex pro přípravu liposomů extruzí.

Zařízení jsou vyráběna pro 10, 100 a 800 ml liposomální suspenze, (využití stlačeného plynu – obvykle dusík).

Mezi další sekundární procesní metody vhodné pro laboratorní i průmyslovou přípravu patří vysokotlaká homogenizace a mikrofluidizace. Na obrázku vlevo je laboratorní vysokotlaký homogenizátor Avestin B3 a vpravo je laboratorní mikrofluidizér ML110 (Microfluidics). Mikrofluidizace je metodou umožňující volbou tlaku připravit liposomy o požadované velikosti i v kontinuálním režimu práce.



Obr. 12 Vysokotlaký homogenizátor a mikrofluidizér.

Oblíbenou sekundární procesní metodou pro přípravu SUV liposomů v laboratorním měřítku je použití homogenizace ultrazvukem. V tomto případě je nutné vzorek chladit a pracovat v inertní atmosféře, protože může docházet k oxidaci lipidů. Výhodou je možnost pracovat s malými objemy vzorků liposomů. Vzorek může být ponořen v nádobce do ultrazvukového homogenizátoru (příprava větších objemů) nebo homogenizován speciální sondou (viz. obrázek 12) pro zpracování menších objemů.



Obr. 13 Ultrazvukový homogenizátor.

1.3. LIPOSOMÁLNÍ NOSIČE

Do liposomů může být enkapsulována celá řada agens různého fyzikálně-chemického charakteru. Lipofilní látky jsou inkorporovány do lipidové dvojvrstvy a hydrofilní látky jsou enkapsulovány do vnitřního vodného prostředí. V závislosti na použité metodě můžeme připravit liposomy o různé velikosti, počtu lamel (unilamelární, oligo- nebo multilamelární vesikuly) a s různými fyzikálními a chemickými vlastnostmi, které mohou značně ovlivnit množství enkapsulované látky.

Pro farmaceutickou oblast jsou liposomy jako nosiče velmi zajímavé z následujících důvodů:

1. snadná enkapsulace hydrofilních a hydrofobních léčiv
2. příprava preparátů z přirozených lipidů, které jsou snadno biodegradabilní a málo toxické
3. příprava liposomů o různé velikosti a morfologii
4. snížení nežádoucích účinků léčiv

5. umožnění specifického transportu léčiv do cílového orgánu nebo tkáně
6. řízení lokalizace a postupné uvolňování léku

Mezi základní parametry charakterizující enkapsulaci látky do liposomů patří:

enkapsulovaný objem ($\mu\text{l}/\mu\text{mol}$ lipidů) je skutečný membránou uzavřený objem látky vztažený na jednotku lipidů.

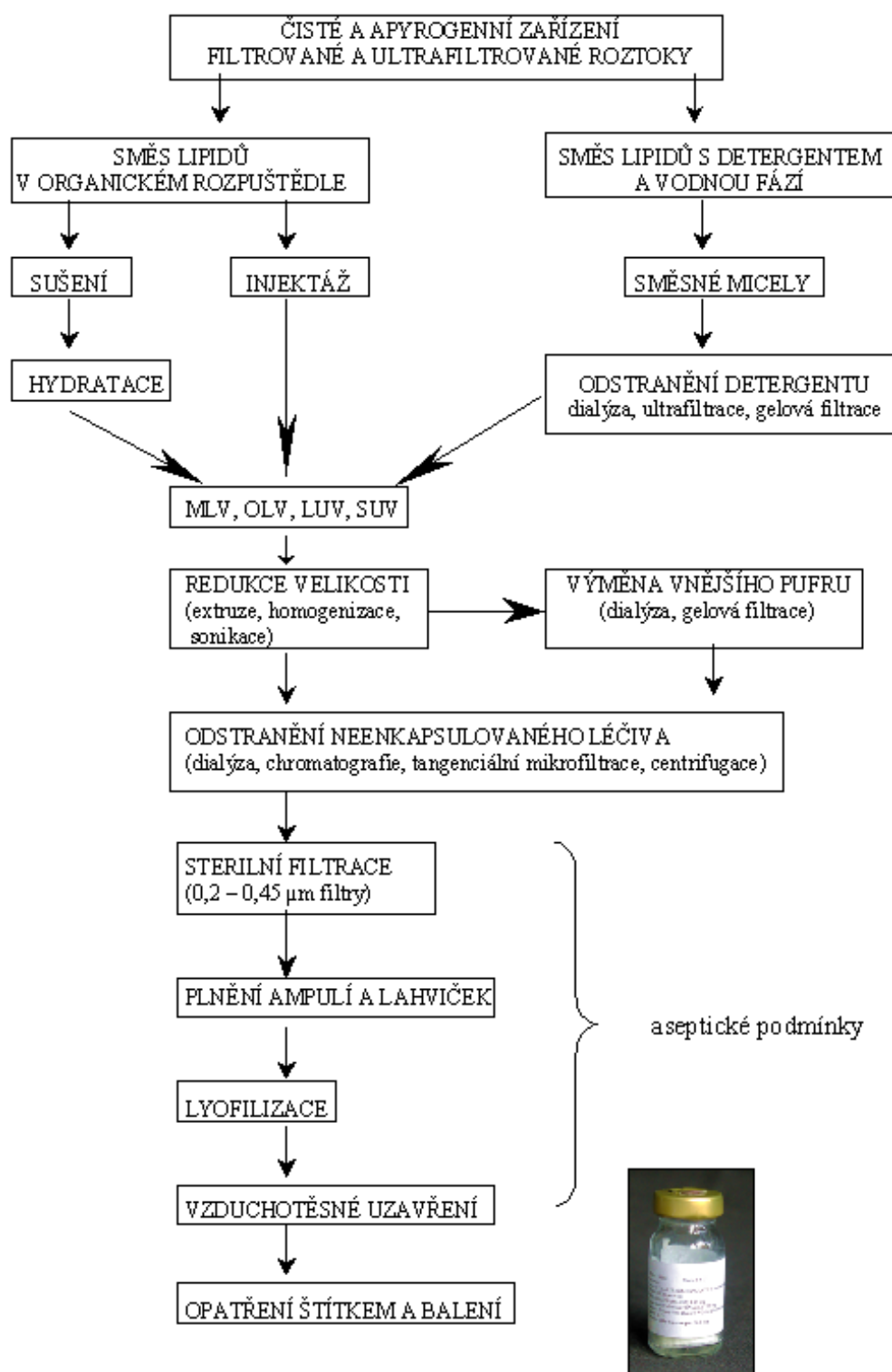
enkapsulační kapacita ($\mu\text{l}/\mu\text{mol}$ lipidů) je maximální množství látky, které může být enkapsulováno liposomy vztažené na mol lipidů a na rozdíl od enkapsulační účinnosti nezávisí na koncentraci lipidů.

enkapsulační účinnost (%) je experimentálně stanovený podíl enkapsulované látky v liposomu k jejímu původnímu množství a je vyjádřena v % enkapsulované látky.

Pro MLV a SUV se enkapsulovaný objem obvykle pohybuje kolem $0,5 \mu\text{l}/\mu\text{mol}$, u LUV kolem $30 \mu\text{l}/\mu\text{mol}$. Enkapsulace hydrofilních léčiv roste v pořadí: $\text{MLV} < \text{SUV} < \text{LUV}$. Pro léčebné aplikace jsou obvykle používány homogenní LUV o velikosti 80–200 nm. Velké liposomy ($5 \mu\text{m}$) jsou méně stabilní, podléhají rychlé opsonizaci a následné fagocytóze. V případě hydrofobních látek, jsou pro enkapsulaci využívány zejména MLV, které mohou do svých lipidových dvojvrstev pojmout větší množství látky než SUV nebo LUV.

Vzhledem k faktu, že liposomy jsou dnes využívány jako nosiče v celé řadě medicínských preparátů (např. antibiotika, cytostatika, vakcíny), je zde pro názornost zpracováno schéma průmyslové výroby takových preparátů.

1.3.1. Průmyslová technologie přípravy liposomů



Obr. 14 Základní schéma přípravy liposomálních preparátů pro farmaceutické využití.

Pro průmyslovou přípravu liposomů je nezbytná snadná dostupnost výchozích lipidů a ostatních vstupních surovin v přijatelné kvalitě. Výrobní proces musí být reprodukovatelný z hlediska požadovaného složení lipidní kompozice, distribuce velikosti liposomů a enkapsulační účinnosti. Liposomální preparáty musí být chráněny a stabilizovány proti fyzikálním, chemickým a mikrobiologickým vlivům nejen během technologického procesu, ale i následně během dlouhodobého skladování. Kontrola kvality a stability je sledována laboratorními analýzami (Tab. I). Laboratorní postupy a metodika je vypracována na úrovni standardních operačních postupů, což je nezbytné pro průmyslovou výrobu liposomů a uvedení liposomálních preparátů na trh.

Tab. 1 Kontrola kvality liposomálních preparátů.

ROZBOR	METODA/CÍL
Charakteristika	
pH	pH metr
osmolarita	osmometr
koncentrace fosfolipidů	HPLC/obsah lipidního fosforu
složení fosfolipidů	TLC, HPLC
koncentrace cholesterolu	HPLC
koncentrace léčiva	příslušná metoda
Chemická stabilita	
pH	pH metr
oxidace fosfolipidů	GLC/složení MK; konjugované dieny
hydrolýza fosfolipidů	HPLC, TLC/koncentrace MK
oxidace cholesterolu	HPLC, TLC
degradace antioxidantu	HPLC, TLC
Fyzikální stabilita	
distribuce velikosti liposomů	DLS, Coulter Counter, světelná mikroskopie, laserová difrakce, GCE
povrchový náboj, pH	měření zeta-potenciálu, pH elektrody
počet lamel	SAXS, NMR
obsah neenkapsulovaného léčiva	GEC, IEC, protaminová precipitace
únik léčiva indukovaný tělními tekutinami	GEC, IEC, protaminová precipitace
Biologická charakterizace	
sterilita	mikrobiální kontaminace
pyrogenicita	LAL test
toxická	monitoring pokusných zvířat/přežívání, histologie, patologie

DLS (dynamic light scattering) – dynamický rozptyl světla, GEC (gel exclusion chromatography) – chromatografie stérické výluky, GLC (gas-liquid chromatography) – plynová chromatografie, IEC (ion exchange chromatography) – iontově výměnná chromatografie, LAL (Limulus Amoebocyte Lysate) test, MK – mastné kyseliny, NMR (nuclear magnetic resonance) – nukleární magnetická rezonance, SAXS (small angle X-ray scattering) – rozptyl X-paprsků pod malým úhlem, TLC (thin layer chromatography) – tenkovrstvá chromatografie.

1.4. ZÁVĚR

Z doložených prací je zřejmé, jak rozsáhlá problematika je spojena s přípravou a fyzikálně-chemickým testováním liposomálních preparátů. Jedná se o velmi komplexní soubor metod a instrumentace pro jejich provádění. Zároveň je vyžadována vysoká kvalifikace experimentátorů v celé řadě chemických oborů. Pro přípravu liposomů byla navržena a zkonstruována celá řada zařízení, která byla dovedena do fáze experimentálních vzorků a prototypů. Detailní popis metod a zařízení je v příložených publikacích.

Na pracovišti VÚVeL byl tento soubor metod zvládnut a byla získána instrumentace do laboratoře Imunofarmakologie. V rámci PGS studia byli vyškoleni pracovníci schopní tyto komplexí metody používat. Metodické zázemí bylo využito pro vývoj experimentálních terapeutik a vakcín na bázi liposomů, jak je ukázáno v dalších dvou kapitolách.

Pracoviště se dostalo mezi respektované laboratoře s liposomální tematikou a je na seznamu laboratoří, které registruje International Liposome Society.

K udržení vysoké úrovně v oblasti biokompatibilních nanomateriálů je ovšem nutné neustále zdokonalovat a rozšiřovat metodické zázemí a instrumentaci, což se děje s podporou komplexních grantů a s využitím projektu OPVK, který umožňuje vysílat studenty a mladé pracovníky na špičková pracoviště do zahraničí.

1.4.1. Publikace k tématu kapitoly

ANALYTICAL BIOCHEMISTRY 218, 352-357 (1994)

Fast-Protein Liquid Chromatography System as a Tool for Liposome Preparation by the Extrusion Procedure

Jaroslav Turánek

Department of Immunology, Veterinary Research Institute, Hudcova 70, 621 32 Brno, Czech Republic

Received March 25, 1993

Employment of fast-protein liquid chromatography (FPLC) system and a high-pressure filtration cell is described for the production of liposomes by the rapid extrusion technique. The system allows processing of up to 50 ml liposomal suspension in one batch at a defined temperature and applied pressure of up to 4.5 MPa. This relatively simple technique is applicable in any laboratory equipped with FPLC or HPLC systems. © 1994 Academic Press, Inc.

Liposomes, or vesicles, are microscopic membrane-like spherical structures consisting of one or more concentric lipid bilayers enclosing aqueous compartments and having various applications in biology and medicine.

Liposomes are classified by whether the sequestered aqueous volume is enclosed by one (unilamellar) or more (oligolamellar, multilamellar) bilayers (1). Unilamellar vesicles are divided into small unilamellar vesicles with a large curvature and large unilamellar vesicles with a low curvature and hence the properties are similar to those of a flat surface.

Multilamellar vesicles (MLV)¹ are liposomes prepared by the technique of rehydration of a thin lipid film. MLV is a very heterogeneous group in terms of size and morphology (1,2).

Liposomes are rapidly becoming accepted as pharmaceutical agents which may improve the therapeutical activity of a wide variety of compounds. Consequently, there is growing demand for easily reproducible and efficient preparation methods on both a laboratory and an industrial scale. A number of reviews and monographs have summarized studies of liposome production and

¹ Abbreviations used: MLV, multilamellar vesicle; FTMLV, frozen-thawed multilamellar vesicle; FPLC, fast-protein liquid chromatography.

352

properties, their use as carriers for drugs and antigens, and their interaction with a variety of cell types (1-5). The rapid extrusion technique was developed for the

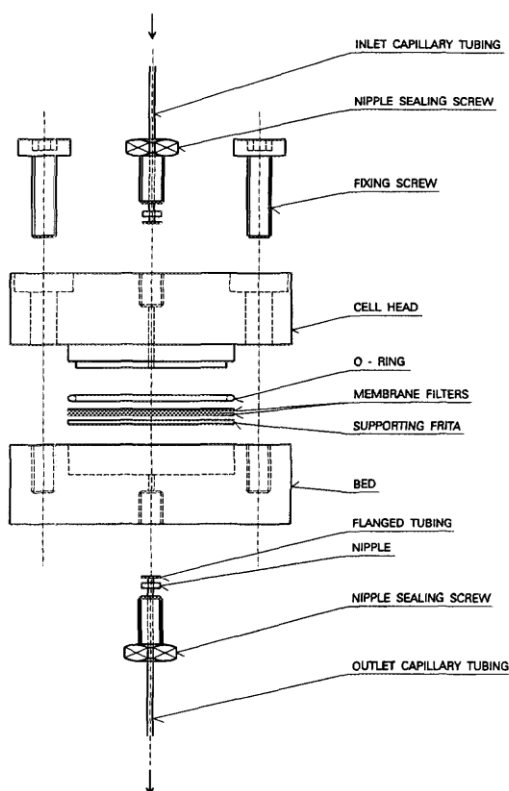


FIG. 1. High-pressure filtration cell.

0003-2697/94 \$6.00
Copyright © 1994 by Academic Press, Inc.
All rights of reproduction in any form reserved.

production of homogeneously sized unilamellar or oligolamellar vesicles by utilizing polycarbonate filters with pore sizes ranging from 30 to 400 nm. The unilamellarity and trapping efficiencies of the vesicles can be significantly enhanced by freezing and thawing the multilamellar vesicles prior to extrusion. The procedure is applicable particularly when very high lipid concentrations (up to 400 mg/ml) are used. In such a case, the extrusion of the frozen-thawed multilamellar vesicles (FTMLV) through 100- to 400-nm filters results in trapping efficiencies of 56–80%, respectively. Liposomes were extruded by the application of nitrogen pressure introduced via a standard gas cylinder fitted with a high-pressure (0–27.5 MP_a) regulator (6–8).

A highly sophisticated FPLC system to be utilized in connection with high-pressure filtration cell for liposome preparation by the rapid extrusion technique is described in this paper.

MATERIALS AND METHODS

Lipids

An egg yolk phospholipid mixture was purified according to Singleton *et al.* (9) and stored in sealed ampules at –20°C until use.

Preparation of Multilamellar Liposomes

The lipid mixture in chloroform solution (200 or 400 mg in 6 ml) was deposited onto the wall of a round-bot-

tom flask (250 ml) by removal of the organic solvent on a rotary evaporator (40°C, 4 h). The dried lipid film was then hydrated with the aqueous phase (150 mM NaCl, 20 mM Hepes, pH 7.4, which had been filtered through a 0.22- μ m filter) under continuous mixing on a mechanical reciprocal shaker for 2 h. The frozen-thawed MLV system (7,8) was obtained by freezing the MLVs in liquid nitrogen and thawing them in a 30°C water bath, repeating the cycle five times.

Electron Microscopy

Micrographs were prepared using the negative staining technique (3% ammonium molybdate solution). A transmission electron microscope BS 500 (Tesla, Czech Republic) was used. All photographs were printed at the final magnification $\times 54,000$. The diameter of the discollapsed sphere times 0.75 was equated to the diameter of the equivalent sphere (6). Apparent liposome diameters were assigned to specific size intervals. At least 300 vesicles were measured for each extruded fraction in two separate experiments.

The scanning electron microscope, BS 300 (Tesla), was used for measuring the actual pore size of membrane filters. Samples of filters were spattered with gold using the Polaron 11 HD apparatus (Polaron).

Extrusion of Liposomes through Membrane Filters

A high-pressure Plexiglas filtration cell was designed to accept two stacked filters 24–25 mm in diameter (Fig.

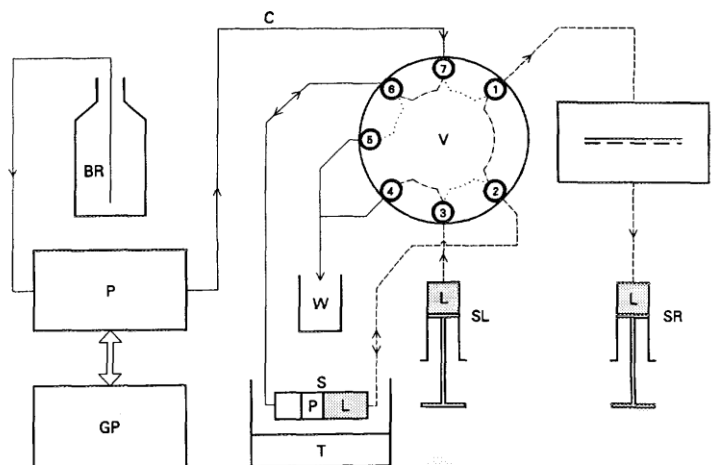


FIG. 2. Adaptation of the FPLC system for the liposome extrusion technique: BR, buffer reservoir; P, pump P-500; GP, gradient programmer GP-250; C, Teflon capillary tubing (1.8 \times 0.8-mm o.d. \times i.d.); W, waste vessel; V, valve V7; 1–7, inputs/outputs; S, Superloop; P, piston; L, liposomes; T, thermostat; F, high-pressure filtration cell; SL, syringe (loading position); SR, syringe (recipient position); valve position, loading, - - - - - extrusion). Working of system described in text.

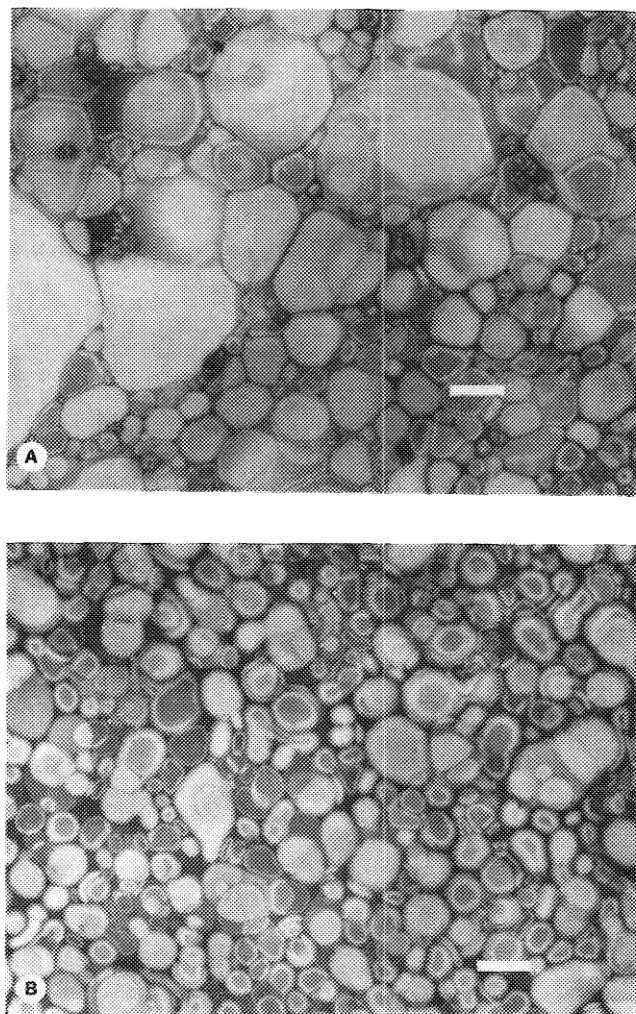


FIG. 3. Negative stain electron micrographs of vesicles prepared by repeated extrusion of multilamellar frozen and thawed vesicles (5 ml, 200 mg/ml egg yolk phospholipid mixture) through polycarbonate filters: (A) unextruded, (B) extruded through 0.4- μm filter pore, and (C) extruded through 0.1- μm filter pore. Bar indicates 200 nm.

1) and withstand pressures of up to 5.0 MPa (upper limit for FPLC) without any difficulties. A fine fritta support effectively protected the membrane filters and no breakage occurred in any of the experiments performed at high pressure. The geometry of the cell keeps its dead space at a minimum to avoid dilution when

small volumes of liposome suspension are injected. The total dead space is about 250 μl (50 μl above the filter and 200 μl in the fritta support). Isopore membranes (Millipore) with pore sizes 0.4, 0.2, and 0.1 μm were used and pressures of up to 4.5 MPa were applied.

FPLC (Pharmacia, Sweden) was used as the program-

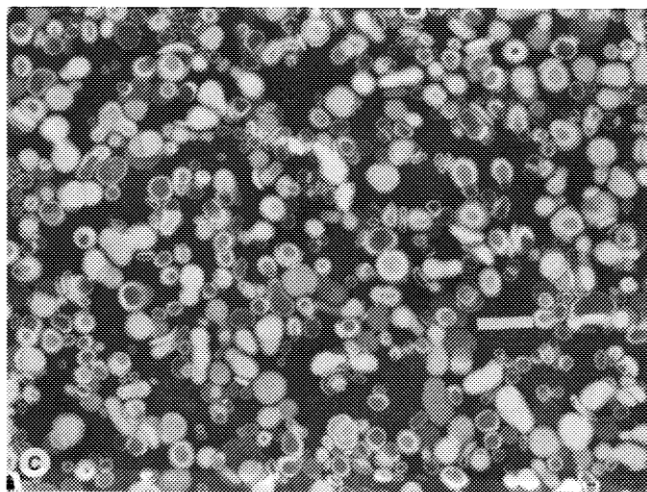


FIG. 3—Continued

mable pressure delivery system. The arrangement of the pressure cell and FPLC for liposome extrusion is shown in Fig. 2. Small volumes of a liposome suspension (up to 4 ml) were loaded into the sample loop through the valve V-7 (Pharmacia), while larger volumes (up to 50 ml) were loaded into Superloop (Pharmacia), submerged together with the cell and recipient syringe in a thermostated water bath Julabo 6A (Julabo, Germany) when other than an ambient temperature was demanded.

Syringes were used for the injection and collection of the liposome suspension. The pressure cell was connected to the V-7 valve by means of tubing connectors and capillary Teflon tubing (1.8×0.5 mm) (Pharmacia). Both the desired flow rate and the extruded volume for a single run were programmed by the gradient programmer GP-250 (Pharmacia).

MLVs (200 mg phospholipid/ml) were prepared in presence of $1 \mu\text{Ci}$ [^{14}C]sucrose in the aqueous phase as the labeled marker to determine trapped volumes (7). Extrusion of frozen and thawed MLV through membrane filters was performed in the labeled medium as indicated above. Nontrapped marker was removed from MLV and FTMLV by centrifugation (10,000 *g*, 30 min, 4°C) and from extruded vesicles by ultracentrifugation (100,000 *g*, 45 min, 4°C). Sedimented vesicles were resuspended in marker-free aqueous phase and the centrifugation was repeated. Trapped [^{14}C]sucrose was es-

timated using Tri-Carb 1600 CA liquid scintillation counter (Packard). Calculated trapped volumes are expressed as microliters of trapped volume per micromole of phospholipid.

RESULTS AND DISCUSSION

Photographs in Fig. 3 illustrate the decrease of liposome diameters in accordance with decreasing pore sizes of filters used for extrusion. Figure 3A shows a heterogeneous frozen-thawed MLV system in which all types of liposomes are present. Extrusion through a $0.4\text{-}\mu\text{m}$ filter (Fig. 3B) eliminates vesicles larger than 200 nm. Two maxima are evident in Fig. 4. The size of the majority of liposomes (50%) ranged between 78 and 147 nm. The second maximum (43%) represents the size range 36–77 nm. Extrusion through a $0.2\text{-}\mu\text{m}$ filter eliminated vesicles above 150 nm (Fig. 4). Liposomes of the size range 36–91 nm (76%) were the most abundant.

Vesicles larger than 120 nm were eliminated when $0.1\text{-}\mu\text{m}$ filters were used for extrusion (Fig. 3C), the largest proportion of liposomes (86%) coming in the size range 20–77 nm (Fig. 4).

Data summarized in Table 1 allow the conclusion that getting over the critical pressure is necessary for the extrusion of vesicles through filter pores. The flow rate per area unit value $V_s = v/S$ ($\text{ml}/\text{min} \cdot \text{cm}^2$) has been introduced to compare various cells and filter types. The critical pressure is strongly dependent on filter pore size and the transition temperature of the lipid

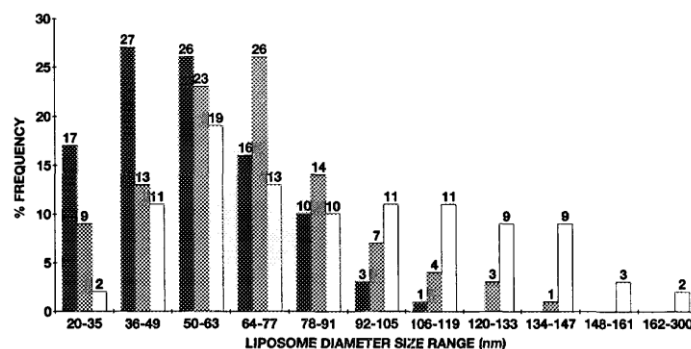


FIG. 4. Size distribution determined by negative stain electron microscopy of frozen and thawed multilamellar vesicles extruded through polycarbonate filters. Vesicles were prepared as detailed under Materials and Methods. Black—MLV extruded through 0.1- μ m filter; gray—MLV extruded through 0.2- μ m filter; white—MLV extruded through 0.4- μ m filter.

used. Estimated critical pressures for extrusion of liposomes (5 ml, 200 mg/ml egg yolk phospholipid mixture) at 20°C and pore sizes 0.4, 0.2, and 0.1 μ m are given in Table 1. Actual pore sizes, measured by electron microscopy, reached 60–70% of the declared value and this fact is reflected in the mean diameter of liposomes.

Trapped volumes for MLV, FTMLV, and FTMLV extruded through filters with various pore sizes are shown in Table 2. It is evident that freezing and thawing of MLV makes for a 10-fold increase in the entrapped volume. Freezing and thawing causes dehydration of the phospholipid bilayer and is responsible for defects in the bilayer structure and the ensuing changes of morphology of MLV and an increase in trapped volume (8,10,11). Extrusion of FTMLV makes for a decrease of liposome diameters (see Fig. 4) which is accompanied by a decrease in trapped volume.

Temperature is crucial for liposomes composed of phospholipids below their transition temperature. Indeed, the estimated critical pressure for multilamellar

vesicles prepared from a soya phospholipid mixture (100 mg/ml) at 20°C and 0.1- μ m pore size was 4.4 MPa (nearly the upper pressure limit for FPLC). Temperature elevation to 40°C (above solid-to-fluid transition) results in a decrease of the critical pressure to 2.5 MPa (unpublished observation), which is similar to that necessary for the egg phospholipid mixture used.

FPLC System Modification

Connection of the high-pressure filtration cell to the FPLC system in our experiments proved to be a convenient application of the rapid extrusion technique on laboratory scale. Even if operated manually, the non-tedious preparation of 5 ml of a liposomal suspension (100–400 mg/ml) did not take more than 15 min for 10 extrusion runs. One batch of liposomal suspension (50 ml, 100 mg/ml egg yolk phospholipid mixture, 0.2- μ m filter) was produced in test experiments when the 50-ml Superloop was connected. This paper provides basic

TABLE 1
Dependence of Back Pressure on Flow Rate and Pore Size for Egg Yolk Phospholipid Liposomes

Filter pore size (μ m)		Flow rate (ml/min)	Flow rate per area (ml/min \cdot cm ²)	Pressure (MP _a)	Critical pressure at 20°C (MP _a)
Declared	Measured				
0.4	0.28	3	1.00	0.5	0.4–0.5
		5	1.63	0.5	
		10	3.26	0.6	
0.2	0.12	3	1.00	0.9	0.8–0.9
		5	1.63	0.1	
		10	3.26	1.2	
0.1	0.06	3	1.00	2.2	2.0–2.2
		5	1.63	2.3	
		10	3.26	3.0	

TABLE 2
Trapped Volumes of Liposomes Prepared
from Egg Yolk Phospholipid

Liposomes	Filter pore size (μm)		Trapped volume $\mu\text{l}/\mu\text{mol}$ phospholipid
	Declared	Measured	
MLV	—	—	0.23 ± 0.06
FTMLV	—	—	2.6 ± 0.5
Extruded FTMLV	0.4	0.28	2.2 ± 0.3
	0.2	0.12	1.5 ± 0.2
	0.1	0.06	1.1 ± 0.2

knowledge which can be helpful in employing the BioPilot System (Pharmacia) for fully automated large-scale production of liposomal preparations by the rapid extrusion technique.

ACKNOWLEDGMENTS

I thank Dr. B. Šmíd for the excellent electron micrographs of liposomes, and Mr. J. Kudrna for scanning electron microscopy of membrane filters.

REFERENCES

1. Deamer, D. W., and Uster, P. S. (1983) in *Liposomes* (Ostro, M. J., Ed.), pp. 27-51, Marcel Dekker, New York/Basel.
2. Cullis, P. R., Hope, M. J., Bally, M. B., Madden, T. P., and Mayer, L. D. (1987) in *Liposomes: From Biophysics to Therapeutics* (Ostro, M. J., Ed.) pp. 39-69, Marcel Dekker, New York/Basel.
3. Woodle, M. C., and Papahadjopoulos, D. (1989) in *Methods in Enzymology*, Vol. 171, pp. 193-217, Academic Press, San Diego.
4. Lopez-Berenstein, G., and Fidler, I. J., Eds. (1989) in *Liposomes in the Therapy of Infectious Diseases and Cancer*, A. R. Liss, New York.
5. Yagi, K., Ed. (1986) in *Medical Application of Liposomes*, Japan Scientific Societies Press, Tokyo.
6. Olson, F., Hunt, C. A., Szoka, F. C., Vail, W. J., and Papahadjopoulos, D. (1979) *Biochim. Biophys. Acta* **557**, 9-23.
7. Hope, M. J., Bally, M. B., Webb, G., and Cullis, P. R. (1985) *Biochim. Biophys. Acta* **812**, 55-65.
8. Mayer, L. D., Hope, M. J., and Cullis, P. R. (1986) *Biochim. Biophys. Acta* **858**, 161-168.
9. Singleton, W. S., Gray, M. S., Brown, M. L., and White, J. L. (1965) *J. Am. Oil Chem. Soc.* **42**, 53-55.
10. Wilschut, J., and Hoekstra, D. (1986) *Chem. Phys. Lipids* **40**, 145-166.
11. Mayer, L. D., Hope, M. J., Cullis, P. R., and Janoff, A. S. (1985) *Biochim. Biophys. Acta* **817**, 193-196.

Linkup of a Fast Protein Liquid Chromatography System with a Stirred Thermostated Cell for Sterile Preparation of Liposomes by the Proliposome–Liposome Method: Application to Encapsulation of Antibiotics, Synthetic Peptide Immunomodulators, and a Photosensitizer

Jaroslav Turánek,* Dana Záluská,† and Jiří Neča*

*Veterinary Research Institute, Hudcova 70, 621 32 Brno, Czech Republic; and †Lachema Joint-Stock Company, Institute of Fine Chemicals Karásek 28, 621 33 Brno, Czech Republic

Received June 21, 1996

The proliposome–liposome method is based on the conversion of the initial proliposome preparation into a liposome dispersion by dilution with the aqueous phase. This technique is characterized by an extremely high entrapment efficiency and is suitable for the encapsulation of a wide range of drugs with different water and alcohol solubility. A description of a home-made stirred thermostated cell and its linkup with an FPLC system for a rapid and automated preparation of multilamellar liposomes under strictly controlled conditions (temperature, dilution rate, and schedule) is presented. The highly reproducible procedure yields multilamellar liposomes with a high encapsulation efficiency for various drugs. Carboxyfluorescein, as a model hydrophilic compound, was entrapped with an efficiency of $81 \pm 2\%$. The antibiotics neomycin and gentamycin were entrapped with efficiencies of 65 and 69%, respectively. Synthetic immunomodulators adamantylamide dipeptide, muramyl dipeptide, and β -D-GlcNAc-norMurNAc-1-Abu-D-isoGln were entrapped with efficiencies of 87, 62, and 85%, respectively. The photosensitizer mesotetra-(parasulfophenyl)-porphin was entrapped with an efficiency of 65%. The cell has been designed for laboratory-scale preparation of liposomes (300–1000 mg of phospholipid per run) in a procedure taking less than 90 min. The method can be readily scaled up and linked with secondary processing methods, such as pressure extrusion through polycarbonate filters. © 1997 Academic Press

Liposomes, i.e., microscopic membrane-like spherical structures consisting of one or more concentric lipid bilayers enclosing aqueous compartments, have be-

come a useful tool and model in various areas of science and liposomal drugs are available commercially (1). Liposomes were adopted by numerous researchers as the vehicle of choice for drug and vaccine delivery and targeting (2, 3). Liposomes are classified in terms of the number of bilayers enclosing the sequestered aqueous volume into unilamellar, oligolamellar, and multilamellar vesicles. Unilamellar vesicles are divided into small unilamellar vesicles (SUV) with a large curvature, and large unilamellar vesicles (LUV) with a low curvature and hence with properties similar to those of a flat surface. Multilamellar vesicles (MLV)¹ are liposomes representing a heterogeneous group in terms of size and morphology (4).

Size, morphology, and lipid composition endow liposomes with different properties in terms of stability, targeting to various tissues, entrapment efficiency for hydrophilic and hydrophobic drugs, etc.

A variety of procedures for the preparation of various types of liposomes have been described and summarized in several reviews and monographs (5, 6). The conventional method of hydration of a lipid film with subsequent freezing and thawing of liposomes is the method of choice for the preparation of MLV. Extrusion of MLV through polycarbonate filters with various pore sizes is an easy way of obtaining oligolamellar or unilamellar liposomes with various size distributions (4, 7). In our previous paper (8), we described the construction

¹ Abbreviations used: MLV, multilamellar vesicles; PL, proliposome–liposome method; CF, carboxyfluorescein; AdDP, adamantylamide dipeptide; MDP, muramyl dipeptide; DDD, β -D-GlcNAc-norMurNAc-1-Abu-D-isoGln; TFA, trifluoroacetic acid; TPPS₄, mesotetra-(parasulfophenyl)-porphin; PC, phosphatidylcholine; FTMLV, frozen-thawed multilamellar vesicles.

of a high-pressure cell and its linkup with an FPLC system for laboratory-scale production of liposomes by the rapid extrusion technique (up to 50 ml of liposome suspension per one run).

In this paper we present a description of a stirred thermostated cell and its linkup with an FPLC system for a rapid production of multilamellar liposomes by the proliposome–liposome method (PL), which is based on the conversion of the initial proliposome preparation into a liposome dispersion by dilution under strictly controlled conditions. This technique is characterized by an extremely high entrapment efficiency, when compared with other methods based on passive entrapment, and is suitable for the encapsulation of a wide range of drugs with various water and alcohol solubilities (9).

The method can be readily scaled up and linked with secondary processing methods, such as extrusion through polycarbonate filters for the preparation of oligolamellar and unilamellar liposomes.

The cell is a prospective tool for modelling the processes of industrial-scale preparation of liposomes.

MATERIALS AND METHODS

Stirred Cell and Its Linkup with FPLC

A schematic drawing and the actual appearance of a disassembled cell are shown in Figs. 1 and 2, respectively. The acrylic body of the thermostatic jacket was designed to accept a centrifugal tube (Corning 50 ml), and two O-rings were used to seal the tube in the thermostatic chamber. The diluting solution is delivered through a teflon capillary (1.8 o.d. \times 0.5 i.d. mm), and a sterile filter (0.22 μ m, Millipore) removes residual particles and microorganisms to maintain the preparation sterile. A Teflon body accepts the filter and protects the capillary from unwanted bending. A magnetic stirrer hangs on the flanged end of the capillary. The stirrer with turbine-like blades is shaped to reach the conical part of the tube near its bottom. The blades are arranged to lift the suspension up from the bottom and maintain homogeneity especially during the first step of dilution when the proliposome mixture is viscous. The body of the stirrer is made of teflon and pieces of Teflon-coated ferrite are inserted into its arms. Another sterile filter closes the pressure–compensation hole and protects the interior from airborne contamination. When a run is finished, the head of the cell is removed and the tube is closed with an original lid.

The linking of the cell with a programmable system for the delivery of the diluting solution is shown in Fig. 3. We used an FPLC system (Pharmacia, Sweden) for accurate flow rate programming. The fraction collector Frac 100, connected with the peristaltic pump P1 (Pharmacia, Sweden) or another adequate system, can be used to ensure a defined flow rate even if the two-step dilution method is used and to stop the pump at

the end of the run. The thermostat Julabo 6A (Julabo, Germany) was used to maintain a constant cell temperature.

Preparation of Proliposome Mixture and Conversion into Liposomes

The egg yolk phosphatidylcholine preparation Lipoid E 80 (Lipoid, Germany) was used in our experiments. A proliposome mixture was prepared using a modification of the method described by Perrett *et al.* Briefly, the lipids (300 mg of solid yellowish grains) were dissolved in pure warm ethanol (240 mg, 50°C) and cooled to room temperature. Water phase was added according to the pattern lipid:ethanol:water (100:80:X, w/w/w). Tris–HCl (25 mM, pH 7.2) was used as the water phase and the value X was 200 in most experiments (600 mg of water phase). The compounds to be entrapped were dissolved in the water phase and added at this step. Water-insoluble compounds are preferably dissolved in ethanol together with phospholipids. The opaque viscous mixture was heated to 60°C for 10 min and then allowed to cool to room temperature yielding a proliposome mixture. The latter was transferred into the stirred cell. The cell was sterilized with 70% ethanol at 50°C for 60 min before use. The proliposome mixture was converted into a liposome suspension by continuous dilution with the water phase (total volume of 39 ml) at a defined flow rate and temperature (23°C). The two-step dilution was accomplished by continual addition of 3 ml of the water phase at a flow rate of 100 μ l/min in the first step and 36 ml of the water phase at 1000 μ l/min in the second step. The water phase used for dilution was free of the compound to be entrapped. The sterility of the product was checked by culture on blood agar (37°C, 96 h).

Preparation of Frozen and Thawed Multilamellar Vesicles

The lipid mixture, dissolved in chloroform (200 mg in 6 ml), was deposited onto the wall of a round-bottom flask (250 ml) by removal of the solvent in a rotary evaporator (40°C, 4 h). The dried lipid film was then hydrated with the aqueous phase (150 mM NaCl, 20 mM Hepes, pH 7.2, previously filtered through a 0.22- μ m filter) under continuous mixing on a mechanical reciprocal shaker for 2 h. The frozen–thawed MLV system (7) was obtained by freezing the MLVs in liquid nitrogen, thawing them in a 30°C water bath, and repeating the cycle five times.

Assay of Encapsulation Efficiency

5,6-Carboxyfluorescein (Molecular Probes) was quantified spectrophotometrically on the luminescence spectrometer LS 50 (Perkin–Elmer) at 470 nm (excita-

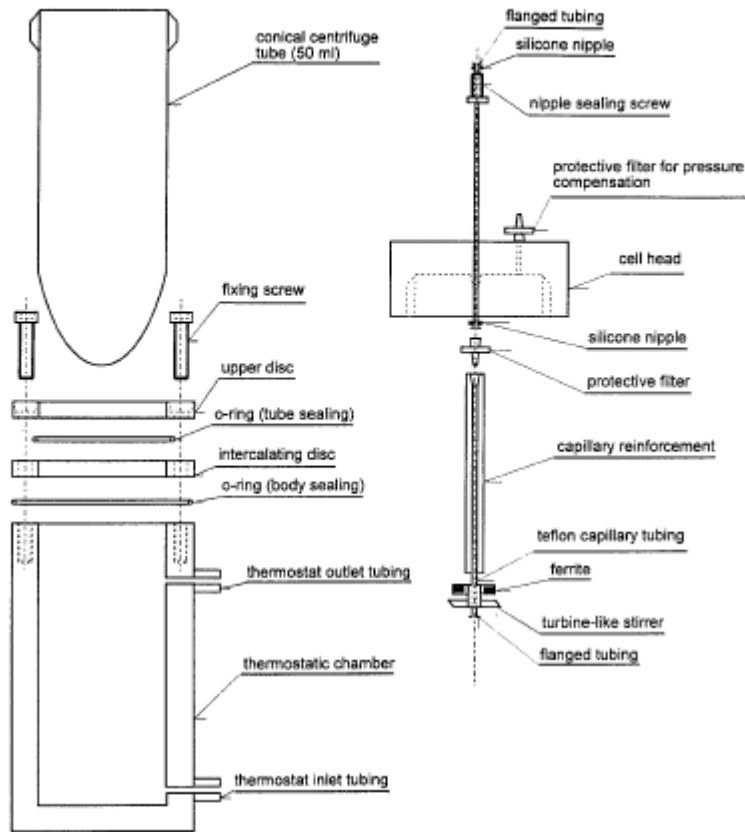


FIG. 1. Schematic drawing of the stirred thermostated cell.

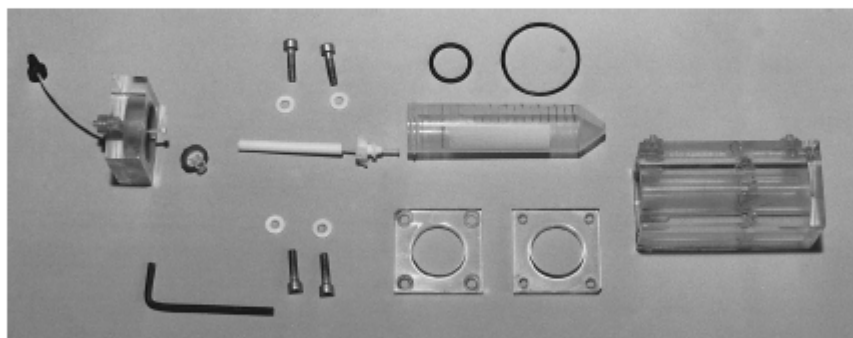


FIG. 2. Photograph of a disassembled cell.

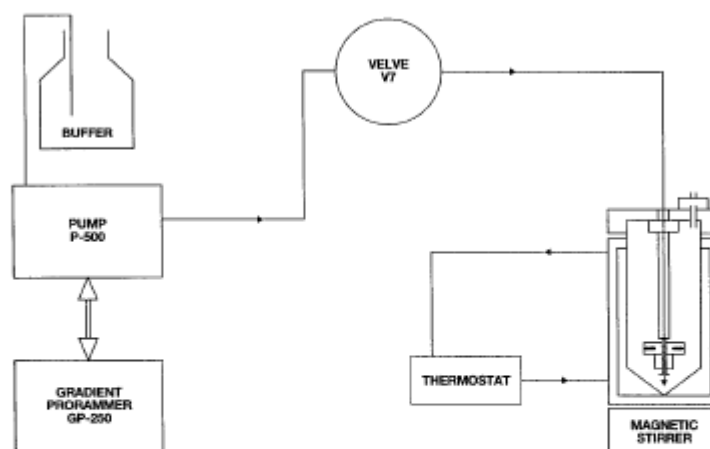


FIG. 3. Schematic drawing of linkup of the cell with FPLC. Operation described in text.

tion) and 520 nm (emission). The efficiency of entrapment was calculated using the equation

$$\% \text{ Entrapment} = C/A \times 100.$$

The validity of the calculation was checked using the equation

$$A = B + C,$$

where A is total (i.e., free and encapsulated) CF in the liposomal suspension, B is free (nonencapsulated) CF, and C is encapsulated CF.

The synthetic immunomodulators adamantylamide dipeptide (AdDP) (Léčiva, Prague, Czech Republic), muramyl dipeptide (MDP) and β -D-GlcNAc-norMurNAc-L-Ábu-D-isoGln (DDD) (a gift from Dr. M. Ledvina, Institute of Organic Chemistry and Biochemistry, Prague) were assayed by HPLC using the chromatographic system Waters consisting of the Waters 600 gradient pump, the Waters 717 plus autoinjector, the Waters 996 diode array detector, and the Waters 474 fluorescence detector. The system was controlled by the program Millennium 2010. All the analyses were run on the column NOVA-PAC C 18 ($4 \mu\text{m}$, $150 \times 3.9 \text{ mm}$, precolumn $20 \times 3.9 \text{ mm}$). Methanol:water (0.1% TFA) was used as the mobile phase for the analysis of AdDP (ratio 45:55) and MDP and DDD (ratio 10:90). The immunomodulators were detected at 203 nm and the obtained UV spectra were matched against the spectra of standards. In the case of DDD, two peaks of anomers appeared in the chromatogram. Both peaks were used for the calculation. The antibiotics gentamycin and neomycin (Sigma) were analyzed by precolumn derivat-

ization with *O*-phthalaldehyde and detected by a fluorescence detector set at 340 nm/455 nm Ex/Em (10, 11).

The photosensitizer mesotetra-(parasulfophenyl)porphyrin (TPPS₄) (kindly provided by Lachema Company, Brno, Czech Republic) was assayed spectrophotometrically at 410 nm using the standard addition method.

Total masses of free and entrapped drugs were determined and used for the calculation of encapsulation efficiency. Drugs entrapped in liposomes were separated from free ones by centrifugation ($15,000g$, 20 min, 4°C). The liposomes were solubilized with TRITON (1% final concentration) to release the entrapped drugs for the assay.

Determination of Captured Volume

Captured volume, defined as the volume of the entrapped discontinuous aqueous phase per mass unit of the lipid phase and expressed in microliters per micromole of phospholipid, was determined as described by Armengol and Esterlich (12) with a minor modification. Briefly, the concentration of CF in the proliposome mixture and in the diluting buffer was $500 \mu\text{M}$. Nonentrapped CF was separated from the liposomes by centrifugation ($15,000g$, 20 min, 4°C), the liposomes were washed twice and resuspended in CF-free buffer to obtain the concentration of 1 mg phospholipid per 1 ml. An aliquot of the liposomes was solubilized with TRITON (final concentration 1%) and the concentration of CF was determined spectrofluorometrically using a calibration curve of a CF standard dilution series covering the range 10–1000 nM of CF.

The captured volume was calculated using the equation

$$V_c = M/C \times L,$$

where V_e is entrapped volume (in $\mu\text{l}/\mu\text{mol}$), M is total mass of CF in the washed liposome preparation, C is initial concentration of CF in the diluting buffer and the proliposome-liposome mixture, and, L is total mass of lipid in the purified preparation.

Electron Microscopy

Electron micrographs were made using the negative staining technique (3% ammonium molybdate solution). The transmission electron microscope BS 500 (Tesla, Czech Republic) was used. The final magnification of the micrograph prints was $36,000\times$.

Particle-Size Analysis by Photon Correlation Spectroscopy

Light-scattering analyses of liposomal preparations were done on the photon correlation spectrometer N4 Plus (Coulter Electronics, USA). Samples of liposomal preparations (0.7 mg phospholipid/ml) were analyzed at 20.0°C and an angle of 90° . A size distribution analysis of the data was done according to the instrument manual.

Statistical Analyses

One-way analysis of variance (ANOVA) with Newman-Keuls posttest contrasts for comparisons of flow rates and entrapment efficiencies of CF. The unpaired two-tail t test was used for the comparison of entrapment efficiency for PL vs FTMLV. The statistical software used was GraphPad PRISM, V.2.00 (GraphPad Software, Inc. San Diego, CA).

RESULTS

Effect of Composition of Proliposome Mixture on Entrapment Efficiency

The entrapment efficiency of the liposomes formed following the dilution of the proliposome mixtures to a final volume of 40 ml was plotted as a function of the weight of the aqueous phase present in the initial proliposome mixtures. A typical plot showing the efficiency of entrapment of CF by Lipoid 80 E liposomes is presented in Fig. 4. The region of maximum entrapment efficiency was mapped in detail. In the case of Lipoid 80 E, a high entrapment efficiency was obtained with the proliposome composition lipid:ethanol:water = 100:80:150–230 (w/w/w). The composition of the proliposome mixture lipid:ethanol:water = 100:80:200 was used for further studies. The liposomes prepared of a proliposome mixture with this composition yielded the entrapment efficiency of $81 \pm 2\%$ for CF (five separate preparations). A negatively stained electron micrograph of liposomes prepared by the proliposome-liposome method is shown in Fig. 5A. Heterogeneity of the liposomal preparation in terms of size, lamellarity and

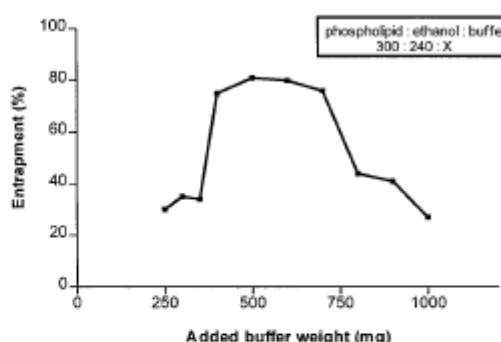


FIG. 4. Plot of entrapment percentage of carboxyfluorescein as a function of weight of buffer (X) incorporated in the initial proliposome mixture. For details, see the Materials and Methods.

morphology can be clearly seen. Multicentric liposomes are also present.

Size distribution processor analysis revealed a bimodal distribution of liposome sizes and weights. In terms of the weight distribution, the major fraction (95.5%) represents vesicles with a size of 1736 ± 383 nm and the minor fraction (4.5%) represents vesicles with a size of 170 ± 46 nm. Graphical presentation of the result of size distribution analysis of liposomes is shown in Fig. 5B.

Entrapped Volume

Entrapped volumes of frozen-thawed MLV prepared by the hydration of a lipid film and of liposomes prepared by the proliposome-liposome method were compared. The values of $1.83 \pm 0.07 \mu\text{l}/\mu\text{mol}$ phospholipid and $1.26 \pm 0.06 \mu\text{l}/\mu\text{mol}$ phospholipid were found for the former and the latter, respectively.

Effect of Dilution Rate on Entrapment Efficiency

As can be seen from data given in Table 1, the dilution speed exerts only a weak effect on the entrapment efficiency. The preparation of liposomes by two-step dilution with flow rates of $100 \mu\text{l}/\text{min}$ (first step) and $1000 \mu\text{l}/\text{min}$ (second step) takes only about 70 min. The whole procedure, including the preparation of the proliposome mixture, takes 90 min. The upper limit for the flow rate was not tested and, as a matter of fact, results from flow characteristics of the $0.22\text{-}\mu\text{m}$ filter used for the maintenance of interior sterility.

Effect of Transformation Temperature on Entrapment Efficiency

The dependence of entrapment efficiency on the transformation temperature is shown in Fig. 6. A dramatic decrease in entrapment efficiency was observed at tem-

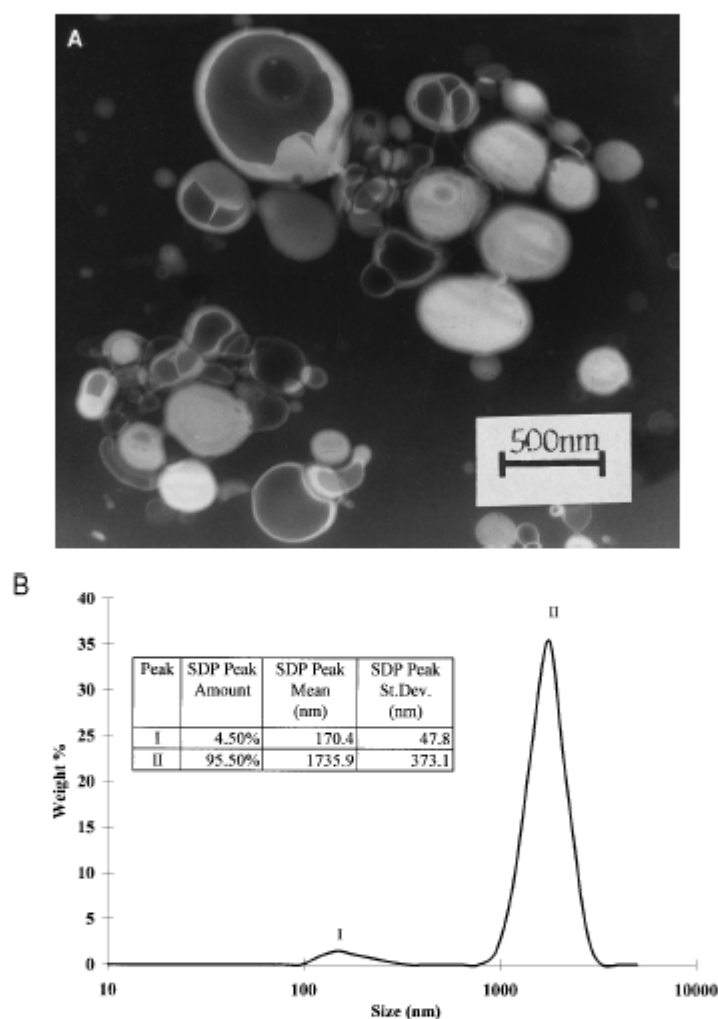


FIG. 5. (A) Negatively stained electron micrograph of liposomes prepared by the proliposome-liposome method. Bar, 500 nm. (B) Size distribution of Lipoid E80 liposomes prepared by proliposome-liposome method plotted in terms of weight (%).

peratures below 30°C and the efficiency rose only slowly when the temperature was increased above 30°C.

Comparison of Entrapment Efficiency for Selected Drugs of FTMLV and PL Liposomes

The entrapment efficiencies for synthetic immunomodulators and glycosidic antibiotics are summarized in Table 2. Both types of liposomes showed a high entrapment efficiency for the hydrophobic AdDP. The hydrophilic MDP and DDD were entrapped with a similar efficiency by FTMLV liposomes. Compared with AdDP

or DDD, the entrapment efficiency of PL liposomes for MDP was lower by approx 20%. Neomycin and gentamycin were entrapped with similar efficiencies by PL liposomes, but entrapment efficiencies of FTMLV liposomes for the two antibiotics were different. TPPS₄ was entrapped with the same efficiency by any of the liposome types.

Sterility of Liposomal Preparations

No bacterial contamination was detectable after 96 h of culture on blood agar in any of the liposomal preparations under study.

TABLE 1

Effect of Flow Rate on Entrapment Percentage of Carboxyfluorescein in Two-Step Dilution of a Proliposome Mixture

Flow rate (ul/min) phase 1/phase 2	% Entrapment		
	N	Mean	St. Dev.
A 20/20	4	74	1.4
B 20/200	4	76	1.8
C 20/400	4	75	1.5
D 20/1000	4	76	2.0
E 100/1000	4	81*	1.8
F 400/1000	4	74	1.4

* The significantly different result from all other means ($P = 0.05$, based on post-ANOVA Newman-Keuls contrasts).

DISCUSSION

The proliposomal concept is suitable for *in situ* liposome preparation, minimizing the problems associated with the storage of liposomal preparations. This concept is based on various principles, such as deposition of lipids on soluble supports with a large surface area (e.g., sorbitol and sodium chloride) or the commercially available Natipide II, a vesicular gel formed by liposomes supplied by Nattermann Phospholipid (13–15).

The method described by Perrett *et al.* (9), which is based on proliposomal preparation of hydrated stacked bilayer sheets in a water-ethanol solution, is simple and practical. Generally, the organization of a lipid/ethanol/water mixture can be described in terms of a three-phase diagram which can be divided into the following three principal areas: lipid dissolved in aqueous ethanol, hydrated bilayers suspended in aqueous ethanol, and a liposomal area. Spontaneous formation of liposomal suspensions is accomplished by the addition of excess aqueous phase to a lipid mixture. The boundaries between the areas in the three-phase diagram should be determined for any particular lipid composition. The major component of Lipoid E 80, which we used for the preparation of liposomes, is phosphatidylcholine (PC). Therefore, we used the published three-phase diagram for PC (9), changing only the proportion of the water phase in the proliposome mixture to find the optimal encapsulation efficiency. The pattern ethanol:lipid:water of the optimized proliposome composition was 100:80:200 (w/w/w). However, maximum was in the range 150 to 230 weight units for the aqueous phase (see Fig. 4), i.e., at a position similar to that postulated by Perrett (9) for pure PC. Moreover, the optimized composition of the proliposome mixture was in the proliposome area of the three-phase diagram for PC. That means that the boundaries between liposomes and precipitated bilayers for pure PC and Lipoid E 80 are similar.

The physical state of the proliposome mixtures is

strongly temperature-dependent and the thermal cycle used for the transformation of the proliposome mixture is decisive for the resulting encapsulation efficiency. It should be noted that the transition temperature for egg yolk lecithin membranes is within the range -15 to -7°C ; hence, the transition from the solid (gel) to the liquid-crystal phase does not affect the process of liposome formation at the temperatures used in our experiments. The solubility of lipids in aqueous ethanol increases markedly with rising temperature. This strong temperature dependence is an important feature of the proliposome system. Mixtures at the boundary of the proliposome region can convert from their original proliposome form into liposomes on cooling. Our experiments have confirmed considerable effects of heating temperature on encapsulation efficiency. We have found that a break point lay at 30°C . Below 30°C there was a steep decrease in entrapment efficiency for CF. The entrapment efficiency of 73% remained constant in the range of 30 – 45°C and increased slowly to 82% when the temperature rose to 60°C . These results are in a good accordance with the temperature-dependent increase in the isotropic component in ^{31}P NMR (9), reflecting an increase in nonbilayer organized molecules of phospholipids.

The design of the cell allows an easy assembly and linkup with FPLC or other delivery systems. Most components used in the construction can be found in any laboratory or are listed in catalogues of major suppliers of laboratory utensils. A programmable delivery system, such as FPLC, is very useful for comfortable and precise work giving highly reproducible results. Supposing that the encapsulation efficiency might be influenced by changing the rate of the proliposome-liposome transformation, which depends on the flow rate of the aqueous phase, we investigated this system using a two-step dilution method. Proliposomes convert into liposomes during the first step and the concentration

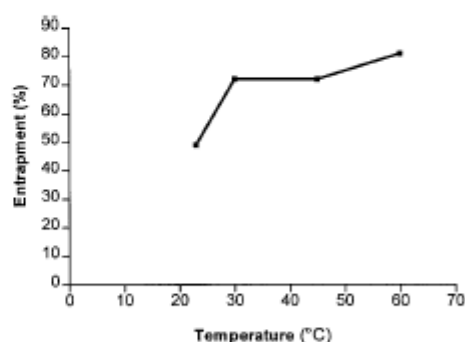


FIG. 6. Effect of transformation temperature on entrapment percentage of carboxyfluorescein in two-step dilution of a proliposome mixture. For details, see Materials and Methods.

TABLE 2
Comparison of Entrapment Efficiencies of FTMLV and PL Liposomes for Selected Drugs

Drugs to be entrapped in mg/300 mg phospholipid			% Entrapment			
			Proliposome-liposome		FTMLV	
			Mean	SD	Mean	SD
A	AdDP	2.28	87*	2.2	78	3.2
B	MDP	1.56	62*	2.8	36	4.7
C	DDD	1	85*	2.8	32	4.1
D	Neomycin	30	65*	1.7	36	3.9
E	Gentamycin	30	69*	2.2	52	4.2
F	6-Carboxyfluorescein	1	81*	1.5	52	3.9
G	TPPS ₄	1.3	65	1.5	62	4.0

* The significant differences from the corresponding results obtained by the FTMLV method ($P < 0.001$, based on t tests).

of ethanol bound to liposomes is reduced to 0.5% in the second step. As shown in Table 1, changes of dilution speed in the first and the second steps had no marked effects on the encapsulation efficiency. An optimum was found at 100 $\mu\text{l}/\text{min}$ for the first and 1000 $\mu\text{l}/\text{min}$ for the second steps. At these flow rates, the procedure was completed within 70 min. The somewhat lower encapsulation efficiency found for the slow-dilution step (20 $\mu\text{l}/\text{min}$) could have resulted from the release of CF from liposomes, because the procedure took 10 to 33 h. The flow rate is limited by the throughput of the filter (in the second dilution step) and by a decrease in encapsulation efficiency (in the first dilution step).

In our experiments, the proliposome-liposome method was used for the encapsulation of various drugs and comparisons were made with FTMLV. The values 1.26 $\mu\text{l}/\mu\text{mol}$ (CF as a marker) for entrapped volume and $81 \pm 2\%$ (CF as a marker) for entrapment efficiency are comparable with 1.5 $\mu\text{l}/\mu\text{mol}$ (inulin as a marker) for entrapped volume and $77.7 \pm 5.7\%$ (CF as a marker) entrapment efficiency published by Perrett (9). It should be noted that the higher entrapped volume in FTMLV liposomes (1.83 $\mu\text{l}/\mu\text{mol}$) was not associated with a higher encapsulation efficiency (52% for CF). Other drugs, too, were encapsulated more effectively into liposomes prepared by the PL method. The only exception was AdDP, which was encapsulated with a relatively high efficiency, probably owing to the hydrophobic character of the adamantyl moiety. The entrapped volume of our FTMLV liposomes, prepared from Lipoid E80, was lower than that published by Mayer *et al.* (1.83 vs 3.07 $\mu\text{l}/\mu\text{mol}$) for PC (77% entrapment with ^{22}Na as a marker) and the same concentration of lipids (200 mg/ml). We can conclude that entrapment efficiencies for Lipoid E80 FTMLV liposomes would be proportionate to entrapped volumes and that the value of 46% should be reached for small hydrophilic compounds. With the exception of AdDP and TPPS₄, the entrapment efficiencies of all the tested compounds varied around this value within $\pm 10\%$. It

is evident that not only the passive entrapment of the aqueous phase, reflected in entrapped volume, but also interactions of a particular compound with hydrophobic or polar parts of lipids markedly enhance the efficiency of entrapment. Vesiculation of lipid bilayers and sealing of the membrane are critical steps in the formation of liposomes. Unstable transient structures appear during the formation of liposomes, a process that is difficult to investigate. A unifying model, based on a bilayered phospholipid fragment, was proposed by Lasic (17). No data describing the transformation of proliposomes (dispersed floccules of lamellar phase) into liposomes were found in available literature. Also unclear are the existence and possible role of bilayered phospholipid fragments in that process. We assume that a relatively high lipid concentration and the large surface area of the lamellar phase in the proliposome mixture are responsible for high entrapment efficiencies for various drugs.

It can be concluded that the cell described in this paper has proved suitable for a rapid, sterile, and highly reproducible production of liposomes by the proliposome technique. The method was successfully applied to the encapsulation of various drugs. Variations of some parameters can release a hidden potential of versatility of this method. Replacement of ethanol with other organic solvents (glycerol), a temperature jump during the preparation, and freeze-drying of liposomes with a high ethanol concentration after the first dilution step are examples of modifications that are being investigated currently.

ACKNOWLEDGMENTS

This work was supported by the Ministry of Industry and Trade (Grant MP-3310/22/94), the Ministry of Agriculture (Grant RE-5559), and the Grant Agency of the Czech Republic (Grant 508-94-1050). We thank Dr. Bedřich Šmíd for the electron micrograph of liposomes and Mr. Jindřich Prokeš for manufacturing some parts of the stirred cell.

REFERENCES

1. Gregoriadis, G. (1995) *Tibtech* **13**, 527-537.
2. Lopez-Berenstein, G., and Fidler, I. J. (1989) *Liposomes in the Therapy of Infectious Diseases and Cancer*, Liss, New York.
3. Alving, C. R. (1991) *J. Immunol. Methods* **140**, 1-13.
4. Cullis, P. R., Hope, M. J., Bally, M. B., Madden, T. P., and Mayer, L. D. (1987) *in* *Liposomes: From Biophysics to Therapeutics* (Ostro, M. J., Ed.), pp. 39-69, Dekker, New York/Basel.
5. Woodle, M. C., and Papahadjopoulos, D. (1988) *in* *Methods in Enzymology*, Vol. 171, pp. 193-217, Academic Press, San Diego.
6. Gregoriadis, G. (1992) *Liposome Technology*, CRC Press, Boca Raton, FL.
7. Hope, M. J., Bally, M. B., Webb, G., and Cullis, P. R. (1985) *Biochim. Biophys. Acta* **812**, 55-65.
8. Turánek, J. (1994) *Anal. Biochem.* **218**, 352-357.
9. Perrett, S., Golding, M., and Williams, P. (1991) *J. Pharm. Pharmacol.* **43**, 154-161.
10. Agarwal, V. G. (1989) *J. Liquid Chromatogr.* **12**, 3265-3277.
11. Shaikh, B., Jackson, J., and Guyer, G. (1991) *J. Chromatogr.* **571**, 189-198.
12. Armengol, X., and Estelrich, J. (1995) *J. Microencap.* **12**, 525-535.
13. Payne, N. I., Timmins, P., Ambrose, Ch. V., Ward, M. D., and Ridgway, F. (1986) *J. Pharm. Sci.* **75**, 325-329.
14. Payne, N. I., Browning, I., and Hynes, Ch. A. (1986) *J. Pharm. Sci.* **75**, 330-333.
15. Röding, J. (1990) *Seifen-Öle-Fette-Wachse* **14**, 509-515.
16. Mayer, L. D., Hope, M. J., Cullis, P. R., and Janoff, A. S. (1985) *Biochim. Biophys. Acta* **817**, 193-196.
17. Lasic, D. D. (1988) *Biochem. J.* **256**, 1-11.

[9] Preparation of Sterile Liposomes by Proliposome-Liposome Method

By JAROSLAV TURÁNEK, ANDREA KAŠNÁ, DANA ZÁLUSKÁ and JIŘÍ NEČA

Introduction

Liposomes are microscopic membrane-like spherical structures consisting of one or more concentric lipid bilayers enclosing aqueous compartments, and have become a useful tool and model in various areas of science. Commercial liposomal drugs are already available.¹ Liposomes were adopted by numerous researchers as the vehicle of choice for drug and vaccine delivery and targeting.^{2,3}

Liposomes are classified in terms of the number of bilayers enclosing the sequestered aqueous volume into unilamellar, oligolamellar, and multilamellar vesicles. Unilamellar vesicles can be divided into small unilamellar vesicles (SUVs) with a large curvature, and large unilamellar vesicles (LUVs) with a low curvature, and hence with properties similar to those of a flat surface. Multilamellar vesicles (MLVs) are liposomes representing a heterogeneous group in terms of size and morphology.⁴ Lipid composition, size, and morphology are variables determining the fate of liposomes in the biological milieu; therefore selection of a suitable method of preparation of liposomal drugs is of importance for both design of animal experiments and future successful marketing of the product.

A variety of procedures for the preparation of different types of liposomes have been developed and summarized in several reviews and monographs, including this series.^{5,6} These methods have been classified for convenience into three categories: (1) mechanical dispersion methods, such as hand shaking or vortexing, sonication, and high-pressure homogenization, (2) detergent-solubilizing dispersion methods including solubilized lecithin dispersion with sodium cholate or octylglucoside, and (3) solvent dispersion methods such as ethanol injection, ether infusion, and

¹ G. Gregoriadis, *Trends Biotechnol.* **13**, 527 (1995).

² G. Lopez-Berestein and I. J. Fidler, "Liposomes in the Therapy of Infectious Diseases and Cancer." A. R. Liss, New York, 1989.

³ C. R. Alving, *J. Immunol. Methods* **140**, 1 (1991).

⁴ P. R. Cullis, M. J. Hope, M. B. Bally, T. P. Madden, and L. D. Mayer, in "Liposomes: From Biophysics to Therapeutics" (M. J. Ostro, ed.), p. 39. Marcel Dekker, New York, 1987.

⁵ M. C. Woodle and D. Papahadjopoulos, *Methods Enzymol.* **171**, 193 (1988).

⁶ G. Gregoriadis, "Liposome Technology." CRC Press, Boca Raton, FL, 1992.

reversed-phase evaporation. These primary processes can be linked with the secondary processes, such as high-pressure homogenization or extrusion through polycarbonate filters with various pore sizes, which are easy ways of obtaining oligolamellar or unilamellar liposomes with various size distributions.^{4,7-11}

Ethanol solvent dispersion (ethanol injection method) has some drawbacks, including low encapsulation efficiency and restriction of lipid composition owing to limitations in the solubility of some lipids in ethanol.

The proliposome-liposome method is based on proliposomal preparation of hydrated stacked bilayer sheets in a water-ethanol solution. Generally, the organization of a lipid-ethanol-water mixture can be described in terms of a three-phase diagram that can be divided into the following principal areas: lipid dissolved in aqueous ethanol, hydrated bilayers suspended in aqueous ethanol, and a liposomal area. Spontaneous formation of liposomal suspensions is accomplished by addition of excess aqueous phase to a lipid mixture.

This technique is simple and practical and is characterized by an extremely high entrapment efficiency, when compared with other methods based on passive entrapment. The technique is suitable for encapsulation of a wide range of drugs with various water and alcohol solubilities.^{12,13}

In this chapter we describe a stirred thermostatted cell and its link-up with a liquid delivery system for the rapid production of multilamellar liposomes by the proliposome-liposome method, which is based on the conversion of the initial proliposome preparation into a liposome dispersion by dilution under strictly controlled conditions. The cell has been designed for laboratory-scale preparation of liposomes (300-1000 mg of phospholipid per run) in a procedure taking less than 90 min and can be readily scaled up and linked with secondary processing methods, such as extrusion through polycarbonate filters for the preparation of oligolamellar and unilamellar liposomes.

The cell is a prospective tool for modeling the processes of industrial-scale preparation of liposomes.

⁷ M. J. Hope, M. B. Bally, G. Webb, and P. R. Cullis, *Biochim. Biophys. Acta* **812**, 55 (1985).

⁸ J. Turánek, *Anal. Biochem.* **218**, 352 (1994).

⁹ N. Berger, A. Sachse, J. Bender, R. Shubert, and M. Brandl, *Int. J. Pharm.* **223**, 55 (2001).

¹⁰ R. Barnadas-Rodríguez and M. Sabés, *Int. J. Pharm.* **213**, 175 (2001).

¹¹ T. Schneider, A. Sachse, G. Rößling, and M. Brandl, *Int. J. Pharm.* **117**, 1 (1995).

¹² S. Perrett, M. Golding, and P. Williams, *J. Pharm. Pharmacol.* **43**, 154 (1991).

¹³ J. Turánek, D. Záluská, and J. Neča, *Anal. Biochem.* **249**, 131 (1997).

Experimental Procedures

Stirred Cell and Its Link-up with Thermostat and Delivery Pump

A schematic drawing and the actual appearance of a disassembled cell are shown in Fig. 1 and 2A, respectively. The acrylic body of the thermostatic jacket has been designed to accept a centrifuge tube (50 ml; Corning, Corning, NY) and two O-rings are used to seal the tube in the thermostatic chamber. The diluting solution is delivered through a Teflon capillary (1.8 mm o.d. \times 0.5 mm i.d.), and a sterile filter (0.22 μ m; Millipore, Prague, Czech Republic) removes residual particles and microorganisms to maintain the preparation sterile. A Teflon body (capillary reinforcement) protects the capillary from unwanted bending (Fig. 2B). A magnetic stirrer hangs loosely on the flanged end of the capillary. The stirrer, with turbine-like blades, is shaped to reach the conical part of the tube near its bottom. The blades are arranged to lift the suspension up from the bottom and maintain homogeneity, especially during the first step of dilution when the proliposome mixture is viscous. The body of the stirrer is made of Teflon and pieces of Teflon-coated ferrite are inserted into its arms (Fig. 2C). A polypropylene frit closes the pressure-compensation hole and protects the interior from airborne contamination. When a run is finished, the head of the cell is removed and the tube is closed with its original lid.

The actual appearance of linking of the cell with a programmable system for delivery of the diluting solution is shown in Fig. 3. A schematic drawing of the arrangement is presented in Fig. 4. We use a fast protein liquid chromatography (FPLC) system (Pharmacia, Uppsala, Sweden) or a peristaltic pump for accurate flow rate programming. The fraction collector (Frac-100; Pharmacia) connected with the peristaltic pump (P1; Pharmacia) or another adequate system can be used to ensure a defined flow rate even if the two-step dilution method is used, and to stop the pump at the end of the run. The thermostat (Julabo U3; Julabo, Seelbach, Germany) is used to maintain constant temperature during the procedure.

Preparation of Proliposome Mixture and Its Conversion into Liposomes

The egg yolk phosphatidylcholine preparation Lipoid E 80 (Lipoid, Ludwigshafen, Germany) is used in our experiments. A proliposome mixture is prepared by a modification of the method described by Perrett *et al.*¹² Briefly, the lipids (300 mg of solid yellowish grains) are dissolved in pure warm ethanol (240 mg, 50°) and cooled to room temperature. Water phase is added at a lipid:ethanol:water ratio of 10:8:*X* (w/w/w). Tris-HCl (20 mM, pH 7.2) is used as the water phase; the value *X* = 20 is

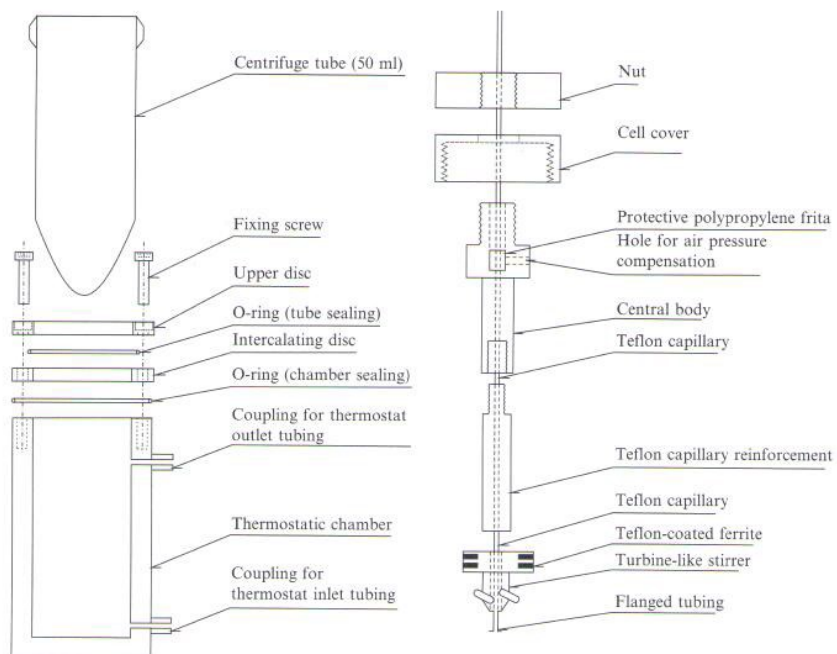


FIG. 1. Schematic drawing of the stirred thermostatted cell.

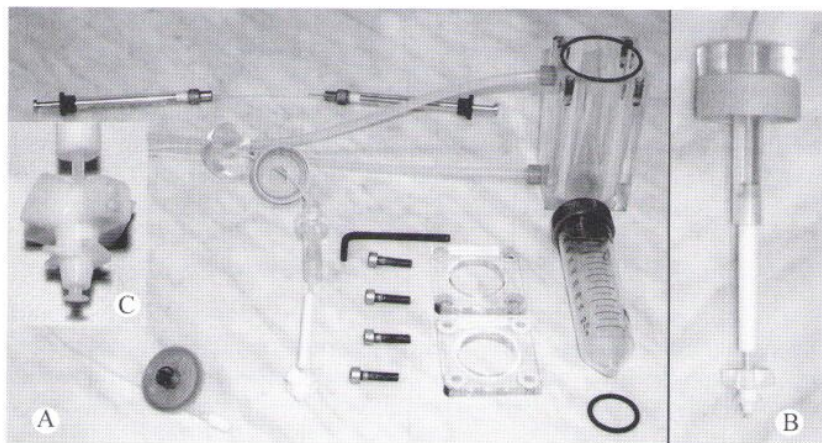


FIG. 2. A disassembled cell (A), assembled cell head with stirrer (B), and detail of stirrer (C).



FIG. 3. Entire system for the preparation of liposomes by the proliposome-liposome method.

used in most experiments (600 mg of water phase). The compounds to be entrapped are dissolved in the water phase and added at this step. Poorly water-soluble compounds are preferably dissolved in ethanol together with phospholipids. Thorough mixing of an ethanol solution of phospholipids with the water phase is achieved by the use of two high-pressure glass syringes, parts of the hand-operated miniextruder supplied by Avestin (Toronto, ON, Canada) or Avanti Polar Lipids (Alabaster, AL) linked with short Teflon capillary tubing (Fig. 2). The water phase with compounds to be entrapped is injected quickly from one syringe into the second syringe containing the ethanol solution of phospholipids. This process is repeated rapidly several times to get a homogeneous preparation. The opaque viscous mixture is heated to 60° (transformation temperature) for 10 min in a sterile Eppendorf tube and then allowed to cool to room temperature, yielding a proliposome mixture. The proliposome mixture is transferred into the stirred cell and converted into a liposome suspension by continuous dilution with the water phase (total volume of 39 ml) at a defined flow rate and temperature. The two-step dilution, which is the most effective dilution mode with respect to encapsulation efficiency and

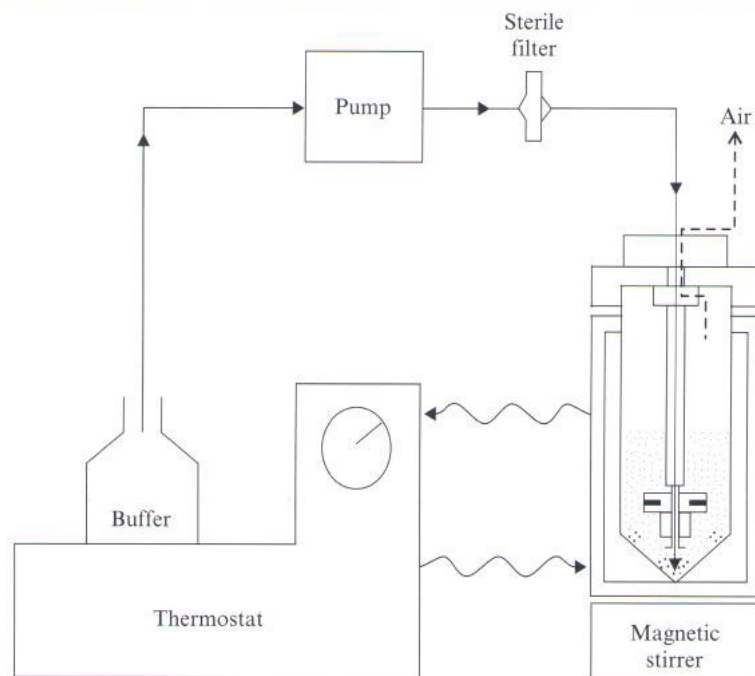


FIG. 4. Schematic drawing of link-up of the cell thermostat and pump. Operation is described in text.

duration of the procedure, is accomplished by continual addition of 3 ml of the water phase at a flow rate of 100 $\mu\text{l}/\text{min}$ in the first step and 36 ml of the water phase at 1000 $\mu\text{l}/\text{min}$ in the second step.¹³

Assay of Encapsulation Efficiency for 5,6-Carboxyfluorescein

5,6-Carboxyfluorescein (CF; Molecular Probes, Eugene, OR) is quantified spectrofluorimetrically in a luminescence spectrometer (LS 50B; PerkinElmer, Prague, Czech Republic) at 470 nm (excitation) and 520 nm (emission). Free 5,6-carboxyfluorescein is separated from liposome-entrapped CF by centrifugation (45,000g, 20 min, 4°). Liposomes are solubilized with Triton X-100 [final concentration, 1% (w/v)] to release the entrapped drug for assay. The entrapment efficiency is calculated by the equation

$$\text{Percent entrapment} = \left(\frac{C}{A} \right) \times 100$$

and the validity of the calculation is checked by the equation

$$A = B + C$$

where A is total (i.e., free and encapsulated) CF in the liposomal suspension, B is free (nonencapsulated) CF, and C is encapsulated CF.

Effect of Proliposome Mixture Composition on Entrapment Efficiency

The entrapment efficiency of the liposomes formed after dilution of proliposome mixtures to a final volume of 40 ml is plotted as a function of the weight of the aqueous phase present in the initial proliposome mixtures. A typical plot showing the efficiency of entrapment of CF by Lipoid 80 E liposomes is presented in Fig. 5. The region of maximum entrapment efficiency has been mapped in detail. A high entrapment efficiency is obtained with a proliposome lipid:ethanol:water composition of 10:8:15–23 (w/w/w). The proliposome lipid:ethanol:water composition of 10:8:20 (w/w/w) has been used for further studies. Liposomes prepared from a proliposome mixture with this composition yielded an entrapment efficiency of $81 \pm 2\%$ for CF (five separate preparations). A negatively stained electron micrograph of liposomes prepared by the proliposome-liposome method is shown in Fig. 6A. Heterogeneity of the liposomal preparation in terms of size, lamellarity and morphology can be seen clearly. Multicentric liposomes are also present.

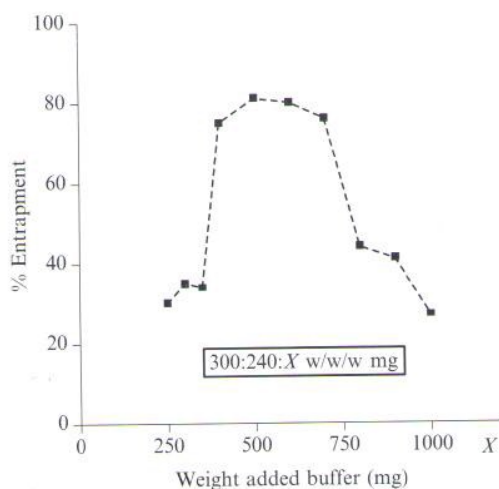


FIG. 5. Plot of entrapment percentage of carboxyfluorescein as a function of weight of buffer (X) incorporated in the initial proliposome mixture [phospholipid:ethanol:buffer = 300:240: X (w/w/w, mg)]. For details see Experimental Procedures.

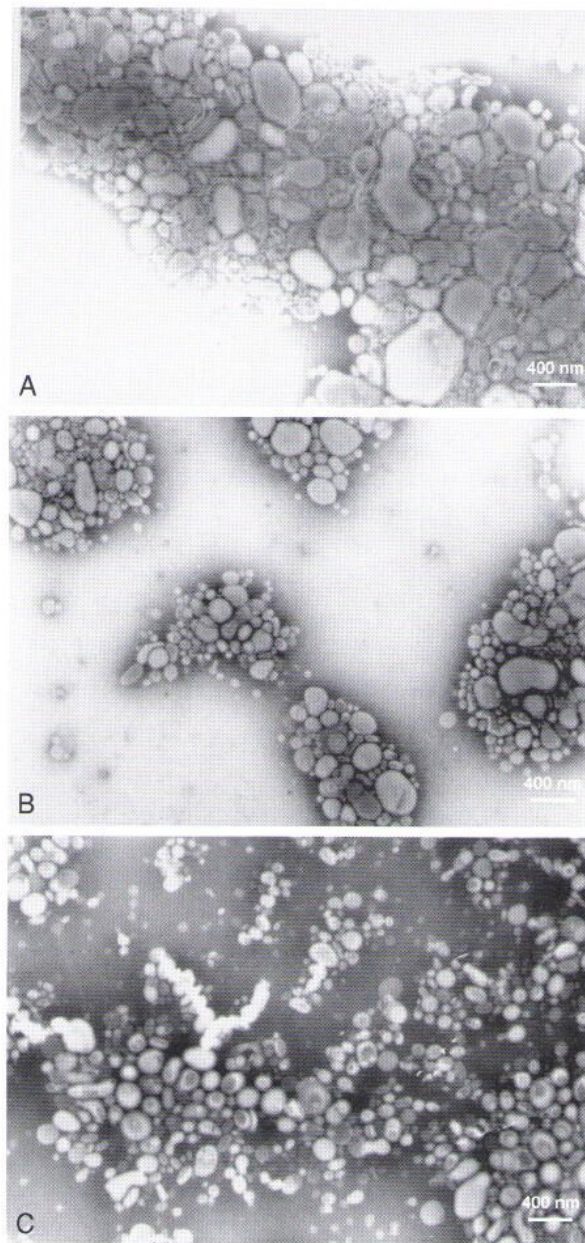


FIG. 6. Electron micrographs of negatively stained liposomes prepared by the proliposome–liposome method. (A) Nonextruded proliposomes; (B) proliposomes extruded through $0.4\text{-}\mu\text{m}$ filters; (C) proliposomes extruded through $0.2\text{-}\mu\text{m}$ filters. Liposomes are stained with 3% ammonium molybdate solution.

Assay of Encapsulation Efficiency for Tested Drugs

The synthetic immunomodulators adamantylamide dipeptide (AdDP) (Lachema, Brno, Czech Republic), muramyl dipeptide (MDP), and β -D-GlcNAc-norMurNAc-L-Abu-D-isoGln (DDD) (obtained by courtesy of M. Ledvina, Institute of Organic Chemistry and Biochemistry, Prague, Czech Republic) is assayed with a high-performance liquid chromatography (HPLC) chromatographic system (Waters, Milford, MA), including a Waters 600 gradient pump, a Waters 717 Plus autoinjector, a Waters 996 diode array detector, a Waters 474 fluorescence detector, and the program Millennium 2010. All the analyses are run on a Waters NOVA-PAC C₁₈ column (4 μ m, 150 \times 3.9 mm; precolumn, 20 \times 3.9 mm). Methanol-water (0.1% trifluoroacetic acid, TFA) is used as the mobile phase for the analysis of AdDP (ratio, 45:55) and MDP and DDD (ratio, 10:90). The immunomodulators are detected at 203 nm and the obtained ultraviolet (UV) spectra are matched against the spectra of standards. DDD yields two anomer peaks in the chromatogram, which are both used for the calculation.

The antibiotics gentamicin and neomycin (Sigma, Prague, Czech Republic) are analyzed by precolumn derivatization with *o*-phthalaldehyde and detected by a fluorescence detector set at 340 nm (excitation) and 455 nm (emission).^{14,15} The photosensitizer meso-tetra-(*p*-sulfophenyl)porphine (TPPS₄) (kindly provided by Lachema Company) is assayed spectrophotometrically at 410 nm, using the standard addition method. Total masses of free and entrapped drugs are determined and used for the calculation of encapsulation efficiency. Free drugs are separated by centrifugation (45,000g, 20 min, 4°). The liposomes are solubilized with Triton X-100 [final concentration, 1% (w/v)] to release the entrapped drugs for the assay.

Comparison of Entrapment Efficiency for Selected Drugs of Frozen-and-Thawed MLVs and Liposomes Prepared by Proliposome-Liposome Method

Preparation of Frozen-and-Thawed Multilamellar Vesicles. The lipid mixture, dissolved in chloroform (200 mg in 6 ml), is deposited onto the wall of a round-bottom flask (250 ml) by removal of the solvent in a rotary evaporator (40°, 4 h). The dried lipid film is then hydrated with the aqueous phase [150 mM NaCl, 20 mM HEPES (pH 7.2) previously filtered through a 0.22- μ m pore size filter] under continuous mixing on a

¹⁴ V. G. Agarwal, *J. Liq. Chromatogr.* **12**, 3265 (1989).

¹⁵ B. Shaikh, J. Jackson, and G. Guyer *J. Chromatogr.* **571**, 189 (1991).

TABLE I
COMPARISON OF ENTRAPMENT EFFICIENCIES OF FTMLV AND PL LIPOSOMES FOR
SELECTED DRUGS

Drug to be entrapped (mg/300 mg phospholipid)		Percent entrapment			
Drug	Amount	Proliposome-liposome		FTMLV	
		Mean	SD	Mean	SD
A: AdDP	2.28	87 ^a	2.2	78	3.2
B: MDP	1.56	62 ^a	2.8	36	4.7
C: DDD	1	85 ^a	2.8	32	4.1
D: Neomycin	30	65 ^a	1.7	36	3.9
E: Gentamicin	30	69 ^a	2.2	52	4.2
F: 6-Carboxyfluorescein	1	81 ^a	1.5	52	3.9
G: TPPS ₄	1.3	65	1.5	62	4.0

Abbreviations: FTMLV, Frozen-and-thawed multilamellar vesicle; PL, proliposome-liposome.

^a Significant difference from the corresponding results obtained by the FTMLV method ($p < 0.001$, based on t tests).

mechanical reciprocal shaker for 2 h. The frozen-and-thawed MLV system⁷ is obtained by freezing the MLVs in liquid nitrogen and thawing them in a 30° water bath, and repeating the cycle five times.

The entrapment efficiencies for synthetic immunomodulators and glycosidic antibiotics are summarized in Table I. Both types of liposomes show a high entrapment efficiency for the hydrophobic AdDP. The hydrophilic MDP and DDD are entrapped with a similar efficiency by frozen-and-thawed MLV (FTMLV) liposomes. Compared with AdDP or DDD, the entrapment efficiency of PL liposomes for MDP is lower by approximately 20%. Neomycin and gentamicin are entrapped with similar efficiencies by PL liposomes, but entrapment efficiencies of FTMLV liposomes for the two antibiotics are different. TPPS₄ is entrapped with the same efficiency by any of the liposome types.

Determination of Captured Volume. Captured volume, which is defined as the volume of the entrapped discontinuous aqueous phase per mass unit of the lipid phase and is expressed in microliters per micromole of phospholipid, is determined as described by Armengol and Estelrich¹⁶ with a minor modification. Briefly, the concentration of CF in the proliposome mixture and in the diluting buffer is 500 μ M. Nonentrapped CF is

¹⁶ X. Armengol and J. Estelrich, *J. Microencapsulation* **12**, 525 (1995).

separated from the liposomes by centrifugation (45,000g, 20 min, 4°) and the liposomes are washed twice and resuspended in CF-free buffer to obtain a concentration of 1 mg of phospholipid per milliliter. An aliquot of the liposomes is solubilized with Triton X-100 [final concentration, 1% (w/v)] and the concentration of CF is determined spectrofluorimetrically, using a calibration curve of a CF standard dilution series covering a 10–1000 nM range for CF.

The captured volume is calculated by the equation

$$V_e = \frac{M}{CL}$$

where V_e is the entrapped volume ($\mu\text{l}/\mu\text{mol}$), M is the total mass of CF in the washed liposome preparation, C is the initial concentration of CF in the diluting buffer and proliposome–liposome mixture, and L is the total mass of lipid in the purified preparation.

Entrapped volumes of frozen-thawed MLVs prepared by hydration of a lipid film and of liposomes prepared by the proliposome–liposome method (without extrusion) are compared. The values of 1.83 ± 0.07 and $1.26 \pm 0.06 \mu\text{l}/\mu\text{mol}$ phospholipid have been found for the former and the latter, respectively.

Electron Microscopy. Electron micrographs are made by the negative staining technique (3% ammonium molybdate solution). A transmission electron microscope (BS 500; Tesla, Brno, Czech Republic) is used. The final magnification of the micrograph prints is $\times 25,200$. The micrographs of some liposomal preparations are presented in Fig. 6.

ζ Potential Measurement and Particle Size Analysis by Photon Correlation Spectroscopy. Light-scattering analyses of liposomal preparations are done with a photon correlation spectrometer (Zetasizer 3000; Malvern Instruments, Malvern, UK). Samples of liposomal preparations (phospholipid, 0.7 mg/ml) are analyzed at 25.0°. ζ potential measurement and a size distribution analysis of the data are done according to the instrument manual.

The ζ potentials of the liposomes prepared from Lipoid E 80 are -18 ± 2.3 mV (20 mM Tris-HCl, pH 7.2) and -4.3 ± 1.7 mV (phosphate-buffered saline).

Effect of Transformation Temperature on Entrapment Efficiency. The physical state of the proliposome mixtures is strongly temperature dependent and the thermal cycle used for the transformation of the proliposome mixture is decisive for the resulting encapsulation efficiency. It should be noted that the transition temperature for egg yolk lecithin membranes is within the range -15 to -7° , and hence the transition from the solid (gel) phase to the liquid-crystal phase does not affect the process

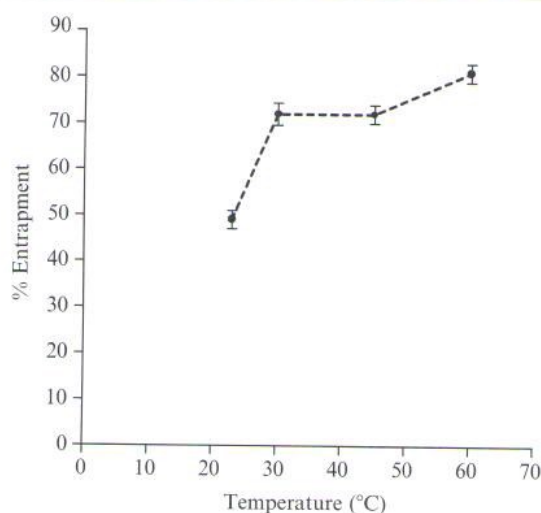


FIG. 7. Effect of transformation temperature on entrapment percentage of carboxyfluorescein in a two-step dilution of a proliposome mixture. For details see Experimental Procedures.

of liposome formation at the temperatures used in our experiments. The solubility of lipids in aqueous ethanol increases markedly with rising temperature. This strong temperature dependence is an important feature of the proliposome system. Mixtures at the boundary of the proliposome region can convert from their original proliposome form into liposomes on cooling.

The break point has been found to be 30°. Below 30° there is a steep decrease in entrapment efficiency for CF. The entrapment efficiency of 73% remains constant in the range of 30–45° and increases slowly to 82% when the temperature rises to 60°. These results are in good accordance with the temperature-dependent increase in the isotropic component in ^{31}P nuclear magnetic resonance (^{31}P NMR),¹² reflecting an increase in non-bilayer-organized molecules of phospholipids.¹² The dependence of entrapment efficiency on the transformation temperature is shown in Fig. 7.

Statistical Analyses

An unpaired two-tail *t* test is used to compare the entrapment efficiency for PL liposomes versus FTMLVs. Statistical software includes Prism, version 2.00 (GraphPad Software, San Diego, CA).

Extrusion of Proliposomes

The proliposomes can be extruded with a hand-operated device, such as the miniextruder supplied by Avanti Polar Lipids, through polycarbonate filters of pore sizes 0.6, 0.4, and 0.2 μm . This procedure was used in some studies on the effect of extrusion on particle size and polydispersity of the final liposomal preparation. The proliposomes are extrudable up to a pore size of 0.2 μm . Higher pressures during the extrusion through a 0.1- μm pore size filter or ultrasonication result in disorganization of proliposomes (tightly packed bilayer sheets) and their transformation into a viscous dispersion of phospholipids. Proliposomes represent transient metastable structures and a high pressure probably induces dehydration of bilayers and metamorphosis back into the amorphous state.

We have found that extrusion of proliposomes influences both the final size and polydispersity of the resultant liposomes. The smaller the filter pores used, the smaller the size and the lower the polydispersity of liposomes obtained. The results obtained by electron microscopy (Fig. 6) and light-scattering measurement (Fig. 8) show a good accordance.

Sterility Testing

The cell is sterilized with 60% ethanol at 60° for 15 min before use. *Staphylococcus aureus* (A-positive strain 722 obtained from the Food Research Institute, University of Wisconsin, Madison, WI) is maintained in glycerol broth at -20° and 24-h-old cultures grown on blood agar plates at 37° are used as a model for experimental contamination of the cell (10^6 CFU) before sterilization. The sterility of the product is checked by culture on blood agar plates (37°, 96 h). No bacterial contamination was detectable after 96 h of culture on blood agar in any of the liposomal preparations under study.

Concluding Remarks

We present a description of a stirred thermostatted cell and its link-up with a liquid delivery system for the rapid production of multilamellar liposomes by the proliposome-liposome method, which is based on the conversion of the initial proliposome preparation into a liposome dispersion by dilution under strictly controlled conditions. The design of the cell allows easy assembly and link-up with FPLC or other delivery systems that facilitate full control of the process, giving highly reproducible results. Most components used in the construction can be found in any laboratory or

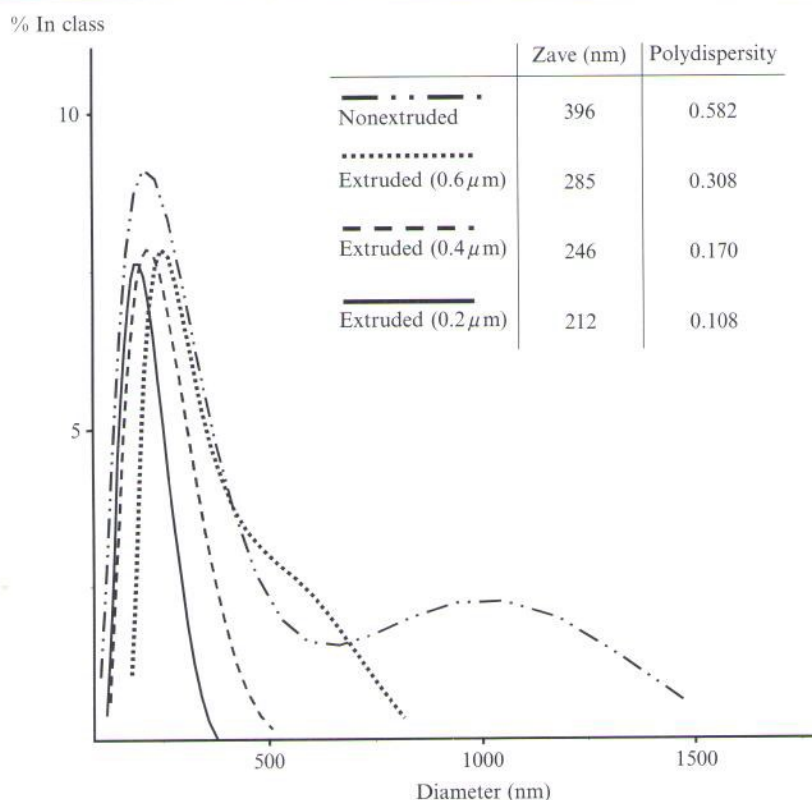


FIG. 8. Size distribution of liposomes prepared from nonextruded and extruded proliposomes.

are listed in catalogs of major suppliers of laboratory utensils. Larger quantities of proliposomes (above 1 ml in total volume, 300–1000 mg of phospholipids) can be easily prepared directly in the cell by mixing an ethanol solution of phospholipids with the water phase at the desired flow rate and temperature. The liposomes are produced according to good manufacturing practice (GMP) and are sterile. The cell has been designed for laboratory-scale preparation of liposomes (300–1000 mg of phospholipid per run) by a procedure taking less than 90 min. The method can be readily scaled up and linked with secondary processing methods, such as extrusion through polycarbonate filters for the preparation of oligolamellar and unilamellar liposomes.

The cell is a prospective tool for modeling of processes of industrial-scale preparation of liposomes.

Vesiculation of lipid bilayers and sealing of the membrane are critical steps in the formation of liposomes. Unstable transient structures appear during the formation of liposomes by a process that is difficult to investigate. A unifying model, based on a bilayered phospholipid fragment, has been proposed by Lasic.¹⁷ No data describing the mechanism of transformation of proliposomes (dispersed floccules of lamellar phase) into liposomes have been found in the available literature. Also unclear are the existence and possible role of bilayered phospholipid fragments in that process. We assume that a relatively high lipid concentration and the large surface area of the lamellar phase in the proliposome mixture are responsible for high entrapment efficiencies for various drugs.

Variations of some parameters influencing the structure of proliposomes (e.g., phospholipid composition, addition of small amount of detergent, temperature, pH and ionic strength, and addition of glycerin or saccharides) and the process of vesiculation (decreasing of ethanol concentration by, e.g., dilution, dialysis, or evaporation at lower pressure) can release a hidden potential of versatility of this method with respect to size, morphology, and entrapment efficiency of final liposomal preparations.

The method has been successfully applied in our laboratory for the encapsulation of various drugs. Prospective candidates for entrapment into liposomes prepared by this technique are particularly lipophilic derivatives (e.g., modified by long acyl chain, cholesterol, or phospholipid) of muramyl dipeptide with immunostimulating activities.¹⁸ This method is also applicable to large-scale preparation of cationic liposomes and plasmid DNA-liposome complexes for DNA vaccine preparation.

Acknowledgments

This work was supported by the Ministry of Agriculture of the Czech Republic (MZE-M03-99-01). We thank M.V. Dr. Bedřich Šmid, Dr. Sc., for preparation of the electron micrographs of liposomes, Andrea Tománková and Irena Trnečková for preparation of pictures, and Mr. Jindřich Prokeš for manufacturing some parts of the stirred cell.

¹⁷ D. D. Lasic, *Biochem. J.* **256**, 1 (1988).

¹⁸ J. Turánek, D. Záluská, M. Hoffer, A. Vacek, M. Ledvina, and J. Ježek, *Int. J. Immunopharmacol.* **19**, 611 (1997).



Contents lists available at ScienceDirect

Analytical Biochemistry

journal homepage: www.elsevier.com/locate/yabio

Immobilization of histidine-tagged proteins on monodisperse metallochelation liposomes: Preparation and study of their structure

Josef Mašek^a, Eliška Bartheldyová^a, Zina Korvasová^a, Michaela Škrabalová^a, Štěpán Koudelka^a, Pavel Kulich^a, Irena Kratochvílová^b, Andrew D. Miller^c, Miroslav Ledvina^d, Milan Raška^e, Jaroslav Turánek^{a,*}

^a Department of Pharmacology, Toxicology, and Immunotherapy, Veterinary Research Institute, 621 32 Brno, Czech Republic

^b Institute of Physics, Czech Academy of Sciences, 182 21 Prague, Czech Republic

^c Imperial College Genetic Therapies Centre, Department of Chemistry, Imperial College, London SW7 2AZ, UK

^d Institute of Organic Chemistry and Biochemistry, Czech Academy of Sciences, 166 10 Prague, Czech Republic

^e Department of Immunology, Faculty of Medicine and Dentistry, Palacky University, 771 47 Olomouc, Czech Republic

ARTICLE INFO

Article history:

Received 15 June 2010

Received in revised form 2 August 2010

Accepted 16 August 2010

Available online 21 August 2010

Keywords:

Liposome

Proteoliposome

Detergent removal method

Recombinant protein

Metallochelation

Atomic force microscopy (AFM)

Transmission electron microscopy (TEM)

Dynamic light scattering (DLS)

Confocal microscopy

ABSTRACT

Liposomes represent a biocompatible platform for the construction of self-assembling proteoliposomes using nickel or zinc metallochelation. Potential applications of such structures consist in the development of new biocompatible vaccination nanoparticles and drug delivery nanoparticle systems. Here, we describe the design and construction of a flow-through ultrafiltration cell suitable for the preparation of monodisperse liposomes enabled for metallochelation and, hence, the formation of proteoliposomes. The linkage of the cell with a fast protein liquid chromatography system facilitates automation of the procedure, which fits the criteria for upscaling. Proof-of-concept experiments are performed using a mixture of egg phosphatidyl choline and nickel-chelating lipid DOGS-NTA-Ni (1,2-dioleoyl-sn-glycerol-3-[[N(5-amino-1-carboxypentyl)iminodiacetic acid]succinyl](nickel salt)) to formulate proteoliposomes with proteins attached by metallochelation, including histidine (His)-tagged recombinant green fluorescent protein and gp120 (derived from HIV-1 Env). These model proteoliposomes are characterized by gel permeation chromatography and by dynamic light scattering. Transmission electron microscopy and immunogold staining are used to characterize surface-bound proteins, revealing the tendency of gp120 to form microdomains on liposome surfaces. These microdomains possess a two-dimensional crystal-like structure that is seen more precisely by atomic force microscopy.

© 2010 Elsevier Inc. All rights reserved.

Liposomes represent the oldest nanoparticle systems described for applications in biological studies as model membranes and in medicine. Over 44 years, liposomes have been shown to be suitable drug delivery systems for applications ranging from cosmetics and dermatology through to medical applications in anti-infection therapy, anticancer therapy, and veterinary vaccination [1]. Liposome-based vaccines have been around for approximately 30 years, and numerous liposome variants have been developed, some with evident immune-stimulatory properties and attractive safety profiles, hence resulting in registered products on the market or preparations in advanced stages of clinical testing (e.g., hepatitis A, Epaxal).

Liposomes represent an almost ideal carrier/delivery systems for the components of synthetic vaccines due to their ready biodegradability and their ability to retain/incorporate a variety of essential vaccine components simultaneously, even components possessing

quite different physicochemical properties (different size, hydrophobicity, charge, etc.). Different synthetic vaccine components can be encapsulated within the aqueous cavities of liposomes (if hydrophilic) or associated with liposome bilayers (if at least partially hydrophobic in character). Furthermore, essential components can be attached to either internal or external outer leaflet membrane by electrostatic, covalent, or metallochelation interactions. The most diverse synthetic vaccine components are typically adjuvants needed to provoke innate immune reactions (e.g., monophosphoryl lipid A, CpG oligonucleotides, muramyl dipeptide and analogues). In addition, these can be combined with antigens needed to provoke specific immunity such as soluble or membrane proteins. Finally, the liposome may present ligands to assist functional delivery of antigens and adjuvants to antigen-presenting cells necessary to invoke immunostimulation [2]. The laboratory and industrial procedures for the liposome preparation have been established, and liposomes have been approved by the US Food and Drug Administration for biomedical applications. The potential for the participation

* Corresponding author. Fax: +420 5 4121 1229.
E-mail address: turanek@vri.cz (J. Turánek).

of liposome-based recombinant vaccines in the human and veterinary vaccine market is very promising [3].

There have been a few reports concerning the metallochelation of recombinant proteins to liposomes. The implementation typically requires an insertion of a metallochelation lipid into the outer leaflet membrane of liposome bilayers that interacts selectively in the presence of metal ions (e.g., nickel ions) with a 4- to 6-amino-acid residue histidine tail (His tag)[†] expressed at the N or C terminus of a recombinant protein of interest such as a putative antigen. The reversible character and high affinity of the metallochelation are very useful for the construction of various self-assembled supramolecular structures useful for the construction of experimental synthetic vaccines [4,5]. Here, we describe the design and construction of a special flow-through stirred ultrafiltration cell linked to a fast protein liquid chromatography (FPLC) system for the automated production of unilamellar highly monodisperse liposomes using the detergent removal method [6]. A simplified procedure for the preparation of mixed lipid-detergent micelles (both containing and not containing nickel-chelating lipids) was developed, and liposomes were formed in the cell during the ultrafiltration step, which guaranteed a sustained and well-defined removal of detergent and facilitated a well-reproducible conversion of the micelles into liposomes. The preparation of monodisperse liposomes is of crucial importance to our investigation of the interaction of recombinant His-tagged proteins with liposomes enabled by metallochelation of the proteins. We also describe the optimization of liposome formulation parameters and processes for the preparation of metallochelating proteoliposomes as well as structural investigations by dynamic light scattering (DLS), *sn*-glycero-3-phosphocholine (GPC), transmission electron microscopy (TEM), atomic force microscopy (AFM), and confocal microscopy.

Materials and methods

Materials

Egg phosphatidyl choline (EPC, purity of 99%), 1,2-dioleoyl-*sn*-glycero-3-phosphoethanolamine-*N*-(1issamine rhodamine B sulfonyl) (LR-PE), and 1,2-dioleoyl-*sn*-glycero-3-[[N(5-amino-1-carboxypentyl)imino]diacetic acid]succinyl (nickel salt) (DOGS-NTA-Ni) (Fig. 1) lipids were purchased from Avanti Polar Lipids (Birmingham, AL, USA). A 20-nm membrane filter Anotop 10 and a 0.2- μ m membrane filter Anotop 10 LC were purchased from Whatman. A membrane ultrafilter Amicon YM-10 was purchased from Amicon-Millipore. Sodium cholate, tetrahydrofuran, 6-carboxyfluorescein (6-CF), and all other chemicals were purchased from Sigma.

Preparation of micelles

EPC was solubilized in ethanol (600 mg/ml). Sodium cholate was solubilized in appropriate buffer to the final concentration of 20 mM. This solution was filtered through the 0.2- μ m membrane filter Anotop 10 LC and the 20-nm membrane filter Anotop 10. The ethanolic solution of EPC and the aqueous detergent solution

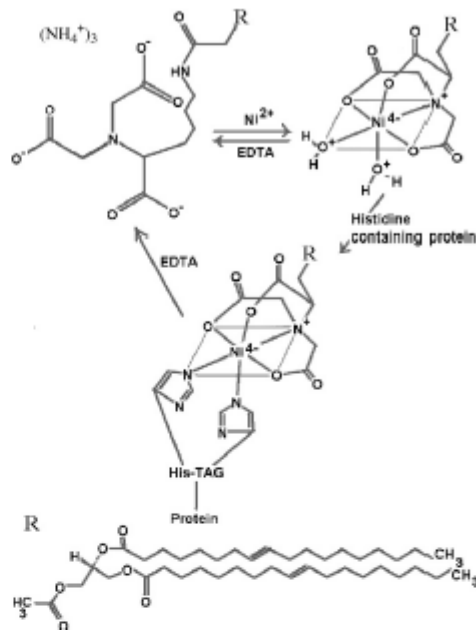


Fig. 1. Structural formulas of lipids for metallochelation and illustration of interaction between metallochelation center and His tag of recombinant proteins.

were mixed at the ratio of 1:30 (v/v) and stirred for 30 min by electromagnetic stirrer at room temperature while light-protected by plastic cap. The initial molar ratio of cholate to lipid was 2:1. The prepared micelles were filtered through 0.2- μ m sterile filter, and their size was measured by the DLS instrument NanoSizer NS (Malvern, Worcestershire, UK). The prepared micelles were used immediately or stored overnight in plugged vials at 4 °C for next-day experiments. Due to the generally small particle size of the resulting micelles, the arrangements were done to avoid any interference of contaminating larger particles (unrelated to micelles) at the size measurement. Therefore, all of the solutions were thoroughly filtered and the cuvettes were excessively cleaned.

Preparation of micelles with DOGS-NTA-Ni

DOGS-NTA-Ni lipid (1 mg) was dissolved in 40 μ l of tetrahydrofuran (THF), and an appropriate amount of EPC lipid was dissolved in ethanol. Then the solutions were mixed to reach the final ratio of 95 M% EPC and 5 M% DOGS-NTA-Ni. The solution of micelles was prepared by the dispersion of ethanol/THF (66:33, v/v) lipid solution in 20 mM sodium cholate to obtain a desired cholate/lipid ratio.

Ultrafiltration cell

The flow-through stirred ultrafiltration cell was designed to accept 25-mm ultrafiltration membrane discs and withstand the pressure necessary for the ultrafiltration (up to 4 bars). No leakage was found up to 40 bars. It is a limit for the FPLC system that is 10 times higher than the maximal pressure limit of the ultrafiltration membranes (4 bars). The ultrafiltration membrane YM-10 was

[†] Abbreviations used: His tag, histidine tail; FPLC, fast protein liquid chromatography; DLS, dynamic light scattering; GPC, *sn*-glycero-3-phosphocholine; TEM, transmission electron microscopy; AFM, atomic force microscopy; EPC, egg phosphatidyl choline; LR-PE, 1,2-dioleoyl-*sn*-glycero-3-phosphoethanolamine-*N*-(1issamine rhodamine B sulfonyl); DOGS-NTA-Ni, 1,2-dioleoyl-*sn*-glycero-3-[[N(5-amino-1-carboxypentyl)imino]diacetic acid]succinyl (nickel salt); 6-CF, 6-carboxyfluorescein; THF, tetrahydrofuran; PBS, sodium phosphate buffer; GFP, recombinant green fluorescent protein; MBL, mannan binding lectin; EDTA, ethylenediamine tetraacetic acid; HPLC, high-performance liquid chromatography; UV, ultraviolet; UV/Vis, UV/visible; CSLM, confocal scanning laser microscopy; HPMC, hydroxypropylmethylcellulose; CMC, critical micelle concentration; 2D, two-dimensional; PDI, polydispersity index; N-NTA₂-DTPA, N-(nitrilotriacetic acid)-di(2-ethylamino) complex.

selected owing to its low nonspecific protein binding properties, resistance to detergents and urea, and good flow rate characteristics (0.15–0.20 ml/min/cm² at 3.9 bars), which enable reaching relatively rapid removal of detergent. The design of the cell facilitates simple loading and taking up the sample, removal of bubbles, and vigorous stirring to eliminate concentration polarization. Fig. 2 displays a schema of the cell, the linkage of the cell to the FPLC system, and a photograph of the entire system with details of the cell.

The course of concentration in dependence on the duration of ultrafiltration in the fixed-volume flow-through cell is described by Eq. (1). For low-molecular-weight substances, Eq. (1) could be reduced to Eq. (2) if (i) the rejection coefficient *R* for a particular substance and the ultrafiltration membrane is close to zero and (ii) polarization of concentration during the process of ultrafiltration is negligible and, hence, does not affect the value of *R*. The small size of cholate molecule fulfills criterion (i), and the fixed

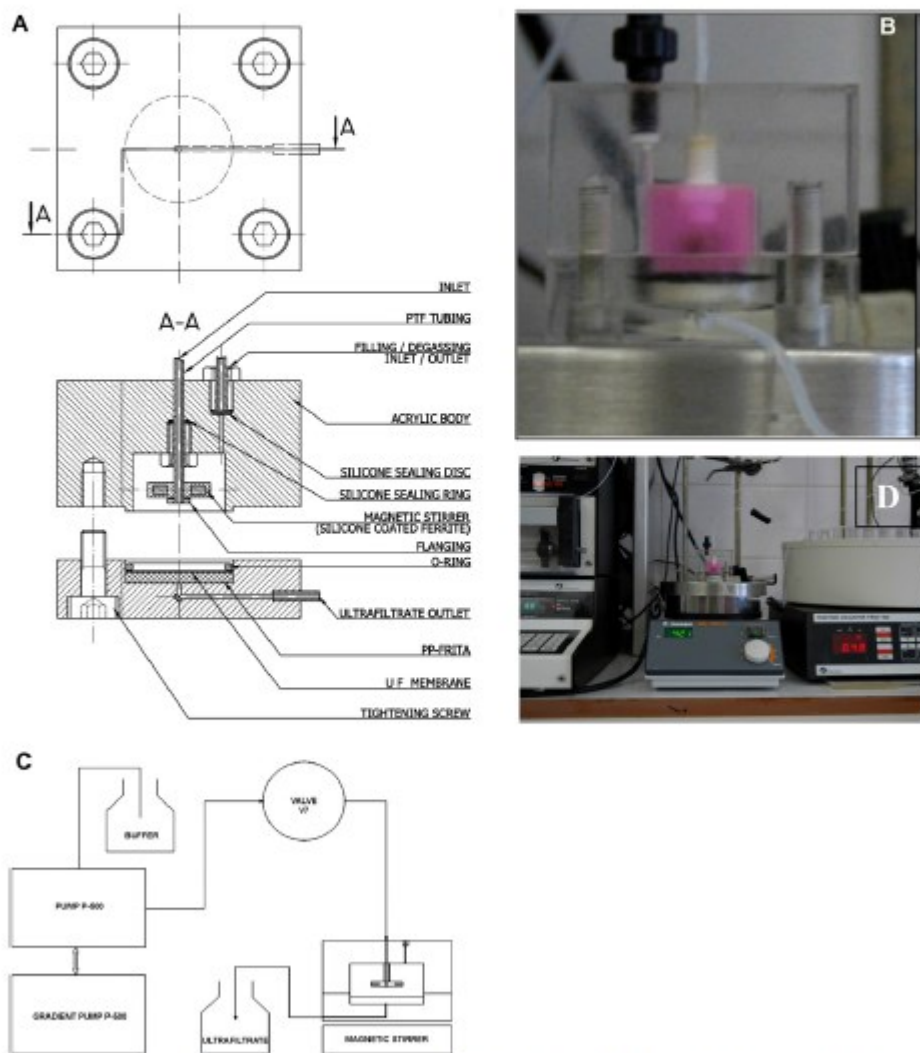


Fig. 2. System for preparation of liposomes by removal of detergent using ultrafiltration. (A) Schematic illustration of the ultrafiltration cell. (B) Photograph of the ultrafiltration cell in detail (pink LR-PE-labeled liposomes inside the cell). (C) Schematic illustration of the linkage of the ultrafiltration cell with the FPLC system. (D) Photograph of the system. (For interpretation of the reference to color in this figure legend, the reader is referred to the Web version of this article).

volume of the sample in the cell together with vigorous stirring minimizes the influence of criterion (ii):

$$C_t = c_1 \cdot e^{-\zeta(t-R)/V_0} \quad (1)$$

$$C_t = c_1 \cdot e^{-\zeta t/V_0} \quad (2)$$

where c_t is the concentration of the substance at time t , c_1 is the initial concentration of the substance, ζ is the flow rate of buffer, t is the time of ultrafiltration, V_0 is the cell volume (4.6 ml), and R is the rejection coefficient $\ln(c_1/c_0)/\ln(V_0/V_t)$.

For low-molecular-weight compounds passing freely through ultrafiltration membrane, R could be set to zero and Eq. (1) is simplified to Eq. (2), where c_t is the final solute concentration in the retentate, c_0 is the initial solute concentration, V_0 is the initial sample volume, and V_t is the final retentate volume.

For the fixed volume flow-through cell, c_t is c_0 , c_0 is c_1 , V_t represents the theoretical fraction V_t of the V_0 (cell volume) that was not completely rinsed at time t , and $V_t = V_0 e^{-\zeta t}$.

Preparation of liposomes

The ultrafiltration cell of the volume of 4.6 ml was filled with the solution of the mixed micelles and linked to the FPLC system (Pharmacia, GE Healthcare). During the liposome preparation process, the solution in the cell was stirred at a frequency of 400 rpm and the flow rate of buffer was set on 0.02 ml/min. At this flow rate, no increase of the pressure inside the cell occurred. The membrane filter YM-10 (Amicon–Millipore) could be reused up to nine times. Afterward, it must be replaced due to a decrease of flow rate and an increase of the pressure inside the cell above 0.3 MPa.

To investigate the influence of lipid concentration on the size and polydispersity of the liposomes, the lipid concentrations of 1, 10, 25, and 50 mg/ml and the corresponding concentrations of sodium cholate (20, 20, 50, and 100 mM in sodium phosphate buffer [PBS]) were applied. To determine the influence of the ionic strength on the size and polydispersity of the liposomes, 20 mM PBS and 20 mM PBS with 300 mM sodium chloride were used. The waste fractions were collected, and the time course of the concentrations of 6-CF, LR-PE, total lipid, and sodium cholate were determined.

Recombinant proteins

Recombinant green fluorescent protein (rGFP) was obtained from Apronex (Prague, Czech Republic).

gp120 + MBL

The recombinant protein gp120 + MBL was prepared as described previously [7]. In brief, synthetic codon-optimized HIV-1 clade B gp120 DNA fragment (coding for the protein fragment delineated by the sequences AEKL and RVVQ) behind mannan binding lectin (MBL) complementary DNA (cDNA) fragment representing the first exon (N-terminal 62 aa delineated by the sequences MSLF-KGEP) was cloned into a mammalian expression vector pcDNA3.1+/V5-His (Invitrogen) expressing gp120 + MBL in fusion with V5 and His epitopes (Invitrogen).

The recombinant plasmid was transfected into human embryonic kidney cells 293T17 (American Type Culture Collection [ATCC], Manassas, VA, USA) using FuGene6 (Roche Applied Science, Indianapolis, IN, USA), and the recombinant protein was purified from culture supernatant using the NiNTA agarose according to the manufacturer's suggestions (Qiagen).

Preparation of proteoliposomes and their characterization by DLS

The solution of rgp120 in PBS (Dogs–Ni/Gp120 M ratio of 10:1, 1.3 mg total lipid:1 mg gp120) was added to the prepared EPC/DOGS–NTA–Ni liposomes. The mixture was stirred for 20 min. The hydrodynamic diameters of the liposomes and proteoliposomes were determined by the DLS instrument NanoSizer NS (Malvern) at 25 °C. A silica cuvette of 45 μ l volume (Hellma, Müllheim, Germany) was used. The release of the bound rgp120 from the liposomes was accomplished by the addition of ethylenediaminetetraacetic acid (EDTA) to the final concentration of 1 mM.

Characterization of liposomes and proteoliposomes

Fluorescence assay of lipid, GFP, and 6-CF

The solution of fluorescence micelles and 6-CF was used to determine the time course of the concentration of the lipid and low-molecular-weight species in the ultrafiltration cell and ultrafiltrate during the process of liposome formation. The micellar solution containing a lipid mixture of 99.5% EPC and 0.5% LR-PE, the total lipid concentration of 10 mg/ml, was prepared by dispersion of ethanolic lipid solution in 20 mM sodium cholate solution as described above. 6-CF was dissolved in PBS and mixed with the micellar solution to the final concentration of 10 mM. The fluorescence in the waste fractions (permeated from the ultrafiltration cell) was determined using a spectrofluorimeter (LS-B 55, PerkinElmer). The fluorescence at 492/530 nm (6-CF) and 568/607 nm (LR-PE) was measured. The excitation and emission slots were 2.5 nm. The data from the spectrofluorimeter were normalized.

Sodium cholate assay

Sample preparation. Fractions (1.5 ml) of the permeate from the ultrafiltration cell were collected, and the concentration of sodium cholate was determined by high-performance liquid chromatography (HPLC) analysis.

HPLC analysis. Sodium cholate was assayed using an analytical column (EclipseXDB–C18, 4.6 \times 150 mm, 5 μ m, Agilent Technologies) at 25 °C at a flow rate of 0.9 ml/min. Prior to use, the mobile phase consisting of acetonitrile and 0.02% acetic acid in water (50:50, v/v) was degassed by sonication. 10- μ l volumes of the sample were injected, and the ultraviolet (UV) detector was set on 192 nm. The elution time of sodium cholate was 3.6 min [8].

Determination of lipid concentration. The lipid concentration was measured by a UV/visible (UV/VIS) spectrophotometer (Uvicon XL, Bio-Tec Instruments) using Stewart's method [9].

Gel permeation chromatography. The quantification of His-tagged GFP attached to the DOGS–NTA–Ni liposomes was carried out by gel permeation chromatography. The fraction of nonbound protein was separated from the liposomal GFP using the FPLC system (Pharmacia, GE Healthcare). The separation conditions were as follows: column, Superose 6 (prep grade) filled in Tricorn 5/200 column (Pharmacia, GE Healthcare); flow rate, 0.2 ml/min; mobile phase, PBS; injected volumes, 25 μ l; detection wavelength, 254 nm. Eluted fractions (0.25 ml) were collected with a fraction collector, and the concentration of GFP was determined by a fluorescence spectrophotometer (LS-55B, PerkinElmer) at 488 nm (excitation) and 520 nm (emission).

Transmission electron microscopy. The liposome structures were determined using a Philips Morgagni transmission electron microscope (EM Philips 208 S, Morgagni software, FEI, Brno, Czech Republic). All samples were negatively stained by 2% (w/w) ammonium molybdate (pH 6.8).

Immunogold labeling of gp120 proteoliposomes. Nonbound gp120 was separated from the proteoliposomes by gel permeation chromatography using a Superose 6 column. The fraction of proteoliposomes was concentrated in a centrifugation tube (cutoff of 30 kDa) and incubated with monoclonal anti-V5 antibody for 1 h at 37 °C. Then 10 nm colloidal gold-protein A conjugate was added. After 12 h of incubation, proteoliposomes were observed by an electron microscope.

Atomic force microscopy. The topography of the liposomes was investigated by AFM. The AFM measurements were performed with an NTEGRA Prima NT MDT system (Ireland) under ambient conditions. The tip-sample surface interaction monitored the van der Waals force between the tip and the surface; this may be either the short-range repulsive force (in contact mode) or the longer range attractive force (in noncontact mode or tapping mode). The AFM measurements on the liposomes were performed using the tapping mode. The sample was scanned under the soft CSG 10 type of probe. The tapping mode consisted of oscillating the cantilever at its resonance frequency (14–28 kHz) and lightly tapping the tip on the surface during scanning.

Confocal scanning laser microscopy. Confocal scanning laser microscopy (CSLM) was used for the observation of GFP binding onto the surface of the metallochelating liposomes and for the proof of the preservation of fluorescence as a marker of rGFP native state. Large liposomes (size ~1 µm) for the CSLM study were prepared according to the method of lipid film hydration followed by a thawing-freezing step and subsequent extrusion through the filter of 1000-nm pore size [10,11]. The lipid composition was the same as used for the preparation of the monodisperse liposomes by detergent removal as described above. GFP was added (20 µg GFP/1 mg lipid) to the prepared liposomes, and the prepared proteoliposomes were immobilized in the hydroxypropylmethylcellulose (HPMC) gel by mixing the liposomal suspension with HPMC solution (final concentration of HPMC was 2%). The sample was observed by a confocal scanning microscope (Leica SP-2) at the following parameters: excitation laser 488 nm (power of 20%), and optoacoustic filter set at emission spectrum of 505–530 nm.

Results

Preparation of micelles

Mixing of EPC solubilized in ethanol with sodium cholate solubilized in the buffer produced uniformly sized micelles. The size of the micelles was not markedly dependent on the lipid concentration (Table 1). However, slight dependence on the ionic strength of the buffer was found (Table 2). The procedure of the direct preparation of micelles was simple in comparison with the indirect method based on resolubilization of the preformed liposomes. The produced micelles were easily filterable through the 0.2-µm membrane filter Anotop 10 LC and the 20-nm membrane filter Anotop 10. The filtration step did not cause any decrease of the

Table 2
Effect of ionic strength on the size of micelles.

Buffer	Size (nm)	Peak width (nm)
20 mM PBS + 0 mM NaCl	4.9	1.33
20 mM PBS + 150 mM NaCl	6.2	1.36
20 mM PBS + 300 mM NaCl	6.7	1.72

Note: The size of the highest percentage occurrence (the maximum of the number distribution curve) is shown.

phospholipid content (as measured by phospholipid content assay [results not shown]) and facilitated the preparation of sterile mixed micelles in both laboratory and large scale.

Preparation of micelles with DOGS-NTA-Ni

DOGS-NTA-Ni lipid was not directly soluble in ethanol; therefore, a small amount of THF (50 µl/1 mg DOGS-NTA-Ni) was used to dissolve it. No precipitate was formed after mixing the THF solution of DOGS-NTA-Ni lipid with other components, such as ethanolic solution of EPC, followed by the addition of the cholate aqueous solution. The size of the resulting final micelles was identical to the size of the micelles prepared of only EPC.

Flow-through ultrafiltration cell

The validity of the theoretical curve describing the removal of low-molecular-weight components from the flow-through ultrafiltration cell was experimentally verified by 6-CF as a fluorescent marker. The correlation between the theoretical and experimental curves is obvious (Fig. 3), and a slight positive deviation is caused by the repulsion between 6-CF and the ultrafiltration membrane. This fact means that R is not exactly equal to zero and the repulsion is not negligible. The simple exponential decay curve for cholate is complicated by the equilibrium between free and micelle/liposome-associated cholate. This is reflected by an increase of the concentration of cholate at the beginning of ultrafiltration. After reaching the critical micelle concentration (CMC), presumably free cholate was presented in solution and the experimental curve correlated well with the theoretical one (Fig. 3). The residual concentration of sodium cholate in liposomes was assayed by HPLC and shown to be below 0.3% of total lipid at the end of ultrafiltration. A possible leakage of phospholipids during the ultrafiltration procedure was assayed by Stewart's method (total phospholipids) and by the spectrofluorimetric method (LR-PE as the phospholipid marker). Both methods confirmed that neither phospholipids nor fluorescence-labeled phospholipids leaked out of the cell during the liposome preparation procedure.

Preparation of liposomes

The transformation of micelles into liposomes during the ultrafiltration removal of cholate was measured by DLS. The removal of cholate induced a formation of disc micelles that was reflected by

Table 1
Effect of lipid concentration on the size of micelles and liposomes.

Lipid concentration (mg/ml)	Micelles size (nm)			Liposomes size (nm)		
	Max. int.	Max. vol.	Max. num.	Max. int.	Max. vol.	Max. num.
1	5.3	5.0	4.8	42.2	40.2	38.1
10	6.0	5.6	5.2	79.8	61.7	48.4
25	5.2	4.7	4.3	75.4	57.4	44.2
50	5.5	5.2	4.9	67.5	54.6	44.8

Note: Size of micelles and liposomes is expressed in terms of maxima of intensity, volume, and number. Lipid concentration represents initial concentration in micelle solution used for preparation of liposomes.

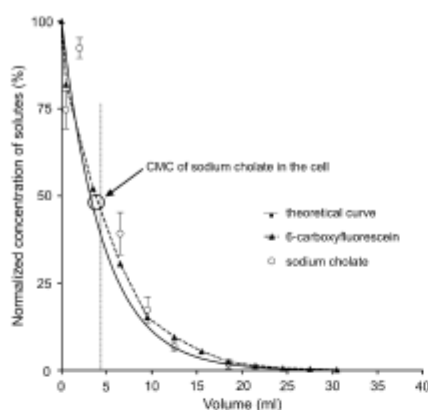


Fig. 3. Normalized concentration time course of 6-CF and sodium cholate in the ultrafiltration cell during ultrafiltration. The dashed vertical line indicates the volume of the cell. The circle indicates the point when the CMC of sodium cholate was reached during ultrafiltration run.

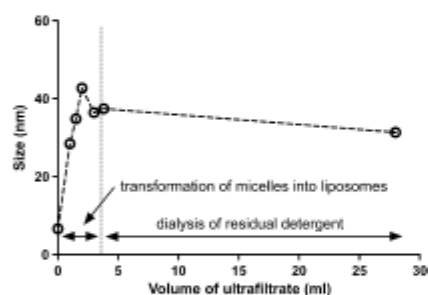


Fig. 4. Transformation of micelles into liposomes during ultrafiltration monitored by DLS. The dashed vertical line indicates the ultrafiltrate volume when the CMC of sodium cholate was reached. This line divides the flow-through volume axis into the left area, where micelles do predominantly exist and are transformed into liposomes, and the right area, where liposomes represent the main lipid form and residual detergent and ethanol/THF are continuously removed by the process of ultrafiltration.

an increase of the micelle size and eventually by a formation of liposomes (Fig. 4). The process of liposome formation had been completed before the CMC of cholate was reached, as shown by the dashed vertical line in Fig. 4. This line divides the flow-through volume axis into the left area, where micelles do predominantly exist and are transformed into liposomes, and the right area, where liposomes represent the main lipid form and residual detergent and ethanol/THF are continuously removed by the process of ultrafiltration.

Effect of various parameters on final size distribution of liposomes

The process of liposome formation is controlled by three parameters: temperature, flow rate (i.e., rate of detergent removal), and buffer composition. The experiments were performed at room temperature, and the speeding up of the detergent removal by an increased flow rate was limited by the flow characteristics of the

ultrafiltration membrane used. A decrease of the flow rate resulted in only a time-consuming procedure without any significant effect on the size (results not shown). Therefore, the influence of ionic strength was studied as the most applicable parameter. An increased NaCl concentration in the buffer resulted in substantially larger size of the prepared liposomes without affecting their monodispersity (Fig. 5). The observation of the prepared liposomes by TEM revealed their unilamellar character, and both TEM and AFM confirmed the monomodal size distribution with very low polydispersity (Fig. 6).

Preparation and characterization of GFP proteoliposomes

rGFP–His tag was used as a suitable marker protein that is easy to be quantified at a low concentration by spectrofluorimetry and is not prone to precipitate in a solution that is void of solubilizers such as imidazole and urea. Preformulated metalchelating liposomes were mixed with rGFP–His tag at various protein/lipid ratios and then separated by GPC on a Superose 6 column. Free versus liposome-bound protein was quantified by spectrofluorimetry. GPC elution profiles of empty liposomes and proteoliposomes are presented in Fig. 7A. Nearly all protein is bound to the liposomes at the protein/DOGS–NTA–Ni molar ratio of 1:40. The size, or rather the hydrodynamic radius, of the proteoliposomes was slightly higher than that of the empty liposomes, as is obvious from the smaller elution volume. The increase of the hydrodynamic radius of the proteoliposomes was also confirmed by DLS (Fig. 7B). Considering the value of $R_H = 2.82$ nm for GFP, the increase of the liposomal size of approximately 7–10 nm is in good accordance with the estimated increase of approximately 113 nm for the liposomes with their surface homogeneously covered by GFP. The binding capacity of DOGS–NTA–Ni liposomes (5 M% of total phospholipid) for rGFP was found to be approximately 25 μ g of protein/mg total phospholipid (Fig. 7C).

The structure of DOGS–NTA–Ni liposomes and rGFP proteoliposomes was studied by TEM, and the layer of protein on the liposomal surface was clearly visible (Fig. 7D). Confocal microscopy confirmed a native fluorescence state of rGFP bound to the liposomal surface (Fig. 7D).

Preparation and characterization of recombinant gp120 + MBL proteoliposomes

Binding of rgp120 to the metalchelating liposomes was followed by the DLS method, which showed a significantly larger size

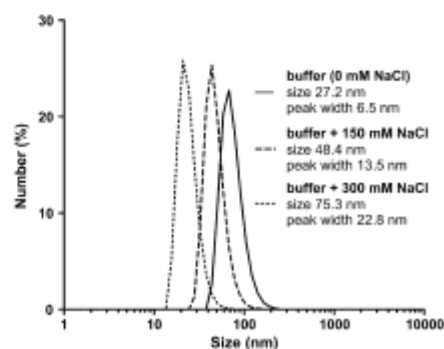


Fig. 5. Size distribution of liposomes prepared in buffer with increasing ionic strength. Buffer: 20 mM PBS.

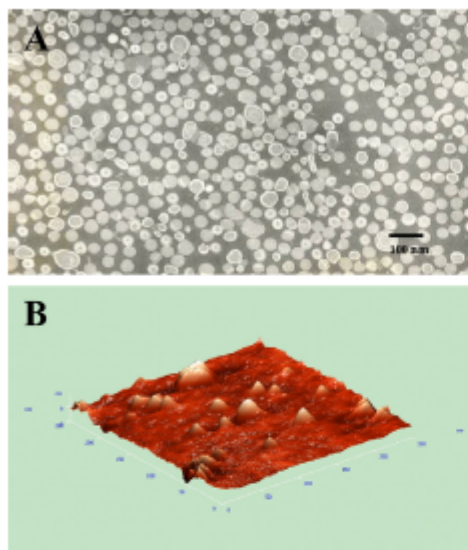


Fig. 6. Visualization of liposomes by TEM and AFM. (A) TEM micrographs of monodisperse liposomal preparation. (B) AFM micrographs of monodisperse liposomal preparation.

of the proteoliposomes as compared with the original plain ones (Fig. 8A). The addition of EDTA resulted in a release of the bound protein from the liposomes, and afterward the value of the liposome size was identical to that of the original plain liposomes (data not shown). When the liposomes void of metallochelating lipid DOGS-NTA-Ni or containing only DOGS-NTA without Ni^{2+} were mixed with rgp120, no change in their size was detected by DLS. These data indicated that the nonspecific binding of the protein was negligible. The localization of rgp120 on the liposomal surface was directly confirmed by TEM. This observation revealed that the bound rgp120 protein tends to form two-dimensional (2D) domains. These structures were also visualized by immunogold staining (Fig. 8B). AFM showed that on the large liposomes with low curvature (150–250 nm), big 2D protein domains or 2D protein crystals are formed (Fig. 8C).

Discussion

Flow-through ultrafiltration cell and preparation of monodisperse liposomes by detergent removal method

When essentially unilamellar monodisperse liposomes of spherical shape are needed (a prerequisite for a precise monitoring of the proteoliposome formation by DLS) the detergent removal method is preferred over the other methods. The mild conditions given by this method are advantageous for the preparation of proteoliposomes, especially for the reconstruction of membrane proteins [12] such as viral or bacterial antigens and recombinant His-tagged proteins that are often prone to precipitation. There are many variants of the detergent removal method, including the dilution of the solution of mixed micelles, gel permeation chromatography, a simple dialysis or a controlled one in a special apparatus for flow dialysis, cross-flow filtration, and adsorption on

beads [13]. The application of the flow-through ultrafiltration cell represents a new approach to the detergent removal method. The flow-through ultrafiltration cell employs “forced dialysis” and gives a better control over the process. The main advantage of this method is the possibility to use the cell as a reactor in which we can run complex procedures of liposome preparation. It means that various components could be added at the right time (e.g., proteins and peptides, modifying glycolipids, sugars for postforming modification, fluorescent markers and postlabeling) by an automatic way through the injection system of the FPLC/HPPLC instrument. The process of removal of low-molecular-weight components could be stopped for a required period or enhanced/retarded by simple changes of the flow rate. In addition, the linkage of the cell with systems such as FPLC facilitates the automation of the whole procedure and manipulation with the sample. The full control over the dialysis rate and the removal of the undesired residuals (e.g., detergent, organic solvents, protein solubilizers) is ensured, and various steps such as the addition of required components through an injection valve during various stages of liposome formation are easy to perform without breaching the sterile conditions. In this case, the sterile filter inserted in front of the cell inlet ensures that the sterility is kept during the whole process (Fig. 2 [filter not shown in the scheme]). The outlet capillary is easy to link with various detectors (e.g., fluorescence, UV/VIS), and the compounds in the effluent from the cell could be monitored online. Small fiber-optic probes could be inserted inside the cell to monitor the online processes of liposome formation and modification. Last but not least, the cell enables concentrating the final liposomal preparation by a reduction of the volume by switching the inlet from FPLC to a pressurized nitrogen bomb to perform a simple ultrafiltration. The low dead volume of the cell is of great importance for the preparation of liposomes and proteoliposomes in small laboratory scale. However, this arrangement also enables very easy upscaling of the whole technology. Precise control over the rate of the detergent removal yielded the final liposomal preparation of high monodispersity (polydispersity index [PDI] within the range of 0.05–0.06), which was reached routinely (Fig. 6). This monodispersity was better than those values obtained by the dialysis method performed in the dialysis bags or slides (Pierce) or in a stirred dialyzing cell (PDI ~0.08–0.12) (results not shown). The preparation of homogeneous mixed micelles by simply mixing the aqueous solution of cholate detergent with the ethanolic solution of lipids followed by filtration represents another significant improvement in simplifying this method. The preparation of the mixed micelles by the solubilization of the preformed liposomes [6,13] is tedious, and the elimination of the liposome preparation step, including the consequent resolubilization, is of importance for a possible industrial application. Moreover, ethanol, cholate, and THF are acceptable for the pharmaceutical industry, and their residuals (including traces of THF used for the solubilization of the chelating lipid DOGS-NTA) are removed quantitatively by the second ultrafiltration step.

The size of the mixed micelles (~5–6 nm [see Table 1]) used by us for the preparation of liposomes is in good correlation with Small’s mixed micellar model proposing the structure of a small phospholipid bilayer disc stabilized at its hydrophobic edges by the molecules of cholate [13,14]. The process of the formation of the monodisperse liposomes is in good accordance with the proposed kinetic model of the micelle-vesicle transition based on rapid formation of disc-like intermediate micelles followed by growth of these micelles up to their critical size and their subsequent closure to form vesicles. In addition, the strong dependence of the end state liposome size on the NaCl concentration confirmed the theoretical prediction based on the kinetic model [15]. Because the process of liposome formation is controlled by kinetics and not thermodynamics, the control over the rate of detergent removal is

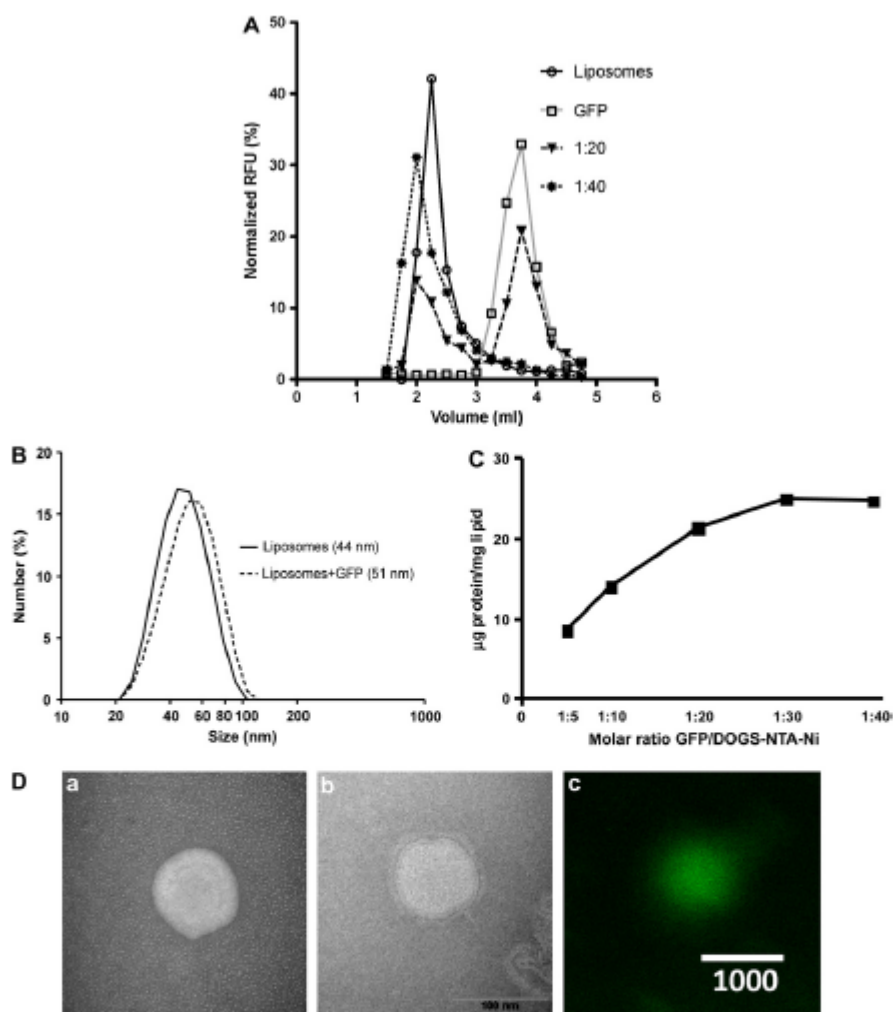


Fig. 7. Association of rGFP-His with EPC/DOGS-NTA-Ni liposomes analyzed by GPC (A), DLS (B), fluorescence spectrometry (C), and TEM and confocal microscopy (D). (A) GPC Superose 6 elution profiles of naked liposomes (○) and rGFP-His-proteoliposomes (□) at the protein/DOGS-NTA-Ni molar ratios of 1:20 (▲) and 1:40 (●). (B) Size distribution of naked liposomes and rGFP-His-proteoliposomes analyzed by DLS. (C) Metalchelation binding capacity of DOGS-NTA-Ni liposomes for rGFP-His ($\mu\text{g protein/mg total lipid}$). (D) TEM micrographs of the structure of naked liposomes (a) and rGFP-His-proteoliposomes (b) and confocal microscopic picture of rGFP-His-proteoliposomes (c). The arrow indicates rGFP-His located on liposome surface (b). Images (a) and (b) are of the same magnification.

of great importance and the application of a flow-through ultrafiltration cell is advantageous. The final size of the liposomal preparation could be controlled by ionic strength of the buffer used for the preparation of the micelles (see Fig. 5). An increase of the NaCl concentration reduces the CMC of cholate and shields the negative charge of the mixed micelles. These two factors are responsible for the formation and stabilization of the large discoid bilayer micelles that are transformed into the larger liposomes [13]. Various addi-

tives, such as bilayer stabilizing sugars (e.g., sucrose) and recombinant protein solubilizers (e.g., urea, guanidine), are compatible with this method and can shift the size of the liposomes into the required range [16]. Some recombinant proteins (e.g., circoviral envelope protein), which tend to precipitate in the absence of stabilizing buffers (imidazole and urea stabilizing buffer), were successfully linked onto metalchelating liposomes by a one-step procedure based on the addition of the protein into the mixed

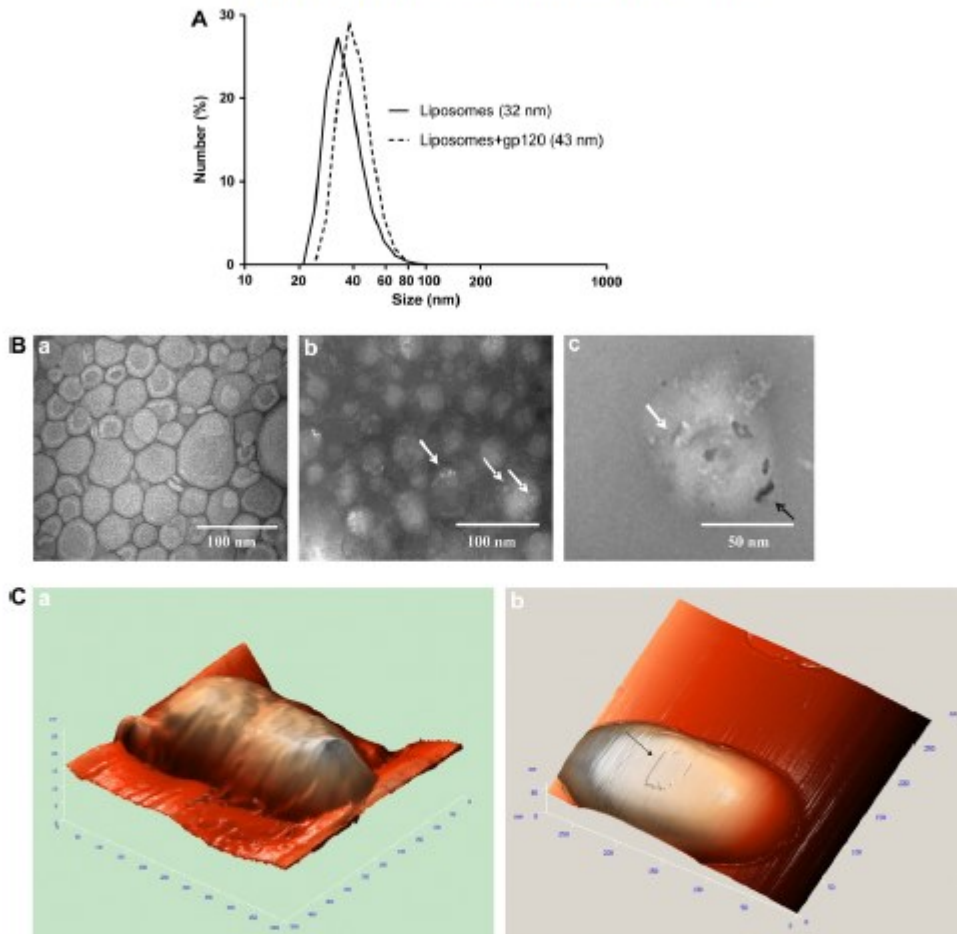


Fig. 8. Characterization of HIV-1 rgp120 proteoliposomes by DLS, TEM, and AFM. (A) Size distribution of naked liposomes and rgp120 proteoliposomes measured by DLS. (B) TEM visualization liposomes: a - plain liposomes, b - liposomes with bound rgp120 proteins (white arrows), c - immunogold staining of rgp120 bound onto liposomal surface (white arrow - protein cluster; black arrow - rgp120 marked by immunogold particles). (C) AFM visualization of liposome: a - plain liposome, b - liposome with rgp120 protein (the arrow indicates the domain of protein 2D crystal).

micelle solution prepared in protein stabilizing buffer and transforming into proteoliposomes during the ultrafiltration procedure (J. Turánek, unpublished results).

Proteoliposomes

There are only few references reporting the metalochelating bond implemented in the construction of liposome-based supra-molecular structures as vaccine carriers [5,17]. In these references, the authors showed a biological effect in vitro and in vivo in the mouse melanoma model. However, the structures of these peptide liposomes and proteoliposomes were not studied in detail, and there is no evidence that the presented schematic drawings correspond to the real structures formed by various

proteins with regard to the precise orientation and, hence, interaction in the 2D region on the liposomal surface. A relatively homogeneous coating of the liposomal surface was demonstrated for small model proteins such as rGFP (Fig. 7D, image d), and rOspC antigen (J. Turánek, unpublished results). These data are in good accordance with the simple schematic concept based on the random distribution on the liposomal surface. Moreover, the binding did not affect the native conformation of rGFP, as demonstrated by the preserved fluorescence characteristics (Fig. 7D, image c). On the other hand, some proteins can form on the liposomal surface higher structures such as 2D crystal domains, as found for HIV-1-derived rGP120 (Fig. 8) or hair-like structures, which we observed by TEM and AFM on rHSP-90 proteoliposomes (J. Turánek, unpublished results).

Although heterogeneity (higher PDI) of liposomes does not necessarily affect a potential application, the precise DLS measurement of liposome-protein coupling requires that the liposomes be highly monodisperse in their size, which could be reached by the method presented here. These liposomes are also advantageous for GPC analysis of both protein coupling and the stability of the proteoliposomes. This was documented for rGFP (Fig. 7A). The increase of the liposomal size due to the linkage of rGFP and covering the liposomal surface should theoretically amount to 11.3 nm with respect to the R_H of GFP, which is 2.82 nm [18]. The DLS experimental data showed an increase of approximately 7–10 nm, in good accordance with the theoretical model as well as the structures revealed by TEM (Fig. 7D, images a and b). The fact that we were able to demonstrate the small size difference between the plain and protein-covered liposomes at so good a correlation of the GPC and DLS data (Fig. 7A and B) is a result of the high monodispersity of the liposomes employed in this study.

With respect to a potential application to the construction of vaccines and drug targeting systems, the question of *in vitro* and especially *in vivo* stability is of great importance. This problem could be divided into two fields: (i) the stability of the liposomes themselves and (ii) the effect of the components present in biological fluids (e.g., proteins, ions) on the stability of the metalchelating bond. It is beyond the scope of this study to thoroughly address this particular question. However, the GPC data indicated good *in vitro* stability of the rGPC proteoliposomes during the chromatographic process when they experience the shear stress and dilution. The study by Rüger and coworkers shows that the single-chain Fv DOGS-NTA-Ni liposomes are unstable in human plasma and that most single-chain Fv fragments (anti-CD105) are released from the liposomal surface, resulting in the loss of the specific targeting performance to the cells expressing surface protein endoglin (CD105) [19]. Our experiments dealing with rGFP proteoliposomes also revealed the destabilization effect of serum, as detected by the GPC procedure. However, rOspC proteoliposomes were shown to be stable under the same conditions (J. Turánek, unpublished results).

On the other hand, Ni-NTA₃-DTDA (Ni-(nitrilotriacetic acid)-ditetradecylamine complex) liposomes with single-chain Fv fragments (anti-CD11c) bound onto the liposomal surface were able to target dendritic cells *in vitro* as well as *in vivo* [17]. The application of the three-functional chelating lipid Ni-NTA₃-DTDA probably endows the metalchelating bond with a higher *in vivo* stability. *In vivo* activity (immunogenicity) was also demonstrated for antigens associated with immunostimulatory complex (ISCOM) particles via metalchelating lipid dipalmitoyliminodiacetic acid [4] and a peptide antigen associated with liposomes via DOGS-NTA-Ni [5]. In general, metal ions, physicochemical character of the metalchelating lipids, and their surface density on the particles belong to the factors that could be optimized to get required *in vivo* stability.

Conclusions

We have demonstrated the first use of flow-through ultrafiltration to prepare essentially monodisperse liposomes by the detergent removal method. The linkage of the cell with the FPLC system facilitates automation of the procedure, which fits the criteria for upscaling. These liposomes are enabled for metalchelation of proteins, mediated by nickel or zinc ions, and represent a biocompatible platform for the construction of self-assembly proteoliposomes. Potential applications of such nanostructures can be as a platform for the development of vaccination nanoparticles

and drug delivery nanoparticle systems [2,5]. For the first time, the ultrastructure of proteoliposomes is demonstrated using AFM, TEM, and immunogold staining. The linkage of recombinant His-tagged proteins onto the surface of metalchelation liposomes can induce the formation of microdomain structures such as the 2D crystalline state observed with rgp120 (derived from HIV-1) postmetalchelation. Such structures are precisely distinguishable by AFM. Such knowledge of structure and physicochemical characteristics of proteoliposomes and their surface-bound proteins is of great importance for the development of vaccination nanoparticles, particularly where optimization of the immune response against bound antigenic proteins is concerned.

Acknowledgments

This work was supported by the following: grant GAČR P305/10/1951 to J.T.; grant MZE 0002716202 to J.T.; grants from the Academy of Sciences of the Czech Republic (projects KAN200520703 and 32-KAN200100801) to J.T., L.K. and M.L., and from the Ministry of Education, Youth, and Sports of the Czech Republic (MSM6198959223) to M.R. The authors thank Jan Mašek for the preparation of schematic drawings.

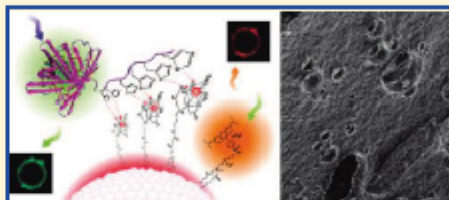
References

- [1] G. Gregoriadis, Engineering liposomes for drug delivery: progress and problems, *Trends Biotechnol.* 128 (1995) 527–532.
- [2] J.G. Altin, C.R. Parish, Liposomal vaccines: targeting the delivery of antigen, *Methods* 40 (2006) 39–52.
- [3] J. de Bekker, S. Capocchi, D. Semar, R. Rappoldi, M. Pizzi, Two years into reverse vaccinology, *Vaccine* 21 (2003) 608–610.
- [4] J. Malliaros, C. Quinn, F.H. Arnold, M.J. Pearce, D.P. Drane, T.L. Stewart, R.J. Macfarlan, Association of antigens to ISCOMATRIX adjuvant using metal chelation leads to improved CTL responses, *Vaccine* 22 (2004) 3968–3975.
- [5] G.G. Chikh, W.M. Li, M.P. Schutze-Redelmeier, J.C. Meunier, M.R. Bally, Attaching histidine-tagged peptides and proteins to lipid-based carriers through use of metal-ion-chelating lipids, *Biochim. Biophys. Acta* 1567 (2002) 204–212.
- [6] O. Zumbusch, H.G. Weder, Liposomes of controllable size in the range of 40 to 180 nm by defined dialysis of lipid-detergent mixed micelles, *Biochim. Biophys. Acta* 640 (1981) 252–262.
- [7] M. Kaška, Z. Mokřová, J. Novák, Z. Hol, L. Novák, J. Bozja, R.W. Compans, C. Yang, J. Mestecky, Delivery of DNA HIV-1 vaccine to the liver induces high and long-lasting humoral immune responses, *Vaccine* 26 (2008) 1541–1551.
- [8] R. Pecklíka, T. Purmann, R. Schubert, Cross-flow filtration: an improved detergent removal technique for the preparation of liposomes, *Int. J. Pharm.* 162 (1998) 177–183.
- [9] J.C.M. Stewart, Colorimetric determination of phospholipids with ammonium ferrioxalate, *Anal. Biochem.* 104 (1980) 10–14.
- [10] J. Turánek, Fast protein liquid chromatography system as a tool for liposome preparation by the extrusion procedure, *Anal. Biochem.* 218 (1994) 352–357.
- [11] L.D. Mayer, M.J. Hope, P.R. Gillis, Vesicles of variable sizes produced by a rapid extrusion procedure, *Biochim. Biophys. Acta* 858 (1986) 161–166.
- [12] J.L. Rigaud, D. Lévy, Reconstitution of membrane proteins into liposomes, *Methods Enzymol.* 372 (2003) 65–85.
- [13] R. Schubert, Liposome preparation by detergent removal, *Methods Enzymol.* 367 (2003) 46–70.
- [14] D.M. Small, Chemistry, in: P.P. Nair, D. Krüchensky (Eds.), *The Bile Acids: Chemistry, Physiology, and Metabolism*, Plenum, New York, 1971, pp. 249–356.
- [15] J. Leng, S.J.J. Eggehaaf, M.E. Gies, Kinetic pathway of spontaneous vesicle formation, *Europhys. Lett.* 59 (2002) 311–317.
- [16] A. Walter, G. Kuehl, K. Bames, G. VanderWaelde, The vesicle-to-micelle transition of phosphatidylcholine vesicles induced by nonionic detergents: effects of sodium chloride, sucrose, and urea, *Biochim. Biophys. Acta* 1508 (2000) 20–33.
- [17] C.I. van Broekhoven, C.R. Parish, C. Demange, W.J. Britton, J.G. Altin, Targeting dendritic cells with antigen-containing liposomes: a highly effective procedure for induction of antitumor immunity and for tumor immunotherapy, *Cancer Res.* 64 (2004) 4357–4365.
- [18] B.R. Terry, E.K. Matthews, J. Haseloff, Molecular characterization of recombinant green fluorescent protein by fluorescence correlation microscopy, *Biochem. Biophys. Res. Commun.* 21 (1996) 21–27.
- [19] R. Riggs, D. Müller, A. Fahr, R.E. Kosterman, *In vitro* characterization of binding and stability of single-chain Fv Ni-NTA-liposomes, *J. Drug Target.* 14 (2006) 576–582.

Preparation of Metallochelating Microbubbles and Study on Their Site-Specific Interaction with rGFP-HisTag as a Model Protein

Róbert Lukáč,^{†,‡} Zuzana Kauerová,^{†,‡} Josef Mašek,[†] Eliška Bartheldyová,[†] Pavel Kulich,[†] Štěpán Koudelka,[†] Zina Korvasová,[†] Jana Pločková,[†] František Papoušek,[†] František Kolář,[†] Roland Schmidt,[§] and Jaroslav Turánek^{*,†}[†]Department of Pharmacology, Toxicology and Immunotherapy, Veterinary Research Institute, Brno, Czech Republic[‡]Institute of Physiology, Academy of Sciences of the Czech Republic, Prague, Czech Republic[§]Hitachi High-Technologies Europe GmbH, Krefeld, Germany

ABSTRACT: The histidine–metallochelating lipid complex is one of the smallest high affinity binding units used as tools for rapid noncovalent binding of histidine tagged molecules, especially recombinant proteins. The advantage of metallochelating complex over protein–ligand complexes (e.g., streptavidin–biotin, glutathiontransferase–glutathion) consists in its very low immunogenicity, if any. This concept for the construction of surface-modified metallochelating microbubbles was proved with recombinant green fluorescent protein (rGFP) containing 6His-tag. This protein is easy to be detected by various fluorescence techniques as flow cytometry and confocal microscopy. Microbubbles (MB) composed of DPPC with various contents of metallochelating lipid DOGS-NTA-Ni were prepared by intensive shaking of the liposome suspension under the atmosphere of sulfur hexafluoride. For this purpose, the instrument 3M ESPE CapMix was used. Various techniques (static light scattering, flow cytometry, and optical microscopy) were compared and used for the measurements of the size distribution of MB. All three methods demonstrated that the prepared MB were homogeneous in their size, and the mean diameter of the MB in various batches was within the range of 2.1–2.8 μm (the size range of 1–10 μm). The presence of large MB (8–10 μm) was marginal. Counting of MB revealed that the average amount of MB prepared of 10 mg of phospholipid equaled approximately 10^9 MB/mL. Lyophilized MB were prepared with saccharose as a cryoprotectant. These MB were shown to be stable both *in vitro* (the estimated half-life of the MB in bovine serum at 37 °C was 3–7 min) and *in vivo* (mouse). The stability of the MB was affected by molar content of DOGS-NTA-Ni. DPPC-based metallochelating MB provided a clear and very contrast image of the ventricular cavity soon after the injection. Site selective and stable binding of rGFP-HisTag (as a model of His-tagged protein) onto the surface of metallochelating MB was demonstrated by confocal microscopy.



■ INTRODUCTION

Lipid-based carrier systems represent drug vehicles composed of physiological lipids such as phospholipids, cholesterol, cholesterol esters, and triglycerides as well as synthetic auxiliary lipids that enable to provide the lipid particles, especially their surface, with a special function. Self-assembling lipid carriers offer many advantages, e.g., controlled release, selective interaction with target cells, and simple manufacture. Lipid-coated gas-filled microbubbles (MB) represent a new class of drug delivery systems with both diagnostic and therapeutic application.¹ Considering drug delivery and targeting, the main advantage of microbubble application is a reduction of undesired side effects such as toxicity.² Furthermore, the diagnostic application of ultrasound imaging using MB has become highly popular because ultrasound is a noninvasive and relatively low-cost tool. It uses portable, real-time imaging equipment and also avoids hazardous ionizing radiation.^{2,3}

Considering MB themselves, they are small (typically 1–8 μm in diameter) microspheres filled with high-molecular-weight gases like perfluorocarbons or sulfur hexafluoride, which results in decreased solubility and prolonged lifespan of the MB within the circulation.² Until now, MB have been characterized by optical microscopy,⁴ static light scattering,⁶ and flow cytometry.^{4,5} Following the reported studies, we applied all the mentioned methods, and moreover, we attempted to preserve the MB using lyophilization, as described in a previous liposome study.⁷

Recently, targeting ligands that have been widely used in cardiovascular system and tumor diagnosis and therapy (reviewed by Liu et al.³) were attached to the surface of the MB.

Received: November 24, 2010

Revised: January 21, 2011

Published: March 18, 2011

Reversible interactions based on biotin-avidin/streptavidin pairs were implemented to provide the surface of the MB with the capability of attaching certain targeting ligands, e.g., monoclonal antibodies.

The histidine-metallochelating lipid complex is one of the smallest high-affinity binding units available as tools for rapid noncovalent binding of histidine tagged molecules, especially recombinant proteins. The advantage of metallochelating complex over protein-ligand complexes (e.g., streptavidin-biotin, glutathione transferase-glutathione) consists in its very low immunogenicity, if any. There have been only a few reports concerning the metallochelation of recombinant His-tagged proteins to nano- and microparticles, mainly liposomes.^{9–10}

The preparation of such structures typically requires an insertion of a metallochelating lipid into the outer leaflet membrane of the liposome bilayer that interacts selectively in the presence of metal ions (such as nickel, zinc, or cobalt ions) with a 4–6 amino acid residue of histidine tail (His-tag) expressed at the N- or C-terminus of a recombinant protein of interest as a targeting ligand or therapeutic agent. The reversible character of the bond, fast binding kinetics at room temperature, and high affinity of metallochelation are very useful features for the construction of various self-assembled reversible supramolecular structures.

The principle of metallochelating bond could be applied also to MB, and according to our knowledge, this is the first time when the metallochelating bond is implemented in the construction of proteoMB. To prove this concept, experiments were carried out using a mixture of DPPC and nickel-chelating lipid DOGS-NTA-Ni as metallochelating lipid in order to formulate proteoMB with proteins attached by metallochelation bond. His-tagged recombinant green fluorescent protein (rGFP-HisTag) was used as a model protein for following structural studies. We developed a method for the preparation of metallochelating MB as a novel platform for the construction of targeted MB or other microbubble-based supramolecular structures. These MB were studied by TEM, SEM, light and confocal microscopy, flow cytometry, and static light scattering. Biocompatibility and ultrasound contrast imaging of these MB were tested in mice using the ultrasound imaging system.

MATERIALS AND METHODS

Microbubble Preparation and Characterization. *Chemicals.* Lipids: 1,2-Dipalmitoyl-*sn*-glycero-3-phosphocholine (DPPC), 1,2-dioleoyl-*sn*-glycero-3-phosphoethanolamine-*N*-(carboxyfluorescein) (CF-PE), 1,2-dioleoyl-*sn*-glycero-3-phosphoethanolamine-*N*-(lissamine Rhodamine B sulfonyl) (Liss-PE), and metallochelating lipid 1,2-dioleoyl-*sn*-glycero-3-[[*N*-(5-amino-1-carboxypentyl)iminodiacetic acid]succinyl] (nickel salt) (DOGS-NTA-Ni) were purchased from Avanti Polar Lipids (Birmingham, AL).

Recombinant HisTag green fluorescent protein (rGFP) was obtained from Apronex (Prague, Czech Republic).

MB (Vevo MicroMarker, batch QA907) commercially available from BRACCO Res. SA (Geneva, Switzerland) were used as a reference for the *in vivo* heart imaging by ultrasound.

Preparation of Liposomes. Liposomes were prepared by the lipid film hydration method. In brief, liposomes were composed of DPPC and/or appropriate amounts of auxiliary lipids (fluorescence-labeled lipids and metallochelating lipid). Lipids were dissolved in chloroform and mixed properly. The mixture was subsequently transferred into a round-bottomed flask, and the solvent was removed via rotary evaporation at 37 °C. The lipid layer was hydrated by adding PBS solution up to



Figure 1. Equipment for preparation of MB: (A) capsule mixing device (3M ESPE CapMix) and the small bomb with sulfur hexafluoride (SF₆) linked with three-way valve and syringe for filling vials. (B) Sealed vial with dispersion of MB under a SF₆ atmosphere.

the final lipid concentration of 10 mg/mL at the temperature of 55 °C in water bath. Afterward, the DPPC liposomes were rapidly frozen in liquid nitrogen and thawed in 55 °C water bath five times. The resulting liposome suspension was digestsively extruded through 400 and 200 nm polycarbonate membrane filters (Whatman; Brentford, UK) at 55 °C using an Avanti Mini-Extruder (Avanti Polar Lipids). Thereafter, the suspension was measured by Zeta Sizer NanoZS (Malvern) to check that the size of the produced liposomes is within the range of 192–205 nm.

Preparation of MB. The liposome suspension (0.75 mL) was transferred into a hermetic vial (the volume of 1.5 mL). The vial was filled with sulfur hexafluoride gas (Messer Schweiz, AG) and mixed intensively for 30 s using 3M ESPE CapMix (capsule mixing device) (3M ESPE, AG). The apparatus for filling the vials and the mixing device is shown in Figure 1. Fluorescence-labeled MB were prepared from a lipid mixture containing DPPC and appropriate fluorescence lipid at the concentration of 0–5 mol %. Residual lipid structures (liposomes and aggregates of collapsed MB shells) were separated from MB by low-speed centrifugation, removing the upper MB containing layer (without foam) and resuspending MB in appropriate buffer (PBS). The procedure was repeated three times. MB with bound rGFP were prepared by addition of rGFP solution (6 μg; 0.2 μmol) to 100 μL of metallochelating microbubble suspension (content of DOGS-NTA-Ni metallochelating lipid was 0.4 μmol). After 1 min of incubation at 25 °C, 100 μL of the rGFP-MB was washed twice by PBS to remove residues of ruptured MB and non-microbubble lipids. This procedure allows obtaining clear background in confocal microscopy.

Efficacy of Liposome-to-MB Conversion. The lipid concentration in liposomes and MB was measured by UV/vis spectrophotometer Uvicon XL (Bio-Tec Instrument) using Stewart's method.¹¹ After conversion of liposomes to MB, the vials were centrifuged at low speed to separate the MB from aqueous phase that contains residual non-microbubble structures. The samples (20 μL) were taken up from the sealed vial by a syringe. The needle was positioned near to bottom to get the sample from the aqueous phase below the layer containing the MB. This aqueous phase contains residual liposomes and nonbubble structures.

The conversion rate was calculated according to equation

$$E_{\text{conv}} (\%) = (C_t - C_d) / C_t \times 100\%$$

where E_{conv} is the efficiency of liposomes-to-MB conversion, C_t the content of total lipid, and C_d the content of residual nonbubble lipid.

The theoretical number of monodispersed MB prepared from one mol of DPPC is expressed by equation

$$N_b = N_A a / 4\pi r^3$$

where N_b is the number of MB prepared from 1 mol of lipid, N_A the Avogadro number (6.02×10^{23} molecules/mol), a the effective area of the hydrophilic group for particular lipid (0.65 nm^2 for DPPC), and $4\pi r^2$ the surface of a microbubble ($r = \text{microbubble radius}$).

Provided that a monodisperse microbubble system is considered (diameter of $2.8 \mu\text{m}$; $r = 1.4 \mu\text{m}$), the number of MB can theoretically be 1.6×10^{16} per 1 mol of saturated phosphatidyl choline (e.g., DPPC or DSPC). The theoretical number of MB (prepared of 10 mg of DPPC (MW 734 Da)) is about 2.16×10^{11} .

MB Characterization by Light Epifluorescent and Confocal Laser Scanning Microscopy. The size and concentration of the MB were determined by optical microscopy (Nikon Eclipse TE200). The microbubble samples were taken directly from the vial, diluted 100 times in PBS, and observed at room temperature. Images were captured in both bright-field and fluorescence modes using LUCIA software (Laboratory Imaging, Czech Republic). The objective Nikon LWD 20 \times was used to capture the images of the MB. To obtain absolute counts of MBs, the Barker counting chamber was employed, and the captured pictures of the MB were evaluated for the size distribution by LUCIA software. A true confocal scanner, Leica TCS SP2 microscope, was used to determine the structure of the MB labeled by headgroup fluorescence labeled lipids (CF-PE, Liss-PE) as well as the MB with bound rGFP.

MB Characterization by TEM and SEM. The size and structure of the MB as well as the liposomes were determined by a Philips Morgagni transmission electron microscope (EM Philips 208 S, MORGAGNI software, FEI, CZ). All samples of MB were negatively stained by 2% (w/w) ammonium molybdate (pH 6.8). The sample of lyophilized MB was fixed to the SEM stub by Plano silver DAG. Images of uncoated samples were taken with the upper secondary electron detector of the Hitachi cold field emission scanning electron microscope SU8000 providing a resolution of 1.4 nm at 1 kV. In order to avoid charging artifacts, an accelerating voltage of 1.5 kV and a probe current of $\sim 15 \text{ pA}$ was selected. Additionally, all images were recorded in the charge suppression or fast integration scan mode.

Static Light Scattering (SLS). A HORIBA LA 950 laser diffraction particle size distribution analyzer was used to determine the microbubble size distribution. At first, the method was optimized by Megabead NIST Traceable Particle Size Standards (Polysciences, Inc., Warrington, PA) from 1, 3, 6, 10 to 15 μm . The 1.0% suspension of polystyrene microspheres in water was diluted by degassed and filtered PBS and measured. Microbubble sample (5–30 μL , 1–10 mg phospholipid/mL) was injected into cuvette-type fraction cell (filled with 10 mL of PBS) equipped with magnetic stirrer to prevent nonhomogeneous distribution owing to flotation of MB. All samples were measured immediately after the application into the cuvette and were analyzed both for number- and volume-weighted size distribution.

Flow Cytometry. In this method, a FACSCalibur cell analyzer (Becton-Dickinson, Franklin Lakes, NJ) was used to characterize microbubble fluorescence intensity (FL), light scattering profiles (FSC and SSC), and microbubble concentration. Voltage and gain settings for FSC, SSC, and FL were adjusted to delineate the microbubble populations from instrument and sample noise. Megabead NIST Traceable Particle Size Standards (Polysciences, Inc., Warrington, PA) from 1, 3, 6, 10 to 15 μm were used for the size distribution analyses. BD Tracount tubes (BD Biosciences) containing a known number of fluorescent polystyrene beads were used according to the instructions of the manufacturer. Absolute counts of MB were calculated by determining the ratio of beads to microbubble population and then multiplying this ratio by the number of beads in the tube. Subsequent data analysis was done using CellQuest Pro (Becton-Dickinson, Franklin Lakes, NJ).

Counting of Microbubbles by Cell Counter. BC-2800 VET (Mindray, China) was used to count the microbubbles and to analyze

their size. The microbubbles were washed two times by PBS and measured with dilution factor of 5.

Lyophilization. Before lyophilization, saccharose powder (molar ratio DPPC:saccharose = 1:5) was added to 500 μL of microbubble suspension (total lipid concentration of 10 mg/mL) composed of DPPC and various concentrations (0–5 mol %) of DOGS-NTA-Ni. The vials were frozen at $-80 \text{ }^\circ\text{C}$ in a freezer and then lyophilized using the Lyovac GT2 instrument (Fin-Aqua, Finland). First, the samples were placed into the drying chamber precooled to $-45 \text{ }^\circ\text{C}$. The lyophilization procedure was running for 24 h at 8 Pa. After this period of time, the second drying step was applied at $25 \text{ }^\circ\text{C}$ for 12 h under 20 Pa. When the lyophilization process was finished, the gasket sealed samples were evacuated and refilled with sulfur hexafluoride by flushing with gas injected through septum. Residual water was below 1% as assayed by Karl Fisher titration. The lyophilized MB were reconstituted by addition of 500 μL of degassed and filtered water, and the hydrated preparation was gently mixed by rotation of the vial by hand.

Stability of MB in Serum. The MB used for stability tests in serum were prepared by the standard way at the lipid concentration of 2 mg/mL. For reference, 50 μL of either liposome suspension used for microbubble generation or a microbubble sample was added to 3 mL of serum. The suspensions were placed into the sealed polycarbonate fluorescence plastic cuvette (10 mm, 4 mL) and tempered to $37 \text{ }^\circ\text{C}$. Quantification of the MB in the samples was carried out by light microscopy. The samples were taken every 5 min (interval 0–20 min), and photographs of three visual fields were acquired (at least 100 MB per field) and evaluated by LUCIA software (Laboratory Imaging, Czech Republic).

In vivo Ultrasound Imaging of Mouse Heart. The lyophilized MB were reconstituted by 0.5 mL of sterile PBS and left 10 min to hydrate, and 50 μL of this sample was injected via the cannulated right jugular vein to adult mice anesthetized by 2% isoflurane (Aerane; Bacter). For a comparison, commercial MB by Bracco were used as a standard. The preparation was diluted with PBS according to the manufacturer's instructions. The imaging of heart was performed using ultrasonic system Vevo 770 (VisualSonics, Toronto, Canada) equipped with 25 MHz probe RMV-707-B working in the contrast mode (frame frequency 110 Hz). The left ventricle was observed in long axis view before, during, and after the injection of MB. After the experiment, the anesthetized animals were killed by cervical dislocation.

Software Used. GraphPad Prism 5 software was used for statistical analyses and preparation of graphs.

RESULTS AND DISCUSSION

Characterization of MB by Microscopy Techniques. Liposome-to-microbubble conversion of DPPC liposomes (unlabeled or labeled by fluorescence lipids) with or without DOGS-NTA-Ni was proved by light and fluorescence microscopy. Optical microscopy enabled a direct visual inspection of the yielded MB, which appeared as dark spheres with bright centers (Figure 2A,B). The analysis of the bright-field images using LUCIA software revealed that the size distribution of freshly produced MB in various batches ranged from 1 to 10 μm with the mean diameter in the range of 2–3 μm . The MB concentration determined by Barker cell counting showed that the average amount of MB (prepared of 1 mg of phospholipid) equaled approximately to $(1-3) \times 10^8$ MB/mL. In fluorescence mode of microscopy, MB appeared as bright rings with dark centers, clearly showing narrow lipid shell labeled by CF-PE. The preparation was free of lipid aggregates or collapsed bubbles (Figure 2B), as determined by fluorescence microscopy. A detailed structure of the MB was obtained by TEM

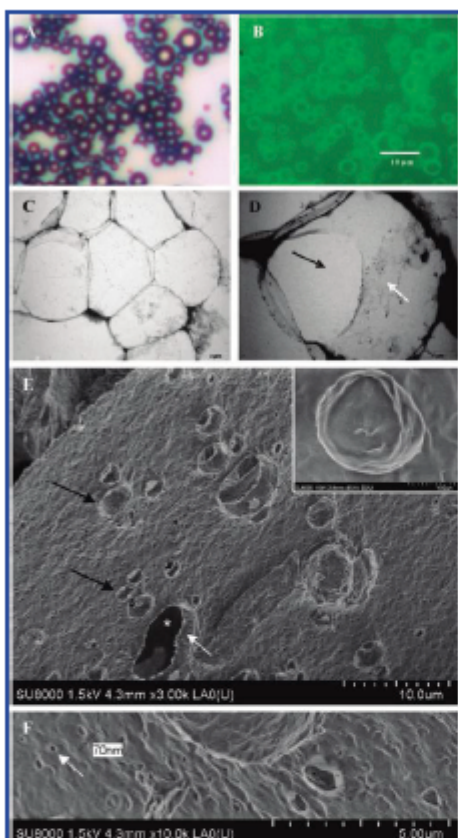


Figure 2. Pictures of MB obtained by various imaging techniques: (A) Light microscopy of DPPC/1% DOGS-NTA-Ni MB with carboxy-fluorescein-PE (1%). (B) The same MB as in (A) observed by epifluorescence microscopy. (C) TEM of MB. During desiccation of the sample in the vacuum interior of electron microscope, the MB are pressed to each other, which results in the deformed polygonal shape. (D) TEM detailed picture of MB. Some liposome-like structures persist in the microbubble preparation and could be found attached to their surface (white arrow). The opening in the microbubble results probably from microexplosion during evacuation in TEM tube (black arrow). (E) SEM picture of lyophilized microbubbles. Intact MB (black arrows), crushed MB shell (white arrow), hollow inside of MB (white asterisk). Inset: details of the surface of lyophilized MB. (F) Residual liposome embedded in matrix (white arrow). Distance between two black line segments is 70 nm.

(Figure 2C,D). The high-resolution TEM pictures showed that residual liposome-like structures persist in microbubble preparation and could be found also attached to the surface of some MB. This fact is not taken into account by many researchers in the field, and this data is not shown in the literature. The TEM also revealed an opening in a microbubble owing to microexplosion

during evacuation in TEM tube. During desiccation of the sample in the electron microscope, the MB are pressed to each other, which results in the deformed polygonal shape (Figure 2C,D).

Characterization of Size Distribution of MB by Flow Cytometry, Optical Microscopy, and Static Light Scattering. *Characterization by Flow Cytometry.* Flow cytometry proved itself to be a very useful method for a precise characterization of the size distribution of MB as well as for a precise and rapid counting of the MB. The data were in a good agreement with those obtained by optical microscopy (Table 1). Moreover, a precise resolution of the multimodal distribution of MB was achieved by flow cytometry even if SLS was not able to resolve it (compare Figure 3B with Figure 3D). The minute amount of large MB (around 10 μm) was also well recognized. The limit size of the large MB was clearly around 10 μm as confirmed by Megabeed NIST Traceable Particle Size Standards ranging from 1 to 15 μm . This data was confirmed by light microscopy.

Optical Microscopy. Figure 3C shows a size distribution profile of MB as evaluated by optical microscopy. The multimodal distribution is recognized, however, not so precisely as in the case of flow cytometry. In optical microscopy, the number of evaluated bubbles is smaller than in flow cytometry; therefore, the multimodal distribution is not so precisely pronounced. On the other hand, direct examination and counting of real MB as objects is a great advantage of this method.

Static Light Scattering. As the main advantage over the other SLS instruments, HORIBA LA 950 enables to measure in a relatively small cuvette (10 mL) with magnetic stirring to prevent changes in the distribution of MB in laser beam area owing to flotation. Microbubble size distribution by number as determined by HORIBA LA 950 ranged approximately from 1 to 18 μm with the mean around $4 \pm 1.8 \mu\text{m}$ (Figure 3D). These data were not in a perfect correlation with the light microscopy and flow cytometry data (Table 1). In principle, the SLS technique tends to overestimate larger bubbles. We have found a tendency to overestimate larger MB; hence, the mean of the size distribution has shown slightly larger values compared with those determined by light microscopy or flow cytometry. Moreover, this method is very sensitive to the presence of residual liposomes and lipid aggregates formed from burst bubbles. Therefore, some samples were not analyzed correctly, and the obtained data reflected not only the presence of MB.

Counting by Cell Counter. The number of microbubbles assayed by this method was in a good agreement with both FACS and microscopy techniques. Size distribution data are comparable with those obtained by static light scattering (Table 1).

In conclusion, even if the evaluation of light microscopy data was more tedious in comparison to flow cytometry and SLS, we chose this method as the most precise because direct visual examination eliminates errors due to counting the nonbubble structures, which are inevitably present in the sample.

Preparation of Metallochelating MB. The effect of DOGS-NTA-Ni on the preparation and stability of DPPC MB was studied in order to optimize the lipid composition. DOGS-NTA-Ni did not affect the conversion of liposomes into MB up to the concentration of 4 mol % in the lipid mixture (Figure 4). This concentration is high enough to provide a full coverage of the surface with His-tagged recombinant protein.

Table 1. Comparison of Microscopy, Static Light Scattering, Flow Cytometry, and Cell Counter with Respect to Determination of MB Size Distribution and Concentration^a

method of measurement	concn of MB [MB/mL] × 10 ⁸	av size of MB [μm]	minimal size [μm]	maximal size [μm]
light microscopy	2.53	2.17	0.93	9.99
static light scattering	DNP	4.09	2.1	16.92
flow cytometry	1.78	2.04	0.64	10.96
cell counter	2.04	3.86	1.68	7.26

^a MB = microbubbles, MB = composed of DPPC (1 mg/mL), DNP = determination is not possible, and ND = not determined.

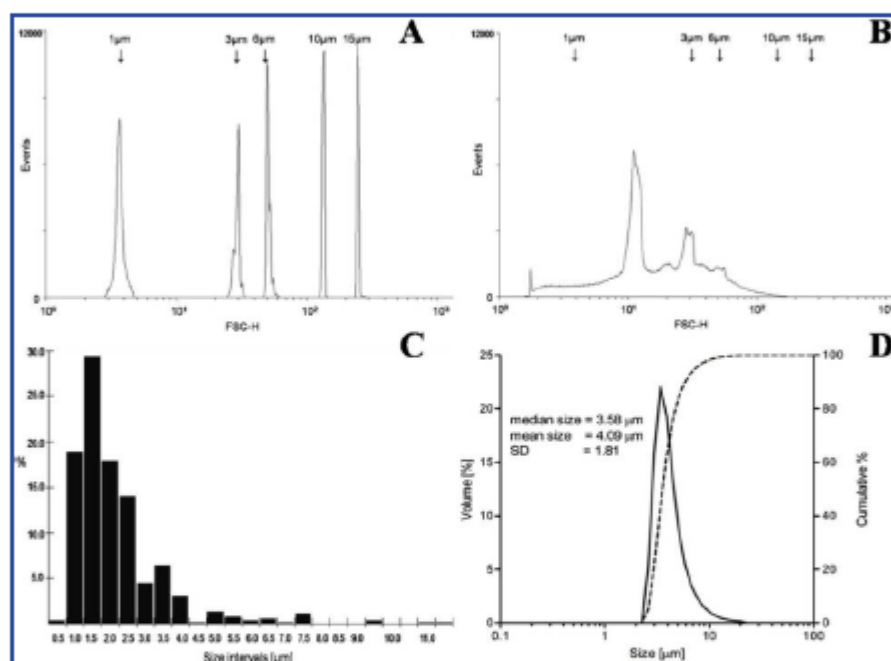


Figure 3. Comparison of size distribution analyses performed by flow cytometry, optical microscopy, and static light scattering. MB were prepared of DPPC/1% DOGS-NTA-Ni (lipid concentration of 10 mg/mL): (A) Positions of standards in forward scattering plot (flow cytometry analysis). (B) Size distribution profile of DPPC/1% DOGS-NTA-Ni MB (flow cytometry analysis). (C) Histogram of DPPC/1% DOGS-NTA-Ni MB obtained by optical microscopy. (D) Graph of size distribution measured by static light scattering (HORIBA LA 950 SLS instrument).

Generally, 1 mol % of metallochelating lipid is sufficient for this purpose.¹⁰ No significant effect on the size distribution was found by light microscopy, SLS, and flow cytometry (results not shown).

Efficacy of Liposomes-to-MB Conversion. The efficacy of the liposomes-to-MB conversion process was found to be around $6.5 \pm 4\%$ (based on the measurement of the lipid concentration by Stewart's method) for all tested compositions with the exception of DPPC/5% DOGS-NTA-Ni liposomes that exhibited a lower stability and the conversion was around 0.2–0.5%. This could be owing to the limited miscibility of DPPC (saturated lipid) with DOGS-NTA-Ni (unsaturated lipid), which results in a decreased stability of such a monolayer. This data based on the

measurement of the content of phospholipids in microbubble and nonmicrobubble structures is in a good agreement (within the order of magnitude) with the theoretical calculations showing that the theoretical number of monodisperse 2.8-μm MB (prepared of 10 mg of DPPC) is about 2.16×10^{11} MB. The number of MB in our preparations was within the range of $(1-3) \times 10^9$ (10 mg of phospholipid). The precision of the calculation is, of course, affected by the fact that a real system is not monodisperse; hence, the theoretical number of the monodisperse MB does not fit the theoretical number for a real systems with a various degree of polydispersity. Moreover, some portion of non-microbubble lipid is presented also in microbubble fraction owing to simple physical association with the MB (see

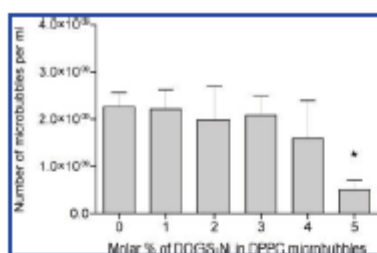


Figure 4. Influence of DOGS-NTA-Ni on the effectiveness of formation of DPPC MB. DPPC MB were prepared with addition of DOGS-NTA-Ni (0–5 mol %), and the effectiveness of liposome-to-microbubble conversion process was expressed as the number of MB per 10 mg of lipid. The number of MB was evaluated by optical microscopy. *: $p \geq 0.95$.

TEM micrographs, Figure 2D). This fact affects the calculation of the number of MB based on the microbubble and non-microbubble lipid assay by Stewart's method.

Lyophilization of MB. Lyophilization is a preferable method for the preparation of long-term storage form of MB. We tested saccharose as an acceptable cryoprotective compound often used for lyophilization of liposomes.¹² Saccharose powder (molar ratio Lipid (DPPC/0–4 mol % DOGS-NTA-Ni):saccharose = 1:5) was found to be effective to preserve the MB during lyophilization and ensuing reconstitution by hydration. Table 2 shows the data for DPPC and DPPC–1 mol % DOGS-NTA-Ni. About 35% of MB were preserved after the lyophilization and rehydration process. No significant differences were found within the group composed of DPPC/0–4 mol % DOGS-NTA-Ni lipids. The mean size of the reconstituted MB was similar to that of the same sample prior to lyophilization. The size limit of the large MB was shifted by about 1 μm toward the larger ones. This effect could have been caused by a fusion of small amount of MB during rehydration. The picture of MB embedded in saccharose matrix after the lyophilization process is shown in Figure 2E. The microbubbles appeared as spherical hollow objects that are a little bit wrinkled owing to lyophilization process. Some of them were crashed by manipulation with the lyophilizate during preparation of the sample; therefore, the very thin fragile lipid shell as well as the inside of MB is well visible. Also, residual liposomes which were not converted into MB are clearly visible embedded in the matrix around the MB (Figure 2F).

In Vitro Stability of DPPC/DOGS-NTA-Ni Metallochelating MB in Serum. The stability of MB in 100% bovine serum at 37 °C was tested by light microscopy. MB were obviously present more than 20 min, and the estimated half-life of the MB in bovine serum was more than 20 min for DPPC and DPPC/DOGS-NTA-Ni 1 mol % and about 5–8 min for DPPC/DOGS-NTA-Ni 3 and 5 mol %. The stability of the MB was affected by a content of DOGS-NTA-Ni. With an increasing concentration of DOGS-NTA-Ni, the stability slightly decreased (Figure 5). During the incubation with serum, no significant effect on the mean size and the size distribution was observed (Table 3). The *in vitro* stability of MB in concentrated serum is a prerequisite for the *in vivo* stability within blood circulation system. The destabilizing effect of DOGS-NTA-Ni at the concentration higher than 4–5 mol % is indicative of possible phase separation of DPPC and DOGS-NTA-Ni lipids. It results in inhomogeneities in lipid monolayer, which destabilizes the MB shell. It is also

Table 2. Effect of Lyophilization on Number and Size Distribution of DPPC and DPPC/DOGS-NTA-Ni MB^a

lipid composition	MB status (before/after lyophilization)	concn of MB [MB/ml]	av size of MB [μm]	minimal size [μm]	maximal size [μm]
DPPC	before	3.575×10^8	2.17 ± 0.85	0.93	6.89
	after	1.23×10^8	2.54 ± 1.44	1.19	7.93
1% DOGS-NTA-Ni	before	3.25×10^8	2.02 ± 0.68	1.04	5.13
	after	1.175×10^8	2.11 ± 0.89	1.19	6.55

^a Lipid concentration was 1 mg/mL.

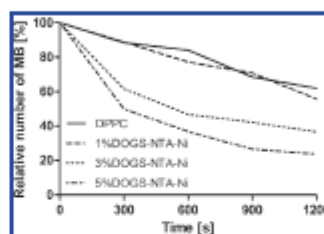


Figure 5. *In vitro* stability of DPPC/DOGS-NTA-Ni metallochelating MB in serum. DPPC MB with 0, 1, 3, and 5 mol % of DOGS-NTA-Ni were incubated in bovine serum (100%) at 37 °C, and the decrease of their number was quantified by optical microscopy. The data were normalized and plotted as percentage of MB number versus time (s).

reasonable to suppose that high surface concentration of metallochelating function in DOGS-NTA-Ni phase-separated islands results in nonspecific interaction with serum proteins destabilizing MB. These aspects will be subjected to further research with the aim to improve *in vivo* stability of metallochelating MB.

In vivo Visualization and Stability of MB. Figure 6 shows typical images of the left ventricle in a long axis view before and after the intravenous injection of DPPC-based MB and commercial MB (Bracco) in anesthetized mice. In both cases, no adverse effect on breathing and heart function was observed. DPPC-based MB provided a clear and very contrast image of the ventricular cavity soon after the injection. In comparison with the MB by Bracco, which are stabilized by poly(ethylene glycol), pure DPPC-based MB exhibited a lower stability in the circulation (the contrast disappeared after 1–2 min, while the MB by Bracco yielded the contrast picture for up to 10 min). For instance, Levovist and SonoVue have a half-life of 78 s and 5 min, respectively. An adequate *in vivo* bubble half-life is a major requirement for imaging as well as ultrasound facilitated drug targeting. In fact, an unpredictable release profile would lead to a lack of control of the drug release, regardless of a passive or active mechanism of MB targeting. As mentioned above, the bubble size is also a critical parameter that must be controlled and kept in the range of 1–7 μm , preferably around 3 μm . The MB larger than 6–8 μm would be trapped in the lung capillaries, and the bubbles smaller than 1 μm would be less stable and less ultrasound responsive.¹³ Our DPPC-based MB fulfill these requirements.

Table 3. Size Distribution of DPPC/DOGS-NTA-Ni MB during Incubation in Bovine Serum at 37 °C and Stability of MB Size (Measured in 0, 5, 10, 15, and 20 min)

lipid composition	av size [μm]	minimal size [μm]	maximal size [μm]
prepared MB (DPPC)	2.9 \pm 1.7	1.1	11.6
0 min	3.0 \pm 1.6	0.9	9.5
5 min	2.9 \pm 1.6	1.2	11.0
10 min	2.7 \pm 2.0	0.9	9.2
15 min	2.6 \pm 1.4	0.9	10.4
20 min	2.6 \pm 1.5	1.0	8.0
prepared MB (1% DOGS-NTA-Ni)	2.7 \pm 1.3	1.3	9.8
0 min	2.7 \pm 1.6	1.0	7.5
5 min	2.9 \pm 1.6	1.0	8.7
10 min	2.7 \pm 2.0	1.0	6.2
15 min	2.6 \pm 1.4	0.8	5.3
20 min	2.6 \pm 1.5	1.1	7.9
prepared MB3% DOGS-NTA-Ni	2.3 \pm 0.8	1.0	5.9
0 min	2.2 \pm 1.1	1.0	8.7
5 min	2.1 \pm 0.7	1.0	4.5
10 min	2.1 \pm 0.8	1.0	4.3
15 min	2.0 \pm 1.2	1.0	4.7
20 min	2.2 \pm 0.8	1.3	4.2
prepared MB5% DOGS-NTA-Ni	2.4 \pm 1.0	0.7	7.3
0 min	2.5 \pm 1.0	1.0	5.2
5 min	2.3 \pm 0.9	1.0	5.0
10 min	2.5 \pm 1.0	1.2	5.9
15 min	2.3 \pm 0.8	1.2	4.5
20 min	2.5 \pm 1.1	1.2	5.1

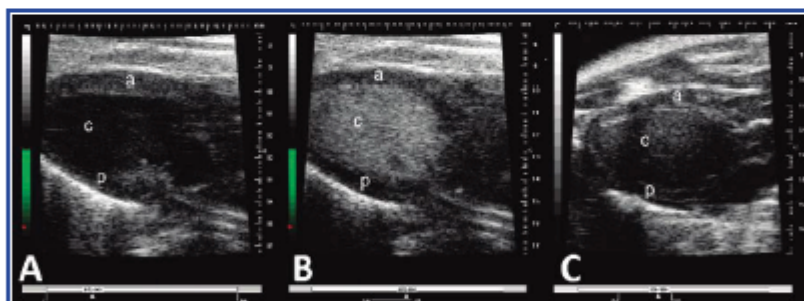


Figure 6. Ultrasound contrast images of the mouse heart in a long axis view. (A) Without MB. (B) After the intravenous administration of DPPC/1% DOGS-NTA-Ni MB. (C) After the intravenous administration of commercial MB by Bracco. c: left ventricle cavity; a: left ventricle anterior wall; p: left ventricle posterior wall.

Binding of rGFP-HisTag onto the Surface of Metallochelating MB. The rGFP-HisTag molecule bound onto the surface of metallochelating liposomes was directly detected by TEM (Figure 7A,B). Fluorescence of rGFP was used to prove binding of this protein onto the MB (Figure 7C). The binding did not affect the native conformation of rGFP as demonstrated by the preserved fluorescence characteristics of the protein. Homogeneous population of highly fluorescent rGFP MB was detected by flow cytometry (Figure 7G).

Non-specific binding of rGFP on both DPPC liposomes as well as MB lacking DOGS-NTA-Ni was observed neither by flow

cytometry nor by confocal microscopy. Confocal microscopy confirmed colocalization of bound rGFP-HisTag (green fluorescence) with the lipids forming microbubble monolayer. The monolayer was marked with Liss-PE (red fluorescence) (Figure 7D–F). Confocal microscopy revealed that a small fraction of MB had also attached liposomes or residual lipid structures of collapsed MB on their surface (as seen in Figure 7D–F). This is in a good agreement with the electron microscopy data (Figure 2D).

Affinity metallochelating binding is based on complexes of bound metal ions (preferably nickel but cobalt, manganese, or

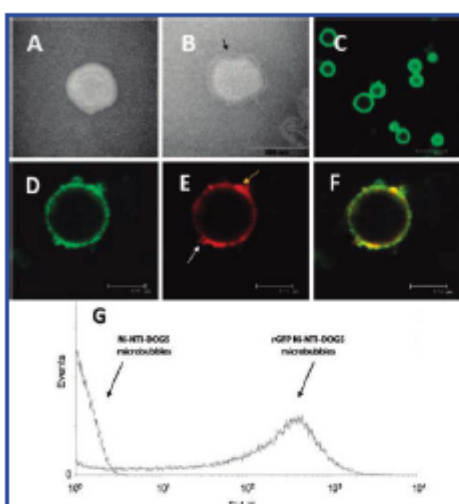


Figure 7. Structure of metallochelating liposomes and MB with bound rGFP-HisTag. (A) TEM micrograph of the structure of plain liposomes. (B) TEM micrograph of the structure of rGFP-His-tag proteoliposomes (the arrow indicates rGFP-His-tag located on the liposome surface). (C) Confocal microscopic picture of rGFP-HisTag-metallochelating MB revealing the localization of functional rGFP on their surface (green fluorescence). (D) Detailed confocal microscopic picture of rGFP (green fluorescence) localized on the surface of a MB. (E) Detailed confocal microscopic picture of Liss-PE (red fluorescence) localized on the surface of a MB (white arrow indicates the lipid membrane aggregate (residuum of a ruptured MB) adsorbed on the surface of a MB; yellow arrow indicates a cluster of residual liposomes attached to the surface of a MB). (F) Merged picture demonstrating colocalization of rGFP-His-tag with MB shell labeled with Liss-PE. (G) Flow cytometry analysis of rGFP-His-tag DOGS-NTA-Ni MB (green fluorescence) and DOGS-NTA-Ni MB (no fluorescent).

zinc could be used also), to which the polyhistidine-tag binds with micromolar affinity. The main advantage of this metallochelating binding is the site-specific immobilizations of proteins. This feature is highly demanded especially in the field of molecular recognition comprising biosensors, oriented surfaces, and targeted drug carriers.

Investigations with single-molecule experiments using scanning force microscopy revealed that His-tags form various types of complexes, which significantly differ in stability and energy profile along their dissociation pathway.^{14,15} With respect to a potential application of metallochelating bond to the construction of targeted MB, the question of *in vitro* and especially *in vivo* stability is of great importance. This problem could be divided into two fields: first, the stability of the MB themselves and, second, the effect of the components present in biological fluids (e.g., proteins and ions) on the stability of the metallochelating bond. It is beyond the scope of this study to address thoroughly this particular question. However, the *in vivo* data indicated that the stability of DPPC-based MB in circulation is lower than that found for the MB stabilized in lyophilizate by poly(ethylene glycol) as cryoprotectant (SonoVue MB). With the sterically

stabilized MB (e.g., by application of poly(ethylene glycol)-phosphatidylcholine as the component modifying the surface of microbubbles), the immobilization of His tag protein on such a sterically protected surface could be greatly hampered by the inaccessibility of the His-tag caused by steric hindrance as described for the interaction of His-tag proteins with metallochelating affinity chromatography media.¹⁶ In this case, the metallochelating function (e.g., NTA) should be positioned at the end of PEG chain to be easily accessible to His-tag. It implies a design and synthesis of new metallochelating lipids fulfilling this specific demand and, hence, being more suitable for the construction of metallochelating MB. The lipid part of the molecule should be optimized to provide miscibility with the lipids used for the formation of the microbubble shell. The role of the spacer with metallochelating function is to provide high affinity binding of His-tag. Compared with the strong interactions reported for the complexes of avidin and biotin ($K_D = 10^{-14}$ M), the affinity of the hexahistidine peptide to Ni-NTA is more than a factor of 10^5 lower ($K_D = 10^{-9}$ M). A limited accessibility of the tag caused by a steric hindrance or electrostatic interactions are possible explanations for the decrease in binding affinity for the Ni²⁺/6His-tagged protein complex ($K_D \approx 10^{-6}$ M).¹⁷ Because there are no data in the literature dealing with metallochelating MB, we have to estimate the possible stability of the metallochelating bond according to a few papers dealing with metallochelating liposomes. The study by Rieger et al. shows that the single-chain Fv DOGS-NTA-Ni liposomes are unstable in human plasma and that most of single-chain Fv fragments are released from the liposomal surface.¹⁸ However, our experiments dealing with rOspC His-tag/DOGS-NTA-Ni proteoliposomes demonstrated their relative stability under the same conditions (Turánek, unpublished results). Similarly, Ni-NTA3-DTDA liposomes with single-chain Fv fragments (antiCD11c) bound onto the liposomal surface were able to target dendritic cells *in vitro* as well as *in vivo*.^{19,20} The application of the three-functional chelating lipid Ni-NTA3-DTDA probably endows the metallochelating bond with a higher *in vivo* stability. Generally, metal ions, physicochemical character of the metallochelating lipids, and their surface density on the particles belong to the factors that could be optimized to get a required *in vivo* stability.

CONCLUSION

At present, the histidine-metallochelating lipid complex is one of the smallest high affinity binding units used as tools for rapid noncovalent binding of histidine tagged molecules, especially recombinant proteins. The advantage of metallochelating complex over protein-ligand complexes (e.g., streptavidin-biotin, glutathione transferase-glutathione) consists in its site-specific binding and very low immunogenicity, if any. We proved usefulness of this concept for the construction of surface modified MB on the model of metallochelating MB with bound rGFP, which is easy to be detected by various techniques as flow cytometry and confocal microscopy.

In vivo application of DPPC-based metallochelating MB to mice demonstrated biocompatibility and good contrast imaging comparable with that of the commercial product SonoVue (Bracco). Stabilization of the metallochelating MB preparation by lyophilization is feasible, and the *in vivo* stability is within the range of phospholipid-based MB (Levovist or SonoVue). An application of monolayer stabilizers like PEG-40 stearate, Phosphoric F68, or Polysorbate 80 could further improve the *in vitro* and

in vivo stability. The main improvement is expected to be obtained by application of novel metallochelating lipids that are designed to be incorporated into the microbubble monolayer. To design such metallochelating lipids, several essential aspects must be taken into account: stabilization effect of the lipid part on the monolayer, high affinity of the metallochelating function linked to the accessory lipid part, and a suitable spacer (e.g., various PEG spacers) for effective binding of larger molecules onto sterically stabilized MB. The design and synthesis of these biocompatible metallochelating lipids is in progress.

AUTHOR INFORMATION

Corresponding Author

*Phone + 420 5 3333 1311; Fax + 420 5 4121 1229; e-mail turanek@vri.cz

Author Contributions

[†]Contributions of the first two authors are equal.

ACKNOWLEDGMENT

This work was supported by following grants: Grant Agency of the Academy of Sciences of the Czech Republic GAAV KAN200520703 to J.T., F.P., and F.K.; Grant Agency of the Academy of Sciences of the Czech Republic GAAV KAN200100801 to J.T.; Grant Agency of the Czech Republic GACR P304/10/1951 to J.T.; and Grant No. MZE 0002716202 to J.T. The authors thank Asst Professor Milan Raška, Ph.D., for the schema of metallochelating microbubble in the table of contents graphic.

REFERENCES

- (1) Rawat, M.; Singh, D.; Sami, S.; SARAF, S. *Yakushaku Zasshi* 2008, 128, 269–280.
- (2) Hemot, S.; Klibanov, A. L. *Adv. Drug Delivery Rev.* 2008, 60, 1153–1166.
- (3) Liu, Y.; Miyoshi, H.; Nakamura, M. *J. Controlled Release* 2006, 114, 89–99.
- (4) Feshitan, J. A.; Chen, C. C.; Kwan, J. J.; Borden, M. A. *J. Colloid Interface Sci.* 2009, 329, 316–324.
- (5) Nicholson, J. K.; Stein, D.; Mai, T.; Mack, R.; Hubbard, M.; Denny, T. *Clin. Diagn. Lab. Immunol.* 1997, 4, 309–313.
- (6) Rapoport, N.; Gao, Z.; Kennedy, A. *J. Natl. Cancer Inst.* 2007, 99, 1095–1106.
- (7) Slow, L. F.; Rades, T.; Lim, M. H. *Cytobiology* 2007, 55, 210–221.
- (8) Malliaros, J.; Quinn, C.; Arnold, F. H.; Pease, M. J.; Dunn, D. P.; Stewart, T. L.; Macfarlan, R. I. *Vaccine* 2004, 22, 3968–3975.
- (9) Chláb, G. G.; Li, W. M.; Schutze-Radelmeier, M. P.; Meunier, J. C.; Bally, M. B. *Biomater. Biotechnol. Acta* 2002, 1567, 204–212.
- (10) Mašek, J.; Barthelidyová, E.; Korvasová, Z.; Štrábalová, M.; Koudelka, S.; Kulich, P.; Kratochvílová, I.; Müller, A. D.; Ledtma, M.; Raška, M.; Turánek, J. *Anal. Biochem.* 2011, 408, 95–104.
- (11) Stewart, J. C. M. *Anal. Biochem.* 1980, 104, 10–14.
- (12) Koudelka, S.; Mašek, J.; Neutřil, J.; Turánek, J. *J. Pharm. Sci.* 2010, 99, 2434–2443.
- (13) Cavallieri, F.; Zhou, M.; Ashokkumar, M. *Curr. Top. Med. Chem.* 2010, 10, 1198–1210.
- (14) Schmitt, L.; Ludwig, M.; Gaus, H. E.; Tampé, R. *Biomater. J.* 2000, 78, 3275–3285.
- (15) Conti, M.; Falini, G.; Samorì, B. *Angew. Chem. Int. Ed.* 2000, 39, 215–218.
- (16) Miras, R.; Cullif, M.; Catty, P.; Guillaud, F.; Mintz, E. *Protein Expr. Purif.* 2001, 22, 299–306.
- (17) Nieba, L.; Nieba-Axmann, S. E.; Persson, A.; Hämmäläinen, M.; Edebratt, F.; Hansson, A.; Lidholm, J.; Magnusson, K.; Karlsson, A. F.; Plückthun, A. *Anal. Biochem.* 1997, 252, 217–228.
- (18) Rüger, R.; Müller, D.; Fahr, A.; Kontermann, R. E. *J. Drug Target.* 2006, 14, 576–582.
- (19) van Broekhoven, C. L.; Parish, C. R.; Demangel, C.; Bittton, W. J.; Altin, J. G. *Cancer Res.* 2004, 64, 4357–4365.
- (20) Knecht, S.; Ricklin, D.; Eberle, A. N.; Ernst, B. *J. Mol. Recognit.* 2009, 22, 270–279.

2. HYDROFILNÍ A HYDROFOBNÍ LÁTKY, SURFAKTANTY: FORMULACE A INTERAKCE S MEMBRÁNAMI

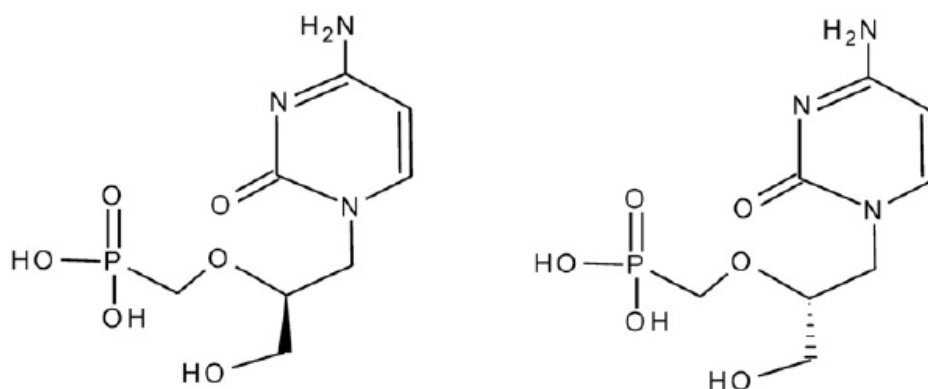
Farmakologicky aktivní látky vyvolávají v organismu svůj účinek celou řadou mechanismů. Zmíním zde ty mechanismy, které jsou relevantní látkám studovaným v přiložených publikacích. Pro dosažení místa cíleného účinku musí molekula farmaka překonat v organismu celou řadu bariér, zejména bariéry tvořené lipidními membránami buněk a jejich organel. Zákonitosti distribučních pochodů farmaka v organismu lze odvodit od základních fyzikálně-chemických vlastností molekul konkrétního farmaka. Pro distribuci v organismu, ale i pro resorpci a vylučování má rozhodující význam rozpustnost látky ve vodném prostředí. Tento základní parametr má vliv také na lékovou formulaci léčiv, která je rozhodující pro optimalizaci biodistribuce a tím i léčebného účinku. Z hlediska rozpustnosti lze tedy farmaka rozdělit na tři skupiny.

2.1. LÁTKY ROZPUSTNÉ VE VODĚ (HYDROFILNÍ LÁTKY)

Pokud se jejich kinetiky neúčastní některý transportní systém (proteinový nosič), pak se špatně vstřebávají po orálním podání a po parenterální aplikaci se distribuují jen v extracelulárním prostoru. Hydrofilní látky mohou do buňky vstupovat buď selektivně s pomocí aktivního nebo pasivního transportu, pinocytózou nebo difusí přes membránu. Dva posledně zmíněné mechanismy vyžadují pro navození účinku vysokou lokální koncentraci farmaka a její delší časové trvání.

Při enkapsulaci těchto látek do liposomů dochází k jejich distribuci ve vodné fázi liposomálních vesikulů a jejich koncentrace odpovídá koncentraci v hydratačním roztoku, použitým pro přípravu liposomů.

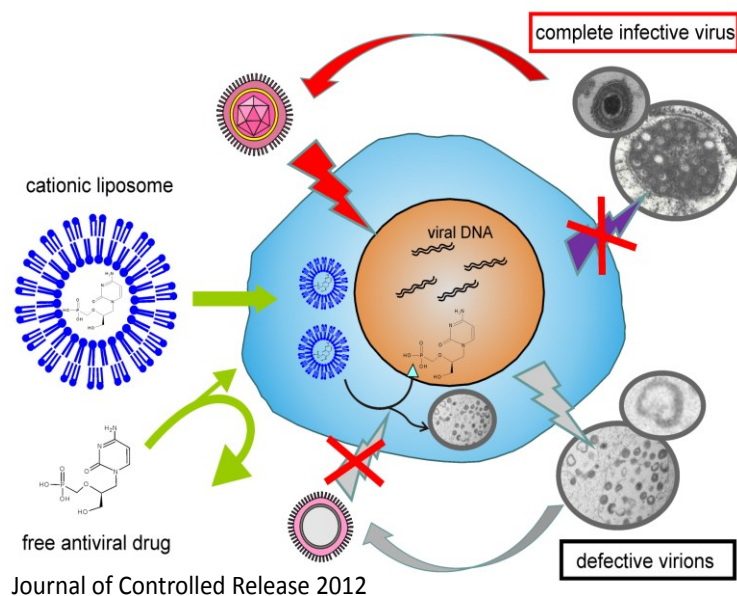
Jako příklad těchto látek, které byly studovány, je antivirotikum cidofovir, které vyvinul prof. Antonín Holý. Tato látka má fosfátovou skupinu a její soli jsou velmi dobře rozpustné ve vodě. Hlavní překážkou pro její účinek na intracelulární cíl – virovou DNA polymerázu – je přechod přes buněčnou membránu. Cidofovir ((S)-1-(3-hydroxy-2-fosfonylmethoxypropyl)-cytosin (HPMPC) představuje novou třídu širokospektrálních antivirotik a je aktivní proti širokému spektru herpesvirů. Virová DNA polymeráza je 8-600 krát citlivější vůči inhibici cidofovirem než lidské DNA polymerázy alfa, beta a gama. Výrazný a dlouho trvající antivirální účinek cidofoviru je přisuzován perzistenci jeho intracelulárních derivátů, které po další fosforylaci jsou zadržovány v buňce a mohou tak dlouhodobě inhibovat virovou DNA polymerázu.



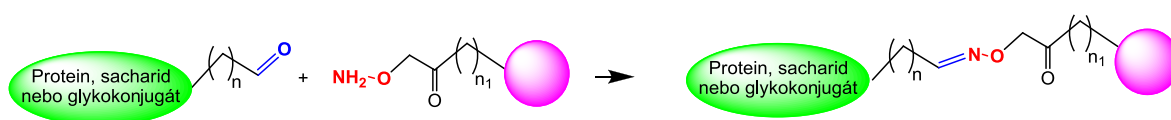
Obr. 15 Vzorec cidofoviru (L a R optické izomery, R isomer je neaktivní).

Vzhledem k mechanismu účinku cidofoviru (intracelulární virová DNA polymeráza) jsou pro enkapsulaci vhodné liposomy, které jsou snadno internalizovány do buněk. Pro cílení liposomů k některým typům buněk (zejména hepatocyty) jsou vhodné kationické liposomy připravované z kationických lipidů s nízkou cytotoxicitou nebo liposomy povrchově modifikované některými ligandy jako např. fragmenty kyseliny hyaluronové, pro které existují na hepatocytech specifické receptory. Ve spolupráci s ÚOCHB byly takovéto kationické lipidy navrženy a syntetizovány (společný český patent a podaná přihláška PCT). V *in vitro* modelech byl prokázán antivirální účinek cidofoviru enkapsulovaného v kationických liposomech na bovinní herpesvirus. Obecné schéma principu cílení antivirotik do cytoplasmy buněk je schematicky naznačeno na obrázku. Dále byly připraveny aktivní lipidy s aminoxy skupinou pro selektivní orientovanou vazbu sacharidů na liposomy, což umožnilo přípravu originálních liposomů povrchově modifikovaných různými fragmenty kyseliny hyaluronové (patentová přihláška v přípravě). Cílení těchto liposomů k hepatocytům, buňkám imunitního systému a nádorovým liniím je v současnosti intenzivně studováno.

Kationické liposomy pro cílení antivirotik

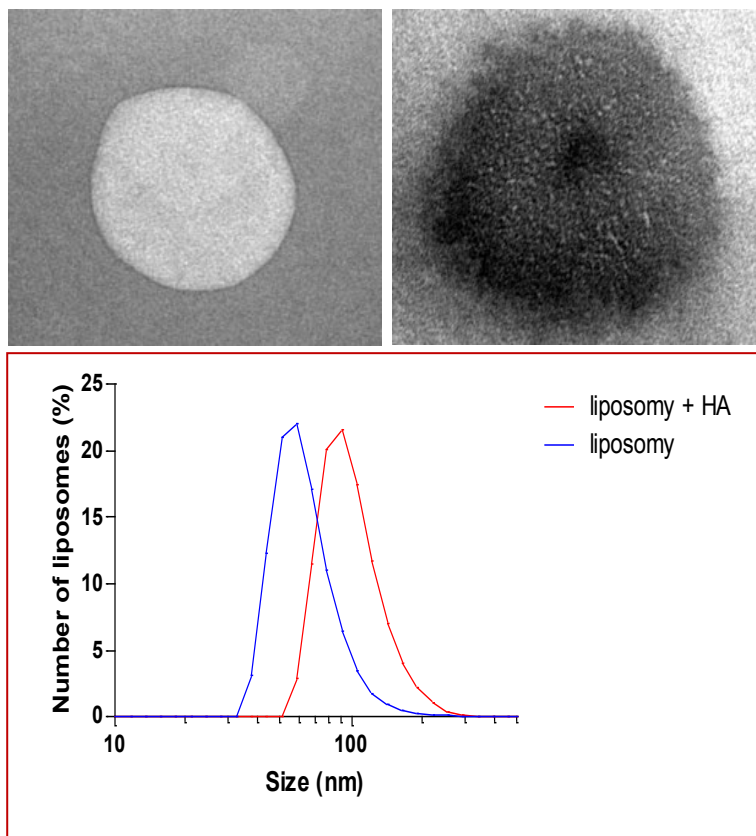


Obr. 16 Schéma cílení antivirotik do cytoplasmy buněk pomocí kationických liposomů. Liposomy umožní dosáhnout dostatečnou koncentraci antivirotika v buňce díky přenosu přes bariéru tvořenou cytoplasmatickou membránou. Tento systém je zejména vhodný pro cílení antivirotik do orgánů jako jsou játra (potenciální aplikace při terapii hepatididy).



Obr. 17 Biokonjugační reakce využívající lipidů s aminoxy skupinou pro selektivní vazbu ligandů nesoucích aldehydickou skupinu

Schéma naznačuje chemickou reakci, která vede k navázání polysacharidu na povrch liposomu s lipidy nesoucími aminoxy skupinu.



Obr. 18 Liposom v TEM

Transmisní elektronová mikroskopie ukazuje liposom (pravý obrázek) a liposom s navázanou kyselinou hyaluronovou (levý obrázek). Spodní graf ukazuje distribuce velikosti liposomů a liposomů s navázanou kyselinou hyaluronovou (HA) pomocí dynamického rozptylu světla.

2.1.1. Podané patentové přihlášky k tématu kapitoly

- Drašar, L., Ledvina, M., Korvasová, Z., Turánek, J. Lipopolyaminy sperminového typu pro konstrukci liposomálních transfekčních systémů. PV 2012-20; 303963 (2012)
- Ledvina, M., Drašar, L., Turánek, J., Korvasová, Z. Lipopolyamines of spermine type for construction of liposomal transfection systems. PCT/CZ2013/000004; EP2802556 A1 (2014)

2.1.2. Publikace k tématu kapitoly



Antiviral effect of HPMP (Cidofovir®), entrapped in cationic liposomes: *In vitro* study on MDBK cell and BHV-1 virus

Zina Korvasová^{a,1}, Lukáš Drašar^{b,1}, Josef Mašek^a, Pavlína Turánek Knotigová^a, Pavel Kulich^a, Ján Matiašovic^a, Kamil Kovařík^a, Eliška Bartheldyová^a, Štěpán Koudelka^a, Michaela Škrabalová^a, Andrew D. Miller^d, Antonín Holý^c, Miroslav Ledvina^{c,*}, Jaroslav Turánek^{a,*}

^a Veterinary Research Institute, Department of Toxicology, Pharmacology and Immunotherapy, Brno, Czech Republic

^b Institute of Chemical Technology, Department of Chemistry of Natural Compounds, Prague, Czech Republic

^c Institute of Organic Chemistry and Biochemistry, Czech Academy of Sciences, Prague, Czech Republic

^d Imperial College London, Imperial College Genetic Therapies Centre, Department of Chemistry, London, UK; King's College London, Institute of Pharmaceutical Science, London

ARTICLE INFO

Article history:

Received 7 September 2011

Accepted 27 January 2012

Available online 2 February 2012

Keywords:

Cationic lipids

BHV-1 virus

Cidofovir

HPMP

Antiviral drugs

ABSTRACT

We designed and synthesised a series of new cationic lipids based on spermine linked to various hydrophobic anchors. These lipids could be potentially useful for the preparation of stable cationic liposomes intended for the construction of drug targeting systems applicable in the field of anticancer/antiviral therapy, vaccine carriers, and vectors for the gene therapy. Low *in vitro* toxicity was found for these compounds, especially for LD1, in several cell lines. The delivery of both a fluorescence marker (calcein) and antiviral drugs into cells has been achieved owing to a large extent of internalization of cationic liposomes (labelled by Lyssamine-Rhodamine PE or fluorescein-PE) as demonstrated by fluorescent microscopy and quantified by flow cytometry. The bovine herpes virus type 1 (BHV-1) virus infection *in vitro* model using MDBK cells was employed to study the effect of the established antiviral drug HPMP (Cidofovir®) developed by Prof. A. Holý. Inhibition of BHV-1 virus replication was studied by quantitative RT-PCR and confirmed by both Hoffman modulation contrast microscopy and transmission electron microscopy. We found that *in vitro* antiviral activity of HPMP was significantly improved by formulation in cationic liposomes, which decreased the viral replication by about 2 orders of magnitude.

© 2012 Elsevier B.V. All rights reserved.

1. Introduction

Cidofovir ((S)-1-(3-hydroxy-2-phosphonylmethoxypropyl)-cytosine abbreviated as HPMP) represents a new class of broad-spectrum antiviral agents that are active against a broad range of herpes viruses and exhibit rather slow cellular kinetics; particularly noteworthy is that the active metabolites are retained intracellularly for a very long time. Cidofovir targets viral DNA polymerase and prevents transcription. Because the viral polymerase is 8 to 600 times more sensitive than human DNA alpha, beta, and gamma polymerases, the active ingredient, Cidofovir diphosphate, is able to specifically target viral replication processes. A notable feature of HPMP is that it confers a long lasting antiviral activity both *in vitro* and *in vivo*. A single application of HPMP after virus adsorption can establish an antiviral effect that can last 7 days in a cell culture or animal

models. This long-lasting antiviral effect of HPMP has been attributed to the persistence of its active intracellular derivatives [1].

The cell membrane represents a main barrier for the entry of negatively charged drugs based on nucleotides, oligonucleotides as well as various DNA constructs for gene therapy. Neutral or lipophilic prodrugs were synthesised to improve intracellular delivery but new problems arose regarding their low solubility [2]. The intracellular activity of certain antiviral agents, including antisense oligonucleotides, acyclic nucleoside phosphonates, and protease inhibitors, is enhanced when they are delivered in liposome-encapsulated form [3]. We have designed and synthesised new cationic lipids useful for the preparation of stable liposomes. Low *in vitro* toxicity was found for several cell lines and high intracellular localisation of cationic liposomes labelled by lyssamine-rhodamine phosphatidyl ethanolamine (LysRhod-PE) or fluorescein phosphatidyl ethanolamine (F-PE) was observed by fluorescent microscopy and quantified by flow cytometry.

The *in vitro* model of bovine herpes virus (BHV-1) infection of MDBK cells was used to study the effect of the established antiviral drug Cidofovir® (HPMP) developed by Prof. A. Holý. BHV-1 (strain M218) (an important pathogen of cattle, which causes a variety of respiratory and genital tract infections such as infectious rhinotracheitis (IBR)) is a useful model for *in vitro* testing because it is not

* Correspondence to: J. Turánek, Veterinary Research Institute, Hudcova 70, 621 32 Brno, Czech Republic. Tel.: +420 5 3333 1311; fax: +420 5 4121 1229.

E-mail addresses: ledvina@uochb.cas.cz (M. Ledvina), turanek@vri.cz (J. Turánek).

¹ Contribution of the two first authors was equal.

transmittable to human [4]. Inhibition of BHV-1 virus replication was studied by quantitative RT-PCR and confirmed by transmission electron microscopy (TEM) and optical microscopy. We found that *in vitro* antiviral activity of HPMPC was significantly improved by formulation in cationic liposomes, which increased the inhibition of viral replication *in vitro* by about 2 orders of magnitude.

2. Materials and methods

2.1. HPMPC

[(S)-1-(3-hydroxy-2-phosphorylmethoxypropyl)-cytosine] (Cidofovir® Vistide® (Fig. 1A) is an antiviral drug which is an inhibitor of viral DNA polymerase. The compound was synthesised as described by Holy et al. [5] [(R)-1-(3-hydroxy-2-phosphorylmethoxypropyl)-cytosine, the inactive optical isomer, was used as a negative control.

2.2. Cationic lipids

The syntheses of the target lipopolyamines of the spermine type (Fig. 1, Structures LD1, LD2, LD3, and LD4) were based on the condensation of N^2,N^3,N^4 -tris-(*tert*-butoxycarbonyl)-spermine with pentafluorophenyl ester of carboxy-terminated hydrophobic structure and subsequent splitting off the *tert*-butoxycarbonyl protecting groups. The syntheses of the target lipopolyamines and analytical data which confirm the structure of the prepared compounds are given in Supplementary material (S1).

2.3. Liposome preparation and characterization

Cationic liposomes were prepared by lipid film hydration technique and extrusion through polycarbonate filters 0.1 μm . EPC and a specific LD cationic lipid and antiviral drug HPMPC (acidic form) in the molar ratio of 4:1:1 were dissolved in chloroform. The solution

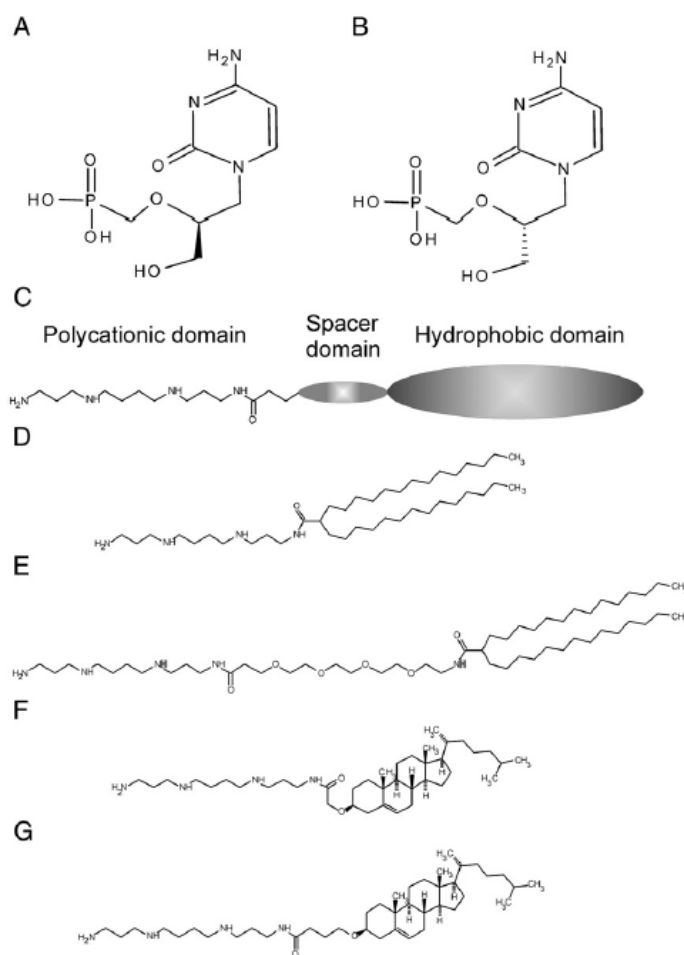


Fig. 1. Structural formula of antiviral drug HPMPC and cationic lipids. A) (S)-1-(3-hydroxy-2-phosphorylmethoxypropyl)-cytosine (active optical isomer) Cidofovir®. B) (R)-1-(3-hydroxy-2-phosphorylmethoxypropyl)-cytosine (inactive optical isomer). C) General formula of cationic lipids. D) LD1 N^2 -(2-Tetradecylhexadecanoyl)-1,12-diamino-4,9-diazadodecane. E) LD2 N^1 -[N-(2-Tetradecylhexadecanoyl)-15-amino-4,7,10,13-tetraoxapentadecanoyl]-1,12-diamino-4,9-diazadodecane. F) LD3 N^1 -(Cholest-5-en-3 β -yloxyacetyl)-1,12-diamino-4,9-diazadodecane. G) LD4 N^1 -[4-(Cholest-5-en-3 β -yloxy)butanoyl]-1,12-diamino-4,9-diazadodecane.

was dried to form a film in a round bottomed flask under reduced pressure at 40 °C in a rotary evaporator. Phosphate buffered saline was added to the film to get the final concentration of 20 mg/ml. Then the liposomes were frozen–thawed four times and extruded through polycarbonate filters 200 nm. Free non-entrapped antiviral drug was separated by 24-h dialysis.

Fluorescence-labelled liposomes were prepared by the same procedure as described above. The composition of lipids was as follows: fluorescent lipid N-lissamine Rhodamine B sulfonyl PE (0.1 mol% of total lipid) was dissolved in chloroform together with EPC and cationic lipids LD (molar ratio EPC:LD of 4:1). The lipid film was prepared and hydrated by phosphate buffered saline with 100 μ M calcein, the liposome morphology was modified by freezing–thawing and extrusion processes. The final concentration of the lipids in the liposomal preparation was 20 mg/ml. Non-entrapped fluorescence marker calcein was separated by dialysis carried out overnight in a refrigerator.

The size distribution and zeta potential of the liposomes were measured using photon correlation spectroscopy (Nanosizer ZS, Malvern).

2.4. In vitro cytotoxicity

MTT (Sigma) was used as an indicator of cell viability as determined by its mitochondria-dependent reduction to formazan. We used 4 kinds of cell cultures; each of them was plated at a density of 2.5×10^5 cells/ml in 96-well plates for 24 h and subsequently exposed to the tested compounds. Cationic lipids LD1, LD2, LD3, and LD4 were tested at the concentration range of 0.4–100 μ M, exposure time was 24 h. The volume of 20 μ l of MTT ($2.5 \text{ g} \cdot \text{l}^{-1}$) was added to each well and the plates were incubated for 3 h at 37 °C. The formed blue-formazan reaction product was dissolved in 110 μ l of 10% SDS. The absorbance of the formazan solution was measured at 540 nm using a reader Synergy II (BioTek, USA).

2.5. Characterization of liposomes and efficiency of encapsulation

The concentration of the entrapped HPMPc was determined by spectrophotometric assay after lysis of the dialysed liposomes with 20 mM cholic acid. The UV absorbance of the sample solution was measured at 272 nm (the extinction coefficient $\epsilon = 9,000$ at pH = 7.0) [6].

2.6. Tissue culture

Madin-Darby bovine kidney (MDBK) cells were grown in Eagle's minimal essential medium (EMEM) supplemented with antibiotics, fungizone, and 10% fetal calf serum (FCS). The serum concentration was reduced to 2% for the growth of the virus and for the antiviral tests. The cells were cultured at 37 °C in a humidified atmosphere containing 5% CO₂.

MDBK cell culture was carried out in Dulbecco's modified Eagle's medium (D-MEM) to which bicarbonate buffer and antibiotic had been added and which was supplemented with fetal calf serum as appropriate. The cell culture was maintained at 37 °C in a humidified incubator with an atmosphere of air plus 5% CO₂.

2.7. Virus strain

BHV-1 isolates (LA-2, V 132, V 19, M218) were tested for sensitivity towards the antiviral drug HPMPc. The isolate M218 [7,8] was evaluated as the most suitable for in vitro studies with respect to HPMPc concentration-dependent sensitivity and hence this strain was used throughout this study. Virus working stock was prepared by infecting a monolayer of MDBK cells at low multiplicity of infection. The working stock, passage 5, had an infectivity of 1×10^9 plaque-forming units/ml. They were stored at –70 °C in aliquots until used.

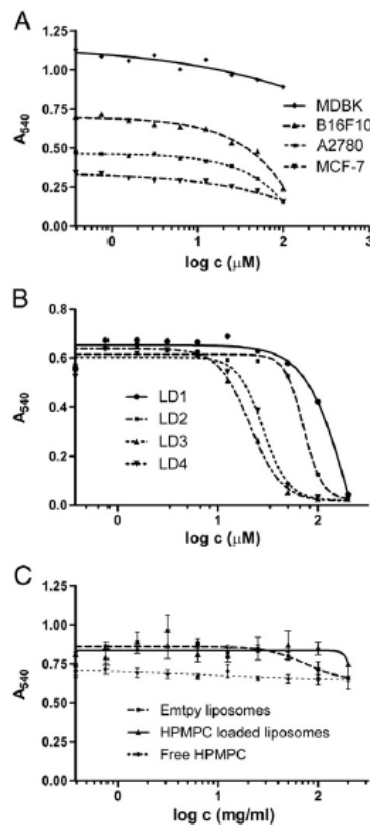


Fig. 2. Cytotoxicity of cationic lipids and liposomes *in vitro*. A) cytotoxic effect of cationic lipid LD1 on various cell lines. B) cytotoxic effect of cationic lipids on MDBK cell line. C) comparison of cytotoxicity of plain and HPMPc-loaded cationic liposomes (EPC:LD1 80:20 mol%) towards MDBK cell line.

2.8. Flow cytometry

After the microscopical evaluation, the cell culture was further analyzed by flow cytometry. The cells were incubated with fluorescent liposomes (calcein and LysRhod-PE) for 1, 3, and 6 h. The samples were then measured on BD FACS Array equipped with an argon-ion laser at 488 nm and 532 nm.

2.9. Antiviral activity of various formulations of HPMPc

MDBK cell culture was incubated for 6 h with liposomal or free HPMPc (50 μ M, 25 μ M, 12.5 μ M in well). Then medium was changed in the wells and 20 μ l of BHV-1 virus preparation (the titre ranged from 10^{-3} to 10^{-9} plaque-forming units) was added to the wells. For each liposome concentration, triplicate for each dilution of virus was prepared. Cells were incubated with BHV-1 strain for 40 h. Then a microscopic analysis and RT-PCR quantification were carried out.

2.10. Quantitative real time PCR (QRT-PCR)

The concentration of viral DNA in samples was quantified by QRT-PCR. A method was established for the measurement of BHV-1 DNA concentration in culture supernatants. This assay was shown to be highly specific and reproducible. The assay was then applied to the

measurement of the reduction of BHV-1 DNA levels in the presence of increasing concentrations of Cidofovir® (HPMPC) and decreasing titre of BHV-1 virus. For more details see Supplementary material (S2).

3. Results

3.1. Cationic lipids

3.1.1. *In vitro* cytotoxicity

Cytotoxicity of new cationic lipids was tested on MDBK cells (which were used in *in vitro* viral model) and on several cancer cell lines. The lowest cytotoxicity was demonstrated by the compound LD1 ($IC_{50} > 100 \mu\text{M}$) (Fig. 2B). Thus, this compound was selected for further *in vitro* studies. The relatively low cytotoxicity of this compound was confirmed also on other cell lines (Fig. 2A). Both cationic lipids with a B30 hydrophobic tail (LD1 and LD2) exerted lower cytotoxicity than those cationic lipids with cholesteryl hydrophobic tail. Neither plain cationic liposomes nor free or liposomal HPMPC exerted cytotoxic effect in the tested range of concentration (Fig. 2C).

3.2. Physico-chemical characterization of liposomes

The lipid film hydration method followed by extrusion through $0.1 \mu\text{m}$ polycarbonate filters produced monodisperse liposomes as demonstrated by TEM (Fig. 3A). The size of the liposomes composed of 0–20% of LD1 was around 80–90 nm and $PDI \approx 0.12$. The increase of the LD1 content (to 30%) significantly influenced the size of the liposomes. These liposomes were smaller in size (55–60 nm; $PDI \approx 0.1$) (Fig. 3B).

Zeta-potential of the liposomes increased with an increased content of cationic lipid LD1, as expected (Fig. 3C). The values of zeta-potential for 20 and 30% of LD1 were high enough to prevent any aggregation of the liposomes when stored in refrigerator. The similar

course of zeta-potential versus a content of cationic lipid was obtained for all the tested cationic liposomes (results not shown).

MTT test was used to measure the *in vitro* toxicity as described in the section Material and Methods.

Due to the strong positive charge of spermine and negative charge of HPMPC we expected a positive effect of the electrostatic interaction on the encapsulation efficacy of cationic liposomes. Indeed, the encapsulation efficacy increased significantly with an increase of LD1 content in the liposomes (Fig. 3D). In comparison to plain EPC liposomes (zeta-potential of 6 mV), the liposomes with 20 and 30% of LD1 demonstrated an increase in the encapsulation efficacy 2.5 and 3 times, respectively. This enormous improvement is indicative of a strong effect of electrostatic forces on the encapsulation efficacy.

3.3. Interaction of cationic liposomes with MDBK cells

Cationic liposomes composed of both commercial (e.g., DoDab, DC cholesterol – results not shown) and our LD cationic lipids interacted strongly with MDBK cells and were internalized more intensively in comparison with EPC liposomes. This was demonstrated both by flow cytometry and fluorescence microscopy (Fig. 4A and B inset). The incorporation of cationic liposomes reached its maximum after about 6 h (Fig. 4B). The course of the concentration of the internalized cationic liposomes revealed saturation kinetics, too with a limit of about 10–25 $\mu\text{g}/\text{ml}$ (total lipid) (Fig. 4C). The incorporation of cationic liposomes was rapid and effective even if low concentration of liposomes (1 $\mu\text{g}/\text{ml}$; 1 h of incubation) was used. Around 85% of cells were found positive for the cationic liposomes labelled by Lys-Rhod PE after 1 h of exposure. At higher concentrations, more than 97% of cells were found positive (Fig. 4D). DoDab and DC-cholesterol liposomes (cationic liposome concentration of 1 $\mu\text{g}/\text{ml}$) resulted only in 5 and 26% of positive cells, respectively, after 1 h of incubation (results not shown).

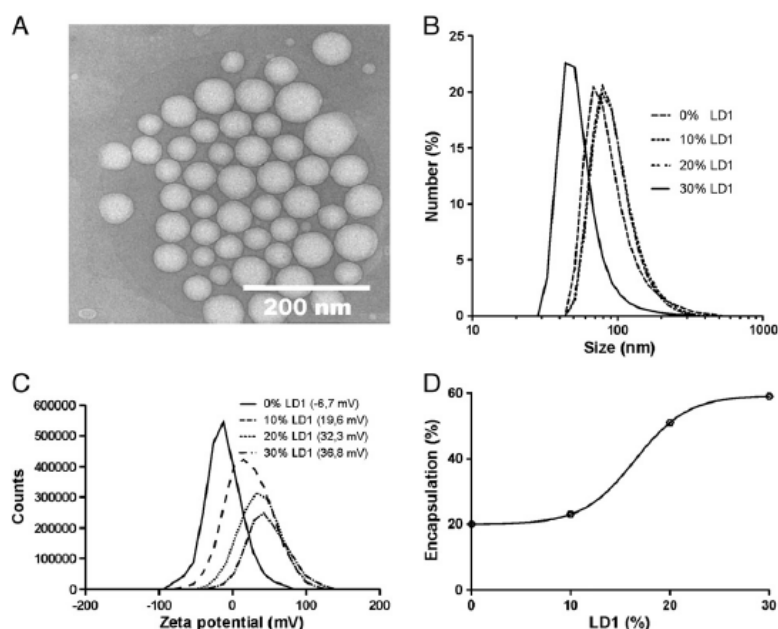


Fig. 3. Physico-chemical characterization of cationic liposomes. A) TEM of cationic liposomes composed of 20% LD1. B) Size distribution of liposomes composed of EPC and 0; 10; 20 and 30 mol% of LD1 (Dynamic light scattering). C) Distribution of zeta-potential of liposomes composed of EPC and 0; 10; 20 and 30 mol% of LD1 (microelectrophoresis and Doppler velocimetry). D) Effect of positive surface charge on encapsulation efficacy of HPMPC (liposome composition: EPC and 0; 10; 20 and 30 mol% of LD1).

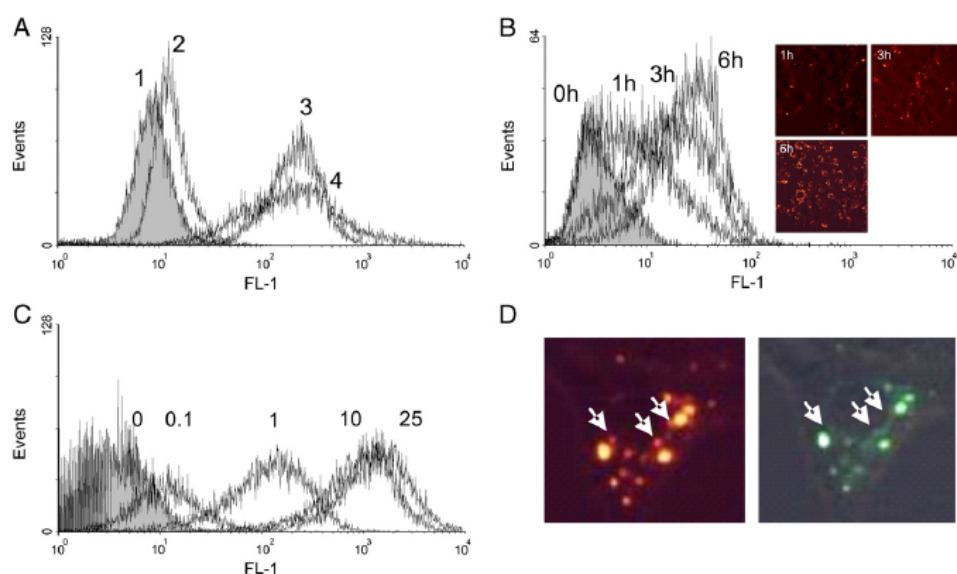


Fig. 4. Interaction of cationic liposomes with MDBK cells as determined by fluorescence microscopy and flow cytometry. Liposomes labelled by F-PE or LysRhod PE and composed of particular LD lipids (20%, 16 $\mu\text{g}/\text{ml}$) were incubated for 6 h with MDBK cells and the internalization was measured by flow cytometry. Neutral noncationic liposomes prepared of EPC served as a control (2 – neutral EPC liposomes). A) Effect of particular cationic lipids on the internalization of cationic liposomes into MDBK cells as determined by flow cytometry. Liposomes were marked by F-PE (exposure time 6 h). 1 – control MDBK cells; 2 – neutral EPC liposomes; 3 – LD1 cationic liposomes; 4 – LD3 cationic liposomes. Data on LD2 and LD4 are similar to those of LD1 and LD3, respectively. Therefore, they were omitted to keep a clarity of the graph. B) Effect of exposure time on the internalization of LD1 cationic liposomes into MDBK cells as determined by flow cytometry. Exposure time 1, 3, and 6 h. (liposomes marked by F-PE). Inset: fluorescence microscopy pictures of MDBK cells with the internalized liposomes. Pictures were taken at 1, 3, and 6 h of exposition. C) Effect of the concentration of LD1 cationic liposomes (total lipid 0.1, 1.0, 10.0, and 25.0 μM) on the internalization of the cationic liposomes in MDBK cells as determined by flow cytometry. LysRhod-PE-labelled cationic liposomes were used in this experiment. D) Localisation of LysRhod-PE-labelled cationic liposomes (red) with encapsulated hydrophilic fluorescence marker calcein (green) in MDBK cells (cationic liposomes composed of 20% LD and 80% EPC). The internalization of fluorescence-labelled liposomes (red) into MDBK cells and a release of calcein into cytoplasm are evident. The liposomes which released their calcein content into cytoplasm are marked by arrows.

3.4. The intracellular localisation of liposomes

Liposomes double stained with LysRhod-PE (lipid marker) and calcein (anionic soluble marker of the liposome interior) were used to study the fate of liposomes in MDBK cells. The liposomes were found accumulated in cytoplasm. Individual liposomes as well as large fluorescence structures were observed. Co-localization of red and green fluorescence showed that the liposomes were stable enough to preserve their content during incubation in medium and were able to deliver it into cells. After 3 h of incubation, some liposomes in cytoplasm released their content (fluorescent marker calcein) into cytoplasm, as demonstrated by a disappearance of green fluorescence of the liposomal content while red fluorescence of a liposomal membrane was observed. Slight green fluorescence of cytoplasm stained with the released calcein was observed as well (Fig. 4D).

3.5. In vitro effect of free and liposomal HPMPc on suppression of viral replication

3.5.1. Cytopathic effect

The antiviral effect of free and liposomal HPMPc was evaluated by microscopy. Both free and liposomal HPMPc produced significant suppression of cytopathic effect induced by BHV-1 virus in MDBK cell monolayer (Fig. 5). Compared to control cells (Fig. 5A), where all the untreated cells infected with BHV-1 virus were in a late stage of apoptosis and the monolayer was destroyed (Fig. 5B), the cells treated with liposomal HPMPc were of normal morphology and their nucleoli were clearly visible in the nucleus (Fig. 5C). The monolayer was preserved almost unimpaired with rare holes in it. Free

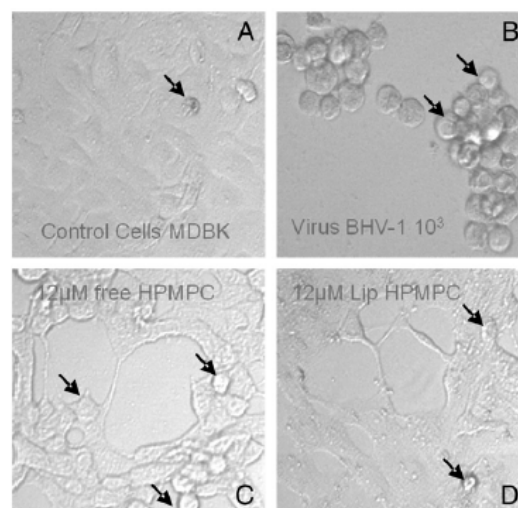


Fig. 5. In vitro effect of free and liposomal HPMPc on cytopathic effect induced by BHV-1 virus in MDBK cells. Cationic liposomes were composed of LD1 (20 mol%). Microscopic evaluation of cytopathic effect of BHV-1 virus on MDBK cells treated with free and liposomal HPMPc was done on T200 Nikon, Hofmann modulation contrast. The virus titre was 10^{-3} PFU, exposure time was 40 h (cells in various stages of apoptosis are marked by arrows). A) control untreated MDBK cells. B) infected cells without treatment. C) infected cells treated with free HPMPc (12 μM). D) infected cells treated with liposomal HPMPc (12 μM).

HPMPC at the same concentration prevented a strong damage of the cell monolayer as well. However, many cells were found to be in a preapoptotic stage (initiation of de-adherence and detachment accompanied by initiation of slight swelling of cells in monolayer) (Fig. 5D).

3.6. Quantification of viral replication by quantitative real time PCR (QRT-PCR)

In the first experiment we compared the antiviral activity of free forms of (R) HPMPC (inactive optical isomer) and (S) HPMPC (active optical isomer) up to the concentration of 50 μM . As expected, the R form did not suppress the viral replication at all and the (S) form suppressed the viral replication in the range of one order of magnitude. The antiviral activity of the R form was not observed even if HPMPC was encapsulated in the liposomes (results not shown).

In the second experiment we tested the effect of the content of cationic lipid on the antiviral effect of liposomal HPMPC. The optimal content of cationic LD1 lipid was around 20% (i.e., 80% EPC and 20% cationic lipid) and these liposomes demonstrated the highest inhibition effect (Fig. 6A). HPMPC encapsulated in neutral EPC liposomes was not very potent and this data were in accordance with the flow cytometry data on the internalization of these liposomes in MDBK cells (Fig. 4A). Other cationic lipids (LD2, 3, and 4) demonstrated a pattern similar to that presented in Fig. 6A for LD1 (data not shown).

In vitro antiviral effect of the optimal liposomal formulation of HPMPC (20% LD1 and 80% EPC) was compared with that of free HPMPC, plain cationic liposomes, and infected control cells. A broad range of virus titre was used for the infection of MDBK cells. In comparison to the control, plain liposomes demonstrated a slight antiviral effect only at the lowest virus titre used for the infection. At a lower virus titre used for the infection, liposomal HPMPC was about 100 times more effective than the free drug as regards the inhibition of BHV-1 replication in MDBK cells (Fig. 6B).

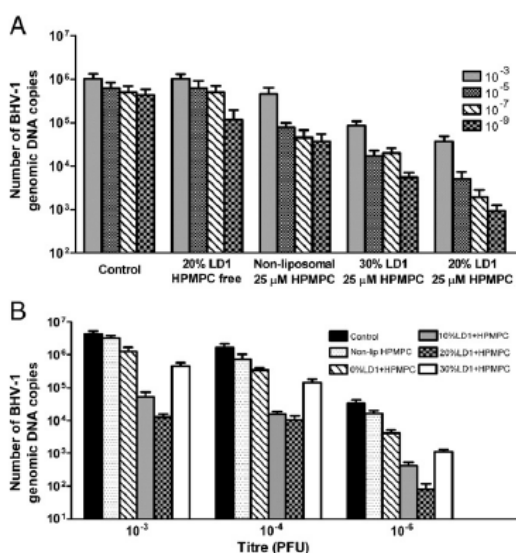


Fig. 6. Inhibition of BHV-1 replication in MDBK cells quantified by QRT-PCR. Representative data from one series of experiments are based on triplicates. A) Effect of liposome composition on the antiviral effect of liposomal HPMPC. LD1 cationic lipid (0, 10, 20, and 30 mol%) was used for the preparation of liposomes. Liposomal and free HPMPC at a concentration of 50 μM , virus titre used for the infection of 10^{-3} , 10^{-4} , and 10^{-5} PFU. B) Comparison of antiviral effect of plain liposomes, free HPMPC, and liposomal HPMPC at a broad range of viral titre (10^{-3} , 10^{-4} , 10^{-5} , 10^{-7} , and 10^{-9} PFU). LD1 lipid (20%) was used for the preparation of cationic liposomes (HPMPC of 25 μM).

3.7. Inhibition of viral replication studied by TEM

Typical signs of BHV-1 infection of MDBK cells are as follows: a disappearance of nucleoli together with chromatin, a massive accumulation of immature 120–550 intranuclear regular viral capsids in inclusion bodies (viral capsids are arranged in paracrystalline arrays) a presence of maturing particles in cytoplasmic vacuoles and, finally, a release of mature viruses with DNA in capsids into extracellular matrix.

This is clearly documented in Fig. 7A,B,C. The application of HPMPC in the liposomal formulation reduced significantly the number of virions in nucleus. Nucleoli were not destroyed and less than 30 immature viral particles as well as the absence of paracrystalline arrays were observed in nucleus. The maturation of viral particles inside vacuoli was suppressed and defective viral particles were observed both in vacuoli and in extracellular matrix (Fig. 7D,E,F). These observations are in good accordance with the data obtained by a microscopic observation of the cytopathic effect as well as with the quantification of viral replication by QRT-PCR. The effect of free drug on maturation of BHV-1 viruses is documented by TEM in the Supplementary material (S3).

4. Discussion

4.1. Cationic liposomes as drug delivery systems

Selective functional delivery of membrane-impermeable molecules from sites of administration to desired target sites of action in cells of an organ of interest has long been a goal that would improve the therapeutic potential of many drugs. Certain antiviral drugs including antisense oligonucleotides and small interfering RNAs (siRNAs), acyclic nucleoside phosphonates, and protease inhibitors are polar drug agents that act directly on intracellular targets. However, biopharmaceutical agents and membrane-impermeable drugs suffer from a huge limitation. Although undeniably effective at their target site(s) of action in the body, these agents are either inappropriately soluble and/or too unstable to reach a target site of interest in the body without assistance. In short, these drug agents each require a purpose-designed “vector system” that (1) assists such drug agents to overcome solubility problems and/or the biological barriers that stand in their way of reaching target disease sites in the body, and (2) which can also mediate functional delivery and release of these drug agents once target sites were reached. In principle, synthetic nanotechnology products based upon liposomes are ideal vector systems to target drug agents to disease lesions of interest in the body with minimum effective doses and hence minimum (if any) potential drug-related side effects. The combination of drug agents with synthetic nanotechnologies has the capacity to bring about a healthcare revolution focused on thousands of new but currently inaccessible therapeutic targets leading to the creation of highly effective, next-generation, personalized pharmaceutical products.

Liposomes are formed by lipid self-assembly when appropriate amphiphilic lipids are mixed together in an organic solvent at an appropriate molar ratio and then arranged or formulated into uni- or multi-lamellar vesicles each with a single aqueous cavity by any one of a number of methods including reverse-phase evaporation (REV), dehydration-rehydration (DRV), and extrusion [8,9]. Lipid molecular shape is an important determinant of both liposome size and the possibility that micelles are formed in preference to liposomes. Indeed, according to their structure and local environment, lipids encourage a formation of different mesophases. However, the mesophase preferred for a liposome formation is L_{α} -lamellar mesophase. Cationic liposomes represent an important variation formulated with an appropriate molar ratio of a synthetic cationic lipid (cytofectin) that confers a net positive charge on vesicular membranes. Cationic

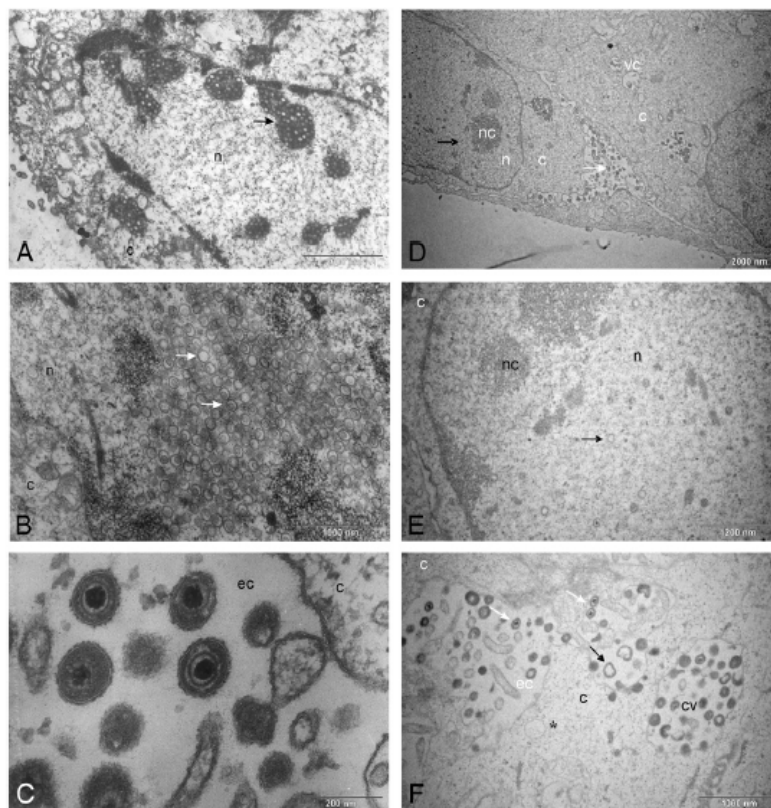


Fig. 7. Replication of BHV-1 viruses in the MDBK cells studied by TEM. Replication of herpes viruses in MDBK cells, which were treated with 50 μ M liposomal HPMPC. Mature herpes viruses occur in the extracellular compartment (EC). Pictures were taken by TEM Philips 208 S Morgagni. A) Large inclusions of BHV-1 virus particles in nucleus of untreated control cells (black arrow), c cytoplasm, n nucleus. B) Detail of an inclusion of BHV-1 virus particles in nucleus. Individual virions marked by white arrows. C) BHV-1 virus particles in extracellular space (ec) (untreated cell culture). D) View of the MDBK cells with defective virus particles inside the nucleus (black arrow) and in extracellular space (white arrow). Nucleoli (nc) are well preserved. The cells were treated with liposomal HPMPC. E) Detail of nucleus (n) with preserved nucleoli (nc). Immature or defective virions are dispersed in nucleus (n) (an immature virion is marked by a black arrow). No inclusions are formed inside nucleus. F) Detail picture of cytoplasmic vacuoli (cv) and extracellular space (ec) with defective virions (black arrow). Sporadic maturing virions (white arrows) are visible in cytoplasm (c), mostly in vacuoles (cv) and in extracellular space (ec). A liposome preserved in cytoplasm is marked by asterisk.

liposomes are capable of complex interactions with large nucleic acids such as plasmid DNA (pDNA) resulting in the formation of lipoplex nanoparticles (LD nanoparticles) that consist of a multilamellar core comprising multiple $L_{\alpha 1}$ fluid mesophase cationic bilayer membranes separated by layers of equispaced DNA helices. This core appears surrounded by a bilamellar liposome-retaining layer. Apparently, lipoplex nanoparticles with the capacity to attain an inverse hexagonal H_{II} mesophase structure are the most efficient at mediating functional delivery of pDNA into cells. Consequently, such lipoplex nanoparticles are generally unstable with respect to colloidal aggregation in biological fluids. Therefore, they have little ability to affect a substantial functional nucleic-acid delivery *in vivo*. However, they certainly have a role *in vitro* and *ex vivo* [8,9]. Smaller nucleic acids such as oligonucleotides may also benefit from cationic liposome-mediated functional delivery to cells *in vitro* or *ex vivo*. Indeed, the potency of an antisense oligonucleotide acting on human endothelial cells *in vitro* can be increased by at least 1000-fold with cationic liposome mediation. This results from the increased cell entry of oligonucleotides and an improved intracellular distribution of the oligonucleotide [10]. So far, only a limited number of studies have reported the encapsulation of a single nucleotide-based antiviral drug. These studies had different goals and showed conflicting data

about antiviral effects. Neutral liposomes with the encapsulated antiviral drug foscarnet were studied in an *in vitro* model and no substantial increase of antiviral activity was found against the cytomegalovirus infection in comparison with the free drug. It could be mainly due to the weak interaction of liposomes with embryonic fibroblasts and low foscarnet content in the liposomes or indeed poor intracellular release characteristics [11]. The goal of our work here was to determine whether the entrapment of the antiviral nucleotide drug Cidofovir® - HPMPC into cationic liposomes could improve its antiviral properties *in vitro*. New cationic lipids (CZ national patent applied 2012) were designed and synthesised to decrease cytotoxicity and improve stability of the negatively charged nucleotide-based antiviral drugs. Our design principles were based upon the need to develop cationic lipids that tend to form $L_{\alpha 1}$ fluid mesophase cationic bilayer in the expectation that such systems should retain liposome integrity and entrap Cidofovir® - HPMPC nucleotide (within the central aqueous cavity of each cationic liposome) without resulting in uncontrolled aggregation that might blunt the efficiency of cationic liposome-mediated delivery of nucleotides to cells. Therefore, the preferred hydrophobic lipid moieties were a branched B30 fatty acid giving rise to the cationic lipids LD1 and LD2 (Fig. 1) or cholesterol thereby giving rise to cationic lipids LD3 and LD4 (Fig. 1). These

cationic lipids were then formulated with EPC as a co-lipid. EPC tends to form $L_{\alpha 1}$ fluid mesophase bilayer like the hydrophobic lipid moieties of the LD cationic lipid series owing to a cylindrical molecular shape. In contrast, since successful functional delivery of larger nucleic acids such as pDNA requires cationic liposomes to interact with the nucleic acids to form lipoplex nanoparticles, the cationic liposome lipid composition in this case should allow for more structural plasticity and mesophase interconversion. Hence, dioleoyl L- α -phosphatidylethanolamine (DOPE) that is known to favour inverse hexagonal H_{II} mesophase structures owing to its inverse conical molecular shape is frequently used as a co-lipid. In support of these design principles, we have observed in preliminary experiments that cationic liposomes prepared of commercially available lipids (*N*-[1-(2,3-dioleoyloxy)propyl]-*N,N,N*-trimethyl ammonium chloride [DOTMA], 1,2-dioleoyloxy-3-(trimethylammonio)propane [DOTAP] as well as 3- β -[*N,N,N*-dimethyl-aminoethane] carbamoyl]cholesterol [DC-Chol]) were not as effective mediators of Cidofovir® delivery to cells as LD1-containing cationic liposomes (more than one order of magnitude lower *in vitro* antiviral effect). On the other hand, cationic liposomes comprising LD1 or LD2 formulated with DOPE did not enable a high effective transfection of cells with pDNA (coding green fluorescent protein [GFP]) as well as cationic liposomes prepared with DOTMA, DOTAP or DC-Chol (results not shown).

4.2. Toxicity of cationic liposomes

A general issue with the application of cationic liposomes, both *in vitro* and *in vivo*, is their potential for toxicity and cytotoxicity. Cationic lipids used for the gene therapy are composed of three basic domains: a positively charged head group, a hydrophobic chain, and a linker that joins the polar and non-polar regions. The polar and hydrophobic domains of cationic lipids may dramatically affect both transfection and toxicity levels [12]. Indeed, the cytotoxicity of some commercially available lipids is a major hurdle in their application *in vivo* [13]. This toxicity has been attributed to their unnatural, non-biodegradable nature. The amphiphile incorporation in cell membranes produces pores and disrupts signalling by inhibition of protein kinase C, too [14]. Generally, the disruption of membranes and production of reactive oxygen species (ROS) are supposed to be responsible for the cationic-lipid mediated toxicity. In this case, mitochondria seem to be the most sensitive organelles. The need to minimize the toxicity of the lipids has constituted a priority for this field of research. The use of biodegradable lipids is one of the suggested approaches. Hence, LD1 could be a prototype of fully biodegradable cationic lipid which does not destabilise biological membranes.

4.3. *In vitro* antiviral effect of liposomal Cidofovir

Considering that more than 1000 capsids may be produced within a single nucleus, the amount of the nuclear membrane required for budding of virus is enormous. Cells infected with BHV-1 disintegrate in the course of virus multiplication, which is reflected by the morphological changes in the cell monolayer that is diagnostic for a cytopathic effect. The rapidity of the cell disintegration suggests dramatic distortions within the nucleus and/or at the nuclear envelope. Although the integrity of membranous compartments was lost to various extents in cells shown to be intact or healthy by light microscopy, intact plasma membranes and fragmented nuclei or nuclei with peripheral chromatin condensation, capsids, and membranous inclusions could be seen.

Herpes simplex viruses (HSVs) comprise the capsid containing the viral genome, the viral envelope consisting of a lipid bilayer with embedded glycoproteins, and tegument proteins filling the space between the capsid and the envelope. DNA double strands formed during replication are packed into capsids built of proteins imported from the cytoplasm. The capsids are transported to the nuclear periphery. Their pathway through the nucleocytoplasmic barrier and

the acquisition of tegument and envelope are yet not fully understood [15–17]. We are delighted with the observed effects of cationic liposome mediation on Cidofovir® - HPMPC antiviral effects in MDBK cells. There appears to be a substantial reduction in numbers of observed viral capsids in the nucleus. In addition, the synthesis of viral DNA plus its incorporation into capsids is prevented owing to the inhibition of viral DNA polymerase. Taking into account the strong reduction of the number of capsids in cell nuclei, there may be a positive regulation loop between viral DNA synthesis and proteo-synthesis of capsid proteins. Considering the slight inhibition of virus DNA synthesis/replication observed at the low virus titres used for *in vitro* infection (Fig. 6), the cationic lipid may also interfere with some part of virus assembly pathway.

4.4. Possible applications of liposomal Cidofovir

Very recently, Coremans described an effective treatment of anogenital condylomata acuminata in human patients by Cidofovir® - HPMPC. Complete or partial responses were observed in 65% of patients ($n = 46$). Still, dose-related mild to moderate application-site reactions were seen in 39% of patients, although no systemic toxicities were noted [18]. Topical applications of Cidofovir® - HPMPC in a suitable formulation could improve the treatment of viral diseases affecting mucosa and with much reduced side effects. There are only few studies concerned with liposomal Cidofovir. There is an example describing the application of liposomal Cidofovir for the treatment of viral retinitis. Remarkable prolonged anti-viral effects were observed in a rabbit model of HSV-1 retinitis. One intravitreal injection (100 μ g) of liposomal Cidofovir appears to have a remarkably potent and prolonged antiviral effect (up to 4 months) in this experimental model. Since Cidofovir® - HPMPC is even more potent against cytomegalovirus than HSV-1, liposomal Cidofovir may prove to be a more effective local therapy for AIDS patients with cytomegalovirus retinitis [19].

Recently, antineoplastic activity of Cidofovir encapsulated in cationic liposomes against primary effusion lymphoma (PEL), a B-cell neoplasm associated with human herpes virus-8 (HHV-8) infection was demonstrated. This *in vitro* study suggests that liposomal delivery allows a release of HPMPC into BCL-1 cells enabling an unexpected antineoplastic activity of this drug even at lower doses [20].

However, our next steps will be to consider how to develop Cidofovir® - HPMPC for the treatment of hepatitis B virus (HBV) infections *in vivo*. As regards this task, we hope to learn from the experience of the team of Miller who succeeded to design a lipid-based, pH-triggered, PEGylated siRNA-nanoparticle system for the functional delivery of chemically unmodified, anti-HBV siRNA constructs to liver hepatocytes *in vivo* [21]. Nanoparticles of uniform small sizes of 80–100 nm in diameter were prepared and administered to HBV transgenic mice resulting in the suppression of HBV infection markers by up to 3-fold relative to controls over a 28-day period. We anticipate that this system could be adapted with cationic lipids LD1 and/or LD2 for the *in vivo* delivery of Cidofovir® - HPMPC intended for the treatment of HBV infection in liver. We are currently working towards this objective.

5. Conclusion

New cationic lipids based on spermine could be potentially useful for the preparation of stable cationic liposomes intended for the construction of drug targeting systems applicable in the field of anticancer/antiviral therapy, genetic vaccines and gene therapy. Cationic lipid formulation of antiviral drugs could be developed for both local and systemic application. This liposomal system enables also co-encapsulation of siRNA-based antiviral drugs to enhance the *in vivo* antiviral effect. The concept was proved in BHV-1 virus infection *in vitro* model by the application of an established antiviral drug

HPMPC (Cidofovir®). The preparation of liposomes with co-entrapped siRNA and Cidofovir is in progress as well as studies on both local and systemic application of this delivery system for the gene therapy and chemotherapy of viral infections and cancer.

Supplementary materials related to this article can be found online at doi: 10.1016/j.jconrel.2012.01.040.

Acknowledgements

This work was supported by following grants: GAČR P304/10/1951 to J.T. and M.L.; Grant No. MZE 0002716202 to J.T., grants from the Academy of Sciences of the Czech Republic (projects KAN200520703 and 32-KAN200100801) to J.T. and M.L. Authors thank to MVDr. Bedřich Šmíd, CSc., for the valuable consultations on TEM results.

References

- [1] E. De Clercq, The therapeutic potential of HPMPC as an antiviral drug, *Rev. Med. Virol.* 3 (1993) 85–96.
- [2] S. Vrbkova, M. Dracinsky, A. Holy, Synthesis of phosphonomethoxyethyl or 1,3-bis(phosphonomethoxy)propan-2-yl lipophilic esters of acyclic nucleoside phosphonates, *Tetrahedron* 63 (2007) 11391–11398.
- [3] N. Duzgunes, S. Simoes, V. Slepishkin, E. Pretzer, D. Flasher, I.J. Salem, G. Steffan, K. Konopka, M.C. Pedrosa deLima, Delivery of Antiviral Agents in Liposomes, in: N. Duzgunes (Ed.), *Methods in Enzymology: Liposomes*, Part E, Vol. 391, Elsevier/Academic Press, San Diego, 2005, pp. 351–373.
- [4] L. Turin, S. Russo, G. Poli, BHV-1: New molecular approaches to control a common and widespread infection, *Mol. Med.* 5 (1999) 261–284.
- [5] A. Holy, I. Rosenberg, H. Dvorakova, Acyclic nucleotide analogs – Synthesis of (3-hydroxy-2-phosphonylmethoxypropyl) derivatives of heterocyclic bases, *Collect. Czechoslov. Chem. Commun.* 54 (1989) 2470–2501.
- [6] M. Serpi, I.S. Krylov, V.M. Zakharova, C.E. McKenna, Synthesis of Peptidomimetic Conjugates of Cyclic Nucleoside Phosphonates, *Curr. Protoc. Nucleic Acid Chem.* 43 (2010) 15.4.1–15.4.13.
- [7] F.G. Burleson, T.M. Chambers, D.L. Wiedbrauk, *Virology: a Laboratory Manual*, Academic Press, Inc., San Diego, 1992.
- [8] K. Kostarelos, A.D. Miller, Synthetic, self-assembly ABCD nanoparticles; a structural paradigm for viable synthetic non-viral vectors, *Chem. Soc. Rev.* 34 (2005) 970–994.
- [9] A.D. Miller, Towards safe nanoparticle technologies for nucleic acid therapeutics, *Tumori* 94 (2008) 234–245.
- [10] C.F. Bennett, M.Y. Chiang, H.D. Chan, J.E. Shoemaker, C.K. Mirabelli, Cationic lipids enhance cellular uptake and activity of phosphorothioate antisense oligonucleotides, *Mol. Pharmacol.* 41 (1992) 1023–1033.
- [11] J.J. Bergers, R.U. Henggeb, S.V. Snijders, L.A.J.M. Bakker-Woudenberg, Inhibition of cytomegalovirus late antigen expression and cytomegalovirus replication in human fibroblasts and differentiated monocytic cells by liposome-encapsulated foscarnet, *J. Control. Release* 47 (1997) 163–171.
- [12] H. Lv, S. Zhang, B. Wang, S. Cui, J. Yan, Toxicity of cationic lipids and cationic polymers in gene delivery, *J. Control. Release* 114 (2006) 100–109.
- [13] A. El-Aneel, An overview of current delivery systems in cancer gene therapy, *J. Control. Release* 94 (2004) 1–14.
- [14] R. Bottega, R.M. Epan, Inhibition of protein kinase C by cationic amphiphiles, *Biochemistry* 31 (1992) 9025–9030.
- [15] P. Wild, M. Engels, C. Sem, K. Tobler, U. Ziegler, E.M. Schraner, E. Loeffle, M. Ackermann, M. Mueller, P. Walther, Impairment of Nuclear Pores in Bovine Herpesvirus 1-infected MDBK Cells, *J. Virol.* 79 (2005) 1071–1083.
- [16] F.J. Rixon, Structure and assembly of herpesviruses, *Semin Virol.* 4 (1993) 135–144.
- [17] M. Homman-Loudiyi, K. Hulthenby, W. Britt, C. Soderberg-Naucler, Envelopment of human cytomegalovirus occurs by budding into Golgi-derived vacuole compartments positive for gB, Rab 3, trans-Golgi network 46, and mannosidase II, *J. Virol.* 77 (2003) 3191–3203 Erratum 77 (2003) 8179.
- [18] G. Coremans, V. Margaritis, R. Snoeck, J. Wyndaele, E. De Clercq, K. Geboes, Topical Cidofovir (HPMPC) Is an Effective Adjuvant to Surgical Treatment of Anogenital Condylomata Acuminata, *Dis. Colon Rectum* 46 (2003) 1103–1109.
- [19] B.D. Kuppermann, K.K. Assil, C. Vuong, G. Besen, C.A. Wiley, E. De Clercq, G. Bergeron-Lynn, J.D. Connor, M. Pursley, D. Munguia, W.R. Freeman, Liposome-encapsulated (S)-1-(3-hydroxy-2-phosphonylmethoxypropyl) cytosine for long-acting therapy of viral retinitis, *J. Infect. Dis.* 173 (1996) 18–23.
- [20] B. Ruozi, G. Riva, D. Belletti, G. Tosi, F. Forni, A. Mucci, P. Barozzi, M. Luppi, M.A. Vandelli, Cidofovir-loaded liposomes: an in vitro study using BCBL-1 cell line as a model for primary effusion lymphoma, *Eur. J. Pharm. Sci.* 41 (2010) 254–264.
- [21] S. Carmona, M.R. Jorgensen, S. Kolli, C. Crowther, F.H. Salazar, P.L. Marion, M. Fujino, Y. Natori, M. Thanou, P. Arbuthnot, A.D. Miller, Controlling HBV replication in vivo by intravenous administration of triggered PEGylated siRNA-nanoparticles, *Mol. Pharm.* 6 (2009) 706–717.



Antiviral activities of 2,6-diaminopurine-based acyclic nucleoside phosphonates against herpesviruses: *In vitro* study results with pseudorabies virus (PrV, SuHV-1)

Darina Zouharova^{a,1}, Ivana Lipenska^{a,1}, Martina Fojtikova^{a,1}, Pavel Kulich^a, Jiri Neca^a, Michal Slany^a, Kamil Kovarcik^a, Pavlina Turanek-Knotigova^a, Frantisek Hubatka^a, Hana Celechovska^a, Josef Masek^a, Stepan Koudelka^{a,b}, Lubomir Prochazka^a, Ludek Eyer^a, Jana Plockova^a, Eliska Bartheldyova^a, Andrew D. Miller^c, Daniel Ruzek^{a,d}, Milan Raska^{a,e}, Zlatko Janeba^f, Jaroslav Turanek^{a,*}

^a Veterinary Research Institute, Department of Pharmacology and Immunotherapy, Brno, Czech Republic

^b International Clinical Research Center, St. Anne's University Hospital, Brno, Czech Republic

^c King's College London, Institute of Pharmaceutical Science, London, United Kingdom, and GlobalAcorn Ltd., London, United Kingdom

^d Institute of Parasitology, Biology Centre of the Czech Academy of Sciences, and Faculty of Science, University of South Bohemia, Ceske Budejovice, Czech Republic

^e Palacky University of Olomouc, Faculty of Medicine, Department of Immunology, Czech Republic

^f Institute of Organic Chemistry and Biochemistry, The Czech Academy of Sciences, Prague, Czech Republic

ARTICLE INFO

Article history:

Received 1 December 2015

Received in revised form 13 January 2016

Accepted 14 January 2016

Keywords:

Pseudorabies
Acyclic nucleoside phosphonates
DNA viruses
Cidofovir
Antiviral drugs
DNA polymerase

ABSTRACT

Pseudorabies virus (PrV), a causative agent of Aujeszky's disease, is deadly to most mammals with the exception of higher primates and men. This disease causes serious economic losses among farm animals, especially pigs, yet many European countries are today claimed to be Aujeszky's disease free because of the discovery of an efficient vaccination for pigs. In reality, the virus is still present in wild boar. Current vaccines are neither suitable for dogs nor are there anti-PrV drugs approved for veterinary use. Therefore, the disease still represents a high threat, particularly for expensive hunting dogs that can come into close contact with infected boars. Here we report on the anti-PrV activities of a series of synthetic diaminopurine-based acyclic nucleoside phosphonate (DAP-ANP) analogues. Initially, all synthetic DAP-ANPs under investigation are shown to exhibit minimal cytotoxicity by MTT and XTT tests (1–100 μM range). Thereafter *in vitro* infection models are established using PrV virus SuHV-1, optimized on PK-15 and RK-13 cell lines. Out of the six DAP-ANP analogues tested, analogue VI functionalized with a cyclopropyl group on the 6-amino position of the purine ring proves the most effective antiviral DAP-ANP analogue against PrV infection, aided by sufficient hydrophobic character to enhance bioavailability to its cellular target viral DNA-polymerase. Four other DAP-ANP analogues with functional groups introduced to the C2-position are shown ineffective against PrV infection, even with favourable hydrophobic properties. Cidofovir[®], a drug approved against various herpesvirus infections, is found to exert only low activity against PrV in these same *in vitro* models.

© 2016 Elsevier B.V. All rights reserved.

1. Introduction

Pseudorabies, also known as "Aujeszky's disease", is an acute, frequently fatal disease caused by PrV, also known as suid

herpesvirus 1 (SuHV-1), which belongs to the genus *Varicellovirus*, in the Alphaherpesvirinae subfamily of the family *Herpesviridae* (Pomeranz et al., 2005). Among the most known viruses in the *Varicellovirus* genus are varicellazoster virus (VZV), bovine herpesvirus 1 (BHV-1) and equine herpesvirus 1 (EHV-1) (McGeoch and Cook, 1994). PrV is a pathogen spread mostly among swine and is lethal for almost all mammals except for higher primates and humans. Only wild pigs are able to survive infection and they serve as a natural reservoir of PrV. Dogs, especially hunting dogs, can be infected with this virus by close

* Corresponding author at: Department of Pharmacology and Immunotherapy, Veterinary Research Institute Hudcova 70 621 00 Brno, Czech Republic.

E-mail address: turanek@vri.cz (J. Turanek).

¹ These authors contributed equally to this work.

Consumption of contaminated raw pork or offal is another source of fatal infection in farm and companion dogs (Zhang et al., 2015; Cay and Letellier, 2009). Much has been discovered so far about PrV neurovirulence, neuropathogenesis, the properties of viral proteins involved in those processes, and genome sequences. PrV has also been used as a model herpesvirus to study virus biology and may be used for tracing neural pathways (Pomeranz et al., 2005). While in swine, PrV is transferred to various organs by viremic and lymphatic pathways (Wittmann et al., 1980), there is no evidence of viral replication in the tissues of experimentally infected dogs, except for in tissues of the nervous system. Therefore, the non-neural tissue damage in infected dogs is primarily induced indirectly by PrV. Histological findings in the central nervous systems (CNS) of PrV-infected dogs were found to be restricted to the brainstem (Zhang et al., 2015). Secondary findings of cardiac lesions were made in both the naturally and experimentally PrV-infected dogs (Olson and Miller, 1986). At present only vaccines for swine are available for the prophylaxis of Aujeszky's disease in pig farms. Inactivated vaccines are not effective in dogs and attenuated vaccines are lethal for dogs as well as for farm animals like lambs and sheep (Kong et al., 2013; Van Alstine et al., 1984). Some attempts to develop recombinant protein (rPrV) and DNA vaccines for swine were described in literature. Many of the rPrV vaccine candidates that have been reported in literature albeit they have not been further pursued so are not yet commercially available (Krishnan, 2000; Dong et al., 2014; Kim et al., 2008; Van Rooij et al., 2010). Despite the significant progress made, the efficacy of potentially safe DNA vaccines requires considerable improvement owing to the high mortality rate from the disease in vaccinated animals (Woodland, 2004; Yoon et al., 2006; Fischer et al., 2003).

In the case of chemotherapy, there are no currently approved veterinary drugs against Aujeszky's disease, and there are only limited reports concerning inhibition studies focused on inhibition of PrV proliferation by various preparations. Some natural compounds have been found to be effective *in vitro* against various herpesviruses, but failed against PrV (De Almeida et al., 1998). *In vitro* inhibition of PrV replication was demonstrated for combination of Acyclovir and Ribavirin (Pancheva, 1991). The antiviral effects of lithium chloride and natural compound diammonium glycyrrhizinate were demonstrated *in vitro* on VERO cells (Sui et al., 2010). Several nucleotide based drugs like bromovinyl deoxyuridine, acyclovir and 2'-nor-2'-deoxyguanosine have been studied as *in vitro* inhibitors and in mice models *in vivo*. Mice survival was most prolonged post administration of 2'-nor-2'-deoxyguanosine (Field, 1985).

Recently, a new largescale method for synthesis of antiretroviral agent 9-[2-(*R*)-(phosphonomethoxy) propyl]-2,6-diaminopurine, (*R*)-PMPDAP, was developed (Krecmerova et al., 2013) and used for synthesis of analogues of diaminopurine-based acyclic

2012). We tested these compound *in vitro* various herpesviruses, especially strains resistant against established antiviral drugs, including PrV which is of importance in veterinary medicine. Two of these DAP-ANP analogues were found to be highly active against PrV in model *in vitro* cell culture studies, while Cidofovir[®], a marketed drug active against many viruses including herpes, adeno, polyoma, papilloma, poxviruses and retroviruses (De Clercq, 1998; De Clercq, 2002), only exerted low anti PrV activity. This is the first study focused on the antiviral effects of DAP-ANP analogues against PrV.

2. Materials and methods

2.1. Syntheses and structure of nucleotide analogues

A series of 6 DAP-ANP analogues (Table 1 and Fig. 1) differing in their hydrophobicity and substitution in the side chain were synthesized according to previously reported methods (Krecmerova et al., 2013; Holy et al., 1999; Jansa et al., 2012; Holy et al., 2001; Jansa et al., 2011). Cidofovir[®] (active compound (*S*)-HPMPC); (*S*)-1-[3-hydroxy-2-(phosphonylmethoxypropyl)]cytosine as well as its inactive (*R*)-isomer were kindly gifted by prof. Antonín Holý.

2.2. Chromatographic analyses HPLC-MS/MS and hydrophobicity of tested compounds expressed as capacity factor

Sample analyses were performed by using high performance liquid chromatography in tandem with mass spectrometry. An Agilent 1200 chromatographic system (Agilent Technologies, Germany), consisting of binary pump, vacuum degasser, auto sampler, UV detector and thermostat column compartment, was used. Separation of modified nucleotides was carried out using Zorbax Eclipse Plus, 2.1 × 150 mm, 3.5 μm particle size column (Agilent Technologies, USA) under isocratic conditions. Mobile phase contained 0.8% of methanol and 0.1% of formic acid in water. The flow rate of the mobile phase was 0.25 ml/min, the column temperature was set at 40°C. UV detector was used for determination of nucleotides capacity factors. A triple quadrupole mass spectrometer Agilent 6410 Triple Quad LC/MS (Agilent Technologies, USA) with an electrospray interface (ESI) was used for quantification of tested compounds in cells. The mass spectrometer was operated in the positive ion mode. Multiple reaction monitoring (MRM) with the mass transitions *m/z* 329.1–191.2, 216.9, 247.0 and 281.2 was used. Relative hydrophobicity of tested compounds was expressed as capacity factor *k'* to compare their potential to penetrate cell membranes.

2.3. In vitro testing—tissue culture

MDCK, MDBK, PK-15, RK-13, VERO cell lines were tested to select appropriate cell line for *in vitro* assays. Cell line PK-15 and RK-13 were selected as the best model with respect to virus multiplication and sensitivity for XTT/MTT cytotoxicity tests. The data obtained on these cell lines gave long term coherent results. The cultures were grown in Dulbecco's minimal essential medium (DMEM/High Glucose, HyClone, Thermo Scientific) supplemented with antibiotics, fungizone and 10% foetal bovine serum (FBS). The cells were cultured at 37 °C in a humidified atmosphere containing 5% CO₂ (HERAcell 150i CO2 incubator, Thermo Scientific, Germany).

2.4. In vitro testing—virus strain

SuHV-1 CAPM V-166 isolate was obtained from the Collection of Pathogenic Microorganisms (Veterinary Research Institute, Brno) and was used throughout these experiments. This isolate was

Table 1
Molecular formulae and weight of chosen antiviral compounds.

Compound	Molecular formula	Molecular weight (Da)
I	C ₁₂ H ₁₂ N ₆ O ₄ P	288
II	C ₁₂ H ₁₂ N ₆ O ₅ PNa ₂	362
III	C ₁₀ H ₁₀ N ₆ O ₅ P	318
IV	C ₁₀ H ₁₀ N ₆ O ₄ P	302
V	C ₁₁ H ₁₀ N ₆ O ₅ PF ₃	365
VI	C ₁₁ H ₁₂ N ₆ O ₄ P	328
CIDOFOVIR	C ₁₂ H ₁₄ N ₄ O ₅ P	279

Note: I: 9-[2-(phosphonomethoxy) ethyl]-2,6-diaminopurine; II: (S)-9-[2-hydroxy-3-(phosphonomethoxy) propyl]-2,6-diaminopurine; III: (R)-9-[3-hydroxy-2-(phosphonomethoxy) propyl]-2,6-diaminopurine; IV: (R)-9-[2-(phosphonomethoxy) propyl]-2,6-diaminopurine; V: (R,S)-9-[3,3,3-trifluoro-2-(phosphonomethoxy) propyl]-2,6-diaminopurine; VI: N 6-cyclopropyl-9-[2-(phosphonomethoxy) ethyl]-2,6-diaminopurine.

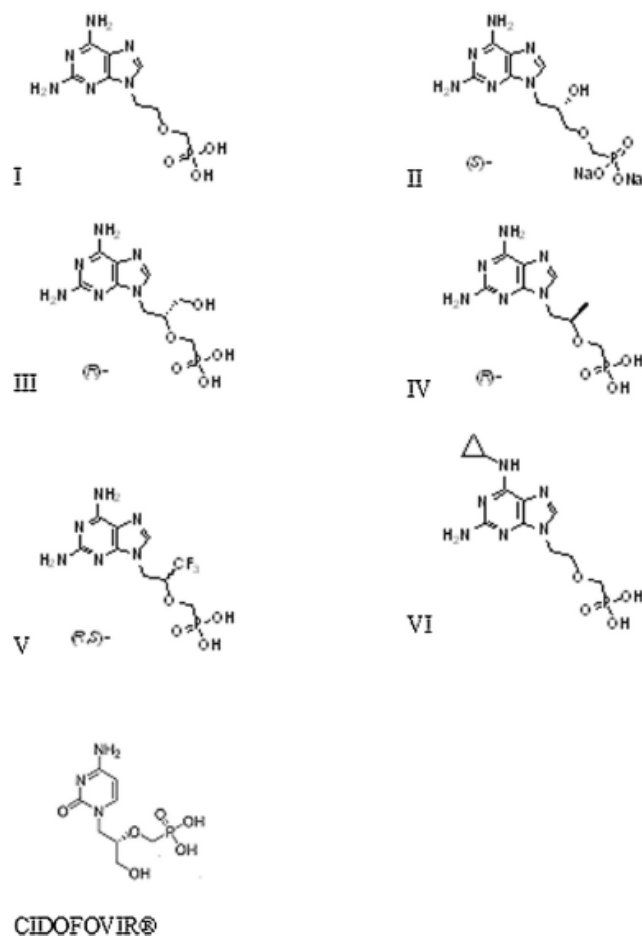


Fig. 1. Structural formulae of tested DAP-ANP analogues.

found to be the most aggressive *in vitro* against tested cell lines. Virus working stock was prepared by infecting a monolayer of cells at low multiplicity of infection and stored at -70°C in aliquots until used. Working solution of virus was prepared at the titre of 10^{-5} PFU.

2.5. *In vitro* cytotoxicity

MTT (Sigma–Aldrich) or XTT Cell Viability Kit (Cell Signalling Technology) test were used to determine cell viability. The test was performed according to manual provided by the producer. All kinds of cell cultures were plated at a density of 1.5×10^5 cells/ml (100 μl per well) in 96-well plates for 24 h and subsequently exposed to tested compounds. Antivirals were tested at the concentration range of 0.78–100 μM , exposure times were 24 h. The volume of 20 μl of MTT (2.5 g/l) was added to each well and

plates were incubated for 3 h at 37°C , then 100 μl 10% SDS was added and incubated 24 h at room temperature. In case of XTT (solubilisation step based on SDS was omitted), 50 μl was added to each well and plates were incubated for 24 h at 37°C . The absorbance of the formazan solution at MTT was measured at 540 nm and at XTT at 450 nm using ELx800 Absorbance Microplate Reader (BioTek Instruments Ltd., USA) and analysed through Gen5 Data Analysis Software (BioTek Instruments Ltd.). Cytotoxicity data were confirmed by direct observation by optical microscopy (Eclipse TS200, Nikon, China) (Li et al., 2008, 2009).

2.6. Assaying of antiviral activity—XTT test

Cell cultures were plated at density of 1.5×10^5 cells/ml (100 μl of cells in each well) in 96-well plates for 24 h and subsequently exposed to tested compounds. Virus SuHV-1CAPM V-166 isolate

was added (titre 10^{-5} PFU) into each well 4 h later. After 6 days of incubation with virus the cell viability was determined by XTT test.

2.7. Inhibition of replication of viral DNA assayed by quantitative PCR

DNA isolation was done using DNeasy Blood & Tissue Kit (QIAGEN) following the producer's protocol. DNA isolation was based on a manufacturer protocol (DNeasy Blood & Tissue, QIAGEN) slightly modified to include mechanical homogenization with zirconia/silica beads (0.2 mm) in a MagNA Lyser instrument (Roche, Mannheim, Germany) at 6400 rpm for 60 s (Slana et al., 2010). The isolated DNA was used as a template for the duplex qPCR assay. The detection of Pseudorabies virus was achieved via primers and probes specific for gB gene (Accession KF711983). Primers (gB718F 5'-ACAAGTTCAGGCCACATCTAC-3'; gB812R 5'-GTCYGTGAAGCGGTTCGTGAT-3') were adopted from Ma et al. (2008) while probe was newly designed (gBprobe1 5'-FAM-ACGTCATCGTCACGACCGTGTGGTC-Cy5-3'). Previously published internal amplification control (IAC) was introduced to eliminate false negative samples (Slana et al., 2008). A typical optimized reaction mixture (total volume 20 μ l) contained 1×480 Probe master qPCR Kit (Roche), 10 pmol of the primer set, 2 pmol of the gB probe, 3.5 pmol of the IAC probe, 0.2 U of Uracil DNA Glycosylase (Roche), 5×10^2 copies of IAC diluted in TE buffer and 5 μ l of DNA template. Each run consisted of the following steps: initial denaturation at 95 °C for 7 min and 47 cycles at 95 °C for 5 s, 56 °C for 30 s and 72 °C for 10 s. The instrument LightCycler 480, (Roche, Switzerland) was used for qPCR analyses of viral DNA. Inhibition curves were calculated by the software PRISM version 5.0 (GraphPad, USA).

2.8. Quantification of tested drugs in cells in vitro—cell preparation

Cell cultures of PK-15 line were plated at density of 2×10^5 cells/ml (3 ml of cells in each well) in 6-well plates for 24 h and subsequently exposed to tested compounds (10 μ M concentration of compounds). After certain intervals of time (0 h; 1 h; 1.5 h; 2 h; 4 h; 8 h; 24 h) the cells were rinsed with PBS (phosphate buffered saline) and harvested by scraping and centrifuged (2800 rpm, 2 min) and the supernatant was discarded.

2.9. Penetration of drugs into cells and assay of intracellular concentration

Cells (samples in triplicates) were resuspended in 500 μ l methanol and sonicated for 1 min (SonoPlus 200, Bandelin, Germany). 50 μ l of the mixture was taken for the protein quantification (BCA method—Pierce BCA Protein Assay Kit, Thermo SCIENTIFIC), which is correlated to the amount of cells. The rest of the mixture was centrifuged, the supernatant was used for quantification of tested drugs by HPLC-MS/MS as described above.

2.10. Transmission electron microscopy—ultrathin section method

3% Glutaraldehyde-fixed PK-15 cells untreated or treated by 10 μ l and 50 μ l within ATV exposed to PrV were centrifuged at 800 rpm. The pellets were rinsed in Milonig buffer, post-fixed in 1% OsO₄ solution in Milonig buffer, dehydrated in 50, 70, 90, 100% acetone, embedded in Epon-Durcupan mixture (Epon 812 Serva; Durcupan, ACM Fluka) and polymerized at 60 °C for 72 h. Ultrathin sections (the thickness of 60 nm) were cut with glass knives on UC 7 ultramicrotome (UC 7, Leica, Austria). The sections were contrasted by 2% aqueous uranyl acetate and 1% aqueous lead citrate. The sections were examined under a Philips EM 208 S Morgagni transmission electron microscope (FEI, Czech Republic).

3. Results

3.1. Chromatographic separation and hydrophobicity of tested compound

The hydrophobicity of tested DAP-ANP analogues was measured to get a better insight into the ability of various analogues to penetrate through the cell membrane. Hydrophobicity of each compound was estimated by HPLC and expressed in terms of a capacity factor k' as defined below (see Table 2). This method is sensitive and relatively simple to allow comparison of various structural modifications in various positions with respect to their contribution to the overall hydrophobicity of the molecule. The expected hydrophobicity of tested compounds based on their structural formulae is in a good agreement with the capacity factor k' calculated from chromatographic data (Fig. 2 and Table 2). Tested DAP-ANP analogues possessed a range of hydrophobicities as measured by their corresponding capacity factors (Table 2). Analogues I, II and III possessed very similar hydrophobicities. Therefore, addition of 2'-hydroxyl (II) or 2'-hydroxymethyl (III) functionalities did not change hydrophobicities very much compared with parent analogue I. On the other hand, 2'-methyl (IV) and especially 2'-trifluoromethyl (V) functionalizations had more profound effects on analogue hydrophobicities. The most hydrophobic analogue VI was modified by cyclopropylation of the 6-amino group of the purine ring. An overlay of chromatograms for individual compounds is presented (Fig. 2).

3.2. Characterisation of in vitro cytotoxic effect of DAP-ANP analogues

All tested DAP-ANP analogues, including Cidofovir[®] as a positive control, were found not cytotoxic against PK-15 and RK-13 cell lines within the concentration range 1–100 μ M and 24 h exposition time. Both XTT and MTT tests gave the same results which were in a good accordance with direct observation by optical microscopy (*data not shown*). Representative data on viability of PK-15 cells treated by compound I or VI is presented at Fig. 3. These analogues demonstrated significant antiviral activity on both cell lines although differing in their hydrophobicities.

3.3. Antiviral effect of the tested compounds

The XTT test was used for prescreening antiviral activities of the DAP-ANP analogues with Cidofovir[®] as positive control. Analogues II, III and IV were not able to protect cells against viral infection resulting in visible cytopathic effects and decreases in local cell viabilities. As expected, optical isomer (*R*)-HPMPC was inactive in both cell lines, while Cidofovir[®] was inactive in PK-15 cell line and weakly active at 100 μ M concentration in RK-13 cell line (*data not shown*). Analogues I and VI were able to inhibit significant cytopathic effect caused by PrV infection. Therefore, these two

Table 2
Hydrophobicities of DAP-ANP analogues expressed as capacity factors.

Compound	Capacity factor k'	STD
I	0.747	0.006
II	0.695	0.012
III	0.724	0.008
IV	2.114	0.017
V	7.698	0.030
VI	9.040	0.035

Mobile phase: 0.8% of methanol and 0.1% of formic acid in water. The flow rate: 0.25 ml/min. The column temperature was set at 40 °C. UV detector was used for determination for capacity factors of nucleotides; capacity factor k' is expressed as $k' = R_t/R_0$ where is R_t retention time, and R_0 is dead volume (R_t for non retained standard).

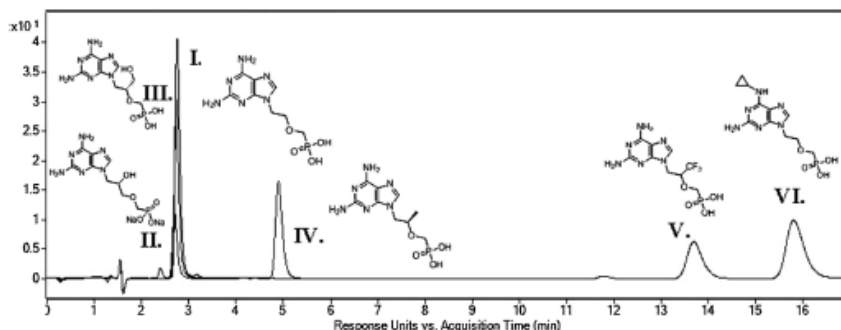


Fig. 2. HPLC separation of individual analogues (chromatographic conditions are described in Section 2). Analogues I, II and III were eluted in similar R_f , therefore the chromatogram was prepared as overlay of individual separations for analogues I, II, III, and chromatogram of the mixture of analogues IV, V and VI.

compounds were advanced to more detailed viral replication assays making use of qPCR. Indeed, viral DNA replication was inhibited by both analogues I a VI in dose dependent manner as demonstrated by qPCR analyses (Fig. 4). Indeed only compounds I and VI were able to inhibit viral DNA replication in a concentration dependent manner (Fig. 4) leading to essentially total inhibition of viral DNA replication at higher concentrations of both, reducing the level of residual viral DNA by approx. six orders of magnitude to detection limit. IC_{50} were estimated to be in submicromolar range and their selectivity index was estimated to be higher than 100 for compound I and higher than 1000 for compound VI ($SI \geq 100/IC_{50}$). In comparison, *S* optical isomer of HPMPIC reduced the level of viral DNA in RK-13 cells by only two orders of magnitude at a concentration of $100 \mu\text{M}$ (data not shown).

The antiviral effects of analogues I and VI were confirmed by optical microscopy, which demonstrated preservation of cell monolayers and significant reductions in cytopathic effects induced by PrV. Infected control cells lost monolayer organisation, and were observed dead or in final stages of apoptosis characterised by disintegration of nucleus and release of cytoplasm. Cells treated with analogues I or VI remained adherent, nuclei were of normal appearance with 1–4 nucleoli and cells exhibited well organised structures. Some cellular debris originating from dead cells was observable on cell monolayers, which is an event common during long term cultivation. Micrographs (Fig. 5) clearly demonstrate the antiviral effects of analogue VI ($10 \mu\text{M}$) on the PK-15 cell line.

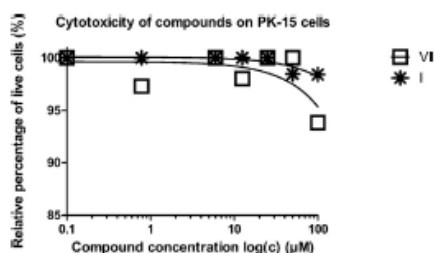


Fig. 3. Viability of PK-15 cells treated by DAP-ANP analogues I and VI. PK-15 cells were exposed for 24 h to DAP-ANP analogues I or VI within the concentration range of 0.8–100 μM . Viability was assayed by XTT test (triplicate setting) and confirmed by optical microscopy. Owing to logarithmic scale of concentration, point at 0.1 μM represents untreated controls without added drugs.

3.4. Demonstration of antiviral effects at subcellular levels by electron microscopy

Electron microscopy was used to confirm viral replication and cessation of viral replication in tissue culture. Typical signs of massive production of viruses were found in the nuclei of control infected cells. Typical clusters of crystalline arrayed capsids are seen in nuclei (Fig. 6C). Virus particles are shed into medium or directly transmitted to neighbouring cells by exocytosis–endocytosis mechanism (Fig. 6B). Morphological changes in cell structures are also typical for virus induced apoptosis. Finally detachment of cells, condensation of chromatin, disappearance of nucleoli, destruction of nuclei and of nuclear membranes are well recognisable (Fig. 6B, C, E). By contrast, cells treated with either analogue I or VI were protected against massive viral infection damage and virus induced apoptosis (Fig. 6F). In a small portion of cells the process of viral replication was induced, but most viral particles produced appeared defective and probably without encapsulated DNA (Fig. 6G, H). These electron microscopy data confirmed results obtained by XTT viability tests (Fig. 3), qPCR (Fig. 4) and optical microscopy (Fig. 5).

3.5. Penetration of drug into cells as assayed by HPLC-MS/MS

The concentration of tested DAP-ANP analogues in cells was assayed by HPLC-MS/MS. Cellular penetration of drugs into cells typically obeys simple saturation kinetic and is a rapid process. A representative curve for hydrophobic analogue VI is presented (Fig. 7B) showing how analogues VI reached approx 90% saturation in 2 h.

Hydrophobic analogue V as well VI was also found to penetrate cells rapidly in comparison to the more hydrophilic analogues I, II, III, IV and positive control (*S*)-HPMPIC (Fig. 7A). Curiously, although both DAP-ANP analogues I and VI were the most potent antiviral agents, yet analogue I accumulated much less readily into target cells than VI given that I is much more hydrophilic in character than VI. Therefore, increasing hydrophobicity did not appear to correlate directly with increasing antiviral efficacy.

4. Discussion

Viral DNA-polymerase is an established molecular target for antiviral drugs directed against herpesviruses. The effectiveness of antiviral drugs such as ganciclovir and acyclovir that act at the viral DNA-polymerase is well documented in literature against

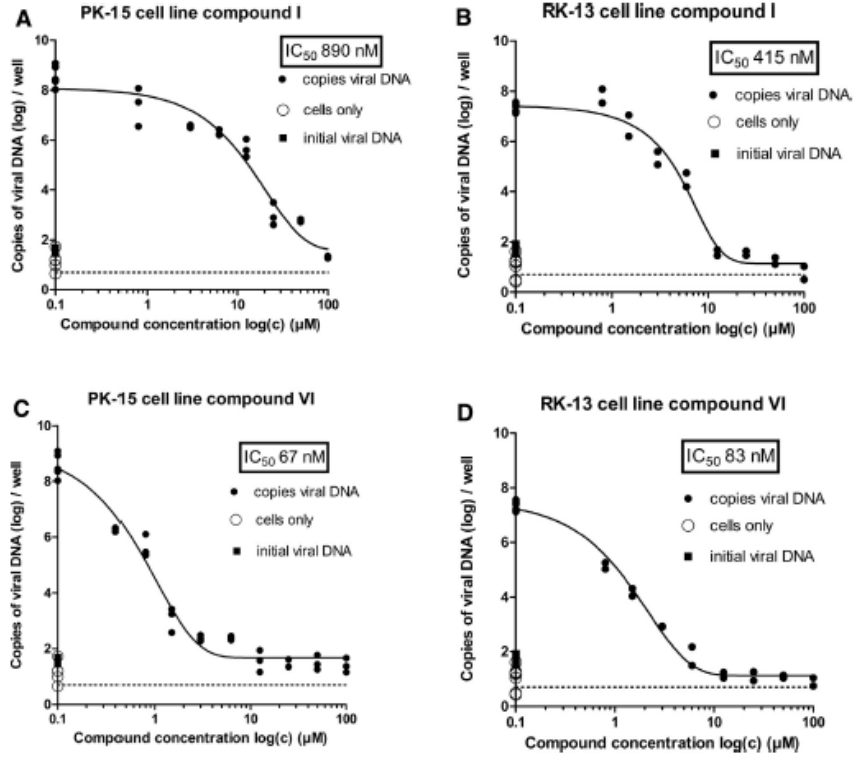


Fig. 4. qPCR assay of inhibitory effect of compound I (Fig. 4A, B) a VI (Fig. 4C, D) on replication of viral DNA. Dashed lines represent detection limit of the qPCR method for PrV DNA. Assays were run in triplicates (PK-15 cells) or duplicates (RK-13 cells). Full squares represent values of viral DNA (the number of copies per reaction) added to cell culture to initiate infection. Theoretically, these values represent maximal possible level of residual viral DNA assayed by qPCR if replication is totally inhibited. Open circles represent negative control (cells without added virus). Full circles represent copies of viral DNA in infected cells.

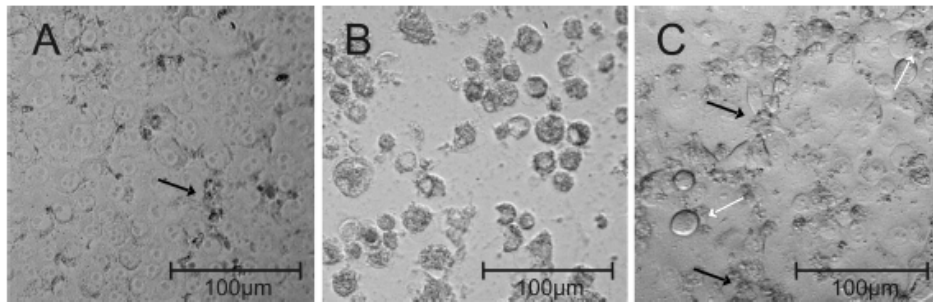


Fig. 5. Cytopathic effect induced by PrV in PK-15 cells and protective effect of analogue VI at 10 µM concentration. (A) control PK-15 cells exhibit intact and well-organised monolayer. Nuclei with 1–4 nucleoli are recognisable, black arrow marks debris upon cell monolayer; (B) destruction of cell monolayer induced by PrV. The most of the cells are shrivelled as the sign of the final stage of necrosis; (C) cells treated by 10 µM concentration of compound VI. Necrotic morphology is observed in some cells, but the cell monolayer is preserved; black arrows mark locations of cell debris, white arrows pick out necrotic cells. Micrographs were taken at day 6 after inoculation of tissue culture by virus.

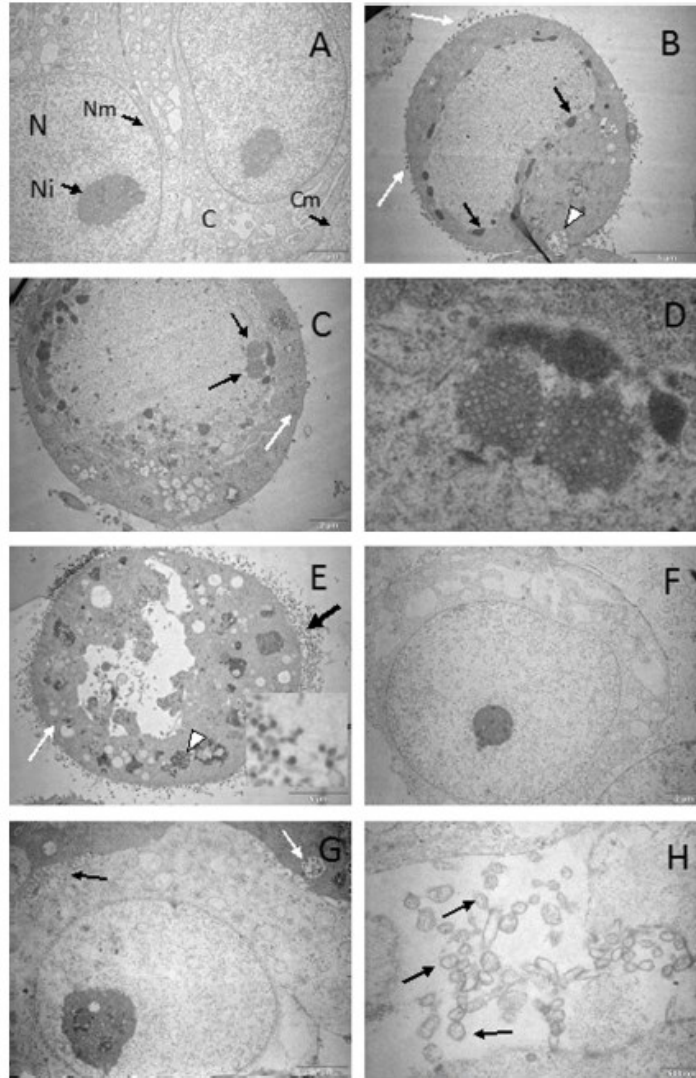


Fig. 6. Inhibition of viral replication in PK-15 cells demonstrated by electron microscopy. (A) Control untreated and uninfected PK-15 cells. (N—nucleus; Ni—nucleoli; Nm—nuclear membrane; C—cytoplasm; Cm—cytoplasm membrane). (B) PK-15 cells infected by PrV. Chromatin is condensed close to the rest of the nuclear membrane (black arrow), nucleoli have disappeared, the cell has lost adherence, complete viral particles are shed into medium (white arrows), note the vacuoli with viral particles which are directly transported into a neighbour cell (white arrow head). (C) PK-15 cells infected by PrV. Two clusters of crystalline arrayed capsids (capsids of A type) are seen in the nucleus (black arrows). (D) Detail from (C). Two clusters of crystalline arrayed capsids (black arrows) are positioned close to the rest of condensed nuclear DNA (black arrowhead). In some capsids the process of incorporation of viral DNA starts (note black dot inside the capsid). (E) Massive shedding of viral particles from PK-15 cells. Cell has lost adherence, the nucleus is completely destroyed and vacuoli are filled with matured viral particles (white arrowhead). Some immature and mature viral particles are presented in cytoplasm (white arrow) and matured viral particles are released from the cell into the medium in large numbers (thick black arrows). Insert shows matured viral particles shed into medium. (F) PK-15 cells treated with compound VI (10 µM) and infected with PrV. The observed cell is in a monolayer surrounded by other cells. No pathological changes are observable in nucleus or in cytoplasm. Viral particles are not observed in most cells. (G) PK-15 cells treated with compound VI (10 µM) and infected with PrV. Small portion of cells become infected and produce viral particles. The production is not massive and infection does not cause pathological changes in the nuclei and cytoplasm of most of cells. Only a small number of apoptotic cells are observed and the monolayer is kept intact. The viral particles produced are in large portion defective in DNA content. Viral particles are seen in vacuoli (white arrow) and released into intercellular spaces (black arrows). (H) Detail of viral particles produced by PK-15 cell treated with analogue VI (10 µM). Most of the particles are defective and do not contain viral DNA (black arrows).

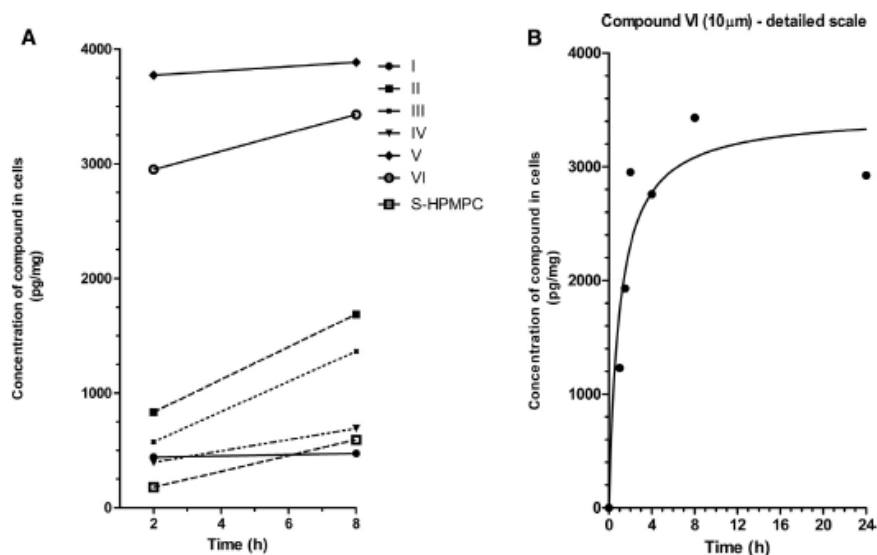


Fig. 7. Penetration of drug into cells as assayed by HPLC-MS/MS. (A) Intracellular concentration of tested DAP-ANP analogues in PK-15 cells at time 2 and 8 h of incubation. PK-15 cells were incubated in triplicates for 2 and 8 h with tested compounds (10 μ M). Obtained samples were analysed by HPLC-MS/MS (details are described in Section 2). (B) Penetration of analogue VI into PK-15 cells. PK-15 cells were incubated in triplicate for various times with analogue VI (10 μ M). Obtained samples were analysed by HPLC-MS/MS (details are described in Section 2).

herpesvirus infections in both human and animals (Garré et al., 2007; De Clercq et al., 2006). Overall we have tested about 30 acyclic nucleoside phosphonate (ANP) analogues looking for active molecules grouped according to their nucleobase structure into various structural families. Here we report on the screening of six bespoke diaminopurine-based acyclic nucleoside phosphonate (DAP-ANP) analogues. Of these, two analogues I and VI (Fig. 1) were found active against PrV infection and were studied in more detail.

In *in vitro* infection assays, penetration of drugs through cell membranes is a primary obstacle to reaching cellular targets. In our previous paper we have shown that entrapment of Cidofovir into cationic liposomes can significantly improve antiviral effects *in vitro* against BHV-1 (Korvasova et al., 2012). The primary reason for this was that nanocarriers like liposomes can facilitate drug delivery to cells by promoting improved internalization into cells by endocytosis. Alternatively, ANPs have been rendered more bioavailable to their cellular targets by preparation of prodrugs increasing their hydrophobic character through esterification of their phosphonate moieties. Indeed, hydrophobicity is a crucial factor that correlates with cell penetration in the absence of transmembrane transport mechanisms. For this reason, increasing drug hydrophobicity can be an important way to improve drug bioavailability to cellular targets *in vitro* and even *in vivo*.

Here we observe that the two analogues V and VI are rendered more hydrophobic than parent DAP-ANP analogue I by introduction of C2'-CF₃- and N²-cyclopropyl moieties respectively. Yet the most active DAP-ANP analogues were actually found to be parent analogue I and N-cyclopropyl analogue VI (compare Table 2, Figs. 2, 4 and 7A). Having said this, apparent cellular IC₅₀ values estimated from PrV cellular infection models (Fig. 4) clearly demonstrate that analogue VI is 10-fold more effective than parent I. On the other hand, analogue VI appears to be 10-fold more bioavailable to target in cells than parent I (Fig. 7A). It cannot be determined for now

whether higher hydrophobicity or lower inhibitory constant K_i (or both) are responsible for higher antiviral activity of compound VI in comparison to compound I. Therefore we would suggest that both analogue I and VI are in fact likely to have equivalent levels of efficacy once at target. Accordingly, the importance of ensuring optimal drug bioavailability to target is clear in order to optimise drug performance. All cell lines tested in preliminary experiments (MDCK, MDBK, PK-15, RK-13, VERO) were susceptible towards PrV viral strain SuHV-1/CAPM V-166 and cytopathic effects were observed after virus inoculation in all cases. On the other hand, all tested DAP-ANP analogues did not exhibit cytotoxicity towards any of these cell lines. Therefore, it can be assumed, that analogues I and VI are selective inhibitors of viral DNA polymerase, but not eukaryotic host cell DNA polymerase.

Viral infections of cell lines PK-15 and RK-13 were studied in detail in each case since both represent standard model tissue culture models for *in vitro* PrV infection. The course of viral infection documented by electron microscopy (Fig. 6B–E) is in accordance with data published by others in PrV-infected cell cultures (Klupp et al., 2001; Klupp et al., 2005; Robbins et al., 1986) or pig's tissues (Aleman et al., 2003). Contrary to some publications (Aleman et al., 2003), production of I-particles appeared low. The multiplication of PrV in cell lines was documented by electron microscopy and qPCR, including the presence of crystal-like arrays of capsids in nuclei, viral particles plus agglomerates of tegument protein in cellular cytoplasm, and shedding of complete viral particles into extracellular medium followed by apoptosis of the infected cells. In non-treated cells the numbers of copies of viral DNA reached the value of 10^6 – 10^7 (6 days after cultivation) (Fig. 4). Administration of analogues I and VI was seen to reduce the number of copies of viral DNA to basal levels comparable to DNA levels in viral inoculum added to cell culture. Inhibition of viral DNA replication was also accompanied by a reduction in numbers

of viral particles in cells and culture medium. Proteins of late phase of virus replication cycle were not found present. Furthermore, nuclear capsid and aggregates of tegument proteins—typical products of late phase of viral replication – were not observable in cells treated by the active compounds either. All these facts implicate the inhibition of viral DNA polymerase resulting in suppressed replication of viral DNA, as expected for ANP analogues related to the well established inhibitors of viral DNA polymerase such as Cidofovir[®]. Intriguingly, when Cidofovir[®] was evaluated in the assays described here, mild antiviral activity was seen (viral DNA replication was reduced by 1–2 order of magnitude at 100 μ M concentration) against both bovine herpesvirus BHV-1 (Korvasova et al., 2012) and PrV (*data not shown*), whereas analogues I and VI (as well as II, III, IV and V) were not active *in vitro* against BHV-1 in MDBK cells. Such selectivity is of interest for future studies on structural relationship between herpesvirus DNA-polymerases and different classes of ANP inhibitors.

Although antiviral chemotherapy has become a standard practice in treatment of herpesvirus infection in humans, the veterinary use of antiviral drugs is rare. Treatment of feline herpesvirus-1 infections could be mentioned as an example (Williams et al., 2005). Nucleotide based drugs like bromovinyl deoxyuridine, acyclovir and 2'-nor-2'-deoxyguanosine were tested for their anti-PrV effect *in vitro* and *in vivo* using lab mice. Substantial prolongation of mouse survival has been demonstrated with 2'-nor-2'-deoxyguanosine (Field, 1985). Correspondingly, while there has been intensive research running in the field of PrV vaccine development, only limited attention has been focused on antiviral drug therapy. Currently most published studies are focused on *in vitro* experiments. These include the use of the herb *Houttuynia cordata* belonging to traditional Chinese herb medicine that was tested *in vitro* (Ren et al., 2011) as well as Glycyrrhizin, the most important bioactive compound of licorice root (Glycyrrhiza radix), that was used in combination with lithium chloride (Sui et al., 2010). Direct antiviral effects have yet to be demonstrated in *in vivo* model experiments. In our case, now that antiviral effects have been demonstrated *in vitro*, with minimal cytotoxicities, and lead analogues I and VI are now ready for studies with the mouse model of Aujeszky's disease, followed by early stage "clinical" studies with dogs infected by PrV. Anti-viral drug therapy of Aujeszky's disease in dogs is a real challenge because of the short time between the first symptoms of infection and death (1–3 days) and the tendency of PrV to replicate inside of neurons (Kramer and Enquist, 2013; Zhang et al., 2015). Accordingly, anti-viral drugs should be administered as soon as first symptoms of disease are observed although this will lead to little improvement unless the drugs are properly bioavailable to the sites of PrV replication in the nuclei of neurons as well. Another important aspect of future potential treatment should also be the preservation of neuro-motoric function of treated dogs and suppression of viral reactivation. These aspects are of importance in general too in the treatment of other herpesviruses infections.

5. Conclusion

Two 2,6-diaminopurine-based acyclic nucleoside phosphonates (DAP-ANPs) were selected as promising structures for further development into potential drugs with antiviral activity against PrV. *In vitro* data demonstrated considerable antiviral activity by both analogues I and VI although the greater bioavailability of VI to target appeared to promote a 10-fold drop in apparent cellular IC₅₀ compared with I. Further modification of the purine 6-amino functional groups is of interest to prepare future ANPs that might be more effective even than analogue VI. On the other hand, the sorts of functionalizations of the acyclic bridge moiety from purine to phosphonate that gave rise to inactive

analogues, II, III, IV and V did not appear to promote antiviral activities at all so can be disregarded going forward. *In vivo* studies with analogue I and VI will now be progressed in order to demonstrate antiviral activity and safety in the standard murine model of PrV infection.

Conflicts of interest

None.

Acknowledgements

By this paper we would like to revere the memory of prof. Antonín Holý, deceased in 2012, who pioneered the field of antiviral drugs at the Institute of Organic Chemistry and Biochemistry, Prague and whose world-wide scientific influence was appreciated.

Project CENATOX, Grant Agency of Czech Republic, GAP503/12/G147 (Jaroslav Turánek); the Ministry of Education, Youth and Sports CZ.1.07/2.3.00/20.0164 (Jaroslav Turánek, Milan Raška), MZE0002716202 Czech Ministry of Agriculture; postdoc position of Štěpán Koudelka was supported by the European Social Fund and the State Budget of the Czech Republic—Project FNUSA-ICRC, Support for Neurological Research and Development Teams through Postdoc Position Formations CZ.1.07/2.3.00/30.0043.

Luděk Eyer, Michal Slaný, Kamil Kovářčík and Daniel Růžek were supported by a project LO1218, with financial support from the MEYS of the Czech Republic under the NPU I program.

The team headed by Jaroslav Turánek, Daniel Růžek, Milan Raška and Andrew D. Miller are obligated to the Ministry of Education, Youth and Sports for supporting the project "FIT" (Pharmacology, Immunotherapy, nanoToxicology).

References

- Aleman, N., Quiroga, M.J., Lopez-Pena, M., Vazquez, S., Guerrero, F.H., Nieto, J.M., 2003. L-Particle production during primary replication of pseudorabies virus in the nasal mucosa of swine. *J. Virol.* 77, 5657–5667.
- Cay, A.B., Letellier, C., 2009. Isolation of Aujeszky's disease virus from two hunting dogs in Belgium after hunting wild boars. *Vlaams Diergeneeskundig Tijdschrift* 78, 194–195.
- De Almeida, A.P., Miranda, M.M.F.S., Simoni, L.C., Wigg, M.D., Lagrota, M.H.C., Costa, S.S., 1998. Flavonol monoglycosides isolated from the antiviral fractions of *Persea americana* (Lauraceae) leaf infusion. *Phytother. Res.* 12, 562–567.
- De Clercq, E., 1998. Antiviral agents that are active against CMV: potential of cidofovir for the treatment of CMV and other virus infections. *Monogr. Virol. Basel.* Karger 21, 193–214.
- De Clercq, E., 2002. Gidofovir in the treatment of poxvirus infections. *Antiviral Res.* 55, 1–13.
- De Clercq, E., Brancale, A., Hodge, A.V., Field, H.J., 2006. Antiviral Chemistry & Chemotherapy's current antiviral agents FactFile 2006 (1st edition). *Antivir. Chem. Chemother.* 17, 113–166.
- Dong, B., Zariwaga, D.S., Ren, X., 2014. An overview of live attenuated recombinant pseudorabies viruses for use as novel vaccines. *J. Immunol. Res.* 824630.
- Field, H.J., 1985. Chemotherapy of Aujeszky's disease (pseudorabies) in the mouse by means of nucleoside analogues: bromovinyldeoxyuridine, acyclovir, and dihydropropoxymethylguanine. *Antiviral Res.* 5, 157–168.
- Fischer, L., Barzu, S., Andreoni, C., Buisson, N., Brun, A., Audonnet, J.C., 2003. DNA vaccination of neonate piglets in the face of maternal immunity induces humoral memory and protection against a virulent Pseudorabies virus challenge. *Vaccine* 21, 1732–1741.
- Garré, B., Van der Meulen, K., Nugent, J., Neyts, J., Croubels, S., De Backer, P., Nauwynck, H., 2007. *In vitro* susceptibility of six isolates of equine herpesvirus 1 to acyclovir, ganciclovir, cidofovir, adefovir, PMEDAP and foscarnet. *Vet. Microbiol.* 122, 43–51.
- Holý, A., Guenter, J., Dvorakova, H., Masojdkova, M., Andrei, G., Snoeck, R., Balzarini, J., De Clercq, E., 1999. Structure–antiviral activity relationship in the series of pyrimidine and purine N-[2-(2-phosphonomethoxy)ethyl] nucleoside analogues 1. Derivatives Substituted at the carbon atoms of the base. *J. Med. Chem.* 42, 2064–2086.
- Holý, A., Votruba, I., Tloustova, E., Masojdkova, M., 2001. Synthesis and cytostatic activity of N-[2-(Phosphonomethoxy)alkyl] derivatives of N⁶-substituted adenines 2,6-diaminopurines and related compounds. *Collect. Czech Chem. Commun.* 66, 1545–1592.

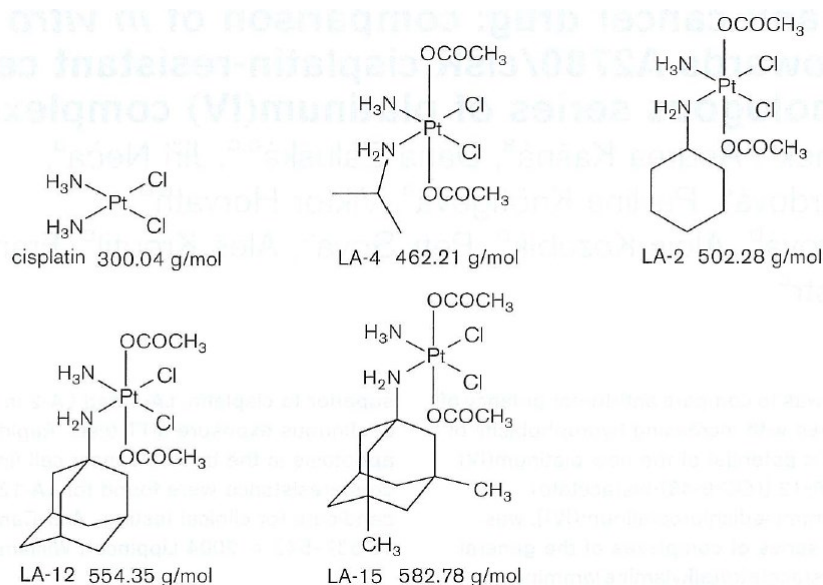
- Jansa, P., Kolman, V., Kostinova, A., Dracinsky, M., Mertlikova-Kaiserova, H., Janeba, Z., 2011. Efficient synthesis and biological properties of the 2'-trifluoromethyl analogues of acyclic nucleosides and acyclic nucleoside phosphonates. *Collect. Czech Chem. Commun.* 76, 1187–1198.
- Jansa, P., Baszczynski, O., Prochazkova, E., Dracinsky, M., Janeba, Z., 2012. Microwave-assisted hydrolysis of phosphonate diesters: an efficient protocol for the preparation of phosphonic acids. *Green Chem.* 14, 2282–2288.
- Kim, S.J., Kim, H.K., Han, Y.W., Aleyas, A.G., George, J.A., Yoon, H.A., Yoo, D.J., Kim, K., Eo, S.K., 2008. Multiple alternating immunizations with dna vaccine and replication incompetent adenovirus expressing gB of pseudorabies virus protect animals against lethal virus challenge. *J. Microbiol. Biotechnol.* 18, 1326–1334.
- Klupp, B.G., Granzow, H., Karger, A., Mettenleiter, T.C., 2005. Identification, subviral localization, and functional characterization of the pseudorabies virus UL17 protein. *J. Virol.* 79, 13442–13453.
- Klupp, B.G., Granzow, H., Mundt, E., Mettenleiter, T.C., 2001. Pseudorabies virus UL57 gene product is involved in secondary envelopment. *J. Virol.* 75, 8927–8936.
- Kong, H., Zhang, K., Liu, Y., Shang, Y., Wu, B., Liu, X., 2013. Attenuated live vaccine (Bartha-K16) caused pseudorabies (Aujeszky's disease) in sheep. *Vet. Res. Commun.* 37, 329–332.
- Korvasova, Z., Drasar, L., Masek, J., Turanek, J., Knotigova, P., Kulich, P., Matiasovic, J., Kovarik, K., Bartheldyova, E., Koudelka, S., Skrabalova, M., Miller, A.D., Holy, A., Ledvina, M., Turanek, J., 2012. Antiviral effect of HPMPC (Gidofvir®), entrapped in cationic liposomes: In vitro study on MDBK cell and BHV-1 virus. *J. Control Release* 160, 330–338.
- Kramer, T., Enquist, L.W., 2013. Directional spread of alphaherpesviruses in the nervous system. *Viruses* 5, 678–707.
- Kremerova, M., Jansa, P., Dracinsky, M., Sazelova, P., Kasicka, V., Neyts, J., Auwerx, J., Kiss, E., Goris, N., Stepan, G., Janeba, Z., 2013. 9-[2-(R)-(phosphonomethoxy)propyl]-2,6-diaminopurine (R)-PMPDAP and its prodrugs: optimized preparation, including identification of by-products formed, and antiviral evaluation in vitro. *Bioorg. Med. Chem.* 21, 1199–1208.
- Krishnan, B.R., 2000. Current status of DNA vaccines in veterinary medicine. *Adv. Drug Deliv. Rev.* 43, 3–11.
- Li, X., Turanek, J., Knotigova, P., Kudlackova, H., Masek, J., Pennington, D.B., Rankin, S.E., Knuton, B.L., Lehmler, H.J., 2008. Synthesis and biocompatibility evaluation of fluorinated: single-tailed glucopyranoside surfactants. *New J. Chem.* 32, 2169–2179.
- Li, X., Turanek, J., Knotigova, P., Kudlackova, H., Masek, J., Pennington, D.B., Rankin, S.E., Knuton, B.L., Lehmler, H.J., 2009. Hydrophobic tail length: degree of fluorination and headgroup stereochemistry are determinants of the biocompatibility of (fluorinated) carbohydrate surfactants. *Colloids Surf. B Biointerfaces* 73, 65–74.
- Ma, W., Kelly, M., Lager, K.M., Richt, J.A., Stoffregen, W.A., Zhou, F., Yoon, K.J., 2008. Development of real-time polymerase chain reaction assays for rapid detection and differentiation of wild-type pseudorabies and gene-deleted vaccine viruses. *J. Vet. Diagn. Invest.* 20, 440–447.
- McGeoch, D.J., Cook, S., 1994. Molecular phylogeny of the alphaherpesvirinae subfamily and a proposed evolutionary timescale. *J. Mol. Biol.* 22, 9–22.
- Olson, G.R., Miller, L.D., 1986. Studies on the pathogenesis of heart lesions in dogs infected with pseudorabies virus. *Can. J. Vet. Res.* 50, 245–250.
- Pancheva, S.N., 1991. Potentiating effect of ribavirin on the anti-herpes activity of acyclovir. *Antiviral Res.* 16, 151–161.
- Pomeranz, L.E., Reynolds, A.E., Hengartner, C.J., 2005. Molecular biology of pseudorabies virus: impact on neurovirology and veterinary medicine. *Microbiol. Mol. Biol. Rev.* 69, 462–500.
- Ren, X., Su, X., Yin, J., 2011. The effect of Houduanyia cordata injection on pseudorabies herpesvirus (Pv) infection in vitro. *Pharm. Biol.* 49, 161–166.
- Robbins, A.K., Whealy, M.E., Watson, R.J., Enquist, L.W., 1986. Pseudorabies virus gene encoding glycoprotein gIII is not essential for growth in tissue culture. *J. Virol.* 59, 635–645.
- Slana, I., Kaevska, M., Kralik, P., Horvathova, A., Pavlik, I., 2010. Distribution of *Mycobacterium avium* subsp. *avium* and M: a, hominis suis in artificially infected pigs studied by culture and IS901 and IS1245 quantitative real time PCR. *Vet. Microbiol.* 144, 437–443.
- Slana, I., Kralik, P., Kralova, A., Pavlik, I., 2008. On-farm spread of *Mycobacterium avium* subsp. *paratuberculosis* in raw milk studied by IS900 and F57 competitive real-time quantitative PCR and culture examination. *Int. J. Food Microbiol.* 128, 250–257.
- Sui, X., Yin, J., Ren, X., 2010. Antiviral effect of diammonium glycyrrhizinate and lithium chloride on cell infection by pseudorabies herpesvirus. *Antiviral Res.* 85, 346–353.
- Van Alstine, W., Anderson, T., Reed, D., Wheeler, J., 1984. Vaccine induced pseudorabies in lambs. *J. Am. Vet. Med. Assoc.* 185, 409–410.
- Van Rooij, E.M., Rijsewijk, F.A., Moonen-Leusen, H.W., Bianchi, A.T., Rziha, H.J., 2010. Comparison of different prime-boost regimes with DNA and recombinant Orf virus based vaccines expressing glycoprotein D of pseudorabies virus in pigs. *Vaccine* 28, 1808–1813.
- Williams, D.L., Robinson, J.C., Lay, E., Field, H., 2005. Efficacy of topical acyclovir for the treatment of feline herpetic keratitis: results of a prospective clinical trial and data from in vitro investigations. *Vet. Rec.* 157, 254–257.
- Wittmann, G., Jakubik, J., Ahd, R., 1980. Multiplication and distribution of Aujeszky's disease (pseudorabies) virus in vaccinated and non-vaccinated pigs after intranasal infection. *Arch. Virol.* 66, 227–240.
- Woodland, D.L., 2004. Jump-starting the immune system: prime-boosting comes of age. *Trends Immunol.* 25, 98–104.
- Yoon, H.A., Aleyas, A.G., George, J.A., Park, S.O., Han, Y.W., Kang, S.H., Cho, J.G., Eo, S.K., 2006. Differential segregation of protective immunity by encoded antigen in DNA vaccine against pseudorabies virus. *Immunol. Cell Biol.* 84, 502–511.
- Zhang, L., Zhong, C., Wang, J., Lu, Z., Liu, L., Yang, W., Iyuu, Y., 2015. Pathogenesis of natural and experimental pseudorabies virus infections in dogs. *Virus* 12, 44

2.2. LÁTKY ROZPUSTNÉ V NEPOLÁRNÍCH ROZPOUŠTĚDLECH (HYDROFOBNÍ, LIPOFILNÍ LÁTKY)

Tyto látky se v závislosti na svém koeficientu rozpustnosti (rozdělovacím koeficientu) oktanol/voda váží na jiné hydrofobní struktury (hydrofobní domény transportních proteinů, lipidní struktury v buňkách – membrány, tukové kapénky). Obecně se hromadí v tukových tkáních, pokud nejsou rychle metabolizovány a vyloučeny z těla. Z farmakologického hlediska je problém jejich malá rozpustnost a tendence tvořit agregáty nebo krystaly. Z hlediska lékové formy pro parenterální aplikace je nezbytné sledovat dva hlavní cíle: a) stabilní systém solubilizace farmaka, který brání tvorbě krystalů nebo agregátů; b) cílení farmaka do místa určení – v případě nádorů – pasivní nebo aktivní cílení pomocí nanopartikulární formulace a případně povrchové modifikace částic, která zajistí dlouhodobou cirkulaci v krevním řečišti, penetraci fenestracemi v endoteliální výstelce kapilár nádorové vaskulatury. Zde se opět uplatnily liposomy, jako vhodný systém pro přípravu nanopartikulárních nosičů lipofilních léčiv. Výzkum byl zaměřen na tři rozdílné typy lipofilních látek s protinádorovým účinkem.

2.2.1. Hydrofobní komplexy cis platiny

Protinádorová léčiva na bázi cisplatiny jsou nedílnou součástí celé řady protinádorových chemoterapeutických postupů. Bylo syntetizováno více než 1000 různých komplexů s cílem snížit vedlejší nežádoucí účinky a potlačit vznik rezistence nádorů na cisplatinu po opakované chemoterapii. Obecně přijímaným mechanismem působení cisplatinových cytostatik je poškození DNA a indukce apoptózy. Výzkum nových komplexů cisplatiny probíhal v rámci dlouhodobé spolupráce s podnikem Lachema, později Pliva-Lachema a.s. Byla navržena a připravena série komplexů cisplatiny v oxidačním čísle II a IV. Tyto komplexy se lišily svojí hydrofobicitou v závislosti na velikosti a struktuře uhlovodíkového ligandu. Strukturní vzorce platinových komplexů v oxidačním čísle IV jsou na následujícím obrázku.



Obr. 19 Cis-platina komplexy Pt IV se vzrůstající hydrofobicitou.

Studie cytotoxického účinku byly prováděny na více než šedesáti různých nádorových liniích a jejich resistantních variantách. Prokázali jsme, že hlavním faktorem cytotoxického účinku nového komplexu označovaného jako LA-12, je rychlá penetrace přes buněčnou membránu, jeho vysoká reaktivita s DNA a také thiolovými skupinami, obtížné opravení poškozené DNA buněčnými reparačními systémy a rychlé navození apoptózy. Podstatným zjištěním byla také zanedbatelná zkřížená rezistence vůči LA-12. Faktor rychlé penetrace přes buněčnou membránu se ukazoval jako klíčový pro rychlé navození apoptózy.

Látka LA-12 je však velmi málo rozpustná (50 μ g/ml) a tudíž nevhodná pro parenterální aplikaci. Solubilizace bylo dosaženo pomocí β -hydroxypropy-cyklodextrinu a tyto inkluzní komplexy byly také vhodné pro intravenózní aplikaci. Symetrická hydrofobní skupina adamantylového ligandu velmi dobře zapadne do hydrofobní kavity cyklodextrinu a tento inkluzní komplex je poměrně stabilní.

Pro formulaci LA-12 do liposomů se ukázala limitující právě snadná penetrace přes membrány, která omezovala stabilitu liposomálních preparátů spolu s reaktivitou samotné látky. LA-12 je tak názorným příkladem, jak lipofilní modifikace výrazně zvyšuje účinek farmaka. Na druhé straně je také příkladem typu látek, pro které je obtížné vyvinout liposomální formulaci.

2.2.1.1. Podané patentové přihlášky k tématu kapitoly

- Zak, F.; Mistr, A.; Poulouva, A.; Melka, M.; Turanek, J.; Zaluska, D. Platinum complex (II), its preparation and therapeutic application. PCT/CZ99/00014; US 6350737 B1(2002)
- Zak, F.; Mistr, A.; Poulouva, A.; Melka, M.; Turanek, J.; Zaluska, D. Platinum complex (II), its preparation and therapeutic application. PCT/CZ99/00014; EP 1082329 B1 (2003)
- Zak, F.; Mistr, A.; Poulouva, A.; Melka, M.; Turanek, J.; Zaluska, D. Platinum complex (IV), its preparation and therapeutic application. PCT/CZ1999/000015; US 6503943 B1 (2003)
- Zak, F.; Mistr, A.; Poulouva, A.; Melka, M.; Turanek, J.; Zaluska, D. Platinum complex (IV), its preparation and therapeutic application. PCT/CZ1999/000015; EP1082330B1 (2003)

Brief Articles

Platinum(IV) Complex with Adamantylamine as Nonleaving Amine Group: Synthesis, Characterization, and in Vitro Antitumor Activity against a Panel of Cisplatin-Resistant Cancer Cell Lines

František Žák,[†] Jaroslav Turánek,^{*†} Aleš Kroutil,[†] Petr Sova,[†] Adolf Mistr,[†] Anna Poullová,[†] Petr Mikolín,[†] Zdirad Žák,[§] Andrea Kašná,[†] Dana Záluská,^{†,‡} Jiří Neča,[†] Lenka Šindlerová,[§] and Alois Kozubík^{||}

PLIVA-Lachema a.s., Karásek 1, 621 33 Brno, Czech Republic; Department of Immunology, Veterinary Research Institute, Hudcova 70, 621 33 Brno, Czech Republic; Department of Inorganic Chemistry, Masaryk University, Kotlářská 2, 611 37 Brno, Czech Republic; and Institute of Biophysics, The Academy of Sciences of the Czech Republic, Královopolská 135, 61265 Brno, Czech Republic

Received March 31, 2003

Procedure of the synthesis is described for new platinum(IV) drug LA-12 [(OC-6–43)-bis(acetato)(1-adamantylamine)amminedichloroplatinum(IV)]. The X-ray diffraction analysis shows that the structure is created by molecules with octahedral arrangement of ligands around a platinum atom and contains one H₂O molecule that is not a part of the coordination sphere of platinum. This new drug is more reactive with glutathione than cisplatin and is lacking cross-resistance with cisplatin as proven on the panel of cancer cell lines.

Introduction

Clinical tests with cisplatin began in 1972, and this drug is included in the basic armament in antitumor chemotherapy. There are two major limitations of cisplatin in anticancer therapy. The first, it has serious adverse effects (nephrotoxicity, neurotoxicity, severe nausea and vomiting, ototoxicity) and second, many tumors exhibit resistance, either ab initio (e.g., non-small-cell lung cancer and colon cancer) or it is acquired during therapy (e.g., small-cell lung cancer or ovarian cancer).¹ The phenomenon of drug resistance is very complex, and little information is available on how disparate mechanisms are coordinated with each other.

The development of orally active platinum drugs led to synthesis of several compounds, some of which are in Phase II evaluation. The leading compound is Pt(IV) complex JM-216, [(OC-6–43)-bis(acetato)amminedichloro-(cyclohexylamine)platinum(IV)], which entered clinical testing in 1992.¹ We have synthesized a series of platinum complexes with bulky hydrophobic ligands. The platinum(IV) complex (OC-6–43)-bis(acetato)(1-adamantylamine)amminedichloroplatinum(IV) (Figure 1) expressed a rapid and high cytotoxic effect without cross-resistance to cisplatin, and the mode of synthesis was acceptable with respect to industrial manufacturing. Therefore, this compound was selected for the further evaluation.

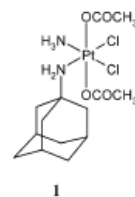
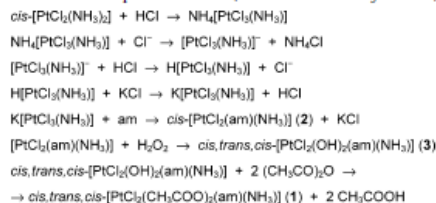


Figure 1. Structural formula of new anticancer platinum drug **1**.

Scheme 1. Preparation of **1** (am = 1-adamantylamine)

Results and Discussion

Chemistry. Scheme 1 shows the reactions involved in the synthesis of the tested substance (OC-6–43)-bis(acetato)(1-adamantylamine)amminedichloroplatinum(IV), coded as LA-12.

A complex with platinum (oxidation state II) was prepared from Cossa's salt and 1-adamantylamine. After purification, the complex was oxidized by a dilute solution of hydrogen peroxide at high temperature and consequently acetylated with acetic anhydride at ambient temperature. The final product was obtained as an

* Corresponding author: RNDr. Jaroslav Turánek, CSc., Veterinary Research Institute, Laboratory of Immunopharmacology and Immunotoxicology, Hudcova 70, 621 32 Brno, Czech Republic. Phone: +420 5 4132 1241, Fax: +420 5 4121 1229, e-mail: turanek@vri.cz.

[†] PLIVA-Lachema a.s.

[‡] Veterinary Research Institute.

[§] Masaryk University.

^{||} The Academy of Sciences of the Czech Republic.

anhydrous substance from a acetone–ether system and contains only one contaminant at a 0.25% level. The platinum complex was chromatographically pure (purity > 99.5%). The composition of **1** as determined by elemental analysis showed a good agreement between the theoretical and actual values.

The band assignment in IR spectroscopy was performed based on data from the literature² and is in accordance with possible vibrations of structural units in the complexes under study. The results of NMR measurements and their interpretations were compared with data from the literature regarding measurements of platinum complex JM-216.³ It enabled the assignment of the structure *cis,trans,cis*-[PtCl₂(CH₃COO)₂(C₁₀H₁₅NH₂)(NH₃)] to **1**.

The structure is formed by octahedral molecules, as expected, with a water molecule outside the coordination sphere of Pt. In the crystal structure, the molecules are arranged in layers with no apparent bonding between them. However, within one layer the molecules are bonded by a system of both intra- and intermolecular hydrogen bonds via NH₂ and H₂O hydrogens. The structure of **1** can be compared with (*OC*-6-43)-bis-(acetato)ammine-dichloro(cyclohexylamine)platinum(IV) (JM-216),⁴ both having the same coordination sphere around Pt atom. While the Pt–ligand distances for both compounds are the same within 3σ, there are some differences in corresponding interatomic angles. Generally, the angles in the coordination sphere of JM-216 tend to be more even, 86.7–94.3° and 174.7–178.3° as compared with **1**, 81.5–95.2° and 172.1–178.0°. The most apparent difference is in a mutual orientation of the acetato groups. In JM-216, the angle between the best planes through both acetato groups is 76.2° while in **1** these groups are almost eclipsed, the angle being 9.9°. The ammonia nitrogen is thus almost equidistant from both carbonyl oxygens which lead to much stronger intramolecular H-bonds between ammonia hydrogens and carbonyl oxygens in our structure. Corresponding donor–acceptor distances are 2.65(1) and 2.79(1) Å as compared with those in JM-216, 2.78(3) and 2.84(3) Å, respectively.

Biological Activities. Platinum complexes are known to react readily with sulfur ligands; hence, elevated cellular glutathione (GSH) may reduce the cytotoxicities of platinum drugs. However, the evidence for the involvement of GSH- and GSH-dependent enzymes in platinum drug resistance still remains equivocal. The role of GSH in modulating Pt(IV) drug cytotoxicity has not been investigated extensively.⁵

We have found **1** much more reactive toward glutathione than cisplatin. Velocity constants for pseudo-first order are in Supporting Information. This high reactivity is unique for **1** and was not found within the set of tested platinum(II) and (IV) drugs (e.g. oxaliplatin, JM-216, **2**) (unpublished results). The reason for this high reactivity is not clear at present, but we speculate that structure of water molecules surrounding the bulky hydrophobic symmetrical adamantylamine ligand can affect the reaction with glutathione and other thiols.

Antitumor Evaluation. We tested cytotoxicity of the new platinum complex **1** on a panel of cisplatin resistant cancer cell lines to find boundaries of cisplatin cross-resistance. Results and used cell lines are summarized

Table 1. Cytotoxicity of Pt Complexes against Cisplatin-Resistant Tumor Cell Lines (24 h continual exposure)

cancer cell line	IC ₅₀ (μM)	
	cisplatin	1
chronic myelogenous leukaemia K562	>80	3
chronic myelogenous leukaemia KG-1	48	2
acute myelogenous leukaemia ML-2	>80	1
mouse melanoma B16	>80	6
colon cancer HT-29N	>80	12
colon cancer HT29	50	8
colon cancer HCT116	>80	9
lung carcinoma A427	63	6
breast carcinoma HBL100	63	6
breast carcinoma MCF-7	71	8
lung carcinoma CORL23/CTR	>80	25
ovarian carcinoma A2780	4	4
ovarian carcinoma A2780/cis	40	3
ovarian carcinoma A2780/cis90	>80	7

in the Table 1. The cytotoxic effect of **1** is rapid and strong in comparison with cisplatin. Only lung large cell carcinoma cell line CORL23/CTR, which is cisplatin-resistant and slow-growing, demonstrated relatively a higher degree of resistance toward **1**, even if lower than toward cisplatin. High cytotoxic effect against leukaemic, melanoma, and colorectal cancer cell lines is promising for the perspective application in therapy of corresponding tumors.

Ovarian epithelial cancer cell line A2780 is a well described model for studies of the cisplatin resistance. The resistant sublines, prepared by gradual treatment with cisplatin, are available, and some mechanisms of resistance are described. **1** has proven also very low cross-resistance with cisplatin in both A2780/cis and A2780/cis90 sublines. In the case of A2780/cis90 subline we have seen some increase in IC₅₀ from 4 μM to 7 μM, but this is not a dramatic change when compared to cisplatin, where a 13-fold increase of IC₅₀ was observed (Table 1). There was no cisplatin cross-resistance with intermediate resistant A2780/cis. Interestingly, we have found substantial cross-resistance on the A2780 and A2780/cis90 pair of cell lines for JM-216 platinum(IV) complex (unpublished result) and cross-resistance was published also for another new generation platinum(II) complex ZD0473 [(*SP*-4-3)-amminedichloro(2-methylpyridine)platinum(II)] (Phase II 2002) on the A2780 and A2780/cis pair.⁶

We have also compared the effect of various exposure times on IC₅₀, because various protocols are used by researchers for estimating IC₅₀. Longer exposure time (72 or 96 h) is giving lower IC₅₀, but this value is inevitably affected by exhaustion of nutrients and growth factors from the medium. Short exposure time (24 h) can underestimate the cytostatic effect in slow-growing cell lines or cell lines with longer period required for induction of the executive phase of apoptosis. The sensitive A2780 cell line exerted a sudden drop of IC₅₀ for both tested drugs after 48 h incubation, and prolongation of incubation time to 72 h did not affect IC₅₀ significantly. It might be linked with reaching confluency after 48 h of incubation. In comparison with A2780 cells the A2780/cis cells were slower growing and no sudden decrease in IC₅₀ was observed. Cytostatic effect of LA-12 on the A2780/cis cell line was increasing during exposure time but remained in the same order of magnitude.

Conclusions

In summary, the synthesis of new platinum(IV) drug **1** [(OC-6-43)-bis(acetato)(1-adamantylamine)amminedichloroplatinum(IV)] with bulky hydrophobic ligand was developed. This new drug demonstrated high cytotoxic effect in cisplatin-resistant cancer cell lines and no cross-resistance with cisplatin was seen. Studies on physical-chemical features of **1** and their relations to high cytotoxicity toward cancer cell lines are central to our further investigations of platinum complexes with bulky hydrophobic ligands. Experiments are running to find cellular target and pathways leading the cancer cells to apoptosis after the exposure to this drug.

Experimental Section

Synthesis of Platinum Complexes. Synthesis of (OC-6-43)-Bis(acetato)(1-adamantylamine)amminedichloroplatinum(IV) (1). The Cossa's salt was prepared from cisplatin by method described by Oksanen.^{7,8}

The solution (8.72 g, 57.65 mmol) of 1-adamantylamine in 80 mL of ethanol was added under stirring to the filtered solution (20.0 g i.e., 54.56 mmol) of Cossa's salt. All operations with free amine were performed in inert atmosphere (predominantly nitrogenous). After 5 h of stirring at 50 °C and cooling of the reaction mixture to laboratory temperature, the insoluble fraction was separated, washed with ethanol, and dried. The filter cake was mixed with 200 mL of dimethylformamide (DMF) and then filtered. The crude product was precipitated from a yellow-orange filtrate with 760 mL of 0.5 M HCl, separated, and washed with diluted HCl of the above concentration and ethanol. After air-drying, the crude product was precipitated from the mentioned system DMF/0.5 M HCl as described above. The yield following drying in a vacuum dryer was 15.0 g (63.3%) of (SP-4-3)-(1-adamantylamine)amminedichloroplatinum(II) (**2**). Anal. (C₁₀H₂₀Cl₂N₂Pt) Then 14.0 g (32.24 mmol) of **2** was resuspended in 54.5 mL of water, and 40 mL of 30% H₂O₂ was added within 50 min. The system was maintained at a reaction temperature of 80 °C for another 50 min. After cooling to laboratory temperature, the crude product was separated, washed with water, and dried in a vacuum-dryer. This procedure was followed by extraction of impurities to DMF, separation of the solid fraction, and washing of the filter cake with DMF and acetone. After being dried in a vacuum dryer, 12.0 g (79.5%) of (OC-6-43)-(1-adamantylamine)amminedichlorodihydroxoplatinum(IV) (**3**) (anal. (C₁₀H₂₂Cl₂N₂O₂Pt)) was obtained. Then 10.8 g (23.06 mmol) of **3** was resuspended in 85 mL of acetic anhydride at laboratory temperature. The reaction mixture was stirred at dark for 48 h, and then the solid fraction was separated and washed with acetic anhydride and diethyl ether. After being dried in a vacuum dryer until a constant weight, 9.7 g (76.1%) of crude product **1** was obtained with 98.5% purity according

to HPLC. Purification consisted of the product extraction with methanol followed by recrystallization. It was performed by precipitation from an acetone-ether system with a yield 80%. Anal. (C₁₄H₂₆Cl₂N₂O₄Pt) C, H, N, Cl. IR (ν, cm⁻¹) 3450 (br), 3300 (w), 3175 (m), 3095 (m, br), 2900 (s), 2850 (w), 1660 (s), 1600 (s), 1370 (m), 1305 (s), 1280 (s), 707 (m). ¹H NMR (MeOD) δ 2.05 (s, CH₃, 6H), 2.04–2.03 (br, CH₂, 6H), 1.74–1.67 (m, CH₂, 6H), 2.08 (br, CH, 3H); ¹³C NMR (MeOD) δ 182.91 (C=O), 23.42 (CH₃), 59.10 (CNH₂), 42.07 (CH₂), 36.94 (CH₂), 31.13 (CH).

Acknowledgment. This work was supported by the Ministry of Industry and Trade of the Czech Republic, Contract No. PZ-Z2/29, "New Medicines for Cancer Therapy". Partial support was obtained from the Ministry of Agriculture, Contract No. M-03-99-01, and Grand Agency of Czech Republic, Contract No. 305/01/0418

Supporting Information Available: X-ray analysis of Pt(IV) complex, methods of in vitro anticancer evaluation, and inhibition curves. This material is available free of charge via the Internet at <http://pubs.acs.org>.

References

- (1) Kelland, L. R. The development of orally active platinum drugs. In *Cisplatin: Chemistry and Biochemistry of a Leading Anti-cancer Drug*; Lippert, B., Ed.; Wiley-VCH: Weinheim, Germany, 1999; pp 497–521.
- (2) Nakamoto, K. *Infrared and Raman Spectra of Inorganic and Organic Compounds*, 5th ed.; John Wiley & Sons: New York, 1977.
- (3) Barnard, Ch. F. J.; Vollano, J. F.; Chaloner, P.; Dewa, S. Z. Studies on the Oral Anticancer Drug JM-216: Synthesis and Characterization of Isomers and Related Complexes. *Inorg. Chem.* **1996**, *35*, 3280–3284.
- (4) Neidle, S.; Snook, Ch. F. Bis(acetato)amminedichloro(cyclohexylamine)platinum(IV), an orally active anticancer drug. *Acta Crystallogr.* **1995**, *C51*, 822–824.
- (5) Mistry, P.; Kelland, L. R.; Abel, G.; Sidhar, S.; Harrap, K. R. The relationships between glutathione, glutathione-S-transferase and cytotoxicity of platinum drugs and melphalan in eight human ovarian carcinoma cell lines. *Br. J. Cancer* **1991**, *64*, 215–220.
- (6) Rogers, P.; Boxall, F. E.; Allott, C. P.; Stephens, T. C.; Kelland, L. R. Sequence-dependent synergism between the new generation platinum agent ZD0473 and paclitaxel in cisplatin-sensitive and -resistant human ovarian carcinoma cell lines. *Eur. J. Cancer* **2002**, *38*, 1653–1660.
- (7) Oksanen, A.; Leskela, M. Synthesis of Ammonium Trichloroammineplatinate(II) Improved through Control of Temperature. *Acta Chim. Scand.* **1994**, *48*, 485–489.
- (8) Oksanen, A. A novel characterization of structure of 'Cossa's salt' K₂(NH₄)_{2-x}-[PtCl₂NH₃]-H₂O by crystallographic comparison with the stoichiometric compounds K[PtCl₂NH₃]-H₂O and NH₄[PtCl₂NH₃]-H₂O. *Inorg. Chim. Acta* **1997**, *260*, 53–60. JM030858+



New platinum(IV) complex with adamantylamine ligand as a promising anti-cancer drug: comparison of *in vitro* cytotoxic potential towards A2780/cisR cisplatin-resistant cell line within homologous series of platinum(IV) complexes

Jaroslav Turánek^a, Andrea Kašná^a, Dana Záluská^{a,c}, Jiří Neěa^a, Veronika Kvardová^a, Pavlína Knötigová^a, Viktor Horváth^b, Lenka Šindlerová^b, Alois Kozubík^b, Petr Sova^c, Aleš Kroutil^c, František Žák^c and Adolf Mistr^c

The aim of this study was to compare anti-tumor potency of platinum(IV) complexes with increasing hydrophobicity of their ligands. Cytotoxic potential of the new platinum(IV) complex, coded as LA-12 [(OC-6-43)-bis(acetato)(1-adamantylamine)amminedichloroplatinum(IV)], was compared within the series of complexes of the general formula (OC-6-43)-bis(acetato)(alkylamine)amminedichloroplatinum(IV). Alkylamine ligands with increasing hydrophobicity were: isopropylamine, cyclohexylamine, 1-adamantylamine and 3,5-dimethyl-1-adamantylamine. Particular platinum(IV) complexes were coded as LA-4, LA-2 (known as JM-216), LA-12 and LA-15, respectively. Cytotoxicity was tested with the microplate tetrazolium (MTT) assay on the panel of cancer cell lines and the results were verified by microscopy. HPLC was used to measure hydrophobicity, stability of complexes in various buffers and velocity constants for their reactivity with glutathione. Platinum(IV) complexes with bulky hydrophobic ligands (LA-12 and LA-15) demonstrated about one order higher velocity constant for pseudo-first-order reaction with glutathione in comparison to cisplatin, LA-4 and LA-2, whose velocity constants were close to those measured for cisplatin and related platinum(II) complexes. Cytotoxicities of LA-12 and LA-15 towards cisplatin-resistant epithelial carcinoma A2780/cisR were

superior to cisplatin, LA-4 and LA-2 in both 24- and 72-h continuous exposure MTT tests. Rapid induction of apoptosis in the treated cancer cell lines and no cisplatin cross-resistance were found for LA-12, which is a candidate for clinical testing. *Anti-Cancer Drugs* 15:000-000 © 2004 Lippincott Williams & Wilkins.

Anti-Cancer Drugs 2004, 15:000-000

Keywords: A2780, cancer cell line, cisplatin, glutathione, multidrug resistance, new platinum(IV) drug

^aVeterinary Research Institute, Department of Immunology, Hudcova 70, 621 33 Brno, Czech Republic, ^bInstitute of Biophysics, the Academy of Sciences of the Czech Republic, Královopolská 135, 61286 Brno, Czech Republic and ^cPLIVA-Lachema, Karásek 1, 621 33 Brno, Czech Republic.

Sponsorship: This work was supported by the Ministry of Industry and Trade of the Czech Republic, contract no. PZ-22/99 'New Medicines for Cancer Therapy'. Partial support was obtained from the Ministry of Agriculture, contract no. MO-03-99-01, and Grand Agency of Czech Republic, contract no. 305/01.0418.

Correspondence to: J Turánek, Veterinary Research Institute, Laboratory of Immunopharmacology and Immunotoxicology, Hudcova 70, 621 32 Brno, Czech Republic
Tel: +420 5 3333 1311; fax: +420 5 4121 1229;
e-mail: turanek@vri.cz

Received 16 December 2003 Revised form accepted 22 January 2004

Introduction

Many different analogs of cisplatin have been synthesized with the hope of reducing toxic side-effects to overcome multidrug resistance and to facilitate the preparation of a suitable formulation for application. About 1000 complexes have been studied in various laboratories so far, but only 10–20% of them turned out to be active against cancer cells in preclinical studies. A novel series of ammine/amine platinum(IV) dicarboxylate complexes represents the first class of complexes prepared as oral agents. Among them, JM216 [(OC-6-43)-bis(acetato)amminedichloro(cyclohexylamine)platinum(IV)] has been found to show significant antitumor activity via the oral route and now it is currently in phase II/III trials [1–3].

Preclinical *in vitro* studies of the new hydrophobic platinum(IV) complex (OC-6-43)-bis(acetato)(1-adamantylamine)amminedichloroplatinum(IV), coded as LA-12, showed that the complex is very efficient against many cancer cell lines resistant towards cisplatin [4] and its favorable *in vivo* toxicological profile is auspicious for human application.

To address some question on the effect of the hydrophobic ligand on the cytotoxicity of platinum(IV) complexes, their stability in various media and reactivity towards biological thiols, we have prepared platinum(IV) complexes forming a homologous series with respect to hydrophobicity and bulkiness of ligands.

Materials and methods

Chemicals

Cisplatin [CDDP, (SP-4-2)-diamminedichloroplatinum(II)].

JM-216 [(OC-6-43)-bis(acetato)amminedichloro(cyclohexylamine)platinum(IV)], coded in this article as LA-2.

LA-4 [(OC-6-43)-bis(acetato)amminedichloro(isopropylamine)platinum(IV)].

LA-12 [(OC-6-43)-bis(acetato)(1-adamantylamine)amminedichloroplatinum(IV)].

LA-15 [(OC-6-43)-bis(acetato)(3,5-dimethyl-1-adamantylamine)amminedichloroplatinum(IV)].

The platinum(IV) complexes were synthesized and kindly donated by PLIVA-Lachema (Brno, Czech Republic). The structural formulae are shown in Figure 1.

MTT-based cytotoxicity test

We used the microplate tetrazolium (MTT) assay [5,6] to measure the cytotoxicity of the tested drugs in cells in exponential growth phase. The cells were seeded on 96-well flat-bottom microplates at densities of $2.5\text{--}3.0 \times 10^4/\text{ml}$, $100\ \mu\text{l}/\text{well}$, and let to grow for 16–24 h in culture medium (RPMI supplemented with 10% fetal calf serum). The drugs dissolved in phosphate-buffered saline (PBS) (total volume $20\ \mu\text{l}$) were added to wells and the cytotoxic effect was evaluated after 24 and 72 h of exposure to the concentration range $0.3\text{--}160\ \mu\text{M}$.

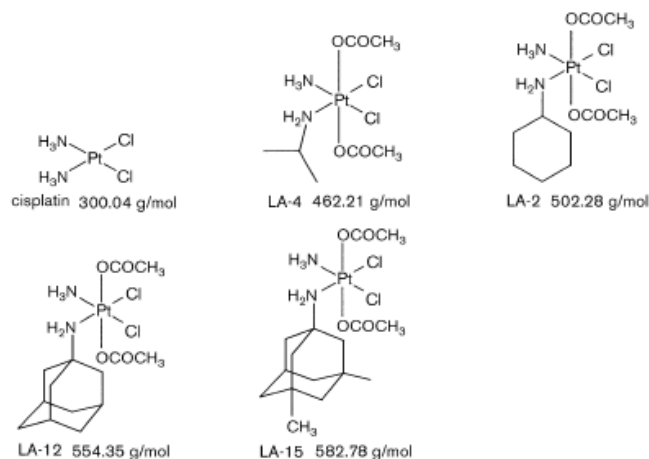
MTT (Sigma, Czech Republic) was dissolved in PBS at a concentration of $5\ \text{mg}/\text{ml}$ and sterilized by filtration.

MTT solution was added into all wells of 96-well flat-bottom microplates with cells at a dose of $20\ \mu\text{l}/\text{well}$. The plates were incubated at 37°C and $5\% \text{CO}_2$ for 3 h. To enhance the dissolution of dark-purple crystals of formazan, $110\ \mu\text{l}$ of 10% SDS in PBS (final pH 5.5) was added to all wells. The microtiter plates were stored in a light-tight box at room temperature and evaluated the next day using the micro-plate reader iEMS (Labsystem, Finland) at $540\ \text{nm}$. All experiments were performed in triplicates.

Cancer cell lines

Cancer cell lines having $\text{IC}_{50} \geq 40\ \mu\text{M}$ (for cisplatin, 24 h continual exposure) were selected from the panel of cancer cell lines tested in our laboratory and were used for the study of cross-resistance. Highly resistant A2780/cis90 ($\text{IC}_{50} \sim 90\ \mu\text{M}$ for cisplatin, 24 h exposure) was established from A2780/cis ($\text{IC}_{50} \sim 40\ \mu\text{M}$ for cisplatin) during 15 months by cultivation in medium with increasing concentrations of cisplatin ($1\text{--}12\ \mu\text{M}$). HBL100, MCF-7 (breast carcinoma and adenocarcinoma), HT-29, HT-29N and HCT-116 (colon carcinoma and adenocarcinoma) were obtained from the Masaryk Memorial Institute of Oncology (Brno). K-562 (chronic myelogenous leukemia), KG-1 (chronic myelogenous leukemia), ML-2 (acute myelogenous leukemia) and B16 (mouse melanoma) were obtained from the Institute of Hematology and Blood Transfusion, Prague. A427, CORL23/CTR (cisplatin resistant) (lung large cell

Fig. 1



Structural formulae of the tested platinum complexes.

carcinoma), A2780, A2780/cis (ovarian carcinoma) were purchased from ECACC.

The cell lines were grown in RPMI 1640 medium (Sigma) supplemented with 10% fetal calf serum (Gibco, Czech Republic), 50 µg/ml penicillin, 50 µg/ml streptomycin, 100 µg/ml neomycin and 300 µg/ml L-glutamine. A2780 cell line and its cisplatin resistant sublines were cultivated in RPMI 1640 medium supplemented with insulin (40 IU/100 ml of medium).

The cytotoxicity of LA-12 against cancer cell lines was examined by the MTT test, and the results were confirmed by Hoffman modulation contrast and fluorescent microscopy (epifluorescent inverted microscope T200; Nikon, Japan) exposing morphological changes of the cells treated with platinum complexes. Propidium iodide and YO-PRO-1 (Molecular Probes, Eugene, OR) were used to distinguish dead or apoptotic cells from vital living ones [7].

Reactivity with glutathione

Reactivity of platinum complexes with glutathione was determined as a velocity constant for the pseudo-first-order reaction at pH 7.5 (20 mM sodium phosphate, 150 mM NaCl), 37 °C, 1 mM glutathione. Concentration of platinum complex in reaction mixture was 10 µM. Samples of reaction mixture were analyzed by HPLC and reaction was monitored in 30-min intervals for 3 h. Cisplatin was analyzed on the column Zorbax NH₂, 25 cm × 4.6 mm. Mobile phase: 90% methanol, 10% water; flow rate 1 ml/min; 25 °C. Chromatographic conditions for analysis of LA-2, LA-4, LA-12 and LA-15 are described in the following section. Reaction conditions were chosen to approximate the *in vivo* conditions with respect to reactant concentrations, pH and ions.

Hydrophobicity of platinum complexes

Hydrophobicity of platinum complexes was estimated by HPLC and expressed as the capacity factor *k* for each complex. Chromatographic separations were run on the column ABZ plus Supelcosil LC-18-S, 150 × 3 mm, 5 µm (Supelco, Prague, Czech Republic). Mobile phase: 40% methanol in water. Flow rate: 0.5 ml/min. Temperature: 40 °C. Detection: UV 210 nm. Instrument: Waters chromatographic system consisting of the Waters 600 gradient pump, the Waters 717 plus autoinjector and the Waters 996 diode array detector. The system was controlled by the programme Millennium 2010. Mobile phase: methanol with water in the ratio 41:59 (v/w), flow rate 0.7 ml/min, room temperature, detection at 206 nm.

Stability of platinum complexes in various media

Stability of platinum(IV) complexes LA-4, LA-2, LA-12 and LA-15 (10 µM) was tested after 24 h incubation in various media at pH 7.2, 37 °C (Media: 50 mM sodium

phosphate buffer, pH 7.2, 50 mM Tris-HCl, pH 7.2, PBS, pH 7.2). The contents of platinum(IV) complexes were analyzed by HPLC and expressed as a percentage of the original concentration.

Statistics

Survival curves, IC₅₀ and velocity constants were calculated by the programme GraphPad Prism, version 3.03. (GraphPad Software, San Diego, CA).

Results

Hydrophobicity of platinum complexes

Hydrophobicities of platinum complexes were measured to get a better insight into the effect of the hydrophobic ligand on the ability of various drugs to penetrate through the cell membrane. Hydrophobicity of platinum complexes was estimated by HPLC and expressed as the capacity factor *k'* for each complex. This method is sensitive and relatively simple to allow comparison of various ligands with respect to their contribution to the overall hydrophobicity of various platinum complexes within the homologous set. The expected hydrophobicities of platinum complexes based on their structural formulae are in a good agreement with the capacity factor *k* calculated from chromatographic data (Fig. 1 and Table 1).

Stability of platinum complexes in various media

The platinum complexes lose their chloride ligands in media containing low concentrations of chloride to form positively charged monoqua and diaqua species which migrate much faster on chromatographic reverse phase column. The comparison within the set of platinum(IV) complexes showed that there were no substantial differences among them with regard to stabilities in media with both low and high chloride contents (50 mM phosphate buffer versus PBS). Stabilities in PBS were somewhat higher, as expected. Replacement of chloride by water in the platinum(IV) complexes was more rapid in Tris-HCl buffer in comparison to phosphate buffer. Results are summarized in Table 2.

Reactivity of platinum complexes with glutathione

Platinum(IV) complexes LA-12 and LA-15 with bulky hydrophobic adamantylamine or 3,5-dimethyl-1-adamantylamine ligands exerted about one order higher velocity constant for the pseudo-first-order reaction with glu-

Table 1 Hydrophobicity of platinum complexes expressed as capacity factor *k*

Platinum complex	Capacity factor <i>k'</i>
Cisplatin	0.00
LA-4	0.41
LA-2	2.30
LA-12	9.54
LA-15	40.95

Table 2 Stability of platinum(IV) complexes LA-4, LA-2, LA-12 and LA-15 after 24 h incubation in various media at pH 7.2, 37°C

Medium	Platinum(IV) complex (% of original content)			
	LA-4	LA-2	LA-12	LA-15
Phosphate buffer	86.1	88.3	83.0	81.4
TRIS	71.1	72.7	72.0	71.3
PBS	88.3	92.3	88.4	93.3

Media: 50 mM sodium phosphate buffer, pH 7.2, 50 mM Tris-HCl, pH 7.2, PBS, pH 7.2.

Table 3 Velocity constants for the pseudo-first-order reaction of platinum drugs with glutathione

Platinum drug	Velocity constant (s ⁻¹)
Cisplatin	3.23×10^{-5}
LA-4	2.20×10^{-5}
LA-2	2.56×10^{-5}
LA-12	3.28×10^{-4}
LA-15	3.53×10^{-4}

Velocity constant for the pseudo-first-order reaction at pH 7.5 (20 mM sodium phosphate, 150 mM NaCl), 37°C, 1 mM glutathione. Concentration of platinum complexes in reaction mixture was 10 µM.

Table 4 Effect of pH on the velocity constants for pseudo first order reaction of LA-12 complex with glutathione

	pH	
	6.5	7.5
$k (\times 10^{-4} \text{ s}^{-1})$	1.37	3.28

Velocity constant for the pseudo-first-order reaction at pH 6.5 and 7.5 (20 mM sodium phosphate, 150 mM NaCl), 37°C, 1 mM glutathione. Concentration of platinum complexes in reaction mixture was 10 µM.

tathione in comparison to cisplatin, LA-4 and LA-2. Results are shown in Table 3. The values of velocity constants for cisplatin, LA-4 and LA-2 were very close to those ones measured for platinum(II) complexes related, with respect to the same alkylamine ligands, to LA-2, LA-4, LA-12 and LA-15 (results not shown). Reactivity of LA-12 was studied at pH 6.5 and 7.5 to get experimental evidence on higher reactivity of S^- in comparison to SH function in glutathione. The obtained data (Table 4) supported the view that S^- is more efficient than SH with respect to nucleophilic attack of the central platinum atom.

Antitumor evaluation

We tested cytotoxicities of a new platinum complex LA-12 on the panel of cisplatin-resistant cancer cell lines to find the boundaries of cisplatin cross-resistance. Cytostatic effects of LA-12 after 24 h exposure were compared with those of cisplatin and LA-2, which represent drugs of clinical relevance or drug in clinical trials, respectively. Results are summarized in Table 5. The cytotoxic effect of LA-12 on cisplatin-resistant cell lines is rapid and strong in comparison to cisplatin and LA-2. Lung large

Table 5 Cytotoxicity of cisplatin, LA-2 and LA-12 platinum complexes against cisplatin-resistant tumor cell lines

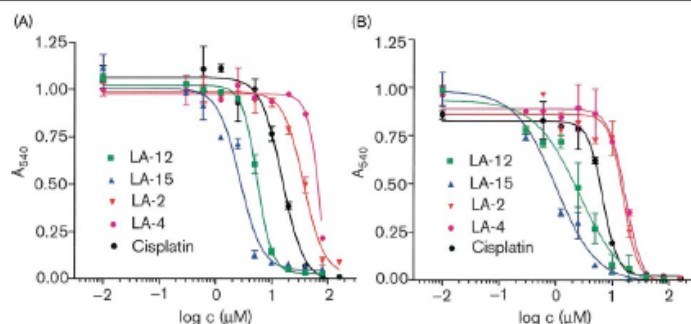
Cancer cell lines	IC50 (µM)		
	Cisplatin	LA-12	LA-2
K562	>80	3	63
KG-1	48	2	63
ML-2	>80	1	56
B16	>80	6	>80
HT29N	>80	12	>80
HT29	50	8	70
HCT116	>80	9	>80
A427	63	6	13
HBL100	63	6	>80
MCF7	71	8	70
CORL23/CTR	>80	25	56
A2780	9	6	37
A2780cis40	40	3	39
A2780cis90	>80	5	34

IC₅₀ was calculated for 24 h exposure time.

cells carcinoma cell line CORL23/CTR, which is cisplatin resistant and slow growing, showed the highest degree of resistance towards LA-12, even if lower than towards both compared drugs. A427 (cisplatin-resistant lung large cell carcinoma) was the only cell line sensitive to LA-2 in a 24-h exposure test. LA-12 did not demonstrate cisplatin cross-resistance within the series of A2780 cell sublines (Table 5). The cisplatin-resistant A2780 sublines represent the types of cisplatin-resistant cells in which several mechanisms of resistance are well balanced; hence, we have used these cell lines to compare the cytostatic effect of various platinum(IV) complexes. Both short continuous exposure (24 h) and long continuous exposure (72 h) were used to compare cytostatic effects of various platinum(IV) complexes. Cisplatin non-resistant parent epithelial ovarian carcinoma cell line A2780 demonstrated high sensitivity towards LA-12 and LA-15. Surprisingly, LA-2 and LA-4 were not as effective as cisplatin in both 24- and 72-h exposure experiments. The difference in cytotoxicity between LA-2 and LA-4 became negligible after 72 h exposure. Dose-response curves are shown in Figure 2.

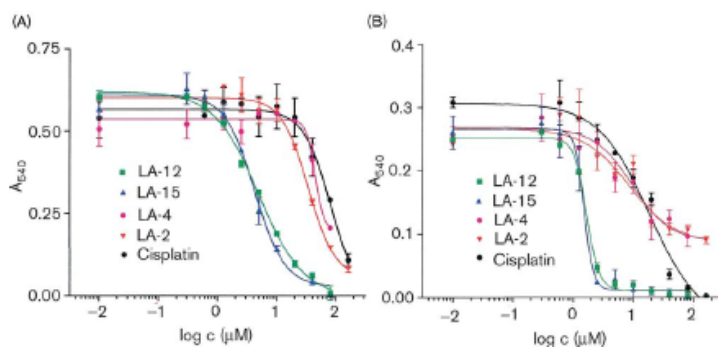
The cisplatin high-resistant cell line A2780/cis90 did not demonstrate substantial differences in sensitivity towards platinum(IV) complexes in comparison with the cisplatin-sensitive A2780 parental cell line. A great difference was only seen in the sensitivity towards cisplatin. It was found for both the cisplatin-sensitive A2780 parental cell line and the high-resistant cell line A2780/cis90 cell subline, that within the series of the tested platinum(IV) complexes the cytotoxic effect was in direct proportion to their hydrophobicity. In contrast to LA-12, LA-15 and cisplatin, both LA-4 and LA-2 did not prevent a substantial fraction of A2780/cis90 cells from survival after 72 h exposure (Fig. 3). Results obtained by the MTT assay were confirmed by microscopy (results not shown).

Fig. 2



Dose-response cytotoxicity curves for the cisplatin-sensitive ovarian epithelial carcinoma A2780 cell line treated with various platinum(IV) complexes and cisplatin. (A) Continual exposure to various complexes for 24 h. (B) LA-12 (IC_{50} 5.5 μ M), LA-15 (IC_{50} 2.7 μ M), LA-2 (IC_{50} 36.6 μ M), LA-4 (IC_{50} 67.9 μ M) and cisplatin (IC_{50} 8.7 μ M). (C) Continual exposure to various complexes for 72 h. (D) LA-12 (IC_{50} 2.6 μ M), LA-15 (IC_{50} 1.0 μ M), LA-2 (IC_{50} 15.6 μ M), LA-4 (IC_{50} 12.2 μ M) and cisplatin (IC_{50} 6.9 μ M).

Fig. 3



Dose-response cytotoxicity curves for the cisplatin-resistant ovarian epithelial carcinoma A2780/cis90 cell line treated with various platinum(IV) complexes and cisplatin. (A) Continual exposure to various complexes for 24 h. (B) LA-12 (IC_{50} 4.7 μ M), LA-15 (IC_{50} 4.2 μ M), LA-2 (IC_{50} 33.9 μ M), LA-4 (IC_{50} 65.0 μ M) and cisplatin (IC_{50} 83.8 μ M). (C) Continual exposure to various complexes for 72 h. (D) LA-12 (IC_{50} 1.2 μ M), LA-2 (IC_{50} 19.4 μ M), LA-4 (IC_{50} 18.3 μ M) and cisplatin (IC_{50} 18.4 μ M).

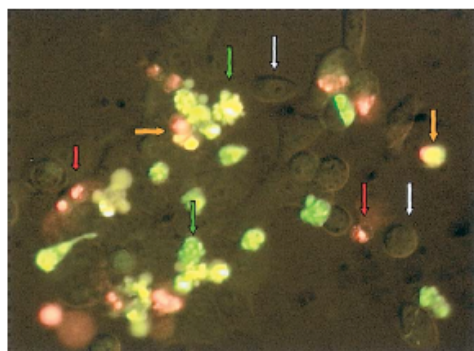
Morphological changes of cancer cell lines after treatment by platinum complexes were observed by fluorescent microscopy. Well-developed morphological symptoms of apoptosis, such as a forming of blebs and increased permeability of the cell membrane to YO-PRO-1, were seen in dying cells. Photographs of apoptotic HCT-116 cells are presented in Figure 4.

Discussion

With various platinum(II) complexes, an increase in ligand hydrophobicity is positively correlated with an

increase of cytotoxic effects due to enhanced penetration of particular platinum complexes via non-specific diffusion to the cancer cells [8]. We have obtained a similar correlation within the set of platinum(IV) complexes for both cisplatin-sensitive and -resistant A2780 cancer cell lines. However, mere correlation between hydrophobicity and cytotoxic effects of platinum drugs is a simplification which does not take into account possible specific interactions of ligands with cellular structures, especially with the proteins involved in recognition and repair of platinum-DNA adducts. The hydrophobic character and

Fig. 4



Morphology of HCT116 exposed to 10 μ M LA-12 for 4 h. Various stages of apoptotic cells were stained by YO-PRO-1 (green arrows). Well-developed blebs and apoptotic bodies are apparent. Dead cells are stained red by propidium iodide (secondary necrosis) (red arrows). Vital cells (white arrows) are not stained and remain adherent. The cells in the transition phase between apoptosis and secondary necrosis are stained by both dyes (orange arrows).

the structure of a particular ligand inevitably influences the structure of the molecules of water solvating the hydrophobic platinum complex. Differences in the structure of the water coat could be responsible for different reactivities of platinum(IV) complexes with glutathione. Approximately one order higher reactivity of LA-12 and LA-15 with glutathione, in comparison to cisplatin, LA-2, LA-4 and other related platinum(II) complexes (results not shown), represents data pointing to the relevancy of the water coat to the reactivity of platinum complexes. The comparison of X-ray crystallographic data showed only minor differences between LA-12 and LA-2 (JM216) with respect to the bond length and angles [4]. However, the geometry of solvated complexes in the water environment may be different from those seen by X-ray crystallography.

Octahedral platinum(IV) complexes undergo ligand substitution reactions that are slow compared to those of their platinum(II) analogs and have been considered as the compounds which are unable to react directly with DNA [9,10]. It was shown that reactivity of hydroxoplatinum(IV) complexes with glutathione is low in comparison with chloroplatinum(IV) complexes [11]. Because the hydrophobic ligands did not change the velocity of the chloride substitution reaction in platinum(IV) complexes, as seen from the results on their stability after 24 h incubation in various media at pH 7.2, 37°C (Table 2), the differences in reactivity with glutathione were not related to the different stability of chloroplatinum(IV) complexes.

The anti-tumor activity of platinum(IV) compounds has been suggested to require *in vivo* reduction to the kinetically more labile, and therefore reactive, platinum(II) derivatives [17,18]. The presence of reduced glutathione is required for the reaction of tetraplatin with DNA *in vitro*. It was postulated that platinum(IV) complexes are activated intracellularly by glutathione or other intracellular reducing agents [11,12]. On the other hand, there is evidence that platinum(IV) species can enter cells and react with DNA [10]. With respect to involvement of glutathione in activation of platinum(IV) complexes, the role of glutathione in the resistance of cancer cells towards cisplatin-based drugs is equivocal, and results based on a simple correlation between intracellular level of glutathione and cytotoxicity are misleading. A more significant role of glutathione is linked with an organic anion pump, multidrug resistance protein (MRP), which could be involved in cisplatin resistance. High expression of MRP2 was found in the A2780/cis70 cell line together with increased levels of glutathione, whose conjugates are the substrates for this ATP-driven pump [9]. The ovarian epithelial carcinoma cell line A2780 and the cisplatin-resistant A2780/cis90 subline represent the types of cisplatin-resistant cells in which several mechanism of resistance are well coordinated [9]. Cisplatin-resistant A2780/cis70 cells demonstrated enhanced efflux as compared to parent A2780 cells [13]. In spite of that, cytotoxic effects of LA-12 and LA-15 towards cisplatin-resistant A2780/cis90 cells were strong and rapid. It can be explained by rapid penetration through the cell membrane, activation by glutathione and interaction with DNA. Rapid induction of apoptosis, when the first morphological changes were seen after 3–4 h of incubation (Fig. 4), implicates that LA-12 and LA-15 can activate pro-apoptotic pathways immediately after entering the cell and forming DNA adducts. Such a rapid onset of apoptosis in treated cells can avoid the replication bypass.

In conclusion, the phenomenon of drug resistance is very complex and little information is available on how disparate mechanisms are coordinated with each other. Resistance to cisplatin is multifactorial and in general it may consist of mechanisms either limiting the formation of DNA adducts and/or increasing the tolerance of DNA adducts. It has been shown that the tolerance to cisplatin-induced damage of DNA was the fundamental mechanism which caused increased cisplatin resistance in some ovarian carcinoma cell lines. Resistance towards cisplatin displayed by the cisplatin-resistant A2780 cell subline could not be solely explained by enhanced repair of the lesions, but was more likely related to some mechanisms of damage tolerance [14–16]. Both signaling and executive mechanisms of apoptosis can be suppressed in cisplatin-resistant cancer cells to induce the tolerance towards DNA damage. LA-12 proved to be very

cytotoxic in the 24-h MTT test against various cancer cells representing different types of cancer and employing different mechanisms of cisplatin-resistance towards cisplatin (Table 5). The strong cytotoxic effect is relevant to the presence of bulky hydrophobic ligands in the platinum(IV) complex. Further studies on the mechanism of cytotoxic effects of LA-12 are focused on its interaction with DNA, the DNA repair system and apoptotic pathways. Highly cytotoxic effects against leukemic, melanoma and colorectal cancer cell lines is promising for the prospective application of the therapy of the corresponding tumors.

References

- Kelland LR. The development of orally active platinum drugs. In: Lippert B (editor): *Cisplatin: Chemistry and Biochemistry of a Leading Anticancer Drug*. Wiley-VCH: Weinheim; 1999, pp. 497–521.
- Kelland LR, Murer BA, Abel G, Gandomenico CM, Mistry P, Harap KR. Ammine/amine platinum(IV) dicarboxylates: a novel class of platinum complex exhibiting selective cytotoxicity to intrinsically cisplatin-resistant human ovarian carcinoma cell lines. *Cancer Res* 1992; **52**:822–828.
- Neidke S, Snook CHF. Bis(acetato)amminedichloro(cyclohexylamine) platinum(IV), an orally active anticancer drug. *Acta Crystallogr* 1995; **51**:822–824.
- Žák F, Turánek J, Kroužil A, Šova P, Mistr A, Poulková A, et al. Platinum(IV) complex with adamantylamine as non-leaving amine group: synthesis, characterization, and *in vitro* antitumour activity against the panel of cisplatin resistant cancer cell lines. *J Med Chem*; in press.
- Mosmann T. Rapid colorimetric assay for cellular growth and survival: application for proliferation and cytotoxicity assays. *J Immunol Methods* 1983; **65**:55–63.
- Bank U, Reinhold D, Ansoorge S. Measurement of cellular activity by means of the MTT-test. *Allegy Immunol* 1991; **37**:119–123.
- Idzorek T, Estaquier J, De Bols F, Ameisen J-C. YO-PRO-1 permits cytofluorometric analysis of programmed cell death (apoptosis) without interfering with cell viability. *J Immunol Methods* 1995; **185**:249–258.
- Moeller N, Kangroo BS, Puscasu I, Mock Ch, Krebs B, Wolff JEA. Rational design of platinum chemotherapeutic drugs: hydrophobicity increases cytotoxicity. *Anticancer Res* 2000; **20**:4435–4440.
- Fery KV, Hamilton TC, Johnson SW. Increased nucleotide excision repair in cisplatin-resistant ovarian cancer cells. *Biochem Pharmacol* 2000; **60**:1305–1313.
- Erabec V. DNA modification by antitumor platinum and ruthenium compounds: their recognition and repair. *Prog Nucleic Acid Res Mol Biol* 2002; **71**:1–68.
- Raynaud R, Boxall FE, Goddard P, Barnard ChF, Burrell BA, Kelland LR. Metabolism, protein binding and *in vivo* activity of the oral platinum drug JM216 and its biotransformation products. *Anticancer Res* 1996; **16**:1857–1862.
- Eastman A. Glutathione mediated activation of anticancer platinum(IV) complexes. *Biochem Pharmacol* 1987; **30**:4177–4178.
- Kool M, de Haas M, Sheffer G L, Scheper R J, van Eijk MJT, Juijn JA, et al. Analysis of expression of cMOAT (MRP2), MRP3, MRP4 and MRPS, homologues of the multidrug resistance-associated protein gene (MRP1), in human cancer cell lines. *Cancer Res* 1997; **57**:3537–3547.
- Johnson SW, Laub PB, Breesley JS, Ozols RF, Hamilton TC. Increased platinum–DNA damage tolerance is associated with cisplatin resistance and cross-resistance to various chemotherapeutic agents in unrelated human ovarian cancer cell lines. *Cancer Res* 1997; **57**:850–856.
- Henkels KM, Turchi JJ. Induction of apoptosis in cisplatin-sensitive and -resistant human ovarian cancer cell lines. *Cancer Res* 1997; **57**:4488–4492.
- Johnson SW, Swiggard PA, Handel LM, Brennan JM, Godwin AK, Ozols RF, et al. Relationship between platinum–DNA adduct formation and removal and cisplatin cytotoxicity in cisplatin-sensitive and cisplatin resistant human ovarian-cancer cells. *Cancer Res* 1994; **54**:5911–5916.



High effectiveness of platinum(IV) complex with adamantylamine in overcoming resistance to cisplatin and suppressing proliferation of ovarian cancer cells in vitro

Alois Kozubík^{a,*}, Viktor Horváth^{a,b,1}, Lenka Švihálková-Šindlerová^{a,c,1},
Karel Souček^a, Jiřina Hofmanová^a, Petr Sova^d, Aleš Kroutil^d,
František Žák^d, Adolf Mistr^d, Jaroslav Turánek^e

^aLaboratory of Cytokinetics, Institute of Biophysics, Academy of Sciences of the Czech Republic, Královopolská 135, 61265 Brno, Czech Republic

^bDepartment of Comparative Animal Physiology and General Zoology, Faculty of Science, Masaryk University, Kotlářská 2, 61137 Brno, Czech Republic

^cResearch Centre for Environmental Chemistry and Ecotoxicology, Faculty of Science, Masaryk University, Kamenice 126/3, 62500 Brno, Czech Republic

^dPLIVA – Lachema a.s., Karásek 1, 62133 Brno, Czech Republic

^eDepartment of Immunology, Veterinary Research Institute, Hudcova 70, 62132 Brno, Czech Republic

Received 26 July 2004; accepted 10 September 2004

Abstract

[(OC-6-43)-bis(acetato)(1-adamantylamine)amminedichloroplatinum(IV)], coded as LA-12, is an octahedral platinum(IV) complex containing a bulky hydrophobic ligand – adamantylamine. The use of bulky hydrophobic amines as non-leaving ligands, may increase uptake of the compound by the cancer cells. Therefore, the effects of LA-12 on sensitive (A2780) and cisplatin resistant (A2780cis) ovarian cancer cell lines were investigated and compared to those of cisplatin. IC₅₀ and IC₉₀ concentrations of LA-12 were 6- (A2780) or 18-fold (A2780cis) lower than those for cisplatin (MTT assay). Equitoxic concentrations (IC₅₀ or IC₉₀) of both compounds caused a significant and similar time- and dose-dependent inhibition of cell proliferation and an increase in the number of floating cells which corresponded to the decrease of total cell viability. A different type and dynamics of cell cycle perturbation after cisplatin and LA-12 treatment were detected. Exposure to LA-12 resulted in transient accumulation of A2780 and A2780cis cells in S phase, while cisplatin caused G₂/M arrest in sensitive and S phase arrest in resistant cells. A relatively low rate of apoptosis after exposure to IC₅₀ or IC₉₀ of both complexes was observed, markedly higher in resistant A2780cis cells. Western blot analysis indicated a concentration-dependent p53 level increase in both lines (higher after cisplatin treatment). PARP cleavage was observed only in A2780cis cells. In conclusion, LA-12 was found to be significantly more efficient than cisplatin, and it was able to overcome the acquired cisplatin resistance (showing resistance factor 2.84-fold lower than those for cisplatin). In spite of the low rate of apoptosis, LA-12 caused increase of p53 level and cell cycle perturbations in the ovarian cancer cell lines studied.

© 2004 Elsevier Inc. All rights reserved.

Keywords: Cisplatin; LA-12; Cytotoxicity; Cell cycle perturbations; Apoptosis; Ovarian cancer

Abbreviations: cis-DDP, cis-diamminedichloroplatinum(II); LA-12, (OC-6-43)-bis(acetato)(1-adamantylamine)amminedichloroplatinum(IV); JM216, (OC-6-43)-bis(acetato)amminechloro(cyclohexylamine)platinum(IV); cisplatin (50 or 90), LA-12 (50 or 90), IC₅₀ or IC₉₀ drug concentrations that cause 50% or 90% inhibition of cell proliferation; Pt(II), planar and four coordinate platinum complex; Pt(IV), octahedral and six coordinate platinum complex; PI, propidium iodide; MTT, 3-(4,5-dimethylthiazol-2-yl)-2,5-diphenyltetrazolium bromide; DAPI, 4,6-diamidino-2-phenyl-indole dihydrochloride; DABCO, 1,4-diazabicyclo-[2.2.2]octane; PARP, poly(ADP-ribose)polymerase; HRP, horseradish peroxidase; PAGE, polyacrylamide gel electrophoresis

* Corresponding author. Tel.: +420 5 41517182; fax: +420 5 41211293.

E-mail address: kozubik@ibp.cz (A. Kozubík).

¹ The contributions by these authors should be considered equal.

1. Introduction

Cisplatin [*cis*-diamminedichloroplatinum(II)] (Fig. 1) is currently one of the three most widely utilized antitumour drugs, with high efficiency in treating testicular and ovarian cancers [1,2]. Despite its strong antitumour activity, cisplatin therapy can lead to a number of side effects such as nephrotoxicity, neurotoxicity, and emesis. The toxicity of cisplatin limits the dose that can be given to patients. These facts together with the aim to find platinum-based derivatives with higher antitumour activity and overcoming resistance of many tumour types have led many investigators to attempt the synthesis and characterization of new platinum (Pt) analogues. Since the early studies by Rosenberg et al. [3] it has been known that Pt(IV) complexes can display antitumour properties.

Pt(IV) compounds which contain lipophilic non-leaving ligands have generally greater lipophilicity than currently used Pt(II) derivatives [4] which could enable them to overcome cisplatin resistance caused by a decreased Pt accumulation in target cancer cells [5,6]. The lack of cross-resistance with cisplatin reported for some Pt(IV) compounds and the clinical development of the first orally active platinum derivative-JM216 [7,8] have helped to increase the interest in this type of platinum compounds. Pt(IV) complexes are much more inert to ligand substitution reactions than their Pt(II) counterparts [9], and offer some pharmacological advantages in comparison with cisplatin [10,11].

(*OC*-6-43)-bis(acetato)(1-adamantylamine)amminedichloroplatinum(IV), coded as LA-12 (Fig. 1), represents an octahedral platinum(IV) complex, containing a bulky non-leaving hydrophobic ligand-adamantylamine. LA-12 was synthesized by the method described previously [12]. The presence of cyclic amines reduces the toxicity of platinum compounds, especially for large rings like cyclopentylamine [13].

With this background Žák et al. [12] designed and synthesized a series of platinum(IV) complexes with amino derivatives of adamantane as one of its six ligands. According to the evaluation of *in vitro* antitumour activity of adamantylamine Pt(IV) complexes, LA-12 displayed

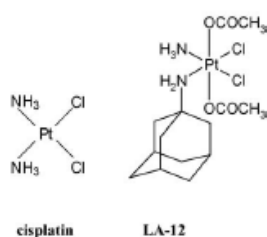


Fig. 1. Chemical structures of cisplatin [*cis*-diamminedichloroplatinum(II)] and LA-12 [(*OC*-6-43)-bis(acetato)(1-adamantylamine)amminedichloroplatinum(IV)].

the highest biological effect from the panel of Pt(IV) evaluated complexes with the general formula (*OC*-6-43)-bis(acetato)(alkylamine)amminedichloroplatinum(IV) on the model of ovarian cancer cell lines, parent cisplatin sensitive A2780, and A2780cis (with acquired cisplatin resistance). In addition, LA-12 has shown a higher cytotoxicity than JM216 in the *in vitro* MTT test for mitochondrial activity on A2780 and A2780cis cells [4]. Therefore, we aimed to study in more detail the cytotoxicity, cell cycle perturbations, and the type of cell death induced by the LA-12 derivative in sensitive and cisplatin resistant ovarian cancer cell lines.

2. Materials and methods

2.1. Materials

Cisplatin (*cis*-DDP, *cis*-diamminedichloroplatinum(II); FW 300.1) (Sigma–Aldrich Corp.) and LA-12 [(*OC*-6-43)-bis(acetato)(1-adamantylamine)amminedichloroplatinum(IV); FW 552.4] (PLIVA-Lachema a.s.) were dissolved in DMSO (Sigma–Aldrich Corp.). The stock solutions of cisplatin and LA-12 were freshly prepared before use. The final concentration of DMSO in cell culture medium did not exceed 0.2%.

2.2. Cell lines and culture

The A2780 (parent cisplatin sensitive) and A2780cis (with acquired cisplatin resistance) ovarian carcinoma cell lines, obtained from the European Collection of Animal Culture (ECAC) [14–16], were grown in RPMI 1640 medium (Sigma–Aldrich Corp.) supplemented with gentamycin (50 µg/ml; Serva) and 10% heat inactivated fetal bovine serum (PAN Biotech GmbH). The cells were cultivated in a humidified incubator at 37 °C in a 5% CO₂ atmosphere, and subcultured twice a week with a plating density of 1:4. The acquired resistance of A2780cis cells was maintained by supplementing the medium with 1 µM cisplatin every second passage. For the experiments, the cells were seeded at a density of 30,000 cells/cm².

2.3. Cytotoxicity assay

The cells were seeded in 96-well tissue culture plates. After overnight incubation, the cells were treated for 72 h with the derivatives studied. Then 10 µl of MTT (2.5 mg/ml; Sigma–Aldrich Corp.) was added to each well and incubated for 4 h in culture conditions. At the end of the incubation period the medium was removed, the formazan product was dissolved in 50 µl of 10% Triton X-100 in 0.1 M HCl, and optical densities were measured at 570 nm using a microplate spectrophotometer reader (ASYS Hitech GmbH). The reading values were converted to the percentage of control (% cell survival). Cytotoxic

effects were expressed as IC₅₀ and IC₉₀, which were the concentrations inducing 50% and 90% inhibition of metabolic activity of the cells treated, respectively.

2.4. Cell number, floating cell quantification, and viability assay

The cells were seeded in 60 mm tissue culture dishes (30,000 cells/cm²). After overnight incubation, the cells were treated with the calculated IC₅₀ and IC₉₀ concentration of cisplatin or LA-12 for 24 h, 48 h, and 72 h. The numbers of cells were determined using a Coulter Counter[®] ZM (Beckman-Coulter). The attached and floating cells were counted separately, and the amount of floating cells was expressed as the percentage of the total cell number. Total cell viability (attached + floating) was analysed using staining with 0.15% eosin via light microscopy.

2.5. Cell cycle analysis

At each time points, floating cells were collected and attached cells were harvested by trypsinization (trypsin/EDTA in PBS; PAN Biotech GmbH), total (floating + attached) cells were washed twice in PBS (4 °C), fixed in 70% ethanol, and stored at 4 °C. The PBS washed cells were subsequently rinsed with 0.2 M phosphate-citrate buffer at pH 7.8 according to Darzynkiewicz et al. [17] – after pelleting the cells were stained with 200 µl staining solution (20 µg PI/ml PBS + ribonuclease A (DNA free; 5 U/ml); both Sigma–Aldrich Corp.) for 30 min at 37 °C in the dark. The DNA content of the cells was analysed using flow cytometry (FACSCalibur[™], Becton Dickinson, 488 nm argon laser for excitation). For each sample, 1.5 × 10⁴ cells were acquired, and the percentages of cells in the individual cell cycle phases were analysed using ModFit 2.0 software (Verity Software House). Single cells were identified and gated by pulse-code processing of the area and the width of the fluorescence signal. Cell debris was excluded by appropriate increase of the forward scatter threshold.

2.6. Fluorescence microscopy of apoptotic morphology and DNA fragmentation analysis

At each time point, the samples for apoptotic cell quantification (nuclear morphology analysis) were harvested by trypsinization and collected floating and harvested attached cells were washed twice in PBS. The total cells, fixed in 70% ethanol, were stained with DAPI (Sigma–Aldrich Corp.; final concentration 1 µg/ml) for 30 min at room temperature in the dark. After incubation, the cells were centrifuged, mixed with Mowiol 40–88 solution (for mounting of the cells under coverslips) (Sigma–Aldrich Corp.) with DABCO as an anti-bleaching treatment of the DAPI-stained cells (0.6%, Sigma–Aldrich

Corp.) and mounted under coverslips. The incidence of apoptotic bodies was evaluated by fluorescence microscopy (Olympus IX-70; Olympus). The apoptotic index was counted from at least 200 cells.

Subsequently, DNA fragmentation analysis was performed. At 72 h time point, 2 × 10⁶ cells treated with cisplatin or LA-12 with IC₅₀ and IC₉₀ concentrations were washed twice with PBS (4 °C) and subsequently DNA isolation was performed using the Invisorb Apoptosis Detection Kit I (Invitex; Invitex GmbH). Gel electrophoresis was performed in 1.5% agarose (Sigma–Aldrich Corp.), using 1 kbp DNA ladder as a marker (MBI Fermentas). DNA was stained with SYBR Green I (Molecular Probes, Inc.) and scanned by Storm (Molecular Dynamics, Amersham Biosciences).

2.7. Western blot analysis

At each time point, the treated cells were harvested, washed twice in cold PBS and lysed in lysis buffer (100 mM Tris–HCl, pH 7.4; 1% SDS; 10% glycerol and protease inhibitor cocktail (P2714, Sigma–Aldrich Corp.)) for 10 min on ice. The cell lysates were sonicated (Soni-fier[®] B-12, Branson Ultrasonics Corp.) and centrifuged. The protein concentration of the samples was determined using a detergent-compatible protein assay (Bio-Rad Laboratories, Inc.). The samples were diluted to the same concentration and equal amounts (20 µg proteins) with 0.01% bromophenol blue and 1% 2-mercaptoethanol were separated on 7.5% SDS-polyacrylamide gel, and blotted onto a PVDF membrane (Millipore Corp.) in a transfer buffer containing 192 mM glycine, 25 mM Tris, and 10% methanol. The membranes were blocked overnight in TBS (20 mM Tris–HCl, pH 7.6; 150 mM NaCl) containing 0.05% Tween 20 and 5% non-fat milk at 4 °C. Then the blots were washed with TBS-Tween and incubated with rabbit polyclonal anti-PARP (#sc-7150, 1:1000, Santa Cruz) or mouse monoclonal anti-p53 (DO-1, 1:2000; [18]) primary antibodies for 2 h at room temperature. The membranes were incubated with secondary anti-mouse IgG (#NA931, 1:3000) and anti-rabbit IgG (#NA934, 1:6000; both Amersham Biosciences) antibodies conjugated with horseradish peroxidase for 1 h after washing in TBS-Tween. Detection of the antibody reactivity was performed with an enhanced chemiluminescence detection kit ECL+ (Amersham Biosciences) and visualized on X-ray films (AGFA-Gevaert N.V.). Equal sample loading was verified by immunodetection of β-actin (A5441, 1:10,000, Sigma–Aldrich Corp.) or staining of PVDF membrane with 0.1% amido black (in 1:3:6 (v/v/v) of acetic acid, methanol and water) for non-specific visualization of proteins. Quantification of visualized bands was performed by densitometry using AIDA software (Advanced Image Data Analyzer; Raytest) allowing assessment of increases in the expression of protein levels compared with untreated controls.

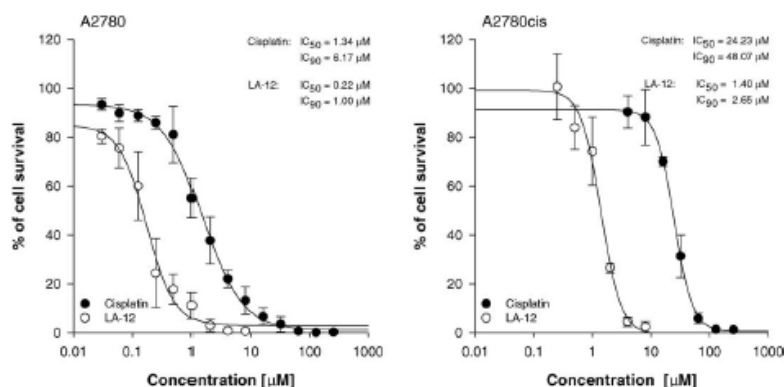


Fig. 2. Time- and dose-response effects on the survival of A2780 and A2780cis cancer cell lines. The effects after 72 h exposure to cisplatin or LA-12 in a concentration range between 0.3 μM and 256 μM were determined by MTT assay. The calculated drug concentrations inhibiting metabolic activity of cells by 50% (IC_{50}) and 90% (IC_{90}) are displayed for both derivatives. The results are expressed as mean \pm standard deviations (S.D.) of at least three independent experiments; all concentrations were tested in three replicates.

2.8. Statistical analysis

All the data are expressed as the means \pm S.D. of at least three independent experiments. With all statistical analyses, the associated probability (p value) of $<5\%$ was considered as significant. Comparisons between the groups were calculated using One-way Analysis of Variance followed by the Tukey range test (*, #). If the variances were non-homogenous, Mann-Whitney U -test analysis was used (\times). All statistical analyses were calculated by the software Statistica for Windows, V. 6.1 (StatSoft, Inc.). The dose-response curves were analysed by the software SigmaPlot[®], V. 8.0 (SPSS International B.V.).

3. Results

3.1. Cytotoxicity of the drugs

Exposure to the compounds in a concentration range between 0.3 μM and 256 μM resulted in a dose-dependent inhibition of cell survival in both A2780 and A2780cis cell lines (Fig. 2). After 72 h treatment, IC_{50} and IC_{90} values of LA-12 were 6.09-fold and 6.17-fold lower, respectively, in A2780 cells, and 17.31-fold and 18.14-fold lower, respectively, in A2780cis cells, than those of cisplatin. Displayed effects were also characterized by the value of resistance factor which is defined as the ratio of IC_{50} concentration

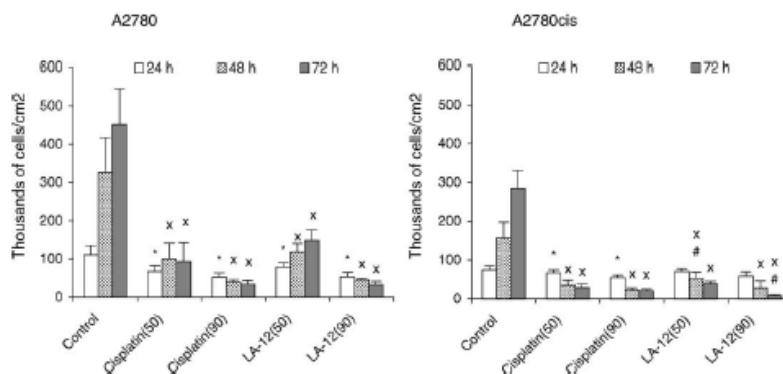


Fig. 3. Effects of equitoxic concentrations of cisplatin or LA-12 on cell growth. The A2780 or A2780cis cells were untreated (control) or sustained treated with IC_{50} and IC_{90} concentrations of cisplatin or LA-12 and harvested at 24 h, 48 h, and 72 h. The cells collected were measured for the number of attached cells per surface area of culture dish (cm^2). The results are expressed as mean \pm standard deviations (S.D.) of at least three independent experiments. The symbols (*), (\times) denote significant difference ($p < 0.05$) from untreated control, (#) denote significant difference ($p < 0.05$) between equitoxic cisplatin and LA-12 effects.

values of the derivative in resistant A2780cis cells to sensitive parent A2780 cells. Cisplatin showed a resistance factor 18.08 while resistance factor of LA-12 was 6.36. It means that LA-12 overcomes cisplatin resistance in A2780cis cells showing a resistance factor 2.84-fold lower than those for cisplatin.

3.2. Determination of cellular growth and viability

In order to confirm the higher effectiveness of LA-12 found by MTT metabolic assay, the effects of equitoxic concentrations (IC_{50} and IC_{90}) of both compounds on the total cell number, percentage of floating cells and viability were investigated.

As shown in Fig. 3, IC_{50} and IC_{90} concentrations of LA-12 and cisplatin caused a similarly time- and concentration-dependent decrease in the number of attached cells per cm^2 significantly different from the untreated control at all the time points studied in A2780 and A2780cis cells.

Parallely, a significant increase in the percentage of floating A2780 and A2780cis cells was detected in all studied groups (Fig. 4a). After 72 h, in cisplatin resistant A2780cis cells the effect of IC_{90} of LA-12 on both parameters was even significantly greater than that of cisplatin. The total cell number (adherent and floating cells together) was also significantly decreased after drug treatment without significant differences between equitoxic concentrations of cisplatin and LA-12 (data not shown).

These results corresponded with the time- and concentration-dependent decrease in cell viability compared with untreated control cells (Fig. 4b), in which no significant differences in cisplatin versus LA-12 effects were recorded, either.

3.3. Cell cycle perturbations

An analysis of cell cycle perturbations was performed in A2780 and A2780cis cells exposed to IC_{50} concentrations

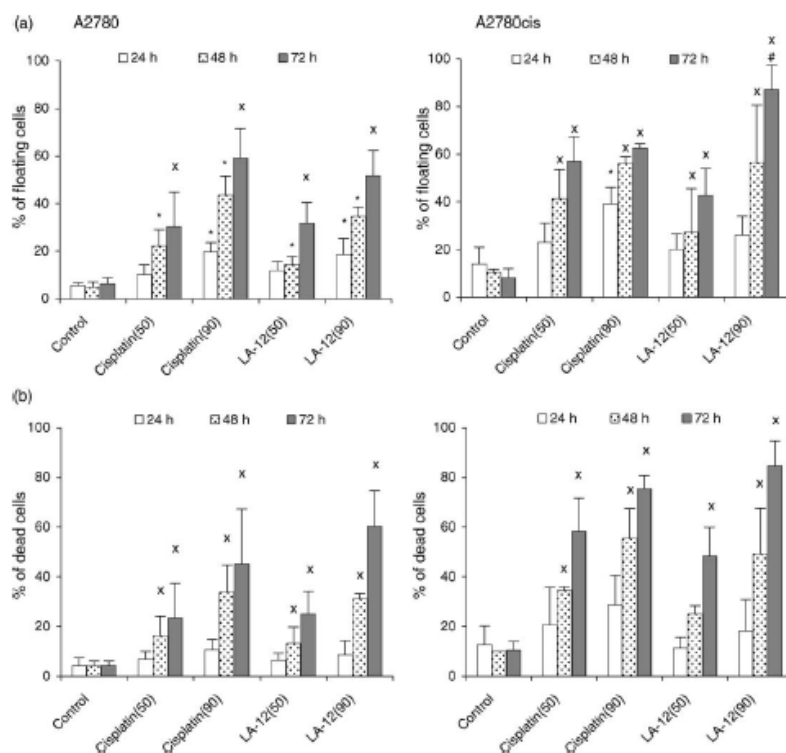


Fig. 4. Effects of equitoxic concentrations of cisplatin or LA-12 on the percentage of floating cells and viability. The A2780 and A2780cis cells were untreated (control) or sustained treated with IC_{50} and IC_{90} concentrations of cisplatin or LA-12 and harvested at 24 h, 48 h, and 72 h. The percentage of floating cells in relation to the total number of cells per dish was determined (a). Viability was measured in the total amount collected (floating + attached) of cells by eosin staining (b). The results are expressed as mean \pm standard deviations (S.D.) of at least three independent experiments. The symbols (*), (#) denote significant difference ($p < 0.05$) from untreated control; (#) denote significant difference ($p < 0.05$) between equitoxic cisplatin and LA-12 concentrations.

of cisplatin or LA-12 at 24 h, 48 h, and 72 h of drug exposure. The results of the cell cycle distribution for one representative experiment are shown in Fig. 5. Comparison of the cisplatin versus LA-12 effects in sensitive A2780 cells showed several significant differences. At the 24 h time point, cisplatin caused transient accumulation of cells in the G₂/M-phase of the cell cycle while LA-12 induced accumulation of cells in the S-phase fraction. At the other time points, there were no significant differences compared to controls. On the other hand, resistant A2780cis cells were arrested in the S-phase of the cell cycle after treatment with both cisplatin and LA-12 at the 24 h time interval, cisplatin being more effective (Fig. 5). This block was shifted to G₂/M-phase in later time intervals.

3.4. Nuclear morphology

A concentration- and time- dependent increase in the percentage of A2780 and A2780cis cells with apoptotic morphology in comparison to the untreated control cells was observed (Fig. 6). While for cisplatin treated cells the significance of the increase was proved already after 48 h, LA-12 did not significantly increase apoptosis until 72 h. That is why cisplatin showed a significantly higher rate of apoptosis in comparison with LA-12 in the 48 h interval. However, this difference was balanced out after 72 h. Generally, the percentage of apoptotic sensitive A2780 cells was low (about 5–8% maximum) after treatment with both drugs, and it was about two to four times higher (about 15–20%) in resistant A2780cis cells.

3.5. Analysis of DNA fragmentation

In order to investigate whether nuclear fragmentation observed after the treatment of cells was associated with DNA fragmentation typical of apoptosis, the agarose gel electrophoresis of extracted genomic DNA from both control and drug-treated cells (72 h sustained treatment with IC₅₀ or IC₉₀ concentrations) was performed (Fig. 7). DNA in A2780 and A2780cis cells appeared as a band of high molecular size corresponding to genomic DNA. However, no typical 180-base pair integer oligonucleosome “DNA ladder” that would be indicative of intranucleosomal cleavage was detected in any samples. DNA appeared unspecifically degraded as a smudge in both A2780 and A2780cis cells after the 72 h treatment with cisplatin or LA-12.

3.6. PARP and p53 expression

In order to compare the pathway leading to the induction of A2780 and A2780cis cell death in response to DNA damage caused by cisplatin or LA-12, the expression of the tumour suppressor p53 and poly-ADP ribose polymerase (PARP) cleavage was examined by Western blotting.

In A2780 cells, only the full-length PARP (113 kDa) was observed in all tested groups and time points of drug exposure (Fig. 8a, left panel). In contrast, in A2780cis cells (Fig. 8a, right panel) the same treatments were associated with time- and concentration-dependent cleavage of full-length PARP. While the cisplatin effect of IC₅₀ was apparent already after 24 h, after LA-12 (IC₅₀) treatment the PARP fragment (89 kDa) was not apparent until 48 h. At the 72 h time point, PARP fragmentation was observed after cisplatin and LA-12 treatment with both IC₅₀ and IC₉₀ concentrations.

Fig. 8b displays the expression levels of p53 protein after treatment of A2780 (left panel) or A2780cis cells (right panel) with IC₅₀ or IC₉₀ concentrations of cisplatin or LA-12. In comparison with the untreated control, a concentration-dependent increase in p53 levels was observed in both cell lines studied. However, in comparison to that with LA-12, treatment with cisplatin caused a markedly higher expression of p53 protein levels in both cancer cell lines. Densitometric quantification of visualized bands of p53 level is presented in Fig. 8c. In comparison with untreated control significantly ($p < 0.05$) higher expression of p53 was detected for both derivatives in both cell lines. At the same time significant increase of p53 expression after cisplatin treatment in comparison with LA-12 in both cell lines was detected. In these experiments time- and concentration-dependent results were proved.

4. Discussion

In the present study the ability of the Pt(IV)-complex LA-12 to induce cytotoxicity, cell cycle perturbations, and cell death in ovarian cancer cell lines A2780 (parent cisplatin sensitive) and A2780cis (with acquired cisplatin resistance) has been characterized and compared to the well established anticancer drug – cisplatin. LA-12 exhibited the highest antitumour activity in vitro from the panel of evaluated platinum(II) and (IV) complexes with adamantane in the MTT test of cytotoxicity on both ovarian cancer cell lines tested (our unpublished results). Moreover, LA-12 was able to overcome the acquired resistance to cisplatin in A2780cis cells (showing a resistance factor of 2.84-fold lower than those of cisplatin). The efficacy of the LA-12 complex to produce similar or higher cytotoxicity than cisplatin in lower determined IC₅₀ or IC₉₀ concentrations was confirmed in several other parameters including decrease in the total and attached cell numbers, increase of the percentage of floating cells, and decrease of cell viability. The ability to overcome the resistance was similar to JM216 and JM221, the first Pt(IV)-containing anticancer agents for oral administration that have been evaluated in a number of intrinsic and acquired cisplatin resistant cell lines. These compounds displayed a lack of cross-resistance with cisplatin, particularly in those cases where reduced platinum accumulation played a dominant

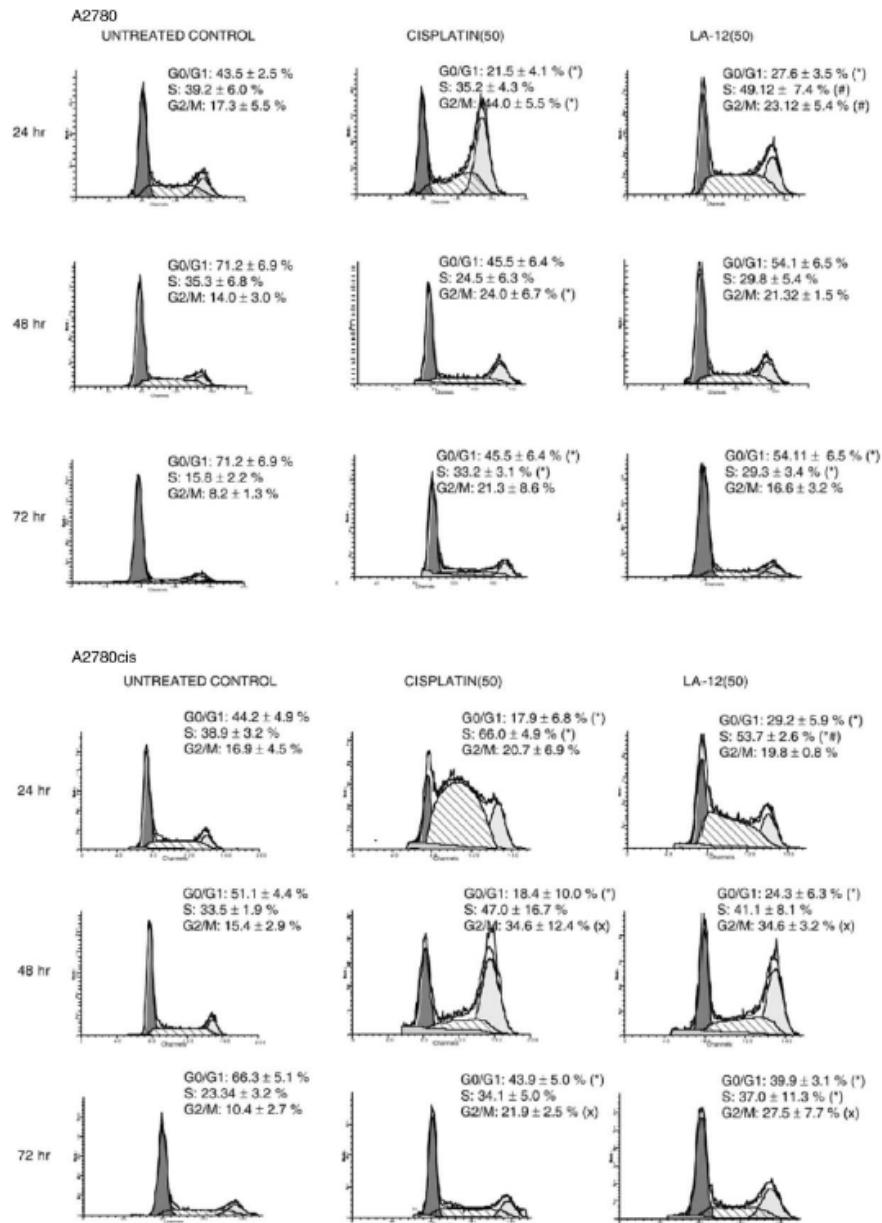


Fig. 5. Effects of IC₅₀ concentrations of cisplatin or LA-12 on cell cycle distribution. Untreated (control) cells or cells treated for 24 h, 48 h, and 72 h were harvested, fixed, stained with propidium iodide and assessed for cell cycle distribution by FACS analysis. One representative time course of A2780 and A2780cis cell cycle distribution histograms as analysed by ModFit™ 2.0 software is reported. The estimated percentages of A2780 or A2780cis cells in different phases of the cell cycle are shown. Dark grey color filling represents G0/G1-phase, hatched filling S-phase and light grey color filling G2/M-phase of modeled cell cycle. The results are expressed as mean ± standard deviations (S.D.) of at least three independent experiments. The symbols (*), (x) denote significant difference (*p* < 0.05) from untreated control; (#) denote significant difference (*p* < 0.05) between equitoxic cisplatin and LA-12 concentrations.

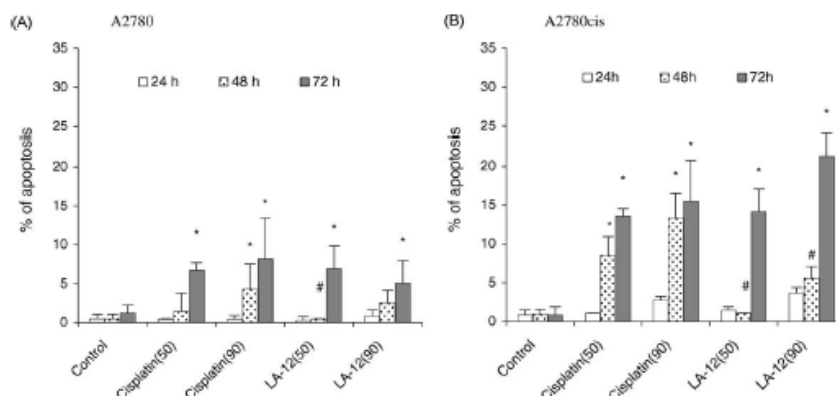


Fig. 6. The percentages of apoptotic cells (apoptotic index) as determined by DAPI staining. The A2780 or A2780cis cells were untreated (control) or treated with IC_{50} and IC_{90} concentrations of cisplatin or LA-12 and harvested at 24 h, 48 h and 72 h. The results are expressed as mean \pm standard deviations (S.D.) of at least three independent experiments. The symbols (*), (#) denote significant difference ($p < 0.05$) from untreated control; (#) denote significant difference ($p < 0.05$) between equitoxic cisplatin and LA-12 concentrations.

role [5,6]. This suggests that the greater lipophilic nature of Pt(IV) compounds [4] might help to overcome the cisplatin resistance that is primarily due to a decreased Pt accumulation.

Activation of cell cycle checkpoints is a general cellular response after exposure to cytotoxic agents. These checkpoints become activated in order to enable some critical cellular functions, such as DNA repair, to be performed before the cell cycle may resume [19]. Previous flow cytometric studies have indicated that cisplatin and other platinum agents predominantly inhibit cell cycle progression at S- and/or G_2/M -phase, independent of drug concentration in a range of $(1-5) \times IC_{50}$ [20]. Our results point out possible reasons of differences between cisplatin and LA-12 at the level of cell cycle regulation and cell death induction. We detected a different type and dynamics of cell cycle perturbation of these compounds. Moreover, differences were observed between the response of cisplatin sensitive A2780 and resistant A2780cis cells. While cisplatin blocked sensitive A2780 cells in the G_2/M -phase and resistant A2780cis cells in the S-phase, LA-12 blocked both types of cells in the S-phase only. The cell cycle arrest was found to be transient, which is a typical response to a number of cytotoxic agents, including cisplatin [20,21]. Our findings are consistent with other reports describing transient S- and G_2/M -phase arrests after other platinum-containing agents in a number of cell lines [20,22] or slowed progression through the S-phase following cisplatin treatment [23]. The differences in the extent and duration of G_2/M arrest observed in studies with different cell lines could depend on differences in the cellular capacity for DNA repair [24].

Our previous results showed that a high concentration ($10 \mu M$) of LA-12 can induce rapid (4 h) apoptosis in

colorectal cancer cells HCT116 [4]. However, the amount of apoptotic ovarian cancer cells after treatment with IC_{50} and IC_{90} doses of LA-12 was low and similar to cisplatin. In general, it was markedly higher in cisplatin resistant A2780cis cells. No detected "DNA ladder" and the appearance of smears of non-specifically degraded DNA confirmed the induction of a low rate of apoptosis in both

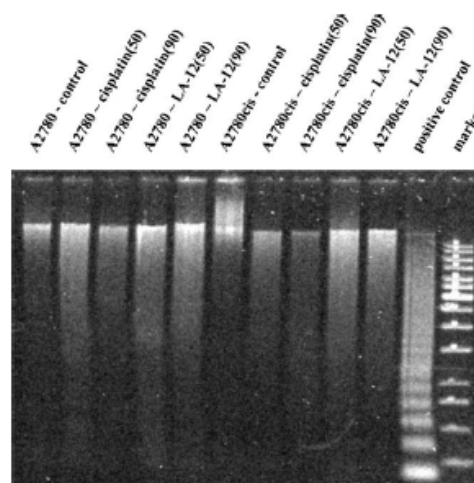


Fig. 7. Agarose gel electrophoresis of genomic DNA isolated from untreated control and cisplatin or LA-12 treated A2780 and A2780cis cells for 72 h with IC_{50} or IC_{90} concentrations of the drugs. The extracted DNA was subjected to gel electrophoresis. One representative experiment out of three is reported. Positive control (HL-60 cells treated with $10 \mu M$ etoposide for 4 h).

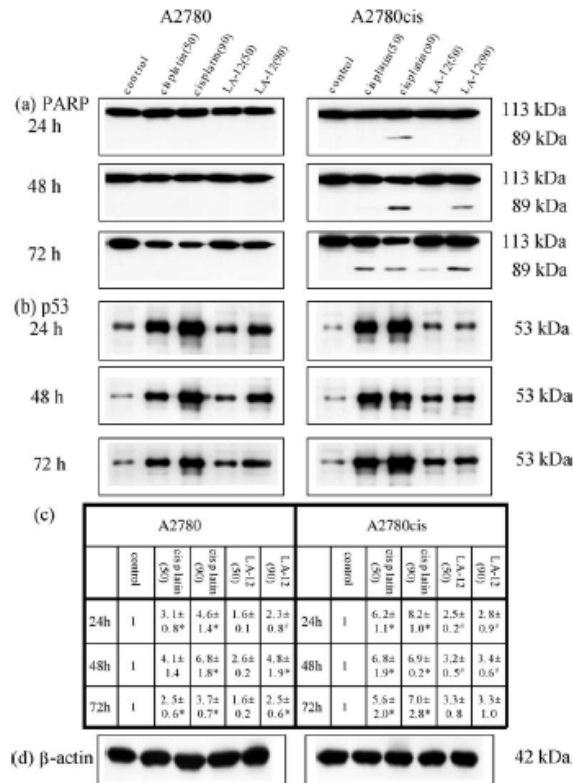


Fig. 8. Western blot analyses of (a) PARP (upper panel) and (b) p53 (middle panel) protein levels in A2780 (left panel) and A2780cis cells (right panel). The cells were not exposed (untreated controls) or exposed to IC₅₀ or IC₃₀ concentrations of cisplatin or LA-12 and harvested at 24 h, 48 h, and 72 h of sustained drug treatment. One representative experiment of at least three is presented. Table (c) contains values of p53 expression quantified by densitometry (mean ± S.D. of at least three independent experiments). The symbols (*) denote significant difference ($p < 0.05$) from untreated control; (#) denote significant difference ($p < 0.05$) between equitoxic cisplatin and LA-12 effects. Equal loading is documented by detection of (d) β -actin (bottom panel).

studied cell lines after exposure to both drugs. To clarify this type of apoptotic response in more detail, cleavage of PARP and expression of p53 protein were investigated.

PARP, a 113-kDa nuclear protein, has been among the first proteins shown to be specifically cleaved during apoptosis [25]. PARP cleavage to the 89 kDa fragment was observed in diverse models of apoptosis [26–28] and it is considered to be a sensitive parameter of apoptosis even when only limited numbers of cells in the total population undergo apoptosis [29]. In our experiments, time- and concentration-dependent PARP cleavage was detected only in cisplatin resistant A2780cis cells. Moreover, it was detected earlier after cisplatin than after LA-12 treatment.

Our results corresponded to the fact that although A2780 cells are the most sensitive ovarian cell line to cisplatin, they show the lowest percentage of apoptosis (6–14%) [30]

and display low levels of DNA degradation [31]. They are also in agreement with Henkels and Turchi [31], who reported different processing of apoptosis between the sensitive A2780 and resistant A2780cis cell lines in response to cisplatin. While in A2780 cells low caspase-3 activation and a very small increase in cytoplasmic cytochrome *c* was detected, in resistant A2780cis cells a dramatic increase of both parameters was observed. Moreover, they have found evidence for an alternative apoptotic pathway in A2780 cells by demonstrating increased FADD expression in response to cisplatin treatment. This supports a model in which cisplatin-induced programmed cell death in the cisplatin-sensitive A2780 and -resistant A2780cis cells proceeds via caspase-3 independent and -dependent pathways, respectively. The lack of DNA fragmentation in our experiments may also be due to the fact that apoptosis may occur in earlier time points. Thus, after 72 h, we

observed mainly secondary necrosis (our unpublished results from PI/Hoechst viable staining and evaluating by fluorescence microscopy). Therefore, no apoptotic DNA could be extractable with a consequence of no intranucleosomal fragmentation with typical DNA laddering on gel.

Since p53 protein is implicated in apoptosis induction and modulation of the cell cycle, as a result of cellular response to DNA damage [32], we analysed whether the cell cycle perturbations and induction of cell death by cisplatin or the LA-12 complex in A2780 and A2780cis cells were associated with changes in the expression levels of this protein. An accumulation of p53 in response to cisplatin that could be connected with its prolonged half-time [33] has been observed in a majority of tumour cells, thus supporting the view that the wild-type p53 protein may inhibit cell growth to allow DNA repair, and in case of irreparable damage, initiate apoptotic cell death [34]. Our data showed that while the A2780 and A2780cis cell lines appear to differ in their p53-dependent apoptotic response to Pt-DNA adducts, transient S or G₂/M arrests in the cell cycle displayed no apparent correlation with p53 induction. The levels of p53 expression remained elevated during the whole interval of cisplatin or LA-12 treatment with IC₅₀ as well as IC₉₀ concentrations in both A2780 and A2780cis cells. Moreover, higher levels of p53 expression were found in both cell lines after treatment with cisplatin compared to equitoxic concentrations of LA-12. This may be due to the fact that cisplatin caused primarily DNA damage and the biochemical mechanisms of its cytotoxicity involve the binding of the drug mainly to the DNA in the cell nucleus and the subsequent induction of cell death. This may occur not only via apoptosis [35] but in our ovarian cancer cell lines A2780 and A2780cis also via some kind of alternative cell death as seen from results of Henkels and Turchi [31]. They postulated caspase-3-dependent and -independent pathways in cisplatin induced apoptosis for these cells. Both ovarian cancer cell lines (parental and resistant) treated with cisplatin or LA-12 exhibited either signs of apoptosis (DAPI staining) or necrosis and secondary necrosis (PI/Hoechst 33342 viable staining evaluated by fluorescence microscopy, our unpublished results) as demonstrated in our experiments, in selected time-points. On the other hand, the mechanism of the LA-12 effect may predominantly involve the binding of the drug also to non-DNA targets such as cytoplasmic and nuclear proteins producing DNA-protein crosslinks (our unpublished results). Differences in cell cycle perturbations and lower expression of p53 after LA-12 versus cisplatin treatment are very important findings and they are currently under investigation in our laboratory.

In summary, the Pt(IV) adamantane complex LA-12 is characterized by significantly higher cytotoxicity than cisplatin in both parent cisplatin sensitive A2780 and cisplatin resistant A2780cis ovarian cancer cell lines and overcomes the acquired resistance to cisplatin. We con-

clude that apoptosis is probably not the major type of cell death caused by LA-12 in doses around IC₅₀ and IC₉₀ in these cell lines, even though this platinum complex strongly increases the expression level of p53 protein. These facts could be associated with cell cycle perturbations. An important finding is the different dynamics of LA-12 effects on cell cycle and apoptosis compared to cisplatin. Based on our results, octahedral platinum(IV) derivative, LA-12, was selected for further evaluation, in which a more detailed analysis of cell cycle modulation and cell death pathways will be realized.

Acknowledgements

This work was supported by the grant No. 305/01/0418 of the Grant Agency of the Czech Republic, by the IGA grant No. S 5004009 of the Academy of Sciences of the Czech Republic, by the grant No. K 5011112, and by the Ministry of Industry and Trade of the Czech Republic, Contract No. PZ-Z2/29, "New Medicines for Cancer Therapy". The authors wish to thank Jaromíra Netíková, Jiřina Holá, Iva Lišková, and Martina Urbánková for superb technical assistance; Bořivoj Vojtěšek for providing p53 antibody, Ladislav Červený for correcting the English version of this paper and Jan Vondráček for critical reading of the manuscript.

References

- [1] Weiss RB, Christian MC. New cisplatin analogues in development. A review. *Drugs* 1993;46:360–77.
- [2] Gordon M, Hollander S. Review of platinum anticancer compounds. *J Med* 1993;24:209–65.
- [3] Rosenberg B, Van Camp L, Grimley EB, Thomson AJ. The inhibition of growth or cell division in *Escherichia coli* by different ionic species of platinum(IV) complexes. *J Biol Chem* 1967;242:1347–52.
- [4] Turánek J, Kasna A, Zašuska D, Neca J, Kvardova V, Knotigova P, et al. New platinum(IV) complex with adamantylamine ligand as a promising anti-cancer drug: comparison of in vitro cytotoxic potential towards A2780/cisR cisplatin-resistant cell line within homologous series of platinum(IV) complexes. *Anticancer Drugs* 2004;15:537–43.
- [5] Kelland LR, Murrer BA, Abel G, Giandomenico CM, Mistry P, Harrap KR. Ammine/amine platinum(IV) dicarboxylates: a novel class of platinum complex exhibiting selective cytotoxicity to intrinsically cisplatin-resistant human ovarian carcinoma cell lines. *Cancer Res* 1992;52:822–8.
- [6] Harrap KR. Initiatives with platinum- and quinazoline-based antitumor molecules. *Cancer Res* 1995;55:2761–8.
- [7] Kelland LR, Abel G, McKeage MJ, Jones M, Goddard PM, Valenti M, et al. Preclinical antitumor evaluation of bis-acetato-ammine-dichloro-cyclohexylamine platinum(IV): an orally active platinum drug. *Cancer Res* 1993;53:2581–6.
- [8] Rose WC, Crosswell AR, Schurig JE, Casazza AM. Preclinical antitumor activity of orally administered platinum (IV) complexes. *Cancer Chemother Pharmacol* 1993;32:197–203.
- [9] Giandomenico CM, Abrams MJ, Murrer BA, Vollano JF, Rheinheimer MI, Wyer SB, et al. Carboxylation of kinetically inert platinum(IV) hydroxy complexes. an entrée into orally active platinum(IV) anti-tumor agents. *Inorg Chem* 1995;34:1015–21.

- [10] O'Neill CF, Ormerod MG, Robertson D, Titley JC, Cumber-Walshwee Y, Kelland LR. Apoptotic and non-apoptotic cell death induced by cis and trans analogues of a novel ammine(cyclohexylamine) dihydroxodichloroplatinum(IV) complex. *Br J Cancer* 1996;74:1037–45.
- [11] Perez JM, Camazon M, Alvarez-Valdes A, Quiroga AG, Kelland LR, Alonso C, et al. Synthesis, characterization and DNA modification induced by a novel Pt(IV)-bis(monoglutarate) complex which induces apoptosis in glioma cells. *Chem Biol Interact* 1999;117:99–115.
- [12] Žák F, Turánek J, Kroutil A, Sova P, Mistr A, Poulová A, et al. Platinum(IV) complex with adamantylamine as non-leaving amine group: synthesis, characterization, and in vitro antitumor activity against the panel of cisplatin resistant cancer cell lines. *J Med Chem* 2004;47:761–3.
- [13] Connors TA, Cleare MJ, Harrap KR. Structure-activity relationships of the antitumor platinum coordination complexes. *Cancer Treat Rep* 1979;63:1499–502.
- [14] Masuda H, Ozols RF, Lai GM, Fojo A, Rothenberg M, Hamilton TC. Increased DNA repair as a mechanism of acquired resistance to cis-diamminedichloroplatinum (II) in human ovarian cancer cell lines. *Cancer Res* 1988;48:5713–6.
- [15] Hamilton TC, Young RC, Ozols RF. Experimental model systems of ovarian cancer: applications to the design and evaluation of new treatment approaches. *Semin Oncol* 1984;11:285–98.
- [16] Behrens BC, Hamilton TC, Masuda H, Grotzinger KR, Whang-Peng J, Louie KG, et al. Characterization of a cis-diamminedichloroplatinum(II)-resistant human ovarian cancer cell line and its use in evaluation of platinum analogues. *Cancer Res* 1987;47:414–8.
- [17] Darzynkiewicz Z, Juan G, Li X, Gorczyca W, Murakami T, Traganos F. Cytometry in cell necrobiology: analysis of apoptosis and accidental cell death (necrosis). *Cytometry* 1997;27:1–20.
- [18] Vojtesek B, Bartek J, Midgley CA, Lane DP. An immunochemical analysis of the human nuclear phosphoprotein p53. New monoclonal antibodies and epitope mapping using recombinant p53. *J Immunol Methods* 1992;151:237–44.
- [19] Pucci B, Kasten M, Giordano A. Cell cycle and apoptosis. *Neoplasia* 2000;2:291–9.
- [20] Nguyen HN, Sevin BU, Averette HE, Perras J, Ramos R, Angioli R, et al. Comparison of cytotoxicity and cell kinetic perturbations of 5 platinum compounds in gynecologic cancer cell-lines. *Int J Oncol* 1993;3:375–82.
- [21] Hofmann J, O'Connor PM, Jackman J, Schubert C, Ueberall F, Kohn KW, et al. The protein kinase C inhibitor ilmofosine (BM 41440) arrests cells in G2 phase and suppresses CDC2 kinase activation through a mechanism different from that of DNA damaging agents. *Biochem Biophys Res Commun* 1994;199:937–43.
- [22] Eliopoulos AG, Kerr DJ, Herod J, Hodgkins L, Krajewski S, Reed JC, et al. The control of apoptosis and drug resistance in ovarian cancer: influence of p53 and Bcl-2. *Oncogene* 1995;11:1217–28.
- [23] Vaisman A, Varchenko M, Said I, Chaney SG. Cell cycle changes associated with formation of Pt-DNA adducts in human ovarian carcinoma cells with different cisplatin sensitivity. *Cytometry* 1997;27:54–64.
- [24] Sorenson CM, Eastman A. Influence of cis-diamminedichloroplatinum(II) on DNA synthesis and cell cycle progression in excision repair proficient and deficient Chinese hamster ovary cells. *Cancer Res* 1988;48:6703–7.
- [25] Kaufmann SH. Induction of endonucleolytic DNA cleavage in human acute myelogenous leukemia cells by etoposide, camptothecin, and other cytotoxic anticancer drugs: a cautionary note. *Cancer Res* 1989;49:5870–8.
- [26] Hayakawa A, Wu J, Kawamoto Y, Zhou YW, Tanuma S, Nakashima I, et al. Activation of caspase-8 is critical for sensitivity to cytotoxic anti-Fas antibody-induced apoptosis in human ovarian cancer cells. *Apoptosis* 2002;7:107–13.
- [27] Kaufmann SH, Desnoyers S, Ottaviano Y, Davidson NE, Poirier GG. Specific proteolytic cleavage of poly(ADP-ribose) polymerase: an early marker of chemotherapy-induced apoptosis. *Cancer Res* 1993;53:3976–85.
- [28] Tewari M, Quan LT, O'Rourke K, Desnoyers S, Zeng Z, Beidler DR, et al. Yama/CPP32 beta, a mammalian homolog of CED-3, is a CrmA-inhibitable protease that cleaves the death substrate poly(ADP-ribose) polymerase. *Cell* 1995;81:801–9.
- [29] Duriez PJ, Shah GM. Cleavage of poly(ADP-ribose) polymerase: a sensitive parameter to study cell death. *Biochem Cell Biol* 1997;75:337–49.
- [30] Kolfischoten GM, Hulscher TM, Schrier SM, van Houten VM, Pinedo HM, Boven E. Time-dependent changes in factors involved in the apoptotic process in human ovarian cancer cells as a response to cisplatin. *Gynecol Oncol* 2002;84:404–12.
- [31] Henkels KM, Turchi JJ. Cisplatin-induced apoptosis proceeds by caspase-3-dependent and -independent pathways in cisplatin-resistant and -sensitive human ovarian cancer cell lines. *Cancer Res* 1999;59:3077–83.
- [32] Hartwell LH, Kastan MB. Cell cycle control and cancer. *Science* 1994;266:1821–8.
- [33] Yazlovitskaya EM, DeHaan RD, Persons DL. Prolonged wild-type p53 protein accumulation and cisplatin resistance. *Biochem Biophys Res Commun* 2001;283:732–7.
- [34] Eastman A. Activation of programmed cell death by anticancer agents: cisplatin as a model system. *Cancer Cells* 1990;2:275–80.
- [35] Gonzales VM, Fuertes MA, Alonso C, Perez JM. Is cisplatin-induced cell death always produced by apoptosis? *Mol Pharmacol* 2001;59:657–63.

Apoptosis and inhibition of gap-junctional intercellular communication induced by LA-12, a novel hydrophobic platinum(IV) complex

Lubomír Procházka^a, Jaroslav Turánek^{a,*}, Radek Tesařík^a, Pavlína Knotigová^a,
Pavlína Polášková^a, Zdeněk Andrysík^b, Alois Kozubík^b, František Žák^c,
Petr Sova^c, Jiri Neuzil^{d,c}, Miroslav Machala^a

^a Veterinary Research Institute, Department of Immunology, Brno, Czech Republic

^b Institute of Biophysics, Academy of Sciences of the Czech Republic, Brno, Czech Republic

^c PLIVA-Lachema a.s., Research and Development, Brno, Czech Republic

^d School of Medical Science, Apoptosis Research Group, Griffith University, Southport, QLD, Australia

^e Molecular Therapy Group, Institute of Molecular Genetics, Academy of Sciences of the Czech Republic, Prague, Czech Republic

Received 20 February 2007, and in revised form 20 March 2007

Available online 9 April 2007

Abstract

A new hydrophobic platinum(IV) complex, LA-12, a very efficient anticancer drug lacking cross-resistance with cisplatin (CDDP), is now being tested in clinical trials. Here we investigated the apoptogenic activity of LA-12 and its effect on gap-junctional intercellular communication (GJIC) in the rat liver epithelial cell line WB-F344. LA-12 induced apoptosis much more efficiently than did CDDP due to a combination of rapid penetration into the cell and attack on DNA, leading to fast activation of p53 and caspase-3. Exposure of WB-F344 cells to LA-12 led to rapid induction of the time- and dose-dependent decrease in GJIC. On the molecular level, loss of GJIC induced by LA-12 was mediated by activation of extracellular signal-regulated kinase (ERK)-1 and ERK-2, as demonstrated by the use of inhibitors of ERK activation. Inhibition of GJIC was linked to rapid hyperphosphorylation of connexin-43 and disappearance of connexon clusters from membranes, which was not observed in the case of CDDP.

© 2007 Elsevier Inc. All rights reserved.

Keywords: Cisplatin; LA-12; Gap-junctional intercellular communication; Connexin-43; MEK/ERK pathway; WB-F344 cells

Cisplatin (CDDP¹) and cisplatin-based complexes belong to well established armament in anticancer chemotherapy, which has two major characteristics. Firstly, CDDP is one of the most toxic anticancer drugs and sec-

ondly, many tumours exhibit CDDP resistance, either *ab initio* (e.g., non-small-cell lung and colon cancer) or acquired during therapy (e.g., small-cell lung or ovarian cancer) [1]. Many different analogues of CDDP have been synthesised with the hope of reducing toxic side-effects and overcoming multidrug resistance [1].

PLIVA-Lachema researchers designed and synthesised a new hydrophobic platinum(IV) complex [(OC-6-43)-bis(acetato)(1-adamantylamine)amminedichloroplatinum (IV)], coded as LA-12, which is more toxic to cancer cells than CDDP and efficiently kills CDDP-resistant cancer cells [2–4], as also documented in pre-clinical studies [5,6]. Moreover, it has been shown that LA-12, although being superior in killing cancer cells, does not possess the high

* Corresponding author. Fax: +420 5 4121 1229.

E-mail address: turanek@vri.cz (J. Turánek).

¹ Abbreviations used: CDDP (cisplatin), (SP-4-2)-diamminedichloroplatinum(II); cx43, connexin-43; DBaP, dibenzo[a,l] pyrene; ERK, extracellular signal-regulated kinase; GJIC, gap-junctional intercellular communication; LA-12, (OC-6-43)-bis(acetato)(1-adamantylamine)amminedichloroplatinum(IV); MTT, 3-(4,5-dimethylthiazol-2-yl)-2,5-biphenyl-tetrazolium bromide; PARP, poly(ADP-ribose)polymerase; PMSF, phenylmethylsulphonyl fluoride; TPA, phorbol ester (12-O-tetradecanoylphorbol 13-acetate); transplatin, (SP-4-1)-diamminedichloroplatinum(II).

deleterious side-effects associated with application of CDDP, with the maximum tolerated dose in the mouse as high as 1 g/kg [6]. This third-generation platinum(IV)-based anticancer drug is in the phase I clinical trial.

The role of gap-junctional intercellular communication (GJIC) in cancer biology and drug resistance is now studied to understand the phenomena responsible for the failure of cancer treatment on one hand and association of inhibition of GJIC with carcinogenesis on the other hand [7]. Gap junctions are formed by protein subunits known as connexins and are found in large numbers in most tissues. These channels mediate electrical and chemical coupling between cells. GJIC, together with other communication mechanisms, control cell proliferation, differentiation, apoptosis, and adaptive response to endogenous and exogenous signals. GJIC is required for completion of embryonic development, maintenance of tissue homeostasis, and regulation of normal cell growth [8–10]. Thus far, 20 members of the connexin family have been described, of which connexin-43 (cx43) is a widespread short-lived protein [11,12]. Connexins are regulated by multiple mechanisms, including MAP kinase-dependent phosphorylation [13–15] as well as lysosomal and proteasomal degradation [16,17].

We have been interested in the molecular mechanism by which platinum-based anticancer drugs induce cell death. Besides the established mechanisms, evidence shows that CDDP toxicity is also modulated by a MAP kinase pathway, for example contributing to cytochrome c release [18,19], though opposing data have been also reported [20]. In spite of no definitive understanding the mechanism of the link between the functional status of connexins and regulation of apoptosis, there are emerging data suggesting that CDDP can also affect GJIC, possibly by regulating the MAP kinase-dependent phosphorylation of specific sites on cx43, although the data are inconclusive [14,15].

Expression of cx43 and the functional status of GJIC were documented in human ovarian surface epithelial cells and ovarian carcinomas *in vivo* and *in vitro* as the major gap-junctional protein [21]. Secondary transfer of molecules, e.g. glutathione, from resistant to sensitive cells may induce the transfer of drug resistance [22]. A contribution of a bystander effect based on connexin to the overall tumour drug resistance is not clear. Albeit, experimental evidence was published that Ca^{+2} is the most probable cell-killing signal pervading through gap junctions [23,24].

We used the rat liver epithelial cell line WB-F344 expressing cx43 and wild type p53, to study the effect of CDDP and the platinum(IV) complex LA-12 on GJIC inhibition and apoptosis. To our knowledge, this is the first study addressing this topic.

Materials and methods

Chemicals

Cisplatin [CDDP, (SP-4-2)-diamminedichloroplatinum(II)] and a new platinum(IV) complex LA-12, [(OC-6-43)-bis(acetato)(1-adamantyl-

amine)amminedichloroplatinum(IV)], were synthesised by PLIVA-Lachema, Brno, Czech Republic. Chemical structures of both platinum complexes are presented in Fig. 1A. Fluorescent dye Lucifer Yellow and Hoechst 33258, MTT, 12-O-tetradecanoylphorbol-13-acetate (TPA), dibenz[*a,h*] pyrene (DBaP), were purchased from Sigma–Aldrich (Prague, Czech Republic), as were other chemicals unless indicated otherwise. Chemical inhibitors used were: SP600125, GF 109203x (Sigma), U0126 (Calbiochem), SB202190 and AG 1478 (Alexis).

LA-12 and cisplatin were mixed with β -cyclodextrin in molar ratio 1:3 and dissolved in DMEM and sonicated.

GJIC inhibition assay

WB-F344 rat liver epithelial cells, a kind gift from Dr. James E. Trosko [25], were cultured in DMEM supplemented with pyruvate (110 mg/L), 10 mM Hepes, and 10% fetal bovine serum. Confluent cells, grown in 24-well plates, were exposed to CDDP or LA-12. After the exposure, a modified protocol of scrape-loading dye transfer assay (SL/DT) was used to assess GJIC [26]. The cells were washed twice with PBS, the fluorescent dye (Lucifer Yellow, 0.05 w/v in PBS) was added, and the cells were scraped using an adapted chisel-like surgical steel blade. After 4 min, the cells were washed twice with PBS. The migration of the dye from the scrape line was measured using an inverted epifluorescent microscope (T 200, Nikon, Japan). Three independent experiments were carried out in duplicates; at least three scrapes per well were evaluated. The ratio of GJIC inhibition related to the negative control was evaluated and expressed in percentage (fraction of control, %FOC). Morphological changes of the confluent layer of WB-F344 cells were assessed during the exposure to the platinum complexes using a microscope equipped with the Hoffman modulation contrast. Typical apoptotic morphology (blebs and prolapses of cytoplasm, apoptic bodies and shrunken cells) was easily distinguishable in WB-F344 cells treated with toxic doses of the platinum drugs.

Cytotoxicity test

Cells were grown in DMEM supplemented with pyruvate (110 mg/L), 10 mM Hepes, and 10% fetal bovine serum. Cells were seeded in 96-well flat-bottom microplates at the density $2.5\text{--}3 \times 10^4$ per mL, 100 μ L per well, and were grown for 16–24 h. The drugs (20 μ L) were added to the wells and the cytotoxic effect was evaluated after 24 h of exposure to the drugs at 0.3–80 μ M.

The MTT assay [27,28] was used to measure cytotoxic effects of the tested drugs on the WB-F344 cells. MTT (Sigma) was dissolved in PBS at the concentration of 5 mg/mL and sterilised by filtration. The MTT solution was added into the wells of 96-well flat-bottom microplates with cells at the dose of 20 μ L per well. The plates were incubated at 37 °C and 5% CO₂ for 3 h. To enhance the dissolution of the dark-purple crystals of formazan, 110 μ L of 10% SDS in PBS (final pH 5.5) were added to all wells. The microtitre plates were stored in a light-tight box at room temperature and evaluated on the next day using the microplate reader iEMS (Labsystem, Turku, Finland) at 540 nm. All experiments were performed in triplicates.

Immunostaining of connexin-43

The cells were cultured to confluency on glass coverslips in four-well plates, treated with the tested compound and fixed in methanol/acetone 1:1 for 20 min at –20 °C. Cells were incubated with PBS containing 3% bovine serum albumin and 5% dried non-fat milk and 0.1% Tween for 1 h and subsequently with anti-cx43 antibody (Sigma) and with FITC coupled anti-rabbit IgG [29]. The coverslips were mounted on glass slides with the Vectashield® Hard Set mounting medium. Immunofluorescence images were captured using the inverted epifluorescent microscope T 200 equipped with a digital camera (CCD-1300, Nikon, Japan) and the LUCIA software (LIM, Czech Republic).

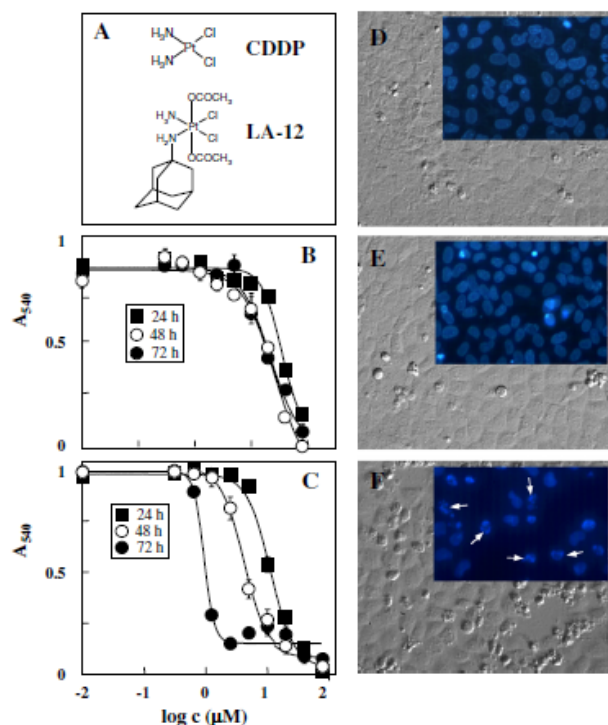


Fig. 1. Dose-response cytotoxicity curves and time course of morphological changes of WB-F344 monolayer after treatment with CDDP and LA-12. (A) Shows the structure of CDDP and LA-12. WB-F344 cells were seeded and exposed to CDDP (B) or LA-12 (C) as shown and cytotoxicity was assessed using the MTT assay as described in Materials and methods. WB-F344 cells were seeded and left untreated (D) or were exposed to 10 μM LA-12 for 4 h (E) and 7 h (F), and their images were then taken using Hoffmann contrast microscopy. The insets show nuclei of the cells after staining with Hoechst 33258 and visualisation using an epifluorescence microscope. The IC_{50} values for CDDP were 35.5 μM , 26.9 μM , and 19.9 μM (exposure time 24 h, 48 h, and 72 h respectively). The IC_{50} values for LA-12 were 10 μM , 2.7 μM , and 0.7 μM (exposure time 24 h, 48 h, and 72 h respectively).

Western blotting

Cells were grown in 6-well plates to the same confluency as for the SL/DT assay, treated as required, and harvested in 120 μL of the lysis buffer (1 mM NaF, 1 mM Na_3VO_4 , 1 mM PMSF, 1% Triton X-100, 10 mM Tris, 0.1% SDS). The samples were then sonicated, and the protein concentration determined using the bicinchoninic acid method and the iEMS reader. The samples were then diluted with the reducing sample buffer to equal protein levels and boiled for 3 min. Extraction and SDS-PAGE separation of proteins was performed as published earlier [30].

Phosphorylation of cx43

Protein extraction, SDS-PAGE and Western blotting of cx43 were performed according to the described methods [9]. Anti-cx43 polyclonal IgG (Sigma), recognising the C-terminal segment of the cytoplasmic domain corresponding to the amino acid residues 363–382, was used for immunostaining the cx43 protein transferred to a nitrocellulose membrane. Detection was performed using the solution of 0.03% (w/v) diaminobenzidine and 0.1% H_2O_2 in PBS. Cx43 immunoreactive bands were designated P0 (unphosphorylated connexin), P1, P2, and P3 (phosphorylated connexins) according to the nomenclature recommended by Matesic et al. [29]. The sample extracts from the WB-F344 cells treated with 20 nM TPA were used as a positive control for highly phosphorylated cx43 (P2,

P3) to compare the extent of connexin phosphorylation after the treatment of WB-F344 cells with the platinum compounds.

Activation of Erk

Cells were deprived of serum for 24 h to reduce the background levels of ERK activity. For detection of phosphorylated Erk1 and Erk2, the PVDF membrane was incubated with an anti-phospho-Erk polyclonal IgG in 5% milk for 3 h (New England Biolabs, Beverly, MA, USA). The Erk protein bands were detected using the ECL kit (Amersham Bioscience, UK).

p53 (ser15), PARP, β -actin

Other proteins were detected using the following antibodies: anti-p53(ser15) IgG (Cell Signalling), anti-PARP IgG (Cell Signalling) and anti- β -actin IgG (Sigma). Detection was performed using the ECL kit as described above.

Hoechst staining

WB-F344 cells were grown to confluency in a 6-well plate with 2.5 ml media per well and treated as specified, after which 125 μL of 1% Triton

X-100 in PBS was added per well, and the cells were left for 3 min and Hoechst 33258 stain (Sigma) then added at the final concentration of 2 $\mu\text{g/ml}$. After 3 min, the cells were spun down (200g, 5 min) and observed in an epifluorescence microscope.

Statistics

Lucifer Yellow diffusion zones were evaluated using the LUCIA imaging analyses software. The ratio of GJIC inhibition related to the negative control was evaluated and expressed in percentage (fraction of control, %FOC). The cytotoxicity curves were constructed and the IC_{50} values calculated using the GraphPad PRISM software (GraphPad Software, Inc. San Diego, CA).

Results and discussion

Previous reports showed that LA-12 was much more toxic to cancer cells than the prototypic drug CDDP (see structures of the drugs in Fig. 1A). Fig. 1B and C shows that this is also the case for the rat liver epithelial cell line WB-F344, revealing higher efficacy of LA-12 by ~ 2 orders of magnitude. Fig. 1D–F shows Hoffmann modulation contrast and fluorescence microscopy of control and LA-12-exposed WB-F344 cells after staining with Hoechst 33258, revealing significant changes in the nuclear morphology of the cells following incubating with LA-12. High cytotoxic potential of LA-12 is also reflected by its strong effect of the exposure time on the IC_{50} values in comparison to CDDP, and by a very sharp transition from non-toxic to toxic concentrations of LA-12 (Fig. 1B and C). Contrary to other platinum(II) or (IV) complexes (e.g. cisplatin, oxaliplatin, carboplatin, and satraplatin) tested in our laboratory, rapid initiation of apoptosis in cancer cell lines occurred at relatively low levels of LA-12 [2–4].

Treatment of WB-F344 cells with lower concentrations of LA-12 (1 or 10 μM) neither disturbed the cell monolayer nor increased the number of apoptotic cells within 4 h of treatment. Fig. 1D–F shows Hoffmann contrast microscopy pictures of the monolayer of control WB-F344 cells and cells exposed to 10 μM LA-12. The monolayer was intact at least for 4 h. After 7 h of exposure the rips surrounded by high number of cells in apoptosis appeared in the monolayer. Morphological signs of apoptosis were well developed. Fluorescence staining with Hoechst 33258 showed significant changes in the nuclear morphology of the cells (see inserts in Fig. 1D–F following incubation with 10 μM LA-12. After a 9 h exposure, the monolayer was completely destroyed and a high number of cells were in various stages of apoptosis (micrograph not shown).

Increased number of cells displaying morphological changes specific for early stage of apoptosis and a number of rips in the monolayer were seen after a 3-h exposure of the cells to high concentrations of LA-12 (80 μM). In contrast to LA-12, more than 9 h were needed for high concentrations of CDDP (80 μM) to see the first morphological signs of apoptosis and appearance of the first rips in the cell monolayer (micrograph not shown).

Since the nuclear fragmentation of WB-F344 cells exposed to LA-12 as shown in Fig. 1F is reminiscent of apoptotic morphology, we carried out experiments whose aim was to confirm or rule out the apoptotic type of cell death. One general feature of apoptosis is activation of caspases, which then cleave the so-called ‘death substrate’ in a specific manner. One of the caspases activated during apoptosis is caspase-3, which efficiently cleaves PARP into two specific fragments [31]. As shown in Fig. 2A, LA-12 caused PARP fragmentation after 6 h of treatment, suggestive of a typical apoptogenic activity. Since CDDP is known to induce apoptosis by activation of the transcriptional activity of p53 due to formation of adducts with genomic DNA, we studied whether the superior toxicity of LA-12 was due to faster kinetics of p53 activation, as documented by phosphorylation of the protein on Ser15. Fig. 2B reveals that LA-12 caused Ser15 phosphorylation and thereby activation of p53 in WB-F344 cells as soon as within 60 min, while CDDP exerted this effect much later, i.e. 22 h after addition to the cells. The intensity of p53 phosphorylation was comparable to that observed with DBaLP, which was used as a positive control [32]. These results confirm the apoptotic type of cell death induced by LA-12 and indicate that it occurs with fast kinetics, most likely due to rapid activation of p53.

While there has been extensive research into the role of p53 in apoptosis induction by CDDP and similar compounds, little is known about the effect of these agents on

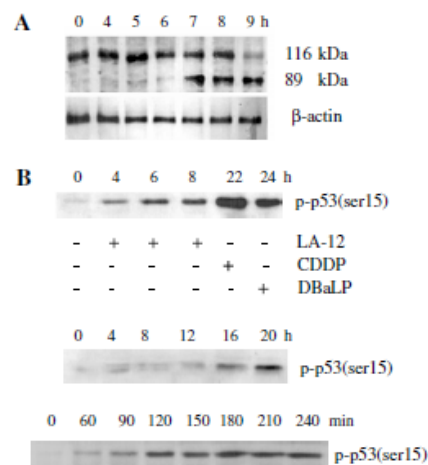


Fig. 2. LA-12 induces apoptosis and causes p53 phosphorylation. (A) WB-F344 cells were exposed to 10 μM LA-12 for the time periods indicated and inspected using Western blotting for the cleavage of PARP. (B) WB-F344 cells were treated with 10 μM LA-12, 30 μM CDDP or 100 nM DBaLP for the periods shown and assessed for p53 phosphorylation at Ser15 by Western blotting. The middle part of (B) shows p53 phosphorylation in cells exposed to 30 μM CDDP and the bottom part of (B) shows p53 phosphorylation in cells exposed to 10 μM LA-12 in earlier phases of the experiment. DBaLP was used as a positive control.

GJIC, although it has been shown that compounds like CDDP may suppress intercellular communication [14,15]. We therefore studied if LA-12 affects GJIC in an established model, the cell line WB-F344, using the Lucifer Yellow diffusion assay. As documented in Fig. 3, CDDP exerted only a low effect on GJIC at concentrations of up to 80 μM , while LA-12 showed an $\sim 40\%$ and almost 100% inhibition at 10 μM at 30 min and 2 h, respectively. Fig. 3C shows the sigmoidal curves for GJIC inhibition by exposure of the cells to LA-12, which allowed to calculate the EC_{50} values to be 12.3 and 6 μM for the 2- and 3-h exposure, respectively. Transplatin, the non-cytotoxic platinum complex, was used as a negative control. The IC_{50} value for transplatin was $>160 \mu\text{M}$, and incubation of the WB-F344 cells with transplatin (80 μM) for 24 h did not induce any morphological changes. Moreover, transplatin did not induce any inhibition of GJIC at the dose of 80 μM (data not shown).

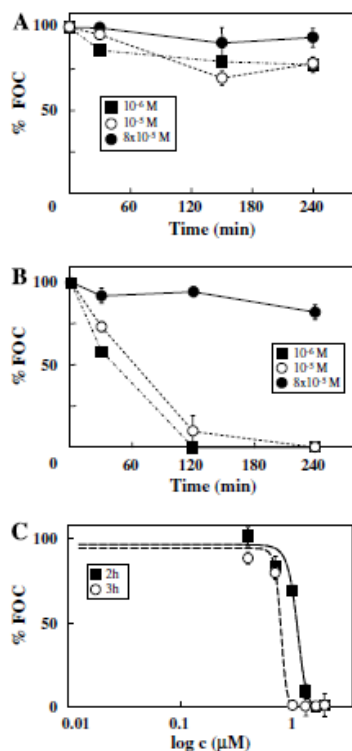


Fig. 3. LA-12 inhibits intercellular communication. WB-F344 cells were exposed to CDDP (A) and LA-12 (B) at concentrations and for times shown and assessed for GJIC by the Lucifer Yellow diffusion method as detailed in Materials and methods. (C) Shows the effect of different concentrations of LA-12 on GJIC following 2- and 3-h exposure. There was no effect of CDDP on inhibition of GJIC, so the graph for CDDP was omitted. The IC_{50} values are 12 μM for 2 h and 6 μM for 3 h of treatment.

These results indicate that the ability of LA-12 to inhibit GJIC may reflect the high apoptogenic activity of LA-12 in contrast to CDDP. The effect of LA-12 on GJIC inhibition is in a good correlation with the cytotoxic data shown in Fig. 1B and C. We have also found a direct correlation between cytotoxicity and inhibition of GJIC in the homologous series of platinum(II) and (IV) based drugs (unpublished results), but LA-12 is unique among them with respect to induction of rapid onset of apoptosis in various cancer cell lines at concentrations relevant to levels found in sera of CDDP-treated patients.

Due to the time needed for penetration of LA-12 into the cells, interaction with DNA, formation and recognition of DNA-platinum adducts leading to triggering irreversible pro-apoptotic signals, LA-12 required more than 30 min to induce significant inhibition of gap junctions in the WB-F344 cells (Fig. 3B). The GJIC inhibition induced by LA-12 was a relatively slow process when compared to the effect of non-genotoxic xenobiotics, e.g. low-molecular-weight polycyclic aromatic hydrocarbons, which inhibit GJIC within 15–30 min after exposure, or phorbol esters such as TPA inducing inhibition of GJIC within 5 min. This rapid onset of GJIC inhibition induced by TPA or polyaromatic hydrocarbons is caused by direct interactions with protein kinases and a consequent activation of intracellular signal transduction pathways [29,30].

The assay used for assessment of GJIC inhibition is based on diffusion of the fluorescent dye Lucifer Yellow across rows of WB-F344 cells via connexin channels connecting the cells. Fig. 4 documents this assay and clearly shows that LA-12 suppressed diffusion of the dye relative to the control. TPA, used as a positive control [33], exerted similar inhibition on Lucifer Yellow diffusion, while the inhibitory activity of LA-12 was overcome by the MEK1/2 inhibitor U0126 added to cells at 20 μM and 30 min before LA-12. That the MEK pathway, but not several other signalling pathways, may be involved in inhibition of GJIC in the case of LA-12 is documented in Table 1. It indicates that within the inhibitors tested, only the MEK1/2 inhibitor U0126 exerted an effect. Moreover, results in Table 1 suggest that the effect of the MEK1/2 inhibitor may involve phosphorylation of an important component of GJIC, cx43.

We then followed the fate of cx43 in WB-F344 cells exposed to LA-12, since an earlier report revealed its ubiquitination and degradation following its hyperphosphorylation [16]. Hyperphosphorylation of cx43 induced by LA-12 or TPA effected also relocalisation of cx43 from the membrane into the cytosol. Immunostaining of connexon clusters showed their rapid disappearance from cell membrane after treatment with TPA or LA-12 (Fig. 6). Relocalisation of cx43 was also prevented by application of the inhibitor U0126.

We further investigated a possible link between the effect of LA-12 on components of the MEK pathways, ERK1 and ERK2, and on the phosphorylation status of cx43, since it has been shown that hyperphosphorylation of cx43 via the

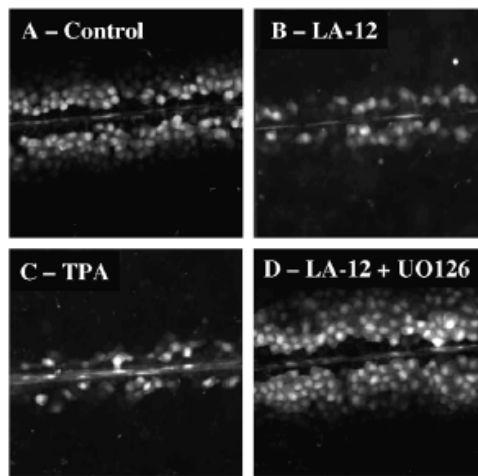


Fig. 4. LA-12 inhibits GJIC communication through the MEK/ERK pathway. WB-F344 cells were exposed for 3 h to 10 μ M LA-12 without (B) and with 30-min pre-incubation with 20 μ M UO126 (D). (A) Shows the negative control (β -cyclodextrin exposure) and (C) the positive control (exposure to 20 nM TPA for 30 min). Following treatment, the cells were stained with Lucifer Yellow as detailed in Materials and methods and visualised by epifluorescence microscopy using a 100-fold magnification.

MEK pathway causes GJIC inhibition [16,29]. Fig. 5A shows Western blots documenting that, indeed, LA-12 caused ERK-dependent phosphorylation of cx43. Thus, exposure of WB-F344 cells to LA-12 resulted in phosphorylation of both ERK1 and ERK2 and in hyperphosphorylation of cx43 (appearance of the band designated cx43 P2), which was abrogated by UO126. A very similar pattern was observed in the case of TPA that is known to activate ERK and inhibit GJIC via cx43 hyperphosphorylation. On the other hand, in corresponding experiments, we did not observe any alteration of the phosphorylation status of cx43 in the presence of CDDP, although the drug caused activation of ERK, albeit at a later stage (Fig. 5B). A good correlation of the data presented in Figs. 4 and 5 imply that activation of ERK and subsequent phosphorylation of cx43 and its relocalisation from the cell membrane (Fig. 6) is responsible for GJIC inhibition induced by LA-12.

Activation of ERK was also found to be important for induction of apoptosis by CDDP in various cell lines [14] and inhibition of the MEK/ERK pathway by UO126 can protect cells against toxic effect of CDDP [15]. We tested a possible role of the ERK pathway activation in WB-F344 cells for the toxicity of CDDP and LA-12. We found that application of UO126 decreased apoptosis in WB-F344 cell treated with CDDP (Fig. 7) but no effect was observed for LA-12 (data not shown). Taken together, activation of ERK1/2 by LA-12 is connected to inhibition of GJIC but, in contrast to CDDP, might not be essential for induction of apoptosis.

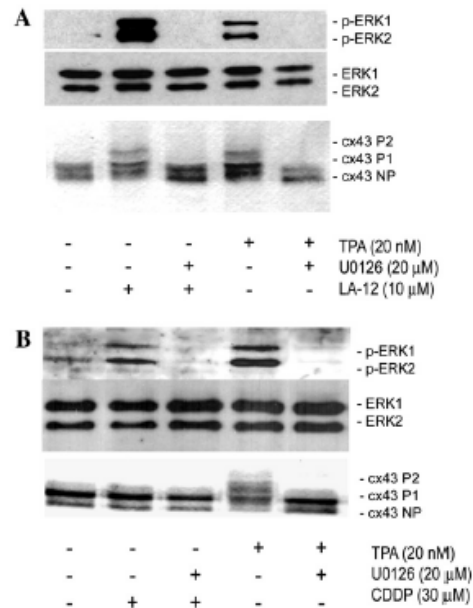


Fig. 5. LA-12 causes hyperphosphorylation of cx43 via ERK activation. WB-F344 cells were exposed to 10 μ M LA-12 for 2 h (A) or 30 μ M CDDP for 12 h (B) in the absence or presence of 20 μ M UO126. Exposure to 20 nM TPA was used as a positive control. Following treatment, the cells were probed by Western blotting for phosphorylated cx43, and for total and phosphorylated ERK1/2, as detailed in Materials and methods.

Table 1
Delineation of pathways affected by LA-12

Pathway	Treatment	GJIC status	Cx43 phosphorylation status
MEK	U0126 + LA-12	Functional	Basal
	U0126 + TPA	Functional	Basal
PKC	GF109203x + LA-12	Inhibited	Hyperphosphorylated
	GF109203x + TPA	Functional	Basal
EGFR	AG1478 + LA-12	Inhibited	Hyperphosphorylated
	AG1478 + TPA	Inhibited	Hyperphosphorylated
p38	SB202190 + LA-12	Inhibited	Hyperphosphorylated
	SB202190 + TPA	Inhibited	Hyperphosphorylated
JNK	SP600125 + LA-12	Inhibited	Hyperphosphorylated
	SP600125 + TPA	Inhibited	Hyperphosphorylated

WB-F344 cells were exposed to 10 μ M LA-12 for 2 h and to 10 nM TPA for 30 min following 30-min pre-incubation with 20 μ M UO126, 10 μ M GF109203x, 10 μ M AG1478, 10 μ M SB202190 or 200 nM SP600125, and the cx43 phosphorylation status was evaluated as detailed in Materials and methods. The GJIC status has been assigned as functional or inhibited under the conditions of the experiment as indicated by the Lucifer Yellow method (see Materials and methods).

The efficacy of LA-12 to induce apoptosis and inhibit GJIC may be due to its faster accumulation in target cells, including those resistant to CDDP, and due to very fast

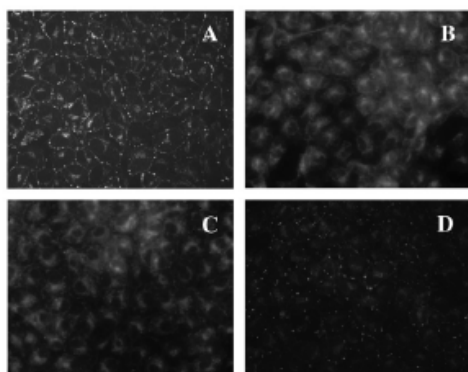


Fig. 6. LA-12 causes internalisation of cx43. WB-F344 cells were allowed to reach confluence, after which they were treated with the vehicle (control cells, A), 10 nM TPA for 30 min (B) and 10 μ M LA-12 for 2 h alone (C) or following a 30-min pre-incubation with 20 μ M U0126 (D). The cells were then fixed and immunostained for cx43. The images were acquired using epifluorescence microscopy.

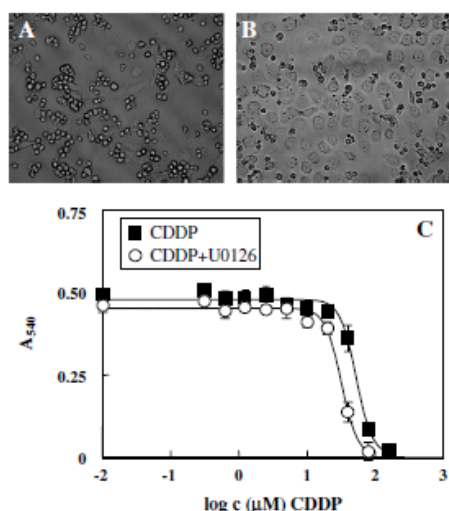


Fig. 7. Inhibitory effect of U0126 on apoptosis induced by CDDP in WB-F344 cells. Micrographs show WB-F344 cells treated with 40 μ M CDDP for 48 h (A) or 40 μ M CDDP + 20 μ M U0126 (B). Pictures were obtained using Hoffman modulation contrast microscopy. (C) Shows cytotoxicity curves for WB-F344 cells treated with CDDP for 48 h with or without pre-treatment with 20 μ M U0126. The IC₅₀ values are 27 μ M for CDDP and 47 μ M for the cells pre-treated with U0126.

formation of adducts with DNA bases (unpublished results). Rapid connection between the DNA injury signal and pro-apoptotic pathways is probably responsible for the strong *in vitro* cytotoxic effects of LA-12. Hyperphosphory-

lation of cx43 via activation of the MEK/ERK pathway results in disappearance of connexons and inhibition of GJIC in WB-F344 cells treated with toxic doses of LA-12. On the other hand, treatment of cells with non-toxic doses of LA-12 ($\leq 1 \mu$ M) did not cause any inhibition of GJIC. These data indicate that disturbance of tissue homeostasis due to inhibition of GJIC may be linked to direct cytotoxic effects of platinum drugs, rather than to an indirect effect found for some carcinogens, such as TPA or polyaromatic tumour promoters. The possible role of the rapid inhibition of GJIC as a feed-back signal magnifying apoptotic pathway is a topic for future research in the intriguing field of cell proliferation and apoptosis.

Acknowledgments

This work was supported by a grant of the Ministry of Industry and Trade of the Czech Republic, Contract No. PZ-Z2/29, "New Medicines for Cancer Therapy", and a grant the Ministry of Agriculture of the Czech Republic (Grant No. MZE 0002716201) and IGA Acad. Sci. Czech Republic (No. IQS500040507).

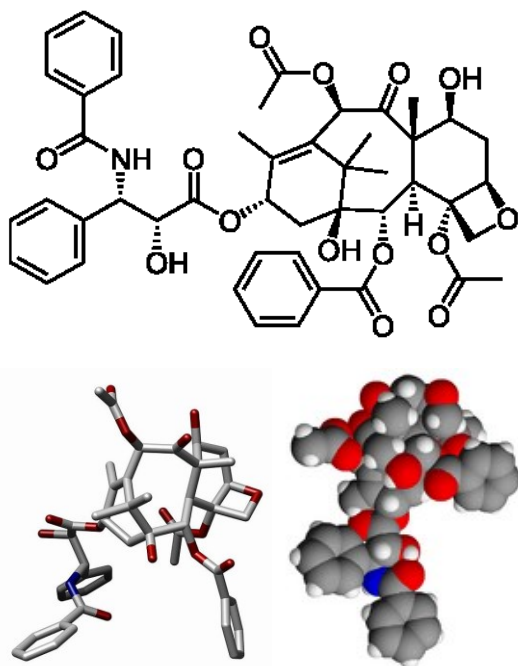
References

- [1] L.R. Kelland, in: B. Lippert (Ed.), *Chemistry and Biochemistry of a Leading Anticancer Drug*, Wiley-VCH, Weinheim, Germany, 1999, pp. 497–521.
- [2] F. Žák, J. Turánek, A. Kroutil, P. Sova, A. Mistr, A. Poulková, P. Mikolín, Z. Žák, A. Kašná, D. Záluská, J. Neča, L. Šindlerová, A. Kozubík, *J. Med. Chem.* 47 (2004) 761–763.
- [3] J. Turánek, A. Kašná, D. Záluská, J. Neča, V. Kvardová, P. Knöžigová, V. Horváth, L. Šindlerová, A. Kozubík, P. Sova, A. Kroutil, F. Žák, A. Mistr, *Anticancer Drugs* 15 (2004) 537–543.
- [4] A. Kozubík, V. Horváth, L. Šviháková-Šindlerová, K. Souček, J. Hofmanová, P. Sova, A. Kroutil, F. Žák, A. Mistr, J. Turánek, *Biochem. Pharmacol.* 69 (2005) 373–383.
- [5] P. Sova, A. Mistr, A. Kroutil, F. Žák, P. Pouckova, M. Zadinova, *Anticancer Drugs* 17 (2006) 201–206.
- [6] P. Sova, A. Mistr, A. Kroutil, F. Žák, P. Pouckova, M. Zadinova, *Anticancer Drugs* 16 (2005) 653–657.
- [7] J.E. Trosko, C.C. Chang, *Mutat. Res.* 480–481 (2001) 219–229.
- [8] J.E. Trosko, C.C. Chang, B. Upham, M. Wilson, *Toxicol. Lett.* 102–103 (1998) 71–78.
- [9] J.E. Trosko, C.C. Chang, M.R. Wilson, B. Upham, T. Hayashi, M. Wade, *Methods* 20 (2000) 245–264.
- [10] D.W. Laird, J.S. Saez, in: E.L. Hertzberg (Ed.), *Advances in Molecular and Cell Biology*, Vol. 30, Elsevier B.V., 2000, pp. 99–128.
- [11] G. Sohl, K. Willecke, *Cardiovasc. Res.* 62 (2004) 228–232.
- [12] D.W. Laird, *Biochem. J.* 394 (2006) 527–543.
- [13] P.D. Lampe, A.F. Lau, *Int. J. Biochem. Cell. Biol.* 36 (2004) 1171–1186.
- [14] X. Wang, J.L. Martindale, N.J. Holbrook, *J. Biol. Chem.* 275 (2000) 39435–39443.
- [15] S.K. Jo, W.Y. Cho, S.A. Sung, H.K. Kim, N.H. Won, *Kidney Int.* 67 (2005) 458–466.
- [16] H. Qin, Q. Shao, S.A. Igdouma, M.A. Alaoui-Jamali, D.W. Laird, *J. Biol. Chem.* 278 (2003) 30005–30014.
- [17] E. Leithe, E. Rivedal, *J. Biol. Chem.* 279 (2004) 50089–50096.
- [18] M.S. Park, M. De Leon, P. Devarjan, *J. Am. Soc. Nephrol.* 13 (2002) 858–865.
- [19] W. Woessmann, X. Chen, A. Borkhardt, *Cancer Chemother. Pharmacol.* 50 (2002) 397–404.

- [20] A. Mandic, K. Viktorsson, T. Heiden, J. Hansson, M.C. Shoshan, *Melanoma Res.* 11 (2001) 11–19.
- [21] E.A. Hanna, S. Umhauer, S.L. Roshong, M.P. Piechocki, M.J. Fernstrom, J.D. Fanning, R.J. Ruch, *Carcinogenesis* 20 (1999) 1369–1373.
- [22] O.S. Frankfurt, D. Seckinger, E.V. Sugarbaker, *Cancer Res.* 51 (1991) 1190–1195.
- [23] V.A. Krutovskikh, C. Piccoli, H. Yamasaki, *Oncogene* 21 (2002) 1989–1999.
- [24] R. Jensen, P.M. Glazer, *Proc. Natl. Acad. Sci. USA* 101 (2004) 6134–6139.
- [25] M. Tsao, J.D. Smith, K.G. Nelson, J.W. Grisham, *Exp. Cell Res.* 154 (1984) 38–52.
- [26] M.H. El-Fouly, J.E. Trosko, C.C. Chang, *Exp. Cell Res.* 168 (1987) 422–430.
- [27] T. Mosmann, *J. Immunol. Methods* 65 (1983) 55–63.
- [28] U. Bank, D. Reinhold, S. Ansorge, *Allerg. Immunol.* 37 (1991) 119–123.
- [29] D.F. Matesic, H.L. Rupp, W.J. Bonney, R.J. Ruch, J.E. Trosko, *Mol. Carcinog.* 10 (1994) 226–236.
- [30] A.M. Rummel, J.E. Trosko, M.R. Wilson, B. Upham, *Toxicol. Sci.* 49 (1999) 232–240.
- [31] M. Los, M. Mozoluk, D. Ferrari, A. Stepczynska, C. Stroh, A. Renz, Z. Herceg, Z. Wang, K. Schulze-Osthoff, *Mol. Biol. Cell* 13 (2002) 978–988.
- [32] Z. Andrysiak, M. Machala, K. Chramostova, J. Hofmanova, A. Kozubik, J. Vondracek, *Toxicol. Appl. Pharmacol.* 211 (2006) 198–208.
- [33] E. Leithe, V. Cruciani, T. Sanner, S.O. Mikalsen, E. Rivedal, *Carcinogenesis* 24 (2003) 1239–1245.

2.2.2. Paclitaxel

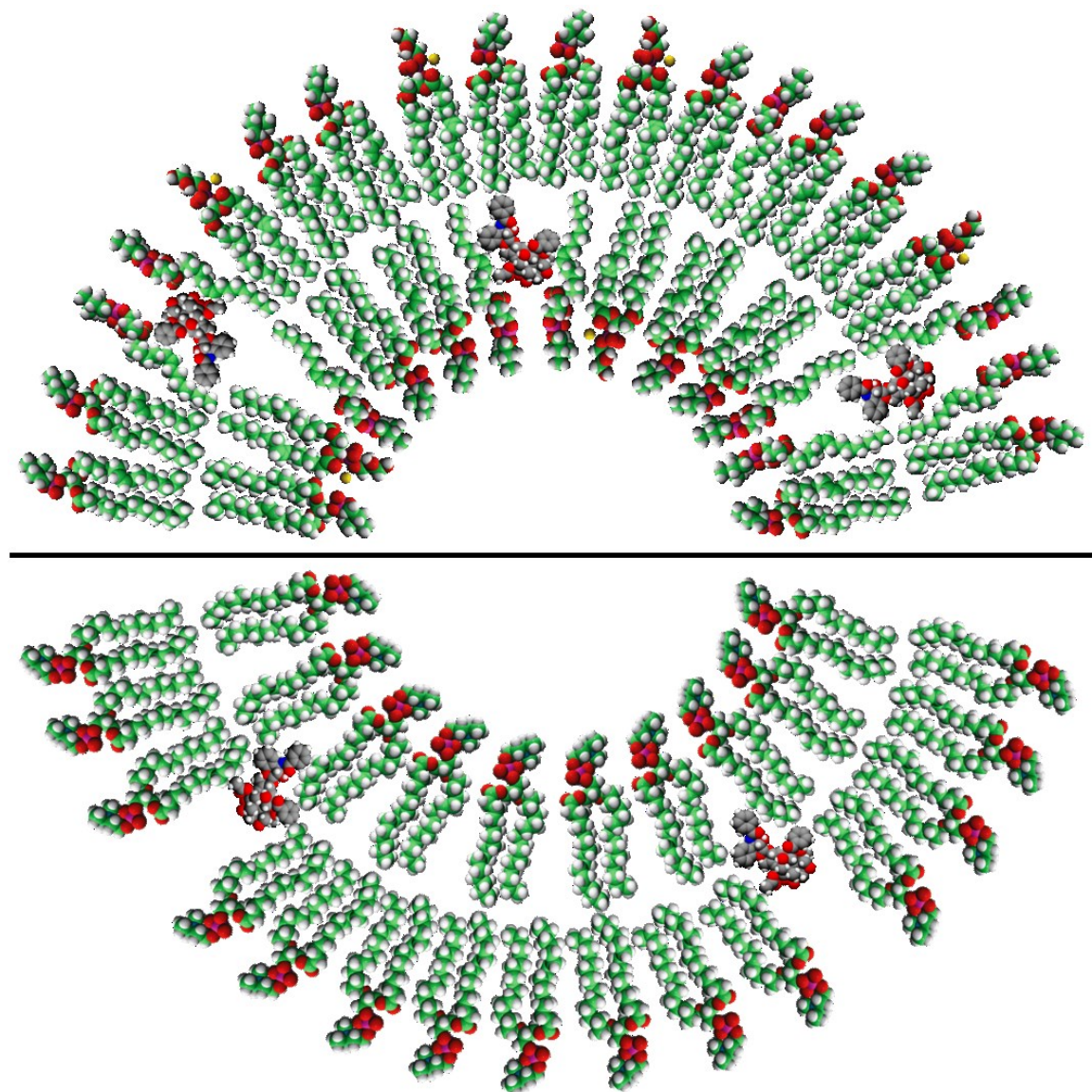
Paclitaxel představuje zavedené farmakum pro léčbu zejména ovariálního karcinomu. Mechanismus účinku spočívá ve vazbě na tubulin a inhibici depolymerace mikrotubulů, což vede v konečném důsledku k apoptóze buňky. Molekula paclitaxelu je poměrně objemná asymetrická lipofilní struktura a ve vodném prostředí je málo rozpustná. Paclitaxel snadno krystalizuje a vytváří jehlicové krystaly a krystalové drúzy. Tyto vlastnosti jsou pro injekční parenterální aplikaci nevhodné a byla testována celá řada způsobů, jak vyvinout vhodnou lékovou formu. Byly syntetizovány rozpustné deriváty ve formě prolečiv, byly testovány solubilizační systémy na bázi cyklodextrinů, biokompatibilních polymerů, emulzí a, proteinových nanočástic, byly připraveny nanokrystaly a různé nanokapsule. V klinické praxi je používána formulace na bázi Cremofor®, což je olejová emulze vykazující však vedlejší toxické účinky. Nově jsou na trhu preparáty na bázi proteinových albuminových nanočástic (Abraxane) a samozřejmě také preparáty na bázi liposomů (např. Lipusu, registrován v Číně).



Obr. 20 Strukturální vzorec paclitaxelu a prostorové modely molekuly paclitaxelu

V případě paclitaxelu slouží liposomy jako solubilizátor (paclitaxel je zabudován a vlastně solubilizován v hydrofobní části fosfolipidové membrány) a zároveň jako cílený nosič. Zabudování poměrně velké a nesymetrické molekuly paclitaxelu do lipidní

membrány liposomů představuje určitý stérický problém. Není tedy divu, že dochází k narušení struktury fosfolipidové membrány liposomů a enkapsulační kapacita je u klasických liposomů kolem tří molárních procent. Další zvyšování koncentrace paclitaxelu vede k destabilizaci systému a vypadávání paclitaxelu z membrány a následné tvorbě jehlicových krystalů, což je z hlediska intravenózní aplikace nepřijatelné.



Obr. 21 Schéma umístění molekuly paclitaxelu ve fosfolipidové membráně.

V horní části je paclitaxel enkapsulován v hydrofobní kapse z lysofosfocholinu. V dolní části je fosfolipidová dvojvrstva narušena vmezeřením paclitaxelu, výsledkem je nízká enkapsulační kapacita klasických liposomů.

Zvýšení enkapsulační kapacity pro paclitaxel je možné změnou lipidního složení liposomálních membrán s využitím lipidů tvořících „hydrofobní kapsy“, do kterých se může vměstnat molekula paclitaxelu. Takové kapsy tvoří například lysofosfolipidy nebo cardiolipin.

Zkoumali jsme možnost přípravy stabilních liposomů s enkapsulovaným paclitaxelem s využitím lysolipidů. V tomto případě jsme dosáhli více než dvojnásobné enkapsulační účinnosti v porovnání s klasickými liposomy. Tento systém je vhodný pro přípravu jak pasivně, tak aktivně targetovaných liposomů. Protinádorový účinek byl prokázán na myším modelu plicního melanomu, kdy bylo možné podávat extrémně vysoké dávky paclitaxelu v liposomech, neboť tato formulace paclitaxelu byla netoxická ve srovnání s paclitaxelem solubilizovaným v Cremoforu®.

Liposomes With High Encapsulation Capacity for Paclitaxel: Preparation, Characterisation and *In Vivo* Anticancer Effect

ŠTĚPÁN KOUDELKA, PAVLÍNA TURÁNEK-KNÖTIGOVÁ, JOSEF MAŠEK, ZINA KORVASOVÁ, MICHAELA ŠKRABALOVÁ, JANA PLOCKOVÁ, ELIŠKA BARTHELDYOVÁ, JAROSLAV TURÁNEK

Department of Vaccinology and Immunotherapy, Veterinary Research Institute, Hudcova 70, 621 00 Bno, Czech Republic

Received 30 June 2009; revised 15 September 2009; accepted 22 September 2009

Published online 10 November 2009 in Wiley InterScience (www.interscience.wiley.com). DOI 10.1002/jps.21992

ABSTRACT: Paclitaxel (PTX) is approved for the treatment of ovarian and breast cancer. The commercially available preparation of PTX, Cremophor EL[®] is associated with hypersensitivity reactions in spite of a suitable premedication. In general, the developed liposomal PTX formulations are troubled with low PTX encapsulation capacity (maximal content, 3 mol%) and accompanied by PTX crystallisation. The application of "pocket-forming" lipids significantly increased the encapsulation capacity of PTX in the liposomes up to 10 mol%. Stable lyophilised preparation of PTX (7 mol%) encapsulated in the liposomes composed of SOPC/POPG/MOPC (molar ratio, 60:20:20) doped with 5 mol% vitamin E had the size distribution of 180–190 nm (PDI, 0.1) with ζ -potential of -31 mV. Sucrose was found to be a suitable cryoprotectant at the lipid:sugar molar ratios of 1:5–1:10. This liposomal formulation did not show any evidence of toxicity in C57BL/6 mice treated with the highest doses of PTX (100 mg/kg administered as a single dose and 150 mg/kg as a cumulative dose applied in three equivalent doses in 48-h intervals). A dose-dependent anticancer effect was found in both hollow fibre implants and syngenic B16F10 melanoma mouse tumour models. © 2009 Wiley-Liss, Inc. and the American Pharmacists Association *J Pharm Sci* 99:2309–2319, 2010

Keywords: paclitaxel; liposomes; extrusion; particle size; lyophilisation; stability; melanoma; B16F10; hollow fibre implants; nanotechnology

INTRODUCTION

PTX is one of the most important compounds that emerge from a natural source. This drug is approved for the treatment of ovarian and breast cancer and is one of the most exciting anticancer molecules currently available.^{1,2} However, a suitable drug formulation still remains a problem, because PTX has a low therapeutic index owing to its high lipophilic character and correspondingly low solubility in water. The commercially available injectable

preparation Taxol[®] is a sterile solution of PTX in Cremophor EL[®] (polyethoxylated castor oil) and dehydrated alcohol. Present day cancer chemotherapy with PTX is associated with hypersensitivity reactions in spite of a suitable premedication with corticosteroids and anti-histamines.³ Hence, the development of an improved delivery system for PTX is of high importance. Current approaches to the improvement are focused mainly on the development of formulations that are devoid of Cremophor EL[®], investigation of the possibility of a large-scale preparation and questing for a longer-term stability. These different approaches have shown some promising possibilities to replace Taxol[®] by a less irritable preparation such as: (a) micelle formulations,⁴ (b) water-soluble prodrug preparations,⁵ (c) enzyme-activatable prodrug preparations conjugated with antibodies or albumin,^{6,7} (d) parenteral emulsions,⁸ (e) microspheres,⁹ (f) cyclodextrins¹⁰ and (g) nanocrystals.¹¹ However, none of these alternatives has reached the stage of replacing Taxol[®] in the clinic yet. Nonliposomal formulations of PTX based on protein-bound particles (Abraxane[®]) were recently approved by FDA. The present-day situation in PTX drug formulations is well reviewed by Hennenfent and Govindan.¹²

Additional Supporting Information may be found in the online version of this article.

Štěpán Koudeřka and Pavlína Turánek-Knötigová contributed equally to this work.

Abbreviations: EE_{PTX}, encapsulation efficiency of paclitaxel; DLS, dynamic light scattering; MOPC, 1-oleoyl-2-hydroxy-*sn*-glycero-3-phosphatidylcholine; POPG, 1-oleoyl-2-hydroxy-*sn*-glycero-3-phosphatidylglycerol; MTD, maximum tolerated dose; PEG-POPE, 1-palmitoyl-2-oleoyl-*sn*-glycero-3-phosphoethanolamine-*N*-(poly(ethyleneglycol)²⁰⁰⁰); PDI, polydispersity index; POPG, 1-palmitoyl-2-oleoyl-*sn*-glycero-3-phosphatidylglycerol; PTX, paclitaxel; SOPC, 1-stearoyl-2-oleoyl-*sn*-glycero-3-phosphatidylcholine.

Correspondence to: Jaroslav Turánek (Telephone: +420-5-3333-1311; Fax: +420-5-4121-1229; E-mail: turanek@vri.cz)

Journal of Pharmaceutical Sciences, Vol. 99, 2309–2319 (2010)
© 2009 Wiley-Liss, Inc. and the American Pharmacists Association



Liposomes, lipid membrane vesicles, represent potentially versatile drug carriers for a wide range of drugs.¹³ Recent advances in this area have led to the development of some products for human medicine, for example, amphotericin and liposomal doxorubicin,¹⁴ and many other liposomal formulations of drugs are in various stages of clinical trial. Various liposome-based PTX formulations were developed in order to improve the drug therapeutic efficiency and to eliminate its negative side-effects. Within the range of the liposomal PTX prepreparates, different approaches had been designed, which has resulted in the preparation of conventional liposomes,^{15,16} sterically stabilised liposomes,^{17,18} immunoliposomes,^{19,20} cationic liposomes,^{21,22} and magneto-liposomes.²³ The liposomal PTX formulations have been successfully tested on various experimental *in vivo* models. In comparison with PTX in Cremophor EL[®], the liposomal PTX was shown to exhibit a lower toxicity, higher efficiency and an increased MTD. However, the maximal achieved encapsulation capacity of the conventional liposomal formulations for PTX was only about 3 mol%. There have been reports to suggest that the PTX encapsulation can be further increased using lysophospholipids in the liposome formulation. These lipids increase the membrane bilayer fluidity and create bilayer "pockets," in which the hydrophobic molecules such as PTX can be encapsulated.²⁴ Yet, no studies have been reported on PTX encapsulated in pocket-forming liposomes as regards their physical-chemical stability as well as biological activity. In this study we investigated the usability of pocket-forming lipids for the preparation of stable and nontoxic PTX liposomes. This basic liposomal carrier could be used for the development and construction of next generation of advanced targeted PTX delivery system. We report improvements in this approach leading to a new optimal liposomal PTX formulation (7 mol% PTX) that is well tolerated and efficient for the treatment of experimental cancer in mouse models. Moreover, this formulation is stable in the lyophilised form during storage.

MATERIALS AND METHODS

Chemicals

Lipids comprising SOPC, MOPC, POPG, PEG-POPE and MOPG were purchased from (Avanti Polar Lipids Alabaster, AL). Vitamin E was obtained from Sigma-Aldrich (Prague, Czech Republic). PTX (purity of 97%, HPLC) was purchased from Houser Chemical Research Inc. (Boulder, CO). All the organic solvents used (reagent or HPLC grade) were from Sigma-Aldrich (Czech Republic).

Methods for the Preparation of PTX Liposomal Formulations

The preparation of the liposomes by lyophilisation from 2-methyl-butan-2-ol was done as described in literature.¹⁵ Briefly, lipids, vitamin E and PTX were solubilised in 2-methyl-butan-2-ol (Sigma-Aldrich, Czech Republic). The mixture of lipids and PTX (12 mg/mL; the total volume of 1 mL) was frozen at -80°C and lyophilised for 24 h in a Lyovac GT2 instrument (Finaqua, Finland). Stepwise hydration of the lipids in PBS was accomplished via step-by-step addition of an aqueous phase to the lyophilisate (20- μL additions during 20 min, total volume of 200 μL) under continual magnetic stirring. After lipid hydration, the volume was adjusted to 1 mL in total and optional extrusion through 0.2- μm polycarbonate filters was performed.

Liposomes containing vitamin E and PTX were prepared by the proliposome-liposome method and by hydration of a lipid film followed by extrusion through 0.2- μm polycarbonate filters in an analogous way to that described previously by Turánek et al.^{25,26} The hand operated device Mini-Extruder (Avanti Polar Lipids Alabaster, AL) was used for the extrusion of small volumes of liposomes (up to 1 mL). Large volumes of the liposomes were extruded by means of a high pressure cell (Millipore Billerica, MA) linked with FPLC instrument (Pharmacia, Uppsala, Sweden).²⁶ The liposomes were prepared of SOPC, POPG and MOPC according to the general composition formula: molar ratio SOPC/POPG/MOPC, 80-X:X:20; where X is 0, 10, 20 or 30 mol% (cf. Tab. 1). The content of PTX was 7 mol%. The freezing and thawing step was omitted in order to prepare oligolamellar liposomes with low water content.

Table 1. Lipids Used for the Preparation of Conventional and Sterically Stabilised Liposomal PTX Formulations

Preparate Formulation	Lipid Composition (Molar Ratio)		
	SOPC	POPG	MOPC
Conventional Liposomes			
1	80	0	20
2	70	10	20
3	60	20	20
4	50	30	20
Preparate Formulation	Lipid Composition (Molar Ratio)		
Sterically Stabilised Liposomes	SOPC	PEG-POPE	MOPC
5	75	5	20

Cryoprotective Effect of Various Disaccharides

The extruded (0.2 μm) liposomal PTX samples were mixed with cryoprotectants (lactose, mannitol, sucrose and trehalose) in various molar ratios (1:1, 1:5 and 1:10) and then lyophilised for 24 h. The effectiveness of particular oligosaccharides as cryoprotectants was evaluated on the basis of the following parameters: the preservation of the original size and the lack of PTX crystals after lyophilisate reconstitution.

Analyses of the PTX Levels

Prior to the chromatographic analysis, the liposomal PTX samples were ultracentrifuged (Beckman-Coulter Prague, Czech Republic, Avanti J-30I) at 100,000 $\times g$ for 30 min to separate the liposome fraction from the supernatant. All samples were lyophilised, redissolved in methanol and analysed by HPLC. The encapsulation efficiency (EE_{PTX}) was calculated according to the following equation:

$$EE_{\text{PTX}} (\%) = \frac{m_{\text{LIP-PTX}}}{m_{\text{TOTAL-PTX}}} \times 100 \quad (1)$$

where $m_{\text{LIP-PTX}}$ is the molar quantity of PTX that remains liposome-associated and $m_{\text{TOTAL-PTX}}$ is the total molar quantity of PTX.

The chromatography procedure was carried out using a Waters system (Milford, MA) composed of a 717 plus auto-injector, a 600 gradient pump and a 996 diode array detector. A Nova-Pak (C18, 150 mm in length, 3.9 mm ID, 4- μm particle size) stainless-steel analytical column was attached. The mobile phase consisting of acetonitrile and water (45:55, v/v) was degassed prior to use. The separation was carried out isocratically, the temperature was set on 35°C and the flow rate was 1.1 mL/min. The detector wavelength was 229 nm. Millennium 2010 programme was applied to the data collection and integration. The determination of the PTX levels was carried out according to the modified procedure by Song et al.²⁷

Liposome Size and ζ -Potential Determination

The size distribution and ζ -potential of the liposomal preparations were determined by DLS and microelectrophoresis using a Zetasizer Nano ZS (Malvern, UK). The measurements were carried out at 25°C with the liposomal concentration of 1 mg/mL in PBS. The disposable cells were used for the ζ -potential measurements. The size of the liposomes was expressed as the distribution by volume and by number.

Transmission Electron Microscopy

Electron micrographs were made using Philips-Morgagni transmission electron microscope (EM

Philips 208S, MORGAGNI software, FEI, CZ). All samples were negatively stained by 2% ammonium molybdate (pH 6.8).

Paclitaxel Crystallisation

The presence of PTX crystals in various liposomal preparations was determined by the phase contrast microscopy using an Eclipse 600 microscope (Nikon, Tokyo, Japan).

Cancer Cell Lines

B16F10 cancer cell lines were obtained from the Interlab Cell Line Collection (Milano, Italy). The cell lines were grown in RPMI 1640 medium (Sigma, Prague, Czech Republic) supplemented with 10% of foetal calf serum (Gibco, Czech Republic), 50 $\mu\text{g/mL}$ penicillin, 50 $\mu\text{g/mL}$ streptomycin and 300 $\mu\text{g/mL}$ L-glutamine. B16F10 cells were applied into C57BL/6 mice and the subline with a high metastatic potential was prepared by the *ex vivo* recultivation from the lung metastatic foci.

Experimental Animals

C57BL/6 (20–22 g) mice (female) obtained from ANLAB Ltd. (Prague, Czech Republic) were free of known pathogens at the time of the experiment. Standard pellet diet and water were given *ad libitum*. The research was conducted according to the principles enunciated in the Guide for the Care and Use of Laboratory Animals issued by the Czech Society for Laboratory Animal Science.

MTT-Based Cytotoxicity Test

The MTT [3-(4,5-dimethylthiazol-2-yl)-2,5-diphenyl-tetrazolium bromide] dye conversion assay^{28,29} was used with some modifications³⁰ to measure the cytotoxicity of free PTX, “empty” liposomes and the optimal liposomal PTX formulation. All samples were measured in triplicates. The results of the MTT test were confirmed by Hoffman modulation contrast and fluorescent microscopy (epifluorescent inverted microscope T200, Nikon) looking for the morphological changes of the cells treated with various preparations.

Toxicity of Liposomal PTX and “Empty” Liposomes

The potential toxic effects of “empty” liposomes were tested on the mice C57BL/6 (20–22 g, 10 per group). These mice were used also for the B16F10 melanoma cancer model. A dose of 200 μL (5, 10, 20 or 40 mg

phospholipids per dose) was administered i.v. in 15 s via a tail vein injection. The toxicity of our optimal liposomal PTX formulation was tested in the same way. The Berlin weight gain test was used as the method for the evaluation of the toxic effects.³¹

The typical symptoms of toxicity including motoric disorder, respiratory problems, apathy, horrent fur, behavioural changes, anorexia and loss of body mass were scored for the individual mouse immediately after the application of the drugs as well as within the following 10 days.

Hollow Fibre Implants Mouse Model

Hollow fibre implant model is useful for rapid *in vivo* screening of anticancer drugs against various animal and human cancer cell lines without the need to use nude mice.^{32,33} The cells inside the hollow fibre are protected against the attack of the host immune system and this model represents the pure chemotherapeutic effect of the preparation. Polyvinylidene Difluoride (mPVDF) hollow fibres, molecular weight cut-off of 500 kDa, interior diameter of 1.0 mm (CELMAX[®] Implant Membrane, Spectrum Laboratories, Inc. Rancho Dominguez, CA) were used in these studies. The fibres were cut into pieces of 24-cm lengths and processed according to the producer instruction (CELMAX[®] Implant Membrane, Instruction for use, Spectrum Laboratories, Inc.). Loading of the fibres with cells and their surgical implantation were done according to the published procedures.^{32,34} The mice were anaesthetised with etomidate sulphate (0.6 mg per mouse i.p.) (Hypnomidate, Janssen Pharmaceutica). Hollow fibres were implanted intraperitoneally using aseptic surgical procedures. A small incision was made on the *linea alba*. A 0.5-cm skin incision exposed the peritoneum that was incised 2 mm to allow the hollow fibre to be passaged into the abdomen. The fibres were inserted in the craniocaudal direction on the right side of the peritoneal cavity. The peritoneum and skin were closed by surgical suture (SEIDE[®]E, 2 metric 3-0 USP, Resorba, Germany). Three fibres were implanted into each mouse. Illustrative demonstration of the procedure is presented in the supporting information to this manuscript.

Treatment of the Mice Bearing the Hollow Fibre Implants Filled With B16F10 Melanoma

The C57BL/6 mice (20–22 g, 3 per group) with the hollow fibre implants containing B16F10 melanoma were treated at the days 1, 3 and 5 with the optimal liposomal PTX formulation via the tail vein. Two experimental groups of the mice were arranged and the cumulative doses of 75 and 150 mg PTX/kg (three

equivalent doses, the interval of 48 h) were applied, respectively. The mice in the control group were treated with “empty” liposomes using the same lipid dose as the group receiving the cumulative dose of 150 mg PTX/kg. Three fibres filled with the cells and maintained in tissue culture medium in 6-well microplate served as the *in vitro* positive control.

Growth Assay

On the day 6, the hollow fibre implants were retrieved from the mice and the samples were assayed for viable cell mass by a stable-endpoint MTT dye conversion assay. The fibres were incubated in 6-well plates (3 fibres/well) with 3 mL complete RPMI 1640 (37°C) containing 1 mg/mL MTT (Sigma–Aldrich, St. Louis, MO) for 4 h at 37°C in 5% CO₂. Thereafter, the MTT solution was aspirated and the fibres were washed with 2 mL saline containing 2.5% protamine sulphate (Sigma–Aldrich, USA) overnight at 4°C. A second washing was performed with 2 mL saline containing 2.5% protamine sulphate for 4 h at 4°C. Then the fibres were removed from protamine sulphate, individually wiped, placed in 24-well plate (1 fibre/well), cut in half and dried overnight at the laboratory temperature. SDS (0.2 mL of 10% solution) was added to each well to extract the formazan and the plates were agitated for 4 h at the laboratory temperature. The extracts were transferred into 96-well plates and the optical density at the wavelength of 540 nm was determined. Blank controls consisted of the hollow fibres filled with complete medium and handled in the same way as the cell-filled samples.

Treatment of the Mice Bearing Lung Metastases of B16F10 Melanoma

The murine B16F10 melanoma cell line used for the cytotoxicity testing described above is endowed with a high metastatic potential for lung, therefore it was used to generate the *in vivo* mouse metastatic melanoma models. C57BL/6 mice (20–22 g, 5 per group) were injected with 5×10^5 B16F10 melanoma cells i.v. via the tail vein. Four days later, the mice of the group I, II and III were treated with the optimal liposomal PTX formulation at the cumulative doses of 25, 50 and 100 mg PTX/kg, respectively (four equivalent doses, the interval of 48 h). The mice in the control group IV were treated with the “empty” liposomes using the same lipid dose as used in the group III, and the mice of the group V were untreated controls. On the day 20 after the injection of the melanoma cells, the mice were sacrificed by decapitation, the lungs were removed, fixed in Bouin's solution and both sides of the lung were photographed under stereomicroscope SMZ-2T (Nikon). The

enlarged photographs were scored for the metastatic foci by visual enumeration. We preferred this endpoint to that of a traditional survival experiment in order to diminish morbidity in the terminal stage of the disease. Moreover, the enumeration of the metastatic foci is difficult in later stages of the disease due to the enlargement and fusion of the foci, and the destruction of the lung tissue by tumour growth.³⁵

Statistics

The programme GraphPad PRISM, V.4 (GraphPad Software, Inc., San Diego, CA) was used to calculate the cytotoxicity curves and IC_{50} . Newman-Keuls Multiple Comparison Test was used for the statistical analyses of the *in vivo* anticancer effect in both the hollow fibre implants and the syngenic B16F10 melanoma mouse cancer models. Statistical analysis using one-way ANOVA test was used for the encapsulation efficiency, size distribution and ζ -potential studies. For these parameters expressed as the mean \pm standard deviation, the determined data represent triplicate of samples.

RESULTS

Comparison of Various Methods for the Preparation of Liposomal PTX

The first method evaluated was the hydration of a lipid film. The lipid films were prepared with an initial PTX content of 7 mol% and then hydrated with 10 mM HEPES (pH 7.2) at 25°C for 60 min. Although no PTX crystals were observed, EE_{PTX} values of $91 \pm 0.8\%$ were assayed by HPLC. When the proliposome-liposome method was used, PTX was dissolved in ethanol solution at 60°C for 10 min. No thermal decomposition of PTX was detected by HPLC but the final EE_{PTX} values were $80 \pm 1.1\%$ and some crystallisation was observed. In these experiments, the best results were obtained with lyophilisation of a powderised lipid-PTX mixture from 2-methylbutan-2-ol followed by hydration in PBS at 25°C for 60 min. The EE_{PTX} values of $94 \pm 0.6\%$ were determined by HPLC and PTX crystallisation was not observed over several days. This is why we chose this method for further studies. Moreover, it is very convenient for simultaneous preparation of large amounts of multiple samples differing in lipid composition.

The liposomes were prepared of SOPC, POPG and MOPC according to the general composition formula: molar ratio SOPC/POPG/MOPC, 80-X:X:20; where X is 0, 10, 20 or 30 mol%. Different liposomal PTX formulations were prepared separately by lyophilisation

of a powderised lipid-PTX from 2-methylbutan-2-ol with subsequent hydration in PBS, which was followed by extrusion through polycarbonate filters of 0.2- μ m pore size using a hand operated Mini-Extruder. The resulting average size of the liposomes was in the range of 175–195 nm with the PDI of 0.11 ± 0.02 , as measured by DLS. The presence of POPG increased the negative value of ζ -potential of the liposomal PTX particles and helped to optimise the EE_{PTX} values (Fig. 1). Sterically stabilised liposomal PTX formulations were prepared by substituting PEG-POPE (5 mol%) for POPG. The ζ -potential was reduced to -7 ± 1.8 mV but EE_{PTX} values became $85 \pm 1.3\%$. The optimal liposomal PTX formulation was found to be: molar ratio SOPC/POPG/MOPC, 60:20:20 with 7 mol% PTX. The influence of the storage temperature (4 or 37°C) on the liposomal PTX samples was investigated. The size of the liposomal particles and the crystalline state of PTX was monitored daily by DLS and by phase contrast microscopy, respectively. Based on these measurements, the optimal liposomal PTX formulation was once again found to be: molar ratio SOPC/POPG/MOPC, 60:20:20 with 7 mol% PTX (Tab. 2).

Vitamin E and Cryoprotectants

Vitamin E (0, 5, 10 and 15 mol%) was added to the liposomal PTX formulation comprising SOPC/POPG/

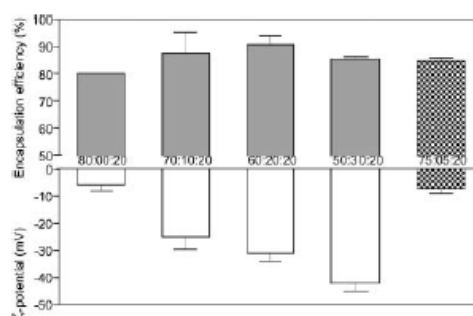


Figure 1. Effect of negatively charged POPG on the encapsulation efficiency and ζ -potential of the liposomal PTX formulations. The liposomes were prepared of SOPC, POPG and MOPC according to the general composition formula: molar ratio SOPC/POPG/MOPC, 80-X:X:20; where X is 0, 10, 20 or 30 mol% (full bars). The data corresponding to the sterically stabilised liposomes prepared of SOPC/PEG-POPE/MOPC (molar ratio, 75:0:20) are denoted by squared bars. The encapsulation efficiency was determined by HPLC (see Materials and Methods Section). ζ -potential was measured in PBS at 25°C. *Statistically not significant ($p < 0.05$) for the encapsulation efficiency of PTX.

Table 2. Influence of the Lipid Composition on the Crystallisation of PTX from the Liposomal PTX Formulations

Storage		SOPC/POPG/MOPC (Molar Ratio)				SOPC/PEG-POPE/MOPC (Molar Ratio)
Time	Temperature	80:00:20	70:10:20	60:20:20	50:30:20	75:05:20
i.a.p.	4°C/37°C	–	–	–	–	–
1st day	4°C/37°C	–/–	–/–	–/–	–/–	–/–
2nd day	4°C/37°C	+/+/+	–/–	–/–	–/–	+/+
4th day	4°C/37°C	+/+/+/+	+/+	–/+	+/+	+/+/+
7th day	4°C/37°C	+/+/+/+	+/+/+	+/+	+/+/+	+/+/+

i.a.p., immediately after preparation.

The amount of the PTX needles in the optical field was scored by the phase contrast microscopy.

–, no crystals; +, sporadic crystals; ++, several crystals; +/+, plenty of crystals.

MOPC at 60:20:20 molar ratio with 7 mol% PTX. As mentioned above, these formulations were prepared by lyophilisation from 2-methyl-butan-2-ol. The size of the liposomal PTX formulation containing 15 mol% of vitamin E tended to be smaller and the ζ -potential also decreased in comparison with the formulations containing lower amounts of vitamin E (Tab. 3). The cryoprotectants, lactose, sucrose and trehalose were found to be almost equal with respect to their cryoprotective effects on the liposomes stabilised with vitamin E (5 mol%). As regards the preservation of the original size of liposomes, mannitol had no cryoprotective effect (Fig. 2). The minimal cryoprotective lipid:sugar molar ratio was found to be 1:5. Sucrose was chosen for further experiments as the low cost cryoprotectant approved for clinical application. In the presence of sucrose (lipid:sucrose molar ratio, 1:5), the lyophilised liposomal PTX formulation containing vitamin E (5 mol%) was found to be stable for at least 6 months during the storage at 4°C. These results were obtained by the measurements of the size distribution, ζ -potential, the lack of PTX crystals and the EE_{PTX} values after the reconstitution of the lyophilised liposomal preparations. Moreover, neither significant changes in the size of the liposomes (Fig. 3A) nor PTX crystals were seen immediately after the reconstitution as well as during next 40 days of storage at 4°C. The multilamellar structure of the PTX liposomes is visible on the

electron microscopy micrograph (Fig. 3B). Hence, the composition comprising SOPC/POPG/MOPC at the molar ratio of 60:20:20 with 7 mol% PTX and 5 mol% vitamin E was found to be the optimal liposomal PTX formulation.

In Vitro Toxicity

“Empty” liposomes of the composition SOPC/POPG/MOPC (molar ratio, 60:20:20) with 5 mol% vitamin E were prepared by lyophilisation from 2-methyl-butan-2-ol. Afterwards, the toxicity was evaluated by the MTT test (24-h exposure). No toxicity was seen on B16F10 cancer lines up to the dose of 20 ± 1.2 mg lipid/mL. This is in contrast to the mixed micelles prepared from the lysophospholipid mixture MOPC/MOPG (molar ratio, 80:20), which were toxic for B16F10 cancer lines at the concentrations $> 200 \pm 4$ μ g/mL. We also compared the *in vitro* cytotoxic effects of the liposomal PTX with free PTX. In terms of the PTX doses, the IC_{50} values for free PTX were shown to be very similar to the values of the optimal liposomal PTX formulation prepared by lyophilisation from 2-methyl-butan-2-ol. For the tested cancer cell line B16F10, both free and liposomal PTX demonstrated similar cytotoxicity curves with IC_{50} equals to 20 ± 1 nM.

Table 3. Influence of Various Molar Percentage of Vitamin E on the Size and ζ -Potential of the Liposomal PTX Formulation

Parameter	Mol% Vitamin E ^a			
	0	5	10	15
Encapsulation efficiency (%)	79.8 \pm 0.4	94.7 \pm 3.8	93.4 \pm 0.8	94.4 \pm 0.9
ζ -Potential (mV)	–31.3 \pm 3.2	–28.4 \pm 4.5	–33.5 \pm 3.8	–24.9 \pm 3.1
Average size (nm)	190 \pm 2	176 \pm 6	194 \pm 6	129 \pm 5

The liposomal composition was SOPC/POPG/MOPC (molar ratio, 60:20:20) with 7 mol% PTX. The size distribution and ζ -potential were measured in PBS. The polydispersity index was 0.11 ± 0.01 for all the liposomal preparations.

^aEach data point represents the mean \pm SD ($n = 3$).

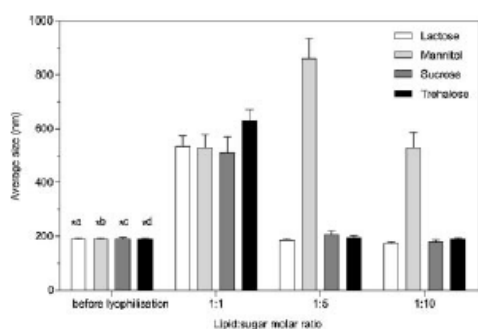


Figure 2. Effect of various cryoprotective sugars on the physical stability of the lyophilised liposomal PTX formulation after reconstitution. Lactose, mannitol, sucrose and trehalose were used as the cryoprotectants for the lyophilisation of the PTX liposomes. Lipid:sugar molar ratios of 1:1, 1:5 and 1:10 were tested. Liposomes extruded ($0.2\ \mu\text{m}$) in the solution of the tested sugars were used as the controls of the size prior to lyophilisation. ^{a,c,e,d}Statistically significant versus 1:1 ($p < 0.05$) and not statistically significant versus 1:5, 1:10 ($p < 0.05$). ^bStatistically significant versus 1:1, 1:5, 1:10 ($p < 0.05$).

In Vivo Toxicity

The optimal liposomal PTX formulation was administered to mice by tail vein injections. There were no outward signs of toxicity even up to very high single doses of PTX ($100\ \text{mg/kg}$; $\approx 2\ \text{mg PTX/mouse}$). The typical symptoms of toxicity based on the Berlin test (e.g., motoric disorder, respiratory problems, apathy, horrent fur, behavioural changes and a loss of body weight) were observed neither immediately after the application nor during the following 10 days. Any toxic side effects were also not seen in the groups with the implanted hollow fibres (the maximal cumulative dose of $150\ \text{mg PTX/kg}$, three equivalent doses) or in the experimental group injected with tumour cells and treated with four doses (the maximal cumulative dose of $100\ \text{mg PTX/kg}$) of our optimal liposomal PTX formulation (groups I, II, III) or "empty" liposomes (group IV).

Anticancer Effect in Hollow Fibre Implants Mouse Model

The cells in the hollow fibres placed in tissue culture medium (*in vitro* control) grew similarly to those implanted into mice (*in vivo* control). There was no statistically significant difference between this two control groups. The application of the optimal liposomal PTX formulation suppressed the growth of B16F10 melanoma cells in the dose-dependent manner (Fig. 4). Due to the surgical intervention

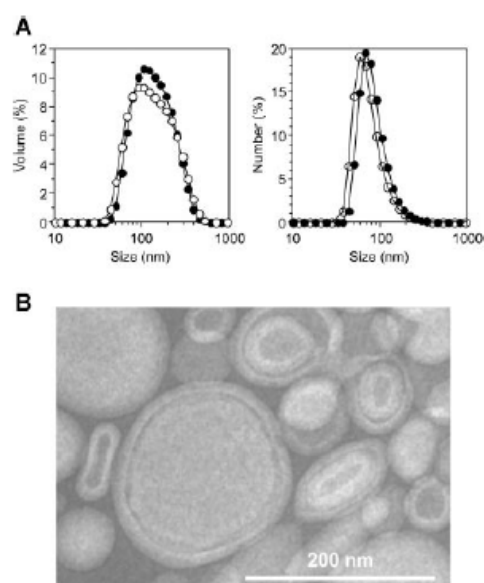


Figure 3. (A) Size distribution of the PTX liposomes prior to lyophilisation and after the lyophilisate reconstitution. The average size of $139 \pm 5\ \text{nm}$ with the PDI of 0.13 ± 0.02 (measured by DLS) was obtained prior to lyophilisation (full circles). After the lyophilisate reconstitution (empty circles), the average size was $136 \pm 4\ \text{nm}$ with the PDI of 0.15 ± 0.01 . These values are not statistically significant for both parameters ($p < 0.05$) average size as well as PDI. (B) Representative TEM photography of the PTX liposomes.

required for the insertion of the hollow fibre implants, it was of interest to follow the potential effects of liposomal PTX on the healing of the surgical wounds. We did not observe any adverse effects (inflammation, ulceration, abnormal cicatrisation or re-opening of the cut) of the liposomal PTX on the wound healing that was proceeding in a normal and comparable manner in both the control C57BL/6 mice and the animals treated with liposomal PTX.

Anticancer Effect in Syngenic Mouse Melanoma Model

The optimal liposomal PTX formulation showed an obvious dose-dependent anti-metastatic effect. The typical appearance of the lungs with black metastatic foci is presented in Figure 5A. No metastases were found in liver or spleen of the mice from any PTX treated group. However, metastases were found in the ovaries of some mice belonging to the control groups IV or V. Numerous fused metastatic foci were

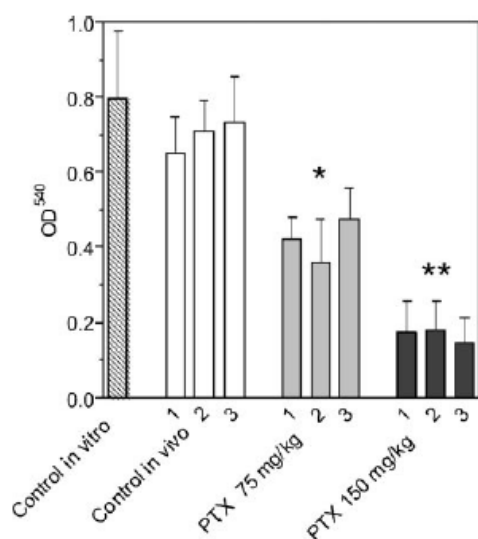


Figure 4. Suppressive effect of liposomal PTX on the growth of B16F10 cancer cells in the hollow fibre implants applied into C57BL/6 mice. C57BL/6 mice (20–22 g, 3 per group) with the hollow fibre implants containing B16F10 melanoma were treated at the day 1, 3 and 5 with the optimal liposomal PTX formulation via the tail vein. Two experimental groups of the mice were arranged and the cumulative doses of 75 and 150 mgPTX/kg (three equivalent doses, interval of 48 h) were applied, respectively. *Statistically significant versus *in vivo* and *in vitro* Controls ($p < 0.001$). **Statistically significant versus *in vivo* and *in vitro* Controls ($p < 0.001$) and the group treated with 75 mgPTX/kg ($p < 0.001$).

also observed in the control groups IV or V but there was no difference between these two control groups with respect to the expansion of melanoma in lungs (Fig. 5B).

DISCUSSION

Preparation of PTX Liposomal Formulation

Low encapsulation capacity of liposomal PTX formulations prepared from conventional lipid composition is known to be a limiting factor for their application. The maximal achievable content of PTX is 3 mol% relative to the total lipids.³⁶ We developed a stable liposomal preparation capable to encapsulate at least 7 mol% of PTX based on the pocket-forming lipids. The example of such lipids are lysophospholipids which asymmetric molecules form cavities—pockets in the liposomal membrane bilayer.

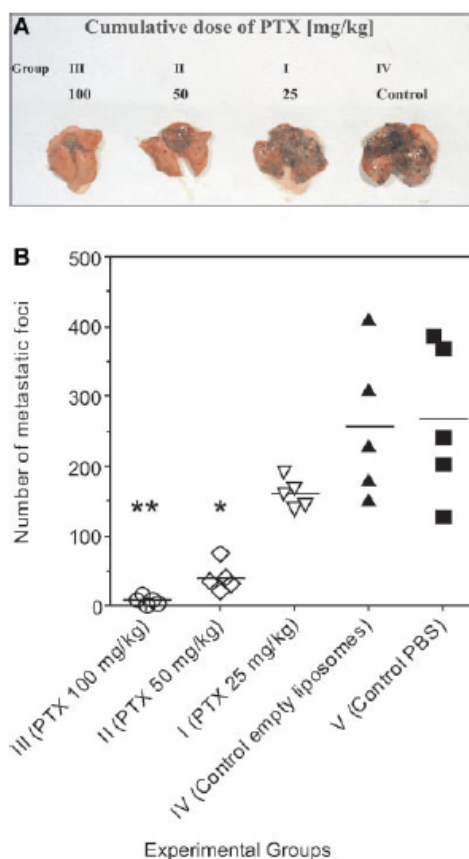


Figure 5. Expanses of lung metastases of B16F10 melanoma cells in the mice treated with various doses of PTX liposomes. (A) Representative photographs of the lungs from various experimental groups. Expanses of lung metastases in the control group V (mice treated by PBS) were similar to those of the group IV (photograph not shown). (B) The number of the metastatic foci in the lungs extracted at the day 20 from the mice treated with PTX liposomes. The cumulative doses of 100, 50 and 25 mgPTX/kg (four equivalent doses, interval of 48 h) were applied in the groups III, II and I, respectively. Empty liposomes were applied in the group IV. The group V represents the PBS treated control. *Statistically significant versus the groups V, IV ($p < 0.001$) and I ($p < 0.05$). **Statistically significant versus the groups V, IV ($p < 0.001$) and I ($p < 0.01$).

These hydrophobic pockets can accommodate bulky hydrophobic molecule of PTX. Higher encapsulation capacity and efficiency as well as physical-chemical stability occurs as the consequence of PTX-pocket

interaction of these PTX liposomes in comparison with the other ones. Due to the possible competition of cholesterol with PTX for the lipid-formed pockets in liposomes, the use of the latter one was avoided. The effect of cholesterol on the reduction of the encapsulation capacity of conventional liposomes for PTX has been reported as well.³⁷ During the storage period, PTX tends to crystallise apart from the liposomes.³⁸ Moreover, the conventional liposomes were found to be more stable than the corresponding sterically stabilised ones.¹⁷ Our composition was found to be the optimal with respect to the development of stable formulations appropriate for long-term storage. The lipid composition we have used is also able to encapsulate up to 10 mol% PTX. However, at such high levels of PTX (9–10 mol%), the corresponding liposomal systems are physically unstable as regards the disintegration and aggregation (results not shown). Therefore, PTX tends to crystallise spontaneously and the preparation does not prove useful for long-term storage in solution.

Lyophilisation from 2-methyl-butan-2-ol, in our hands, has proven to be a simple and robust method with respect to the preparation of the liposomal PTX samples. This method is convenient for rapid screening to find an optimal lipid composition for long-term storage of liposomal PTX. This is gratifying since a preparation procedure for long-term stable liposomal PTX formulations combining the methods of hydration of lipid film, lyophilisation from 2-methyl-butan-2-ol, sonication and second lyophilisation has been described as too complicated and expensive for the industrial applications.³⁹ The optimal formulation comprising SOPC/POPG/MOPC (molar ratio, 60:20:20) with 7 mol% PTX and 5 mol% vitamin E should be more acceptable since the preparation procedure is much simpler. The proliposome-liposome method is also of relevance for the industrial application. The small amount of PTX crystals formed during the procedure could be removed by the filtration/extrusion step and the liposomal preparation could be sterilised by final microfiltration.

Toxicity of PTX Liposomes

Lysophospholipids are biologically active compounds that destabilise biomembranes. We found *in vitro* toxicity of lysophospholipid micelles against B16F10 and other cancer cell lines (results not shown). Therefore, we did not continue to develop the PTX formulation based on the lysophospholipid micelles, even if this system in our hands allowed the encapsulation capacity of up to 20 mol%. Lysophosphatidylcholine has also been shown to be toxic to the eye lens in organ culture.⁴⁰ In order to eliminate the possible *in vivo* toxicity of lysophospholipids, we

added vitamin E into our optimal liposomal formulation. The effect of antioxidant properties of vitamin E on the membrane stabilisation has been reported.⁴¹ Vitamin E is recognised as a membrane stabilisation agent keeping bilayer structure of liposomal membrane in presence of high concentration of lysolipids, which were used for pocket-forming in which the molecule of PTX is embedded. Moreover, vitamin E as antioxidant is protective for both male and female reproductive organs. These organs are the main target of cytotoxic effect of various anticancer drugs including PTX.⁴² It has been also found that vitamin E inhibits the lysophosphatidylcholine induced endothelial dysfunction.⁴³ *In vitro*, the liposomes containing lysophospholipids and vitamin E were not toxic to various cell lines at the doses up to 20 mg/mL (results not shown). *In vivo*, neither "empty" liposomes, nor our optimal liposomal PTX formulations were associated with any signs of toxicity as established by the Berlin test. The low toxicity of our optimal liposomal PTX formulation correlates well with our *in vitro* data and also with other reported *in vivo* data for various liposomal formulations.^{15,40,44} Protective effect of liposome encapsulation on PTX developmental toxicity in the rat was also demonstrated. These findings are very important for possible application in anticancer treatment during human pregnancy.⁴⁵ The highest single dose of PTX used for the treatment of the mice was about 100 mg/kg, and the highest cumulative dose was about 150 mg/kg (three equivalent doses, the interval between two doses was 48 h). These applied doses still did not reach the MTD. Higher doses were difficult to apply owing to the limits for the i.v. applicable volume in mice (100 μ L) as well as with respect to the impossibility to apply more than four doses by i.v. route via tail vein. Therefore, our optimal liposomal PTX formulation outperforms Taxol[®] where the MTD is about 20–25 mg/kg.^{9,10,15,39,40,44} Very important finding is that no adverse effects (inflammation, ulceration, abnormal cicatrisation or re-opening of the cut) was observed with respect to the wound healing in the mice undergoing surgical intervention required for the insertion of the hollow fibre implants. This feature could be important for future application to cancer patients who are often treated by a combination of surgery and chemotherapy.

In this study we were not focused on the effect of the treatment on impairing of haemopoiesis. This topic is going to be addressed by a separate paper. In our recent paper on the new potent anticancer drug α -tocopheryl maleamide, which was found to be toxic as free drug *in vitro* for GM-progenitors and *in vivo* general toxicity was found, we demonstrated that its liposomal formulation completely abrogates these side-effects and, moreover, a slight dose-dependent

stimulation of bone-marrow proliferation was demonstrated together with no leucopenia or neutropenia observed.⁴⁶

In Vivo Anticancer Effect

The B16 melanoma has been a particularly useful tool for the experimental studies on tumour and host properties involved in metastasis.^{47,48} The syngenic B16F10 melanoma cell line has a high potential for lung metastases via the blood-borne route and is an excellent model to determine *in vitro* and *in vivo* efficacy of liposomal PTX.^{35,49} Good correlation was found between the data obtained from both hollow fibre and metastatic cancer models. Our optimal liposomal PTX formulation was well tolerated at high doses and the anticancer effect was obvious in melanoma-bearing mice. The treatment brought significant reductions in lung metastases, when high cumulative doses were administered (100 or 50 mg PTX/kg). At lower doses of PTX (25 mg/kg), an extensive dissemination of metastases in lungs was observed. Nevertheless, the number of the metastatic foci was lower in comparison with the controls. Application of PTX formulated in Taxol[®] at the dose of 20 mg/kg (close to MTD) exhibited no effect on metastasis in lungs (results not shown).

In conclusion, the application of "pocket-forming" lipids significantly increased the encapsulation capacity of PTX in liposomes at least up to 7 mol%, which is more than twice the level achieved previously in the liposomes developed by various research groups. Physical stability of PTX liposomes was achieved by lyophilisation and this technology is applicable for potential industrial production. Suppressed crystallisation of PTX in liposomal suspension together with a low toxicity of the liposomal PTX formulation allowed applying high doses of PTX, which were necessary to induce a significant therapeutic effect against melanoma in the mice B16F10 melanoma model. MTD (in mice) of liposomal PTX was above 150 mg/kg (cumulative dose) and 100 mg/kg (single dose). In this parameter liposomal PTX significantly outperforms Taxol[®] 20–22 mg/kg). This basic non-toxic lipid-pocket containing liposomal carrier could be used for construction of next generation of advanced PTX delivery systems for neovascular targeting therapy based on cationic liposomes. All our data suggest that this new formulation shows a very useful safety and efficacy profiles and could be favourable for clinical applications.

ACKNOWLEDGMENTS

This work was supported by a grant from the Ministry of Agriculture of the Czech Republic (the grant No.

MZE 0002716202) to J.T. The authors thank to Dr. Pavel Kulich for the preparation of TEM micrographs. We gratefully acknowledge the critical comments on the manuscript by Prof. Theresa Allen (University of Alberta, Canada).

REFERENCES

- Wani MC, Taylor HL, Wall ME, Coggon P, Mcphail AT. 1971. Plant antitumor agents 6. Isolation and structure of taxol, a novel antileukemic and antitumor agent from *Taxus brevifolia*. *J Am Chem Soc* 93:2325–2327.
- Schiff PB, Horwitz SB. 1980. Taxol stabilizes microtubules in mouse fibroblast cells. *Proc Natl Acad Sci* 77:1561–1565.
- Rowinsky EK, Donehower RC. 1995. Taxol therapy—Paclitaxel (Taxol). *N Engl J Med* 332:1004–1014.
- Lee SC, Kim C, Kwon IC, Chung H, Jeong SY. 2003. Polymeric micelles of poly(2-ethyl-2-oxazoline)-block-poly(epsilon-caprolactone) copolymer as a carrier for paclitaxel. *J Control Release* 89:437–446.
- Feng X, Yuan YJ, Wu JC. 2002. Synthesis and evaluation of water-soluble paclitaxel prodrugs. *Bioorg Med Chem Lett* 12:3301–3303.
- Liu CH, Strobl JS, Bane S, Schilling JK, McCracken M, Chatterjee SK, Rahim-Bata R, Kingston DGI. 2004. Design, synthesis, and bioactivities of steroid-linked taxol analogues as potential targeted drugs for prostate and breast cancer. *J Nat Prod* 67:152–159.
- Dosio F, Arpicco S, Brusa P, Stella B, Cattel L. 2001. Poly(ethylene glycol)-human serum albumin-paclitaxel conjugates: Preparation, characterization and pharmacokinetics. *J Control Release* 76:107–117.
- Lundberg BB, Risovic V, Ramaswamy M, Wasan KM. 2003. A lipophilic paclitaxel derivative incorporated in a lipid emulsion for parenteral administration. *J Control Release* 86:93–100.
- Ruan G, Feng SS. 2003. Preparation and characterization of poly(lactic acid)-poly(ethylene glycol)-poly(lactic acid) (PLA-PEG-PLA) microspheres for controlled release of paclitaxel. *Biomaterials* 24:5037–5044.
- Sharma US, Balasubramanian SV, Straubinger RM. 1995. Pharmaceutical and physical-properties of paclitaxel (taxol) complexes with cyclodextrins. *J Pharm Sci* 84:1223–1230.
- Merisko-Liversidge E, Sarpotdar P, Bruno J, Hajj S, Wei L, Peltier N, Rake J, Shaw JM, Pugh S, Polin L, Jones J, Corbett T, Cooper E, Liversidge GG. 1996. Formulation and antitumor activity evaluation of nanocrystalline suspensions of poorly soluble anticancer drugs. *Pharm Res* 13:272–278.
- Hennenfent KL, Govindan R. 2006. Novel formulations of taxanes: A review. Old wine in a new bottle? *Ann Oncol* 17: 735–749.
- Hofheinz RD, Gnad-Vogt SU, Beyer U, Hochhaus A. 2005. Liposomal encapsulated anticancer drugs. *Anticancer drugs* 16:691–707.
- Abraham SA, Waterhouse DN, Mayer LD, Cullis PR, Madden TD, Bally MB. 2005. The liposomal formulation of doxorubicin. *Methods Enzymol* 391:17–97.
- Sharma A, Mayhew E, Bolcsak L, Cavanaugh C, Harmon P, Janoff A, Bernacki RJ. 1997. Activity of paclitaxel liposome formulations against human ovarian tumor xenografts. *Int J Cancer* 71:103–107.
- Zhang JA, Anyarambhatla G, Ma L, Ugwu S, Xuan T, Sardone T, Ahmad I. 2005. Development and characterization of a novel Cremophor (R) EL free liposome-based paclitaxel (LEP-ETU) formulation. *Eur J Pharm Biopharm* 59:177–187.

17. Crosasso P, Ceruti M, Brusa P, Arpico S, Dosio F, Cattel L. 2000. Preparation, characterization and properties of sterically stabilized paclitaxel-containing liposomes. *J Control Release* 63:19–30.
18. Yang T, Cui FD, Choi MK, Cho JW, Chung SJ, Shim CK, Kim DD. 2007. Enhanced solubility and stability of PEGylated liposomal paclitaxel: In vitro and in vivo evaluation. *Int J Pharm* 338:317–326.
19. Yang T, Choi MK, Cui FD, Kim JS, Chung SJ, Shim CK, Kim DD. 2007. Preparation and evaluation of paclitaxel-loaded PEGylated immunoliposome. *J Control Release* 120:169–177.
20. Yang T, Choi MK, Cui FD, Lee SJ, Chung SJ, Shim CK, Kim DD. 2007. Antitumor effect of paclitaxel-loaded PEGylated immunoliposomes against human breast cancer cells. *Pharm Res* 24:2402–2411.
21. Kunstfeld R, Wickenhauser G, Michaelis U, Teifel M, Umek W, Naujoks K, Wolff K, Petzelbauer P. 2003. Paclitaxel encapsulated in cationic liposomes diminishes tumor angiogenesis and melanoma growth in a “humanized” SCID mouse model. *J Invest Dermatol* 120:476–482.
22. Strieth S, Nussbaum CF, Eichhorn ME, Fuhrmann M, Teifel M, Michaelis U, Berghaus A, Dellian M. 2008. Tumor-selective vessel occlusions by platelets after vascular targeting chemotherapy using paclitaxel encapsulated in cationic liposomes. *Int J Cancer* 122:452–460.
23. Zhang JQ, Zhang ZR, Yang H, Tan QY, Qin SR, Qiu XL. 2005. Lyophilized paclitaxel magnetoliposomes as a potential drug delivery system for breast carcinoma via parenteral administration: In vitro and in vivo studies. *Pharm Res* 22:573–583.
24. Needham D, Sarpal RS. 1998. Binding of paclitaxel to lipid interfaces: Correlations with interface compliance. *J Liposome Res* 8:147–163.
25. Turánek J, Kasna A, Zaluska D, Neca J. 2003. Preparation of sterile liposomes by proliposome-liposome method. *Methods Enzymol* 367:111–125.
26. Turánek J. 1994. Fast-protein liquid-chromatography system as a tool for liposome preparation by the extrusion procedure. *Anal Biochem* 218:352–357.
27. Song D, Hsu LF, Au JLS. 1996. Binding of taxol to plastic and glass containers and protein under in vitro conditions. *J Pharm Sci* 85:29–31.
28. Mosmann T. 1983. Rapid colorimetric assay for cellular growth and survival: Application to proliferation and cytotoxicity assays. *J Immunol Methods* 65:55–63.
29. Bank U, Reinhold D, Ansgar S. 1991. Measurement of cellular activity by means of the MTT-test. *Allerg Immunol* 37:119–123.
30. Turánek J, Kasna A, Zaluska D, Neca J, Kvardova V, Knotigova P, Horvath V, Sindlerova L, Kozubik A, Sova P, Kroutil A, Zak FE, Mistr A. 2004. New platinum (IV) complex with adamantylamine ligand as a promising anti-cancer drug: Comparison of in vitro cytotoxic potential towards A2780/cisR cisplatin-resistant cell line within homologous series of platinum (IV) complexes. *Anticancer drugs* 15:537–543.
31. Berlin BS. 1962. Test for biologic safety of Arlael A. *Ann Allergy* 20:472–479.
32. Hall LM, Krauthauser CM, Wexler RS, Hollingshead MG, Slee AM, Kerr JS. 2000. The hollow fiber assay: Continued characterization with novel approaches. *Anticancer Res* 20:903–911.
33. Decker S, Hollingshead M, Bonomi CA, Carter JP, Sausville EA. 2004. The hollow fibre model in cancer drug screening: The NCI experience. *Eur J Cancer* 40:821–826.
34. Hollingshead MG, Alley MC, Camalier RF, Abbott BJ, Mayo JG, Malspeis L, Grever MR. 1995. In-vivo cultivation of tumor cells in hollow fibers. *Life Sci* 57:131–141.
35. Parhar RS, Lala PK. 1987. Amelioration of B16F10 melanoma lung metastasis in mice by a combination therapy with indomethacin and interleukin-2. *J Exp Med* 165:14–28.
36. Wu J, Liu Q, Lee RJ. 2006. A folate receptor-targeted liposomal formulation for paclitaxel. *Int J Pharm* 316:148–153.
37. Yang T, Cui FD, Choi MK, Lin HX, Chung SJ, Shim CK, Kim DD. 2007. Liposome formulation of paclitaxel with enhanced solubility and stability. *Drug Del* 14:301–308.
38. Immordino ML, Brusa P, Arpico S, Stella B, Dosio F, Cattel L. 2003. Preparation, characterization, cytotoxicity and pharmacokinetics of liposomes containing docetaxel. *J Control Release* 91:417–429.
39. Sharma A, Mayhew E, Straubinger RM. 1993. Antitumor effect of taxol-containing liposomes in a taxol-resistant murine tumor model. *Cancer Res* 53:5877–5881.
40. Libondi T, Menzione M, Auricchio G. 1985. In vitro effect of α -tocopherol on lysophosphatidylcholine-induced lens damage. *Exp Eye Res* 40:661–666.
41. Atkinson J, Epand RF, Epand RM. 2008. Tocopherols and tocotrienols in membranes: A critical review. *Free Radical Bio Med* 44:739–764.
42. Kadota T, Chikazawa H, Kondoh H, Ishikawa K, Kawano S, Kuroyanagi K, Hattori N, Sakakura K, Koizumi S, Hiraiwa E, Kohmura H, Takahashi N. 1994. Toxicity studies of paclitaxel (T). Single dose intravenous toxicity in rats. *J Toxicol Sci* 19:1–9.
43. Murohara T, Ikeda H, Katoh A, Takajo Y, Otsuka Y, Haramaki N, Imaizumi T. 2002. Vitamin E inhibits lysophosphatidylcholine-induced endothelial dysfunction and platelet activation. *Antioxid Redox Sign* 4:791–798.
44. Cabanes A, Briggs KE, Gokhale PC, Treat JA, Rahman A. 1998. Comparative in vivo studies with paclitaxel and liposome-encapsulated paclitaxel. *Int J Oncol* 12:1035–1040.
45. Scialli AR, Waterhouse TB, Desesso JM, Rahman A, Goeringer GC. 1997. Protective effect of liposome encapsulation on paclitaxel developmental toxicity in the rat. *Teratology* 56:305–310.
46. Turánek J, Wang XF, Knotigova P, Koudelka S, Dong LF, Vrublova E, Mahdavian E, Prochazka I, Sangsura S, Vacek A, Salvatore BA, Neuzil J. 2009. Liposomal formulation of α -tocopheryl maleamide: In vitro and in vivo toxicological profile and anti cancer effect against spontaneous breast carcinomas in mice. *Toxicol Appl Pharmacol* 237:249–257.
47. Loch-Neckel G, Nemen D, Puhl AC, Fernandes D, Stimarniglio MA, Silva MA, Hangai M, Silva MCS, Lemos-Senna E. 2007. Stealth and non-stealth nanocapsules containing camptothecin: In vitro and in vivo activity on B16F10 melanoma. *J Pharm Pharmacol* 59:1359–1364.
48. Lavi G, Voronov E, Dinarello CA, Apte RN, Cohen S. 2007. Sustained delivery of IL-1Ra from biodegradable microspheres reduces the number of murine B16 melanoma lung metastases. *J Control Release* 123:123–130.
49. Yoshiura K, Nishishita T, Nakaoka T, Yamashita N, Yamashita N. 2009. Inhibition of B16 melanoma growth and metastasis in C57BL mice by vaccination with a syngeneic endothelial cell line. *J Exp Clin Oncol* 28:13.



Review

Liposomal paclitaxel formulations

Štěpán Koudelka^a, Jaroslav Turánek^{a,b,*}^a Department of Toxicology, Pharmacology and Immunotherapy, Veterinary Research Institute, Brno, Czech Republic^b Department of Pharmacology, Faculty of Medicine, Masaryk University, Brno, Czech Republic

ARTICLE INFO

Article history:

Received 14 May 2012

Accepted 7 September 2012

Available online 15 September 2012

Keywords:

Paclitaxel

Liposome

Drug targeting

Drug delivery systems

Anti-cancer drugs

ABSTRACT

Over the past three decades, taxanes represent one of the most important new classes of drugs approved in oncology. Paclitaxel (PTX), the prototype of this class, is an anti-cancer drug approved for the treatment of breast and ovarian cancer. However, notwithstanding a suitable premedication, present-day chemotherapy employing a commercial preparation of PTX (Taxol®) is associated with serious side effects and hypersensitivity reactions. Liposomes represent advanced and versatile delivery systems for drugs. Generally, both *in vivo* mice tumor models and human clinical trials demonstrated that liposomal PTX formulations significantly increase a maximum tolerated dose (MTD) of PTX which outperform that for Taxol®. Liposomal PTX formulations are in various stages of clinical trials. LEP-ETU (NeoPharm) and EndoTAG®-1 (Medigene) have reached the phase II of the clinical trials; Lipusu® (Luye Pharma Group) has already been commercialized. Present achievements in the preparation of various liposomal formulations of PTX, the development of targeted liposomal PTX systems and the progress in clinical testing of liposomal PTX are discussed in this review summarizing about 30 years of liposomal PTX development.

© 2012 Elsevier B.V. All rights reserved.

Contents

1. Introduction	323
2. Solubilization and delivery systems for paclitaxel	323
3. Liposomes as delivery systems	324
3.1. Interaction of paclitaxel with liposomal bilayers	324
3.2. Liposomal paclitaxel formulations	325
3.3. Pharmacokinetics and biodistribution of liposomal paclitaxel	325
4. Conventional liposomes	325
4.1. Paclitaxel encapsulated in conventional liposomes	325
4.2. Paclitaxel encapsulated in pocket-forming liposomes	327
5. Functionalized liposomes	327
5.1. Paclitaxel encapsulated in pegylated liposomes (long-circulating liposomes)	327
5.1.1. Application of pegylated paclitaxel-containing liposomes in metronomic chemotherapy	328
5.2. Paclitaxel encapsulated in ligand-targeted liposomes	328

Abbreviations: G-P, paclitaxel solubilized in Cremophor EL®; DCP, di-cetylphosphate; DEPC, di-1-acyloxy phosphatidyl choline; DIPC, di-1-acyloxy phosphatidyl choline; DIPE, di-1-acyloxy phosphatidyl ethanolamine; DIPC, di-1-acyloxy phosphatidyl glycerol; DLTs, dose-limiting toxicities; DMPC, dimyristoyl phosphatidyl choline; DMPG, dimyristoyl phosphatidyl glycerol; DOTAP, dioleoyl trimethylammonium propane; DOPC, dioleoyl phosphatidyl choline; DPPC, dipalmitoyl phosphatidyl choline; DSPE-PEG, distearoyl phosphatidyl ethanolamine-polyethylene glycol; DSPE-mPEG, distearoyl phosphatidyl ethanolamine-methoxy polyethylene glycol; EPC, egg phosphatidyl choline; EPR, enhanced permeability and retention; FA, folic acid; FDA, Food and Drug Administration; FGF(s), fibroblast growth factor(s); FR, folate receptor; HA, hyaluronic acid; HEPC, hydrogenated egg phosphatidyl choline; HER-2, human epidermal growth factor receptor-2; HCC, hepatocellular carcinoma; HSPC, hydrogenated soybean phosphatidyl choline; HUVEC, human umbilical vein endothelial cells; i.v., intravenous; i.p., intraperitoneal; IRs, infusion-related reactions; LEP, liposome-encapsulated paclitaxel; LEP-ETU, liposome-encapsulated paclitaxel formulation developed and marketed by NeoPharm; MOPC, oleoyl-hydroxy phosphatidyl choline; MLV(s), multilamellar vesicle(s); MRI, magnetic resonance imaging; MTD(s), maximum tolerated dose(s); NRP-1, neuropilin-1; NSCLC, non-small cell lung cancer; OQLCS, octadecyl-quaternized lysine-modified chitosan; PC, phosphatidyl choline; PEG, polyethylene glycol; PG, phosphatidyl glycerol; PL(s), phospholipid(s); POPC, palmitoyl-oleoyl phosphatidyl choline; PRC, People's Republic of China; PTX, paclitaxel; RD, recommended dose; RES, reticuloendothelial system; RHAMM, receptor for hyaluronan-mediated motility; SCID, severe combined immunodeficiency; SPC, stearyl-caproyl phosphatidyl choline; SOPC, stearyl-oleoyl phosphatidyl choline; α -TAS, α -tocopheryl acid succinate; TATp, transactivating transcriptional activator peptide.

* Corresponding author at: Department of Toxicology, Pharmacology and Immunotherapy, Veterinary Research Institute, Hudcova 70, 621 00 Brno, Czech Republic. Tel.: +420 533 331 311.

E-mail address: turanek@vri.cz (J. Turánek).

0168-3659/\$ – see front matter © 2012 Elsevier B.V. All rights reserved.
<http://dx.doi.org/10.1016/j.jconrel.2012.09.006>

5.2.1.	Folate-receptor-targeted paclitaxel liposomes	328
5.2.2.	HER-2-targeted paclitaxel liposomes	328
5.2.3.	Peptide-targeted paclitaxel liposomes	328
5.2.4.	Hyaluronan-targeted paclitaxel liposomes	329
5.3.	Paclitaxel encapsulated in cationic liposomes	329
5.4.	Paclitaxel encapsulated in thermosensitive liposomes	329
5.5.	Paclitaxel encapsulated in magnetoliposomes	330
6.	Toxicity and anti-tumor activity of liposomal paclitaxel	330
7.	Clinical trials	330
8.	Conclusion	332
	Acknowledgments	332
	References	332

1. Introduction

Taxanes are complexes of diterpenoid natural products and semi-synthetic analogs. Presently, these drugs belong to prominent anti-cancer agents used for combined chemotherapy [1]. Paclitaxel (Fig. 1) (PTX, the chemical name is 5 β ,20-epoxy-1,2 α ,4,7 β ,10 β ,13 α -hexahydroxytax-11-en-9-one 4,10-diacetate 2-benzoate 13-ester with (2R,3S)-N-benzoyl-L-phenylisoserine), the prototype of this class, emerges from a natural source [2]. This drug is approved for the treatment of breast and ovarian cancer. PTX was found to be effective in treating a broad spectrum of advanced human cancer including breast and ovarian cancer as well as non-small cell lung carcinoma (NSCLC), melanoma and head and neck cancer (see for review) [3].

The commercial PTX preparation (Taxol®) is formulated in the vehicle composed of Cremophor EL® (polyethoxylated castor oil used as a solubilizing surfactant) and dehydrated ethanol, which provides a homogeneous preparation. In the clinical application, PTX is usually administered as a 3-hour and 24-hour infusion representing a total dose of 135–175 mg/m² of the body every 3 weeks [4]. However, the present-day chemotherapy employing Taxol® is accompanied by serious problems. One of the major problems associated with this formulation is the fact, that the diluted Cremophor EL®/ethanol vehicle is toxic [5]. The negative side effects include serious hypersensitivity reactions, nephrotoxicity and neurotoxicity [6]. PTX solubilized in Cremophor EL® (Cr-P) shows also an incompatibility with the plastic components of the administration

sets [7,8]. Furthermore, the short-term stability of PTX upon dilution with aqueous media can result in possible drug precipitation [9].

It follows that the clinical application of Taxol® is connected with problems of incompatibility and instability. Special requirements regarding a proper filter device as well as appropriate containers and infusion bags for the storage and administration of the drug have to be fulfilled.

2. Solubilization and delivery systems for paclitaxel

Present-day cancer chemotherapy with PTX is associated with hypersensitivity reactions in spite of a suitable premedication with corticosteroids and anti-histamines [3]. Hence, the development of an improved delivery system for PTX is of high importance. Current approaches to the improvement are focused mainly on the development of formulations that are devoid of Cremophor EL®, investigation of the possibility of a large-scale preparation and a request for a longer-term stability. These different approaches have shown some promising possibilities to replace Taxol® by a less irritable preparation such as: (a) micelle formulations [10], (b) water-soluble prodrug preparations [11], (c) enzyme-activatable prodrug preparations conjugated with antibodies or albumin [12,13], (d) parenteral emulsions [14], (e) microspheres [14,15], (f) cyclodextrins [16], and (g) nanocrystals [17]. Only Abraxane® (albumin nanoparticle-based PTX preparation) and Lipusu® (liposomal PTX approved by State FDA of China) have entered the field of clinical applications. Generally, liposomes and protein nanoparticles represent a promising

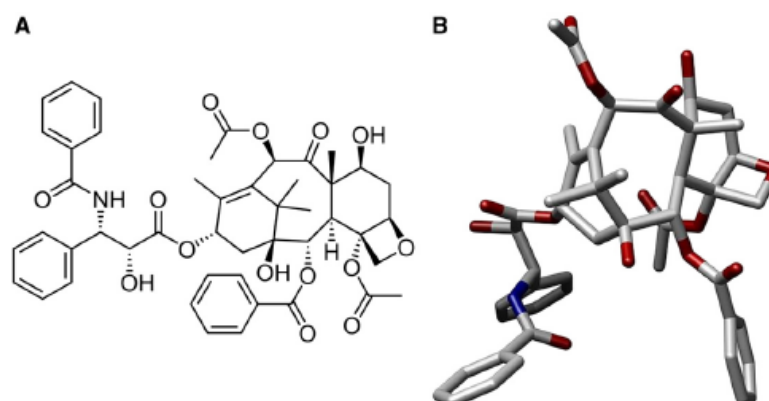


Fig. 1. A) Structural formula of PTX molecule, and B) 3D crystal structure of PTX molecule.

approach to the optimization of PTX delivery. Their commercialization is at the doorstep of modern drug delivery market.

3. Liposomes as delivery systems

The numerous anti-cancer agents that have a high cytotoxic effect on the tumor cells *in vitro* exhibit a remarkable decrease of the selective anti-tumor effect for *in vivo* procedures applicable in the clinical treatment. One of the significant limitations of the anti-cancer drugs, PTX is not an exception, is their low therapeutic index, i.e. the dose required to produce an anti-tumor effect is toxic to normal tissues. The low therapeutic index of these drugs results from the inability to achieve therapeutic concentrations at the specific target sites (e.g. tumors). Further, it results from the non-specific toxicity to normal tissues such as bone marrow, renal, gastrointestinal tract, and cardiac tissue and also from the problems associated with a preparation of a suitable formulation of the drugs [18].

Liposomes represent versatile and advanced nanodelivery systems for a wide range of biologically active compounds [19]. These relatively non-toxic systems have a considerable potential to entrap

both hydrophobic and hydrophilic drugs. The entrapment of the drug into the liposomes is used to bypass the frequent generic toxicity associated with the drug [20,21]. Thus, it represents a very effective route that enhances the drug therapeutic effect. The final amount of the encapsulated drug is affected by a selection of an appropriate preparation method providing a preparation of liposomes of various size, lamellarity and physico-chemical properties [22]. The modification of liposomes permits a passive or active targeting of the tumor site. This effect enables an efficient drug payload into the malignant cells of tumor, while the non-malignant cells become minimally impacted.

3.1. Interaction of paclitaxel with liposomal bilayers

The bulky hydrophobic and asymmetric molecule of PTX could be entrapped within the liposomal phospholipid (PL) bilayers. The positioning of the unshapely molecule of PTX entrapped in the bilayer of liposomes (Fig. 2) represents a meta-stable stage which tends to turn into a more stable crystalline form. Liposomes by their nature also represent a meta-stable system.

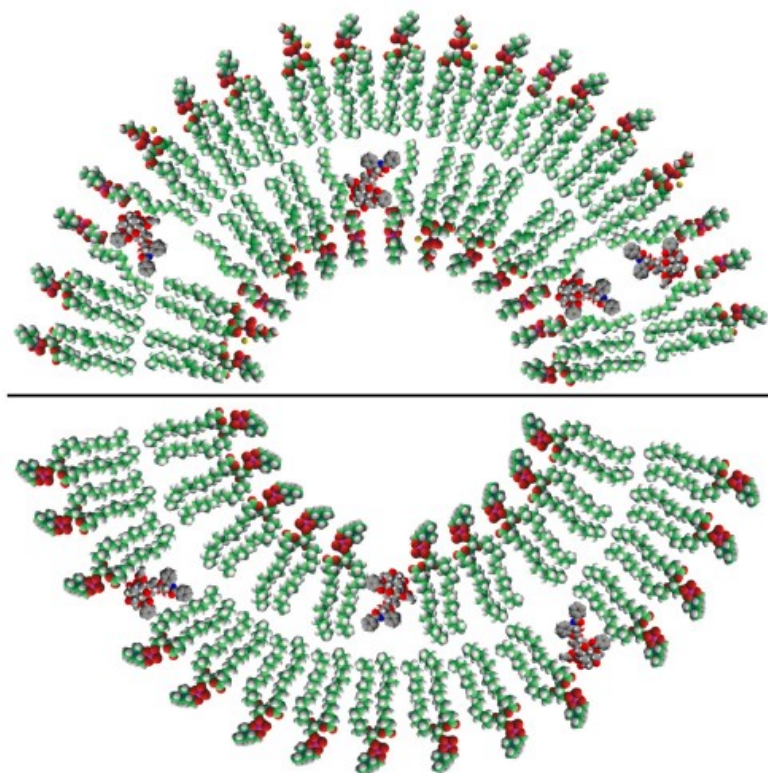


Fig. 2. Arrangement of the encapsulated PTX in different lipid membrane bilayers of the liposomal carrier. The upper part shows the molecule of PTX encapsulated in the liposomal bilayer which is composed of unsaturated- and lyso-lipids. These lipids increase the bilayer fluidity and create bilayer "pockets" in which the bulky hydrophobic molecule of PTX is embedded. Such a liposomal composition enables to encapsulate up to 15 mol% of PTX. The lower part demonstrates the molecule of PTX which is encapsulated in the liposomal bilayer composed of saturated DPPC-based lipids. The incorporation of PTX into the saturated membranes disturbs the structure of the membrane bilayer. At higher drug concentrations, the molecule of PTX is forced out of the bilayer and needle-like crystals of PTX are formed in the liposome formulation. This effect results in a low encapsulation capacity of PTX (3–4 mol%) and in a short stability of the liposomes.

They tend to fuse and form multilamellar vesicles (MLVs) and non-vesicular structures. The aqueous/lipid phase separation of self-assembled PLs in the bilayer is linked with phenomena of phase transition. All these processes can affect the PL microenvironment stabilizing the molecule of PTX in the bilayer and subsequently induce an undesirable crystallization of PTX. With respect to the phase transition, the procedures like freezing, lyophilization and rehydration are critical and can destabilize the liposomal PTX preparation. Partitioning of PTX into the saturated PL bilayers results in changes of membrane physical properties such as phase-transition temperatures and a PL-order parameter, that are different from those observed for unsaturated and charged PL bilayers. PTX incorporated into the saturated PLs changes their thermotropic phase behavior; it reduces the PL order parameter (i.e., has a "fluidizing" effect) in the gel phase of the PL bilayers. On the contrary, partitioning of PTX into unsaturated fluid PL bilayers has a slight "rigidifying" effect [23–25].

3.2. Liposomal paclitaxel formulations

The preparation of an optimal PTX formulation requires important considerations such as the optimization of the liposomal composition, the balance of the PTX amount encapsulated in the liposomes (drug/lipid molar ratio) and the stability of the prepared PTX liposomes during storage in aqueous media [26]. As mentioned above, main characteristics of the molecule of PTX are asymmetry, bulkiness, hydrophobicity, low solubility and tendency to crystallization in aqueous milieu. All these factors affect the final design and preparation of a suitable drug formulation.

Liposomes provide suitable environment, which enhances the solubility of the hydrophobic molecule of PTX by the association of the drug within membrane bilayers. Commonly prepared formulations of PTX-liposomes were able to encapsulate the highest achievable content of PTX (3–4 mol%). Generally, elevating portions of encapsulated PTX reduce the stability of a liposomal PTX formulation due to PTX crystallization. The stability of PTX-liposomes in the aqueous phase is predominantly affected by a liposomal composition. Hydrated PTX-liposomes were found to be stable within week- or month-periods, while the lyophilized PTX liposomal formulations demonstrated a prolonged stability (years). The encapsulation of PTX into liposomes enhances the drug therapeutic efficacy, thus, the same therapeutic effect could be reached by a decreased PTX-dose. On the other hand, the MTD of liposome-encapsulated PTX (LEP) is increased compared with the Taxol® [26].

3.3. Pharmacokinetics and biodistribution of liposomal paclitaxel

The extended release of PTX from the liposomes after intravenous (i.v.) application depends on the morphology and composition of a particular liposomal carrier. Multilamellar sterically stabilized liposomes would be the most stable formulations. The drug released from the circulating liposomes binds rapidly to the serum proteins (presumably to serum albumin and α_1 -acid glycoprotein, minor portion is bound to lipoproteins) [27,28] and subsequently follows the same pharmacokinetic processes and fate as the drug administered as Taxol®. The distribution of the drug between the protein-bound and free fractions is well characterized and 89–98% of PTX is bound, hence, the possible blood cell uptake (erythrocytes and platelets) of PTX is low [27,29–31].

The non-linearity of LEP pharmacokinetics could be related to the retention of PTX within the liposomes and sequestration by the reticuloendothelial system (RES). This fact suggests that kinetics of the drug transfer from the central compartment to the peripheral tissue compartments is delayed for liposomal formulations (i.e., the release of PTX from liposomes is not instantaneous upon administration). This modulation of the drug release rate by liposomes seems to

impact the tissue distribution of PTX and may explain the formulation-dependent differences in toxicity and anti-tumor efficacy. As a result, the proposed changes in tissue distribution of PTX due to the liposome encapsulation may provide an explanation for the observed increase in the MTD for LEP in comparison with Cr-P vehicle [32].

RES represents a major mechanism for clearance of circulating liposomes. LEP is taken-up by the spleen and lung to a greater extent than Cr-P. In the lungs, the drug concentration peaked at 40 and 10 μg PTX/g for LEP and Cr-P, respectively. In the spleen, the drug concentration peaked at 70 and 12 μg PTX/g for LEP and Cr-P, respectively. The uptake of LEP into the spleen was higher in comparison with the lungs. The higher drug levels achieved with LEP persisted for approximately 2.5 to 3 h. Subsequently, lung levels declined more quickly for LEP than for Cr-P suggesting that a substantial portion of the liposome-deposited lung dose was not in the free (released) form. In the liver, drug concentrations were similar for both formulations, with peak levels about 10 μg PTX/g. Other tissues, skin, kidneys, adipose, muscle, brain, and bone marrow showed a greater tissue exposure for Cr-P. This fact is in good accordance with higher bone marrow toxicity of Cr-P and following leucopenia [33].

The morphology, stability and functionalization of liposomal PTX formulation undoubtedly affect the pharmacokinetics and biodistribution pathways and consequently the MTD and the anti-cancer effect. Possible pathways of LEP are presented in Fig. 3.

4. Conventional liposomes

Conventional liposomes are usually composed of neutral or/and negatively charged PLs and cholesterol is also often presented. However, after administration, these liposomes are quickly captured and accumulated by phagocytic cells of the RES. The prime organs of liposomal accumulation are the liver and the spleen due to their rich blood supply and the abundance of tissue-resident phagocytic cells [34].

4.1. Paclitaxel encapsulated in conventional liposomes

Various lipid compositions of PLs like DMPC, DMPG, and cholesterol were screened to find a stable liposomal formulation suitable for encapsulation of PTX. MLVs having constant PTX/lipid weight ratio (1:15) were prepared by a lipid film hydration. The presence of PTX crystals or microaggregates of PTX–lipid complex was observed in all the preparations independently of the lipid composition. However, the mixtures of PC/PG (molar ratio between 7:3 and 9:1) together with the addition of 5% cholesterol gave sub-optimal results [35]. Further, the preparation of liposomal formulation composed of PC/PG (molar ratio, 9:1) containing PTX (molar ratio, 1:33) was developed. The liposomes were prepared by a combination of the methods of lipid film hydration, lyophilization from *tert*-butyl alcohol, and sonication. The prepared PTX liposomes were physically stable and the initial PTX content remained unchanged during storage for more than 2 months at 4 °C and 1 month at 20 °C [36]. Other mixture of PLs and hydrophobic excipients was optimized to prepare physical stable particles without any evidence of PTX crystals. The liposomes were prepared by lipid film hydration followed by sonication and extrusion of MLVs. The composition of PC/DMPG (molar ratio, 7:3) together with 40 mol% cholesterol and 25 mol% α -tocopherol was able to encapsulate 3 mol% PTX. The liposomes had a mean size of 100 nm and were morphologically stable up to 75 days at 4 °C [37]. Cholesterol was tested as a rigidifying agent to prolong the stability of PC liposomes containing PTX. The liposomes were prepared by lipid film hydration followed by extrusion through 0.2 μm filters. However, the increased portions of cholesterol in the liposomes decreased the amount of incorporated PTX. The encapsulation efficiency of PTX decreased below 40% as a consequence of the competition of PTX and cholesterol for the hydrophobic space in the

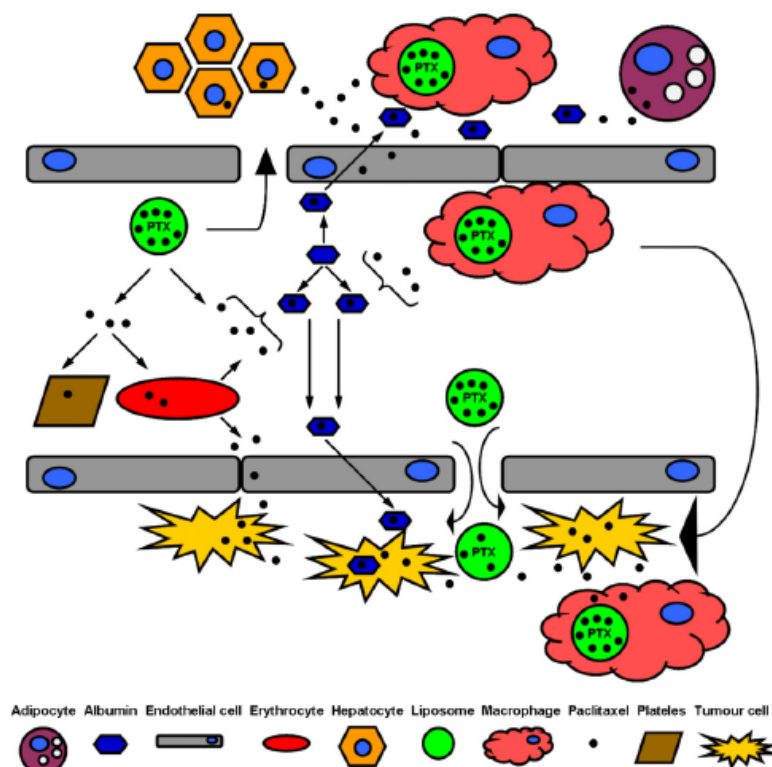


Fig. 3. Biodistribution pathways of PTX. After administration, liposomal PTX can enter various pathways. These pathways and the biodistribution of PTX are determined by various factors, e.g. character of liposomes (such as steric stabilization), morphology (size and lamellarity), and lipid composition. 1) PTX could be released from the liposomes which are used as a non-toxic biocompatible solubilizer of the drug. The free drug interacts with serum proteins, presumably with albumin. PTX is then transported into the tumor cells or into some somatic cells (e.g. adipocytes). These cells can form a depot for the drug. A small portion of free PTX can directly penetrate into the tumor cells and into the somatic cells. Erythrocytes and platelets can also form a depot for PTX. 2) Liposomal PTX can penetrate through fenestrations of the tumor vasculature. In the tumor, the liposomal drug is accumulated and subsequently released in the vicinity of the tumor cells and the tumor endothelial cells. They are the target for PTX. Liposomal PTX could be also internalized into the tumor cells. Liposomes penetrate through the liver fenestrations. The drug is accumulated and detoxified by enzymatic pathways of cytochrom P450 in the liver. 3) Liposomal PTX could be also internalized by phagocytes (e.g. macrophages). These cells can provide a selective transport and subsequent release of the drug in the tumor.

lipid bilayer. Finally, an optimal addition of cholesterol was found to be 10 mol% with respect to liposomal stabilization up to 10 weeks [38]. Saturated PLs with an extending fatty acid chain (DMPC, DPPC and DSPC) and negatively charged DMPC (molar ratio, 9:1) encapsulating PTX (3 mol%) were used for the preparation of liposomes by lipid film hydration followed by sonication. The drug encapsulation efficacy was higher for liposomes with DMPC and DPPC (96%) than for those with DSPC (70%), while the liposome size increased from 143, 157 to 185 nm for DMPC, DPPC and DSPC, respectively. All these formulations retained about 93% of the initial PTX concentration during 4-day incubation at 4 °C in PBS. Moreover, the delivery of PTX by liposomes to MCF-7 breast cancer cells resulted in a significant increase of the intracellular PTX level and was more efficient in arresting cells in mitosis in comparison with PTX delivered by Taxol® [39].

LEP formulations were also developed in the form of lipid-PTX lyophilizates. This approach significantly eliminates the problem of long-term stability of liposomal PTX formulations in aqueous milieu.

After a reconstitution, the liposomes prepared of DEPC/DMPC/SCPC (molar ratio, 1:1:0.9) containing PTX (3 mol%) were stable for 24 h [40]. The physico-chemical stability of the lyophilized PTX liposomes was monitored during storage. MLVs prepared of PC, cholesterol and vitamin E could be diluted up to 0.5 mg PTX/ml and still PTX crystal-free liposomes were observed. In the samples stored at 4 °C up to 5 months, the level of PL degradation products was negligible and no PTX decomposition or precipitation was found [41]. A novel lyophilized PTX formulation marked as LEP-ETU (NeoPharm) was prepared of DOPC/cardioliipin/cholesterol (molar ratio, 9:0.5:0.5) and α -tocopheryl acid succinate (α -TAS) with PTX/lipids (molar ratio, 1:33). At these liposomes, the original liposomal size was preserved and a stable content of each particular lipid as well as PTX was found up to 12 months at 2–8 °C and 25 °C. Upon lyophilizate reconstitution, neither precipitation of PTX nor any changes in original size were observed for 72 h at 2–8 °C and 25 °C. Moreover, this formulation could be reliably diluted to 0.25 mg PTX/ml [42].

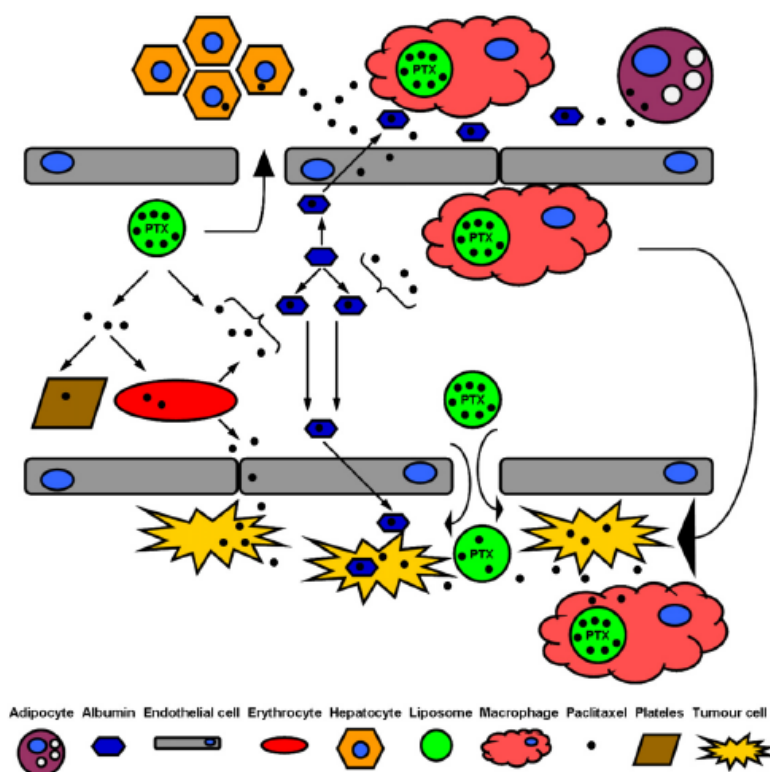


Fig. 3. Biodistribution pathways of PTX. After administration, liposomal PTX can enter various pathways. These pathways and the biodistribution of PTX are determined by various factors, e.g. character of liposomes (such as steric stabilization), morphology (size and lamellarity), and lipid composition. 1) PTX could be released from the liposomes which are used as a non-toxic biocompatible solubilizer of the drug. The free drug interacts with serum proteins, presumably with albumin. PTX is then transported into the tumor cells or into some somatic cells (e.g. adipocytes). These cells can form a depot for the drug. A small portion of free PTX can directly penetrate into the tumor cells and into the somatic cells. Erythrocytes and platelets can also form a depot for PTX. 2) Liposomal PTX can penetrate through fenestrations of the tumor vasculature. In the tumor, the liposomal drug is accumulated and subsequently released in the vicinity of the tumor cells and the tumor endothelial cells. They are the target for PTX. Liposomal PTX could be also internalized into the tumor cells. Liposomes penetrate through the liver fenestrations. The drug is accumulated and detoxified by enzymatic pathways of cytochrom P450 in the liver. 3) Liposomal PTX could be also internalized by phagocytes (e.g. macrophages). These cells can provide a selective transport and subsequent release of the drug in the tumor.

lipid bilayer. Finally, an optimal addition of cholesterol was found to be 10 mol% with respect to liposomal stabilization up to 10 weeks [38]. Saturated PLs with an extending fatty acid chain (DMPC, DPPC and DSPC) and negatively charged DMPG (molar ratio, 9:1) encapsulating PTX (3 mol%) were used for the preparation of liposomes by lipid film hydration followed by sonication. The drug encapsulation efficacy was higher for liposomes with DMPC and DPPC (96%) than for those with DSPC (70%), while the liposome size increased from 143, 157 to 185 nm for DMPC, DPPC and DSPC, respectively. All these formulations retained about 93% of the initial PTX concentration during 4-day incubation at 4 °C in PBS. Moreover, the delivery of PTX by liposomes to MCF-7 breast cancer cells resulted in a significant increase of the intracellular PTX level and was more efficient in arresting cells in mitosis in comparison with PTX delivered by Taxol® [39].

LEP formulations were also developed in the form of lipid-PTX lyophilizates. This approach significantly eliminates the problem of long-term stability of liposomal PTX formulations in aqueous milieu.

After a reconstitution, the liposomes prepared of DEPC/DMPC/SCPC (molar ratio, 1:1:0.9) containing PTX (3 mol%) were stable for 24 h [40]. The physico-chemical stability of the lyophilized PTX liposomes was monitored during storage. MLVs prepared of PC, cholesterol and vitamin E could be diluted up to 0.5 mg PTX/ml and still PTX crystal-free liposomes were observed. In the samples stored at 4 °C up to 5 months, the level of PL degradation products was negligible and no PTX decomposition or precipitation was found [41]. A novel lyophilized PTX formulation marked as LEP-ETU (NeoPharm) was prepared of DOPC/cardioliipin/cholesterol (molar ratio, 9:0.5:0.5) and α -tocopheryl acid succinate (α -TAS) with PTX/lipids (molar ratio, 1:33). At these liposomes, the original liposomal size was preserved and a stable content of each particular lipid as well as PTX was found up to 12 months at 2–8 °C and 25 °C. Upon lyophilizate reconstitution, neither precipitation of PTX nor any changes in original size were observed for 72 h at 2–8 °C and 25 °C. Moreover, this formulation could be reliably diluted to 0.25 mg PTX/ml [42].

The endeavor to develop a PTX formulation for an inhalation application led to encapsulation of PTX into DLPC vesicles (weight ratio, 1:10). The procedure was based on lyophilization from *tert*-butanol followed by nebulization. The prepared MLVs were of final size of $0.23 \pm 0.17 \mu\text{m}$ and a microscope analysis revealed no PTX crystals. A single-dose application of liposomes (5 mg PTX/kg) by aerosol was compared with an *i.v.* administration. After the aerosol application, levels of PTX were started to be analyzed 5 min after the 30-min aerosol inhalation. The concentration of PTX in lungs ranged from 5.5 to 23.1 $\mu\text{g/g}$ of the tissue during first 25 min. It was followed by a slow decrease to the initial value which remained the same until the end of an observation period of 3 h. For the *i.v.* administration, the concentration of PTX in lungs reached up to 11.7 $\mu\text{g/g}$ of the tissue within 1 min but then it fell down to 0.8 $\mu\text{g/g}$ during 4 min. In addition, the dose applied by aerosol technology (5 mg PTX/kg) was substantially lower than the frequently used doses for *i.v.* or intraperitoneal (*i.p.*) administration (≥ 20 mg PTX/kg) to induce an anti-tumor effect [43].

4.2. Paclitaxel encapsulated in pocket-forming liposomes

The application of pocket-forming lipids can significantly increase the encapsulation capacity of liposomes for PTX. The examples of such lipids are lysophospholipids whose asymmetric molecules form cavities-pockets in the liposomal membrane bilayer. These hydrophobic pockets can accommodate the bulky hydrophobic molecule of PTX and the encapsulation capacity could be increased up to 15 mol% [44].

Based on the pocket-forming lipids, a stable lyophilized formulation encapsulating PTX (7 mol%) in liposomes composed of SOPC/POPG/MOPC lipids (molar ratio, 60:20:20) and vitamin E (5 mol%) was developed. The physical stability of PTX liposomes, morphology of MLVs and original size of 180 nm as well as suppressed PTX crystallization was preserved for 6 months at 4 °C. A significant reduction of lung metastasis was achieved by the application of liposomal PTX (100 and 50 mg/kg) in melanoma bearing mice. The side effects of liposomal PTX were negligible in comparison with Taxol®, whose toxic dose was about 20–25 mg PTX/kg. Besides, both single doses of 100 mg PTX/kg and a cumulative dose of 150 mg PTX/kg (4 equivalent doses, 48-h period) were well tolerated without any signs of toxicity [45].

5. Functionalized liposomes

Liposomes represent a versatile drug delivery system that could be endowed with other properties improving their targeting towards the tumors. Several approaches and examples are presented below.

5.1. Paclitaxel encapsulated in pegylated liposomes (long-circulating liposomes)

Rapid clearance of the conventional liposomes by RES represents one of the major disadvantages in the drug delivery. This problem was solved by employing the long-circulating liposomes. The grafting of conventional liposomes with an inert and biocompatible polymer such as polyethylene glycol (PEG) leads to the formation of a protective and hydrophilic layer on the liposomal surface [46]. The surface modification reduces a clearance of liposomes by the cells of RES and apparently prolongs the half-life of liposomes during circulation [47]. The long-circulating liposomes are also referred to as pegylated, sterically stabilized or stealth liposomes. It was demonstrated that the permeability of the capillary endothelium in the tumors is increased in comparison with normal tissues [48]. The macromolecules are passively accumulated to greater extent for longer period in the tumor than in the non-malignant capillary endothelium. This phenomenon is referred to as an enhanced permeability and retention (EPR) effect

[49]. Small long-circulating liposomes (100 nm) demonstrated a higher frequency of encountering permeable capillaries of the tumor and extravasating into the fenestrated tumor tissue. This accumulation of long-circulating liposomes with encapsulated drugs by EPR effect represents a passive targeting mechanism enhancing the drug delivery and drug therapeutic potential [50].

Liposomal formulations containing 4 mol% of PTX were prepared either as conventional ones made up of PC/PG/cholesterol (molar ratio, 9:1:2) or as pegylated ones composed of PC/PG/cholesterol/DSPE-PEG (molar ratio, 9:1:2:0.7). However, both types of liposomes were physically stable only for less than 1 day in the hydrated state at 4 °C and retained only 50% of the initial PTX content [51]. Conventional and pegylated liposomes were prepared by extrusion of MLVs producing PTX liposomes with a mean size of 120 nm. The inclusion of cholesterol at more than 20% caused a PTX precipitation and liposome destabilization. The conventional PTX liposomes were found to be more stable than corresponding pegylated ones [52].

However, the pegylated PTX liposomes were long-circulating showing a half-life time of 48.6 h against 9.3 h for the conventional ones. It is a result of a reduced clearance of the pegylated PTX liposomes. Their biodistribution demonstrated a considerable decrease in PTX uptake in RES-containing organs (liver and spleen) after 0.5 and 3 h in comparison with their conventional counterparts in Balb/c mice model [52]. The biodistribution effect of PTX was evaluated after *i.v.* administration of 7.5 mg PTX/kg (single dose) of Taxol®, conventional and pegylated PTX liposomes in mice model bearing tumor xenograft. Cr-P was rapidly accumulated and cleared by the liver, spleen and lung, while PTX liposomes exhibited a prolonged half-life of 1.6-fold and 7.1-fold for the conventional and pegylated formulation, respectively. In tumor, after 6 and 24 h the PTX concentration of pegylated liposomes (0.4 and 0.1 $\mu\text{g/g}$) was significantly higher than that of the conventional liposomes (0.1 and 0.03 $\mu\text{g/g}$) and Cr-P (0.05 $\mu\text{g/g}$ and cleaved). In case of pegylated PTX liposomes, the drug concentration in tumor after 6 h was higher than that in spleen, lung, heart, kidney and brain. The accumulation of the pegylated PTX liposomes after *i.v.* administration of 7.5 mg PTX/kg (3 cumulative doses in 4-day intervals) in tumor resulted in a significant inhibition of the tumor growth as compared with the other preparations at the end of the observation period of 60 days. Long circulation time and slow release of PTX from pegylated liposomes offers a chance for PTX to be attained at tumor through EPR effect and maintain the effective therapeutic level for a long-time period via a depot effect. The passive tumor targeting was demonstrated by an application of pegylated PTX liposomes of an appropriate size of <200 nm [53]. The composition of lipids comprising EPC, HEPc, cholesterol and DSPE-mPEG was optimized to improve the encapsulation capacity of PTX and prepare stable pegylated liposomes. The addition of cholesterol allowed a preparation of small-sized liposomes with high drug incorporation. The presence of pegylated PL provided a steric stabilization of the liposomes. Increasing portions of HEPc (25 to 82 mol%) have led to an increased average diameter of the liposomes (113 to 203 nm), meanwhile, the encapsulation efficacy of PTX gradually decreased (69 to 37%). Based on these results, the liposomal formulation of EPC/HEPC/cholesterol/DSPE-mPEG (molar ratio, 15:5:2:1) was found to be optimal. Liposomes were prepared by sonication of MLVs followed by extrusion through 0.2 μm filters. The maximum encapsulation capacity of stable liposomes during the preparation was observed to be 20 mol%. Above this content, PTX accelerated liposome destabilization, needle-like precipitates and aggregated liposomes were observed. Liposomes encapsulating up to 15 mol% of PTX retained the initial drug content and the original size (about 140 nm) for 6 months at 4 °C. Moreover, *i.v.* administration of liposomal PTX (40 mg/kg) caused neither acute toxicity nor mice death, which Taxol® at the corresponding dose did [54]. For the *in vivo* studies utilizing Colon-26 solid tumor-bearing mice, it was confirmed that PEG-coated PTX liposomes delivered a significantly higher amount of PTX to tumor tissue and provided more excellent anti-tumor effect than PEG naked PTX liposomes [55].

These results suggest that PEG liposomes would serve as a potent PTX delivery vehicle for the future cancer chemotherapy and represent a suitable platform for the development of targeted liposomal PTX systems.

5.1.1. Application of pegylated paclitaxel-containing liposomes in metronomic chemotherapy

Metronomic chemotherapy or frequent administration at doses much lower than MTD represents an alternative approach of treatment in comparison with common strategy employing MTD chemotherapy of the drug. As an advantage, this strategy represents a lower toxicity and metronomic regimen could maximize the growth-limiting effects as well as the anti-angiogenic properties. The pegylated PTX liposomes and Taxol® formulation were used to evaluate the effect of metronomic and MTD treatment on the tumor growth inhibition and anti-angiogenic activity. The nude Balb/c mice bearing MDA-MB-231 cells were started to be treated after 11th day of xenograft implantation. PTX formulations were administered at 15 mg PTX/kg on the 11th, 15th, 19th and 23rd day and at 6 mg PTX/kg every day from the 11th to 15th day as well as the 22nd to 26th day for MTD and metronomic chemotherapy, respectively. On the 32nd day, mice were sacrificed and the tumor volume was quantified. Generally, the tumor growth in the groups of metronomic and MTD pegylated PTX liposomes as well as MTD Taxol® demonstrated the same inhibition effect, while significant tumor progression was observed for the metronomic administration of Taxol®. The metronomic application of pegylated PTX liposomes was the most efficient in anti-angiogenic activity as determined by microvessel density assessment. These results indicate that frequent administration of pegylated PTX liposomes had an anti-angiogenic effect that blocked the blood supply and may be more effective in suppressing tumor growth in vivo [56].

5.2. Paclitaxel encapsulated in ligand-targeted liposomes

Another attempt to overcome the limitations associated with the conventional liposomes was the development of ligand-targeted liposomes also referred to as immunoliposomes [57]. Because long-circulating liposomes demonstrate a minimal affinity to normal tissues they provide a biologically inert and safe platform for the design of advanced drug delivery systems. Ligand-targeted liposomes employ certain targeting groups conjugated to the surface of long-circulating liposomes for selective delivery of the encapsulated drug to the desired site of action (active targeting). The targeting groups used include antibody molecules or their fragments, naturally occurring or synthetic ligands such as peptides, carbohydrates, glycoproteins or receptor ligands, i.e. generally a molecule that selectively recognizes and binds to a target antigen selectively expressed by the tumor cells. The active targeting increases the specificity of the interaction of a liposome-encapsulated drug with the target cells as well as the amount of the drug delivered [58].

5.2.1. Folate-receptor-targeted paclitaxel liposomes

Liposomes (3 mol% PTX) targeting folate receptor (FR), which is frequently overexpressed by epithelial cancer cells, were prepared and characterized. FR-targeted PTX liposomes were composed of DPPC/DMPG/DSPE-mPEG/DSPE-PEG-folate (molar ratio, 85.5:9.5:4.5:0.5). Formulations developed as lyophilizates prepared by extrusion of MLVs had the final mean size of 93 nm with PTX incorporation efficacy of 98%. Upon lyophilizate rehydration, the liposomes exhibited a particle stability and drug retention over 72 h at 4 °C. The enhanced cellular uptake and liposome internalization by KB oral carcinoma cells expressing FR was demonstrated for FR-targeted PTX liposomes in comparison with their non-targeted counterpart [59].

5.2.2. HER-2-targeted paclitaxel liposomes

The human epidermal growth factor receptor-2 (HER-2) represents a target for the delivery of PTX by liposomes to breast cancer

cells. Herceptin monoclonal HER-2 antibody coupled with pegylated liposomes represents a suitable strategy for active tumor targeting mediated via HER-2 expressing cancer. After 2-h in vitro incubation, the cellular uptake of the pegylated HER-2 targeted PTX liposomes by breast cancer cells BT-474 and SK-BR-3 expressing HER-2 was found to be twice higher than that for the pegylated HER-2 non-targeted PTX liposomes. In the case of MDA-MB-231 cancer cells with low-abundant HER-2 factor, the cellular uptake was comparable for both types of liposomes [60]. Specific tumor uptake of PTX was evaluated after i.v. application of the pegylated HER-2 non-targeted and pegylated HER-2 targeted PTX liposomes in breast carcinoma xenograft mouse model. In BT-474 cells, pegylated HER-2 targeted PTX liposomes showed a significantly higher drug concentration ratio of tumor to plasma compared with the pegylated non-targeted PTX liposomes. However, this HER-2 selective tumor distribution was not observed in MDA-MB-231 cells with low-abundant HER-2 factor. The anti-tumor effect of the pegylated HER-2 targeted PTX liposomes was superior to the Cr-P and to the pegylated non-targeted PTX liposomes in mouse bearing BT-474 breast cancer, whereas for the MDA-MB-231 mouse model, the anti-tumor efficacy was comparable for both types of liposomes [61].

5.2.3. Peptide-targeted paclitaxel liposomes

Vascular endothelial growth-factor receptors such as neuropilin-1 (NRP-1) and alpha V integrins represent effective vascular targets expressed by endothelial cells. Novel peptides, the first one containing two individual neovessel-specific motifs like Arg-Gly-Asp (RGD) and Ala-Thr-Trp-Leu-Pro-Pro-Arg (ATWLPPR) and the second one integrin-targeted possessing only RGD motif, were synthesized to provide specific target binding. Dual-targeted or single-targeted liposomes (< 100 nm) composed of PC/cholesterol/DSPE-mPEG (molar ratio, 9:1:0.5) encapsulating 3 mol% PTX had peptide anchored via palmitic acid into the lipid membrane bilayer. The release of PTX was lower than 2% of the initial drug concentration during 24 h. The cytotoxic effect and ligand-mediated internalization of liposomes was tested on A549 (human lung carcinoma) and HUVEC (human umbilical vein endothelial cells) both expressing alpha V integrins and NRP-1. The lowest value of IC₅₀ was observed for dual-targeted PTX liposomes in comparison with PTX liposomes single-targeted, non-targeted and Taxol® indicating an advanced binding activity and specificity to the target. The specific cellular uptake of dual-targeted liposomes was significantly higher than that for other formulations. Different liposomal PTX formulations were administered into xenograft mouse models bearing A549 cells to evaluate the anti-tumor efficacy in vivo. The mean tumor weight was determined to be 1622 mg for an untreated control at the end of the experimental period of 60 days. The anti-tumor activity of PTX liposomes expressed as the mean tumor weight was found to be 608 mg, 439 mg, and 296 mg for the non-targeted, single-targeted, and dual-targeted liposomes, respectively, [62,63]. This concept of RGD peptide targeting was also developed for the construction of targeted PTX liposomes. They were prepared by covalent conjugation of RGD peptide with pegylated lipid of long-circulating PTX liposomes [64].

Another example of targeting is represented by an application of cationic PTX liposomes in combination with attached fibroblast growth factors (FGFs). FGFs are small polypeptide growth factors playing important roles in complex biological events such as angiogenesis and tumor formation. These peptides were explored for liposomal drug targeting in neovascular therapy [65]. FGF receptors, overexpressed on the surface of variety of tumor cells and on tumor neovasculature, represent potential targets for tumor and vascular targeting. A novel truncated basic RGF (tbRGF) peptide was attached by electrostatic force onto the surface of cationic liposomes composed of DOTAP/cholesterol (molar ratio, 1:1) encapsulating PTX. For in vivo tumor model, the peptide-targeted cationic PTX liposomes prolonged the retention time and demonstrated a significantly 2.6-fold and

7.2-fold higher tumor accumulation than two other used formulations, non-targeted liposomes and Taxol®, respectively. In this case, the underlying mechanisms involve the steps as follows: liposomes slowly accumulated in tumor tissue, ultimately reaching a high level in tumor due to EPR effect and tbFGF-modified liposomes enhanced the accumulation via the ligands against the receptors that were overexpressed on the surface of the tumor cells, resulting in a slow drug release to tumor sites [66].

A new chitosan derivative, octadecyl-quatemed lysine-modified chitosan (OQLCS), possesses an amino group to which functional groups such as folic acid (FA) or transactivating transcriptional activator peptide (TATp) could be attached. FA could be selectively bound to folate receptor (FR), a 38 kDa glycosyl-phosphatidyl inositol-anchored cell surface receptor, which is frequently overexpressed by epithelial cancer cells. TATp, cell-penetrating peptide, is an effective transport carrier possessing the ability to facilitate an efficient uptake of various cargos ranging from small peptide sequences to large biomolecules like liposomes and polymers. Polymeric liposomes composed of FA-OQLCS/OQLCS/cholesterol (weight ratio, 1:1:1) attaching TATp (weight ratio TATp/liposome, 1:4) onto the liposomal surface were capable to load up to 26 wt% of PTX. The inclusion of PTX higher than 11 wt% resulted in a poor encapsulation efficacy. Thus, for further experiments the liposomes with 11 wt% of PTX were prepared. Original liposome mean size of 60 nm was preserved for 2 months. In the first 2 days, a precipitation of PTX about 40% was observed. It was followed by a drug release up to 80% after 2 weeks at 37 °C. In addition, almost all PTX discharged from the Taxol® formulation already within 2 days [67]. A composition similar to that of FA-OQLCS/PEG-OQLCS/cholesterol (weight ratio, 2:3:1) attaching TATp was also used for the construction of polymeric liposomes (FA-TATp-PLs) loading 10 wt% of PTX. Significantly higher uptake of these liposomes for FR-positive KB nasopharyngeal epidermal carcinoma cells than that for FR-negative A549 human lung carcinoma cells was observed by confocal laser microscopy. In vivo anti-tumor activity of PTX loaded in FA-TATp-PLs was evaluated at SCID mice bearing KB cells. Drug administration repeating every 3 days was followed by a quantification of tumor volume until the 27th day. The average tumor volume of the mice after the treatment period with 5 and 10 mg/kg PTX loaded in FA-TATp-PLs was 4.2 and 4.8 times lower than that of the mice treated with 5 and 10 mg/kg Taxol®, respectively. The effective tumor-growth inhibition by PTX loaded in FA-TATp-PLs could be explained by a combination of a selective uptake by KB cells, the EPR effect and an efficient delivery through the transmembrane ability of TATp [68].

5.2.4. Hyaluronan-targeted paclitaxel liposomes

A frequent overexpression of CD44 (a receptor for hyaluronic acid (HA)) and CD168 (a receptor for hyaluronan-mediated mobility (RHAMM)) on many types of tumors offers further possibility of targeting by the naturally-occurring high-molecular-weight HA [69,70]. HA, a naturally-occurring glycosaminoglycan, is one of the main components of the extracellular matrix. HA is also known as a bioadhesive compound capable of binding with high affinity to cell surface, intracellular receptors, extracellular matrix components and also to itself [71]. In the tumor cells, binding of HA to its receptors is involved in the tumor growth and spreading. Cancer-cell proliferation and metastatic processes are regulated by CD44 [72,73].

Mixing of DLPE/DLPG lipids (molar ratio, 9:1) for the encapsulation of PTX resulted in self-assembling into nanoparticle-like clusters which were subsequently coated with HA. The prepared structures were of spherical shape having final size of 300 nm. For in vitro experiments, the particles were found to deliver PTX selectively into the mouse colorectal cancer cells (CT-26), expressing CD44, in a CD44-dependent manner. Injected systemically to mice bearing CT-26 solid tumors, this drug delivery system demonstrated a high safety profile and tumor-site accumulation. PTX-particles act as long-circulating tumor targeted particles with half-life of 6 h compared with 10 min

for Taxol®. Under the same conditions, the PTX-particles (5 mg PTX/kg) induced tumor arrest and were as potent as a 4-fold higher dose for Taxol®. It was also observed that these particles reduce PTX liver and spleen accumulation and induction of pro-inflammatory cytokines was lower in comparison with Taxol® [74].

5.3. Paclitaxel encapsulated in cationic liposomes

Targeting of the vasculature has several advantages over targeting of tumors. There are no physiological barriers for endothelial cells. Thus, for drug delivery systems, the vasculature is more easily accessible than tumor cells. The destruction of a few capillary endothelial cells can affect a large number of tumor cells. Finally, the endothelial cells are genetically stable and do not become resistant to the therapy [75]. The high proliferation rate of these cells provides them with a selective target for anti-tumor drugs [76]. The concept of anti-angiogenic therapy is based on the inhibition of endothelial cell proliferation, whereas vascular targeting destroys tumor microvasculature producing malnutrition and accumulation of metabolites. Thus, a neovessel is an attractive target since angiogenesis is necessary for a tumor growth and metastasis. Cationic liposomes were found to be selective for targeting the tumor endothelial cells. The positive charge of their surface determines the distribution of liposomes into the vascular tumor compartment. The encapsulation of the anti-tumor drug into the cationic liposomes represents a novel approach to the selective drug delivery that employs the vascular targeting for the tumor therapy [77,78].

PTX was loaded into cationic liposomes prepared of cationic lipid DOTAP and dioleic-derived PLs. They were of the final size of 180–200 nm. The hamster melanoma A-Mel-3 was implanted into Syrian golden hamster. The experimental animals were treated with the dose of 5 mg PTX/kg by i.v. infusion. The rhodamine-labeled cationic PTX liposomes were shown to be accumulated at the tumor to normal tissue ratio of 3:1, as observed by in vivo fluorescence microscopy imaging. The anti-tumor activity was evaluated by quantification of the tumor volume at the end of the 23-day observation period. The tumor growth was found to be only 1.7% for the cationic LEP, while 10% for the empty cationic liposomes and 11% for Cr-P. Moreover, the occurrence of the lymph node metastases was significantly delayed by the cationic LEP in comparison with the other formulations used [79]. The selective and efficient delivery of PTX encapsulated in the cationic liposomes (EndoTAG®-1 also known as LipoPac® or MBT-0206) was also reported for other experimental models. The liposomes were found to successfully decrease the tumor angiogenesis and melanoma growth in humanized SCID murine model [80] as well as to impair the functional tumor microvasculature in Syrian golden hamsters bearing A-Mel-3 melanoma [81]. The neovascular targeting was also tested for the treatment of prostate cancer [82]. This approach represents a new method for the treatment by reducing the primary tumor mass. Moreover, it provides an additional effect in suppression of angiogenesis in comparison with the conventional treatment.

5.4. Paclitaxel encapsulated in thermosensitive liposomes

Thermosensitive liposomes encapsulating PTX were prepared using EPC and cholesterol in combination with ethanol. The prepared liposomes had a phase transition temperature of 43 °C. The in vivo efficacy of the thermosensitive PTX liposomes was determined in B16F10 murine melanoma transplanted into C57Bl/6 mice in combination with local hyperthermia. A significant reduction of tumor volume and an increase in survival time were observed in tumor-bearing mice treated with a combination of hyperthermia and thermosensitive PTX liposomes compared with animals treated with an equivalent dose of Cr-P with or without hyperthermia [83]. Another approach was based on a thermosensitive pluronic acid (Pluronic®

F127) hydrogel in which PTX-containing liposomes were embedded. This system was developed for hydrophobic anti-cancer agents to be used in parenteral formulations for treating local cancers. A thermoreversible hydrogel based on F127 containing liposomal PTX can be utilized for controlled drug delivery and enhanced drug uptake in cancer cells [84].

5.5. Paclitaxel encapsulated in magnetoliposomes

Magnetite (Fe_3O_4) nanoparticles have been explored for various biomedical applications. The applications include the use of magnetite nanoparticles in cell labeling/cell separation, magnetofection to facilitate gene delivery, as contrast agents for magnetic resonance imaging (MRI), to induce local hyperthermia in response to an external alternating magnetic field to selectively destroy cancer cells, and as a magnetically targeted carrier system in drug delivery applications. PL vesicles encapsulating magnetic nanoparticles (liposome complexes) have been prepared for targeting a drug to a specific organ using a magnetic force as well as for local hyperthermia therapy. Liposome complexes represent also an ideal platform for use as contrast agents of magnetic resonance imaging (MRI).

Liposomal formulation of PTX was also developed as lyophilized magnetoliposomes. Ultrafine magnetite (Fe_3O_4 , 50 nm) was encapsulated into liposomes composed of HSPC, cholesterol, DCP and α -tocopherol (molar ratio, 62:31:7:2.5) using reverse-phase evaporation followed by sonication. Although negatively charged DCP provides electrostatic repulsion and cholesterol improves the stability, liposome aggregation and drug precipitation were observed upon storage (15–25 °C, 3 months). Further, the liposome stability was extended for 6 months by a lyophilization process as determined by the encapsulation efficacy, size distribution and morphology. In vivo biodistribution suggested that magnetoliposomes were distinctively localized in the tumor tissues having obvious tumor-targeting and sustained-release effect, which have a good responsiveness to external magnetic field. Neither erythrocytalysis nor agglomeration phenomenon was observed after incubation of magnetoliposomes with red cell suspension [85]. This concept of liposomal PTX magnetoliposomes was subsequently upgraded as chitosane-coated liposome complexes with 10 nm Fe_3O_4 nanoparticles encapsulating PTX [86].

Further progress in magnetoliposome applications as drug delivery systems is associated with a development of instruments able to focus them by magnetic field. At present, such instruments are available only for mice or rats.

6. Toxicity and anti-tumor activity of liposomal paclitaxel

In animal models, LEP formulations demonstrate lower toxicity and equal anti-tumor efficacy as the clinical formulation of Taxol®. The toxicity and anti-tumor activity of LEP and Cr-P was tested in vitro and in vivo on various mouse models bearing tumor xenograft. The incorporation of PTX into liposomes not only eliminates the hypersensitivity reactions associated with the Cremophor EL® vehicle but also decreases the toxicities that arise from the drug's pharmacological action [87,88]. A reduction of toxicity towards critical normal tissues results in a substantial elevation of the MTD. The impact of these changed parameters on the therapeutic index is striking in PTX-resistant tumors like colon tumor model or melanoma [36,45].

In vitro, the toxicity of LEP and Cr-P was found to be similar for the tested P388 and L1210 leukemia cells. In vivo, LEP exhibited reduced side effects and enhanced drug efficacy [89]. To examine the toxicity of Cr-P and LEP formulation, a comparative in vivo study was carried out. For Cr-P administered *iv.*, a cumulative PTX dose of 325 mg/kg on 3 consecutive days caused 100% mortality at the 3rd day. At LEP, no mortality for the murine L1210 leukemia model was observed [87]. A dose-dependent character of the toxicity and anti-tumor effect of

PTX formulated either in liposomes or in Cremophor EL® was investigated after *ip.* administration in DBA-2 mice bearing P388 leukemia. The Cr-P and LEP were administered as cumulative PTX doses (3 equivalent doses in consecutive days) of 40–120 mg/kg and 40–300 mg/kg, respectively. LEP exhibits lower cumulative toxicity than Cr-P. By the encapsulation of PTX in liposomes, the acute toxicity associated with Cremophor EL® was eliminated [90]. The growth-inhibitory activity of LEP was retained in vitro against a variety of tumor cell lines. In vivo, LEP was found to be well tolerated in mice model. MTD for this formulation was 200 mg PTX/kg for both *iv.* and *ip.* administration. This significantly outperforms the MTD for Cr-P that was reported to be 30 mg PTX/kg (*iv.*) and 50 mg PTX/kg (*ip.*) [91].

PTX-sensitive A121a human ovarian tumor was subcutaneously applied in nude mice. The treatment procedure with LEP and Cr-P resulted in a similar anti-tumor effect. However, LEP was better tolerated after *iv.* administration [88]. LEP formulation was used to suppress the growth of PTX-resistant Colon-26 murine tumor implanted in the Balb/c mice. The Cr-P was found to be in-effective in the inhibition of the tumor growth at the doses close to MTD (30 mg PTX/kg). On the contrary, LEP reduced the tumor progression at the doses that would be lethal, if PTX was applied in Cremophor EL® [36,92].

As it was reported, PTX administration has a severe embryotoxic effect. It could be partially attributable to the toxicity associated with Cremophor EL® vehicle. The embryotoxicity of LEP and Cr-P was tested in the chick embryo model. The injections of PTX at the doses up to 30 μg were applied into the eggs. At the Cr-P, the dose of 1.5 μg PTX/egg caused an embryotoxic effect in 60% of the tested eggs. On the contrary, a 20-fold higher dose of LEP formulation was necessary to produce the same toxicity effect [93]. Similarly, LEP was found to reduce PTX-associated embryotoxicity in rats. Wistar rats were *iv.* treated at the doses of 2 and 10 mg/kg of PTX in liposome and Cremophor EL® on the 8th day of pregnancy. At the dose of 10 mg PTX/kg of Cr-P, the maternal and embryonal toxicity was observed. Three of seven rats died and all of the embryos in the survived rats were resorpted. LEP at 10 mg PTX/kg was associated with none maternal death, only some malformations occurred in the survived fetuses. At the dose of 2 mg PTX/kg of Cr-P, the fetal weight was decreased and resorption increased. The malformations were prominent at the PTX doses of 2 mg/kg of Cr-P and 10 mg/kg of LEP. It is obvious that the encapsulation of PTX into liposomes provides a significant reduction of the drug and vehicle associated embryotoxicity. These results have important implications for the therapy with PTX during human pregnancy [94].

7. Clinical trials

PTX is a promising anti-tumor agent with poor water solubility. It is effective in treatment of various cancers, especially ovarian and breast cancer. Taxol® represents a currently available preparation of PTX produced by Bristol-Myers Squibb. The administration of this preparation has serious side effects. The extensive clinical use of PTX is somewhat lagging behind due to the lack of appropriate delivery systems. There is a need for alternative delivery systems for PTX that would not have any side effects. Liposomal PTX formulations are in various stages of clinical trials. LEP-ETU (NeoPharm) and EndoTAG®-1 (Medigene) have reached the phase II of the clinical trials; Lipusu® (Luye Pharma Group) has already been commercialized.

The first LEP preparation was composed of EPC, cardiolipin, cholesterol, and α -TAS. The liposomes were supplied as a lyophilizate by Pharmacia (Nerviano, Italy). The parameters such as MTD, recommended dose (RD), dose-limiting toxicities (DLTs), pharmacokinetics, and the anti-tumor effect of LEP were evaluated in weekly scheduled phase I study. Prior to the treatment, all of the 14 patients with refractory solid malignancies were premedicated. Subsequently, they received LEP infusion (90–150 mg PTX/m²) over 45 min once a week for 6 out of 8 weeks. One patient experienced DLTs at 150 mg

PTX/m². He received less than 70% of the intended cumulative dose. A stabilization of the disease was documented only in 2 patients for the 8 weeks. The whole blood clearance of total PTX was similar to Taxol®. However, this trial was discontinued upon completion of enrolment of 150 mg PTX/m² cohort. The assessment of pharmacokinetics and the clinical data suggested that this LEP was unlikely to have any advantage over Taxol® [95]. Further efforts to eliminate toxicities associated with Taxol®, to improve the drug safety profile and to enhance the PTX therapeutic efficacy led to the development of LEP formulation (marked LEP-ETU) by NeoPharm. The phase I study was designed to determine MTD, DLTs, pharmacokinetics and anti-tumor effects of LEP-ETU. The whole of 25 adult patients with advanced incurable cancer (breast, colon, and ovarian) were treated by LEP-ETU infusion (135–375 mg PTX/m²) for 90 min every 21 days (6 cycles). To prevent infusion-related reactions (IRRs), the initial patients (135–225 mg PTX/m²) were premedicated on the day of infusion. The later patients (225–375 mg PTX/m²) were not premedicated. Multiple infusions without IRRs were completed in 75% patients. The most frequent adverse events were fatigue, nausea, anemia, hypoesthesia, and neutropenia. DLTs occurred at 375 mg PTX/m² and consisted of febrile neutropenia and neuropathy. MTD was determined to be 325 mg PTX/m². LEP-ETU at 325 mg PTX/m² provided an acceptable neutropenic events relative to those observed for Taxol® at 175 mg PTX/m². An evidence of anti-tumor activity was observed as a partial response and stable disease at 3 and 11 patients, respectively [32,96–99]. The protection against toxicities relating to free PTX and the encouraging data regarding the tumor response enabled a successful progression of LEP-ETU into the phase II of the clinical testing for the treatment of metastatic breast cancer. NeoPharm conducted a multicenter, open-label trial of LEP-ETU at 5 centers in India. A total of 35 patients were enrolled. They received a dose of 275 mg PTX/m² without routine prophylactic premedication for IRRs every 3 weeks (6 cycles). Overall tumor responses with fully audited data were as follows: 16 patients with tumor response including 15 partial responses and 1 complete response; 10 patients with stable disease; 9 subjects with progressive disease. LEP-ETU was well tolerated. No significant IRRs were observed, as indicated by the low extent of adverse events even at the absence of prophylactic premedication. The research continues to evaluate whether to extend the trial phase II of LEP-ETU or to start phase III of randomized trials with Taxol® used as a comparing agent in metastatic breast cancer patients. The goal is to embark the process of regular approval of LEP as an effective modality for the treatment of cancer patients as early as possible [100].

The second PTX preparation was based on cationic LEP. The delivery of cationic LEP to the tumor vasculature in combination with chemotherapy affecting the proliferating tumor cells represents an effective two-component anti-tumor therapy. Generally, anti-angiogenic drugs themselves cannot eradicate tumors completely. A remarkable anti-tumor effect can be achieved by combining anti-angiogenic tumor therapy with conventional cytotoxic radio- or chemo-therapy. Tumor endothelial cell apoptosis and intra-tumoral thrombosis was found to be induced by cationic LEP. This therapy supports vascular targeting as an underlying mechanism [101]. This novel therapeutic strategy was first realized by the development of EndoTAG®-1 preparation by Medigene. This preparation comprised PTX encapsulated in cationic lipid complexes based on liposomes composed of DOPC/DOTAP and the drug (molar ratio, 45/50/5) [102]. EndoTAG®-1 is currently tested in the phase II of trials against various types of solid tumors. Medigene recently announced interim results of EndoTAG®-1 against inoperable, locally advanced or metastasized pancreatic cancer. In this study, gemcitabine monotherapy was randomized against different doses of EndoTAG®-1 in combination with gemcitabine. Median survival in the group receiving the highest dose of EndoTAG®-1 exceeded the median survival of the control group by 30%. The survival was even higher in patients who received EndoTAG®-1 over a longer period and repeatedly [102].

A case study on a successful treatment of a patient suffering from progressive hepatocellular carcinoma (HCC) was reported. This HCC is the third most common cause of cancer deaths. In the patient, EndoTAG®-1 stopped tumor progression for 9 months [102]. In another study, patients with advanced cancer and liver metastasis were treated by EndoTAG®-1. Generally, EndoTAG®-1 was well tolerated. Common side effects were fatigue and hypersensitivity reactions. Nine of 18 patients had a stable disease after a first treatment cycle. Four patients without progression of a disease continued the treatment [103].

The third liposomal PTX preparation, Lipusu® (paclitaxel liposome for injection, Luye Pharma Group), was developed by Sike Pharmaceutical (Nanjing, Jiangsu, PRC). This preparation was approved by the State FDA of China. Lipusu® is the first commercially available PTX formulation to be marketed. It represents a natural extract from Yew used in the treatment of ovarian, breast, NSCLC, gastric and head and neck cancer. The application of a liposome technology resolved the issues of PTX insolubility and eliminated the use of solvents causing toxic side-effects. Advanced drug delivery by liposomes reduced the side-effects to blood pressure, the medulla, peripheral blood and the liver after injection. These improvements enable to apply higher drug doses leading to an enhanced drug efficacy. The advanced drug distribution has led to an increased tolerance of PTX in patients. Moreover, the lyophilized preparation provides flexible storage conditions for LEP.

A clinical study was performed to obtain an optimal premedication protocol for Lipusu®. Lipusu® as a component of combined chemotherapy was administered at 175 mg PTX/m² (triweekly or weekly divided) to patients with solid tumors as follows: advanced NSCLC (30%), gastric cancer (30%), breast cancer (27%), esophagus cancer (11%), head and neck cancer (2%). Generally, the authors recommended a premedication prior to Lipusu® as follows: (1) methylprednisolone 40 mg, administered i.v. 30 min before Lipusu®, granisetron 30 min before chemotherapy, and (2) dexamethasone 2.25–3 mg taken orally 12 and 2 h before Lipusu®, granisetron 30 min before chemotherapy [104]. Thirteen of NSCLC patients with malignant pleural effusions were enrolled into the phase I clinical study. The treatment was realized by instillation of LEP (125 mg PTX/m²) into the pleural cavity through a catheter during 30 min. As regards the efficacy, no significant difference between LEP and Taxol® was observed. The toxicity of LEP was much lower than that of Taxol®. Anaphylaxis, peripheral nerve toxicity, nausea and vomiting never occurred in patients treated with LEP. In contrast, anaphylaxis and peripheral nerve toxicity were the major side-effects in patients treated with Taxol®. In addition, the symptoms of diarrhea, anemia, neutropenia, thrombocytopenia, hepatotoxicity and chest pain were all mild after the intrapleural LEP application and were easily controlled. All these symptoms became more severe in the patients treated with Taxol®. The intra-pleural administration of LEP could maximize the treatment effect of local disease while minimizing a systemic toxicity. To confirm this finding, a phase II study of a large number of patients was recommended [105,106].

Abraxane® (albumin nanoparticle-bound PTX) is the only non-liposomal preparation of PTX which reached the market [107]. The preparation was developed by Abraxis BioScience. This company was acquired by Celgene in 2010. Abraxane® was approved for the treatment of metastatic breast cancer in 2005. Albumin nanoparticle formulation allows PTX to penetrate into tumors more easily and makes the drug to be more tolerated than Taxol® [108]. Abraxane® significantly improved the response rate in NSCLC patients in comparison with the generic chemotherapy by PTX drug. However, according to the data from phase III of the study, Abraxane® did not retard tumor growth or help lung cancer patients live longer [109]. Hair loss, nerve pain, unusual sensations (burning or tingling), changes in the heart rhythm and weakness were side effects, even if reported in small portion of patients.

8. Conclusion

It was demonstrated that liposomal carriers are superior to Taxol® as regards the delivery of PTX. Presently, two liposomal formulations are in clinical trials and close to commercialization. The preparations based on conventional liposomes represent the first generation of LEP. There is no doubt that patients will benefit from the improved therapeutic effect of these modern drug delivery systems. It seems that conventional liposomes represent a non-toxic solubilization system rather than a real targeted drug delivery system. The second generation of LEP is based on functionalized liposomes (cationic or ligand-targeted). They are under the development in various stages of preclinical and clinical trials. This great progress in the development of LEP preparations demonstrates the versatile and unique properties of liposomes as drug carriers. The impact of both the therapeutic effectiveness and the price of LEP suggests a near-future success on the drug delivery market.

Acknowledgments

This work was supported by the following grants: the Grant Agency of the Czech Republic (GAP304/10/1951) to J.T. and (GAP503/12/G147), the Grant Agency of the Academy of Sciences of the Czech Republic (KAN200100801) to J.T., the Ministry of Agriculture of the Czech Republic (MZE0002716202), and the Ministry of Education, Youth and Sports of the Czech Republic (CZ.1.07/2.3.00/20.0164) to J.T. The authors thank Dr. Jana Plocková for her assistance in the preparation of the manuscript.

References

- LB. Michaud, V. Valero, G. Hortobagyi, Risks and benefits of taxanes in breast and ovarian cancer, *Drug Saf.* 23 (2000) 401–428.
- M.C. Wani, H.L. Taylor, M.E. Wall, P. Coggon, A.T. McPhail, Plant antitumor agents 6. Isolation and structure of taxol, a novel antileukemic and antitumor agent from *Taxus brevifolia*, *J. Am. Chem. Soc.* 93 (1971) 2325–2327.
- E.K. Rowinsky, R.C. Donehower, Drug therapy—Paclitaxel (Taxol), *N. Engl. J. Med.* 332 (1995) 1004–1014.
- I. Kramer, A. Heuser, Paclitaxel pharmaceutical and pharmacological issues, *Eur. Hosp. Pharm.* 1 (1995) 37–41.
- R.T. Donr, Pharmacology and toxicology of Cremophor EL diluent, *Ann. Pharmacother.* 28 (1994) 511–514.
- R.B. Weiss, R.C. Donehower, P.H. Wiernik, T. Ohnuma, R.J. Gralla, D.L. Trump, J.R. Baker, D.A. Vanecko, D.D. Vonhoff, B. Leyland-Jones, Hypersensitivity reactions from taxol, *J. Clin. Oncol.* 8 (1990) 1263–1268.
- M.C. Allwood, H. Martin, The extraction of diethylhexylphthalate (DEHP) from polyvinyl chloride components of intravenous infusion containers and administration sets by paclitaxel injection, *Int. J. Pharm.* 127 (1996) 65–71.
- S.C. Kim, H.J. Yoon, J.W. Lee, J.W. Yu, E.S. Park, S.C. Chi, Investigation of the release behavior of DEHP from infusion sets by paclitaxel-loaded polymeric micelles, *Int. J. Pharm.* 293 (2005) 303–310.
- Q.Y. Xu, L.A. Trissel, J.F. Martinez, Stability of paclitaxel in 5% dextrose injection or 0.9% sodium chloride injection at 4, 22 or 32 degrees C, *Am. J. Hosp. Pharm.* 51 (1994) 3058–3060.
- S.C. Lee, C. Kim, I.C. Kwon, H. Chung, S.Y. Jeong, Polymeric micelles of poly(2-ethyl-2-oxazoline)-block-poly(epsilon-caprolactone) copolymer as a carrier for paclitaxel, *J. Control. Release* 89 (2003) 437–446.
- X. Feng, Y.J. Yuan, J.C. Wu, Synthesis and evaluation of water-soluble paclitaxel prodrugs, *Bioorg. Med. Chem. Lett.* 12 (2002) 3301–3303.
- F. Dosio, S. Arpicco, P. Brusa, B. Stella, L. Cattel, Poly(ethylene glycol) human serum albumin-paclitaxel conjugates: preparation, characterization and pharmacokinetics, *J. Control. Release* 76 (2001) 107–117.
- C.H. Liu, J.S. Strobl, S. Bane, J.K. Schilling, M. McCracken, S.K. Chatterjee, R. Rahim-Bata, D.G. Kingston, Design, synthesis and bioactivities of steroid-linked taxol analogues as potential targeted drugs for prostate and breast cancer, *J. Nat. Prod.* 67 (2004) 152–159.
- B.B. Lundberg, V. Risovic, M. Ramaswamy, K.M. Wasan, A lipophilic paclitaxel derivative incorporated in a lipid emulsion for parenteral administration, *J. Control. Release* 86 (2003) 93–100.
- G. Ruan, S.S. Feng, Preparation and characterization of poly(lactic acid)-poly(ethylene glycol)-poly(lactic acid) (PLA-PEG-PLA) microspheres for controlled release of paclitaxel, *Biomaterials* 24 (2003) 5037–5044.
- U.S. Sharma, S.V. Balasubramanian, R.M. Straubinger, Pharmaceutical and physical properties of paclitaxel (taxol) complexes with cyclodextrins, *J. Pharm. Sci.* 84 (1995) 1223–1230.
- E. Merisko-Liversidge, P. Sarptodar, J. Bruno, S. Hajji, L. Wei, N. Peltier, J. Rake, J.M. Shaw, S. Pugh, L. Pollin, J. Jones, T. Corbett, E. Cooper, G.G. Liversidge, Formulation and antitumor activity evaluation of nanocrystalline suspensions of poorly soluble anticancer drugs, *Pharm. Res.* 13 (1996) 272–278.
- A. Sharma, U.S. Sharma, Liposomes in drug delivery: progress and limitations, *Int. J. Pharm.* 154 (1997) 123–140.
- R.D. Hofheinz, S.U. Ghad-Vogt, U. Beyer, A. Hochhaus, Liposomal encapsulated anticancer drugs, *Anticancer Drugs* 16 (2005) 691–707.
- S. Koudelka, J. Masek, J. Neuzil, J. Turánek, Lyophilized liposome-based formulations of alpha-tocopheryl succinate: preparation and physico-chemical characterization, *J. Pharm. Sci.* 99 (2010) 2434–2443.
- M. Tattersall, S. Clarke, Developments in drug delivery: implications for cancer care, *Curr. Opin. Oncol.* 15 (2003) 293–299.
- S.B. Kulkarni, G.V. Betageri, M. Singh, Factors affecting microencapsulation of drugs in liposomes, *J. Microencapsul.* 12 (1995) 229–246.
- S.V. Balasubramanian, R.M. Straubinger, Taxol-lipid interactions—taxol-dependent effects on the physical properties of model membranes, *Biochemistry* 33 (1994) 8941–8947.
- C. Bernsdorff, R. Reszka, R. Winter, Interaction of the anticancer agent Taxol (TM) (paclitaxel) with phospholipid bilayers, *J. Biomed. Mater. Res.* 46 (1999) 141–148.
- M.R. Wenk, A. Fahr, R. Reszka, J. Seelig, Paclitaxel partitioning into lipid bilayers, *J. Pharm. Sci.* 85 (1996) 228–231.
- R.M. Straubinger, S.V. Balasubramanian, Preparation and characterization of taxane-containing liposomes, *Methods Enzymol.* 391 (2005) 97–117.
- G.N. Kumar, U.K. Walle, K.N. Bhalla, T. Walle, Binding of taxol to human plasma, albumin and alpha-1-acid glycoprotein, *Res. Commun. Chem. Pathol. Pharmacol.* 80 (1993) 337–344.
- E. Sykes, K. Woodburn, D. Decker, D. Kessel, Effects of Cremophor-EL on distribution of taxol to serum lipoproteins, *Br. J. Cancer* 70 (1994) 401–404.
- A. Sparreboom, O. van Tellingen, W.J. Nooljen, J.H. Beijnen, Tissue distribution, metabolism and excretion of paclitaxel in mice, *Anticancer Drugs* 7 (1996) 78–86.
- A. Sparreboom, L. van Zuylen, E. Brouwer, W.J. Loos, P. de Bruijn, B. Gelderblom, M. Pillay, K. Nooter, G. Stoter, J. Verweij, Cremophor EL-mediated alteration of paclitaxel distribution in human blood: clinical pharmacokinetic implications, *Cancer Res.* 59 (1999) 1454–1457.
- M.D. Wild, U.K. Walle, T. Walle, Extensive and saturable accumulation of paclitaxel by the human platelet, *Cancer Chemother. Pharmacol.* 36 (1995) 41–44.
- G.J. Fetterly, T.H. Grøeås, J.W. Sherman, J. Dal, A. Gahrn, D. Iecromte, J. Fiedler-Kofly, N. Damjanov, M. Bshman, M.P. Kane, E.H. Rubin, A.R. Tan, Pharmacokinetic/pharmacodynamic modeling and simulation of neutropenia during phase I development of liposome-entrapped paclitaxel, *Clin. Cancer Res.* 14 (2008) 5856–5863.
- G.J. Fetterly, R.M. Straubinger, Pharmacokinetics of paclitaxel-containing liposomes in rats, *AAPS PharmSci* 5 (2003).
- T.M. Allen, C. Hansen, Pharmacokinetics of health versus conventional liposomes—effect of dose, *BBA-Biomembr.* 1068 (1991) 133–141.
- F. Sampedro, J. Partika, P. Santalo, A.M. Molinspujol, J. Bonal, R. Perez-Soler, Liposomes as carriers of different new lipophilic antitumor drugs—a preliminary report, *J. Microencapsul.* 11 (1994) 309–318.
- A. Sharma, E. Mayhew, R.M. Straubinger, Antitumor effect of taxol-containing liposomes in a taxol-resistant murine tumor model, *Cancer Res.* 53 (1993) 5877–5881.
- M.F. Shieh, I.M. Chu, C.J. Lee, P. Kan, D.M. Hau, J.J. Shieh, Liposomal delivery system for taxol, *J. Ferment. Bioeng.* 83 (1997) 87–90.
- T. Yang, F.D. Cui, M.K. Choi, H.X. Lin, S.J. Chung, C.K. Shim, D.D. Kim, Liposome formulation of paclitaxel with enhanced solubility and stability, *Drug Deliv.* 14 (2007) 301–308.
- M. Heney, M. Alipour, D. Vergidis, A. Omri, C. Mugabe, J. Thang, Z. Sountres, Effectiveness of liposomal paclitaxel against MCF-7 breast cancer cells, *Can. J. Physiol. Pharmacol.* 88 (2010) 1172–1180.
- A. Sharma, E. Mayhew, I. Bolesak, C. Cavanaugh, P. Harmon, A. Janoff, R.J. Bernacki, Activity of paclitaxel liposome formulations against human ovarian tumor xenografts, *Int. J. Cancer* 71 (1997) 103–107.
- C. Holvoet, Y.V. Heyden, G. Lories, J. Paizier-Vercammen, Preparation and evaluation of paclitaxel-containing liposomes, *Pharmazie* 62 (2007) 126–132.
- J.A. Zhang, G. Anyambhadra, L. Ma, S. Ugoni, T. Xuan, T. Sardone, I. Ahmad, Development and characterization of a novel Cremophor (R) EL free liposome-based paclitaxel (LEP-ETU) formulation, *Eur. J. Pharm. Biopharm.* 59 (2005) 177–187.
- N.V. Koshkina, J.C. Waldrep, L.E. Roberts, E. Golunski, S. Melton, V. Knight, Paclitaxel liposome aerosol treatment induces inhibition of pulmonary metastases in murine renal carcinoma model, *Clin. Cancer Res.* 7 (2001) 3258–3262.
- D. Needham, R.S. Sarpal, Binding of paclitaxel to lipid interfaces: correlations with interface compliance, *J. Liposome Res.* 8 (1998) 147–163.
- S. Koudelka, J. Turánek-Knigova, J. Masek, Z. Korvasova, M. Skrabalova, J. Plockova, E. Bartheldyova, J. Turánek, Liposomes with high encapsulation capacity for paclitaxel: preparation, characterisation and in vivo anticancer effect, *J. Pharm. Sci.* 99 (2010) 2309–2319.
- M.C. Woodle, D.D. Lasic, Sterically stabilized liposomes, *BBA-Biomembr.* 1113 (1992) 171–199.
- P.S. Uster, T.M. Allen, B.E. Daniel, C.J. Mendez, M.S. Newman, G.Z. Zhu, Insertion of poly(ethylene glycol) derivatized phospholipid into pre-formed liposomes results in prolonged in vivo circulation time, *FEBS Lett.* 386 (1996) 243–246.
- R.K. Jain, Transport of molecules across tumor vasculature, *Cancer Metastasis Res.* 6 (1987) 559–593.
- H. Maeda, Y. Matsumura, Tumorotropic and lymphotropic principles of macromolecular drugs, *Crit. Rev. Ther. Drug Carrier Syst.* 6 (1989) 193–210.

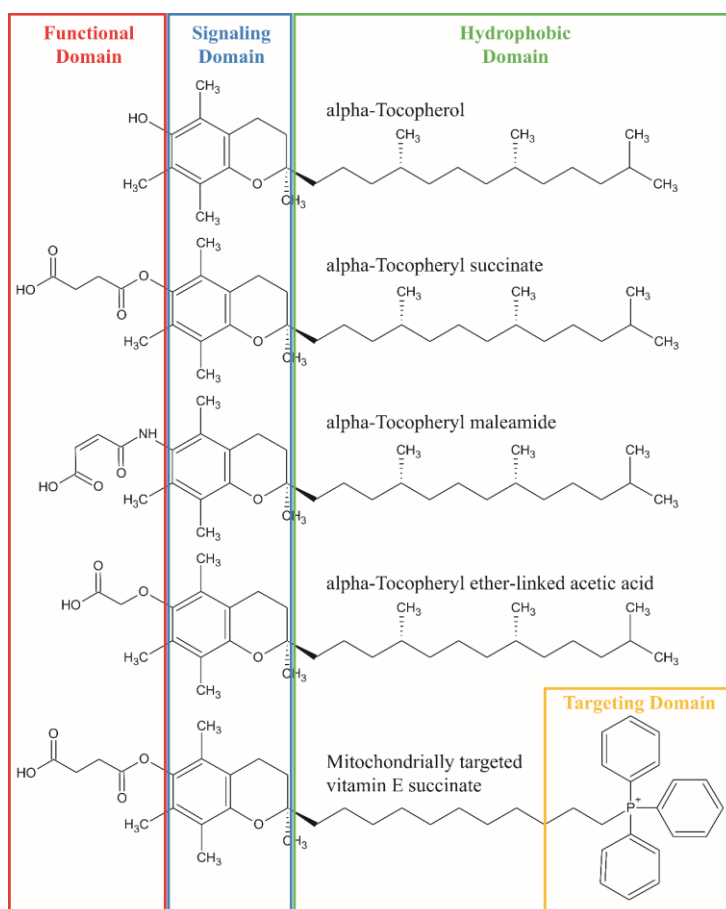
- [50] F. Yuan, M. Dellian, D. Fukumura, M. Leung, D.A. Berk, V.P. Torchilin, R.K. Jain, Vascular permeability in a human tumor xenograft – molecular-size dependence and cutoff size, *Cancer Res.* 55 (1995) 3752–3756.
- [51] M.J. Immordino, P. Brusa, S. Arpicco, B. Stella, F. Dosio, L. Gattell, Preparation, characterization, cytotoxicity and pharmacokinetics of liposomes containing docetaxel, *J. Control. Release* 91 (2003) 417–429.
- [52] P. Grossi, M. Ceppi, P. Brusa, S. Arpicco, F. Dosio, L. Gattell, Preparation, characterization and properties of sterically stabilized paclitaxel-containing liposomes, *J. Control. Release* 63 (2000) 19–30.
- [53] T. Yang, F.D. Cui, M.K. Choi, J.W. Cho, S.J. Chung, C.K. Shim, D.D. Kim, Enhanced solubility and stability of PEGylated liposomal paclitaxel: in vitro and in vivo evaluation, *Int. J. Pharm.* 338 (2007) 317–326.
- [54] P. Kan, C.W. Tsao, A.J. Wang, W.C. Su, H.F. Liang, A liposomal formulation able to incorporate a high content of paclitaxel and exert promising anticancer effect, *J. Drug Deliv.* (in press), <http://dx.doi.org/10.1155/2011/629234>.
- [55] Y. Yoshizawa, Y. Kono, K. Ogawara, T. Kimura, K. Higaki, PEG liposomalization of paclitaxel improved its in vivo disposition and anti-tumor efficacy, *Int. J. Pharm.* 412 (2011) 132–141.
- [56] Y. Huang, X.M. Chen, B.X. Zhao, X.Y. Ke, B.J. Zhao, X. Zhao, Y. Wang, X.A. Zhang, Q. Zhang, Antiangiogenic activity of sterically stabilized liposomes containing paclitaxel (SSL-PTX): in vitro and in vivo, *AAPS PharmSciTech* 11 (2010) 752–759.
- [57] S. Zalipsky, C.B. Hansen, D.E. deMenezes, T.M. Allen, Long-circulating polyethylene glycol-grafted immunoliposomes, *J. Control. Release* 39 (1996) 153–161.
- [58] P. Sapa, T.M. Allen, Ligand-targeted liposomal anticancer drugs, *Prog. Lipid Res.* 42 (2003) 439–462.
- [59] J. Wu, Q. Liu, R.J. Lee, A folate receptor-targeted liposomal formulation for paclitaxel, *Int. J. Pharm.* 316 (2006) 148–153.
- [60] T. Yang, M.K. Choi, F.D. Cui, J.S. Kim, S.J. Chung, C.K. Shim, D.D. Kim, Preparation and evaluation of paclitaxel-loaded PEGylated immunoliposome, *J. Control. Release* 120 (2007) 169–177.
- [61] T. Yang, M.K. Choi, F.D. Cui, S.J. Lee, S.J. Chung, C.K. Shim, D.D. Kim, Antitumor effect of paclitaxel-loaded PEGylated immunoliposomes against human breast cancer cells, *Pharm. Res.* 24 (2007) 2402–2411.
- [62] S.Y. Meng, B. Su, W. Li, Y.M. Ding, L.A. Tang, W. Zhou, Y. Song, H.Y. Li, C.C. Zhou, Enhanced antitumor effect of novel dual-targeted paclitaxel liposomes, *Nanotechnology* 21 (2010).
- [63] S.Y. Meng, B. Su, W. Li, Y.M. Ding, L.A. Tang, W. Zhou, Y. Song, C.C. Zhou, Integrin-targeted paclitaxel nanoliposomes for tumor therapy, *Med. Oncol.* 28 (2011) 1180–1187.
- [64] H. Zhao, J.C. Wang, Q.S. Sun, C.J. Luo, Q. Zhang, RGD-based strategies for improving antitumor activity of paclitaxel-loaded liposomes in nude mice xenografted with human ovarian cancer, *J. Drug Target.* 17 (2009) 10–18.
- [65] T. Terada, M. Mizobata, S. Kawakami, E. Yamashita, M. Hashida, Optimization of tumor-selective targeting by basic fibroblast growth factor-binding peptide grafted PEGylated liposomes, *J. Control. Release* 119 (2007) 262–270.
- [66] X.H. Wang, L.Y. Deng, X.A. Chen, H.Y. Pei, L.L. Gai, X. Zhao, Y.Q. Wei, L.J. Chen, Truncated BFGF-mediated cationic liposomal paclitaxel for tumor-targeted drug delivery: improved pharmacokinetics and biodistribution in tumor-bearing mice, *J. Pharm. Sci.* 100 (2011) 1196–1205.
- [67] P.Q. Zhao, H.J. Wang, M. Yu, S.Z. Cao, F. Zhang, J. Chang, R.F. Niu, Paclitaxel-loaded, folic acid-targeted and TAT-peptide-conjugated polymeric liposomes: in vitro and in vivo evaluation, *Pharm. Res.* 27 (2010) 1914–1926.
- [68] R.F. Niu, P.Q. Zhao, Y.J. Yuan, S.Z. Cao, F. Zhang, J. Chang, Preparation, characterization, and antitumor activity of paclitaxel-loaded folic acid modified and TAT peptide conjugated PEGylated polymeric liposomes, *J. Drug Target.* 19 (2011) 373–381.
- [69] D. Peer, R. Margalit, Tumor-targeted hyaluronan nanoliposomes increase the antitumor activity of liposomal doxorubicin in syngeneic and human xenograft mouse tumor models, *Neoplasia* 6 (2004) 343–353.
- [70] V.M. Platt, P.C. Szoka, Anticancer therapeutics: targeting macromolecules and nanocarriers to hyaluronan or CD44, a hyaluronan receptor, *Mol. Pharm.* 5 (2008) 474–486.
- [71] N. Yerushalmi, R. Margalit, Hyaluronic acid-modified bioadhesive liposomes as local drug depots: effects of cellular and fluid dynamics on liposome retention at target sites, *Arch. Biochem. Biophys.* 349 (1998) 21–26.
- [72] A. Bartolazzi, R. Peach, A. Aruffa, I. Stamenkovic, Interaction between CD44 and hyaluronate is directly implicated in the regulation of tumor-development, *J. Exp. Med.* 180 (1994) 53–66.
- [73] M.B. Penno, J.T. August, S.B. Baylin, M. Mabry, R.I. Limmoila, V.S. Lee, D. Grotteau, X.L. Yang, C. Rosada, Expression of CD44 in human lung tumor, *Cancer Res.* 54 (1994) 1381–1387.
- [74] I. Rivkin, K. Cohen, J. Koffler, D. Melikhov, D. Peer, R. Margalit, Paclitaxel-clusters coated with hyaluronan as selective tumor-targeted nanovectors, *Biomaterials* 31 (2010) 7106–7114.
- [75] T. Boehm, J. Folkman, T. Browder, M.S. O'Reilly, Antiangiogenic therapy of experimental cancer does not induce acquired drug resistance, *Nature* 390 (1997) 404–407.
- [76] J. Denekamp, Endothelial cell-proliferation as a novel approach to targeting tumor therapy, *Br. J. Cancer* 45 (1982) 136–139.
- [77] J. Denekamp, The tumour microcirculation as a target in cancer therapy: a clearer perspective, *Eur. J. Clin. Invest.* 29 (1999) 733–736.
- [78] G. Thurston, J.W. McLean, M. Rizen, P. Baluk, A. Haskell, T.J. Murphy, D. Hanahan, D.M. McDonald, Cationic liposomes target angiogenic endothelial cells in tumors and chronic inflammation in mice, *J. Clin. Invest.* 101 (1998) 1401–1413.
- [79] M. Schmitt-Sody, S. Strieth, S. Krasnici, B. Sauer, B. Schulze, M. Teifel, U. Michaelis, K. Naujoks, M. Dellian, Neovascular targeting therapy: Paclitaxel encapsulated in cationic liposomes improves antitumoral efficacy, *Clin. Cancer Res.* 9 (2003) 2335–2341.
- [80] R. Kunstfeld, G. Wickelmaier, U. Michaelis, M. Teifel, W. Uemek, K. Naujoks, K. Wolff, P. Petzelbauer, Paclitaxel encapsulated in cationic liposomes diminishes tumor angiogenesis and melanoma growth in a “humanized” SCID mouse model, *J. Invest. Dermatol.* 120 (2003) 476–482.
- [81] S. Strieth, M.E. Eichhorn, B. Sauer, B. Schulze, M. Teifel, U. Michaelis, M. Dellian, Neovascular targeting chemotherapy: encapsulation of paclitaxel in cationic liposomes impairs functional tumor microvasculature, *Int. J. Cancer* 110 (2004) 117–124.
- [82] C. Bode, L. Trojan, C. Weiss, B. Kraenzlin, U. Michaelis, M. Teifel, P. Alken, M.S. Michel, Paclitaxel encapsulated in cationic liposomes: a new option for neovascular targeting for the treatment of prostate cancer, *Oncol. Rep.* 22 (2009) 321–326.
- [83] D. Sharma, T.P. Chelvi, R. Rahman, Thermoresponsive liposomal taxol formulation: heat-mediated targeted drug delivery in murine melanoma, *Melanoma Res.* 8 (1998) 240–244.
- [84] S.F. Nie, W.L.W. Hsiao, W.S. Pan, Z.J. Yang, Thermoresponsive pluronic (R) F127-based hydrogel containing liposomes for the controlled delivery of paclitaxel: in vitro drug release, cell cytotoxicity, and uptake studies, *Int. J. Nanomedicine* 6 (2011) 151–166.
- [85] J.Q. Zhang, Z.R. Zhang, H. Yang, Q.Y. Tan, S.R. Qin, X.L. Qiu, Jytoplasmic paclitaxel magnetoliposomes as a potential drug delivery system for breast carcinoma via parenteral administration: In vitro and in vivo studies, *Pharm. Res.* 22 (2005) 573–583.
- [86] M.J. Kim, D.H. Jang, Y.I. Lee, H.S. Jung, H.J. Lee, Y.H. Cho, Preparation, characterization, cytotoxicity and drug release behavior of liposome-encapsulated paclitaxel/Fe₃O₄ nanoparticles, *J. Nanosci. Nanotechnol.* 11 (2011) 889–893.
- [87] A. Cabanes, K.E. Briggs, P.C. Gokhale, J.A. Treat, A. Rahman, Comparative in vivo studies with paclitaxel and liposome-encapsulated paclitaxel, *Int. J. Oncol.* 12 (1998) 1035–1040.
- [88] A. Sharma, R.M. Straubinger, I. Ojima, R.J. Bernacki, Antitumor efficacy of taxane liposomes on a human ovarian tumor xenograft in nude athymic mice, *J. Pharm. Sci.* 84 (1995) 1400–1404.
- [89] M.H. Bartoli, M. Boitard, H. Fessi, H. Briel, J.P. Devissaguet, F. Picot, F. Pussieux, In vitro and in vivo antitumoral activity of free, and encapsulated taxol, *J. Microencapsul.* 7 (1990) 191–197.
- [90] A. Sharma, U.S. Sharma, R.M. Straubinger, Paclitaxel-liposomes for intracavitary therapy of intraperitoneal P388 leukemia, *Cancer Lett.* 107 (1996) 265–272.
- [91] A. Sharma, R.M. Straubinger, Novel taxol formulations – preparation and characterization of taxol-containing liposomes, *Pharm. Res.* 11 (1994) 889–896.
- [92] R.M. Straubinger, A. Sharma, M. Murray, E. Mayhew, Novel taxol formulations: taxol-containing liposomes, *J. Natl. Cancer Inst. Monogr.* 15 (1993) 69–78.
- [93] A.R. Scialli, J.M. Desesso, A. Rahman, S.R. Hursain, G.C. Goering, Embryotoxicity of free and liposome-encapsulated taxol in the chick, *Pharmacology* 51 (1995) 145–151.
- [94] A.R. Scialli, T.B. Waterhouse, J.M. Desesso, A. Rahman, G.C. Goering, Protective effect of liposome encapsulation on paclitaxel developmental toxicity in the rat, *Teratology* 56 (1997) 305–310.
- [95] O. Soepenberg, A. Sparreboom, M.J.A. de Jonge, A.S.T. Planting, G. de Heus, W.J. Loos, C.M. Hartman, C. Bowden, J. Verweij, Real-time pharmacokinetics guiding clinical decisions: phase I study of a weekly schedule of liposome with solid encapsulated paclitaxel in patients tumours, *Eur. J. Cancer* 40 (2004) 681–688.
- [96] N. Damjanov, M.N. Fishman, J.L. Steinberg, G.J. Fetterly, A. Haas, A. Gahrn, C. Lauay, J.L. Dul, J.W. Sherman, E.H. Rubin, Final results of a phase I study of liposome entrapped paclitaxel (LEP-ETU) in patients with advanced cancer, *J. Clin. Oncol.* 23 (2005) 147.
- [97] M.N. Fishman, Y. Elsayed, N. Damjanov, J.L. Steinberg, J.J. Mahany, J.A. Nieves, S.P. Wanaski, J.L. Dul, J.W. Sherman, Phase I study of liposome entrapped paclitaxel (LEP-ETU) in patients with advanced cancer, *J. Clin. Oncol.* 22 (2004) 154.
- [98] M.N. Fishman, Y.A. Elsayed, N. Damjanov, J.L. Steinberg, J.J. Mahany, J.A. Nieves, S.P. Wanaski, J.L. Dul, J.W. Sherman, Safety and tolerability of liposome entrapped paclitaxel (LEP-ETU) administered with and without premedication in patients with advanced cancer, *Ann. Oncol.* 15 (2004) 108.
- [99] A.R. Tan, A.R. Hanauske, H. Gelderblom, M.E. Scheulen, L.J. Van Warmerdam, H. Rosing, G.J. Fetterly, V.S. Shu, J.W. Sherman, E.H. Rubin, Results of a clinical pharmacokinetic (PK) bioequivalence (BE) study of liposomal paclitaxel (LEP-ETU) versus paclitaxel (T) in patients with advanced cancer, *J. Clin. Oncol.* 24 (2006) 83.
- [100] NeoPharm presents the phase II data of liposome-entrapped paclitaxel (LEP) in patients with metastatic breast cancer, http://www.drugs.com/clinical_trials/neo-pharm-presents-phase-ii-data-liposome-entrapped-paclitaxel-lep-patients-metastatic-breast-cancer-8758.html [24-3-2012].
- [101] S. Strieth, C.F. Nussbaum, M.E. Eichhorn, M. Fuhrmann, M. Teifel, U. Michaelis, A. Berghaus, M. Dellian, Tumor-selective vessel occlusions by platelets after vascular targeting chemotherapy using paclitaxel encapsulated in cationic liposomes, *Int. J. Cancer* 122 (2008) 452–460.
- [102] M. Christopeit, G. Lenz, R. Forspointner, K. Bartelheim, R. Kuhnbad, K. Naujoks, A. Schallhorn, Nine months to progression using four-th line liposomally encapsulated paclitaxel against hepatocellular carcinoma, *Chemotherapy* 54 (2008) 309–314.
- [103] U. Fasol, A. Frost, M. Buchert, J. Arends, U. Fiedler, D. Schan, J. Scheuempflug, K. Mross, Vascular and pharmacokinetic effects of EndoTAG-1 in patients with advanced cancer and liver metastasis, *Ann. Oncol.* 23 (2012) 1030–1036.

- [104] Q. Zhang, X.E. Huang, L.L. Gao, A clinical study on the premedication of paclitaxel liposome in the treatment of solid tumors, *Biomed. Pharmacother.* 63 (2009) 603–607.
- [105] X.H. Wang, J.C. Zhou, Y.S. Wang, Z.Y. Zhu, Y. Lu, Y.Q. Wei, L.J. Chen, A phase I clinical and pharmacokinetic study of paclitaxel liposome infused in non-small cell lung cancer patients with malignant pleural effusions, *Eur. J. Cancer* 46 (2010) 1474–1480.
- [106] X.H. Wang, H. Zheng, Z.Y. Zhu, Y.Q. Wei, L.J. Chen, Clinical pharmacokinetics of paclitaxel liposome with a new route of administration in human based on the analysis with ultra performance liquid chromatography, *J. Pharm. Sci.* 99 (2010) 4746–4752.
- [107] FDA approval for nanoparticle paclitaxel, [http://www.cancer.gov/cancertopics/druginfo/ila-nanoparticle-paclitaxel\(24-3-2012\)](http://www.cancer.gov/cancertopics/druginfo/ila-nanoparticle-paclitaxel(24-3-2012)).
- [108] K. Garber, Improved paclitaxel formulation hints at new chemotherapy approach, *J. Natl. Cancer Inst.* 96 (2004) 90–91.
- [109] W.J. Gradishar, S. Tjulandit, N. Davidson, H. Shaw, N. Desai, P. Bhar, M. Hawkins, J. O'Shaughnessy, Phase III trial of nanoparticle albumin-bound paclitaxel compared with polyethylated castor oil-based paclitaxel in women with breast cancer, *J. Clin. Oncol.* 23 (2005) 7794–7803.

2.2.3. Deriváty vitamínu E s protinádorovým účinkem

α -Tokoferyl sukcinát (α -TOS) je semisyntetickým analogem vitamínu E s poměrně selektivním účinkem na nádorové buňky a protinádorovým účinkem *in vivo*. Byla syntetizována řada jeho analog, které se vyznačují resistencí vůči esterázám, neboť obsahují těžce štěpitelné eterové nebo amidové vazby. α -Tokoferyl maleamid (α -TAM) představuje jedenu z těchto nových látek a vyznačuje se řádově vyšší cytotoxicitou *in vitro* a protinádorovým účinkem *in vivo* na myších nádorových modelech.

Závažným omezením použití těchto látek pro léčbu nádorů je jejich nízká rozpustnost ve vodných roztocích. Jejich hydrofobní charakter tedy předurčuje lékovou formulaci. Experimentální formulace pro podání *i.v.*, nebo *i.p.* způsobem (solubilizace v roztoku etanolu, DMSO nebo olejových emulzích) jsou přípustné pro studium protinádorového účinku na myších modelech, avšak jsou zcela nevhodné pro humánní intravenózní aplikace. Vesikulární formy nebo různé micelární formy s využitím vhodných surfaktantů (např. polyetylen glykol) byly připraveny a testovány na myších jako případné vhodné formulace pro využití v humánní medicíně.

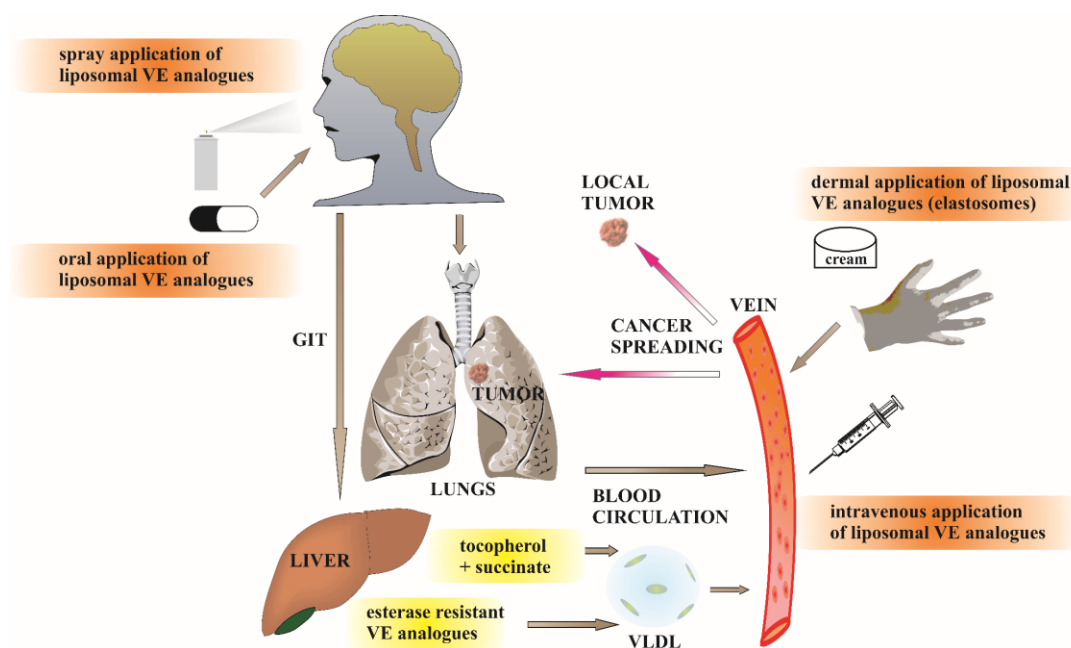


Obr. 22 Strukturální vzorce některých derivátů vitamínu E s protinádorovým účinkem.

Zejména příprava vesikulárních struktur metodou spontánní vesikulace se jeví jako vhodnou metodou pro přípravu lékové formy. Problémy u tohoto přístupu vyvstávají s dlouhodobou stabilitou preparátů a toxicitou některých derivátů po *i.v.* aplikaci (např. α -tokoferyloxalát). Tato toxicita může souviset s extrémně vysokým záporným povrchovým nábojem těchto částic a jejich nestabilitou v krvi. Zřejmě může docházet k aktivaci komplementu, tvorbě mikroembolií a dalším nežádoucím jevům.

I v případě derivátů tokoferolu se ukázalo, že použití liposomů je vhodnou alternativou pro vývoj bezpečné lékové formy, která splňuje i další kritéria kladená na farmaceutický preparát pro *i.v.* aplikaci.

V této oblasti se nám podařilo vyvinout technologii přípravy stabilního liposomálního preparátu α -TOS a α -TAM. Liposomální preparáty obou látek byly také testovány s výborným výsledkem na myších nádorových modelech. Podařilo se zachovat výrazný protinádorový účinek a zcela eliminovat nežádoucí účinky, které byly zjištěny u předchozích formulací α -TAM. Liposomální forma především eliminovala imunotoxický účinek (zejména na kostní dřeň) čímž se otvírá možnost využít tyto látky pro kombinovanou imuno- a chemo-terapii nádorů. Praktická aplikace ve veterinární medicíně je směřována k léčbě nádorů mléčné žlázy u fen. První terapeutické aplikace byly zaměřeny na intratumorové podání. Výsledky na dvou fenách prokázaly destrukci cévního zásobování nádoru, stagnaci růstu a ohraničení nádoru. Průběh terapie byl podobný situaci na myším modelu spontánních nádorů mléčné žlázy. Jednoznačné ohraničení nádoru po aplikaci liposomálních derivátů vit E efekty umožnilo jeho snadné chirurgické odstranění. Kombinace derivátů vit E s molekulárními adjuvans otevírá cestu k imunoterapii nádorů s využitím intratumorové aplikace. Liposomy zde sehrávají roli nosiče tvořícího depot terapeutik. Masivní apoptóza nádorových buněk a uvolnění nádorových antigenů v přítomnosti molekulárního adjuvans je předpokladem pro navození protinádorové imunity, která eliminuje metastatická ložiska, nedostupná chirurgickému odstranění nebo intratumorové aplikaci terapeutika. Intratumorová aplikace (přímá injekce do nádoru, transdermální přenos do podkožních nádorů pomocí dermatologických krémů) umožňuje dosáhnout vysokých koncentrací chemoterapeutika v nádoru a přitom eliminovat dosažení toxických dávek v ostatních orgánech. Terapii můžeme vymezit pojmem „chemoterapií indukovaná protinádorová imunita“. Celkový přehled je na obrázku 22.



Obr. 23 Způsob podání liposomálních analog vitamínu E

Zacílení nádorové tkáně může být dosaženo různými způsoby podání léčiva. Orální aplikace pomocí kapsulí naplněných liposomy s enkapsulovanými protinádorovými deriváty vitamínu E představuje nejjednodušší způsob podání. Orální aplikace však vyžaduje použití látek s resistantní vůči hydrolytickým enzymům v trávicím traktu (éterové nebo amidové vazby spojující dikarboxylovou kyselinu s tokoferolem). Transdermální lokální aplikace je vhodná pro léčbu kožních nádorů nebo nádorů lokalizovaných v podkoží. Elastické liposomy (elastic liposomec, transferosomes, elastosomes) jsou vhodné pro tento způsob aplikace, neboť umožňují akcelarovat přechod účinné látky přes bariéru tvořenou *stratum corneum*. Využití sprejové formy liposomálních derivátů vitamínu E je vhodné pro přímé cílení plicních nádorů a pro přenos účinných látek do oběhového systému. Obejití hepatopankreatického okruhu je další výhodou tohoto způsobu aplikace při případném cílení protinádorových chemoterapeutik do mozku. Po parenterální aplikaci (i.v.) mohou liposomální deriváty vitamínu E vstoupit do různých transportních drah. Tyto dráhy a biodistribuce účinné látky jsou podmíněny faktory jako například typem liposomů (stérická stabilizace), morfologie (velikost a lamelarita) a lipidní kopozicí (stability, povrchový náboj). Liposomy mohou penetrovat skrz fenestrace v endoteliálních buňkách nádorové vaskulatury a kumulovat se v nádoru, kde jsou postupně uvolňovány v blízkosti nádorových buněk a endoteliálních buněk nádorové vaskulatury. Zejména destrukce nádorové vaskulatury vede k potlačení růstu nádoru a jeho zániku. (Adaptováno z naší práce *Journal of Controlled Release.*, 2015 Volume: 207 Pages: 59-69)

2.2.3.1 Publikace k tématu kapitoly

Journal of Controlled Release 207 (2015) 59–69



Contents lists available at ScienceDirect

Journal of Controlled Release

journal homepage: www.elsevier.com/locate/jconrel



Review

Liposomal delivery systems for anti-cancer analogues of vitamin E



Stepan Koudelka^{a,b,*}, Pavlina Turanek Knotigova^a, Josef Masek^a, Lubomir Prochazka^a, Robert Lukac^a, Andrew D. Miller^c, Jiri Neuzil^{d,e}, Jaroslav Turanek^{a,*}

^a Department of Pharmacology and Immunotherapy, Veterinary Research Institute, Brno, Czech Republic

^b International Clinical Research Center, St. Anne's University Hospital Brno, Brno, Czech Republic

^c Institute of Pharmaceutical Science, King's College London, London, United Kingdom

^d School of Medical Science, Griffith University, Southport, Qld, Australia

^e Institute of Biotechnology, Academy of Sciences of the Czech Republic, Prague, Czech Republic

ARTICLE INFO

Article history:

Received 14 January 2015
Received in revised form 3 April 2015
Accepted 5 April 2015
Available online 7 April 2015

Keywords:

Alpha-tocopheryl succinate
Analogues of vitamin E
Anti-cancer drugs
Apoptosis
Drug delivery systems
Drug targeting
Liposome
Nanomedicine

ABSTRACT

Pro-apoptotic analogues of vitamin E (VE) exert selective anti-cancer effect on various animal cancer models. Neither suitable formulation of α -tocopheryl succinate (α -TOS), representative semi-synthetic VE analogue ester, nor suitable formulations of the other VE analogues for clinical application have been reported yet. The major factor limiting the use of VE analogues is their low solubility in aqueous solvents. Due to the hydrophobic character of VE analogues, liposomes are predetermined as suitable delivery system. Liposomal formulation prevents undesirable side effects of the drug, enhances the drug biocompatibility, and improves the drug therapeutic index. Liposomal formulations of VE analogues especially of α -TOS and α -tocopheryl ether linked acetic acid (α -TEA) have been developed. The anti-cancer effect of these liposomal VE analogues has been successfully demonstrated in pre-clinical models in vivo. Present achievements in: (i) preparation of liposomal formulations of VE analogues, (ii) physico-chemical characterization of these developed systems and (iii) testing of their biological activity such as induction of apoptosis and evaluation of anti-cancer effect are discussed in this review.

© 2015 Elsevier B.V. All rights reserved.

Contents

1. Introduction	60
2. Alpha-tocopheryl succinate and vitamin E analogues	60
2.1. Biological activity of alpha-tocopheryl succinate	60
2.1.1. Apoptogenic activity of alpha-tocopheryl succinate and other vitamin E analogues	60
2.2. Resistance and alpha-tocopheryl succinate	61
2.3. Physico-chemical properties of alpha-tocopheryl succinate	62
3. Solubilization and delivery systems for alpha-tocopheryl succinate	62
4. Liposomal delivery systems for vitamin E analogues	62
4.1. Interaction of VE analogues with liposomal bilayers	63
4.2. Liposomal formulations of vitamin E analogues	64
4.2.1. Vitamin E analogues entrapped in conventional liposomes	64
4.2.2. Vitamin E analogues entrapped in pH-sensitive liposomes	65
4.2.3. Vitamin E analogues entrapped in liposomes for aerosol delivery	65
4.3. Administration routes for delivery of liposomal vitamin E analogues	66

Abbreviations: ABC, ATP binding cassette; DCs, dendritic cells; DMSO, dimethyl sulfoxide; DIPC, dilauryl phosphatidylcholine; DOPE, dioleoyl phosphatidylethanolamine; EPC, egg phosphatidylcholine; EPR, enhanced permeability and retention; ETP, etoposide; FBS, fetal bovine serum; FDA, Food and Drug Administration; GFP, green fluorescent protein; GIT, gastro-intestinal tract; GTH, glutathione; HSPC, hydrogenated soy phosphatidylcholine; IC₅₀, the half inhibitory concentration; Im, intramuscular; INF- γ , interferon-gamma i.p., intraperitoneal; i.t., intratumoral; i.v., intravenous; mitoVES, mitochondrially-targeted vitamin E succinate; MLVs, multilamellar vesicles; MRP1, multidrug resistance protein 1; PC, phosphatidylcholine; PE, phosphatidylethanolamine; PE-PEG, phosphatidylethanolamine-polyethylene glycol; PEG, polyethylene glycol; PL, phospholipid; PSVs, pH-sensitive vesicles; RES, reticulo-endothelial system; s.c., subcutaneous; SPC, soy phosphatidylcholine; SLNs, small unilamellar vesicles; α -TAM, α -tocopheryl maleamide; α -TEA, α -tocopheryl ether linked acetic acid; α -TGA, α -tocopheryl acetate; α -TOG, α -tocopheryl glucopyranoside; α -TOH, α -tocopherol; α -TOM, α -tocopheryl maleate; α -TOS, α -tocopheryl succinate; α -TPGS, α -tocopheryl polyethylene glycol succinate; TPP, triphenyl phosphonium; VE, vitamin E; VES, vitamin E succinate; VLDL, very low density lipoprotein.

* Corresponding authors at: Department of Pharmacology and Immunotherapy, Veterinary Research Institute, Hudcova 70, 621 00 Brno, Czech Republic.

E-mail addresses: koudelka@vri.cz (S. Koudelka), uranek@vri.cz (J. Turanek).

<http://dx.doi.org/10.1016/j.jconrel.2015.04.003>
0168-3659/© 2015 Elsevier B.V. All rights reserved.

5. Cancer immunotherapy and alpha-tocopheryl succinate	67
6. Conclusion	67
Acknowledgments	67
References	67

1. Introduction

Vitamin E (VE) is a generic term used for a lipid-soluble group of the related compounds of tocopherols and tocotrienols. Their molecules share common structure composed of chromanol head and phytyl tail. Owing to its character, VE tends to associate with hydrophobic domains of various structures like biomembranes and proteins. A major biological function of VE is to protect polyunsaturated lipids of membranes against oxidation [1]. It has been reported that products of phospholipid (PL) hydrolysis such as lysoPLs together with VE form complexes. The formed complexes tend to stabilize PL bilayers and prevent membrane disintegration by detergent-like actions of lysoPLs [2]. The isomers of biological importance are tocopherols of which α -tocopherol (α -TOH) is the most potent vitamin. α -Tocopheryl succinate (α -TOS) is a semi-synthetic prototype of α -TOH representing the most developed VE analogue. α -TOS is extensively studied as the model agent used in various biological and physico-chemical experiments.

Pro-apoptotic VE analogues were found to induce cell apoptosis and demonstrated anti-proliferative activity in vitro [3–5]. It has been reported that pro-apoptotic VE analogues exert selective toxicity towards the cancer cells with low toxicity to the non-cancer cells [6–9]. Recent studies documented the cytotoxic effects of α -TOS in various experimental models against broad spectrum of cancer including breast, lung, prostate and colon cancer as well as mesothelioma, neuroblastoma and melanoma [10–16]. Higher selectivity of α -TOS toxicity to various cancer cells in vitro and the more effective prevention of tumor growth prolonging survival in vivo contribute to attractive employment of α -TOS as novel type of anti-cancer agent.

It has been also reviewed that VE analogues could be applicable for the delivery of other anti-cancer drugs. α -Tocopheryl polyethylene glycol succinate (α -TPGS), α -TOS and α -TOH were used as solubilization excipients, prodrug conjugates or carriers for paclitaxel, topotecan, doxorubicin and docetaxel delivery [17].

2. Alpha-tocopheryl succinate and vitamin E analogues

The structural molecule of α -TOH and its analogues can be divided into several functionally different domains. Each domain is responsible for individual function of particular VE analogue [18] (Fig. 1).

2.1. Biological activity of alpha-tocopheryl succinate

The biological activity of α -TOS is encountered with pro-vitamin/vitamin effect. After entering the bloodstream, α -TOS is associated with lipoproteins and transported into tumor microvasculature [19]. In the tumor, α -TOS exerts pro-apoptotic activity resulting in tumor growth inhibition. Lipoproteins carrying α -TOS are also cleared during passage through the liver where α -TOS is hydrolyzed by competent esterases. The cleavage product, α -TOH, is partially excreted in bile and partially shuttled into nascent lipoproteins. The nascent lipoproteins enriched with α -TOH are then re-secreted into the bloodstream. The system with additional α -TOH promotes anti-inflammatory and anti-oxidant defenses [20,21].

The anti-oxidant activity of α -TOH is eliminated by esterification with succinic acid. The presence of succinate group endows α -TOS with apoptogenic activity. The lack or low activity of specific esterases essential for hydrolysis of α -TOS in cancer cells results in inhibition of cell proliferation. α -TOS induces the release and relocation of

pro-apoptotic signals yielding mitochondrial destabilization and dysfunction leading to programmed cell death [22,23]. On the contrary, esterase activity was observed in non-cancer cells [24]. Agents bearing esteric bond are specific for cancer cells, while non-cancer cells become relatively intact. Over 60 compounds analogous to α -TOS have been synthesized. These analogues were tested for induction of apoptosis in various cancer cells to find the more efficient pro-apoptotic drugs. Some of the novel VE analogues exhibited IC_{50} in low micromolar range. The serious problem encountered when the apoptogenic activity was maximized by structure modification resulted in the loss of selectivity for cancer cells in vitro or cancer tissue in pre-clinical models [25]. For example, the highly apoptogenic α -tocopheryl oxalate was toxic to immuno-compromised mice and α -tocopheryl maleamide (α -TAM) was toxic to non-cancer cells in vitro [26,27].

2.1.1. Apoptogenic activity of alpha-tocopheryl succinate and other vitamin E analogues

It has been reported that α -TOS induces significant apoptotic activity in about 50 cancer cell lines [8]. For B16 murine melanoma, about 50% growth inhibition without any cell death for 9.4 μ M of α -TOS was observed, while almost 100% lethality was caused by 18.8 μ M of α -TOS [28]. Apoptogenic activity of free and vesiculated α -TOS was tested on murine Lewis lung 3LL cells. The IC_{50} of 34 and 56 μ M was determined for vesiculated and free α -TOS, respectively. Cells exposed to vesiculated α -TOS underwent apoptosis earlier probably due to enhanced interaction of cancer cells with particles formed by α -TOS vesiculation [14]. α -Tocopheryl maleate ester (α -TOM) was found to exhibit far more efficient apoptogenic activity than its α -TOS counterpart in vitro [29]. A novel class of VE amide analogues with amide bond linking the functional domain to the chromanol head was synthesized. Owing to the non-hydrolysable amide bond, α -tocopheryl amides were more efficient in apoptosis induction than the corresponding α -tocopheryl esters [30]. For example, observed IC_{50} for Jurkat T lymphoma cells was 2 μ M for α -TAM, while for α -TOM it was 10-fold higher [31]. In vitro cytotoxic effect of VE analogues on various cancer cells followed the order of α -TAM > α -TOM > α -TOS \gg α -TOH. For human Meso-2 mesothelioma, human breast MCF-7 carcinoma and B16F10 murine melanoma, the corresponding IC_{50} were found to be 2, 5 and 13 μ M for α -TAM, 22, 27 and 35 μ M for α -TOM, and 43, 61 and 64 μ M for α -TOS, respectively. Any cytotoxicity for the redox-active α -TOH was not observed [27,31]. Replacement of hydroxyl group by acetate group generates α -tocopheryl acetate (α -TOA) analogue. However, any apoptogenic activity for α -TOA was not observed as well [5]. α -Tocopheryl ether-linked acetic acid (α -TEA) represents synthetic VE analogue with non-hydrolysable acetic acid moiety attached to the chromanol head by ether linkage. Like α -TOS, α -TEA is capable to induce apoptosis in various human cancer including breast, cervical, ovarian, prostate, colon and lung cells. For ovarian cancer cells, the IC_{50} of 5–20 μ M was determined [32]. Mitochondrially-targeted VE succinate (mitoVES) represents mitochondrially-targeted version of VES with cytotoxic activity enhancing the selectivity for cancer cells as well as the efficacy to reduce tumors in pre-clinical models. MitoVES was synthesized by its tagging with the delocalized cationic group triphenyl phosphonium (TPP), as pioneered for redox-active substances [33]. MitoVES was found 40-fold more apoptogenic efficient than α -TOS un-targeted. The corresponding IC_{50} of 0.5 and 20 μ M in Jurkat T lymphoma cells was assessed for mitoVES and α -TOS, respectively [34].

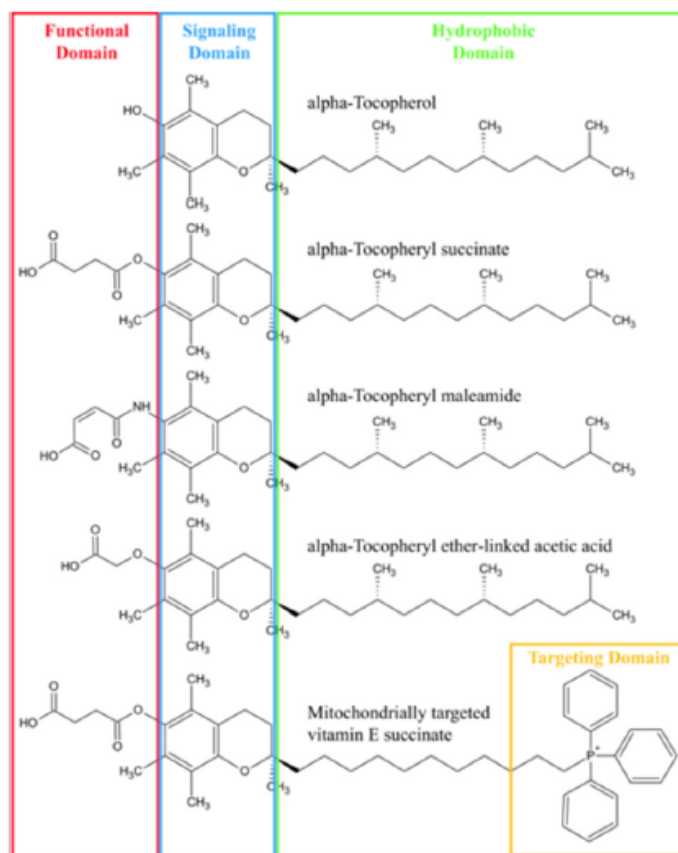


Fig. 1. Chemical structures of VE analogues with their domains in the molecule. Functional domain is responsible for redox activity of α -TOH, while for VE analogue esters, amides or ethers it endows the compound with apoptogenic activity. Signaling domain is involved in the regulation of certain apoptotic signaling pathways. Hydrophobic domain mediates docking of the compound in biological membranes or lipoproteins. Targeting domain is represented by triphenyl phosphonium (TPP) attached to α -TOS molecule enhancing mitochondrial accumulation of mitoVES.

2.2. Resistance and α -tocopheryl succinate

Long-term administration of α -TOS to cancer cells induces their resistance to α -TOS as well as cross-resistance to other VE analogues such as α -TEA or α -TAM via up-regulation of ATP-binding cassette A1 (ABCA1) [35]. ABCA1 represents one of the members of the ABC transporter superfamily. Altered accumulation or bioavailability of pro-apoptotic VE analogues inside cancer cells is one of the major mechanisms involved in their resistance. It is the balance between active uptake and active efflux mediated by TAP and SCARB1, ABCA1 transporters determining the susceptibility of lung and prostate cancer cells to α -TOS [11,36]. It was previously shown that mitochondrial targeting of α -TOS overcomes transporter mediated chemo-resistance and also reduces tumors that were resistant to α -TOS [35].

Multidrug resistance protein 1 (MRP1) is another member of ABC superfamily transporters that is involved in chemo-resistance in cancer patients. MRP1 acts as efflux pump and transports broad range of organic anions and neutral drugs conjugated to anions such as glutathione

(GTH) [37]. Agents capable to decrease the intracellular GTH level may alleviate MRP1-related chemo-resistance in glioblastomas by reducing its availability for generating drug-GTH conjugates in MRP1-overexpressing cells. Overexpression of MRP1 was frequently observed in human glioblastoma cells (e.g., T98G). It has been found that exposition of T98G cells to α -TOS reduced intracellular GTH concentration, modulated MRP1 activity and improved accumulation of etoposide (ETP), a MRP1 substrate drug [38]. The cytotoxic effect of ETP in T98G cells was improved by pre-incubation with 60 μ M α -TOS for 72 h. For these cells, α -TOS decreased the IC_{50} of ETP from 31.6 to 6.3 μ M. This improvement was not observed in human glioblastoma cells that do not express MRP1. Anti-cancer drugs formulated in liposomes could be used to enhance accumulation of drugs in the brain after systemic accumulation [39]. Liposomal ETP and α -TOS could be a feasible approach to reduce chemo-resistance via α -TOS effect to reduce GTH concentration and improve ETP accumulation. Liposomes containing α -TOS and ETP were developed. In vitro treatment of T98G cells by liposomal ETP and α -TOS showed superior

synergistic cytotoxicity in comparison to liposomal ETP. The cytotoxic effect of liposomal ETP was similar to free ETP. Liposomal α -TOS did not affect cell proliferation except at the highest doses used [38].

2.3. Physico-chemical properties of α -tocopheryl succinate

Structural modification of α -TOH with succinyl moiety results in the amphiphilic character of α -TOS. Incorporation of α -TOS within the PL vesicles increases surface charge because the terminal carboxylic group of α -TOS is ionized at physiological pH [40]. The terminal group of α -TOS responds to pH changes. Under alkaline conditions, α -TOS spontaneously forms self-assembled vesicles of multilamellar character [41,42]. The shift of pH from 9 to 4 induces membrane phase transition. Vesicular structure formed out of the lamellar phase is transformed into hexagonal II phase. Phase transformation occurred as a consequence of attenuated hydrophilicity of the membrane surface caused by protonation of the ionized carboxylic group. Corresponding to this phenomenon, the increase of vesicular size as well as the shift of negative charge to electroneutral values was reported [43,44] (Fig. 2).

3. Solubilization and delivery systems for α -tocopheryl succinate

Suitable formulations of the pro-apoptotic VE analogues have not been invented yet. Inherent low solubility of VE analogues in the aqueous environment is the main obstacle on the way to simple application form. The hydrophobic character of VE analogues predetermines the design and strategy for their formulations. Various approaches have been employed for the preparation of delivery systems of VE analogues, especially for well-studied α -TOS. Solubilization of α -TOS in ethanol, dimethylsulfoxide (DMSO) or oil emulsions was used for the application of the drug in mouse tumor models [20,45,46]. However, it has been reported that as few as one or two injections of the therapeutic dose of α -TAM solubilized in DMSO caused rapid death of experimental animals (Balb/c, C57Bl and FVB/N *c-neu* mice). After i.v. administration of the drug, mixing of blood plasma and α -TAM solubilized in DMSO produced copuscular structures having high negative charge responsible for mice toxicity [27]. Spontaneous vesiculation of TRIS or sodium salts of α -TOS and other dicarboxylic acid analogues was used for preparation of the

drug formulation [24,47,48]. Vesiculated VE analogues preserved its cytotoxic effect. However, in vivo toxicity of these vesiculated forms was reported for some VE analogues, e.g., α -tocopheryl oxalate [26]. Polyethylene glycol (PEG) has gained attention as drug conjugate owing to its solubility in water, biocompatibility and non-toxic properties [49]. Conjugation of α -TOS with PEG-1000 provided formulation of the drug with enhanced biocompatibility. Pegylated α -TOS showed higher anti-cancer efficacy to human A549 lung carcinoma implanted in nude mice than the corresponding non-pegylated α -TOS formulation [50].

In general, administration of VE analogues solubilized in organic solvents causes un-avoidable formation of aggregates responsible for local inflammation and embolization. Studies designed in such wrong way can drive conclusion on toxicity and in-efficacy of VE analogues, as done in the paper by Ireland [51]. Moreover, the observed rapid or delayed toxic effect was not caused owing to the drug itself but by the physical stage of the drug formulation causing formation of toxic aggregates immediately after i.v. or i.p. administration. The other problem encountered is physical destabilization of vesicular structures of the drugs and formation of non-vesicular phase. Destabilization could be induced by increased body temperature, interaction with blood components or by simple dilution of the drugs solubilized in organic solvent during i.v. administration. Non-vesicular phase is prone to form aggregates in the cardiovascular system during circulation. These aggregates are the cause of serious side effects and death of treated animals [27]. Formulations of VE analogues that retain biological activity of the drug, especially if the anti-cancer effect is preserved while the possible toxicity associated with inappropriate drug formulation is reduced or minimized represent a doorstep for the development of clinically relevant delivery systems of VE analogues.

4. Liposomal delivery systems for vitamin E analogues

Numerous anti-cancer drugs exhibit high cytotoxic potential towards cancer cells in vitro. However, the lack of selective anti-cancer effect in vivo precludes their extensive application in the clinical treatment. Another major problem limiting the use of anti-cancer drugs is their low therapeutic index. Low therapeutic index results from several factors such as the non-specific cytotoxicity of the drug which is critical to normal

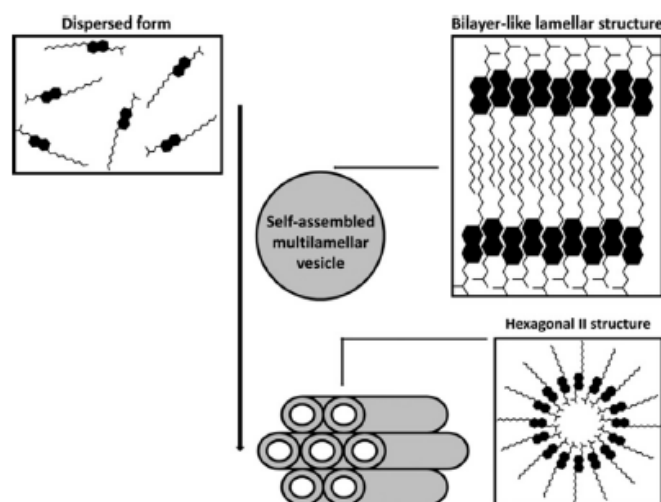


Fig. 2. Self-assembled structures of α -TOS upon pH induction. Dispersion of free drug under alkaline conditions produces self-assembled vesicular formulation having lamellar character. Multilamellar vesicles undergo destabilization under acidic conditions and subsequently they are inverted into hexagonal II phase. The black arrow indicates acidification of aqueous phase.

tissues (cardiac, gastrointestinal, renal tissue and bone marrow), the problems associated with preparation of inappropriate drug formulation having undesirable effects, and the inability to achieve therapeutic drug concentrations at the target tissue (e.g., tumor) [52]. The use of FDA approved liposomal carriers for delivery of VE analogues having selective cytotoxicity towards cancer represents promising concept to be developed for potential application in human cancer therapy.

Liposomal drug delivery systems are based on established industrial technologies. Liposomes themselves represent non-toxic biocompatible nanoparticles approved by FDA for application in human medicine. Liposomes, self-assembled membrane-like spherical vesicles, have considerable potential for entrapment of lipophilic and hydrophilic agents [53]. Entrapment of the drug into the liposomes is used to bypass the frequent toxicity associated with the drug or inappropriate drug formulation (e.g., toxicity of paclitaxel formulated in Cremophor) [54,55]. It

also represents a very effective route that enhances the drug therapeutic effect [56]. Preparation procedures and surface modifications enable production of liposomes for various applications. The final amount of the entrapped drug is affected by selection of appropriate preparation methods. Liposomal formulation of desired composition, morphology, size distribution and surface modification can be tailored for targeting to cells of interest [57] (Fig. 3).

To design the effective drug delivery, it is important to formulate drug in liposomal systems having efficient biodistribution and bioavailability. Formulation of hydrophobic drugs into conventional liposomes represents non-toxic solubilization system. However, rapid clearance of conventional liposomes by reticulo-endothelial system (RES) is one of the major disadvantages in drug delivery. Due to rich blood supply and abundance of tissue-resident macrophages, conventional liposomes are primarily accumulated by phagocytic cells of RES in liver and spleen [58]. Grafting of conventional liposomes by inert and biocompatible PEG reduces rapid clearance of liposomes and apparently prolongs their circulation [59,60]. Small pegylated liposomes (<200 nm) demonstrated higher frequency of extravasation into the fenestrated tumor tissue by enhanced permeation and retention (EPR) effect. Accumulation of pegylated liposomes with entrapped drugs by EPR effect represents passive targeting mechanism improving the drug delivery [61]. Pegylated liposomes demonstrated minimal affinity to normal tissues providing biologically inert and safe platform for the design of advanced drug delivery systems. Ligand-targeted liposomes employ certain targeting groups conjugated to the surface of pegylated liposomes. Ligands are represented by molecules that selectively recognize and bind to target antigen selectively expressed by the tumor cells. This active targeting increases the specificity of interaction of liposome-entrapped drug with the target, the amount of the drug delivered and the drug therapeutic potential [62].

4.1. Interaction of VE analogues with liposomal bilayers

Numerous studies were realized to determine location of α -TOH within the PL bilayers [63]. Interaction of phenoxyl hydroxy group by hydrogen bond to either carbonyl or phosphate oxygen of PL locates the chromanol head of α -TOH close to the aqueous interface. Phetyl chain extends into the bilayer center parallel to PL hydrocarbon chains [63,64]. Acylation of α -TOH with acetate group increases the molecule hydrophobic character by the presence of non-polar methyl group and by minimization of hydrogen bonding capacity of the molecule. Position of α -TOA seems to be located in the more hydrophobic region than for α -TOH which does not perturb the interfacial region [65]. Esterification of α -TOH with succinyl moiety adds free carboxyl group at the end of four carbon chains. The extension increases the overall molecule length and probably places the chromanol head deeper into the PL bilayer. The free carboxyl group of α -TOS is located in the hydrophilic interfacial region where it increases the membrane surface charge [40]. Association of α -tocopheryl glucopyranoside (α -TOG) with phosphatidylcholine (PC) bilayers positioned the chromanol head of α -TOG into the hydrophilic area by electrostatic interaction with choline nitrogen. Bulky hydrophilic sugar unit protruding above PC bilayer was surrounded by water molecules of the aqueous phase [66]. Structural modification of α -TOH either with non-polar or polar groups generates VE analogues having different incorporations within PL bilayer. Non-polar modification intensifies the hydrophobic character of the drug, embeds the molecule deeper into the hydrophobic area of the bilayer and minimizes hydrogen bond interactions. Replacement of hydroxyl group by hydrophilic moiety can result in different penetrations of the whole molecule into the bilayer. Ionisable hydrophilic moiety responds to changes in pH and induces surface charge which can stabilize membrane structures. Incorporation of various VE analogues results in their different packings within the PLs influencing the entrapment capacity and stability of membrane bilayers.

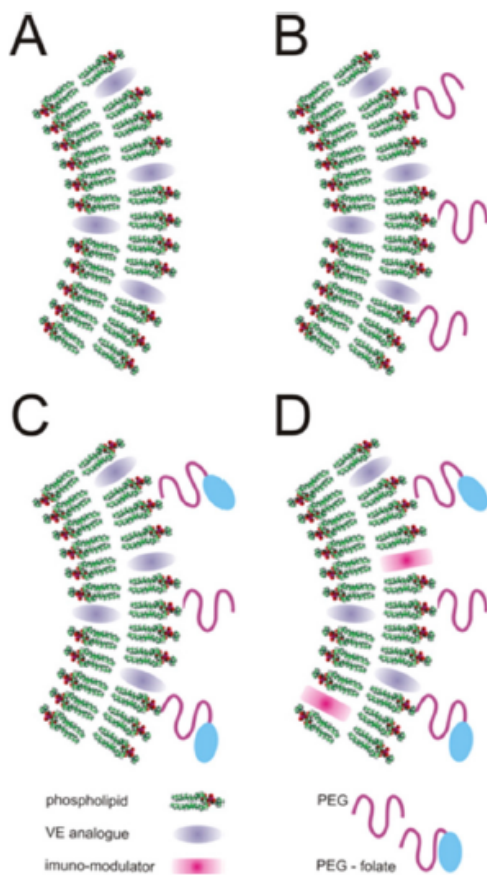


Fig. 3. Various modifications of liposomal delivery systems for VE analogues. A) Conventional liposomes represent non-toxic solubilization delivery systems for VE analogues. B) grafting of liposomal surface with PEG polymer prolongs the liposome circulation and enhances the passive targeting. C) conjugation of targeting ligands (e.g., folate) with PEG onto the external surface of long-circulating liposomes provides specific delivery to the desired tumor site (active targeting). D) co-entrapment of molecular immuno-modulators (e.g., lipophilic MDP analogues, CpG oligonucleotides or MPLA) into the ligand-targeted liposomes represents novel combined immuno-/chemo-therapy approach.

The incorporation and entrapment capacities of egg phosphatidylcholine (EPC) bilayers for α -TOS were investigated. The concentration of α -TOS was elevated up to 20 mol% of the drug with respect to EPC content. Stability of EPC liposomes was not affected up to 15 mol% of α -TOS. Phase separation and formation of non-liposomal structures were observed for liposomes containing higher than 20 mol% of α -TOS [67]. Stability of soy phosphatidylcholine (SPC) bilayers loaded with α -TOA was tested. Phase separation (liposomes versus oil/water phase) was not observed for α -TOA content up to 40 mol%. Particles having a size of 70 nm were stable at room temperature for 72 h. For α -TOA content above 48 mol%, the particle size increased to 220 nm and phase separation was observed at room temperature within 24 h. The highest aqueous volume of 0.46 L/mol was determined for 23 mol% of α -TOA content [68]. Formation of emulsion induced by α -TOA was tested for liposomes composed of saturated PLs. The presence of α -TOA up to 3 mol% in saturated bilayers did not affect liposome stability. Additions of α -TOA decreased polarity in the hydrophobic bilayer region and drug incorporation did not affect the bilayer stability. Excess of α -TOA over 60 mol% was repelled, formed hydrophobic α -TOA core between the inner and outer leaflets of bilayer and produced emulsion. Similarly to previously published results by Asal, entrapped volume decreased to 0.1 L/mol for α -TOA content above 23 mol% [69].

4.2. Liposomal formulations of vitamin E analogues

Hydrophobic character and low aqueous solubility of VE analogues predetermine liposomes as suitable nanodelivery systems. Liposomes provide favorable environment enhancing the solubility of hydrophobic drugs. Multilamellar vesicles (MLVs) with low aqueous volume containing multiple membrane bilayers demonstrated effective capacity for incorporation of VE analogues [27,67,69]. The amount of entrapped VE analogues and composition of PLs could be optimized to keep stable formulation. Overloading of PL entrapment capacity by VE analogues produces phase separation and co-existence of liposomal and non-liposomal structures. Extending fatty acid chains in PLs promote incorporation of hydrophobic drugs into the bilayers. Saturated PLs forming rigid bilayers enable entrapment of low amount of hydrophobic drugs due to the high surface density of bilayers at low temperatures. Cholesterol improves entrapment of hydrophobic drugs only if the input of the drug is less than the drug entrapment capacity [57]. Prolonged stability, suppressed aggregation and fusion are achieved by electrostatic repulsion of charged liposomes in the hydrated stage. For α -TOS, the presence of charged PLs in liposomes is not necessary because the molecule of α -TOS is negatively charged at physiological pH. Development of lyophilized formulations offers advantage of the prolonged stability of liposomes during year-period [70,71]. Liposome technology enables preparation of MLVs which the size could be easily controlled by application of secondary processing techniques such as extrusion, sonication, microfluidization or high pressure homogenization. Generally, the composition of liposomal carrier, the balance of the drug entrapped in liposomes (drug/lipid molar ratio) and the stability of liposomal drug formulation represent critical parameters to be considered to design the optimal formulation of VE analogues.

The realized experiments regarding the liposomal formulations of VE analogues were preliminarily focused on testing of cytotoxicity in vitro and evaluation of anti-cancer effect in vivo. The preparation procedures, physico-chemical characterization and monitoring of the liposome stability during prolonged storage period were not consistently studied.

4.2.1. Vitamin E analogues entrapped in conventional liposomes

Conventional formulation of α -TOS and PC (molar ratio, 3:17) liposomes was developed in the form of lyophilizate. Homogeneous population of liposomes was prepared by lipid film hydration followed by extrusion of MLVs through 0.2 μ m filters. Lyophilization of α -TOS liposomes was accomplished in the presence of sucrose (lipid/sucrose

molar ratio, 1:5) to prolong the stability of formulation. Major physico-chemical parameters of the stability were monitored during a 6-month storage. Physical stability, constant liposome morphology and size distribution as well as stable contents of PC and entrapped α -TOS were preserved by sucrose used as cryoprotectant and stabilizer of the lyophilizate [67]. To overcome cytotoxicity associated with administration of drugs in inappropriate formulation (free α -TAM solubilized in DMSO) and to solve the low aqueous solubility of the drugs, α -TOS and α -TAM were formulated in PC liposomes (molar ratio, 3:17). Liposomes were prepared by lipid film hydration followed by extrusion of MLVs. The final liposome size of 130 nm was determined. Entrapment up to 15 mol% of α -TOS did not cause any phase separation. In spite of some in vitro toxicity of free α -TOS or α -TAM towards stimulated mice or human peripheral blood lymphocytes, neither α -TOS (100 mg/kg) nor α -TAM (25 mg/kg) formulated in liposomes affected the leukocyte count in peripheral blood within 3 weeks following their administration in Balb/c mice. Tumor growth inhibition was demonstrated by i.v. application of liposomal α -TOS (15 μ M) and liposomal α -TAM (1.5 μ M) administered on days 0, 4, 7, and 13 in FVB/N c-neu transgenic mice with spontaneous breast carcinoma. Liposomal formulations of both VE analogues applied by i.v. route proved the anti-cancer efficacy while acute toxicity and immunotoxicity of α -TAM were eliminated by the drug entrapment [27]. Sonication of α -TOS dispersion and hydration of lipid film composed of α -TOS and EPC (molar ratio, 1.7:1) were the methods used for preparation of vesiculated and liposomal drug formulations. Extrusion through 0.1- μ m filters reduced the particle size to 95 and 88 nm for α -TOS vesicles and α -TOS liposomes, respectively. Particle stability was studied by dynamic light scattering in the presence of slightly acidic pH of 6, divalent cations (3 mM) and 50% fetal bovine serum (FBS) at 37 °C for 24 h. Neutralization of negatively charged α -TOS and collapse of vesicular structure followed by aggregation was observed for 3-mM divalent cations and 50% FBS incubations. The size of vesiculated α -TOS increased to 300 nm. Physical stabilization of α -TOS was supported by the drug incorporation within bilayers of EPC liposomes. Free, vesiculated and liposomal α -TOS prevented in vitro proliferation of melanoma B16F1 cells in a dose- (0–50 μ M) and time- (12–48 h) dependent manner. Of these formulations, liposomal α -TOS demonstrated significantly higher inhibition efficacy than its vesiculated and free counterpart. Unlike vesiculated and free α -TOS, liposomal α -TOS did not cause erythrocyte hemolysis at 37 °C for 24 h. Undesirable side effect of the drug causing hemolysis was eliminated by entrapment of α -TOS into liposomes. Anti-cancer effect of α -TOS formulations was evaluated on melanoma B16F1 cell-bearing mice. Four days after cell implantation, α -TOS dose of 10 μ M was administered by i.v. five times every three days. On the 20th day, tumor volume was quantified. In comparison to untreated control, the tumor growth was inhibited by 70% and 79% for vesiculated α -TOS and liposomal α -TOS, respectively. Moreover, liposomal α -TOS exhibited improved intra-tumoral distribution as observed by confocal laser scanning microscopy. Enhanced delivery of α -TOS by liposomes altered the drug biodistribution and promoted the drug accumulation in tumor [72]. Other conventional PC liposomes loaded with α -TOS were made by combination of lipid film formation followed by anionic surfactant hydration and detergent dialysis to obtain small unilamellar vesicles (SUVs). Liposomal α -TOS promoted apoptosis and decreased viability of hamster cheek pouch carcinoma cells (HCPC-1) in vitro. After the 12-h exposure to 7 μ M of α -TOS, cell viability decreased to 51% for α -TOS un-assisted, while to 21% for liposomal α -TOS owing to enhanced fusion of SUVs with the cell membrane and subsequent release of the entrapped α -TOS [73]. Phosphatidylethanolamine-PEG (PE-PEG) was used to modify the surface of conventional liposomes. The modified liposomes composed of hydrogenated SPC, cholesterol and α -TOS had size of 100 nm and demonstrated prolonged circulation in comparison to free α -TOS after i.v. administration in mice [74].

The developed conventional liposomes were found to stabilize the hydrophobic molecule of α -TOS. Formulation of α -TAM into the conventional liposomes eliminated the drug cytotoxicity in vitro and

proved *in vivo* anti-cancer efficacy while immunotoxicity was eliminated. Application of extrusion was convenient to control the final size of liposomes for *in vivo* administration.

4.2.2. Vitamin E analogues entrapped in pH-sensitive liposomes

Phosphatidylethanolamine (PE) has a small head group occupying the smaller volume in comparison to the hydrocarbon chains. Resulting cone shape of PE obstructs to form lamellar phase and has tendency to revert into the hexagonal phase. The vesicles prepared only of pH-sensitive PE do not form stable liposomal structures at physiological pH. Entrapment of amphiphilic molecules with negatively charged group promotes electrostatic repulsion to form stable liposomes at physiological pH. Acidification of pH-sensitive liposomes triggers protonation of carboxylic group of amphiphilic molecule leading to strengthening of molecule hydrophobic character. Acidic environment reverts PE into the hexagonal phase leading to destabilization of liposomes (fusion and aggregation) and release of the entrapped material. Selection of amphiphilic stabilizer as well as its content with respect to PE influences cellular internalization, pH sensitivity and stability in biological fluids [75]. Tumors exhibit acidic environment in comparison to the normal tissues, thereby causing such pH-sensitive formulations appropriate delivery systems more selective for cancer cells [75,76].

Lipid composition, particle stability and leakage of entrapped marker upon pH changes was tested for pH-sensitive liposomes composed of PE and α -TOS. Shift of induced leakage of carboxyfluorescein from pH of 7 to 6 was observed for liposome composition of molar ratio of PE/ α -TOS from 9:1 to 7:3. Increasing content of α -TOS acts as stabilizer to promote liposome stability and retention of entrapped marker in slightly acidified environment. However, for pH below 6, the increase of liposome size and leakage of entrapped marker were observed for all the tested compositions as consequence of increased membrane permeability and liposome fusion [77]. Other formulations of pH-sensitive vesicles (PSVs) were developed as pegylated ones and as conventional ones. Pegylated PSVs were composed of α -TOS TRIS salt with 8 mol% of α -TOS-PEG conjugate. Conventional PSVs made up of α -TOS TRIS salt were prepared by detergent removal followed by extrusion through 0.22- μ m filters. The mean size of 165 nm and ζ -potential of -75 mV was assessed for conventional PSVs. TEM revealed bilayer structure of the vesicles. Hydrophilic marker calcein entrapped in the conventional PSVs was released (30, 75 and 95%) in the pH-dependent manner (6.4, 5.4 and 4.4) during 10 min. Prolonged incubation was accompanied by precipitation of conventional PSVs. Acidification of conventional PSVs altered lamellar structure of α -TOS vesicles leading to leakage of entrapped calcein. Addition of 2, 4, 6 and 8 mol% of neutral molecule of α -TOS-PEG to conventional PSVs was found decrease mean size to 145, 121, 98 and 101 nm as well as ζ -potential to -45 , -31 , -10 and -1 mV. Stability of pegylated PSVs was determined upon calcium-induced fusion. Content of α -TOS-PEG higher than 6 mol% in PSVs had protective effect to prevent fusion even if the incubation with 10 mM calcium was extended to 24 h at 37 °C. At such level, PEG shielded negatively charged groups on the surface and promoted stability of PSVs. Pharmacokinetics of calcein formulated as free, conventional or pegylated PSVs was evaluated on Kunming mice model. Pegylated PSVs demonstrated 7.3 and 6.5-fold prolonged half-time in comparison to free and conventional formulation, respectively [78]. From the point of view of α -TOS activity, this agent can act as liposome entrapped anti-cancer drug exhibiting cytotoxic effect as well as stabilizer of PE in pH-sensitive liposomes owing to its amphiphilic character. Moreover, pH-sensitive delivery system constructed of PE and α -TOS offers advance for combined or synergistic anti-cancer treatment by co-entrapment of hydrophilic anti-cancer drugs.

4.2.3. Vitamin E analogues entrapped in liposomes for aerosol delivery

Aerosol delivery of liposomal hydrophobic chemotherapeutic drugs was shown to increase drug concentrations in lungs and organs in comparison to oral or *im* application. Administration by aerosol was shown very effective against pulmonary metastasis of

melanoma and osteocarcinoma in mice [79,80]. Because α -TEA and α -TOS have hydrophobic character, aerosol delivery of their liposomal formulations was chosen as potentially effective and clinically relevant application for anti-cancer therapy. For these studies, mouse mammary 66 cl-4-GFP cells originally derived from spontaneously arising adenocarcinoma were transfected with green fluorescent protein (GFP). Preliminary results showed arrest of DNA synthesis and apoptosis induction by α -TEA and α -TOS *in vitro* [81]. After implantation in mice, 66 cl-4-GFP cells generated aggressive tumor growth with metastases to lungs and lymph nodes.

Liposomal formulation of α -TEA was prepared by entrapment of the drug into dilauroyl PC (DLPC) vesicles (weight ratio, 1:3) by lyophilization from *tert*-butanol. Prior to use, lyophilizate was rehydrated and subsequent nebulization produced 2- μ m particles for aerosol treatment. Conventional formulation was made by solubilization of α -TEA in ethanol followed by mixing with peanut oil (volume ratio, 1:8) for gavage application. Nine days after *s.c.* implantation of 66 cl-4-GFP cells, mice treatment was started. A total dose of 612 μ g of α -TEA per mouse was applied by aerosol within 17 days. For gavage, a total dose of 65 mg α -TEA per mouse was applied within 13 days. Quantification of final volumes revealed significant tumor reduction by liposomal α -TEA aerosol (325 ± 55 mm³) in comparison to untreated mice (915 ± 115 mm³). Fluorescence examination of lungs detected 11 ± 4 and 102 ± 17 microscopic metastases (<20 μ m) for mice treated by liposomal α -TEA aerosol and mice untreated, respectively. Gavage administration of conventional oily-based α -TEA formulation was ineffective to prevent tumor burden [82]. Based on successful inhibition of tumor burden in mice cancer model, liposomal formulations of α -TEA and α -TOS were prepared as previously described [82]. Generation of aerosol produced 2- μ m particles. Any physical or chemical alterations of liposomal VE analogues were not observed during this process. For gavage treatment, rehydrated liposomal lyophilizates had a size of 4–10 μ m. Nine days after *s.c.* cell implantation, daily dose of 36 μ g and 6.4 mg of particular VE analogue was administered by aerosol or gavage within 21 days. Liposomal α -TEA and liposomal α -TOS delivered by aerosol prevented tumor growth having final volumes about 400 mm³. For untreated control, final tumor volume of 1000 mm³ was assessed. Similarly to tumor inhibition, fluorescent lung metastases were reduced to 31 and 44 by liposomal α -TEA and liposomal α -TOS aerosol treatments, respectively. For untreated mice control, 77 fluorescent lung metastases were detected. Lymph node metastases were reduced by liposomal α -TEA aerosol, while by liposomal α -TOS aerosol did not. Gavage treatment by liposomal α -TEA reduced tumor growth and lung metastases similarly like liposomal α -TEA aerosol. Liposomal α -TOS applied by gavage involves transport through intestinal tract. Esterases cleaved ester bond in α -TOS even if liposome entrapped. Products of hydrolysis include succinic acid and α -TOH that both do not exhibit anti-cancer effect and metastasis elimination [81]. It can be concluded that probably poor absorption of liposomal α -TEA by gastrointestinal tract (GIT) reduced the drug bioavailability even if α -TEA remained intact after gavage administration. Significantly higher doses of α -TEA were found to be administered by gavage to induce anti-cancer effect in comparison to α -TEA delivered by aerosol [81]. Combined chemotherapy by liposomal α -TEA aerosol and cisplatin applied *i.p.* was evaluated on immuno-compromised NU/NU mice bearing human ovarian cisplatin-resistant A2780/cp70 carcinoma. Daily dose of 36 μ g of liposomal α -TEA in combination with 5 mg/kg of cisplatin administered weekly was the only treatment reducing growth of small preformed tumors. Large preformed tumors were more efficiently inhibited by liposomal α -TEA (72 μ g daily) with cisplatin (5 mg/kg weekly) than either liposomal α -TEA or cisplatin single treatments. Metastasis in lungs and lymph nodes were significantly reduced by liposomal α -TEA combined with cisplatin treatment. Synergistic anti-cancer effect was observed even if platinum-resistant tumor was used [83]. The developed aerosol formulation of liposomal α -TEA was successfully combined with liposomal 9-nitro-camptothecin, liposomal paclitaxel or celecoxib to

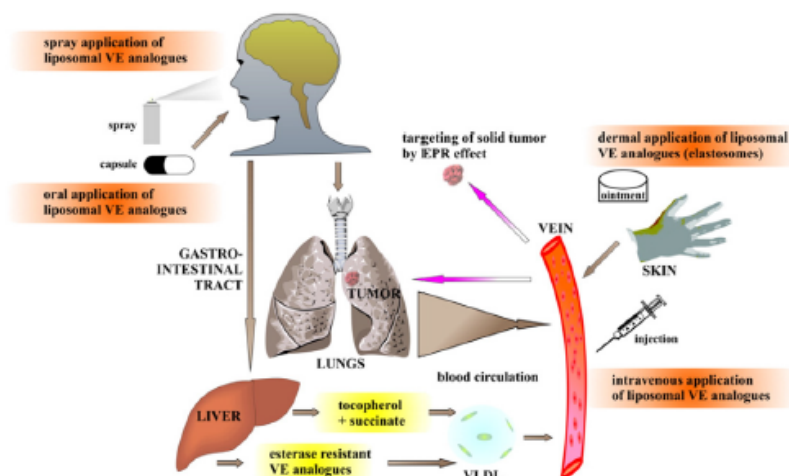


Fig. 4. Administration routes for liposomal delivery of VE analogues. Various routes of administration can be used to reach the targeted tissue or tumor. Spraying of liposomal VE analogues is a suitable route for the direct targeting of lung cancer as well as for the delivery of VE analogues into the brain circulation. The bypassing of hepato-pancreatic port and the directing of VE analogues into the brain circulation are the advantages of this administration route. Oral application of biopolymer-coated liposomes or acidic-resistant capsules filled by liposomal VE analogues represents simple administration route. The oral application may be feasible in the case of VE analogues having ether or amide bonds linking dicarboxylic acid to the tocopherol. These analogues of VE are not hydrolyzed after absorption in the intestines. Transdermal local application of liposomal formulation of VE analogues can be used for the treatment of skin tumors or subcutaneous tumors. Transferosomes (elastic liposomes) are of interest for purposes owing to their improved penetration through stratum corneum. After parenteral administration (i.v.), liposomal VE analogues can enter various pathways. These pathways and the biodistribution of VE analogues are determined by various factors, e.g., character of liposomes (steric stabilization), morphology (size and lamellarity) or lipid composition. In the bloodstream, VE analogues are redistributed between liposomes and the blood components (cellular and protein elements). Liposomal VE analogues can penetrate through fenestrations of the tumor vasculature. In the tumor, liposomal drug is accumulated and subsequently released in the vicinity of the tumors and the tumor endothelial cells.

reduce tumor burden as well as lung and lymph node metastases in various animal cancer models [84–87].

4.3. Administration routes for delivery of liposomal vitamin E analogues

Various routes for administration of liposomal VE analogues could be used to reach the specific local or systemic effect (Fig. 4).

Aerosol spraying is suitable for the direct targeting of lung cancer or for the drug delivery into the circulation. Lungs represent attractive target due to non-invasive administration via aerosols, avoidance of the first-pass metabolism, high drug bioavailability and availability of huge surface area for local drug action and systemic drug absorption [88,89]. Targeting the aerosol to conducting or peripheral airways could be accomplished by altering the size of aerosol particles and by the inspiratory flow rate. In general, particles of 10–5 µm are deposited in the large conducting airways and oropharyngeal region. Particles of 1–5 µm inhaled in the small airways achieve substantial alveolar deposition [90,91]. Pulmonary drug delivery for systemic absorption requires smaller size of aerosol particles to ensure peripheral drug penetration. Formulation of liposomal anti-cancer VE analogues for aerosol delivery α-TEA and α-TOS has been developed (see Section 4.2.3).

Oral delivery is considered to be one of the most abundant and traditional way of drug delivery. Administration of liposomes by oral route is problematic due to their low stability under the physiological conditions of GIT. The major destabilizing factors are acidic pH in the stomach, the presence of bile salts and pancreatic enzymes in the GIT. The use of saturated lipids and the presence of cholesterol improve the liposome rigidity and thus reduce the possibility of enzymatic degradation [92]. Enhanced stability could be also achieved by modification of liposomal surface by biopolymers such as PEG, chitosan or collagen [93–95]. Moutardier prepared liposomes coated with collagen for the oral delivery of hydrophobic anti-cancer drugs like vincristine and methotrexate for the treatment of colorectal cancer [94]. On the other hand,

oral administration of acidic-resistant capsules filled with liposomal VE analogues represents also simple way of application. Toxicological data were reviewed and they are available for some VE analogues owing to their extensive use as food additives [96]. However, this route is not effective for VE analogue esters because of their rapid degradation by intestinal esterases. Esterase resistant VE analogues having ether or amide bond represent feasible way to overcome this problem [31,82]. However, the selection, design and development of the drug specific carrier system represent state-of-art and require thorough understanding of the physicochemical drug properties and the drug behavior in physiological conditions [97].

Transdermal local administration could be used for the treatment of skin and subcutaneous tumors. Unfortunately, the barrier nature of the skin presents significant obstacle for most drugs to be delivered into and through it [98]. It has been found that PC enhances transdermal delivery by lowering the permeability barrier of the skin. Changes in the ultra-structure of the intercellular lipids were observed after application of the PC vesicles suggesting enhanced penetration [99]. Owing to the conical shape of dioleoyl PE (DOPE) and lysoPC, liposomes containing these lipids penetrated deeper into the densely-packed stratum corneum [100]. Small-sized liposomes can accelerate transdermal penetration of drug. Liposomes having size about 30 nm promoted faster penetration of α-TOA in comparison to 150-nm liposomes [101]. Transferosomes represent advanced transdermal delivery systems for the drugs. These elastic liposomes are usually composed of PC and edge activators (e.g., surfactants) which provide ultra-deformation of liposomes. Transferosomes could be reversibly deformed to allow passing through the narrow constriction which are 5–10 times lower than their own diameter without any loss of the entrapped material. Transdermal hydration gradient produce force to drive transferosomes through the intact stratum corneum into the epidermis [102]. The ultra-deformable liposomes have been already tested for the transdermal delivery of hydrophobic anti-cancer drug methotrexate [103].

Parenteral/intravenous administration comprises various drug pathways determined by character of liposomal delivery systems. Small liposomes can penetrate through the liver fenestrations. In the liver, drug is accumulated, transformed by enzymatic pathways and secreted in the form of very low density lipoprotein (VLDL) particles into the blood circulation. Liposomal VE analogues can also penetrate through fenestrations of the tumor vasculature. In the tumor, liposomal drug is accumulated by EPR effect and subsequently released in the vicinity of the tumor cells.

5. Cancer immunotherapy and alpha-tocopheryl succinate

An interesting approach of cancer treatment is represented by cancer immunotherapy which attempts to stimulate the immune system to reject and eliminate tumors. To date, cancer immunotherapy employing only non-liposomal formulations of α -TOS adjuvant such as drug solubilized in ethanol or vesicular drug form have been published.

Dendritic cells (DCs) represent potential candidates to design cell-based vaccines for cancer immunotherapy. The ability of DCs to process and present tumor antigens to T lymphocytes ($CD4^+$ and $CD8^+$) activates immune responses against cells expressing tumor antigens [104]. The use of appropriate immuno-stimulating molecules like Toll or NOD receptor ligands can significantly stimulate the efficacy of DC-based cancer vaccines. α -TOS was chosen to be the promising anti-cancer drug with selective toxicity to cancer cells and low immunotoxicity in vivo [27]. Adjuvant effect of α -TOS solubilized in ethanol vehicle combined with DCs was evaluated on C57BL/6 mice bearing murine Lewis lung 3LL cells. Tumor volume about 30 mm^3 was formed 10 days after the cell implantation. Mice received 200 mg/kg of α -TOS solubilized in ethanol by i.t. or i.p. route on the 10th, 14th, 18th day. On the 22nd day, tumor volumes were quantified. Tumors in control mice (ethanol vehicle, i.p./i.t.) grew progressively ($1800 \pm 237 \text{ mm}^3$, i.p. and $2000 \pm 296 \text{ mm}^3$, i.t.), while mice treated by α -TOS showed tumor inhibition ($376 \pm 39 \text{ mm}^3$, i.p. and $401 \pm 22 \text{ mm}^3$, i.t.). For combined treatment with α -TOS (200 mg/kg, i.p./i.t.), dose of DCs (1×10^6) was i.t. administered on the 12th, 16th, 20th day. Tumor volume was quantified on the 30th day. Therapy with α -TOS + DCs ($78 \pm 18 \text{ mm}^3$) was more efficient than either α -TOS ($471 \pm 68 \text{ mm}^3$) or DCs. However, this treatment had limited effect on formation of visible lung metastases. Subcutaneous administration of DCs represent common vaccination procedure, therefore application of DCs, s.c./i.t. and α -TOS, i.p. was evaluated. At the end of therapy (28th day), tumor volumes were quantified as follows: 98 ± 29 , 99 ± 10 , 493 ± 75 and $514 \pm 138 \text{ mm}^3$ for DCs, s.c. + α -TOS, i.p., DCs, i.t. + α -TOS, i.p., DCs and α -TOS, respectively. Intra-tumoral or s.c. application of DCs demonstrated similar tumor inhibition. Secretion of interferon-gamma (INF-) was determined because its content is coincident to response of T lymphocytes ($CD4^+$ and $CD8^+$) stimulated by DCs. Stimulation is involved in immune activation and tumor growth inhibition. T lymphocytes ($CD4^+$ and $CD8^+$) from mice treated with DCs, s.c. + α -TOS, i.p. produced significantly higher amount of INF- ($2224 \pm 39 \text{ pg/ml}$ and $319 \pm 4 \text{ pg/ml}$) than for those treated with α -TOS ($586 \pm 4 \text{ pg/ml}$ and $189 \pm 2 \text{ pg/ml}$), DCs ($204 \pm 2 \text{ pg/ml}$ and $161 \pm 3 \text{ pg/ml}$) and ethanol control ($79 \pm 1 \text{ pg/ml}$ and $80 \pm 1 \text{ pg/ml}$), respectively. Local (i.t.) or systemic (i.p.) administration of α -TOS significantly inhibited growth of 3LL tumor growth in C57BL/6 mice. Synergetic effect of α -TOS and DCs was achieved by α -TOS-mediated apoptosis in cancer cells whose antigens were presented by DCs to enhance immune response on mice model in vivo. Positive correlation was observed between tumor growth inhibition and INF- production by T lymphocytes isolated from mice spleens treated with α -TOS + DCs. Anti-cancer activity of α -TOS + DCs was superior to α -TOS resulting in complete tumor regression in some cases [46]. Solubilization of α -TOS in ethanol was replaced by more potentially clinically relevant adjuvant of vesiculated α -TOS formulation. Chemo-immuno-therapy using vesiculated α -TOS in combination with

DCs vaccination were successfully applied to reduce the growth of primary lung and mammary tumors [14,105].

6. Conclusion

α -TOS and the other VE analogues with a potent pro-apoptogenic activity demonstrated efficient cytotoxic activity in vitro and anti-cancer effect in vivo on various experimental animal models. The lack of immunotoxicity of liposomal formulations and the possibility to be used with other anti-cancer drugs offer interesting opportunity for the combined chemo- and immuno-therapy. More data from the experimental, epidemiological and finally clinical studies are necessary for the next active investigation of these highly promising agents that may be established as routine anti-cancer drugs. Development of safe formulations which preparation can be applicable for industrial scale production is the assumption for future clinical trials.

Acknowledgments

This work was supported by the following grants: the Grant Agency of Czech Republic GAP503/12/G147 (JT), the Ministry of Education, Youth and Sports CZ.1.07/2.3.00/20.0164 (JT) and in part by the BIOCEV – European Regional Development Fund CZ.1.05/1.1.00/02.01/09 (JN). SK was supported by the European Social Fund and the State Budget of the Czech Republic – Project FNUSA-ICRC, Support for Neurological Research and Development Teams through Postdoc Position Formations CZ.1.07/2.3.00/30.0043. Support of Global Acorn (ADM) is kindly acknowledged.

References

- [1] K. Fukuzawa, K. Matsura, A. Tokumura, A. Suzuki, J. Terano, Kinetics and dynamics of singlet oxygen scavenging by alpha-tocopherol in phospholipid model membranes, *Free Radic. Biol. Med.* 22 (1997) 923–930.
- [2] S. Uramo, M. Kitahara, Y. Kato, Y. Hasegawa, M. Matsuo, Membrane stabilizing effect of vitamin E — existence of a hydrogen bond between alpha-tocopherol and phospholipids in bilayer liposomes, *J. Nutr. Sci. Vitaminol.* 36 (1990) 513–519.
- [3] Z. Djuric, L.K. Heilbrun, S. Lababidi, C.K. Everett-Bauer, M.W. Faries, Growth inhibition of MCF-7 and MCF-10A human breast cells by alpha-tocopheryl hemisuccinate, cholesterol hemisuccinate and their ether analogs, *Cancer Lett.* 111 (1997) 133–139.
- [4] W.P. Yu, B.G. Sanders, K. Kline, RRR-alpha-tocopheryl succinate inhibits EL4 thymic lymphoma cell growth by inducing apoptosis and DNA synthesis arrest, *Nutr. Cancer* 27 (1997) 92–101.
- [5] W.P. Yu, M. Simmons-Menchaca, A. Gapor, B.G. Sanders, K. Kline, Induction of apoptosis in human breast cancer cells by tocopherols and tocotrienols, *Nutr. Cancer* 33 (1999) 26–32.
- [6] M.W. Faries, M.B. Fortuna, C.K. Everett, J.D. Smith, D.F. Trent, Z. Djuric, The selective antiproliferative effects of alpha-tocopheryl hemisuccinate and cholesterol hemisuccinate on murine leukemia cells result from the action of the intact compounds, *Cancer Res.* 54 (1994) 3346–3351.
- [7] J. Neuzil, T. Weber, N. Gellert, C. Weber, Selective cancer cell killing by alpha-tocopheryl succinate, *Br. J. Cancer* 84 (2001) 87–89.
- [8] J. Neuzil, M. Tomasetti, A.S. Mellick, R. Alleva, B.A. Salvatore, M. Birringer, M.W. Faries, Vitamin E analogues: a new class of inducers of apoptosis with selective anti-cancer effects, *Curr. Cancer Drug Targets* 4 (2004) 355–372.
- [9] T. Weber, M. Lu, L. Andera, H. Lahm, N. Gellert, M.W. Faries, V. Korinek, W. Sattler, D.S. Ucker, A. Terman, A. Schroder, W. Erl, U.T. Brunk, R.J. Coffey, C. Weber, J. Neuzil, Vitamin E succinate is a potent novel antineoplastic agent with high selectivity and cooperativity with tumor necrosis factor-related apoptosis-inducing ligand (Apo2 ligand) in vivo, *Clin. Cancer Res.* 8 (2002) 863–869.
- [10] K.T. Barnett, F.D. Fokum, M.P. Malafa, Vitamin E succinate inhibits colon cancer liver metastases, *J. Surg. Res.* 106 (2002) 292–298.
- [11] A. Hrzienjak, H. Reicher, A. Wintersperger, B. Steinecker-Frohniwieser, P. Sedlmayr, H. Schmidt, T. Nakamura, E. Malle, W. Sattler, Inhibition of lung carcinoma cell growth by high density lipoprotein-associated alpha-tocopheryl succinate, *Cell. Mol. Life Sci.* 61 (2004) 1520–1531.
- [12] M.P. Malafa, F.D. Fokum, A. Mowlavi, M. Abusief, M. King, Vitamin E inhibits melanoma growth in mice, *Surgery* 131 (2002) 85–91.
- [13] M.P. Malafa, F.D. Fokum, J. Andoh, L.T. Neitael, S. Bandyopadhyay, R. Zhan, M. Iizumi, E. Furuta, E. Horvath, K. Watabe, Vitamin E succinate suppresses prostate tumor growth by inducing apoptosis, *Int. J. Cancer* 118 (2006) 2441–2447.
- [14] L.V. Ramanathapuram, T. Hahn, S.M. Dial, E.T. Akporiaye, Chemo-immunotherapy of breast cancer using vesiculated alpha-tocopheryl succinate in combination with dendritic cell vaccination, *Nutr. Cancer* 53 (2005) 177–193.
- [15] M. Stapelberg, N. Gellert, E. Swettenham, M. Tomasetti, P.K. Witting, A. Procopio, J. Neuzil, Alpha-tocopheryl succinate inhibits malignant mesothelioma by disrupting the fibroblast growth factor autocrine loop, *J. Biol. Chem.* 280 (2005) 25369–25376.

- [16] E. Swettenham, P.K. Witting, B.A. Salvatore, J. Neuzil, Alpha-tocopheryl succinate selectively induces apoptosis in neuroblastoma cells: potential therapy of malignancies of the nervous system, *J. Neurochem.* 94 (2005) 1448–1456.
- [17] N. Duhem, F. Danhier, V. Preat, Vitamin E based nanomedicines for anti-cancer drug delivery, *J. Control. Release* 182 (2014) 33–34.
- [18] J. Neuzil, K. Kagedal, L. Andera, C. Weber, U.T. Brunk, Vitamin E analogs: a new class of multiple action agents with anti-neoplastic and anti-atherogenic activity, *Apoptosis* 7 (2002) 179–187.
- [19] H.J. Kayden, M.G. Traber, Absorption, lipoprotein transport, and regulation of plasma concentrations of vitamin E in humans, *J. Lipid Res.* 34 (1993) 343–358.
- [20] J. Neuzil, H. Massa, Hepatic processing determines dual activity of alpha-tocopheryl succinate: a novel paradigm for a shift in biological activity due to pro-vitamin-to-vitamin conversion, *Biochem. Biophys. Res. Commun.* 327 (2005) 1024–1027.
- [21] P.J. Prussiner, H. Lindner, O. Glatzer, H. Reicher, G.M. Kostner, A. Wintersperger, E. Malle, W. Sattler, Lipoprotein-associated alpha-tocopheryl succinate inhibits cell growth and induces apoptosis in human MCF-7 and HBL-100 breast cancer cells, *Biochim. Biophys. Acta* 1485 (2000) 129–144.
- [22] J. Neuzil, T. Weber, A. Schroder, M. Lu, G. Ostermann, N. Gellert, G.C. Mayne, B. Olejnicka, A. Negre-Salvayre, M. Sticha, R.J. Coffey, C. Weber, Induction of cancer cell apoptosis by alpha-tocopheryl succinate: molecular pathways and structural requirements, *FASEB J.* 15 (2001) 403–415.
- [23] S. Yamamoto, H. Tamai, R. Iihisaka, T. Kanra, K. Arita, H. Kobuchi, K. Utsumi, Mechanism of alpha-tocopheryl succinate-induced apoptosis of promyelocytic leukemia cells, *Free Radic. Res.* 33 (2000) 407–418.
- [24] M.A. Timmerstein, X.K. Ge, C.R. Ellis, M.W. Fariss, Administration of the tris salt of alpha-tocopheryl hemisuccinate inactivates CYP2E1, enhances microsomal alpha-tocopherol levels and protects against carbon tetrachloride-induced hepatotoxicity, *Free Radic. Biol. Med.* 26 (1999) 825–835.
- [25] J. Neuzil, M. Tomasetti, Y. Zhao, L.F. Dong, M. Birringer, X.F. Wang, P. Low, K. Wu, B.A. Salvatore, S.J. Ralph, Vitamin E analogs, a novel group of "mitocans," as anticancer agents: the importance of being redox-silent, *Mol. Pharmacol.* 71 (2007) 1185–1199.
- [26] K. Kogure, S. Manabe, I. Suzuki, A. Tokumura, K. Fukuzawa, Cytotoxicity of alpha-tocopheryl succinate, malonate and oxalate in normal and cancer cells in vitro and their anti-cancer effects on mouse melanoma in vivo, *J. Nutr. Sci. Vitaminol.* 51 (2005) 382–387.
- [27] J. Turanek, X.F. Wang, P. Knotigova, S. Koudelka, L.F. Dong, E. Vrublova, E. Mahdavian, L. Prochazka, S. Sangsura, A. Vacek, B.A. Salvatore, J. Neuzil, Liposomal formulation of alpha-tocopheryl maleamide: in vitro and in vivo toxicological profile and anticancer effect against spontaneous breast carcinomas in mice, *Toxicol. Appl. Pharmacol.* 237 (2009) 249–257.
- [28] K.N. Prasad, J. Edwards-Prasad, Effects of tocopherol (vitamin E) and succinate on morphological alterations and growth-inhibition in melanoma cells in culture, *Cancer Res.* 42 (1982) 550–555.
- [29] M. Birringer, J.H. Eytina, B.A. Salvatore, J. Neuzil, Vitamin E analogues as inducers of apoptosis: structure-function relation, *Br. J. Cancer* 88 (2003) 1948–1955.
- [30] E. Mahdavian, S. Sangsura, G. Landry, J. Eytina, B.A. Salvatore, A novel synthesis of tocopheryl amines and amides, *Tetrahedron Lett.* 50 (2009) 19–21.
- [31] A. Tomic-Vatic, J. Eytina, J. Chapman, E. Mahdavian, J. Neuzil, B.A. Salvatore, Vitamin E amides, a new class of vitamin E analogues with enhanced proapoptotic activity, *Int. J. Cancer* 117 (2005) 188–193.
- [32] K. Anderson, M. Simmons-Menchaca, K.A. Lawson, J. Atkinson, B.G. Sanders, K. Kline, Differential response of human ovarian cancer cells to induction of apoptosis by vitamin E succinate and vitamin E analogue, alpha-TEA, *Cancer Res.* 64 (2004) 4263–4269.
- [33] M.P. Murphy, R.A.J. Smith, Targeting antioxidants to mitochondria by conjugation to lipophilic cations, *Annu. Rev. Pharmacol. Toxicol.* 47 (2007) 629–656.
- [34] L.F. Dong, V.J.A. Jameson, D. Tilly, J. Cerny, E. Mahdavian, A. Marin-Hernandez, L. Hernandez-Esquivel, S. Rodriguez-Enriquez, J. Stursa, P.K. Witting, B. Stantic, J. Rohlena, J. Truksa, K. Kluckova, J.C. Dyason, M. Ledvina, B.A. Salvatore, R. Moreno-Sanchez, M.J. Coster, S.J. Ralph, R.A.J. Smith, J. Neuzil, Mitochondrial targeting of vitamin E succinate enhances its pro-apoptotic and anti-cancer activity via mitochondrial complex II, *J. Biol. Chem.* 286 (2011) 3717–3728.
- [35] L. Prochazka, S. Koudelka, L.F. Dong, J. Stursa, J. Goodwin, J. Neza, J. Slavik, M. Gganek, J. Masek, K. Kluckova, M. Nguyen, J. Turanek, J. Neuzil, Mitochondrial targeting overcomes ABCA1-dependent resistance of lung carcinoma to alpha-tocopheryl succinate, *Apoptosis* 18 (2013) 286–299.
- [36] J. Ni, X.Q. Wen, Y. Yao, H.C. Chang, Y. Yin, M. Zhang, S.Z. Xie, M. Chen, B. Simons, P. Chang, A. di Sant'Agnese, E.M. Messing, S.Y. Yeh, Tocopherol-associated protein suppresses prostate cancer cell growth by inhibition of the phosphoinositide 3-kinase pathway, *Cancer Res.* 65 (2005) 9807–9816.
- [37] G. Jedlitschky, L. Leier, U. Buchholz, M. Center, D. Keppler, ATP-dependent transport of glutathione-S-conjugates by the multidrug resistance-associated protein, *Cancer Res.* 54 (1994) 4833–4836.
- [38] Y.H. Kang, E.M. Lee, H.J. Youk, S.H. Kim, H.J. Lee, Y.G. Park, S.J. Lim, Potentiation by alpha-tocopheryl succinate of the etoposide response in multidrug resistance protein 1-expressing glioblastoma cells, *Cancer Lett.* 217 (2005) 181–190.
- [39] J. Yoshida, M. Mizuno, Clinical gene therapy for brain tumors: Liposomal delivery of anti-cancer molecule to glioma, *J. Neuro-Oncol.* 65 (2003) 261–267.
- [40] J.B. Massey, Interfacial properties of phosphatidylcholine bilayers containing vitamin E derivatives, *Chem. Phys. Lipids* 109 (2001) 157–174.
- [41] A.S. Janoff, C.L. Kurtz, R.L. Jablonski, S.R. Minchey, L.T. Boni, S.M. Gruner, P.R. Cullis, L.D. Mayer, M.J. Hope, Characterization of cholesterol hemisuccinate and alpha-tocopherol hemisuccinate vesicles, *Biochim. Biophys. Acta* 941 (1988) 165–175.
- [42] M.Z. Lai, N. Duzgunes, F.C. Szoka, Effects of replacement of the hydroxyl group of cholesterol and tocopherol on the thermotropic behavior of phospholipid-membranes, *Biochemistry* 24 (1985) 1646–1653.
- [43] L.T. Boni, W.R. Perkins, S.R. Minchey, L.E. Boleak, S.M. Gruner, P.R. Cullis, M.J. Hope, A.S. Janoff, Polymorphic phase-behavior of alpha-tocopherol hemisuccinate, *Chem. Phys. Lipids* 54 (1990) 193–203.
- [44] K. Kogure, S. Hamada, M. Kizaki, H. Takemasa, A. Tokumura, I. Suzuki, K. Fukuzawa, Structural characteristic of terminal dicarboxylic moiety required for apoptogenic activity of alpha-tocopheryl esters, *Biochim. Biophys. Acta* 1672 (2004) 93–99.
- [45] A. Basu, B. Grossie, M. Bennett, N. Mills, V. Imrhan, Alpha-tocopheryl succinate (alpha-TOS) modulates human prostate LNCaP xenograft growth and gene expression in BALB/c nude mice fed two levels of dietary soybean oil, *Eur. J. Nutr.* 46 (2007) 34–43.
- [46] L.V. Ramanathapuram, J.J. Koble, D. Bearss, C.M. Payne, K.T. Trevor, E.T. Akporiaye, Alpha-tocopheryl succinate sensitizes established tumors to vaccination with non-matured dendritic cells, *Cancer Immunol. Immunother.* 53 (2004) 580–588.
- [47] K. Kogure, S. Manabe, S. Hama, A. Tokumura, K. Fukuzawa, Potentiation of anti-cancer effect by intravenous administration of vesiculated alpha-tocopheryl hemisuccinate on mouse melanoma in vivo, *Cancer Lett.* 192 (2003) 19–24.
- [48] X.W. Teng, N.M. Davies, C. Fukuda, R.L. Good, M.W. Fariss, Pharmacokinetics and tissue distribution of alpha-tocopheryl succinate formulations following intravenous administration in the rat, *Biopharm. Drug Dispos.* 26 (2005) 195–203.
- [49] R.B. Greenwald, Z.H. Choe, J. McGuire, C.D. Conover, Effective drug delivery by PEGylated drug conjugates, *Adv. Drug Deliv. Rev.* 55 (2003) 217–250.
- [50] H.J. Youk, E. Lee, M.K. Choi, V.J. Lee, J.H. Chung, S.H. Kim, C.H. Lee, S.J. Lim, Enhanced anticancer efficacy of alpha-tocopheryl succinate by conjugation with polyethylene glycol, *J. Control. Release* 107 (2005) 43–52.
- [51] D.J. Ireland, H.T. Kissick, M.W. Bellharz, Alpha-tocopheryl succinate: toxicity and lack of anti-tumor activity in immuno-competent mice, *Food Chem. Toxicol.* 46 (2008) 508–512.
- [52] A. Sharma, U.S. Sharma, Liposomes in drug delivery: progress and limitations, *Int. J. Pharm.* 154 (1997) 123–140.
- [53] R.D. Hofheinz, S.J. Gnad-Vogt, U. Beyer, A. Hochhaus, Liposomal encapsulated anti-cancer drugs, *Anti-Cancer Drugs* 16 (2005) 691–707.
- [54] S. Koudelka, P. Turánek Knotigová, J. Mašek, Z. Korvasová, M. Škrabalová, J. Ploková, J. Bartheldyová, J. Turánek, Liposomes with high encapsulation capacity for paclitaxel: preparation, characterisation and in vivo anticancer effect, *J. Pharm. Sci.* 99 (2010) 2309–2319.
- [55] S. Koudelka, J. Turanek, Liposomal paclitaxel formulations, *J. Control. Release* 163 (2012) 322–334.
- [56] M. Tattersall, S. Clarke, Developments in drug delivery: implications for cancer care, *Curr. Opin. Oncol.* 15 (2003) 293–299.
- [57] S.B. Kulkarni, G.V. Betageri, M. Singh, Factors affecting microencapsulation of drugs in liposomes, *J. Microencapsul.* 12 (1995) 229–246.
- [58] T.M. Allen, C. Hansen, Pharmacokinetics of stealth versus conventional liposomes – effect of dose, *Biochim. Biophys. Acta* 1068 (1991) 133–141.
- [59] P.S. Uster, T.M. Allen, B.E. Daniel, C.J. Mendez, M.S. Newman, G.Z. Zhu, Insertion of poly(ethylene glycol) derivatized phospholipid into pre-formed liposomes results in prolonged in vivo circulation time, *FEBS Lett.* 386 (1996) 243–246.
- [60] M.C. Woodle, D.D. Lasic, Sterically stabilized liposomes, *Biochim. Biophys. Acta* 1113 (1992) 171–199.
- [61] F. Yuan, M. Dellian, D. Fukumura, M. Leunig, D.A. Berk, V.P. Torchilin, R.K. Jain, Vascular permeability in a human tumor xenograft – molecular-size dependence and cutoff size, *Cancer Res.* 55 (1995) 3752–3756.
- [62] P. Sapra, T.M. Allen, Ligand-targeted liposomal anti-cancer drugs, *Prog. Lipid Res.* 42 (2003) 439–462.
- [63] P.J. Quinn, Localization of vitamin E in membranes, in: P.J. Quinn, V.E. Kagan (Eds.), *Subcellular Biochemistry: Fat-Soluble Vitamins*, Plenum Press Inc., New York, 1998, pp. 319–343.
- [64] P.J. Quinn, Is the distribution of alpha-tocopherol in membranes consistent with its putative functions? *Biochem. Mosc.* 69 (2004) 58–66.
- [65] J. Villalain, F.J. Aranda, J.C. Gomez-Fernandez, Calorimetric and infrared spectroscopic studies of the interaction of alpha-tocopherol and alpha-tocopheryl acetate with phospholipid-vesicles, *Eur. J. Biochem.* 158 (1986) 141–147.
- [66] G. Neupert, P. Polewski, M. Marikiewicz, P. Walejko, S. Witkowski, K. Polewski, Partition of tocopheryl glucopyranoside into liposome membranes studied by fluorescence methods, *Biophys. Chem.* 146 (2010) 92–97.
- [67] S. Koudelka, J. Masek, J. Neuzil, J. Turanek, Lyophilised liposome-based formulations of alpha-tocopheryl succinate: preparation and physico-chemical characterization, *J. Pharm. Sci.* 99 (2010) 2434–2443.
- [68] Y. Asai, Structural differences in aqueous dispersions of alpha-tocopheryl acetate and phosphatidylcholine upon varying their molar fractions, *Pharmazie* 59 (2004) 849–853.
- [69] K. Kawakami, Y. Nishihara, K. Hirano, Liposome/emulsion transition induced by alpha-tocopheryl acetate, *Langmuir* 15 (1999) 7454–7460.
- [70] L.M. Crowe, J.H. Crowe, A. Rudolph, C. Womersley, L. Appd, Preservation of freeze-dried liposomes by trehalose, *Arch. Biochem. Biophys.* 242 (1985) 240–247.
- [71] J.A. Zhang, G. Anyarambhatla, L. Ma, S. Ugwu, T. Xuan, T. Sardone, I. Ahmad, Development and characterization of a novel Cremophor (R) EL free liposome-based paclitaxel (LEP-ETU) formulation, *Eur. J. Pharm. Biopharm.* 59 (2005) 177–187.
- [72] S. Hama, S. Utsumi, Y. Fukuda, K. Nakayama, Y. Okamura, H. Tsuchiya, K. Fukuzawa, H. Harashima, K. Kogure, Development of a novel drug delivery system consisting of an antitumor agent tocopheryl succinate, *J. Control. Release* 161 (2012) 843–851.
- [73] X.B. Gu, J.L. Schwartz, X.W. Pang, Y.F. Zhou, D.A. Sirosi, R. Sridhar, Cytotoxicity of liposomal alpha-tocopheryl succinate towards hamster cheek pouch carcinoma (HCP-1) cells in culture, *Cancer Lett.* 239 (2006) 281–291.
- [74] H. Harar, J. Gorin, H. Shmeeda, A. Gabizon, Characterization of a liposomal formulation of alpha-tocopherol succinate for cancer therapy, *Ann. Oncol.* 18 (2007) 38.

- [75] H. Karanth, R.S.R. Murthy, pH-sensitive liposomes – principle and application in cancer therapy, *J. Pharm. Pharmacol.* 59 (2007) 469–483.
- [76] S. Simoes, J.N. Moreira, C. Fonseca, N. Duzgunes, M.C.P. deLima, On the formulation of pH-sensitive long circulation times, *Adv. Drug Deliv. Rev.* 56 (2004) 947–965.
- [77] H. Iizumoto, E. Kanaoka, K. Hirano, pH-Sensitive liposomes composed of tocopherol hemisuccinate and of phosphatidylethanolamine including tocopherol hemisuccinate, *Biochim. Biophys. Acta* 1213 (1994) 343–348.
- [78] H. Xu, Y.H. Deng, K.Q. Wang, D.W. Chen, Preparation and characterization of stable pH-sensitive vesicles composed of alpha-tocopherol hemisuccinate, *AAPS PharmSciTech* 13 (2012) 1377–1385.
- [79] V. Knight, N.V. Koshkina, J.C. Waldrep, B.C. Giovannella, B.E. Gilbert, Anticancer effect of 9-nitrocampothecin liposome aerosol on human cancer xenografts in nude mice, *Cancer Chemother. Pharmacol.* 44 (1999) 177–186.
- [80] N.V. Koshkina, B.E. Gilbert, J.C. Waldrep, A. Seryshev, V. Knight, Distribution of camptothecin after delivery as a liposome aerosol or following intramuscular injection in mice, *Cancer Chemother. Pharmacol.* 44 (1999) 187–192.
- [81] K.A. Lawson, K. Anderson, M. Simmons-Menchaca, J. Atkinson, L.Z. Sun, B.G. Sanders, K. Kline, Comparison of vitamin E derivatives alpha-TEA and VES in reduction of mouse mammary tumor burden and metastasis, *Exp. Biol. Med.* 229 (2004) 954–963.
- [82] K.A. Lawson, K. Anderson, M. Menchaca, J. Atkinson, L.Z. Sun, V. Knight, B.E. Gilbert, C. Conti, B.G. Sanders, K. Kline, Novel vitamin E analogue decreases syngeneic mouse mammary tumor burden and reduces lung metastasis, *Mol. Cancer Ther.* 2 (2003) 437–444.
- [83] K. Anderson, K.A. Lawson, M. Simmons-Menchaca, L.Z. Sun, B.G. Sanders, K. Kline, Alpha-TEA plus cisplatin reduces human cisplatin-resistant ovarian cancer cell tumor burden and metastasis, *Exp. Biol. Med.* 229 (2004) 1169–1176.
- [84] P. Latimer, M. Menchaca, R.M. Snyder, W.P. Yu, B.E. Gilbert, B.G. Sanders, K. Kline, Aerosol delivery of liposomal formulated paclitaxel and vitamin E analog reduces murine mammary tumor burden and metastases, *Exp. Biol. Med.* 234 (2009) 1244–1252.
- [85] K.A. Lawson, K. Anderson, R.M. Snyder, M. Simmons-Menchaca, J. Atkinson, L.Z. Sun, A. Bandyopadhyay, V. Knight, B.E. Gilbert, B.G. Sanders, K. Kline, Novel vitamin E analogue and 9-nitro-campothecin administered as liposome aerosols decrease syngeneic mouse mammary tumor burden and inhibit metastasis, *Cancer Chemother. Pharmacol.* 54 (2004) 421–431.
- [86] S.B. Riedel, S.M. Fischer, B.G. Sanders, K. Kline, Vitamin E analog, alpha-tocopherol ether-linked acetic acid analog, alone and in combination with celecoxib, reduces multiplicity of ultraviolet-induced skin cancers in mice, *Anti-Cancer Drugs* 19 (2008) 175–181.
- [87] S. Zhang, K.A. Lawson, M. Simmons-Menchaca, L.Z. Sun, B.G. Sanders, K. Kline, Vitamin E analog alpha-TEA and celecoxib alone and together reduce human MDA-MB-435-RL-GFP breast cancer burden and metastasis in nude mice, *Breast Cancer Res. Treat.* 87 (2004) 111–121.
- [88] H.M. Mansour, Y.S. Rhee, X.A. Wu, Nanomedicine in pulmonary delivery, *Int. J. Nanomedicine* 4 (2009) 299–319.
- [89] P. Zarogoulidis, E. Chatzaki, K. Porpodis, K. Domvri, W. Hohenforst-Schmidt, E.P. Goldberg, N. Karamanos, K. Zarogoulidis, Inhaled chemotherapy in lung cancer: future concept of nanomedicine, *Int. J. Nanomedicine* 7 (2012) 1551–1572.
- [90] N.R. Labiris, M.B. Dolovich, Pulmonary drug delivery. Part II: the role of inhalant delivery devices and drug formulations in therapeutic effectiveness of aerosolized medications, *Br. J. Clin. Pharmacol.* 56 (2003) 600–612.
- [91] N.R. Labiris, M.B. Dolovich, Pulmonary drug delivery. Part I: physiological factors affecting therapeutic effectiveness of aerosolized medications, *Br. J. Clin. Pharmacol.* 56 (2003) 588–599.
- [92] P.S. Hiremath, K.S. Soppimath, G.V. Betageri, Proliposomes of esomeprazole for improved oral delivery: formulation and in vitro evaluation using PAMPA, Caco-2 and rat intestine, *Int. J. Pharm.* 380 (2009) 96–104.
- [93] H. Li, J.H. Song, J.S. Park, K. Han, Polyethylene glycol-coated liposomes for oral delivery of recombinant human epidermal growth factor, *Int. J. Pharm.* 258 (2003) 11–19.
- [94] V. Moutardier, F. Tosini, P. Vlieghe, L. Cara, J.R. Depero, T. Clerc, Colloidal anticancer drugs bioavailabilities in oral administration models, *Int. J. Pharm.* 260 (2003) 23–38.
- [95] H. Takeuchi, Y. Matsui, H. Sugihara, H. Yamamoto, Y. Kawashima, Effectiveness of submicron-sized, chitosan-coated liposomes in oral administration of peptide drugs, *Int. J. Pharm.* 303 (2005) 160–170.
- [96] M.Z. Fiume, Final report on the safety assessment of tocopherol, tocopheryl acetate, tocopheryl linoleate, tocopheryl linoleate/oleate, tocopheryl nicotinate, tocopheryl succinate, dioleoyl tocopheryl methylsilanol, potassium ascorbyl tocopheryl phosphate, and tocophersolan, *Int. J. Toxicol.* 21 (2002) 51–116.
- [97] K. Thariki, R.P. Gangwal, A.T. Sangamwar, S. Jain, Oral delivery of anticancer drugs: challenges and opportunities, *J. Control. Release* 170 (2013) 15–40.
- [98] G.M. Maghraby, B.W. Barry, A.C. Williams, Liposomes and skin: from drug delivery to model membranes, *Eur. J. Pharm. Sci.* 34 (2008) 203–222.
- [99] A. Kato, Y. Ishibashi, Y. Miyake, Effect of egg yolk lecithin on transdermal delivery of bunazosin hydrochloride, *J. Pharm. Pharmacol.* 39 (1987) 399–400.
- [100] M. Kirjavainen, A. Urtti, I. Jaaskelainen, T.M. Suhonen, P. Paronen, R. Valjakka-Koskela, J. Kiesvaara, J. Monkkonen, Interaction of liposomes with human skin in vitro – the influence of lipid composition and structure, *Biochim. Biophys. Acta* 1304 (1996) 179–189.
- [101] R. Natsuki, Y. Morita, S. Osawa, Y. Takeda, Effects of liposome size on penetration of di-tocopherol acetate into skin, *Biol. Pharm. Bull.* 19 (1996) 758–761.
- [102] R. Rajan, S. Jose, V.P. Mukund, D.T. Vasudevan, Transferosomes – a vesicular transdermal delivery system for enhanced drug permeation, *J. Adv. Pharm. Technol. Res.* 2 (2011) 138–143.
- [103] J.Y. Fang, P.F. Liu, C.M. Huang, Decreasing systemic toxicity via transdermal delivery of anticancer drugs, *Curr. Drug Metab.* 9 (2008) 592–597.
- [104] T. Fukao, Dendritic cell-based anticancer vaccination: has it matured, *Trends Immunol.* 23 (2002) 231–232.
- [105] L.V. Ramanathapuram, T. Hahn, M.W. Graner, E. Katsanis, E.T. Akporiaye, Vesiculated alpha-tocopheryl succinate enhances the anti-tumor effect of dendritic cell vaccines, *Cancer Immunol. Immunother.* 55 (2006) 166–177.



Contents lists available at ScienceDirect

Free Radical Biology & Medicine

journal homepage: www.elsevier.com/locate/freeradbiomed

Original Contribution

Mitochondrial targeting of α -tocopheryl succinate enhances its pro-apoptotic efficacy: A new paradigm for effective cancer therapy

Lan-Feng Dong^{a,*}, Victoria J.A. Jameson^b, David Tilly^c, Lubomir Prochazka^d, Jakub Rohlena^e, Karel Valis^e, Jaroslav Truksa^e, Renata Zobalova^{a,e}, Elahe Mahdavian^f, Katarina Kluckova^e, Marina Stantic^a, Jan Stursa^g, Ruth Freeman^a, Paul K. Witting^h, Erik Norbergⁱ, Jacob Goodwin^a, Brian A. Salvatore^f, Jana Novotna^e, Jaroslav Turanek^d, Miroslav Ledvina^g, Pavel Hozak^j, Boris Zhivotovskiyⁱ, Mark J. Coster^c, Stephen J. Ralph^a, Robin A.J. Smith^b, Jiri Neuzil^{a,e,*}

^a School of Medical Science, Griffith University, Southport, QLD 4222, Australia^b Department of Chemistry, University of Otago, Dunedin, New Zealand^c Eskitis Institute for Cell and Molecular Therapies, Griffith University, Nathan, QLD, Australia^d Veterinary Research Institute, Brno, Czech Republic^e Institute of Biotechnology, Academy of Sciences of the Czech Republic, Prague, Czech Republic^f Department of Chemistry and Physics, Louisiana State University Shreveport, Shreveport, LA 71115, USA^g Institute of Biochemistry and Organic Chemistry, Academy of Sciences of the Czech Republic, Prague, Czech Republic^h Discipline of Pathology, Bosch Research Institute, Sydney Medical School, University of Sydney, Sydney, NSW, Australiaⁱ Institute of Environmental Medicine, Karolinska Institute, Stockholm, Sweden^j Institute of Molecular Genetics, Academy of Sciences of the Czech Republic, Prague, Czech Republic

ARTICLE INFO

Article history:

Received 30 December 2010

Revised 16 February 2011

Accepted 25 February 2011

Available online 12 March 2011

Keywords:

Mitochondrial targeting

Triphenyl phosphonium

Reactive oxygen species

Apoptosis, Anti-cancer agents

Free radicals

ABSTRACT

Mitochondria are emerging as intriguing targets for anti-cancer agents. We tested here a novel approach, whereby the mitochondrially targeted delivery of anti-cancer drugs is enhanced by the addition of a triphenylphosphonium group (TPP⁺). A mitochondrially targeted analog of vitamin E succinate (MitoVES), modified by tagging the parental compound with TPP⁺, induced considerably more robust apoptosis in cancer cells with a 1–2 log gain in anti-cancer activity compared to the unmodified counterpart, while maintaining selectivity for malignant cells. This is because MitoVES associates with mitochondria and causes fast generation of reactive oxygen species that then trigger mitochondria-dependent apoptosis, involving transcriptional modulation of the Bcl-2 family proteins. MitoVES proved superior in suppression of experimental tumors compared to the untargeted analog. We propose that mitochondrially targeted delivery of anti-cancer agents offers a new paradigm for increasing the efficacy of compounds with anti-cancer activity.

© 2011 Elsevier Inc. All rights reserved.

Mitochondria have become a focus of research as emerging targets for anti-cancer drugs [1–5]. We recently proposed the term “mitocans” for small compounds with anti-cancer activity that destabilize mitochondria, which results in apoptosis induction, often

selectively affecting cancer cells, and classified them into several groups according to their molecular targets and mechanism of action [6].

Mitocans from the vitamin E (VE) group, epitomized by the redox-silent α -tocopheryl succinate (α -TOS), selectively induce apoptosis in cancer cells [6–9] and suppress the growth of many types of carcinomas in preclinical models [10–14]. At the molecular level, α -TOS acts as a Bcl-2 homology domain 3 (BH3) mimetic [15], effectively sensitizing cancer cells to other drugs. More importantly, α -TOS and other apoptogenic VE analogs induce apoptosis by affecting the mitochondrial complex II (CI). The VE analogs interfere with the function of ubiquinone (UbQ) [16] as the natural acceptor for electrons generated by the succinate dehydrogenase activity of CI during conversion of succinate to fumarate [17].

Previous reports showed that adding a triphenylphosphonium (TPP⁺) group onto antioxidant compounds further enhanced their

Abbreviations: BH3, Bcl-2 homology domain 3; CI, complex II; ChIP, chromatin immunoprecipitation; DHE, dihydroethidium; DMPQ, 5,5-dimethyl-1-pyrroline N-oxide; EPR, electron paramagnetic resonance; MIM, mitochondrial inner membrane; MitoQ, mitochondrially targeted coenzyme Q; MitoVES, mitochondrially targeted vitamin E succinate; MOM, mitochondrial outer membrane; NS, nonsilencing; ROS, reactive oxygen species; SOD, superoxide dismutase; TEM, transmission electron microscopy; α -TOS, α -tocopheryl succinate; TPP⁺, triphenylphosphonium; UbQ, ubiquinone; USI, ultrasound imaging; VE, vitamin E; VES, vitamin E succinate.

* Corresponding authors at: School of Medical Science, Griffith University, Southport, QLD 4222, Australia. Fax: +61 2 555 28804.

E-mail addresses: ldong@griffith.edu.au (L.-F. Dong), j.neuzil@griffith.edu.au (J. Neuzil).

0891-5849/\$ – see front matter © 2011 Elsevier Inc. All rights reserved.
doi:10.1016/j.freeradbiomed.2011.02.032

activity by promoting their selective mitochondrial uptake driven by the mitochondrial membrane potential [18,19]. Therefore, we decided to modify mitocans, exemplified by VE succinate (VES), in a similar manner, anticipating that tagged agents accumulate in the mitochondrial inner membrane (MIM), providing a greater apoptogenic efficacy than the prototypic, untargeted α -TOS. Here we show that TPP⁺ tagging of the hydrophobic chain of apoptogenic VE analogs indeed significantly increased their efficacy in killing cancer cells, while maintaining their selectivity for malignant cells, translating into their superior anti-cancer effect. We propose this as a new paradigm of efficient cancer therapy.

Materials and methods

Cell culture and treatment

The following cell lines used in this study were obtained from the ATCC, unless specified otherwise: human T lymphoma Jurkat, Bax⁻ Jurkat, and Bax⁻/Bak⁻ Jurkat cells [20]; human mesothelioma cells Mes02, Ist-Mes, Ist-Mes-2, and MM-BI [21]; human breast cancer cells MCF7 (erbB2-low) and MDA-MB-453 (erbB2-high) and MCF7_{D09} cells with transcriptionally inactive p53 [22]; human colorectal cells HCT116; human neuroblastoma TetN21 cells [23]; human non-small-cell lung carcinoma cells H1299; human cervical cancer cells HeLa; mouse mesothelioma cells AE17 [24]; human nonmalignant mesothelial cells Met-5A; human fibroblasts A014578; rat ventricular myocyte-like cells HL1 [25]; and mouse atrial myocyte-like cells H9c2. The murine breast cancer cells NeuTL were prepared from breast carcinomas of transgenic PVB/N *c-neu* mice [26]. Jurkat cells deficient in Bak were prepared by stable transfection of parental Jurkat cells with a plasmid coding for BAK short-hairpin RNA (shRNA), and the lack of expression of Bak was verified by Western blotting (not shown). Jurkat cells were grown in the RPMI medium, and DMEM was used for other malignant and nonmalignant cell lines unless specified otherwise, supplemented with 10% fetal calf serum and antibiotics. HL1 cells, maintained in fibronectin/gelatin-coated dishes, were grown in Claycomb medium supplemented with noradrenalin [25]. The cells were exposed to mitochondrially targeted vitamin E succinate (MitoVES) and other agents prepared as will be published elsewhere.

Assessment of IC₅₀, apoptosis, and reactive oxygen species (ROS) generation

Toxicity of the various analogs toward cancer and nonmalignant cells was assessed on the basis of IC₅₀ values determined using the standard MTT assay. Apoptosis level was assessed using the annexin V/propidium iodide method [27]. Cell death was, in some cases, assessed using the crystal violet method, as follows: cells were placed into 96-well plates at 10,000 cells per well. The next day the medium

was replaced with fresh medium containing increasing concentrations of MitoVES. The crystal violet staining was performed after 24 h by fixing the cells with 2% paraformaldehyde for 30 min, washing three times with PBS, staining with 0.05% crystal violet, washing three times with PBS, and subsequently solubilizing in 1% SDS. The final absorbance measurement was determined at 595 nm using the Tecan Infinity plate reader.

Cellular ROS were detected with the probe dihydroethidium (DHE; Molecular Probes) by flow cytometry or by trapping with 5,5-dimethyl-1-pyrroline *N*-oxide (DMPO; Sigma) using electron paramagnetic resonance (EPR) spectroscopy [27]. ROS generation was also assessed using the TetN21 cells transiently transfected with pHyPer-Mito (Evrogen), a plasmid coding for the mitochondrially targeted redox sensor OxyR, which shifts its fluorescence at increased levels of hydrogen peroxide [28]. Formation of hydrogen peroxide was assessed by time-lapse analysis using confocal microscopy.

Isolation of mitochondria and gel filtration chromatography

Cells (1.2×10^8) were treated with MitoVES for various periods and harvested. The pellet was resuspended in 0.5 ml of ice-cold hypotonic fractionation buffer (25 mM Tris at pH 7.4, 2 mM EDTA, 5 mM MgCl₂, 10 mM KCl, 125 mM sucrose, 1 mM phenylmethylsulfonyl fluoride, plus a protease inhibitor cocktail) and left on ice for 10 min. The swollen cells were lysed using a glass homogenizer (Kontes Glass). The isotonicity of each sample was achieved by addition of 250 μ l of ice-cold hypertonic fractionation buffer with 0.5 M sucrose. Organelles and unbroken cells were centrifuged at 900 g for 10 min, followed by centrifugation of the supernatant at 1700 g for 5 min. The remaining supernatant was then centrifuged at 15,000 g for 10 min and the mitochondrial pellet lysed in a buffer comprising 25 mM Hepes, pH 7.5, 0.3 M NaCl, and 2% Chaps. The mitochondrial lysate was centrifuged at 19,000 g for 5 min and loaded onto the Superdex-200 10/300 preparation grade column (separation range ~600–10 kDa; Amersham Biosciences) equilibrated with the 2% Chaps lysis buffer (see above). Proteins were eluted at 0.3 ml/min and fractions of 0.5 ml collected and mixed with 3 \times Laemmli reducing sample buffer and boiled. The samples were then analyzed by SDS-PAGE followed by Western blotting for Bax and Bak.

RT-PCR and qPCR

The amount of target mRNA was assessed by RT-PCR and qPCR. Total RNA was isolated using the Aurum RNA Total Mini Kit including the DNase treatment step (Bio-Rad) and reverse-transcribed using the Revertaid First Strand cDNA Synthesis Kit (Fermentas) according to the manufacturer's instructions (1–5 μ g total RNA per 20 μ l reaction mixture). RT-PCR was carried out using the standard procedure. For qPCR, cDNA corresponding to 12 ng starting total RNA was diluted

Table 1
Primers used for qPCR and RT-PCR.

Gene	Primers	
	Forward	Reverse
BCL-2	5'-GCTCATGCTCTGGAGAGCG-3'	5'-GGGCGCTACAGTTCACAA-3'
BCL-X ₂	5'-GGGATG GGGTAAACTG GGGT-3'	5'-CAAAAGTATCCAGCCCG-3'
MCL-1	5'-TAA GGA GAA ACG GACT GCG-3'	5'-ACCAGCTCTACTCCAGCAA-3'
BAX	5'-TCCCGATCGCTTGAGACA-3'	5'-CGGGTTTCATCCAGGATCC-3'
BAK	5'-GCTATGACTCAGAGTTCAGACCA-3'	5'-CAATTGATGCCACTCTCAACAG-3'
BAD	5'-CAACCA GCAGCAGCCATCAT-3'	5'-AAA CTGTCACATCTCCCG-3'
BID1	5'-AGCTCA GGAACACAGCCGGT-3'	5'-GACATCA CGGAGCAAGCA-3'
BID2	5'-GATGAGCTGAGACTGATGG-3'	5'-CACTGTCCGAGCTCATGAA-3'
BIM	5'-GACATTTCTCTCTGGCTG-3'	5'-CCACCGGAGGCATCTTCTG-3'
NOXA	5'-TGTA GTTGGCATCTCCCGC-3'	5'-CTCGACTTCCAGCTCTGCTG-3'
PUMA	5'-CCAACGTGAGCACTAGCCT-3'	5'-ACAGGATTCCAGTCTGGCC-3'
PO	5'-TCGACAATGGCAGCATCTAC-3'	5'-ATCCGCTCCACAGCAAGG-3'

with water to 4.5 μ l, 0.5 μ l of the combined 10 μ M forward and reverse primers was added, and, finally, 5 μ l of 2 \times SYBR Green JumpStart Taq Ready Mix (Sigma) was added, and the reaction was carried out on a Bio-Rad CFX96 real-time thermal cycler using three-step PCR (98 $^{\circ}$ C for 5 s, 60 $^{\circ}$ C for 15 s, 72 $^{\circ}$ C for 25 s) for 40 cycles followed by melting curve analysis. Primers were designed on the intron/exon boundaries to prevent DNA amplification and are listed in Table 1. *P0* was used as the housekeeping gene.

Western blotting

Proteins in whole-cell lysates and cytosolic, nuclear, and mitochondrial fractions, prepared by standard methods, were separated using SDS–polyacrylamide gel electrophoresis before Western blotting was performed. Antibodies for the following proteins were used: Cyt c, Smac/Diablo, Bax, Bcl-x_l, Bim L, Bim EL, Puma, Cox4, FoxO1, Mst1, phospho-Mst1 (Thr183) (Cell Signaling), AIF, Bcl-2, p53, p21^{Waf1/Cip1} (Santa Cruz Biotechnology), Mcl-1 (BD Pharmingen), Bak (Upstate Biotechnology), and Noxa (Alexis). Anti-actin IgG or anti-lamin IgG (both Sigma) was used as a loading control.

Analysis of Bak and Bax conformational changes

MitoVES-induced exposure of the N-terminus of Bak was assessed using the epitope-specific antibody directed against the amino acid sequence 1–57 of the Bak protein (clone Ab-1; Calbiochem) [29]. The active conformation of Bax was estimated using anti-Bax IgG (clone 6A7; Sigma) directed against amino acids 12–24 [30]. Cells grown in a six-well plate were exposed to MitoVES, harvested, fixed with 0.25% paraformaldehyde, incubated with the primary antibody diluted 1:50 in digitonin (100 μ g/ml in PBS) and with FITC-labeled secondary antibody diluted 1:75 in digitonin–PBS, and analyzed by flow cytometry using “live gating” to exclude cellular debris.

Chromatin immunoprecipitation (ChIP) analysis

The ChIP assay was performed using a ChIP kit with enzymatic shearing (Active Motif). Briefly, nuclei isolated from 4×10^7 MitoVES-treated or control Jurkat cells were sheared for 10 min using the Enzymatic Shearing Cocktail, precleared by incubation with protein G beads to reduce the nonspecific background (10 μ l of precleared chromatin was saved as input), and incubated overnight at 4 $^{\circ}$ C on a rotator with anti-FoxO1 IgG or a nonspecific rabbit IgG (both from Santa Cruz Biotechnology) as a negative control. In the next step, the antibody complexes were precipitated by incubation with protein G beads and after several washes eluted by a solution of SDS and NaHCO₃. Nucleoprotein complexes were then de-cross-linked by an overnight incubation at 65 $^{\circ}$ C and treatment with RNase A and proteinase K. The resulting DNA molecules were purified using the DNA purification minicolumns. Five microliters of purified DNA was used for RT-PCR and qPCR analysis with the following NOXA primers: forward 5'-TGATGTTGGCATCTCCGCGC-3', reverse 5'-CTCGACTTC-CAGCTCTGCTG-3'.

Knockdown of Bak and Mst1

The Bak protein was knocked down stably using shRNA. In brief, Jurkat cells were electroporated (10^7 cells with 40 μ g DNA; 1 pulse of 325 V for 15 ms; ECM830 square electroporator from BTX) in the presence of a plasmid carrying *BAK* or nonsilencing (NS) shRNA (SureSilencing shRNA plasmid; SA Biosystems). Four different shRNA plasmids were used. Before transfection, the plasmid's original puromycin resistance was replaced with Geneticin resistance. The cells were selected for ~1 month in the presence of 1 mg/ml G418, tested by Western blotting, and used in experiments.

MCF7 cells were transfected using the FUGENE transfection reagent and the anti-human *Mst1* Mission shRNA cloned into the pLKO.1-puro vector, clone NM_006282.2-829s1c1 (Sigma). The shRNA sequence was CCGGCCAGAGCTATGGTCAGATAACCTCGAGGT-TATCTGACCATAGCTCTGGTTTITG. Cells were selected with 0.5 μ g/ml puromycin for 2 weeks and individual clones chosen on the basis of diminished expression of *Mst1* assessed by qPCR and Western blotting.

Confocal microscopy

For acquisition of images with the fluorescently labeled MitoVES (MitoVES-F), NeuTL cells were grown on coverslips, stained with MitoTracker red (Molecular Probes), incubated with 10 μ M MitoVES_{1-5-F} for 30 min, counterstained with Hoechst 33342, and inspected in a confocal microscope.

Transmission electron microscopy (TEM)

Cells were subjected to TEM after being processed as described [27].

Mouse tumor experiments

The FVB/N *c-neu* mice carrying the rat *HER-2/neu* proto-oncogene driven by the MMTV promoter on the H-2^d FVB/N background [18] were used in this study. The animals form spontaneous ductal breast carcinomas at the age of 7–9 months. Tumors were also established in immunocompromised, athymic (Balb c *nu/nu*) mice by injecting HCT116 cells subcutaneously at 5×10^6 cells per animal.

Animals were regularly checked by ultrasound imaging (USI) using the Vevo770 USI apparatus equipped with the 30- μ m resolution RMV708 scan head (VisualSonics) as detailed elsewhere [16,31–33]. As soon as tumors reached ~40 mm³, the animals were treated by ip injection of 1–2 μ mol MitoVES or 10–15 μ mol α -TOS in corn oil containing 4% EtOH every 3–4 days. Control mice were injected with an equal volume (100 μ l) of the excipient only. Progression of tumor growth was assessed every 3–4 days using USI, which enables three-dimensional reconstruction of tumors and precise quantification of their volume.

All animal experimentation was performed according to the guidelines of the Australian and New Zealand Council for the Care and Use of Animals in Research and Teaching and was approved by the Griffith University Animal Ethics Committee.

Statistics

All data shown are mean values of three independent experiments (unless stated otherwise) \pm SD. Statistical significance was assessed using Student's *t* test and differences were considered significant at $p < 0.05$.

Results

We synthesized and tested several compounds derived from VE by the addition of the TPP⁺ group (Fig. 1). MitoVES, the prototypic mitochondrially targeted racemic VES with an 11-carbon linker between the chromanol and the TPP⁺ group induced >90% apoptosis at 50 μ M within 3–10 h in various cancer cell lines and was still apoptogenic at 1 μ M (Fig. 2A). Equimolar α -TOS or VES (an analog of α -TOS lacking methyl groups in the aliphatic chain) was significantly less efficient than MitoVES (Fig. 2B). Addition of TPP⁺ to the succinyl moiety of α -TOS via a four-carbon spacer (VES4TPP) did not enhance the activity of the parental agent (Fig. 2B), suggesting that in this case TPP⁺, while mediating mitochondrial delivery, masked the free carboxyl group essential for the apoptogenic activity of the compound

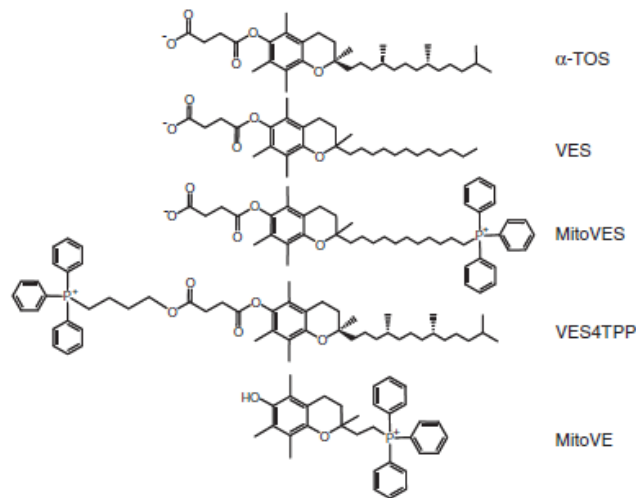


Fig. 1. Structures of compounds used in the study.

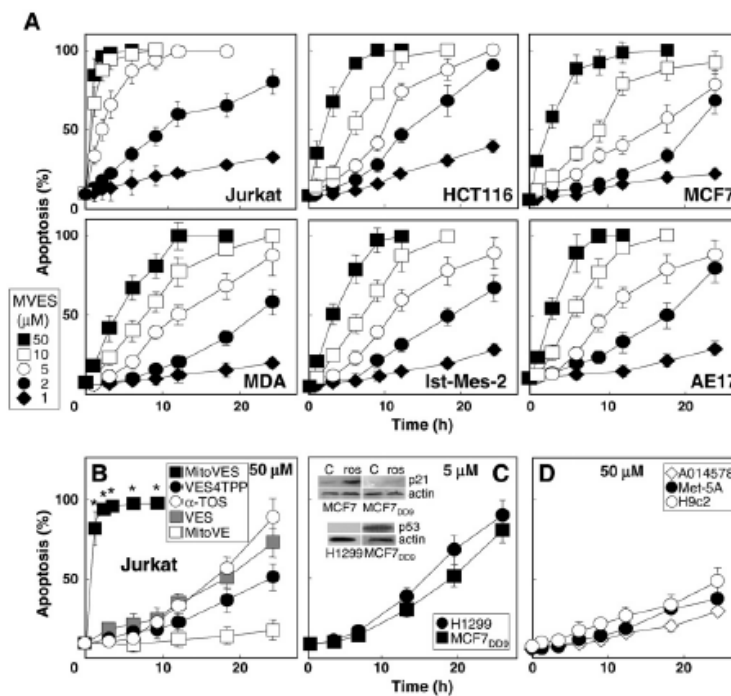


Fig. 2. MitoVES causes efficient apoptosis selectively in malignant cells. (A) The malignant Jurkat, HCT116, MCF7, MDA-MB-453 (MDA), Ist-Mes-2, and AE17 cells were exposed to MitoVES at the concentrations shown. (B) Jurkat cells were exposed to 50 μ M MitoVES, VES4TPP, α -TOS, VES, or MitoVE. (C) H1299 and MCF7_{ccc} cells were exposed to 5 μ M MitoVES. (D) Fibroblasts A014578, the nonmalignant mesothelial cells Met5A, and the cardiomyoblasts H9c2 were exposed to 50 μ M MitoVES. In all cases, the cells were evaluated for apoptosis level. The inset in (C) shows the expression of p21 in MCF7 and MCF7_{ccc} cells, after exposure to roscovitine (ros; a drug promoting p53 stability), and p53 in H1299 and MCF7_{ccc} cells. The data shown are mean values \pm SD ($n = 3$), the images are representative of three independent experiments. * $p < 0.05$, significant difference between cells treated with MitoVES and cells treated with the other agents.

Table 2
IC₅₀ values of VE analogs for apoptosis in various malignant and nonmalignant cell lines.

Cell type ^a	MitoVES	α -TOS	VES 4TPP
Jurkat	0.48 ± 0.1	18 ± 3 ^b	21 ± 5
MM-BI	1.4 ± 0.3	26 ± 4	n.d. ^c
Mes02	2.4 ± 0.5	29 ± 5	28 ± 6
Ist-Mes	2.2 ± 0.3	24 ± 5	n.d.
Ist-Mes-2	1.1 ± 0.25	21 ± 3	n.d.
AE17	3.1 ± 0.7	33 ± 5	n.d.
MCF7	1.9 ± 0.5	22 ± 4	19 ± 3
MCF7 _{D09}	2.8 ± 0.9	25 ± 6	n.d.
MDA-MB-453	3.3 ± 0.7	28 ± 5	n.d.
NeuTL	2.1 ± 0.5	65 ± 8	n.d.
HCT116	2.8 ± 0.8	31 ± 6	n.d.
H1299	4.9 ± 1.1	39 ± 6	n.d.
HeLa	0.44 ± 0.07	69 ± 7.5	n.d.
A014578	67 ± 10.4	>100	>100
H9c2	54 ± 8.3	>100	>100
HL1	48 ± 6.2	>100	>100
Met5A	21 ± 4.5	69 ± 8	n.d.

^a Jurkat cells were treated at 0.5 × 10⁷/ml, other cell lines were treated at ~60% confluency.

^b The IC₅₀ values were derived from viability curves using the MTT viability assay and are expressed in micromolar.

^c n.d., not determined.

[12,34]. VE with a short aliphatic chain, modified by addition of TPP⁺ to its phytol chain (MitoVE) [18], did not show any effect (Fig. 2B). The data for MitoVES and α -TOS showed similar trends in the IC₅₀ values,

with MitoVES more effective (>10- to 30-fold) than its untagged counterpart (Table 2). MitoVES efficiently killed lung cancer cells deficient in p53 (line H1299) as well as breast cancer cells with transcriptionally inactive p53 (line MCF7_{D09}) (Fig. 2C), demonstrating p53 independence of apoptosis induced by the agent. Compared to cancer cells, MitoVES was much less effective in inducing apoptosis in nonmalignant cells, such as fibroblasts, cardiomyoblasts, and non-malignant mesothelial cells (Fig. 2D). The IC₅₀ values of MitoVES for nonmalignant cell types were 1–2 orders of magnitude greater than those determined for the cancer cells (Table 2). Collectively, these results demonstrate considerably greater potency of MitoVES for killing in a range of cancer cell types compared to α -TOS without loss of selectivity.

Mitochondrial ROS production is emerging as an important mechanism in the mitocan-induced activation of apoptosis to kill cancer cells [35]. EPR spectroscopy and flow cytometry revealed ROS accumulation in the presence of MitoVES, which was suppressed by the mitochondrially targeted UbQ (MitoQ) [18] or superoxide dismutase (SOD) (Figs. 3A and B). The two antioxidants also suppressed MitoVES-induced apoptosis (Fig. 3B), implicating a role for ROS in the process. To assess the kinetics of ROS generation, we utilized the Tet21N neuroblastoma cells transiently transfected with pHyPer-dMito. The level of mitochondrial hydrogen peroxide was monitored using a confocal microscope that allows real-time visualization of ROS generation. Exposure of the cells to MitoVES resulted in the appearance of ROS within 5 min after addition of the

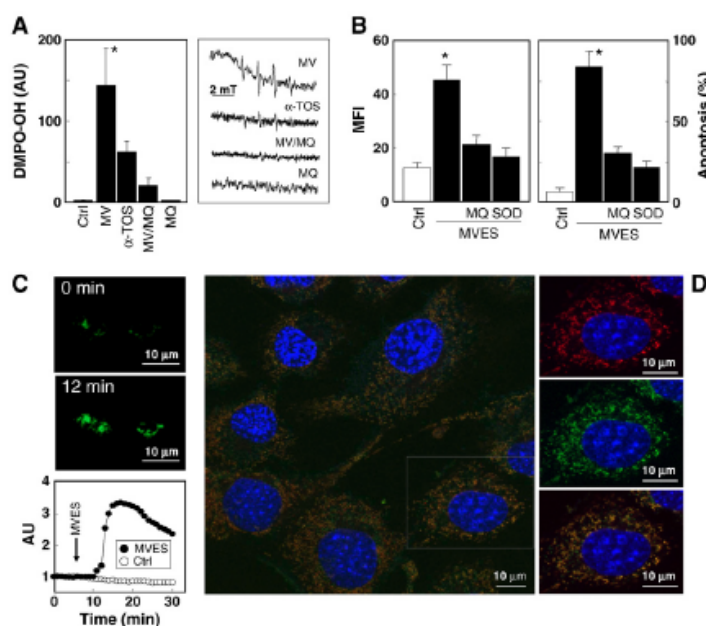


Fig. 3. MitoVES triggers rapid generation of ROS and localizes to mitochondria. (A, B) Jurkat cells were exposed to 50 μ M α -TOS or 5 μ M MitoVES (MV) for 2 h (A, left) or 12 h (B, right), in the presence of MitoQ (MQ; 2 μ M, 1 h pretreatment) or SOD (PEG-SOD, 750 units/mg, cotreatment) and assessed for ROS generation by (A) EPR spectroscopy and DMPO (AU, arbitrary units) or (B) flow cytometry (mean fluorescence intensity, MFI) and DHE (left) and for (B) apoptosis induction (right). (C) Tet21N cells grown on coverslips were transiently transfected with pHyPer-dMito and placed on the stage of a live-confocal microscope. After 16 h, 10 μ M MitoVES was added to the cells. Images were taken each 1 min and the level of green fluorescence was evaluated. The arrow indicates addition of MitoVES. The images show green fluorescence in two cells before and 12 min after addition of MitoVES. (D) NeuTL cells were labeled with MitoTracker red, supplemented with 20 μ M MitoVES-F, and observed by confocal microscopy. The image on the left shows a cluster of cells labeled with Hoechst 33342 to visualize nuclei (blue), MitoTracker red to show mitochondria (red), and MitoVES-F to indicate the localization of the agent (green). The boxed cells are shown in detail on the right with blue/red, blue/green, and an overlay of the three colors. The data shown are mean values \pm SD ($n = 3$); the images are representative of three independent experiments. The data in (C) are derived from one experiment representative of three independent experiments. * $p < 0.05$, significant difference between cells treated with MitoVES only and the other treatments as well as control cells.

stressor, indicating a very rapid response (Fig. 3C). The structure of MitoVES, i.e., its TPP⁺ group, determines the accumulation of the agent in mitochondria because of the high negative potential at the matrix face of the MIM. To unequivocally document mitochondrial localization of the agent, we prepared its green fluorescent analog, MitoVES-F, by attachment of fluorescein to the free carboxylic group of MitoVES. The murine breast cancer NeuT cells pretreated with MitoTracker red were then supplemented with MitoVES-F and inspected by confocal microscopy. Fig. 3D documents that MitoVES accumulated predominantly in mitochondria, validating our strategy of targeting anti-cancer compounds to mitochondria by tagging them with the cationic TPP⁺ group.

We next tested whether apoptosis induced by MitoVES is dependent on mitochondria. Exposure of Jurkat cells and their Bax^{-/-} counterparts to 50 μ M α -TOS or 5 μ M MitoVES resulted in efficient apoptosis in the two sublines. In contrast, when the Bax^{-/-}/Bak^{-/-} cells were exposed to α -TOS, cell death was delayed by ~24 h, and MitoVES was ineffective (Fig. 4A). TEM revealed delayed morphological changes characteristic of cell death in Bax^{-/-}/Bak^{-/-} Jurkat cells exposed to α -TOS but no morphological alterations were evident in the presence of MitoVES (Fig. 4B), demonstrating Bax/Bak dependence of the process. The apoptosis-resistant Bax^{-/-}/Bak^{-/-} Jurkat cells responded to MitoVES with ROS accumulation (Fig. 4C), indicating that ROS generation precedes apoptosis. In the wild-type Jurkat cells, the MitoVES-induced apoptosis was suppressed by a caspase-9 but not a caspase-8 inhibitor (Fig. 4D), further pointing to mitochondria as critical mediators of MitoVES-triggered apoptosis.

Given the role of Bax/Bak in MitoVES-induced apoptosis, we next studied the mechanism of mitochondrial outer membrane (MOM) channel formation. First, we observed cytosolic translocation of cytochrome c (Cyt c) and Smac/Diablo, and mitochondrial translocation of Bax, in Jurkat cells exposed to MitoVES, but not in their Bax^{-/-}/Bak^{-/-} counterparts. No mobilization of the AIF protein was observed in either cell line (Fig. 5A). Gel filtration of mitochondrial lysates of

MitoVES-treated cells followed by Western blotting indicated formation of oligomers of Bak and Bax (Fig. 5B). However, only the Bak protein revealed a significant conformational change, as shown by conformation-specific antibodies using flow cytometry. Moreover, the substantial conformational change in the Bak protein was seen already at 4 h, at which stage no change was observed for the Bax protein (Fig. 5C). Because this suggests a major role for Bak in the mitochondrial channel formation, we prepared Bak-deficient Jurkat cells by stable transfection of the parental cells with BAK shRNA. Of the four shRNAs used, three efficiently suppressed the Bak protein, with BAK shRNA3 showing no expression of Bak, and BAK shRNA1 and shRNA4 showing low levels of the protein (Fig. 5D, inset). The sublines with low or no expression of Bak were relatively resistant to MitoVES, in particular at its lower concentrations (Fig. 5D), indicating the dominant role of Bak in apoptosis induced by MitoVES.

We next tested the level of Bcl-2 family proteins critical for modulation of mitochondrial homeostasis in cells exposed to MitoVES, of which the BH3-only proteins Noxa and Puma showed increased mRNA levels, but only Noxa was increased at the protein level (Figs. 6A and B). In addition, levels of the Mcl-1 protein decreased in MitoVES-treated cells (Fig. 6B). The model for Bak channel formation involves upregulation of Noxa, which displaces the antiapoptotic protein Mcl-1 or Bcl-x_L from its association with Bak [36]. Because MitoVES induces Noxa expression, we studied its transcriptional regulation and found that it was controlled by the FoxO1 protein, as evidenced by the ChIP analysis (Fig. 6C). This assay, coupled with qPCR analysis, revealed 2.3-fold higher binding of the FoxO1 protein to the NOXA promoter in MitoVES-exposed cells. We also found that MitoVES activated the Mst1 kinase, which is known to phosphorylate FoxO1 (Fig. 6D) [37,38]. To further document a role for Mst1 in apoptosis induced by MitoVES, we knocked down the protein in MCF7 cells and exposed them to the agent. Fig. 6E reveals that lowering the level of the kinase Mst1 caused higher resistance of the

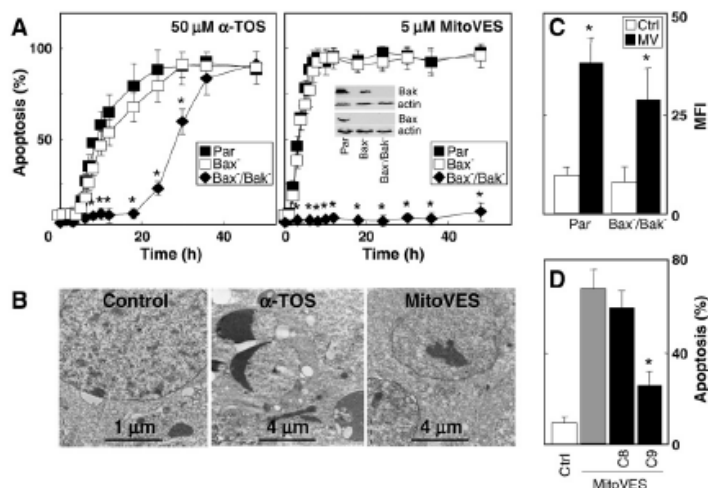


Fig. 4. MitoVES-induced apoptosis is dependent on mitochondria. Parental (Par), Bax^{-/-}, and Bax^{-/-}/Bak^{-/-} Jurkat cells were exposed to 50 μ M α -TOS or 5 μ M MitoVES for (A) the times shown, (B) 36 h, or (C) 2 h and assessed for (A) apoptosis induction, (B) morphological alterations using TEM, and (C) ROS accumulation using flow cytometry. The inset in (A) shows the status of the expression of the Bax and/or Bak proteins in parental, Bax^{-/-}, and Bax^{-/-}/Bak^{-/-} cells. (D) Jurkat cells were exposed to 5 μ M MitoVES in the presence of 25 μ M caspase-8 inhibitor (IETD-FMK) or caspase-9 inhibitor (LEHD-FMK) for 5 h and assessed for apoptosis level. The data shown are mean values \pm SD (n=3); the images are representative of three independent experiments. *p < 0.05, significant difference between Bax^{-/-}/Bak^{-/-} cells and parental or Bax^{-/-} cells (A), cells treated with MitoVES and control cells (C), and cells treated with MitoVES in the presence or absence of a caspase-9 inhibitor (D).

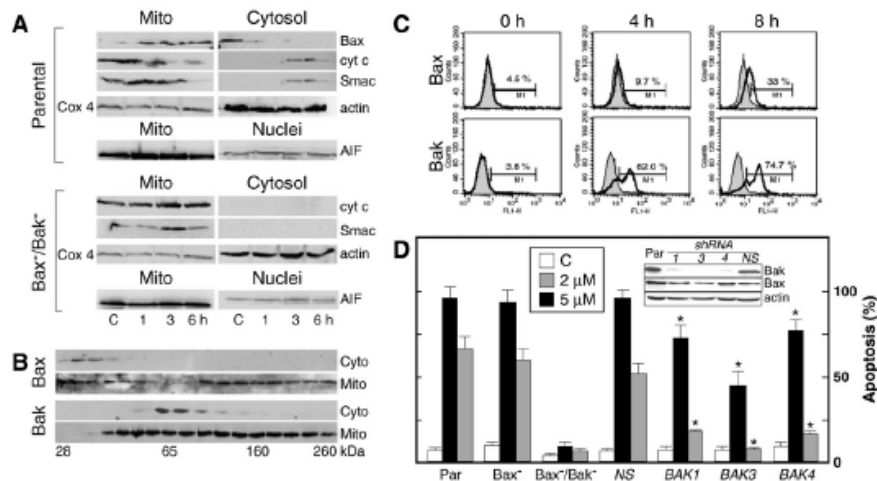


Fig. 5. MitoVES-dependent apoptosis is mediated preferentially by Bak. (A) Parental and Bak^{+/}/Bak⁻ Jurkat cells were exposed to 5 μM MitoVES; fractionated into the mitochondrial, cytosolic, and nuclear compartments; and assessed by Western blotting for the levels of Bax, Cyt c, Smac/Diablo, and AIF. (B) Jurkat cells were exposed to 5 μM MitoVES for 12 h, the mitochondrial fraction was lysed and subjected to fractionation by size-exclusion chromatography, and the individual fractions were probed by Western blotting for the presence of the Bax or Bak proteins. (C) Jurkat cells were treated with 5 μM MitoVES and assessed for conformational change of the Bax or Bak protein using specific antibodies and flow cytometry. (D) Parental, Bak⁻, and Bak^{+/}/Bak⁻ Jurkat cells and Jurkat cells stably transfected with NS or BAK shRNAs with different expression of the Bak protein (inset) were exposed to 2 or 5 μM MitoVES for 9 h and assessed for apoptosis. The data shown are mean values ± SD (n = 3); the images are representative of three independent experiments. *p < 0.05, significant difference between the level of apoptosis in cells stably transfected with BAK shRNA and with NS shRNA exposed to the same level of MitoVES.

cells to killing by MitoVES. These results suggest a role for the Mst1/FoxO1/Noxa axis in the formation of a Bak channel in cancer cells exposed to MitoVES.

To assess the effect of MitoVES on tumors, two preclinical models were used, including the FVB/N *c-neu* transgenic mice with spontaneous ductal breast carcinomas driven by high expression of the oncogene *erbB2* in mammary epithelial cell [26] and nude mice with xenografts derived from HCT116 cells. After tumors reached ~40 mm³, the mice were treated by ip administration of either MitoVES at 1–2 μmol or α-TOS at 15 μmol per animal per dose. Fig. 7 shows that MitoVES very efficiently suppressed carcinoma growth (>90% in both models), in some cases causing tumors to diminish in size. This effect of MitoVES was much stronger than when α-TOS was used at 10-fold higher concentration, indicating the superior effect of the mitochondrially targeted analog.

Discussion

In industrialized countries, the number of deaths from neoplastic disease has surpassed the number of deaths from cardiovascular pathologies [39], and the future trend is grim [40]. While there has been some success in treating certain types of cancer, many recur and/or remain highly resilient to therapy and some, such as malignant mesothelioma, offer virtually no therapeutic modality [41]. Frequent mutations make the cancer landscape highly heterogeneous, allowing escape from immune tumor surveillance or therapeutic interventions, as well as making the design of targeted anti-cancer drugs challenging [42–44]. The widely used conventional anti-cancer therapies utilize mechanisms such as DNA intercalation, microtubule disruption, or folate inhibition and can offer great benefits, especially in combination. However, the same therapies show relatively little specificity for cancer cells and often result in severe side effects. On the other hand, the specific and successful agents such as Trastuzumab or Imatinib are targeted at certain subsets of cancers and are therefore suitable only for selected groups of patients.

This study investigated the possibility of delivering drug candidates specifically to mitochondria because these organelles are emerging as new and intriguing targets for cancer treatment [1–5,45]. It is becoming increasingly clear that cancer cell mitochondria differ from those in normal cells [4,46]. Our previous work has shown that the mitocan α-TOS, targeting the mitochondrial respiratory chain to induce apoptosis [16], selectively eliminates cancer cells while leaving noncancerous cells relatively unaffected [6]. α-TOS, however, is a partially hydrophobic molecule with the potential to be distributed not only to mitochondria but also to other (sub)cellular membranes. We therefore hypothesized that specific mitochondrial delivery could increase both its efficacy and its specificity. Recent pioneering work by Murphy and Smith [47] revealed a strategy for achieving efficient delivery of hydrophobic redox-active compounds to mitochondria, more specifically to the MIM, by joining the cationic TPP⁺ group onto the aliphatic chain of agents such as UbQ or VE, considerably enhancing their bioactivity. Incorporation of cationic lipophilic compounds such as MitoVES inside tumor mitochondria is favored by the development of a higher electrical gradient (by 20–60 mV vs normal cell mitochondria), which in turn promotes increased lipophilic cation accumulation [48].

Modification of mitocans from the VE group by conjugation with TPP⁺, exemplified by the mitochondrially targeted VES MitoVES, enhanced the apoptogenic efficacy of the parental compound by a factor of 1–2 logs. Preferential mitochondrial localization of MitoVES was documented by inspecting cells preloaded with MitoTracker red and incubated with a fluorescent variant of the agent, using confocal microscopy. We documented that mitochondria were crucial for apoptosis induced by MitoVES, in particular by showing that Bak⁻/Bak^{+/} Jurkat cells were resistant to MitoVES, while they were still induced into cell death, albeit delayed, when exposed to α-TOS.

Of particular importance is the rapid action with which MitoVES induces the cascade of reactions ultimately resulting in apoptosis. This is evidenced by time-lapse imaging of the generation of ROS in cancer cells transiently transfected with pHyPer-dMito, whose product, the

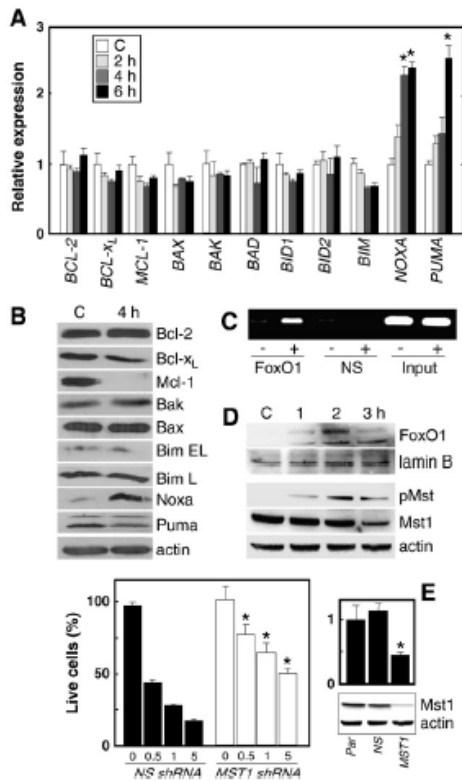


Fig. 6. MitoVES-induced apoptosis involves transcriptional upregulation of the Noxa protein. Jurkat cells were exposed to 5 μ M MitoVES and assessed for the level of Bcl-2 family members by (A) qPCR and (B) Western blotting. (C) Jurkat cells were exposed to 5 μ M MitoVES for 2 h and the nuclear fraction was analyzed for binding of FoxO1 protein to the NOXA promoter using the ChIP assay. (D) Jurkat cells were exposed to MitoVES at 5 μ M for the times indicated, and Western blotting was used to probe the nuclear fraction for the level of the FoxO1 protein and the whole cell lysate for the levels of total Mst1 and pMst. (E) MCF7 cells stably transfected with NS or MST1 shRNA were exposed to MitoVES for 24 h at the concentrations shown (μ M) and assessed for cell death using the crystal violet method. The graph on the right shows the level of expression of MST1 transcript assessed by qPCR in parental (Par) cells and in cells transfected with NS or MST1 shRNA. The Western blot indicates substantial lowering of the Mst1 protein in the transfected cells (upper row) with actin used as a loading control (lower row). The data shown in (A) are mean values \pm SD ($n=3$), the data in (E) mean values \pm SEM ($n=3$); the images are representative of three independent experiments. * $p<0.05$, significant difference between gene expression in control and MitoVES-treated cells in (A), between the percentage of live cells in corresponding samples of cells transfected with NS and MST1 shRNA in (E) (left) and between the level of mRNA in parental cells or cells transfected with NS shRNA and in cells transfected with MST1 shRNA in (E) (right).

redox-sensitive OxyR, increases fluorescence in the presence of hydrogen peroxide [28], and exposed to MitoVES. We observed an increase in the green fluorescence of the cells 5 min after addition of the drug, which was followed by its plateau some 5–10 min later (Fig. 3C). Our experiments also clearly show that the oxidative burst induced in cancer cells by MitoVES is due to the fact that this drug targets CII [49], as we similarly found earlier for α -TOS. Importantly, too, we observed that an uncoupler considerably lowered apoptosis induced by MitoVES but not α -TOS in cancer cells [49], documenting

the importance of mitochondrial potential for the targeting of MitoVES into the MIM.

Our results also help explain the molecular mechanism of the drug-induced MOM pore formation and indicate that in response to MitoVES, the Bak protein has a major role in forming channels in the MOM. This is supported by results revealing that Bax-deficient cancer cells are susceptible to MitoVES, whereas Bak-deficient cells are rather resistant to the agent. Formation of the Bak channel in cells exposed to MitoVES is probably regulated by the BH3-only protein Noxa. This process involves the transcriptional factor FoxO1, which itself is activated by the Mst1 kinase, in agreement with the published literature [37,38]. We propose that Noxa liberates Bak from its association with the antiapoptotic proteins such as Mcl-1, allowing efficient formation of the Bak channel [36]. This mechanism is further supported by the observed reduction in levels of the Mcl-1 protein detected in cells treated with MitoVES, which is compatible with reports showing proteasomal degradation of Mcl-1 occurring after the levels of Noxa become elevated [50] and is compatible with our recent findings for α -TOS [51].

To document the superior anti-cancer effects of MitoVES, we utilized two models of cancer, i.e., the FVB/N *c-neu* transgenic mice with spontaneous formation of HER2-high breast carcinomas [26] and nude mice with HCT116 cell-derived xenografts. Using the very precise USI-based evaluation of the tumor kinetics, MitoVES was >10-fold more efficient than the nontargeted α -TOS in both models [2,12,16]. This indicates a high anti-cancer efficacy of MitoVES that can be ascribed to its preferential association with mitochondria.

We conclude that MitoVES is an epitome of a new type of mitocans with a high level of apoptogenic activity. Hence, in principle, direct targeting of cancer cell mitochondria by MitoVES is expected to overcome many of the problems found with other drug targets for which genetic analyses have revealed a large degree of complexity and heterogeneity among individual types of cancer [52,53], with the implied difficulty in finding relatively universal treatments without serious side effects. The safety and eligibility of MitoVES as a payload with lipophilic TPP⁺ as a pharmacophor for delivery are accentuated by phase I/II trials in which MitoQ-containing TPP⁺ was used to treat patients with neurological disorders or hepatitis with no adverse effects even after more than 1 year of supplementation [54,55]. Thus, we propose that MitoVES, and the mitochondrially targeted mitocans in general, shows the potential to fulfill the promise of broadly applicable, selective anti-cancer drugs. Clinical trials using MitoVES are, therefore, imminent.

Acknowledgments

We thank Dr. I. Scheffler for the B1 and B9 cells, Dr. H. Rabinowich for the Bak^{-/-} and Bax^{-/-}/Bak^{-/-} Jurkat cells, Dr. E. Gottlieb for the HCT116^{DDP-GFP} cells, Dr. W. Claycomb for the HL1 cells, Dr. B. Vojtesek for the H1299 and MCF7^{DDP} cells, Dr. D. Spitz and Dr. F. Domann for pCR3.1-SDHC, Dr. J. Hancock for pEGFP-C3-H-Ras, and Dr. K. Lukyanov for pHyPer-dMito. This work was supported by grants from the Australian Research Council, the Cancer Council Queensland, the National Breast Cancer Foundation, the Grant Agency of the Czech Republic (204/08/0811, P301/10/1937), the Grant Agency of the Academy of Sciences of the Czech Republic (IAA500520702, KJB500970904, KAN200520703) to J.N., the Griffith Institute of Health Grant to L.F.D., the Otago University Research Grants Committee to R. A.J.S., the Swedish Research Council, the Swedish and the Stockholm Cancer Societies, the Swedish Childhood Cancer Foundation, the EC FP-6 (Chemores) and the FP-7 (Apo-Sys) programs to B.Z., the Grant Agency of the Czech Republic (GP204/09/P632) to L.P., the Grant Agency of the Academy of Sciences of the Czech Republic (200100801) to M.L., the Grant Agency of the Academy of Sciences of the Czech Republic (KJB500970904) to K.V., Grant MZE 0002716202 to J.T., and Grant P20RR016456 from the National Center

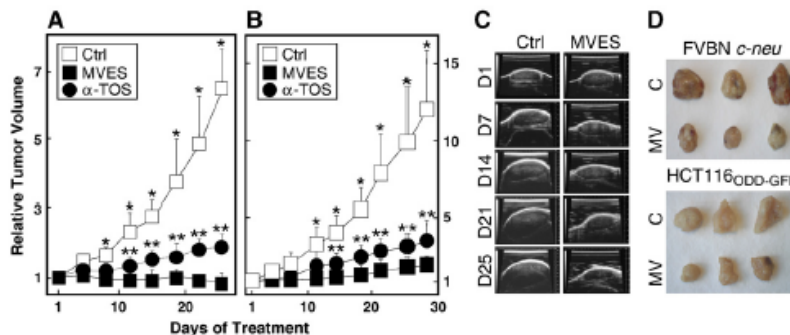


Fig. 7. MitoVES suppresses tumor progression. (A) FVB/N *c-neu* mice with breast carcinomas and (B) Balb *c nu/nu* mice with xenografts derived from HCT 116 cells were treated by ip injection of 1–2 μ mol MitoVES or 15 μ mol α -TOS per mouse every 3–4 days, and tumors were visualized and their volume was quantified using USI. (C) Representative ultrasound images of tumors of control and MitoVES-treated *c-neu* mice acquired at the days shown. (D) Images of tumors excised at the end of the experiment. Data from USI quantification of tumor volume are mean values \pm SD ($n=5-7$). Typical photographic images are shown from each sample. * $p < 0.05$, significant difference between control and MitoVES-treated animals, ** $p < 0.05$, significant difference in the tumor volumes of animals treated with MitoVES and α -TOS.

for Research Resources to E.M. and B.A.S. This work forms parts of the Ph.D. theses of R.F., R.Z., K.K., V.J.A.J., and M.S. L.P. was supported in part by funds from the Apoptosis Research Group, Griffith University (Southport, QLD, Australia).

References

- Fantin, V. R.; Leder, P. Mitochondriotoxic compounds for cancer therapy. *Oncogene* **25**:4787–4797; 2006.
- Fulda, S.; Galluzzi, L.; Kroemer, G. Targeting mitochondria for cancer therapy. *Nat. Rev. Drug Discov.* **9**:447–464; 2010.
- Gogvadze, V.; Orrenius, S.; Zhivotovskiy, B. Mitochondria in cancer cells; what is so special about them? *Trends Cell Biol.* **18**:165–173; 2008.
- Moreno-Sánchez, R.; Rodríguez-Enríquez, S.; Marín-Hernández, A.; Saavedra, E. Energy metabolism in tumor cells. *FEBS J.* **274**:1393–1418; 2007.
- Trachootham, D.; Alexandre, J.; Huang, P. Targeting cancer cells by ROS-mediated mechanisms: a radical therapeutic approach? *Nat. Rev. Drug Discov.* **8**:579–591; 2009.
- Neuzil, J.; Dong, L. F.; Ramanathapuram, L.; Hahn, T.; Chladova, M.; Wang, X. F.; Zabolova, R.; Prochazka, L.; Gold, M.; Freeman, R. E., et al. Vitamin E analogues: a novel group of mitocans, anti-cancer agents that act by targeting mitochondria. *Mol. Aspects Med.* **28**:607–645; 2007.
- Neuzil, J.; Weber, T.; Gellert, N.; Weber, C. Selective cancer cell killing by α -tocopherol succinate. *Br. J. Cancer* **84**:87–89; 2001.
- Yu, W.; Sanders, B. G.; Kline, K. RRR- α -Tocopherol succinate-induced apoptosis of human breast cancer cells involves Bax translocation to mitochondria. *Cancer Res.* **63**:2483–2491; 2003.
- Zhang, Y.; Ni, J.; Messing, E. M.; Chang, E.; Yang, C. R.; Yeh, S. Vitamin E succinate inhibits the function of androgen receptor and the expression of prostate-specific antigen in prostate cancer cells. *Proc. Natl. Acad. Sci. USA* **99**:7408–7413; 2002.
- Hahn, T.; Szabo, L.; Gold, M.; Ramanathapuram, L.; Hurlley, L. H.; Akporiaye, E. T. Dietary administration of the pro-apoptotic vitamin E analogue α -tocopheryl succinate inhibits metastatic murine breast cancer. *Cancer Res.* **66**:9374–9378; 2006.
- Malafa, M. P.; Fokum, F. D.; Mowlavi, A.; Abusief, M.; King, M. Vitamin E inhibits melanoma growth in mice. *Surgery* **131**:85–91; 2002.
- Neuzil, J.; Weber, T.; Schröder, A.; Lu, M.; Ostermann, G.; Gellert, N.; Mayne, G. C.; Olejnicka, B.; Nègre-Salvayre, A.; Sicha, M., et al. Induction of apoptosis in cancer cells by α -tocopheryl succinate: molecular pathways and structural requirements. *FASEB J.* **15**:403–415; 2001.
- Stapelberg, M.; Gellert, N.; Swettenham, E.; Tomasetti, M.; Witting, P. K.; Prompito, A.; Neuzil, J. α -Tocopheryl succinate inhibits malignant mesothelioma by disrupting the FGF autocrine loop: the role of oxidative stress. *J. Biol. Chem.* **280**:25369–25376; 2005.
- Weber, T.; Lu, M.; Andera, L.; Iahm, H.; Gellert, N.; Fariss, M. W.; Korinek, V.; Sattler, W.; Ucker, D. S.; Terman, A., et al. Vitamin E succinate is a potent novel anti-neoplastic agent with high tumor selectivity and cooperativity with tumor necrosis factor-related apoptosis-inducing ligand (TRAIL, Apo2L) in vivo. *Clin. Cancer Res.* **8**:863–869; 2002.
- Shiau, C. W.; Huang, J. W.; Wang, D. S.; Weng, J. R.; Yang, C. C.; Lin, C. H.; Li, C.; Chen, C. S. Tocopheryl succinate induces apoptosis in prostate cancer cells in part through inhibition of Bcl-2/Bcl-2 function. *J. Biol. Chem.* **281**:11819–11825; 2006.
- Dong, L. F.; Low, P.; Dyason, J.; Wang, X. F.; Prochazka, L.; Witting, P. K.; Freeman, R.; Swettenham, E.; Valis, K.; Liu, J., et al. α -Tocopheryl succinate induces apoptosis by targeting ubiquinone-binding sites in mitochondrial respiratory complex II. *Oncogene* **27**:4324–4333; 2008.
- Sun, F.; Huo, X.; Zhai, Y.; Wang, A.; Xu, J.; Su, D.; Bardam, M.; Rao, Z. Crystal structure of mitochondrial respiratory membrane protein complex II. *Cell* **121**:1043–1057; 2005.
- Kelso, G. F.; Porteous, C. M.; Gullter, C. V.; Hughes, G.; Porteous, W. K.; Ledgerwood, E. C.; Smith, R. A.; Murphy, M. P. Selective targeting of a redox-active ubiquinone to mitochondria within cells: antioxidant and antiapoptotic properties. *J. Biol. Chem.* **276**:4588–4596; 2001.
- Smith, R. A.; Porteous, C. M.; Gane, A. M.; Murphy, M. P. Delivery of bioactive molecules to mitochondria in vivo. *Proc. Natl. Acad. Sci. USA* **100**:5407–5412; 2003.
- Wang, G. Q.; Wlcekowski, E.; Goldstein, L. A.; Wang, G. Q.; Wlcekowski, E.; Goldstein, L. A.; Gastan, B. R.; Rabinowitz, A.; Gambetta, A.; Li, S.; Fang, B.; Yin, X. M.; Rabinovich, H. Resistance to granzyme B-mediated cytochrome c release in B-lymphoid cells. *J. Exp. Med.* **194**:1325–1337; 2001.
- Pass, H. I.; Stevens, E. J.; Oe, H.; Tsokos, M. G.; Abati, A. D.; Fetsch, P. A.; Mew, D. J.; Pogrebnik, H. W.; Matthews, W. J. Characteristics of nine newly derived mesothelioma cell lines. *Ann. Thorac. Surg.* **59**:835–844; 1995.
- Kotala, V.; Uldrijan, S.; Horlyk, M.; Tribusek, M.; Strnad, M.; Vojtesek, B. Potent induction of wild-type p53-dependent transcription in tumour cells by a synthetic inhibitor of cyclin-dependent kinases. *Cell. Mol. Life Sci.* **58**:1333–1339; 2001.
- Gogvadze, V.; Norberg, E.; Orrenius, D.; Zhivotovskiy, B. Involvement of Ca^{2+} and ROS in α -tocopheryl succinate-induced mitochondrial permeabilization. *Int. J. Cancer* **127**:1823–1832; 2010.
- Jackaman, C.; Bundell, C. S.; Kimmear, B. F.; Smith, A. M.; Filion, P.; van Hagen, D.; Robinson, B. W.; Nelson, D. J. IL-2 intratumoral immunotherapy enhances CD8⁺ T cells that mediate destruction of tumor cells and tumor-associated vasculature: a novel mechanism for IL-2. *J. Immunol.* **171**:5051–5063; 2003.
- Claycomb, W. C.; Lamson, N. A.; Stallworth, B. S.; Egeland, D. B.; Delcarpio, J. B.; Bahinski, A.; Izzo, N. J. HL-1 cells: a cardiac muscle cell line that contracts and retains phenotypic characteristics of the adult cardiomyocyte. *Proc. Natl. Acad. Sci. USA* **95**:2979–2984; 1998.
- Guy, C. T.; Webster, M. A.; Schaller, M.; Parsons, T. J.; Cardiff, R. D.; Muller, W. J. Expression of the neu protooncogene in the mammary epithelium of transgenic mice induces metastatic disease. *Proc. Natl. Acad. Sci. USA* **89**:10578–10582; 1992.
- Weber, T.; Dalen, H.; Andera, L.; Nègre-Salvayre, A.; Augé, N.; Sicha, M.; Lore, A.; Terman, A.; Witting, P. K.; Higuchi, M., et al. Mitochondria play a central role in apoptosis induced by α -tocopheryl succinate, an agent with anticancer activity. *Biochemistry* **42**:4277–4291; 2003.
- Belousov, V. V.; Fradkov, A. F.; Lulyanov, K. A.; Staroverov, D. B.; Shakhbazov, K. S.; Tersikh, A. V.; Lulyanov, S. Genetically encoded fluorescent indicator for intracellular hydrogen peroxide. *Nat. Methods* **3**:281–286; 2006.
- Griffiths, G. J.; Dubrez, L.; Morgan, C. P.; Jones, N. A.; Whitehouse, J.; Corfe, B. M.; Dive, C.; Hickman, J. A. Cell damage-induced conformational changes of the pro-apoptotic protein Bak in vivo precede the onset of apoptosis. *J. Cell Biol.* **144**:903–914; 1999.
- Hsu, Y. T.; Youle, R. J. Nonionic detergents induce dimerization among members of the Bcl-2 family. *J. Biol. Chem.* **272**:13829–13834; 1997.
- Dong, L. F.; Freeman, R.; Liu, J.; Zabolova, R.; Marín-Hernández, A.; Stantic, M.; Rohlena, J.; Rodríguez-Enríquez, S.; Valis, K., et al. Suppression of tumor growth in vivo by the mitocan α -tocopheryl succinate requires respiratory complex II. *Clin. Cancer Res.* **15**:1593–1600; 2009.
- Dong, L. F.; Swettenham, E.; Eliasson, J.; Wang, X. F.; Gold, M.; Medunic, V.; Stantic, M.; Low, P.; Prochazka, L.; Witting, P. K., et al. Vitamin E analogs inhibit angiogenesis by selective apoptosis induction in proliferating endothelial cells: the role of oxidative stress. *Cancer Res.* **67**:11906–11913; 2007.

- [33] Wang, X. F.; Birringer, M.; Dong, L. F.; Veprek, P.; Iow, P.; Swettenham, E.; Stantic, M.; Yuan, L. H.; Zabolova, R.; Wu, K., et al. A peptide adduct of vitamin E succinate targets breast cancer cells with high erbB2 expression. *Cancer Res.* **67**:3337–3344; 2007.
- [34] Birringer, M.; EyTrna, J. H.; Salvatore, B. A.; Neuzil, J. Vitamin E analogues as inducers of apoptosis: structure-function relationship. *Br. J. Cancer* **88**: 1948–1955; 2003.
- [35] Ralph, S. J.; Rodríguez-Enríquez, S.; Neuzil, J.; Moreno-Sánchez, R. Bioenergetic pathways in tumor mitochondria as targets for cancer therapy and the importance of the ROS-induced apoptotic trigger. *Mol. Aspects Med.* **31**:29–59; 2010.
- [36] Willis, S. N.; Chen, L.; Dawson, G.; Wei, A.; Naik, E.; Fletcher, J. I.; Adams, J. M.; Huang, D. C. Pro-apoptotic Bak is sequestered by Mcl-1 and Bcl-2, but not Bcl-2, until displaced by BH3-only proteins. *Genes Dev.* **19**:1294–1305; 2005.
- [37] Lehtinen, M. K.; Yuan, Z.; Bossa, P. R.; Yang, Y.; Villén, J.; Becker, E. R.; DiBacco, S.; de la Iglesia, N.; Gygi, S.; Blackwell, T. K.; Bonni, A. A conserved MST-FOXO signaling pathway mediates oxidative-stress responses and extends life span. *Cell* **125**:987–1001; 2006.
- [38] Oberer, P.; Geiger, K.; Ambros, P. E.; Meister, B.; Austerlechner, M. J. ROR1L1-mediated expression of Noxa and Bim induces apoptosis via the mitochondria in neuroblastoma cells. *Cell Death Differ.* **14**:534–547; 2007.
- [39] Twombly, R. Cancer surpasses heart disease as leading cause of death of all but the very elderly. *J. Natl. Cancer Inst.* **97**:330–331; 2005.
- [40] Jemal, A.; Siegel, R.; Xu, J.; Ward, E. Cancer statistics, 2010. *CA Cancer J. Clin.* **60**: 277–300; 2010.
- [41] Fennell, D. A.; Gaudino, G.; O'Byrne, K. J.; Mutti, L.; van Meerbeek, J. Advances in the systemic therapy of malignant pleural mesothelioma. *Nat. Clin. Pract. Oncol.* **5**: 136–147; 2008.
- [42] Chan, C. W.; Housseau, F. The kiss of death by dendritic cells to cancer cells. *Cell Death Differ.* **15**:58–69; 2008.
- [43] Dunn, G. P.; Bruce, A. T.; Ikeda, H.; Old, L. J.; Schreiber, R. D. Cancer immunoeediting: from immunosurveillance to tumor escape. *Nat. Immunol.* **3**:991–998; 2002.
- [44] Rodríguez-Nieto, S.; Zhivotovskiy, B. Role of alterations in the apoptotic machinery in sensitivity of cancer cells to treatment. *Curr. Pharm. Des.* **12**:4411–4425; 2006.
- [45] Neuzil, J.; Wang, X. F.; Dong, L. F.; Iow, P.; Ralph, S. J. Molecular mechanism of 'mitocan'-induced apoptosis in cancer cells epitomizes the multiple roles of reactive oxygen species and Bcl-2 family proteins. *FEBS Lett.* **580**:5125–5129; 2006.
- [46] Galluzzi, L.; Morselli, E.; Kepp, O.; Vitale, I.; Rigoni, A.; Vacchelli, E.; Michaud, M.; Zischka, H.; Castedo, M.; Kroemer, G. Mitochondrial gateways to cancer. *Mol. Aspects Med.* **31**:1–20; 2010.
- [47] Murphy, M. P.; Smith, R. Targeting antioxidants to mitochondria by conjugation to lipophilic cations. *Annu. Rev. Pharmacol. Toxicol.* **47**:629–656; 2007.
- [48] Rodríguez-Enríquez, S.; Marín-Hernández, A.; Gallardo-Pérez, J. C.; Carreño-Fuentes, L.; Moreno-Sánchez, R. Targeting of tumor energy metabolism. *Mol. Nutr. Food Res.* **33**:29–48; 2009.
- [49] Dong, L. F.; Jameson, V. J. A.; Tilly, D.; Cerny, J.; Mahdavian, E.; Marín-Hernández, A.; Hernández-Esquivel, I.; Rodríguez-Enríquez, S.; Witting, P. K.; Stantic, B., et al. Mitochondrial targeting of vitamin E succinate enhances its pro-apoptotic and anti-cancer activity via mitochondrial complex II. *J. Biol. Chem.* **286**:3717–3728; 2011.
- [50] Willis, S. N.; Fletcher, J. I.; Kaufmann, T.; van Delft, M. F.; Chen, L.; Czabotar, P. E.; Jerino, H.; Lee, E. F.; Fairlie, W. D.; Bouillet, P., et al. Apoptosis initiated when BH3 ligands engage multiple Bcl-2 homologs, not Bax or Bak. *Science* **315**:776–777; 2007.
- [51] Prochazka, L.; Dong, L. F.; Valis, K.; Freeman, R.; Ralph, S. J.; Turanek, J.; Neuzil, J. α -Tocopherol succinate causes mitochondrial permeabilization by preferential formation of Bak channel. *Apoptosis* **15**:782–794; 2010.
- [52] Jones, S.; Zhang, X.; Parsons, D. W.; Lin, J. C.; Leary, R. J.; Angenendt, P.; Mankoo, P.; Carter, H.; Kamiyama, H.; Jimeno, A., et al. Core signaling pathways in human pancreatic cancers revealed by global genomic analyses. *Science* **321**:1801–1806; 2008.
- [53] Parsons, D. W.; Jones, S.; Zhang, X.; Lin, J. C.; Leary, R. J.; Angenendt, P.; Mankoo, P.; Carter, H.; Siu, I. M.; Gallia, G. L., et al. An integrated genomic analysis of human glioblastoma multiforme. *Science* **321**:1807–1812; 2008.
- [54] Cane, E. J.; Orr, D. W.; Keogh, G. F.; Gibson, M.; Lockhart, M. M.; Frampton, C. M.; Taylor, K. M.; Smith, R. A.; Murphy, M. P. The mitochondria-targeted anti-oxidant mitoquinone decreases liver damage in a phase II study of hepatitis C patients. *Liver Int.* **30**:1019–1026; 2010.
- [55] Snow, B. J.; Rolfe, F. L.; Lockhart, M. M.; Frampton, C. M.; O'Sullivan, J. D.; Fung, V.; Smith, R. A.; Murphy, M. P.; Taylor, K. M. A double-blind, placebo-controlled study to assess the mitochondria-targeted antioxidant MitoQ as a disease-modifying therapy in Parkinson's disease. *Mov. Disord.* **25**:1670–1674; 2010.

α -Tocopheryl succinate causes mitochondrial permeabilization by preferential formation of Bak channels

Lubomir Prochazka · Lan-Feng Dong ·
Karel Valis · Ruth Freeman · Stephen J. Ralph ·
Jaroslav Turanek · Jiri Neuzil

Published online: 9 March 2010
© Springer Science+Business Media, LLC 2010

Abstract Mitocans are drugs selectively killing cancer cells by destabilizing mitochondria and many induce apoptosis via generation of reactive oxygen species (ROS). However, the molecular events by which ROS production leads to apoptosis has not been clearly defined. In this study with the mitocan α -tocopheryl succinate (α -TOS) the role of the Bcl-2 family proteins in the mechanism of malignant cell apoptosis has been determined. Exposure of several different cancer cell lines to α -TOS increased expression of the Noxa protein, but none of the other proteins of the Bcl-2 family, an event that was independent of the cellular p53 status. α -TOS caused a profound conformational change in the pro-apoptotic protein, Bak, involving oligomerization in all cell types, and this also applied to the Bax protein, but only in non-small cell lung cancer cells. Immunoprecipitation studies indicated that α -TOS activates the two BH1-3 proteins, Bak or Bax, to form high molecular weight complexes in the mitochondria. RNAi knockdown revealed that Noxa and Bak are required for α -TOS-induced apoptosis, and the role of Bak was

confirmed using Bak- and/or Bax-deficient cells. We conclude that the major events induced by α -TOS in cancer cells downstream of ROS production leading to mitochondrial apoptosis involve the Noxa-Bak axis. It is proposed that this represents a common mechanism for mitochondrial destabilization activated by a variety of mitocans that induce accumulation of ROS in the early phases of apoptosis.

Keywords Vitamin E succinate · Apoptosis · Bak · Noxa · Mitochondria · Permeabilization

Abbreviations

BH3	Bcl-2 homology domain-3
CII	Complex II
Cox IV	Cytochrome c oxidase subunit IV
DHE	Dihydroethidium
ECL	Enhanced chemiluminescence
MOM	Mitochondrial outer membrane
RNAi	RNA interference
ROS	Reactive oxygen species
Q-PCR	Quantitative real-time PCR
siRNA	Short interfering RNA
STS	Staurosporin
α -TEA	α -Tocopheryloxyacetic acid
α -TOS	α -Tocopheryl succinate
TRAIL	TNF-related apoptosis-inducing ligand
VE	Vitamin E

L. Prochazka (✉) · J. Turanek
Veterinary Research Institute, Hudcova 70, 621 00 Brno,
Czech Republic
e-mail: lubomir.pr@gmail.com

L.-F. Dong · R. Freeman · J. Neuzil (✉)
Apoptosis Research Group, School of Medical Science and the
Griffith Institute of Health and Medical Research, Griffith
University, Parklands Avenue, Southport, QLD 4222, Australia
e-mail: j.neuzil@griffith.edu.au

K. Valis · J. Neuzil
Molecular Therapy Group, Institute of Biotechnology,
Czech Academy of Sciences, Prague, Czech Republic

S. J. Ralph
Genomic Research Centre, School of Medical Science,
Griffith University, Southport, QLD, Australia

Introduction

α -Tocopheryl succinate (α -TOS) is a tumor-selective drug activating intrinsic apoptosis [1, 2] by targeting the

mitochondrial complex II (CII; succinate dehydrogenase) triggering subsequent production of reactive oxygen species (ROS) [3, 4]. The importance of ROS accumulation in apoptosis induction by α -TOS was established in that higher levels of apoptosis in cancer cell lines were directly associated with greater ROS production [5]. In addition, antioxidants, such as the mitochondrially targeted coenzyme Q, suppressed the anti-cancer cell toxicity of the vitamin E (VE) analog [6, 7].

Several mechanisms have been suggested to explain α -TOS induced apoptosis, mostly involving mitochondrial destabilization [8]. It has also been reported that the VE analog acts as a Bcl-2 homology-3 (BH3) mimetic, since it interacted with the BH3 domain of the Bcl-2 family proteins, disrupting the interaction between Bak, Bcl-x_L, and Bcl-2 in prostate cancer cells [9]. Another report suggested α -TOS induced translocation of Bax into mitochondria in breast cancer cells, although the mechanism of this process was not defined [10]. These results led to the proposal that ROS production induced the dimerization of Bax, followed by its mitochondrial mobilization [11], perhaps helping to explain the events occurring in α -TOS-challenged cells [8, 12]. However, the precise mechanisms of mitochondrial translocation and/or activation of apoptogenic Bcl-2 family proteins triggered by α -TOS remained unclear.

A hallmark of mitochondrial apoptosis is the permeabilization of the mitochondrial outer membrane (MOM) involving two Bcl-2 protein family members, the BH3 domain proteins, Bak and Bax with at least one of these two proteins shown to be necessary for pore formation in the MOM [13–15]. In most cases, MOM permeabilization is triggered by activation of BH3 proteins, either by increasing their expression or via the BH3-only proteins Noxa, Puma, Bim, or Bid. It has been proposed that the BH3 proteins are liberated from their heterodimeric association with members of the pro-survival Bcl-2 family or they can be directly activated [16–18]. From this point of view, it is of interest that α -tocopheryloxyacetic acid (α -TEA), an ether analog of VE, was previously shown to kill breast cancer cells via a pathway involving upregulation of the BH3-only protein, Noxa [19].

Activation of the Bak and Bax proteins corresponds to conformational changes, which involve exposure of the N-terminus of these proteins [20, 21] and their subsequent oligomerization in the MOM [22]. ROS-dependent dimerization of Bax protein via disulfide bond formation has also been proposed as one mechanism for Bax activation [11]. According to another hypothesis, the BH3 proteins may polymerize at their ends or interact with lipids of the MOM, with ensuing MOM destabilization or lipid pore formation [13, 23–25]. In addition to Bax and Bak, the BH3 domain protein, Bok (also known as Diva) can also cause MOM permeabilization. However, since Bok is

restricted to a small number of malignant tissues, it is irrelevant for most types of cancer cells [26].

Because individual types of cancers are complex and can differ considerably in their array of DNA mutations, harboring different sets of genetic changes [27, 28], it will be very unlikely to cure cancer with drugs targeted to only a few gene products or single pathways involved in tumor survival [29]. The importance of mitocans, epitomized by VE analogs (in particular the prototypic α -TOS), as anti-cancer agents that target mitochondria to trigger apoptosis [3, 4, 8, 12] is that mitochondrial function is a universal cellular requirement. Thus, mitochondria are prime targets and transmitters of apoptosis which if selectively activated in cancer cells would provide an effective treatment for a variety of different tumors. It is this imperative which makes it critical to understand in greater detail the molecular mechanisms by which VE analogs cause permeabilization of the MOM, a paradigm that may be utilized for efficient therapy of many different cancers [30, 31].

Materials and methods

Cell culture and treatment

Jurkat T lymphoma cells, the Bak⁻/Bax⁻ and Bax⁻ Jurkat cells [32], the p53-deficient H1299 non-small cell lung cancer cell line [33], as well as the MCF7 breast adenocarcinoma cell line and its p53-transcriptionally inactive sub-line (MCF7_{DD9}) [34] were grown in RPMI-1640 medium supplemented with antibiotics and 10% FBS. Jurkat cells were treated with α -TOS (Sigma) (for structure see Fig. 1) at 5×10^5 cells per ml, and the adherent H1299, MCF7 and MCF7_{DD9} cells at 80–90% confluency. α -TOS was always freshly prepared in ethanol as a stock solution that was added to the cell cultures so that the concentration of ethanol in the medium did not exceed 0.1% (v/v). In some cases, the cells were pre-incubated (1 h) with 1 μ M mitochondrially targeted coenzyme Q (MitoQ; for structure, see Fig. 1) [35].

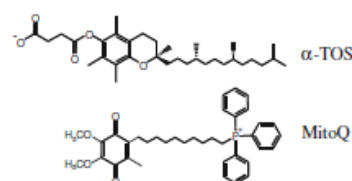


Fig. 1 Structures of α -tocopheryl succinate (α -TOS) and mitochondrially targeted coenzyme Q (MitoQ)

Western blot analysis

The following antibodies were used: anti-Bak IgG (clone Ab-1) (Calbiochem); anti-Bak IgG (NT) and anti-Bax IgG (NT) (both from Upstate Biotechnology); anti-Bax IgG (6A7), anti-p53 IgG (DO-1) (both from Sigma); anti-Noxa IgG (Alexis); anti-Mcl-1 IgG (clone 22) (BD Pharmingen); anti-actin IgG (C-2), anti-cytochrome c IgG (A-8), anti-Bcl-2 IgG (C-2), anti-Bid IgG (5C9), anti-Bad IgG (C-7) were all from Santa Cruz; anti-Bcl-x_L IgG, anti-Bim IgG, anti-Cox IV IgG and anti-Puma IgG were from Cell Signaling).

To obtain whole cell lysates, cells were centrifuged at $300 \times g$ for 5 min and washed twice with ice-cold PBS. The pellet was resuspended in whole cell lysis buffer (10 mM TRIS at pH 7.4, 1 mM NaF, 1 mM Na₃VO₄, 1 mM PMSF, 0.1% SDS, 1% Triton X-100, plus protease inhibitor cocktail), frozen, thawed and sonicated. Aliquots were used to estimate the level of total protein using the BCA method (Pierce). The samples were then diluted in loading buffer and boiled for 4 min. Proteins were resolved by SDS-PAGE and transferred to PVDF or nitrocellulose membranes (GE Healthcare). After probing with a specific primary antibody and horseradish peroxidase-conjugated secondary antibody, the bands were detected by the enhanced chemiluminescence (ECL) kit or the Advanced ECL kit (both GE Healthcare) using either a gel documentation system (Bio-Rad) or X-ray film (AGFA).

Isolation of mitochondria and gel filtration chromatography

Cells (1.2×10^8) were left untreated or treated with an appropriate concentration of α -TOS, human recombinant TNF-related apoptosis-inducing ligand (TRAIL) [36] or staurosporine (STS) for different periods, harvested and washed twice with ice-cold PBS. The final pellet was resuspended in 500 μ l of ice-cold hypotonic fractionation buffer (25 mM Tris at pH 7.4, 2 mM EDTA, 5 mM MgCl₂, 10 mM KCl, 125 mM sucrose, 1 mM PMSF, plus protease inhibitor cocktail), and left on ice for 10 min. The swollen cells were broken using a glass homogenizer (Kontes Glass Co.). The isotonicity of each sample was achieved by addition of 250 μ l of ice-cold hypertonic fractionation buffer containing 500 mM sucrose. Organelles and unbroken cells were centrifuged at $900 \times g$ for 10 min, followed by centrifugation of the supernatant at $1,700 \times g$ for 5 min. The remaining supernatant was then centrifuged at $15,000 \times g$ for 10 min and the mitochondrial pellet lysed in a buffer comprising 25 mM HEPES, pH 7.5, 300 mM NaCl and 2% CHAPS. The mitochondrial lysate was centrifuged at $19,000 \times g$ for 5 min and

loaded onto the Superdex-200 10/300 Preparation Grade column (Amersham Biosciences). The column was equilibrated with the 2% CHAPS lysis buffer (see above). The proteins were eluted at 0.3 ml/min, and fractions of 0.5 ml were collected and mixed with 3-times concentrated Laemmli reducing sample buffer and boiled. The samples were then analyzed by SDS-PAGE and western blotting.

Assessment of apoptosis and ROS accumulation

Apoptosis was evaluated by flow cytometry (FACS Calibur, BD Bioscience) using the annexin-V FITC and propidium iodide method, essentially as described [2]. ROS accumulation was assessed using the fluorescent probe dihydroethidium (DHE) essentially as detailed elsewhere [2].

Analysis of Bak and Bax conformational changes

Drug-induced exposure of the N-terminus of Bak was assessed using the epitope-specific antibody directed against the amino acid sequence 1-57 of the Bak protein (clone Ab-1) [37]. The active conformation of Bax was estimated using anti-Bax IgG (clone 6A7) directed against amino acids, 12-24, which only cross-reacts with the active/mitochondrially localized Bax protein domain [20]. Cells grown in a 6-well plate were exposed to various concentration of α -TOS, STS (positive control for inducing Bak and Bax conformational changes) [37, 38] or TRAIL, after which they were harvested, washed with ice-cold PBS, and fixed with 0.25% paraformaldehyde. The cells were then washed with ice-cold PBS and incubated with primary antibody diluted 1:50 in digitonin (100 μ g/ml of PBS) for 30 min, which was followed by a 30 min incubation with an FITC-labeled secondary antibody diluted 1:75 in digitonin-PBS, and analyzed by flow cytometry using 'live gating' to exclude cellular debris.

Immunoprecipitation

Pelleted mitochondria were resuspended in 1 ml of immunoprecipitation lysis buffer (1% CHAPS, 150 mM NaCl, protease inhibitors cocktail, 25 mM HEPES, pH 7.4), left on ice for 30 min before centrifugation at $16,000 \times g$ for 3 min. A 20 μ l aliquot of the supernatant was used for the BCA protein level assay while the rest of the lysate was pre-cleared with 1 μ l of mouse serum (protein concentration 4 mg/ml) and 20 μ l of Protein G-conjugated agarose beads (Santa Cruz) at 4°C for 30 min. The Protein G agarose beads with the bound

immunoglobulins were spun down at $1,000 \times g$ for 5 min and the remaining supernatant comprised pre-cleared lysate. The lysate was then diluted to the final protein concentration of 300 $\mu\text{g}/\text{ml}$. A 1 ml aliquot of the lysate was incubated with 2 μg of mouse monoclonal anti-Mcl-1 or rabbit polyclonal anti-Bcl-x_L or anti-Bim IgG at 4°C for 3 h under gentle agitation followed by addition of 20 μl of Protein G-conjugated agarose beads and incubated overnight at 4°C. The Protein G beads were then pelleted at $1,000 \times g$ for 5 min, washed 4 times with the immunoprecipitation lysis buffer, resuspended in 40 μl of 1.5 times concentrated reducing sample loading buffer and boiled for 5 min. The samples were then centrifuged to remove the Protein G beads and the supernatant was loaded onto a gel for SDS/PAGE. Co-immunoprecipitated proteins bound to Mcl-1, Bcl-x_L or Bim were detected using specific antibodies and western blotting. Pure lysis buffer handled in parallel with the real samples, pre-cleared and containing antibodies was used as a negative control.

Quantitative real-time PCR

Total RNA was extracted with the TRI reagent (MRC) and reverse-transcribed to cDNA using oligo dT primers and the M-MLV reverse transcriptase (Invitrogen). Quantitative real-time PCR (Q-PCR) was performed using the LightCycler 480 instrument (Roche) operated using 95°C for 15 min; 50x: 95°C for 15 s, 58°C for 30 s, 72°C for 30 s and melting analysis was performed from 60 to 95°C. Each PCR reaction mixture of 10 μl contained 5 μl of the SYBRgreen Master Mix (Invitrogen), 0.5 μl cDNA, and forward and reverse primers at the concentration of 0.8 μM . Relative quantification of target genes expression was performed using the formula described elsewhere [39]. β -Actin was used as a house-keeping gene.

PCR primers were as follows; *Noxa*: forward 5'-CTG TCC GAG GTG CTC CAG TT-3' and reverse 5'-TCC TGA GTT GAG TAG CAC AC-3'; *Puma*: forward 5'-CCA AAC GTG ACC ACT AGC CT-3' and reverse 5'-ACA GGA TTC ACA GTC TGG GC-3'; *Mcl-1*: forward 5'-TAA GGA CAA AAC GGG ACT GG-3' and reverse 5'-ACC AGC TCC TAC TCC AGC AA-3'; *Bcl-2*: forward 5'-TGC ACC TGA CGC CCT TCA C-3' and reverse 5'-AGA CAG CCA GGA GAA ATC AAA CAG-3'; *Bcl-x_L*: forward 5'-GTA AAC TGG GGT CGC ATT GT-3' and reverse 5'-TGC TGC ATT GTT CCC ATA GA-3'; *Bak*: forward 5'-GCT ATG ACT CAG AGT TCC AGA CCA-3' and reverse 5'-CAA TTG ATG CCA CTC TCAAAC AG-3'; *Bax*: forward 5'-AGA GGA TGA TTG CCG CCG T-3' and reverse 5'-CAA CCA CCC TGG TCT TGG ATC-3'; *Bim*: forward 5'-GCA CAT TTC CCT CTG GCC TG-3' and reverse 5'-CCC ACG GGA GGC ATA CTT TCT G-3'

β -actin: forward 5'-AAT CTG GCA CCA CAC CTT CT-3' and reverse 5'-AG CAC AGC CTG GATAGC AAC-3'.

RNA interference

H1299 and MCF7 cells were modified by silencing the expression of the Noxa, Bim, Mcl-1, Bax and Bak proteins using short interfering RNA (siRNA) essentially as described elsewhere [40]. In brief, cells were grown at 30% confluence in the absence of antibiotics and incubated with individual siRNAs pre-incubated with Lipofectamine-2000-supplemented OptiMEM medium. *Bak* siRNA, *Bim* siRNA and *Mcl-1* siRNA (Ambion), and *Bax* siRNA (Santa Cruz Biotechnology) were used at 60 nM, *Noxa* siRNA (Santa Cruz Biotechnology) at 20 nM and the control (scrambled) siRNA (Santa Cruz Biotechnology) at 20 or 60 nM. After 7 h, the OptiMEM medium was replaced with complete RPMI medium without antibiotics. After an additional 24 h, the cells were transferred into a 96-well flat bottom test plate or into 12-well plates and grown for another 24 h, and assessed for the levels of individual proteins and for cytotoxicity induced by α -TOS.

MTT cytotoxicity test

The MTT colorimetric assay [41] was used to assess the cytotoxic effects of α -TOS on siRNA-transfected cells. MTT (Sigma) was dissolved in PBS at 2.5 mg/ml and sterile-filtered. 20 μl of the MTT solution were added into each well of the 96-well plate with siRNA-transfected cells treated with various concentrations of α -TOS for 24 h. The plates were then incubated at 37°C in 5% CO₂ for 3 h, 100 μl of 10% SDS was then added into each well, and the plates were then stored overnight in the dark at room temperature, after which they were analysed for absorbance at 540 nm using a microplate reader (Synergy II; Biotek). All experiments were performed in triplicate. The value of IC₅₀ and the 95% confidence interval of the mean were calculated using GraphPad PRISM 5.00 software (GraphPad Software) and non-linear regression to establish dose-response inhibitory curves. The data sets were compared by Extra sum-of-squares F test based on traditional statistical hypothesis testing.

Statistics

The acquired data, unless otherwise stated, were analyzed using the GraphPad PRISM 5.00 software. The data represents the mean \pm SEM of three independent experiments. The symbol ** denotes $P < 0.05$. Images are representative of at least three independent experiments.

Results

We had previously shown that cancer cells treated with α -TOS died independently of their p53 status as exemplified by the p53^{-/-} HCT116 colorectal carcinoma cell line [36]. These studies have been extended here to p53 null cancer cells of different origin confirming that the p53 protein is redundant for apoptosis induced by the VE analog (Fig. 2). For these studies, the cell lines expressing wild type p53 protein included Jurkat (T lymphoma) and MCF7 (breast carcinoma) cell lines, whereas the non-small cell lung carcinoma cell line, H1299, is p53-deficient and the breast carcinoma cell line, MCF7_{DD9}, has a transcriptionally silent p53. α -TOS induced apoptosis at concentrations ranging between 50 and 80 μ M within 24 h in all the cell lines tested, with only slight differences in the capacity of α -TOS towards the p53 null cell lines with all showing cytochrome c release (Fig. 2).

To obtain a greater understanding of the mechanism leading to activation of apoptosis by α -TOS and the role of mitochondria in the process [2–4, 9, 37, 42–45], the role of the Bcl-2 family proteins indispensable for apoptosis induction/progression was examined [13, 14]. First, Q-PCR was used to estimate mRNA levels for the pro- and anti-apoptotic Bcl-2 family members, including *Bax*, *Bak*, *Noxa*, *Puma*, *Bim*, *Mcl-1*, *Bcl-2* and *Bcl-x_L*. The only genes showing a significant response to α -TOS-induced stress with increased mRNA levels were *Noxa* and *Puma* (Fig. 3). We next examined α -TOS-induced protein expression of Noxa and Puma by western blot analysis, which confirmed increased levels of Noxa, but not the Puma protein and no

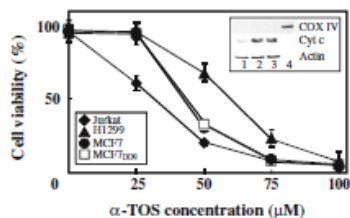


Fig. 2 α -TOS kills cancer cells regardless of their p53 status. The wild type p53 Jurkat and MCF7 cells, the p53-null H1299 cells and MCF7_{DD9} cells with transcriptionally silent p53 were exposed to increasing concentrations of α -TOS for 24 h and the apoptosis levels analyzed by flow cytometry using the annexin V-FITC/propidium iodide method and the results are expressed as the percent cell viability relative to non-treated cells. The insert documents the level of cytochrome c release in control Jurkat cells (1) and cells exposed to 50 μ M α -TOS for 7 (2) or 8 h (3). Actin was used as a loading control for the cytosolic fraction, while COX IV was used to document the purity of the cytosolic fraction. Sample 4 documents the presence of COX IV solely in the mitochondrial subfractions. Data shown represent mean \pm SEM ($n = 3$), western blot images are representative of at least three independent experiments

Springer

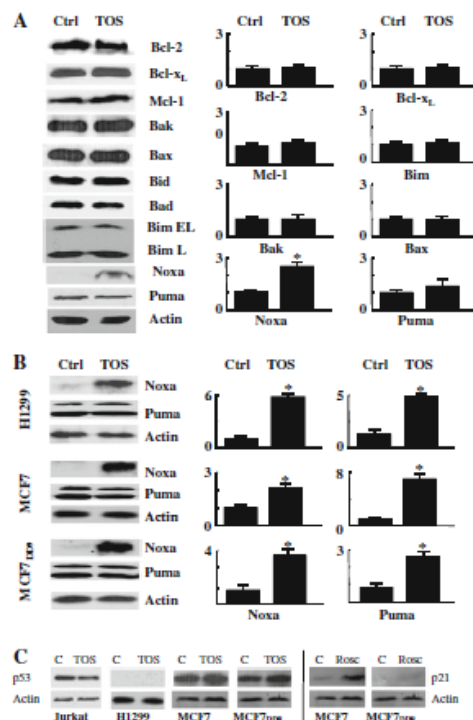


Fig. 3 α -TOS enhances expression of the BH3-only protein Noxa independently of cellular p53 status. Jurkat T lymphoma **a** and other cell lines **b** represented by MCF7 with wild-type p53, p53-deficient H1299 cells and MCF7_{DD9} cells with transcriptionally silent p53 were treated with α -TOS (see below) and assessed for the expression of Bcl-2 family proteins **a** or only Noxa and Puma **b** using Q-PCR and Western blotting. Jurkat cells were exposed to 50 μ M α -TOS for 6 h, H1299 cells to 80 μ M α -TOS for 12 h, and MCF7 and MCF7_{DD9} cells to 50 μ M α -TOS for 15 h. **c** The control and α -TOS-treated cells were also probed by western blotting for p53 or p21 protein levels in the case of MCF7 wt and MCF7_{DD9} cells and the cells were treated with 20 μ M Roscovitine for 20 h as a control for p53 dependent upregulation of p21 protein. Actin was used as a marker of equal protein loading for western blotting and as a house-keeping gene for Q-PCR. The Q-PCR data represent mean \pm SEM ($n = 3$). The symbol ** denotes significant differences between control and treated cells with $P < 0.05$. Western blot images are representative of at least three independent experiments

changes in the levels of other Bcl-2 family proteins (Fig. 3). Importantly, the increase in expression of Noxa occurred independently of the p53 status of the cells, as the single BH3 only member of the Bcl-2 family upregulated in response to α -TOS in both the p53-null H1299 cells and in the MCF7_{DD9} cells with transcriptionally silent p53 (Fig. 3).

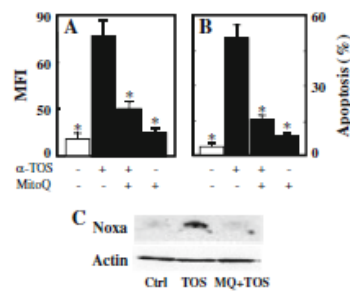


Fig. 4 ROS play a role in Noxa upregulation and apoptosis induction by α -TOS. Jurkat cells were pre-incubated, as indicated, for 1 h with 1 μ M MitoQ, exposed to 50 μ M α -TOS, and assessed for accumulation of ROS using the fluorescent probe DHE (a; 1-h exposure), apoptosis using the annexin V-FITC kit (b; 12-h exposure) and Noxa protein expression by western blotting (c; 4-h exposure). The data in panels A and B represent mean \pm SEM ($n = 3$), the images in panel C are representative of three independent experiments

In the next set of experiments we tested the premise that apoptosis induced by α -TOS and Noxa upregulation are a result of generation of ROS. Further, we tested the possibility that the increase of Noxa expression is downstream of ROS generation. This is suggested by our previous results showing that ROS are generated within 1 h in cancer cells exposed to α -TOS [2, 3, 7] and we documented it in this study by experiments in which MitoQ was used as a scavenger of ROS. Results presented in Fig. 4 document high levels of ROS in Jurkat cells exposed to α -TOS for 1 h, which was suppressed by MitoQ (Fig. 4a). The ROS scavenger also suppressed apoptosis induction (Fig. 4b) and Noxa protein upregulation (Fig. 4c). These results therefore support a causal relationship in α -TOS-challenged cells between early ROS accumulation, Noxa upregulation and apoptosis induction.

Since Noxa protein upregulation is accepted as one of several possible cellular processes that precede MOM permeabilization [17], pore formation was examined. Before the MOM pore can be formed, its components (usually Bak and/or Bax) must be conformationally activated. In accordance with earlier reports [20, 37, 38], flow cytometry of permeabilized cells using antibodies directed against epitopes exposed on the surface of 'activated' Bax and Bak proteins can be utilized to assess the extent of conformational changes of Bak and Bax proteins in individual cell lines. STS (0.5 μ M) was used as a positive control for the activation of Bak and Bax proteins in Jurkat cells, and TRAIL (250 ng/ml) was used for similar purposes in the other cell lines [45]. All the cell lines tested in this study responded to α -TOS treatment by undergoing conformational changes in Bak protein, whereas the Bax conformation remained unchanged in

Jurkat cells, was slightly altered in MCF7 and was highly modified in H1299 cells (Fig. 5). The observed conformational changes of Bax protein were not regulated by p53, since we observed prominent activation of the protein in the p53-null H1299 cells and only slight changes in the MCF7_{DD9} cells with transcriptionally silent p53 (Fig. 5).

Given the conformational changes detected in Bak protein from all cell lines tested and in Bax protein from some of the cell lines, we next investigated the extent of oligomerization of Bak or Bax in response to α -TOS. Gel filtration chromatography and mild buffer conditions were used to separate purified mitochondrial lysates from control cells and cells treated with the VE analog using a Superdex-200 column to separate macromolecules from 3 to 600 kDa. Individual fractions were collected and analyzed by western blotting for the presence of anti-Bak IgG- and anti-Bax-IgG-reactive proteins. In agreement with the results above showing conformational change (Fig. 5), we observed anti-Bak IgG-reactive proteins in high molecular weight (HMW) fractions in all cell lines studied following their exposure to α -TOS, whereas only H1299 cells showed anti-Bax IgG-reactive proteins in HMW fractions when exposed to the VE analog (Fig. 6). Further, we observed very weak Bax-positive bands in the HMW fractions from mitochondrial lysates of MCF7 and MCF7_{DD9} cells (Fig. 6), consistent with low levels of conformational change detected in these cells (Fig. 5). The results show that mitochondria from cells treated with α -TOS, as well as with TRAIL or STS contain significant amounts of Bak protein in HMW fractions of up to 260 kDa. In the control cell samples, Bak protein was present only in the low MW fractions (50–80 kDa), consistent with the proposal that Bak remains functionally inactive, bound in heterodimeric complexes with Mcl-1 or Bcl-x_L in these cells [17]. On the other hand, Bax protein was detected in HMW fractions in the cell lines (except for H1299 cells) only after treatment with TRAIL or STS. Bax protein in its inactive state largely resides in the monomeric form in the cytosol. However, initial analysis of fractions of mitochondrial lysates from non-treated and α -TOS treated cells did not contain sufficient Bax protein present to allow detection using standard ECL reagents. Consequently, Advanced ECL detection kits were used and with greater sensitivity revealed the presence of the Bax protein in the low MW fractions corresponding to 20–50 kDa in control cells as well as in α -TOS-treated cells. These low MW forms likely correspond to either the monomeric form of Bax loosely attached to the mitochondrial membrane or the heterodimer in complex with anti-apoptotic members of the Bcl-2 family.

The above results indicated a prominent role for the Bak protein in α -TOS-induced cell death. Next, the α -TOS

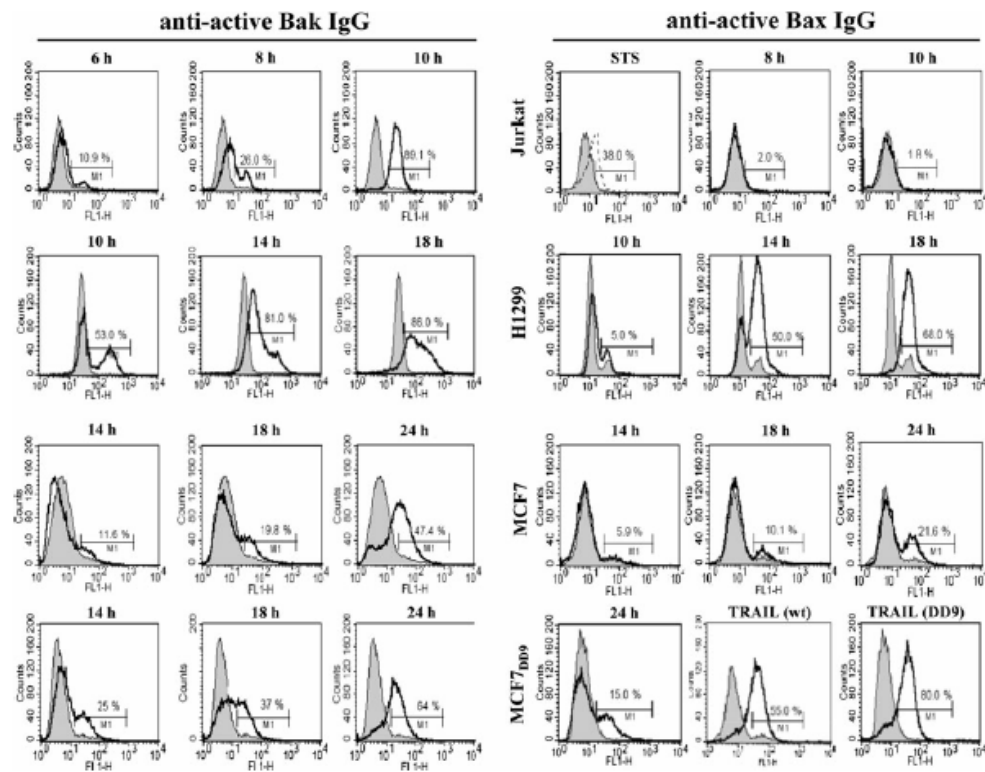


Fig. 5 α -TOS activates BHI-3 proteins. Jurkat, MCF7 and MCF7^{DDP} cells were treated with 50 μ M α -TOS, and H1299 cells with 80 μ M α -TOS for the indicated time points. The cells were then analyzed for conformational changes of the Bak and Bax proteins as described in the Experimental section. Treatment with 500 nM STS for 4 h or 250 ng/ml TRAIL for 6 h was used as a positive control for

conformational changes of the Bax protein. Following the treatment, permeabilized whole cells were reacted with anti-Bak IgG or anti-Bax IgG recognizing the activated form of the proteins due to their altered conformation, and the level of this change was assessed by flow cytometry. Filled histograms represent untreated cells, empty histograms represent α -TOS treated cells

induced increase in levels of Noxa was examined for its role in Bak channel formation leading to apoptosis. For these studies, samples of mitochondrial lysates prepared from α -TOS-treated or control H1299 cells were immunoprecipitated with antibodies against the anti-apoptotic Bcl-2 family protein Mcl-1 or Bcl-x_L, both of which are known to interact with BHI-3 and BHB-only proteins. The Noxa protein was found to co-immunoprecipitate with Mcl-1 in samples from α -TOS-treated cells but not control cells (Fig. 7). No Noxa protein was detected in the Bcl-x_L immunoprecipitates. Surprisingly, the amount of Bak protein co-immunoprecipitated with Mcl-1 was significantly higher in α -TOS-treated cells than in the control cells (Fig. 7). A similar or even greater difference between treated and non-treated cells was observed in Bcl-x_L

immunoprecipitates, where the amount of associated Bak was also higher in α -TOS treated cells. Moreover, Bcl-x_L was also co-immunoprecipitated with Bax protein from treated cells and not from the control cells.

Bim, as another BH3 protein of interest was analyzed for its interaction following α -TOS treatment and was found associated with Bak, but not Bax after α -TOS treatment (Fig. 7). The two splice variants of Bim protein, BimEL and BimL, were detected in the mitochondria of the treated cells at significantly greater levels than in control cells (Fig. 7). From these results, it is concluded that α -TOS upregulates the Noxa protein that binds Mcl-1 and also causes translocation of Bim into mitochondria that together leads to activation of Bak to form pores in the MOM.

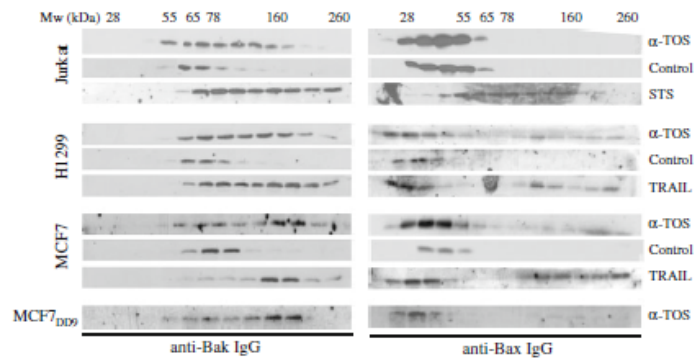


Fig. 6 α -TOS induces Bak oligomerization in the mitochondrial membrane. Proteins of mitochondrial lysates (100 μ g) derived from control cells and cells treated with α -TOS (Jurkat cells, 50 μ M, 12 h; H1299 cells, 80 μ M, 20 h; MCF7 and MCF7_{DD9} cells, 50 μ M, 24 h) were fractionated using gel filtration through a Superdex 200 Preparation Grade column. Individual fractions were collected and

probed by western blotting for the presence of Bak and Bax proteins. Treatment with 500 nM STS for 6 h was used as a positive control for Bak and Bax oligomerization in Jurkat cells. Treatment with TRAIL at 250 ng/ml for 10 h was used as a positive control for Bak and Bax oligomerization in H1299, MCF7 and MCF7_{DD9} cells

Although the results presented above documented the involvement of the Noxa-Bak axis in apoptosis [46] induced in various cancer cell lines by α -TOS, more definitive evidence was sought identifying the role of the BH3 proteins. For this, use was made of Bax^{-/-}/Bak^{-/-} Jurkat cells as well as those lacking only the Bax protein. Exposure of these cells as well as their Bax/Bak-proficient counterparts revealed that Bax^{-/-} and the parental Jurkat cells were equally susceptible to α -TOS-induced apoptosis, while the Bax^{-/-}/Bak^{-/-} cells were resistant, at least over the first 24 h of treatment. Similar observations were made when the three different Jurkat cell lines were exposed to TRAIL (Fig. 8), consistent with a previous report [47]. While these results confirm the importance of Bak and/or Bax proteins for fast induction of apoptosis, we observed delayed cell death in the Bax^{-/-}/Bak^{-/-} cells (Fig. 8). The nature and the molecular mechanism of the delayed death of the double-deficient cells are unclear at this stage and under investigation in our laboratory.

To further determine the roles of Bcl-2 proteins in apoptosis induced in cancer cells by α -TOS, RNA interference (RNAi) was used to knock down expression of proteins of interest and the resulting change in the IC₅₀ values for cellular responses to α -TOS in the RNAi-treated cells assayed using MTT. Exposure of cells to individual siRNA duplexes resulted in substantially reduced levels of the targeted proteins, i.e. Bak, Bax, Bim, Noxa and Mcl-1 (Fig. 9a). Downregulation of the Bak protein in MCF7 cells shifted the 24 h IC₅₀ value from ~65 to ~100 μ M (Fig. 9b) and the 40 h IC₅₀ value from ~45 to ~70 μ M (data not shown). Combining *Bak* and *Noxa* siRNA treatment or using either siRNA alone produced similar effects

in the H1299 cells becoming more resistant to α -TOS (Fig. 9c). Knocking down Bax had no effect on the susceptibility of the cells to α -TOS (Fig. 9c). Surprisingly, downregulation of Bim did not yield statistically significant difference in 24 h IC₅₀. Importantly, downregulation of the anti-apoptotic Mcl-1 protein significantly increased susceptibility of H1299 cells to α -TOS (Fig. 9c). These results confirm the importance of the Noxa-Bak-Mcl-1 axis in apoptosis induced in cancer cells by α -TOS.

Discussion

Redox-silent VE analogs epitomized by the prototypic α -TOS belong to the anti-cancer drugs termed 'mitocans' [1, 8, 48] which induce apoptosis in cancer cells, often in a selective manner by mitochondrial destabilization. Mitocans comprise 8 groups of compounds that destabilize mitochondria by utilizing different mechanisms [48, 49]. We have placed VE analogs into group 2 [9], containing BH3 mimetics, and group 5 comprising agents interfering with the electron redox chain [3, 4]. We and others have documented that VE analogs cause high level accumulation of ROS in the early stages of apoptosis [2–7, 42, 44, 50] leading to mitochondrial destabilization, involving regulation of the Bcl-2 family proteins [2, 10, 51]. However, the precise molecular bases for the link between ROS accumulation and mitochondrial destabilization have not been identified. Although many inducers of apoptosis cause ROS accumulation followed by pore formation in the MOM, surprisingly, how these events link together has until now not been clear [52].

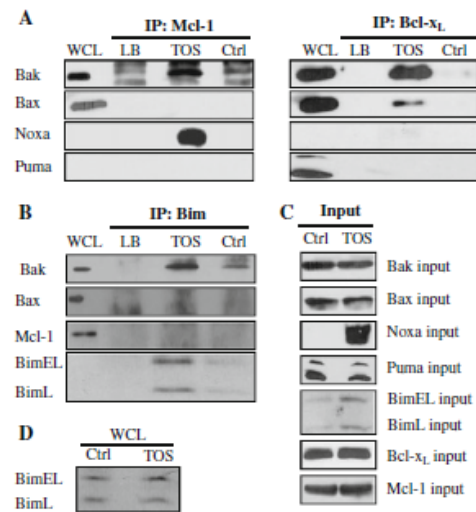


Fig. 7 Immunoprecipitation of selected Bcl-2 family members confirms α -TOS induced interactions among the Bcl-2 family. Mitochondrial lysates of H1299 cells were analyzed by antibody pull-down and western blotting as shown. Ctrl: non-treated cells; TOS: α -TOS-treated cell samples with the antibodies as indicated. LB: immunoprecipitation using lysis buffer as a control for antibody cross-reactivity. WCL: whole cell lysates as positive control for Bak, Bax or other proteins as indicated. **a** Right hand panel shows proteins co-immunoprecipitating with Mcl-1. The left hand panel shows proteins co-immunoprecipitating with Bcl-x_L. **b** Only Bak protein co-immunoprecipitated with Bim in mitochondrial lysates from α -TOS treated cells. **c** The levels of protein expressed in samples of whole mitochondrial lysates. **d** Comparison of levels of Bim protein expressed in whole cell lysates from α -TOS treated versus non-treated cells

In this study, the role of the Bcl-2 family proteins in permeabilization of the MOM during α -TOS-induced apoptosis of cancer cell lines has been determined. Results with different wild-type and inactive p53 cancer cells were consistent and extended our previous findings that the VE analog induced apoptosis independently of the p53 status in the HCT116 colon cancer cell line [36]. Recently, it was reported that α -TEA, an ether analog of α -TOS, also induced apoptosis independently of p53, by upregulating the BH3-only protein Noxa, although the precise mechanism of MOM formation was not determined [19]. We show here that α -TOS causes increased expression of the *Noxa* and *Puma* mRNA, both independently of p53. However, only the *Noxa* gene is upregulated at the protein level, while that of *Puma* is not increased, indicating possible differences in the post-transcriptional regulation of the *Noxa* and *Puma* proteins. Although *Puma* upregulation at the mRNA and not protein level to the best of our

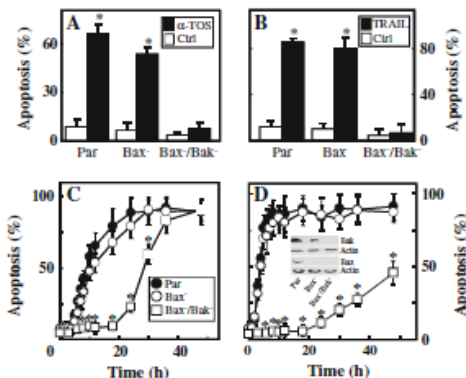


Fig. 8 Susceptibility of Bax- and/or Bak-deficient cells to α -TOS-induced apoptosis. Panels **a** and **b** Levels of apoptosis in the parental, Bax⁻ or Bax⁻/Bak⁻ Jurkat cells treated for 12 h with 50 μ M α -TOS or 20 ng/ml TRAIL as indicated in panels **c** and **d**: Time dependent increase in apoptosis of parental, Bax⁻ or Bax⁻/Bak⁻ Jurkat cells treated with 50 μ M α -TOS or 20 ng/ml TRAIL as indicated. The inset panel in **d** shows levels of proteins as indicated in the respective Jurkat cell populations. The extent of apoptosis was estimated by flow cytometry using the annexin V-FITC/propidium iodide assay. The data represent mean \pm SEM of three independent experiments. The symbol ** denotes significant differences with $P < 0.05$

knowledge has not been reported before, the underlying mechanism for these events will require further studies.

The 'indirect model' [17] for pore formation in the MOM involving the Bcl-2 family proteins proposes a role for BH3-only proteins (e.g. Noxa, Puma, Bim), in apoptosis induction in eukaryotic cells, that are upregulated leading to the activation by subsequently displacing and liberating the pro-apoptotic Bak or Bax proteins from their complexes with anti-apoptotic Bcl-2 family members (such as Bcl-2, Bcl-x_L or Mcl-1). The Mcl-1 protein, which lacks the BH4 domain but contains a PEST sequence, has been proposed to undergo proteasomal degradation in the course of liberating Bak and/or Bax proteins that then form pores in the MOM [53, 54]. However, the results presented here suggest that degradation of the Mcl-1 protein following Noxa upregulation did not occur in any of the cell lines tested. These results are similar to those from other studies documenting that the Mcl-1 protein does not need to be degraded in order to be functionally inactivated during the apoptotic process. For example, this has been reported for apoptosis induction by camptothecin involving Noxa upregulation in H1299 and HeLa cells [55], Bim-induced apoptosis in MCF7 cells [56], γ -secretase inhibitor GSI-induced apoptosis in HCT116 cells [46], or the proteasomal inhibitor bortezomid in B-cell lymphoma [57].

It was proposed that destabilization of the Mcl-1 protein may involve its JNK-dependent phosphorylation [58].

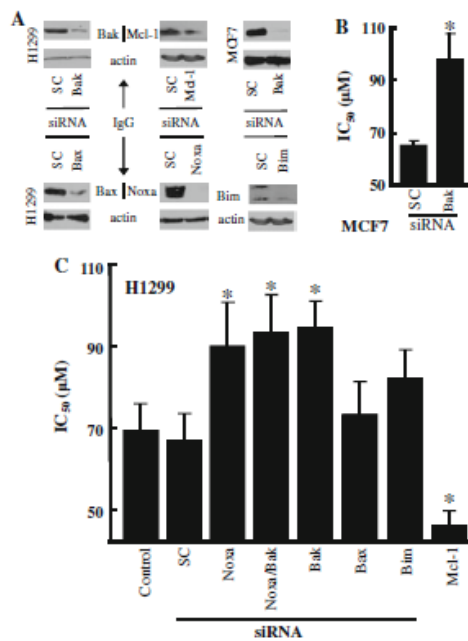


Fig. 9 Knocking down Noxa and Bak desensitizes cancer cells to α -TOS-induced apoptosis. **a** Efficacy of downregulation of the Bak, Bax, Bim, Noxa and Mcl-1 proteins in H1299 and MCF7 cells using siRNA knock down. Actin was used as a standard for protein loading. **b** Change in the IC₅₀ value for α -TOS of MCF7 cells pre-treated with scrambled (SC) siRNA or Bak siRNA. **c** Changes in the IC₅₀ value for α -TOS of H1299 control cells or cells pre-treated with scrambled (SC), Noxa, Bak, Bax, Bim or Mcl-1 siRNA, or with Bak plus Noxa siRNA. Data show the mean \pm 95% confidence interval, and the symbol '*' denotes statistically significant differences from control cells with $P < 0.05$

We tested this premise in our system using the JNK inhibitor SP600125. Since we found that this did affect α -TOS-induced apoptosis in neither Jurkat nor H1299 cells (data not shown), we did not pursue this pathway any further in our studies.

Co-immunoprecipitation of Mcl-1 complexed with Noxa or Bak, Bcl-x_L with Bak and of Bim with Bak in H1299 cells showed that Mcl-1/Noxa and, rather surprisingly, Mcl-1/Bak and Bcl-x_L/Bak interactions were more abundant in the α -TOS-treated than in the control cells. This kind of result was very surprising, since co-IP experiments of this type of proteins usually give opposite results. Explanation of this, however, may lie in the definition of the 'direct model' for Bax and Bak activation [18, 59–61]. Central to this model is the concept that Bak and Bax sequestered by the anti-apoptotic Bcl-2 proteins represent only a fraction of the total Bak and Bax protein

pools when these pro-apoptotic proteins are activated either spontaneously or by some unspecified mechanisms [18, 62]. Co-immunoprecipitation experiments presented here indicate that α -TOS-induced activation of Bak and Bax may cause their sequestration by Mcl-1 and Bcl-x_L, respectively, until a saturation point is surpassed allowing accumulation of the active forms of Bak and Bax. Moreover, the Noxa protein, upregulated by treating cancer cells with α -TOS not only could compete with activated Bak for the hydrophobic BH3 binding groove of Mcl-1 [63] or Bcl-x_L [64] making Bak freely available, but could also possibly displace Bim from its complex with Mcl-1, allowing Bim to act as a direct co-activator of Bak or Bax [46]. Unexpectedly, we did not detect any interaction between Bim and Mcl-1, although Bim accumulated in mitochondria and interacted with the Bak protein, which was the first time observed (and also tested in H1299 cells) direct interaction of the wt Bim and Bak protein to the best of our knowledge. The co-IP results suggest that increased level of the Bim protein associated to the mitochondria of α -TOS treated H1299 cells probably directly relates to the increased number of the Bak protein detected in co-IP WB. α -TOS perhaps aims Bim at mitochondria without any other direct effect on the self-interaction of Bim and Bak. Similarly, Noxa does not seem to disrupt, at least in our study in H1299 cells, the pre-formed anti-apoptotic Bak/Mcl-1, Bak/Bcl-x_L or even Bax/Bcl-x_L complexes and rather competes with the BH1-3 proteins for the Mcl-1 protein.

The results obtained in this study better fit a model where the excessive unsequestered monomers of activated Bak protein (and Bax protein in the case of H1299 cells), are then free to self-interact, forming a pore triggering the apoptotic cascade downstream of mitochondria. In the case of the non-small cell lung carcinoma H1299 or A549 cells, which express high levels of the Mcl-1 protein, Mcl-1 can significantly prolong the apoptotic process induced by various pro-apoptotic stimuli including cisplatin, etoposide, UV irradiation or calcium ionophores [65] with similar results also shown for hematopoietic cells [66]. We propose that α -TOS sensitizes Mcl-1-overexpressing cells to a variety of pro-apoptotic stimuli, in a similar manner to that shown for cells treated with the topoisomerase I inhibitor CPT-11 which also acted to increase expression of the Noxa protein [67].

Both the indirect and direct activation models share a common denominator: any major disruption of the dynamic balance between the anti-apoptotic Bcl-2 family proteins and the BH3 pro-apoptotic proteins favoring unsequestration of the latter triggers the intrinsic apoptotic process. It has been published that a conformational change of the BH1-3 proteins is important for aggregation of these proteins and for their targeting to the MOM, where they

eventually form a pore that allows the apoptotic cascade to proceed [21, 22]. In this study, we used antibodies recognizing epitopes exposed only on the activated states of BH1-3 proteins. However, the detection of the activation epitope on the Bak protein (documented by using the specific antibody Ab-1) unlike that found for the Bax protein (utilizing the 6A7 antibody) does not necessarily mean that the Bak MOM pore will be formed [20, 21]. Thus the recognition of the N-terminal activation epitope of the Bak protein by the Ab-1 antibody may detect only the 'priming' stage for Bak functional activation. We have observed the activation or 'priming' of Bak in all cell lines tested, and this correlated with the process of α -TOS-induced Bak MOM pore formation. By contrast, the Bax protein was fully activated only in the H1299 cells suggesting a relatively similar importance for these two proteins to mediate α -TOS-induced apoptosis in the non-small cell lung carcinoma cell line. The MCF7 and MCF7_{DD9} cells showed only slight levels of Bax activation, occurring after most of the Bak protein had been activated which suggests a higher level of functional importance for the Bak protein in breast cancer cells.

After epitope activation or 'priming' of the BH1-3 proteins, they oligomerize due to interaction of activated monomers via their BH3 domains within the MOM, becoming detectable in higher molecular weight fractions of mitochondrial lysates [68]. Our results demonstrate that the Bak protein oligomerizes in mitochondria after α -TOS treatment in all tested cell lines, since it was only then detected in fractions >160 kDa. Our data from FPLC analysis of the mitochondrial lysates of cells treated with α -TOS (Fig. 6) indicate that the Bak protein complexes formed are homo-oligomeric, since Bax protein was not found in these same fractions. Conversely, the results observed in the H1299 cells indicate that the Bax protein oligomers do not contain Bak protein. These observations rule out hetero-oligomerization of the Bak and Bax proteins during cancer cell apoptosis induced by VE analogs.

Our data for Bak oligomerization are consistent with and further explained by recent reports, documenting that following an apoptogenic signal, two Bak monomers initially form a homodimer by way of generation of disulphide bridges, which is followed by higher homo-oligomeric structures that results in formation of a Bak channel in the MOM [69, 70]. We propose that this step occurs following Noxa upregulation in cancer cells exposed to α -TOS, which gives initially higher levels of ROS that themselves not only cause increased expression of the Noxa protein but, following Noxa-mediated departure of Bcl-2 family anti-apoptotic proteins from Bak, but also catalyse formation of the Bak-Bak dimers.

Conformational changes of Bak protein has been shown to occur during apoptosis induced by VE analogs in

prostate cancer cells via a BH3 mimetic like mode of action [9]. However, we did not observe a similar activity induced by α -TOS in the cell lines used in our experiments. Unlike the report by Shiao and colleagues, who observed disruption of Bak-Mcl-1 or Bak-Bcl-x_L interaction in prostate cancer cells treated with α -TOS [9], we found that the Bak protein did immunoprecipitate with Mcl-1 and Bcl-x_L in MCF7 (data not shown) and in H1299 cells exposed to α -TOS. Therefore, the BH3 mimetic-like activity of VE analogs may be cell-type specific, dose related or both. Notwithstanding, we suggest that the BH3 mimetic-like activity of VE analogs should make a significant contribution by sensitizing cancer cells to apoptosis induction by other agents, particularly in cell lines over-expressing the anti-apoptotic Bcl-2 family proteins. However, the major role of VE analogs in apoptosis induction can be ascribed to the accumulation of high levels of ROS in the exposed cells, which translates to mitochondrial destabilization, as delineated in this report.

The requirement of the Bak protein and involvement of Mcl-1/Bak axis in α -TOS-induced apoptosis was confirmed by RNAi against Bak and Mcl-1 while knocking down of the Bax protein did not significantly affect the IC₅₀ values of α -TOS, at least in H1299 cells. We observed an increase in the IC₅₀ value in cells exposed to the VE analogue following knock down of the Bak or Noxa protein levels. Probably the most direct evidence for the importance of the Bak protein in apoptosis induced by α -TOS, at least for the Jurkat T lymphoma cells, comes from experiments comparing wild-type cells with cells deficient in both Bak and Bax or either one of these two proteins. The results clearly indicate that Jurkat cells containing the Bak protein are susceptible to apoptosis while the Bax protein appears not to be critical.

We have recently documented that the target of VE analogs is the mitochondrial CII [3, 4, 44], and this has been supported by others (Gogvadze et al., personal communication). Thus, α -TOS displaces ubiquinone from CII, such that electrons, generated due to conversion of succinate to fumarate at CII [71], cannot be intercepted and give rise to superoxide [72]. The resulting ROS then cause mitochondrial destabilization by a mechanism that has previously not been clarified. According to the data shown here, we propose a model whereby ROS leads to transcriptional upregulation of the BH3-only protein Noxa that may cooperate with Bim and results in unsequestration, activation and oligomerization of the BH1-3 protein Bak, with ensuing formation of a pore in the MOM. The α -TOS-triggered ROS accumulation that causes transcriptional upregulation of Noxa is dependent on the FOXO family of transcription factors and is the subject of ongoing research (K.V. et al., unpublished results).

In conclusion, we document here that redox-silent VE analogs, epitomized by α -TOS, destabilize mitochondria by

promoting formation of MOM pores. To the best of our knowledge, this is the first report defining the molecular mechanism triggered by mitocan induced ROS accumulation in cancer cells leading to mitochondrial activated apoptosis.

Acknowledgements Jurkat Bax⁻/Bak⁻ and Jurkat Bax⁻ cells were provided by H. Rabinowicz (University of Pittsburgh, Pittsburgh, PA, USA), H1299 and MCF7_{DO9} cells by Dr. B. Vojtesek (Masaryk Memorial Institute, Bmo, Czech Republic), and human recombinant TRAIL by Dr. L. Andera (Institute of Molecular Genetics, Academy of Sciences of the Czech Republic, Prague, Czech Republic). This work was supported in part by grants from the Australian Research Council (to J.N. and P.K.W.), the Queensland Cancer Fund, the National Breast Cancer Foundation, the Grant Agency of the Academy of Sciences of the Czech Republic KAN200520703, IAA5005220602 and IAA5005200602 to J.N., by Concept Grant AV0250520514 awarded by the Academy of Sciences of the Czech Republic, by a grant from Ministry of Agriculture of the Czech Republic (Grant No. MZE 0002716202) to J.T. and by a grant from the Grant agency of the Czech Republic 204/09/P632 to L.P. L.P. was supported in part by the Apoptosis Research Group (Griffith University).

References

- Neuzil J, Dong LF, Ramanathapuram L et al (2007) Vitamin E analogues as a novel group of mitocans: anti-cancer agents that act by targeting mitochondria. *Mol Asp Med* 28:607–645
- Weber T, Dalen H, Andera L et al (2003) Mitochondria play a central role in apoptosis induced by alpha-tocopheryl succinate, an agent with an antineoplastic activity: comparison with receptor-mediated pro-apoptotic signaling. *Biochemistry* 42:4277–4291
- Dong LF, Low P, Dyason JC et al (2008) α -Tocopheryl succinate induces apoptosis by targeting ubiquinone-binding sites in mitochondrial respiratory complex II. *Oncogene* 27:4324–4335
- Dong LF, Freeman R, Liu J et al (2009) Suppression of tumor growth in vivo by the mitocan α -tocopheryl succinate requires respiratory complex II. *Clin Cancer Res* 15:1593–1600
- Kang YH, Lee E, Choi MK et al (2004) Role of reactive oxygen species in the induction of apoptosis by α -tocopheryl succinate. *Int J Cancer* 112:385–392
- Allegra R, Tomasetti M, Andera L et al (2001) Coenzyme Q blocks biochemical but not receptor-mediated apoptosis by increasing mitochondrial antioxidant protection. *FEBS Lett* 503:46–50
- Stapelberg M, Gellert N, Swettenham E et al (2005) α -Tocopheryl succinate inhibits malignant mesothelioma by disrupting the fibroblast growth factor autocrine loop. *J Biol Chem* 280:25369–25376
- Neuzil J, Wang XF, Dong LF, Low P, Ralph SJ (2006) Molecular mechanism of 'mitocan'-induced apoptosis in cancer cells epitomizes the multiple roles of reactive oxygen species and Bcl-2 family proteins. *FEBS Lett* 580:5125–5129
- Shiau CW, Huang JW, Wang DS et al (2006) α -Tocopheryl succinate induces apoptosis in prostate cancer cells in part through inhibition of Bcl-x₁/Bcl-2 function. *J Biol Chem* 281:11819–11825
- Yu WP, Sanders BG, Kline K (2003) RRR- α -tocopheryl succinate-induced apoptosis of human breast cancer cells involves Bax translocation to mitochondria. *Cancer Res* 63:2483–2491
- D' Alessio M, De Nicola M, Coppola S et al (2005) Oxidative Bax dimerization promotes its translocation to mitochondria independently of apoptosis. *Faseb J* 19:1504–1506
- Neuzil J, Dyason JC, Freeman R et al (2007) Mitocans as anti-cancer agents targeting mitochondria: lessons from studies with vitamin E analogues, inhibitors of complex II. *J Bioenerg Biomembr* 39:65–72
- Wei MC, Zong WX, Cheng EHY et al (2001) Proapoptotic BAX and BAK: a requisite gateway to mitochondrial dysfunction and death. *Science* 292:727–730
- Reed JC (2006) Proapoptotic multidomain Bcl-2/Bax-family proteins: mechanisms, physiological roles, and therapeutic opportunities. *Cell Death Differ* 13:1378–1386
- Lindsten T, Ross AJ, King A et al (2000) The combined functions of proapoptotic Bcl-2 family members Bak and Bax are essential for normal development of multiple tissues. *Mol Cell* 6:1389–1399
- Korsmeyer SJ, Wei MC, Saito M, Weller S, Oh KJ, Schlesinger PH (2000) Pro-apoptotic cascade activates BID, which oligomerizes BAK or BAX into pores that result in the release of cytochrome c. *Cell Death Differ* 7:1166–1173
- Willis SN, Fletcher JL, Kaufmann T et al (2007) Apoptosis initiated when BH3 ligands engage multiple Bcl-2 homologs, not Bax or Bak. *Science* 315:856–859
- Brunelle JK, Letai A (2009) Control of mitochondrial apoptosis by the Bcl-2 family. *J Cell Sci* 122:437–441
- Wang P, Yu WP, Hu ZZ et al (2008) Involvement of JNK/p73/NOXA in vitamin E analog-induced apoptosis of human breast cancer cells. *Mol Carcinogen* 47:436–445
- Hsu YT, Youle RJ (1997) Nonionic detergents induce dimerization among members of the Bcl-2 family. *J Biol Chem* 272:13829–13834
- Griffiths GJ, Corfe BM, Savory P et al (2001) Cellular damage signals promote sequential changes at the N-terminus and BH-1 domain of the pro-apoptotic protein Bak. *Oncogene* 20:7668–7676
- Zhang LL, Shimizu S, Sakamaki K, Yonehara S, Tsujimoto Y (2004) A caspase-8-independent signaling pathway activated by fas ligation leads to exposure of the Bak N terminus. *J Biol Chem* 279:33865–33874
- Kuwana T, Mackey MR, Perkins G et al (2002) Bid, Bax, and lipids cooperate to form supramolecular openings in the outer mitochondrial membrane. *Cell* 111:331–342
- Schafer B, Quispe J, Choudhary V et al (2009) Mitochondrial outer membrane proteins assist bid in bax-mediated lipid pore formation. *Mol Biol Cell* 20:2276–2285
- Hardwick JM, Polster BM (2002) Bax, along with lipid conspirators, allows cytochrome c to escape mitochondria. *Mol Cell* 10:963–965
- Lee RM, Chen J, Matthews CP, McDougall JK, Neiman PE (2001) Characterization of NRI3-related human cell death regulator, Boo/Diva, in normal and cancer tissues. *Biochim Biophys Acta* 1520:187–194
- Jones S, Zhang XS, Parsons DW et al (2008) Core signaling pathways in human pancreatic cancers revealed by global genomic analyses. *Science* 321:1801–1806
- Parsons DW, Jones S, Zhang XS et al (2008) An integrated genomic analysis of human glioblastoma Multiforme. *Science* 321:1807–1812
- Hayden EC (2008) Cancer complexity slows quest for cure. *Nature* 455:148
- Reed JC, Pellecchia M (2005) Apoptosis-based therapies for hematologic malignancies. *Blood* 106:408–418
- Green DR, Kroemer G (2005) Pharmacological manipulation of cell death: clinical applications in sight? *J Clin Invest* 115:2610–2617
- Wang GQ, Wiecek E, Goldstein LA et al (2001) Resistance to granzyme B-mediated cytochrome c release in Bak-deficient cells. *J Exp Med* 194:1325–1337

33. Giaccone G, Battey J, Gazdar AF, Oie H, Draoui M, Moody TW (1992) Neuromedin-B is present in lung-cancer cell-lines. *Cancer Res* 52:2732s–S2736s
34. Kotala V, Uldrijan S, Horky M, Trbusek M, Strnad M, Vojtesek B (2001) Potent induction of wild-type p53-dependent transcription in tumour cells by a synthetic inhibitor of cyclin-dependent kinases. *Cell Mol Life Sci* 58:1333–1339
35. Kelso GF, Porteous CM, Coulter CV et al (2001) Selective targeting of a redox-active ubiquinone to mitochondria within cells: antioxidant and antiapoptotic properties. *J Biol Chem* 276:4588–4596
36. Weber T, Lu M, Andera L et al (2002) Vitamin E succinate is a potent novel antineoplastic agent with high selectivity and cooperativity with tumor necrosis factor-related apoptosis-inducing ligand (Apo2 ligand) in vivo. *Clin Cancer Res* 8:863–869
37. Griffiths GJ, Dubrez L, Morgan CP et al (1999) Cell damage-induced conformational changes of the pro-apoptotic protein bak in vivo precede the onset of apoptosis. *J Cell Biol* 144:903–914
38. Mandic A, Viktorsson K, Molin M et al (2001) Cisplatin induces the proapoptotic conformation of Bak in a Delta MEKK1-dependent manner. *Mol Cell Biol* 21:3684–3691
39. Pfaffl MW (2001) A new mathematical model for relative quantification in real-time RT-PCR. *Nucleic Acids Res* 29:e45
40. Swettenham E, Witting PK, Salvatore BA, Neuzil J (2005) α -Tocopheryl succinate selectively induces apoptosis in neuroblastoma cells: potential therapy of malignancies of the nervous system? *J Neurochem* 94:1448–1456
41. Mosmann T (1983) Rapid colorimetric assay for cellular growth and survival—application to proliferation and cytotoxicity assays. *J Immunol Meth* 65:55–63
42. Neuzil J, Weber T, Schroder A et al (2001) Induction of cancer cell apoptosis by α -tocopheryl succinate: molecular pathways and structural requirements. *FASEB J* 15:403–415
43. Alleva R, Benassi MS, Tomasetti M et al (2005) α -Tocopheryl succinate induces cytostasis and apoptosis in osteosarcoma cells: the role of E2F1. *Biochem Biophys Res Commun* 331:1515–1521
44. Dong LF, Swettenham E, Eliasson J et al (2007) Vitamin E analogues inhibit angiogenesis by selective induction of apoptosis in proliferating endothelial cells: the role of oxidative stress. *Cancer Res* 67:11906–11913
45. Baksh S, Tommasi S, Fenton S et al (2005) The tumor suppressor RASSF1A and MAP-1 link death receptor signaling to bax conformational change and cell death. *Mol Cell* 18:637–650
46. Han J, Goldstein LA, Hou W, Rabinowich H (2007) Functional linkage between NOXA and Bim in mitochondrial apoptotic events. *J Biol Chem* 282:16223–16231
47. Han J, Goldstein LA, Gastman B et al (2004) Differential involvement of Bax and Bak in TRAIL-mediated apoptosis of leukemic T cells. *Leukemia* 18:1671–1680
48. Neuzil J, Tomasetti M, Zhao Y et al (2007) Vitamin E analogs, a novel group of “mitocans”, as anticancer agents: the importance of being redox-silent. *Mol Pharmacol* 71:1185–1199
49. Ralph SJ, Neuzil J (2009) Mitochondria as targets for cancer therapy. *Mol Nutr Food Res* 53:9–28
50. Wang XF, Birringer M, Dong LF et al (2007) A peptide conjugate of vitamin E succinate targets breast cancer cells with high ErbB2 expression. *Cancer Res* 67:3337–3344
51. Zhao Y, Li R, Xia W, Neuzil J, Lu Y, Zhang H, Zhao X, Zhang X, Sun C, Wu K (2010) Bid integrates intrinsic and extrinsic signaling in apoptosis induced by α -tocopheryl succinate in human gastric carcinoma cells. *Cancer Lett* 288:42–49
52. Gogvadze V, Orrenius S, Zhivotovsky B (2008) Mitochondria in cancer cells: what is so special about them? *Trends Cell Biol* 18:165–173
53. Chen L, Willis SN, Wei A et al (2005) Differential targeting of prosurvival Bcl-2 proteins by their BH3-only ligands allows complementary apoptotic function. *Mol Cell* 17:393–403
54. Czabotar PE, Lee EF, van Delft MF et al (2007) Structural insights into the degradation of Mcl-1 induced by BH3 domains. *Proc Natl Acad Sci USA* 104:6217–6222
55. Mei YD, Xie CW, Xie W, Tian X, Li M, Wu M (2007) Noxa/Mcl-1 balance regulates susceptibility of cells to camptothecin-induced apoptosis. *Neoplasia* 9:871–881
56. Lee EF, Czabotar PE, van Delft MF et al (2008) A novel BH3 ligand that selectively targets Mcl-1 reveals that apoptosis can proceed without Mcl-1 degradation. *J Cell Biol* 180:341–355
57. Pérez-Galán P, Roué G, Villamor N, Montserrat E, Campo E, Colomer D (2006) The proteasome inhibitor bortezomib induces apoptosis in mantle-cell lymphoma through generation of ROS and Noxa activation independent of p53 status. *Blood* 107:257–264
58. Kang MH, Wan Z, Kang YH, Spoto R, Reynolds CP (2008) Mechanism of synergy of N-(4-hydroxyphenyl)retinamide and ABT-737 in acute lymphoblastic leukemia cell lines: Mcl-1 inactivation. *J Natl Cancer Inst* 100:580–595
59. Letai A, Bassik MC, Walensky LD, Sorcinelli MD, Weiler S, Korsmeyer SJ (2002) Distinct BH3 domains either sensitize or activate mitochondrial apoptosis, serving as prototype cancer therapeutics. *Cancer Cell* 2:183–192
60. Marani M, Tenev T, Hancock D, Downward J, Lemoine NR (2002) Identification of novel isoforms of the BH3 domain protein Bim which directly activate Bax to trigger apoptosis. *Mol Cell Biol* 22:3577–3589
61. Merino D, Giam M, Hughes PD et al (2009) The role of BH3-only protein Bim extends beyond inhibiting Bcl-2-like pro-survival proteins. *J Cell Biol* 186:355–362
62. Fletcher JL, Meusburger S, Hawkins CJ et al (2008) Apoptosis is triggered when prosurvival Bcl-2 proteins cannot restrain Bax. *Proc Natl Acad Sci USA* 105:18081–18087
63. Day CL, Chen L, Richardson SJ, Harrison PJ, Huang DCS, Hinds MG (2005) Solution structure of prosurvival Mcl-1 and characterization of its binding by proapoptotic BH3-only ligands. *J Biol Chem* 280:4738–4744
64. Sattler M, Liang H, Nettlesheim D et al (1997) Structure of Bcl-x_L-Bak peptide complex: Recognition between regulators of apoptosis. *Science* 275:983–986
65. Song LX, Coppola D, Livingston S, Cress D, Haura EB (2005) Mcl-1 regulates survival and sensitivity to diverse apoptotic stimuli in human non-small cell lung cancer cells. *Cancer Biol Ther* 4:267–276
66. Zhou P, Qian LP, Kozopas KM, Craig RW (1997) Mcl-1, a Bcl-2 family member, delays the death of hematopoietic cells under a variety of apoptosis-inducing conditions. *Blood* 89:630–643
67. Okumura K, Huang SB, Sinicrope FA (2008) Induction of Noxa sensitizes human colorectal cancer cells expressing mcl-1 to the small-molecule Bcl-2/Bcl-x_L inhibitor, ABT-737. *Clin Cancer Res* 14:8132–8142
68. Dewson G, Kratina T, Sim HW et al (2005) To trigger apoptosis, Bak exposes its BH3 domain and homodimerizes via BH3: groove interactions. *Mol Cell* 30:369–380
69. Wang H, Takemoto C, Akasaka R et al (2009) Novel dimerization mode of the human Bcl-2 family protein Bak, a mitochondrial apoptosis regulator. *J Struct Biol* 166:32–37
70. Dewson G, Kratina T, Czabotar P, Day CL, Adams JM, Kluck RM (2009) Bak activation for apoptosis involves oligomerization of dimers via their $\alpha 6$ helices. *Mol Cell* 36:696–703
71. Sun F, Huo X, Zhai YJ et al (2005) Crystal structure of mitochondrial respiratory membrane protein complex II. *Cell* 121:1043–1057
72. Adam-Vizi V, Chinopoulos C (2006) Bioenergetics and the formation of mitochondrial reactive oxygen species. *Trends Pharmacol Sci* 27:639–645

Lyophilised Liposome-Based Formulations of α -Tocopheryl Succinate: Preparation and Physico-Chemical Characterisation

ŠTĚPÁN KOUDELKA,¹ JOSEF MAŠEK,¹ JIRI NEUZIL,^{2,3} JAROSLAV TURÁNEK¹

¹Department of Vaccinology and Immunotherapy, Veterinary Research Institute, Hudcova 70, 621 32 Bmo, Czech Republic

²Apoptosis Research Group, School of Medical Science, Griffith Institute of Health and Medical Research, Griffith University, Southport, 4222 Qld, Australia

³Molecular Therapy Group, Institute of Biotechnology, Academy of Sciences of the Czech Republic, Prague, Czech Republic

Received 25 June 2009; revised 16 September 2009; accepted 4 October 2009

Published online 28 December 2009 in Wiley InterScience (www.interscience.wiley.com). DOI 10.1002/jps.22002

ABSTRACT: α -Tocopheryl succinate (α -TOS) is a semisynthetic analogue of α -tocopherol with selective toxicity to the cancer cells and anticancer activity *in vivo*. Yet, no suitable formulation of α -TOS for medical application has been reported. Various formulations, for example, solutions in organic solvents, oil emulsions and vesicles prepared by spontaneous vesiculation, polyethylene glycol conjugates and liposomes of various compositions have been tested. We developed and characterised a stable lyophilised liposome-based α -TOS formulation. α -TOS (15 mol%) was incorporated into large oligolamellar vesicles (OLVs) composed of soy phosphatidylcholine (SPC) by the method of lipid film hydration followed by extrusion through polycarbonate filters. Stabilised liposomal formulation was prepared by lyophilisation in the presence of sucrose (molar ratio lipid/sucrose, 1:5). The size distribution of the liposomes (130–140 nm, polydispersity index 0.14) as well as the stable lipid and α -TOS contents were preserved during storage in the lyophilised form at 2–8°C for at least 6 months. The data indicate good physical and chemical stability of the lyophilised preparation of α -TOS liposomes that can be used in clinical medicine. © 2009 Wiley-Liss, Inc. and the American Pharmacists Association *J Pharm Sci* 99:2434–2443, 2010

Keywords: vitamin E analogues; liposome; extrusion; α -tocopheryl succinate; lyophilisation; stability; cancer; apoptosis; nanotechnology; particle size

INTRODUCTION

Proapoptotic analogues of VE have been reported to exert selective toxicity to malignant cells and very low negative side effect.^{1,2} The prototypic member of this group of agents, α -TOS, is a redox-silent, semisynthetic succinyl ester of α -TOH.³ The VE analogue has been shown to exert antiproliferative activity⁴ and induces cell apoptosis *in vitro*.⁵ The antitumour effects of α -TOS in various experimental models of cancer have also been documented.^{6–8}

Thus far, no suitable formulations of proapoptotic analogues of VE have been reported. From the clinical

point of view, the main disadvantage of these agents is their very low solubility in the aqueous environment. The hydrophobic character of VE analogues predetermines the strategy for their formulations. Different approaches to the preparation of delivery systems of α -TOS have been investigated. These procedures employed the drug solubilisation in organic solvents such as ethanol and dimethylsulphoxide^{9,10} or in oil emulsions,^{11–16} spontaneous vesiculation of the drug itself¹⁷ and the sodium¹⁸ or TRIS¹⁹ salts of the agents, conjugates of the drugs with polyethylene glycol^{20,21} and liposomal formulation of the agents.²² Development of an optimal delivery system for α -TOS needs to focus on the preparation of formulations of the VE analogue that would be stable during long-term storage, and that would retain its biological activity and would be useful for clinical application.

Liposomes, lipidic membranous vesicles, represent advanced and versatile nanodelivery systems for wide range of biologically active compounds.²³ These relatively nontoxic systems have considerable potential for the entrapment of both lipophilic and

Abbreviations: α -TOH, α -tocopherol; α -TOS, α -tocopheryl acid succinate; DLS, dynamic light scattering; LPC, lysophosphatidylcholine; MLV, multilamellar vesicle; OLV, oligolamellar vesicle; PDI, polydispersity index; SPC, soy phosphatidylcholine; VE, vitamin E.

Correspondence to: Jaroslav Turánek (Telephone: +420-5-3333-1311; Fax: +420-5-4121-1229; E-mail: turanek@vri.cz)

Correspondence to: Jiri Neuzil (Telephone: +61-7-5552-9109; Fax: +61-7-5552-4888; E-mail: j.neuzil@griffith.edu.au)

Journal of Pharmaceutical Sciences, Vol. 99, 2434–2443 (2010)
© 2009 Wiley-Liss, Inc. and the American Pharmacists Association

2434 JOURNAL OF PHARMACEUTICAL SCIENCES, VOL. 99, NO. 5, MAY 2010



hydrophilic drugs.²⁴ α -TOS can be easily incorporated into lipid membrane bilayers of liposomal vesicles. The relatively simple procedure allows production of liposomes for various applications. Therefore, entrapment of the drug in liposomes represents a very effective route that enhances its therapeutic effect. Liposomal formulation of α -tocopheryl maleamide (α -TAM), an esterase-resistant analogue of the ester α -tocopheryl maleate,²⁵ was reported to eliminate the acute toxicity associated with administration of the free VE analogue.²⁶

The physico-chemical stability of liposomal nanoparticles depends on their composition and structure. Physical modifications of liposomes, including fusion and aggregation of the particles, as well as increase of the membrane permeability and the drug release can occur as the consequences of chemical degradation of the liposomal system.²⁷ Lyophilisation in the presence of cryoprotectants (e.g. saccharides) is a process that stabilises the liposomal products for the purpose of long-term storage. Saccharides protect the liposomal integrity, enhance the retention of the drug entrapped in the liposomes and prevent degradation of the liposomal components.^{28,29}

The aim of this study was to develop an optimal lyophilised formulation of liposomal α -TOS. The preparation of the lyophilised liposomal α -TOS formulation, its physico-chemical characterisation and the evaluation of stability during 6-month storage period were investigated. At month-storage intervals, the following parameters of the stability of the liposomal samples were determined: particle size distribution, ζ -potential, lipid content, drug content and drug entrapment efficiency.

MATERIALS AND METHODS

Chemicals

α -TOS, α -tocopheryl acetate (α -TOA) and α -TOH were purchased from Sigma-Aldrich (Prague, Czech Republic). SPC (purity of 95%) and LPC were obtained from Avanti Polar Lipids (Alabaster, AL). The following chemicals were acquired from Fluka (Prague, Czech Republic): ferrous chloride quadrhydrate ($\text{FeCl}_2 \cdot 4\text{H}_2\text{O}$), ammonium thiocyanate (NH_4SCN), cupric sulphate (CuSO_4), phosphoric acid (H_3PO_4), sucrose and cumene hydroperoxide. All organic solvents used (reagent or HPLC grade) were purchased from Sigma-Aldrich. In all experiments, MilliQ water was used (Millipore, Prague, Czech Republic).

Preparation of α -TOS Liposomal Formulation

OLVs were prepared by the thin-film hydration method followed by extrusion through polycarbonate filters as previously described.^{30,31} Briefly, the

mixture of SPC and α -TOS was dissolved in chloroform and transferred into a round-bottom flask. To find the optimal composition, the lipid/ α -TOS molar ratios of 95:5; 90:10; 85:15 and 80:20 were tested. The organic solvent was removed using the rotary vacuum evaporator Laborota 4000 (Heidolph, Kelheim, Germany) yielding a dry thin lipid film (40°C, 4 h). The lipid film was then hydrated with an aqueous phase (20 mM HEPES buffer, pH 7.20, 0.2 μm filtered) and converted to the suspension of MLVs (lipid concentration of 10 mg/mL) by continuous shaking (30 min). The freezing and thawing step was omitted in order to preserve the oligolamellar morphology of the liposomes with a low internal volume of the water phase. MLVs were then sequentially extruded seven times through polycarbonate filters (Whatman, Alabaster, AL) of various pore sizes (400, 200, 100, 80 and 50 nm) at room temperature to find the optimal extrusion procedure yielding the population of OLVs. The polycarbonate filters (diameter of 25 mm) were inserted into the high-pressure filtration cell, which was linked to the FPLC system (Pharmacia, Uppsala, Sweden) that controlled the flow rate and provided the high pressure.³¹

Preparation of the Lyophilisate

The extruded liposomes were mixed with the appropriate amount of sucrose and sterilised by filtration through 0.22- μm filters (Millex-MP Filter Unit; Millipore). The lipid/sucrose molar ratios were 1:1, 1:3, 1:5, 1:7 and 1:10. Aliquots of the liposomal preparation (10 mg/mL of total lipid content) were filled into 20-mL sterile vials. These vials with 1.5 mL of liposomes were frozen at -80°C in a freezer and then lyophilised using the Lyovac GT2 instrument (Finn-Aqua, Tuusula, Finland). The samples were placed into the drying chamber precooled to -45°C . The lyophilisation procedure was run for 24 h at 8 Pa. After this period, a second drying step was applied at 25°C for 12 h under 20 Pa. The lyophilised samples were stored at $2-8^\circ\text{C}$ for further characterisation and stability studies.

Liposome Size and ζ -Potential Determination

The size distribution and ζ -potential of the liposomes (lipid concentration of 10 mg/mL) were determined by DLS and microelectrophoresis using a Zetasizer Nano ZS instrument (Malvern, Worcestershire, UK). The He-Ne laser in the equipment operated at the wavelength of 633 nm. The measurements were carried out at 25°C using the scattering angle of 173° for the determination of size distribution. Data were analysed in terms of the average size and the PDI.

The ζ -potential values were determined in the disposable cell by assessing the velocity of the liposomes in the electric field. To convert the electrophoretic

mobility into the ζ -potential values, the Smoluchowski constant $f(K_n) = 1.5$ was applied using the DT software (Malvern). The measurements took place at 25°C in 20 mM HEPES buffer used as the dispersant.

Characterisation of Liposomes by Transmission Electron Microscopy

The size and morphology of liposomes containing α -TOS were studied by transmission electron microscopy (TEM) using a negative staining method. The liposomes were placed on the carbon-coated copper grid and then stained with 2% ammonium molybdate solution. The stained samples were characterised using a Philips-Morgagni electron microscope (EM Philips 208 S, MORGAGNI software, FEI, Brno, Czech Republic).

Lipid Quantification

For each particular preparation, the final lipid concentration in the liposomal samples and in the lipid extracts was determined according to the Stewart method based on the quantification of the complex formed by phospholipids with ammonium ferriothiocyanate in the organic solution.³²

Lipid Extraction Procedure and Lysophospholipid Determination

Lipids were extracted from the liposomes according to the Bligh–Dyer³³ two-phase extraction method. Chloroform was removed on the rotary evaporator and the dry residuum was redissolved in the mixture of chloroform and methanol (2:1, v/v). Aliquots of 5 μ L (overall lipid content \sim 45 μ g) of the total lipid redissolved extracts were applied on the TLC silica gel 60 F₂₅₄ plates (Merck, Darmstadt, Germany). Separation of the lysophospholipid from the phospholipid was achieved in the development chamber containing chloroform/methanol/water (65:25:4, v/v/v) as the mobile phase. The developed plates were dried for 5 min at 100°C. Lipids were visualised by bathing the plates in the staining reagent, which was a mixture of 10% CuSO₄ (w/v) and 8% H₃PO₄ (v/v) in water, for 60 s. Subsequently, the plates were heated at 60°C for 15 min, which was followed by an increase in the temperature to 130°C for 15 min. Individual lipids became detectable as brown spots, and their optical densities were evaluated by photodensitometric scanning using the Scanner 3 apparatus equipped with winCATS software (Camag, Muttenz, Switzerland). The lysophospholipid content was expressed as a percentage of the total phospholipid. SPC and LPC were used as standards.

Determination of Hydroperoxide Content

Hydroperoxides in the liposomal samples were determined by the ferric thiocyanate assay with

several modifications. Samples of liposomes (50 μ L) were diluted to 0.5 mL with methanol, and then 0.4 mL of 1.14 mM FeCl₂·4H₂O solution was added. The subsequent addition of chloroform and methanol (0.5 mL each) formed a biphasic system. The sample was then vortexed, and after centrifugation at 2000g for 5 min two clear phases were observed. Solution of 60 mM NH₄SCN (0.2 mL) was added to 0.8 mL of the upper aqueous phase for the development of colour. The samples were analysed at 478 nm using the Uvikon XL spectrophotometer (BioTek, Winooski, USA). The stock solution of 0.19 mM cumene hydroperoxide was used as the standard.

Entrapment Efficiency of α -TOS

Aliquots of 100 μ L of liposomal α -TOS preparations (1 mg/mL α -TOS) were diluted with 20 mM HEPES buffer to the final volume of 2 mL and stirred gently. For the chromatographic analysis, the samples were prepared by ultracentrifugation at 30,000 rpm (108,000g, rotor JA-30.50 Ti, Beckman-Coulter, Fullerton, USA) for 50 min at 4°C (Beckman-Coulter, Avanti J-30I). The supernatant containing the free drug was separated from the sediment. The liposomal sediment was then redispersed in the same volume of 20 mM HEPES buffer. The redispersed sediment and the liposomes that were not centrifuged were frozen at -80°C and then lyophilised for 24 h. Both these parts of the sample were redissolved in the same volume of methanol (2 mL) and vortexed. Aliquots of 10 μ L were injected into the HPLC system. The entrapment efficacy of α -TOS loading into liposomes (EE_{TOS}) was calculated according to the following equation:

$$EE_{\text{TOS}}(\%) = \frac{A_{\text{LIP-TOS}}}{A_{\text{TOTAL-TOS}}} \times 100 \quad (1)$$

where $A_{\text{LIP-TOS}}$ represents the amount of α -TOS that remains associated with liposomes and $A_{\text{TOTAL-TOS}}$ is the total amount of α -TOS.

Analysis of α -Tocopheryl Succinate and α -Tocopherol

The chromatography was carried out using a Beckman Gold *Noveau* system composed of a 507 autosampler, a 127 binary gradient pump and a 168 diode array detector. The Agilent Eclipse XDB-C18 (150 mm \times 4.6 mm ID, 4- μ m particle size) stainless-steel analytical column was attached. The acidified mobile phase (0.03% acetic acid) consisting of methanol and water (97:3, v/v) was degassed by sonication prior to use. The separation was carried out isocratically at the flow rate of 1.3 mL/min and ambient temperature. The detector wavelength was set at 206 nm. The Gold *Noveau* software was used for the data collection and analysis. The calibration

graphs were calculated by linear regression analysis of the peak area ratio of the standard and the internal standard versus the drug concentration of the standard. α -Tocopheryl acetate was used as the internal standard.

Determination of Residual Water Content

The residual water content in the lyophilised liposomal α -TOS preparations was determined by Karl Fischer titration method using a volumetric TitroLine KF titrator (Schott Instruments, Mainz, Germany). Known amount of anhydrous methanol was added into container with a syringe to solubilise lyophilised cake of liposomal preparation. This procedure avoided contamination of the sample with airborne moisture. Known amount of solubilised sample was withdrawn by syringe from the container and added to the Karl Fischer titration vessel. The residual moisture content in anhydrous methanol was used as the blank. After the weight of sample in the final container was determined, the percent moisture was calculated. The results represent means of duplicate samples.

Statistics

The software GraphPad PRISM was used for the calculation and preparation of the size distribution and ζ -potential graphs. Statistical analysis using one-way ANOVA (significance level, $p < 0.05$) test was used for the size distribution and ζ -potential studies.

RESULTS

Preparation of Liposomal Formulations of α -TOS

The optimal amount of α -TOS drug entrapped in the SPC liposomes was found to be 15 mol% of total lipid.

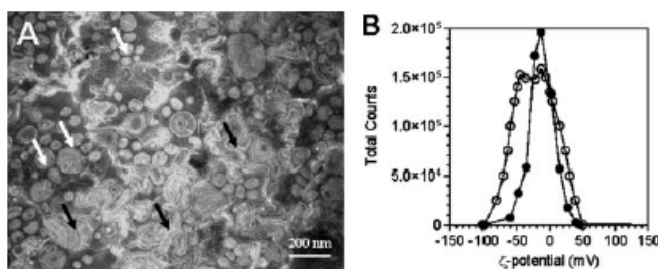


Figure 1. Characterisation of liposomal formulation containing 20 mol% of α -TOS. (A) Phase separation visualised by TEM. White arrows indicate liposomes; black arrows indicate nonliposomal structures. (B) Two peaks of ζ -potential were obtained for the liposomal preparation with 20 mol% of α -TOS (empty circles) characterised by the presence of nonliposomal and liposomal structures. The ζ -potential of the optimised liposomal preparation containing 15 mol% of α -TOS is denoted by the full circles. The ζ -potential values were assessed in 20 mM HEPES buffer.

The concentration of α -TOS higher than 20 mol% with respect to the total lipid leads to the phase separation, as assessed by TEM. The micrograph in Figure 1A documents the presence of liposomal as well as nonliposomal structures. Assessment of the ζ -potential revealed two peaks (Fig. 1B) with the more negative signal attributable to the nonliposomal fraction composed predominantly of negatively charged α -TOS. The liposomal composition of 85 mol% SPC and 15 mol% α -TOS was chosen for further development of the lyophilised liposomal preparations. Final size distribution of the liposomes reflected the pore size of the respective filters used for the extrusion (Tab. 1). Extrusion through the polycarbonate filters of the pore size of 0.2 μ m was found optimal with respect to the final size distribution and pressure/flow rate parameters. Extrusion of up to 50 mL of the liposomal suspension (10 mg/mL of lipid) in one run was facilitated by linking the high-pressure cell to the FPLC system equipped with a superloop. This method produced well-defined preparations of α -TOS liposomes. The final average size of the liposomes was 133 ± 4 nm and the PDI was within 0.14 ± 0.02 , as determined by the DLS assay. The negative ζ -potential of -13.4 ± 1.4 mV for the α -TOS liposomal preparation was obtained in 20 mM HEPES (pH 7.2).

Cryoprotective Effect of Sucrose

The lyophilisation process of liposomal α -TOS preparations in the presence of various additions of sucrose as cryoprotectant was studied in order to enhance the physical stability of the liposomes. The size distribution of the liposomes prior to lyophilisation and after the lyophilisate reconstitution was compared and evaluated using the DLS assay. The protection of the original size of liposomes

Table 1. Final Size Distribution of Optimal Liposome α -TOS Formulation Extruded through Polycarbonate Filters of Different Pore Size

Filter Pore Size (nm)	Average Size (nm)	Polydispersity Index	Size Distribution		
			Intensity (nm)	Volume (nm)	Number (nm)
400	172	0.16	205	202	112
200	140	0.10	157	145	100
100	122	0.08	134	121	91
80	103	0.07	111	98	79
50	89	0.06	92	82	68

Liposomal samples of the lipid concentration of 10 mg/mL were analysed in 20 mM HEPES buffer at 25°C.

(133 ± 4 nm, PDI 0.14 ± 0.02) was the main parameter used to consider the cryoprotective efficiency of sucrose (Fig. 2). When a minimal addition of sucrose was used (molar ratio, 1:1), the liposomes were physically unstable and tended to fuse and thus increased their size. Both the particle size and the PDI (240 ± 24 nm, PDI 0.70 ± 0.16) significantly increased as a consequence of the fusion and aggregation processes. Although the prepared liposomes (molar ratio, 1:3) had acceptable average size (141 ± 4 nm), the PDI was relatively high (0.26 ± 0.05). The minimal molar lipid/sucrose ratio necessary for the optimal stabilisation of the liposomal α -TOS formulations was found to be 1:5, as determined by the DLS assay (size 131 ± 3 nm, PDI 0.14 ± 0.03) and verified by TEM (data not shown). The presence of sucrose at this optimal ratio was sufficient to preserve the morphology and size distribution of the α -TOS liposomal preparation and was chosen for further stabilisation of the formulation. The liposomal samples with elevated amounts of sucrose (molar ratios, 1:7 and 1:10)

exhibited no additional stabilisation effect (size 126 ± 2 nm, PDI 0.13 ± 0.01 and 125 ± 2 nm, PDI 0.14 ± 0.01 , respectively).

Physico-Chemical Characterisation of Liposomal α -TOS

As mentioned above, the liposomal α -TOS formulation was lyophilised with an optimal amount of sucrose (lipid/sucrose molar ratio, 1:5) and then stored at 2–8°C for up to 6 months. The lyophilised samples were reconstituted at 1-month intervals with 20 mM HEPES buffer to give a final concentration of the liposomes with the lipid concentration of 10 mg/mL. The reconstitution step of the lyophilised dry powders was fast, and the rehydrated samples constituted dispersions of liposomes with milky translucent appearance. All physical and chemical parameters of the stability of α -TOS liposomes were assessed both prior to lyophilisation (initial state), immediately after reconstitution of the lyophilisate (time zero), and every month after reconstitution of the lyophilisate. The pH of the reconstituted liposomal preparations did not change from the initial value of 7.20 ± 0.15 during the storage period.

Physical Stability of Liposomes

The process of lyophilisation did not affect the physical stability of the liposomes containing sucrose as the cryoprotectant. The size distribution measurements of the reconstituted liposomes always showed mono-modal distribution. The particle size distribution and the ζ -potential of the liposomes containing α -TOS were 133 ± 4 nm (PDI 0.14 ± 0.02) and -13 ± 1.4 mV, respectively, before lyophilisation and 131 ± 2 nm (PDI 0.14 ± 0.03) and -13 ± 2.0 mV, respectively, after the lyophilisate reconstitution following 6 months of storage (Tab. 2, Fig. 3). The typical phenomenon of the liposome instability that usually results from an increase in the particle size was found neither by TEM nor by DLS evaluation. No significant changes in the ζ -potential of the lyophilised liposomes after the reconstitution were observed. These data document that the initial parameters of the physical stability of the α -TOS

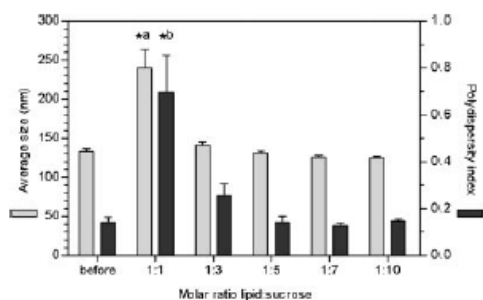


Figure 2. Effect of different lipid/sucrose molar ratios on the physical stability of the lyophilised optimal liposomal α -TOS formulation after reconstitution. The liposomes extruded in the presence of sucrose through a 0.2- μ m polycarbonate filter were used as control of size distribution prior to lyophilisation. ^{a,*},^{b,*}Statistically significant difference versus 'before' and versus '1:3, 1:5, 1:7 and 1:10' ($p < 0.001$).

Table 3. Chemical Stability of Reconstituted Lyophilisates of Optimal α -TOS Liposomal Preparations

Storage Time (Months)	Lipid Content (% of Initial)	Hydroperoxide Content (%)	Lysophospholipid Content (%)
Initial state	100	<0.1	3.9
0	99	<0.1	3.8
1	101	0.1	3.9
2	98	0.3	3.8
3	100	1.3	3.7
4	102	1.0	3.5
5	99	1.9	3.6
6	100	1.6	3.6

The data for hydroperoxide and lysophospholipid content are expressed as percentages of the total lipid concentration in respective samples. All data represent means of duplicate samples. The residual water content (w/w) remained unchanged in the range of 1.2–1.6% up to 6 months during storage (Karl Fischer titration method).

according to Eq. (1). The obtained values of EE_{TOS} of the reconstituted liposomal α -TOS formulations were greater than 90% during the storage period and 92% in the initial preparation. These values indicate a successful α -TOS trapping in liposomes and confirm very good incorporation of the drug into the SPC liposomal membrane bilayers. Monitoring the EE_{TOS} values during the 6-month storage period in a refrigerator has shown no discernible changes in the liposomal content of α -TOS. The content of α -TOS in the liposomes determined by HPLC was within the range of 95–105% of the drug concentration in the initial preparations. The presence and quantity of α -TOH as the degradation product of α -TOS was detected. The level of α -TOH in the preparations was assessed to verify the chemical stability of α -TOS entrapped in the liposomes. The HPLC analysis has proven that the α -TOH content did not exceed 5% of the α -TOS content. The results of the chemical characterisation of the drug are summarized in Table 4.

Table 4. Chemical Stability of α -TOS Entrapped in Liposomes after Reconstitution of the Lyophilisate

Storage Time (Months)	α -TOS Content (% of Initial)	α -TOS Entrapment (%)	α -TOH Content (%)
Initial state	100	92	1.1
0	101	94	1.2
1	103	92	1.6
2	101	95	2.1
3	97	91	2.9
4	98	93	3.9
5	97	94	4.7
6	95	94	4.9

The data for α -TOH content are expressed as percentages of α -TOS concentration in respective samples. All data represent means of duplicate samples.

The residual water content (w/w) remained unchanged in the range of 1.2–1.6% up to 6 months during storage (Karl Fischer titration method).

DISCUSSION

The VE analogue α -TOS and its esterase-resistant analogue α -tocopheryl maleate amide (α -TAM)²⁵ are efficient anticancer drugs as documented by studies on different experimental models of cancer. Their liposomal formulations were found to be well tolerated in mice of various strains and preserved the strong anticancer efficacy of the VE analogues, as shown using the transgenic FVB/N *c-neu* mice with spontaneous breast carcinomas.²⁶ Nonliposomal systems like vesiculated VE analogues formed by spontaneous vesiculation were found to be toxic for some analogues of VE, for example, α -tocopheryl oxalate,¹⁸ or α -TAM.²⁶ Thus, entrapment of such analogues (as shown for α -TAM) minimises the secondary toxicity while the anticancer efficacy remains preserved.²⁶

Stable preparations of α -TOS and similar anticancer agents that could be stored for prolonged periods of time are needed. A plausible approach to this problem is the use of liposomes, which have been utilised as suitable carriers for a variety of drugs and vaccines. Moreover, liposomal technologies are applicable at the industrial scale for the production of sterile preparations suitable for parenteral administration in the clinical setting. Therefore, we developed a method for the preparation of liposomal α -TOS, the drug that has been shown by us and others to exert potent anticancer activities in a variety of preclinical models,^{1,6–9,13–17,34,35} and its lyophilised formulation, which was stable during a 6-month period.

The hydrophobic character and low aqueous solubility of α -TOS predetermine liposomes as suitable delivery systems. The multiple liposomal bilayers in oligolamellar liposomes show an effective capacity for incorporation of α -TOS and they also enhance the solubility of the drug by partitioning of α -TOS among the phosphatidylcholine molecules. We

prepared the optimal liposomal α -TOS formulation by the classical method, which constitutes hydration of a lipid film followed by an extrusion step. This simple process allowed preparation of low-dispersive and homogeneous populations of liposomes. The liposomes were able to encapsulate up to 15 mol% of α -TOS without any negative effect on the stability of the membrane bilayers. At higher molar ratios of α -TOS, phase separation occurred and nonliposomal structures were formed (cf. Fig. 1A). This phase separation limits the encapsulation capacity of the SPC liposomes for α -TOS to <20 molar%.

Other methods for the preparation of liposomal α -TOS were described in literature, for example, combination of the lipid film formation followed by anionic surfactant hydration and detergent dialysis.³⁶ However, this procedure is more time-consuming and no data on phosphatidylcholine/ α -TOS molar ratio have been documented in the literature. Therefore, we favour the method described in this communication.

Application of a secondary processing method, that is, extrusion through polycarbonate filters, was successfully used for the reduction of the final size distribution of the α -TOS liposomal preparations to <150 nm. Liposomes of these sizes are appropriate for intravenous applications, especially their long-circulating versions are suitable for targeting of solid tumours.

Saccharides such as trehalose or sucrose are cryoprotectants known to exert a stabilising effect on liposomal membrane bilayers during lyophilisation.²⁹ In our case, we selected sucrose as the low-cost cryoprotectant suitable for the application in clinical medicine. The saccharides stabilise the liposomal bilayers when the membrane-stabilising water is removed, for example, by drying or by lyophilisation. The protective effect is related to the ability of direct interaction of disaccharides with the polar head-groups of phospholipids by forming hydrogen bonds. The saccharides also form an amorphous and glassy matrix and exhibit low molecular mobility (vitrification). The individual particles become embedded in this state during lyophilisation, and they are also protected from the mechanical damage of the crystalline ice formation.³⁷ The cryoprotectants need a careful optimisation of concentration for effective stabilisation of the liposomal delivery systems.³⁸ We observed that at the lipid/sucrose molar ratio of 1:5, very good morphological as well as chemical stability of the lyophilised preparation was achieved. Similar results were reported for the stability of lyophilised liposomal formulations of the camptothecin-based anticancer drug SN-38.³⁹ TEM observations confirmed that the structure of the oligolamellar liposomes incorporating α -TOS was not changed during storage in the lyophilised stage. This is important

because this type of liposomes is endowed with sustained release of the entrapped drug, since their concentric membranes are slowly degraded and release of the drug from the bilayers is attenuated.⁴⁰

Liposomal formulations of α -TOS have already been reported, although the physico-chemical characterisation of these preparations over a prolonged storage period was not assessed.^{35,41} Lyophilisation/freeze-drying of the liposomal products in the presence of a suitable saccharide cryoprotectant was found to enhance the stability of the dry lyophilisate powders during long-term storage.^{42,43} A major advantage of this process is lyophilisation of liposomes under appropriate cryoprotective conditions. The structural integrity of the liposomes is protected and the potential particle fusion and aggregation are prevented. During the storage period, the α -TOS-containing liposomes maintained their vesicle size unchanged and, upon reconstitution, the original liposome size was always observed. Based on the DLS assay, the liposome size distribution was found to be about 130 nm within 0.14 of PDI (cf. Fig. 3 and Tab. 2).

During freeze-drying, water is removed by sublimation from the liposomal formulation so that possible alterations of the physical and chemical properties during long-term storage, in particular lipid hydrolysis, are minimised.^{44,45} As a consequence of significant lipid hydrolysis, the organisation of the lipid assembly can change from lamellar to the micellar system.⁴⁶ In our α -TOS liposomal preparations, the content of lysophospholipids was not changed during storage (cf. Tab. 3). Another potential problem encountered upon the storage of liposomal preparations is oxidation of lipids, resulting in phospholipid degradation. The primary products of oxidation of lipids in the presence of molecular oxygen are lipid hydroperoxides.⁴⁷ Further, the lipid packaging/organisation in the bilayer is disturbed as a result of lipid oxidation, which results in an increased membrane permeability. We found that in our preparations, the content of lipid hydroperoxides did not exceed 2% of the total lipid during the 6-month storage, and that the increase of the lipid hydroperoxide content occurred during the first 2 months of storage (cf. Tab. 3). The low percentage of hydroperoxides and lysophospholipids in the liposomal preparations following their 6-month storage period are within the limits suggested by Barenholz and Amselem⁴⁸ for liposomal preparations of doxorubicin.

In our liposomal formulation, up to 5% of α -TOH was found as a degradation product of α -TOS during the prolonged storage period. The decomposition of α -TOS during the 6-month storage represented only about 4% of total α -TOS (cf. Tab. 4), which is acceptable from the pharmacological point of view. This decrease of α -TOS content affected neither the ζ -

potential of the liposomes (cf. Tab. 2) nor the pH values of the preparation (results not shown). These results clearly document that α -TOS undergoes only minimal hydrolysis during prolonged storage, making such preparations suitable for clinical application.

In conclusion, we developed methodology for the preparation of lyophilised α -TOS liposomes, as a stable dry-powder formulation. This was achieved by the lyophilisation/freeze-drying process using the optimal amount of amorphous sucrose matrix as the cryoprotectant and stabiliser of the lyophilisate. This preparation is suitable for storage for at least 6 months, since none of the major physico-chemical parameters tested was altered beyond the acceptable limit. In preclinical testing, such liposomal formulations of α -TOS have been proved to be well tolerated by mice after repeated intravenous applications, and the anticancer effect was demonstrated *in vivo* using transgenic FVB/N *c-neu* mice with spontaneous breast carcinomas and the mouse B16F10 melanoma model.²⁶ To summarize, we have developed a formulation of a α -TOS, a promising anticancer drug, which is warranted for testing in clinical trials.

ACKNOWLEDGMENTS

This work was supported in part by the grants from Ministry of Agriculture of the Czech Republic (Grant No. MZE 0002716202) to J.T., the Ministry of Education, Youth and Sport of the Czech Republic (project MSM 0021627502) to S.K. and the Academy of Sciences of the Czech Republic (KAN200520703) to J.N. and J.T. The authors thank to Dr. Jana Plocková for her assistance in the preparation of the manuscript, Dr. Pavel Kulich for the preparation of TEM micrographs and Dr. Josef Slavik for his help with TLC densitometric analyses.

REFERENCES

- Weber T, Lu M, Andera I, Lahm H, Gellert N, Fariss MW, Korinek V, Sattler W, Ucker DS, Terman A, Schroder A, Erl W, Brunk UT, Coffey RJ, Weber C, Neuzil J. 2002. Vitamin E succinate is a potent novel antineoplastic agent with high selectivity and cooperativity with tumor necrosis factor-related apoptosis-inducing ligand (Apo2 ligand) *in vivo*. *Clin Cancer Res* 8:863–869.
- Neuzil J, Weber T, Gellert N, Weber C. 2001. Selective cancer cell killing by α -tocopheryl succinate. *Br J Cancer* 84:87–89.
- Djuric Z, Heilbrun LK, Lababidi S, EverettBauer CK, Fariss MW. 1997. Growth inhibition of MCF-7 and MCF-10A human breast cells by α -tocopheryl hemisuccinate, cholesteryl hemisuccinate and their ether analogs. *Cancer Lett* 111:133–139.
- Neuzil J, Tomasetti M, Zhao Y, Dong LF, Birringer M, Wang XF, Low P, Wu K, Salvatore BA, Ralph SJ. 2007. Vitamin E analogs, a novel group of 'mitocans', as anti-cancer agents: The importance of being redox-silent. *Mol Pharmacol* 71:1185–1199.
- Yu WP, Sanders BG, Kline K. 1997. RRR- α -tocopheryl succinate inhibits EL4 thymic lymphoma cell growth by inducing apoptosis and DNA synthesis arrest. *Nutr Cancer* 27:92–101.
- Malafa MP, Fokum FD, Andoh J, Neitzel LT, Bandyopadhyay S, Zhan R, Iizumi M, Furuta E, Horvath E, Watabe K. 2006. Vitamin E succinate suppresses prostate tumor growth by inducing apoptosis. *Int J Cancer* 118:2441–2447.
- Tomasetti M, Gellert N, Procopio A, Neuzil J. 2004. A vitamin E analogue suppresses malignant mesothelioma in a preclinical model: A future drug against a fatal neoplastic disease? *Int J Cancer* 109:641–642.
- Barnett KT, Fokum FD, Malafa MP. 2002. Vitamin E succinate inhibits colon cancer liver metastases. *J Surg Res* 106:292–298.
- Ramanathapuram LV, Kobie JJ, Bearss D, Payne CM, Trevor KT, Akporiaye ET. 2004. AT α -Tocopheryl succinate sensitizes established tumors to vaccination with non-matured dendritic cells. *Cancer Immunol Immunother* 53:580–588.
- Neuzil J, Massa H. 2005. Hepatic processing determines dual activity of α -tocopheryl succinate: A novel paradigm for a shift in biological activity due to pro-vitamin-to-vitamin conversion. *Biochem Biophys Res Commun* 327:1024–1027.
- Basu A, Grossie B, Bennett M, Mills N, Imrhan V. 2007. AT α -Tocopheryl succinate (α -TOS) modulates human prostate LNCaP xenograft growth and gene expression in BALB/c nude mice fed two levels of dietary soybean oil. *Eur J Nutr* 46:34–43.
- Fariss MW, Bryson KF, Hylton EE, Lippman HR, Stubin CH, Zhao XG. 1993. Protection against carbon tetrachloride-induced hepatotoxicity by pretreating rats with the hemisuccinate esters of tocopherol and cholesterol. *Environ Health Perspect* 101:528–536.
- Wang XF, Birringer M, Dong LF, Veprek P, Low P, Swettenham E, Stantic M, Yuan LH, Zabalova R, Wu K, Ralph SJ, Ledvina M, Neuzil J. 2007. A peptide adduct of vitamin E succinate targets breast cancer cells with high erbB2 expression. *Cancer Res* 67:3337–3344.
- Dong LF, Swettenham E, Eliasson J, Wang XF, Gold M, Medunic Y, Stantic M, Low P, Prochazka L, Witting PK, Turanek J, Akporiaye ET, Ralph SJ, Neuzil J. 2007. Vitamin E analogs inhibit angiogenesis by selective apoptosis induction in proliferating endothelial cells: The role of oxidative stress. *Cancer Res* 67:11906–11913.
- Dong LF, Low P, Dyason J, Wang XF, Prochazka L, Witting PK, Freeman R, Swettenham E, Valis K, Liu J, Zabalova R, Turanek J, Spitz DR, Domann FE, Scheffler IE, Ralph SJ, Neuzil J. 2008. AT α -Tocopheryl succinate induces apoptosis by targeting ubiquinone-binding sites in mitochondrial respiratory complex II. *Oncogene* 27:4324–4335.
- Dong LF, Freeman R, Liu J, Zabalova R, Marin-Hernandez A, Stantic M, Rohlena J, Rodriguez-Enriquez S, Valis K, Butcher B, Goodwin J, Brunk UT, Witting PK, Moreno-Sanchez R, Scheffler IE, Ralph SJ, Neuzil J. 2009. Suppression of tumour growth *in vivo* by the mitocan α -tocopheryl succinate requires respiratory complex II. *Clin Cancer Res* 15:1593–1600.
- Ramanathapuram LV, Hahn T, Graner MW, Katsanis E, Akporiaye ET. 2006. Vesiculated α -tocopheryl succinate enhances the anti-tumor effect of dendritic cell vaccines. *Cancer Immunol Immunother* 55:166–177.
- Kogure K, Manabe S, Suzuki I, Tokumura A, Fukuzawa K. 2005. Cytotoxicity of α -tocopheryl succinate, malonate and oxalate in normal and cancer cells *in vitro* and their anti-cancer effects on mouse melanoma *in vivo*. *J Nutr Sci Vitaminol* 51:392–397.
- Tirmenstein MA, Ge XK, Elkins CR, Fariss MW. 1999. Administration of the tris salt of α -tocopheryl hemisuccinate inactivates CYP2E1, enhances microsomal α -tocopherol levels and protects against carbon tetrachloride-induced hepatotoxicity. *Free Radic Biol Med* 26:825–835.

20. Youk HJ, Lee E, Choi MK, Lee YJ, Chung JH, Kim SH, Lee CH, Lim SJ. 2005. Enhanced anticancer efficacy of α -tocopheryl succinate by conjugation with polyethylene glycol. *J Control Release* 107:43–52.
21. Quin J, Engle D, Litwiller A, Peralta E, Grasch A, Boley T, Hazelrigg S. 2005. Vitamin E succinate decreases lung cancer tumor growth in mice. *J Surg Res* 127:139–143.
22. Jizomoto H, Kanaoka E, Hirano K. 1994. pH-sensitive liposomes composed of tocopherol hemisuccinate and of phosphatidylethanolamine including tocopherol hemisuccinate. *Biochim Biophys Acta* 1213:343–348.
23. Sharma A, Sharma US. 1997. Liposomes in drug delivery: Progress and limitations. *Int J Pharm* 154:123–140.
24. Hofheinz RD, Gnad-Vogt SU, Beyer U, Hochhaus A. 2005. Liposomal encapsulated anti-cancer drugs. *Anticancer Drugs* 16:691–707.
25. Tomic-Vatic A, EyTina JH, Chapmann JM, Mahdavian E, Neuzil J, Salvatore BA. 2005. Vitamin E amides, a new class of vitamin E analogues with enhanced pro-apoptotic activity. *Int J Cancer* 117:118–123.
26. Turanek J, Wang XF, Knotigova P, Koudelka S, Dong LF, Vrablova E, Mahdavian E, Prochazka L, Sangsura S, Vacek A, Salvatore BA, Neuzil J. 2009. Liposomal formulation of α -tocopheryl maleamide: In vitro and in vivo toxicological profile and anticancer effect against spontaneous breast carcinomas in mice. *Toxicol Appl Pharmacol* 237:249–257.
27. Grit M, Crommelin JA. 1993. Chemical-stability of liposomes—Implications for their physical stability. *Chem Phys Lipids* 64:3–18.
28. Crowe LM, Crowe JH, Rudolph A, Womersley C, Appel L. 1985. Preservation of freeze-dried liposomes by trehalose. *Arch Biochem Biophys* 242:240–247.
29. Crowe JH, Crowe LM, Carpenter JF, Wistrom CA. 1987. Stabilization of dry phospholipid-bilayers and proteins by sugars. *Biochem J* 242:1–10.
30. Turanek J, Kasna A, Zaluska D, Neca J. 2003. Preparation of sterile liposomes by proliposome-liposome method. *Methods Enzymol* 367:111–125.
31. Turanek J. 1994. Fast-protein liquid-chromatography system as a tool for liposome preparation by the extrusion procedure. *Anal Biochem* 218:352–357.
32. Stewart JCM. 1980. Colorimetric determination of phospholipids with ammonium ferrioxalate. *Anal Biochem* 104:10–14.
33. Bligh EG, Dyer WJ. 1959. A rapid method of total lipid extraction and purification. *Can J Biochem Physiol* 37:911–917.
34. Neuzil J, Weber T, Schröder A, Lu M, Ostermann G, Gellert N, Mayne GC, Olejnicka B, Nègre-Salvayre A, Sticha M, Coffey RJ, Weber C. 2001. Induction of apoptosis in cancer cells by α -tocopheryl succinate: Molecular pathways and structural requirements. *FASEB J* 15:403–415.
35. Lawson KA, Anderson K, Simmons-Menchaca M, Atkinson J, Sun LZ, Sanders BG, Kline K. 2004. Comparison of vitamin E derivatives α -TEA and VES in reduction of mouse mammary tumor burden and metastasis. *Exp Biol Med* 229:954–963.
36. Gu XB, Schwartz JL, Pang XW, Zhou YF, Sirois DA, Sridhar R. 2006. Cytotoxicity of liposomal α -tocopheryl succinate towards hamster cheek pouch carcinoma (HCPC-1) cells in culture. *Cancer Lett* 239:281–291.
37. Crowe JH, Leslie SB, Crowe LM. 1994. Is vitrification sufficient to preserve liposomes during freeze-drying. *Cryobiology* 31:355–366.
38. Suzuki T, Komatsu H, Miyajima K. 1996. Effects of glucose and its oligomers on the stability of freeze-dried liposomes. *Biochim Biophys Acta* 1278:176–182.
39. Zhang JA, Xuan T, Parmar M, Ma L, Ugwu S, Ali S, Ahmad I. 2004. Development and characterization of a novel liposome-based formulation of SN-38. *Int J Pharm* 270:93–107.
40. New RRC. 1990. Introduction. In: New RRC, editor. *Liposomes: A practical approach*. Oxford: IRL Press. pp 1–32.
41. Kang YH, Lee EM, Youk HJ, Kim SH, Lee HJ, Park YG, Lim SJ. 2005. Potentiation by α -tocopheryl succinate of the etoposide response in multidrug resistance protein 1-expressing glioblastoma cells. *Cancer Lett* 217:181–190.
42. Hinch DK, Zuther E, Hellwege EM, Heyer AG. 2002. Specific effects of fructo- and gluco-oligosaccharides in the preservation of liposomes during drying. *Glycobiology* 12:103–110.
43. Sun WQ, Leopold AC, Crowe LM, Crowe JH. 1996. Stability of dry liposomes in sugar glasses. *Biophys J* 70:1769–1776.
44. Grit M, Desmidt JH, Struijke A, Crommelin DJA. 1989. Hydrolysis of phosphatidylcholine in aqueous liposome dispersions. *Int J Pharm* 50:1–6.
45. Grit M, Underberg WJM, Crommelin DJA. 1993. Hydrolysis of saturated soybean phosphatidylcholine in aqueous liposome dispersions. *J Pharm Sci* 82:362–366.
46. Zuidam NJ, Gouw HKME, Barenholz Y, Crommelin DJA. 1995. Physical (in)stability of liposomes upon chemical hydrolysis—The role of lysophospholipids and fatty acids. *Biochim Biophys Acta* 1240:101–110.
47. Schnitzer E, Pinchuk I, Lichtenberg D. 2007. Peroxidation of liposomal lipids. *Eur Biophys J* 36:499–515.
48. Barenholz Y, Amselem S. 1993. Quality control assays in the development and clinical use of liposome-based formulations. In: Gregoriadis G, editor. *Liposome technology*. Volume I. New York: CRC Press. pp 527–616.



Liposomal formulation of α -tocopheryl maleamide: *In vitro* and *in vivo* toxicological profile and anticancer effect against spontaneous breast carcinomas in mice

Jaroslav Turánek^{a,*}, Xiu-Fang Wang^b, Pavlína Knötigová^a, Štěpán Koudelka^a, Lan-Feng Dong^b, Eva Vrublová^a, Elahe Mahdavian^c, Lubomír Procházka^a, Smink Sangsura^c, Antonín Vacek^a, Brian A. Salvatore^c, Jiri Neuzil^{b,d,*}

^a Department of Vaccinology and Immunotherapy, Veterinary Research Institute, Brno, Czech Republic

^b Apoptosis Research Group, School of Medical Science, Griffith University, Southport, Qld, Australia

^c Department of Chemistry, Louisiana State University, Shreveport, LA, USA

^d Molecular Therapy Group, Institute of Biotechnology, Academy of Sciences of the Czech Republic, Prague, Czech Republic

ARTICLE INFO

Article history:

Received 17 October 2008

Revised 5 January 2009

Accepted 12 January 2009

Keywords:

Vitamin E analogues

Liposome

α -Tocopheryl maleamide

α -Tocopheryl succinate

Apoptosis

Cancer

Mouse cancer model

Ultrasound imaging

Hollow fibers

Immunotoxicity

ABSTRACT

The vitamin E analogue α -tocopheryl succinate (α -TOS) is an efficient anti-cancer drug. Improved efficacy was achieved through the synthesis of α -tocopheryl maleamide (α -TAM), an esterase-resistant analogue of α -tocopheryl maleate. *In vitro* tests demonstrated significantly higher cytotoxicity of α -TAM towards cancer cells (MCF-7, B16F10) compared to α -TOS and other analogues prone to esterase-catalyzed hydrolysis. However, *in vitro* models demonstrated that α -TAM was cytotoxic to non-malignant cells (e.g. lymphocytes and bone marrow progenitors). Thus we developed lyophilized liposomal formulations of both α -TOS and α -TAM to solve the problem with cytotoxicity of free α -TAM (neurotoxicity and anaphylaxis), as well as the low solubility of both drugs. Remarkably, neither acute toxicity nor immunotoxicity implicated by *in vitro* tests was detected *in vivo* after application of liposomal α -TAM, which significantly reduced the growth of cancer cells in hollow fiber implants. Moreover, liposomal formulation of α -TAM and α -TOS each prevented the growth of tumours in transgenic FVB/N *c-neu* mice bearing spontaneous breast carcinomas. Liposomal formulation of α -TAM demonstrated anti-cancer activity at levels 10-fold lower than those of α -TOS. Thus, the liposomal formulation of α -TAM preserved its strong anti-cancer efficacy while eliminating the *in vivo* toxicity found of the free drug applied in DMSO. Liposome-based targeted delivery systems for analogues of vitamin E are of interest for further development of efficient and safe drug formulations for clinical trials.

© 2009 Elsevier Inc. All rights reserved.

Introduction

α -Tocopheryl succinate (α -TOS) is a semi-synthetic analogue of vitamin E (VE) with selective toxicity for cancer cells (Neuzil et al., 2001a) and anti-cancer efficacy *in vivo* (Prasad et al., 2003). A new derivative, α -tocopheryl maleamide (α -TAM), represents a novel class of apoptogenic VE analogues with a non-cleavable amide bond, endowing them with higher pro-apoptotic effects *in vitro* (Tomovic et al., 2005). α -TOS is a potent inducer of apoptosis in a wide

range of human and murine cancer cells (Dalen and Neuzil, 2003; Weber et al., 2002; Neuzil et al., 2001b; Israel et al., 2000; Yu et al., 1997, 1999), while showing limited or no toxicity toward non-malignant cells (Neuzil et al., 2001a; Israel et al., 2000; Yu et al., 1999). In experimental models, α -TOS and its derivatives have been demonstrated to inhibit a variety of cancers (Wang et al., 2006), including breast (Wang et al., 2006; Hahn et al., 2006; Dong et al., 2008) lung (Ramanathapuram et al., 2004) and colon cancer (Barnett et al., 2002; Weber et al., 2002; Neuzil et al., 2001b; Prasad et al., 2003), as well as melanomas (Malafa et al., 2002) and mesotheliomas (Stapelberg et al., 2005; Tomasetti et al., 2004).

A significant limitation of using α -TOS and other VE derivatives is their low solubility in aqueous solvents. Hydrophobic character and low solubility of α -tocopherol and its derivatives pre-determine their drug formulations. Applications of α -TOS in ethanol, DMSO or vegetable oil emulsions by intravenous or intraperitoneal routes are largely restricted to mouse tumour models, with little clinical relevance. Vesiculated forms of α -TOS and various surfactants and solubilizers (e.g. polyethylene glycols) have been tested as suitable formulations for human application. Spontaneous vesiculation of

Abbreviations: CFU-E, erythroid colony-forming unit; ConA, concanavaline A; EPC, egg phosphatidylcholine; GM-CFC, granulocyte-macrophage colony-forming cell; PVDF, polyvinylidene difluoride; α -TAM, α -tocopheryl maleamide; α -TOH, α -tocopherol; α -TOM, α -tocopheryl maleate; α -TOS, α -tocopheryl succinate; USI, ultrasound imaging; VE, vitamin E.

* Corresponding authors. J. Turánek is to be contacted at Veterinary Research Institute, Department of Vaccinology and Immunotherapy, Hudcova 70, 621 32 Brno, Czech Republic. Fax: +420 5 4121 1229. J. Neuzil, Apoptosis Research Group, Griffith Institute of Health and Medical Research, School of Medical Science, Griffith University, Gold Coast Campus, Southport, Qld, Australia. Fax: +61 7 55524888.

E-mail addresses: turanej@vri.cz (J. Turánek), j.neuzil@griffith.edu.au (J. Neuzil).

0041-008X/\$ – see front matter © 2009 Elsevier Inc. All rights reserved.
doi:10.1016/j.taap.2009.01.027

sodium or TRIS salts of α -TOS (Jizomoto et al., 1984) and other dicarboxylic acid analogues has been utilized for drug formulations that are suitable for *i.v.* applications. Anti-cancer effects of vesiculated α -TOS were proven in mouse tumour models, but this formulation does not eliminate *in vivo* toxicity of some potent analogues of VE, such as α -tocopheryl oxalate (Kogure et al., 2005). Some practical problems with long-term stability during storage were also not addressed.

Liposomes represent an advanced and versatile nanodelivery system for drug formulation that can eliminate or suppress organ-specific toxic side-effects of various drugs (Allen, 1997). α -TOS and other vitamin E analogues could be easily incorporated into the lipid bilayers to produce liposomes of various size distribution and surface modification, affecting their half-life, organ distribution and targeting to cancer cells. Recently, successful experimental treatment of pre-established tumours of the highly metastatic murine mammary cancer cell line 4T1 was demonstrated, using combination of chemotherapy with vesiculated α -TOS and dendritic cell-based immunotherapy (Ramanathapuram et al., 2005). Low toxicity and, especially, immunotoxicity of anticancer drugs and their formulations are important requirements for successful combination of chemo- and immunotherapy.

In this paper we present data showing that both α -TOS and the new, highly potent analogue α -TAM, when formulated in liposomes, efficiently induced apoptosis in cancer cells *in vitro* and suppressed tumours in mouse models without secondary toxicity and immunotoxicity.

Materials and methods

Cell culture and treatment. B16F10 mouse melanoma and MCF-7 human breast cancer cell lines were obtained from the European Collection of Cell Cultures. The cells were grown in the RPMI-1640

medium supplemented with 10% of fetal calf serum, 50 μ g/ml penicillin, 50 μ g/ml streptomycin, 100 μ g/ml neomycin, and 300 μ g/ml L-glutamine, and were treated with α -tocopherol (α -TOH), α -TOS (both Sigma), α -tocopheryl maleate (α -TOM) (Birringer et al., 2003) or α -TAM (Tomic-Vatic et al., 2005) (see Fig. 1 for structures of VE and its analogues). Drugs were solubilized in small volume of DMSO and then in PBS (residual concentration of DMSO in medium was below 1%). The concentration range was 0.6–300 μ M, exposure time 24 h.

Preparation of liposomes. Liposomes containing VE analogues in combination with EPC (egg phosphatidylcholine, 99%; Avanti Polar Lipids), were prepared using the proliposome–liposome method, or hydration of a lipid film, followed by extrusion through polycarbonate filters with different pore size in an analogous way to that described earlier (Turánek et al., 2003; Turánek, 1994). The hand-operated mini-extruder (Avanti Polar Lipids) was used for preparation of small volumes of liposomes (up to 1 ml). Large-volume liposomes were extruded using a high-pressure cell attached to the HPLC instrument (GE Healthcare) (Turánek, 1994).

Size and zeta-potential measurements. DLS (dynamic light scattering) and micro-electrophoresis were performed using a NanoSizer SZ (Malvern, UK) to measure the size and zeta-potential of liposome preparations, using phospholipids at 1 mg/ml in PBS and temperature of 25 °C. Disposable cells were used for zeta-potential measurements. The size of the liposomal preparation was expressed as volume distributions (% in class).

MTT-based cytotoxicity assay. The MTT viability assay was used as described (Mosmann, 1983; Bank et al., 1991) to assess the cytotoxicity of VE analogues. The results of the test were confirmed by Hoffman modulation contrast and fluorescent microscopy (Nikon T200 microscope equipped with G2B filter set) to visualize

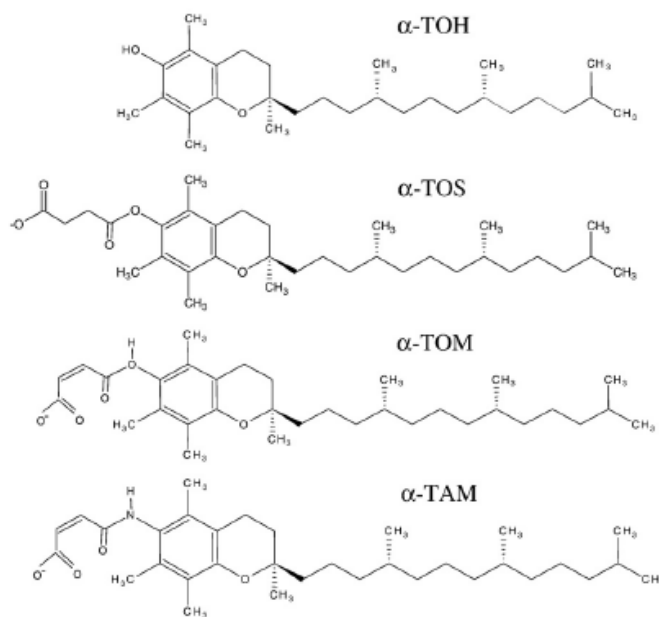


Fig. 1. Structures of VE analogues. The structures of α -tocopherol (α -TOH), α -tocopheryl succinate (α -TOS), α -tocopheryl maleate (α -TOM) and α -tocopheryl maleamide (α -TAM) are shown.

morphological changes of treated cells. Propidium iodide (PI; 5 μM) and YO-PRO-1 (5 μM) (Molecular Probes) were used to distinguish dead or apoptotic cells from living cells (Izdziorek et al., 1995). The exposure time was 24 h.

Cytotoxic effects of VE analogues on ConA-stimulated mouse splenocytes. Standard ^3H -thymidine incorporation test was used to study *in vitro* cytotoxic effects of α -TAM and α -TOS on mouse splenocytes stimulated with concanavaline A (ConA; 10 $\mu\text{g}/\text{ml}$). Briefly, splenocytes were prepared from Balb/c mouse spleen by its homogenization through a fine nylon mesh. Cells density was adjusted to 10^6 cells per ml of the RPMI-1640 medium supplemented with 10% pre-colostral calf serum and antibiotics. Cells were seeded in 96-well plates in triplicate and exposed to α -TOH, α -TOS or α -TAM. The tested drugs were solubilized in DMSO and the final concentration of DMSO in the medium was 0.5% (v/v) or lower. The cells were supplemented with ^3H -thymidine (50 μl , 5 $\mu\text{Ci}/\text{ml}$) 24 h before harvesting, and assessed for ^3H -thymidine incorporation using the TopCount NXT β -counter (Packard Bioscience). Exposure times 24, 48, and 72 h were used to follow the toxic effect on lymphocytes in various stages of activation and proliferation.

In vitro cytotoxic effect of VE analogues on mouse bone marrow GM-CFC. For granulocyte-macrophage colony-forming cell (GM-CFC) determination, bone marrow cells from Balb/c mice were drawn by flushing the femoral bone with IMDM, counted (Model ZN, Coulter Electronics), and kept on ice until used. Femoral marrow cells (10^5 per ml) were plated in triplicate in a semi-solid environment created by a plasma dot containing IMDM plus 20% fetal calf serum, and 3% IL-3-containing conditioned medium (Vacek et al., 1990). Tested compounds (α -TOS or α -TAM) were added into medium and the cultures were incubated for next 7 d in semisolid medium. Colonies of at least 50 cells were scored using a microscope (40 \times magnification).

In vivo cytotoxic effect of α -TOS and α -TAM on GM-CFC from mouse bone marrow and on peripheral blood leucocytes. Balb/c mice (female, 8 per group) were injected *i.v.* with 100 μl of PBS (control), empty liposomes (liposomal control, 1.3 g of PC/kg), liposomal α -TOS (100 or 10 mg/kg) and liposomal α -TAM (25 mg/kg). Four animals from each group were euthanized by cervical dislocation 48 h later and the number of GM progenitors in bone marrow counted as described (Vacek et al., 1990). The other 4 mice in each group were used to assess the effect of VE analogues on peripheral blood count during 3 weeks after drug administration. To do this, 20 μl of blood was taken every week from the tail vein and the number of leucocytes counted (Model ZN, Coulter Electronics).

Berlin test for toxicity of liposomal VE analogues in mice. The Berlin test of general toxicity was used as the method for evaluation of potential toxic effects of VE analogues on Balb/c or C57Bl mice (females). Individual animals (10 per group) treated with given agents were weighed and their behavior monitored for the next 10 d. Mice treated with PBS or empty liposomes were used as control groups. Liposomal preparations were administered *i.v.* or *i.p.* as a single dose (100 mg/kg α -TOS, 25 mg/kg α -TAM) or as 4 repeated doses within 6 d (25 mg/kg per dose α -TOS, 5 mg/kg per dose α -TAM). Typical symptoms of toxicity based on the Berlin test, including motoric disorder, respiratory problems, apathy, horrent fur, behavioral changes and loss of body mass, were monitored daily. The test was complemented by dissection of the euthanized animals and inspection of their organs (weighing, microscopic observation of morphological changes).

Hollow fiber assay for anti-tumour efficacy of VE analogues. Polyvinylidene difluoride (PVDF) hollow fibers (molecular mass cut-off 500 kDa, internal diameter 1 mm) (CELMAX[®] Implant Membrane,

Spectrum Laboratories) were processed according to the manufacturer's instructions. Loading of fibers with cells and their surgical implantation was done according to the published protocol (Hall et al., 2000; Hollingshead et al., 1995). A 5 mm incision on the *linea alba* exposed the peritoneum which was then incised (2 mm) to allow passage of hollow fibers into the abdomen. Three fibers per mouse were inserted in the craniocaudal direction on the right side of the peritoneal cavity.

Balb/c or C57Bl mice (3 per group) with hollow fiber implants containing B16F10 or MCF-7 cancer cell were treated *i.v.* with liposomal α -TAM by tail vein injection. Cumulative doses of 75 mg α -TAM per kg (three equivalent doses of 25 mg/kg applied on days 1, 3 and 5 after implantation of hollow fibers) were applied. The mice in the control group were treated with the same dose of empty liposomes.

On day 6, the hollow fibers were retrieved from the mice and the samples assessed for viable cells using the MTT viability assay. The fibers were incubated in 6-well plates (3 fibers/well) in 3 ml of the complete RPMI 1640 medium, containing 1 mg/ml MTT, for 4 h at 37 $^{\circ}\text{C}$. The MTT solution was then aspirated and the fibers washed with 2 ml saline containing 2.5% protamine sulfate overnight at 4 $^{\circ}\text{C}$. A second wash was performed with 2 ml saline containing 2.5% protamine sulfate, and the fibers maintained at 4 $^{\circ}\text{C}$ for 4 h. The fibers were then placed in a 24-well plate (1 fiber/well), SDS (0.2 ml of 10% solution) added to each well to extract the formazan crystals, and the plates rotated for 4 h at room temperature. The extracted samples were transferred to 96-well plates, and the absorbance was recorded at 540 nm.

Mouse breast cancer experiments. The transgenic FVB/N *c-neu* mice with spontaneous breast carcinomas (Guy et al., 1992) were treated with α -TOS solubilized in DMSO or formulated in liposomes. From 3 months of age, the mice were regularly scanned for tumours using the Vevo770 ultrasound imaging (USI) system (VisualSonics) equipped with the 60 MHz (40 μm resolution) RMV704 scan-head (VisualSonics), essentially as detailed elsewhere (Dong et al., 2007; Wang et al., 2007; Dong et al., 2008). After tumours were detected (typically 10–20 mm³), treatment with α -TOS in DMSO, or liposomal α -TOS or α -TAM commenced. Therapy with α -TAM in DMSO was not attempted since in preliminary toxicity studies, 1 or 2 injections of α -TAM in DMSO at the dose of 0.8 mg per animal (16 mg/kg) killed the test (Balb/c) mice, i.e. at levels 10-fold lower than those of α -TOS used in therapy of mice with experimental tumours and showing minimum toxicity. Mice were injected with α -TOS in DMSO intraperitoneally and with the liposomally formulated agents via the tail vein, with 5 total injections on days 1, 4, 7, 10 and 13. α -TOS in DMSO was injected at 400 mg/kg. Liposomal preparations of α -TOS and α -TAM, comprising 10% (w/w) of the VE analogue and 90% (w/w) EPC, were reconstituted in water so that the preparation contained 2.5% (w/v) liposomes. The average size of the liposomes was 140–145 nm, their polydispersity index in the range of 0.1–0.13. The volume of the liposomal preparation injected per animal was such that every animal received 400 mg/kg α -TOS or 40 mg/kg α -TAM per dose.

Analysis of VE analogues. VE analogues were extracted from liposomes by Bligh-Dyer two-phase extraction (Bligh and Dyer, 1959) chloroform was removed on a rotary evaporator and the dry residuum dissolved in the mobile phase (methanol–water, 99:1, acidified with 3% acetic acid), and subjected to HPLC analysis. The Eclipse XDB-C18 HPLC column (4.6 \times 15 mm, 5 μm) (Agilent) was eluted at 1.2 ml/min using the Beckman System Gold HPLC system. Injected volume: 10 μl . UV detection: 205 nm. α -Tocopheryl acetate (Sigma) was used as the internal standard (20 μg α -tocopheryl acetate per 1 mg of α -TOS). Calibration curve for vitamin E and the tested analogues was linear in the concentration range 1–100 $\mu\text{g}/\text{ml}$. Elution times: α -TOS, 6.1 min; α -TOH, 7.8 min; α -tocopheryl acetate, 11.2 min.

Statistics The program GraphPad PRISM was used for the calculation of cytotoxicity curves and IC_{50} . Newman–Keuls Multiple Comparison Test was used for statistical analysis of haemotoxicity and the hollow fiber studies. For the pre-clinical tumour model, differences in the mean relative tumour size (\pm S.D.) were examined using analysis of covariance (ANCOVA) with days as the covariate. Statistical analyses were performed using the SPSS[®] 10.0 analytical software. Statistical significance was accepted at $p < 0.05$.

Animal safety. Mice were housed and handled according to the rules of the Commission for Animal Welfare of the Ministry of Agriculture of the Czech Republic, and according to the guidelines of the Australian and New Zealand Council for the Care and Use of Animals in Research and Teaching, and were approved by the local Animal Ethics Committees.

Results

Preparation of liposomal VE analogues

We first attempted to prepare various types of liposomes encapsulating the VE analogues α -TOS and α -TAM. Because α -TOS, unlike α -TAM, is commercially available, we optimized the liposomal preparation using the succinyl analogue, and the results were then applied to preparation of liposomal α -TAM. Liposomes composed of EPC could accept up to 15 molar % of α -TOS without affecting the stability of the bilayer. Phase separation was observed by transmission electron microscopy when the concentration of α -TOS in liposomal composition was 20 molar % of total lipid (results not shown). This observation was confirmed by zeta-potential measurements. Two peaks with zeta-potential of -48 and -18 mV (assessed in PBS) were observed confirming non-liposomal and liposomal α -TOS containing structures, respectively. The composition of 90% EPC and 10% α -TOS was chosen for further experiments as optimal with respect to morphological stability of liposomes. Liposomes with well defined size distribution were prepared by application of extrusion through polycarbonate filters with various pore sizes. Small-scale preparations

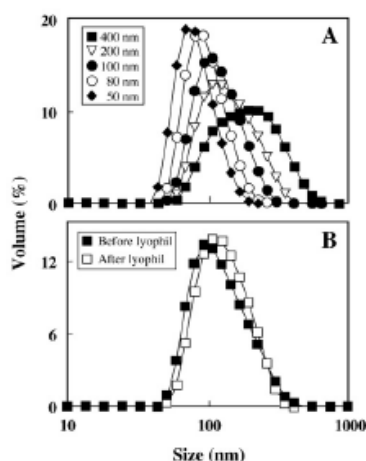


Fig. 2. Preparation of liposomes by extrusion. (A) Liposomes with α -TOS were prepared by extrusion through polycarbonate filters of different pore size and their size distribution was assessed by DLS. (B) α -TOS-containing liposomes prepared by extrusion through a 200 nm filter were assessed for size distribution before lyophilization and after rehydration following a 6-month storage in the refrigerator. Size distribution is expressed in volume (% in class).

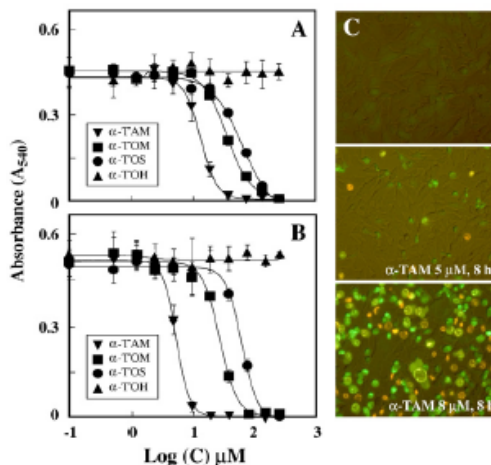


Fig. 3. Cytotoxic effect of VE analogues on cancer cell lines. Human breast carcinoma MCF-7 (A) and mouse melanoma B16F10 cells (B) were exposed for 24 h to α -TOH, α -TOS, α -TOM or α -TAM at the concentrations shown and assessed for MTT activity as detailed in Materials and methods. Media control is set at -1 because of the $\log(c)$ scale. (C) The mouse melanoma B16F10 cells were treated with the vehicle (control cells), or for 8 h with α -TAM at 5 or 8 μ M, and observed under epifluorescence microscope. The fluorescent markers Yo-Pro-1 (green) and PI (red/yellow) were used for visualization of early apoptotic changes and post-apoptotic, secondary necrosis, respectively.

(up to 1 ml) were performed using a hand-operated mini-extruder. Large-scale preparations (10–20 ml) were achieved by application of a high-pressure extrusion cell and the FPLC chromatographic system as the source of high pressure.

Fig. 2A shows fine-tuning of the size distribution with respect to the applied filter pore size. Both techniques used for extrusion produced liposomal preparations of similar quality, therefore the high-pressure extrusion cell linked to the FPLC apparatus was used for the large-scale process (grams of phospholipids). Polycarbonate filters with 0.2 μ m pore size were used to produce monodisperse liposomal preparation (size of 140–145 nm and polydispersity within 0.1–0.13) suitable for i.v. application. The extrusion process was also running at relatively low pressure (~ 1 MPa). Zeta-potential of liposomal α -TOS (10%) in PBS was -12 ± 2 mV.

For long term storage and transport, liposomes were stabilized by lyophilization in the presence of sucrose. The lipid:sucrose molar ratio of 1:5 was found sufficient to preserve the physical (size, polydispersity) and chemical (content of α -TAM or α -TOS) properties of the liposomal preparations. Physical stability of lyophilized liposomal α -TOS after rehydration is shown in Fig. 2B, which demonstrates no changes in the physical stability of the liposomes. Also, there was virtually no difference in the content of α -TAM and α -TOS (as assessed by HPLC) in the lyophilized liposomal samples stored for up to 12 months at 4 $^{\circ}$ C (data not shown).

In vitro cytotoxicity of VE analogues against cancer cell lines

The human breast cancer cell line MCF-7 and the murine melanoma cell line B16F10 were used for testing the effects of α -TOH and its analogues α -TOS, α -TOM and α -TAM. The cytotoxic potential of the four agents is presented in Figs. 3A, B, with the order of α -TAM > α -TOM > α -TOS > α -TOH. No toxicity was observed for the redox-active α -TOH. Similarly, the IC_{50} values followed the same trend, with the lowest ones for α -TAM for both cell lines (Table 1). The

Table 1
IC₅₀ values of the effect of liposomal VE analogues on the viability of MCF-7 and B16F10 cells

Vitamin E analogue	Cancer cell line	
	MCF-7	B16F10
	IC ₅₀ (μM)	
α-TAM	13.3 ^a	5.2
α-TOM	35.5	26.6
α-TOS	63.5	61.5
α-TOH	>300	>300

^a The IC₅₀ values (μM) were calculated from the MTT activity curves (cf. Fig. 3) using the GraphPad PRISM software.

high level of toxicity of α-TAM to cancer cells was confirmed by fluorescence microscopy of B16F10 cells exposed to the VE analogue using the marker of apoptosis YO-PRO-1 and necrosis PI, showing profound appearance of apoptotic morphology of the cells (Fig. 3C).

Cytotoxic effects of VE analogues on ConA-stimulated mouse splenocytes

Mouse splenocytes were stimulated with ConA and exposed for increasing periods of time to α-TOS or α-TAM, and assessed for inhibition of their proliferation. The dose response curves in Fig. 4A demonstrate that the inhibitory effect of α-TAM, was stronger than

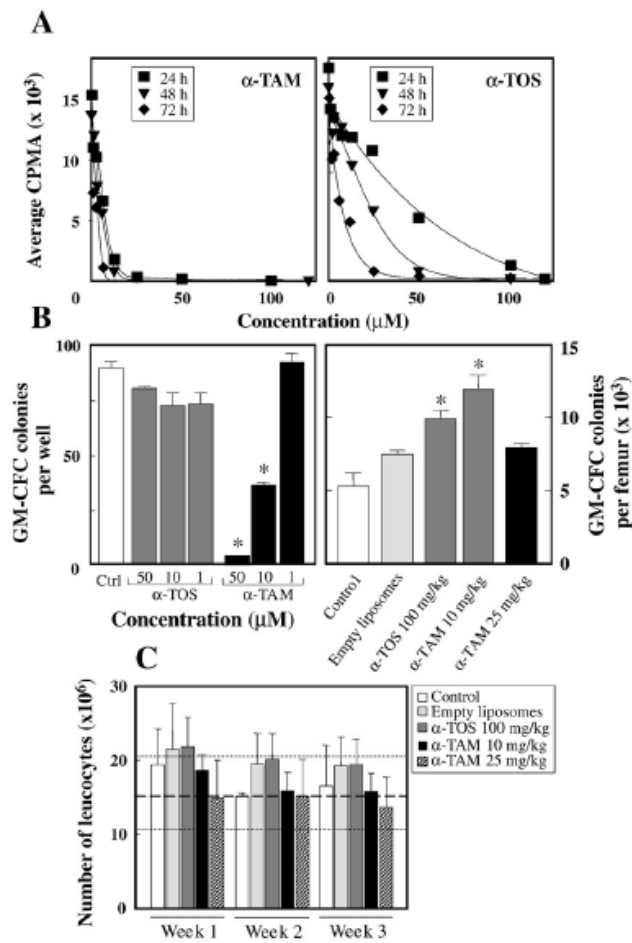


Fig. 4. Liposomal VE analogues are non-toxic to normal cells in vivo. (A) Mouse splenocytes, prepared from Balb/c mice and stimulated with 10 μg/ml ConA as detailed in Materials and methods, were exposed to α-TOS or α-TAM for the time periods and concentration shown, and their proliferation was assessed using the ³H-thymidine incorporation method, expressed in counts per min. (B, left panel). GM progenitors were isolated from Balb/c mouse bone marrow and treated with α-TOS or α-TAM at the concentrations shown, the number of colonies was counted and expressed per individual well. (B, right panel). Balb/c mice were injected i.p. with the vehicle, empty liposomes or liposomal α-TOS or α-TAM at the doses shown, and GM-CFC colonies in bone marrow counted 48 h later and expressed per individual femur (* denotes statistically significant differences with p < 0.05 in comparison to control). (C) Balb/c mice were injected i.v. with the vehicle, empty liposomes or liposomal α-TOS or α-TAM at the doses shown. Small volume of blood (20 μl) was drawn from each animal 1, 2 or 3 weeks later, and the number of leucocytes counted. The dashed horizontal line shows the normal leucocyte blood count in healthy, untreated Balb/c mice, with standard deviation indicated by the dotted lines. No statistical significant differences were found between control and treated groups.

that of α -TOS. This data is consistent with the toxicity of the agents to cancer cells.

In vitro and in vivo cytotoxic effects of VE analogues on GM-CFC from mice bone marrow

We next studied toxicity of free α -TOS and α -TAM to the GM-CFC progenitors *in vitro*. Our results show that α -TOS was non-toxic when applied at doses of up to 50 μ M, while α -TAM, in contrast, was highly toxic at 50 μ M and was also toxic when applied at 10 μ M (Fig. 4B). *In vivo* application of both derivatives as liposomal preparations did not cause any suppression of bone marrow proliferation and decrease in GM-CFC progenitors. On the contrary, we observed 1.5–2.5-fold stimulation of bone marrow proliferation reflected by an increase in GM-CFC progenitors after application of liposomal formulation of both derivatives (Fig. 4B).

Effect of liposomal VE analogues on leukocyte count

Application of neither liposomal α -TOS nor α -TAM affected the leukocyte count in peripheral blood within 3 weeks following their administration in mice, when applied as a single dose at 100 mg/kg α -TOS, or 25 or 10 mg/kg α -TAM (Fig. 4C). Our results demonstrate that the leukocyte counts in mice treated with the two agents administered as liposomal preparations were well within the range of normal leukocyte numbers in mice. Thus, there is a good correlation between *in vivo* effects of liposomal preparations of both VE analogues on bone marrow proliferation (cf. Fig. 4B) and leukocyte count in peripheral blood after *i.v.* application of the agents.

Berlin toxicity test

We studied the general toxicity of liposomal preparations of both α -TOS and α -TAM in mice. Untreated mice and mice treated with empty liposomes were used as controls. Neither of the typical symptoms of toxicity used by the Berlin test, including motoric disorder, respiratory problems, apathy, horrent fur, behavioral changes, anorexia and loss of body mass, were observed immediately after application of the drugs or within the following 10 d in either Balb/c or C57Bl mice. No morphological changes of inner organs were observed after dissection and microscopic examination. Contrary to the liposomal formulation, free α -TAM applied in DMSO at 5 mg/kg caused rapid death of the animals. Symptoms like spasms and heavy breathing pointed to neurotoxicity or anaphylactic reaction. Therefore, we discontinued experiments that involved the use of non-liposomal formulations of α -TAM.

Effect of liposomal α -TAM on hollow fiber model of cancer cell proliferation

The hollow fiber model was used for pre-screening of potential anti-cancer activity of α -TAM *in vivo*. Because of the surgical intervention required for insertion of the hollow fiber implants, it was of interest to follow the potential effects of liposomal α -TAM on healing of surgical wounds. We did not observe any adverse effects (inflammation, ulceration, abnormal cicatrization or re-opening of cut) of liposomal α -TAM on wound healing which proceeded in a normal and comparable manner in both control Balb/c or C57Bl mice and in animals treated with liposomal α -TAM. We next evaluated the effect of liposomal α -TAM on proliferation of MCF-7 and B16F10 cell lines in Balb/c mice. Application of liposomal α -TAM significantly reduced the growth of both cell lines in the implants (Fig. 5A). In the second experiment, we focused on B16F10 cells implanted in young (3–4 months) and old (8–9 months) C57Bl mice. In both groups of animals, liposomal α -TAM suppressed growth of cancer cells in the hollow fiber implants by 50–70%, with somewhat higher efficacy in

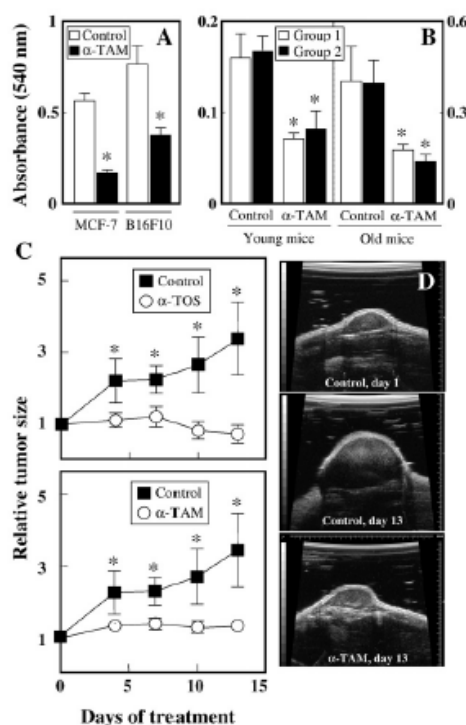


Fig. 5. Liposomal VE analogues inhibit proliferation of cancer cells *in vivo* and suppress breast carcinomas. Hollow fibers were seeded with MCF-7 or B16F10 cells and implanted in the peritoneum of Balb/c mice (A), or with B16F10 cells and implanted in the peritoneum of 3–4 or 8–9 month old C57Bl mice (B), as detailed in Materials and methods. The mice were then injected with 3 doses of liposomal α -TAM at 25 mg/kg of the VE analogue each at 48 h intervals, the hollow fibers removed and proliferation of the cells evaluated using the MTT assay as detailed in Materials and methods. Results of two independent experiments are shown in B (* denotes statistically significant differences with $p < 0.05$ in comparison to control). (C) Transgenic FVB/N *c-neu* transgenic mice with spontaneous breast carcinomas were treated by injection of liposomal α -TOS and α -TAM at doses corresponding to 15 and 15 μ mol of α -TOS and α -TAM, respectively, administered on days 0, 4, 7 and 13, as detailed in Materials and methods. The tumour volume was quantified non-invasively by USI and expressed relative to the initial volume, which was 21 ± 5 mm³. Panel D shows representative images of a control mouse at the onset of the experiment and on day 13, and a mouse treated with liposomal α -TOS on day 13. The data shown are mean values \pm SD ($n = 5$), the symbol *** denotes statistically significant differences with $p < 0.05$.

the older mice (Fig. 5B). No symptoms of toxicity after liposomal α -TAM application were observed in either group of mice.

Anti-cancer effects of liposomal VE analogues in experimental breast cancer

We next assessed the effect of liposomal α -TOS and α -TAM on breast carcinomas in the transgenic FVB/N *c-neu* mice with spontaneous ductal HER2-high breast carcinomas. Liposomal preparations of both α -TOS and α -TAM suppressed breast carcinomas in the *c-neu* mice by 90–100%, when applied in amounts corresponding to approximately 15 μ mol α -TOS and 1.5 μ mol α -TAM per dose (Fig. 5C). Importantly, neither of the two liposomally formulated analogues was toxic to the *c-neu* mice. This is especially encouraging in the case of α -TAM, which is extremely toxic when applied as solution in DMSO.

Discussion

We and others have recently focused on a novel class of anti-cancer agents, redox-silent VE analogues. Of these, the ester α -TOS has been studied most, due to its relatively high apoptogenic activity and selectivity for cancer cells, as well as anti-cancer efficacy in animal models of neoplasia (for review see Neuzil et al., 2007a). In the quest for more efficient pro-apoptotic drugs, over 60 compounds analogous to the prototypic α -TOS have been synthesized and tested for their apoptogenic activity towards cancer cells, some showing IC_{50} values in the low micromolar range (for review see Neuzil et al., 2007b for review). A serious problem encountered when maximizing the apoptogenic activity of compounds by modifying their structure is loss of selectivity for cancer cells *in vitro* or tumour tissue in pre-clinical models. For example, the highly apoptogenic α -tocopheryl oxalate is toxic to immunocompromised mice (Kogure et al., 2005).

We have recently developed a novel group of VE analogues, in which the functional domain is linked to the tocopheryl head group via an amide bond that is not prone to esterase-catalyzed hydrolysis. Furthermore, since peptidases are in general far more discriminating and less promiscuous than esterases, we reasoned that the apoptogenic activity of tocopheryl amides may be more pronounced *in vivo*, thereby increasing the anti-cancer efficacy of the amides vs. the esters (Tomic-Vatic et al., 2005). The IC_{50} value for α -TAM was $\sim 2 \mu M$ for the Jurkat T lymphoma or the Meso-2 mesothelioma cells, while it was about 10-times higher for the corresponding α -TOM. On the other hand, the non-malignant fibroblasts were rather resistant to α -TAM (Tomic-Vatic et al., 2005). However, when we tested α -TAM *in vivo*, in an experiment in which 40 mg/kg (1.5 μmol) of the agent, i.e. ~ 10 -times less than the efficient dose used in mouse models of cancer for α -TOS (Dong et al., 2007; Stapelberg et al., 2005; Malafa et al., 2002; Barnett et al., 2002; Weber et al., 2002; Dong et al., 2008), the amide analogue showed extreme toxicity. Thus, one or two injections of α -TAM in DMSO in Balb/c, C57Bl or FVB/N *c-neu* mice caused death of the animals, associated with severe neurotoxicity and anaphylactic shock. We therefore were not able to proceed in testing this highly apoptogenic amide analogue of VE in pre-clinical models of cancer. Application of liposomal preparations of α -TAM was not accompanied by any sign of toxicity, as assessed using the Berlin toxicity test and gross pathological examination of the animals. This fact is supportive to application of liposomes as carriers for this drug.

Liposomal formulations have been used to administer hydrophobic drugs into the bloodstream (Allen, 1997). This approach offers several advantages. For example, the drug is embedded in the liposomal particles that form an emulsion in the bloodstream, while the 'naked' drug would (at least to some extent) precipitate at the site of administration, possibly resulting in severe local and/or systemic inflammation, activation of the complement and general toxicity. Liposomal preparations also allow for longer half-life of the drug in the bloodstream and better uptake by cancer cells, in particular when the drug is embedded in long-circulating liposomes (Karanth and Murthy, 2007; Gabizon, 1992). An interesting report described the use of pH-sensitive liposomes comprised of α -TOS and phosphatidyl ethanolamine for drug delivery (Jizomoto et al., 1984). Such liposomes are more selective for cancer cells with an acidic pH gradient in the proximity of the plasma membrane (Gerweck and Seetharaman, 1996; Karanth and Murthy, 2007), and we reported that α -TOS, a weak acid, is taken up considerably faster by tumour cells than their non-malignant counterparts (Neuzil et al., 2002). Most importantly, perhaps, liposomes have been used as a delivery vehicle to bypass the frequent generic toxicity of anti-cancer agents (Tattersall and Clarke, 2003; Krishna et al., 1997).

For the above reasons, in particular the last one, we decided to investigate whether VE analogues, represented by α -TOS and α -TAM,

can be used as anti-cancer agents following their liposomal formulation. For this, the method of extrusion was used for liposomal preparation, applying filters of a defined pore size. We chose for further application liposomes containing 10% of the VE analogue prepared by extrusion through a 200-nm filter, with appropriate physical properties including the size distribution and zeta-potential (cf. Fig. 2A). These liposomes also showed very good physico-chemical stability, such as little or no change in the size distribution following lyophilization and reconstitution after prolonged storage (cf. Fig. 2B), and no change in the contents of either of the two VE analogues (see the Results section). Therefore, we exploited the use of liposomes comprising α -TOS and α -TAM mouse models of cancer.

α -TAM, however, strongly suppressed *in vitro* proliferation of ConA-primed mouse splenocytes (cf. Fig. 4A) as well as formation of GM-CSF colonies (cf. Fig. 4B). On the other hand, when injected into the bloodstream of the experimental animals, liposomal α -TOS and α -TAM did not induce suppression of GM-progenitors in the femur. In fact, both agents stimulated proliferation of progenitors by 50–150% (cf. Fig. 4B). This is indicative of the promotion of hematopoiesis by liposomal formulations of VE analogues at doses that have been used to suppress tumours in animal models (Dong et al., 2007; Stapelberg et al., 2005; Malafa et al., 2002; Barnett et al., 2002; Weber et al., 2002; Dong et al., 2008). Elimination of the potential *in vivo* adverse effect on GM-progenitors in the femur by α -TAM, which was indicated by cytotoxic effect found for the 'naked' compound *in vitro*, could be explained by favourable redistribution of the drug incorporated in liposomes, so that the concentration of α -TAM in bone marrow did not reach the toxic levels. Elimination of bone marrow toxicity of some antiviral drugs, e.g. azidothymidine, entrapped in liposomes was well documented in literature (Phillips and Tsoukas, 1992; Garg and Jain, 2006). Moreover, it was found by us and others that liposomes themselves exert slight immunostimulating activity and can also induce stimulation of bone marrow GM-progenitors (Turánek et al. 1997; Kasna et al. 2004). These data can be reconciled with an earlier report, documenting promotion of erythropoiesis by α -TOS (Gogu et al., 1991) as well as toxicity of α -TOS to leukemic cells while not affecting normal hematopoiesis (Freitas et al., in press). The authors showed that α -TOS, when added to bone marrow cells at $\sim 10 \mu M$, stimulated an increase in the number of the erythroid colony-forming unit (CFU-E)-derived colonies, comparable to the effects of 50 mU of erythropoietin or 200 U of IL-3. When applied at 50 mg/kg, α -TOS caused $\sim 75\%$ increase in CFU-E-derived colonies in femur bone marrow cells (Gogu et al., 1991). Collectively, these data indicate that liposomal formulations of both α -TOS and α -TAM can be used safely in experimental mouse models of cancer.

Before assessing the anti-cancer activity of liposomal analogues in a relevant mouse cancer model, we first tested the effect of liposomal α -TAM on the growth of cancer cells in hollow fiber implants in mice (Hall et al., 2000; Hollingshead et al., 1995). Our data reveal a very good response to the VE analogue applied via the tail vein, with up to 90% inhibition of cancer cell proliferation (cf. Figs. 5A, B). Importantly, too, liposomal α -TAM did not exert any discernible toxicity in these animals, as assessed using the Berlin test. This is in sharp contrast to the pilot experiment, in which we injected mice with α -TAM dissolved in DMSO, resulting in rapid death of the animals (see the Results section). The lack of general toxicity of liposomal α -TAM in mice allowed us to move to the ultimate experiment of this project, testing the liposomal formulations of α -TOS and α -TAM in a relevant model of neoplastic disease. We used the transgenic FVB/N *c-neu* mice carrying the rat *HER-2/neu* proto-oncogene driven by the MMTV promoter on the H-2^d FVB/N background, with spontaneous formation of ductal breast carcinomas (Guy et al., 1992). Both liposomal α -TOS and α -TAM reduced the tumour growth by almost 90% (cf. Figs. 5C, D), similarly as shown before for α -TOS solubilized in com oil and injected in the *c-neu* mice with breast carcinomas (Dong et al., 2007;

Wang et al., 2007). In accord with the *in vitro* data, some 10-times lower doses of liposomal α -TAM were needed in comparison to α -TOS to induce comparable anti-tumour effects. Again, and consistent with previous experiments, there was no adverse reaction of the transgenic mice to the liposomal VE analogues during the course of the therapy. These results clearly demonstrate that liposomal formulations eliminate the deleterious generic toxicity inherent to non-liposomal α -TAM. This is in agreement with previously published data for other anti-cancer agents (Tattersall and Clarke, 2003; Krishna et al., 1997).

There are scant reports on pharmacokinetics and tissue distribution of α -TOS and other analogues after *i.v.* administration in vesiculated or liposomal forms. One study showed that α -TOS applied to rats had a half-life of approximately 10 h with a small volume of distribution and low clearance. α -TOS was preferentially accumulated in the lung and liver tissue and associated with cell membrane lipids, especially within the microsomal and mitochondrial membranes (Teng et al., 2005). Considering the toxicity, pharmacokinetics and pharmacodynamics of vitamin E analogues, the physical nature of the applied drugs is an important factor. *In vivo* toxicity of some derivatives of vitamin E could be ascribed to their toxicity toward certain somatic cells when applied at higher concentrations, but, more probably, the rapid onset of acute toxicity is due to the physical nature of the vitamin E derivatives. These hydrophobic compounds dissolved in the organic phase (e.g. DMSO or ethanol) can form nano- and microparticles after injection into water phase. The structure of these particles has not been described in an adequate manner in the literature. According to our experience, after injection of α -TOS ethanolic solution into water phase, the VE analogue forms microparticles and metastable nanoparticles (30–60 nm), which tend to precipitate. The high density of the surface negative charge of these particles could be responsible for activation of the complement and rapid precipitation of the drugs can lead to formation of microparticles inducing embolization in the lungs and the heart. We observed these symptoms in mice that died after *i.v.* application of α -TAM dissolved in DMSO. Intra-peritoneal application of the DMSO-dissolved derivatives appeared to have caused toxic effects due to their precipitation on the surface of inner organs and induction of inflammation in the peritoneum. Fusion of inner organs after *i.p.* application of α -TOS is a good evidence of inflammation in peritoneum and injury to pellicia of inner organs. This supports our view that suitable drug formulation such as using liposomes or other nanoparticulate carriers is useful for getting relevant pre-clinical data. In this study we were not focused on finding the maximal tolerated doses. Instead, the applied doses of liposomal preparations were selected with respect to be effective against cancer but not harmful to the immune system. In other words, we used doses tolerable with respect to immunotoxicity or, more precisely, doses that did not interfere with hematopoiesis. This is also important for the development of future combined immuno-chemotherapy based on co-application of autologous dendritic cells (Ramanathapuram et al., 2004, 2005) or co-application of various immunomodulators (e.g. CpG oligonucleotides, MDP analogues, monophosphoryl lipid A, bacterial extracts etc.).

Studies on pharmacokinetics and pharmacodynamics of liposomal α -TOS and α -TAM and the follow-up to this study will be focused on the role of liposomes and low-density lipoproteins in redistribution of the drugs. Cancer cells express high levels of receptors for very low-density lipoproteins, which represent the best carriers for hydrophobic anti-cancer drugs. After reaching the circulation, α -TOS associates with circulating lipoproteins, which deliver it to the microvasculature of tumour tissue, where it is taken up by cancer cells (Pussinen et al., 2000). Liposomes designed for selective transfer of α -TOS and other anti-cancer VE analogues to serum lipoproteins after *i.v.* application could improve the anti-cancer effect and selectivity of these drugs.

Conclusion

The fundamental outcome of this study is the elimination of acute toxicity of free α -TAM by its incorporation into liposomes. We report here that liposomal formulations of VE analogues α -TOS and α -TAM preserve their anti-cancer efficacy while eliminating any secondary toxicity. The formulation of anti-cancer agents like VE analogues in liposomes makes these drugs selective for cancer cells in pre-clinical models. This is intriguing clinically, since it suggests a feasible approach to the preparation of anti-cancer drugs for application in human patients.

Acknowledgments

This work was supported in part by grants from the Ministry of Agriculture of the Czech Republic (Grant no. MZE 0002716201) to J.T., the National Breast Cancer Foundation of Australia, the Queensland Cancer Fund, the Australian Research Council, and the Academy of Sciences of the Czech Republic (projects A500520602 and KAN200520703) to J.N., and the Louisiana Board of Regents Support Fund Research Competitiveness Subprogram grant for B.A.S. and E.M.

References

- Allen, T.M., 1997. Liposomes – opportunities in drug delivery. *Drugs* 54, 8–14.
- Bank, U., Reinhold, S., Ansoorge, S., 1991. Measurement of cellular activity by means of the MTT test. *Allerg. Immunol.* 37, 119–123.
- Barnett, K.T., Fokum, F.D., Malafa, M.P., 2002. Vitamin E succinate inhibits colon cancer liver metastases. *J. Surg. Res.* 106, 292–298.
- Birringer, M., Eytina, J.H., Salvatore, B.A., Neuzil, J., 2003. Vitamin E analogues as inducers of apoptosis: structure–function relation. *Br. J. Cancer* 88, 1948–1955.
- Bligh, E.G., Dyer, W.J., 1959. A rapid method of total lipid extraction and purification. *Can. J. Biochem. Physiol.* 37, 911–917.
- Dalen, H., Neuzil, J., 2003. α -Tocopheryl succinate sensitises a T lymphoma cell line to TRAIL-induced apoptosis by suppressing NF- κ B activation. *Br. J. Cancer* 88, 153–158.
- Dong, L.F., Swettenham, E., Eliasson, J., Wang, X.F., Gold, M., Medunec, Y., Stantic, M., Low, P., Prochazka, L., Witting, P.K., Turanek, J., Akporiaye, E.T., Ralph, S.J., Neuzil, J., 2007. Vitamin E analogues inhibit angiogenesis by selective induction of apoptosis in proliferating endothelial cells: the role of oxidative stress. *Cancer Res.* 67, 11906–11913.
- Dong, L.F., Low, P., Dyason, J.C., Wang, X.F., Prochazka, L., Witting, P.K., Freeman, R., Swettenham, E., Valls, K., Liu, J., Zabalova, R., Turanek, J., Spitz, D.R., Domann, I.E., Schiedler, S.J., Ralph, S.J., Neuzil, J., 2008. α -Tocopheryl succinate induces apoptosis by targeting ubiquinone-binding sites in mitochondrial respiratory complex II. *Oncogene* 27, 4324–4335.
- Freitas, R.A., Silva Dos Santos, G.A., Gimenes Teixeira, H.L., Scheucher, P.S., Luena-Araujo, A.R., Lima, A.S., Abreu, E., Lima, R.S., Garcia, A.B., Jordão, A.A., Falduto, R.P., Vanniuchi, H., Rego, E.M., in press. Apoptosis induction by (+)- α -tocopheryl succinate in the absence or presence of all-trans retinoic acid and arsenic trioxide in NB4, NB4-R2 and primary APL cells. *Leuk. Res.*
- Gabizon, A.A., 1992. Selective tumor localization and improved therapeutic index of anthracyclines encapsulated in long-circulating liposomes. *Cancer Res.* 52, 891–896.
- Garg, M., Jain, N.K., 2006. Reduced hematopoietic toxicity, enhanced cellular uptake and altered pharmacokinetics of azidothymidine loaded galactosylated liposomes. *J. Drug Target.* 14, 1–11.
- Gerweck, L.E., Seetharaman, K., 1996. Cellular pH gradient in tumor versus normal tissue: potential exploitation for the treatment of cancer. *Cancer Res.* 56, 1194–1198.
- Gogu, S.R., Lertora, J.J.L., George, W.J., Hyslop, N.E., Agrawal, K.C., 1991. Protection of zidovudine-induced toxicity against murine erythroid progenitor cells by vitamin E. *Exp. Hematol.* 19, 649–652.
- Guy, C.T., Webster, M.A., Schaller, M., Parsons, T.J., Cardiff, R.D., Müller, W.J., 1992. Expression of the neu protooncogene in the mammary epithelium of transgenic mice induces metastatic disease. *Proc. Natl. Acad. Sci. USA* 89, 10578–10582.
- Hahn, T., Szabo, I., Gold, M., Ramanathapuram, L., Hurley, L.H., Akporiaye, E.T., 2006. Dietary administration of the proapoptotic vitamin E analogue α -tocopheryl-*o*-succinate add inhibits metastatic murine breast cancer. *Cancer Res.* 67, 1877.
- Hall, L.M., Krauthauser, C.M., Westler, R.S., Hollingshead, M.G., Stee, A.M., Kerr, J.S., 2000. The hollow fiber assay: continued characterization with novel approaches. *Anticancer Res.* 20, 903–911.
- Hollingshead, M.G., Alley, M.C., Camaller, R.F., Abbott, B.J., Mayo, J.G., Malspeis, L., Grever, M.R., 1995. *In vivo* cultivation of tumor-cells in hollow fibers. *Life Sci* 57, 131–141.
- Idziorek, T., Estaquier, J., Debels, F., Ameisen, J.C., 1995. Yop-1 permits cytotoxicometric analysis of programmed cell death (apoptosis) without interfering with cell viability. *J. Immunol. Methods* 185, 249–258.
- Israel, K., Yu, W.P., Sanders, B.C., Klina, K., 2000. Vitamin E succinate induces apoptosis in human prostate cancer cells: role for Fas in vitamin E succinate-triggered apoptosis. *Nutr. Cancer* 36, 90–100.

- Jizomoto, H., Kanaoka, E., Hirano, K., 1984. pH-sensitive liposomes composed of tocopherol hemisuccinate and of phosphatidylethanolamine including tocopherol hemisuccinate. *Biochim. Biophys. Acta* 1213, 343–348.
- Karanth, H., Murthy, R.S.R., 2007. pH-sensitive liposomes – principle and application in cancer therapy. *J. Pharm. Pharmacol.* 59, 469–483.
- Kasna, A., Turanek, J., Vacek, A., Zaluska, D., Knötligova, P., Masek, K., 2004. Restoration of femoral GM-CFC progenitors in sublethally irradiated mice of various ages treated with liposomal adamantylamide dipeptide. *Int. Immunopharmacol.* 4, 1099–1106.
- Kogure, K., Manabe, S., Suzuki, I., Tokumura, A., Fukuzawa, K., 2005. Cytotoxicity of α -tocopherylsuccinate, malonate and oxalate in normal and cancer cells in vitro and their anti-cancer effects on mouse melanoma in vivo. *J. Nutr. Sci. Vitaminol.* 51, 392–397.
- Krishna, R., Dejong, G., Mayer, L.D., 1997. Pulsed exposure of SDZ PSC 833 to multidrug resistant P388/ADR and MCF7/ADR cells in the absence of anticancer drugs can fully restore sensitivity to doxorubicin. *Anticancer Res.* 17, 3329–3334.
- Malafa, M.P., Fokum, E.D., Mowlavi, A., Abusief, M., King, M., 2002. Vitamin E inhibits melanoma growth in mice. *Surgery* 131, 85–91.
- Mosmann, T., 1983. Rapid colorimetric assay for cellular growth and survival – application to proliferation and cytotoxicity assays. *J. Immunol. Methods* 65, 55–63.
- Neuzil, J., Weber, T., Gellert, N., Weber, C., 2001a. Selective cancer cell killing by α -tocopheryl succinate. *Br. J. Cancer* 84, 87–89.
- Neuzil, J., Weber, T., Schröder, A., Lu, M., Ostermann, G., Gellert, N., Mayne, G.C., Olejnicka, B., Nègre-Salvayre, A., Sticha, M., Coffey, R.J., Weber, C., 2001b. Induction of apoptosis in cancer cells by α -tocopheryl succinate: molecular pathways and structural requirements. *FASEB J.* 15, 403–415.
- Neuzil, J., Zhao, M., Ostermann, G., Sticha, M., Gellert, N., Weber, C., Easton, J.W., Brunk, U.T., 2002. α -Tocopheryl succinate, an agent with in vivo anti-tumor activity, induces apoptosis by causing lysosomal instability. *Biochem. J.* 362, 709–715.
- Neuzil, J., Dong, L.F., Ramanathapuram, L., Hahn, T., Chladova, M., Wang, X.F., Zabolova, R., Prochazka, L., Gold, M., Freeman, R., Turanek, J., Akporiaye, E.T., Dyson, J.C., Ralph, S.J., 2007a. Vitamin E analogues as a novel group of mitocans: anti-cancer agents that act by targeting mitochondria. *Mol. Asp. Med.* 28, 607–645.
- Neuzil, J., Tomasetti, M., Zhao, Y., Dong, L.F., Birringer, M., Wang, X.F., Low, P., Wu, K., Salvatore, B.A., Ralph, S.J., 2007b. Vitamin E analogs, a novel group of “mitocans” as anticancer agents: the importance of being redox-silent. *Mol. Pharmacol.* 71, 1185–1199.
- Phillips, N.C., Tsoukas, C., 1992. Liposomal encapsulation of azidothymidine results in decreased hematopoietic toxicity and enhanced activity against murine acquired immunodeficiency syndrome. *Blood* 79, 1137–1143.
- Prasad, K.N., Kumar, B., Yan, X.D., Hanson, A.J., Cole, W.C., 2003. α -Tocopheryl succinate, the most effective form of vitamin E for adjuvant cancer treatment: a review. *J. Am. Coll. Nutr.* 22, 108–117.
- Pussinen, P.J., Lindner, H., Glatter, O., Reichert, H., Kostner, G.M., Wintersperger, A., Malle, E., Sattler, W., 2000. Lipoprotein-associated α -tocopheryl-succinate inhibits cell growth and induces apoptosis in human MCF-7 and HBL-100 breast cancer cells. *Biochim. Biophys. Acta* 1485, 129–144.
- Ramanathapuram, L.V., Koble, J.J., Bearss, D., Payne, C.M., Trevor, K.T., Akporiaye, E.T., 2004. α -Tocopheryl succinate sensitizes established tumors to vaccination with nonmatured dendritic cells. *Cancer Immunol. Immunother.* 53, 580–588.
- Ramanathapuram, L.V., Hahn, T., Dial, S.M., Akporiaye, E.T., 2005. Chemo-immunotherapy of breast cancer using vesiculated α -tocopheryl succinate in combination with dendritic cell vaccination. *Nutr. Cancer* 53, 177–193.
- Stapelberg, M., Gellert, N., Swettenham, E., Tomasetti, M., Witting, P.K., Procopio, A., Neuzil, J., 2005. α -Tocopheryl succinate inhibits malignant mesothelioma by disrupting the fibroblast growth factor autocrine loop. *J. Biol. Chem.* 280, 25369–25376.
- Tattersall, M., Clarke, S., 2003. Developments in drug delivery: implications for cancer care. *Curr. Opin. Oncol.* 15, 293–299.
- Teng, X.W., Davies, N.M., Fukuda, C.H., Good, R.L., Baris, M.W., 2005. Pharmacokinetics and tissue distribution of d- α -tocopheryl succinate formulations following intravenous administration in the rat. *BioPharm. Drug Dispos.* 26, 195–203.
- Tomasetti, M., Gellert, N., Procopio, A., Neuzil, J., 2004. Avitamin E analogue suppresses malignant mesothelioma in a preclinical model: a future drug against a fatal neoplastic disease? *Int. J. Cancer* 109, 641–642.
- Tomic-Vatc, A., Eytina, J., Chapman, J., Mahdavian, E., Neuzil, J., Salvatore, B.A., 2005. Vitamin E amides, a new class of vitamin E analogues with enhanced pro-apoptotic activity. *Int. J. Cancer* 117, 188–193.
- Turanek, J., 1994. Fast-protein liquid-chromatography system as a tool for liposome preparation by the extrusion procedure. *Anal. Biochem.* 218, 352–357.
- Turanek, J., Zaluska, D., Hofer, M., Vacek, A., Ledvina, M., Jezek, J., 1997. Stimulation of haemopoiesis and protection of mice against radiation injury by synthetic analogues of muramyl dipeptide incorporated in liposomes. *Int. J. Immunopharmacol.* 19, 611–617.
- Turanek, J., Kasna, A., Zaluska, D., Neca, J., 2003. Preparation of sterile liposomes by proliposome-liposome method. *Methods Enzymol.* 367, 111–125.
- Vacek, A., Rotkova, D., Bartonicikova, A., 1990. Radioprotection of hematopoiesis conferred by aqueous extract from chlorococcal algae (hastimul) administered to mice before irradiation. *Exp. Hematol.* 18, 234–237.
- Wang, X.F., Dong, L.F., Zhao, Y., Tomasetti, M., Wu, K., Neuzil, J., 2006. Vitamin E analogues as anticancer agents: lessons from studies with α -tocopheryl succinate. *Mol. Nutr. Food Res.* 50, 675–685.
- Wang, X.F., Birringer, M., Dong, L.F., Veprek, P., Low, P., Swettenham, E., Stanic, M., Yuan, L.H., Zabolova, R., Wu, K., Ledvina, M., Ralph, S.J., Neuzil, J., 2007. A peptide conjugate of vitamin E succinate targets breast cancer cells with high ErbB2 expression. *Cancer Res.* 67, 3337–3344.
- Weber, T., Lu, M., Andera, L., Lahm, H., Gellert, N., Fariss, M.W., Korinek, V., Sattler, W., Ucker, D.S., Terman, A., Schroder, A., Erl, W., Brunk, U.T., Coffey, R.J., Weber, C., Neuzil, J., 2002. Vitamin E succinate is a potent novel anti-neoplastic agent with high selectivity and cooperativity with tumor necrosis factor-related apoptosis-inducing ligand (Apo2 ligand) in vivo. *Clin. Cancer Res.* 8, 863–869.
- Yu, W.P., Sanders, B.G., Kline, K., 1997. RRR- α -tocopheryl succinate inhibits E14 thymic lymphoma cell growth by inducing apoptosis and DNA synthesis arrest. *Nutr. Cancer* 27, 92–101.
- Yu, W.P., Simmons-Menchaca, M., Gapor, A., Sanders, B.G., Kline, K., 1999. Induction of apoptosis in human breast cancer cells by tocopherols and tocotrienols. *Nutr. Cancer* 33, 26–32.



ORIGINAL ARTICLE

α -Tocopheryl succinate induces apoptosis by targeting ubiquinone-binding sites in mitochondrial respiratory complex II

L-F Dong¹, P Low², JC Dyason³, X-F Wang¹, L Prochazka^{4,9}, PK Witting⁵, R Freeman¹, E Swettenham¹, K Valis⁶, J Liu¹, R Zobalova^{1,6}, J Turanek⁴, DR Spitz⁷, FE Domann⁷, IE Scheffler⁸, SJ Ralph² and J Neuzil^{1,6}

¹Apoptosis Research Group, School of Medical Science, Griffith University, Southport, Queensland, Australia; ²Genomic Research Centre, School of Medical Science, Griffith University, Southport, Queensland, Australia; ³Institute for Glycomics, Griffith University, Southport, Queensland, Australia; ⁴Department of Immunology, Veterinary Research Institute, Brno, Czech Republic; ⁵ANZAC Medical Research Institute, Concord Hospital, Concord, Sydney, New South Wales, Australia; ⁶Molecular Therapy Group, Institute of Biotechnology, Academy of Sciences of the Czech Republic, Prague, Czech Republic; ⁷Free Radical and Radiation Biology Program, Department of Radiation Oncology, Holden Comprehensive Cancer Center, University of Iowa, Iowa City, IA, USA and ⁸Division of Biology, University of California, San Diego, CA, USA

α -Tocopheryl succinate (α -TOS) is a selective inducer of apoptosis in cancer cells, which involves the accumulation of reactive oxygen species (ROS). The molecular target of α -TOS has not been identified. Here, we show that α -TOS inhibits succinate dehydrogenase (SDH) activity of complex II (CII) by interacting with the proximal and distal ubiquinone (UbQ)-binding site (Q_P and Q_D , respectively). This is based on biochemical analyses and molecular modelling, revealing similar or stronger interaction energy of α -TOS compared to that of UbQ for the Q_P and Q_D sites, respectively. *CybL*-mutant cells with dysfunctional CII failed to accumulate ROS and underwent apoptosis in the presence of α -TOS. Similar resistance was observed when *CybL* was knocked down with siRNA. Reconstitution of functional CII rendered *CybL*-mutant cells susceptible to α -TOS. We propose that α -TOS displaces UbQ in CII causing electrons generated by SDH to recombine with molecular oxygen to yield ROS. Our data highlight CII, a known tumour suppressor, as a novel target for cancer therapy.

Oncogene (2008) 27, 4324–4335; doi:10.1038/onc.2008.69; published online 31 March 2008

Keywords: α -tocopheryl succinate; complex II; ubiquinone-binding sites; reactive oxygen species; apoptosis; anti-cancer drug target

Introduction

Cytotoxic drugs acting by selectively affecting mitochondria in cancer cells, 'mitocans' (Neuzil *et al.*, 2006, 2007; Ralph *et al.*, 2007), are attractive for the treatment of cancer (Ko *et al.*, 2004; Bonnet *et al.*, 2007; Dong *et al.*, 2007; Neuzil *et al.*, 2007). Prime examples of such drugs are α -tocopheryl succinate (α -TOS) (Neuzil *et al.*, 2001a, b), 3-bromopyruvate (3BP) (Geschwind *et al.*, 2002; Ko *et al.*, 2004) and dichloroacetate (DCA) (Bonnet *et al.*, 2007). 3BP inhibits the glycolytic pathway enzyme hexokinase, and succinate dehydrogenase (SDH), suppressing adenosine 5'-triphosphate production and mitochondrial respiration (Ko *et al.*, 2001; Xu *et al.*, 2005). DCA targets cancer cells by inhibiting pyruvate dehydrogenase kinase (Bonnet *et al.*, 2007). Finally, β -phenylethyl isothiocyanate selectively kills cancer cells by eliciting the generation of reactive oxygen species (ROS) (Trachootham *et al.*, 2006).

α -TOS, a redox-silent analogue of vitamin E (VE), causes rapid production of ROS in cancer cells, triggering apoptosis (Weber *et al.*, 2003; Stapelberg *et al.*, 2005; Swettenham *et al.*, 2005; Wang *et al.*, 2005). α -TOS also inhibits the anti-apoptotic function of Bcl-2 and Bcl-x_L by blocking their BH3 domains (Shiau *et al.*, 2006). This may explain, in part, how α -TOS sensitizes cancer cells to other anti-cancer drugs. However, it does not explain how the agent causes accumulation of ROS, obligatory mediators of α -TOS-induced apoptosis. Antioxidants like superoxide dismutase (SOD) or the mitochondrially targeted coenzyme Q (MitoQ) (James *et al.*, 2005, 2007) negate the apoptotic action of α -TOS (Alleva *et al.*, 2001; Weber *et al.*, 2003; Stapelberg *et al.*, 2005). Cancer cells that accumulate low levels of ROS in response to α -TOS are less susceptible to apoptosis (Kogure *et al.*, 2002; Kang *et al.*, 2004; Stapelberg *et al.*, 2005; Swettenham *et al.*, 2005).

The effects of α -TOS on cancer cells, combined with a reduced toxicity towards normal cells, result from a greater antioxidant defence of the latter (Church *et al.*,

Correspondence: Associate Professor J Neuzil, Apoptosis Research Group, School of Medical Science, Griffith University, Gold Coast Campus, Southport, Queensland 9726, Australia.

E-mail: j.neuzil@griffith.edu.au or

Dr SJ Ralph, Genomic Research Centre, School of Medical Science, Griffith University, Southport, Queensland, Australia.

E-mail: s.ralph@griffith.edu.au

⁹Visiting student with the Apoptosis Research Group, School of Medical Science, Griffith University, Southport, Queensland, Australia.

Received 22 October 2007; revised 18 December 2007; accepted 21 February 2008; published online 31 March 2008

1993; Safford *et al.*, 1994; Allen and Balin, 2003; Huang *et al.*, 2006) and/or increased levels of esterases that hydrolyse the pro-oxidant α -TOS by hydrolysis to the redox-active, non-apoptogenic α -TOH (Fariss *et al.*, 2001; Neuzil and Massa, 2005).

The molecular target of α -TOS in cancer cells that results in ROS production has not previously been defined. One possibility how the VE analogue could give rise to ROS and ensuing apoptosis is by interfering with the ROS-generating centres along the mitochondrial electron redox chain. Of particular interest is complex II (CII), since previous data showed that toxicity of α -TOS on cancer cells can be suppressed by MitoQ (Stapelberg *et al.*, 2005; Swettenham *et al.*, 2005) that is known to interact with the ubiquinone (UbQ)-binding sites of CII (James *et al.*, 2005, 2007). Here, we examined the effect of α -TOS on the respiratory chain, identifying the UbQ-binding pockets in CII as the key molecular target for the agent, and propose that its interaction with the UbQ-binding sites results in ROS generation. The UbQ-

binding sites of CII represent a novel, and thus far unrecognized target for anti-cancer drugs.

Results

Cancer cells accumulate ROS and undergo apoptosis when exposed to α -TOS

We first tested if exposure of breast cancer cells to α -TOS caused generation of ROS. The results obtained by flow cytometry (Figures 1a, b) show that both erbB2-low MCF7 and erbB2-high MDA-MB-453 cells accumulated ROS and underwent apoptosis when challenged with α -TOS. Electron paramagnetic resonance (EPR) spectroscopy confirmed ROS generation occurring in cells exposed to α -TOS (Figures 1c and d). Pre-treatment of the cells with MitoQ or their co-treatment with SOD suppressed ROS accumulation and decreased the extent of apoptosis (Figure 1e). MCF7 ρ^0

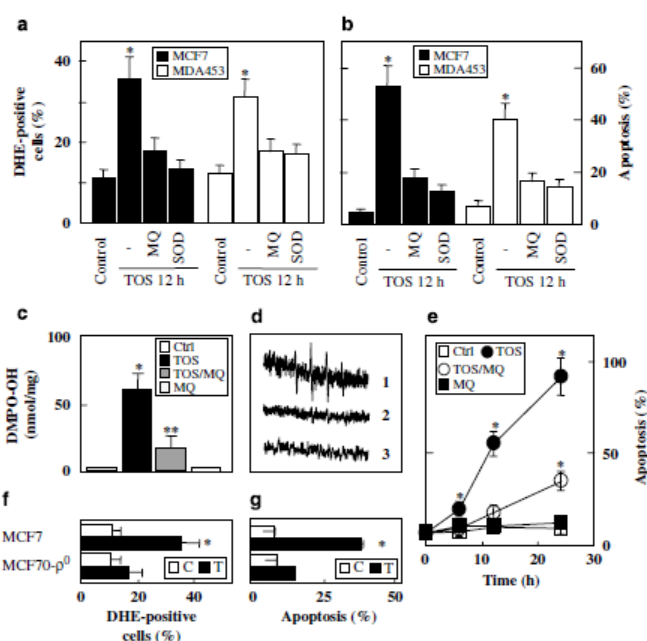


Figure 1 Reactive oxygen species (ROS) generation and induction of apoptosis in cancer cells by α -tocopheryl succinate (α -TOS). ErbB2-low MCF7 and -high MDA-MB-453 cells were exposed to α -TOS at $50\mu\text{M}$ and for times shown, and assessed for dihydroethidium (DHE)- (a) and annexin V-positive cells (%) (b). Jurkat cells were treated with $50\mu\text{M}$ α -TOS for 2h or as shown and assessed for ROS accumulation using electron paramagnetic resonance (EPR) spectroscopy (c, evaluation of the 5,5-dimethyl-1-pyrroline N-oxide (DMPO)-OH adduct level in nmol/mg protein; d, representative EPR spectra of cells exposed to α -TOS in the absence (1) or presence of mitochondrially targeted coenzyme Q (MitoQ) (2) or to MitoQ only (3). (e) The kinetics of apoptosis induction in Jurkat cells exposed to $50\mu\text{M}$ α -TOS in the absence or presence of MitoQ. Control (C) MCF7 parental and ρ^0 cells exposed to $50\mu\text{M}$ α -TOS for 2h (T) were assessed for ROS accumulation (f) and apoptosis (g). Where indicated, the cells were pre-treated for 1h with $2\mu\text{M}$ MitoQ (MQ) or co-treated with SOD (polyethylene glycol (PEG)-SOD, $750\text{U}/\text{mg}$). The data shown represent mean values \pm s.d. ($n = 3$). The symbol $*$ denotes significant difference ($P < 0.05$) in the level of apoptosis and ROS of treated cells compared with the untreated control cell population.

cells with dysfunctional electron redox chain, when exposed to α -TOS, showed relatively low levels of ROS accumulation and the induction of apoptosis was reduced (Figures 1f and g).

α -TOS targets the UbQ-binding pockets on CII

Studies with α -tocopherol (α -TOH) indicated that it could bind to the UbQ site in CII where it acts as a competitive inhibitor of SDH (Yu and Yu, 1983). We thus investigated whether α -TOS, with its related structure but opposing biological activity, interferes with UbQ binding to CII. Using high levels of succinate (20 mM) that is capable of entering cells (Spencer, 1977; Maehara *et al.*, 1988) to promote both SDH activity (Maehara *et al.*, 1988; Berridge and Tan, 1993) and mitochondrial respiration proceeding via CII, NeuTL cells were assayed for SDH activity in the presence or absence of α -TOS. The inhibitors of SDH activity, 3BP (Sanborn *et al.*, 1971) and 3-nitropropionic acid (3NPA) (Scallet *et al.*, 2003), were employed as positive controls. To establish the relationship between inhibition of SDH and 3-(4,5-dimethylthiazol-2-yl)-2,5-diphenyltetrazolium bromide (MTT) reduction, initial experiments with 3BP and 3NPA were performed in the absence of succinate that might otherwise compete for binding to the enzyme, and the results confirmed that 3BP and 3NPA inhibited CII-mediated MTT reduction and that

SDH activity and MTT reduction were closely related (Figure 2a).

Thenoyltrifluoroacetone (TTFA) is an inhibitor of CII that blocks the succinate-dependent MTT reduction by targeting the UbQ-binding sites rather than the SDH enzyme catalytic site (Sun *et al.*, 2005). The CII UbQ sites are situated beneath the active site of SDH, in the transmembrane region of the CII. With high succinate levels as the substrate driving CII-mediated MTT reduction in whole cells, treatment with 3BP, α -TOS or TTFA inhibited MTT reduction in a dose-dependent manner (Figures 2b-d). Pre-incubation of cells with MitoQ, a form of UbQ that preferentially localizes to mitochondria where it binds to CII but not CIII (Kelso *et al.*, 2001; James *et al.*, 2005, 2007), overcame the inhibition in MTT reduction by TTFA and α -TOS, but not by 3BP (Figures 2b-d). These results indicate that α -TOS inhibits SDH activity in a similar manner to TTFA.

Verification that α -TOS inhibits mitochondrial respiratory CII activity

Additional support for the role of α -TOS in inhibiting CII activity was obtained with mitochondrial preparations from rat liver and membrane fractions from *Paracoccus denitrificans*. SDH activity decreased rapidly after treatment with α -TOS (Figure 3). These data

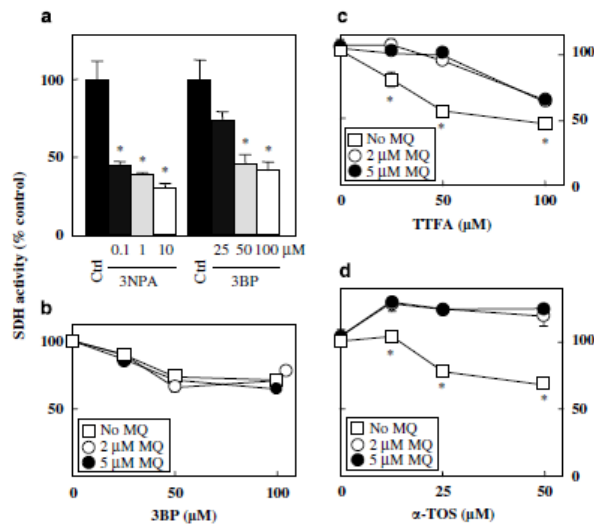


Figure 2 The effect of 3-nitropropionic acid (3NPA), 3-bromopyruvate (3BP), thenoyltrifluoroacetone (TTFA) and α -tocopheryl succinate (α -TOS) on the ability of NeuTL cells to reduce 3-(4,5-dimethylthiazol-2-yl)-2,5-diphenyltetrazolium bromide (MTT). (a) MTT reduction in phosphate-buffered saline (PBS) was assessed after a 4 h co-incubation period in the presence of 3NPA or 3BP used at the concentrations (μ M) shown. (b-d) Cells were pre-incubated for 60 min with mitochondrially targeted coenzyme Q (MitoQ) at the concentrations indicated (Ctrl, 2 or 5 μ M; insert box) before addition of 3BP (0–100 μ M) (b) and assessed for their ability to reduce MTT after a 2 h incubation period. Cells pre-treated with MitoQ were then treated with TTFA (c) and with α -TOS (d) at the concentration shown, and were assessed for their ability to reduce MTT in RPMI containing 20 mM succinic acid (pH 7.4) after a 2 h incubation period. Results are presented as mean reduction (%) of MTT relative to control (untreated) \pm s.d. The symbol "*" denotes significant differences with $P < 0.05$.

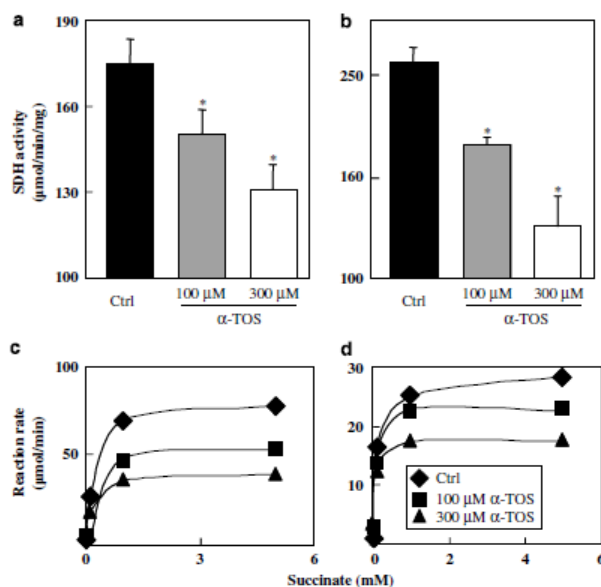


Figure 3 Inhibition of succinate dehydrogenase (SDH)/complex II (CII) activity in isolated rat liver mitochondria (a, c), and *Paracoccus denitrificans* (b, d) by α -tocopheryl succinate (α -TOS). Preparations of mitochondria from rat liver or membranes from *P. denitrificans* were incubated in a reaction mixture facilitating mitochondrial SDH/CII activity ($\mu\text{mol}/\text{min}$ per mg protein) and containing 2,6-dichlorophenol-indophenol + phenazine methosulphate (DCPIP + PMS). Samples in a and b contained succinate and were both treated with α -TOS as indicated. Dose-response curves displaying changes in the reaction rate ($\mu\text{mol}/\text{min}$) for DCPIP were measured as absorbance at 600 nm under different concentrations of succinate as indicated in the absence or presence of α -TOS (c, d). Results are represented as mean values \pm s.d. ($n=3$). The symbol ** indicates values significantly different from the controls with $P<0.05$.

strongly indicate that α -TOS, acting directly on the UbQ site(s) of CII, interferes with the electron flow to phenazine methosulphate (PMS) and 2,6-dichlorophenol-indophenol (DCPIP). In contrast, α -TOS had no effect on NADH dehydrogenase (CI) activity (data not shown), consistent with selective targeting of CII.

Next, we tested whether α -TOS initiated apoptosis in parental Chinese hamster lung fibroblasts (B1 cells), CII-dysfunctional cells (B10 cells) and CII-dysfunctional cells (B9 cells, with a mutation in the gene encoding the succinyl dehydrogenase subunit C (SDHC subunit, *CybL*). B9 cells were less responsive to α -TOS, with lower levels of ROS accumulation (Figure 4a) and diminished SDH activity (Figure 4b) compared to the parental (B1) or B10 cells. B9 cells were also relatively resistant to apoptosis induced by α -TOS (Figure 4c). Reconstitution of CII in the *CybL*-mutant (B9) cells normalized the SDH activity (Figure 4b), and also restored cell sensitivity to α -TOS-induced killing (Figure 4c).

Data obtained with the CII-dysfunctional (B9) and the reconstituted B9 cells were independently verified by treatment of MCF7 cells with four different short-interfering RNAs (siRNA) against *CybL*. Duplexes 1, 3 and 4 substantially suppressed CII activity (Figure 4e),

as well as ROS generation (Figure 4d) and apoptosis induction in response to α -TOS (Figure 4f).

Using a human monoclonal SDHC antibody, we probed the B1, B9 and B10, and the CII-reconstituted Chinese hamster lung fibroblasts (B9_{rec}) for the presence of SDHC. Western blotting analysis (Figures 4h and i) revealed high levels of human SDHC in the B9_{rec} cells and its low level in MCF-7 cells treated with the SDHC siRNAs. The B9 cells with reconstituted CII revealed re-appearance of SDHC. Densitometric evaluation, showed that siRNA treatment of MCF7 cells lowered the level of the SDHC protein by 50–80% (Figure 4j). These data are consistent with the RT-PCR results showing presence of human *SDHC* mRNA in CII-reconstituted cells and low levels of the transcript in MCF7 cells treated with SDHC siRNA (Figure 4g). The siRNA approach was specific for SDHC, since we did not observe any changes in the level of the SDHB subunit protein in the SDHC-treated MCF7 cells (data not shown).

Molecular modelling reveals strong binding of α -TOS to UbQ sites on CII

To rationalize our results, suggesting that α -TOS interacts with CII via the UbQ-binding sites, we

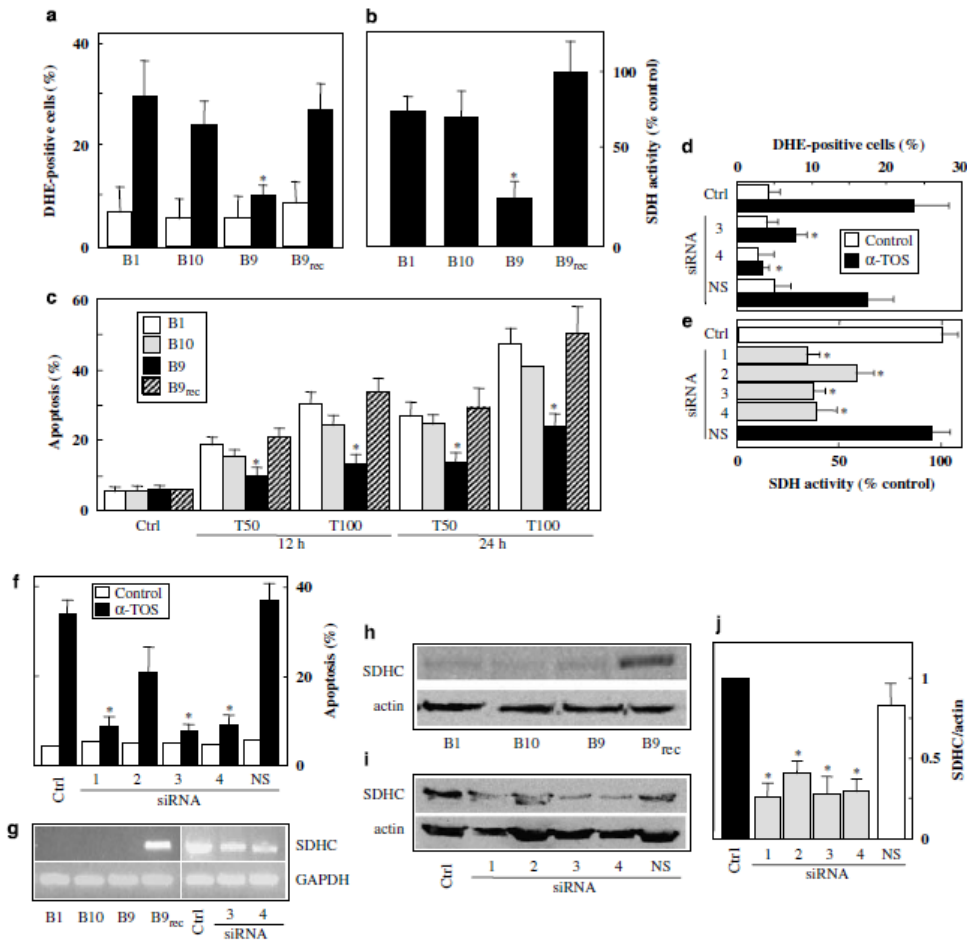


Figure 4 Apoptosis induction by α -tocopheryl succinate (α -TOS) is suppressed in complex II (CII)-dysfunctional cells. Parental (B1), CII-dysfunctional (B10), CII-dysfunctional (*CybL*-mutant; B9) and *CybL*-mutant cells following CII reconstitution by transfection with human *CybL* (B9_{rec}) were exposed to α -TOS 50 μ M and for 24h, unless shown otherwise, harvested and assessed for ROS accumulation (a), succinate dehydrogenase (SDH) activity assessed in whole cells on the basis of 3-(4,5-dimethylthiazol-2-yl)-2,5-diphenyltetrazolium bromide (MTT) reduction with succinate as a substrate (b) and apoptosis (c). MCF7 cells were pre-treated with *CybL* or non-specific (NS) short-interfering RNAs (siRNA), exposed to α -TOS as shown, and assessed for reactive oxygen species (ROS) accumulation (d), SDH activity (e) and apoptosis induction (f). (g) Results of RT-PCR analysis of B1, B10, B9 or B9_{rec} cells as well as *SDHC* siRNA-treated MCF7 cells using human *SDHC* primers. (h) Results of western blotting of B1, B10, B9 and B9_{rec} cells using monoclonal immunoglobulin G (IgG) anti-human SDHC. Western blotting is also shown to document the levels of SDHC in MCF7 cells treated with different *SDHC* siRNA duplexes and with NS siRNA (i), which was evaluated relative to the actin band (j). Results are represented as mean values \pm s.d. ($n = 3$), images are representative of three independent experiments. The symbol '*' indicates values significantly different from the controls with $P < 0.05$.

performed molecular modelling using AutoDock (Morris *et al.*, 1998). The crystal structure of porcine heart mitochondrial CII has been reported (Sun *et al.*, 2005). Since it exhibits high sequence identity with human CII (95–97% for the individual subunits), we used this structure (1ZOY) and the related structure (1ZP0) with

the inhibitor TTFA bound as the basis for our study. Structural analysis revealed the proximal UbQ-binding site (Q_P) and also identified the position of the proposed distal UbQ-binding site (Q_D). To test the feasibility of using AutoDock for this system, we first simulated the binding of UbQ5 to both the Q_P and the proposed Q_D

sites. UbQ5 was chosen as it is of similar size to α -TOS (Figure 5e) and contains a similar number of rotatable bonds (16 and 17, respectively). Figure 5a indicates that UbQ5 docked in Q_P to a deeper position than that observed for the portion of UbQ resolved in the published crystal structure (Sun *et al.*, 2005). UbQ5 was also found to dock into the proposed Q_D site, with the UbQ ring positioned in front of the binding site and the hydrophobic tail located inside the site (Figure 5c).

In the Q_P site, the ring system of α -TOS sits in the same binding pocket as the UbQ ring but is tilted to one side. The succinate ester moiety extended deeper into the binding site protruding down towards the location of the prosthetic haem group. The carboxyl group fits neatly into this pocket and is involved in a bidentate hydrogen bond with Ser42(C) (Figure 5b). Ser42(C) also interacts with the ester oxygen of α -TOS. As befits the hydrophobic nature of the remainder of the α -TOS molecule, all the other interactions with the protein are hydrophobic. Thus, the hydrocarbon side chain loops around and extends out of the Q_P site and along the same channel where the isoprenoid side chain of UbQ5 is located.

In the Q_D site, the phenyl ring system of α -TOS sits towards the bottom of the binding site with the succinate ester moiety extending out the bottom of the site in a similar way to that observed for the head group of the phospholipid visible in the original crystal structure (Figure 5c). The succinate moiety hydrogen bonds to Lys135(D) and Lys128(D) (Figure 5d), while the hydrocarbon side chain loops around the inside of the binding site. The calculated energy of interaction for the docked conformations of α -TOS (Figure 5e) suggested that it can bind at either site. While the binding energy of α -TOS at the Q_P site is slightly less than that of UbQ5, α -TOS would certainly compete with UbQ5. At the Q_D site, α -TOS shows a much stronger binding energy than that of UbQ5 and would be expected to easily displace it from this site (Figure 5e).

We had to use UbQ5 in the modelling study because of the relatively high number of rotatable bonds in α -TOS (17) and UbQ5 (16); adding the full isoprene tail of UbQ10 (with the extra rotatable bonds) makes the AutoDock calculations intractable. Also, data analysis from the published crystal structure only shows electron density for the very start of the isoprenoid chain suggesting that the rest of the tail is not particularly tightly bound at this site (Sun *et al.*, 2005). Therefore, the expected interaction energies of UbQ10 for the two sites will be similar to those calculated for UbQ5.

Apoptosis induced by α -TOS is independent of its BH3 mimetic activity

Shiau *et al.* (2006) reported that VE analogues possess BH3 mimetic activity, interacting with Bcl-2 and Bcl-x_L. To ascertain whether the apoptogenic activity of α -TOS is dependent on this activity, we utilized the BH3 mimetic BH31-2' (Calbiochem, Gibbstown, NJ, USA) (Degterev *et al.*, 2001; Milanesi *et al.*, 2006). Cytotoxicity of α -TOS was assessed in MCF7 cells exposed to

increasing concentrations of BH31-2'. We found that levels $>5\mu\text{M}$ caused mitochondrial destabilization (not shown). Combining BH31-2' ($5\mu\text{M}$) with α -TOS significantly enhanced the sensitivity of the cells to the VE analogue (Figure 6). These data indicate a synergistic effect of BH31-2' and α -TOS, and suggest that the VE analogue induces apoptosis predominantly by other modes than acting as a BH3 mimetic.

α -TOS inhibits tumour growth irrespective of erbB2 status

To demonstrate anti-cancer activity of α -TOS, we first determined whether the VE analogue could suppress tumour growth in an animal model of breast cancer with low erbB2 expression, given that over two-thirds of human breast cancers express low levels of the receptor tyrosine kinase (Slamon *et al.*, 1989). Nude mice were xenotransplanted with MCF7 cells and treated with α -TOS. Data in Figure 7a show that α -TOS repressed tumour growth with a significant decrease in the tumour size. We then tested treatment of erbB2-high breast carcinomas using the transgenic *FVB/N c-neu* mice (Guy *et al.*, 1992). Compared to the controls, the tumours in the α -TOS-treated mice showed a 30–40% reduction in size over the several weeks of treatment. These results suggest a high level of efficacy for α -TOS therapy against breast carcinomas regardless of their erbB-2/HER2 status.

Discussion

It is increasingly recognized that mitochondria are emerging as effective targets that may provide the selectivity needed for potent anti-cancer therapy (Neuzil *et al.*, 2001b; Don and Hogg, 2004). Studies with mitocans have shown exciting potential for cancer therapy since these drugs have limited side effects, and some of these compounds possess specificity for cancer cells (Neuzil *et al.*, 2007).

This study supports a role for α -TOS as a competitive inhibitor of the UbQ site(s) in CII. Our data reveal that both the Q_P and Q_D sites of CII are targets for α -TOS. Binding of the VE analogue at CII promotes ROS generation in cancer cells. The validity of the molecular modelling approach is supported by our identification of several other compounds with strong interaction energies for the CII UbQ site(s) (not shown). Of them, pyridoxal phosphate has been previously identified as a potent inhibitor of SDH activity by competing with UbQ (Choudhry *et al.*, 1985, 1986).

Molecular modelling strongly supports the notion that the binding of α -TOS to CII within the Q_P and Q_D sites is a key to the apoptogenic activity of the agent. These observations were verified by experiments with cells where a mutation in CybL disrupts the CII function and the ability of cells to survive when growing in the presence of succinate. First, *CybL*-mutant cells, unlike their CI-deficient and parental counterparts, failed to accumulate ROS and induce apoptosis when exposed to α -TOS, while reconstitution of functional CII reinstated

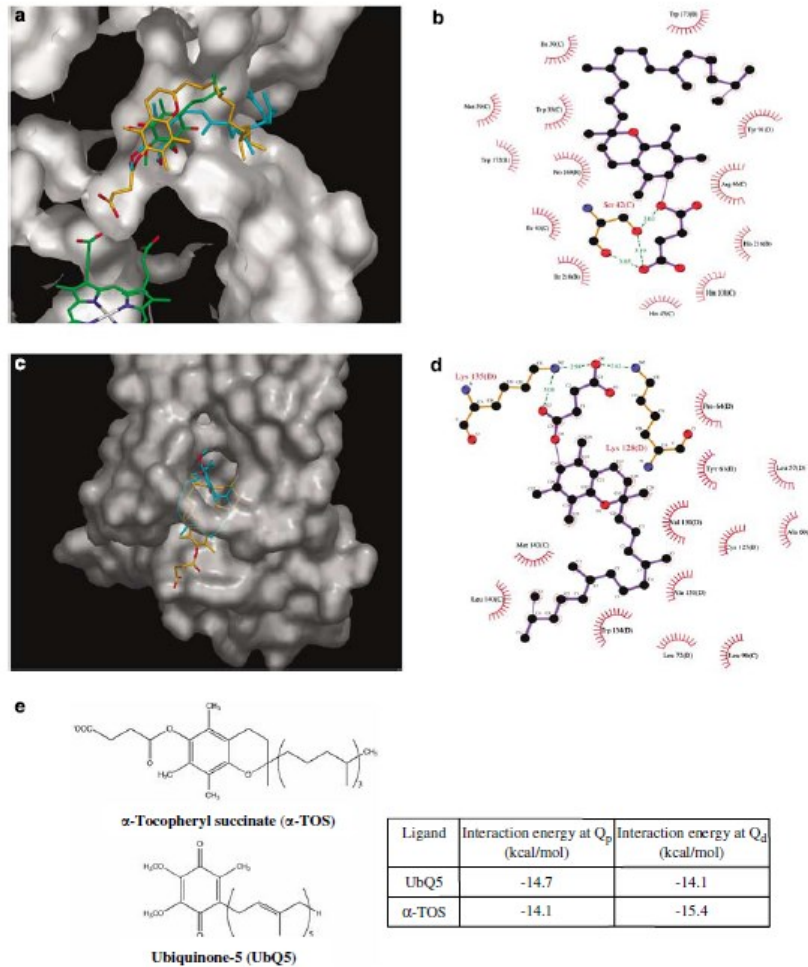


Figure 5 Molecular modelling reveals interaction of α -tocopheryl succinate (α -TOS) with ubiquinone (UbQ)-binding sites in complex II (CII). (a) Cut-away view of the Q_p-binding site showing the haem group (bottom left corner) and the position of UbQ (green carbon atoms) as indicated with arrows. The best-fit conformations of UbQ5 (cyan carbons) and α -TOS (orange carbon atoms) are also shown. (b) Ligplot diagram showing the major interactions between the best-docked conformation of α -TOS and the Q_p-binding site. (c) View of the proposed Q_D-binding site (with overhanging bridge as a translucent surface) showing the best-docked conformations of UbQ5 (cyan carbons) and α -TOS (orange carbons). (d) Ligplot diagram showing the major interactions between the best-docked conformation of α -TOS and the Q_D-binding site. (e) Chemical structures of UbQ5 and α -TOS and a table of interaction energies for the best-ranked docking conformations for UbQ5 and α -TOS in the Q_p and Q_D-binding sites. Images in (a) and (e) were prepared using Astex Viewer (Hartshorn, 2002), while those in (b) and (d) were prepared using Ligplot (Wallace *et al.*, 1995).

susceptibility to the agent. These findings can be reconciled with a study reporting resistance of *CybL*-mutant cells to apoptosis when challenged with various cytotoxic agents (Albayrak *et al.*, 2003). Hence, CII is an important driver of ROS production mediated by cytotoxic drugs. Second, we demonstrate that knocking-down *CybL*

rendered cancer cells resistant to α -TOS-triggered ROS accumulation and apoptosis induction (Figure 4). This is important evidence, since the siRNA approach is an acute insult to the cells, while a knockout cell line can undergo adaptive differential expression of genes, potentially obscuring the direct effect of the knockout genotype.

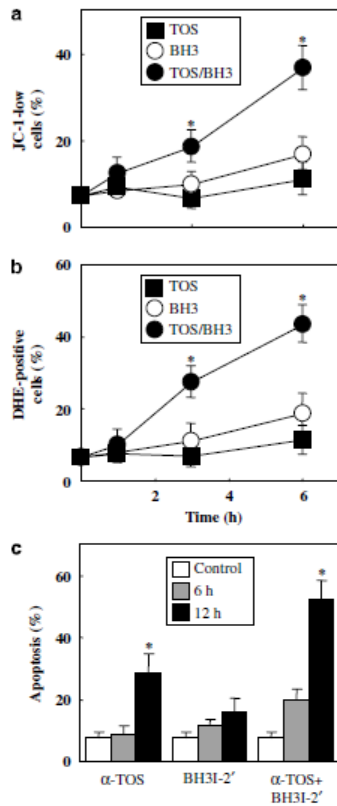


Figure 6 α -Tocopheryl succinate (α -TOS) causes apoptosis independent of its BH3 mimetic activity. MCF7 cells were treated with 5 μ M BH31-2' or exposed to 30 μ M α -TOS following 10 min pre-treatment with 5 μ M BH31-2'. Cells were then assessed for mitochondrial depolarization (a), reactive oxygen species (ROS) generation (b) and apoptosis induction (c). Results are represented as mean values \pm s.d. ($n = 3$). The symbol '*' indicates values significantly different from the controls with $P < 0.05$.

We and others have previously shown α -TOS to be a potent inducer of ROS in cancer cells (Weber *et al.*, 2003; Kang *et al.*, 2004). The α -TOS drug target we have identified as CII of the respiratory chain has been proposed as a contributor to cellular ROS production (McLennan and Degli-Esposti, 2000). Addition of MitoQ to cells did not overcome the 3BP-mediated inhibition of SDH activity since 3BP acts upstream at the site of the SDH catalytic centre. MitoQ overcame both the TTFA- and α -TOS-mediated inhibition of SDH activity. While TTFA binds to both Q_P and Q_D sites in CII (Sun *et al.*, 2005) like α -TOS, it displays less selective toxicity (Zhang *et al.*, 2001) than the VE analogue for killing cancer cells (Neuzil *et al.*, 2001b). Further studies are required to understand this differential specificity.

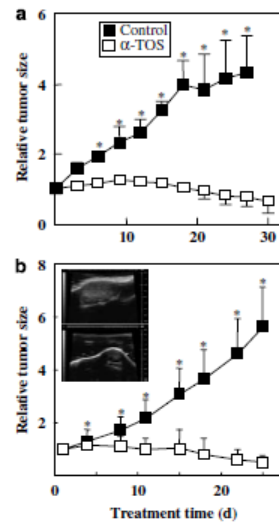


Figure 7 Inhibition of breast cancer in mouse models by α -tocopheryl succinate (α -TOS). (a) Nude mice were inoculated with MCF7 cells and once tumours became established, the animals were treated every 3 days with 10 μ M per mouse of α -TOS dissolved in dimethyl sulphoxide (DMSO) or with DMSO alone, by i.p. injection. Tumour size was measured using callipers and was correlated to the size of the carcinomas at the onset of the therapy. Four animals were used in each group. (b) Female *FVB/N c-neu* mice with small tumours received either 10 μ M α -TOS solubilized in corn oil/4% ethanol ($n = 11$) or the excipient alone (control, $n = 9$) by i.p. injection once every 3 days. Tumour size was quantified using ultrasound imaging (USI). Two independent experiments were conducted. The inset in b shows representative images of tumours acquired by USI in the control (upper image) and treated (lower image) *FVB/N c-neu* mice on day 22 of the experiment. The results shown are mean values \pm s.e.m. The symbol '*' denotes significant differences ($P < 0.05$).

When α -TOS displaces UbQ from its binding site(s) on CII, electrons may no longer be tunnelled down the SDH hydrophilic head on to AD and relayed via the [Fe-S] centres and the haem group to UbQ (Cheng *et al.*, 2006; Tran *et al.*, 2006). Instead, they recombine with molecular oxygen to enhance superoxide anion radical (O_2^-) production that leads to induction of apoptosis in the cancer cell. Although it is possible that ROS generation occurs via the FAD site (Yankovskaya *et al.*, 2003; Gottlieb and Tomlinson, 2005), it cannot be excluded that electrons in the case of a dysfunctional CII, interact with oxygen, which is dissolved in the membrane part of CII (Slane *et al.*, 2006). Another possibility is that electrons move to CI by reverse electron transport, where they form O_2^- (Adam-Vizi and Chinopoulos, 2006). Blocking UbQ binding promotes ROS generation by removing the opportunity of electrons to react with its acceptor (Figure 8). This is strongly supported by studies with the *Caenorhabditis elegans* *mev-1* mutant that can oxidize succinate to

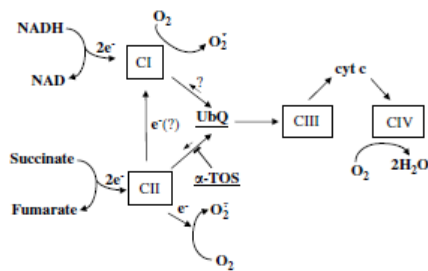


Figure 8 Model for the interference of α -tocopheryl succinate (α -TOS) with the mitochondrial electron chain. The scheme shows the proposed effects of α -TOS with the branching of the electron transport chain in its upstream region and clarifies the point of inhibition by α -TOS as specifically interacting with complex II (CII). It also suggests CII as the possible site of superoxide generation, although its precise location within succinate dehydrogenase (SDH) has not been identified. The possible reverse electron transport from CII to CI is also shown.

fumarate but cannot transfer electrons to UbQ, resulting in increased ROS levels and premature ageing (Ishii *et al.*, 1998). This can be reconciled with a recent study suggesting that the Q_p site is important for electron channelling between UbQ and the juxtapositioned haem group (Zhao *et al.*, 2006), which contributes to stabilization of the transient ubisemiquinone radical (Tran *et al.*, 2006). Interestingly, several human cancers, such as paragangliomas, resulting from genetic disorders due to mutations in CII subunits, including SDHC, may also be induced by increased ROS formation (Niemann and Muller, 2000; Gottlieb and Tomlinson, 2005; Ishii *et al.*, 2005).

Our results are not dissimilar to a recent report documenting selective molecular mechanism of apoptosis induction in cancer cells by adaphostin, a compound that binds to the UbQ reduction (Q₁) site of CIII, resulting in ROS accumulation (Le *et al.*, 2007). That CII is of importance in ROS formation is further evidenced by a recent report showing that non-steroid anti-inflammatory drugs caused ROS generation in cells, of which the majority was derived from CII (Soller *et al.*, 2007). Moreover, ferulenol, a coumarine derivative, has been reported to affect the succinate UbQ reductase by interfering with the UbQ cycle (Lahouel *et al.*, 2007). Given these recent results, more drugs affecting CII are likely to be found in near future.

Although anti-cancer drugs have been described that may target the UbQ sites on the oxidoreductase complexes along the mitochondrial respiratory chain to increase cellular ROS levels and activate apoptosis (Dias and Bailly, 2005; Hall, 2005; Le *et al.*, 2007), α -TOS has an additional feature in that it also disrupts the anti-apoptotic function of Bcl-2 and Bcl-x_L by blocking their BH3-binding domain (Shiau *et al.*, 2006). Hence, α -TOS may prove superior for inducing cancer cell death because of its dual action on two important targets, Q_p and Q_D sites of CII, and the Bcl-2 family proteins, promoting the induction of mitochondrially

mediated apoptosis. This notion is further corroborated by our data revealing sensitization of cancer cells to α -TOS by the BH3 mimetic BH31-2'.

We also show that α -TOS suppresses tumour progression in mouse models of breast cancer regardless of their erbB2 status. This could be explained by α -TOS blocking the CII UbQ-binding sites, thereby causing ROS generation with ensuing induction of apoptosis, acting in a dominant manner downstream of any anti-apoptotic pro-survival activity resulting from the erbB2 receptor tyrosine kinase signalling. This makes the VE analogue a potentially useful anti-cancer agent when dealing with the challenge of breast cancers with high levels of expression of erbB2/HER2 that are rather recalcitrant to therapy (Slamon *et al.*, 1989). Similarly, we recently demonstrated that a peptide conjugate of α -TOS (with relatively high affinity for the erbB2 receptor) effectively kills breast cancer cells (Wang *et al.*, 2007).

To conclude, we present the molecular targets of the intriguing anti-cancer agent α -TOS with low toxicity to non-cancerous tissues (Weber *et al.*, 2002), a compound that acts by selectively affecting mitochondria, organelles that are essential both for life and for unleashing the apoptosis machinery (Newmeyer and Ferguson-Miller, 2003). We identify the UbQ-binding sites of the mitochondrial CII as a new target for anti-cancer drugs, and propose that these results will not only lead to the establishment of VE analogues as efficient anti-cancer agents but also will increase the interest in mitochondrial components as targets that are yet to be fully exploited for selective cancer therapy. Work is presently underway, using *in silico* modelling, to identify lead compounds that induce apoptosis by interfering with the UbQ-binding site(s) of CII and develop them into efficient and selective anti-cancer drugs. Our results on the molecular mechanism of apoptosis induced in cancer cells by α -TOS may be reconciled with our clinical outcome from a mesothelioma patient who has been treated with the VE analogue. The data reveals a significant clinical benefit with α -TOS therapy, causing a reduction in tumour volume and improved the well being of our subject who had a lethal type of neoplastic pathology (Robinson *et al.*, 2005). We are currently preparing to set-up a larger clinical trial in which a cohort of mesothelioma patients will be treated with the mitocan α -TOS.

Materials and methods

Cell culture and treatment

Human breast cancer cells MCF7 with low and MDA-MB-453 with high levels of erbB2, and the murine breast cancer erbB2-high NeuTL cells derived from the *c-neu* mice were cultured in Dulbecco's modified Eagle's media (DMEM) with 10% fetal calf serum (FCS) and antibiotics. Jurkat T lymphoma cells were cultured in RPMI-1640 medium with 10% FCS and antibiotics. MCF7 cells deficient in mtDNA (*mt⁰*) were prepared as described (Weber *et al.*, 2003). CI-dysfunctional (B10 cells) (Seo *et al.*, 1997), CII-dysfunctional (B9 cells with mutant CybL (Oostveen *et al.*, 1995)) and the parental Chinese hamster lung fibroblasts (B1 cells) (Oostveen *et al.*, 1995) were

grown in DMEM with 10% FCS, antibiotics, 10mg/ml glucose and non-essential amino acids.

Assessment of apoptosis, ROS accumulation and membrane potential

Apoptosis was quantified using the annexin V-FITC kit (PharMingen, Franklin Lake, NJ, USA) (Weber *et al.*, 2003). Cellular ROS were detected with the probe dihydroethidium (Molecular Probes, Carlsbad, CA, USA) by flow cytometry (Weber *et al.*, 2003), or by trapping with 5,5-dimethyl-1-pyrroline N-oxide (DMPO; Sigma, St Louis, MO, USA) using EPR spectroscopy (Weber *et al.*, 2003). Cells were also pre-treated for 1 h with 2 μ M MitoQ (James *et al.*, 2005) or co-incubated with SOD (polyethylene glycol-SOD, 750 U/ml; Sigma). The mitochondrial inner transmembrane potential ($\Delta\Psi_m$) was assessed using 5,5',6,6'-tetrachloro-1,1',3,3'-tetraethylbenzimidazolyl-carbocyanine iodide (JC-1; Molecular Probes) (Weber *et al.*, 2003).

SDH activity assay

MTT solutions were prepared by dissolving 2.5 mg/ml MTT (Sigma) in phosphate-buffered saline (PBS) alone or phenol red-free RPMI media with 20 mM succinic acid, pH 7.4. Solutions of 3NPA, α -TOS and MitoQ in ethanol, TFA in dimethyl sulphoxide (DMSO) or 3BP in PBS were added to cells simultaneously with MTT. The drugs were tested in exponential growth phase of cells in 96-well plates using 4–8 replicates per dilution. Cells were also pre-incubated for 1 h with 2 or 5 μ M MitoQ. Final concentrations of ethanol or DMSO in cultures were \leq 0.1% (v/v). Treated and control cells were exposed to MTT for 2 or 4 h at 37 °C and 5% CO₂. Supernatants were removed, except for 30 μ l, before adding 150 μ l DMSO to dissolve the formazan crystals, and absorbance measured at 570 nm.

Preparation of mitochondrial particles

Rat liver mitochondria were freshly prepared as described (Rice and Lindsay, 1997) and stored at –20 °C until used. *P. dentrificans* CCM982 (NCIB 8944) was grown anaerobically at 30 °C in a medium containing 50 mM succinate as the carbon source and 10 mM nitrate as the terminal acceptor. Membranes were prepared as published (Burnell *et al.*, 1975) and stored at –20 °C until used.

Measurement of mitochondrial CI and CII activity

Reduction of the CII substrate DCPIP in the presence of cells or liver mitochondrial preparations was measured at 600 nm (Trounce *et al.*, 1996). Reaction mixtures contained 0.5 mM NADH, 5 mM succinate, 10 mM KCN, 50 μ M DCPIP and 50 μ M PMS. For each assay point, 0.5 mg sample protein was used and α -TOS added as indicated. When measuring the CI (NADH dehydrogenase) activity, PMS was omitted.

RNA interference, cell transfection, western blotting and RT-PCR

The siGENOME ON-TARGETplus set of four duplexes of siRNA oligonucleotides (Dharmacon, Chicago, IL, USA) targeting the *CybL* (*SDHC*) subunit of CII were used. Nonspecific siRNA was used as a negative control. Transfections of MCF7 cells with siRNA were performed as described

References

Accelrys (2001). *Insight II*. Accelrys Inc: San Diego.
Adam-Vizi V, Chinopoulos C. (2006). Bioenergetics and the formation of mitochondrial reactive oxygen species. *Trends Pharmacol Sci* 27: 639–645.

(Stapelberg *et al.*, 2005). B9 cells were transfected using the Topo pCR3.1 Uni plasmid harbouring the *CybL* gene (Slane *et al.*, 2006) and selected as described (Weber *et al.*, 2003). Stably transfected and siRNA-treated cells were assessed for SDH activity and SDHC expression. Western blotting was performed as described (Wang *et al.*, 2007) using anti-SDHC immunoglobulin G (IgG) (clone 3E2; Novus Biologicals, Littleton, CO, USA) with anti- β -actin IgG (Santa Cruz Biotechnology, Santa Cruz, CA, USA) as a loading control. RT-PCR was performed using a standard protocol. The published human *CybL* (Slane *et al.*, 2006) and Chinese hamster glyceraldehyde 3-phosphate dehydrogenase primers (Sever *et al.*, 2004) were used.

Molecular modelling of α -TOS interaction with UbQ binding in CII

For details, see the Supplementary Information.

Animal experiments

Balb/c nu/nu mice were inoculated s.c. with MCF7 cells (2×10^6 cells per mouse). After tumours developed, mice were injected with 10 μ mol α -TOS in DMSO i.p. every 3 days. Control mice were injected with an equal volume of DMSO. Tumour size was estimated with digital callipers.

Transgenic *FVB/N c-neu* mice (Guy *et al.*, 1992) were used with ~70% of the female mice developing spontaneous ductal breast carcinomas within ~7 months. Tumours were quantified by USI using the Vevo770 device fitted with the RMV704 scan-head (VisualSonics) operated at 60 MHz and with 40 μ m resolution (Dong *et al.*, 2007; Wang *et al.*, 2007). Mice received 10 μ mol α -TOS in corn oil/4% ethanol or the vehicle administered i.p. every 3 days. α -TOS therapy of the animals commenced when the tumour volume was ~40 mm³. Animal studies were performed according to the guidelines of the Australian and New Zealand Council for the Care and Use of Animals in Research and Teaching and were approved by the local Animal Ethics Committee.

Statistical analyses

Between-group comparisons were made using mean \pm s.d. and the unpaired Student's *t*-test. Differences in the mean relative tumour size (\pm s.e.m.) was examined using analyses of covariance (ANCOVA) with days as the covariate. Statistical analyses were performed using SPSS 10.0 analytical software. Statistical significance was accepted at $P < 0.05$.

Acknowledgements

We thank Professor RAJ Smith for providing MitoQ, and Professor RK Ralph and Professor JW Eaton for critical reading of the manuscript. This work was supported in part by grants from the National Breast Cancer Foundation, the Queensland Cancer Fund and the Australian Research Council (Discovery Grant DP0453372 to JN and Fellowship DP0343325 to PKW), and a grants from the Academy of Sciences of the Czech Republic (IAA500520702 and KAN2005207203 to JN), and by a grant from the Ministry of Agriculture of the Czech Republic (MZE 0002716201 to JT). DRS and FED were supported by NIH grants RO1-CA100045 (DRS) and NIH RO1-CA73612 (FED).

Albayrak T, Scherhammer V, Schoenfeld N, Braziulis E, Mund T, Bauer MK *et al.* (2003). The tumor suppressor *cybL*, a component of the respiratory chain, mediates apoptosis induction. *Mol Biol Cell* 14: 3082–3096.

- Allen FH. (2002). The Cambridge Structural Database: a quarter of a million crystal structures and rising. *Acta Crystallogr B* **5**: 380–388.
- Allen RG, Balin AK. (2003). Effects of oxygen on the antioxidant responses of normal and transformed cells. *Exp Cell Res* **289**: 307–316.
- Alleva R, Tomasetti M, Andera L, Gellert N, Borghi B, Weber C *et al*. (2001). Coenzyme Q blocks chemical but not receptor-mediated apoptosis by increasing mitochondrial antioxidant protection. *FEBS Lett* **503**: 46–50.
- Berridge MV, Tan AS. (1993). Characterization of the cellular reduction of 3-(4,5-dimethylthiazol-2-yl)-2,5-diphenyltetrazolium bromide (MTT): subcellular localization, substrate dependence, and involvement of mitochondrial electron transport in MTT reduction. *Arch Biochem Biophys* **303**: 474–478.
- Bonnet S, Archer SL, Allalunis-Turner J, Haromy A, Beaulieu C, Thompson R *et al*. (2007). A mitochondria-K⁺ channel axis is suppressed in cancer and its normalization promotes apoptosis and inhibits cancer growth. *Cancer Cell* **11**: 37–51.
- Burnell JN, John P, Whately FR. (1975). The reversibility of active sulphate transport in membrane vesicles of *Paracoccus denitrificans*. *Biochem J* **150**: 527–536.
- Case DA, Pearlman DA, Caldwell JW. (2002). *Amber 7*. University of California: San Francisco.
- Cheng VW, Ma E, Zhao Z, Rothery RA, Weiner JH. (2006). The iron-sulfur clusters in *Escherichia coli* succinate dehydrogenase direct electron flow. *J Biol Chem* **281**: 27662–27668.
- Choudhry ZM, Gavrikova EV, Kotlyar AB, Tushurashvili PR, Vinogradov AD. (1985). Pyridoxal phosphate-induced dissociation of the succinate: ubiquinone reductase. *FEBS Lett* **182**: 171–175.
- Choudhry ZM, Kotlyar AB, Vinogradov AD. (1986). Studies on the succinate dehydrogenating system. Interaction of the mitochondrial succinate-ubiquinone reductase with pyridoxal phosphate. *Biochim Biophys Acta* **850**: 131–138.
- Church SL, Grant JW, Ridnour LA, Oberley LW, Swanson PE, Meltzer PS *et al*. (1993). Increased manganese superoxide dismutase expression suppresses the malignant phenotype of human melanoma cells. *Proc Natl Acad Sci USA* **90**: 3113–3117.
- Degterev A, Lugovskoy A, Cardone M, Mulley B, Wagner G, Mitchison T *et al*. (2001). Identification of small-molecule inhibitors of interaction between the BH3 domain and Bcl-x_L. *Nat Cell Biol* **3**: 173–182.
- Dias N, Bailly C. (2005). Drugs targeting mitochondrial functions to control tumor cell growth. *Biochem Pharmacol* **70**: 1–12.
- Don AS, Hogg PJ. (2004). Mitochondria as cancer drug targets. *Trends Mol Med* **10**: 372–378.
- Dong LF, Swettenham E, Eliasson J, Wang XF, Gold M, Medunic Y *et al*. (2007). Vitamin E analogs inhibit angiogenesis by selective apoptosis induction in proliferating endothelial cells: the role of oxidative stress. *Cancer Res* **67**: 11906–11913.
- Fariss MW, Nicholls-Grzemeski FA, Tirmenstein MA, Zhang JG. (2001). Enhanced antioxidant and cytoprotective abilities of vitamin E succinate is associated with a rapid uptake advantage in rat hepatocytes and mitochondria. *Free Radic Biol Med* **31**: 530–541.
- Geschwind JF, Ko YH, Torbenson MS, Magee C, Pedersen PL. (2002). Novel therapy for liver cancer: direct intraarterial injection of a potent inhibitor of ATP production. *Cancer Res* **62**: 3909–3913.
- Gottlieb E, Tomlinson IP. (2005). Mitochondrial tumour suppressors: a genetic and biochemical update. *Nat Rev Cancer* **5**: 857–866.
- Guy CT, Webster MA, Schaller M, Parsons TJ, Cardiff RD, Muller WJ. (1992). Expression of the neu protooncogene in the mammary epithelium of transgenic mice induces metastatic disease. *Proc Natl Acad Sci USA* **89**: 10578–10582.
- Hall N. (2005). Mitochondria: a novel target for the chemoprevention of cancer. *Apoptosis* **10**: 687–705.
- Hartshorn MJ. (2002). AstexViewer™: an aid for structure-based drug design. *J Comput Aided Mol Des* **16**: 871–881.
- Huang LS, Sun G, Cobessi D, Wang AC, Shen JT, Tung EY *et al*. (2006). 3-Nitropropionic acid is a suicide inhibitor of mitochondrial respiration that, upon oxidation by complex II, forms a covalent adduct with a catalytic base arginine in the active site of the enzyme. *J Biol Chem* **281**: 5965–5972.
- Ishii N, Fujii M, Hartman PS, Tsuda M, Yasuda K, Senoo-Matsuda N *et al*. (1998). A mutation in succinate dehydrogenase cytochrome b causes oxidative stress and aging in nematodes. *Nature* **349**: 694–697.
- Ishii N, Yasuda K, Akatsuka A, Hino O, Hartman PS, Ishii N. (2005). A mutation in the SDHC gene of complex II increases oxidative stress, resulting in apoptosis and tumorigenesis. *Cancer Res* **65**: 203–209.
- James AM, Sharpley MS, Manas AB, Frerman FE, Hirst J, Smith RAJ *et al*. (2007). Interaction of the mitochondria-targeted antioxidant MitoQ with phospholipid bilayers and ubiquinone oxidoreductases. *J Biol Chem* **282**: 14708–14718.
- James EM, Cocheme HM, Smith RA, Murphy MP. (2005). Interactions of mitochondria-targeted and -untargeted ubiquinones with the mitochondrial respiratory chain and reactive oxygen species. Implications for the use of exogenous ubiquinones as therapies and experimental tools. *J Biol Chem* **280**: 21295–21312.
- Kang YH, Lee E, Choi MK, Ku JL, Kim SH, Park YG *et al*. (2004). Role of reactive oxygen species in the induction of apoptosis by α -tocopherol succinate. *Int J Cancer* **112**: 385–392.
- Keiso GF, Porteous CM, Coulter CV, Hughes G, Porteous WK, Ledgerwood EC *et al*. (2001). Selective targeting of a redox-active ubiquinone to mitochondria within cells: antioxidant and antiapoptotic properties. *J Biol Chem* **276**: 4588–4596.
- Ko YH, Pedersen PL, Geschwind JF. (2001). Glucose catabolism in the rabbit VX2 tumor model for liver cancer: characterization and targeting hexokinase. *Cancer Lett* **173**: 83–91.
- Ko YH, Smith BL, Wang Y, Pomper MG, Rini DA, Torbenson MS *et al*. (2004). Advanced cancers: eradication in all cases using 3-bromopyruvate therapy to deplete ATP. *Biochem Biophys Res Commun* **324**: 269–275.
- Kogure K, Hama S, Manabe S, Tokumura A, Fukuzawa K. (2002). High cytotoxicity of α -tocopherol hemisuccinate to cancer cells is due to failure of their antioxidative defense systems. *Cancer Lett* **186**: 151–156.
- Lahouel M, Zini R, Zellagui A, Rhouati S, Carrupt PA, Morin D. (2007). Ferulenol specifically inhibits succinate ubiquinone reductase at the level of the ubiquinone cycle. *Biochem Biophys Res Commun* **355**: 252–257.
- Le SB, Haiker MK, Buhrow S, Wang Q, Flatten K, Padiaditakis P *et al*. (2007). Inhibition of mitochondrial respiration as a source of adaphostin-induced reactive oxygen species and cytotoxicity. *J Biol Chem* **282**: 8860–8872.
- Maehara Y, Kusumoto T, Kusumoto H, Anai H, Sugimachi K. (1988). Sodium succinate enhances the colorimetric reaction of the *in vitro* chemosensitivity test: MTT assay. *Oncology* **5**: 434–436.
- McLennan HR, Degli-Esposti M. (2000). The contribution of mitochondrial respiratory complexes to the production of reactive oxygen species. *J Bioenerg Biomembr* **32**: 153–162.
- Milanesi E, Costantini P, Gambalunga A, Colonna R, Petronilli V, Cabrelle A *et al*. (2006). The mitochondrial effects of small organic ligands of BCL-2: sensitization of BCL-2-overexpressing cells to apoptosis by a pyrimidine-2,4,6-trione derivative. *J Biol Chem* **281**: 10066–10072.
- Morris GM, Goodsell DS, Halliday RS. (1998). Automated docking using a Lamarckian genetic algorithm and empirical binding free energy function. *J Comput Chem* **19**: 1639–1662.
- Neuzil J, Massa H. (2005). Hepatic processing determines dual activity of vitamin E succinate. *Biochem Biophys Res Commun* **327**: 1024–1027.
- Neuzil J, Tomasetti M, Zhao Y, Dong LF, Birringer M, Wang XF *et al*. (2007). Vitamin E analogs, a novel group of 'mitocans', as anti-cancer agents: the importance of being redox-silent. *Mol Pharmacol* **71**: 1185–1199.
- Neuzil J, Wang XF, Dong LF, Low P, Ralph SJ. (2006). Molecular mechanism of 'mitocan'-induced apoptosis in cancer cells epitomizes the multiple roles of reactive oxygen species and Bcl-2 family proteins. *FEBS Lett* **580**: 5125–5129.

- Neuzil J, Weber T, Gellert N, Weber C. (2001a). Selective cancer cell killing by α -tocopheryl succinate. *Br J Cancer* **84**: 87–89.
- Neuzil J, Weber T, Schröder A, Lu M, Ostermann G, Gellert N *et al.* (2001b). Induction of apoptosis in cancer cells by α -tocopheryl succinate: molecular pathways and structural requirements. *FASEB J* **15**: 403–415.
- Newmeyer DD, Ferguson-Miller S. (2003). Mitochondria: releasing power for life and unleashing the machineries of death. *Cell* **112**: 481–490.
- Niemann S, Muller U. (2000). Mutations in SDHC cause autosomal dominant paraganglioma, type 3. *Nat Genet* **26**: 268–270.
- Oostveen FG, Au HC, Meijer PJ, Scheffler IE. (1995). A Chinese hamster mutant cell line with a defect in the integral membrane protein CII-3 of complex II of the mitochondrial electron transport chain. *J Biol Chem* **270**: 26104–26108.
- Ralph SJ, Dyason JC, Freeman R, Dong LF, Prochazka L, Wang XF *et al.* (2007). Mitocans as anti-cancer agents targeting mitochondria: lessons from studies with vitamin E analogues, inhibitors of complex II. *J Bioenerg Biomembr* **39**: 65–72.
- Rice JE, Lindsay JG. (1997). Subcellular fractionation of mitochondria. In: Graham JM, Rickwood D (eds.) *Subcellular Fractionation. A Practical Approach Series*. Oxford University Press: Oxford, UK, pp 107–142.
- Robinson BW, Musk AW, Lake RA. (2005). Malignant mesothelioma. *Lancet* **366**: 397–408.
- Safford SE, Oberley TD, Urano M, St Clair DK. (1994). Suppression of fibrosarcoma metastasis by elevated expression of manganese superoxide dismutase. *Cancer Res* **54**: 4261–4265.
- Sanborn BM, Felberg NT, Hollocher TC. (1971). The inactivation of succinate dehydrogenase by bromopyruvate. *Biochim Biophys Acta* **227**: 219–231.
- Sanner MF. (1999). Python: a programming language for software integration and development. *J Mol Graph Mod* **17**: 57–61.
- Scallet AC, Haley RL, Scallet DM, Duhart HM, Binieda ZK. (2003). 3-Nitropropionic acid inhibition of succinate dehydrogenase (complex II) activity in cultured Chinese hamster ovary cells: antagonism by L-carnitine. *Ann NY Acad Sci* **993**: 305–312.
- Seo BB, Kitajima-Ihara T, Chan EK, Scheffler IE, Matsuno-Yagi A, Yagi T. (1997). Molecular remedy of complex I defects: rotenone-insensitive internal NADH-quinone oxidoreductase of *Saccharomyces cerevisiae* mitochondria restores the NADH oxidase activity of complex I-deficient mammalian cells. *Proc Natl Acad Sci USA* **95**: 9167–9171.
- Sever N, Lee PC, Song BL, Rawson RB, Debose-Boyd RA. (2004). Isolation of mutant cells lacking Insig-1 through selection with SR-12813, an agent that stimulates degradation of 3-hydroxy-3-methylglutaryl-coenzyme A reductase. *J Biol Chem* **279**: 43136–43147.
- Shiau CW, Huang JW, Wang DS, Weng JR, Yang CC, Lin CH *et al.* (2006). Tocopheryl succinate induces apoptosis in prostate cancer cells in part through inhibition of Bcl-x_L/Bcl-2 function. *J Biol Chem* **281**: 11819–11825.
- Slamon DJ, Godolphin W, Jones LA, Holt JA, Wong SG, Keith DE *et al.* (1989). Studies of the HER-2/neu proto-oncogene in human breast and ovarian cancer. *Science* **244**: 707–712.
- Slane BG, Aykin-Burns N, Smith BJ, Kalen AL, Goswami PC, Domann FE *et al.* (2006). Mutation of succinate dehydrogenase subunit C results in increased oxidative stress, and genomic instability. *Cancer Res* **66**: 7615–7620.
- Soller M, Drose S, Brandt U, Brune B, von Knethen A. (2007). Mechanism of thiazolidinedione-dependent cell death in Jurkat T cells. *Mol Pharmacol* **71**: 1535–1544.
- Spencer TL. (1977). The transport and oxidation of succinate by Ehrlich ascites-tumour cells. *Biochem J* **160**: 121–123.
- Stapelberg M, Gellert N, Swettenham E, Tomasetti M, Witting PK, Procopio A *et al.* (2005). Tocopheryl succinate inhibits malignant mesothelioma by disruption of the FGF autocrine signaling loop: mechanism and the role of oxidative stress. *J Biol Chem* **280**: 25369–25376.
- Sun F, Huo X, Zhai Y, Wang A, Xu J, Su D *et al.* (2005). Crystal structure of mitochondrial respiratory membrane protein complex II. *Cell* **121**: 1043–1057.
- Swettenham E, Witting PK, Salvatore BA, Neuzil J. (2005). Tocopheryl succinate selectively induces apoptosis in neuroblastoma cells: potential therapy of malignancies of the nervous system? *J Neurochem* **94**: 1448–1456.
- Trachootham D, Zhou Y, Zhang H, Demizu Y, Chen Z, Pelicano H *et al.* (2006). Selective killing of oncogenically transformed cells through a ROS-mediated mechanism by β -phenylethyl isothiocyanate. *Cancer Cell* **10**: 241–252.
- Tran QM, Rothery RA, Maklashina E, Cecchini G, Weiner JH. (2006). The quinone binding site in *Escherichia coli* succinate dehydrogenase is required for electron transfer to the heme b. *J Biol Chem* **281**: 32310–32317.
- Trounce IA, Kim YL, Jun AS, Wallace DC. (1996). Assessment of mitochondrial oxidative phosphorylation in patient muscle biopsies, lymphoblasts, and transmittochondrial cell lines. *Meth Enzymol* **264**: 484–509.
- Wallace AC, Laskowski RA, Thornton JM. (1995). LIGPLOT: a program to generate schematic diagrams of protein-ligand interactions. *Protein Eng* **8**: 127–134.
- Wang XF, Birringer M, Dong LF, Veprek P, Low P, Swettenham E *et al.* (2007). A peptide adduct of vitamin E succinate targets breast cancer cells with high erbB2 expression. *Cancer Res* **67**: 3337–3344.
- Wang XF, Witting PK, Salvatore BA, Neuzil J. (2005). Tocopheryl succinate induces apoptosis in HER2/erbB2-overexpressing breast cancer cells by signalling via the mitochondrial pathway. *Biochem Biophys Res Commun* **326**: 282–289.
- Weber T, Dalen H, Andera L, Nègre-Salvayre A, Augé N, Sticha M *et al.* (2003). Mitochondria play a central role in apoptosis induced by α -tocopheryl succinate, an agent with anticancer activity. *Biochemistry* **42**: 4277–4291.
- Weber T, Lu M, Andera L, Lahm H, Gellert N, Fariss MW *et al.* (2002). Vitamin E succinate is a potent novel anti-neoplastic agent with high tumor selectivity and cooperativity with tumor necrosis factor-related apoptosis-inducing ligand (TRAIL, Apo2L) *in vivo*. *Clin Cancer Res* **8**: 863–869.
- Word JM, Lovell SC, Richardson JS, Richardson DC. (1999). Asparagine and glutamine: using hydrogen atom contacts in the choice of side-chain amide orientation. *J Mol Biol* **285**: 1735–1747.
- Xu RH, Pelicano H, Zhou Y, Carew JS, Feng L, Bhalla KN *et al.* (2005). Inhibition of glycolysis in cancer cells: a novel strategy to overcome drug resistance associated with mitochondrial respiratory defect and hypoxia. *Cancer Res* **65**: 613–621.
- Yankovskaya V, Horsefield R, Tornroth S, Luna-Chavez C, Miyoshi H, Leger C *et al.* (2003). Architecture of succinate dehydrogenase and reactive oxygen species generation. *Science* **299**: 700–704.
- Yu L, Yu CA. (1983). Inhibitory effect of α -tocopherol and its derivatives on bovine heart succinate-cytochrome c reductase. *Biochim Biophys Acta* **723**: 139–149.
- Zhang JG, Tirmerstein MA, Nicholls-Grzeski FA, Fariss MW. (2001). Mitochondrial electron transport inhibitors cause lipid peroxidation-dependent and -independent cell death: protective role of antioxidants. *Arch Biochem Biophys* **393**: 87–96.
- Zhao Z, Rothery RA, Weiner JH. (2006). Effects of site-directed mutations in *Escherichia coli* succinate dehydrogenase on the enzyme activity and production of superoxide radicals. *Biochem Cell Biol* **84**: 1013–1021.

Supplementary Information accompanies the paper on the Oncogene website (<http://www.nature.com/onc>).

Vitamin E Analogues Inhibit Angiogenesis by Selective Induction of Apoptosis in Proliferating Endothelial Cells: The Role of Oxidative Stress

Lan-Feng Dong,¹ Emma Swettenham,¹ Johanna Eliasson,¹ Xiu-Fang Wang,¹ Mikhal Gold,² Yasmine Medunic,¹ Marina Stantic,¹ Pauline Low,² Lubomir Prochazka,⁴ Paul K. Witting,² Jaroslav Turanek,⁴ Emmanuel T. Akporiaye,³ Stephen J. Ralph,² and Jiri Neuzil^{1a}

¹Apoptosis Research Group and ²Genomic Research Centre, School of Medical Science, Griffith University, Southport, Queensland, Australia; ³Microbiology and Immunology, University of Arizona, Tucson, Arizona; ⁴Veterinary Research Institute, Brno, Czech Republic; ⁵ANZAC Research Institute, Concord Hospital, University of Sydney, Concord, New South Wales, Australia; and ⁶Molecular Therapy Group, Institute of Molecular Genetics, Czech Academy of Sciences, Prague, Czech Republic

Abstract

"Mitocans" from the vitamin E group of selective anticancer drugs, α -tocopheryl succinate (α -TOS) and its ether analogue α -TEA, triggered apoptosis in proliferating but not arrested endothelial cells. Angiogenic endothelial cells exposed to the vitamin E analogues, unlike their arrested counterparts, readily accumulated reactive oxygen species (ROS) by interfering with the mitochondrial redox chain and activating the intrinsic apoptotic pathway. The vitamin E analogues inhibited angiogenesis *in vitro* as assessed using the "wound-healing" and "tube-forming" models. Endothelial cells deficient in mitochondrial DNA (mtDNA) were resistant to the vitamin E analogues, both in ROS accumulation and apoptosis induction, maintaining their angiogenic potential. α -TOS inhibited angiogenesis in a mouse cancer model, as documented by ultrasound imaging. We conclude that vitamin E analogues selectively kill angiogenic endothelial cells, suppressing tumor growth, which has intriguing clinical implications. [Cancer Res 2007;67(24):11906-13]

Introduction

Under physiologic conditions, endothelial cells are suspended in G₀ and proliferate only in response to endothelial injury. In growing tumors, malignant cells secrete a cocktail of mitogens, such as vascular endothelial growth factor (VEGF) and fibroblast growth factor 2 (FGF2), which diffuse from the tumor cell and interact with cognate receptors on preexisting endothelial cells, triggering their proliferation (1). A prerequisite for tumor progression beyond a small initial carcinoma is formation of new blood vessels, a process known as angiogenesis. The stage at which tumor growth stimulates the "switch-to-the-angiogenic-phenotype" is not known. It has been assumed that this occurs at the stage when the diffusion of oxygen and nutrients across the cells is hampered so that a hypoxic core within the growing tumor is formed (2, 3). Because angiogenesis is essential for tumor progression, its

inhibition makes a plausible anticancer strategy (4-6). Several approaches have been used to inhibit tumor angiogenesis and prevent tumor progression, including gene therapy, immunotherapy, or chemotherapy (7-9).

A novel approach to inhibit angiogenesis is selective induction of apoptosis in endothelial cells (10). Hogg and colleagues (11) recently observed that targeting angiogenic endothelial cells by an arsenic derivative efficiently suppressed their proliferation and drove them into apoptosis. This translated to suppression of tumor progression and regression of tissue vascularization (10, 11). The authors showed that the drug interfered with the function of the adenine nucleotide translocator within the mitochondrial inner membrane. This is consistent with the notion that mitochondria are emerging as novel targets for cancer therapy (11-13).

We have defined a class of compounds, mitocans, which suppresses cancer by inducing apoptosis via targeting mitochondria (13). These drugs include a number of cytotoxic agents, such as the above-mentioned arsenic derivative, as well as a group of vitamin E analogues, epitomized by the redox-silent α -tocopheryl succinate (α -TOS), a selective inducer of apoptosis in cancer cells and a potent anticancer agent (14-20). α -TOS and its analogues have been shown to efficiently induce apoptosis by targeting mitochondria, a process involving generation of reactive oxygen species (ROS; refs. 16-19), which also suppresses cancer cell proliferation (18). Recently, we have shown that α -TOS causes ROS generation in cancer cells by displacing ubiquinone in its binding sites on complex II (13). This activity of vitamin E analogues translates to cancer suppression in a variety of preclinical models (15, 20-23).

We observed earlier that α -TOS specifically caused apoptosis in proliferating endothelial cells, being nontoxic to arrested endothelial cells, although the mechanism was not resolved (24). Because this finding is suggestive of selective toxicity of α -TOS for angiogenic endothelial cells, we explored this phenomenon in more detail. Here we present data on the mechanism of greater susceptibility of angiogenic endothelial cells to α -TOS as well as to the ether analogue and link this efficacy to inhibition of tumor angiogenesis *in vivo* in a preclinical model of breast cancer using mice with spontaneous breast carcinomas.

Materials and Methods

Cell culture and treatment. The endothelial-like EAhy926 cells (25) were maintained in DMEM supplemented with 100 μ M hypoxanthine, 0.4 μ M aminopterin, and 16 μ M thymidine. These cells retain properties of endothelial cells, including expression of factor VIII (25).

Note: Supplementary data for this article are available at Cancer Research Online (<http://cancerres.aacrjournals.org/>).

L.-F. Dong and E. Swettenham contributed equally to this work.
Requests for reprints: Jiri Neuzil, Apoptosis Research Group, Heart Foundation Research Centre, School of Medical Science and the Griffith Institute of Health and Medical Research, Griffith University, Southport 9716, Queensland, Australia. Phone: 61-2-555-29109; Fax: 61-2-555-28444; E-mail: jneuzil@griffith.edu.au.

©2007 American Association for Cancer Research.
 doi:10.1158/0008-5472.CCR-07-3034

tube-forming activity, and the propensity to persist in confluent cultures (7). EAhy926 cells deficient in mtDNA (ρ^0 phenotype) were prepared as detailed elsewhere (16). Acquisition of the ρ^0 phenotype was confirmed by lack of expression of cytochrome *c* oxidase subunit II but not subunit IV (data not shown).

The cells were treated under conditions of high, medium, or nil proliferation (40–50%, ~70%, and 100% confluency, respectively). The drugs used (Supplementary Scheme 1) were α -tocopherol (α -TOH), the ester analogue α -TOS (both Sigma), and the orally applicable ether analogue 2,5,7,8-tetramethyl-2R-(4R,8R,12-trimethyltridecyl)-chroman-6-yl-oxyacetic acid (α -tocopheryloxyacetic acid, α -TEA; ref. 22).

Assessment of apoptosis and mitochondrial potential. Apoptosis was estimated routinely by the Annexin V binding method based on phosphatidyl serine externalization at the relatively early phases of programmed cell death, essentially as described elsewhere (16).

Mitochondrial inner transmembrane potential ($\Delta\psi_m$) was estimated using the polychromatic probe 5,5',6,6'-tetrachloro-1,1',3,3'-tetraethylbenzimidazolyl-carbocyanine iodide (JC-1; Molecular Probes) as detailed elsewhere (16).

Evaluation of ROS accumulation, cell proliferation, and cell cycle distribution. Cellular ROS were detected indirectly by flow cytometry using dihydroethidium (DHE; Molecular Probes; ref. 18) and directly by electron paramagnetic resonance (EPR) spectroscopy (16), after treatment of cells with α -TOS or α -TEA. In some experiments, the cells were pretreated for 1 h with 2 μ M of mitochondrially targeted coenzyme Q (MitoQ; ref. 26) or cocultured with superoxide dismutase [polyethylene glycol-superoxide dismutase (PEG-SOD); Sigma S4636] at 750 units/mL.

Cell proliferation was determined using an ELISA colorimetric kit (Roche) to determine the number of cells in S phase of the cell cycle, based on DNA incorporation of 5-bromo-2-deoxyuridine (BrdUrd) using the manufacturer's protocol. For cell cycle analysis, cells were plated in 24-well plates so that they reached ~50%, 70%, and 100% confluency after 24-h recuperation. Cells were then harvested and resuspended in buffer containing sodium citrate (1%), Triton X-100 (0.1%), RNase A (0.05 μ g/mL), and propidium iodide at 5 μ g/mL, incubated in the dark for 30 min at 4°C and analyzed by flow cytometry.

Assessment of complex II (succinate dehydrogenase) activity. Solutions of 3-(4,5-dimethylthiazol-2-yl)-2,5-diphenyltetrazolium bromide (MTT; Sigma) were prepared before use by dissolving 25 mg/mL of MTT in PBS containing 20 mmol/L succinic acid (pH 7.4) as the sole substrate. Stock solutions of tetrahydrofuran (THF; Sigma) in DMSO, and α -TOS and MitoQ in ethanol were prepared. The drugs were tested on EAhy926 cells in the exponential growth phase in 96-well microtiter plates using four to eight replicate wells per drug dilution assayed. To assess the ability of MitoQ to restore MTT reduction, cells were preincubated for 3 h with 3 μ M/L MitoQ. Cells were allowed to reduce MTT for 2 h at 37°C, and absorbance was measured at 570 nm.

Wound-healing and tube-forming activity assessment. Endothelial cells were seeded and cultured to complete confluence. The central region of a monolayer of cells was "wounded" by scraping away cells, generating a denuded 0.5-mm wide stripe. Regrowth of cells was assessed by following the kinetics of filling the gap, visualized under a microscope equipped with a grid in the eyepiece. The healing rate was expressed in μ m/h.

For the tube-forming activity of endothelial cells, formation of capillary-like structures in a three-dimensional setting was assessed, essentially as described elsewhere (7). In brief, 300 μ L of cold Matrigel (BD Biosciences) per well were transferred with a cold tip using a 24-well plate. Matrigel was overlaid with a suspension of EAhy926 cells, so that a total of 200 μ L of complete medium with 5×10^5 cells were added to each well. After 6 h in the incubator, the polygonal structures, made by a network of EAhy926 capillaries was established. The cells were treated and tube-forming activity was estimated by counting the number of complete capillaries connecting individual points of the polygonal structures in a light microscope 24 h after transferring the cells to Matrigel. Three fields in the central area were chosen randomly in every well. The number of capillaries in control cultures was considered 100%.

Cell transfections. EAhy926 cells were transfected with a plasmid harboring the Bcl-x₁-EGFP gene (27) as described elsewhere (16). The cells were maintained in the selection medium for at least five passages, after which they were assessed for expression of the protein by inspection for green fluorescence using a fluorescence microscope or by Western blotting, revealing >95% transfected cells (data not shown).

VE-cadherin expression. Western blotting was performed as reported earlier (16) using anti-VE-cadherin IgG (Santa Cruz). For immunofluorescence microscopy, EAhy926 cells at ~40% or 100% confluency were incubated with anti-VE-cadherin IgG, followed by secondary FITC-conjugated IgG and mounting with 4',6-diamidino-2-phenylindole-containing Vectashield. The cells were inspected in the Leica DMIRE2 fluorescence microscope fitted with deconvolution software.

In vivo experiments. A colony of transgenic *FVB/N202 c-neu* mice carrying the rat *HER-2/neu* proto-oncogene driven by the mouse mammary tumor virus promoter on the H-2^s FVB/N background (28) was established at the Griffith University Animal Facility and maintained under strict inbreeding conditions. Approximately 70% of the female mice develop spontaneous mammary carcinomas with a mean latency of ~7 months. Formation of tumors was monitored by ultrasound imaging using the Vevo770 instrument (VisualSonics) equipped with the VisualSonics RM704 scan head (mean frequency, 60 MHz; resolution, 40 μ m), allowing noninvasive scanning of tumor tissue and tumor volume quantification. Scanning was performed on mice anesthetized using isoflurane with continuous monitoring of the heart rate as reported elsewhere (23). As soon as tumors were detected, the mice were treated by i.p. administration every 3 days of α -TOS dissolved in corn oil/4% ethanol (15 μ M α -TOS per injection per mouse). The kinetics of tumor growth was followed by ultrasound imaging every 3rd day.

The Vevo770 ultrasound imaging device is equipped with the Power Doppler function, which makes it possible to follow circulation in blood vessels. This was applied to assess the extent of angiogenesis in the *FVB/N c-neu* mice carcinomas. The control and treated mice were assessed by ultrasound imaging using the same respiratory gating, and the volume of blood vessels within tumors was expressed as percentage of vascularization of individual tumors.

Results

We first exposed EAhy926 cells at different levels of proliferation to α -TOS and α -TEA. As shown in Fig. 1A and B, endothelial cells at the lowest confluency were most susceptible to apoptosis, whereas arrested endothelial cells showed much greater resistance. Proliferating endothelial cells neither accumulated ROS nor underwent apoptosis when exposed to the redox-active α -TOH (Supplementary Table S1). Both α -TOS and α -TEA also suppressed proliferation of endothelial cells (Fig. 1C and D). The differences in proliferation of endothelial cells were assessed by cell cycle distribution (Supplementary Fig. S1A) revealing only a small S phase subpopulation in the arrested cells, whereas a high number of cells in S phase were found for the 50% proliferating cultures. Supplementary Fig. S1B documents high levels of expression in the confluent endothelial cells of the cell surface protein VE-cadherin involved in cell-cell contact of endothelial cells.

The fact that angiogenic endothelial cells are susceptible to the mitocans α -TOS and α -TEA raises the question of the role of mitochondria in apoptosis induced by vitamin E analogues, with α -TOS known to cause accumulation of ROS in cancer cells. We therefore assessed endothelial cells under conditions of proliferation and arrest for ROS generation as a response to α -TOS or α -TEA. Indeed, proliferating but not arrested endothelial cells responded to the challenge by early accumulation of high levels of ROS, as assessed by flow cytometry (Fig. 2A and B) and EPR spectroscopy (Supplementary Fig. S2). MitoQ and SOD suppressed

ROS generation and apoptosis induction by the vitamin E analogues in angiogenic endothelial cells (Fig. 2C and D).

Next, the role of mitochondria in apoptosis of endothelial cells exposed to α -TOS and α -TEA was investigated. Supplementary Fig. S3A shows that the majority (>97%) of control cells had high $\Delta\Psi_m$, whereas exposing proliferating endothelial cells to either agent resulted in early (within 24 h) dissipation of $\Delta\Psi_m$, occurring in 15% to 20% of the population. Mitochondrial destabilization is generally followed by caspase activation. Supplementary Fig. S3B reveals that caspases were activated in apoptosis induced by the two vitamin E analogues because the pan-caspase inhibitor z-VAD-fmk efficiently inhibited apoptosis in proliferating endothelial cells. We also show here that overexpression in endothelial cells of the antiapoptotic protein Bcl-x_l protected the cells from α -TOS- and α -TEA-induced apoptosis (Supplementary Fig. S3C).

We have shown that vitamin E analogues cause generation of ROS with ensuing induction of apoptosis in cancer cells by interfering with coenzyme Q binding in the mitochondrial complex II. We therefore tested the possibility that α -TOS triggers ROS generation in endothelial cells by interfering with the complex II SDH activity. Table 1 documents that α -TOS and α -TEA inhibited SDH activity similarly, as shown for TTFA, a compound known to displace coenzyme Q in complex II. Inhibition of SDH activity by α -TOS, α -TEA, or TTFA was rescued by MitoQ, which is known to interact with complex II. These data strongly suggest that α -TOS and α -TEA act by interfering with ubiquinone binding of complex II.

We next asked the question whether the propensity of angiogenic endothelial cells to undergo apoptosis, when challenged with vitamin E analogues, translates to inhibition of angiogenesis. We used two experimental approaches to assess angiogenesis *in vitro*, based on the wound-healing and the tube-forming activity assays. In the wound-healing assay, cells were grown to complete confluence and then a central strip of cells was removed, after which regrowth into the cleared space was evaluated (Supplementary Fig. S4). Figure 3A and B show that the healing rate was $\sim 20 \mu\text{m}/\text{h}$ for control cells, ~ 8 and $\sim 3 \mu\text{m}/\text{h}$ for cells exposed to 25 and 37.5 $\mu\text{mol}/\text{L}$ α -TOS, respectively. No regrowth was observed at 50 $\mu\text{mol}/\text{L}$ α -TOS. A dose-dependent inhibition of wound healing was also observed for α -TEA (Fig. 3C and D). Importantly, inhibition of wound healing by the vitamin E analogues was associated with extensive apoptosis induction in the wound zone of the endothelium (Fig. 3B and D). Next, a dose-dependent inhibitory effect on endothelial cell tube-forming activity was observed for α -TOS and α -TEA (Fig. 4). The vitamin E analogues suppressed the tube-forming activity of the endothelial cells by way of apoptosis induction, as found by assessing the cells for apoptosis after their treatment and analysis after retrieval from the Matrigel cultures.

The role of mitochondria in susceptibility of angiogenic endothelial cells to α -TOS was confirmed in experiments in which mtDNA-deficient endothelial cells were exposed to the vitamin E analogue and assessed for ROS accumulation and apoptosis induction by flow cytometry. As documented in Fig. 5A, dividing populations of ρ^0 cells, unlike their parental counterparts, showed reduced levels of ROS. The subconfluent ρ^0 endothelial cells also failed to undergo efficient apoptosis when exposed to α -TOS (Fig. 5B). We were interested whether endothelial cells deficient in mtDNA maintain their wound-healing and tube-forming activity, and, if so, how this is affected by α -TOS. Figure 5C and D reveal that endothelial cells deficient in mtDNA are capable of wound

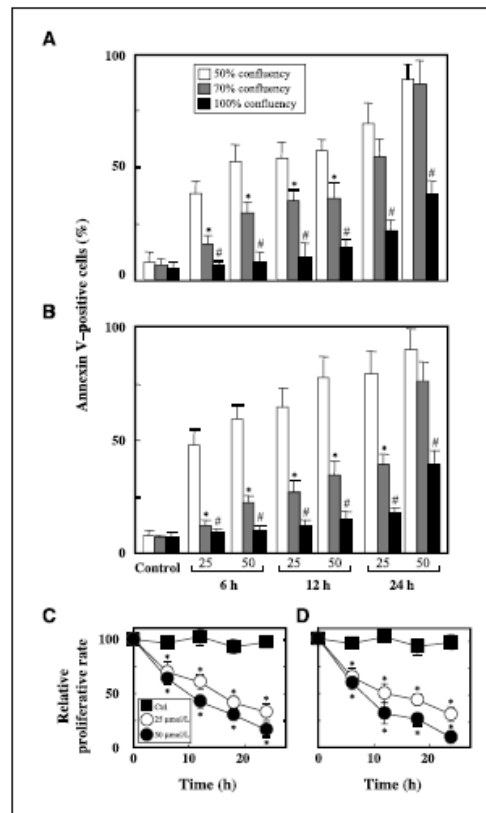
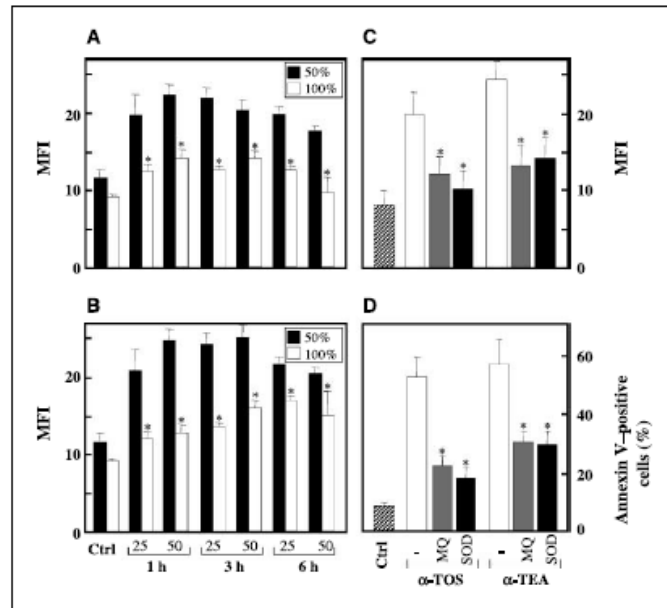


Figure 1. Vitamin E analogues induce apoptosis and inhibit proliferation in angiogenic but not arrested endothelial cells. EAhy926 cells were seeded to reach low ($\sim 50\%$), medium ($\sim 70\%$), and high (100%) confluency. The cells were treated with 25 or 50 $\mu\text{mol}/\text{L}$ α -TOS (A and C) or α -TEA (B and D) for increasing periods of time and assessed for apoptosis induction by the Annexin V binding method (A and B) or proliferation (assessed on 50% confluent cells) by means of BrdUrd incorporation (C and D). Columns, mean ($n = 3$); bars, SD. *, statistically significant differences from 100% confluent cells; #, those from both 100% and 70% confluent cells (A and B). *, statistically significant differences from the controls (ctr); C and D.

healing and tube formation, although at a slower rate than the parental cells. Importantly, the ρ^0 cells maintained the two features of *in vitro* angiogenesis (wound healing and tube formation) even in the presence of α -TOS. These results strongly suggest the importance of normal mitochondrial function for susceptibility of angiogenic endothelial cells to vitamin E analogues.

We next tested whether the inhibitory activity of α -TOS on angiogenesis *in vitro* translates to an *in vivo* situation. Hence, we used the transgenic *FVB/N c-neu* mice that form spontaneous breast ductal carcinomas at the age of ~ 7 months due to mammary tissue-specific overexpression of the receptor tyrosine kinase erbB2 (HER2). In particular, we studied the effect of i.p. administered α -TOS on the kinetics of the tumor growth and

Figure 2. Vitamin E analogues cause accumulation of mitochondria-derived superoxide in angiogenic endothelial cells. EAhy926 cells were seeded at two different densities to achieve ~50% and 100% confluent cells, at which stage they were exposed to α -TOS (A) or α -TEA (B) at 25 and 50 μ mol/L for increasing periods of time. Generation of ROS was assessed after incubating the cells with DHE and estimating mean fluorescence intensity (MFI) using flow cytometry. Proliferating EAhy926 cells were pretreated for 10 min with PEG-SOD (25 units/mL) or 2 h with 3 μ mol/L MitoQ and assessed for ROS accumulation using flow cytometry after 3 h (C) or for apoptosis induction using the Annexin V method after 12-h exposure to 25 μ mol/L α -TOS or α -TEA (D). Columns, mean (n = 3); bars, SD. *, statistically significant differences from 100% confluent cells (A and B); †, statistically significant differences from cells exposed to α -TOS or α -TEA only (C and D).



vascularization of the carcinomas. This was performed using the Power Doppler function of the ultrasound instrument that allows for noninvasive and very precise quantification of the tumor volume and percentage tumor vascularization. Figure 6 documents that α -TOS suppressed growth of the tumor, decreasing the volume of the carcinomas by ~30%. Importantly, the extent of tumor vascularization increased with time in the control mice, whereas it decreased significantly when the animals were treated with the vitamin E analogue. These data link the antitumor efficacy of α -TOS with its propensity to act as an antiangiogenic agent *in vivo*.

Discussion

Our earlier data showed that proliferating endothelial cells, unlike their confluent counterparts, were susceptible to apoptosis induction when exposed to α -TOS (24), but the molecular mechanism had not been resolved. Recent data by Don et al. (10)

are consistent with our findings because they showed that proliferating endothelial cells were susceptible to the mitocan arsenide, whereas growth arrested cells were resistant to the drug, although the reasons for protection of the growth-arrested endothelial cells were not identified.

Our major interest was to understand the molecular mechanism of differential sensitivity of endothelial cells to the clinically interesting vitamin E analogues in relation to their proliferative status. Because *in vivo* endothelial cells in tumors show a high proliferative rate, whereas endothelial cells of normal blood vessels feature a very long half-life before dividing, it can be expected that vitamin E analogues will kill angiogenic endothelial cells in tumors but not endothelial cells of the normal vasculature. Similarly, as shown by Don et al. (10), we also found that proliferating endothelial cells responded to apoptogenic vitamin E analogues by accumulation of relatively high levels of ROS. In the case of agents such as α -TOS, the mechanism of generation of ROS

Concentration (μ mol/L)*	TTFA	TTFA + MitoQ	α -TOS	α -TOS + MitoQ	α -TEA	α -TEA + MitoQ
0	100	100	100	100	100	100
12.5	76.1 \pm 5.3	98.1 \pm 1.9	83.1 \pm 7.9	102.1 \pm 1.1	71.1 \pm 7.9	98.2 \pm 3.1
25	48.3 \pm 6.1	97.1 \pm 2.3	63.2 \pm 8.1	98.9 \pm 4.5	49.1 \pm 8.2	87.9 \pm 7.8
50	41.3 \pm 3.8	78.9 \pm 6.9	48.9 \pm 3.2	79.9 \pm 5.3	38.9 \pm 6.1	74.2 \pm 8.9

*Proliferating endothelial cells were exposed to TTFA, α -TOS, and α -TEA at the concentrations shown for 2 h following, as shown, a 2-h preincubation with 3 μ mol/L MitoQ.

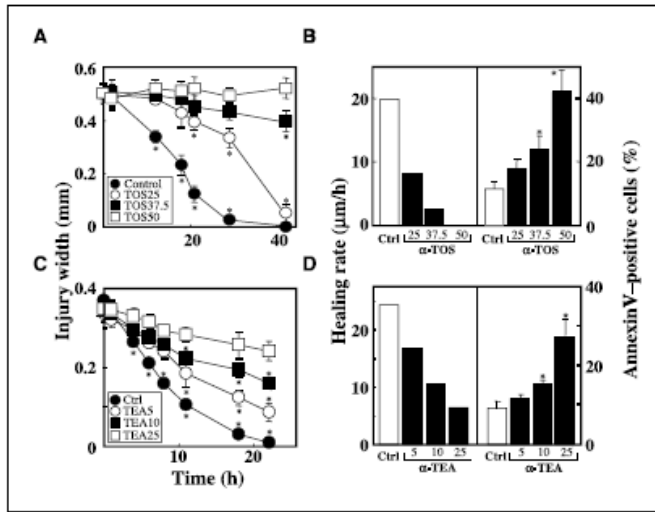


Figure 3. Vitamin E analogues inhibit wound healing. EAhy926 cells were seeded in culture dishes and allowed to reach complete confluency. The central part of the endothelial monolayer was wounded by removing a lane of cells ~0.5 mm across. Gap narrowing by proliferating and migrating cells was then followed in control cultures and in the presence of α -TOS (A and B) or α -TEA (C and D) at concentrations shown ($\mu\text{mol/L}$). At different times, the gap width was assessed in the microscope and plotted as a function of time (A and C). The "healing rate" was estimated from the slopes in A and C and expressed in $\mu\text{m/h}$ (B and D). The level of apoptosis in the wounded cultures of EAhy926 cultures was assessed at 42 h (B and D). Columns and points, mean ($n = 3$); bars, SD. *, statistically significant differences from the controls.

in cancer cells is most likely due to displacement by the vitamin E analogue of ubiquinone in one or both of its binding pockets within the mitochondrial complex II (13). It is therefore probable that the absence of the electron acceptor, ubiquinone, will result in recombination of electrons with molecular oxygen to form superoxide. It has been shown that the absence of complex II [more specifically, the cytochrome B-large, CybL, or the SDH subunit C (SDHC)] due to mutations in *SDHC* results in lower levels of ROS generation when the cells are exposed to α -TOS or

several unrelated inducers of apoptosis, and this is reflected by low levels of apoptosis induction (13, 29). We also assessed the possible role of complex II in apoptosis induction by vitamin E analogues in endothelial cells and found that α -TOS and α -TEA inhibited SDH activity, and that it was restored in the presence of the complex II-interacting MitoQ (30), similarly, as also observed for TTFa, an agent that displaces coenzyme Q in complex II (31). Our data suggest a general mechanism of ROS-mediated induction of apoptosis by vitamin E analogues in both cancer cells and proliferating

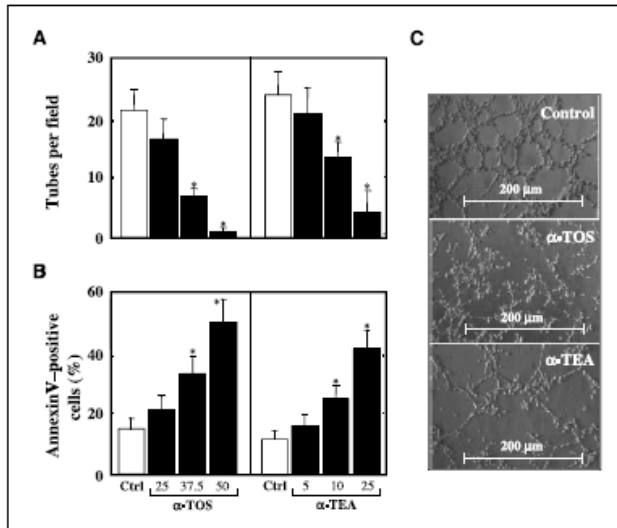
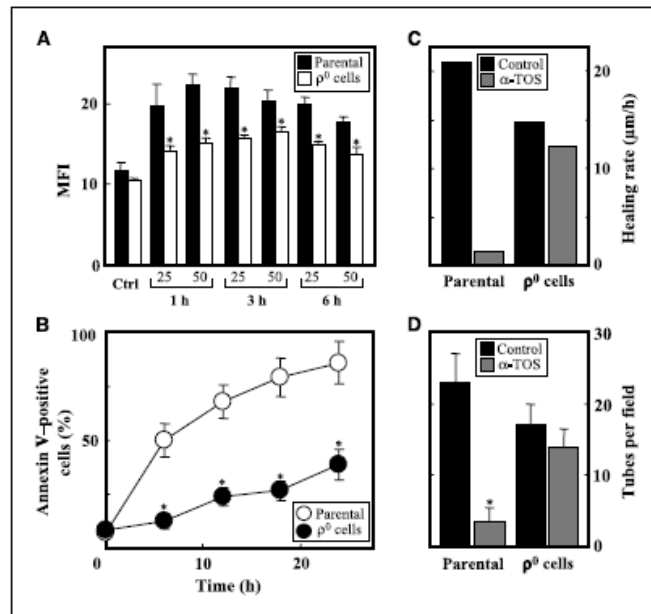


Figure 4. Vitamin E analogues inhibit the tube-forming activity of EAhy926 cells. EAhy926 cells were seeded in 24-well plates with 300 μL of Matrigel per well so that suspension of 200 μL of complete medium with 5×10^5 cells were added to each well. Control cultures as well as those supplemented with α -TOS or α -TEA at concentrations shown ($\mu\text{mol/L}$) were evaluated by counting in a light microscope the number of complete tubes connecting points of individual polygons of the capillary network at 24 h as detailed in Materials and Methods (A). Cells were retrieved after 24 h from Matrigel and assessed for apoptosis induction (B). C, Matrigel cultures at 12 h in the absence of any drug or in the presence of 50 $\mu\text{mol/L}$ α -TOS or 25 $\mu\text{mol/L}$ α -TEA. Columns, mean ($n = 3$); bars, SD; the digital photographs are representative of three independent experiments. *, statistically significant differences from the controls.

Figure 5. EAhy926 cells deficient in mtDNA are resistant to α -TOS. Proliferating parental or mtDNA-deficient (ρ^0) EAhy926 cells were exposed to α -TOS at 25 μ M or as shown and assessed for ROS accumulation using DHE (A) and for apoptosis induction using the Annexin V binding method (B). Parental and mtDNA-deficient endothelial cells were seeded in Petri dishes, allowed to reach confluency, and the endothelium wounded. Regrowth was followed in the absence or presence of 25 μ M α -TOS at 24 h and evaluated as detailed in Materials and Methods (C). Parental and mtDNA-deficient EAhy926 cells were seeded on Matrigel, exposed to 25 μ M α -TOS, and the number of tubes as a read-out of angiogenesis (refer to Materials and Methods for details) counted at 24 h (D). Columns and points, mean ($n = 3$); bars, SD. *, statistically significant differences from parental (A and B) and control cells (D).



endothelial cells, which is based on displacement of coenzyme Q in its binding pocket(s) in the mitochondrial complex II, which results in generation of superoxide. We propose that this site is also likely to be responsible for the antiangiogenic effect of vitamin E analogues by way of binding of vitamin E analogues that displace the natural electron acceptor, resulting in generation of apoptosis-inducing ROS levels.

Not only does the selectivity of vitamin E analogues as agents inducing apoptosis in angiogenic endothelial cells have significant clinical relevance in helping to arrest tumor progression, but also the molecular mechanism as defined here is of major interest and importance. Don et al. (10) reported on selective killing of proliferating endothelial cells by an arsenic derivative. They showed that the angiogenic cells accumulated high levels of ROS, unlike their arrested counterparts. We also observed this in angiogenic endothelial cells exposed to α -TOS and α -TEA. These differences in accumulation of ROS seem central to the susceptibility or resistance of the endothelial cells to apoptosis because eliminating ROS accumulation, such as by coexposure to antioxidants, also suppresses the extent of apoptosis. Numerous compounds have been reported to inhibit angiogenesis by way of killing proliferating endothelial cells or causing their cytostasis. These include anticancer drugs paclitaxel (32, 33) or vinblastine (34), the histone deacetylase inhibitor LBH589 (35), the vascular-targeting compound ZD6126 (36), or the proteasome inhibitor bortezomib (37). Although these agents have been shown to reduce tumors in experimental animals, neither of them has been reported for selective toxicity toward proliferating while being nontoxic to arrested endothelial cells. To the best of our knowledge, this intriguing paradigm has only been shown for the mitocans arsenide (10) and vitamin E analogues (reported here). The

selectivity of apoptosis induction in angiogenic endothelial cells by vitamin E analogues is particularly interesting because vitamin E analogues have shown promise as anticancer agents in several animal models. This is further fueled by our clinical outcome from a mesothelioma patient who has been treated with transdermally applied α -TOS. The data reveal a significant clinical benefit with α -TOS therapy, causing a reduction in tumor volume and improved well-being of our subject who previously was suffering from a lethal neoplastic pathology (38, 39).

The molecular mechanism for the very low levels of ROS accumulation in arrested endothelial cells exposed to vitamin E analogues is not known at present. We can suggest at least two possibilities that could explain this. First, the arrested cells may respond to the stress imposed by vitamin E analogues by generating lower levels of ROS due to a difference in the cellular systems that cause formation of radicals. The other, probably more plausible possibility, is due to potential up-regulation of the antioxidant systems in the resistant, arrested endothelial cells. One enzyme that may be up-regulated is manganese superoxide dismutase (MnSOD). This idea is consistent with reports showing that cells deficient in mtDNA are resistant to apoptosis and show increased expression of MnSOD (40–42). We have also found elevated expression of MnSOD in arrested endothelial cells,⁷ possibly related to higher levels of p53 (43, 44). The molecular mechanism of regulation of MnSOD expression in endothelial cells in relation to their proliferative status is the subject of ongoing studies.

⁷J. Neuzil et al., unpublished data.

Because killing of angiogenic endothelial cells by α -TOS and α -TEA suggests that vitamin E analogues may possess antiangiogenic activity, thereby suppressing tumor progression, we studied the effect of the two agents on angiogenesis *in vitro*. In these experiments, we used the immortalized EAhy926 cells because these cells, unlike the primary endothelial cells with limited life span (usually four to five cell cycle transitions), can be used for up to 100 doublings, while preserving properties of primary endothelial cells including expression of von Willebrand factor or P selectin, as well as formation of tubes in a three-dimensional setting and persistent arrest (7, 25). Our results clearly document the efficacy of α -TOS and α -TEA in inhibiting angiogenesis *in vitro*, as assessed by both the wound-healing and tube-forming approach. Importantly, inhibition of angiogenesis *in vitro* was associated with the induction of apoptosis in the proliferating endothelial cells, which suggests a link between the efficacy of vitamin E analogues to induce apoptosis in proliferating endothelial cells with their antiangiogenic activity.

We also assessed endothelial cells deficient in mtDNA for their susceptibility to α -TOS because ρ^0 cancer cells are resistant to apoptosis (16, 19, 40, 45) and feature an impaired mitochondrial electron redox chain, a major source of ROS generation (46, 47). We found that ρ^0 endothelial cells were relatively resistant to α -TOS-induced apoptosis. We also observed that ρ^0 endothelial cells retained the propensity of normal endothelial cells to undergo wound healing after injury as well as tube forming in Matrigel, and that neither the wound-healing nor the tube-forming activities were

impaired by α -TOS. These are important findings that further support the importance of fully functional mitochondria to make angiogenic endothelial cells susceptible to apoptosis induction by vitamin E analogues.

Lastly, we evaluated the effect of α -TOS on angiogenesis *in vivo*. To do this, we used the transgenic *FVB/N c-neu* mice with spontaneous development of breast carcinomas (28). We have observed recently that analogues of vitamin E coupled to peptides binding the HER2 receptor suppressed progression of these tumors (23). The Vevo770 ultrasound device allows us to visualize and quantify blood vessels so that noninvasive assessment of the kinetics of angiogenesis in tumors treated with a potential inhibitor of angiogenesis can be assessed directly in real time *in vivo*. We found that α -TOS significantly suppressed tumor progression, consistent with our recent report (23), and that this was accompanied by inhibition of angiogenesis. Ultrasound imaging revealed that the percentage of the tumor mass occupied by blood vessels increased in control animals by as much as ~8-fold over the 3 weeks of the experiment in the control animals, whereas it was suppressed by ~50% in mice treated with α -TOS. These data unequivocally document the antiangiogenic property of α -TOS. This result is of clinical relevance because HER2-positive breast cancer is resistant to therapy (48) and because breast cancer accounts for >25% of female cancer patients in the USA, with almost 200,000 new cases and >40,000 deaths predicted for 2007 (49).

Our *in vitro* results suggest that apoptosis is a plausible factor by which vitamin E analogues inhibit angiogenesis. However, we

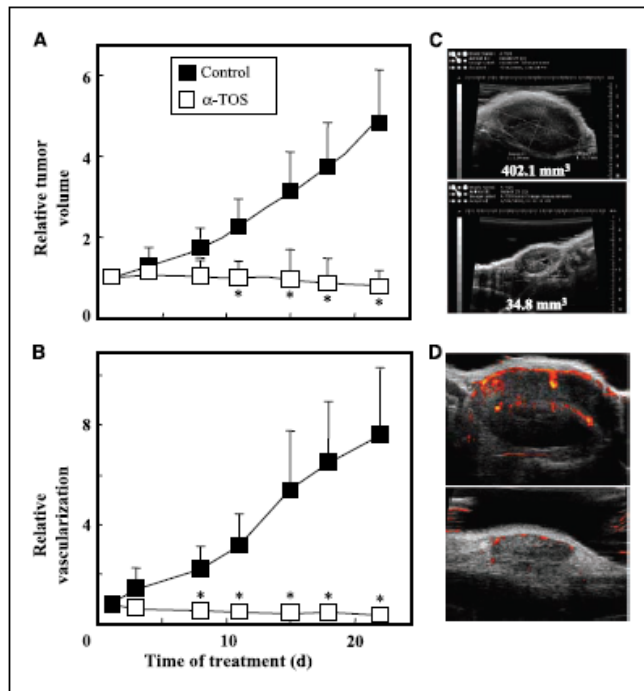


Figure 6. α -TOS suppresses cancer and reduces tumor vascularity. The transgenic *FVB/N c-neu* mice with spontaneous breast carcinomas were treated with α -TOS solubilized in corn oil/4% ethanol administered every 3 to 4 d by i.p. injection. Volume tumors of control and treated mice (A) and vascularity (B) were evaluated using ultrasound imaging fitted with the Power Doppler function and were expressed relative to the initial state. Points, mean ($n = 5-7$); bars, SD. C, representative images of ultrasound imaging of tumors and their vascularization (D) at 22 d of control (top) and α -TOS-treated mice (bottom). *, statistically significant differences from the controls.

cannot rule out other possibilities that may contribute to the overall antiangiogenic activity of the drugs. These include, in particular, the effect of α -TOS on expression of genes by which tumor cells promote angiogenesis, such as VEGF, as shown for breast cancer cells (50), and FGF2, as reported for mesothelioma cells (18, 51). Notwithstanding, apoptosis seems to be an important mechanism by which vitamin E analogues inhibit angiogenesis, thereby inhibiting tumor progression, which is clinically intriguing.

Acknowledgments

Received 8/8/2007; revised 9/13/2007; accepted 10/18/2007.

Grant support: Australian Research Council (J. Neuzil and P.K. Witting); the Queensland Cancer Fund; the National Breast Cancer Foundation; the Grant Agency of the Academy of Sciences of the Czech Republic KAN200520703, IAA5005220602, and IAA500520602 (J. Neuzil); Concept Grant AV0250520514 awarded by the Academy of Sciences of the Czech Republic; and Grant from the Ministry of Agriculture of the Czech Republic (grant No. MZE 0002716201). J. Eliasson was a visiting student at the Apoptosis Research Group (Griffith University) supported by a scholarship from the University of Linköping, Linköping, Sweden. M. Gold was a visiting student at the Apoptosis Research Group (Griffith University) supported by the Bravo! Award from the University of Arizona, Tucson, AZ. L. Prochazka was a visiting student at and in part supported by the Apoptosis Research Group (Griffith University).

The costs of publication of this article were defrayed in part by the payment of page charges. This article must therefore be hereby marked *advertisement* in accordance with 18 U.S.C. Section 1734 solely to indicate this fact.

We thank R. Youle (NIH, Bethesda, MD) for providing the Bcl-xL plasmid and R. Smith (Otago University, Dunedin, New Zealand) for the MitoQ.

References

- Cross MJ, Claesson-Welsh L. FGF and VEGF function in angiogenesis: signalling pathways, biological responses and therapeutic inhibition. *Trends Pharmacol Sci* 2001;22:201-7.
- Folkman J, Shing Y. Angiogenesis. *J Biol Chem* 1992; 267:10931-4.
- Naumov GN, Akslen LA, Folkman J. Role of angiogenesis in human tumor dormancy: animal models of the angiogenic switch. *Cell Cycle* 2006;6:1779-87.
- Hlatky L, Hahnfeldt P, Folkman J. Clinical application of antiangiogenic therapy: microvessel density, what it does and doesn't tell us. *J Natl Cancer Inst* 2002;94:883-93.
- Folkman J. Angiogenesis: an organizing principle for drug discovery? *Nat Rev Drug Discov* 2007;6:273-86.
- Cardinet P. Angiogenesis in life, disease and medicine. *Nature* 2005;438:932-6.
- Alfani A, Marchisone C, Del Grosso F, et al. Inhibition of angiogenesis and vascular tumor growth by interferon-producing cells: A gene therapy approach. *Am J Pathol* 2000;156:1381-93.
- Malacki M, Kolaut P, Proczka R. Angiogenic and antiangiogenic gene therapy. *Gene Ther* 2005;12:59-69.
- Kerbel R, Folkman J. Clinical translation of angiogenesis inhibitors. *Nat Rev Cancer* 2002;2:727-39.
- Don AS, Kisker O, Dilda P, et al. A peptide trivalent arsenical inhibits tumor angiogenesis by perturbing mitochondrial function in angiogenic endothelial cells. *Cancer Cell* 2003;3:497-509.
- Don AS, Hogg PJ. Mitochondria as cancer drug targets. *Trends Mol Med* 2004;10:372-8.
- Fantin VR, Leder P. Mitochondriotoxic compounds for cancer therapy. *Oncogene* 2006;25:4787-97.
- Neuzil J, Dyason JC, Freeman R, et al. Mitocans as anti-cancer agents targeting mitochondria: lessons from studies with vitamin E analogues, inhibitors of complex II. *J Bioenerg Biomembr* 2007;39:65-72.
- Neuzil J, Weber T, Gellert N, Weber C. Selective cancer cell killing by α -tocopheryl succinate. *Br J Cancer* 2001;84:87-9.
- Neuzil J, Weber T, Schröder A, et al. Induction of cancer cell apoptosis by α -tocopheryl succinate: molecular pathways and structural requirements. *FASEB J* 2001;15:403-15.
- Weber T, Dahlen H, Anders L, et al. Mitochondria play a central role in apoptosis induced by α -tocopheryl succinate, an agent with anti-neoplastic activity: comparison with receptor-mediated pro-apoptotic signaling. *Biochemistry* 2003;42:4277-91.
- Yu W, Sanders BG, Kline K. RRR- α -Tocopheryl succinate-induced apoptosis of human breast cancer cells involves Bax translocation to mitochondria. *Cancer Res* 2003;63:4883-91.
- Stapelberg M, Gellert N, Swettenham E, et al. α -Tocopheryl succinate inhibits malignant mesothelioma by disrupting the fibroblast growth factor autocrine loop mechanism and the role of oxidative stress. *J Biol Chem* 2005;280:25369-76.
- Swettenham E, Witting PK, Salvatore BA, Neuzil J. α -Tocopheryl succinate selectively induces apoptosis in neuroblastoma cells potential therapy of malignancies of the nervous system? *J Neurochem* 2005;94:1448-56.
- Weber T, Lu M, Anders L, et al. Vitamin E succinate is a potent novel antineoplastic agent with high selectivity and cooperativity with tumor necrosis factor-related apoptosis-inducing ligand (Apo2 ligand) *in vivo*. *Clin Cancer Res* 2002;8:863-9.
- Malafa MP, Fokum FD, Mowlavi A, Abusief M, King M. Vitamin E inhibits melanoma growth in mice. *Surgery* 2002;131:85-91.
- Hahn T, Szabo I, Gold M, et al. Dietary administration of the proapoptotic vitamin E analogue α -tocopheryloxyacetic acid inhibits metastatic murine breast cancer. *Cancer Res* 2006;66:9374-8.
- Wang XF, Birringer M, Dong LF, et al. A peptide conjugate of vitamin E succinate targets breast cancer cells with high ErbB2 expression. *Cancer Res* 2007;67: 3337-44.
- Neuzil J, Schröder A, von Hundelshausen P, et al. Inhibition of inflammatory endothelial responses by a pathway involving caspase activation and p65 cleavage. *Biochemistry* 2001;40:6886-92.
- Edgell CJ, McDonald CC, Graham JB. Permanent cell line expressing human factor VIII-related antigen established by hybridization. *Proc Natl Acad Sci USA* 1983;80:5734-7.
- Kelso GF, Porteous CM, Coulter CV, et al. Selective targeting of a redox-active ubiquinone to mitochondria within cells: antioxidant and antiapoptotic properties. *J Biol Chem* 2001;276:4588-96.
- Wolter KG, Hsu YT, Smith CL, et al. Movement of Bax from the cytosol to mitochondria during apoptosis. *J Cell Biol* 2003;159:1281-92.
- Guy CT, Webster MA, Schaller M, et al. Expression of the neu protooncogene in the mammary epithelium of transgenic mice induces metastatic disease. *Proc Natl Acad Sci USA* 1992;89:10578-82.
- James AM, Sharpley MS, Manas AB, et al. Interaction of the mitochondria-targeted antioxidant mitoQ with phospholipid bilayers and ubiquinone oxidoreductases. *J Biol Chem* 2007;282:14708-18.
- Sun F, Hao X, Zhai Y, et al. Crystal structure of mitochondrial respiratory membrane protein complex II. *Cell* 2005;121:1043-57.
- Alhayrak T, Scherhammer V, Schoenfeld N, et al. The tumor suppressor cyb1, a component of the respiratory chain, mediates apoptosis induction. *Mol Biol Cell* 2003; 14:3082-96.
- Dicker AP, Williams TL, Iliakis G, Grant DS. Targeting angiogenic processes by combination low-dose paclitaxel and radiation therapy. *Am J Clin Oncol* 2003;26: e45-53.
- Pasquier E, Carre M, Pourroy B, et al. Antiangiogenic activity of paclitaxel is associated with its cytostatic effect, mediated by the initiation but not completion of a mitochondrial apoptotic signaling pathway. *Mol Cancer Ther* 2004;3:1301-10.
- Marimóni D, Nico B, Vacca A, et al. Synergistic inhibition of human neuroblastoma-related angiogenesis by vinblastine and rapamycin. *Oncogene* 2005;24: 6785-95.
- Qian DZ, Kato Y, Shabbeer S, et al. Targeting tumor angiogenesis with histone deacetylase inhibitors: the hydroxamic acid derivative LBH589. *Clin Cancer Res* 2006;12:634-42.
- Hoang T, Huang S, Armstrong E, Etkhof JC, Harari PM. Augmentation of radiation response by the vascular targeting agent ZD6126. *Int J Radiat Oncol Biol Phys* 2006;64:1458-65.
- Nawrocki ST, Sweeney-Gotsch B, Takamori R, McConkey DJ. The proteasome inhibitor bortezomib enhances the activity of docetaxel in orthotopic human pancreatic tumor xenografts. *Mol Cancer Ther* 2004;3: 59-70.
- Robinson BW, Lake RA. Advances in malignant mesothelioma. *N Engl J Med* 2005;353:1591-603.
- Tsioris A, Wilesby RK. Malignant pleural mesothelioma: current concepts in treatment. *Nat Clin Pract Oncol* 2007;4:344-52.
- Park SY, Chang I, Kim JY, et al. Resistance of mitochondrial DNA-depleted cells against cell death: role of mitochondrial superoxide dismutase. *J Biol Chem* 2004;279:7512-20.
- Frøman R, Neuzil J. Role of thioredoxin-1 in apoptosis induction by α -tocopheryl succinate and TNF-related apoptosis-inducing ligand in mesothelioma cells. *FEBS Lett* 2006;580:2671-6.
- Neuzil J, Widen C, Gellert N, et al. Mitochondria transmit apoptotic signals in cardiomyocyte-like cells and isolated hearts exposed to experimental ischemia-reperfusion injury. *Redox Report* 2007;12:148-62.
- Zhang Y, Griffith HC, Sage J, Jacks T, Liu JO. Cell cycle inhibition by the anti-angiogenic agent TNP-470 is mediated by p53 and p21^{WAF1/CIP1}. *Proc Natl Acad Sci USA* 2000;97:6427-32.
- Hussain SP, Amstad P, He P, et al. p53-induced up-regulation of MnSOD and Gpx but not catalase increases oxidative stress and apoptosis. *Cancer Res* 2004;64:2350-6.
- Higuchi M, Aggarwal BB, Yeh ET. Activation of CPP32-like protease in tumor necrosis factor-induced apoptosis is dependent on mitochondrial function. *J Clin Invest* 1997;99:1751-8.
- Chandel NS, Schumacker PT. Cells depleted of mitochondrial DNA (p⁰) yield insight into physiological mechanisms. *FEBS Lett* 1999;454:173-6.
- Levrant J, huase H, Shao ZH, Vanden Hoek TL, Schumacker PT. Cell death during ischemia: relationship to mitochondrial depolarization and ROS generation. *Am J Physiol* 2002;284:H549-58.
- Burstein HJ. The distinctive nature of HER2-positive breast cancers. *N Engl J Med* 2005;353:1652-4.
- Jemal A, Siegel R, Ward E, Murray T, Xu J, Thun MJ. Cancer statistics, 2007. *CA Cancer J Clin* 2007;57: 43-66.
- Malafa MP, Neitzel LT. Vitamin E succinate promotes breast cancer tumor dormancy. *J Surg Res* 2000;93:163-70.
- Neuzil J, Swettenham E, Wang XF, Dong LF, Stapelberg M. α -Tocopheryl succinate inhibits angiogenesis by disrupting paracrine FGF2 signalling. *FEBS Lett* 2007;581:5611-5.



Review

Vitamin E analogues as a novel group
of mitocans: Anti-cancer agents that act
by targeting mitochondria

Jiri Neuzil ^{a,b,*}, Lan-Feng Dong ^a, Lalitha Ramanathapuram ^c,
Tobias Hahn ^c, Miroslava Chladova ^b, Xiu-Fang Wang ^a,
Renata Zobalova ^{a,b}, Lubomir Prochazka ^d, Mikhal Gold ^c,
Ruth Freeman ^a, Jaroslav Turanek ^d, Emmanuel T. Akporiaye ^c,
Jeffrey C. Dyason ^e, Stephen J. Ralph ^f

^a Apoptosis Research Group, School of Medical Science, Griffith University, Southport, Qld, Australia

^b Molecular Therapy Group, Institute of Molecular Genetics, Czech Academy of Sciences, Prague, Czech Republic

^c Department of Immunobiology, University of Arizona, Tucson, AZ, USA

^d Department of Immunology, Veterinary Research Institute, Brno, Czech Republic

^e Institute for Glycomics, Griffith University, Southport, Qld, Australia

^f Genomic Research Institute, School of Medical Science, Griffith University, Southport, Qld, Australia

Received 19 January 2007; revised 12 February 2007; accepted 13 February 2007

Abstract

Mitochondria have recently emerged as new and promising targets for cancer prevention and therapy. One of the reasons for this is that mitochondria are instrumental to many types of cell death and often lie downstream from the initial actions of anti-cancer drugs. Unlike the tumour suppressor gene encoding p53 that is notoriously prone to inactivating

* Corresponding author. Address: Apoptosis Research Group, Heart Foundation Research Centre, School of Medical Science and the Griffith Institute of Health and Medical Research, Griffith University Gold Coast Campus, Southport, Qld, Australia. Tel.: +61 7 55529109; fax: +61 7 55528444.

E-mail address: j.neuzil@griffith.edu.au (J. Neuzil).

mutations but whose function is essential for induction of apoptosis by DNA-targeting agents (such as doxorubicin or 5-fluorouracil), mitochondria present targets that are not so compromised by genetic mutation and whose targeting overcomes problems with mutations of upstream targets such as p53. We have recently proposed a novel class of anti-cancer agents, mitocans that exert their anti-cancer activity by destabilising mitochondria, promoting the selective induction of apoptotic death in tumour cells. In this communication, we review recent findings on mitocans and propose a common basis for their mode of action in inducing apoptosis of cancer cells. We use as an example the analogues of vitamin E that are proving to be cancer cell-specific and may soon be developed into efficient anti-cancer drugs.

© 2007 Elsevier Ltd. All rights reserved.

Keywords: Vitamin E analogues; Mitocans; Mitochondria; Apoptosis; Cancer

Contents

1. Introduction	609
2. Vitamin E analogues as prototypic examples of mitocans	610
2.1. Hexokinase inhibitors	612
2.2. BH3 mimetics	612
2.3. Thiol redox compounds	613
2.4. VDAC/ANT targeting drugs	614
2.5. Electron transport chain targeting drugs	615
2.6. Lipophilic cations targeting inner membrane	615
2.7. Drugs targeting other sites	616
3. Mitochondria as mediators of apoptosis induced by VE analogues	617
3.1. Reactive oxygen species as triggers in apoptosis induction	617
3.2. Mitochondrial proteins as modulators of apoptosis induced by VE analogues	619
3.3. Cells deficient in mtDNA as a model to study apoptosis induced by vitamin E analogues	621
4. Non-mitochondrial signalling during apoptosis induced by VE analogues	621
4.1. Inhibition of cell cycle progression by vitamin E analogues	622
4.2. c-Jun pathway as a target for apoptosis induced by vitamin E analogues	624
4.3. Akt, NF κ B and other pro-survival pathways as a target for VE analogue-induced apoptosis	624
4.4. Sensitisation of cancer cells to TRAIL by modulation of signalling pathways by vitamin E analogues	626
5. Vitamin E analogues as modulators of the immune function	628
6. VE analogues as anti-cancer agents	630
6.1. Drug formulations	630
6.2. Combination of vitamin E derivatives with other anti-cancer drugs	631
7. Perspectives	633
Acknowledgements	634
References	634

1. Introduction

Recent advances in molecular biology and molecular medicine have shed some light on the mechanisms underlying cancer initiation and progression and have helped to promote the design of novel therapeutic strategies. However, curing neoplastic disease still presents a formidable task, owing in part to the cancer cell mutational capacity and the consequent variation exhibited by cancers, even of the same type. Some types of cancer are very difficult to treat (such as erbB2-positive breast carcinomas). Some remain fatal such as malignant mesothelioma (MM), a relatively rare neoplasia arising largely from asbestos exposure and affecting several hundred thousand people worldwide, mostly in industrialised countries. Unless an efficient treatment for these diseases is to be found, all of the patients suffering with these cancers are likely to have significantly reduced life-spans. Furthermore, with the relocation of asbestos related industries into developing countries like China and India and as a result of the >20-year latency of MM, an emergence of such cancers in these countries is assured. These are only a few of the many examples of what remains as a significant health problem. It is imperative that cancer research continues in pursuing the ultimate goal: the efficient treatment of cancers, free of the present problems of associated recurrences and their devastating impact.

We have recently identified a novel group of anti-cancer agents, designated as 'mitocans'. These intriguing compounds have often been relatively effective anti-cancer agents, targeting the mitochondria inside cancer cells. By so doing, they cause mitochondrial destabilisation with the ensuing mobilisation/activation of mitochondrial mediators of apoptosis, including the Bcl-2 family proteins and the downstream apoptotic mediators cytochrome *c*, Smac/Diablo and the apoptosis-inducing ligand (AIF). By targeting mitochondria, these inducers of apoptosis circumvent the frequent mutations at the level of DNA that occur in cancers making them resistant to many established drugs whose mode of action commonly relies on activation of the potent tumour suppressor p53.

A prime example of mitocans is the group of vitamin E (VE) analogues, best represented by α -tocopheryl succinate (α -TOS), a redox-silent form of VE that has been documented to selectively induce apoptosis in cancer cells, while being largely non-toxic to normal cells and tissues (Neuzil et al., 2004). Moreover, α -TOS represents a subgroup of mitocans that act specifically at the level of a novel target for anticancer drugs, the mitochondrial complex II, thereby causing generation of reactive oxygen species (ROS) (Neuzil et al., 2006; Ralph et al., in press). α -TOS also acts as a BH3 mimetic (Shiau et al., 2006), as outlined in detail below. The efficacy of these agents may be further enhanced by modifications that endow them with additional chemico-physical properties resulting in their greater accumulation in cancer cell mitochondria, thereby maximising their apoptogenic activity against cancers.

In this review, we document the latest developments in mitocans, their modes of action in targeting mitochondria and their potential utilisation in cancer therapy. It is worth highlighting that α -TOS as well as several of its analogues have been shown to suppress cancer in several experimental models, including melanomas (Malafa

et al., 2002), mesotheliomas (Tomasetti et al., 2004a; Stapelberg et al., 2005) and erbB2-positive breast carcinomas (Wang et al., 2007). It is believed that these drugs will be established as efficient and selective anti-cancer agents on the clinical level and, more generally, will trigger interest in research into mitocans as anticancer drugs of the future.

2. Vitamin E analogues as prototypic examples of mitocans

Developing improved strategies for selectively killing cancer cells without affecting the normal tissues represents a holy grail in cancer therapy. Such treatments are expected to result in greater patient acceptance because their selective targeting translates to significantly reduced side effects, enabling greater compliance by cancer sufferers with the rigours of undergoing the gambit of chemotherapy. The advent of Trastuzimab as a monoclonal antibody therapy targeting the Her-2 receptor on breast cancer cells and Glivec, a BCR-ABL tyrosine kinase inhibitor used against chronic myelogenous leukaemia and gastrointestinal cancer, has heralded the development of selectively targeted molecular therapies (Baselga, 2006). These novel therapies are driving renewed emphasis in cancer research into therapies that will target the distinguishing properties of cancer cells without affecting normal cells. Past chemotherapies based on disrupting cell division have been notoriously non-specific, targeting all rapidly dividing cell populations in the body. Consequently, these treatments affect normal tissues with high turnover rates, such as the hemopoietic system and the gastrointestinal tract with associated toxic side effects. Both Trastuzimab and Glivec, despite their targeting, have also shown cardiotoxicity, so the hunt continues for improved cancer therapies. An area that is emerging and attracting increasing interest recently is in the design and development of small molecule inhibitors that target the unique properties of cancer cell metabolism thereby causing these cells to die by apoptosis. In particular, amongst the myriad of metabolic drug inhibitors under development is a class of drugs that have been termed 'mitocans' that signifies mitochondrially targeted drugs activating cell death pathways specifically in cancer cells, with low or no toxicity to normal cells (Ralph et al., 2006).

Although a considerable number of drugs have been described to target mitochondria and induce apoptosis of cancer cells, only those whose site of action has been clearly identified will be discussed in the present review. The different subclasses of mitocans encompassing a growing number of drugs are listed in Table 1. The classification relates to the different metabolic reactions associated with the mitochondrial organelle whose function is central to cell survival. Grouping the mitocans into different classes helps to rationalize the growing number of mitocans and is based on the order and level from outside to inside of mitochondria and their site of drug action. If one of these reactions is inhibited inside the cancer cell, then continued survival becomes compromised. The basis for the specificity of these drugs for cancer cells is examined in the following sections where examples from each class are discussed.

2.1. Hexokinase inhibitors

The hexokinases, catalysing the reaction of glucose to glucose-6-phosphate accompanied by hydrolysis of ATP, are predominantly found in cancer cells associated with the outer mitochondrial surface (Mathupala et al., 2006). Here, hexokinases I and II help protect the mitochondrial transmembrane channel formed between the outer membrane porin, VDAC1 and the inner membrane adenine nucleotide transporter, ANT (Ralph et al., 2006; Vyssokikh et al., 2004). The hexokinase association with VDAC helps to prevent the pro-apoptotic molecules like Bax from binding to the outer face of VDAC, suppressing the mitochondrial outer membrane pore (MOMP) and the apoptotic signalling pathway. Hence, 3-bromopyruvate and 2-deoxyglucose as inhibitors of hexokinases are included in the class of mitocans because the inhibition they cause reduces the stability of the hexokinase-VDAC association, thereby increasing the propensity for pro-apoptotic molecules like Bax to bind to VDAC, whose binding then leads to formation of MOMP (Pastorino et al., 2002).

Inactivation of endogenous cyclophilin D by use of a small interference RNA or a cyclophilin inhibitor was found to release hexokinase II from mitochondria and to enhance Bax-mediated apoptosis (Machida et al., 2006). The anti-apoptotic effects of cyclophilin D were cancelled as a result of the detachment of hexokinase II from mitochondria, demonstrating that mitochondrial binding of hexokinase II is essential to the suppression of apoptosis by cyclophilin D. Furthermore, cyclophilin D dysfunction appears to abrogate hexokinase II-mediated suppression of apoptosis, indicating that cyclophilin D is required for the anti-apoptotic activity of hexokinase II (Machida et al., 2006).

Not only does 3-bromopyruvate inhibit hexokinases (Mathupala et al., 2006), but it also inhibits the activity of many other glycolytic pathway enzymes and the citric acid cycle/electron transport component, succinate dehydrogenase (SDH) (Sanborn et al., 1971). A rapid decrease in cellular production of ATP ensues as a result of the metabolic inhibition by 3-bromopyruvate (Ko et al., 2004). A related drug targeting SDH is 3-nitropropionic acid and this inhibition is associated with a large increase in superoxide as a by-product of the electron transport chain inhibition (Bacsi et al., 2006). The production of ROS is a common mechanism whereby the mitocans induce cancer cell apoptosis.

2.2. BH3 mimetics

The class II in the list of mitocans are the BH3 domain mimetics. This is a large class of agents comprising compounds such as the polyphenolic drugs like gossypol, the green tea constituent epigallocatechingallate (EGCG), as well as peptides based on the BH3 domain sequence (O'Neill et al., 2004; van Delft et al., 2006). The BH3 mimetics act by targeting the BH3-binding domain proteins like of Bcl-2 and Bcl-x_L. This action inhibits Bcl-2 and Bcl-x_L, preventing them from binding to Bax and Bak, blocking these pro-apoptotic proteins from forming pores in the outer mitochondrial membrane. Consequently, in the presence of excess BH3 mimetic, when Bax and Bak

are activated by apoptotic signalling, they will be free to form MOMP, thereby inducing apoptosis (Antignani and Youle, 2006; Robey and Hay, 2006). Although Bax and Bak have been shown to form pores either alone or in complex with VDAC (Shoshan-Barmatz et al., 2006), the precise mechanisms for this pore forming process are not yet well defined.

2.3. Thiol redox compounds

Members of the third class of mitocans act by modifying thiol redox states in key molecules regulating the function of the mitochondrial permeability transition and the mitochondrial transmembrane channel proteins, including VDAC and ANT. Both of these proteins, VDAC and ANT, contain two or more Cys residues in the structure of the mammalian forms thereby providing reactive thiol groups whose modification could affect their function. It has been established that the redox state of thiol reactive groups is important for activation of the mitochondrial permeability transition (Costantini et al., 2000; McStay et al., 2002). Consequently, the thiol cross-linkers such as 4,4'-diisothiocyanostilbene/2,2'-disulfonic acid, diamide and phenylarsene oxide affect the VDAC and ANT function and activation of mitochondrial permeability transition (Shafir et al., 1998; Costantini et al., 2000; Madesh and Hajnoczky, 2001; McStay et al., 2002). The adenine nucleotide transporter (ANT) dimerises to form the nucleotide transporter channel (Dahout-Gonzalez et al., 2006). Arsenites also react with mono and dithiol groups, particularly the latter when two thiols are at close proximity, acting to cross-link the thiols together. Several other compounds also target thiol groups of either VDAC or ANT. For example, copper-*o*-phenanthroline has been proposed to dimerise ANT by intermolecular cross-linking of Cys 56 (in the rat sequence) (McStay et al., 2002). It was proposed that phenylarsene oxide, eosin 5-maleimide or diamide form intramolecular cross-links between Cys 160 and Cys 257, restricting ANT in the C-conformation, promoting mitochondrial permeability transition (McStay et al., 2002). Arsenite is much weaker than phenylarsene oxide in modifying the ANT Cys residues (Sahara et al., 2004). However, phenylarsene oxide is a highly toxic compound *in vivo*, is non-selective for cancer versus normal cells (Hirano et al., 2005) and is a strong inhibitor of tyrosine phosphatases as well (Zhang et al., 1992). The glutathionyl peptide trivalent arsenical compound 4-(*N*-(*S*-glutathionylacetyl)amino) phenylarsenoxide (GSAO) inactivates ANT-mediated ATP/ADP transport and triggers Ca²⁺-dependent influx by cross-linking Cys 160 and 257 of ANT. This leads to increased cellular ROS, ATP depletion, mitochondrial depolarization and induction of apoptosis in endothelial cells, and inhibited tumour growth in mice with no apparent side effects (Don et al., 2003). Interestingly, although the para form of GSAO revealed no apparent toxicity in animals undergoing treatment and inhibited tumour growth leading to phase I clinical trials as an anticancer agent (Don et al., 2003), the ortho form was toxic and this was proposed to result from increased accumulation of the drug in normal cells, due to the loss of MDR efflux (Dilda et al., 2005).

Single thiol interacting compounds such as *N*-ethylmaleimide (NEM) can inhibit the mitochondrial permeability transition and this could be either the result of direct

interaction with key Cys residues on ANT or indirectly via reaction with GSH, preventing it from being oxidized and catalysing disulfide bridging between adjacent thiol groups in ANT (McStay et al., 2002).

NEM or monobromobimane, in the 25–50 μM range, preferentially react with GSH, leading to its modification in mitochondria and thereby prevents GSH from being oxidized. As a result, NEM inhibits mitochondrial permeability transition activation by the thiol reactive compounds, diamide or *t*-butylhydroperoxide, implying a role for GSSG in the action of these agents on the permeability transition induced by disulfide cross-linking. Arsenites may have a similar action, modifying and inhibiting the role of glutathione in redox control, such that glutathione based enzymes are unable to function, leading to increases in cellular ROS production. Glutathione *S*-transferase (GST) interacts with ANT in both normal and cancer cells, and becomes dissociated from ANT during apoptosis induction, suggesting that GST/GSH may repress the permeability transition and ANT pore opening (Verrier et al., 2004). This is supported by the observation that increasing the expression of GST in cancer cells renders them more resistant to arsenite induced apoptosis, reducing the levels of ROS (Zhou et al., 2005).

Another group of compounds that belongs in the third class of mitocans are the isothiocyanates, particularly the dietary compounds phenyl ethyl isothiocyanates (PEITC's) (Trachootham et al., 2006; Xiao et al., 2006). Again, these compounds act similarly as thiol modifiers forming adducts with thiol groups on important redox regulators. PEITC's effectively inhibit the glutathione antioxidant system, producing severe ROS accumulation in transformed cells. This excessive ROS output results in oxidative mitochondrial damage, inactivation of redox-sensitive molecules, and massive cell death. In vivo, in cancer models, PEITC was also shown to exhibit therapeutic activity and prolong animal survival.

2.4. VDAC/ANT targeting drugs

Several different mitocans in the fourth class, like the third class, also affect the function of the ANT ion channels and transporters of nucleotides, but in this case, by directly binding and modifying the protein subunit structure. Oligomeric structures comprising VDAC subunits in the outer and ANT subunits in the inner membrane exist in a coupled state forming a channel spanning across the two membranes of the mitochondria (Zalk et al., 2005). Drugs in the fourth class of mitocans directly known to bind to ANT include lonidamine, an indazole carboxylate (Belzacq et al., 2001); bisphosphonates that form cytotoxic ATP analogue-type metabolites (Monkkonen et al., 2006), as well as retinoid like structures such as CD 437 and all-trans retinoic acid (Garattini et al., 2004). Reports of VDAC binding modifiers acting as mitocans could not be found. Cations such as ruthenium red and La^{3+} binding to Ca^{2+} sites on VDAC block channel activity and appear to prevent the activation of MOMP (Gincel et al., 2001). This may be because Ca^{2+} influx via VDAC into the mitochondria is required for the induction of apoptosis and hence, any drug which blocks Ca^{2+} entry, would help prevent apoptosis.

2.5. Electron transport chain targeting drugs

The fifth class of mitocans comprises a large number of different drugs that target the components of the electron transport chain, leading to ROS production and activation of apoptosis in cancer cells. These drugs include α -TOS, the main subject of this review, as well as related drugs such as *N*-(4hydroxyphenyl)retinamide (4HPR, fenretinide). The pro-oxidant mechanisms of 4HPR activity have not been clearly identified, although it is likely to act in the μ M range as an inhibitor of at least one of the complexes along the electron transport chain, requiring mitochondrial respiration for its apoptotic activity (reviewed in Hail et al., 2006). Tamoxifen was shown to induce apoptosis in MCF-7 breast cancer cells at low μ M levels by affecting mitochondrial function and increasing ROS production (Kallio et al., 2005). The target of tamoxifen action was later identified as the FMN site of complex I leading to H₂O₂ production. Resveratrol acts in the μ M range at several different sites from complex I to III along the electron transport chain, probably competing with ubiquinone, and also inhibits the F1 ATPase at low μ M levels (Zini et al., 1999; Gledhill and Walker, 2005). Although resveratrol is considered an antioxidant, it can also act as a pro-oxidant by enhancing ROS production in cells, inducing apoptosis via the mitochondrial pathway (Tinhofer et al., 2001). A methoxy derivative of resveratrol showed even more potent activity in inducing apoptosis in transformed cells (Gossiau et al., 2005). Two additional reports with different cancer cell types further support the ability of resveratrol to act as a mitocan (Sareen et al., 2006; Zunino and Storms, 2006).

2.6. Lipophilic cations targeting inner membrane

The sixth class of mitocans includes molecules that are delocalized lipophilic cations which accumulate at much greater concentrations in the mitochondrial matrix than in the cytoplasm of cells (Smith et al., 2003). These compounds are even more selectively accumulated into the mitochondrial matrix of cancer cells because cancer cells show greater *trans*-membrane potentials across the plasma membrane as well as their content of more polarized mitochondria with a much greater $\Delta\psi_m$ than in non-malignant cells (Davis et al., 1985; Lampidis et al., 1985; Ralph et al., 2006). The target for the lipophilic cation-based mitocans may be one of the inhibitory binding sites on the ATPase (Gledhill and Walker, 2005). One of the earliest members of this class of compounds to be identified for its anti-cancer activity was rhodamine-123 (Bernal et al., 1982). It recently entered phase I clinical trials for prostate cancer and revealed minimal side effects and safe administration at monthly intervals without detectable drug accumulation in the serum of patients (Jones et al., 2005). It is likely that the related compound, Rose Bengal, works in a similar fashion to rhodamine 123 and is also currently in clinical trials as a cancer therapy for metastatic melanoma and recurrent breast cancer, revealing complete remissions in some patients (Provectus PV-10-MM-01, www.ClinicalTrials.gov).

The drug, F16 (Fantin et al., 2002) is a mechanistically more characterized example of this mitocan class and was shown to increase ROS production, depolarize

mitochondria as a weak protonophore, collapsing $\Delta\psi_m$ leading to mitochondrial permeability transition and selective apoptosis of cancer cells when applied in the μM range. In this study, F16 was also reported to inhibit the growth of mammary tumours in mice. MKT-077, a rhodocyanine dye analogue, is another example of this type of mitocan that entered phase I clinical trials although these were terminated due to renal toxicity (Britten et al., 2000). This raises the issue of toxicity with many of the mitocans in class VI. A good example of the potential for toxicity that must be carefully evaluated with this mitocan class is represented by the production of Parkinson's like disease effects caused by the drug MPTP (1-methyl-4-phenyl-1,2,3,6-tetrahydropyridine) after the selective destruction of the nigrostriatal dopaminergic neurons. The toxicity is due to the selective uptake by the dopamine transporters on these cells as well as the metabolite formed by the action of the enzyme, monoamine oxidase B, highly expressed in the dopaminergic neurons. As a result of these two unique properties of the dopaminergic neurons, the mitochondriotoxic drug MPP⁺ (1-methyl-4-phenylpyridinium) is produced which acts as an inhibitor of mitochondrial respiration by blocking the NADH-ubiquinone oxidoreductase site of complex I as well as the likelihood that MPP⁺ is also a protonophore (Davey et al., 1992; Albores et al., 1990) that would collapse the $\Delta\psi_m$, leading to cell destruction. This, together with the non-selective cell toxicity associated with another lipophilic cation and known mitochondrial poison, dequalinium chloride (Gamboa-Vujicic et al., 1993) raises the importance of identifying class VI mitocans that are cancer cell-specific in terms of their uptake and cellular toxicity as recently described in a predictive model based on their structures reported by Trapp and Horobin (2005).

The amphipathic and positively charged α -helical pro-apoptotic peptide (KLAK-LAK)₂ has also been included in this class of mitocans as a delocalised lipophilic cation. However, it must first be coupled to a targeted delivery system for surface receptor binding and uptake into cancer cells, before it is able to function as a mitocan (Ellerby et al., 1999; Fantin et al., 2005). As with the other members of this class of mitocans, the peptide has been shown to dissipate $\Delta\psi_m$ leading to apoptosis, and was found to be very efficient at reducing tumour burdens in animal models (Fantin et al., 2005).

2.7. Drugs targeting other sites

The last class of mitocans contains those whose target site and mechanism of action on the cancer cell mitochondria to bring about apoptosis is not well characterized or at present is unclear. It includes drugs that bind to the peripheral benzodiazepine receptor (PBR) such as PK-11195 and Ro5-4864 (Maaser et al., 2005; James et al., 2006). PBR is also known as the outer mitochondrial membrane translocator protein (Papadopoulos et al., 2006), an 18 kDa mitochondrial protein involved in transport of cholesterol into the mitochondria as the rate-determining, hormone-sensitive step in steroid biosynthesis (Liu et al., 2006) and is important for porphyrin transport and heme synthesis, apoptosis, cell proliferation, anion transport, regulation of the mitochondrial function and immunomod-

ulation. This protein is often found overexpressed in cancer cell types (Pretner et al., 2006; Papadopoulos et al., 2006) and is a potential target for anti-cancer drugs that bind to it, but this is an area of research that has not been well defined as yet. The other drugs included in this class of mitocans are the natural product derived pentacyclic triterpenoids such as betulinic acid and related structures. Betulinic acid and its derivatives have been shown as specifically cytotoxic to a range of tumour cell lines (Kessler et al., 2006; Rzeski et al., 2006), causing rapid increase in ROS production and concomitant dissipation of mitochondrial membrane potential in a dose- and time-dependent manner, which resulted in cell apoptosis (Liu et al., 2004). Betulinic acid was found to be non-toxic up to 500 mg/kg body weight in mice (Alakurtti et al., 2006). The target in the mitochondria for the betulinic acid-related compounds has not been identified and hence, their mechanism for initiating the mitochondrial dysfunction leading to apoptosis remains unknown.

The sesquiterpene lactones are another group within the last class of mitocans encompassing a number of different naturally occurring structures that induce oxidative stress-mediated apoptosis in cancer cells acting in the μM range (Nakagawa et al., 2005) via loss of $\Delta\psi_m$ and induction of ROS (Wen et al., 2002; Kim et al., 2005; Steele et al., 2006). They are also believed to target tumour stem cells whilst not affecting normal cells (Guzman et al., 2005).

3. Mitochondria as mediators of apoptosis induced by VE analogues

3.1. Reactive oxygen species as triggers in apoptosis induction

One of the earliest events resulting from exposure of cells to VE analogues is generation of ROS (Weber et al., 2003). We observed that addition of α -TOS to cancer cells resulted in appreciable accumulation of ROS within 30–60 min, as detected by electron paramagnetic resonance (EPR) spectroscopy using radical traps and by flow cytometry by means of redox-sensitive probes (Weber et al., 2003; Wang et al., 2006; Swettenham et al., 2005). Ottino and Duncan (1997) were first to report accumulation of ROS upon exposure of cancer cells to α -TOS. That ROS are compulsory initiators of apoptosis following challenge of cells with α -TOS has been shown and confirmed by other researchers, reporting that the efficacy with which α -TOS induces apoptosis parallels the level of ROS accumulation and that cells with low antioxidant defences are more vulnerable to α -TOS (Kogure et al., 2002; Kang et al., 2004).

Probably the main reason for generation of ROS by cancer cells upon their exposure to mitocans is related to the mitochondrial targeting nature of these agents because the mitochondria are major cellular sites of respiration. Recent studies suggest that α -TOS binds to the proximal and distal ubiquinone binding pocket of the mitochondrial complex II (Ralph et al., in press; Dong et al., submitted for publication). This notion is based on molecular modelling and biochemical assays that were fuelled by a recent study reporting the crystal structure of porcine complex II (Sun et al., 2005). We propose that by its action, α -TOS would displace ubiquinone within

complex II, so that electrons arising from conversion of succinate to fumarate are no longer accepted by their natural receptor and, instead, interact with molecular oxygen to generate superoxide (Ralph et al., in press). Superoxide will then be converted by superoxide dismutase (SOD) to the highly diffusible hydrogen peroxide that, in the cytosol, can activate the intrinsic apoptotic pathway, inducing events such as the dimerisation of cytosolic Bax via disulfide bridges, resulting in externalisation of the Bax C-terminal membrane-targeting sequence (D'Alessio et al., 2005). We propose that this mechanism could also explain the Bax mitochondrial relocalisation in cancer cells exposed to α -TOS (Neuzil et al., 2006). A second mechanism of apoptosis linked to generation of ROS involves p53 (Sablina et al., 2005). Consistent with this notion, we found that α -TOS activates p53 in mesothelioma cells, resulting in upregulation of p53-dependent genes (Tomasetti et al., 2006). We recently observed that α -TOS causes upregulation of the BH3-only protein, Noxa, that is under transcriptional control of p53, and that an increase in Noxa levels liberated the mitochondrial pro-apoptotic protein Bak, from its sequestered association with the anti-apoptotic Mcl-1 (Neuzil et al., unpublished results).

An interesting aspect of apoptosis induction by α -TOS and the role of ROS come from studies on normal cells. Hence, smooth muscle cells (SMCs) and endothelial cells (ECs) both succumb to α -TOS (Kogure et al., 2001; Neuzil et al., 2001a), although this depends largely on their proliferative status. Thus, proliferating SMCs and ECs, when exposed to α -TOS, respond by ROS generation, probably due to their reduced levels of expression of antioxidant enzymes, such as the mitochondrial SOD (Kogure et al., 2001; Swettenham et al., submitted for publication). The apoptogenic effect of α -TOS on proliferating but not growth-arrested ECs is highly intriguing since it suggests that VE analogues may have potent anti-angiogenic activity, in a similar manner to that reported for arsenite-derived compounds which kill angiogenic cells by interfering with the adenine nucleotide translocator (ANT) of the mitochondrial inner membrane (MIM) (Don et al., 2003).

Mitochondria are vital for providing optimal conditions to allow the continued survival of most eukaryotic cells by mediating energy generation in the form of ATP. Recent studies have revealed that mitochondria also play an important role in programmed cell death (Green and Kroemer, 2004). Mitochondria are also required for apoptosis of cancer cells induced by VE analogues (Neuzil et al., 2004) and hence, these drugs belong to the family of 'mitocans' as agents that initiate programmed cell death by targeting the mitochondria of tumour cells (Ralph et al., 2006).

The initiation of apoptotic pathways leads to destabilization of mitochondria. The initial triggers that play a role in upstream apoptosis from mitochondria induced by VE analogues are not exactly known. However, studies have shown that treatment of cells with α -TOS activates sphingomyelinase (SMase) (Ogretmen and Hannun, 2004), destabilises lysosomes (Neuzil et al., 1999) and causes generation of ROS (Kogure et al., 2002; Weber et al., 2003; Stapelberg et al., 2005; Swettenham et al., 2005; Wang et al., 2005). The first event observed upon exposure of cells to α -TOS is the activation of sphingomyelinase (SMase), an enzyme that converts sphingomyelin, which is a relatively rare lipid constituent of the plasma membrane, to the apopto-

genic lipid second messenger ceramide (Ogretmen and Hannun, 2004). We have shown that SMase was activated within 15–30 min after treating Jurkat cells with α -TOS. This activation could not be suppressed by a pan-caspase inhibitor, zVADfmk, indicating that SMase is a caspase-independent, and likely direct target of the VE analogue (Weber et al., 2003). It is also plausible that the SMase activation may be due to a change in the plasma membrane fluidity upon incorporation of the lipophilic α -TOS, a mechanism that has been recently suggested (Dimanche-Boitrel et al., 2005). Generation of the lipid second messenger, ceramide in cancer cells as a very early response to α -TOS may also help explain the activation of protein phosphatase 2A (PP2A) and the ensuing hypophosphorylation of protein kinase C α occurring in cells exposed to α -TOS, since the drug does not directly target PP2A (Neuzil et al., 2001c). This proposal is in agreement with the previous finding that long-chain ceramides are activators of PP2A (Ruvolo et al., 1999).

Another early event after α -TOS treatment is lysosomal destabilisation (Neuzil et al., 1999). We have also observed that cells deficient in an important lysosomal protein, cathepsin D, were relatively resistant to the VE analogue (Neuzil et al., 2002). Thus, it is highly probable that lysosomal destabilisation is upstream of mitochondria in apoptosis signalling triggered by VE analogues and could amplify the major, mitochondrial pathway rather than bringing the cells to the commitment phase in a mitochondria-independent manner (Neuzil et al., 2004).

The evidence for α -TOS inducing the generation of ROS in cancer cells is substantial (Ottino and Duncan, 1997; Kogure et al., 2002; Weber et al., 2003; Stapelberg et al., 2005; Swettenham et al., 2005; Wang et al., 2005). We observed significant accumulation of ROS in Jurkat cells 1 h after α -TOS challenge, indicating that generation of radicals is a relatively early event when cancer cells are exposed to VE analogues. The major form of ROS produced by the cells in response to α -TOS appears to be superoxide, since addition of superoxide dismutase removed the radicals and also inhibited apoptosis (Kogure et al., 2001; Wang et al., 2005). Furthermore, the site of superoxide generation as well as the target of ROS action is most likely the mitochondria because in studies where cancer cells were pre-treated with the mitochondrially targeted coenzyme Q (Kelso et al., 2001), this agent suppressed radical generation and inhibited apoptosis inducible by the subsequent addition of α -TOS (Alleva et al., 2001; Weber et al., 2003, 2005).

3.2. Mitochondrial proteins as modulators of apoptosis induced by VE analogues

While the identity of the initial triggering events leading to apoptosis induced by VE analogues has not been fully resolved, the events occurring during apoptosis induced by VE analogues down-stream of mitochondria have been described in more detail. Mitochondria are sites of apoptotic signalling factors whose release from the mitochondria promotes the apoptotic response. Thus, the downstream events following mitochondrial destabilisation during apoptosis induced by VE analogues consist of mobilisation of apoptotic mediators, including cytochrome *c*, the apoptosis-inducing factor (AIF) and Smac/Diablo (Neuzil et al., 2004). Cytochrome *c*, upon cytosolic translocation, forms a ternary complex with Apaf-1 and procaspase-9,

resulting in the auto-activation of the initiator caspase-9 with subsequent activation of effector caspase-3, -6 or -7. At this moment the cell enters the so-called point of no return or irreversible phase of the apoptotic pathway (Yamamoto et al., 2003; Neuzil et al., 2001b,c; Weber et al., 2003). This pathway is critically important to the induction of apoptosis by α -TOS (Neuzil et al., 2004).

Smac/Diablo is an important agonist of caspase-dependent apoptotic signalling, as it antagonises members of the family of inhibitor of apoptosis proteins (IAPs including c-IAP1, c-IAP2 and XIAP) that inhibit caspase activity (Du et al., 2000; Verhagen et al., 2000). The expression of IAPs is controlled by the transcription factor, nuclear factor- κ B (NF κ B), whose activity is repressed by α -TOS (Erl et al., 1997; Neuzil et al., 2001a; Dalen and Neuzil, 2003). Hence, cytosolic translocation of Smac/Diablo is likely to promote the inhibition of the cell survival pathways during apoptosis induced by α -TOS and may therefore maximise the apoptogenic potential of resistant cells with high level of expression of the IAP family proteins (Neuzil, 2003; Wang et al., 2005).

Another protein localized in mitochondria that amplifies the apoptosis of cancer cells exposed to VE analogues is the apoptosis-inducing factor (AIF) (Weber et al., 2003). In treated cells, AIF translocates directly into the nuclei, thereby bypassing the caspase activation cascade (Susin et al., 1999). In the nucleus, AIF causes cleavage of chromatin in a caspase-independent manner (Cande et al., 2002). In this way, AIF can circumvent inactivating mutations should they occur in the caspase-dependent signaling or in situations where IAPs are over-expressed, that could render cancer cells more resistant to treatment. The release of AIF could also help mediate α -TOS-induced apoptosis in cells resistant to conventional anti-cancer drugs that are dependent on caspase activation for their anti-cancer effects (Neuzil et al., 2004).

The mitochondrial pro- and anti-apoptotic proteins, including Bax, Bcl-2 and Bcl-x_L, are important factors regulating the mitochondrial apoptotic signalling pathways (Cory et al., 2003). It has been suggested that treatment with α -TOS causes formation of the mitochondrial permeability transition pore (Yamamoto et al., 2003). The permeability transition is likely to be modulated as a result of cross-talk between the mitochondrial pro- and anti-apoptotic proteins (Yamamoto et al., 2003; Weber et al., 2003). For example, the over-expression of Bax sensitised cells to α -TOS-induced apoptosis (Weber et al., 2003; Yu et al., 2003), whereas over-expression of Bcl-2 or Bcl-x_L protected them from this agent. However, protection was not observed when truncated versions of these two proteins lacking the mitochondrial-targeting terminus were used for transfection of the cells (Weber et al., 2003). In a similar manner, down-regulation of Bcl-2 by antisense oligodeoxynucleotide treatment sensitised cells to the VE analogue (Neuzil et al., 2001c; Weber et al., 2003). Furthermore, transfection with a gain-of-function mutant of Bcl-2 (containing Ser 70 substituted by Glu) protected cells, whereas use of a loss-of-function mutant (with Ser 70 substituted by Ala) sensitised cancer cells to α -TOS (Neuzil et al., 2001c). The latter observations can be explained by the fact that PKC-dependent phosphorylation of Ser 70 is known to play a role in the mitochondrial docking of Bcl-2 (Ruvolo et al., 1998).

Recently, another mechanism whereby α -TOS could destabilise mitochondria by targeting the Bcl-2 family protein was reported. Shiao et al. (2006) showed that α -TOS and its several analogues act as BH3 mimetics, by way of binding to the BH3 domain of proteins like Bcl-2 and Bcl-x_L. They showed that in healthy cells, the anti-apoptotic proteins Bcl-2 and Bcl-x_L interacted with the pro-apoptotic Bak, a constituent of the mitochondrial outer membrane, and that this interaction was abolished in the presence of α -TOS. Modeling and biochemical studies revealed that α -TOS was capable of binding to the BH3 binding domain of the anti-apoptotic proteins, blocking their activity. Therefore, we have included the VE analogue amongst the group II mitocans, as examples of BH3 mimetics (cf Table 1).

3.3. Cells deficient in mtDNA as a model to study apoptosis induced by vitamin E analogues

Perhaps the most important evidence for mitochondria as major transmitters of apoptotic signalling induced by VE analogues comes from experiments in which mtDNA-deficient (ρ^0) cells were found to be resistant to α -TOS when compared with the wild-type cells and revertant counterparts (Weber et al., 2003; Wang et al., 2005). It has also been observed that transfection of cancer cells with dominant-negative (DN) caspase-9 or caspase-9 siRNA suppressed apoptosis induced by α -TOS (Weber et al., 2002; Swettenham et al., 2005). Furthermore it has been reported that cancer cells lacking mtDNA (ρ^0 cells) which, as a result, are resistant to apoptosis (Dey and Moraes, 2000), failed to translocate cytochrome *c* in response to α -TOS treatment. By contrast, the parental cells were sensitive to apoptosis induced by this treatment. The resistance exhibited by the ρ^0 cells was associated with low levels of the markers for early apoptotic events including phosphatidyl serine outer plasma membrane externalisation and caspase-3 activation (Weber et al., 2003). Similar resistance by ρ^0 cells has been found for other inducers of apoptosis, such as tumour necrosis factor- α (TNF- α) (Higuchi et al., 1997).

Based on the many observations described in the preceding sections, mitochondria are undoubtedly the most important intracellular organelles for relaying the initial apoptotic signals down-stream to the stage when the cell becomes committed to undergo apoptosis. It is worth mentioning at this point that other organelles may be involved as well in the process of apoptosis induced by VE analogues, such as lysosomes as reported in other studies (Neuzil et al., 1999, 2002). Nonetheless, mitochondria are essential components for transmission of the early apoptogenic events in cells, whose signals are probably amplified by mediators released from organelles like lysosomes or the endoplasmic reticulum. The major pathways of apoptosis induced by VE analogues are outlined and summarised in Fig. 1.

4. Non-mitochondrial signalling during apoptosis induced by VE analogues

Although mitochondria are the major intracellular organelle playing an important role in apoptosis triggered by VE analogues, signalling pathways operating via other

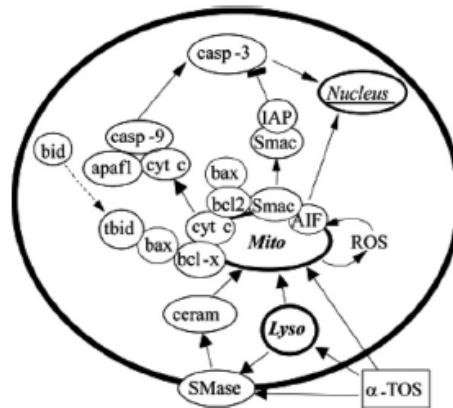


Fig. 1. Possible upstream and downstream intrinsic apoptotic pathways initiated by vitamin E analogues, based largely on experiments with Jurkat cells (adapted from Weber et al., 2003). α -TOS translocates to the cell, activates sphingomyelinase (SMase), giving rise to the formation of the lipid second messenger ceramide, possibly causing also destabilisation of lysosomes. These events converge on destabilisation of the mitochondrial membrane, which is amplified by ROS generation during this process. Mitochondrial membrane destabilisation, likely promoted by leakage by lysosomal proteases, leads to cytosolic relocalisation of pro-apoptotic factors (such as cytochrome *c*, Smac/Diablo or the apoptosis-inducing factor, AIF) that can be regulated by the Bcl-2 family of proteins (including the anti-apoptotic proteins Bcl-2, Bcl-xL or Mcl-1, which can be compromised by the pro-apoptotic Bax, probably mobilised to mitochondria after cleavage of Bid to its pro-apoptotic form tBid). Cytochrome *c*, Apaf-1 and procaspase-9 form apoptosome, a ternary complex resulting in activation of the initiator caspase-9 that, in turn, activates the effector caspases. Smac/Diablo may amplify this process by suppressing the caspase-inhibitory activity of the inhibitor of apoptosis protein (IAP) family members, while AIF transmits the mitochondrial destabilisation directly to nuclear apoptotic events, bypassing the caspase cascade.

organelles such as the lysosomes and endoplasmic reticulum (ER) may also be involved in VE analogue induced apoptosis (Neuzil et al., 1999, 2002). In addition, cytoplasmic signalling involved in the inhibition of cell cycle progression, the c-Jun pathway, regulation of Akt activity and NF κ B pro-survival pathways and sensitisation of cancer cells to TRAIL signalling pathways may also contribute to VE analogue induced apoptosis as described below.

4.1. Inhibition of cell cycle progression by vitamin E analogues

It is very important to understand the mechanisms that link cell cycle control with the induction of apoptosis (Fotadar et al., 1996). In fact, several stages exist during the cell cycle where the cell must assess whether it is prepared or not, before proceeding to the next stage. These are referred to as “checkpoints”, and they occur at the end of G1 before transition to S phase, at the end of S phase and before transition to G2, in G2 before the start of mitosis (M), and again in M phase. Failure to pass any

of the checkpoints leads to an arrest of the cell cycle and potentially induction of the crisis event of apoptosis.

Several reports have implicated the inhibition of cell cycle progression as a means by which VE analogues could induce apoptosis or inhibit proliferation of cancer cells and/or sensitize them to the effects of other anti-cancer drugs. Ni et al. (2003) showed that α -TOS inhibits proliferation of prostate cancer cells by down-regulating expression of several critical cyclins and the cognate cyclin-dependent kinases (CDK), resulting in hypo-phosphorylation of the Rb protein and G1/S arrest. Cell cycle arrest and apoptosis were also induced by α -TOS in osteosarcoma cells via activation of p53 and reduced expression of the transcription factor E2F1, critical for the G1/S transition (Alleva et al., 2006). Further, exposure of osteosarcoma cells to α -TOS promoted a prolonged arrest at the S/G2 border, sensitising the cells to methotrexate-induced apoptosis (Alleva et al., 2005). These findings can be reconciled with an earlier report, in which α -TOS suppressed proliferation of breast cancer cells by inhibiting the E2F1-dependent *trans*-activation via increased binding of cyclin A (Turley et al., 1997).

It has been recently reported that α -TOS significantly inhibited proliferation and induced apoptosis of prostate cancer cell lines (Malafa et al., 2006; Shiau et al., 2006). Daily injection of α -TOS into SCID mice containing xenotransplanted prostate cancer cells significantly suppressed tumour growth as well as lung metastases (Malafa et al., 2006). Apoptosis induction and inhibition of proliferation by α -TOS has also been established for malignant mesothelioma cell lines (Tomasetti et al., 2004a). It was further shown that this action resulted from the selective disruption of the FGF-FGFR autocrine signalling loop, most likely affected by modulation of the E2F1 and *egr-1 trans*-activation in the mesothelioma cell lines (Stapelberg et al., 2004, 2005). These are exciting results since malignant mesotheliomas are untreatable at this stage, particularly given that we obtained a strong anti-mesothelioma effect with α -TOS treatment in xenograft models of this cancer (Tomasetti et al., 2004a; Stapelberg et al., 2005).

Cellular proliferation and apoptosis are intimately coupled, and cell cycle modulators can influence both of these events (Vermeulen et al., 2003). The p53 gene is frequently lost or mutated in many cancers, and lack of functional p53 is accompanied by elevated rates of genomic instability, rapid tumour progression and resistance to anti-cancer drugs and radiotherapy (Weller, 1998). Using three human osteosarcoma cell lines, SAOS and U2OS cells carrying the wild-type p53 gene and the mutant p53 cell line MG63, we showed that α -TOS markedly inhibited cell proliferation only in the MG63 cells (Alleva et al., 2006). In SAOS cells, after 24 h of treatment, α -TOS induced cell accumulation at the S/G2 boundary coincident with a decrease of cells in G1. The U2OS cell line responded to α -TOS treatment by a transient accumulation of cells in the G1 phase. Higher concentrations of α -TOS induced cell death in the wild type p53 cell lines only after 48 h of treatment. In order to evaluate the molecular mechanism involved in the cell cycle arrest caused by α -TOS, expression of the cell cycle regulatory proteins that control the progression from S to G2 phases was examined. Treatment of SAOS and U2OS cells with α -TOS did not affect levels of expression of cyclin A and cyclin E. However, treatment of p53

mutant MG63 cells with α -TOS caused a reduction in both cyclin A and cyclin E protein levels.

The above results reveal that VE analogues, epitomised by α -TOS, exert a potent modulatory activity on cell cycle progression and that cellular responses to this agent differ depending on their p53 activity. Although these differences suggest the possibility of different targets for α -TOS in different cell types, the VE analogue does affect cell cycle progression, and this could act in its own right to inhibit cell proliferation resulting in suppression of tumour growth, and/or amplify the apoptogenic signalling pathways.

4.2. *c-Jun* pathway as a target for apoptosis induced by vitamin E analogues

c-Jun forms homodimers and heterodimers with Fos and other jun-related proteins, which together constitute the AP-1 transcription factor that binds to the TPA response elements (TREs), mediating transcriptional responses to a variety of stimulants. Because of the relationship of *c-Jun* NH₂-terminal kinase (JNK) activity with modulation of apoptotic pathways (Liu and Lin, 2005), the *c-Jun* signaling activation has been investigated in more detail in relation to the effects of α -TOS (Zu et al., 2005). The VE analogue markedly increased levels of expression of the Ask1, GADD45, Sek1, and phospho-Sek1 proteins, of which Ask1 and GADD45 are associated with the cell membrane. Activated Ask1 and GADD45 phosphorylate the Sek1 protein that then leads to phosphorylation of JNK itself. Consistent with these findings, the phosphorylated form of JNK was also noticeably increased, although the expression level of total JNK was not affected. In relation to this effect, the protein Bim, that is normally in the cytosol, translocates during apoptosis to the mitochondrial membrane, where it binds to Bcl-2 and Bcl-x_L. Prior to this translocation, Bim is phosphorylated by JNK (Kirschnek et al., 2005). Thus, JNK activation leads to antagonisation of the anti-apoptotic function of proteins like Bcl-2 and Bcl-x_L, thereby inducing the release of mitochondrial mediators of apoptosis into the cytoplasm.

Activation of JNK by α -TOS has also been shown to occur in gastric cancer cells (Wu et al., 2004), where it may act to amplify the mitochondrial apoptosis signalling pathway, as JNK activation has been shown to do in prostate cancer cells (Zu et al., 2005).

4.3. *Akt*, *NF κ B* and other pro-survival pathways as a target for VE analogue-induced apoptosis

One of the signalling pathways modulated by VE analogues is that of erbB2-Akt. ErbB2 is a receptor tyrosine kinase, a member of the epithelial growth factor receptor super-family and a product of the *c-neu* gene (Roskoski, 2004; Slamon et al., 1989). Cancer cells with high erbB2 expression often show resistance to anti-cancer drug treatment. This tyrosine kinase-linked *trans*-membrane protein is overexpressed in 30–50% of primary breast cancers. The major complication associated with erbB2 overexpression is linked to activation of Akt via the phosphatidylinositol 3-kinase

pathway (Zhou and Hung, 2003; Vivanco and Sawyers, 2002). Akt is a serine/threonine kinase that promotes cellular survival (Dudek et al., 1997). Once activated, Akt exerts anti-apoptotic effects through phosphorylation of several proteins, including Bad (Datta et al., 1997) and caspase-9 (Cardone et al., 1998). Moreover, Akt causes activation of the transcription factor NF κ B (Kane et al., 1999) that controls expression of pro-survival genes such as members of the IAP family (LaCasse et al., 1998). In most non-transformed cells, NF κ B complexes (a heterotrimer composed of p50 and p65 subunits bound to an inhibitor subunit I κ B) are largely cytoplasmic. Activation of NF κ B results in translocation to the nucleus and binding to promoter regions of specific pro-survival genes, such as those coding for IAPs, the caspase-8 inhibitor FLIP and the TRAIL decoy receptor, DcR1. One possibility by which α -TOS may suppress NF κ B-dependent transcription of pro-survival genes is via activation of caspase-3 that would cleave the NF κ B subunit p65, inactivating NF κ B (Neuzil et al., 2001a).

Donapaty et al. (2006) recently reported that α -TOS treatment affects oncogenic Ras activity. α -TOS inhibits the proliferation and induces apoptosis of NIH3T3 cells stably transfected with oncogenic K-Ras or H-Ras. Treatment with α -TOS suppressed the levels of phospho-Akt and phospho-Erk1/2 in oncogenic Ras expressing NIH3T3 cells. These results provide support for further investigation of the chemopreventive and therapeutic potential of α -TOS in tumors, dependent on activated Ras signaling, and identify phospho-Erk and phospho-Akt as potential biomarkers for the action of α -TOS in cancer cells.

We showed that VE analogues induced apoptosis at comparable levels in mouse and human breast cancer cells, regardless of their erbB2 status. One plausible mechanism is that these agents induce the relocation of Smac/Diablo from mitochondria to the cytosol (Wang et al., 2005), where Smac/Diablo binds to IAPs, liberating caspase-3 to execute its apoptotic function (Du et al., 2000). In another report, it was shown that α -tocopheryloxybutyric acid, a compound analogous to α -TOS, induced apoptosis in the erbB2-over-expressing human breast cancer cells MDA-MB-453 by simultaneously inhibiting activation (phosphorylation) of erbB2 and ensuing activation of p38 MAP kinase (Akazawa et al., 2002). Several other studies have shown modulation of the MAP kinase pathway by VE analogues as a way by which these agents induce apoptosis. Interestingly, Kline's group reported that extra-cellular signal-regulated kinases (ERKs) and JNK, but not the p38 MAP kinase, were involved in α -TOS-induced apoptosis in the human breast cancer cells MDA-MB-435 cells leading to activation of the down-stream transcription factors c-Jun and ATF-2 (Yu et al., 2001). It is possible that this pathway is targeted by α -TOS in the erbB2-low MDA-MB-435 cells, while the erbB2-high MDA-MB-453 cells activate their apoptotic machinery by the concerted deregulation of erbB2/Akt and p38 pathways when challenged with VE analogues.

One of the intriguing targets of VE analogues is the pro-survival transcription factor NF κ B (see above). Inhibition of NF κ B activation by α -TOS was first documented in the context of cardiovascular diseases (Erl et al., 1997). It is possible that VE analogues trigger apoptosis resulting in activation of caspase-3 that cleaves the obligatory NF κ B subunit p65, rendering it inactive (Levkau et al., 1999). We

have shown that α -TOS initiates a 'sub-apoptotic' phenotype, under which cells activate their effector caspase but do not enter the commitment phase (Neuzil et al., 2001a), probably because this requires efficient activation of specific cyclin-dependent kinases (Harvey et al., 2000). Regardless of the precise mechanism, inhibition of NF κ B activation by VE analogues has an anti-survival effect, i.e. is pro-apoptotic. These observations support the use of α -TOS as a sensitising agent for other apoptotic inducers. For example, treatment of the Jurkat T lymphoma cells with α -TOS sensitises them to TRAIL-dependent killing (Dalen and Neuzil, 2003).

4.4. Sensitisation of cancer cells to TRAIL by modulation of signalling pathways by vitamin E analogues

TRAIL is a tumor necrosis factor family member that selectively induces apoptosis of cancer but not normal cells (Pitti et al., 1996; Ashkenazi et al., 1999; Shi et al., 2003). TRAIL has been proven relatively safe in "in vivo" studies of rodents and primates compared with other death receptor ligands, TNF and Fas, which induce significant inflammation and tissue injury (Ashkenazi et al., 1999; Walczak et al., 1999). Thus, two unique characteristics of TRAIL have been identified. Firstly, TRAIL can selectively induce apoptosis in tumorigenic or transformed cells, but not in normal cells, highlighting its potential application in cancer treatment. Secondly, in contrast to other members of the TNF family, whose expression is tightly regulated and often only transiently expressed in activated cells, TRAIL mRNA is constitutively expressed in a wide range of tissues (Wiley et al., 1995).

TRAIL is produced either as a type II membrane protein or secreted in a soluble form which binds to its cognate death receptors (DRs), DR4 and DR5, inducing their trimerisation and intracellular recruitment of the adaptor protein Fas-associated death domain (FADD) (Schneider et al., 1997). The death domain (DD), in turn, recruits pro-caspase-8 into a death-inducing signalling complex (DISC) that triggers, autocatalytic cleavage and activation of caspase-8. This leads to activation of the effector caspase-3 (known as the type I death pathway). Alternatively, the death pathway can be further amplified by involvement of the mitochondrial pathway (the type II pathway) (Scaffidi et al., 1998). TRAIL-activated caspase-8 can generate truncated Bid, which mediates the release of cytochrome *c* from mitochondria, leading to the assembly of the apoptosome (comprised of cytochrome *c*, Apaf-1 and pro-caspase-9). Formation of the apoptosome leads to activation of caspase-9, which then activates effector caspases (Zou et al., 1999). In cells killed by the type I death pathway, DISC-activated caspase-8 activates downstream effector caspases and triggers apoptosis. However, in many cell types, the Type II death pathway is activated whereby TRAIL-induced activation of caspase-8 is insufficient to kill without recruiting the mitochondrial apoptotic programme.

A synergistic and cooperative killing effect was observed when TRAIL was combined with α -TOS in treatment of malignant mesothelioma (MM) cells, since the effect was selective for cancer cells (Tomasetti et al., 2004b). MM is a fatal type of neoplasia with poor therapeutic prognosis, largely due to resistance to apoptosis. Impaired apoptotic pathways render MM cells resistant to TRAIL-induced apopto-

sis. Sub-lethal doses of α -TOS significantly decreased the IC_{50} values for TRAIL by a factor of ~ 10 – 100 .

The observation that α -TOS and TRAIL synergise in p53^{wt} MM but not in the p53^{mut} cells suggested a role for p53 in *trans*-activation of the pro-apoptotic genes involved in drug synergism (Tomasetti et al., 2006). The p53 protein is a key component of the cellular 'emergency-response' mechanism (Levine, 1997; Sionov and Haupt, 1999). A variety of stress-associated signals activate p53 to induce growth arrest and/or apoptosis, thereby eliminating damaged and potentially dangerous cells (Lane, 1992). The p53 apoptotic target genes can be divided into two groups, the first group encoding proteins that act through receptor-mediated signalling and the second group encoding proteins involved in regulation of the apoptotic effector proteins. α -TOS induces apoptosis in a p53-independent manner (Weber et al., 2002) but, it also induces the expression and activation of p53 leading to increased expression of DR4 and DR5. Notably, such expression of DRs does not occur in the p53^{mut} MM cells. Studies using siRNA directed at p53 revealed that the p53 protein contributes significantly to the expression of TRAIL DRs. Thus, p53-dependent up-regulation of DR4 or DR5 provides one explanation for the sensitisation of MM cells to TRAIL. In addition, a hypoxic environment efficiently contributes to enhanced expression of DR4 and DR5 via p53 when MM cells are treated with α -TOS (Tomasetti et al., 2006). Regulation of the activity of many transcription factors by redox modulators has been previously described (Sun and Oberley, 1996). Thus, a novel mode of action for α -TOS likely involves reduction of the redox-sensitive amino acid residues on the p53 protein leading to increased DR expression, sensitising MM cells to the effects of TRAIL.

MM cells express both DR4 and DR5 on their surface and increasing their expression with α -TOS could facilitate activation of caspase-8 and cleavage of Bid. A kinetic analysis of TRAIL-induced signalling revealed transient activation of caspase-8 and resulted in low levels of apoptosis. Caspase-8 activation was less pronounced in the presence of TRAIL plus α -TOS although activation of the mitochondria-dependent apoptotic pathway, including Bid cleavage, cytochrome *c* cytosolic mobilisation and caspase-9 activation was observed (Tomasetti et al., 2004b). Bid cleavage induced by combining TRAIL and α -TOS may lead to mitochondrial translocation of Bax, as was shown for α -TOS alone in other cancer models (Weber et al., 2003; Yu et al., 2003). Thus, the elevation of p53 by α -TOS could facilitate TRAIL-induced apoptosis, releasing both Bid and Bax from their sequestration by Bcl-x_L and thereby promote mitochondria-dependent apoptosis.

A cooperative pro-apoptotic effect of α -TOS with immunological apoptogens has also been observed with breast cancer (Yu et al., 1999) and colon cancer cells and in an animal tumour model (Weber et al., 2002). Yu et al. showed that α -TOS converted Fas-resistant cells to become Fas-sensitive via mobilisation of the Fas receptor from the cytosol to the plasma membrane. Moreover, α -TOS enhanced the sensitivity of Jurkat T lymphoma cells to the induction of apoptosis by TRAIL (Dalen and Neuzil, 2003). The transient activation of NF κ B occurred when the cells were exposed to TRAIL and it is known that NF κ B controls expression of pro-survival genes, including FLIP (Kreuz et al., 2001) and IAPs (Degli-Esposti et al., 1997).

α -TOS, by inhibiting the TRAIL-induced transient NF κ B activation, which in turn inhibits expression of pro-survival proteins conferring resistance of cells to TRAIL-induced apoptosis, may be important when α -TOS is used as a co-treatment with TRAIL against TRAIL-resistant cancers.

5. Vitamin E analogues as modulators of the immune function

Although the anti-cancer properties of the VE analogues, α -TOS and α -tocopheryloxyacetic acid (α -TEA) are well documented, we are only now beginning to unravel the underlying molecular mechanisms of action of this family of compounds (Neuzil et al., 2001a,b, 2002; Shun et al., 2004; Lawson et al., 2003, 2004; Anderson et al., 2004). Studies that have examined the mechanisms of α -TOS or α -TEA-induced anti-cancer activity have focused on the pro-apoptotic nature of these analogs (reviewed in Neuzil, 2002; Neuzil et al., 2004; Kline et al., 2001). Less well studied is the potential contribution of the immune system to the in vivo anti-tumor activity of these agents. Our laboratory has pioneered studies that have examined the interplay between these VE analogues and cells of the immune system with the goal of harnessing the unique properties of tumour cell killing and T cell activation to generate an effective anti-tumour response. Similar to the previously reported selective toxicity of these VE compounds towards cancer cells compared to non-cancerous cells, we have also demonstrated that α -TOS is minimally toxic to murine splenic lymphocytes and dendritic cells (DC) both in vitro (Ramanathapuram et al., 2004) and in vivo (unpublished observations) at concentrations that are toxic to tumour cells.

Our laboratory has pioneered the use of α -TOS and α -TEA as adjuvants to improve the efficacy of DC-based cancer vaccines for the treatment of metastatic cancer. DCs are immune cells endowed with the unique ability to efficiently process and present antigens, secreting a variety of important immunostimulatory cytokines. DCs also express critical immune co-stimulatory molecules (Banchereau and Steinman, 1998; Fukao, 2002) necessary for priming anti-tumor T cell responses. These attributes have made DCs prime candidates for the immunotherapy of cancer (Banchereau and Steinman, 1998; Fukao, 2002). When used in combination with *ex vivo* generated, immature DCs for the treatment of established murine Lewis lung and mammary cancers, α -TOS and its more water-soluble, vesiculated form (V α -TOS) acted synergistically with DCs to inhibit the growth of established primary tumors and prolonged survival of the mice (Ramanathapuram et al., 2004, 2005). The impact on tumour metastases in the residual disease setting after primary tumor resection was even more profound (Ramanathapuram et al., 2004), demonstrating the potential utility of this chemo-immunotherapy approach for the prevention or treatment of micrometastatic disease after tumour debulking. The observed clinical responses were strongly correlated with polarization toward a T helper 1 (T_{H1}) immune response evidenced by increased interferon-gamma (IFN- γ) secretion and enhanced tumoricidal activity exhibited by tumor-draining lymph node cells and splenic lymphocytes (Ramanathapuram et al., 2004, 2005).

Although the use of $V\alpha$ -TOS constituted an improvement over α -TOS, the ester bond linking the succinate group to the chroman head in both α -TOS and $V\alpha$ -TOS is susceptible to hydrolytic cleavage by intestinal esterases (Neuzil et al., 2002). This susceptibility makes both forms less desirable for oral delivery because only the intact compound has anti-tumour activity (Burton and Traber, 1990). In contrast, α -TEA, which features an acetic acid moiety attached via a non-hydrolysable ether bond to the chroman head has been shown to exhibit anti-tumour activity when administered by oral gavage to tumour-bearing mice, while α -TOS is ineffective in this setting (Lawson et al., 2003, 2004). With an eye to moving α -TEA chemotherapy to the clinic, we incorporated α -TEA into mouse chow in order to prevent and treat spontaneous metastatic breast cancer. We reported, for the first time, that oral delivery of α -TEA by incorporation into the diet significantly inhibited primary murine mammary tumour growth and dramatically reduced spontaneous metastatic spread of tumour cells to the lung (Hahn et al., 2006). Furthermore, similar to the combination of $V\alpha$ -TOS with DCs, dietary α -TEA therapy was a potent adjuvant when combined with DC vaccination (unpublished observations).

The question that remained to be answered was the mechanism by which these VE analogues augmented the anti-tumour immune responses. We hypothesized that α -TOS and α -TEA induced apoptotic tumour cell death thereby releasing putative tumour antigens and to T lymphocytes. In addition, we speculated that cellular factors released by dying tumor cells caused DC activation, thereby improving their ability to prime tumour-specific T cells. To this end, our studies have shown that supernatant derived from $V\alpha$ -TOS or $V\alpha$ -TEA-treated tumour cells caused upregulation of the co-stimulatory molecules, CD40, CD80 and CD86 on DCs (Ramanathapuram et al., 2004, 2005) that are necessary for efficient activation of T lymphocytes. The phenotypic change in DC maturation status was also accompanied by an increase in the production of interleukin (IL)-12p70, an important cytokine secreted by mature DC that favours the development of a T_{H1} immune response *in vivo* (Welte et al., 1996). Furthermore, we have determined that α -TOS or α -TEA-induced apoptosis of tumour cells induces expression of heat shock proteins (HSPs) including HSP60, HSP70 and HSP90 (Ramanathapuram et al., 2006) which are molecular chaperones that act as “danger signals” alerting antigen presenting cells including DCs of potential damage or infection leading to their activation (Feng et al., 2002; Srivastava, 2002; Basu et al., 2000; Todryk et al., 1999; Bethke et al., 2002; Flohe et al., 2003; Basu and Srivastava, 2001; Somersan et al., 2001; Mosser and Morimoto, 2004). That HSPs released in response to $V\alpha$ -TOS or $V\alpha$ -TEA treatment are at least partially responsible for DC activation, was shown by blocking the cognate HSP receptor CD91 (Basu et al., 2001) on DCs with α_2 -macroglobulin. Treatment of DCs with α_2 -macroglobulin prior to co-incubation with $V\alpha$ -TOS or $V\alpha$ -TEA-derived tumour supernatant resulted in partial inhibition of co-stimulatory molecule expression (Ramanathapuram et al., 2006) and down-regulation of the antigen presenting machinery components, both of which were correlated with decreased ability of DCs to stimulate T cell proliferation (unpublished observations). Taken together, these findings suggest that release of HSPs during α -TOS or α -TEA-induced apoptotic tumour cell death

is a potential mechanism for DC activation that culminates in the induction of a robust anti-tumour response capable of inhibiting primary tumour growth and abrogating metastatic disease.

In summary, the VE analogues, α -TOS and α -TEA appear to employ a two-pronged approach to modulate the immune system; firstly, by direct killing of tumor cells whose antigens can be cross-presented by DCs, and, secondly, by maturation of DCs via HSP-mediated “danger signals”. These pre-clinical studies demonstrate the potential usefulness of combining α -TOS or α -TEA with DC-based vaccines for the treatment of cancer and can be readily translated to the clinic.

6. VE analogues as anti-cancer agents

6.1. Drug formulations

The hydrophobic character and low solubility of tocopherols, exemplified by VE analogues, dictate the formulation of these drugs for administration. Applications of α -TOS in ethanol, dimethylsulphoxide (DMSO) or vegetable oil emulsions by intravenous (i.v.) and intraperitoneal (i.p.) routes are restricted to mouse tumour models and are not suitable for clinical use in humans. Vesiculated forms of α -TOS in liposomes, various surfactants and solubilisers (e.g. polyethylene glycols), and enhancers of transdermal penetration are being tested as formulations applicable for human therapy.

Pharmacokinetic studies of α -TOS in humans and sheep following ingestion have shown it to be absorbed by the epithelial cells of the intestinal villi and completely hydrolysed to α -TOH, which is then secreted in chylomicrons into mesenteric lymph (Cheeseman et al., 1995; Hidioglou and Singh, 1991). α -TOH then enters the bloodstream from where it distributes to other lipoproteins and to peripheral tissues (Kayden and Traber, 1993). The delivery of the intact α -TOS molecule to tissue is essential for its unique anti-cancer activities (Fariss et al., 1993). Oral application, though, may be feasible in the case of ether or amide forms of VE analogues (Lawson et al., 2003; Tomic-Vatic et al., 2005; Hahn et al., 2006), which are not hydrolysed after absorption across the GI tract.

Spontaneous vesiculation of sodium or TRIS salts of α -TOS (Jizomoto et al., 1994) and other dicarboxylic acid analogues are utilised for drug formulations suitable for i.v. application. Anti-cancer effects of vesiculated α -TOS have been proven in mouse tumour models, but this formulation did not eliminate the *in vivo* toxicity of some effective VE analogues, such as α -tocopheryl oxalate (Kogure et al., 2005).

Liposomes represent the oldest and most advanced versatile nanodelivery system for drug formulation (Allen, 1997). α -TOS and other VE analogues can be easily incorporated into lipid bilayers to produce liposomes for various applications. Co-entrapment of α -TOS with other drugs and construction of liposomes targeted to various tumours is an attractive proposition for research into this area. Liposomal formulation could also eliminate or suppress organ-specific toxic side effects (Allen, 1997). We have found that neurotoxicity of the very potent analogue α -TAM

(Tomic-Vatic et al., 2005) was suppressed by incorporation into liposomes when single doses as high as 25 mg/kg or cumulative doses of 100 mg/kg were applicable i.v. into mice (Neuzil et al., unpublished data).

There are only limited studies on the pharmacokinetics and tissue distribution of α -TOS and other analogues after i.v. administration in vesiculated or liposomal forms. Studies with rats showed that α -TOS applied by the i.v. route has a half-life of approximately 10 h with a low volume of distribution (~ 0.56 ml/kg) and low clearance. α -TOS preferentially accumulates in lung and liver tissue and is associated with cell membrane lipids, especially within microsomal and mitochondrial membranes (Teng et al., 2005). α -TOS is also associated with circulating lipoproteins, which carry it to the microvasculature of tumour tissue, where it is taken up by cancer cells (Neuzil and Massa, 2005). Cancer cells overexpress receptors for very low-density lipoproteins, which represent excellent carriers for hydrophobic anticancer drugs. Inhibition of lung carcinoma cell growth by high density lipoprotein-associated α -TOS has been documented both in vitro and in vivo (Pussinen et al., 2000; Hrzjenjak et al., 2004). As such, liposomal compositions designed to selectively transfer α -TOS onto serum lipoproteins after i.v. application could significantly improve the anti-cancer effects of this drug.

The in vitro results with α -TOS incorporated into small unilamellar vesicles ($V\alpha$ -TOS) suggest that interaction of $V\alpha$ -TOS at the membrane level may be partly responsible for ceramide-mediated apoptosis, which is produced by the action of SMase (Gua et al., 2006).

α -Tocopheryl polyethylene glycol succinate (TPGS), a derivative of α -TOS, has been used to enhance the bioavailability of poorly absorbed drugs and as a vehicle for drug delivery systems. TPGS also possesses anti-cancer activity in vitro and in vivo (Youk et al., 2005). TPGS inhibited the growth of human lung carcinoma cells implanted in nude mice as well as in culture, more potently than did α -TOS. The time-dependent uptake of TPGS into cells did not differ from that of α -TOS, indicating that the enhanced antitumour efficacy of TPGS was not due to its increased uptake into cells. Compared with α -TOS, TPGS was more effective in inducing apoptosis and in generation of ROS, suggesting that the superior anti-cancer efficacy of TPGS is associated with its increased ability to induce cell death apoptosis (Youk et al., 2005). TPGS as a pharmacologically active component is an interesting compound for construction of liposomal drug delivery systems.

6.2. Combination of vitamin E derivatives with other anti-cancer drugs

Several examples are given below to demonstrate the potential of α -TOS and its analogues for adjuvant chemotherapy and radiotherapy. α -TOS as a potent inducer of apoptosis in a wide variety of human tumour cells may be a clinically useful drug when used in combination with other anti-cancer drugs. Recent reports that α -TOS could lower the intracellular GSH concentration in Jurkat cells (Weber et al., 2003) opened the door to investigations into whether α -TOS could be an effective sensitizer, enhancing the chemotherapeutic response of cancer cells overexpressing the multidrug resistance (MDR) protein MRP1, which are resistant to many anti-cancer

drugs. Kang et al. reported that α -TOS modulated the MRP1 function and enhanced the response of MRP1-overexpressing glioblastoma cells to etoposide, an MRP1 substrate drug currently being used for chemotherapy of glioblastoma patients, either by co-treatment or by being incorporated in liposomes together with etoposide (Kang et al., 2005). Thus, α -TOS synergistically enhanced the cytotoxic effects of etoposide in MRP1-expressing glioblastoma cells, and the sensitizing effect of α -TOS was shown to be closely related to its ability to modulate MRP1 function. Selectivity of α -TOS in MRP1-expressing cells and enhanced accumulation of VP-16, a well-known MRP1 substrate drug, in MRP1-expressing cells were likely due to lowering of GSH and hence limiting the GSH levels available for conjugation with the drug prior to the efflux.

The potential of the platinum-based chemotherapeutics is limited by several factors, including deleterious side effects and intrinsic or acquired resistance. Although most ovarian tumours respond well to chemotherapeutic drugs and may completely regress, there is a high level of recurrence in the advanced stages of the disease (Rustin et al., 2004). Recurrent tumour growth is a poor prognostic indicator, and second-line chemotherapy often fails, most likely because of acquired resistance to drug therapy. For example, in ovarian cancer, the initial success of cisplatin chemotherapy is often short-lived, as recurrence occurs in most cases (Judson et al., 1999). Anderson et al. (2004) demonstrated that treatment of immunocompromised, athymic mice bearing cisplatin-resistant A2780/cp70-GFP human ovarian cancer cell xenografts with α -TEA, in combination with cisplatin, significantly reduced the tumour burden and inhibited metastasis. In this case, α -TEA was formulated in liposomes (α -TEA/lipid-1,2-dilauroyl-sn-glycero-3-phosphocholine ratio of 1:3 (w/w)) and applied as an aerosol (Anderson et al., 2004).

Camptothecin and its less-toxic derivatives (irinotecan, 9-aminocamptothecin and 9-nitrocamptothecin, 9-NC) have been used clinically for the treatment of several forms of cancer including breast, ovarian, lung, and colorectal tumours (Ulukan and Swaan, 2002). 9-NC is currently in clinical trials for treatment of ovarian and pancreatic cancers, and is being considered for breast cancer therapy (Verschraegen et al., 1999; Konstadoulakis et al., 2001). Although 9-NC possesses impressive anticancer activity, it also exhibits significant toxic effects. Hence, the need to find strategies that might circumvent this problem by combining 9-NC at a lower dosage with another anticancer drug, such as VE analogues, is warranted.

α -TEA and 9-NC, both water-insoluble compounds, were formulated into liposomes using dilauroylphosphatidylcholine and administered by aerosol to deliver doses calculated to be 36 and 0.4 $\mu\text{g}/\text{mouse}$ per day, respectively, together or separately, every day for a week. Combination treatments enhanced anti-proliferative and pro-apoptotic activities in cell culture, and, when the drugs were formulated in liposomes and delivered via aerosol to treat an aggressive and metastatic syngeneic BALB/c murine mammary tumour, there was a significant reduction in tumour volume and lymph node metastasis in comparison to either treatment alone (Lawson et al., 2004). Also, combinations of α -TEA (administered in aerosolised liposomes) and celecoxib, an inhibitor of cyclooxygenase-2 administered in the diet, reduced tumour burden and lung metastasis of MDA-MB-435-FL-GFP breast cancer cell

xenografts in athymic mice better than when either compound was administered separately (Zhang et al., 2004).

Combination of α -TOS and radiotherapy was tested *in vitro* by Jha et al. (1999). They showed that α -TOS treatment for 24 h before, during, and after irradiation for the entire experimental period enhanced the decline in mitotic accumulation caused by γ -irradiation of human tumour cell lines. This effect was not observed for normal cells, such as fibroblasts. These data suggest that the actions of α -TOS, alone or combined with γ -radiation are selective for tumour cells.

7. Perspectives

This review focuses on the recent advances in a promising group of anti-cancer agents, VE analogues. These drugs have been shown to act by selective induction of apoptosis in cancer cells by way of targeting mitochondria. Therefore, they have been classified as mitocans, which is a growing group of small molecules of divergent structures that destabilise mitochondria, thereby suppressing cancer. Mitocans comprise several classes, depending on their particular mode of action. VE analogues belong to class II (BH3 mimetics) and class V (agents interfering with the electron redox chain) of mitocans (cf Table 1). From this point of view, VE analogues are truly unique. Not only do these compounds act by sensitising cancer cells to other inducers of apoptosis whose activity may be compromised by relatively high levels of expression of the anti-apoptotic Bcl-2 family proteins; but they also directly induce apoptosis by way of displacing coenzyme Q in complex II of the mitochondrial electron chain. Therefore, VE analogues, thus far, represent the only group of mitocans that have been clearly shown to act by at least two different modes.

Because of the unique properties of the apoptogenic VE analogues, they can very efficiently induce programmed cell death. Importantly, VE analogues exert this activity selectively in cancer cells. This includes preferential uptake by cancer cells due to the acidic nature of VE analogues such as α -TOS and the acidic environment of the tumour as opposed to normal tissue interstitium. Moreover, normal, non-malignant cells are endowed with high esterase activity that cleaves compounds like α -TOS to the non-apoptogenic, redox active α -TOH, and they also possess better antioxidant defenses, preventing accumulation of ROS that are required to trigger apoptosis in response to VE analogues (Neuzil et al., 2004).

Also for this reason, these agents present a promising group of anti-cancer drugs or adjuvants with no or low toxicity towards normal cells and tissues. Pre-clinical tests indicate the potent anti-cancer efficacy of VE analogues against a variety of types of cancer, including the fatal mesotheliomas and the refractory HER2-positive breast carcinomas. In particular, these latter two groups of patients should provide excellent possibility for using groups for testing VE analogues like α -TOS in the clinic. We believe that 2007 should witness the start of the first human phase I/II clinical trials of VE analogues which will promote more interest in the clinically highly intriguing and biochemically unique compounds redox-silent analogues of vitamin E.

Acknowledgements

This work was supported in part by a grant from the Grant Agency of the Academy of Sciences of the Czech Republic, and by the Institutional Research Concept funds of the Academy of Sciences of the Czech Republic AV0Z50520701 to J.N., and by Ministry of Agriculture of the Czech Republic grant MZE 0002716201 to J.T.

References

- Akazawa, A., Nishikawa, K., Suzuki, K., Asano, R., Kumadaki, I., Satoh, H., Hagiwara, K., Shin, S.J., Yano, T., 2002. Induction of apoptosis in a human breast cancer cell over-expressing ErbB-2 receptor by α -tocopheryloxybutyric acid. *Jpn. J. Pharmacol.* 89, 417–421.
- Alakurti, S., Makela, T., Koskimies, S., Yli-Kauhaluoma, J., 2006. Pharmacological properties of the ubiquitous natural product betulin. *Eur. J. Pharm. Sci.* 29, 1–13.
- Albores, R., Neafsey, E.J., Drucker, G., Fields, J.Z., Collins, M.A., 1990. Mitochondrial respiratory inhibition by *N*-methylated beta-carboline derivatives structurally resembling *N*-methyl-4-phenylpyridine. *Proc. Natl. Acad. Sci. USA* 87, 9368–9372.
- Allen, T.M., 1997. Liposomes: opportunities in drug delivery. *Drugs* 54, 8–14.
- Alleva, R., Tomasetti, M., Andera, L., Gellert, N., Borghi, B., Weber, C., Murphy, M.P., Neuzil, J., 2001. Coenzyme Q blocks chemical but not receptor-mediated apoptosis by increasing mitochondrial antioxidant protection. *FEBS Lett.* 503, 46–50.
- Alleva, R., Benassi, M.S., Tomasetti, M., Gellert, N., Pazzaglia, L., Borghi, B., Picci, P., Neuzil, J., 2005. α -Tocopheryl succinate induces cytostasis and apoptosis in osteosarcoma cells: the role of E2F1. *Biochem. Biophys. Res. Commun.* 331, 1515–1521.
- Alleva, R., Benassi, M.S., Tomasetti, M., Gellert, N., Borghi, B., Neuzil, J., Picci, P., 2006. α -Tocopheryl succinate alters cell cycle distribution sensitising human osteosarcoma cells to methotrexate-induced apoptosis. *Cancer Lett.* 232, 226–253.
- Anderson, K., Lawson, K.A., Simmons-Menchaca, M., Sun, L.Z., Sanders, B.G., Kline, K., 2004. *Exp. Biol. Med.* 229, 1169–1176.
- Antignani, A., Youle, R.J., 2006. How do Bax and Bak lead to permeabilization of the outer mitochondrial membrane? *Curr. Opin. Cell Biol.* 18, 685–689.
- Ashkenazi, A., Pai, R.C., Frong, S., Leung, S., Lawrence, D.A., Marsters, S.A., Blackie, C., Chang, L., McMurtrey, A.E., Hebert, A., DeForge, L., Koumenis, I.L., Lewis, D., Harris, L., Bussiere, J., Koepfen, H., Shahrokhi, Z., Schwall, R.H., 1999. Safety and antitumor activity of recombinant soluble Apo2 ligand. *J. Clin. Invest.* 104, 155–162.
- Bacsi, A., Woodberry, M., Widger, W., Papaconstantinou, J., Mitra, S., Peterson, J.W., Boldogh, I., 2006. Localization of superoxide anion production to mitochondrial electron transport chain in 3-NPA-treated cells. *Mitochondrion* 6, 235–244.
- Banchereau, J., Steinman, R.M., 1998. Dendritic cells and the control of immunity. *Nature* 392, 245–252.
- Baselga, J., 2006. Targeting tyrosine kinases in cancer: the second wave. *Science* 312, 1175–1178.
- Basu, S., Srivastava, P.K., 2001. Fever-like temperature induces maturation of dendritic cells through induction of hsp90. *Int. Immunol.* 15, 1053–1061.
- Basu, S., Binder, R.J., Suto, R., Anderson, K.M., Srivastava, P.K., 2000. Necrotic but not apoptotic cell death releases heat shock proteins, which deliver a partial maturation signal to dendritic cells and activate the NF- κ B pathway. *Int. Immunol.* 12, 1539–1546.
- Basu, S., Binder, R.J., Ramalingam, T., Srivastava, P.K., 2001. CD91 is a common receptor for heat shock proteins gp96, hsp90, hsp70, and calreticulin. *Immunity* 14, 303–313.
- Belzacq, A.S., El Hamel, C., Vieira, H.L., Cohen, I., Haouzi, D., Metivier, D., Marchetti, P., Brenner, C., Kroemer, G., 2001. Adenine nucleotide translocator mediates the mitochondrial membrane permeabilization induced by lonidamine, arsenite and CD437. *Oncogene* 20, 7579–7587.

- Bernal, S.D., Lampidis, T.J., Summerhayes, I.C., Chen, L.B., 1982. Rhodamine-123 selectively reduces clonal growth of carcinoma cells in vitro. *Science* 218, 1117–1119.
- Bethke, K., Staib, F., Distler, M., Schmitt, U., Jonuleit, H., Enk, A.H., Galle, P.R., Heike, M., 2002. Different efficiency of heat shock proteins (HSP) to activate human monocytes and dendritic cells: superiority of HSP60. *J. Immunol.* 169, 6141–6148.
- Britten, C.D., Rowinsky, E.K., Baker, S.D., Weiss, G.R., Smith, L., Stephenson, J., Rothenberg, M., Smetzer, L., Cramer, J., Collins, W., Von Hoff, D.D., Eckhardt, S.G., 2000. A phase I and pharmacokinetic study of the mitochondrial-specific rhodacyanine dye analog MKT 077. *Clin. Cancer Res.* 6, 42–49.
- Burton, G.W., Traber, M.G., 1990. Vitamin E antioxidant activity, biokinetics, and bioavailability. *Annu. Rev. Nutr.* 10, 357–382.
- Cande, C., Cecconi, F., Dessen, P., Kroemer, G., 2002. Apoptosis-inducing factor (AIF): key to the conserved caspase-independent pathways of cell death. *J. Cell. Sci.* 115, 4727–4734.
- Cardone, M.H., Roy, N., Stennicke, H.R., Salvesen, G.S., Franke, T.F., Stanbridge, E., Frisch, S., Reed, J.C., 1998. Regulation of cell death protease caspase-9 by phosphorylation. *Science* 282, 1318–1321.
- Cheeseman, K.H., Holley, A.E., Kelly, F.J., Wasil, M., Hughes, L., Burton, G., 1995. Biokinetics in humans of RRR- α -tocopherol: the free phenol, acetate ester, and succinate ester forms of vitamin E. *Free Radic. Biol. Med.* 19, 591–598.
- Cory, S., Huang, D.C., Adams, J.M., 2003. The Bcl-2 family: roles in cell survival and oncogenesis. *Oncogene* 22, 8590–8607.
- Costantini, P., Belzacq, A.S., Vieira, H.L., Larochette, N., de Pablo, M.A., Zamzami, N., Susin, S.A., Brenner, C., Kroemer, G., 2000. Oxidation of a critical thiol residue of the adenine nucleotide translocator enforces Bcl-2-independent permeability transition pore opening and apoptosis. *Oncogene* 19, 307–314.
- Dahout-Gonzalez, C., Nury, H., Trezeguet, V., Lauquin, G.J., Pebay-Peyroula, E., Brandolin, G., 2006. Molecular, functional, and pathological aspects of the mitochondrial ADP/ATP carrier. *Physiology* 21, 242–249.
- Dalen, H., Neuzil, J., 2003. α -Tocopheryl succinate sensitises T lymphoma cells to TRAIL killing by suppressing NF- κ B activation. *Br. J. Cancer* 88, 153–158.
- D'Alessio, M., De Nicola, M., Coppola, S., Gualandi, G., Pugliese, L., Cerella, C., Cristofanon, S., Civitareale, P., Ciriolo, M.R., Bergamaschi, A., Magrini, A., Ghibelli, L., 2005. Oxidative Bax dimerization promotes its translocation to mitochondria independently of apoptosis. *FASEB J.* 19, 1504–1506.
- Datta, S.R., Dudek, H., Tao, X., Masters, S., Fu, H., Gotoh, Y., Greenberg, M.E., 1997. Akt phosphorylation of BAD couples survival signals to the cell-intrinsic death machinery. *Cell* 9, 231–241.
- Davey, G.P., Tipton, K.F., Murphy, M.P., 1992. Uptake and accumulation of 1-methyl-4-phenylpyridinium by rat liver mitochondria measured using an ion-selective electrode. *Biochem. J.* 288, 439–443.
- Davis, S., Weiss, M.J., Wong, J.R., Lampidis, T.J., Chen, L.B., 1985. Mitochondrial and plasma membrane potentials cause unusual accumulation and retention of rhodamine 123 by human breast adenocarcinoma-derived MCF-7 cells. *J. Biol. Chem.* 260, 13844–13850.
- Degli-Esposti, M.A., Dougall, W.C., Smolak, P.J., Waugh, J.Y., Smith, C.A., Goodwin, R.G., 1997. The novel receptor TRAIL-R4 induces NF- κ B and protects against TRAIL-mediated apoptosis yet retains and incomplete death domain. *Immunity* 7, 813–820.
- Dey, R., Moraes, C.T., 2000. Lack of oxidative phosphorylation and low mitochondrial membrane potential decrease susceptibility to apoptosis and do not modulate the protective effect of Bcl-x_L in osteosarcoma cells. *J. Biol. Chem.* 275, 7087–7094.
- Dilda, P.J., Decollogne, S., Rossiter-Thornton, M., Hogg, P.J., 2005. Para to ortho repositioning of the arsenical moiety of the angiogenesis inhibitor 4-(N-(S-glutathionylacetyl)amino) phenylarsenoxide results in a markedly increased cellular accumulation and antiproliferative activity. *Cancer Res.* 65, 11729–11734.

- Dimanche-Boitrel, M.T., Meurette, O., Rebillard, A., Lacour, S., 2005. Role of early plasma membrane events in chemotherapy-induced cell death. *Drug Resist Update* 8, 5–14.
- Don, A.S., Kisker, O., Dilda, P., Donoghue, N., Zhao, X., Decollogne, S., Creighton, B., Flynn, E., Folkman, J., Hogg, P.J., 2003. A peptide trivalent arsenical inhibits tumor angiogenesis by perturbing mitochondrial function in angiogenic endothelial cells. *Cancer Cell* 3, 497–509.
- Donapaty, S., Louis, S., Forvath, E., Kun, J., Sebtü, S.M., Malafa, M.P., 2006. RRR- α -tocopherol succinate down-regulates oncogenic Ras signalling. *Mol. Cancer Ther.* 5, 309–316.
- Dong, L.F., Low, P., Dyason, J., Wang, X.F., Prochazka, L., Swettenham, E., Tumanek, J., Scheffler, I.E., Ralph, S.J., Neuzil, J., submitted for publication. The mitocan α -tocopherol succinate induces apoptosis by disrupting ubiquinone binding of mitochondrial respiratory complex II.
- Du, C., Fang, M., Li, Y., Li, L., Wang, X., 2000. Smac, a mitochondrial protein that promotes cytochrome *c*-dependent caspase activation by eliminating IAP inhibition. *Cell* 102, 33–42.
- Dudek, H., Datta, S.R., Franke, T.F., Birnbaum, M.J., Yao, R., Cooper, G.M., Segal, R.A., Kaplan, D.R., Greenberg, M.E., 1997. Regulation of neuronal survival by the serine-threonine protein kinase Akt. *Science* 275, 661–665.
- Ellerby, H.M., Arap, W., Ellerby, L.M., Kain, R., Andrusiak, R., Rio, G.D., Krajewski, S., Lombardo, C.R., Rao, R., Ruoslahti, E., Bredesen, D.E., Pasqualini, R., 1999. Anti-cancer activity of targeted pro-apoptotic peptides. *Nat. Med.* 5, 1032–1038.
- Erl, W., Weber, C., Wardemann, C., Weber, P.C., 1997. α -Tocopherol succinate inhibits monocytic cell adhesion to endothelial cells by suppressing NF- κ B mobilization. *Am. J. Physiol.* 273, H634–H640.
- Fantin, V.R., Berardi, M.J., Scorrano, L., Korsmeyer, S.J., Leder, P., 2002. A novel mitochondriotoxic small molecule that selectively inhibits tumor cell growth. *Cancer Cell* 2, 29–42.
- Fantin, V.R., Berardi, M.J., Babbe, H., Michelman, M.V., Manning, C.M., Leder, P., 2005. A bifunctional targeted peptide that blocks HER-2 tyrosine kinase and disables mitochondrial function in HER-2-positive carcinoma cells. *Cancer Res.* 65, 6891–6900.
- Fariss, M.W., Bryson, K.F., Hylton, E.E., Lippman, H.R., Stubin, C.H., Zhao, X., 1993. Protection against carbon tetrachloride-induced hepatotoxicity by pretreating rats with the hemisuccinate esters of tocopherol and cholesterol. *Environ. Health Perspect* 101, 528–536.
- Feng, H., Zeng, Y., Graner, M.W., Katsanis, E., 2002. Stressed apoptotic tumor cells stimulate dendritic cells and induce specific cytotoxic T cells. *Blood* 100, 4108–4115.
- Flohe, S.B., Bruggemann, J., Lendemans, S., et al., 2003. Human heat shock protein 60 induces maturation of dendritic cells versus a Th1-promoting phenotype. *J. Immunol.* 170, 2340–2348.
- Fotadar, R., Diederich, L., Fotadar, A., 1996. Apoptosis and the cell cycle. *Prog. Cell.*
- Fukao, T., 2002. Dendritic-cell-based anticancer vaccination: has it matured? *Trends Immunol.* 23, 231–232.
- Fulda, S., Scaffidi, C., Susin, S.A., Krammer, P.H., Kroemer, G., Peter, M.E., Debatin, K.M., 1998. Activation of mitochondria and release of mitochondrial apoptogenic factors by betulinic acid. *J. Biol. Chem.* 273, 33942–33948.
- Gamboa-Vujčić, G., Emma, D.A., Liao, S.Y., Fuchtnr, C., Manetta, A., 1993. Toxicity of the mitochondrial poison dequalinium chloride in a murine model system. *J. Pharm. Sci.* 82, 231–235.
- Garattini, E., Gianni, M., Terao, M., 2004. Retinoid related molecules an emerging class of apoptotic agents with promising therapeutic potential in oncology: pharmacological activity and mechanisms of action. *Curr. Pharm. Des.* 10, 433–448.
- Gincel, D., Zaid, H., Shoshan-Barmatz, V., 2001. Calcium binding and translocation by the voltage-dependent anion channel: a possible regulatory mechanism in mitochondrial function. *Biochem. J.* 358, 147–155.
- Gledhill, J.R., Walker, J.E., 2005. Inhibition sites in F1-ATPase from bovine heart mitochondria. *Biochem. J.* 386, 591–598.
- Gossiau, A., Chen, M., Ho, C.T., Chen, K.Y., 2005. A methoxy derivative of resveratrol analogue selectively induced activation of the mitochondrial apoptotic pathway in transformed fibroblasts. *Br. J. Cancer* 92, 513–521.

- Green, D.R., Kroemer, G., 2004. The pathophysiology of mitochondrial cell death. *Science* 305, 626–629.
- Gua, X., Schwartz, J.L., Panga, X., Zhou, Y., Siroise, D.A., Sridhar, R., 2006. Cytotoxicity of liposomal α -tocopheryl succinate towards hamster cheek pouch carcinoma (HCPC-1) cells in culture. *Cancer Lett.* 239, 281–291.
- Guzman, M.L., Rossi, R.M., Karnischky, L., Li, X., Peterson, D.R., Howard, D.S., Jordan, C.T., 2005. The sesquiterpene lactone parthenolide induces apoptosis of human acute myelogenous leukemia stem and progenitor cells. *Blood* 105, 4163–4169.
- Hahn, T., Szabo, L., Gold, M., Ramanathapuram, L., Hurley, L.H., Akporiaye, E.T., 2006. Dietary administration of the proapoptotic vitamin E analogue α -tocopheryloxyacetic acid inhibits metastatic murine breast cancer. *Cancer Res.* 66, 9374–9378.
- Hail, N., Lotan, R., 2001. Mitochondrial respiration is uniquely associated with the prooxidant and apoptotic effects of *N*-(4-hydroxyphenyl)retinamide. *J. Biol. Chem.* 276, 45614–45621.
- Hail Jr., N., Kim, H.J., Lotan, R., 2006. Mechanisms of fenretinide-induced apoptosis. *Apoptosis* 11, 1677–1694.
- Harvey, K.J., Lukovic, D., Ucker, D.S., 2000. Caspase-dependent Cdk activity is a requisite effector of apoptotic death events. *J. Cell. Biol.* 148, 59–72.
- Hidiroglou, M., Singh, K., 1991. Plasma α -tocopherol profiles in sheep after oral administration of α -tocopheryl acetate and *D*- α -tocopheryl succinate. *J. Dairy Sci.* 74, 2718–2723.
- Higuchi, M., Aggarwal, B.B., Yeh, E.T., 1997. Activation of CPP32-like protease in tumor necrosis factor-induced apoptosis is dependent on mitochondrial function. *J. Clin. Invest.* 99, 1751–1758.
- Hirano, S., Kobayashi, Y., Hayakawa, T., Cui, X., Yamamoto, M., Kanno, S., Shraim, A., 2005. Accumulation and toxicity of monophenyl arsenicals in rat endothelial cells. *Arch. Toxicol.* 79, 54–61.
- Hrzenjak, A., Reicher, H., Wintersperger, A., Steinecker-Frohnwieser, B., Sedlmayr, P., Schmidt, H., Nakamura, T., Malle, E., Sattler, W., 2004. Inhibition of lung carcinoma cell growth by high density lipoprotein-associated α -tocopheryl-succinate. *Cell. Mol. Life Sci.* 61, 1520–1531.
- James, M.L., Selleri, S., Kassiou, M., 2006. Development of ligands for the peripheral benzodiazepine receptor. *Curr. Med. Chem.* 13, 1991–2001.
- Jha, M.N., Bedford, J.S., Cole, W.C., Edward-Prasad, J., Prasad, K.N., 1999. Vitamin E (*D*- α -tocopheryl succinate) decreases mitotic accumulation in γ -irradiated human tumor, but not in normal, cells. *Nutr. Cancer* 35, 189–194.
- Jizomoto, H., Kanaoka, E., Hirano, K., 1994. pH-sensitive liposomes composed of tocopherol hemisuccinate and of phosphatidylethanolamine including tocopherol hemisuccinate. *Biochim. Biophys. Acta* 1213, 343–348.
- Jones, L.W., Narayan, K.S., Shapiro, C.E., Sweatman, T.W., 2005. Rhodamine-123: therapy for hormone refractory prostate cancer, a phase I clinical trial. *J. Chemother.* 17, 435–440.
- Judson, P.L., Watson, J.M., Gehrig, P.A., Fowler Jr., W.C., Haskill, J.S., 1999. Cisplatin inhibits paclitaxel-induced apoptosis in cisplatin-resistant ovarian cancer cell lines: possible explanation for failure of combination therapy. *Cancer Res.* 59, 2425–2432.
- Kallio, A., Zheng, A., Dahllund, J., Heiskanen, K.M., Harkonen, P., 2005. Role of mitochondria in tamoxifen-induced rapid death of MCF-7 breast cancer cells. *Apoptosis* 10, 1395–1410.
- Kane, L.P., Shapiro, V.S., Stokoe, D., Weiss, A., 1999. Induction of NF- κ B by the Akt/PKB kinase. *Curr. Biol.* 9, 601–604.
- Kang, Y.H., Lee, H., Choi, M.K., Ku, J.L., Kim, S.H., Park, Y.G., Lin, S.J., 2004. Role of reactive oxygen species in the induction of apoptosis by α -tocopheryl succinate. *Int. J. Cancer* 112, 385–392.
- Kang, Y.H., Lee, E., Youk, H.J., Kim, S.H., Lee, H.J., Park, Y.G., Lim, S.J., 2005. Potentiation by α -tocopheryl succinate of the etoposide response in multidrug resistance protein 1-expressing glioblastoma cells. *Cancer Lett.* 217, 181–190.
- Kayden, H.J., Traber, M.G., 1993. Absorption, lipoprotein transport, and regulation of plasma concentrations of vitamin E in humans. *J. Lipid Res.* 34, 343–358.

- Kelso, G.F., Porteous, C.M., Coulter, C.V., Hughes, G., Porteous, W.K., Ledgerwood, E.C., Smith, R.A., Murphy, M.P., 2001. Selective targeting of a redox-active ubiquinone to mitochondria within cells: antioxidant and antiapoptotic properties. *J. Biol. Chem.* 276, 4588–4596.
- Kessler, J.H., Mullauer, F.B., de Roo, G.M., Medema, J.P., 2006. Broad in vitro efficacy of plant-derived betulinic acid against cell lines derived from the most prevalent human cancer types. *Cancer Lett.*
- Kim, J.H., Liu, L., Lee, S.O., Kim, Y.T., You, K.R., Kim, D.G., 2005. Susceptibility of cholangiocarcinoma cells to parthenolide-induced apoptosis. *Cancer Res.* 65, 6312–6320.
- Kirschnek, S., Ying, S., Fischer, S.F., Hacker, H., Villunger, A., Hochrein, H., Hacker, G., 2005. Phagocytosis-induced apoptosis in macrophages is mediated by up-regulation and activation of the Bcl-2 homology domain 3-only protein Bim. *J. Immunol.* 174, 671–679.
- Kitada, S., Leone, M., Sareth, S., Zhai, D., Reed, J.C., Pellecchia, M., 2003. Discovery, characterization, and structure-activity relationships studies of proapoptotic polyphenols targeting B-cell lymphocyte/leukemia-2 proteins. *J. Med. Chem.* 46, 4259–4264.
- Kline, K., Yu, W., Sanders, B.G., 2001. Vitamin E: mechanisms of action as tumor cell growth inhibitors. *J. Nutr.* 131, 161S–163S.
- Ko, Y.H., Smith, B.L., Wang, Y., Pomper, M.G., Rini, D.A., Torbenson, M.S., Hullihen, J., Pedersen, P.L., 2004. Advanced cancers: eradication in all cases using 3-bromopyruvate therapy to deplete ATP. *Biochem. Biophys. Res. Commun.* 324, 269–275.
- Kogure, K., Morita, M., Nakashima, S., Hama, S., Tokumura, A., Fukuzawa, K., 2001. Superoxide is responsible for apoptosis in rat vascular smooth muscle cells induced by α -tocopheryl hemisuccinate. *Biochim. Biophys. Acta* 1528, 25–30.
- Kogure, K., Hama, S., Manabe, S., Tokumura, A., Fukuzawa, K., 2002. High cytotoxicity of α -tocopheryl hemisuccinate to cancer cells is due to failure of their antioxidant defence systems. *Cancer Lett.* 186, 151–156.
- Kogure, K., Manabe, S., Suzuki, K., Tokumura, A., Fukuzawa, K., 2005. Cytotoxicity of α -tocopheryl succinate, malonate and oxalate in normal and cancer cells in vitro and their anti-cancer effects on mouse melanoma in vivo. *J. Nutr. Sci. Vitaminol.* 51, 392–397.
- Konstadoulakis, M.M., Antonakis, P.T., Tsiouloulis, A.G., Stathopoulos, G.P., Manouras, A.P., Mylonaki, D.B., Golemis, B.X., 2001. A phase II study of 9-nitrocamptothecin in patients with advanced pancreatic adenocarcinoma. *Cancer Chemother. Pharmacol.* 48, 417–420.
- Kreuz, S., Siegmund, D., Scheunich, P., Wajant, H., 2001. NF- κ B inducers upregulate cFLIP, a cycloheximide-sensitive inhibitor of death receptor signaling. *Mol. Cell. Biol.* 21, 3964–3973.
- LaCasse, E.C., Baird, S., Korneluk, R.G., MacKenzie, A.E., 1998. The inhibitors of apoptosis (IAPs) and their emerging role in cancer. *Oncogene* 17, 3247–3259.
- Lampidis, T.J., Bernal, S.D., Summerhayes, I.C., Chen, L.B., 1983. Selective toxicity of rhodamine 123 in carcinoma cells in vitro. *Cancer Res.* 43, 716–720.
- Lampidis, T.J., Hasin, Y., Weiss, M.J., Chen, L.B., 1985. Selective killing of carcinoma cells “in vitro” by lipophilic-cationic compounds: a cellular basis. *Biomed. Pharmacother.* 39, 220–226.
- Lane, D.P., 1992. Cancer: p53, guardian of the genome. *Nature* 358, 15–16.
- Lawson, K.A., Anderson, K., Menchaca, M., Atkinson, J., Sun, L.Z., Knight, V., Gilbert, B.E., Conti, C., Sanders, B.G., Kline, K., 2003. Novel vitamin E analogue decreases syngenic mouse mammary tumor burden and reduces lung metastasis. *Mol. Cancer Ther.* 2, 437–444.
- Lawson, K.A., Anderson, K., Snyder, R.M., Simmons-Menchaca, M., Atkinson, J., Sun, L.Z., Bandyopadhyay, A., Knight, V., Gilbert, B.E., Sanders, B.G., Kline, K., 2004. Novel vitamin E analogue and 9-nitro-camptothecin administered as liposome aerosols decrease syngenic mouse mammary tumor burden and inhibit metastasis. *Cancer Chemother. Pharmacol.* 54, 421–431.
- Levine, A.J., 1997. p53 the cellular gatekeeper for growth and division. *Cell* 88, 323–331.
- Levkau, B., Scatena, M., Giachelli, C.M., Ross, R., Raines, E.W., 1999. Apoptosis overrides survival signals through a caspase-mediated dominant-negative NF- κ B loop. *Nat. Cell. Biol.* 1, 227–233.
- Liu, J., Lin, A., 2005. Role of JNK activation in apoptosis: a double-edged sword. *Cell. Res.* 15, 36–42.
- Liu, W.K., Ho, J.C., Cheung, F.W., Liu, B.P., Ye, W.C., Che, C.T., 2004. Apoptotic activity of betulinic acid derivatives on murine melanoma B16 cell line. *Eur. J. Pharmacol.* 498, 71–78.

- Maaser, K., Sutter, A.P., Scherubl, H., 2005. Mechanisms of mitochondrial apoptosis induced by peripheral benzodiazepine receptor ligands in human colorectal cancer cells. *Biochem. Biophys. Res. Commun.* 332, 646–652.
- Liu, J., Rone, M.B., Papadopoulos, V., 2006. Protein–protein interactions mediate mitochondrial cholesterol transport and steroid biosynthesis. *J. Biol. Chem.* 281, 38879–38893.
- Machida, K., Ohta, Y., Osada, H., 2006. Suppression of apoptosis by cyclophilin D via stabilization of hexokinase II mitochondrial binding in cancer cells. *J. Biol. Chem.* 281, 14314–14320.
- Madesh, M., Hajnoczky, G., 2001. VDAC-dependent permeabilization of the outer mitochondrial membrane by superoxide induces rapid and massive cytochrome *c* release. *J. Cell. Biol.* 155, 1003–1015.
- Malafa, M.P., Fokum, F.D., Mowlavi, A., Abusief, M., King, M., 2002. Vitamin E inhibits melanoma growth in mice. *Surgery* 131, 85–91.
- Malafa, M.P., Fokum, F.D., Andoh, J., Neitzel, L.T., Bandyopadhyay, S., Zhan, R., Iizumi, M., Furuta, E., Horvath, E., Watabe, K., 2006. Vitamin E succinate suppresses prostate tumor growth by inducing apoptosis. *Int. J. Cancer* 118, 2441–2447.
- Mathupala, S.P., Ko, Y.H., Pedersen, P.L., 2006. Hexokinase II: cancer's double-edged sword acting as both facilitator and gatekeeper of malignancy when bound to mitochondria. *Oncogene* 25, 4777–4786.
- McStay, G.P., Clarke, S.J., Halestrap, A.P., 2002. Role of critical thiol groups on the matrix surface of the adenine nucleotide translocase in the mechanism of the mitochondrial permeability transition pore. *Biochem. J.* 367, 541–548.
- Miller, W.H., 2002. Molecular targets of arsenic trioxide in malignant cells. *Oncologist* 7, S14–S19.
- Monkkonen, H., Auriola, S., Lehenkaari, P., Kellinsalmi, M., Hassinen, I.E., Vepsäläinen, J., Monkkonen, J., 2006. A new endogenous ATP analog (Apppl) inhibits the mitochondrial adenine nucleotide translocase (ANT) and is responsible for the apoptosis induced by nitrogen-containing bisphosphonates. *Br. J. Pharmacol.* 147, 437–445.
- Moreira, P.I., Custodio, J., Moreno, A., Oliveira, C.R., Santos, M.S., 2006. Tamoxifen and estradiol interact with the flavin mononucleotide site of complex I leading to mitochondrial failure. *J. Biol. Chem.* 281, 10143–10152.
- Mosser, D.D., Morimoto, R.I., 2004. Molecular chaperones and the stress of oncogenesis. *Oncogene* 23, 2907–2918.
- Nakagawa, Y., Iinuma, M., Matsuura, N., Yi, K., Naoi, M., Nakayama, T., Nozawa, Y., Akao, Y., 2005. A potent apoptosis-inducing activity of a sesquiterpene lactone, arucanolide, in HL60 cells: a crucial role of apoptosis-inducing factor. *J. Pharmacol. Sci.* 97, 242–252.
- Neuzil, J., 2002. α -Tocopheryl succinate epitomizes a compound with a shift in biological activity due to pro-vitamin-to-vitamin conversion. *Biochem. Biophys. Res. Commun.* 293, 1309–1313.
- Neuzil, J., 2003. Vitamin E succinate and cancer treatment: a vitamin E prototype for selective antitumour activity. *Br. J. Cancer* 89, 1822–1826.
- Neuzil, J., Massa, H., 2005. Hepatic processing determines dual activity of α -tocopherol succinate: a novel paradigm for a shift in biological activity due to pro-vitamin-to-vitamin conversion. *Biochem. Biophys. Res. Commun.* 327, 1024–1027.
- Neuzil, J., Svensson, I., Weber, T., Weber, C., Brunk, U.T., 1999. α -Tocopheryl succinate-induced apoptosis in Jurkat T cells involves caspase-3 activation, and both lysosomal and mitochondrial destabilisation. *FEBS Lett.* 445, 295–300.
- Neuzil, J., Schröder, A., von Hundelshausen, P., Zerneck, A., Weber, T., Gellert, N., Weber, C., 2001a. Inhibition of inflammatory endothelial responses by a pathway involving caspase activation and p65 cleavage. *Biochemistry* 40, 4686–4692.
- Neuzil, J., Weber, T., Gellert, N., Weber, C., 2001b. Selective cancer cell killing by α -tocopheryl succinate. *Br. J. Cancer* 84, 87–89.
- Neuzil, J., Weber, T., Schröder, A., Lu, M., Ostermann, G., Gellert, N., Mayne, G.C., Olejnicka, B., Nègre-Salvayre, A., Sticha, M., Coffey, R.J., Weber, C., 2001c. Induction of apoptosis in cancer cells by α -tocopheryl succinate: Molecular pathways and structural requirements. *FASEB J.* 15, 403–415.

- Neuzil, J., Zhao, M., Ostermann, G., Sticha, M., Gellert, N., Weber, C., Eaton, J.W., Brunk, U.T., 2002. α -Tocopheryl succinate, an agent with *in vivo* anti-tumour activity, induces apoptosis by causing lysosomal instability. *Biochem. J.* 362, 709–715.
- Neuzil, J., Tomasetti, M., Mellick, A.S., Alleva, R., Salvatore, B.A., Biringer, B., Fariss, M.W., 2004. Vitamin E analogues: a new class of inducers of apoptosis with selective anti-cancer effect. *Curr. Cancer Drug Targets* 4, 267–284.
- Neuzil, J., Wang, X.F., Dong, L.F., Low, P., Ralph, S.J., 2006. Molecular mechanism of 'mitocan'-induced apoptosis in cancer cells epitomizes the multiple roles of reactive oxygen species and Bcl-2 family proteins. *FEBS Lett.* 580, 5125–5129.
- Ni, J., Chen, M., Zhang, Y., Li, R., Huang, J., Yeh, S., 2003. Vitamin E succinate inhibits human prostate cancer cell growth via modulating cell cycle regulatory machinery. *Biochem. Biophys. Res. Commun.* 300, 357–363.
- Ogretmen, B., Hannun, Y.A., 2004. Biologically active sphingolipids in cancer pathogenesis and treatment. *Nat. Rev. Cancer* 4, 604–616.
- O'Neill, J., Manion, M., Schwartz, P., Hockenbery, D.M., 2004. Promises and challenges of targeting Bcl-2 anti-apoptotic proteins for cancer therapy. *Biochim. Biophys. Acta* 1705, 43–51.
- Ottino, P., Duncan, J.R., 1997. Effect of α -tocopherol succinate on free radical and lipid peroxidation levels in BL6 melanoma cells. *Free Radic. Biol. Med.* 22, 1145–1151.
- Papadopoulos, V., Baraldi, M., Guilarte, T.R., Knudsen, T.B., Lacapere, J.J., Lindemann, P., Norenberg, M.D., Nutt, D., Weizman, A., Zhang, M.R., Gavish, M., 2006. Translocator protein (18 kDa): new nomenclature for the peripheral-type benzodiazepine receptor based on its structure and molecular function. *Trends Pharmacol. Sci.* 27, 402–409.
- Pastorino, J.G., Shulga, N., Hoek, J.B., 2002. Mitochondrial binding of hexokinase II inhibits Bax-induced cytochrome *c* release and apoptosis. *J. Biol. Chem.* 277, 7610–7618.
- Pitti, R.M., Marsters, S.A., Ruppert, S., Donahue, C.J., Moore, A., Ashkenazi, A. Induction of apoptosis by Apo-2, ligand, a new member of the tumor necrosis factor cytokine, family, 1996. *J. Biol. Chem.* 271, 12687–12690.
- Pretner, E., Amri, H., Li, W., Brown, R., Lin, C.S., Makariou, E., Defeudis, F.V., Drieu, K., Papadopoulos, V., 2006. Cancer-related overexpression of the peripheral-type benzodiazepine receptor and cytostatic anticancer effects of Ginkgo biloba extract (EGb 761). *Anticancer Res.* 26, 9–22.
- Pussinen, P.J., Lindner, H., Glatter, O., Reicher, H., Gerhard, M., Kostner, H.M., Wintersperger, A., Malle, E., Sattler, W., 2000. Lipoprotein-associated α -tocopheryl-succinate inhibits cell growth and induces apoptosis in human MCF-7 and HBL-100 breast cancer cells. *Biochim. Biophys. Acta* 1485, 129–144.
- Ralph, S.J., Dong, L.F., Low, P., Lawen, A., Neuzil, J., 2006. Mitocans: mitochondria-targeted anti-cancer drugs as improved therapies and related patents. *Recent patent reviews on anti-cancer. Drug Discov.* 1, 305–326.
- Ralph, S.J., Dyason, J., Freeman, R., Dong, L.F., Prochazka, L., Wang, X.F., Immo, E., Scheffler, Neuzil, J., *in press*. Mitocans as anti-cancer agents targeting mitochondria: Lessons from studies with vitamin E analogues, inhibitors of complex II. *J. Bioenerg. Biomembr.*
- Ramanathapuram, L.V., Kobie, J.J., Bearss, D., Payne, C.M., Trevor, K.T., Akporiaye, E.T., 2004. α -Tocopheryl succinate sensitizes established tumors to vaccination with nonmatured dendritic cells. *Cancer Immunol. Immunother.* 53, 580–588.
- Ramanathapuram, L.V., Hahn, T., Dial, S.M., Akporiaye, E.T., 2005. Chemo-immunotherapy of breast cancer using vesiculated α -tocopheryl succinate in combination with dendritic cell vaccination. *Nutr. Cancer* 53, 177–193.
- Ramanathapuram, L.V., Hahn, T., Graner, M.W., Katsanis, E., Akporiaye, E.T., 2006. Vesiculated α -tocopheryl succinate enhances the anti-tumor effect of dendritic cell vaccines. *Cancer Immunol. Immunother.* 55, 166–177.
- Robey, R.B., Hay, N., 2006. Mitochondrial hexokinases, novel mediators of the antiapoptotic effects of growth factors and Akt. *Oncogene* 25, 4683–4696.
- Roskoski, R., 2004. The ErbB/HER receptor protein-tyrosine kinases and cancer. *Biochem. Biophys. Res. Commun.* 319, 1–11.

- Rustin, G.J.S., Bast, R.C., Kelloff, G.J., Barrett, J.C., Carter, S.K., Nisen, P.D., Sigman, C.C., Parkinson, D.R., Ruddon, R.W., 2004. Use of CA-125 in clinical trial evaluation of new therapeutic drugs for ovarian cancer. *Clin. Cancer Res.* 10, 3919–3926.
- Ruvolo, P.P., Deng, X., Carr, B.K., May, W.S., 1998. A functional role for mitochondrial protein kinase C α in Bcl2 phosphorylation and suppression of apoptosis. *J. Biol. Chem.* 273, 25436–25442.
- Ruvolo, P.P., Deng, X., Ito, T., Carr, B.K., May, W.S., 1999. Ceramide induces Bcl2 dephosphorylation via a mechanism involving mitochondrial PP2A. *J. Biol. Chem.* 274, 20296–20300.
- Rzeski, W., Stepulak, A., Szymanski, M., Siffringer, M., Kaczor, J., Wejksza, K., Zdzinska, B., Kandefer-Szerszen, M., 2006. Betulinic acid decreases expression of bcl-2 and cyclin D1, inhibits proliferation, migration and induces apoptosis in cancer cells. *Naunyn Schmiedebergs Arch. Pharmacol.* 374, 11–20.
- Sablina, A.A., Budanov, A.V., Ilyinskaya, G.V., Agapova, L.S., Kravchenko, J.E., Chumakov, P.M., 2005. The antioxidant function of the p53 tumor suppressor. *Nat. Med.* 11, 1306–1313.
- Sahara, N., Takeshita, A., Kobayashi, M., Shigeno, K., Nakamura, S., Shinjo, K., Naito, K., Maekawa, M., Hori, T., Ohnishi, K., Kitamura, K., Naoe, T., Hayash, H., Ohno, R., 2004. Phenylarsine oxide (PAO) more intensely induces apoptosis in acute promyelocytic leukemia and As2O3-resistant APL cell lines than As2O3 by activating the mitochondrial pathway. *Leuk. Lymphoma* 45, 987–995.
- Sanborn, B.M., Felberg, N.T., Hollocher, T.C., 1971. The inactivation of succinate dehydrogenase by bromopyruvate. *Biochim. Biophys. Acta* 227, 219–231.
- Sareen, D., van Ginkel, P.R., Takach, J.C., Mohiuddin, A., Darjatmoko, S.R., Albert, D.M., Polans, A.S., 2006. Mitochondria as the primary target of resveratrol-induced apoptosis in human retinoblastoma cells. *Invest. Ophthalmol. Vis. Sci.* 47, 3708–3716.
- Scaffidi, C., Fulda, S., Srinivasan, A., Friesen, C., Li, F., Tomaselli, K.J., Debatin, K.M., Krammer, P.H., Peter, M.E., 1998. Two CD95 (APO-1/Fas) signaling pathways. *EMBO J.* 17, 1675–1687.
- Schneider, P., Thome, M., Burns, K., Bodmer, J.L., Hofmann, K., Kataoka, T., Holler, N., Tschopp, J., 1997. TRAIL receptors 1 (DR4) and 2 (DR5) signal FADD-dependent apoptosis and activate NF- κ B. *Immunity* 7, 831–836.
- Shafir, I., Feng, W., Shoshan-Barmatz, V., 1998. Voltage-dependent anion channel proteins in synaptosomes of the torpedo electric organ: immunolocalization, purification, and characterization. *J. Bioenerg. Biomembr.* 30, 499–510.
- Shi, J., Zheng, D., Mam, K., Tam, P., Fan, S.T., Xu, R., 2003. TRAIL: a potential agent for cancer therapy. *Curr. Mol. Med.* 3, 727–736.
- Shiau, C.W., Huang, J.W., Wang, D.S., Weng, J.R., Yang, C.C., Lin, C.H., Li, C., Chen, C.S., 2006. α -Tocopheryl succinate induces apoptosis in prostate cancer cells in part through inhibition of Bcl-x_L/Bcl-2 function. *J. Biol. Chem.* 281, 1125–1189.
- Shoshan-Barmatz, V., Israelson, A., Brdiczka, D., Sheu, S.S., 2006. The voltage-dependent anion channel (VDAC): function in intracellular signalling, cell life and cell death. *Curr. Pharm. Des.* 12, 2249–2270.
- Shun, M.C., Yu, W., Gapor, A., Parsons, R., Atkinson, J., Sanders, B.G., Kline, K., 2004. Pro-apoptotic mechanisms of action of a novel vitamin E analog (α -TEA) and a naturally occurring form of vitamin E (δ -tocotrienol) in MDA-MB-435 human breast cancer cells. *Nutr. Cancer* 48, 95–105.
- Sionov, R.V., Haupt, Y., 1999. The cellular response to p53: the decision between life and death. *Oncogene* 18, 6145–6157.
- Slamon, D.J., Godolphin, W., Jones, L.A., Holt, J.A., Wong, S.G., Keith, D.E., Levin, W.J., Stuart, S.G., Udove, J., Ullrich, A., 1989. Studies of the HER-2/neu proto-oncogene in human breast and ovarian cancer. *Science* 244, 707–712.
- Smith, R.A., Porteous, C.M., Gane, A.M., Murphy, M.P., 2003. Delivery of bioactive molecules to mitochondria in vivo. *Proc. Natl. Acad. Sci. USA* 100, 5407–5412.
- Somersan, S., Larsson, M., Fonteneau, J.F., Basu, S., Srivastava, P., Bhardwaj, N., 2001. Primary tumor tissue lysates are enriched in heat shock proteins and induce the maturation of human dendritic cells. *J. Immunol.* 167, 4844–4852.
- Srivastava, P., 2002. Interaction of heat shock proteins with peptides and antigen presenting cells: chaperoning of the innate and adaptive immune responses. *Annu. Rev. Immunol.* 20, 395–425.

- Stapelberg, M., Tomasetti, M., Gellert, N., Alleva, R., Procopio, A., Neuzil, J., 2004. α -Tocopheryl succinate inhibits proliferation of mesothelioma cells by differential down-regulation of fibroblast growth factor receptors. *Biochem. Biophys. Res. Commun.* 318, 636–641.
- Stapelberg, M., Gellert, N., Swettenham, E., Tomasetti, M., Witting, P.K., Procopio, A., Neuzil, J., 2005. α -Tocopheryl succinate inhibits malignant mesothelioma by disrupting the FGF autocrine loop: the role of oxidative stress. *J. Biol. Chem.* 280, 25369–25376.
- Steele, A.J., Jones, D.T., Ganeshaguru, K., Duke, V.M., Yogashangary, B.C., North, J.M., Lowdell, M.W., Kottaridis, P.D., Mehta, A.B., Prentice, A.G., Hoffbrand, A.V., Wickremasinghe, R.G., 2006. The sesquiterpene lactone parthenolide induces selective apoptosis of B-chronic lymphocytic leukemia cells in vitro. *Leukemia* 20, 1073–1079.
- Sun, Y., Oberley, L.W., 1996. Redox regulation of transcriptional activators. *Free Radic. Biol. Med.* 21, 335–348.
- Sun, F., Huo, X., Zhai, Y., Wang, A., Xu, J., Su, D., Bartlam, M., Rao, Z., 2005. Crystal structure of mitochondrial respiratory membrane protein complex II. *Cell* 121, 1043–1057.
- Susin, S.A., Lorenzo, H.K., Zamzami, N., Marzo, I., Snow, B.E., Brothers, G.M., Mangion, J., Jacotot, E., Costantini, P., Loeffler, M., Larochette, N., Goodlett, D.R., Aebbersold, R., Siderovski, D.P., Penninger, J.M., Kroemer, G., 1999. Molecular characterization of mitochondrial apoptosis-inducing factor. *Nature* 397, 441–446.
- Swettenham, E., Witting, P.K., Salvatore, B.A., Neuzil, J., 2005. α -Tocopheryl succinate selectively induces apoptosis in neuroblastoma cells: potential therapy of malignancies of the nervous system? *J. Neurochem.* 94, 1448–1456.
- Swettenham, E., Eliasson, J., Low, P., Wang, X.F., Gold, M., Witting, P.K., Dong, L.F., Turanek, J., Akporiaye, E.T., Ralph, S.J., Neuzil, J., submitted for publication. Vitamin E succinate inhibits angiogenesis by selective apoptosis induction in proliferating endothelial cells.
- Teng, X.W., Davies, N.M., Fukuda, Ch., Good, R.L., Faris, M.W., 2005. Pharmacokinetics and tissue distribution of d- α -tocopheryl succinate formulations following intravenous administration in the rat. *Biopharm. Drug Dispos.* 26, 195–203.
- Tinhofer, I., Bernhard, D., Senfter, M., Anether, G., Loeffler, M., Kroemer, G., Kofler, R., Csordas, A., Greil, R., 2001. Resveratrol, a tumor-suppressive compound from grapes, induces apoptosis via a novel mitochondrial pathway controlled by Bcl-2. *FASEB J.* 15, 1613–1615.
- Todryk, S., Melcher, A.A., Hardwick, N., Linardakis, E., Bateman, A., Colombo, M.P., Stoppacciano, A., Vile, R.G., 1999. Heat shock protein 70 induced during tumor cell killing induces Th1 cytokines and targets immature dendritic cell precursors to enhance antigen uptake. *J. Immunol.* 163, 1398–1408.
- Tomasetti, M., Gellert, N., Procopio, A., Neuzil, J., 2004a. A vitamin E analogue suppresses malignant mesothelioma in a pre-clinical model: a prototype of a future drug against a fatal neoplastic disease? *Int. J. Cancer* 109, 641–642.
- Tomasetti, M., Rippo, M.R., Alleva, R., Moretti, S., Andera, L., Neuzil, J., Procopio, A., 2004b. α -Tocopheryl succinate and TRAIL selectively synergise in induction of apoptosis in human malignant mesothelioma cells. *Br. J. Cancer* 90, 1644–1653.
- Tomasetti, M., Andera, L., Alleva, R., Borghi, B., Neuzil, J., Procopio, A., 2006. α -Tocopheryl succinate induces DR4 and DR5 expression by a p53-dependent route: implication for sensitisation of resistant cancer cells to TRAIL apoptosis. *FEBS Lett.* 580, 1925–1931.
- Tomic-Vatic, A., EyTina, J., Chapman, J., Mahdavian, E., Neuzil, J., Salvatore, B.A., 2005. Vitamin E amides, a new class of vitamin E analogues with enhanced proapoptotic activity. *Int. J. Cancer* 117, 188–193.
- Trachootham, D., Zhou, Y., Zhang, H., Demizu, Y., Chen, Z., Pelicano, H., Chiao, P.J., Achanta, G., Arlinghaus, R.B., Liu, J., Huang, P., 2006. Selective killing of oncogenically transformed cells through a ROS-mediated mechanism by beta-phenylethyl isothiocyanate. *Cancer Cell.* 10, 241–252.
- Trapp, S., Horobin, R.W., 2005. A predictive model for the selective accumulation of chemicals in tumor cells. *Eur. Biophys. J.* 34, 959–966.
- Turley, J.M., Ruscetti, F.W., Kim, S.J., Fu, T., Gou, F.V., Birchenall-Roberts, M.C., 1997. Vitamin E succinate inhibits proliferation of BT-20 human breast cancer cells: increased binding of cyclin A negatively regulates E2F transactivation activity. *Cancer Res.* 57, 2668–2675.

- Tzung, S.P., Kim, K.M., Basanez, G., Giedt, C.D., Simon, J., Zimmerberg, J., Zhang, K.Y., Hockenbery, D.M., 2001. Antimycin A mimics a cell-death-inducing Bcl-2 homology domain 3. *Nat. Cell Biol.* 3, 183–191.
- Ullukan, H., Swaan, W., 2002. Camptothecins: a review of their chemotherapeutic potential. *Drugs* 62, 2039–2057.
- van Delft, M.F., Wei, A.H., Mason, K.D., Vandenberg, C.J., Chen, L., Czabotar, P.E., Willis, S.N., Scott, C.L., Day, C.L., Cory, S., Adams, J.M., Roberts, A.W., Huang, D.C., 2006. The BH3 mimetic ABT-737 targets selective Bcl-2 proteins and efficiently induces apoptosis via Bak/Bax if Mcl-1 is neutralized. *Cancer Cell* 10, 389–399.
- Verhagen, A.M., Ekert, P.G., Pakusch, M., Silke, J., Connolly, L.M., Reid, G.E., Moritz, R., Simpson, R.J., Vaux, D.L., 2000. Identification of DIABLO, a mammalian protein that promotes apoptosis by binding to and antagonizing IAP proteins. *Cell* 102, 43–53.
- Vermelen, K., Berneman, Z.N., Van Bockstaele, D.R., 2003. Cell cycle and apoptosis. *Cell Prolif.* 36, 165–175.
- Verrier, F., Deniaud, A., Lebras, M., Metivier, D., Kroemer, G., Mignotte, B., Jan, G., Brenner, C., 2004. Dynamic evolution of the adenine nucleotide translocase interactome during chemotherapy-induced apoptosis. *Oncogene* 23, 8049–8064.
- Verschraegen, C.F., Gupta, E., Loyer, E., Kavanagh, J.J., Kudelka, A.P., Freedman, R.S., Edwards, C.L., Harris, N., Steger, M., Steltz, V., Giovannella, B.C., Stehlin, J.S., 1999. A phase II clinical and pharmacological study of oral 9-nitrocamptothecin in patients with refractory epithelial ovarian, tubal or peritoneal cancer. *Anticancer Drug* 10, 375–383.
- Vivanco, L., Sawyers, C.L., 2002. The phosphatidylinositol 3-kinase AKT pathway in human cancer. *Nat. Rev. Cancer* 2, 489–501.
- Vysokikh, M., Zorova, L., Zorov, D., Heimlich, G., Jurgensmeier, J., Schreiner, D., Brdiczka, D., 2004. The intra-mitochondrial cytochrome *c* distribution varies correlated to the formation of a complex between VDAC and the adenine nucleotide translocase: this affects Bax-dependent cytochrome *c* release. *Biochim. Biophys. Acta* 1644, 27–36.
- Walczak, H., Miller, R.E., Ariail, K., Gliniak, B., Griffith, T.S., Kubin, M., Chin, W., Jones, J., Woodward, A., Le, T., Smith, C., Smolak, P., Goodwin, R.G., Rauch, C.T., Schuh, J.C., Lynch, D.H., 1999. Tumoricidal activity of tumor necrosis factor-related apoptosis-inducing ligand in vivo. *Nat. Med.* 5, 157–163.
- Wang, X.F., Witting, P.K., Salvatore, B.A., Neuzil, J., 2005. α -Tocopheryl succinate induces apoptosis in HER2/erbB2-overexpressing breast cancer cells by signalling via the mitochondrial pathway. *Biochem. Biophys. Res. Commun.* 326, 282–289.
- Wang, X.F., Dong, L.F., Zhao, Y., Tomasetti, M., Wu, K., Neuzil, J., 2006. Vitamin E analogues as anti-cancer agents: Lessons from studies with α -tocopheryl succinate. *Molecular Nutrition and Food Research* 50, 675–685.
- Wang, X.F., Birringer, M., Dong, L.F., Veprek, P., Low, P., Swettenham, E., Stanic, M., Yuan, L.H., Zabolova, R., Wu, K., Ralph, S.J., Ledvina, M., Neuzil, J., 2007. A peptide adduct of vitamin E succinate targets breast cancer cells with high erbB2 expression. *Cancer Res.* 67, 3337–3344.
- Weber, T., Lu, M., Andera, L., Lahm, H., Gellert, N., Fariss, M.W., Korinek, V., Sattler, W., Ucker, D.S., Terman, A., Schröder, A., Erl, W., Brunk, U., Coffey, R.J., Weber, C., Neuzil, J., 2002. Vitamin E succinate is a potent novel anti-neoplastic agent with high tumor selectivity and cooperativity with tumor necrosis factor-related apoptosis-inducing ligand (TRAIL, Apo2L) in vivo. *Clin. Cancer Res.* 8, 863–869.
- Weber, T., Dalen, H., Andera, L., Nègre-Salvayre, A., Augé, N., Sticha, M., Loret, A., Terman, A., Witting, P.K., Higuchi, M., Plasilova, M., Zivny, J., Gellert, N., Weber, C., Neuzil, J., 2003. Mitochondria play a central role in apoptosis induced by α -tocopheryl succinate, an agent with anticancer activity. Comparison with receptor-mediated pro-apoptotic signaling. *Biochemistry* 42, 4277–4291.
- Weller, M., 1998. Predicting response to cancer chemotherapy: the role of p53. *Cell Tissue Res.* 292, 435–445.

- Welte, T., Koch, F., Schuler, G., Lechner, J., Doppler, W., Heufer, C., 1996. Interleukin-12 is produced by dendritic cells and mediates T helper 1 development as well as interferon- γ production by T helper 1 cells. *Eur. J. Immunol.* 26, 659–668.
- Wen, J., You, K.R., Lee, S.Y., Song, C.H., Kim, D.G., 2002. Oxidative stress-mediated apoptosis. The anticancer effect of the sesquiterpene lactone parthenolide. *J. Biol. Chem.* 277, 38954–38964.
- Wiley, S.R., Schooley, J.K., Smolak, P.J., Din, W.S., Huang, C.P., Nicholl JK Sutherland, G.R., Smith, T.D., Rauch, C., Smith, C.A., 1995. Identification and characterization of a new member of the TNF family that induces apoptosis. *Immunity* 3, 673–682.
- Wolvetang, E.J., Johnson, K.L., Krauer, K., Ralph, S.J., Linnane, A.W., 1994. Mitochondrial respiratory chain inhibitors induce apoptosis. *FEBS Lett.* 339, 40–44.
- Wu, K., Zhao, Y., Li, G.C., Yu, W.P., 2004. c-Jun N-terminal kinase is required for vitamin E succinate-induced apoptosis in human gastric cancer cells. *World J. Gastroenterol.* 10, 1110–1114.
- Xiao, D., Lew, K.L., Zeng, Y., Xiao, H., Marynowski, S.W., Dhir, R., Singh, S.V., 2006. Phenethyl isothiocyanate-induced apoptosis in PC-3 human prostate cancer cells is mediated by reactive oxygen species-dependent disruption of the mitochondrial membrane potential. *Carcinogenesis* 27, 2223–2234.
- Xu, K., Thornalley, P.J., 2001. Involvement of glutathione metabolism in the cytotoxicity of the phenethyl isothiocyanate and its cysteine conjugate to human leukaemia cells in vitro. *Biochem. Pharmacol.* 61, 165–177.
- Xu, R.H., Pelicano, H., Zhou, Y., Carew, J.S., Feng, L., Bhalla, K.N., Keating, M.J., Huang, P., 2005. Inhibition of glycolysis in cancer cells: a novel strategy to overcome drug resistance associated with mitochondrial respiratory defect and hypoxia. *Cancer Res.* 65, 613–621.
- Yamamoto, S., Tamai, H., Ishisaka, R., Kanno, T., Arita, K., Kobuchi, H., Utsumi, K., 2003. Mechanism of α -tocopheryl succinate-induced apoptosis of promyelocytic leukemia cells. *Free Radic. Res.* 33, 407–418.
- Youk, H.J., Lee, E., Choi, M.-K., Lee, Y.J., Chung, J.H., Kim, S.H., Lee, C.H., Lim, S.J., 2005. Enhanced anticancer efficacy of α -tocopheryl succinate by conjugation with polyethylene glycol. *J. Contr. Release* 107, 43–52.
- Yu, W., Israel, K., Liao, Q.Y., Aldaz, C.M., Sanders, B.G., Kline, K., 1999. Vitamin E succinate (VES) induces Fas sensitivity in human breast cancer cells: role for Mr 43,000 Fas in VES-triggered apoptosis. *Cancer Res.* 59, 953–961.
- Yu, W., Liao, Q.Y., Hantash, F.M., Sanders, B.G., Kline, K., 2001. Activation of extracellular signal-regulated kinase and c-Jun-NH₂-terminal kinase but not p38 mitogen-activated protein kinases is required for RRR- α -tocopheryl succinate-induced apoptosis of human breast cancer cells. *Cancer Res.* 61, 6569–6576.
- Yu, W., Sanders, B.G., Kline, K., 2003. RRR- α -tocopheryl succinate-induced apoptosis of human breast cancer cells involves Bax translocation to mitochondria. *Cancer Res.* 63, 2483–2491.
- Zalk, R., Israelson, A., Garty, E.S., Azoulay-Zohar, H., Shoshan-Barmatz, V., 2005. Oligomeric states of the voltage-dependent anion channel and cytochrome *c* release from mitochondria. *Biochem. J.* 386, 73–83.
- Zhang, Z.Y., Davis, J.P., Van Etten, R.L., 1992. Covalent modification and active site-directed inactivation of a low molecular weight phosphotyrosyl protein phosphatase. *Biochemistry* 31, 1701–1711.
- Zhang, S., Lawson, K.A., Simmons-Menchaca, M., Sun, L.Z., Sanders, B.G., Kline, K., 2004. Vitamin E analog α -TEA and celecoxib alone and together reduce human MDA-MB-435-FL-GFP breast cancer burden and metastasis in nude mice. *Breast Cancer Res. Treat.* 87, 111–121.
- Zheng, J., Ramirez, V.D., 1999. Picetannol, a stilbene phytochemical, inhibits mitochondrial F0F1-ATPase activity by targeting the F1 complex. *Biochem. Biophys. Res. Commun.* 261, 499–503.
- Zhou, B.P., Hung, M.C., 2003. Dysregulation of cellular signalling by HER2/neu in breast cancer. *Semin. Oncol.* 30, 38–48.
- Zhou, L., Jing, Y., Styblo, M., Chen, Z., Waxman, S., 2005. Glutathione-S-transferase pi inhibits As2O3-induced apoptosis in lymphoma cells: involvement of hydrogen peroxide catabolism. *Blood* 105, 1198–1203.

- Zini, R., Morin, C., Bertelli, A., Bertelli, A.A., Tillement, J.P., 1999. Effects of resveratrol on the rat brain respiratory chain. *Drugs Exp. Clin. Res.* 25, 87–97.
- Zou, H., Li, Y., Liu, X., Wang, X., 1999. An APAF-1 cytochrome *c* multimeric complex is a functional apoptosome that activates pro-caspase-9. *J. Biol. Chem.* 274, 11549–11556.
- Zu, K., Hawthorn, L., Ip, C., 2005. Up-regulation of c-Jun-NH2-kinase pathway contributes to the induction of mitochondria-mediated apoptosis by α -tocopheryl succinate in human prostate cancer cells. *Mol. Cancer Ther.* 4, 43–50.
- Zunino, S.J., Storms, D.H., 2006. Resveratrol-induced apoptosis is enhanced in acute lymphoblastic leukemia cells by modulation of the mitochondrial permeability transition pore. *Cancer Lett.* 240, 123–134.

2.2.4. Surfaktanty na bázi fluorovaných uhlovodíků se sacharidovou doménou

Tyto látky byly studovány zprvu jako nový typ surfaktantů pro potřeby polymerní chemie a katalýzy. Jejich případné budoucí použití ve farmakologii a medicíně záviselo od jejich biokompatibility. Některé s těchto parciálně fluorovaných látek se jeví na základě in vitro testů jako potenciálně použitelné ve farmakologii a jsou v současnosti testovány jako vhodná sonda pro in vivo zobrazování pomocí magnetické resonance (MRI). Liposomální formulace jsou využitelné pro značení buněk a jejich přesné lokalizace pomocí MRI při buněčné terapii mozkových mrtvic, infarktů a nádorů. Připravujeme také značené liposomy pro studium jejich biodistribuce a lokalizace v místě nádorů.

Tato oblast je relativně velmi nová a biomedicíncké aplikace zatím nejsou doloženy relevantními publikacemi. Publikované práce se týkají zejména studia biokompatibility s využitím in vitro testů a studia fyzikálně-chemických vlastností těchto nových surfaktantů. Dlouhodobá spolupráce v této oblasti probíhá s prof. Lehmlerem z USA.

Synthesis and biocompatibility evaluation of partially fluorinated pyridinium bromides

Sandhya M. Vyas,^a Jaroslav Turánek,^b Pavlína Knötigová,^b Andrea Kašná,^b Veronika Kvardová,^b Venkat Koganti,^c Stephen E. Rankin,^c Barbara L. Knutson^c and Hans-Joachim Lehmler^{*a}

Received (in St Louis, MO, USA) 11th November 2005, Accepted 3rd April 2006

First published as an Advance Article on the web 26th April 2006

DOI: 10.1039/b516039a

Although cationic surfactants are of general interest for a variety of consumer and biomedical applications, only a limited number of partially fluorinated, single-tailed, cationic surfactants have been synthesized. To study the potential usefulness of fluorinated cationic surfactants for these applications we synthesized a series of partially fluorinated pyridinium bromide surfactants. Three 10-perfluoroalkyldecyl pyridinium surfactants were synthesized by coupling a perfluoroalkyl iodide with 9-decene-1-yl acetate using an AIBN mediated radical reaction. The resulting 9-iodo-10-perfluoroalkyldec-1-yl acetates were deiodinated using HI–Zn–EtOH and hydrolyzed using KOH–EtOH to yield the corresponding 10-perfluoroalkyldecanol. The partially fluorinated alcohol was converted into the bromide using Br₂–PPH₃. Alkylation of excess pyridine with the bromides gave the desired 10-perfluoroalkyldecyl pyridinium bromides in good yields. Three 10-perfluoroalkylundecyl surfactants were synthesized using a similar approach with 10-undecenoic acid methyl ester as starting material. Based on an initial *in vitro* toxicity assessment, the toxicity of the partially fluorinated pyridinium surfactants was slightly lower or comparable to benzalkonium chloride, a typically cationic surfactant (with IC₅₀s of tested compounds ranging from 5 to 15 μM). An increase in the length and/or the degree of fluorination of the hydrophobic tail correlated with a mild decrease of cytotoxicity and haemolytic activity. Partially fluorinated pyridinium surfactants may, therefore, be useful for biomedical applications such as components for novel gene and drug delivery systems.

Introduction

Fluorinated surfactants are highly surface active, display weak intermolecular interactions, and typically have only low acute toxicity, properties which make them highly suitable for a large number of technical and, potentially, biomedical applications.¹ Because of these unique properties there is, for example, considerable interest in fluorinated cationic surfactants as templates for the synthesis of ordered porous ceramics.^{2–7} Other ongoing research is focusing on the use of fluorinated surfactants in biomedical applications.^{8,9} Single tailed partially fluorinated surfactants with a variety of non-ionic or zwitterionic head groups, for example carnitine,¹⁰ morpholinophosphate,¹¹ phosphocholine,¹² pyridinium,^{2–7} and carbohydrate^{13–16} head groups, have been synthesized. In contrast to their hydrocarbon counterparts, many partially fluorinated surfactants, especially surfactants with a high degree of fluorination, display low or moderate toxicity in *in vitro* and *in vivo* studies and are, thus, considered to be biocompatible.

Although hydrocarbon cationic surfactants such as benzalkonium chloride (BAC) and hexadecylpyridinium chloride are of considerable interest for a broad range of consumer and biomedical applications (for example, antimicrobial agents in mouthwashes,^{17,18} ophthalmic and contact lens solutions¹⁸ and novel cationic gene or drug delivery systems^{19–21}) only a small number of fluorinated cationic surfactants have been synthesized and their biocompatibility assessed. More work is, therefore, needed to determine how the biocompatibility of a partially fluorinated, cationic surfactant is different from its hydrocarbon analogue and how structural features, for example the chain-length and the degree of fluorination of the hydrophobic tail, influence a surfactant's biocompatibility. The aim of this work was to develop an efficient synthetic route to partially fluorinated pyridinium surfactants and to perform an initial toxicity assessment to test their potential usefulness for novel drug delivery systems and other biomedical applications.

Results and discussion

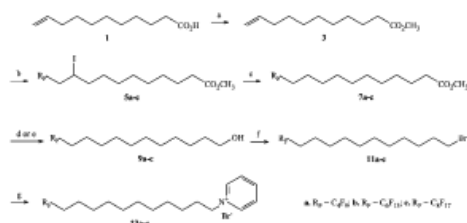
Synthesis

Most partially fluorinated compounds are not available from commercial sources. One crucial step in the synthesis of any partially fluorinated surfactants is, therefore, the synthesis of a functionalized partially fluorinated alkyl chain. Such partially

^a Department of Occupational and Environmental Health, University of Iowa, Iowa City, IA 52242, USA. E-mail: hans-joachim-lehmler@uiowa.edu; Fax: (+1) 3193354290; Tel: (+1) 3193354211

^b Veterinary Research Institute, Department of Immunology, Hudcova 70, 621 33 Brno, Czech Republic

^c Chemicals and Materials Engineering Department, University of Kentucky, Lexington, KY 40536, USA



Scheme 1 a. CH_3OH , PTSA, toluene, Δ ; b. R_FI , AIBN, Δ ; c. HI (55%), Zn, $\text{C}_2\text{H}_5\text{OH}$, Δ ; d. (i) CH_3OH , KOH, Δ , (ii) LiAlH_4 , anhydrous ether, ambient temperature; e. LiAlH_4 , anhydrous ether, ambient temperature; f. PPh_3 , Br_2 , DCM, ambient temperature; g. pyridine, Δ .

fluorinated alkyl moieties are typically synthesized by the coupling of a perfluorinated iodide with an ω -unsaturated hydrocarbon precursor in an AIBN mediated radical reaction.^{22–25} We have utilized this approach to synthesize a series of terminally fluorinated pyridinium bromides.

As shown in Schemes 1 and 2, the iodo methyl esters **5a–c** or iodoacetates **6a–c** were synthesized using this reaction from undecenoic methyl ester **3** or decenol acetate **4**, respectively. Addition of AIBN in multiple portions was a key factor in this reaction. The secondary iodides **5a–c** or **6a–c** were deiodinated using HI–Zn–EtOH without further purification. Hydroiodic acid and zinc were chosen because both reagents are easy to handle and less toxic compared to tributyltin hydride,²⁴ which is typically employed in similar deiodination reactions.

As shown in Scheme 1, the series of methyl esters **7a–c** was converted into the corresponding alcohols **9a–c** by two different routes. Initially the esters **7a–c** were converted into the corresponding, R_F -substituted (*i.e.* partially fluorinated) undecanoic acids²² which were subsequently reduced to the alcohols **9a–c** with lithium aluminium hydride in anhydrous ether (reaction condition **d** in Scheme 1). This approach was chosen because the partially fluorinated acids can be more easily purified by recrystallization from hexanes compared to structurally related partially fluorinated alcohols,^{22,23} thus allowing one to perform the synthesis on a large (100 gram) scale. To further improve the overall yield of the alcohols we optimized the direct reduction of the methyl ester **7a–c** with lithium aluminium hydride (reaction condition **e** in Scheme 1). The direct reduction of the esters **7a–c** increased the yield of



Scheme 2 a. DMAP, AcCl, pyridine, DCM; b. R_FI , AIBN, Δ ; c. HI (55%), Zn, $\text{C}_2\text{H}_5\text{OH}$, Δ ; d. CH_3OH , KOH, Δ ; e. PPh_3 , Br_2 , DCM, ambient temperature; f. pyridine, Δ .

the alcohols **9a–c** from approximately 60% to 70%. In the case of the acetate series, the alcohols **10a–c** were obtained by hydrolysis of the acetate followed by recrystallization from hexane.²³ Typical overall yields of the alcohols **10a–c** were 65–85%.

The alcohols **9a–c** and **10a–c** were brominated using triphenylphosphine and bromine similar to the procedure reported by Naud and co-workers.²⁴ Bromination of the alcohols **9a–c** and **10a–c** with $\text{HBr}/\text{H}_2\text{SO}_4$ also yielded the desired partially fluorinated bromides, but this approach was abandoned because the purification of the bromides is tedious and the yields are low. In the final step of the synthesis excess pyridine and the respective bromides were heated under reflux to yield the corresponding pyridinium bromides **13a–c** and **14a–c**.²⁶

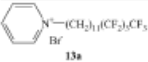
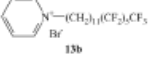
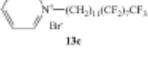
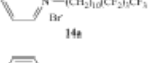
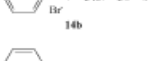
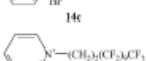
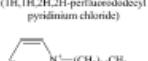
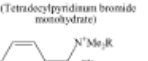
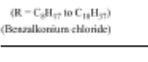
The ^1H NMR spectra of most of the pyridinium bromides showed one singlet around $\delta = 3.1$ ppm which was not related to any group in the compound. The chemical shift of this peak was not consistent, thus suggesting that, like their hydrocarbon analogues, several of the partially fluorinated pyridinium salts form stable monohydrates. This interpretation of the ^1H NMR spectra was further confirmed by D_2O exchange experiments. In addition, the results from the combustion analysis experiments confirm the presence of one water molecule in the pyridinium salts **13a** and **14a–c**.

Cytotoxicity and haemolytic assessments

Despite their importance for a variety of consumer and biomedical applications, only limited information about the toxicity of cationic surfactants, especially fluorinated cationic surfactants, is available.¹⁸ An initial cytotoxicity assessment of all six pyridinium surfactants was therefore performed using the A2780 ovarian carcinoma cell line.²⁷ The IC_{50} values of the pyridinium salts and several other surfactants are summarized in Tables 1 and 2, respectively. The partially fluorinated pyridinium surfactants (**13a–c** and **14a–c**) were highly toxic in the A2780 cancer cell line with IC_{50} values ranging from 5 to 15 μM . These IC_{50} values are comparable to IC_{50} values of typical anticancer agents, *e.g.* platinum complexes.²⁷ The most toxic compounds **13a** and **14a** were also bactericidal against *Salmonella typhimurium* (results not shown). Overall, the low IC_{50} values of **13a–c** and **14a–c** are in agreement with a previous report that highly fluorinated 1*H*,1*H*,2*H*,2*H*,3*H*,3*H*-perfluoroundecyltrialkylammonium salts are toxic in Namalva lymphoblastoid cells with IC_{50} s below 0.16 mM.²⁸

The short-chain pyridinium salts **13a** and **14a** were the most toxic surfactants in this series with toxicities comparable with BAC. Similar results were obtained with several other cell lines (data not shown). The increase in the length of the partially fluorinated tail caused a mild decrease in cytotoxicity, thus suggesting that the toxicity of cationic surfactants can be reduced by introducing a certain degree of fluorination. This hypothesis is further supported by the observation that the partially fluorinated pyridinium surfactant **14a** was less toxic compared to its hydrocarbon analogue tetradecylpyridinium bromide. This hydrocarbon surfactant was the most toxic compound investigated in our study. 1*H*,1*H*,2*H*,2*H*-perfluorododecylpyridinium chloride, a highly fluorinated pyridinium surfactant with a slightly shorter hydrophobic tail compared

Table 1 Haemolytic and cytotoxicity assessment of the partially fluorinated pyridinium bromides **13a–c** and **14a–c** and related cationic fluorocarbon and hydrocarbon surfactants in the A2780 cell line

Compound	A2780 cell line IC ₅₀ [μM]	Haemolysis PBS [μM]	Haemolysis PBS + 20% FBS [μM]
 13a	7.97	62.5	250
 13b	11.1	62.5	250
 13c	14.7	62.5	125
 14a	4.9	62.5	250
 14b	9.3	62.5	125
 14c	11.7	62.5	125
 (1H,1H,2H,2H-perfluorododecyl pyridinium chloride)	31.4	250	>500
 (Tetradecylpyridinium bromide monohydrate)	2.3	62.5	250
 (R = C ₈ H ₁₇ to C ₁₄ H ₂₉) (Benzalkonium chloride)	5.3	125	400


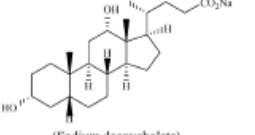
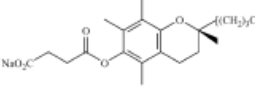
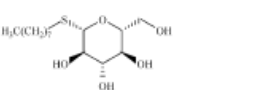
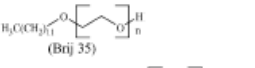
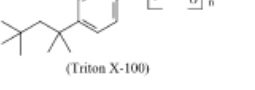
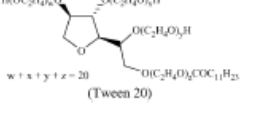
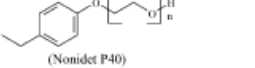
to **14a**, was the least toxic cationic surfactant, an observation that also suggests that an increased degree of fluorination may decrease the cytotoxicity of pyridinium surfactants.

In agreement with previous studies,¹⁸ the partially fluorinated cationic surfactants **13a–c** and **14a–c** (Table 1) were much more toxic compared to typical anionic surfactants and several non-ionic surfactants with a hydrocarbon tail (Table 2). Some non-ionic surfactants, e.g. Triton X-100 or Nonidet P40, were also toxic towards A2780 cells in a range comparable to that of the partially fluorinated pyridinium surfactants. The mechanisms of the relatively high toxicity of cationic surfactants in general and of the partially fluorinated surfactants **13a–c** and **14a–c** in particular most likely involve a disruption of the integrity of the cell membrane. This hypothesis is supported by the fact that the partially fluorinated surfactants are equally toxic in several cell lines and in bacteria, e.g. *Salmonella typhimurium* (data not shown).

Because of the potential biomedical use of the partially fluorinated surfactants **13a–c** and **14a–c** we also investigated their haemolytic activity on rabbit red blood cells in both PBS

and PBS containing 20% fetal bovine serum. As with the cytotoxicity, it is well established that the *in vitro* haemolytic activity of fluorinated surfactants on red blood cells dramatically decreases with increasing degree of fluorination and increasing length of the fluorinated hydrophobic tail.^{11–14,29–31} In contrast, the haemolytic activity of hydrocarbon surfactants typically increases with increasing chain length. The pyridinium surfactants showed significantly stronger haemolytic activity than BAC (Table 1) and the anionic and non-ionic surfactants (Table 2) investigated. This observation is in agreement with the strong haemolytic activity reported for highly fluorinated trialkylammonium salts.³⁵ The lowest concentration of the pyridinium surfactants at which haemolytic activity was observed did not appear to depend on the degree of fluorination and/or the length of the hydrophobic tail. One exception was the highly fluorinated 1H,1H,2H,2H-perfluorododecylpyridinium chloride which exhibited haemolytic activity at concentrations comparable to several anionic and non-ionic surfactants, thus suggesting that, in contrast to the cytotoxicity studies, a significant degree of fluorination may

Table 2 Haemolytic and cytotoxicity assessment of typical anionic and non-ionic surfactants in the A2780 cell line

Compound	A2780 cell line IC ₅₀ [μM]	Haemolysis PBS [μM]	Haemolysis PBS + 20% FBS [μM]
 (Sodium dodecylsulphate)	294	250	>1000
 (Sodium deoxycholate)	243	> 1000	>1000
 (α-tocopheryl succinate)	56	300	> 500
 (Octylthioglucoiside)	680	500	> 500
 (Brij 35)	68	125	>1000
 (Triton X-100)	22.3	830	>1000
 (Tween 20) $w + x + y + z = 20$	260	> 1000	>1000
 (Nonidet P40)	11.2	400	830

be necessary before a protective effect against haemolysis can be observed.

Conclusion

These findings suggest that partial fluorination of the hydrophobic tail of pyridinium and other cationic surfactants may reduce their toxicity and haemolytic activity. This observation is comparable to single tailed non-ionic and zwitterionic surfactants, where partial fluorination of the hydrophobic tail results in a reduction of the toxicity compared to the hydrocarbon analogue. Despite their cytotoxicity, cationic surfactant-lipids are used for the construction of synthetic delivery systems, *e.g.* liposomes, for transfection of cells by DNA/RNA constructs.³² Fluorinated, cationic surfactants may,

therefore, be useful for biomedical applications such as components for novel gene and drug delivery systems.

Experimental

Perfluorinated iodides were purchased from Oakwood Chemical Co. (West Columbia, South Carolina, USA) and used as received. Long-chain hydrocarbon starting materials were purchased from TCI Chemicals (Portland, Oregon, USA). Anhydrous solvents were purchased from Fisher Scientific (Fairlawn, New Jersey, USA). All the ¹H NMR spectra were recorded in CDCl₃ on a multinuclear Bruker Avance 300 Digital NMR spectrometer at 297 K; all chemical shifts are reported in parts per million (ppm) relative to internal tetramethylsilane (Me₄Si), with the residual solvent proton

resonance as internal standard. Coupling constants are given in hertz (Hz). ^{19}F chemical shifts were determined using CFCl_3 as internal standard. Melting points were determined using a Thermal Analysis 2920 Differential Scanning Instrument. Thermograms were recorded using a heating rate of 20°min^{-1} from 20 to 230°C and the temperature maxima of the main phase transitions after one DSC run were determined.²² Mass spectra on non-ionic intermediates were measured at the University of Iowa Mass Spectrometry Facility using a Voyager GC-MS instrument operated at 70 eV in the electron impact mode. The reported fragment peaks correspond to the most abundant ions, in addition to the parent ion(s). Mass spectra of pyridinium salts were recorded at the University of Kentucky Mass Spectrometry Facility using a Bruker Autoflex time-of-flight mass spectrometer equipped with MALDI. Microanalytical data were obtained from Atlantic Micro Lab Microanalysis Service (Atlanta, Georgia, USA). IR spectra were measured with a Thermo Nicolet Nexus 470 FT-IR spectrophotometer.

AIBN mediated coupling reaction (general procedure)

The radical addition of R_fI to undecenoic methyl ester **3**³³ or decenol acetate **4**³⁴ in the presence of AIBN was performed following literature procedures.^{23,35,36} The alkenoic acid methyl ester **3** (98 g, 0.5 mol) or alkenol acetate **4** (91 g, 0.5 mol) and a perfluorinated iodide R_fI ($\text{R}_f = \text{C}_4\text{F}_9$, C_6F_{13} , C_8F_{17} , 0.55 mol) were placed in a 500 ml round bottomed flask equipped with a reflux condenser. The radical initiator AIBN (2 mol%) was added. The reaction mixture was heated to 90°C under stirring. After 30 min, the flask was cooled to room temperature, and another portion of AIBN (2 mol%) was added. The stirred solution was again heated to 90°C , and the entire process was repeated at least two additional times; 3 h were allowed to pass after the final addition of AIBN. The progress of the reaction was monitored by GC and ^1H NMR spectroscopy of small aliquots collected between AIBN additions. The flask was cooled to room temperature, and the crude iodo methyl esters **5a-c** or iodoacetates **6a-c** were used in the next step without further purification.

Terminally perfluorinated esters **7a-c** and acetates **8a-c** (general procedure)

The crude secondary iodides **5a-c** or **6a-c** were dissolved in 150 ml of $\text{C}_2\text{H}_5\text{OH}$ and hydroiodic acid (non-stabilized, 55%, 35 ml, 1.5 mol) was added. Zinc dust (97 g, 1.5 mol) was added very slowly at 0°C . The mixture was refluxed for 6 h and then filtered. The filtrate was evaporated to dryness and re-dissolved in diethyl ether (ca. 200 ml). The solution was washed with water (2×100 ml), saturated aqueous NaHCO_3 solution (1×100 ml), and brine (1×100 ml), and then dried over MgSO_4 . Removal of the solvent afforded the crude terminally fluorinated ester **7a-c** or acetate **8a-c**. The complete conversion was confirmed by ^1H NMR spectroscopy and GC.

Hydrolysis of **7a-c** and **8a-c** (general procedure)

The partially fluorinated esters **7a-c** or acetates **8a-c** were dissolved in 150 ml of $\text{C}_2\text{H}_5\text{OH}$. To this KOH (57 g, 1.5 mol) was added slowly. The reaction mixture was refluxed for six

hours under stirring. After complete conversion it was cooled to 0°C and water was added dropwise. The mixture was acidified with 2N H_2SO_4 and extracted with diethyl ether (3×100 ml). The solution was washed with water (2×100 ml), saturated aqueous NaHCO_3 solution (1×100 ml), and brine (1×100 ml), and then dried over MgSO_4 . Removal of the solvent by rotary evaporation afforded the crude acids or alcohols which were purified by recrystallization with hexane.^{22,23} The analytical data of the acids and alcohol **10b** are in agreement with previously published data.²³

11,11,12,12,13,13,14,14,14-Nonafluorotetradecanol (10a). ^1H NMR δ/ppm 1.34 (m, 12H, $-(\text{CH}_2)_6-$), 1.57 (m, 4H, $\text{R}_f\text{CH}_2\text{CH}_2-$ and $-\text{CH}_2\text{CH}_2\text{OH}$), 1.9–2.4 (m, 2H + OH, $\text{R}_f\text{CH}_2\text{CH}_2-$), 3.66 (t, $J = 6.6$ Hz, 2H, $-\text{CH}_2\text{CH}_2\text{OH}$). ^{13}C NMR δ/ppm 20.1 (t, $J = 4.0$ Hz), 25.7, 29.1, 29.2, 29.3, 29.4, 29.5, 30.8 (t, $J = 22.0$ Hz), 32.7, 62.9. ^{19}F NMR δ/ppm -81.6 (CF_3), -115.1, -124.9, -126.6. GC/MS m/z (relative intensity, %) 358 (M - H_2O , 5), 330 (30), 302 (20), 288 (30). IR(KBr) ν/cm^{-1} 3346 (OH), 2930, 2858, 1235, 1133, 1117, 722.

11,11,12,12,13,13,14,14,15,15,16,16,17,17,18,18-Hepta-decafluorooctadecanol (10c). ^1H NMR δ/ppm 1.35 (m, 12H, $-(\text{CH}_2)_6-$), 1.59 (m, 4H, $\text{R}_f\text{CH}_2\text{CH}_2-$ and $-\text{CH}_2\text{CH}_2\text{OH}$), 1.88 (br s, 1H, OH), 2.08 (m, 2H, $\text{R}_f\text{CH}_2\text{CH}_2-$), 3.68 (t, $J = 6.7$ Hz, 2H, $-\text{CH}_2\text{CH}_2\text{OH}$). ^{13}C NMR δ/ppm 20.0 (t, $J = 3.8$ Hz), 25.7, 29.1, 29.2, 29.3, 29.4, 29.5, 30.8 (t, $J = 22.5$ Hz), 32.7, 62.9. ^{19}F NMR δ/ppm -81.5 (CF_3), -115.1, -122.3 ($3 \times \text{CF}_2$), -123.3, -124.1, -126.7. GC/MS m/z (relative intensity, %) 558 (M - H_2O , 2), 530 (10), 502 (5), 488 (9). IR(KBr) ν/cm^{-1} 3322 (OH), 2933, 2855, 1242, 1205, 1150, 1117, 661.

Reduction of partially fluorinated acids and esters with LiAlH_4 (general procedure)

The partially fluorinated acids or esters (0.15 mol) were dissolved in 50–80 ml of THF and added over 5 min to a slurry of LiAlH_4 (3.8 g, 0.1 mol) in 10 ml THF at 0°C under nitrogen. The mixture was allowed to come to room temperature and was stirred overnight. After complete conversion it was cooled to 0°C and water was added dropwise until the evolution of hydrogen ceased. The mixture was acidified with 2N HCl and extracted with diethyl ether (3×100 ml). The solution was washed with water (2×100 ml), saturated aqueous NaHCO_3 solution (1×100 ml), and brine (1×100 ml), and then dried over MgSO_4 . Removal of the solvent by rotary evaporation afforded the crude alcohols (**9a-c**), which were purified by chromatography on silica gel (hexane-ethyl acetate = 9:1) or recrystallization with hexane. Typical yields ranged from 80–85%. The analytical data of **9a-c** are in agreement with previously published data.²⁴

Terminally perfluorinated bromides **11a-c** and **12a-c** (general procedure)

Triphenylphosphine (24.2 g, 0.13 mol) and bromine (7 ml, 0.13 mol) were dissolved in 50 ml of anhydrous methylene chloride at 0°C . After 30 min, a DCM solution of the alcohol (**9a-c** or **10a-c**, 0.1 mol in 25 ml of DCM) was added, and the solution was stirred at room temperature for 15 h. The solution was poured into ice water (300 ml). The product was extracted with

diethylether (4 × 100 ml). The solution was washed with water (2 × 100 ml), saturated aqueous NaHCO₃ solution (1 × 100 ml), and brine (1 × 100 ml), and then dried over MgSO₄. Removal of the solvent by rotary evaporation afforded the crude bromide (**11a-c**, **12a-c**), which was purified by chromatography on silica gel (hexane-ethyl acetate = 9:1) or recrystallization with hexane.^{22,23} Yields were typically 70–75%. The analytical data of **11a-c** are in agreement with previously published data.²⁴

11,11,12,12,13,13,14,14,14-Nonafluorotetradecyl bromide (12a). ¹H NMR δ/ppm 1.24 (m, 12H, -(CH₂)₆-), 1.53 (m, 2H, R_FCH₂CH₂-), 1.79 (m, 2H, -CH₂CH₂Br), 1.98 (m, 2H, R_FCH₂CH₂-), 3.34 (t, *J* = 6.9 Hz, 2H, -CH₂CH₂Br). ¹³C NMR δ/ppm 20.2 (t, *J* = 4.0 Hz), 28.3, 28.9, 29.2, 29.3, 29.4, 29.5, 30.9 (t, *J* = 22.0 Hz), 33.0, 33.9. ¹⁹F NMR δ/ppm -81.6 (CF₃), -115.1, -125.1, -126.6. GC/MS *m/z* (relative intensity, %) 438 (M - 1, < 1), 317 (23), 303 (30), 151 (12), 137 (100), 135 (96). IR(KBr) ν/cm⁻¹ 2930, 2854, 1283, 1236, 1134.

11,11,12,12,13,13,14,14,15,15,16,16,16-Heptafluorohexadecyl bromide (12b). ¹H NMR δ/ppm 1.3 (m, 12H, -(CH₂)₆-), 1.56 (m, 2H, R_FCH₂CH₂-), 1.83 (m, 2H, -CH₂CH₂Br), 2.02 (m, 2H, R_FCH₂CH₂-), 3.38 (t, *J* = 6.8 Hz, 2H, -CH₂CH₂Br). ¹³C NMR δ/ppm 20.7 (t, *J* = 4.0 Hz), 28.1, 28.7, 29.0, 29.2, 29.3, 29.3, 30.9 (t, *J* = 22.2 Hz), 32.8, 34.0. ¹⁹F NMR δ/ppm -81.3 (CF₃), -114.9, -122.5, -123.4, -124.1, -126.7. GC/MS *m/z* (relative intensity, %) 538 (M - 1, < 1), 417 (14), 403 (20), 151 (12), 137 (100), 135 (95). IR(KBr) ν/cm⁻¹ 2932, 2858, 1241, 1207, 1145.

11,11,12,12,13,13,14,14,15,15,16,16,17,17,18,18,18-Heptafluorooctadecyl bromide (12c). ¹H NMR δ/ppm 1.32 (m, 12H, -(CH₂)₆-), 1.60 (m, 2H, R_FCH₂CH₂-), 1.86 (m, 2H, -CH₂CH₂Br), 2.07 (m, 2H, R_FCH₂CH₂-), 3.40 (t, *J* = 6.8 Hz, 2H, -CH₂CH₂Br). ¹³C NMR δ/ppm 20.3 (t, *J* = 4.0 Hz), 28.4, 28.9, 29.3, 29.4, 29.5, 29.5, 31.1 (t, *J* = 21.9 Hz), 33.1, 33.9. ¹⁹F NMR δ/ppm -81.4 (CF₃), -114.9, -122.4 (3 × CF₂), -123.3, -124.1, -126.7. GC/MS *m/z* (relative intensity, %) 638 (M - 1, < 1), 517 (13), 503 (20), 151 (10), 137 (100), 135 (96). IR(KBr) ν/cm⁻¹ 2937, 2854, 1246, 1205, 1151.

General procedure for pyridinium bromides **13a-c** and **14a-c**²⁶

Bromides (**12a-c**, **13a-c**, 0.1 mol) and anhydrous pyridine (41 ml, 0.5 mol) were refluxed for 10 hours. A white precipitate was obtained after addition of ether to the cold reaction mixture. The filtrate was washed thoroughly with ether and recrystallized twice from acetone. Typical yields were 80–85% (py = H₅C₅N⁺).

12,12,13,13,14,14,15,15,15-Nonafluoropentadecylpyridinium bromide monohydrate (13a). Mp 25.5 °C (minor phase transition), 45.0 °C. ¹H NMR δ/ppm 1.2–1.5 (m, 14H, -(CH₂)₇-), 1.57 (m, 2H, R_FCH₂CH₂-), 1.9–2.1 (m, 4H, R_FCH₂CH₂- and -CH₂CH₂-py), 3.2 (br s, OH), 4.98 (t, *J* = 7.5 Hz, 2H, -CH₂CH₂-py), 8.24 (t, *J* = 6.3 Hz, 2H, H-3,5), 8.63 (t, *J* = 7.8 Hz, 1H, H-4), 9.50 (d, *J* = 5.7 Hz, 2H, H-2,6). ¹³C NMR δ/ppm 19.91 (t, *J* = 3.7 Hz), 25.93, 28.90, 28.93, 29.02, 29.04, 29.17, 29.24, 30.67 (t, *J* = 21.8 Hz), 31.82, 61.93, 128.41, 145.00, 145.11. ¹⁹F NMR δ/ppm -81.6 (CF₃), -115.1,

-125.0, -126.6. MS *m/z* (calcd) 452 (452). IR(KBr) ν/cm⁻¹ 2928, 2856, 1233, 1133. Anal. calcd for C₂₀H₂₇F₉NBr · H₂O: C 43.63; H 5.27; N 2.54. Found: C 43.45; H 5.27; N 2.50%.

12,12,13,13,14,14,15,15,16,16,17,17-Heptafluorohexadecylpyridinium bromide (13b). Mp 61.0 °C, 75.6 °C. ¹H NMR δ/ppm 1.2–1.6 (m, 14H, -(CH₂)₇-), 1.57 (m, 2H, R_FCH₂CH₂-), 1.9–2.1 (m, 4H, R_FCH₂CH₂- and -CH₂CH₂-py), 5.05 (t, *J* = 7.2 Hz, 2H, -CH₂CH₂-py), 8.24 (t, *J* = 6.6 Hz, 2H, H-3,5), 8.62 (t, *J* = 7.8 Hz, 1H, H-4), 9.70 (d, *J* = 5.7 Hz, 2H, H-2,6). ¹³C NMR δ/ppm 19.89 (t, *J* = 3.6 Hz), 25.89, 28.88, 28.90, 28.99, 29.11, 29.13, 29.20, 30.66 (t, *J* = 21.8 Hz), 31.94, 61.77, 128.41, 145.14 (2 × C). ¹⁹F NMR δ/ppm -81.7 (CF₃), -115.2, -122.8, -123.6, -124.4, -126.9. MS *m/z* (calcd) 552 (552). IR(KBr) ν/cm⁻¹ 2925, 2855, 1239, 1205, 1144, 1123. Anal. calcd for C₂₂H₂₇F₁₃NBr: C 41.77; H 4.27; N 2.21. Found: C 41.64; H 4.29; N 2.07%.

12,12,13,13,14,14,15,15,16,16,17,17,18,18,19,19-Heptafluorononadecylpyridinium bromide (13c). Mp 78.1 °C. ¹H NMR δ/ppm 1.2–1.6 (m, 14H, -(CH₂)₇-), 1.62 (m, 2H, R_FCH₂CH₂-), 1.9–2.1 (m, 4H, R_FCH₂CH₂- and -CH₂CH₂-py), 5.07 (t, *J* = 7.2 Hz, 2H, -CH₂CH₂-py), 8.22 (t, *J* = 6.6 Hz, 2H, H-3,5), 8.59 (t, *J* = 7.8 Hz, 1H, H-4), 9.63 (d, *J* = 5.4 Hz, 2H, H-2,6). ¹³C NMR δ/ppm 20.20 (t, *J* = 3.6 Hz), 26.19, 29.19, 29.31, 29.42 (2 × C), 29.50 (2 × C), 30.68 (t, *J* = 22.4 Hz), 32.21, 62.19, 127.63, 145.30, 145.36. ¹⁹F NMR δ/ppm -81.2 (CF₃), -114.8, -122.3 (3 × CF₂), -123.1, -124.0, -126.6. MS *m/z* (calcd) 652 (652). IR(KBr) ν/cm⁻¹ 2922, 2854, 1245, 1204, 1147, 1115. Anal. calcd for C₂₄H₂₇F₁₇NBr: C 39.36; H 3.68; N 1.91. Found: C 39.39; H 3.66; N 1.80%.

11,11,12,12,13,13,14,14,14-Nonafluorotetradecylpyridinium bromide monohydrate (14a). Mp—broad phase transition at ambient temperature; determination of the onset of this transition was not possible. ¹H NMR δ/ppm 1.2–1.5 (m, 12H, -(CH₂)₆-), 1.60 (m, 2H, R_FCH₂CH₂-), 1.9–2.1 (m, 4H, R_FCH₂CH₂- and -CH₂CH₂-py), 3.1 (br s, OH), 5.00 (t, *J* = 7.2 Hz, 2H, -CH₂CH₂-py), 8.25 (t, *J* = 6.6 Hz, 2H, H-3,5), 8.63 (t, *J* = 7.8 Hz, 1H, H-4), 9.51 (d, *J* = 6.0 Hz, 2H, H-2,6). ¹³C NMR δ/ppm 20.00 (t, *J* = 3.6 Hz), 26.02, 28.97, 28.99, 29.11, 29.18, 29.20, 30.67 (t, *J* = 22.4 Hz), 31.95, 62.05, 128.58, 145.07, 145.32. ¹⁹F NMR δ/ppm -81.6 (CF₃), -115.1, -125.0, -126.6. MS *m/z* (calcd) 438 (438). IR(KBr) ν/cm⁻¹ 2930, 2852, 1234, 1214, 1194, 1133. Anal. calcd for C₁₉H₂₅F₉NBr · H₂O: C 42.53; H 4.85; N 2.61. Found: C 42.51; H 4.96; N 2.67%.

11,11,12,12,13,13,14,14,15,15,16,16,16-Pentadecafluorohexadecylpyridinium bromide monohydrate (14b). Mp 54.9 °C, 73.0 °C. ¹H NMR δ/ppm 1.2–1.5 (m, 12H, -(CH₂)₆-), 1.60 (m, 2H, R_FCH₂CH₂-), 1.9–2.1 (m, 4H, R_FCH₂CH₂- and -CH₂CH₂-py), 2.5 (br s, OH), 4.99 (t, *J* = 7.6 Hz, 2H, -CH₂CH₂-py), 8.20 (t, *J* = 6.6 Hz, 2H, H-3,5), 8.57 (t, *J* = 7.8 Hz, 1H, H-4), 9.52 (d, *J* = 5.6 Hz, 2H, H-2,6). ¹³C NMR δ/ppm 19.91 (t, *J* = 3.6 Hz), 25.89, 28.87 (2 × C), 29.00, 29.06, 29.08, 30.67 (t, *J* = 22.2 Hz), 31.85, 61.93, 128.41, 145.00, 145.11. ¹⁹F NMR δ/ppm -81.5 (CF₃), -115.0, -122.6, -123.6, -124.2, -126.8. MS *m/z* (calcd) 538 (538). IR(KBr)

ν/cm^{-1} 2922, 2843, 1253, 1217, 1175, 1146. Anal. calcd for $\text{C}_{21}\text{H}_{25}\text{F}_{13}\text{NBr} \cdot \text{H}_2\text{O}$: C 39.62; H 4.25; N 2.20. Found: C 39.95; H 4.18; N 2.24%.

11,11,12,12,13,13,14,14,15,15,16,16,17,17,18,18-Hepta-decafluorooctadecylpyridinium bromide monohydrate (14c). Mp 68.7 °C. ^1H NMR δ/ppm 1.2–1.6 (m, 12H, $-(\text{CH}_2)_6-$), 1.58 (m, 2H, $\text{R}_F\text{CH}_2\text{CH}_2-$), 1.9–2.1 (m, 4H, $\text{R}_F\text{CH}_2\text{CH}_2-$ and $-\text{CH}_2\text{CH}_2-\text{py}$), 2.7 (br s, OH), 5.01 (t, $J = 7.6$ Hz, 2H, $-\text{CH}_2\text{CH}_2-\text{py}$), 8.21 (t, $J = 6.6$ Hz, 2H, H-3,5), 8.59 (t, $J = 7.8$ Hz, 1H, H-4), 9.53 (d, $J = 5.6$ Hz, 2H, H-2,6). ^{13}C NMR δ/ppm 20.15 (t, $J = 3.6$ Hz), 26.15, 29.13 (2 \times C), 29.27, 29.33, 29.35, 30.90 (t, $J = 21.75$ Hz), 32.12, 62.14, 128.68, 145.43, 145.58. ^{19}F NMR δ/ppm -81.4 (CF_3), -115.0, -122.5 (3 \times CF_2), -123.1, -124.1, -126.8. MS m/z (calcd) 638 (638). IR(KBr) ν/cm^{-1} 2921, 2853, 1253, 1209, 1169, 1139. Anal. calcd for $\text{C}_{23}\text{H}_{25}\text{F}_{17}\text{NBr} \cdot \text{H}_2\text{O}$: C 37.50; H 3.6; N 1.90. Found: C 37.49; H 3.60; N 1.88%.

Assessment of cytotoxicity

Cancer cell lines

The A2780 ovarian carcinoma cell line (ECACC) was selected from a panel of cancer cell lines used for testing in our laboratory.²⁷ The cell line was grown in RPMI 1640 medium (Sigma, Czech Republic) supplemented with 10% of fetal calf serum (Gibco, Czech Republic), 40 IU of insulin per 100 ml of medium, 50 $\mu\text{g ml}^{-1}$ penicillin, 50 $\mu\text{g ml}^{-1}$ streptomycin, 100 $\mu\text{g ml}^{-1}$ neomycin, and 300 $\mu\text{g ml}^{-1}$ L-glutamine as reported previously.²⁷ Cultures were maintained in a humidified incubator at 37 °C and 5% CO_2 .

MTT-based cytotoxicity test

The MTT assay^{37,38} was used to assess the cytotoxicity of the pyridinium salts in cells in the exponential growth phase. In short, cells were seeded on 96-well flat-bottom microplates at the density $2.5\text{--}3.0 \times 10^4$ per ml, 100 μl per well, and allowed to grow for 16 to 24 hours in culture medium. The pyridinium salts dissolved in PBS (total volume of 20 μl) were added to wells and the cytotoxic effect was evaluated after 24 hours of exposure over a concentration range from 0.3 μM to 250 μM using the MTT assay. Benzalkonium chloride (BAC) (Sigma-Aldrich), a cationic surfactant employed in cosmetics as a foaming and cleaning agent and bactericide, was used as a reference compound.

MTT (Sigma Chemical Co., Czech Republic) was dissolved in PBS at a concentration of 5 mg ml^{-1} and sterilized by filtration. MTT solution was added into all wells of 96-well flat-bottom microplates with cells in a dose of 20 μl per well. The plates were incubated for 3 h. To enhance the dissolution of dark-purple crystals of formazan, 110 μl of 10% SDS in PBS (final pH 5.5) were added to all wells. The microtitre plates were stored in a light-tight box at room temperature, evaluated on the next day using a well-plate spectrophotometer reader iEMS MF (Labsystems, Turku, Finland) at 540 nm and the IC_{50} (i.e. the molar concentration which produces 50% of the maximum possible inhibitory response) values were calculated from the dose response curves. All experiments were performed in triplicate and IC_{50} values were

calculated using GraphPad PRISM V.3.00 (GraphPad Software Inc., San Diego, CA).

The results from the MTT assay were further confirmed by Hoffman modulation contrast and fluorescent microscopy (epifluorescent inverted microscope T200, Nikon, Japan) exposing morphological changes of the cells treated with various pyridinium salts. Propidium iodide and YO-PRO-1 (Molecular Probes, Oregon, USA), were used to distinguish dead or apoptotic cells from vital living ones (data not shown).³⁹

Haemolytic activity

Rabbit red blood cells (2% in PBS) were used to perform standard haemolytic tests in both PBS and PBS containing 20% fetal bovine serum. Concentration ranges of tested compounds were from 1 μM to 1 mM. The released haemoglobin was quantified using a well-plate spectrophotometer reader iEMS MF (Labsystems, Turku, Finland) at 540 nm after two hours incubation of red cells with a particular compound at 37 °C. Data were expressed as the lowest concentration of surfactants causing haemolysis.

Acknowledgements

We thank Mr John Snyder (Department of Chemistry, The University of Iowa) for helpful discussions of the NMR experiments and Dr Paul Bummer (College of Pharmacy, University of Kentucky) for access to the DSC instrument. This material is based upon work supported by the National Institute of Environmental Health Sciences (ES12475) and the National Science Foundation (NIRT 0210517). This work was also supported by grants from the Ministry of Agriculture of the Czech Republic (grant No. MZE-0002716201) and NAZV QF 3115. Its contents are solely the responsibility of the authors and do not necessarily represent the official views of the funding agencies.

References

- 1 E. Kissa, *Fluorinated surfactants and repellents*, Marcel Dekker, New York, 2001, vol. 97.
- 2 G. Osei-Prempeh, H.-J. Lehmler, B. L. Knutson and S. E. Rankin, *Microporous Mesoporous Mater.*, 2005, **85**, 16.
- 3 B. Tan, H.-J. Lehmler, S. M. Vyas, B. L. Knutson and S. E. Rankin, *Chem. Mater.*, 2005, **17**, 916.
- 4 S. E. Rankin, B. Tan, H.-J. Lehmler, K. P. Hindman and B. L. Knutson, *Microporous Mesoporous Mater.*, 2004, **73**, 197.
- 5 B. Tan, A. Dozier, H.-J. Lehmler, B. L. Knutson and S. E. Rankin, *Langmuir*, 2004, **20**, 6981.
- 6 B. Tan, H.-J. Lehmler, S. M. Vyas, B. L. Knutson and S. E. Rankin, *Nanotechnology*, 2005, **16**, S502.
- 7 K. Ghosh, H.-J. Lehmler, S. E. Rankin and B. L. Knutson, *Langmuir*, 2005, **21**, 6145.
- 8 H.-J. Lehmler, P. M. Bummer and M. Jay, *CHEMTECH*, 1999, **29**, 7.
- 9 J. G. Riess, *J. Fluorine Chem.*, 2002, **114**, 119.
- 10 J. B. Nivet, M. Le Blanc and J. G. Riess, *Eur. J. Med. Chem.*, 1991, **26**, 953.
- 11 V. M. Sadler, F. Jeanneau, M. P. Krafft, J. Rabal and J. G. Riess, *New J. Chem.*, 1998, **22**, 609.
- 12 M.-P. Krafft, J.-P. Rolland, P. Vierling and J. G. Riess, *New J. Chem.*, 1990, **14**, 869.
- 13 A. Milius, J. Greiner and J. G. Riess, *New J. Chem.*, 1991, **15**, 337.
- 14 L. Zarif, J. Greiner, S. Pace and J. G. Riess, *J. Med. Chem.*, 1990, **33**, 1262.
- 15 L. Zarif, J. Greiner and J. G. Riess, *J. Fluorine Chem.*, 1989, **44**, 73.

- 16 J. Greiner, A. Milius and J. G. Riess, *Tetrahedron Lett.*, 1988, **29**, 2193.
- 17 F.-A. Pitten and A. Kramer, *Arzneim.-Forsch.*, 2001, **51**, 588.
- 18 H. P. Drobeck, Current topics on the toxicity of cationic surfactants, in *Cationic Surfactants (Surfactant Science Series)*, ed. J. Cross and E. J. Singer, Marcel Dekker, New York, 1994, vol. 53, p. 61.
- 19 J.-H. S. Kuo, M.-S. Jan, C.-H. Chang, H.-W. Chiu and C.-T. Li, *Colloids Surf., B*, 2005, **41**, 189.
- 20 T. Bramer, M. Paulsson, K. Edwards and K. Edsman, *Pharm. Res.*, 2003, **20**, 1661.
- 21 C. Tondre and C. Caillet, *Adv. Colloid Interface Sci.*, 2001, **93**, 115.
- 22 H.-J. Lehmler, M. O. Oyewumi, M. Jay and P. M. Bummer, *J. Fluorine Chem.*, 2001, **107**, 141.
- 23 H.-J. Lehmler and P. M. Bummer, *J. Fluorine Chem.*, 2002, **117**, 17.
- 24 C. Naud, P. Calas, H. Blancou and A. Commeyras, *J. Fluorine Chem.*, 2000, **104**, 173.
- 25 M. Graupe, T. Koini, V. Y. Wang, G. M. Nassif, R. Colorado, Jr, R. J. Villazana, H. Dong, Y. F. Miura, O. E. Shmakova and T. R. Lee, *J. Fluorine Chem.*, 1999, **93**, 107.
- 26 T. Asakawa, H. Hisamatsu and S. Miyagishi, *Langmuir*, 1995, **11**, 478.
- 27 J. Turanek, A. Kasna, D. Zaluska, J. Neca, V. Kvardova, P. Knofigova, V. Horvath, L. Sindlerova, A. Kozubik, P. Sova, A. Kroutil, F. Zak and A. Mistr, *Anti-Cancer Drugs*, 2004, **15**, 537.
- 28 J. B. Nivet, R. Bernelin, M. Le Blanc and J. G. Riess, *Eur. J. Med. Chem.*, 1992, **27**, 891.
- 29 J. G. Riess, S. Pace and L. Zarif, *Adv. Mater.*, 1991, **3**, 249.
- 30 F. Guillod, J. Greiner and J. G. Riess, *Chem. Phys. Lipids*, 1995, **78**, 149.
- 31 M. P. Krafft, P. Vierling and J. G. Riess, *Eur. J. Med. Chem.*, 1991, **26**, 545.
- 32 D. D. Lasic, *Liposomes in Gene Delivery*, CRC Press, Boca Raton, 1997.
- 33 S. Ravi, D. Padmanabhan and V. R. Mandapur, *J. Indian Inst. Sci.*, 2001, **81**, 299.
- 34 K. E. Murphy and A. H. Hoveyda, *J. Am. Chem. Soc.*, 2003, **125**, 4690.
- 35 N. O. Brace, *J. Chem. Soc.*, 1962, 4491.
- 36 N. O. Brace, *J. Fluorine Chem.*, 1982, **20**, 313.
- 37 T. Mosmann, *J. Immunol. Methods*, 1983, **65**, 55.
- 38 U. Bank, D. Reinhold and S. Ansoerge, *Allergy Immunol.*, 1991, **37**, 119.
- 39 T. Idziorek, J. Estaquier, F. De Bels and J.-C. Ameisen, *J. Immunol. Methods*, 1995, **185**, 249.

Synthesis and biocompatibility evaluation of fluorinated, single-tailed glucopyranoside surfactants†

Xueshu Li,^a Jaroslav Turánek,^{a,b} Pavlína Knötigová,^b Hana Kudláčková,^b Josef Mašek,^b D. Brant Pennington,^c Stephen E. Rankin,^c Barbara L. Knutson^c and Hans-Joachim Lehmler^{a*}

Received (in Durham, UK) 2nd April 2008, Accepted 31st July 2008

First published as an Advance Article on the web 19th September 2008

DOI: 10.1039/b805015e

Partially fluorinated non-ionic surfactants are of interest for a range of biomedical applications, such as the pulmonary administration of drugs using reverse water-in-perfluorocarbon microemulsions. We herein report the synthesis and characterization of a series of partially fluorinated β -D-glucopyranoside surfactants from the respective alcohols and peracetylated β -D-glucopyranoside using $\text{BF}_3 \cdot \text{Et}_2\text{O}$ as catalyst. The surfactant packing parameter of the fluorinated surfactants ranged from 0.472 to 0.534 (MOPAC calculations) or 0.562 to 0.585 (calculated from literature values), which is comparable to surfactants with a similar partially fluorinated tail. Based on an initial biocompatibility assessment, the β -D-glucopyranoside surfactants have low toxicities in the B16F10 mouse melanoma cell line and comparatively low haemolytic activities towards rabbit red blood cells. The fluorinated surfactants appear to be less toxic towards cells in culture and to have a lower haemolytic activity compared to their hydrocarbon analogs. Furthermore, an increasing degree of fluorination appears to reduce both the cytotoxicity and the haemolytic activity. Similar structure–activity relationships have been reported for other partially fluorinated surfactants. Overall, these findings suggest that the surfactants may be useful for biomedical applications, such as novel drug delivery systems.

Introduction

Surfactants with a partially fluorinated tail of the general structure $(\text{CH}_2)_m\text{C}_n\text{F}_{2n+1}$ have unique physicochemical properties, such as high surface activity and weak molecular interactions.¹ Furthermore, perfluorinated tails are larger and stiffer compared to hydrocarbon tails. For example, the limiting molecular areas of perfluorinated and hydrocarbon chains at the air–water interface are 30 and 20 Å², respectively.^{2,3} This difference in physicochemical properties and molecular geometry allows (partially) fluorinated surfactants to self-assemble in supramolecular structures that are distinctively different from those observed for their hydrocarbon analogues.⁴ They tend to self-assemble more easily and to form better organized and more stable systems than their hydrocarbon counterparts.⁵

Partially fluorinated surfactants are of interest for biomedical applications, such as pulmonary drug delivery,^{6,7} because of these unique properties. A variety of single tailed partially fluorinated surfactants with different headgroups, for

example carnitine,⁸ (di-)morpholinophosphate,^{9,10} phosphocholine,¹¹ pyridinium¹² and carbohydrate^{5,13} headgroups, have been synthesized, and their biocompatibility has been assessed using *in vitro* and *in vivo* approaches. There is evidence that partially fluorinated surfactants in general display low to moderate acute toxicity compared to their hydrocarbon analogues.⁵ Partially fluorinated surfactants with a perfluorooctyl or perfluorodecyl group in the hydrophobic tail have particularly low toxicities. In addition, the haemolytic activity of partially fluorinated surfactants is low despite their high surface activity.⁵

Some fluorinated surfactants form stable, reverse water-in-perfluorocarbon (micro-)emulsions.^{14–18} These emulsions are of particular interest for the perfluorocarbon-assisted pulmonary administration of drugs^{6,7} because perfluorocarbon-insoluble drugs can be administered by dissolving them in the aqueous core of the reverse (micro-)emulsion. For example, some dimorpholinophosphate surfactants form reverse (micro-) emulsions that are highly fluid and have a water content of up to 30 vol% at a surfactant concentration of 2% (w/v).¹⁹ In addition, these reverse (micro-)emulsions appear to be biocompatible *in vitro* and *in vivo*.^{19,20} However, all other reverse water-in-perfluorocarbon (micro-)emulsions investigated to date are based on perfluorinated surfactants (e.g., poly(oxyethylene) derivatives) that are not biocompatible.^{15–18} Therefore, there is considerable need for novel partially fluorinated surfactants that are biocompatible and have the potential to form stable, reverse water-in-perfluorocarbon (micro-)emulsions.

^a Department of Occupational and Environmental Health, University of Iowa, Iowa City, IA 52242, USA.

E-mail: hans-joachim-lehmler@uiowa.edu; Fax: 3193354290; Tel: 3193354211

^b Veterinary Research Institute v.v.i., Department of Vaccinology and Immunotherapy, Brno, Czech Republic. E-mail: turanek@vri.cz

^c Chemicals and Materials Engineering Department, University of Kentucky, Lexington, KY 40506, USA

† Electronic supplementary information (ESI) available: Detailed characterization of compounds 6b,c,e,f, 7b,c,e,f, 8b,c,e,f and 9b,c,e,f. See DOI: 10.1039/b805015e

Building on earlier studies with partially fluorinated carbohydrate surfactants,⁵ the present study describes the synthesis and characterization of a series of partially fluorinated β -D-glucopyranoside surfactants. In addition, this study evaluates their toxicity in a cell culture model as well as their haemolytic activity in comparison to the analogous hydrocarbon surfactants.

Results and discussion

Surfactant packing parameters of β -D-glucopyranosides

Although it is difficult to predict if a partially fluorinated surfactant forms reverse water-in-perfluorocarbon microemulsions,⁵ the molecular geometry of a surfactant is one important determinant of the self-assembled structures formed by a surfactant. One possible way to describe the molecular geometry of a surfactant is the surfactant packing parameter $P = v/(a_0 l_c)$ (where v is the volume of the hydrophobic chain, a_0 is the area of the polar head group and l_c is the length of the hydrophobic chain).^{4,21} To guide us with the selection of promising target molecules, we calculated the surfactant packing parameter for several β -D-glucopyranosides using either MOPAC or published values for v , a_0 and l_c .^{4,22} In addition, we calculated the surfactant packing parameters of two dimorpholinophosphate surfactants which have been shown to form stable, reverse water-in-perfluorocarbon (micro-)emulsions.^{14,19} The results of these calculations are shown in Table 1.

The volumes, tail lengths and surfactant parameters calculated with the two different approaches differed significantly from each other. Similarly, Giulieri and Krafft reported significant differences between published and experimental values for v and l_c .⁴ Despite these discrepancies, the calculated surfactant packing parameters allowed a comparison of the molecular geometry of glucopyranoside and dimorpholinophosphate surfactants and the identification of trends. Independent of the approach used, the surfactant packing parameters of both types of surfactants were similar, and near the packing parameter value that would be associated with ideal cylindrical micelles ($P = 0.5$).²¹ For the MOPAC results, P for the glucopyranosides was slightly larger than the P for dimorpholinophosphate surfactants, while the converse was suggested from the experimental data due to the smaller experimental dimorpholinophosphate headgroup area.⁴ Furthermore, P of the partially fluorinated glucopyranoside surfactants increased slightly with increasing degree of fluorination, whereas P for the hydrocarbon glucopyranoside surfactants did not change with increasing chain length. Overall, the surfactant packing parameters shown in Table 1 suggest that partially fluorinated glucopyranoside and dimorpholinophosphate surfactants have a similar molecular geometry. Therefore, glucopyranosides **8a-f** were synthesized for further studies because they may also form reverse water-in-perfluorocarbon microemulsions.

Synthesis

The synthesis of several fluorinated β -D-glucopyranosides has been reported in the literature.²³⁻²⁵ The hydrocarbon spacer

between the glucose moiety and the terminal perfluoroalkyl group of these surfactants is short, with two,²³ three²⁶⁻²⁸ or six^{24,25} methylene groups. To the best of our knowledge, glucopyranoside surfactants with longer hydrocarbon spacers have not been synthesized previously. The following section describes the synthesis of the partially fluorinated β -D-glucopyranosides **8a-f**, which were selected based on their surfactant packing parameters.

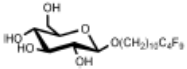
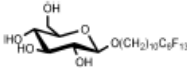
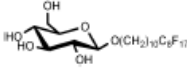
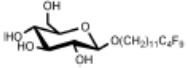
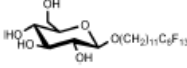
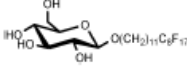
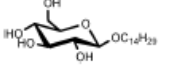
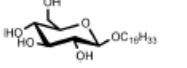
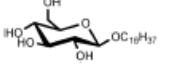
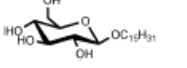
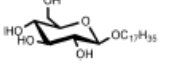
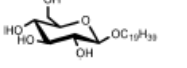
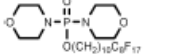
First, a series of partially fluorinated alcohols with the general structure $C_mF_{2m+1}(CH_2)_nOH$ ($m = 4, 6$ and 8 , $n = 10$ and 11) were synthesized from decenol (**1**) or 10-undecenoic acid (**2**), respectively.¹² As shown in Scheme 1, the two starting materials were converted into the corresponding acetate or methyl ester, and the hydrocarbon precursor was coupled with a perfluorinated iodide in an AIBN mediated radical reaction.²⁹⁻³² The resulting secondary iodides were deiodinated with HI/Zn/EtOH and converted into the respective alcohol **3** either by saponification or by reduction with LAH.

Subsequently, the fluorinated alcohols **3a-f** and the corresponding hydrocarbon analogues **4a-f** were reacted with peracetylated β -D-glucopyranoside (**5**) to obtain the peracetylated glucopyranosides **6a-f** and **7a-f**. This glycosylation reaction can be performed using a number of Lewis acids, for example $SnCl_4$,^{33,34} $ZnCl_2$ ³⁵ or $BF_3 \cdot Et_2O$.^{24,36-39} as catalysts. Initial experiments showed that reaction of the fluorinated alcohols **3** with **5** in the presence of $ZnCl_2$ or $AlCl_3$ required long reaction times and high reaction temperatures, which led to the formation of mixtures of the α - and β -anomers of the desired peracetylated glucopyranosides **6a-f**. In contrast, $BF_3 \cdot Et_2O$ gave the desired β -anomers of the glucopyranosides **6a-f** and **7a-f** in 40-55% yield when low reaction temperatures (<5 °C) and short reaction times (<3 h) were employed. The glycosylation products obtained under these conditions typically contained traces of α -anomer (<1%) as determined by ¹H NMR. This small amount of the α -anomer was considered acceptable for the intended application of these compounds as surfactants in biomedical applications. The thermodynamically more stable α -anomers were obtained when the reaction temperature was raised to 30 °C and the reaction time was extended to 10 h (data not shown). No other products, for example 2-, 3-, 4- or 6-(*F*-)alkyl glucopyranosides, were formed according to TLC and ¹H NMR analysis.

In the final step of the synthesis, the (*F*-)alkylated peracetylated β -D-glucopyranosides **6a-f** and **7a-f** were deacetylated using NaOMe in absolute methanol, followed by neutralization with Dowex[®] 50W \times 8-100 ion exchange resin.³⁸ The crude product was purified by column chromatography on silica gel followed by recrystallization from acetone. The pure glucopyranosides **8a-f** and **9a-f** were obtained with yields ranging from 92 to 98%.

In a preliminary study we also investigated a different route to the desired glucopyranosides to improve the overall yields of the synthesis. Analogous to published syntheses that employ bromo-sugars and an alcohol as starting materials,^{40,41} we reacted 2,3,4,6-tetraacetyl- α -D-glucopyranosyl bromide (**10**) with a partially fluorinated alcohol in the presence of Ag_2CO_3 in DCM at 0 °C (Scheme 2). However, instead of the desired glucopyranoside **6e**, we obtained the fluorinated

Table 1 Surfactant packing parameter P^d of the glucopyranosides **8a-f** and their hydrocarbon analogues **9a-f**

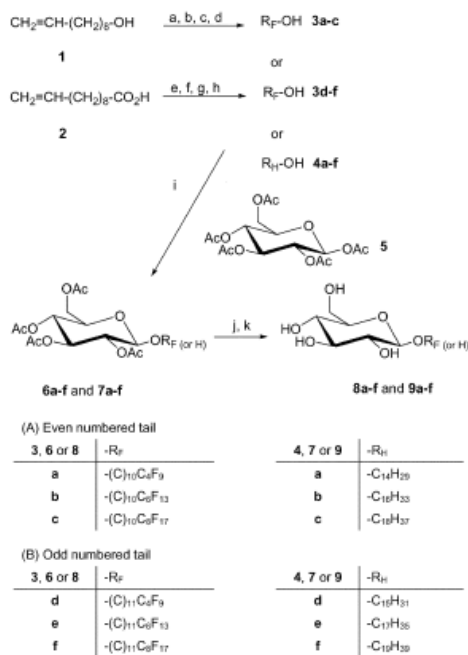
Entry	Structure	MOPAC calculation results				
		Area, $a_0/\text{\AA}^2$	Volume, $v^0/\text{\AA}^3$	Length, $l_c/\text{\AA}$	P	P^d
8a		41	357	18.5	0.472	0.566
8b		41	426	21.1	0.493	0.579
8c		41	495	23.7	0.510	0.589
8d		41	394	19.7	0.488	0.562
8e		41	469	22.3	0.513	0.575
8f		41	545	24.9	0.534	0.585
9a		41	307	18.2	0.410	0.488
9b		41	350	20.7	0.413	0.490
9c		41	394	23.2	0.415	0.492
9d		41	332	19.5	0.415	0.489
9e		41	376	21.9	0.418	0.491
9f		41	420	24.4	0.419	0.492
10a		50	495	23.7	0.419	0.618

(continued on next page)

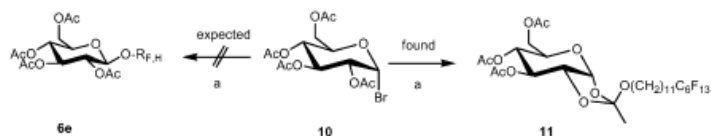
Table 1 (continued)

Entry	Structure	MOPAC calculation results				
		Area, $a_0/\text{\AA}^2$	Volume, $v/\text{\AA}^3$	Length, $\ell/\text{\AA}$	P	P^d
10b		50	545	24.9	0.438	0.614

^a Surfactant packing parameter $P = v/(a_0\ell)$, where a_0 is the area of the polar head group, v is the volume of the hydrophobic chain, and ℓ is the length of the hydrophobic chain.^{42,43} ^b The volume v (\AA^3) from MOPAC correlations was calculated as $22.1n_H + 37.7n_F$ (n_H odd) or $21.9n_H + 34.5n_F$ (n_H even), where n_H = the number of hydrogenated and n_F = the number of fluorinated carbons. ^c The length ℓ (\AA) from MOPAC correlations was calculated as $0.86 + 1.24n_H + 1.3n_F$. ^d Surfactant packing parameter P calculated using published values for a_0 , v and ℓ .^{42,43}



Scheme 1 Synthesis of perfluoroalkyl and alkyl β -D-glucopyranosides. **Reagents and conditions:** (a) DMAP, Ac-Cl, pyridine, DCM; (b) $\text{F}(\text{CF}_2)_m\text{I}$ ($m = 4, 6$ or 8), AIBN; (c) HI (55%), Zn, $\text{C}_2\text{H}_5\text{OH}$; (d) CH_3OH , KOH; (e) CH_3OH , PTSA, toluene; (f) $\text{F}(\text{CF}_2)_m\text{I}$ ($m = 4, 6$ or 8), AIBN; (g) HI (55%), Zn, $\text{C}_2\text{H}_5\text{OH}$; (h) LiAlH_4 , anhydrous ether, ambient temperature; (i) BF_3/OEt_2 (48%), anhydrous DCM, 0°C to ambient temperature, 3 h; (j) MeONa/MeOH , 0°C to ambient temperature; (k) Dowex[®] 50W $\times 8$ -100 ion-exchange resin.



Scheme 2 Synthesis of orthoester **11**. **Reagents and conditions:** (a) **3e**, Ag_2CO_3 , DCM, 0°C to ambient temperature.

1,2-orthoacetate **11** in 80% yield. Based on the chemical shifts of the H-1' proton at 5.70 ppm, the 1,2-orthoacetate **11** is the *exo* isomer (*exo*: δ 5.72 ppm vs. *endo*: δ 5.59 ppm⁴²). Similarly, Tsui and Gorin have reported the formation of 1,2-orthoacetates as side products (21–34% yield) under comparable reaction conditions.⁴² The lower yield in that study may be due to the shorter chain length of the alcohols employed (\leq C-8).

Melting points of (*F*)-alkyl glucopyranosides

Glucopyranosides are compounds that form both thermotropic liquid crystalline phases upon heating and lyotropic liquid crystalline phases upon addition of solvents such as water.^{43–45} As a result of this complex phase behaviour, a range of melting points has been reported in the literature for alkyl β -D-glucopyranosides. To investigate the thermotropic properties of the partially fluorinated glucopyranosides, the phase transitions of the glucopyranosides **8a–f** and **9a–f** were investigated using differential scanning calorimetry (DSC). The phase transitions determined by DSC were in agreement with the melting points measured with a MeTemp apparatus.

As shown in Fig. 1, both hydrocarbon and fluorocarbon glucopyranosides displayed at least two phase transitions. The main phase transitions were observed at temperatures ranging from 69 to 116 $^\circ\text{C}$. A minor phase transition observed at temperatures from 145 to 190 $^\circ\text{C}$ corresponds to the clearing temperatures reported for long-chain hydrocarbon glucopyranosides^{43,44} and probably represents a transition from an anisotropic liquid crystalline phase to an isotropic liquid phase.

While the phase transition temperatures for the even numbered glucopyranosides **8a–b** and **9a–b** were almost the same, the respective phase transition temperatures for the highly fluorinated glucopyranoside **8c** were clearly higher compared to the corresponding hydrocarbon analogue **9c** (Fig. 1(A)). Similarly, the partially fluorinated glucopyranosides with an odd number of carbon atoms in the hydrophobic tail (**8d–f**)

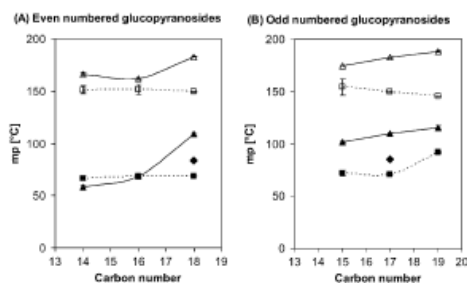


Fig. 1 Comparison of the phase transition maxima of perfluoroalkyl and alkyl β -D-glucopyranosides with an (A) even (8a-c and 9a-c) and (B) odd number (8d-f and 9d-f) of carbon atoms in the hydrophobic tail (\blacktriangle and \triangle = fluoroalkyl; \blacksquare and \square = alkyl; closed symbols = major phase transition; open symbols = minor phase transition; \blacklozenge represents the maximum of a second phase transition observed for alkyl glucopyranosides 9e and 9e). Values shown are the experimental mean \pm one standard deviation of at least three DSC experiments.

displayed higher phase transition temperatures compared to their hydrocarbon analogues 9d-f (Fig. 1(B)). In comparison, the melting points of the partially fluorinated β -D-glucopyranosides 8a-f are lower compared to fluorinated hydrocarbon spacers $-(\text{CH}_2)_m\text{C}_m\text{F}_{2m+1}$, $m = 4, 6$ and 8).^{26,28}

These differences in the phase transition temperatures between hydrocarbon and fluorocarbon β -D-glucopyranosides are a result of the perfluoroalkyl terminus in the hydrophobic tail. Due to the larger steric demand of the fluorine atom, perfluoroalkyl chains are more rigid, which allows a more efficient packing in the solid state. As a consequence, the melting point of the glucopyranosides 8c-f was higher compared to the corresponding hydrocarbon analogues 9c-f. Similar trends in phase transition temperatures have been reported for other partially fluorinated compounds, such as partially fluorinated, long-chain carboxylic acids with the general structure $\text{F}_{2m+1}\text{C}_m(\text{CH}_2)_{10}\text{COOH}$ ($m = 4, 6$ and 8)²⁹ or fluorinated β -D-glucopyranosides with a short hydrocarbon spacer.^{26,28}

Biological studies

An initial cytotoxicity assessment of the glucopyranoside surfactants 8a-f and 9a-f was performed using the B16F10 mouse melanoma cell line.⁴⁶ Haemolytic activities, both in the presence and absence of 20% serum, were determined using rabbit red blood cells.¹² Octylthioglucooside was used as a positive control for the cytotoxicity studies and the determination of haemolytic activities. Cytotoxicities and haemolytic activities, expressed as EC_{50} values, are summarized in Table 2 for all compounds under investigation. Representative cytotoxicity curves for surfactants 8c, 8e and 9e are presented in Fig. 2.

The partially fluorinated glucopyranosides 8a-b and 8d-e were moderately toxic, with EC_{50} values ranging from 179 to 311 μM . These EC_{50} values are comparable to the EC_{50} values of the analogous hydrocarbon derivatives 9a-d, which ranged

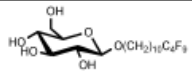
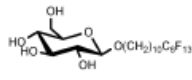
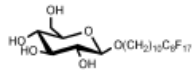
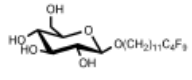
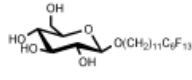
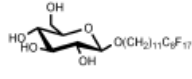
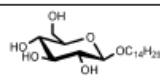
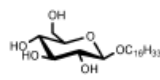
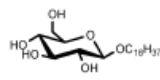
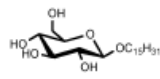
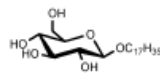
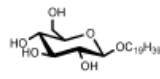
from 190 to 600 μM . This is in contrast to the positive control, octylthioglucooside (OTG), which showed significant cytotoxicity over the same concentration range. Similarly, partially fluorinated surfactants derived from maltose,⁴⁷ mannitol,⁴⁸ sorbitan,⁴⁸ sucrose,⁴⁹ trehalose,⁴⁹ and xylitol⁵⁰ also display moderate-to-low toxicity in cells in culture, with EC_{50} typically > 100 μM . In contrast, glucopyranosides with shorter fluorinated chains (≤ 12 carbon atoms) appear to be more cytotoxic than glucopyranosides 8a-f.²⁵ For example, 7,7,8,8,9,9,10,10,11,11,12,12,12-tridecafluorododecyl- β -D-glucopyranoside was cytotoxic at concentrations of 50 μM .

The two glucopyranosides 8e and 8f with the perfluoroethyl terminus were even less toxic than 8a-b and 8d-e, with EC_{50} values > 1.5 mM. Similarly, the cytotoxicity of fluorinated pyridinium surfactants has been shown to decrease with an increasing degree of fluorination.¹² One possible explanation for this decrease in cytotoxicity is a lower cellular uptake due to the hydrophobic and lipophobic perfluoroalkyl terminus of the hydrophobic tail. This interpretation is supported by a recent study that showed no cellular uptake of a highly fluorinated galactopyranoside in the B16 melanoma cell line.²⁵ However, there is also evidence that fluorinated surfactants readily partition into model membranes,^{2,51-53} and, thus, should be able to enter cells in culture. Therefore, cellular uptake studies are necessary to determine if the glucopyranosides 8c and 8f can indeed partition through cell membranes.

The results from the MTT assay were further confirmed by Hoffman modulation contrast microscopy (Fig. 3). In agreement with the results from the MTT assay, treatment of B16F10 cells with high concentrations of surfactant 8c (24 h, 1.5 mM) surfactant neither altered cell growth nor induced morphological changes in comparison to the control (Fig. 3(A) and (B)). In contrast, surfactants 8e and 9e induced retardation in cell proliferation and caused an abnormal prolonged morphology of the cells at a concentration close to the EC_{50} (Fig. 3(C) and (D)). In addition, both surfactants induced apoptosis in a significant number of cells. No viable cells were observed at high concentrations (1.5 mM) of 8e and 9e (Fig. 3(E) and (F)). Only necrotic cells and cellular debris were evident at these high concentrations. Fluorescence staining with PI and YO-PRO-1 showed only a small portion of B16F10 cells in early or late stage of apoptosis in control cells (Fig. 3(G)) but significant amount of cells treated with 8e at concentration close to the EC_{50} were in various stages of apoptosis (see Fig. 3(H)).

In addition to the cytotoxicity experiments, the haemolytic activity of all surfactants was assessed using rabbit red blood cells.¹² The glucopyranosides 8a-f and 9a-f were haemolytic at low millimolar concentrations. The haemolytic activity decreased for both groups of surfactants in the presence of serum, with EC_{50} values > 15 mM for 8a-f in the presence of serum and > 5 mM for 9a-f in the absence of serum. Furthermore, the hydrocarbon glucopyranosides 9a-f had a higher haemolytic activity compared to their fluorinated analogues 8a-f. Similar observations have been reported for various other fluorinated surfactants.^{5,12,47-50} In addition, the haemolytic activity decreased for structurally related glucopyranosides (*i.e.*, 8a-d with ten and 8d-f with eleven methylene groups in the hydrocarbon spacer) with increasing

Table 2 Assessment of cytotoxicity and haemolytic activity of partially fluorinated glucopyranosides and their hydrocarbon analogues in the B16F10 cell line.^{12,46}

Entry	Structure R _{(F or H)-β-D-Glu}	Cytotoxicity, EC ₅₀ /μM	Haemolytic activity, EC ₅₀ ^a /mM	
			Without serum	20% Serum
8a		194	> 20 (10%)	>20 (10%)
8b		311	> 20 (25%)	20
8c		> 1500	> 20	>20
8d		190	15	20
8e		179	> 20	>20
8f		> 1500	> 20	>20
Hydrocarbon surfactants				
9a		250	10	15
9b		300	> 20 (30%)	>20
9c		190	> 20 (10%)	>20
9d		230	5	15
9e		230	15	>20 (5%)
9f		600	> 20	>20
OTG	Octylthiogluco-side	20	0.5	3

^a Data in parenthesis represent the percentage haemolysis at a 20 mM concentration of the respective glucopyranoside.

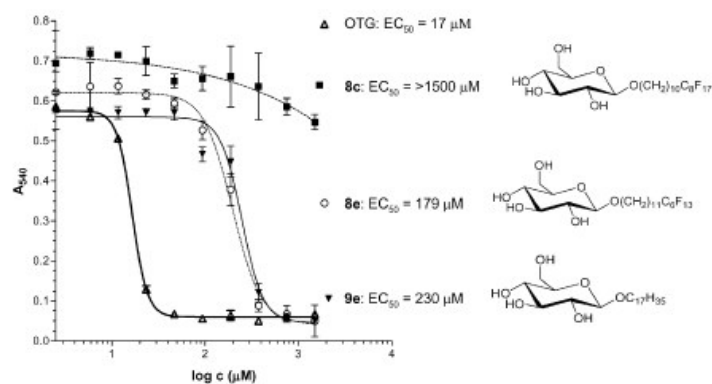


Fig. 2 Cytotoxic effect of glucopyranosides **8c**, **8e** and **9e** in the B16F10 mouse melanoma cell line. B16F10 cells were exposed for 24 h to the respective glucopyranoside at the concentrations shown and assessed for MTT activity as described in the Experimental section. A representative hydrocarbon surfactant, octylthioglucoside (OTG), is shown for comparison.

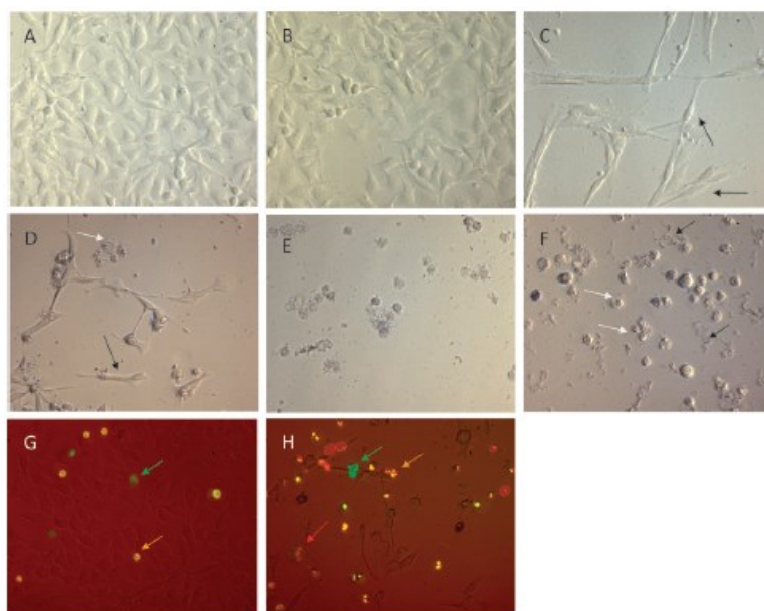


Fig. 3 Cytotoxic effect of glucopyranosides **8e**, **8e** and **9e** in the B16F10 mouse melanoma cell line. The B16F10 cells were treated for 24 h with (A) the vehicle (PBS + 1% DMSO) or with glucopyranoside (B) **8e** (1.5 mM), (C) **8e** (250 μ M, black arrows indicate abnormal spindle-shaped cells), (D) **9e** (250 μ M, black arrow indicate abnormal spindle-shaped cell, white arrow indicate typical necrotic cell), (E) **8e** (1.5 mM) or (F) **9e** (1.5 mM, black arrows indicate cellular debris, white arrows indicate necrotic cells). The fluorescent markers Yo-Pro-1 (green) and PI (red/yellow) were used for the visualization of early apoptotic changes and post-apoptotic secondary necrosis in B16F10 cells treated for 24 h with (G) vehicle (green arrows indicate early stage of apoptosis, orange arrows indicate late stage of apoptosis) or (H) **8e** (250 μ M, green arrows indicate early stage of apoptosis, orange arrows indicate late stage of apoptosis, red arrows indicate secondary necrosis). The cells were observed under an epifluorescent microscope.

length of the perfluoroalkyl terminus. This anti-haemolytic effect of an increasing degree of fluorination has been reported previously for a number of structurally diverse surfactants.^{5,12,47–50}

Conclusions

A series of β -D-glucopyranoside surfactants with (F)-alkyl chain lengths ranging from 14 to 19 carbon atoms was synthesized in good yields from the respective alcohols and peracetylated β -D-glucopyranoside (**5**) using $\text{BF}_3 \cdot \text{Et}_2\text{O}$ as catalyst. Similar to other partially fluorinated surfactants, an increasing degree of fluorination reduced their toxicity and haemolytic activity. Because of their biocompatibility as well as their molecular geometry (*i.e.*, the surfactant packing parameter), the partially fluorinated glucopyranoside surfactants **8a–e** are of particular interest for biomedical applications, such as the pulmonary administration of drugs using reverse water-in-perfluorocarbon (micro-)emulsions.^{6,7}

Experimental

Calculation of surfactant packing parameters of (F)-alkyl β -D-glucopyranosides

The geometry of each molecule was optimized using MOPAC as implemented in Chem3D Ultra 9.0 (CambridgeSoft).⁵⁴ Molecular volumes were calculated as COSMO volumes, and tail lengths were measured directly from the optimized geometry as the length from the O atom to the terminal atom in the tail. Tail length and volume correlations were developed for hydrocarbon and fluorocarbon surfactants in the series. Areas were determined by determining volumes for a series of at least three surfactants with the same head group and using a linear correlation between tail length and volume to determine the head volume (from the intercept). The area was then calculated assuming a spherical head geometry (which may not be reasonable for dimorpholinophosphate surfactants). The alternative calculations were based on experimental areas and correlations between carbon number and bond lengths and tail volumes.^{4,22}

Synthesis of (F)-alkyl β -D-glucopyranosides

The long-chain hydrocarbon starting materials **1** and **2** were purchased from TCI Chemicals (Portland, Oregon, USA). Pentaacetyl- β -D-glucopyranose (**5**), the long chain alkyl alcohols **4a–f** and anhydrous dichloromethane were obtained from Fisher Scientific (Fairlawn, New Jersey, USA). Perfluorinated iodides were purchased from Oakwood Chemical Co. (West Columbia, South Carolina, USA). The ^1H and ^{13}C NMR spectra were recorded on a multinuclear Bruker Avance 300 or Bruker DRX 400 Digital NMR Bruker spectrometers at ambient temperature. Due to their poor solubility, NMR spectra of long-chain glucopyranosides were recorded at 318 K. All ^1H and ^{13}C chemical shifts are reported in parts per million (ppm) relative to internal tetramethylsilane. ^{13}C signals of the glucose moiety were assigned as described previously.³⁶ ^{19}F spectra were recorded using the Bruker Avance 300 with CFCl_3 as internal standard. The mass spectra

were measured at the University of Iowa Mass Spectrometry Facility. High-resolution mass spectra (HR-MS) were measured using an Autospec ESI-MS instrument and ESI mass spectra were recorded using a ThermoFinnigan LCQ Deca mass spectrometer. Elemental analyses were obtained from Atlantic Micro Lab Microanalysis Service (Atlanta, Georgia, USA). Melting points were determined using a MeTemp apparatus and are uncorrected. In addition, the maxima of the major phase transitions of all glucopyranosides was determined using differential scanning calorimetry (DSC) from 0 to 200 °C with a 10 °C min^{-1} ramp.^{29,45} All reactions were monitored by thin layer chromatography, followed by visualization with anisaldehyde- H_2SO_4 .⁵⁵ The detailed characterization of representative compounds with odd and even numbered tails is shown in the text below (the detailed characterization of the remaining compounds is available as ESI†).

General procedure for the synthesis of perfluoroalkyl and alkyl 2,3,4,6-tetra-O-acetyl- β -D-glucopyranosides (**6a–f** and **7a–f**)³⁸

Boron trifluoride diethyl ether complex (10.0 mmol, 48% w/w) in 5 mL dry dichloromethane was added dropwise to a solution of pentaacetyl- β -D-glucopyranose **5** (5.0 mmol) and the corresponding alcohol **3a–f** or **4a–f** (6.0 mmol) in 15 mL dry dichloromethane at 0 °C. The reaction mixture was stirred at 0 °C for 2 h and allowed to slowly warm to ambient temperature. Dichloromethane (20 mL) was added and the mixture was washed with saturated NaHCO_3 solution (3×15 mL) and brine (2×15 mL). The organic phase was dried over anhydrous Na_2SO_4 , filtered, and the solvent was removed under reduced pressure. The residue was purified by column chromatography on silica gel with hexane and ethyl acetate as eluent (hexane-ethyl acetate = 3 : 1). The product was obtained as a white solid or a yellowish viscous liquid with moderate yields ranging from 46 to 55%.

Perfluoroalkyl 2,3,4,6-tetra-O-acetyl- β -D-glucopyranosides

11,11,12,12,13,13,14,14,14-Nonafluorotetradecyl-2,3,4,6-tetra-O-acetyl- β -D-glucopyranoside (6a). Viscous liquid; yield, 55%; ^1H NMR (300 MHz, CDCl_3): δ /ppm 1.1–1.3 (m, 12H, $6 \times \text{CH}_2$), 1.45 (m, 4H, H-2' and H-9'), 1.8–2.0 (m, 14H, $4 \times \text{CH}_3\text{CO}$ and H-10'), 3.35 (m, 1H, H-1'a), 3.59 (m, 1H, H-5), 3.76 (m, 1H, H-1'b), 4.00 (d, 1H, $J_{6a,6b} = 12.0$ Hz, H-6a), 4.16 (dd, 1H, $J_{6a,6b} = 12.0$ Hz, $J_{5,6b} = 4.7$ Hz, H-6b), 4.39 (d, 1H, $J = 8.0$ Hz, H-1), 4.84 (dd, 1H, $J_{1,2} = 8.0$ Hz, $J_{2,3} = 9.5$ Hz, H-2), 4.96 ("t", 1H, $J \sim 9.9$ Hz, H-4), 5.09 ("t", 1H, $J \sim 9.5$ Hz, H-3). ^{13}C NMR (75 MHz, CDCl_3): δ /ppm 20.0 (C-9'), 20.5 ($4 \times \text{CH}_3\text{CO}$), 25.8 (C-3'), 29.0–29.4 (C-2', C-4' to C-8'), 30.7 (t, $J = 21$ Hz, C-10'), 62.0 (C-6), 68.5 (C-4), 70.0 (C-1'), 71.3 (C-2), 71.7 (C-5), 72.8 (C-3), 100.8 (C-1), 169.1, 169.4, 170.2, 170.5 ($4 \times \text{COCH}_3$). ^{19}F NMR (282 MHz, CDCl_3): δ /ppm –81.6 (CF_3), –115.1 (CF_2), –124.9 (CF_2), –126.6 (CF_2). Positive-ion ESI-MS peak at m/z 729 ($[\text{M} + \text{Na}]^+$).

12,12,13,13,14,14,15,15,15-Nonafluoropentadecyl-2,3,4,6-tetra-O-acetyl- β -D-glucopyranoside (6d). Viscous liquid; yield, 51%; ^1H NMR (300 MHz, CDCl_3): δ /ppm 1.1–1.3 (m, 14H, $7 \times \text{CH}_2$), 1.44 (m, 4H, H-2' and H-10'), 1.8–2.0 (m, 14H, $4 \times \text{CH}_3\text{CO}$ and H-11'), 3.34 (m, 1H, H-1'a), 3.60 (ddd, 1H,

$J_{4,5} = 9.8$ Hz, $J_{5,6a} = 2.4$ Hz, $J_{5,6b} = 4.5$, H-5), 3.74 (m, 1H, H-1'^b), 4.10 (dd, 1H, $J_{6a,6b} = 12.2$ Hz, $J_{5,6a} = 2.3$ Hz, H-6a), 4.15 (dd, 1H, $J_{6a,6b} = 12.2$ Hz, $J_{5,6b} = 4.7$ Hz, H-6b), 4.38 (d, 1H, $J = 8.0$ Hz, H-1), 4.84 ("t", 1H, $J \sim 8.4$ Hz, H-2), 4.95 (dd, 1H, $J_{1,2} = 8.0$ Hz, $J_{2,3} = 9.5$ Hz, H-4), 5.08 ("t", 1H, $J \sim 9.4$ Hz, H-3). ¹³C NMR (75 MHz, CDCl₃): δ /ppm 20.0 (C-10'), 20.4 (4 × CH₃CO), 25.7 (C-3'), 29.0–29.5 (C-2', C-4' to C-9'), 30.6 (t, $J = 22$ Hz, C-11'), 61.9 (C-6), 68.5 (C-4), 70.0 (C-1'), 71.3 (C-2), 71.7 (C-5), 72.8 (C-3), 100.8 (C-1), 169.0, 169.3, 170.1, 170.5 (4 × COCH₃). ¹⁹F NMR (282 MHz, CDCl₃): δ /ppm –81.6 (CF₃), –115.1 (CF₂), –124.9 (CF₂), –126.6 (CF₂). Positive-ion ESI-MS peak at m/z 743 ([M + Na]⁺).

Alkyl 2,3,4,6-tetra-*O*-acetyl- β -D-glucopyranosides

Tetradecyl-2,3,4,6-tetra-*O*-acetyl- β -D-glucopyranoside (7a)^{38,56}. White solid; mp 63–64 °C (lit.: 57–84 °C^{56,57}); yield, 51%; ¹H NMR (300 MHz, CDCl₃): δ /ppm 0.88 (t, 3H, $J = 7.0$ Hz, H-14'), 1.1–1.4 (m, 22H, 11 × CH₂), 1.56 (m, 2H, H-2'), 1.9–2.1 (4 × s, 12H, 4 × CH₃CO), 3.48 (dt, 1H, $J_{1'a,1'b} = 9.6$ Hz, $J_{1'a,2'} = 6.6$ Hz, H-1'a), 3.69 (ddd, 1H, $J_{4,5} = 9.8$ Hz, $J_{5,6a} = 2.5$ Hz, $J_{5,6b} = 4.7$, H-5), 3.86 (dt, 1H, $J_{1'a,1'b} = 9.6$ Hz, $J_{1'a,2'} = 6.6$ Hz, H-1'a), 4.13 (dd, 1H, $J_{6a,6b} = 12.2$ Hz, $J_{6a,5} = 2.5$ Hz, H-6a), 4.26 (dd, 1H, $J_{6a,6b} = 12.2$ Hz, $J_{5,6b} = 4.7$ Hz, H-6b), 4.48 (d, 1H, $J_{1,2} = 8.0$ Hz, H-1), 4.98 (dd, 1H, $J_{1,2} = 8.0$ Hz, $J_{2,3} = 9.5$ Hz, H-2), 5.09 ("t", 1H, $J \sim 9.6$ Hz, H-4), 5.21 ("t", 1H, $J \sim 9.4$ Hz, H-3). ¹³C NMR (75 MHz, CDCl₃): δ /ppm 14.3 (C-14'), 20.8–20.9 (4 × CH₃CO), 22.9 (C-13'), 26.1 (C-3'), 29.5–29.9 (C-2', C-4' to C-11'), 32.1 (C-12'), 62.2 (C-6), 68.7 (C-4), 70.4 (C-1'), 71.6 (C-2), 71.9 (C-5), 73.0 (C-3), 101.0 (C-1), 169.4, 169.6, 170.5, 170.9 (4 × COCH₃). Positive-ion ESI-MS peak at m/z 567 ([M + Na]⁺).

Pentadecyl-2,3,4,6-tetra-*O*-acetyl- β -D-glucopyranoside (7d)⁶. White solid; mp 68–69 °C; yield, 53%; ¹H NMR (300 MHz, CDCl₃): δ /ppm 0.88 (t, 3H, $J = 7.0$ Hz, H-15'), 1.1–1.4 (m, 24H, 12 × CH₂), 1.56 (m, 2H, H-2'), 2.0–2.1 (4 × s, 12H, 4 × CH₃CO), 3.47 (dt, 1H, $J_{1'a,1'b} = 9.7$ Hz, $J_{1'a,2'} = 6.7$ Hz, H-1'a), 3.69 (ddd, 1H, $J_{4,5} = 9.9$ Hz, $J_{5,6a} = 2.5$ Hz, $J_{5,6b} = 4.7$, H-5), 3.86 (dt, 1H, $J_{1'a,1'b} = 9.7$ Hz, $J_{1'a,2'} = 6.4$ Hz, H-1'a), 4.13 (dd, 1H, $J_{6a,6b} = 12.3$ Hz, $J_{6a,5} = 2.5$ Hz, H-6a), 4.26 (dd, 1H, $J_{6a,6b} = 12.3$ Hz, $J_{5,6b} = 4.6$ Hz, H-6b), 4.48 (d, 1H, $J_{1,2} = 7.9$ Hz, H-1), 4.98 (dd, 1H, $J_{1,2} = 7.9$ Hz, $J_{2,3} = 9.6$ Hz, H-2), 5.08 ("t", 1H, $J \sim 9.7$ Hz, H-4), 5.21 ("t", 1H, $J \sim 9.4$ Hz, H-3). ¹³C NMR (75 MHz, CDCl₃): δ /ppm 14.3 (C-15'), 20.8–20.9 (4 × CH₃CO), 22.9 (C-14'), 26.0 (C-3'), 29.5–29.9 (C-2', C-4' to C-12'), 32.2 (C-13'), 62.3 (C-6), 68.7 (C-4), 70.5 (C-1'), 71.6 (C-2), 72.0 (C-5), 73.1 (C-3), 101.1 (C-1), 169.5, 169.6, 170.5, 170.8 (4 × COCH₃). Positive-ion ESI-MS peak at m/z 581 ([M + Na]⁺).

General procedure for the synthesis of perfluoroalkyl and alkyl β -D-glucopyranosides (8a–f and 9a–f)⁸. A solution of sodium methoxide (5 mmol) in methanol (5 mL) was added dropwise to a solution of the respective tetraacetylated glucopyranoside **6a–f** or **7a–f** (2 mmol) in methanol (10 mL) and the mixture was stirred at ambient temperature for 1 h. The reaction mixture was neutralized by addition of Dowex[®]

50W × 8-100 ion exchange resin (2.0 g). The ion exchange resin was filtered off and the solvent was removed under reduced pressure. The crude product was purified by recrystallization from acetone or column chromatography on silica gel (eluent: DCM–MeOH = 8 : 1), followed by recrystallization from acetone, to give the products as white solids in high yields ranging from 92 to 98%.

Perfluoroalkyl β -D-glucopyranosides

11,11,12,12,13,13,14,14,14-Nonafluorotetradecyl- β -D-glucopyranoside (8a). White solid; mp 59–61 °C; mp (DSC) 58.43 ± 1.76 °C, 166.19 ± 1.51 °C; yield, 95%; ¹H NMR (300 MHz, CD₃OD): δ /ppm 1.3–1.5 (m, 12H, 6 × CH₂), 1.6–1.7 (m, 4H, H-2' and H-9'), 2.18 (m, 2H, H-10'), 3.22 ("t", 1H, $J \sim 8.3$ Hz, H-2), 3.3–3.4 (m, 3H, H-3, H-4 and H-5), 3.57 (m, 1H, H-1'a), 3.70 (dd, 1H, $J_{6a,6b} = 11.9$ Hz, $J_{5,6b} = 5.1$ Hz, H-6a), 3.8–4.0 (m, 2H, H-6b and H-1'b), 4.29 (d, 1H, $J_{1,2} = 7.7$ Hz, H-1). ¹³C NMR (75 MHz, CD₃OD) δ /ppm 21.3 (C-9'), 27.1 (C-3'), 30.2–30.9 (C-2', C-4' to C-8'), 31.7 (t, $J = 22$ Hz, C-10'), 62.8 (C-6), 70.9 (C-1'), 71.8 (C-4), 75.1 (C-2), 78.0 (C-5), 78.1 (C-3), 104.4 (C-1). ¹⁹F NMR (282 MHz, CD₃OD) δ /ppm –81.0 (CF₃), –114.1 (CF₂), –124.0 (CF₂), –125.7 (CF₂). Anal. Calc. for C₂₀H₃₁F₉O₆: C 44.61, H 5.80. Found: C 44.39, H 5.68%. HR-MS of [M + Na]⁺ m/z : Calc. 561.1875, Found. 561.1880.

12,12,13,13,14,14,15,15-Nonafluoropentadecyl- β -D-glucopyranoside (8d). White solid; mp 98–99 °C; mp (DSC) 101.57 ± 0.88 °C, 174.57 ± 0.07 °C; yield, 98%; ¹H NMR (400 MHz, CD₃OD): δ /ppm 1.3–1.4 (m, 14H, 7 × CH₂), 1.6–1.7 (m, 4H, H-2' and H-10'), 2.18 (m, 2H, H-11'), 3.22 ("t", 1H, $J \sim 8.0$ Hz, H-2), 3.3–3.4 (m, 3H, H-3, H-4 and H-5), 3.58 (m, 1H, H-1'a), 3.70 (dd, 1H, $J_{6a,6b} = 11.9$ Hz, $J_{5,6b} = 5.3$ Hz, H-6a), 3.8–4.0 (m, 2H, H-6b and H-1'b), 4.29 (d, 1H, $J_{1,2} = 7.8$ Hz, H-1). ¹³C NMR (100 MHz, CD₃OD) δ /ppm 21.3 (C-10'), 27.1 (C-3'), 30.2–30.9 (C-2', C-4' to C-9'), 31.8 (t, $J = 22$ Hz, C-11'), 62.9 (C-6), 70.9 (C-1'), 71.8 (C-4), 75.2 (C-2), 77.9 (C-5), 78.3 (C-3), 104.4 (C-1). ¹⁹F NMR (282 MHz, CD₃OD) δ /ppm –81.0 (CF₃), –114.1 (CF₂), –124.0 (CF₂), –125.7 (CF₂). Anal. Calc. for C₂₁H₃₃F₉O₆: C 45.65, H 6.02. Found: C 44.97, H 6.11%. HR-MS of [M + Na]⁺ m/z : Calc. 575.2031, Found. 575.2041.

Alkyl β -D-glucopyranosides

Tetradecyl- β -D-glucopyranoside (9a)^{38,44}. White powder; mp 69–71 °C (lit.: 64.8 °C⁴⁴); mp (DSC) 66.96 ± 2.52 °C, 151.47 ± 3.97 °C; yield, 95%; ¹H NMR (300 MHz, CD₃OD): δ /ppm 0.90 (m, 3H, $J = 6.9$ Hz, H-14'), 1.3–1.4 (m, 22H, 11 × CH₂), 1.63 (m, 2H, H-2'), 3.31 ("t", 1H, $J \sim 8.9$ Hz, H-2), 3.2–3.4 (m, 3H, H-3, 4 and 5, overlapped with residue proton of CD₃OD), 3.57 (m, 1H, H-1'a), 3.71 (dd, 1H, $J_{6a,6b} = 12.0$ Hz, $J_{5,6a} = 5.0$ Hz, H-6a), 3.8–4.0 (m, 2H, H-6b and H-1'b), 4.28 (d, 1H, $J_{1,2} = 7.7$ Hz, H-1). ¹³C NMR (75 MHz, CD₃OD) δ /ppm 14.4 (C-14'), 23.7 (C-13'), 27.1 (C-3'), 30.4–30.8 (C-2', C-4' to C-11'), 33.0 (C-12'), 62.9 (C-6), 71.0 (C-1'), 71.8 (C-4), 75.2 (C-2), 77.9 (C-5), 78.2 (C-3), 104.4 (C-1). Anal. Calc. for C₂₀H₄₀O₆: C 63.80, H 10.71. Found: C 63.97, H 10.67%. HR-MS of [M + Na]⁺ m/z : Calc. 399.2723, Found. 399.2735.

Pentadecyl- β -D-glucopyranoside (9d). White powder; mp 75–77 °C; mp (DSC): 72.27 \pm 2.85 °C, 154.32 \pm 7.84 °C; yield, 95%; ^1H NMR (300 MHz, CD_3OD): δ /ppm 0.90 (m, 3H, $J = 7.0$ Hz, H-15'), 1.2–1.4 (m, 24H, $12 \times \text{CH}_2$), 1.63 (m, 2H, H-2'), 3.19 ("t"), 1H, $J \sim 8.9$ Hz, H-2), 3.2–3.4 (m, 3H, H-3, 4 and 5, overlapped with residue proton of CD_3OD), 3.57 (m, 1H, H-1'a), 3.71 (dd, 1H, $J_{6a,6b} = 12.0$ Hz, $J_{5,6a} = 5.2$ Hz, H-6a), 3.8–4.0 (m, 2H, H-6b and H-1'b), 4.27 (d, 1H, $J_{1,2} = 7.7$ Hz, H-1). ^{13}C NMR (75 MHz, CD_3OD) δ /ppm 14.4 (C-15'), 23.7 (C-14'), 27.1 (C-3'), 30.4–30.8 (C-2', C-4' to C-12'), 33.0 (C-13'), 62.9 (C-6), 71.0 (C-1'), 71.8 (C-4), 75.2 (C-2), 77.8 (C-5), 78.2 (C-3), 104.4 (C-1). Anal. Calc. for $\text{C}_{21}\text{H}_{42}\text{O}_6$: C 64.58, H 10.84. Found: C 64.06, H 10.64%. HR-MS of $[\text{M} + \text{Na}]^+$ m/z : Calc. 413.2879. Found. 413.2870.

Synthesis of orthoester 11

Ag_2CO_3 (5 mmol) was added to a solution of 2,3,4,6-tetraacetyl- α -D-glucopyranosyl bromide (**10**)⁵⁸ in anhydrous DCM (10 mL) at 0 °C under a nitrogen atmosphere. The mixture was stirred for 10 min and alcohol **3e** (5 mmol) in anhydrous DCM (10 mL) was added slowly. After 3 h, additional DCM (20 mL) was added, the reaction mixture was filtered and the solvent removed under reduced pressure. The yellowish residue was purified by column chromatograph on silica gel with hexane and ethyl acetate (3 : 1, v/v) as eluent.

3,4,6-Tri-O-acetyl-1,2-[1-(12,12,13,13,14,14,15,15,16,16,17,17,17-tridecafluoroheptadecyloxy)ethylidene]- α -D-glucopyranose. White powder; mp 82–83 °C; yield, 80%; ^1H NMR (300 MHz, CDCl_3): δ /ppm 1.27 (m, 14H, $7 \times \text{CH}_2$), 1.56 (m, 4H, H-2' and H-10'), 1.71 (s, 3H, CH_3), 2.04–2.11 (m, 11H, $3 \times \text{CH}_3\text{CO}$ and H-11'), 3.46 (t, 2H, $J = 6.6$ Hz, H-1'), 3.96 (m, 1H, H-5), 4.19 (m, 2H, H-2 and H-6aHH), 4.30 (m, 1H, H-6b), 4.90 (m, 1H, H-4), 5.17 ("t"), 1H, $J = 2.7$ Hz, H-3), 5.70 (d, 1H, $J = 5.2$ Hz, H-1). ^{13}C NMR (75 MHz, CDCl_3) δ /ppm 20.3 (C-3'), 20.9–20.1 ($3 \times \text{CH}_3\text{CO}$ and CH_3), 26.3 (C-10'), 29.3–29.9 (C-2', C-4' to C-9'), 31.1 (t, $J = 22$ Hz, C-11'), 63.3 (C-6), 63.9 (C-1'), 67.1 (C-5), 68.4 (C-4), 70.3 (C-3), 73.2 (C-2), 97.1 (C-1), 121.5 (=C(CH_3)OR), 169.4, 169.9, 170.9 ($3 \times \text{COCH}_3$). ^{19}F NMR (282 MHz, CDCl_3): δ /ppm –81.3 (CF₃), –114.9 (CF₂), –122.5 (CF₂), –123.4 (CF₂), –124.1 (CF₂), –126.7 (CF₂). Anal. Calc. for $\text{C}_{31}\text{H}_{41}\text{F}_{13}\text{O}_{10}$: C 45.37, H 5.04. Found: C 45.40, H 5.05%.

Assessment of cytotoxicity

Cancer cell line. The B16F10 mouse melanoma cell line (ECACC) was selected from a panel of cancer cell lines used for testing in our laboratory. The cell line was grown in D-MEM medium (Sigma, Czech Republic) supplemented with 10% of fetal calf serum (Gibco, Czech Republic), 50 mg L⁻¹ penicillin, 50 mg L⁻¹ streptomycin, 100 mg L⁻¹ neomycin, and 300 mg L⁻¹ L-glutamine as reported previously.^{12,46} Cultures were maintained in a humidified incubator (Shellab, Sheldon, OR, USA) at 37 °C and 5% CO₂.

MTT-based cytotoxicity test. The MTT assay^{59,60} was used to assess the cytotoxicity of the glucopyranosides in cells in the exponential growth phase. In short, cells were seeded on 96-well flat-bottom microplates at the density

2.5–3.0 $\times 10^4$ mL⁻¹, 100 μL per well, and allowed to grow for 16–24 h in culture medium. The tested compounds were first dissolved in DMSO (Sigma, Czech Republic) and then in sterile PBS. Final concentrations of DMSO in samples were below 1%. PBS with DMSO (1 and 5%) served as control. No cytotoxicity of 1% DMSO in PBS was observed. Glucopyranosides dissolved in sterile PBS (total volume of 20 μL) were added to each well and the cytotoxic effect was evaluated after 24 h of exposure over a concentration range from 6 μM to 1.5 mM using the MTT assay. Octylthioglucooside (Roche) was used as a positive control.

MTT (Sigma Chemical Co., Czech Republic) was dissolved in PBS at a concentration of 5 mg mL⁻¹ and sterilized by filtration. MTT solution was added into all wells of 96-well flat-bottom microplates with cells in a dose of 20 μL per well. The plates were incubated for 3 h. To enhance the dissolution of dark-purple crystals of formazan, 110 μL of 10% SDS in PBS (final pH 5.5) were added to all wells. The microtitre plates were stored in a light-tight box at room temperature, evaluated on the next day using a well-plate spectrophotometer reader EL 800 (BioTek, USA) at 540 nm and the EC₅₀ (i.e. the molar concentration which produces 50% of the maximum possible inhibitory response) values were calculated from the dose response curves. All experiments were performed in triplicate and EC₅₀ values were calculated using GraphPad PRISM V.4.00 (GraphPad Software Inc., San Diego, CA).

The results from the MTT assay were further confirmed by Hoffman modulation contrast microscopy (epifluorescent inverted microscope T200, Nikon, Japan) exposing morphological changes of the cells treated with various surfactants. Propidium iodide (PI) and YO-PRO-1 (Molecular Probes, Oregon, USA) were used to distinguish dead or apoptotic cells from vital living ones.⁶¹

Haemolytic activity. Rabbit red blood cells (2% in PBS) were used to perform standard haemolytic tests in both PBS and PBS containing 20% fetal bovine serum (Gibco). The surfactants were tested in concentration range extending from 40 μM to 20 mM. The tested compounds were dissolved in DMSO and added into PBS. Maximal final concentration of DMSO in PBS was 5% for 20 mM concentration of tested compound. This concentration of DMSO did not cause any haemolysis in control red blood cells. After 2 h incubation of red cells with a particular compound at 37 °C, the released haemoglobin was separated from red blood cells by centrifugation (700 g, 10 min, three washes) and quantified using a well-plate spectrophotometer reader EL 800 (BioTek, USA) at 540 nm. Data are expressed as the lowest concentration of surfactant causing 50% haemolysis.

Acknowledgements

The authors thank Dr Paul Bummer (University of Kentucky) for access to the DSC instrument. This work was supported by grants from the National Institute of Environmental Health Sciences (ES12475), the National Science Foundation (NIRT 0210517), the US Department of Agriculture Biomass Research and Development Initiative (Grant Agreement

68-3A75-7-608) and the Department of Energy Development and Independence, Energy and Environment Cabinet of The Commonwealth of Kentucky. Additional support was provided by grants from the Ministry of Agriculture of the Czech Republic (grant No. MZE-0002716201) and NAZV QF-3115 to J. T. Its contents are solely the responsibility of the authors and do not necessarily represent the official views of the funding agencies.

References

- 1 J. G. Riess, *J. Fluorine Chem.*, 2002, **114**, 119.
- 2 M. Arora, P. M. Bummer and H.-J. Lehmler, *Langmuir*, 2003, **19**, 8843.
- 3 H.-J. Lehmler and P. M. Bummer, *Biochim. Biophys. Acta*, 2004, **1664**, 141.
- 4 F. Giulieri and M.-P. Krafft, *Colloids Surf., A*, 1994, **84**, 121.
- 5 J. G. Riess and J. Greiner, *Carbohydr. Res.*, 2000, **327**, 147.
- 6 H.-J. Lehmler, P. M. Bummer and M. Jay, *CHEMTECH*, 1999, **29**, 7.
- 7 H.-J. Lehmler, *Expert Opin. Drug Delivery*, 2007, **4**, 247.
- 8 J. B. Nivet, M. Le Blanc and J. G. Riess, *Eur. J. Med. Chem.*, 1991, **26**, 953.
- 9 H. M. Courrier, M. P. Krafft, N. Butz, C. Porte, N. Frossard, A. Remy-Kristensen, Y. Mely, F. Pons and T. F. Vandamme, *Biomaterials*, 2003, **24**, 689.
- 10 V. M. Sadtler, F. Jeanneaux, M. P. Krafft, J. Rahal and J. G. Riess, *New J. Chem.*, 1998, **22**, 609.
- 11 M.-P. Krafft, J.-P. Rolland, P. Vierling and J. G. Riess, *New J. Chem.*, 1990, **14**, 869.
- 12 S. M. Vyas, J. Turanek, P. Knoetigova, A. Kasna, V. Kvardova, V. Koganti, S. E. Rankin, B. L. Knutson and H.-J. Lehmler, *New J. Chem.*, 2006, **30**, 944.
- 13 R. Miethchen and M. Hein, *Carbohydr. Res.*, 2000, **327**, 169.
- 14 H. M. Courrier, T. F. Vandamme and M. P. Krafft, *Colloids Surf., A*, 2004, **244**, 141.
- 15 K.-V. Schubert and E. W. Kaler, *Colloids Surf., A*, 1994, **84**, 97.
- 16 P. LoNostro, S.-M. Choi, C.-Y. Ku and S.-H. Chen, *J. Phys. Chem. B*, 1999, **103**, 5347.
- 17 G. Mathis, P. Leempoel, J. C. Ravey, C. Selve and J. J. Delpuech, *J. Am. Chem. Soc.*, 1984, **106**, 6162.
- 18 C. Ceschin, J. Roques, M. C. Malet-Martino and A. Lattes, *J. Chem. Technol. Biotechnol.*, 1985, **35A**, 73.
- 19 V. M. Sadtler, M. P. Krafft and J. G. Riess, *Angew. Chem., Int. Ed. Engl.*, 1996, **35**, 1976.
- 20 H. M. Courrier, F. Pons, J. M. Lesinger, N. Frossard, M. P. Krafft and T. F. Vandamme, *Int. J. Pharm.*, 2004, **282**, 131.
- 21 J. N. Israelachvili, D. J. Mitchell and B. W. Ninham, *J. Chem. Soc., Faraday Trans. 2*, 1976, **72**, 1525.
- 22 B. J. Boyd, C. J. Drummond, I. Krodkiewska and F. Grieser, *Langmuir*, 2000, **16**, 7359.
- 23 J. Greiner, A. Milius and J. G. Riess, *Tetrahedron Lett.*, 1988, **29**, 2193.
- 24 M. C. Z. Kasuya, R. Cusi, O. Ishihara, A. Miyagawa, K. Hashimoto, T. Sato and K. Hatanaka, *Biochem. Biophys. Res. Commun.*, 2004, **316**, 599.
- 25 M. C. Z. Kasuya, A. Ito, R. Cusi, T. Sato and K. Hatanaka, *Chem. Lett.*, 2005, **34**, 856.
- 26 M. Hein, R. Miethchen, D. Schwaebisch and C. Schick, *Liq. Cryst.*, 2000, **27**, 163.
- 27 M. Hein and R. Miethchen, *Tetrahedron Lett.*, 1998, **39**, 6679.
- 28 M. Hein, R. Miethchen and D. Schwaebisch, *J. Fluorine Chem.*, 1999, **98**, 55.
- 29 H.-J. Lehmler, M. O. Oyewumi, M. Jay and P. M. Bummer, *J. Fluorine Chem.*, 2001, **107**, 141.
- 30 H.-J. Lehmler and P. M. Bummer, *J. Fluorine Chem.*, 2002, **117**, 17.
- 31 C. Naud, P. Calas, H. Blancou and A. Commeyras, *J. Fluorine Chem.*, 2000, **104**, 173.
- 32 M. Graupe, T. Koini, V. Y. Wang, G. M. Nassif, R. Colorado, Jr, R. J. Villazana, H. Dong, Y. F. Miura, O. E. Shmakova and T. R. Lee, *J. Fluorine Chem.*, 1999, **93**, 107.
- 33 S. Konstantinovic, B. Dimitrijevic and V. Radulovic, *Indian J. Chem., Sect. B: Org. Chem. Incl. Med. Chem.*, 2002, **41**, 598.
- 34 V. Vill, T. Böcker, J. Thiem and F. Fischer, *Liq. Cryst.*, 1989, **6**, 349.
- 35 Y. Yuasa and Y. Yuasa, *Org. Process Res. Dev.*, 2004, **8**, 405.
- 36 Z. Petrovic, S. Konstantinovic and A. Spasojevic, *Indian J. Chem., Sect. B: Org. Chem. Incl. Med. Chem.*, 2004, **43**, 132.
- 37 V. Ladmiral, G. Mantovani, C. G. J., S. Cauet, J. L. Irwin and D. M. Haddleton, *J. Am. Chem. Soc.*, 2006, **128**, 4823.
- 38 G. Milkereit, M. Morr, J. Thiem and V. Vill, *Chem. Phys. Lipids*, 2004, **127**, 47.
- 39 V. Vill, H. M. von Minden, M. H. J. Koch, U. Seydel and K. Brandenburg, *Chem. Phys. Lipids*, 2000, **104**, 75.
- 40 C. L. Stevens, G. H. Ransford, J. Nemeo, J. M. Cahoon and P. M. Pillai, *J. Org. Chem.*, 1974, **39**, 298.
- 41 H. Paulsen and M. Paal, *Carbohydr. Res.*, 1985, **137**, 39.
- 42 D. S. K. Tsui and P. A. J. Gorin, *Carbohydr. Res.*, 1985, **144**, 137.
- 43 V. Vill, H. M. von Minden, M. H. J. Koch, U. Seydel and K. Brandenburg, *Chem. Phys. Lipids*, 2000, **104**, 75.
- 44 V. Adasch, B. Hoffmann, W. Milius, G. Platz and G. Voss, *Carbohydr. Res.*, 1998, **314**, 177.
- 45 H. Kiwada, H. Niimura, Y. Fujisaki, S. Yamada and Y. Kato, *Chem. Pharm. Bull.*, 1985, **33**, 753.
- 46 J. Turanek, A. Kasna, D. Zaluska, J. Neca, V. Kvardova, P. Knoetigova, V. Horvath, L. Sindlerova, A. Kozubik, P. Sova, A. Kroutil, F. Zak and A. Mistr, *Anti-Cancer Drugs*, 2004, **15**, 537.
- 47 A. Milius, J. Greiner and J. G. Riess, *New J. Chem.*, 1991, **15**, 337.
- 48 L. Zanf, J. Greiner and J. G. Riess, *J. Fluorine Chem.*, 1989, **44**, 73.
- 49 S. Abouhilale, J. Greiner and J. G. Riess, *J. Am. Oil Chem. Soc.*, 1992, **69**, 1.
- 50 L. Zarif, J. Greiner, S. Pace and J. G. Riess, *J. Med. Chem.*, 1990, **33**, 1262.
- 51 H.-J. Lehmler, M. Jay and P. M. Bummer, *Langmuir*, 2000, **16**, 10161.
- 52 H.-J. Lehmler and P. M. Bummer, *Colloids Surf., B*, 2005, **44**, 74.
- 53 H.-J. Lehmler and P. M. Bummer, *J. Lipid Res.*, 2005, **46**, 2415.
- 54 J. J. P. Stewart, Fujitsu Limited, Tokyo, Japan, 2000.
- 55 M. C. Kasuya, M. Ikeda, K. Hashimoto, T. Sato and K. Hatanaka, *J. Carbohydr. Chem.*, 2005, **24**, 705.
- 56 Z. Li, L. Cai and M. Cai, *Synth. Commun.*, 1992, **22**, 2121.
- 57 D. Tickle, A. George, K. Jennings, P. Camilleri and A. J. Kirby, *J. Chem. Soc., Perkin Trans. 2*, 1998, 467.
- 58 P. R. Andriana, W. Xie, H. N. Cheng, L. Qiao, D. J. Murphy, Q.-M. Gu and P. G. Wang, *Org. Lett.*, 2002, **4**, 1863.
- 59 T. Mosmann, *J. Immunol. Methods*, 1983, **65**, 55.
- 60 U. Bank, D. Reinhold and S. Ansoerg, *Allerg. Immunol.*, 1991, **37**, 119.
- 61 T. Idziorek, J. Estaquier, F. De Bels and J.-C. Ameisen, *J. Immunol. Methods*, 1995, **185**, 249.



Contents lists available at ScienceDirect

Colloids and Surfaces B: Biointerfaces

journal homepage: www.elsevier.com/locate/colsurfb

Hydrophobic tail length, degree of fluorination and headgroup stereochemistry are determinants of the biocompatibility of (fluorinated) carbohydrate surfactants

Xueshu Li^a, Jaroslav Turánek^{b,*,**}, Pavlína Knötičková^b, Hana Kudláčková^b, Josef Mašek^b, Sean Parkin^c, Stephen E. Rankin^d, Barbara L. Knutson^d, Hans-Joachim Lehmler^{a,*,8}

^a Department of Occupational and Environmental Health, University of Iowa, Iowa City, IA 52242, USA

^b Veterinary Research Institute v.v.i., Department of Vaccinology and Immunotherapy, Brno, Czech Republic

^c Department of Chemistry, University of Kentucky, Lexington, KY 40506, USA

^d Department of Chemical and Materials Engineering, University of Kentucky, Lexington, KY 40506, USA

ARTICLE INFO

Article history:

Received 16 April 2009

Received in revised form 28 April 2009

Accepted 28 April 2009

Available online 5 May 2009

Keywords:

Cytotoxicity

Haemolytic activity

Surfactant–lipid interactions

DPPC

Fluorescence anisotropy

ABSTRACT

A series of hydrocarbon and fluorocarbon carbohydrate surfactants with different headgroups (i.e., gluco-, galacto- and maltopyranoside) and (fluorinated) alkyl tails (i.e., C₇ and C₁₄ to C₂₀) was synthesized to investigate trends in their cytotoxicity and haemolytic activity, and how surfactant–lipid interactions of selected surfactants contribute to these two measures of biocompatibility. All surfactants displayed low cytotoxicity (EC₅₀ = 25 to >250 μM) and low haemolytic activity (EC₅₀ = 0.2 to >3.3 mM), with headgroup structure, tail length and degree of fluorination being important structural determinants for both endpoints. The EC₅₀ values of hydrocarbon and fluorocarbon glucopyranoside surfactants displayed a “cut-off” effect (i.e., a maximum with respect to the chain length). According to steady-state fluorescence anisotropy studies, short chain (C₇) surfactants partitioned less readily into model membranes, which explains their low cytotoxicity and haemolytic activity. Interestingly, galactopyranosides were less toxic compared to glucopyranosides with the same hydrophobic tail. Although both surfactant types only differ in the stereochemistry of the 4-OH group, hexadecyl gluco- and galactopyranoside surfactants had similar apparent membrane partition coefficients, but differed in their overall effect on the phase behaviour of DPPC model membranes, as assessed using steady-state fluorescence anisotropy studies. These observations suggest that highly selective surfactant–lipid interactions may be responsible for the differential cytotoxicity and, possibly, haemolytic activity of hydrocarbon and fluorocarbon carbohydrate surfactants intended for a variety of pharmaceutical and biomedical applications.

© 2009 Elsevier B.V. All rights reserved.

1. Introduction

Self-assembled supramolecular nano- and micro-structures (such as liposomes, microemulsions and microbubbles) of simple, single-tailed carbohydrate surfactants with a hydrocarbon or a partially fluorinated hydrophobic tail are of interest for a number of pharmaceutical and biomedical applications. Hydrocarbon carbohydrate surfactants have been studied as solubilising agents in aqueous formulations and offer several advantages compared to classical polyoxyethylene-based surfactants, including comparatively high purity, biodegradability and production from renewable sources [1,2]. Fluorinated, carbohydrate-based surfactants are of interest for pharmaceutical applications, such as novel perfluoro-

rocarbon compound (PFC)-based drug delivery systems [3–5]. In particular reverse water-in-PFC (micro-)emulsions are investigated for the pulmonary administration to the diseased lung [4–6]. These reverse emulsions allow the delivery of a well-defined dose of pharmaceutical agents directly to the diseased lung via the airways, for example during liquid ventilation [6,7], without adversely impairing gas exchange in the lung [4–6]. Because of this broad range of pharmaceutical and biomedical applications, there is considerable interest in developing new, biocompatible carbohydrate-based surfactants.

Despite their potential use in a range of pharmaceutical application, structure–toxicity relationships of hydrocarbon and fluorocarbon carbohydrate surfactants in general and simple gluco-, galacto- and maltopyranoside surfactants in particular are poorly developed, especially in mammalian systems. Only a few reports have investigated the toxicity and haemolytic activities of hydrocarbon [1,2,8,9] and fluorocarbon surfactants [10–15] with carbohydrate headgroups. Limited studies of the effect of different carbohydrate surfactants on model membranes [16] and the

* Corresponding author. Tel.: +1 319 335 4211; fax: +1 319 335 4290.

** Corresponding author. Tel.: +420 5 3333 1311; fax: +420 5 4121 1229.

E-mail addresses: turanek@vri.cz (J. Turánek), hans-joachim-lehmler@uiowa.edu (H.-J. Lehmler).

In vitro haemolytic activity [2] suggest that the headgroup and the hydrophobic tail are both important structural determinants of surfactant–lipid interactions and, thus, toxicity and haemolytic activity. There is also evidence that an increasing degree of fluorination reduces both toxicity and haemolytic activity compared to the corresponding hydrocarbon surfactant [10–15]. However, it is unclear if carbohydrate surfactants also display a “cut-off effect” in biological activities (e.g., a maximum in activity based on chain length) that is characteristic of many non-ionic surfactants [17]. Little is also known about the interaction of carbohydrate surfactants with model membranes and biological lipid assemblies. This is an important gap in our knowledge because surfactants that have a high affinity for lipid membranes may adversely affect membrane permeability, fluidity, curvature and, ultimately, membrane function.

Most of the above mentioned studies are limited to a comparatively small number of commercially available carbohydrate surfactants, thus limiting efforts to understand if general trends in cytotoxicity and haemolytic activity are related to surfactant–lipid interactions. Here we investigate the cytotoxicity and haemolytic activity of a series of hydrocarbon and fluorocarbon gluco-, galacto- and maltopyranoside surfactants *In vitro* to identify structural factors (e.g., chemical structure of the headgroup, length and degree of fluorination of the hydrophobic tail) influencing both measures of biocompatibility. Subsequently, the membrane partitioning behaviour of selected surfactants is investigated to aid in our understanding of general trends in cytotoxicity and haemolytic activity.

2. Materials and methods

2.1. General methods

The long-chain hydrocarbon starting material **1a** and **1b** were purchased from TCI Chemicals (Portland, Oregon, USA). Pentaacetyl- β -D-glucopyranose (**4**), the long chain alkyl alcohols **3** and anhydrous dichloromethane were obtained from Fisher Scientific (Fairlawn, New Jersey, USA). Perfluorinated iodides were purchased from Oakwood Chemical Co. (West Columbia, South Carolina, USA). Heptyl- β -D-glucopyranoside (**β -13a**) was purchased from EMD Biosciences Inc. (San Diego, CA, USA). The synthesis and characterization of all other carbohydrate surfactants (Scheme 1) is described in detail in the supporting material. L- α -Dipalmitoylphosphatidylcholine (DPPC, >99%) was purchased from Avanti Polar Lipid (Alabaster, AL, USA); 1,6-Diphenyl-1,3,5-hexatriene (DPH, >99%), was purchased from Molecular Probes (Eugene, OR). Chloroform (>99.9%) and tetrahydrofuran (THF, >99.9%) were purchased from Fisher Scientific. Deionized ultrafiltered water (DIUF) was obtained using a MILLI-Q system (Millipore, Billerica, Massachusetts, USA).

2.2. Assessment of cytotoxicity

2.2.1. Cancer cell line

The B16F10 mouse melanoma cell line (Interlab Cell Line Collection, Milano, Italy) was selected from a panel of cancer cell lines used for testing in our laboratory. The cell line was grown in D-MEM medium (Sigma Chemical Co., Czech Republic) supplemented with 10% of fetal calf serum (Gibco, Czech Republic), 50 mg L⁻¹ penicillin, 50 mg L⁻¹ streptomycin, 100 mg L⁻¹ neomycin, and 300 mg L⁻¹ L-glutamine as reported previously [18,19]. Cultures were maintained in a humidified incubator at 37 °C and 5% CO₂.

2.2.2. MTT-based cytotoxicity test

The MTT assay [20,21] was used to assess the cytotoxicity of the glucopyranosides in cells in the exponential growth phase.

In short, cells were seeded on 96-well flat-bottom microplates at the density 2.5–3.0 × 10⁵ per mL, 100 μ L per well, and allowed to grow for 16–24 h in culture medium. The tested compounds were first dissolved in DMSO (Sigma, Czech Republic) and then in sterile PBS. Final concentrations of DMSO in samples were below 1%. PBS with DMSO (1 and 5%) served as control. No cytotoxicity of 1% DMSO in PBS was observed. Glycopyranosides dissolved in sterile PBS (total volume of 20 μ L) were added to each well and the cytotoxic effect was evaluated after 24 h of exposure over a concentration range from 1 μ M to 250 μ M using the MTT assay. Octylthioglycoside (Roche, Czech Republic) was used as a positive control.

MTT (Sigma Chemical Co., Czech Republic) was dissolved in PBS at a concentration of 5 mg mL⁻¹ and sterilized by filtration. MTT solution was added into all wells of 96-well flat-bottom microplates with cells in a dose of 20 μ L per well. The plates were incubated for 3 h. To enhance the dissolution of dark-purple crystals of formazan, 110 μ L of 10% SDS in PBS (final pH 5.5) were added to all wells. The microtiter plates were stored in a light-tight box at room temperature, evaluated on the next day using a well-plate spectrophotometer reader Synergy 2 (BioTek, USA) at 540 nm and the EC₅₀ values (i.e. the molar concentration which produces 50% of the maximum possible inhibitory response) were calculated from the dose response curves. All experiments were performed in triplicate and EC₅₀ values were calculated using GraphPad PRISM V.4.00 (GraphPad Software Inc., San Diego, California, USA).

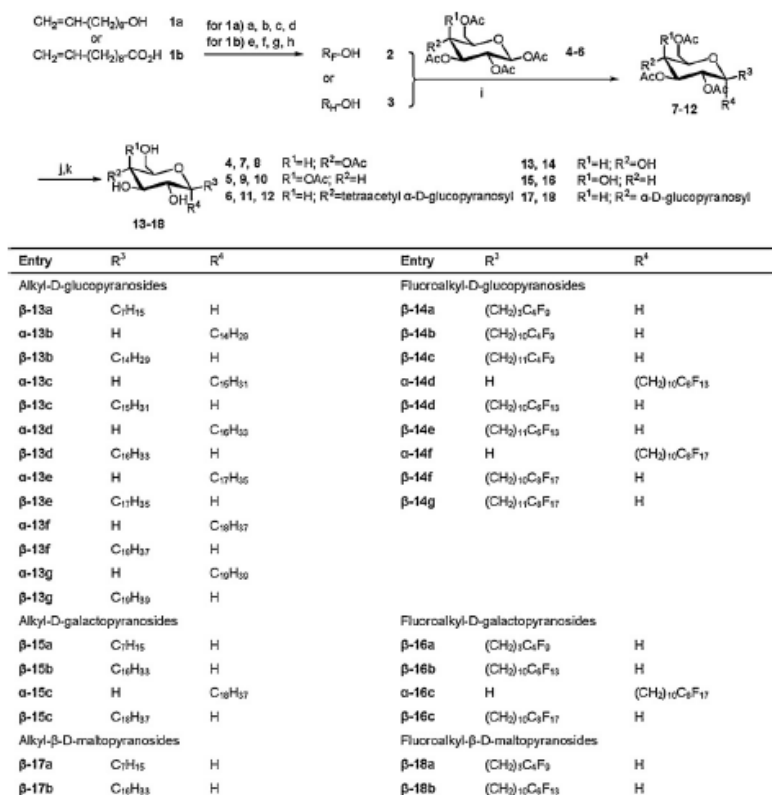
2.2.3. Haemolytic activity

Rabbit red blood cells (2% in PBS) were used to perform standard haemolytic tests in both PBS and PBS containing 20% fetal bovine serum (Gibco). The surfactants were tested in concentration range extending from 7 μ M to 3.3 mM. The tested compounds were dissolved in DMSO and added into PBS. Maximal final concentration of DMSO in PBS was 5% for 20 mM concentration of tested compound. This concentration of DMSO does not cause any haemolysis in control red blood cells. After 2 h incubation of red cells with a particular compound at 37 °C, the released haemoglobin was separated from red blood cells by centrifugation (700 g, 10 min, three washes) and quantified using a well-plate spectrophotometer reader EL 800 (BioTek, Winooski, Vermont, USA) at 540 nm. Data are expressed as the lowest concentration of surfactant causing 50% haemolysis.

2.3. Fluorescence anisotropy studies

2.3.1. Preparation of DPH-labelled DPPC vesicles

Multilamellar vesicles (MLVs) of DPPC containing increasing concentration (0–20 μ M) of carbohydrate surfactants and DPH with the lipid-to-DPH molar ratio of 500:1 were prepared [22]. In short, 250 μ L of a DPPC solution (1 mM in chloroform), 2 μ L of a DPH solution (0.25 mM in THF) and the appropriate volume of a solution of carbohydrate surfactant **β -13a**, **β -13d** or **β -15b** (1 mM in chloroform) were mixed well before removing the solvent using a rotary evaporator under reduced pressure at 30 °C. After being dried under a high vacuum for 2 h to remove solvent traces, the resulting films were hydrated with 1 mL of ultra-pure water well above the phase transition temperature of DPPC ($T > 50$ °C) for 1 h. Subsequently, the liposome suspensions were vortexed for 3 min to uniformly disperse the MLVs. Large unilamellar vesicles (LUVs) were obtained from the MLVs by extruding the suspension 15 times through a double-stacked polycarbonate membrane filter (pore size: 100 nm) using a LiposFast extruder (Avestin Inc., British Columbia, Canada) at 50 °C. The resulting lipid dispersions were stored at room temperature and used within 24 h of preparation. The final working samples were prepared by diluting the 100 μ L of the LUV suspensions with 2400 μ L of ultra-pure water.



Scheme 1. Synthesis and chemical structure of perfluoroalkyl and alkyl glycosides. ((a) DMAP, Ac-Cl, pyridine, DCM; (b) F(CF₂)_mI, AIBN; (c) HI (55%), Zn, C₂H₅OH; (d) CH₃OH, KDH; (e) CH₃OH, PTSA, toluene; (f) F(CF₂)_mI (m = 4,6 or 8), AIBN; g. HI (55%), Zn, C₂H₅OH; (h) LiAlH₄, anhydrous ether, ambient temperature; (i) BF₃/OEt₂ (48%), anhydrous DCM (α-anomer: 0 °C for 20 min, then 30 °C for 10 h; β-anomer: 0 °C for 2 h, then warmed to ambient temperature); (j) MeONa/MeOH, 0 °C to ambient temperature; (k) Dowex®50W × 8–100 ion-exchange resin).

2.3.2. Measurement of steady-state anisotropy

Steady-state DPH fluorescence anisotropy experiments with the final working solutions were carried out using a LS55 Luminescence Spectrometer from PerkinElmer (Shelton, CT, USA) as described previously [22]. In short, the cuvette chamber was thermally controlled using a PerkinElmer PTP-1 Peltier System (Shelton, CT, USA). The solutions were mixed continuously with a small magnetic stir bar at low speed. The steady-state DPH anisotropy within the DPPC bilayer was determined at $\lambda_{\text{ex}} = 350$ nm and $\lambda_{\text{em}} = 452$ nm with an excitation and emission slit width of 10 nm. For the fluorescence experiment, the samples were equilibrated at 50 °C for 15 min and subsequently cooled to 20 °C with a rate of 0.2 °C/min. DPH anisotropy values (r) were calculated from Eq. (1) as follows,

$$r = \frac{I_{\text{VV}} - G \times I_{\text{VH}}}{I_{\text{VV}} + 2G \times I_{\text{VH}}} \quad (1)$$

where I_{VV} and I_{VH} are the values of the fluorescence intensity measured with both polarizers in vertical (VV) orientations or with the excitation polarizer in vertical and emission polarizer in horizontal position (VH), respectively. G is a correction factor for differences in sensitivity of the detection system for vertically and horizon-

tally polarized light. T_m , the temperatures at the midpoint of the phase transition were determined from plots of absolute fluorescence anisotropy as a function of temperature [22]. All fluorescence experiments were carried out in triplicate.

2.3.3. Calculation of apparent partition coefficients

The partition coefficients K of the surfactant between DPPC bilayers and the aqueous phase were calculated based on shifts in melting temperature [22,23] according to the equation

$$-\Delta T_m = \frac{R \cdot T_{m,0}^2}{\Delta H_m} \frac{K \cdot C_A}{55.5 + K \cdot C_L} \quad (2)$$

where $T_{m,0}$ represents the phase transition temperature without additives and ΔT_m (i.e., $T_m - T_{m,0}$) is the changes of the melting temperature according to DPPC vesicles without additives. ΔH_m is the enthalpy change associated with the phase transition (31.38 kJ·mol⁻¹) [24] and R is the gas constant (8.314 J·K⁻¹·mol⁻¹). C_L and C_A denote the total lipid concentration and the concentration of additive (surfactant), respectively.

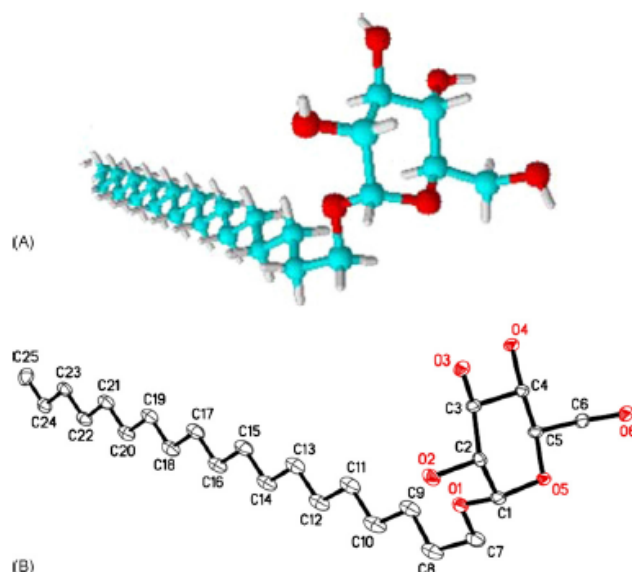


Fig. 1. Molecular structures of nonadecyl α -D-glucopyranoside (α -13g). (A) 3D Structure obtained by geometry optimization using the AM1 semi-empirical molecular orbital method [15]. (B) Crystal structure showing the atom-labelling scheme. Displacement ellipsoids are drawn at 50% probability level.

3. Results

3.1. Synthesis

To further explore structure–toxicity relationships of simple, single-tailed carbohydrate surfactants and to investigate their interaction with (model) membranes, we synthesized and characterized a series of 34 α - and β -gluco-, galacto- and maltopyranosides and 4 mixtures containing the α - and β -anomers of the respective surfactants (Scheme 1). All surfactants were synthesized from a fluorinated alcohol **2** and the appropriate peracetylated carbohydrate (**4–6**) as described previously for β -glucopyranoside surfactants [15]. In short, the fluorinated alcohols **2** were prepared from 9-decen-1-ol (**1a**) or undecenoic acid (**1b**) in four steps as described earlier [15,19]. Subsequently, peracetylated gluco- (**7** and **8**),

galacto- (**9** and **10**) or maltopyranosides (**11** and **12**) were obtained by reacting the fluorinated alcohols **2** (or the corresponding hydrocarbon analogues **3**) with the corresponding peracetylated β -D-gluco- (**4**), β -D-galacto- (**5**) or β -maltopyranosides (**6**) using $\text{BF}_3 \cdot \text{Et}_2\text{O}$ as catalyst [13,25–28]. The respective α - and β -anomers were obtained by controlling the reaction temperature and time (β -anomers: $<5^\circ\text{C}$ and $<3\text{ h}$; α -anomers: 30°C and 10 h). In the final step of the synthesis, the (*F*-)alkylated peracetylated carbohydrates **7–12** were deacetylated using NaOMe in absolute methanol, followed by neutralization with Dowex[®] 50W $\times 8$ –100 ion exchange resin [27]. The surfactants were obtained in moderate-to-good yields and are $>95\%$ pure. Molecular structures of nonadecyl α -D-glucopyranoside (α -13g) obtained by geometry optimization using the AM1 semi-empirical molecular orbital method or crystal structure analysis are shown in Fig. 1.

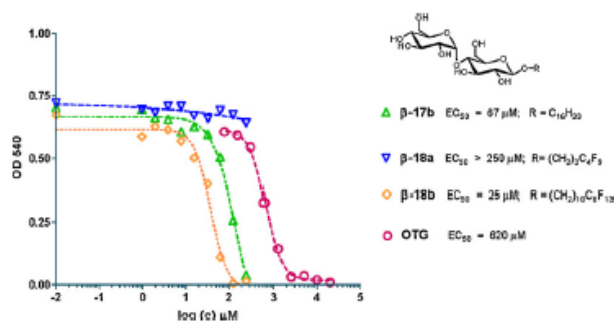
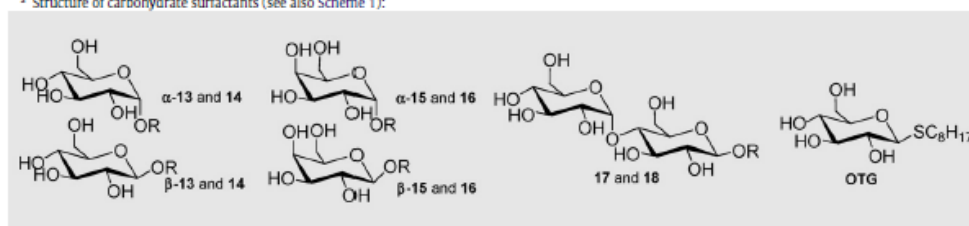


Fig. 2. Cytotoxic effect of maltopyranosides β -17b, β -18a and β -18b in the B16F10 mouse melanoma cell line. B16F10 cells were exposed for 24 h to the respective carbohydrate surfactants at the concentrations shown and assessed for MTT activity as described under materials and methods. A representative hydrocarbon surfactant, octylthioglucooside (OTG), is shown for comparison.

Table 1
Assessment of cytotoxicity and haemolytic activity of partially fluorinated carbohydrate surfactants and their hydrocarbon analogues in B16F10 cell line^a.

Entry	Structure of tails	Cytotoxicity EC ₅₀ (μM)	Haemolytic activity EC ₅₀ (mM) Without serum	20% serum
Alkyl glucopyranosides				
α-13b	C ₁₄ H ₂₉	53	2.5	>3.3 (30%)
α-13c	C ₁₅ H ₃₁	67	>3.3 (20%)	>3.3
α-13d	C ₁₆ H ₃₃	70	>3.3 (20%)	>3.3
α-13e	C ₁₇ H ₃₅	37	>3.3 (25%)	>3.3
α-13f	C ₁₈ H ₃₇	>250	>3.3	>3.3
α-13g	C ₁₉ H ₃₉	>250	>3.3	>3.3
β-13a	C ₇ H ₁₅	>250	>3.3	>3.3
β-13b ^b	C ₁₄ H ₂₉	41	1.7	2.5
β-13c ^b	C ₁₅ H ₃₁	38	0.8	2.5
β-13d ^b	C ₁₆ H ₃₃	50	>3.3 (30%)	>3.3
β-13e ^b	C ₁₇ H ₃₅	38	2.5	>3.3 (5%)
β-13f ^b	C ₁₈ H ₃₇	32	>3.3 (10%)	>3.3
β-13g ^b	C ₁₉ H ₃₉	100	>3.3	>3.3
(α+β)-13b ^c	C ₁₄ H ₂₉	62	0.8	1.7
(α+β)-13g ^d	C ₁₉ H ₃₉	>250	>3.3 (5%)	>3.3
Perfluoroalkyl glucopyranosides				
α-14d	(CH ₂) ₁₀ C ₆ F ₁₃	47	>3.3 (5%)	>3.3
α-14f	(CH ₂) ₁₀ C ₈ F ₁₇	>250	>3.3	>3.3
β-14a	(CH ₂) ₃ C ₄ F ₉	>250	>3.3	>3.3
β-14b ^e	(CH ₂) ₁₀ C ₆ F ₁₃	32	>3.3 (10%)	>3.3 (10%)
β-14c ^e	(CH ₂) ₁₁ C ₈ F ₁₇	32	2.5	>3.3
β-14d ^e	(CH ₂) ₁₀ C ₆ F ₁₃	52	>3.3 (25%)	>3.3
β-14e ^e	(CH ₂) ₁₁ C ₈ F ₁₇	30	>3.3	>3.3
β-14f ^e	(CH ₂) ₁₀ C ₈ F ₁₇	>250	>3.3	>3.3
β-14g ^e	(CH ₂) ₁₁ C ₈ F ₁₇	>250	>3.3	>3.3
(α+β)-14a ^e	(CH ₂) ₃ C ₄ F ₉	>250	>3.3	>3.3
(α+β)-14g ^f	(CH ₂) ₁₁ C ₈ F ₁₇	>250	>3.3	>3.3
Alkyl galactopyranosides				
α-15c	C ₁₈ H ₃₇	>250	>3.3	>3.3
β-15a	C ₇ H ₁₅	>250	>3.3	>3.3
β-15b	C ₁₆ H ₃₃	>250	>3.3 (40%)	>3.3
β-15c	C ₁₈ H ₃₇	>250	>3.3 (20%)	>3.3
Perfluoroalkyl galactopyranosides				
α-16c	(CH ₂) ₁₀ C ₆ F ₁₃	>250	>3.3 (10%)	>3.3
β-16a	(CH ₂) ₃ C ₄ F ₉	>250	>3.3	>3.3
β-16b	(CH ₂) ₁₀ C ₆ F ₁₃	>250	>3.3 (20%)	>3.3 (5%)
β-16c	(CH ₂) ₁₀ C ₈ F ₁₇	>250	>3.3 (5%)	>3.3
Alkyl maltopyranosides				
β-17a	C ₇ H ₁₅	>250	>3.3	>3.3
β-17b	C ₁₆ H ₃₃	67	0.03	0.15
Perfluoroalkyl maltopyranosides				
β-18a	(CH ₂) ₃ C ₄ F ₉	>250	>3.3	>3.3
β-18b	(CH ₂) ₁₀ C ₆ F ₁₃	25	1.7	2.5
Positive control				
OTG	Octylthioglucoside	620	0.5	3

^a Structure of carbohydrate surfactants (see also Scheme 1):



^b The data have been reported previously [15].

^c α-13b: β-13b = 1: 4.

^d α-13g: β-13g = 1: 2.

^e α-14a: β-14a = 1: 6.

^f α-14g: β-14g = 1: 1.

3.2. Cytotoxicity in the B16F10 mouse melanoma cell line

An initial cytotoxicity assessment of all 34 alkyl- and fluoro-alkyl carbohydrate surfactants (plus 4 mixtures of α - and β -anomers) was performed using the B16F10 mouse melanoma cell line to assess their overall biocompatibility and gain insights into structure-toxicity relationships. The cytotoxicities of the test compounds, expressed as EC_{50} values, are summarized in Table 1. Representative cytotoxicity curves for maltopyranosides surfactants **β -17b**, **β -18a** and **β -18b** are presented in Fig. 2. The C_{14} to C_{17} hydrocarbon α - (**α -13b-e**) and β -glucopyranosides (**β -13b-e**) showed mild cytotoxicity, with EC_{50} values in the range of 37–70 μ M. The C_{18} and C_{19} α -glucopyranosides **α -13f** and **α -13g** did not show a cytotoxic effect in the concentration range investigated, whereas the corresponding β -glucopyranosides **β -13f** and **β -13g** were moderately toxic. Mixtures of α - and β -glucopyranosides **13b** and **13g** had cytotoxicities that were similar to the toxicity of the pure α - and β -anomers. The cytotoxicity of β -glucopyranosides with short C_7 alkyl (**β -13a**) or fluorinated alkyl chains (**β -14a**) was insignificant and comparable to the positive control, octylthioglucoside (EC_{50} >250 μ M). α - and β -glucopyranosides with partially fluorinated C_{14} to C_{17} alkyl chains (**α -14d** and **β -14b-e**) had EC_{50} values that were comparable to the corresponding hydrocarbon derivatives. Glucopyranosides with the highest degree of fluorination (i.e., **α -14f** and **β -14f-g**) were not cytotoxic, with EC_{50} values >250 μ M, whereas the hydrocarbon C_{18} and C_{19} β -glucopyranosides **β -13f** and **β -13g** were moderately cytotoxic (EC_{50} values of 32 and 100 μ M, respectively).

In contrast to the gluco- and maltopyranosides (see below), all surfactants based on α - (**α -15c** and **α -16c**) or β -galactose (**β -15a-c** and **β -16a-c**) were nontoxic, with EC_{50} values >250 μ M. This is a surprising observation considering the structural similarity between the gluco- and galactopyranosides.

The EC_{50} values of β -maltopyranosides with C_{16} alkyl (**β -17b**) and C_{16} fluoroalkyl chains (**β -18b**) were 67 and 25 μ M, respectively, which is within the range observed for the structurally related C_{16} glucopyranosides. β -Maltopyranosides with a short C_7 alkyl (**β -17a**) or C_7 fluoroalkyl chain (**β -18a**) were nontoxic within the concentration range investigated (EC_{50} >250 μ M), which is also comparable to the EC_{50} values observed with analogous C_7 gluco- and galactopyranosides.

3.3. Haemolytic activity

Much higher concentrations of the surfactants were generally needed to induce haemolysis. In fact, most carbohydrate surfactants displayed no *in vitro* haemolytic activity, with EC_{50} values >3.3 mM (Table 1). Only a few surfactants were slightly haemolytic, with EC_{50} ranging from 0.8 to 2.5 mM. This moderate haemolytic activity was suppressed by the addition of serum, which is known to have a protective effect on cell membranes in the presence of surfactants. No correlation was observed between the haemolytic activity and the cytotoxicity.

The alkyl α -glucopyranosides **α -13b-e** showed a slight indication of haemolysis at 3.3 mM concentrations, whereas the long-chain derivatives **α -13f** and **α -13g** were not haemolytic in the concentration range under investigation. This is in contrast to the alkyl β -glucopyranosides **β -13b** and **β -13c**, which appeared to have slightly more haemolytic activity compared to the corresponding α -glucopyranosides. The C_7 glucopyranosides **β -13a** and **β -14a** were essentially nonhaemolytic at concentrations below 3.3 mM. In contrast, the positive control, octylthioglucoside, showed significant haemolytic activity in the concentration range investigated, with an EC_{50} of 0.5 mM. Partially fluorinated α - and β -glucopyranosides **14** displayed slightly lower haemolytic activities compared to their hydrocarbon analogues.

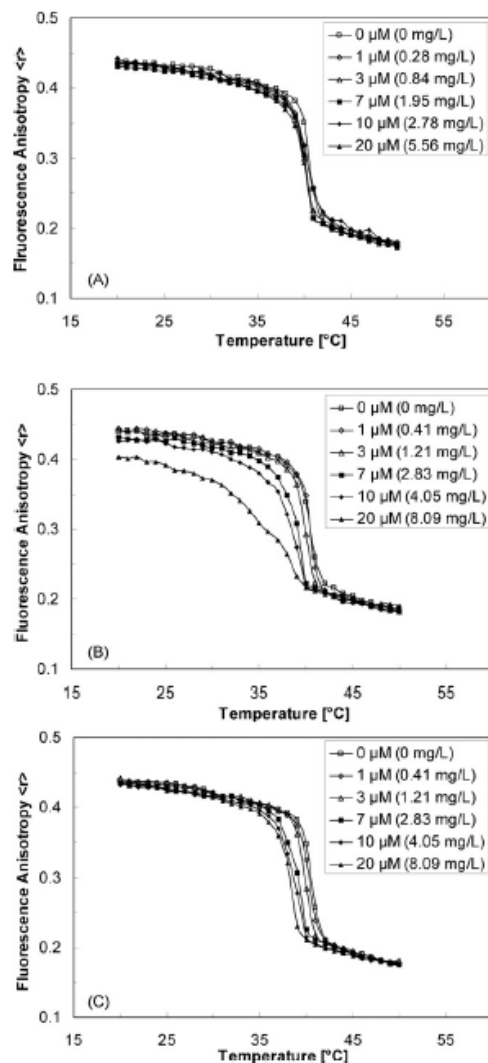


Fig. 3. Temperature-dependent changes of DPH fluorescent anisotropy in DPPC bilayers for selected concentrations of carbohydrate surfactants **β -13a** (A), **β -13d** (B) or **β -15b** (C), respectively. Samples containing 10 μ M of DPPC were cooled from 50 to 20 $^\circ\text{C}$ at a rate of 0.2 $^\circ\text{C}/\text{min}$. The excitation and emission wavelengths are 350 nm and 452 nm, respectively. The excitation and emission slit widths are both 10 nm.

Hydrocarbon and fluorocarbon surfactants based on α - and β -galactose (**α -15c** or **β -15a-c** and **α -16c** or **β -16a-c**, respectively) were slightly less haemolytic compared to analogous glucopyranosides. In contrast to the corresponding β -glucopyranosides [15], the partially fluorinated tail conveyed little-to-no protection against haemolysis.

Like other C_7 carbohydrate surfactants, both β -maltopyranoside C_7 surfactants (**β -17a** and **β -18a**) were nonhaemolytic, whereas the

C_{16} maltopyranoside surfactant **β -17b** was the most haemolytic compound under investigation. The high haemolytic activity of **β -17b** was substantially suppressed by addition of serum. Introduction of a partially fluorinated C_{16} chain (**β -18b**) suppressed haemolytic activity by more than one order of magnitude. The relatively high haemolytic activity of **β -17b** suggests a specific effect of this surfactant on red cell membranes compared to other carbohydrate surfactants.

3.4. Assessment of membrane partition behaviour using steady-state fluorescence anisotropy

The partitioning of carbohydrate surfactants into model or cell membranes is expected to alter membrane properties, such as fluidity and/or curvature. These changes may explain the trends in cytotoxicity and haemolytic activity. To test this hypothesis, we studied the effect of three hydrocarbon surfactants, **β -13a**, **β -13d** and **β -15b**, on dipalmitoylphosphatidylcholine (DPPC) model membranes using 1,6-diphenyl-1,3,5-hexatriene (DPH) fluorescence anisotropy. Measurements of the fluorescence anisotropy (r) (Eq. (1)) are extensively used to study the effect of small molecules on membrane behaviour by assessing changes in the rotational diffusion of the fluorophore (i.e., DPH) that are thought to correlate with the fluidity of the membrane [29].

Fig. 3 shows the temperature-dependent change in the fluorescent anisotropy (r) of DPH-labelled DPPC bilayers for selected concentrations of the respective carbohydrate surfactant. Upon cooling, the DPPC model membrane displayed a characteristic, sharp change in the fluorescence anisotropy. This change in the fluorescence anisotropy indicates a significant change in the fluidity of the bilayer due to the transition from the liquid-crystalline to the gel-phase of DPPC. The midpoint of this change in (r) corresponds to the major phase transition temperature (T_m) of DPPC. The width of the phase transition can be calculated from the on- and offset of the change in (r). Similar to other small molecules, T_m decreased and the transition width increased with increasing concentrations of all three carbohydrate surfactants. The increase in the transition width was especially significant for the C_{16} glucopyranoside **β -13d**.

As shown in Fig. 4, the decrease in T_m differed significantly between the three surfactants. The T_m of hexadecyl β -D-glucopyranoside (**β -13d**) decreased linearly over the entire concentration range investigated (0–20 μ M), whereas the structurally similar hexadecyl β -D-galactopyranoside (**β -15b**) displayed a linear decrease in T_m up to a surfactant concentration of 7 μ M and an approximately constant T_m at concentrations ≥ 10 μ M. In contrast, the short-tailed surfactant, heptyl β -D-glucopyranoside (**β -13a**), decreased the phase transition temperature of DPPC only

slightly over the same concentration range. The membrane partition coefficients calculated using equation 2 from the depression of T_m increased in the order heptyl β -D-glucopyranoside (**β -13a**, 4.61×10^4 , $R^2 = 0.98$) \ll hexadecyl β -D-glucopyranoside (**β -13d**, 2.78×10^5 , $R^2 = 0.99$) $<$ hexadecyl β -D-galactopyranoside (**β -15b**, 5.15×10^5 , $R^2 = 0.99$).

4. Discussion

In the present study we investigate general trends in the cytotoxicity and haemolytic activity of a series of 34 hydrocarbon and fluorocarbon carbohydrate surfactants. Subsequently, the membrane partition behaviour of selected surfactants was investigated *in vitro* to assess if surfactant–lipid interactions play a role in the observed trends in cytotoxicity and haemolytic activity.

4.1. Cytotoxicity in cells in culture—structure–toxicity relationships

Only limited information about the cytotoxicity of carbohydrate surfactants in mammalian cell culture models have been published. Several studies have reported that partially fluorinated, carbohydrate-based surfactants are not toxic at high micromolar to low millimolar concentrations, whereas the corresponding hydrocarbon analogues display considerable toxicity [10–14]. Unfortunately, these studies typically did not report an EC_{50} value, which makes it difficult to investigate structure–toxicity relationships and to compare studies using different cell lines. Furthermore, these studies investigated only a few surfactants with glucose, galactose or maltose headgroups. Therefore, we determined the cytotoxicity of all 34 surfactants using the B16F10 mouse melanoma cell line (Table 1 and Fig. 2) to investigate structure–toxicity relationships.

The most intriguing finding of this study is that the EC_{50} values of the hydrocarbon and fluorocarbon glucopyranosides **13** and **14** displayed a maximum with respect to chain length, i.e., the hydrocarbon and fluorocarbon C_{14} to C_{17} glucopyranosides showed mild cytotoxicity, whereas the short (C_7) and long-chain (C_{18} and C_{19}) glucopyranosides, including octylthioglycoside as positive control, were less toxic, with most EC_{50} values > 250 μ M. The EC_{50} values of the small number of maltopyranosides **17** and **18** investigated suggest that the cytotoxicity of this class of carbohydrate surfactants may also display a maximum in EC_{50} values with respect to chain length. Although similar trends have been reported for the biological activity of many surface active compounds in non-mammalian model systems, especially for compounds with anaesthetic and antimicrobial activity [17], a “cut-off” effect in the biological activities has not been reported previously for carbohydrate surfactants in general and fluorinated carbohydrate surfactants in particular.

The existence of a “cut-off” effect is surprising because the membrane permeability of organic compounds is proportional to their hydrophobicity (e.g., assessed by the octanol–water partition coefficient or the hydrophile–lipophile balance). Assuming that the biological activity (e.g., cytotoxicity) correlates with the membrane permeability (and, thus, the cellular uptake), the toxicity of the surfactants is expected to increase (and not to decrease) with increasing length of the hydrophobic tail. The low toxicity of C_7 surfactants and the moderate toxicity of C_{14} to C_{17} surfactants are consistent with this expectation. However, the low toxicity of most C_{18} and C_{19} surfactants and the galactopyranosides **15** and **16** suggests that the membrane permeability is not the only determinant of the cytotoxicity, especially after a comparatively long exposure of 24 h. Several other factors, such as decreasing aqueous and lipid solubility, decreasing critical micelle concentration (as measure of hydrophobicity and detergency), increasing binding

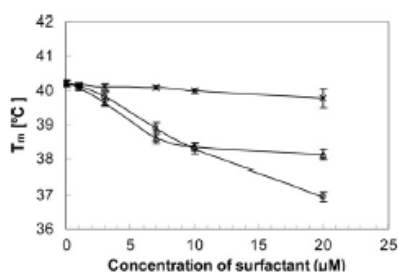


Fig. 4. T_m as a function of the increasing concentration of carbohydrate surfactants **β -13a** (x), **β -13d** (o) or **β -15b** (Δ). T_m , the temperatures at midpoint of the phase transition, was determined from plots of absolute fluorescence anisotropy values as a function of temperature. All fluorescence experiments were carried out at least in triplicate.

to proteins in the cell culture medium (e.g., albumin) or decreasing diffusion through the cell membrane with increasing tail length and increasing degree of fluorination, are likely to play a role [17,30]. Independent of the factors ultimately contributing to the low toxicity of the long-chain surfactants in cells in culture, our results suggest that the length and the degree of fluorination of the hydrophobic tail are important determinants of their toxicity.

Another intriguing observation is the low toxicity of the galactopyranoside surfactants **15** and **16** compared to the corresponding glucopyranoside surfactants **13** and **14**. Similarly, Kasuya and co-workers reported that 3,3,4,4,5,5,6,6,7,7,8,8,9,9,10,10,11,11,12,12,12-heneicosafuoro-dodecyl- β -D-glucopyranoside was nontoxic in the B16 melanoma cell line at a concentration of 50 μ M (48 h exposure), whereas the corresponding β -D-galactopyranoside displayed some toxicity at the same concentration [14]. These findings show that not only the length of the hydrophobic tail and the degree of fluorination [10–15], but also the stereochemistry of the polar headgroup are important determinants of the cytotoxicity of carbohydrate surfactants. Specifically, the absolute configuration of the hydroxyl group at the C-4 position determines the cytotoxicity of gluco- versus galactopyranoside surfactants in the B16F10 mouse melanoma cell line.

Since analogous gluco- and galactopyranoside surfactants have a comparable headgroup size, the differences in the EC_{50} values between these two surfactant groups suggest selective mechanism(s) of toxicity. In agreement with this interpretation, the low toxicity of all surfactants suggests that their cytotoxic effect is not due to the massive disruption of the phospholipid membrane. Instead, it is more likely that the cytotoxic effect is a result of more or less selective interactions of the surfactants with lipid rafts. These interactions impair the function of membrane proteins, which results in the activation of pathways inducing apoptosis and/or necrosis. This hypothesis is supported by our earlier study showing that the glucopyranosides **β -13e** and **β -14e** induced apoptosis in B16F10 cells [15]. Similarly, other surfactants have been shown to cause a ligand-independent clustering of death receptors, such as Fas, in membrane rafts, which provides scaffolds for the coupling of adaptor and effector proteins involved in apoptosis [31]. The selectivity of these complex surfactant–lipid and surfactant–protein interactions is affected both by the structure of the hydrophobic tail and the structure and stereochemistry of the polar headgroup.

4.2. Haemolytic activity

At haemolytic concentrations, surfactants directly destabilize the cell membrane and alter the anchoring of the cytoskeleton complex to the cell membrane, followed by massive release of the cell content [8,9,32]. Therefore, it is not surprising that, in comparison to the cytotoxic effect, much higher concentrations of the surfactants (>3.3 mM; Table 1) were typically needed to induce haemolysis. Furthermore, serum was protective against haemolysis due to binding of the surfactants to albumin, which lowers the free concentration of the surfactants and minimizes its partitioning into the cell membrane. The only exception was the C_{16} maltopyranoside surfactant **β -17b**, which was the most haemolytic compound under investigation. Similarly, the corresponding C_{12} maltopyranoside has been reported to be a potent haemolytic agent and causes lysis of human erythrocytes at concentrations as low as 58 μ M [9].

Some limited structure–activity relationships have been reported for the haemolytic activity of carbohydrate surfactants. Their haemolytic activity depends on the headgroup, the length of the hydrophobic tail and the degree of fluorination. For example, the haemolytic activity of short-chain surfactants (C_8 to C_{12}) decreases with decreasing size of the carbohydrate headgroup (disaccharide > monosaccharide headgroup) and flexibility of

the headgroup (pyranoside > straight polyhydroxylated chain), but increases with increasing tail length [1,33]. In contrast, a fluorinated tail protects against haemolysis, with high micromolar or low millimolar concentrations typically displaying no haemolytic activity [10,12,34]. In agreement with these earlier studies, maltopyranosides displayed more haemolytic activity compared to gluco- and galactopyranosides and a fluorinated tail protected against haemolysis by β -glucopyranosides and maltopyranosides. In conclusion, the haemolytic activity of the surfactants investigated herein is not a concern for *in vivo* applications because of the high concentrations (>3.3 mM) needed to induce haemolysis *in vitro* and the strong protective effect of serum.

4.3. Membrane partition behaviour

Our studies of the cytotoxicity and haemolytic activity suggest that carbohydrate surfactants with short (C_7) hydrophobic tail are less toxic and display comparatively low haemolytic activity compared to surfactants with C_{14} to C_{17} tails (Table 1). For example, the short-tail surfactant **β -13a** was not toxic in cells in culture (EC_{50} > 250 μ M) and not haemolytic (EC_{50} > 3.3 mM) in the concentration range investigated in this study, whereas long-chain surfactant **β -13d** was both toxic and haemolytic in the same concentration range. In contrast, all short-chain and most long-chain galactopyranosides, such as **β -15b**, displayed no cytotoxicity and little-to-no haemolytic activity in the concentration range studied. One possible explanation for the low cytotoxicity and low haemolytic activity of, for example, **β -13d** and **β -15b** is a poor tendency of both compounds to partition into cell membranes. To test this hypothesis, we studied the effect of three hydrocarbon surfactants, **β -13a**, **β -13d** and **β -15b**, on dipalmitoylphosphatidylcholine (DPPC) bilayers using fluorescence anisotropy measurements. DPPC bilayers were selected because they are frequently used to study the membrane partition behaviour of organic compounds [35].

The changes in the phase behaviour of the DPPC model membranes were characteristic for the incorporation of many small molecules into phospholipid bilayers and indicated a loss of cooperativity in the bilayer at micromolar concentrations. Specifically, T_m decreased and the transition width increased with increasing concentrations of all three carbohydrate surfactants. A similar effect of a C_{12} glucopyranoside and several other short chain carbohydrate surfactants on DPPC model membranes has been reported previously [16]. However, there were distinct differences in the effect of **β -13d** versus **β -15b** on T_m , which supports the above mentioned hypothesis that carbohydrate surfactants can interact selectively with lipid rafts in (model-)cell membranes, thus inducing a toxic effect at different concentrations and by different modes of action. Furthermore, the apparent membrane partition coefficients increased in the order heptyl β -D-glucopyranoside (**β -13a**) \ll hexadecyl β -D-glucopyranoside (**β -13d**) \sim hexadecyl β -D-galactopyranoside (**β -15b**). The smaller membrane partition coefficient of **β -13a** and its minimal influence on the phase transition behaviour of DPPC bilayers indicate that short-chain (C_7) carbohydrate surfactants have only a small tendency to partition into cell membranes. The partition coefficients of the long-chain surfactants **β -13d** and **β -15b** were higher compared to **β -13a**, which is in agreement with other studies reporting an increasing tendency of surface active compounds to partition into (model) membranes [30]. Interestingly, the partition coefficients of **β -13d** and **β -15b** were of the same order of magnitude. Together these observations suggest that the low toxicity of the C_7 surfactants is a result of the small partition coefficient of these surfactants, independent of the headgroup. In contrast, the low toxicity of galactopyranosides **14** and **15** is not correlated with simple physicochemical properties, such as the membrane partition coefficient. Instead, differences in the three-dimensional structure of the

headgroup (i.e., galactose versus glucose) and, possibly, the interaction of **β -15b** (and other long-chain galactopyranosides) with phospholipids molecules in a (model) membrane play, as suggested above, a role in the toxicity of these two surfactant groups. The later hypothesis is supported by the different trend in the depression of T_m of **β -15b** versus **β -13d** (Fig. 4).

5. Conclusions

The chain length, the degree of fluorination and the headgroup structure are important determinants of the cytotoxicity and the haemolytic activity of non-ionic carbohydrate surfactants. Of particular interest is the "cut-off" effect observed in the initial biocompatibility assessment of the hydrocarbon and fluorocarbon glucopyranoside surfactants (i.e., the cytotoxicity of these carbohydrate surfactants displayed a maximum at hydrophobic tail length ranging from C_{14} to C_{17}). To the best of our knowledge, this is the first time that such a "cut-off" effect has been reported in a mammalian cell culture system for carbohydrate surfactants in general and fluorinated surfactants in particular. Furthermore, the cytotoxicity of surfactants with glucose versus galactose headgroups depended on the stereochemistry in the C-4 position of the pyranoside. Studies of the surfactant–lipid interactions suggest that short chain surfactants are a lower tendency to partition into lipid membranes, which may explain their lower toxicity compared to C_{14} to C_{17} surfactants. C_{16} surfactants with glucose and galactose headgroups appear to have comparable membrane partition coefficients, but affect membrane phase behaviour (i.e., T_m) differently at surfactant concentrations $>10 \mu\text{M}$. The later finding clearly indicates that the cytotoxicity of the carbohydrate surfactants is due to highly specific surfactant–lipid interactions. This interpretation of our results is further supported by the fact that haemolysis of red blood cells occurs at much higher concentrations. Overall, these findings suggest that membrane partition behaviour and specific surfactant–lipid interactions are important determinants of the biocompatibility of simple carbohydrate-based surfactants investigated for a range of pharmaceutical and biomedical applications.

Acknowledgements

This work was supported by grants from the National Institute of Environmental Health Sciences (ES12475), the National Science Foundation (NIRT 0210517), the U.S. Department of Agriculture Biomass Research and Development Initiative (Grant Agreement 68-3A75-7-608) and the Department of Energy Development and Independence, Energy and Environment Cabinet of The Commonwealth of Kentucky. Additional support was provided by grants from the Ministry of Agriculture of the Czech Republic (grant No. MZE-0002716202) and NAZV QF-3115 to JT. Its contents are solely the responsibility of the authors and do not necessarily represent the official views of the funding agencies.

Appendix A. Supplementary data

Supplementary data associated with this article can be found, in the online version, at doi:10.1016/j.colsurfb.2009.04.023.

References

- [1] E. Söderlind, M. Wollbratt, C. von Corswant, The usefulness of sugar surfactants as solubilizing agents in parenteral formulations, *Int. J. Pharm.* 252 (2003) 61–71.
- [2] E. Söderlind, L. Karlsson, Haemolytic activity of maltopyranoside surfactants, *Eur. J. Pharm. Biopharm.* 62 (2006) 254–259.
- [3] J.G. Riess, M.P. Krafft, Fluorocarbons and fluorosurfactants for *in vivo* oxygen transport (blood substitutes), imaging, and drug delivery, *MRS Bull.* 24 (1999) 42–48.
- [4] H.-J. Lehmler, Perfluorocarbon compounds as vehicles for pulmonary drug delivery, *Expert Opin. Drug Deliv.* 4 (2007) 247–262.
- [5] H.-J. Lehmler, P.M. Bummer, M. Jay, Liquid ventilation—a new way to deliver drugs to diseased lungs? *Chemtech* 29 (1999) 7–12.
- [6] T.H. Shaffer, M.R. Wolfson, L.C. Clark, Liquid ventilation, *Pediatr. Pulmonol.* 14 (1992) 102–109.
- [7] M.R. Wolfson, T.H. Shaffer, Liquid ventilation: an adjunct for respiratory management, *Paediatr. Anaesth.* 14 (2004) 15–23.
- [8] B. Isomaa, H. Haegerstrand, G. Paatero, A.C. Engblom, Permeability alterations and anti-hemolysis induced by amphiphiles in human erythrocytes, *Biochim. Biophys. Acta* 860 (1986) 510–524.
- [9] B. Isomaa, H. Haegerstrand, G. Paatero, Shape transformations induced by amphiphiles in erythrocytes, *Biochim. Biophys. Acta* 899 (1987) 93–103.
- [10] A. Milus, J. Greiner, J.G. Riess, Synthesis of *off*-alkylated glycosides as surfactants for *in vivo* uses. Effects of the length of the hydrocarbonated spacer in the aglycone on klings-knorr reaction, surface activity and biological properties, *New J. Chem.* 15 (1991) 337–344.
- [11] L. Zarif, J. Greiner, J.G. Riess, Perfluoroalkylated monoesters of 1,4-d-sorbitan, isosorbide, and isomannide: new surfactants for biomedical applications, *J. Fluorine Chem.* 44 (1989) 73–85.
- [12] L. Zarif, J. Greiner, S. Pace, J.G. Riess, Synthesis of perfluoroalkylated xylitol ethers and esters: new surfactants for biomedical uses, *J. Med. Chem.* 33 (1990) 1262–1269.
- [13] M.C.Z. Kasuya, R. Cusi, O. Ishihara, A. Miyagawa, K. Hashimoto, T. Sato, K. Hatanaka, Fluorous-tagged compound: a viable scaffold to prime oligosaccharide synthesis by cellular enzymes, *Biochem. Biophys. Res. Commun.* 316 (2004) 599–604.
- [14] M.C.Z. Kasuya, A. Ito, R. Cusi, T. Sato, K. Hatanaka, Cellular uptake and saccharide chain elongation of "fluoro-amphiphilic" glycosides, *Chem. Lett.* 34 (2005) 856–857.
- [15] X. Li, J. Turánek, P. Knötičková, H. Kudláčková, J. Mašek, D.B. Pennington, S.E. Rankin, B.L. Knutson, H.-J. Lehmler, Synthesis and biocompatibility evaluation of fluorinated, single-tailed glucopyranoside surfactants, *New J. Chem.* 32 (2008) 2169–2179.
- [16] B. Rozycka-Rozzak, B. Jurczak, K.A. Wilk, Effects of nonionic sugar surfactants on the phase transition of dppc membranes, *Thermochim. Acta* 453 (2007) 27–30.
- [17] P. Balgavy, F. Devinsky, Cut-off effects in biological activities of surfactants, *Adv. Colloid Interf. Sci.* 66 (1996) 23–63.
- [18] J. Turánek, A. Kasna, D. Zaluska, J. Neca, V. Kvardova, P. Knötičková, V. Horvath, L. Sindlerova, A. Kozubik, P. Sova, A. Kroutil, F. Zak, A. Mistr, New platinum(IV) complex with adamantylamine ligand as a promising anti-cancer drug: comparison of *in vitro* cytotoxic potential towards a2780/cisplatin-resistant cell line within homologous series of platinum(IV) complexes, *Anti-Cancer Drugs* 15 (2004) 537–543.
- [19] S.M. Vyas, J. Turánek, P. Knötičková, A. Kasna, V. Kvardova, V. Koganti, S.E. Rankin, B.L. Knutson, H.-J. Lehmler, Synthesis and biocompatibility evaluation of partially fluorinated pyridinium bromides, *New J. Chem.* 30 (2006) 944–951.
- [20] T. Mosmann, Rapid colorimetric assay for cellular growth and survival: application to proliferation and cytotoxicity assays, *J. Immunol. Methods* 65 (1983) 55–63.
- [21] U. Bank, D. Reinhold, S. Ansoorge, Measurement of cellular activity by means of the mtt color test. Optimization of the method, *Allerg. Immunol.* 37 (1991) 119–123.
- [22] W. Xie, I. Kania-Korwel, P.M. Bummer, H.-J. Lehmler, Effect of potassium perfluorooctanesulfonate, perfluorooctanoate and octanesulfonate on the phase transition of dipalmitoylphosphatidylcholine (dppc) bilayers, *Biochim. Biophys. Acta* 1768 (2007) 1299–1308.
- [23] T. Inoue, T. Iwanaga, K. Fukushima, R. Shimozawa, Effect of sodium octanoate and sodium perfluorooctanoate on gel-to-liquid-crystalline phase transition of dipalmitoylphosphatidylcholine vesicle membrane, *Chem. Phys. Lipids* 46 (1988) 25–30.
- [24] R.L. Biltonen, D. Lichtenberg, The use of differential scanning calorimetry as a tool to characterize liposome preparations, *Chem. Phys. Lipids* 64 (1993) 129–142.
- [25] Z. Petrovic, S. Konstantinovic, A. Spasojevic, BF₃ etherate-induced formation of *C*-16-alkyl β -D-glucopyranosides, *Ind. J. Chem.* 43B (2004) 132–134.
- [26] V. Ladmiral, G. Mantovani, G.J. Clarkson, S. Cauet, J.L. Irwin, D.M. Haddleton, Synthesis of neoglycopolymers by a combination of "click chemistry" and living radical polymerization, *J. Am. Chem. Soc.* 128 (2006) 4823–4830.
- [27] G. Milkereit, M. Morr, J. Thiem, V. Vill, Thermotropic and lyotropic properties of long chain alkyl glycopyranosides part iii: Ph-sensitive headgroups, *Chem. Phys. Lipids* 127 (2004) 47–63.
- [28] V. Vill, H.M. von Minden, M.H.J. Koch, U. Seydel, K. Brandenburg, Thermotropic and lyotropic properties of long chain alkyl glycopyranosides. Part I: monosaccharide headgroups, *Chem. Phys. Lipids* 104 (2000) 75–91.
- [29] J.R. Lakowicz, Principles of Fluorescence Spectroscopy, Springer Science+Business Media, New York, 2006.

- [30] F. Kamp, J.A. Hamilton, How fatty acids of different chain length enter and leave cells by free diffusion, *Prostaglandins Leukot. Essent. Fatty Acids* 75 (2006) 149–159.
- [31] F. Mollinedo, C. Gajate, Fas/cd95 death receptor and lipid rafts: new targets for apoptosis-directed cancer therapy, *Drug Resistance Updates* 9 (2006) 51–73.
- [32] H. Haegerstrand, B. Isomaa, Morphological characterization of exovesicles and endovesicles released from human erythrocytes following treatment with amphiphiles, *Biochim. Biophys. Acta* 1109 (1992) 117–126.
- [33] E. Soederlind, L. Karlsson, Haemolytic activity of maltopyranoside surfactants, *Eur. J. Pharm. Biopharm.* 62 (2006) 254–259.
- [34] S. Abouhilale, J. Greiner, J.G. Riess, Perfluoroalkylated fatty acid monoesters of trehalose and sucrose for biomedical applications: remarkable emulsifying properties of 6-O-[3'-(perfluorooctyl)propanoyl]trehalose, *J. Am. Oil Chem. Soc.* 69 (1992) 1–8.
- [35] K. Lohner, Effects of small organic molecules on phospholipid phase transitions, *Chem. Phys. Lipids* 57 (1991) 341–362.

2.2.5. Senzory pro testování cytotoxického účinku farmak v modelech *in vitro*

Využití piezoelektrických krystalů pro sledování fyzikálně-chemických procesů je moderním přístupem v současných analytických metodách, které směřují k miniaturizaci detekčních systémů a k využití funkcionalizovaných nanomateriálů. Využití těchto senzorů pro monitorování účinku farmak a dalších látek *in vitro* na některé funkce buněk je nově rozvíjenou oblastí s vysokým aplikačním potenciálem. Metoda je vhodná pro studium vlivu farmak na stimulaci či inhibici buněčného růstu, rozpoznávání a adhezi na povrchy přirozených a umělých materiálů, migraci buněk a tvorbu konfluentních buněčných povrchů.

První publikované práce byly zaměřeny na modifikaci zlatých elektrod biokompatibilními matricemi a ověření funkčnosti systému na některých buněčných liniích (např. epiteliální buňky WB F344, melanom B16F10). Byly zkonstruovány měřicí cely pro práci s buňkami a jejich funkčnost byly testovány na modelu inhibice buněčného růstu působením cytotoxických a cytostatických látek.

Vzhledem k rychlému vývoji v oblasti miniaturizace těchto technologií a vývoji nových nanomateriálů, lze se očekávat rychlý vývoj v této oblasti. Z tohoto důvodu bude pokračovat intenzivní výzkum na využití těchto biosenzorů ve spolupráci s MU a CEITEC.

2.2.5.1. Publikace k tématu kapitoly



Available online at www.sciencedirect.com



Biosensors and Bioelectronics 22 (2007) 1896–1901

**BIOSENSORS
&
BIOELECTRONICS**

www.elsevier.com/locate/bios

Adhesion of eukaryotic cell lines on the gold surface modified with extracellular matrix proteins monitored by the piezoelectric sensor

Zdenka Fohlerová^{a,b}, Petr Skládal^{a,*}, Jaroslav Turánek^b

^a Department of Biochemistry, Masaryk University, Kotlářská 2, 61137 Brno, Czech Republic

^b Department of Immunopharmacology and Immunotoxicology, Veterinary Research Institute, Hudcova 70, 62132 Brno, Czech Republic

Received 24 April 2006; received in revised form 1 August 2006; accepted 9 August 2006

Available online 18 September 2006

Abstract

The piezoelectric sensor (quartz crystal microbalance, QCM) was used to monitor cell adhesion in real time. Two cell lines, rat epithelial cells (WB F344) and lung melanoma cells (B16F10) were used. The cells were adhered and grown on the gold surface of the sensor pre-coated with adsorbed layer of extracellular matrix proteins as vitronectin and laminin. The process of cell attachment and spreading on the gold surface was continuously monitored and displayed by changes of the resonant frequency Δf and resistance ΔR values of the piezoelectric resonators. The initial phase of cell attachment and spreading induced a decrease of frequency and increase of resistance relating viscoelastic properties of the cell monolayer on the sensing surface. The steady-state of both shifts was achieved after a few hours. The presence and state of cells on the surface was confirmed by fluorescent microscopy. The obtained results demonstrate that the piezoelectric sensor is suitable for studies of the cell adhesion processes. Thus obtained cell-based biosensor has potential for identification and screening of biologically active drugs and other biomolecules affecting cellular shape and attachment.

© 2006 Elsevier B.V. All rights reserved.

Keywords: Quartz crystal microbalance; Cell adhesion; Extracellular matrix; Apoptosis; Fluorescence microscopy

1. Introduction

Studies of biochemical and physiological activities in living cell cultures have attracted considerable interest during the recent years. The classical methods of studying cytotoxicity effects and cell adhesion and their interaction with e.g. extracellular matrix (ECM) proteins as fibronectin, laminin and vitronectin (Grinnell and Feld, 1982; Curtis and Forrester, 1984; Hayman et al., 1985) are performed using the cultivation of cells on a microtitration plate, the evaluation is carried out using the optical microscopy and cell counting methods and provide only qualitative information about the cells. The new sensing methods have been introduced that provide quantitative information about the cellular adhesion, growth and migration. In this way, detailed information about the effect of various chemical compounds affecting cell morphology and metabolic state became easily accessible (Marx et al., 2001; Arndt et al., 2004). These methods generally called as cell-based biosensors allow evalu-

ating response of the cells in real time, continuously and without additional potentially disturbing intracellular labels and probes. Moreover, the other approaches for transduction of cellular signals were discussed elsewhere (Pancrazio et al., 1999). Various types of cells include macrophages (Kowolenko et al., 1990), fibroblasts (Giaever and Keese, 1993), epithelial (Marx et al., 2003) and endothelial (Marx et al., 2005) cells, the studies performed include kinetics of the adhesion as well as the cell dying process. The monitoring was realized by sensitive techniques such as electrical cell-substrate impedance sensing ECIS (Xiao and Luong, 2003), piezoelectric sensors (Wegener et al., 1998) and impedance analysis of piezoelectric resonators (Wegener et al., 2000).

It is well known that the operation of piezoelectric resonators in liquid phase includes both mass change induced frequency shifts and density or viscosity effects of the surrounding liquid layer as well (Kanazawa and Gordon, 1985). Thus, when mammalian cells attach to the surface, reversible frequency shifts are observed which do not obey the simple Sauerbrey equation (Sauerbrey, 1959), but the signal instead originates from viscoelastic changes close to the surface. Therefore, for a more detailed information related to the cell–surface interaction, it

* Corresponding author. Tel.: +42 5 49497010; fax: +42 5 41211214.
E-mail address: skladal@chemi.muni.cz (P. Skládal).

is necessary to measure additional parameters as resistance R (Marx et al., 2003), dissipation factor D (Fredriksson et al., 1998a,b) or even better apply the rather complex impedance analysis (Li et al., 2005). The process of cell adhesion is monitored in real-time and non-invasively and provides information about different molecular mechanisms responsible for cell attachment and spreading. A better insight into various physiological processes such as cell differentiation during development, tissue regeneration and cell migration in tumor metastasis (Poste and Fidler, 1980) becomes available.

In this work, we studied and compared the ability of two different cells – liver epithelial and lung melanoma derived lines – to adhere on the gold electrode of the piezoelectric sensor. The electrode was pre-coated with an adsorbed protein layer of ECM such as laminin and vitronectin before exposing it to the culture medium. Experimental procedures were performed in the serum containing medium and the changes of resonant frequency f and resistance R values were measured. The cell attachment and spreading on the surface is mostly characterized by the decrease of frequency and the increase of resistance values (Zhou et al., 2000; Muratsugu et al., 1997). It is commonly suggested that the cells can be treated neither as an adsorbed rigid mass nor as entirely viscous materials. Here, it was demonstrated an interesting event that the cell attachment on the surface modified with laminin induced an increase of frequency.

2. Materials and methods

2.1. Cell cultures and growth conditions

Two different anchorage dependent cell lines were chosen for the study. Cells were cultured in the standard conditions in a stock flask (10 cm^2) in a humidified incubator with 5% CO_2 /95% air atmosphere at 37°C . The rat liver epithelial cells WB F433 were cultured using the D-MEM medium (Dulbecco's modified Eagle's medium, Sigma) supplemented with 10% (v/v) fetal bovine serum (Gibco), 100 unit/l penicillin, 0.1 g/l streptomycin and 4 mg/l gentamycin (all from PAA Laboratories, Austria), 2 g/l NaHCO_3 and 1.2 g/l HEPES (both from Sigma). The lung melanoma cells B16F10 were grown in the RPMI 1640 medium (Sevapharma, Czech Republic). This culture medium was additionally supplemented with 0.6 g/l glutamine, 10% (v/v) fetal bovine serum, 0.1 g/l pyruvate, 100 unit/l penicillin, 0.1 g/l streptomycin and 4 mg/l gentamycin. The pH value was adjusted at 7.4 in both types of media. The culture medium was exchanged twice a week and routine subculturing of the confluent cell layer was performed using standard trypsinization, 0.05% (w/v) trypsin-EDTA procedure. The confluence represents the state of cells grown to maximum capacity within the given space, when intercellular surface contacts inhibit further growth. Resuspended cells in the medium were used for the seeding onto either the piezosensor surface or microtitration plate.

2.2. Measurements with piezoelectric sensors

The schema of the measuring device is depicted in Fig. 1. The measurements were realized using the active oscillator-based

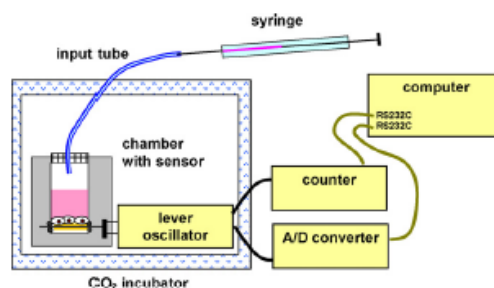


Fig. 1. Schematic diagram of the experimental set-up. The cells applied by capillary using the Hamilton syringe are seeded to the surface of the resonator pre-coated with different materials. The measurement chamber and the oscillator are placed inside the thermostated CO_2 incubator. The piezosensor is connected to the lever oscillator providing Δf and ΔR values measured by the counter and A/D converter, respectively.

method. The AT-cuts of optically smooth quartz crystal (3 cm^2) with fundamental resonant frequency of 10 MHz and with gold electrodes (0.2 cm^2) on both sides were obtained from ICM (International Crystal Manufacturing Company, Oklahoma City, OK). The crystal was inserted in the Teflon-made batch chamber (ICM), which was adapted for our requirements. The chamber was covered by a polyethylene frit to prevent evaporation of the medium. The cell suspension was applied through a thin Teflon capillary by using the Hamilton syringe, total volume inside the cell was 0.2 ml. The lever oscillator (ICM) was used to drive the piezoelectric resonator at the fundamental frequency. This circuit provided resonance frequency and resistance-proportional voltage signals, which were simultaneously monitored using the universal frequency counter (UZ 2400, Grundig Electronics, Germany) and custom-made analog input module (16 bit resolution, based on a PIC microcontroller), respectively. Both signal processing units were linked through RS232C interfaces to a standard PC/Windows computer with the own LabTools program for data display, storage and editing. The relative resistance changes were obtained after calibration of the measuring set-up with standard resistors as suggested by the manufacturer (ICM).

The crystal regeneration was realized by subsequent washing steps of chromic-sulphuric acid, 10% sodium hydroxide, water and acetone. The assembled measuring chamber was sterilized for 20 min in the autoclave before each experiment. At the beginning, $100\ \mu\text{l}$ of the medium was introduced to provide stable f and R baselines. Then $100\ \mu\text{l}$ of cell suspension was added to the chamber. The process of cell attachment was monitored over several hours at the constant temperature 37°C and 5% CO_2 .

2.3. Electrode coating and cell adhesion assay

The surfaces pre-coated with ECM proteins (either vitronectin or laminin, both from Sigma) were used for the cell adhesion. The complete protein adsorption on the gold surface with laminin ($2\ \mu\text{g}/\text{cm}^2$) dissolved in PBS and vitronectin ($0.1\ \mu\text{g}/\text{cm}^2$) dissolved in deionized was realized for 2 h in the incubator. After washing the electrode with sterile deionized

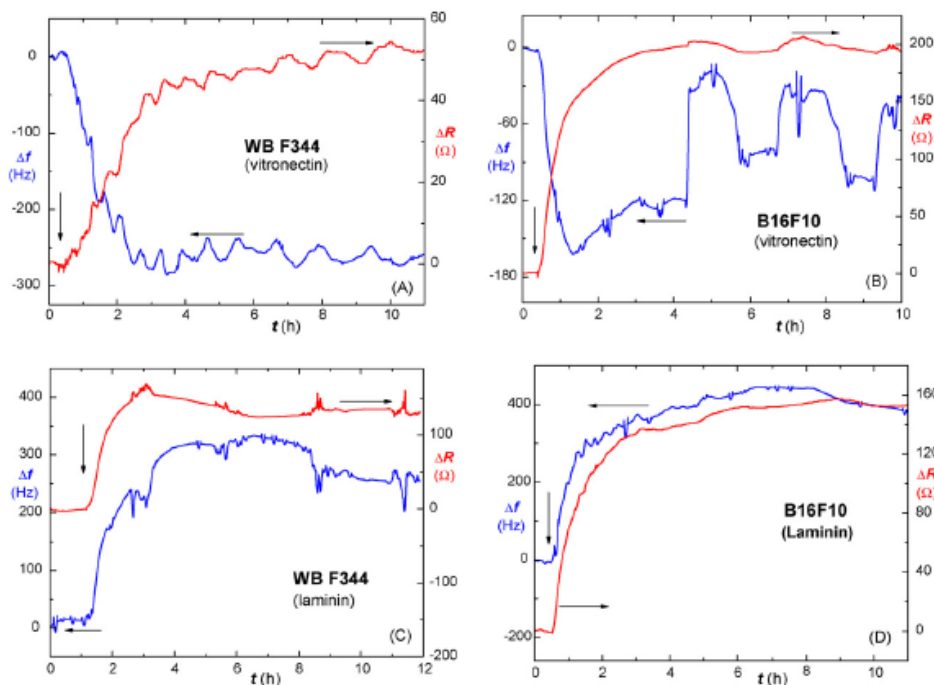


Fig. 2. Cultivation of the WB F344 (A and C) and B16F10 (B and D) cell lines on the surface of gold electrodes of the piezoelectric quartz crystal modified with either vitronectin (A and B) or laminin (C and D). Changes of the resonance frequency (Δf) and resistance (ΔR) recorded in time; initial volume of the medium was 100 μ l. The vertical arrow marks the addition of cells, 100 μ l of medium containing (per 1 ml) cells: 4.2×10^5 WB F344 (A), 4.0×10^5 B16F10 (B), 5.0×10^5 WB F344 (C) and 5.6×10^5 B16F10 (D).

water, 100 μ l of the culture medium was injected to the chamber and the frequency and voltage baselines were recorded. Then, the cell adhesion process was monitored after inoculation of 100 μ l of the cell suspension into the chamber. Cells were counted using the hemacytometry (Central Development Workshop, Brno) before each experiment.

2.4. Fluorescent detection

Direct cell detection on the sensing surface was performed using the fluorescent dye specific for mitochondria MitoTracker Red CMXRos (Molecular Probes). The probe was used at 50 nM concentration and stained cells were observed using the fluorescent microscope Nikon Eclipse E 600, excitation and emission wavelengths were 579 and 599 nm, respectively. Fluorescent images were acquired using the embedded CCD camera.

3. Results and discussion

3.1. Attachment of WB F344 and B16F10 cells on vitronectin

Vitronectin is a major cell adhesion protein in plasma and it is also present in the extracellular matrix of tissues. Interactions

of cells with the ECM proteins are mediated by adhesion of the cellular transmembrane receptors of the integrin superfamily that recognize peptide motifs, such as Arg-Gly-Asp (RGD), which are presented on the surface of ECM proteins. The experimental measurement was focused on the ability of both cell lines to bind through the integrin-mediated adhesion on the vitronectin and their viability on such surface. The interaction of cells with the surface was monitored using relative changes of both Δf and ΔR as parameters providing more information about the adhesion. After stabilization of the baseline signals in the presence of medium only, the cells were injected to the chamber. To allow a better comparison, similar number of cells ($\sim 4 \times 10^5$ cells/ml) was added to the chamber in each case. Thus obtained experimental traces are presented in Fig. 2A and B.

The addition of cells (vertical arrows) initiated decrease of frequency and increase of resistance, as could be commonly expected for increased surface viscoelasticity in the presence of cells. However, the starting phase of the cell sedimentation, attachment and spreading was completed within 2 h for WB F344 cells, but significantly faster, within 1 h, for B16F10 cells, based on the frequency. Later, the frequency remained stable for WB F344 (mean value around -260 Hz) while resistance was slightly increasing ($0.7 \Omega/h$) reaching 55 Ω at the end of

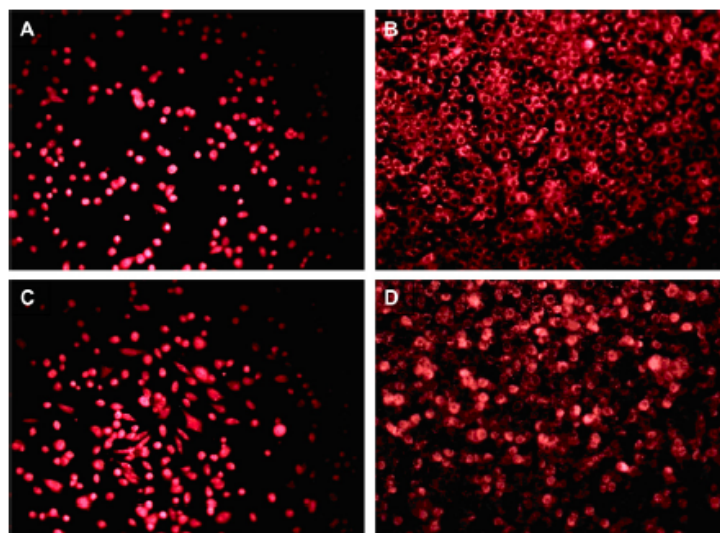


Fig. 3. Fluorescence photomicrographs of WB F344 (A and C) and B16F10 cells (B and D) after adhesion on the sensing surface of resonators modified with either vitronectin (A and B) or laminin (C and D), the corresponding interaction traces were shown in Fig. 2. The adhered cells were stained using the mitochondria-specific probe MitoTracker Red CMX Ros. The width of images corresponds to 700 μm . The detailed description is provided in the text.

the experiment (Fig. 2A). Both Δf and ΔR exhibited periodic fluctuations with amplitudes of 30 Hz and 5 Ω , respectively, the periodicity was increasing from 30 min at the beginning to 90 min at the end. For B16F10 the maximum frequency response of -162 Hz observed after 1 h was followed by the increase to -120 Hz and then quite large fluctuations of frequency (60–80 Hz) appeared with periodicity of 150 min. Surprisingly, the accompanying fluctuations of resistance were much smaller (10 Ω) considering the rather high mean ΔR value of 200 Ω . For both cell lines, the described fluctuations were observed repeatedly and also after more than 10 h later of the presented measurements (data not shown). The fluctuations were not associated with instrumental disturbance e.g. thermostat heating or CO_2 supply on/off switches as was confirmed in control experiments. We assume that the observed local changes of signal could be linked to the cell motion and different metabolic activities of cells near the sensing surface. One can also consider the possibility of a partial evaporation of the culturing medium from the chamber, though this was not noticed in control measurements. Similar periodic fluctuations of frequency might be found also in the literature, e.g. in the case of endothelial cells adhering on gold in the presence of serum proteins (Marx et al., 2001).

At the end of measurement, the chamber was washed, the attached cells were stained with the fluorescent probe, the piezoelectric sensor was removed and microscopic fluorescent image was obtained (Fig. 3). The used MitoTracker probe available in the oxidized form was able to stain mitochondria of living cells and also cells in the pre-apoptotic state. Thus, the WB F344 cells

(Fig. 3A) were detected clearly in the apoptotic state, the surface was occasionally covered with individual round-shaped cells containing the accumulated dye, no internal structure of the cells was visible and cell–cell interactions were clearly missing. On the other hand, the B16F10 cells (Fig. 3B) formed a monolayer consisting of spread viable cells contacting each other. The internal cell structure demonstrated the contrast black area of nucleus. This confluent layer of cells was covering completely the gold surface and together with external intercontacts of cells significantly affected resistance of the sensing crystals, which was four times higher compared to the sensor with WB F344 cells. Furthermore, one could assume that the WB F344 cells died shortly after their firm attachment on the surface (around 2–3 h). It was possible that the cells were firmly contacting surface but not spreading and only staying attached in the rounded shape, without forming cell–cell contacts and gradually dying. However, this process was not accompanied by significant changes of either frequency or resistance.

Regarding the previously observed fluctuations of frequency in the case of the B16F10 cells, these should be most probably associated with cell division occurring in a close contact with the sensing surface. On the contrary, the smaller and faster fluctuations of signals obtained for the WB F344 cells should be attributed to cells only loosely contacting the surface; however, the growth of such cells was probably faster compared to the cells tightly adhering to the surface. Evidently, vitronectin is a suitable modifier promoting growth of the B16F10 cells on the surface of gold, but it is not suitable for the WB F344 cells.

3.2. Attachment of WB F344 and B16F10 cells on laminin

The gold coated with adsorbed laminin was tested as an alternative surface for cell adhesion. Laminin is known as an important component of the basal lamina which anchors epithelium to the underlying connective tissue. The experimental procedure was the same as above for vitronectin. The adhesion curves for both cell lines are shown in Fig. 2C and D. To our surprise, after the addition of cells ($\sim 5.5 \times 10^5$ cell/ml) into the measuring chamber, an increase of resistance was monitored as expected, but the recorded frequency started increasing reaching +320 Hz for WB F344 and +450 Hz for B16F10 cell lines. This behavior was obtained repeatedly using either same or different initial cell loadings. The resistance increases peaked at 166 Ω and stabilized around 130 Ω for the WB F344 cells, for B16F10 the resistance was gradually increasing and stabilized around 150 Ω . The following fluorescent detection of the attached cells showed mostly apoptotic cells with few cells in the pre-apoptotic phase (non-circular shape) in the case of WB F344 (Fig. 3C). As previously observed with vitronectin, it is possible that the WB F344 cells exhibited deficiency of expressed receptors required for both tested ECM proteins and consequently the environmental conditions for their viability were insufficient and thus the cells gradually died. On the other hand, a nice confluent layer was obtained for the B16F10 cell line (Fig. 3D).

The observed increase of frequency obtained for cells adhering on laminin layer is rather peculiar. The layer of laminin itself is stable in the presence of cultivation medium only, as stable baselines (1 h) were obtained for both resistance and frequency (Fig. 2C, the part before the addition of cells). The increase of frequency itself usually indicates release of some material from the sensing surface; this should however be accompanied with a decrease of resistance, and the obtained resistance change was a significant increase, fully corresponding with cell adherence on the surface. From other studies (Marx et al., 2005) it was apparent that ECM without the cell does not exhibit any significant energy dissipation so the resistance shift must be attributed to the presence of cells. One could hypothesize that the adhering cells are interacting with adsorbed laminin, changing significantly its surface orientation. Consequently, the viscoelastic properties of the originally oriented or rigid laminin layer might become relaxed through interaction with the surface of cells and frequency increases. Alternatively, the added cells might temporarily interact with the adsorbed laminin, partially becoming firmly attached to the surface and partially leaving again to the solution and extracting laminin from the surface; this would decrease the surface mass and frequency should go up; the resistance increase will result from the attached cells.

The increase of frequency accompanying adhesion of epithelial cells was noticed also by others (Wegener et al., 1998; Marxer et al., 2003), however, no definitive explanation was provided. In our case, this phenomenon is clearly related with the type of the ECM matrix modifying the sensing surface; the same cell lines exhibited this anomalous behavior only with laminin, but not with vitronectin deposited on the surface. A better insight to the behavior of cells observed in the case of laminin might be

obtained using gold modified with covalently attached laminin, which would be firmly fixed to the surface; such experiments are planned for future.

3.3. Resistance versus frequency plots for cell adhesion

For a better interpretation of the observed results and different viscoelastic behavior of both cell types, the time-series frequency and resistance plots shown in Fig. 2 were replotted as resistance versus frequency dependences. As was described elsewhere (Zhou et al., 2000), when cells adhere to the sensor surface, they produce a reversible frequency shift. Most studies have suggested that cells adhered to the sensing surface do not act as elastic mass therefore they do not obey the simple Sauerbrey equation, a relationship that relates adhering elastic mass to the linearly decreasing Δf shift and $\Delta R = 0$. The cells not only affect Δf but also dissipate energy causing both Δf decreases and significant ΔR increases. Thus, cells attached to the sensor surface cannot be treated like an adsorbed rigid mass and not as entirely viscous materials, but as a combination of both interactions.

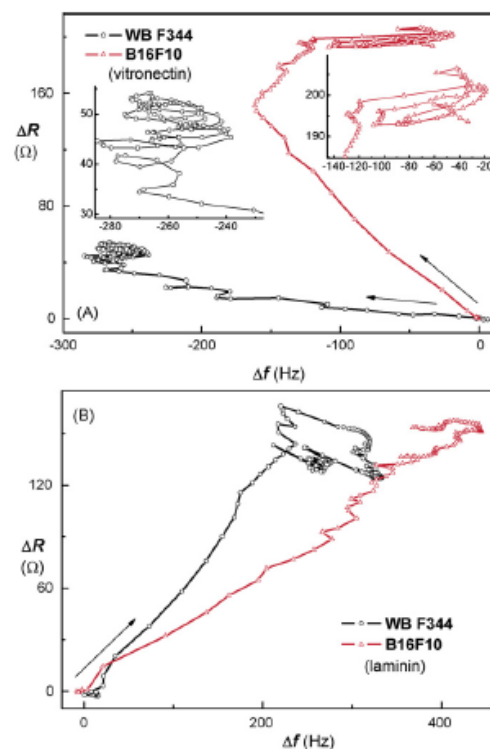


Fig. 4. The replot of the time-series data from Fig. 2 as dependences of resistance ΔR on the resonant frequency Δf changes observed in the case of either vitronectin (A) or laminin (B) coated surfaces.

The measured raw data were averaged 30-times, i.e. one new point now represents a 5 min interval, in order to remove random short-time fluctuations of signals. As can be seen, the initial phase consisting of rather distant points corresponds to the process of sedimentation and adherence of cells on the sensing surface, spreading and establishing contacts with the pre-adsorbed proteins, cell proliferation starts in later phases. The shape of the curves presented in Fig. 4A corresponds with similar dissipation versus frequency plots published previously (Li et al., 2005). As regards the dependences obtained with increasing frequencies, the similar measurements in the literature did not include resistance monitoring (Wegener et al., 1998; Marxer et al., 2003) so that direct comparison is complicated.

In the case of the vitronectin-modified sensors, the obtained curves exhibited quite interesting fine structure after the initial adhesion of cells (Fig. 4A). The original periodic fluctuations of resistance and frequency now appear as progressing spirals, resulting from the phase shifts of frequency and resistance peaks. This fine structure is shown in the enlarged inset graphs of Fig. 4A. We believe that the observed minor changes correspond with either metabolic or morphologic state of the cell. This hypothesis is however hard to implement for the laminin-coated sensors, where no 'reasonable' fine structure in the R - f plots was apparent (Fig. 4B). Thus, R - f diagrams very clearly demonstrate that the B16F10 cells exhibited more pronounced viscoelastic behavior producing more dissipating effects than the WB F344 cells; this was indicated as a large change of the ΔR values. In opposite, the WB F344 cells produced the large change of resonant frequency as was apparent for the vitronectin-coated surfaces. The frequency increases on the laminin-coated surface should be further examined with differently constructed laminin layers.

4. Conclusions

The piezoelectric quartz crystals operated in the active mode were used for adhesion studies of epithelial WB F344 and lung melanoma B16F10 derived anchorage dependent cell lines. The cell adhesion was promoted through modification of the sensing surface using pre-adsorbed vitronectin and laminin. The behavior of both cell lines was different; the WB F344 cells were confirmed on the surface using fluorescent staining; however, the cells were not viable but rather isolated and clearly in the apoptotic state. On the other hand, the B16F10 appeared fully viable on both types of surfaces forming confluent layers. The monitored parameters—changes of resonance frequency and resistance of the resonators were followed in real time. Frequency decrease and resistance increase accompanied cell adhesion on the surface with vitronectin. The laminin interaction with adhering both WB F344 and B16F10 cells resulted in the increase of both frequency and resistance; the increased frequency possibly results from rearrangement of the laminin sublayer or its partial release upon binding of cells.

From the methodological point of view, the combined frequency and resistance monitoring allowed to study minor details apparent as fine structure of the resistance versus frequency plots. Further correlation of the observed results with independent techniques is required for complete interpretation and understanding of the observed signals. The proposed combination of the piezoelectric transducer with adhered cells seems to be highly promising for construction of cell-based biosensors, especially after expansion of the current single-channel measurements into multisensing formats. In this way, the testing of physiologically active substances and environmental stress factors affecting cell morphology will be easily realized.

Acknowledgments

This work was supported by grants from the Czech Ministry of Agriculture (MZE 0002716201), the Czech Ministry of Education (MSM 0021622413) and from the European Union (QLK3-CT-2001-00244, project CELLSSENS).

References

- Arndt, S., Seebach, J., Psathaki, K., Galla, H.J., Wegener, J., 2004. *Biosens. Bioelectron.* 19, 583–594.
- Curtis, A.S.G., Forrester, J.V., 1984. *J. Cell Sci.* 71, 17–35.
- Fredriksson, C., Kihlman, S., Kasemo, B., Steel, D.M., 1998a. *J. Mater. Sci. Mater. Med.* 9, 785–788.
- Fredriksson, C., Kihlman, S., Rodahl, M., Kasemo, B., 1998b. *Langmuir* 14, 248–251.
- Giaever, I., Keese, C.R., 1993. *Nature (London)* 366, 591–592.
- Grinnell, F., Feld, M.K., 1982. *J. Biol. Chem.* 257 (9), 4888–4893.
- Hayman, E.G., Pierschbacher, M.D., Ruoslahti, E., 1985. *J. Cell Biol.* 100, 1948–1954.
- Kanazawa, K.K., Gordon, J., 1985. *Anal. Chim. Acta* 175, 99–105.
- Kowalenko, M., Keese, C.R., Lawrence, D.A., Giaever, I., 1990. *J. Immunol. Methods* 127, 71–77.
- Li, J., Thielmann, Ch., Reuning, U., Johannsmann, D., 2005. *Biosens. Bioelectron.* 20, 1333–1340.
- Marx, K.A., Zhou, T., Montrone, A., McIntosh, D., Braunhut, S.J., 2005. *Anal. Biochem.* 343, 23–34.
- Marx, K.A., Zhou, T., Montrone, A., Schulze, H., Braunhut, S.J., 2001. *Biosens. Bioelectron.* 16, 773–782.
- Marx, K.A., Zhou, T., Warren, M., Braunhut, S.J., 2003. *Biotechnol. Prog.* 19, 987–999.
- Marxer, C.G., Coen, M.C., Greber, T., Greber, U.F., Schlapbach, L., 2003. *Anal. Bioanal. Chem.* 377, 578–586.
- Muratsugu, M., Romanschin, A.D., Thompson, M., 1997. *Anal. Chim. Acta* 342, 23–29.
- Pancrazio, J.J., Whelan, J.P., Borkholder, D.A., Ma, W., Stenger, D.A., 1999. *Ann. Biomed. Eng.* 27, 697–711.
- Poste, G., Fidler, I.J., 1980. *Nature* 283, 139–146.
- Sauerbrey, G., 1959. *Z. Phys.* 155, 206–222.
- Wegener, J., Janshoff, A., Galla, H.J., 1998. *Eur. Biophys. J.* 28, 26–37.
- Wegener, J., Seebach, J., Janshoff, A., Galla, H.J., 2000. *Biophys. J.* 78, 2821–2833.
- Xiao, C., Luong, J.H.T., 2003. *Biotechnol. Prog.* 19, 1000–1005.
- Zhou, T., Marx, K.A., Warren, M., Schulze, H., Braunhut, S.J., 2000. *Biotechnol. Prog.* 16, 268–277.



The cell adhesion and cytotoxicity effects of the derivate of vitamin E compared for two cell lines using a piezoelectric biosensor

Zdenka Fohlerová^a, Jaroslav Turánek^b, Petr Skládal^{a,c,*}

^a Department of Biochemistry, Masaryk University, Kotlářská 2, 61137 Brno, Czech Republic

^b Veterinary Research Institute, Brno, Czech Republic

^c CEITEC MU, Masaryk University, Brno, Czech Republic

ARTICLE INFO

Article history:

Received 2 July 2012

Received in revised form 19 August 2012

Accepted 21 August 2012

Available online 28 August 2012

Keywords:

Quartz crystal microbalance

Fluorescence microscopy

Cell adhesion

Extracellular matrix

Apoptosis

Vitamin E

ABSTRACT

The quartz crystal microbalance (QCM) was used to construct a piezoelectric biosensor utilizing rat liver epithelial cells (WB F344) and lung melanoma cells (B16F10) as biorecognition elements. The cells adhered on the gold surface modified by either hydrophobic polystyrene or fibronectin. The simultaneous monitoring of changes in the resonant frequency Δf and the resistance ΔR corresponded with the mass and viscoelastic properties of the adhered cells. In addition, the bound cells were stained using fluorescent probes to evaluate their viability on the non-transparent gold surface. Furthermore, this piezoelectric biosensor was used for monitoring of drug-induced apoptosis initiated by micromolar concentrations of α -tocopherol amidomalate (α -TAM), a potential anticancer drug. The characteristic features of apoptosis as shrinkage and disintegration of cell–cell contacts could be monitored by QCM. The decrease of frequency and increase of resistance characterized gradual death of cells that was confirmed by fluorescence microscopy. The results indicate that the piezoelectric biosensor can be used for the real-time study of the cell adhesion and the screening of biologically active drugs affecting cellular behaviour.

© 2012 Elsevier B.V. All rights reserved.

1. Introduction

Many important physical and chemical processes involving cells can be associated with the changes of the mass and/or the viscoelastic behaviour of the surface bound materials and so observed by the well-known piezoelectric quartz crystal microbalance (QCM). Initially, QCM devices were used to measure molecules in the gas phase; the measured resonance frequency shift of the piezoelectric resonator was directly proportional to the adsorbed mass according to the Sauerbrey equation [1]. Further, QCM was developed as a sensing tool operating in the liquid phase; in this case, only one side of the quartz crystal is contacting with the surrounding liquid. This configuration was adopted in different applications in electrochemistry [2,3]. The operations in the liquid required to determine the mass-induced frequency shift and additional physical properties, such as density and viscosity of the liquid [4]. More recently, QCM has been applied as the biosensor to study various macromolecular systems as DNA hybridization [5], DNA–drug binding [6], viruses, bacteria, proteins [7–9] and small molecules as drugs [10], hormones [11] and pesticides [12]. QCM was also successfully applied in biological processes involving mammalian cells as the

biorecognition element, e.g. cellular adhesion, growth, migration and drug stimulation [13–15]. In many studies, scientists have worked with the different anchorage dependent cell types including fibroblastic V79 cells, osteoblasts, MDCK I and II cells, human ovarian cancer cell lines and many others [16–19]. Besides this, various parameters such as frequency [20,21], dissipation factor [22], impedance parameters [18,19,23], transient decay time constant and maximal oscillation amplitude [24] were measured and related to the cellular events.

In this work, QCM was applied for the real-time monitoring of the cells adhesion process of two different cells lines including rat liver epithelial cells (WB F344) and lung melanoma cells (B16F10). Their ability to adhere on the gold electrode pre-coated with the hydrophobic polystyrene, protein of extracellular matrix (ECM) such as fibronectin and the native gold electrode was compared. Experiments were performed in serum-containing medium and the frequency f (Hz) and auto gain control voltage (AGC) U (directly proportional to the resistance R of QCM) provided by the lever oscillating circuit was recorded.

The attachment and spreading of cells on the surface is complex process that requires the contacts among neighbouring cells and with the surface bound extracellular matrix as well. The specificity of the cell adhesion comes from combinatorial expression and interactions among a large number of adhesion receptors such as integrins, and induction relies on diffusible ligands binding to receptor, on the cell–cell contacts and on the cell–matrix adhesion.

* Corresponding author at: Department of Biochemistry, Masaryk University, Kotlářská 2, 61137 Brno, Czech Republic.
E-mail address: skladal@chemi.muni.cz (P. Skládal).

The studies, where cell adhesion is monitored in real-time and non-invasively, provide information about the different molecular mechanisms responsible for cell attachment and spreading, thus giving the valuable information for various physiological processes such as cell differentiation, tissue regeneration and cell migration in tumour metastasis [25]. When cells adhere and grow on the sensor surface, they produce a reversible frequency shift. The frequency shift related to the mass on the sensor does not obey the simple Sauerbrey equation because cells do not behave either as a rigid layer or a viscous mass. Therefore, the additional parameters such as resistance and dissipation factor are commonly measured [26]. In the second part of our experiments, the apoptosis of both WB F344 and B16F10 cells were induced by the newly tested derivative of vitamin E called α -tocopherol amidomaleate (α -TAM) [27,28]. α -TAM and other derivatives of vitamin E are supposed to act through their pro-apoptotic effect on the cells and thus they appear as promising anticancer drugs. The mechanism is dependent on their structure and consists in the activation of signal pathways including MAP kinases and destabilization of mitochondrial membrane subsequently releasing cytochrome c, activation of caspases and induction of apoptosis. Because of the alterations in cell shape and viscoelastic properties of adsorbed surface mass, QCM technique seems to be the suitable and sensitive method for the detection of apoptosis. QCM provides the interesting and quantitative information about the mechanism of cell adhesion and the important view into the drug-induced apoptosis monitored in real time and without any labels.

2. Materials and methods

2.1. Quartz crystal microbalance

The 10 MHz quartz crystal (diameter 1.5 cm) with gold electrodes (0.5 cm) on both sides was supplied by ICMC (Oklahoma City, OK). The crystal was inserted between two silicon O-rings inside the Teflon chamber (ICMC). The chamber placed inside the thermostatic incubator was covered by polyethylene frit to limit evaporation of the culture medium and to allow the access of CO₂. The initial suspension of cells was applied through a thin capillary passing through the frit using a Hamilton syringe. The frequency and the AGC voltage of the resonator were simultaneously recorded using the universal frequency counter (UZ 2400, Grundig Electronics, Germany, 1 Hz resolution) and the digital millivoltmeter card 4060 (National Instruments, Austin, TX), respectively. The own software (LabTools) served for data storage and evaluation. The resistance R values (in Ω) were calculated from the polynomial equation (Origin, Microcal) obtained from the calibration curve generated using serially connected known resistances as suggested in the ICMC literature [29], $R = A + B_1U + B_2U^2$, where the parameters $A = -13,909$, $B_1 = 15,563$ and $B_2 = -4057$ were determined using calibrating resistances in series with the resonator.

2.2. Cell cultures

The experiments were performed with two different anchorage dependent cell lines. Cells were cultured in a stock flask in a humidified incubator with 5% CO₂/95% air atmosphere at 37 °C. The WB F433 cells were cultured using the D-MEM medium (Dulbecco's modified Eagle's medium, Sigma) supplemented with 10% (v/v) foetal bovine serum (Gibco), 100 units/l penicillin and 0.1 g/l streptomycin (PAA Laboratories, Austria), 4 mg/l gentamycin (PAA), 2 g/l NaHCO₃ (Sigma) and 1.2 g/l HEPES (Sigma). The B16F10 cells were cultured in the RPMI 1640 medium (Sevapharma, Czech Rep.). This culture medium was additionally supplemented with 0.6 g/l glutamine, 100 ml/l foetal bovine serum, 0.1 g/l pyruvate, 100 unit/l

penicillin, 0.1 g/l streptomycin and 4 mg/l gentamycin, pH was adjusted at 7.4. Before experiments, cells were washed twice in phosphate buffer saline (PBS) and trypsinized with 0.05% (w/v) trypsin-EDTA for 5 min at 37 °C. Cells were then re-suspended in the culture medium and used for the seeding into either the QCM cell or microplates.

2.3. Electrode coating and cell inoculation

Cleaned electrodes of the QCM sensor were modified with fibronectin (100 μ g/ml in PBS) and polystyrene (10 mg/ml in toluene) to improve cell adhesion on gold surface. Water washing steps were followed by the addition of 100 μ l of culture medium to obtain the baseline signal. Subsequently, 100 μ l of the cell suspension was inoculated into the chamber and cultured under the condition mentioned above.

2.4. Visualization of cells on the electrode

The mitochondria specific fluorescence dye MitoTracker Red CMXRos (50 nM, Molecular Probes) stained and confirmed the presence of cells on the electrode using the Olympus BX41 microscope.

2.5. Effects of drugs on cells

When the confluent layer of cell was established on the QCM sensor, α -TAM was added to the final concentration of 300 μ M; the stock solution contained 5% ethanol, resulting in <1% ethanol in the final medium; this amount effected neither the cell viability nor the QCM signals. The Δf and ΔR shifts were monitored for several hours. The QCM output was compared with the simultaneous experiment made on the microplate and followed by fluorescence detection of the apoptotic and/or necrotic cells by Yo-Pro 1 and propidium iodide realized with 1 h interval.

3. Results and discussion

3.1. Adhesion of cells on the fibronectin coated gold

Initially, the medium containing serum in the absence of cells was used to establish the baseline at the 37 °C giving a reference state of the frequency and the resistance. The following addition of 3.5×10^5 cells/ml caused the typical decrease of frequency and increase of resistance (Fig. 1A). In the next 2 h, cells were round and become spreading on the surface, resulting in the steepness of the measured frequency curve. Then the cells started proliferation or slowly died. The steady state was achieved about ten hours after the cell addition and the following fluorescence microscopy confirmed the confluence monolayer for both cell types. However, a partial de-attachment was observed for the B16F10 cells (Fig. 1A), WB F344 cells response remained stable. The reason for this difference was probably the larger size of the B16F10 cells which occupied entire surface after spreading and the excess of non-attached cells was turning dead. Looking on the alternative R - f plot (Fig. 1B), a better insight into the viscoelastic behaviour of cells was obtained. In principle, if the pure elastic mass is adsorbed on the sensor, no resistance change is observed due to the fact that the energy of the damped oscillations is saved in the system. The cells appear as viscoelastic and thus the resistance shift can be recorded since the energy of oscillations is lost due to the frictional force. The graph suggesting that the B16F10 cells exhibited higher viscoelastic influence on the sensor compared to the WB F344 cells. A larger change of surface resistance seems responsible for this observation. The frequency change was very similar for both cell lines.

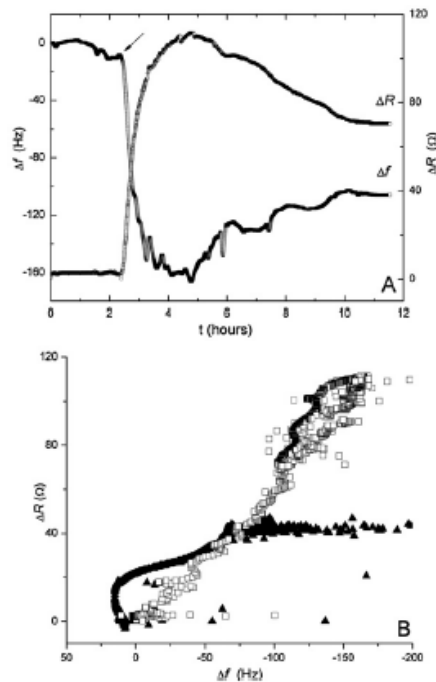


Fig. 1. Time dependent change of frequency and resistance during the adhesion of B16F10 cells on the gold surface modified with fibronectin (A). The R-f plot of the B16F10 (\square) and WB F344 cells (\blacktriangle) showing the viscoelastic behaviour of two different cell lines (B).

The fibronectin exhibited promoting effects for the cell adhesion resulting in a stable coverage.

3.2. Adhesion of WB F344 and B16F10 cells on the hydrophobic polystyrene

In the study described by Fredriksson et al. [22], the cells adhering on the hydrophobic and hydrophilic polystyrene were investigated. The author suggested that the QCM response differs both with cell types on the same surface and with the same type of cells on different surfaces. Furthermore, the presence of serum in the medium exhibited significant effects, too.

Here, 3.5×10^5 cells/ml were seeded on the hydrophobic polystyrene coated on the surface of QCM. The expected decrease of frequency and increase of resistance was observed but immediately after a short period frequency increased and the resistance decreased (data not shown). The changes of both measured parameters corresponded with the de-attachment of cells as confirmed by the fluorescence microscopy. It appears that the polystyrene-modified surface was not suitable for the studied cell lines.

Similarly, the cells were seeded directly on the bare gold surface of the QCM electrode. The results suggested that the cells attached on the surface probably because of the present pre-adsorbed serum proteins but the time stability was not proved.

As was previously described by Marx et al. [20], the Δf and ΔR shift values depend on the cell type and reflect the number of firmly attached cells and the viscoelastic properties of the adsorbed layer. Further changes of the QCM shift parameters after achieving the

steady state of both values depended upon a number of factors effecting of the cellular shape, attachment and metabolic state. van Kooten et al. [30] described that anchorage-dependent living cells do not attach well to surfaces possessing hydrophobic character. This observation was proved by Marx [20] and confirmed here, when the cells adhered on the native and hydrophilic treated gold surfaces were compared.

3.3. α -TAM induced apoptosis measured with QCM

The main part of work tested the performance of a cellular biosensor, containing 4×10^5 cells/ml seeded on the fibronectin coated surface. This served for the monitoring of α -TAM induced apoptosis. The QCM output was compared with the simultaneous experiment carried out using the common microplate assay and the apoptotic kit containing Yo-Pro 1 (detection of apoptotic cells) and propidium iodide (detection of necrotic cells). The apoptosis is accompanied by the change in the cell morphology and therefore it should be observable using the QCM biosensor.

When the steady state for both measured parameters of the sensor with cells was achieved, α -TAM was added to the QCM cell and microplate wells at the final concentration equal to $300 \mu\text{mol/l}$. The time dependent changes of the frequency and the resistance were monitored for 12 h (Fig. 2A and B). The addition of α -TAM caused at the beginning the steep decrease of the frequency and the increase of the resistance. This disturbance was caused by the addition of the drug as was confirmed by the control experiment in the absence of cells. The following changes in the frequency and the

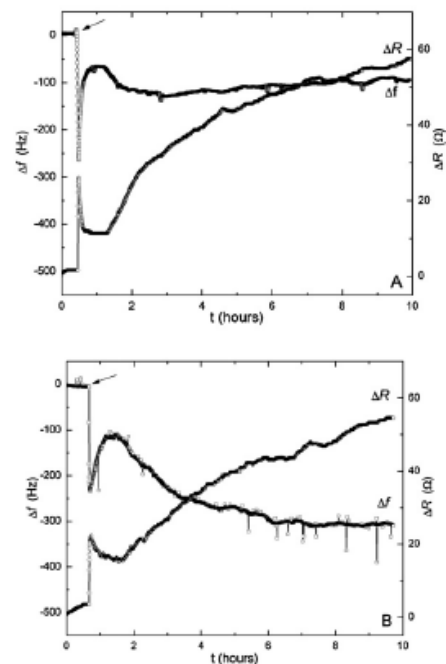


Fig. 2. The apoptosis of B16F10 cells (A) and WB F344 cells (B) initiated by the addition (arrow) of the pro-apoptotic drug α -TAM. The responses correspond with the morphology of apoptotic and necrotic cells detected by fluorescence microscopy. Time dependent signals – frequency and resistance from the piezoelectric biosensor.

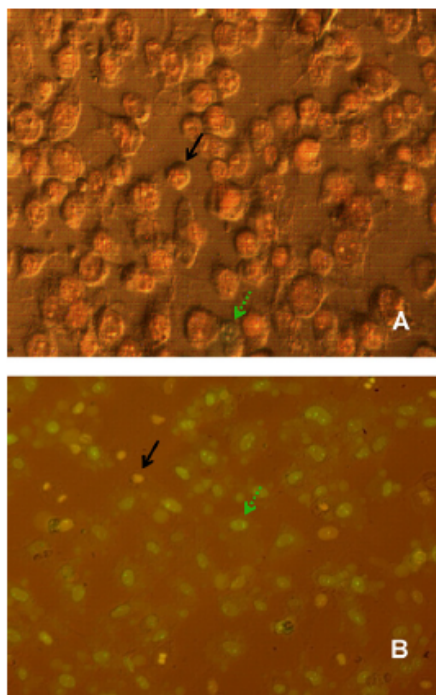


Fig. 3. Fluorescence microscopy image of the B16F10 cells (A) and WB F344 cells (B) stained with Yo-Pro 1 (dashed green arrows) and propidium iodide (black arrows). Images were taken 3 h (B16F10 cells) and 7 h (WB F344 cells) after the addition of 300 μ M α -TAM.

resistance were observed in time and compared with microscopical observations. The decrease of frequency accompanied by increasing resistance corresponds with gradual cellular change in morphology and viscoelastic properties typical for the apoptosis. The apoptotic cells turned heavier as the frequency gradually decreased. While the Δf shift was stable, the ΔR values still slowly increased at the end of the plotted data which probably means that the cells were still partially active and did not turned completely rigid. The frequencies were stabilized in 7 h for WB F344 cells and in 3 h for B16F10 cells. The major differences in measured signals are primarily in the frequency shift of both cell lines. The $\Delta f = 100$ Hz (B16F10 cells) and $\Delta f = 300$ Hz (WB F10 cells) can be explained by the dissimilar morphology and structures of cells. Time-dependent comparison of the fluorescence microscopy of cells cultured on the microplate and QCM signals confirmed our expectation. The images of gradual apoptosis were taken each hour. The time when the frequency signals were getting stable (i.e. 7 and 3 h for WB F344 and B16F10 cells) corresponded with fluorescence images (Fig. 3) of fully apoptotic and necrotic cells. Thus the B16F10 cells were liable to apoptosis more quickly due to their higher sensitivity to tested substance than WB F344 cells.

4. Conclusion

The piezoelectric transducer served as a simple and versatile tool for monitoring and quantification of the attachment and spreading of the anchorage dependent cells to a solid substrate.

The continuous operation in real time, no need for labelling and sensitive detection of viscoelastic properties of the interfacial layer allowed achieving detailed information compared to the standard microplate cultivation techniques where only the end of the process is measured. As indicated previously [31], the cell type, surface modification, cell number and cultivation conditions exhibit significant effects on the measured frequency and resistance shifts. The biomolecules exhibiting effects on the morphology and the viscoelastic properties of cells can be easily followed.

Acknowledgement

This work was supported by the project "CEITEC – Central European Institute of Technology" (CZ.1.05/1.1.00/02.0068) from European Regional Development Fund.

References

- [1] G. Sauerbrey, Verwendung von Schwingquartzen zur Wägung dünner Schichten und zur microwägung, *Zeitschrift für Physik* 155 (1959) 206–222.
- [2] H. Xu, J.B. Schlenoff, Kinetics, isotherms and competition in polymer adsorption using the quartz crystal microbalance, *Langmuir* 10 (1995) 241–245.
- [3] T.W. Schneider, D.A. Buttry, Electrochemical quartz crystal microbalance studies of adsorption and desorption of self-assembled monolayers of alkyl thiols on gold, *Journal of the American Chemical Society* 115 (1993) 12391–12397.
- [4] K.K. Kanazawa, J. Gordon, The oscillation frequency of a quartz resonator in contact with a liquid, *Analytica Chimica Acta* 175 (1985) 99–105.
- [5] N. Fawcett, J.A. Evans, L. Chien, L. Flowers, Nucleic acid hybridization detected by piezoelectric resonance, *Analytical Letters* 21 (1988) 1099–1114.
- [6] L. Pope, S. Allen, M. Davies, C. Roberts, S. Tendler, P. Williams, Probing DNA duplex formation and DNA–drug interactions by the quartz crystal microbalance technique, *Langmuir* 17 (2001) 8300–8304.
- [7] R. Vaughan, C.K. Sullivan, G.G. Guilbault, Development of QCM immunosensors for the detection of *Listeria monocytogenes*, *Enzyme and Microbial Technology* 29 (2001) 636–638.
- [8] A.J.C. Eun, L. Huang, F.T. Chew, F.Y. Sam, S.K. Wong, Detection of two orchid viruses using QCM immunosensors, *Journal of Virological Methods* 99 (2002) 71–79.
- [9] S. Imai, H. Mizuno, M. Suzuki, T. Takeuchi, E. Tamiya, F. Mashige, A. Ohkubo, I. Karube, Total urinary protein sensor based on a piezoelectric quartz crystal, *Analytica Chimica Acta* 340 (1994) 65–70.
- [10] J. Haláček, A. Makower, P. Skládal, F.W. Scheller, Highly sensitive detection of cocaine using a piezoelectric immunosensor, *Biosensors and Bioelectronics* 17 (2002) 1045–1050.
- [11] M. Zhihong, L. Xiaohui, F. Weiling, A new sandwich-type assay of estrogen using piezoelectric immobilized with estrogen response element, *Analytical Communications* 36 (1999) 281–283.
- [12] J. Horáček, P. Skládal, Improved direct piezoelectric biosensor operating in liquid solution for the competitive label-free assay of 2,4-dichlorophenoxyacetic acid, *Analytica Chimica Acta* 347 (1997) 43–50.
- [13] J. Fatišon, F. Azari, N. Tufenkji, Real-time QCM-D monitoring of cellular responses to different cytomorphic agents, *Biosensors and Bioelectronics* 26 (2011) 3207–3212.
- [14] K. Zhou, K.A. Marx, A.H. Dewilde, D. McIntosh, S.J. Braunhut, Dynamic cell adhesion and viscoelastic signatures distinguish normal from malignant human mammary cells using quartz crystal microbalance, *Analytical Biochemistry* 421 (2012) 164–171.
- [15] M. Saitakis, E. Gizeli, Acoustic sensors as a biophysical tool for probing cell attachment and cell/surface interactions, *Cellular and Molecular Life Sciences* 69 (2012) 357–371.
- [16] C. Xiao, J.H.T. Luong, On-line monitoring of cell growth and cytotoxicity using electric cell-substrate impedance sensing, *Biotechnology Progress* 19 (2003) 1000–1005.
- [17] J. Redepenning, T.K. Schlesinger, E.J. Mechalke, D.A. Puleo, R. Bizios, Osteoblast attachment monitored with a quartz crystal microbalance, *Analytical Chemistry* 65 (1993) 3378–3381.
- [18] J. Wegener, J. Seebach, A. Janshoff, H.J. Galla, Analysis of the composite response of shear wave resonators to the attachment of mammalian cells, *Biophysical Journal* 78 (2000) 2821–2833.
- [19] J. Li, Ch. Thielmann, U. Reuning, D. Johannsmann, Monitoring of integrin-mediated adhesion of human ovarian cancer cells to model protein surfaces by quartz crystal resonators: evaluation in the impedance analysis mode, *Biosensors and Bioelectronics* 20 (2005) 1333–1340.
- [20] K.A. Marx, T. Zhou, A. Montrone, D. McIntosh, S.J. Braunhut, Quartz crystal microbalance biosensor study of endothelial cells and their extracellular matrix following cell removal: evidence for transient cellular stress and viscoelastic changes during detachment and the elastic behavior of the pure matrix, *Analytical Biochemistry* 343 (2005) 23–34.
- [21] K.A. Marx, T. Zhou, M. Warren, S.J. Braunhut, Quartz crystal microbalance study of endothelial cell number dependent differences in initial adhesion and

- steady-state behavior: evidence for cell–cell cooperativity in initial adhesion and spreading, *Biotechnology Progress* 19 (2003) 987–999.
- [22] C. Fredriksson, S. Kihlman, M. Rodahl, B. Kasemo, The piezoelectric quartz crystal mass and dissipation sensor: a means of studying cell adhesion, *Langmuir* 14 (1998) 248–251.
- [23] S. Arndt, J. Seebach, K. Psathaki, H.J. Galla, J. Wegener, Bioelectrical impedance assay to monitor changes in cell shape during apoptosis, *Biosensors and Bioelectronics* 19 (2004) 583–594.
- [24] C.G. Marxer, M.C. Coen, T. Greber, U.F. Greber, L. Schlapbach, Cell spreading on quartz crystal microbalance elicits positive frequency shifts indicative of viscosity changes, *Analytical and Bioanalytical Chemistry* 377 (2000) 578–586.
- [25] G. Poste, I.J. Fidler, The pathogenesis of cancer metastasis, *Nature* 283 (1980) 139–146.
- [26] T. Zhou, K.A. Marx, M. Warren, H. Schulze, S.J. Braunhut, The quartz crystal microbalance as a continuous monitoring tool for the study of endothelial cell surface attachment and growth, *Biotechnology Progress* 16 (2000) 268–277.
- [27] J. Neuzil, Vitamin E succinate and cancer treatment: a vitamin E prototype for selective antitumour activity, *British Journal of Cancer* 89 (2003) 1822–1826.
- [28] M. Birringer, J.H. Eytina, B.A. Salvatore, J. Neuzil, Vitamin E analogues as inducers of apoptosis: structure–function relation, *British Journal of Cancer* 88 (2003) 1948–1955.
- [29] K.O. Wessendorf, The lever oscillator for use in high resistance resonator applications, *Frequency Control Symposium*, in: 47th Proceedings of the 1993 IEEE International, 1993, pp. 711–717.
- [30] T.G. van Kooten, J.M. Moorlag, J.M. Schakenraad, H.C. van der Mie, H.J. Busscher, Influence of substratum wettability on the strength of adhesion of human fibroblasts, *Biomaterials* 13 (1992) 897–904.
- [31] Z. Fohlerová, P. Skládal, J. Turánek, Adhesion of eukaryotic cell lines on the gold surface modified with extracellular matrix proteins monitored by the piezoelectric sensor, *Biosensors and Bioelectronics* 22 (2007) 1896–1901.

Biographies

Zdenka Fohlerová, MSc, is completing her doctoral studies at the Department of Biochemistry, Masaryk University, Brno. She is focused on the research of cell-based biosensors and visualization of cells using atomic force microscopy.

Jaroslav Turánek after obtaining PhD degree from University of J.E. Purkyně in Brno in 1987 joined the Veterinary Research Institute in Brno. He currently heads the Laboratory of immunopharmacology and Immunotoxicology. His research interests include liposomes as nano-carriers for antiviral and anticancer drugs, antigens and adjuvans and immunomodulating agents.

Petr Skládal joined Masaryk University in Brno (Czech Republic) in 1988 after receiving the MSc degree, he completed the PhD degree in 1992, and in 1999 he was appointed as the Associated Professor at the Department of Biochemistry where he heads the Laboratory of Biosensors. In 2006, he founded also the Nanobiotechnology Laboratory at the National Center of Biomolecular Research and CEITEC MU. His research interests include bioanalytical application of piezoelectric sensors, development of immunosensors and bioaffinity studies using biosensors.

2.3. ZÁVĚR

Série publikovaných prací ukázala na vhodnost liposomů jako nosičových systémů pro hydrofilní a hydrofobní farmaka. Pro jejich studium budou rozvíjeny také nové metody testování, které jsou založeny na využití biosenzorů na bázi piezoelektrických krystalů.

3. LIPOSOMY PRO KONSTRUKCI REKOMBINANTNÍCH VAKCÍN

Vakcinologie představuje komplexní multidisciplinární obor, který je založen jak na velmi racionálních teoretických základech, tak dosud na empirickém přístupu. Pozoruhodný pokrok v imunologii a genetice přispěl k pochopení funkcí imunitního systému na molekulární a buněčné úrovni. Tyto nové poznatky společně s rozvojem rekombinantních technologií, biotechnologií a dostupností nových biokompatibilních materiálů, zejména mikro a nanomateriálů, vedou k výraznému pokroku ve vývoji a produkci moderních rekombinantních vakcín.

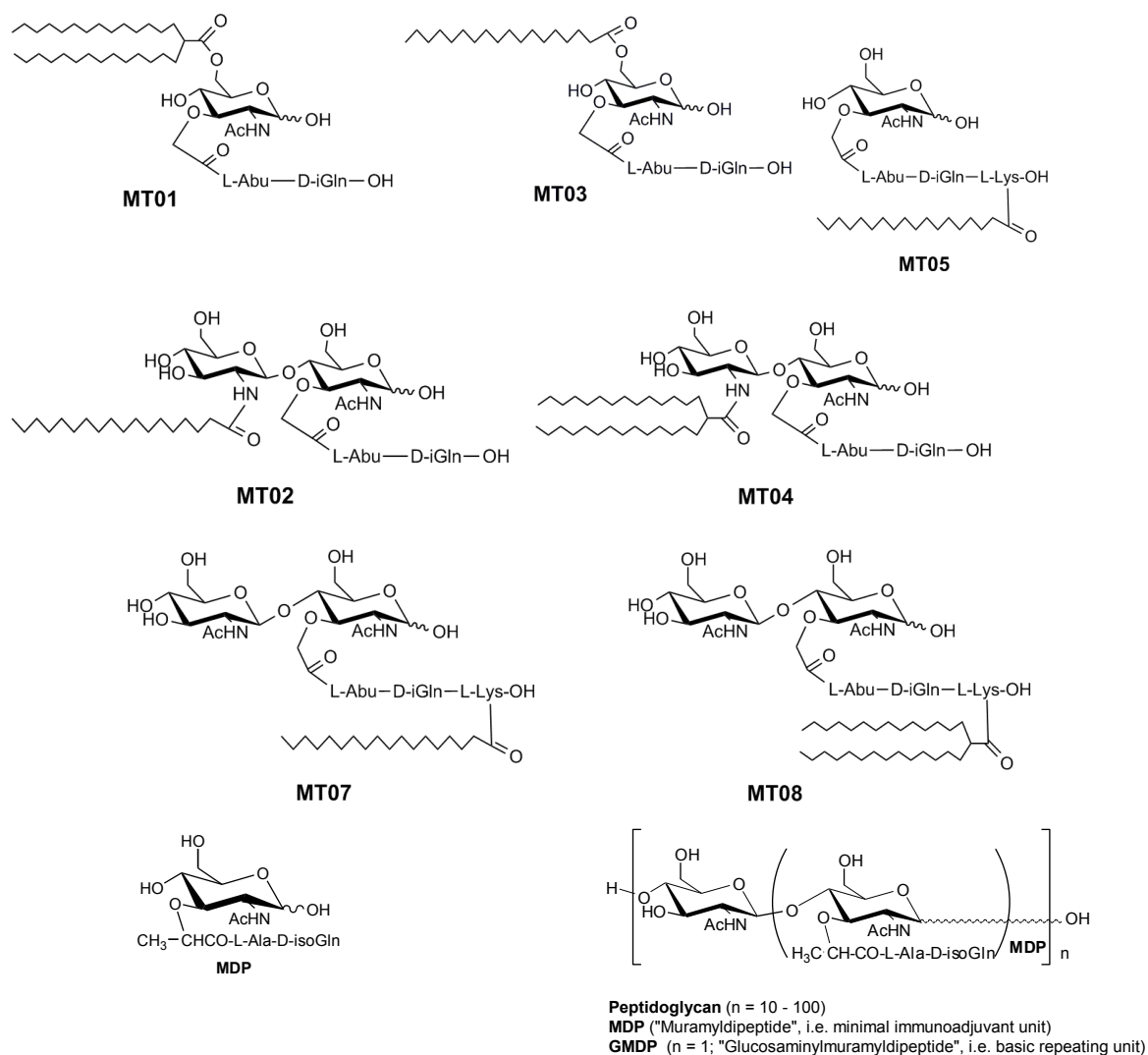
Subjednotkové vakcíny a rekombinantní vakcíny, jako jejich speciální odnož jsou moderním směrem ve vývoji vakcín a výrazným přínosem vakcinologie k léčbě infekčních, autoimunních a nádorových onemocnění.

Vývoj těchto nových vakcín je založen na identifikaci vhodných antigenů a jejich epitopů. Základními otázkami je jaký antigen prezentovat imunitnímu systému a jak má být tento antigen prezentován. Klíčovými faktory, které jsou řešeny ve výzkumu, jsou a) vyhledávání antigenů, jejich modifikace a příprava rekombinantními technologiemi; b) vhodná formulace antigenu; c) výběr a vývoj bezpečných a účinných adjuvans; d) způsob podání vakcíny s důrazem na minimální invazivitu aplikace a potřebu speciálně školeného personálu. Faktorem, který pohání výzkum v oblasti rekombinantních vakcín je bezpečnost, cena a krátká doba pro vývoj vakcín proti novým patogenům, nebo v případě chřipky nutnost rychlé obměny antigenů kvůli antigennímu driftu a vzniku reasortantů.

V oblasti vývoje moderních vakcín patří liposomy pro svoji biokompatibilitu a versatilitu k jedním z nejúspěšnějších mikro a nanoparticulárním systémům. Na trhu jsou již liposomální vakcíny proti chřipce (Inflexal® V, firma Crucell) a hepatitidě A (Epaxal®; firma Crucell). Celá řada liposomálních vakcín proti infekčním a nádorovým chorobám je v různých stádiích klinického testování.

Výzkum v této oblasti jsme směřovali na vývoj originálních plně syntetický adjuvans na bázi normuramylových glykopeptidů. Tento výzkum byl prováděn ve spolupráci s Ústavem organické chemie a biochemie, AV ČR, Praha (Dr. M. Ledvina) a

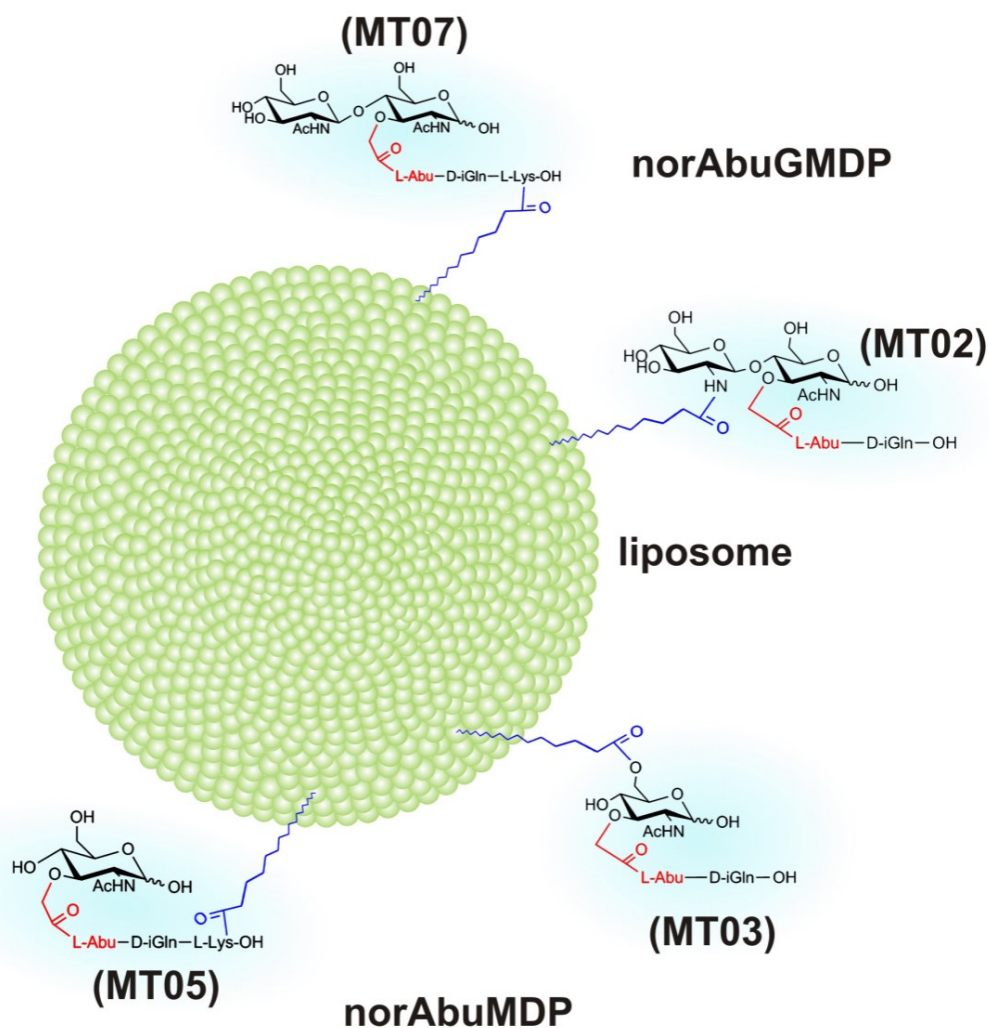
vyústil v podání národních a mezinárodních patentů, které chrání tato nová adjuvans. Zároveň byla vytvořena spin off Mendel Therapeutics. s.r.o. pro komercializaci výsledků. Na obrázku je série syntetických adjuvans, která jsou dnes testována pro použití ve vakcínách ve spolupráci s Bioveta a.s. a dalšími zahraničními pracovišti. Tyto látky se vyznačují potlačenou pyrogenitou a bezpečností otestovanou na celé řadě zvířecích druhů (myš, morče, skot, prase, pes, kočka, králík).



Obr. 24 Syntetická analoga Muramyl Dipeptidu (MDP) odvozená od peptidoglykanu.

Liposomální formulace syntetických adjuvans byly testovány jako stimulatory nespecifické imunity v různých *in vivo* modelech a byla prokázána jejich účinnost při potlačení experimentální kryptosporidiózy novorozeneých kůzlat, nebo regeneraci kostní

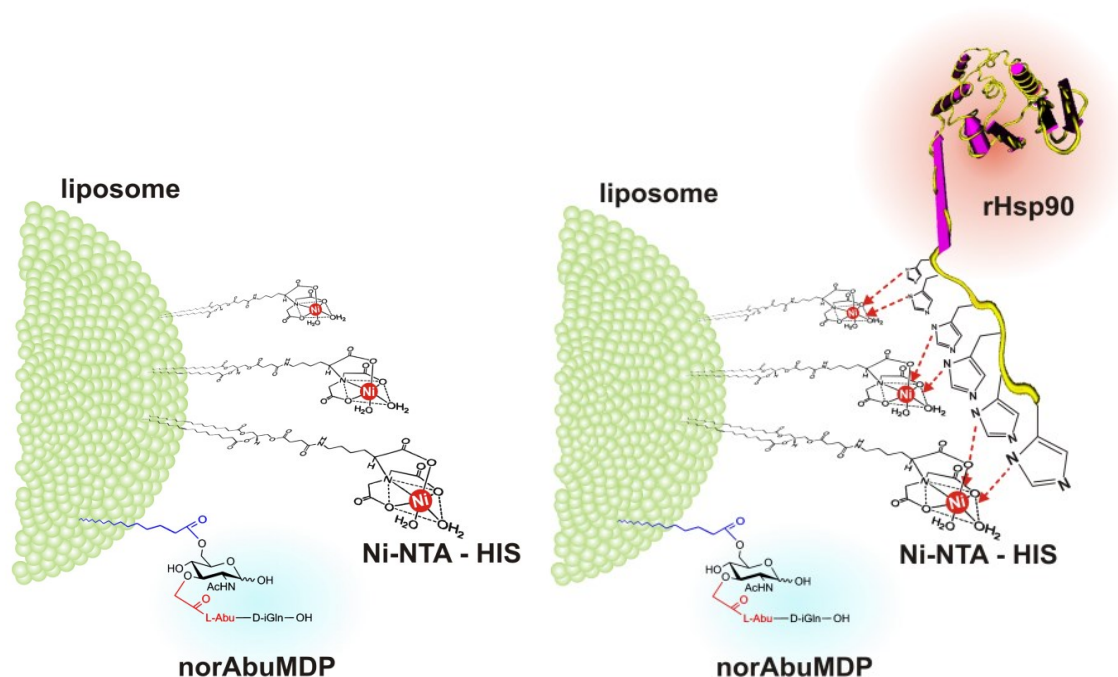
dřeně subletálně ozářených myši. Na myším modelu byla také prokázána stimulace imunitního systému a stimulace hemopoézy po letálním ozáření.



Obr. 25 Schematická struktura liposomálních imunostimulátorů s povrchově vázanými hydrofobními analogy normuramylových glykopeptidů.

Pro konstrukci experimentálních vakcín jsme se zabývali liposomy a vyvinuli speciální metalochelatační nanoliposomální nosiče s inkorporovanými lipofilizovanými deriváty na bázi norAbuMDP a norAbuGMDP. Technologie přípravy jsou popsány v publikacích v kapitole „Metody přípravy liposomů“. Tyto metalochelatační liposomální nosiče jsou vhodné pro směrované nekovalentní navázání rekombinantních antigenů s HisTag kotvou. V případě potřeby lze využít karbodiimidu pro převedení nekovalentní

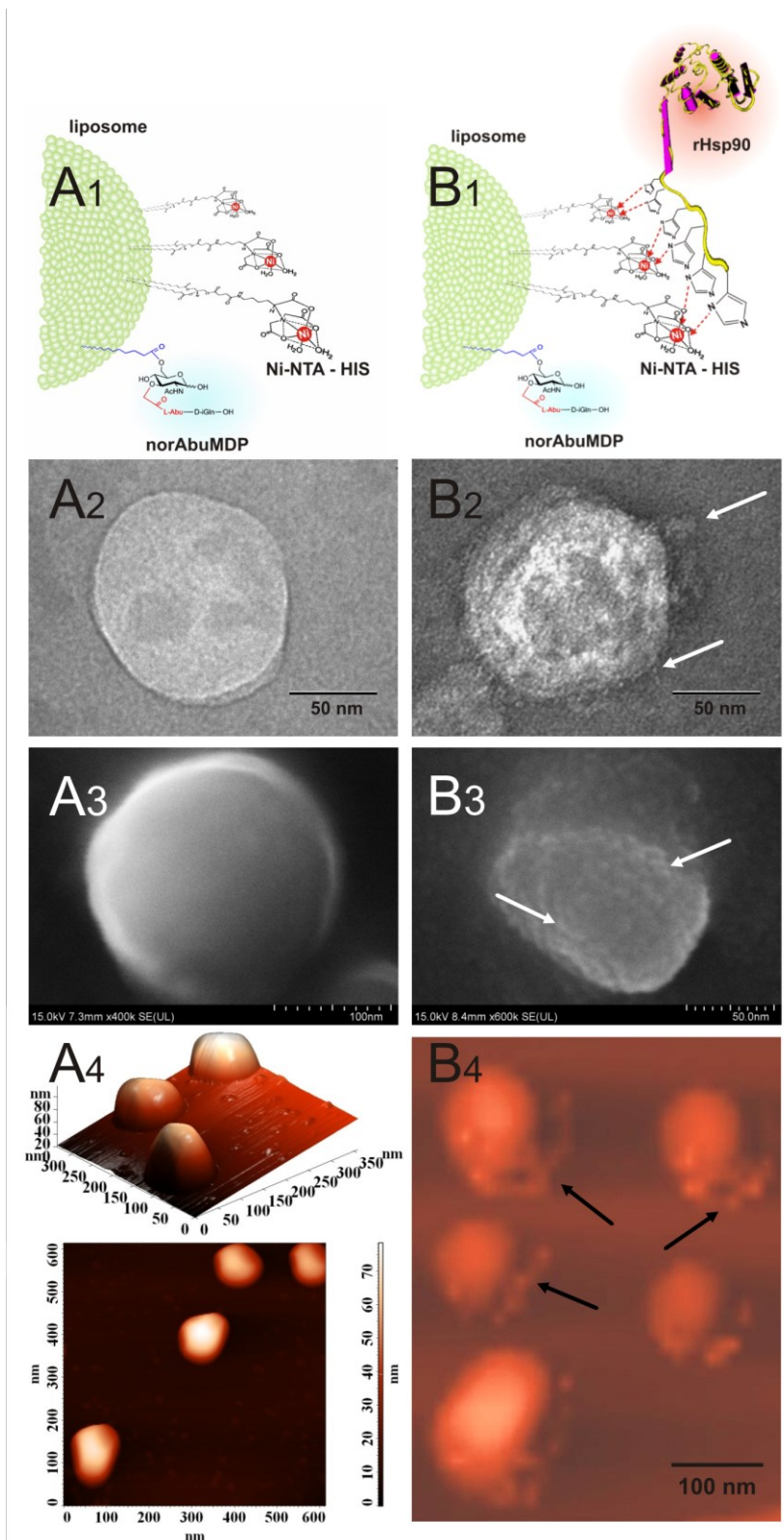
metalochelatační vazby na kovalentní vazbu se zachováním precizní orientace proteinu na povrchu liposomální lipidní dvojvrstvy. Vyvinutý systém nanoliposomálních nosičů je v současnosti jedním z nových systémů testovaným pro vývoj rekombinantní chimérické vakcíny proti borelióze.



Obr. 26 Schématické zobrazení metalochelatačního nanoliposomálního nosiče pro konstrukci rekombinantních vakcín.

Volný nosič (vlevo) a nosič s navázaným rekombinantním proteinem (vpravo). Specifická metalochelatační vazba umožňuje dosáhnout precizní orientace molekul rekombinantního proteinu na povrchu liposomů.

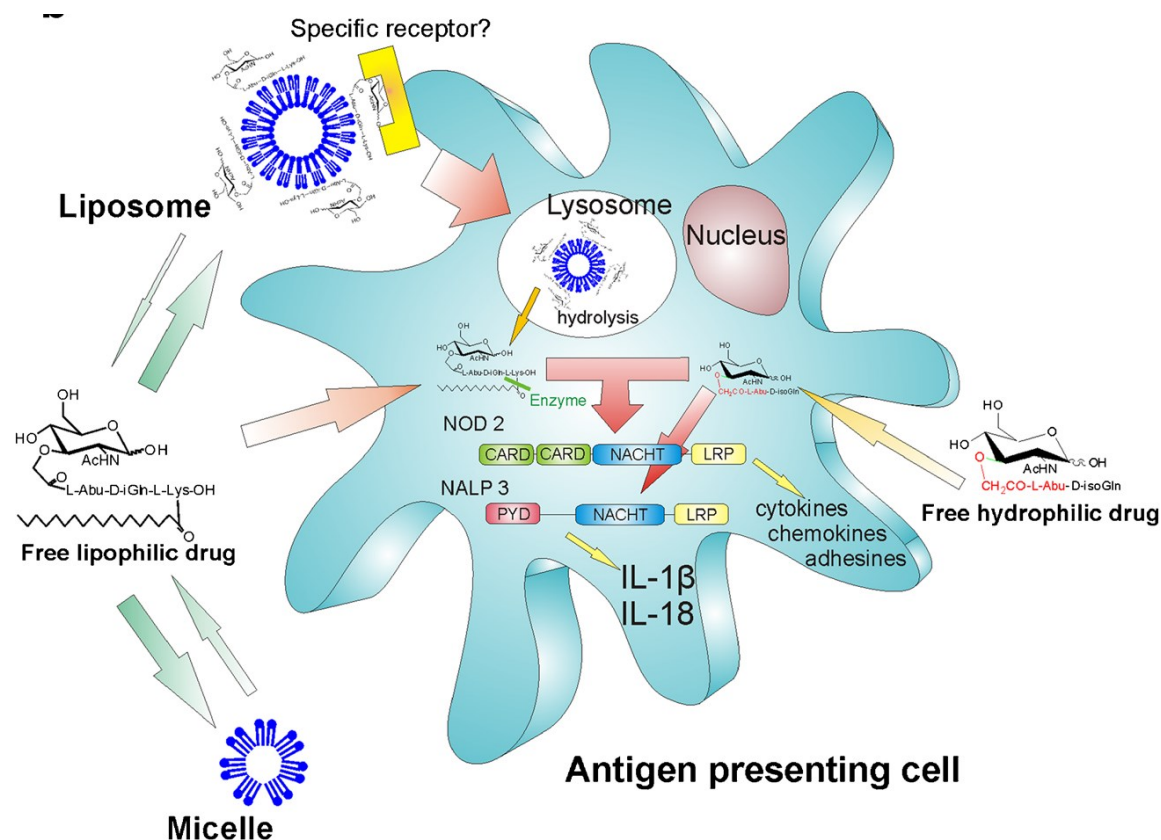
Na následujícím obrázku jsou zobrazeny struktury proteoliposomů, které byly potvrzovány moderními mikroskopickými metodami (TEM, SEM a AFM) v kombinaci s gelovou permeační chromatografií, PAGE a imunoblotingem.



Obr. 27 Struktury proteoliposomů zobrazené moderními mikroskopickými metodami.

Na obrázku je struktura liposomálních nosičů (A) a odpovídajících proteoliposomů (B) zobrazených mikroskopickými metodami (TEM, SEM a AFM). Šipky naznačují jednotlivé molekuly vázaného proteinu (rHSP 90).

Princip mechanismu účinku liposomálních molekulárních adjuvans na bázi normuramylových glykopeptidů je vyjádřen na obrázku 27. Klíčem je cílení k intracelulárním receptorům NOD 2 a ke komplexu inflamasomu NLRP 3. Tato oblast je v současnosti intenzivně studována na našem oddělení.



Obr. 28 Schéma možných farmakokinetických drah pro deriváty na bázi normuramylových glykopeptidů.

Různé modifikace molekul norAbuMDP/GMDP pomocí lipidních struktur vede k expozici různých částí molekuly na povrchu liposomů. V závislosti na koncentraci určitého analogu v dvojvrstvě mohou být vytvořeny nové molekulární vzorce, které jsou rozpoznány receptory na buňkách imunitního systému a vedou ke zvýšené internalizaci liposomů. Buněčná membrána je bariérou pro volné hydrofilní látky, které tak nepronikají snadno do buňky a nedosáhnou dostatečné koncentrace nutné k aktivaci intracelulárním receptorům (*situace in vivo*). Hydrofobní deriváty tvoří micely, u nichž je nesnadné predikovat stabilitu v biologickém prostředí kvůli komplexnosti interakcí. Předpokládá se přímá interakce s buněčnou membránou a penetrace do buňky. Liposomální formulace hydrofilních i lipofilních derivátů je relativně stabilní v biologickém prostředí a je dokumentována endocytóza/fagocytóza buňkami imunitního systému. Ve srovnání s volnými látkami, liposomální formulace tvoří depot v tkáni a zvyšuje významně koncentraci

účinné látky v buňce. Pro aktivaci intracelulárních receptorů je zřejmě zapotřebí odstranění lipidních struktur z molekuly pomocí lysozomálních a cytoplasmatických enzymů, které rozštěpí esterové vazby mezi glykopeptidovou částí a hydrofobním zbytkem. Důležitost tohoto kroku nebyla v současnosti dostatečně rozpoznána a pochopena. Citlivost různých derivátů k působení hydrolytických enzymů a komplexnost celého procesu aktivace receptorů NOD1/2 a NLRP 3 může vysvětlovat různorodost účinků lipofilních derivátů MDP.

Bezpečnost liposomálních vakcína a nových syntetických adjuvans byla testována na prasatech po *i.d.* aplikaci a srovnána s olejovými adjuvans, která mohou způsobovat nekrotické léze a záněty. Liposomální experimentální vakcíny nezpůsobovaly po *i.d.* aplikaci nežádoucí vedlejší účinky, což je důležité zejména pro zamýšlené budoucí aplikace v humánní medicíně. Srovnání vedlejších účinků olejové vakcíny a liposomálního preparátu po *i.d.* aplikaci praseti je doloženo na obrázku. Bezpečnost liposomální formulace vakcíny proti borelióze byla prokázána také na štěňatech a koťatech (spolupráce s firmou Bioveta a.s. v rámci projektu TAČR Rekombinantní multiepitopová vakcína proti borelióze pro veterinární aplikace).



Obr. 29 Srovnání vedlejšího účinku syntetických a olejových adjuvans po *i.d.* aplikaci.

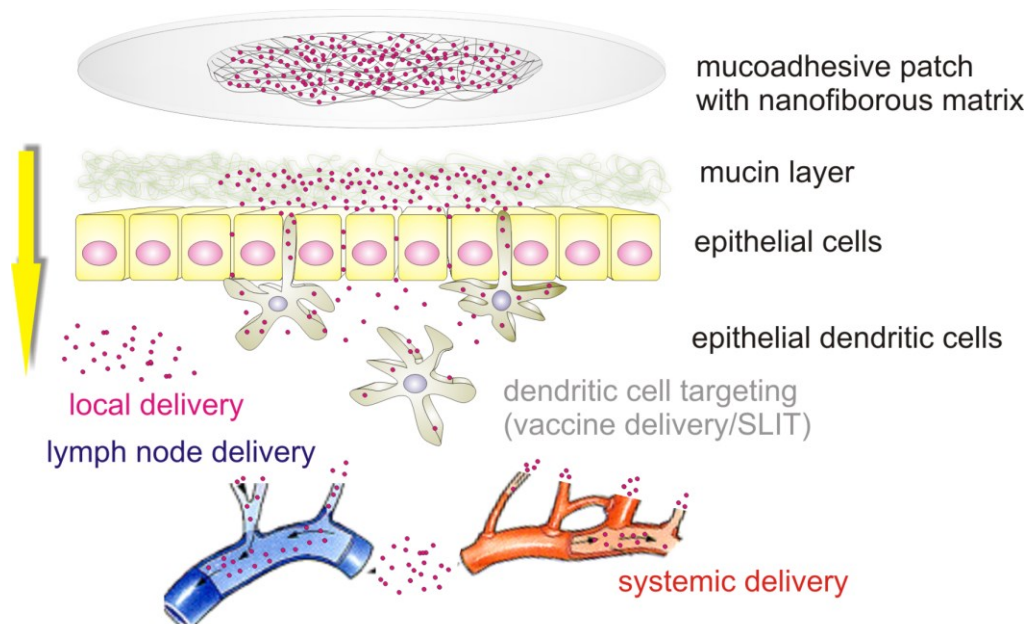
Oblast po *i.d.* aplikaci olejové vakcíny a liposomálního preparátu u prasete.

3.1. NOVÝ SMĚR VÝZKUMU REKOMBINANTNÍCH VAKCÍN

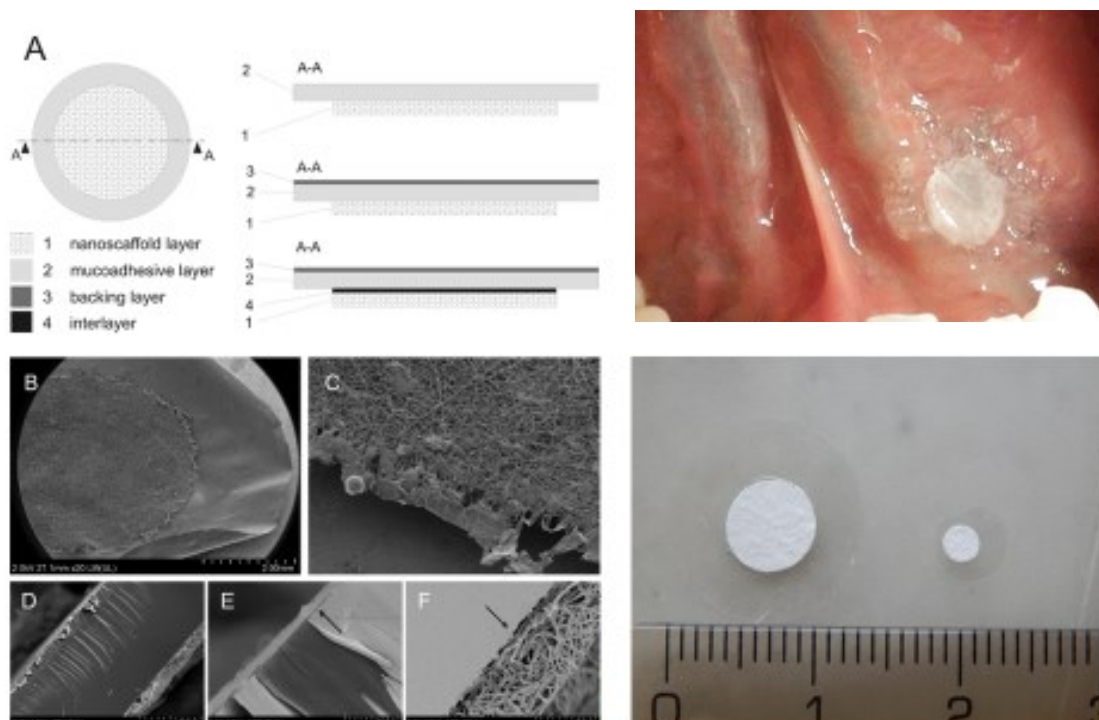
Další směřování výzkumu v oblasti moderních rekombinantních vakcín je do oblasti mukózních vakcín s využitím biokompatibilních nanotextilií založených na

technologii nanovláken. Jedná se o zcela novou oblast, ve které jsme průkopníky. Technologické, aplikační a bezpečnostní faktory favorizují tento typ vakcín pro budoucí použití jak ve veterinární, tak humánní medicíně. Jednoznačnou výhodou sublinguální aplikace vakcín je neinvazivnost a snadnost podání, bezpečnost aplikace, schopnost navodit mukózní a systémovou imunitní odpověď, což je základ pro úspěšnou vakcinaci u celé řady infekcí (nejnověji u viru zika). Dalším významným rysem je snadná technologická proveditelnost výroby a nízká hmotnost skladovací formulace (významné pro distribuci vakcíny v obtížně dostupných oblastech třetího světa). Jedná se o prioritní výzkum našeho oddělení a jsou připravovány projekty základního a aplikovaného výzkumu ve spolupráci s tuzemskými (UP Olomouc, BTÚ, FZÚ, TUL) a zahraničními pracovišti (King's College, University of Kent, Pasteur Institute, Institute of René Descartes).

Klíčovými kroky pro dosažení úspěchu v oblasti sublinguální imunizace jsou: a) systém pro sublinguální aplikaci antigenů; b) hodná formulace antigenu a delivery systém; c) vhodná adjuvans a jejich formulace. Náš příspěvek se týká všech tří částí. Liposomální molekulární adjuvans a formulace antigenu jsou popsány v předchozích kapitolách. Originální mukoadhesivní systém pro sublinguální aplikace. Hlavním účelem mukoadhesivního systému je udržet po delší dobu antigen na sublinguální sliznici a umožnit jeho penetraci do sublinguální tkáně, kde je rozpoznán dendritickými buňkami a dopraven do drénujících mízních uzlin. Mukoadhesivní systém udržuje vysoký koncentrační gradient antigenu a brání jeho odplavení mukozními sekrecemi z místa aplikace. Schematicky je zobrazen princip na obrázku 28 a vzhled mukoadhesivních filmů a jejich aplikace na sublinguální mukózu je na obrázku 29. Ukázka struktury nanovláken s navázanými liposomy je na obrázku 30.

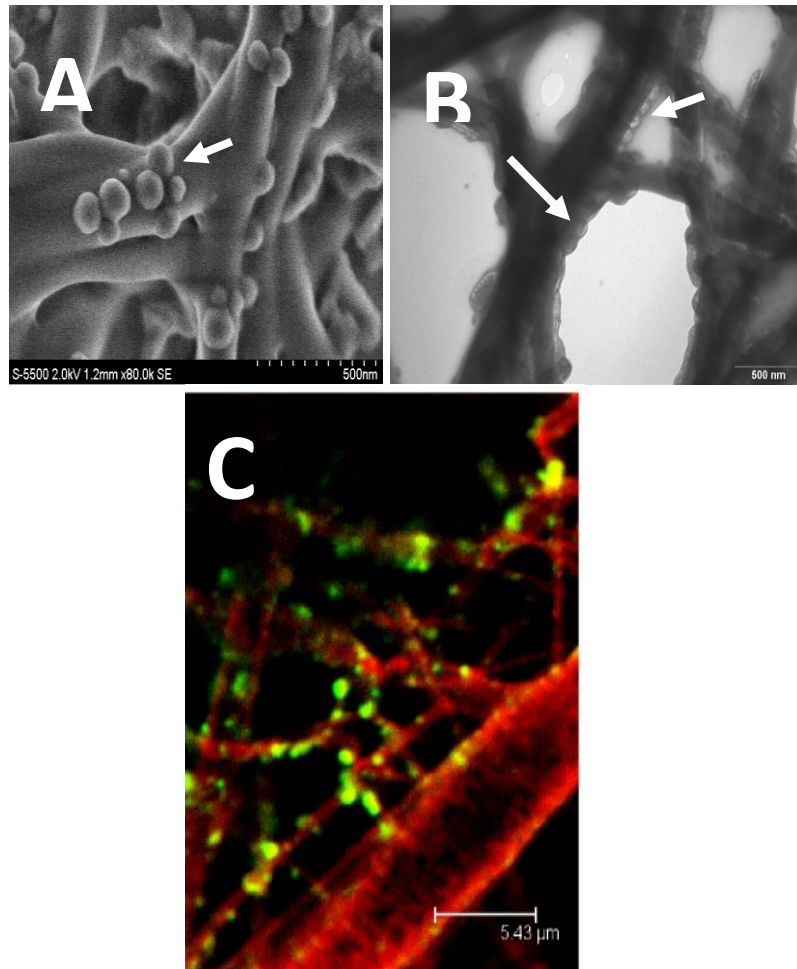


Obr. 30. Schéma sublinguální imunizace



Obr. 31. Schematické a skutečné zobrazení struktury mukoadhesivních filmů na bázi nanovláken.

A) schéma mukoadhesivních filmů, B-F) snímky struktury pomocí skenovací elektronové mikroskopie. Aplikace filmu na sublinguální mukózu (snímek vpravo nahoře); vzhled mukoadhesivních filmů pro aplikace na velká zvířata a malé hlodavce (snímek vpravo dole).



Obr. 32 Ukázka struktury nanovláken s navázanými liposomy.

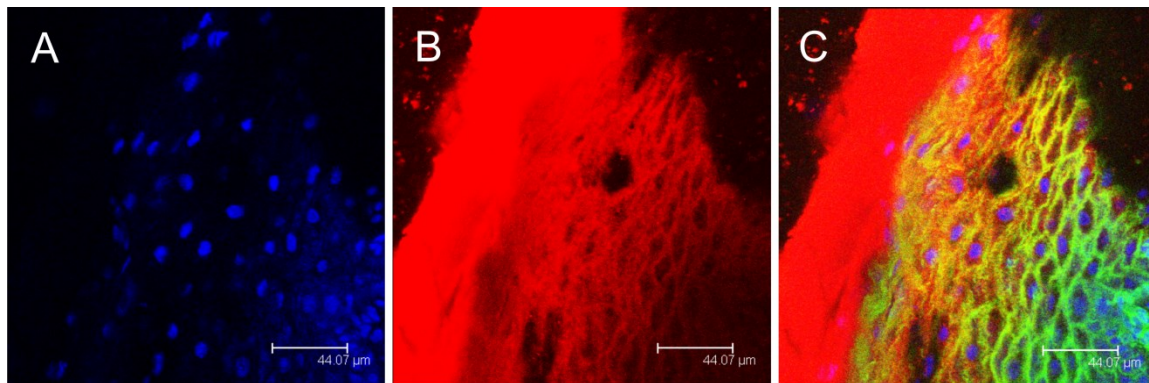
Snímky byly pořízeny skenovací a transmisní elektronovou mikroskopií (A, B) a konfokální mikroskopií (C). Jsou zřetelně patrné liposomy navázané na povrch nanovlákn. V případě konfokální mikroskopie byly použity metalochelatační proteoliposomy s rGFP (zelená fluorescence) a fluorescenční lipid pro označení nanovláken (červená fluorescence). Šípky označují liposomy na povrchu nanovláken.

Aplikace fluorescenčně značených liposomů nebo polymerních nanočástic na sublinguální mukózu pomocí mukoadhesivních filmů prokázala rychlou paracelulární penetraci, pohlcení dendritickými buňkami a dopravu do drénujících mízních uzlin, což je základní předpoklad pro navození imunitní reakce proti takto podaným antigenům. Experimentální potvrzení našich předpokladů bylo dosaženo pomocí prasečího modelu. Histologické preparáty byly vyšetřeny pomocí konfokální mikroskopie a byla potvrzena paracelulární penetrace nanočástic do hlubších vrstev stratifikované sublinguální mukózy a dopravení nanočástic do drénujících mízních uzlin. Fluorescenční nanočástice byly nalezeny v T a B oblasti mízních uzlin, kam byly dopraveny dendritickými buňkami (obr. 31).

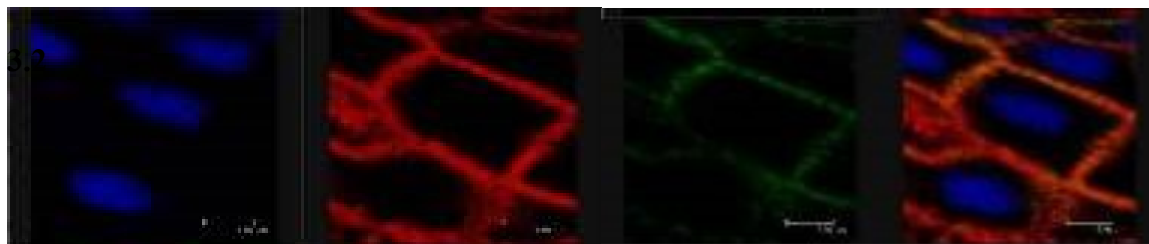
Obr. 33. Průkaz penetrace fluorescenčních nanočástic do sublinguálních tkáně a mizních uzlin po sublinguálním podání s využitím mukoadhesivních filmů (snímky byly pořízeny konfokálním mikroskopem).

modrá – buněčná jádra; červená – nanočástice; zelená – aktin

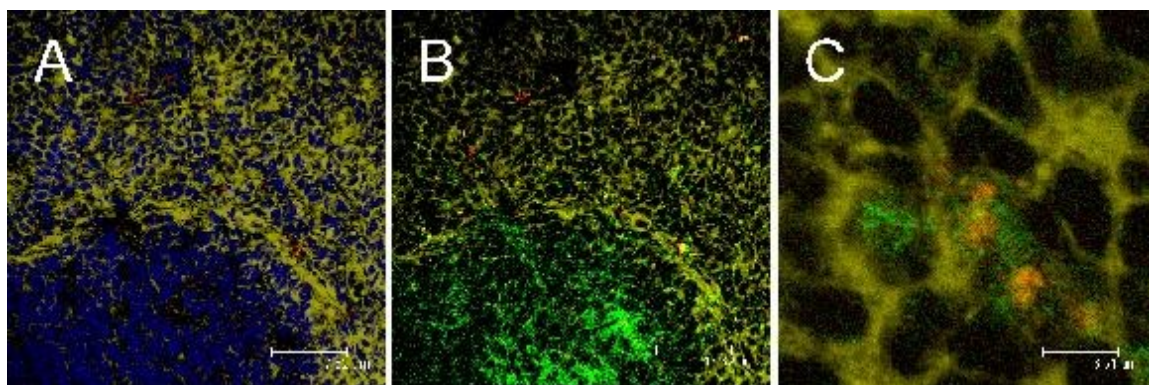
Penetrace nanočástic (nanoliposomy) do sublinguální mukózy



Detail zobrazení paracelulárního průniku nanočástic submukózní vrstvou epitelálních buněk



Průkaz doručení nanočástic do T a B zóny drénujících mizních uzlin



A) řez mizní uzlinou s vyznačením jader T a B zóny. Červeně fluoreskující částice jsou patrné v obou zónách.

B) řez mizní uzlinou s vyznačením lymfocytů T a B zóny (SLA II antigen)

C) Detailní zobrazení dendritických buněk s internalizovanými fluorescenčními liposomy (T zóna)

modrá – buněčná jádra; červená – nanočástice; žlutozelená – aktin; zelená – SLA II antigen (prasečí lymfocyty)

3.2. ZÁVĚR

Ucelený systém pro sublinguální vakcinace představuje moderní aplikaci nanotechnologie pro medicínální aplikace. Vyvinutý systém má potenciál průlomové technologie, pro kterou razíme název „Technologie tištěných vakcín“. Ve spolupráci s českými (UP Olomouc a TU Liberec) a zahraničními partnery (Global Acorn, UK) byla podána přihláška mezinárodního patentu (J. Turánek, J. Mašek, M. Raška, R. Lukáč, P. Knotigová, D. Lubasová, A.D.Miller Mucoadhesive carriers of particles, method of preparation and uses thereof PCT/GB2015/052833) a do časopisu Biomaterials byl podán rukopis s názvem „Multi-layered nanofibrous mucoadhesive films for buccal and sublingual administration of drug-delivery and vaccination nanoparticles - important step towards effective mucosal vaccines“. V rámci výzvy vlády Spojeného Království Velké Británie a Seerního Irska byl podán mezinárodní projekt na vývoj vakcíny proti viru zika a jsou připravovány výzkumné projekty se zahraničními partnery na rozvoj této technologie v rámci výzvy HORIZON 2020. V roce 2016 plánujeme se zahraničním partnerem založení start-up pro komercializaci technologie tištěných vakcín.

3.2.1. Publikace k tématu kapitoly

Immunology Letters, 39 (1994) 157–161
0165 - 2478 / 94 / \$ 7.00 © 1994 Elsevier Science B.V. All rights reserved

IMLET 02074

Adjuvant effect of liposomes and adamantylamide dipeptide on antigenicity of entrapped synthetic peptide derived from HIV-1 transmembrane region glycoprotein gp41

Jaroslav Turánek^{a,*}, Miroslav Toman^a, Jan Novák^b, Viktor Krchňák^c and Pavla Hořavová^a

^aVeterinary Research Institute, Hudecova 70, 621-32 Brno, Czech Republic; ^bInstitute of Sera and Vaccines, Koruní 108, 100-103 Praha-10, Czech Republic; ^cInstitute of Organic Chemistry and Biochemistry, Czech Academy of Sciences, Flemingovo náměstí 2, Praha-6, Czech Republic

(Received 25 October 1993; accepted 23 November 1993)

1. Summary

The synthetic peptide antigen (Ag) (the primary structure Tyr-Leu-Lys-Asp-Gln-Gln-Leu-Leu-Gly-Ile-Trp-Gly-Cys-Ser-Gly-Lys-Leu-Ile-Cys-Thr derived from the envelope glycoprotein gp41 of the human immunodeficiency virus type 1 (HIV-1) and exerting specificity with all HIV-1-positive sera available in the Czech Republic (and also in a panel of 10,000 sera from WHO)) was conjugated with bovine serum albumin (BSA) and encapsulated into liposomes. Adjuvant activities of liposomes with various lipid compositions were compared with Freund's complete adjuvant (FCA) and with aluminium hydroxide (AL). The immune response to BSA-Ag liposomes with co-entrapped adamantylamide dipeptide (AdDP) was comparable with that of FCA in terms of longevity and levels of specific antibodies in mouse sera.

2. Introduction

Liposomes are microscopic membrane-like structures consisting of one or more concentric lipid bilayers enclosing an equal number of aque-

ous compartments and having various uses in biological studies [1]. Since 1974, liposomes have been recognized as potent immunological adjuvants for a wide variety of antigens [see reviews 2,3]. The progress in liposome technology, peptide synthesis, synthesis of new immunoadjuvants and also in the knowledge of the antigenic structure of proteins and factors regulating immune responses have made liposomes an attractive adjuvant candidate for the preparation of synthetic vaccines which are defined at molecular level and, therefore, potentially safe. An enhancement of immunogenicity can be attained by co-entrapment of an adjuvant.

Adamantylamide-L-alanyl-D-isoglutamine (AdDP, for adamantylamide dipeptide) belongs to a group of desmuramyl MDP (muramyl dipeptide) derivatives able to protect an organism from some viral infections [4]. This hybrid entity combines pertinent components of both an antiviral and an immunomodulator in a single synthetic compound missing side effect (pyrogenicity, edemagenicity, effect on the sleep) which are inherent to a great number of MDP derivatives [5].

In this study, the immunogenicity of a model liposomal vaccine containing a synthetic peptide antigen derived from envelope glycoprotein gp41 of the HIV-1 was compared with those of Freund's complete adjuvant (FCA) and aluminium hydroxide (AL) antigen formulations.

Key words: Glycoprotein 41; Adamantylamide dipeptide; Synthetic peptide antigen; HIV-1; Liposome; (Mouse)

*Corresponding author.

SSDI 0165-2478(93)E0165-9

157

3. Materials and Methods

3.1. Preparation of synthetic peptides

Peptides were prepared by continuous-flow solid-phase multiple peptide synthesis [6] on *p*-methyl-benzhydrylamine resin using the Fmoc/*t*-Bu protection strategy. Fmoc groups were removed by piperidine, condensation was performed by HOBt esters, and the coupling reaction was monitored with bromophenol blue [7]. Side-chain protecting groups were removed by trifluoroacetic acid and the completed peptides were split off the resin in liquid hydrogen fluoride. Crude peptides were purified by gel filtration on Sephadex G-15. The purified peptides displayed correct amino acid compositions and showed the expected molecular peak in fast atom bombardment mass spectroscopy.

Amino acid sequences of peptides were derived from envelope gp41 protein products of the LAV isolate of the HIV-1 [8] so as to include domains predicted as responsible for the humoral immune response to the native viral proteins [9]. The peptide antigen with the sequence position 598–617 and primary structure Tyr-Leu-Lys-Asp-Gln-Gln-Leu-Leu-Gly-Ile-Trp-Gly-Cys-Ser-Gly-Lys-Leu-Ile-Cys-Thr was selected from 14 different synthetic decapeptides covering the region within 586–631 envelope glycoprotein gp41 sequence position with constant shift by two amino acids.

Specificity of the antigen was checked with all the HIV-1-positive sera available in Czech Republic and also in a panel of 10,000 sera from WHO.

For easy handling and improving antigenicity the peptide was coupled to bovine serum albumin (BSA) by the glutaraldehyde method and used in this form in immunological studies.

3.2. ELISA on plates

ELISA was carried out by the standard solid-phase method. The peptides were used either in a free form or coupled to BSA (SERVA). Microelisa plates (Nunc for free and Dynatech for BSA-conjugated peptides) were coated with the respective peptides (1 µg/well) in bicarbonate buffer (pH 9.6) at room temperature for 1 h. Free binding sites were saturated with 1% BSA or glycine in

the same buffer. The BSA or glycine solution was removed after 1 h at room temperature; serum diluted 1:50 was added into each well and the plates were incubated at room temperature for 1 h. After several washings, peroxidase-conjugated swine antibody to mouse Ig diluted 1:2500 was added. The colour reaction was developed by the incubation with *o*-phenylenediamine (Sigma). The anti 598–617 gp41 peptide antibodies in mouse sera were assayed only in plates coated with free peptide antigens and the remaining binding sites were saturated with glycine. The specificity of free and conjugated peptide antigens was checked in plates saturated with BSA. Detailed ELISA procedure was described by Vestergaard et al. [10].

3.3. Phospholipids

Sigma liposome kit positive (63 µmol of phosphatidylserine, 18 µmol dicetylphosphate, 9 µmol cholesterol) and Sigma liposome kit negative (63 µmol of phosphatidylserine, 18 µmol stearylamine, 9 µmol cholesterol) (Sigma) were used for the preparation of liposomes.

An egg yolk phospholipid mixture (EPM) was purified as described by Singleton [11] and stored in sealed ampules at –20°C until used for liposome preparation. The composition of EPM was assayed as 70% of phosphatidylserine; 24.6% of phosphatidylethanolamine; 4% of sphingomyeline; 0.1% esters of cholesterol; 0.7% of triglycerides.

3.4. Preparation of liposomes

Frozen-thawed multilamellar vesicles (FTMLV) [12,13] were prepared by the hydration of the 160 mg of lipid film, prepared in a round-bottom flask by removal of chloroform on a rotary evaporator with aqueous phase (150 mM NaCl, 20 mM HEPES, pH 7.4, sterilized by filtration through 0.22 µm filter) containing the antigen and alternatively immunoadjuvant compounds to be co-entrapped. After continuous mixing on a mechanical reciprocal shaker for 2 h, FTMLV were obtained by freezing the multilamellar vesicles (MLV) in liquid nitrogen and thawing them in a 30°C water bath, repeating the cycle 5 times. Vesicles extruded through 0.2 µm filter (VET200),

which share more uniform size distribution, were prepared from FTMLV [12–14]. The FPLC system and a high-pressure filtration cell were used [15]. The non-entrapped material was removed by centrifugation (10,000 × g, 20 min) of the liposomal suspension completed to 5 ml with the buffer used for hydration. The procedure was repeated twice to remove the non-entrapped material completely.

3.5. Efficiency of association

The amounts of BSA-Ag associated with liposomes were measured by gamma counting using BSA-Ag radioiodinated by the chloramine T method [16].

3.6. Preparation of other adjuvant formulations

Aluminium hydroxide-adsorbed antigen (AL-BSA-Ag) was prepared using the adjuvant AL-SPAN-OIL (USOL, Prague, Czech Republic) following the manufacturer's instructions. The BSA-Ag solution or liposomal BSA-Ag formulation (2 ml) with appropriate antigen concentration were mixed with 2 ml of AL and then with 6 ml of SPAN-OIL. The animals were injected subcutaneously with 0.5 ml of the vaccine.

The FCA (Difco) formulation was prepared by mixing 2 ml of BSA-Ag solution with 2 ml of FCA following the manufacturer's detailed instructions.

3.7. Animal immunization experiments

Female Balb/c mice 8–9-week-old mice (Veter-

inary Research Institute, Brno) weighing 20–22 g were used in immunization experiments. Animals were primed subcutaneously in groups of fifteen with 0.2 ml of the respective vaccines. Only the AL formulations were injected with the dosage of 0.5 ml. Three weeks later, the mice were boosted with the same antigen formulation. Three animals of the each group were killed on the 21st, 35th, 42nd, 49th and 56th day after priming, and specific antibodies in sera were quantified by ELISA.

4. Results

4.1. Entrapment of BSA-Ag into liposomes

Entrapment rates of ¹²⁵I-labelled BSA-Ag are summarized in Table 1. A significantly higher encapsulation efficiency is evident in the case of FTMLV when compared with MLV. An approximately 50% efficiency was presumed for AdDP as an analogy of that assayed for muramyl dipeptide and its analogues (unpublished results). Encapsulation efficiencies obtained with EPM (160 mg of lipids in 1 ml of aqueous phase) agreed well with results published by other authors [12].

4.2. Adjuvant activity of liposomes

Initial experiments were carried out to define the amount of antigen with which liposomes could exhibit adjuvant activity, using two dosages of BSA-Ag (1 and 0.1 µg of net peptide antigen) injected as the liposomal, FCA or AL formulations.

No responses were observed at the dose of 0.1

TABLE 1

DEPENDENCE OF PHOSPHOLIPID/ANTIGEN RATIO ON ENCAPSULATION EFFICIENCY FOR MLV AND FTMLV

Liposomes were prepared by hydration of 160 mg of dry lipid film with 1 ml of 20 mM HEPES + 0.15 M NaCl, pH 7.2, containing various amounts of BSA-Ag conjugate + 1.6 µg of radiolabelled BSA-Ag conjugate. FTMLV were prepared by freezing and thawing of MLV. The cycle was repeated 5 times.

Incorporation (%)	Amount of BSA-Ag/160 mg phospholipids				
	16 mg	1.6 mg	0.16 mg	16 µg	1.6 µg
FTMLV	45.1	49.9	55.7	57.8	22.7
MLV	13.7	15.4	13.9	15.2	9.9

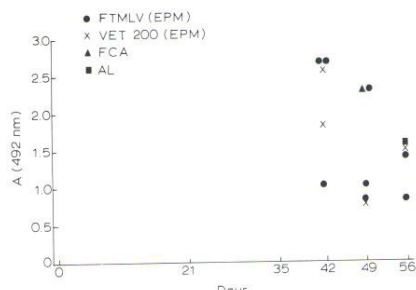


Fig. 1. Immune responses to synthetic peptide antigen (Ag) in a dose of 1 µg/mouse for various BSA-Ag formulations. Results are individual values for each of the treated mice from 3-member groups. A value of 0.05 is accepted as the threshold. Arrows indicate the days of the 1st and 2nd immunizations. For other details see text.

µg of the antigen when any adjuvant was used. Dosage of 1 µg of antigen induced specific antibody production in animals injected with FTMLV or FTMLVET200. Dynamics of specific immune responses in animals immunized with FTMLV or VET200 containing 1 µg of entrapped antigen per dose are shown in Fig. 1.

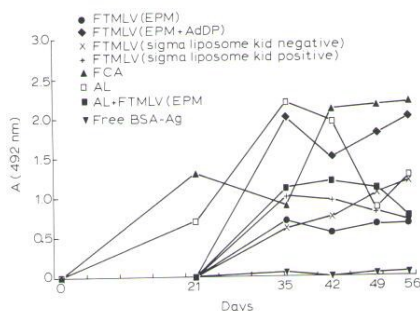


Fig. 2. Comparison of immune responses to synthetic peptide antigen (Ag) (dose: 5 µg/mouse) for various BSA-Ag formulation. Each point represents the mean of 3 tested sera. Arrows indicate the days of the 1st and 2nd immunization. For other details see text.

160

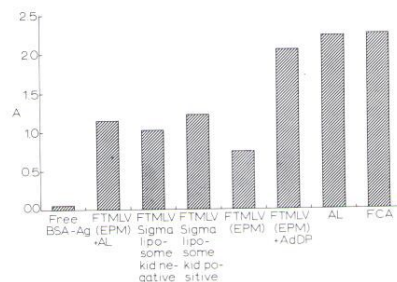


Fig. 3. Comparison of the highest level of specific antibodies against synthetic peptide antigen (Ag), which were reached for each of the BSA-Ag formulations within 21st and 56th days. Values are taken from Fig. 2.

4.3. Comparison of liposomes with other immunological adjuvants

In further immunization experiments we have used a 5 µg dose of antigen, and immunoadjuvant action of FTMLV was compared with those of the FCA, AL-SPAN-OIL and AdDP. The latter adjuvant (16 µg/dose) was administered in a liposomal form co-entrapped with BSA-Ag.

FTMLVs prepared from the commercial Sigma liposome kit (with positive or negative charge) were also tested. Fig. 2 shows the dynamics of immune responses to various formulations of the antigen. The maxima of specific antibody responses reached for each antigen formulation are presented in Fig. 3.

5. Discussion

Experiments with the incorporation of BSA-Ag into liposomes revealed that repeated freezing and thawing the MLV increased the encapsulation efficiency markedly. Our results agreed well with those published by Mayer et al. [12] who reported for FTMLV an encapsulation efficiency of about 40 and 60% for concentrations 100 and 200 mg lipids/ml, respectively. The encapsulation efficiencies obtained in our experiments for BSA-Ag were similar within a wide range of lipid/BSA-Ag ratio.

Initial immunization studies in Balb/c mice have revealed that both liposomal formulations

(FTMLV or VET200) can provoke immune responses at the dose of 1 μg of antigen, which was the threshold dose for the FCA or AL formulations (only sporadic responses were seen). Weaker responses to the VET200 antigen formulation can be attributed to both the low encapsulation efficiency (20%) and a possible decrease of antigen concentration resulting from adsorption on membrane filter used for the extrusion. The liposomes prepared by the extrusion technique were not further included in subsequent experiments owing to the limited amount of the antigen available.

In the immunization experiments with 5 μg of antigen per dose (Fig. 2), the FTMLV prepared from EPM were compared with those prepared from the commercial Sigma liposome kit.

No significant differences were observed among immune responses to antigens entrapped in FTMLV(EPM), FTMLV(Sigma liposome kit negative), FTMLV(Sigma liposome kit positive) or FTMLV(EPM)+AL.

A dramatic increase in immune responses was found in animals immunized with FTMLV(EPM) formulation with co-entrapped AdDP. This antigen formulation was comparable with those containing FCA or AL in terms of intensity of antibody responses. The onset of immune response induced by any of the liposomal formulations was delayed when compared with those following the administration of FCA or AL formulations. Contrary to AL formulation the liposomes with co-entrapped AdDP proved long-term duration of high specific antibody response, comparable with that induced by FCA.

In a study on antibody response to primary and secondary immunization with influenza subunit vaccine, the free AdDP (100 μg /mouse) did not exert an effect on specific antibody titers following the secondary immunization, but its protective power was significant [17].

We have shown that co-entrapment of AdDP and synthetic peptide antigen into liposomes improved their adjuvant action to the level compar-

able with FCA and AL. It may be due to protective effect of liposomes against metabolic degradation of AdDP. Prolongation of elimination half-time may explain why this compound is effective even in very low doses [18].

Liposomal form of AdDP is a promising base for development of synthetic vaccines. Pharmacokinetic profile of liposomal form of AdDP and its antiviral activity is a task for our future research.

References

- [1] Alving, C.R. and Richards, R.L. (1982) in: *The Liposomes* (M. Ostro, Ed.) pp. 1-115, Marcel Dekker, New York.
- [2] Gregoriadis, G. (1990) *Immunol. Today* 11, 89.
- [3] Warren, H.S. and Chedid, L.A. (1988) *CRC Crit. Rev. Immunol.* 8, 83.
- [4] Masihi, K.N., Lange, W., Rohde-Shulz, B. and Mašek, K. (1987) *Int. J. Immunother.* 3, 89.
- [5] Mašek, K. (1988) *Adv. Biosci.* 68, 11.
- [6] Krcňák, V. and Vágner, J. (1990) *Pept. Res.* 3, 182.
- [7] Krcňák, V., Vágner, J., Šafář, P. and Lébl, M. (1988) *Coll. Czech. Chem. Comm.* 53, 2542.
- [8] Wain-Hobson, S., Sonigo, P., Danos, O., Cole, S. and Alizon, M. (1985) *Cell* 40, 9.
- [9] Krcňák, V., Mach, O. and Maly, A. (1989) *Methods Enzymol.* 178, 586.
- [10] Vestergaard, B.F., Graubale, P.C.I. and Spangaard, H. (1977) *Acta Pathol. Microbiol. Scand. (B)* 85, 466.
- [11] Singleton, W.S., Gray, M.S., Brown, M.L. and White, J.L. (1965) *J. Am. Oil Chem. Soc.* 42, 53.
- [12] Mayer, L.D., Hope, M.J. and Cullis, P.R. (1986) *Biochim. Biophys. Acta* 858, 161.
- [13] Hope, M.J., Bally, M.B., Webb, G. and Cullis, P.R. (1985) *Biochim. Biophys. Acta* 812, 55.
- [14] Olson, F., Hunt, C.A., Szoka, F.C., Vail, W.J. and Papahadjopoulos, D. (1979) *Biochim. Biophys. Acta* 557, 9.
- [15] Turánek, J. (1993) *Anal. Biochem.* in press.
- [16] Garvey, J.S., Cremer, N.E. and Sussdorf, D.H. (1977) in: *Methods in Immunology*, pp. 171-182, Benjamin Cummings Publ., MA.
- [17] Masihi, K.N., Lange, W., Schwenke, S., Gast, G., Huchshorn, P., Palache, A. and Masek, K. (1990) *Vaccine* 8, 159.
- [18] Walder, P., Buchar, E., Machková, Z., Vrba, T., Flegel, M., Janků, I. and Mašek, K. (1991) *Immunopharmacol. Immunotoxicol.* 13, 101.



PII: S0192-0561(98)00003-4

STIMULATION OF HAEMOPOIESIS AND PROTECTION OF MICE AGAINST RADIATION INJURY BY SYNTHETIC ANALOGUES OF MURAMYLDIPEPTIDE INCORPORATED IN LIPOSOMES

JAROSLAV TURÁNEK,*|| DANA ZÁLUSKÁ,† MICHAL HOFER,‡ ANTONÍN VACEK,‡
MIROSLAV LEDVINA§ and JAN JEŽEK§

*Veterinary Research Institute, 621 32 Brno, Czech Republic; †Research Institute of Fine Chemicals, 621 33 Brno, Czech Republic; ‡Institute of Biophysics, 612 65 Brno, Czech Republic and §Institute of Organic Chemistry and Biochemistry, 16 610 Prague, Czech Republic

(Received for publication 16 January 1998)

Abstract—Protection from undesirable effects of radiotherapy or chemotherapy, primarily from myelosuppression, remains still a crucial problem to be studied. Attention has been therefore paid to various immunomodulatory agents that through the monocyte/macrophage system induced production of cytokines, which can induce and operate restoration of haemopoiesis and thus act radioprotectively. Some synthetic analogues of MDP free of undesirable side-effects, were synthesized in the Czech Republic. Lipophilic β -D-GlcNstearoyl-(1- > 4)-norMurNAc-L-Abu-D-isoGln (DDD-St) was designed to be easily entrapped into liposomes and this liposomal DDD-St protected efficiently mice against irradiation, when administered i.p., i.v. or s.c. 24 h prior to lethal irradiation (survival rate in the range of 30–80% compared with 0% in control). Especially the subcutaneous application of liposomal DDD-St was very efficient. The parameters characteristic of recovery of haemopoiesis in bone marrow on day 10 after 6.5 Gy irradiation were significantly improved in comparison with the controls. Very high radioprotective effect of s.c. administered liposomal DDD-St can be explained (together with induction of haemopoiesis) by an effective and long-lasting activation of nonspecific immunity, which is able to withhold an onset of septicemia in early days after irradiation. In conclusion, the liposomal DDD-St should be therapeutically beneficial in moderating the haemopoietic damage, which is an undesirable effect of radiotherapy or chemotherapy. © 1998 International Society for Immunopharmacology.

Keywords: liposomes, muramyl dipeptide analogues, radioprotection, haemopoiesis, mouse

INTRODUCTION

Protection from undesirable effects of radiotherapy or chemotherapy, primarily from myelosuppression, remains still a crucial problem to be coped with. Attention has been paid to various immunomodulatory agents that via the monocyte/macrophage system induce the production of cytokines, which induce and control haemopoiesis, and hence can act radio- or chemoprotectively (Fedoročko, 1994; Killion *et al.*, 1992). Muramylpeptides have been found to be highly active *in vitro* and *in vivo* in respect of inducing tumoricidal, antiviral and bactericidal activities. A large variety of analogues of muramyl dipeptide (MDP) have been synthesized and tested in various experimental models (reviewed by Barratt *et al.*, 1995). However, a great majority of

them have side-effects such as pyrogenicity, sleep-promoting and oedemagenic activities, which are shared with MDP (Kleinerman, 1995). Encapsulation of muramyl peptides into liposomes, vesicles composed of one or several lipid bilayers enclosing an aqueous phase, led to the reduction of the side-effects and to improved therapeutic efficacy in *in vitro* and *in vivo* models of tumor cytotoxicity, as well as in experimental microbial infections in mice (Barratt *et al.*, 1995). Targeting of liposomal immunomodulators to macrophages, their internalization via phagocytosis and hence the facilitating of interaction with the intracellular receptor led to a stimulation of macrophage functions (Merhi *et al.*, 1996; Tenu *et al.*, 1989) such as the induction of secretion of IL-1, IL-6 and TNF known to have therapeutic effects on haemopoietic regeneration after irradiation (Neta *et al.*, 1988; Pat-

|| Author to whom correspondence should be addressed.

chen *et al.*, 1991). A relatively high radioprotective activity of liposomal muramyltripeptide phosphatidyl ethanolamine (Ciba-Geigy, Switzerland), as indicated mainly in terms of animal survival, was demonstrated by Fedoročko (1994).

Some synthetic analogues of MDP (Fig. 1), free of undesirable side-effects, were designed and synthesized in the Czech Republic (Ledvina *et al.*, 1989). A study of radioprotective and haemopoietic effect of their free and liposomal forms is presented in this paper.

EXPERIMENTAL PROCEDURES

Animals

Female CBA × C57B1F₁ mice, 12 weeks old and having 20–25 g of weight at the beginning of experiments, were irradiated with a single whole-body doses from ⁶⁰Co gamma-ray source at a dose rate of 0.285 Gy/min (10.0 Gy for survival and 6.5 Gy for recovery of haemopoietic tissues). The preparations were administered i.p., i.v. or s.c. 24 h before irradiation.

Preparation of frozen-and-thawed multilamellar vesicles

Liposomes (frozen-and-thawed multilamellar vesicles, FTMLV) were prepared from the egg-yolk pho-

sphatidylcholine Lipoid 80 E (Lipoid, Germany) by classical method of hydration of lipid film by apyrogenic phosphate buffered saline (PBS) containing compounds to be entrapped (lipophilic β -D-GlcNstearoyl-(1- > 4)-norMurNAc-L-Abu-D-isoGln (DDD-St) or hydrophilic β -D-Glc-(1- > 4)-norMurNAc-L-Abu-D-isoGln (DDD)). The lipid mixture, dissolved in chloroform (200 mg in 6 ml), was deposited onto the wall of a round-bottom flask (250 ml) by removal of the solvent in a rotary evaporator (40 C, 4 h). The dried lipid film was then hydrated with the aqueous phase under continuous mixing on a mechanical reciprocal shaker for 2 h. FTMLV was obtained by freezing the multilamellar vesicles in liquid nitrogen and thawing them in a 30 C water bath, repeating the cycle five times (Hope *et al.*, 1985). For i.v. application the liposomes were extruded through 1.2 μ m Isopore filter (Millipore). The analyses of entrapment efficiency were done by HPLC. DDD-St was entrapped with 99% and DDD with 32% efficiency, respectively (Turánek *et al.*, 1997). In case of DDD, the untrapped drug was removed by centrifugation. DDD-St or DDD preparations (free of liposomal formulations) were appropriately diluted in PBS and administered in desired equimolar dosages in volume of 0.2 ml per animal in a single injection. The same volume of PBS or empty liposomes was applied to control animals.

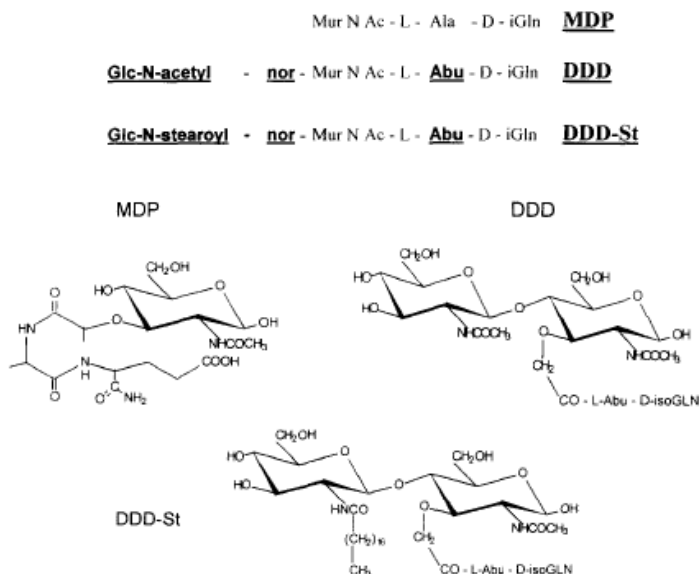


Fig. 1. Synthetic analogues of MDP.

Assay for colony-forming cells

Endogenous spleen colony-forming units (E-CFUs) were measured on day 9 of their development using the method of Till and McCulloch (1961), after 6.5 Gy of the whole-body irradiation (five mice per group).

GM-CFC progenitors

For granulocyte-macrophage colony forming cells (GM-CFC) determination, bone marrow cells from intact mice were drawn by flushing femoral bone with an IMDM medium, counted on Coulter Counter (Model ZN, Coulter Electronics) and kept in a melting ice bath before their use.

Femoral marrow cells were plated in triplicate in a semisolid environment created by a plasma clot in our modification (Vacek *et al.*, 1990), containing the Iscove's modification of Dulbecco's medium (IMDM) plus 20% fetal calf serum (FCS), 10% of colony-stimulating factor (CSF), 10% citrate bovine plasma, and CaCl₂ at a concentration of 1.5 mg/ml.

The cultures were incubated for seven days in a thermostat (Forma Scientific, USA) at 37 °C in a fully humidified atmosphere to 5% CO₂ in air. Colonies of at least 50 cells were scored at 40× magnification. The experiments were repeated three times. The source of stimulating factors (CSF) for growth of colonies was lung conditioned medium (LCM) from mice that had been inoculated intraperitoneally with 5 µg of endotoxin (*Salmonella typhimurium*, Sigma) 3 h before they were exsanguinated (Metcalf, 1984). The dose of growth factors (LCM) was adjusted to a value that supports 90% of maximum colony number in a dose-dependent curve and this dose was used throughout the experiments.

Bone marrow and blood cellularity

Blood leukocytes (samples of blood drawn from an incision of the tail vein) and nucleated cell elements of the femoral bone marrow (femoral diaphyses flushed with saline) were estimated by means of Coulter Counter (Model ZN, Coulter Electronics).

Statistics

Survival was monitored daily and reported as the percentage of animals surviving 30 days after irradiation with lethal dose of 9.5 or 10 Gy. Each treated group in each experiment consisted of 10–15 mice. Survival curves were calculated by programme GraphPad PRISM, V.2.00 (GraphPad Software, Inc., San Diego, CA).

Statistical significance of the differences between individual experimental groups of mice in haemo-

poietic parameters was calculated by analysis of variance.

RESULTS

Radioprotective effect of empty liposomes and analogues of MDP in free and liposomal form were tested in the first series of experiments. The endogenous spleen colony assay (E-CFUs) was used to determine the effects of empty liposomes prepared from phospholipon 80. Significant differences were not seen between the control group (PBS) and the groups to which liposomes (FTMLV) were administered at doses of 5, 25, 50 or 500 mg of phospholipid/kg (results not shown).

Figure 2 shows the effect of free or liposomal immunomodulators on the number of E-CFUs. Free immunomodulators administered at an equimolar dose of 10 µmol/kg did not exert any effect in comparison with the control. Unlike the group treated with free immunomodulators, the groups treated with liposomal immunomodulators showed a significant increase in the number of E-CFUs.

The third experiment in this series focused on the survival of mice treated i.p. with free or liposomal immunomodulators 24 h before irradiation with a

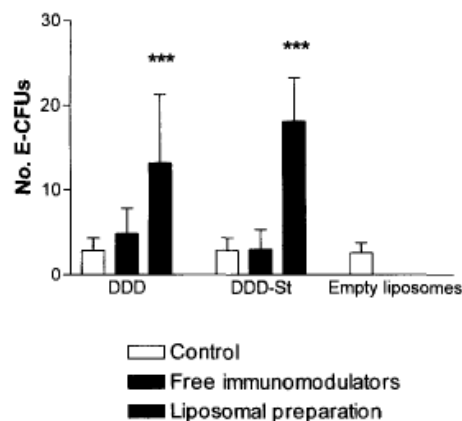


Fig. 2. Effect of DDD and DDD-St in free or liposomal form on endogenous spleen colony formation (E-CFUs) in irradiated mice. Mice, eight animals per group, were administered with 0.2 ml saline or preparation tested by i.p. injection 24 h prior to irradiation (6.5 Gy). Equimolar dosages of synthetic immunomodulators (10 µmol per kg of body weight) were administered. DDD—7.14 mg/kg, DDD-St—9.2 mg/kg, liposomes—500 mg of phospholipids/kg. ****p* < 0.001 sample vs control.

lethal dose of 10 Gy. As shown in Fig. 3 empty liposomes and free DDD did not increase the survival rate when compared with control. Unlike the free hydrophilic DDD, the free lipophilic DDD-St significantly increased the percentage of survival. The administration of liposomal form of DDD-St or DDD to mice resulted in a very high percentage survival (around 80%), efficiencies of the two derivatives being similar. For practical reasons, the lipophilic DDD-St designed to be easily entrapped into liposomes via hydrophobic stearyl arm, was chosen for further study. Further studies of an enhancement of radioresistance and stimulation of haemopoiesis after lethal and sublethal irradiation was focused on this analogue.

In spite of seasonal variations in radiosensitivity of mice, DDD-St exerted a radioprotective effect against lethal irradiation (9.5 or 10 Gy). The highest survival was found in mice given the liposomal preparation of DDD-St. A comparison of radioprotective effects of free and liposomal DDD-St in mice irradiated with lethal doses of 9.5 or 10 Gy is presented in Fig. 4. The highest survival percentage achieved by the treatment with liposomal DDD-St vs free DDD-St corresponds with the parameters characteristic of recovery of haemopoiesis in bone marrow on day 10 after 6.5 Gy

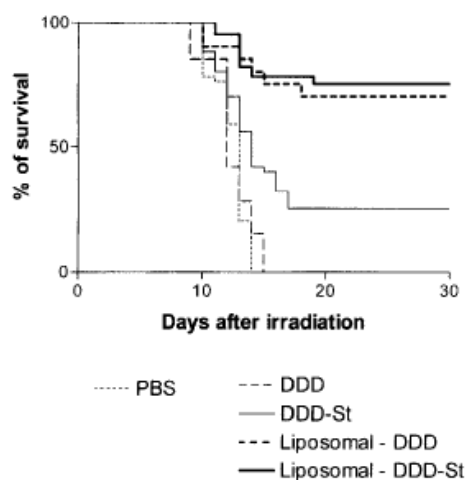


Fig. 3. Survival curves of mice treated i.p. with free or liposomal immunomodulators 24 h before γ -irradiation (10 Gy). Mice, 12–16 animals per group, were administered with 0.2 ml saline or preparation tested by i.p. injection 24 h prior to γ -irradiation (10 Gy). Equimolar dosages of synthetic immunomodulators (10 μ mol per kg of body weight) were administered. DDD—7.14 mg/kg, DDD-St—9.2 mg/kg, liposomes—500 mg of phospholipids/kg.

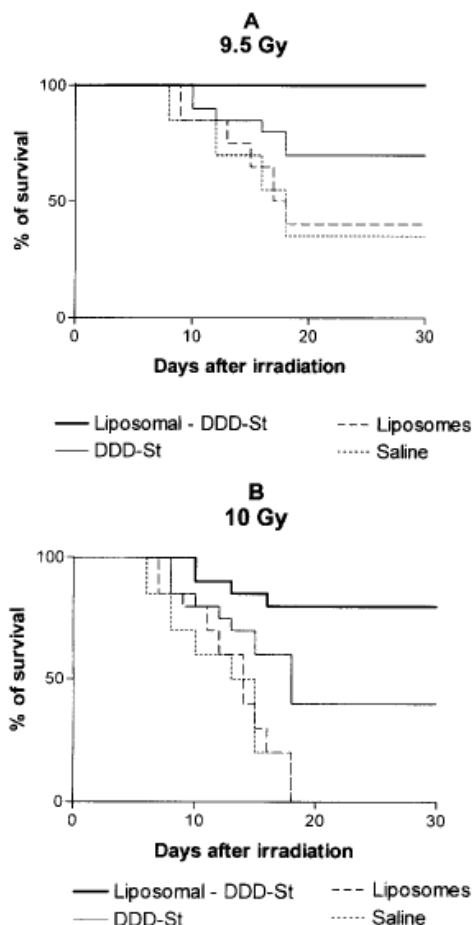


Fig. 4. Survival curves of mice treated i.p. with free or liposomal DDD-St 24 h before γ -irradiation by doses of 9.5 Gy (A) or 10 Gy (B). Mice, 12–16 animals per group, were administered with 0.2 ml saline or preparation tested by i.p. injection 24 h prior to γ -irradiation. Equimolar dosages of synthetic immunomodulators (10 μ mol per kg of body weight) were administered. DDD-St 9.2 mg/kg, liposomes—500 mg of phospholipids/kg.

irradiation. The results are summarized in Table 1. The treatment with free or liposomal DDD-St improved the parameters of haemopoiesis. Significant differences were found only between the group treated with liposomal DDD-St and saline or empty liposomes-treated controls. As far as the number of GM-CFC per femur was concerned, significant improvements were achieved with both preparations.

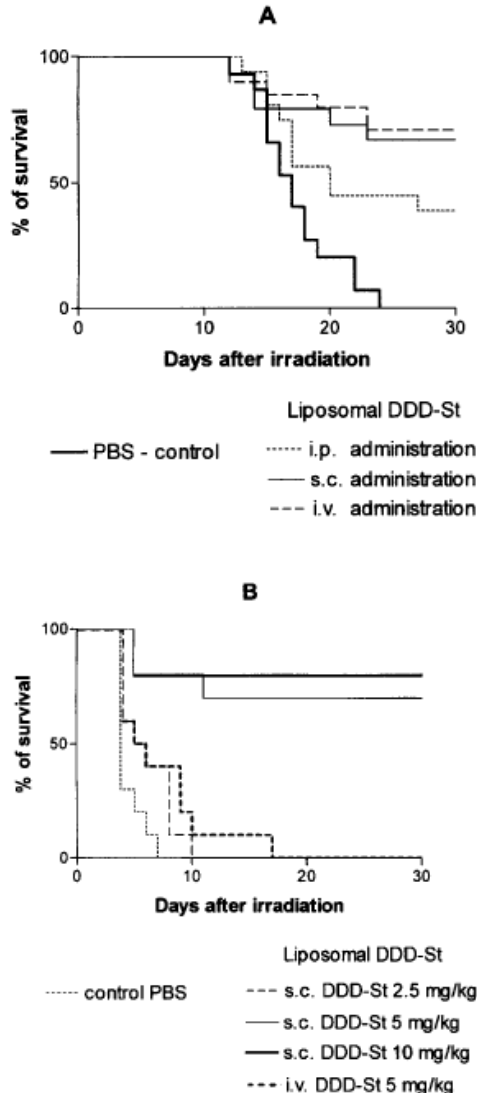


Fig. 5. Effect of i.p., i.v., or s.c. administration of liposomal DDD-St, 24 h before γ -irradiation (10 Gy), on the survival of mice. A. Mice, 10–15 animals per group, were administered via i.p., i.v. or s.c. with 0.2 ml of suspension of liposomal DDD-St (10 μ mol per kg of body weight) 24 h prior to γ -irradiation (10 Gy). DDD-St—9.2 mg/kg, liposomes—500 mg of phospholipids/kg. The experiment was performed during October and November 1996. B. Mice, 10–15 animals per group, were administered via i.v. or s.c. with 0.2 ml of suspension of liposomal DDD-St (10 μ mol per kg of body weight) 24 h prior to γ -irradiation (10 Gy). DDD-St—9.2 mg/kg, liposomes—500 mg of phospholipids/kg. The experiment was performed during March 1997.

Further, the effectiveness of liposomal DDD-St administered via various routes was examined. A comparison of i.p., i.v. and s.c. administrations was done using the optimal doses of liposomal DDD-St defined in pilot experiments. Intravenous and subcutaneous administrations were superior to intraperitoneal administration (Fig. 5). Moreover, the optimal i.v. dose of liposomal DDD-St was 5 mg/kg, which was half of i.p. dose. Differences in efficacy between the i.v. and s.c. administration was negligible in cases when the median of survival time was around day 16. Seasonal variations in radiosensitivity of mice resulted in decrease of the median of survival time and a shift of this value to day 4 owing to a rapid onset of septicemia caused by radiation injury of guts. In such case, surprisingly, s.c. administration was still very effective although i.v. administration did not exert radioprotective effect. In some experiments only prolongation of the median of survival time was observed without being accompanied by increase of percentage of survival (Fig. 5).

DISCUSSION

The precise mechanism(s) of liposomal MDP-analogues radioprotection remain unknown. However, the decrease in radiosensitivity of haemopoietic tissue in immunomodulator-protected mice has been partially attributed to the release of humoral stimulators and CSFs and the stimulation and transition of stem cells into the cell cycle in irradiated mice (Neta, 1988).

Immunomodulation *in vivo* results in activation of macrophages, and consequently other cells of the immune system such as T and NK cells. This activation results in local proliferation of macrophages, increased haemopoiesis, recruitment and monocytes and granulocytes from bone marrow to the periphery, and an enhanced release of acute phase proteins (Murray *et al.*, 1989). These activities are thought to be of major importance for host defense activation against infection.

Activation of macrophages and induction of cytokines production (IL-1, IL-6, TNF and CSF) may indicate that MDP-analogues can accelerate the restoration of functional haemopoietic cells via production of cytokines that stimulate a broad spectrum of progenitor cells and thus being one of the mechanisms leading to earlier haemopoietic recovery after irradiation (Murray *et al.*, 1989; Slordal *et al.*, 1989).

In all our experiments we observed increase in number of E-CFUs in groups of irradiated mice treated with liposomal DDD and DDD-St. Within the period of postirradiation regeneration (3–14 days), there

Table 1. Parameters of haemopoiesis at day 10 after irradiation of mice treated i.p. with free or liposomal DDD-St 24 h prior to γ -irradiation (6.5 Gy). Data represent mean \pm SEM and each point represents 10 animals per group

	Weight of spleen (mg)	No. of E-CFU-S	No. of GM-CFC per femur	No. of leukocytes in 1 μ l of peripheral blood	No. of granulocytes
Control (PBS)	31.5 \pm 0.8	3.1 \pm 0.5	1110 \pm 44	1064 \pm 139	536 \pm 84
Liposomes (500 mg/kg)	37.9 \pm 1.3 ^{mm}	4.4 \pm 0.6	1822 \pm 108	1257 \pm 105	620 \pm 44
DDD-St (10 mg/kg)	34.9 \pm 1.3	4.9 \pm 0.8	4686 \pm 218 ^{mm}	1471 \pm 156	789 \pm 93
DDD-St liposomal (10 mg/kg, 500 mg phospholipid/kg)	41.5 \pm 1.8 ^{mm,n}	10.3 \pm 0.8 ^{mm,jo}	5645 \pm 465 ^{mm}	1625 \pm 132 ⁿ	911 \pm 108 ⁿ

^{mm}p < 0.01 DDD-St liposomal vs control.

ⁿⁿp < 0.01 DDD-St liposomal vs DDD-St.

ⁿp < 0.05 DDD-St liposomal vs control.

^{jo}p < 0.05 DDD-St liposomal vs DDD-St.

were 4- and 5-folds more GM-CFC per femur in DDD-St- and liposomal DDD-St-treated mice, respectively, when compared to control. The study focusing on production of cytokines is in progress.

Since the intracellular receptor for MDP was determined, the site of action of muramyl peptides is believed to be intracellular (Tenu *et al.*, 1989). *In vivo*, experiments with free analogues of MDP are complicated by several factors, which include pharmacokinetically dictated effects such as short-half life owing to rapid clearance, dilution, lack of significant localization at the site of interest, serum protein binding and enzymatic degradation. To overcome some of these disadvantages, liposomes may be used as carriers. As macrophages are believed to be the most important target cells for immunomodulation by analogues of muramyl dipeptide, the use of classical liposomes, which tend to localize in large number in these cells, is quite obvious. By encapsulating analogues of MDP in liposomes, the life-time in the organism is prolonged and high concentrations at the site of action can be reached. The activity of colloidal liposomal delivery system could be explained as follows: liposomes are taken up by macrophages by phagocytosis and concentrated in the lysosomal compartment. Here, the MDP analogues are released from the liposomes (hydrophobic derivatives are eventually metabolized to hydrophilic ones) and can diffuse into the cytoplasm to reach the intracellular receptor (Merhi *et al.*, 1996). Results of our experiments with free and liposomal DDD are in accordance with this concept (Figs 2 and 3). Certain activities of lipophilic DDD-St can be ascribed to prolonged half-life and its ability to penetrate into and through the cell membrane. Significant improvement of its activity in terms of sur-

vival and parameters of haemopoiesis was also achieved by incorporation into liposomes.

Both induction of nonspecific immunity and accelerated restoration of haemopoiesis are responsible for the survival of lethally irradiated mice. Liposomal immunomodulators proved themselves to be effective in induction of nonspecific immune response against infection (Bakker-Woudenberg, 1993). This aspect is of importance in cases when rapid onset of septicemia (within days after irradiation) takes place owing to severe injury of guts caused by irradiation. Very high radioprotective effect of s.c. administered liposomal DDD-St can be explained by an effective and long-lasting activation of nonspecific immunity, which is able to withhold an onset of septicemia in early days after irradiation (see Fig. 5). Subcutaneous application of liposomal DDD-St seems to be very efficient for such reason and also it is considered as a convenient route of administration to humans in the future.

In conclusion, encapsulation of both MDP-analogues into liposomes prolongates their biological half-time and improves targeting to tissue macrophages. Our results are supportive for such explanation and are comparable with those published for liposomal muramyl tripeptide phosphatidylethanolamine (Fedoročko, 1994).

The obtained results suggest that liposomal DDD-St possesses a relatively high radioprotective activity, and as indicated mainly in terms of animal survival, liposomal DDD-St should be therapeutically beneficial in moderating haemopoietic damage as an undesirable effect of radiotherapy or chemotherapy.

Acknowledgements—This work was supported by grants from The Ministry of Industry and Trade MP-3310/22/94 and The Ministry of Agriculture RE-5559.

REFERENCES

- Bakker-Woudenberg, I. A. J. M., Lokerse, A. F., ten Kate, M. T., Meijssen, P. M. B., van Vianen, W. and van Etten, E. W. (1993) Liposomes a carrier of antimicrobial agents or immunomodulatory agents in the treatment of infections. *Eur. J. Clin. Microbiol. Infect. Dis.* **12**, 61–67.
- Barratt, G., Morin, C. and Schuber, F. (1995) Liposomal immunomodulators. In *Liposomes, New Systems and New Trends in Their Applications*, eds F. Puisieux, P. Couvreur, J. Delattre and J. P. Devissaguet, pp. 461–506. Editions de Santé, Paris.
- Fedoročko, P. (1994) Liposomal muramyl tripeptide phosphatidylethanolamine (MTP-PE) promotes haemopoietic recovery in irradiated mouse. *Int. J. Radiat. Biol.* **65**, 465–475.
- Hope, M. J., Bally, M. B., Webb, G. and Cullis, P. R. (1985) Production of large unilamellar vesicles by a rapid extrusion procedure, characterization of size distribution, trapped volume and ability to maintain a membrane potential. *Biochim. Biophys. Acta.* **812**, 55–65.
- Killion, J. J., Kleinerman, E. S., Wilson, M. R., Tanaka, M. and Fidler, I. F. (1992) Sequential therapy with chemotherapeutic drugs and liposome-encapsulated muramyl tripeptide: determination of potential interactions between these agents. *Oncology Research* **4**, 413–418.
- Kleinerman, E. S. (1995) Biologic therapy for osteosarcoma using liposome-encapsulated muramyl tripeptide. *Sarcomas* **9**, 927–938.
- Ledvína, M., Farkaš, J., Zajíček, J., Ježek, J. and Zaoral, M. (1989) An alternative synthesis of O-(2-acetamido-2-deoxy-β-D-glucopyranosyl)-(1 → 4)-N-acetylnormuramoyl-L-α-aminobutanoyl-D-isoglutamine. *Collect. Czech. Chem. Commun.* **54**, 2784–2794.
- Merhi, G., Coleman, A. W., Devissaguet, J.-P. and Barratt, G. M. (1996) Synthesis and immunostimulating properties of lipophilic ester and ether muramyl peptide derivatives. *J. Med. Chem.* **39**, 4483–4488.
- Metcalf, D. (1984) *The Hemopoietic Colony Stimulating Factors*. Elsevier Sci. Publ. Co. Inc. N.Y. pp. 494.
- Murray, J. L., Kleinerman, E. S., Cunningham, J. E., Tatom, J. R., Andrejcio, K., Lepe-Zuniga, J., Lamki, L. M., Resenblum, M. G., Frost, H., Gutterman, J. U., Fidler, I. J. and Krakoff, I. H. (1989) Phase I trial of liposomal muramyl tripeptide phosphatidylethanolamine in cancer patients. *Journal of Clinical Oncology* **7**, 1915–1925.
- Neta, T. (1988) Cytokines in radioprotection and therapy of radiation injury. *Biotherapy* **1**, 41–45.
- Neta, R., Vogel, S. N., Sipe, J. D., Wong, G. G. and Nordan, R. P. (1988) Comparison of *in vivo* effects of human recombinant IL-1 and human recombinant IL-6 in mice. *Lymphokine Research* **7**, 403–412.
- Patchen, M. L., MacVittie, T. J., Williams, J. L., Schwartz, G. N. and Souza, L. M. (1991) Administration of interleukin-6 stimulates multilineage hematopoiesis and accelerates recovery from radiation-induced hematopoietic depression. *Blood* **77**, 472–480.
- Slordal, L., Warren, D. J. and Moore, A. A. S. (1989) Effect of recombinant murine tumor necrosis factor on hemopoietic reconstitution in sublethally irradiated mice. *Journal of Immunology* **142**, 833–835.
- Tenu, J. P., Adams, A., Souvannavong, V., Yapo, A., Petit, J. F. and Douglas, K. (1989) Photoaffinity labelling of macrophages and B lymphocytes using ¹²⁵I-labelled ary-azide derivatives of muramyl dipeptide. *Int. J. Immunopharmacol.* **11**, 653–661.
- Till, J. E. and McCulloch, E. A. (1961) A direct measurement of the radiosensitivity of normal mouse bone marrow cells. *Rad. Res.* **14**, 213–222.
- Turánek, J., Záluská, D. and Neča, J. (1997) Linkup of a fast protein liquid chromatography system with a stirred thermostated cell for sterile preparation of liposomes by the proliposome-liposome method: application to encapsulation of antibiotics, synthetic peptide immunomodulators, and a photosensitizer. *Anal. Biochem.* **249**, 131–139.
- Vacek, A., Rotkovská, D. and Bartoničková, A. (1990) Radioprotection of haemopoiesis conferred by aqueous extract from chlorococcal algae (Ivastimul) administered to mice before irradiation. *Exp. Hematol.* **18**, 234–237.

Stimulation of nonspecific immunity, haemopoiesis and protection of mice against radiation injury by 1-adamantylamide-L-alanyl-D-isoglutamine incorporated in liposomes

Jaroslav Turánek ^{a,*}, Dana Záluská ^a, Antonín Vacek ^b, Petra Borkovcová ^a,
Jitka Thurnvaldová ^a, Luděk Bláha ^a, Karel Mašek ^c

^a Department of Immunology, Veterinary Research Institute, Hudcova 70, 621 32 Brno, Czech Republic

^b Institute of Biophysics, Brno, Czech Republic

^c Institute of Pharmacology, Prague, Czech Republic

Received 14 February 2000; received in revised form 13 June 2000; accepted 1 August 2000

Abstract

1-Adamantylamide-L-alanyl-D-isoglutamine (adamantylamide dipeptide (AdDP)) belongs to a group of desmuramyl muramyl peptide derivatives which are able to protect an organism from some viral infections. Encapsulation of AdDP to egg phosphatidyl choline liposomes and the targeting of this drug to lymphatic node macrophages via subcutaneous (s.c.) administration proved to be the efficient way to protect mice against irradiation when administered s.c., 24 h prior to lethal γ -irradiation (long-term survival rate in the range of 40% compared with 0% in saline or free drug control). Parameters characteristic for the recovery of haemopoiesis in the bone marrow (number of granulocyte-macrophage haemopoietic progenitor cells, granulocyte-macrophage colony forming cells (GM-CFC)) were significantly improved in comparison with the controls and free drug on day 10 after 6.5 Gy irradiation. The haemopoietic effect was observed in the broad application time window (72 h before and 48 h after irradiation). Very high radioprotective effect of s.c. administered liposomal AdDP (L-AdDP) can be explained (together with induction of haemopoiesis) by the effective and long-lasting activation of nonspecific immunity, which withholds the onset of septicemia in early days after irradiation. Induction of nonspecific immunity was proven in *Candida albicans* infectious model. L-AdDP significantly increased both the survival time and score (about 40% survival compared with 0% in controls and free drug).

In conclusion, L-AdDP could be therapeutically beneficial to moderate the haemopoietic damage (undesirable effect of radiotherapy or chemotherapy) and induce the non-specific immunity to support the antimicrobial treatment of immunocompromised patients © 2001 Elsevier Science B.V. All rights reserved.

Keywords: Liposomes; Muramyl dipeptide analogues; Radioprotection; Haemopoiesis; Non-specific immunity; *Candida albicans*; Mouse

* Corresponding author. Tel.: +420-5-4132-1241; fax: +420-5-4121-1229.

E-mail address: turanek@vri.cz (J. Turánek).

1. Introduction

Protection from undesirable effects of radiotherapy or chemotherapy, primarily from myelosuppression, still remains a crucial problem to be coped with. Attention has been paid to various immunomodulatory agents that, via the monocyte/macrophage system, induce the production of cytokines, which induce and control haemopoiesis, and hence can act radio- or chemoprotectively [6,11]. Muramylpeptides have been found to be highly active in vitro and in vivo in respect of inducing tumoricidal, antiviral and bactericidal activities. Various analogues of muramyl dipeptide (MDP) have been synthesized and tested in various experimental models (reviewed by [Ref. 3]). However, most of them have side effects such as pyrogenicity, sleep-promotion and oedemagenic activities, which are shared with MDP [12].

1-Adamantylamide-L-Alanyl-D-isoglutamine (adamantylamide dipeptide (AdDP), Fig. 1) belongs to a group of desmuramyl MDP derivatives, able to protect an organism from some viral infections [14]. This hybrid entity combines components of both an antiviral and immunomodulator effect in a single synthetic compound without side effects (pyrogenicity, edemagenicity, effect on sleep) which are inherent to several MDP derivatives [15].

Encapsulation of muramyl peptides into liposomes, vesicles composed of one or several lipid bilayers enclosing an aqueous phase, reduced the side-effects, improved the therapeutic efficacy in in vitro and in vivo models of tumor cytotoxicity and as well as in experimental microbial infections in mice [3]. Targeting of liposomal immunomodulators to macrophages, their internalization via phagocytosis and hence, the facilitating of interaction with the intracellular receptor led to a stimulation of macrophages [16,24] such as the induction of secre-

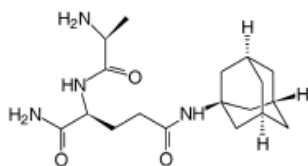


Fig. 1. Structural formula of AdDP.

tion of IL-1, IL-6 and TNF known to have therapeutic effects on haemopoietic regeneration after irradiation [19,21]. A relatively high radioprotective activity of liposomal β -D-GlcNstearoyl-(1 \rightarrow 4)-norMurNAc-L-Abu-D-isoGln (DDD-St) or β -D-Glc-(1 \rightarrow 4)-norMurNAc-L-Abu-D-isoGln (DDD), as indicated mainly in terms of animal survival and number of progenitor cells in femour, was demonstrated by our group [13,25,26]. Effect of in vivo administration of AdDP on proliferation of bone marrow granulocyte-macrophage haemopoietic progenitor cells (GM-CFC) was recently demonstrated [27].

In this paper we have compared the effect of free AdDP and L-AdDP administered via subcutaneous (s.c.) route on the induction of nonspecific immunity and haemopoiesis in the mice models.

2. Experimental

2.1. Animals

Female (C57Bl/6 \times BALB/C) F_1 mice, 12 weeks old and having 23 ± 2 g of weight at the beginning of the experiment, were irradiated with a single whole-body doses from ^{60}Co gamma-ray source at a dose rate of 0.285 Gy/min (10.0 Gy for survival and 6.5 Gy for recovery of haemopoietic tissues). The preparations were administered s.c. at various time before or after irradiation.

Female BALB/cJ, 8 weeks old and having 18–22 g of weight, were used for infectious experiments with *Candida albicans*.

2.2. Chemicals

AdDP was donated by Lachema (Brno, Czech Republic). Purity of other chemicals used in the experiments were of analytical grade or better. Apyrogenicity of preparations (content of lipopolysaccharide) was tested by limulus amoebocyte lysate colorimetric kit QCL-1000 (Bio-Whittaker)

2.3. Preparation of frozen-and-thawed multilamellar vesicles (FTMLV)

Liposomes (FTMLV) were prepared under apyrogenic conditions from the egg-yolk phosphatidyl-

choline (EPC) 99% purity (Avanti Polar Lipids, USA) by the method of hydration of lipid film by apyrogenic phosphate buffered saline (PBS) containing various amounts of AdDP. The lipid mixture, dissolved in chloroform (200 mg in 6 ml), was deposited onto the wall of a round-bottom flask (250 ml) by removal of the solvent in a rotary evaporator (40°C, 4 h). The dried lipid film was then hydrated with the aqueous phase under continuous mixing on a mechanical reciprocal shaker for 2 h. FTMLV was obtained by freezing the multilamellar vesicles in liquid nitrogen and thawing them in a 30°C water bath, repeating the cycle five times [9]. The analyses of entrapment efficiency were done by HPLC. AdDP was entrapped with around 65% efficiency [25,26]. To assure the comparable size distribution, the liposomal preparations were extruded through 1 µm polycarbonate filter. The size of liposomes was around 0.75–1.1 µm, as determined by dynamic light scattering instrument (Zetasizer 3000, Malvern, UK). The untrapped drug was removed by centrifugation. Preparations (free or liposomal formulations) were appropriately diluted in PBS and administered in desired dosages in volume of 0.2 ml/animal in a single injection. The same volume of PBS or empty liposomes was applied to control animals.

2.4. GM-CFC progenitors

For GM-CFC determination, bone marrow cells from intact mice were drawn by flushing femoral bone with an IMDM medium, counted on Coulter Counter (Model ZN, Coulter Electronics) and kept in a melting ice bath before their use.

Femoral marrow cells were plated in triplicate in a semisolid environment created by a plasma clot in our modification [28], containing the IMDM plus 20% fetal calf serum (FCS), 10% of conditioned medium from rmlL-3-producing myeloma cell line [10], the final concentration of rmlL-3 being 1 U/ml (1 U/ml was defined as a concentration of rmlL-3 that yielded a maximum colony number on a concentration dependence curve), 10% citrate bovine plasma and CaCl₂ at a concentration of 1.5 mg/ml.

The cultures were incubated for 7 days in a thermostat (Forma Scientific, USA) at 37°C in a fully humidified atmosphere of 5% CO₂ in air.

Colonies of at least 50 cells were scored at 40× magnification. The experiments were repeated three times. The source of stimulating factors (CSF) for growth of colonies was lung conditioned medium (LCM) from mice that had been inoculated intraperitoneally (i.p.) with 5 µg of endotoxin (*Salmonella typhimurium*, Sigma) 3 h before they were exsanguinated [17]. The dose of growth factors (LCM) was adjusted to a value that supports 90% of maximum colony number in a dose-dependent curve and this dose was used throughout the experiments.

2.5. Bone marrow cellularity

Numbers of nucleated cells per femur were estimated by means of Coulter Counter (Model ZN, Coulter Electronics) after flushing femoral diaphyses with saline.

2.6. Numbers of leukocytes

Number of leukocytes in the peripheral blood were determined by means of a Coulter Counter.

2.7. Postirradiation survival

In lethally irradiated mice (a dose of 10 Gy), the deaths were monitored every day until day 30 after the radiation exposure.

2.8. *C. albicans* infection

C. albicans (strain 2091) was obtained from the Collection of Microorganisms, Masaryk University, Brno. Infectivity of the strain was increased by repeated passage on mice. The infected mice were killed when appeared moribund and *C. albicans* were reisolated from spleen and kidney. Adapted *C. albicans* were lyophilised and third passage was used for i.v. administration to mice (5 × 10⁵ organisms/mouse).

2.9. Statistics

Survival was monitored daily and reported as the percentage of animals surviving 30 days after irradiation or infection. Each treated group in each experiment consisted of 10–15 mice. Survival curves were

calculated by programme GraphPad PRISM, V.2.00 (GraphPad Software San Diego, CA). Statistical significance of the differences between individual experimental groups (five mice) in haemopoietic parameters was calculated by analysis of variance. Logrank test based on Chi-square statistic was used for evaluation of statistical significance of differences between survival curves. *P*-values less than 0.05 were considered statistically significant.

3. Results

In the first series of experiments we have tested, the overall radioprotective effect of preparations ex-

pressed as survival rate of lethally irradiated mice. Fig. 2a shows the effect of AdDP or L-AdDP on the survival of mice treated with s.c. injection 24 h before the lethal irradiation. It is apparent that free AdDP did not effect substantially both survival time and survival score. The effects of empty liposomes and various doses of AdDP (0.91, 1.83, and 3.65 mg/kg) were similar to the control and therefore, they were omitted from the graph. In contrast to free AdDP, the L-AdDP exerted strong concentration-dependent positive effect on both survival half-time and survival (statistically significant differences of L-AdDP compared with both PBS and free AdDP were observed, $p < 0.05$). Seasonal variations in radiosensitivity of mice resulted in decrease of the median of survival time and a shift of this value to days 4–6 because of a rapid onset of septicaemia caused by a severe irradiation injury of guts. In this case, the induction of nonspecific immunity is very important to combat the onset of septicemia. Results presented in Fig. 2b are representative of these cases.

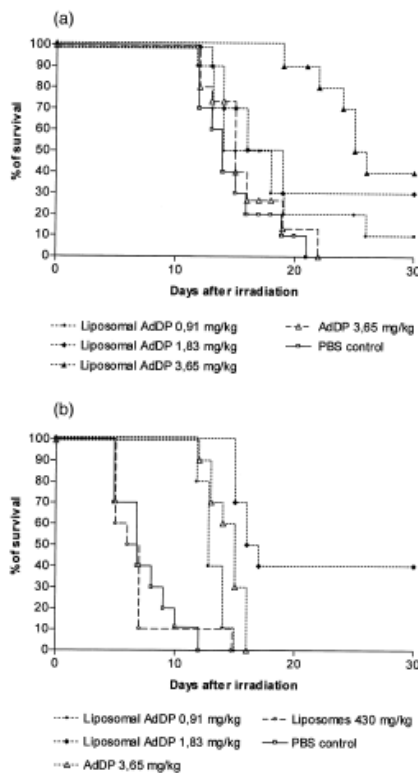


Fig. 2. Survival curves of mice treated s.c. with free and L-AdDP, 24 h before γ -irradiation (10 Gy). (a) Mice, 10 animals/group, were administered with 0.2 ml buffered saline or preparation tested by s.c. injection, 24 h prior to γ -irradiation (10 Gy). The experiment was performed during October 1998. Empty liposomes: 107, 215 or 430 mg/kg EPC. Curves do not differ from that for buffered saline, so they were omitted to keep the clarity of the graph. Doses of free AdDP: 3.65 mg/kg. Curves for doses of 0.91 and 1.83 mg/kg were similar to that of buffered saline and hence were omitted to keep the clarity of the graph. Doses of L-AdDP: AdDP 0.91 mg/kg, EPC 107 mg/kg. AdDP 1.83 mg/kg, EPC 215 mg/kg. AdDP 3.65 mg/kg, EPC 430 mg/kg. *P*-values. PBS vs. AdDP preparations: AdDP: 3.65 mg/kg ($p = 0.2953$), L-AdDP 0.91 mg/kg ($p = 0.0042$), AdDP 1.83 mg/kg ($p = 0.0025$), L-AdDP 3.65 mg/kg ($p < 0.0001$). Free AdDP (3.65 mg/kg) vs. liposomal AdDP: L-AdDP 0.91 mg/kg ($p = 0.0409$), AdDP 1.83 mg/kg ($p = 0.0177$), L-AdDP 3.65 mg/kg ($p < 0.0001$). (b) Mice, 10 animals/group, were administered with 0.2 ml buffered saline or preparation tested by s.c. injection, 24 h prior to γ -irradiation (10 Gy). The experiment was performed during May 1999. Dose of free AdDP: 3.65 mg/kg. Doses of L-AdDP: AdDP 0.91 mg/kg, EPC 107 mg/kg. AdDP 1.83 mg/kg, EPC 215 mg/kg. Doses of empty liposomes: EPC 430 mg/kg. *p*-values. PBS versus AdDP preparations: AdDP: 3.65 mg/kg ($p < 0.0001$), L-AdDP 0.91 mg/kg ($p < 0.0001$), L-AdDP 1.83 mg/kg ($p < 0.0001$). Free AdDP (3.65 mg/kg) versus liposomal AdDP: L-AdDP 0.91 mg/kg ($p = 0.0234$), AdDP 1.83 mg/kg ($p = 0.0036$).

Free immunomodulator prolonged significantly the survival half-life ($p < 0.0001$) but did not affect the survival score. Contrary to free AdDP, the L-AdDP was able to protect about 40% of mice against death of postirradiation infection ($p < 0.05$ L-AdDP vs. free AdDP). The experiments with *C. albicans* infectious model were included in these series to confirm the importance of nonspecific immunity onto radio-protection. Fig. 3 shows results of experiments in which mice were treated with free or L-AdDP before challenging with *C. albicans*. Free AdDP exerted a slight effect on the survival half-time but no survival of animals was observed at the end of experiment. Treatment of mice with L-AdDP led to a significant increase in the survival of infected animals similarly to those levels obtained in the experiments with lethally irradiated mice ($p < 0.001$ L-AdDP vs. AdDP).

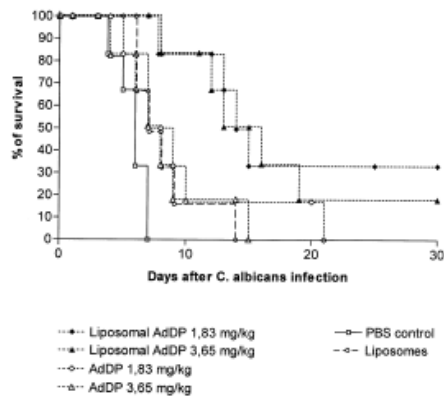


Fig. 3. Survival of female BALB/cJ mice treated s.c. with free or L-AdDP at 24 h before i.v. challenge with *C. albicans* (mice 5×10^5 organisms/mouse). Mice, 10 animals/group, were administered with 0.2 ml of buffered saline or preparations tested. Doses of free AdDP: 1.83 or 3.65 mg/kg. Doses of L-AdDP: AdDP 1.83 mg/kg, EPC 215 mg/kg. AdDP 3.65 mg/kg, EPC 430 mg/kg. Empty liposomes: EPC 430 mg/kg. p -values. PBS versus AdDP preparations: AdDP: 3.65 mg/kg ($p < 0.0001$), AdDP: 1.83 mg/kg ($p < 0.0001$), AdDP: 1.83 mg/kg (AdDP: 3.65 mg/kg ($p < 0.0001$), L-AdDP 3.65 mg/kg ($p < 0.0001$), empty liposomes EPC 430 mg/kg ($p = 0.0004$). Free AdDP (3.65 mg/kg) vs. free AdDP (1.83 mg/kg) $p = 0.795$. Free AdDP (3.65 mg/kg) vs. L-AdDP: L-AdDP 1.83 mg/kg ($p = 0.011$), L-AdDP 3.65 mg/kg ($p < 0.0007$).

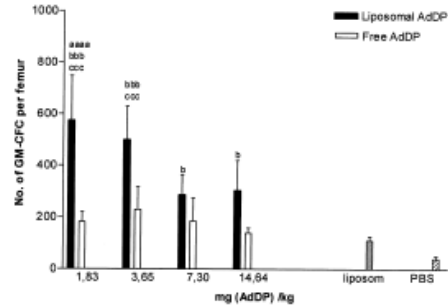


Fig. 4. Effect of various doses of L-AdDP or free AdDP on the number of GM-CFC per femur after sublethal γ -irradiation of mice. Mice, five animals per group, were administered with 0.2 ml buffered saline or preparation tested by s.c. injection 24 h prior to γ -irradiation (6.5 Gy). The day 13 after irradiation, the number of GM-CFC per femour were counted. Liposome control were administered with doses of 430 mg/kg. $^{aaaa} p < 0.0001$ L-AdDP vs. liposome control; $^{bbb} p < 0.001$ L-AdDP vs. PBS; $^{ccc} p < 0.001$ L-AdDP vs. AdDP free; $^b p < 0.05$ L-AdDP vs. PBS.

The second series of experiments were focused on the restoration of haemopoiesis in sublethally irradiated mice treated with AdDP preparations. The num-

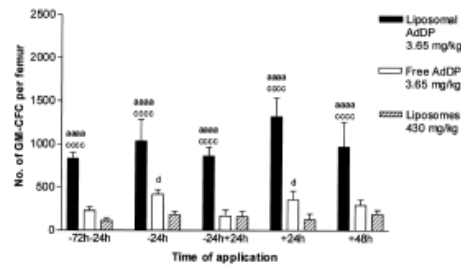


Fig. 5. Timing effect of L-AdDP or free AdDP on the number of GM-CFC per femour after sublethal γ -irradiation of mice. Mice, five animals per group, were administered with 0.2 ml buffered saline or preparation tested by s.c. injection at various times. Groups were treated as follows: (1) two doses at 72 and 24 h prior to, (2) single dose 24 h prior to, (3) two doses 24 h prior to and 24 h after, (4) single dose 24 h after, (5) single dose 48 h after γ -irradiation (6.5 Gy). The day 13 after irradiation, the number of GM-CFC per femour were counted. Liposome control were administered with doses of EPC 430 mg/kg; $^{aaaa} p < 0.0001$ AdDP liposomal vs. liposome control; $^{cccc} p < 0.0001$ AdDP liposomal vs. AdDP free; $^b p < 0.05$ AdDP vs. liposome control.

ber of progenitor cells (GM-CSF) per femur was chosen as the main parameter to consider the activity of various preparations. Dose response effects of liposomal and free AdDP on GM-CFC per femur are presented in Fig. 4. The optimum dose of L-AdDP administered s.c. was found to be about 1.83–3.65 mg/kg (100–200 nmol/mouse). Statistically significant optimum for free AdDP was not found within the range of tested concentrations. The timing effect of application of immunomodulators on GM-CFC per femur was studied in a series of experiments. We have detected that empty liposomes exerted a slight stimulatory effect when compared with PBS-treated controls, but statistical analyses did not support its significance. The empty liposomes were chosen as a control in these series of experiments to discriminate the net effect of L-AdDP from that of empty liposomes. Representative results of these experiments are presented in Fig. 5. The haemopoietic effect of L-AdDP was superior to that of free AdDP in all time intervals. Surprisingly, the postirradiation application of L-AdDP was also very effective.

4. Discussion

The precise mechanism(s) of liposomal MDP-analogues radioprotection remain(s) unknown. However, the decrease in radiosensitivity of haemopoietic tissue in immunomodulator-protected mice has been partially attributed to the release of humoral stimulators and CSFs and the stimulation and transition of stem cells into the cell cycle in irradiated mice [20].

Immunomodulation *in vivo* results in activation of macrophages, and consequently other cells of the immune system such as T and NK cells. This activation results in local proliferation of macrophages, increased haemopoiesis, recruitment of monocytes and granulocytes from bone marrow to the periphery, and an enhanced release of acute phase proteins [18]. These activities are thought to be of major importance for host defence mechanism against infection.

Activation of macrophages and induction of cytokines production (IL-1, IL-6, TNF and CSF) may indicate that MDP-analogues can accelerate the restoration of functional haemopoietic cells via production of cytokines that stimulate a broad spectrum

progenitor cells and thus being one of the mechanisms leading to earlier haemopoietic recovery after irradiation [18,23].

In our previous experiments, we have demonstrated that s.c. application of liposomal DDD-St exerted radioprotective effect in the term of restoration of haemopoiesis and induction of nonspecific immunity [25,26]. Surprisingly, the s.c. route of application was superior to both the intravenous (i.v.) and i.p. administration. In studies dealing with similar topics, the s.c. administration of free or liposomal analogues of MDP were not tested [6] or were not effective [7].

Since the intracellular receptor for MDP was determined, the site of action of muramyl peptides is believed to be intracellular [24]. *In vivo*, experiments with free analogues of MDP are complicated by several factors, which include pharmacokinetically dictated effects such as short half-life owing to rapid clearance, dilution, lack of significant localization at the site of interest, serum protein binding and enzymatic degradation. To overcome some of these disadvantages, liposomes may be used as carriers. As macrophages are believed to be the most important target cells for immunomodulation by analogues of MDP, the use of classical liposomes, which tend to localize in large number in these cells, is quite obvious.

Studies on pharmacokinetic parameters of AdDP showed that this compound resembles hydrophobic derivatives of MDP rather than hydrophilic ones with respect to the half-life of the elimination phase (11–12 h). The most surprising result after the s.c. administration was a very rapid absorption phase with a half-life of 1 min. The distribution phase was about 20 min, i.e., 10 times longer than after an i.v. administration [30]. In our previous study with DDD and DDD-St derivatives, we have postulated that activation of macrophages in local lymphatic nodes draining the side of injection is responsible for strong induction of haemopoiesis and nonspecific immunity. Low efficiency of s.c.-administered free AdDP can be explained, similarly to hydrophilic DDD, by rapid absorption phase. This small molecule is preferentially drained to blood and only a small concentration is achieved in the lymphatic nodes. Moreover, rapid transport through lymphatic nodes decreases the time of drug interaction with macrophages and

hence their activation and subsequent stimulation of the immune response.

By encapsulating AdDP into liposomes, which are efficient lymphotropic drug delivery system, the life-time in the organism is prolonged and high concentrations at the site of action can be reached by s.c. application. Large liposomes tend to stay at the site of injection after s.c. administration, where they can play the role of a depot. To a lesser extent, these liposomes can penetrate through extracellular matrix, reach the lymphatic nodes via lymphatic capillaries and deliver the AdDP content to lymph node macrophages. After phagocytosis, the liposomes are concentrated in the lysosomal compartment from which AdDP is released into the cytoplasm to interact with the intracellular receptor. This concept for MDP analogues was proposed by Merhi et al. [16].

It is not clear how large liposomes can penetrate through the interstitial space consisting of a gel-like matrix of mucopolysaccharides supported by a network of reticular and collagenous fibers. The size of the aqueous channels presented in the matrix are of about 100 nm [22]. This size prevents penetration of liposomes larger than 120 nm and nearly all large liposomes (about 98%) remain at the site of s.c. application [1]. In spite of this restriction, large liposomes labeled with fluorescein or colloidal gold were found in lymphatic nodes and inside of the macrophages [29]. S.c. injection of clodronate entrapped in multilamellar liposomes (macrophage suicide technique) results in depletion of macrophages lining the subcapsular sinus and those in the medulla of regional popliteal lymph nodes [4]. From these experiments, we can conclude that even if a small portion of large liposomes can reach the lymph nodes, the amount is sufficient to deliver AdDP to macrophages in lymph nodes.

Both induction of nonspecific immunity and accelerated restoration of haemopoiesis are responsible for the survival of lethally irradiated mice. Liposomal immunomodulators proved themselves to be effective in induction of nonspecific immune response against infection [2]. This aspect is important in cases when rapid onset of septicemia (within days after irradiation) takes place due to severe injury of guts caused by irradiation. Very high radioprotective effect of s.c. administered L-AdDP can be explained by an effective and long-lasting activation of nonspe-

cific immunity, which is able to withhold an onset of septicemia in early days after irradiation (see Fig. 2b). Studies on hydrophilic and hydrophobic MDP analogues entrapped in liposomes revealed potent stimulatory activity in terms of particle clearing and killing of microbes by the cells of the mononuclear phagocyte system. *C. albicans* infection model was used to demonstrate stimulation of non-specific antimicrobial defence system of the host [5,7]. We detected that L-AdDP was an effective immunostimulator also after s.c. application contrary to MDP analogues used in studies mentioned above.

Haemopoietic effect of free AdDP was studied by Vacek et al. [27] and Hoffer [8]. I.p. administration of free AdDP was used in the studies with lethally and sublethally irradiated mice. I.p. administration of free AdDP required 5–15 times higher doses compared to the s.c. L-AdDP, to achieve 10–25% long-term survival of lethally irradiated mice. In the case of rapid onset of septicemia, no long-term survival was achieved contrary to s.c. L-AdDP. Doses about 5–15 times higher compared to s.c. L-AdDP, were also applied to increase the number of GM-CFC per femur, three to four times, to control after sublethal irradiation. Surprisingly, we have found that the haemopoietic effect of L-AdDP was also very strong when applied 24–48 h after the sublethal irradiation.

The obtained results suggested that L-AdDP possesses a relatively high radioprotective activity, and as indicated, in terms of animal survival, L-AdDP may be therapeutically beneficial in moderating haemopoietic damage, which is an undesirable effect of radiotherapy or chemotherapy. Accordingly, s.c. application of L-AdDP seems to be very efficient and also it is considered as a convenient route of administration to humans in the future. Effect of size and lipid composition of AdDP liposomes on haemopoiesis is now under study.

Acknowledgements

This work was supported by a grant (PZ-Z2/25/97) from The Ministry of Industry and Trade of the Czech Republic. The research was conducted according to the principles enunciated in the Guide for the Care and Use of Laboratory Animals issued by the Czech Society for Laboratory Animal Science.

References

- [1] Allen TM, Hansen CB, Guo LSS. Subcutaneous administration of liposomes: a comparison with intravenous and intraperitoneal routes of injection. *Biochim Biophys Acta*; 1993;1150:9–16.
- [2] Bakker-Woudenberg IATM, Lokense AF, ten Kate MT, Melissen PMB, van Vianen W, van Etten EWM. Liposomes as carriers of antimicrobial agents or immunomodulatory agents in the treatment of infections. *Eur J Clin Microbiol Infect Dis* 1993;12:61–7.
- [3] Baratt G, Morin C, Schuber F. Liposomal immunomodulators. In: Puisieux F, Couvreur P, Delattre J, Devissaguet JP, editors. *Liposomes, new systems and new trends in their applications*. Paris: Editions de Santé, 1995:461–506.
- [4] Delemarre FGA, Kors N, Kraal G, Van Rooijen N. Repopulation of macrophages in popliteal lymph nodes of mice after liposome-mediated depletion. *J Leukocyte Biol* 1990;47:251–7.
- [5] Eppstein DA, VanDerPas JA, Frase-Smith EB, Kurahara CG, Felgner PL, Mathews TR, et al. Liposome-encapsulated muramyl dipeptide analogue enhances non-specific host immunity. *Int J Immunother* 1986;II(2):115–26.
- [6] Fedorčko P. Liposomal muramyl tripeptide phosphatidylethanolamine (MTP-PE) promotes haemopoietic recovery in irradiated mouse. *Int J Radiat Biol* 1994;65:465–75.
- [7] Fraser-Smith EB, Eppstein DA, Larsen MA, Mathews TR. Protective effect of a muramyl dipeptide analog encapsulated in or mixed with liposomes against *Candida albicans* infection. *Infect Immun* 1983;1:172–8.
- [8] Hofer M, Vacek A, Mašek K, Juchelková L, Pipalová I. Adamantylamide dipeptide stimulates hematopoiesis and increases survival in irradiated mice. *Int J Immunopharmacol* 2000;22:91–7.
- [9] Hope MJ, Bally MB, Webb G, Cullis PR. Production of large unilamellar vesicles by a rapid extrusion procedure, characterization of size distribution, trapped volume and ability to maintain a membrane potential. *Biochim Biophys Acta* 1985;812:55–65.
- [10] Karasuyama H, Melchers F. Establishment of mouse cell lines which constitutively secrete large quantities of interleukins 2, 3, 4 or 5 using modified cDNA expression vectors. *Eur J Immunol* 1988;18:97–105.
- [11] Killian JJ, Kleinerman ES, Wilson MR, Tanaka M, Fidler IF. Sequential therapy with chemotherapeutic drugs and liposome-encapsulated muramyl tripeptide: determination of potential interactions between these agents. *Oncol Res* 1992;4:413–8.
- [12] Kleinerman ES. Biologic therapy for osteosarcoma using liposome-encapsulated muramyl tripeptide. *Sarcomas* 1995;9:927–38.
- [13] Ledvina M, Farkaš J, Zajíček J, Ježek J, Zaoral M. An alternative synthesis of O-(2-acetamido-2-deoxy-β-D-glucopyranosyl)-(1 → 4)-N-acetylnoramoyl-L-α-aminobutanoil-D-isoglutamine. *Collect Czech Chem Commun* 1989; 54:2784–94.
- [14] Masihi KN, Lange W, Rohde-Shultz B, Mašek K. Antiviral activity of immunomodulator adamantylamide dipeptide. *Int J Immunother* 1987;3:89–96.
- [15] Mašek K. Immunopharmacological properties of synthetic muramyl peptides and their analogs. In: Masihi KN, Lange W, editors. *Immunomodulators and nonspecific host defence mechanisms against microbial infections*. *Advances in Biochemistry* vol. 68; 1988. p. 11.
- [16] Merhi G, Coleman AW, Devissaguet JP, Barratt GM. Synthesis and immunostimulating properties of lipophilic ester and ether muramyl peptide derivatives. *J Med Chem* 1996;39:4483–8.
- [17] Metcalf D. *The Hemopoietic Colony Stimulating Factors*. New York: Elsevier, 1984. p. 494.
- [18] Murray JL, Kleinerman ES, Cunningham JE, Tatom JR, Andrejcio K, Lepe-Zuniga J, et al. Phase I trial of liposomal muramyl tripeptide phosphatidylethanolamine in cancer patients. *J Clin Oncol* 1989;7:1915–25.
- [19] Neta R, Vogel SN, Sipe JD, Wong GG, Nordan RP. Comparison of in vivo effects of human recombinant IL-1 and human recombinant IL-6 in mice. *Lymphokine Res* 1988;7:403–12.
- [20] Neta T. Cytokines in radioprotection and therapy of radiation injury. *Biotherapy* 1988;1:41–5.
- [21] Mac Patchen ML, Vittie TJ, Williams JL, Schwartz GN, Souza LM. Administration of interleukin-6 stimulates multilineage hematopoiesis and accelerates recovery from radiation-induced hematopoietic depression. *Blood* 1991;77:472–80.
- [22] Porter ChJH. Drug delivery to the lymphatic system. *Crit Rev Ther Drug Carrier Syst* 1997;14:333–93.
- [23] Stordal L, Warren DJ, Moore AAS. Effect of recombinant murine tumor necrosis factor on hemopoietic reconstitution in sublethally irradiated mice. *J Immunol* 1989;142:833–5.
- [24] Tenu JP, Adams A, Souvannavong V, Yapo A, Petit JF, Douglas K. Photoaffinity labelling of macrophages and B lymphocytes using ¹²⁵I-labelled aryl-azide derivatives of muramyl dipeptide. *Int J Immunopharmacol* 1989;11:611–53.
- [25] Turánek J, Záluská D, Neča J. Linkup of a fast protein liquid chromatography system with a stirred thermostated cell for sterile preparation of liposomes by the proliposome-liposome method: application to encapsulation of antibiotics, synthetic peptide immunomodulators, and a photosensitizer. *Anal Biochem* 1997;249:131–9.
- [26] Turánek J, Záluská D, Hofer M, Vacek A, Ledvina M, Ježek J. Stimulation of haemopoiesis and protection of mice against radiation injury by synthetic analogues of muramyl dipeptide incorporated in liposomes. *Int J Immunopharmacol* 1997;19:611–7.
- [27] Vacek A, Hofer M, Mašek K. Effect of in vivo administration of adamantylamide dipeptide on bone marrow granulocyte-macrophage hemopoietic progenitor cells (GM-CFC) and on ability of serum of the treated mice to stimulate GM-CFC colony formation in vitro: comparison with muramyl dipeptide and glucan. *Immunopharmacol Immunotoxicol* 1999;21:1–14.
- [28] Vacek A, Rotkovská D, Bartoničková A. Radioprotection of

- hemopoiesis conferred by aqueous extract from chlorococcal algae (*Ivastimul*) administered to mice before irradiation. *Exp Hematol* 1990;18:234–7.
- [29] Velinova M, Read N, Kirby Ch, Gregoriadis G. Morphological observations on the fate of liposomes in the regional lymph nodes after footpad injection into rats. *Biochim Biophys Acta* 1996;1299:207–15.
- [30] Walder P, Buchar E, Machková Z, Vrba T, Flegel M, Janků I, et al. Pharmacokinetic profile of the immunomodulating compound adamantylamide dipeptide (AdDP), muramyl dipeptide derivative in mice. *Immunopharmacol Immunotoxicol* 1991;13:101–9.



Restoration of femoral GM-CFC progenitors in sublethally irradiated mice of various ages treated with liposomal adamantylamide dipeptide

Andrea Kašná^a, Jaroslav Turánek^{a,*}, Antonín Vacek^b, Dana Záluská^a,
Pavína Knötigová^a, Karel Mašek^c

^aDepartment of Immunology, Veterinary Research Institute, Hudcova 70, 621 32 Brno, Czech Republic

^bInstitute of Biophysics, 612 65 Brno, Czech Republic

^cDepartment of Pharmacology School of Medicine, Charles University, Albertov 4, Prague 2, Czech Republic

Received 6 October 2003; received in revised form 13 November 2003; accepted 4 May 2004

Abstract

In this study we tested the stimulatory effect of adamantylamide-L-alanyl-D-isoglutamine (AdDP) or its liposomal formulation (L-AdDP) on recovery of the granulocyte–macrophage hemopoietic progenitor cells in the bone marrow of sublethally irradiated mice of various ages. Number of GM-CFC progenitors in femur on day 10 was used as a parameter reflecting the stimulatory activity. Mice (aged 3–5 month) pre-treated with AdDP or L-AdDP via s.c. route displayed enhanced recovery of the granulocyte–macrophage hemopoietic progenitor cells at the dose of 5.5 Gy. Overaged mice (2 years) responded to the treatment when the dose was increased to 6.5 Gy, while radiation doses below 5.5 Gy should be used to see the stimulation effect in young mice (6 weeks). Entrapment of AdDP into liposomes enhanced costimulatory activity of sera of treated mice and prolonged this activity at least for 30 h after stimulation, in comparison to the mice treated with free AdDP where the costimulatory activity was spanned only up to 12 h. In conclusion, L-AdDP represents a suitable formulation of AdDP that induced recovery of GM-CFC progenitors in the femur of irradiated mice of various ages. The stimulatory effect depends on the extent of injury to bone marrow hemopoietic microenvironments caused by various doses of γ -irradiation.

© 2004 Elsevier B.V. All rights reserved.

Keywords: Adamantylamide dipeptide; Hemopoiesis; Liposome; Immunomodulator; Radiation

1. Introduction

Adamantylamide dipeptide (AdDP) belongs to the group of desmuramyl peptides [1]. This synthetic

immunomodulatory compound demonstrated high hemopoietic activity besides antitumorous, antiviral [2,3] and antimicrobial activities [4]. Increased hemopoietic activity was also found following intraperitoneal [5] and subcutaneous application of AdDP [6]. Stimulation of non-specific immunity together with recovery of hemopoiesis was shown to be responsible for radioprotective effect found for AdDP and other MDP analogues [6–8].

* Corresponding author. Tel.: +420-5-3333-1311; fax: +420-5-4121-1229.

E-mail address: turanek@vri.cz (J. Turánek).

In our previous studies we found that the encapsulation of AdDP and other MDP analogues into liposomes that are the vesicles composed of one or more phospholipid bilayers enclosing an aqueous phase led to the increase of their biological activities [6,7,9].

Liposomes can act as the transport systems targeting immunomodulatory drugs to immune cells and protecting encapsulated drugs against enzymatic degradation. Liposomes can also form a biodegradable depot for administered drugs [10].

The radiation and large majority of chemotherapeutic agents used in cancer treatment produces the suppression of the host defence system especially through the destruction of lymphoid and bone marrow cells. The enhancement of host defence through a more rapid restoration of hemopoiesis is in patients undergoing radiotherapy and chemotherapy of critical importance since otherwise a number of them are dying from secondary diseases.

The major aim of present paper was to extend our previous observations on hematopoietic and radioprotective effects of AdDP and liposomal AdDP in relation to the age and therefore the effects of these compounds in juvenile, young, adult and aged animals were investigated.

2. Experimental procedures

2.1. Mice

Female (CBAx57Bl6)F1 mice (ANLAB, Brno, Czech Republic) having 14–25 g of weight and age from 6 weeks to 2 years were used for the experiments. Standardised pelleted diet and HCl-treated tap water (pH 2–3) were given ad libitum. The research was conducted according to the principles enunciated in the Guide for Care and Use of Laboratory Animals issued by the Czech Society for Laboratory Animal Science.

The preparations were applied to animals between 9 and 11 a.m. Twenty-four hours after subcutaneous injection of AdDP or L-AdDP (200 nmol in 0.2 ml per mouse), mice were irradiated with single whole-body doses in the range of 3.5–6.5 Gy from ⁶⁰Co gamma-ray source Chisostat (Chirana, Czech Republic) at the dose of 0.285 Gy/min. Mice were killed by cervical dislocations on day 10 after irradiation and the num-

bers of GM-CFC progenitor cells were evaluated in the bone marrow of animals from experimental and control groups (see Section 2.4).

2.2. Chemicals

Adamantylamide-L-alanyl-D-isoglutamine (AdDP) was synthesised and kindly donated by PolyPeptide Laboratories (Praha, Czech Republic). Purities of the other chemicals used in the experiments were of analytical grade or better. Colorimetric kit QCL-1000 (Bio-Whittaker, USA) was used to confirm apyrogenicity of preparations with respect to the content of lipopolysaccharide. The content of endotoxin was found to be below 0.01 EU per mg AdDP.

2.3. Preparation of frozen-and-thawed multilamellar vesicles (FTMLV)

Liposomes were prepared from the egg-yolk phosphatidylcholine (EPC) (99% purity, Avanti Polar Lipids, USA) by the method of hydration of phospholipid film by apyrogenic phosphate-buffered saline (PBS) containing immunomodulator AdDP. Glassware was treated overnight at 180 °C to remove pyrogens. The lipid was dissolved in chloroform (300 mg in 6 ml) and deposited onto the wall of a round-bottom flask (250 ml) by removal of the solvent in a rotary evaporator (40 °C, 4 h). The dried lipid film was then hydrated with the aqueous phase under continuous mixing on a mechanical reciprocal shaker for 2 h. FTMLV was obtained by freezing the multilamellar vesicles in liquid nitrogen and thawing them in a 30 °C water bath, repeating the cycle five times [11]. The analyses of entrapment efficiency were done by HPLC. AdDP was entrapped with around 65% efficiency [7,12]. Preparations of AdDP (free or liposomal formulations) were appropriately diluted in PBS and administered by s.c. route at a dose of 200 nmol/mouse in a single injection (200 µl). Control animals were treated with the same volume of PBS.

2.4. GM-CFC progenitors

For granulocyte-macrophage colony forming cells (GM-CFC) determination, bone marrow cells from intact mice were drawn by flushing of femoral bone with an IMDM medium, counted on Coulter Counter

(Model ZN, Coulter Electronics) and kept in a melting ice bath before their use.

Femoral marrow cells were plated in triplicate in a semisolid environment created by a plasma clot in our modification [13] containing the Iscove's modification of Dulbecco's medium (IMDM) plus 20% foetal calf serum (FCS), 10% of conditioned medium from rmlL-3-producing myeloma cell line [14]. The final concentration of rmlL-3 being 1 U/ml (1 U/ml was defined as a concentration of rmlL-3 that yielded a maximum colony number in preliminary experiments comparing the colony number vs. concentration of rmlL-3), 10% citrate bovine plasma, and CaCl₂ at a concentration of 1.5 mg/ml.

The cultures were incubated for seven days in a thermostat (Forma Scientific, USA) at 37 °C in a fully humidified atmosphere of 5% CO₂ in air. Colonies of at least 50 cells were scored at 40 × magnification.

2.5. Bone marrow cellularity

Numbers of nucleated cells per femur were estimated by means of Coulter Counter (Model ZN, Coulter Electronics) after flushing of femoral diaphyses with saline.

2.6. Colony-stimulating activity (CSA) and costimulating activity (CoSA)

CoSA was determined as the ability of AdDP or L-AdDP, sera of AdDP or L-AdDP treated mice, or conditioned medium from cultures of adherent stromal cells to enhance the number of GM-CFC colonies induced by a suboptimal concentration of rmlL-3 in the above-described GM-CFC assay. The concentration of rmlL-3 was adjusted to a value which yielded one-third of the maximum number of colonies on a dose-dependent curve [15]. Mice sera were taken at various intervals after injection of drugs and their abilities to co-stimulate *in vitro* growth of colonies from granulocyte-macrophage progenitor cells (GM-CFC) were determined. The tested sera were diluted with saline at a ratio 1:2 prior to use.

2.7. Statistics

Statistical analyses were carried out using the programme GraphPad PRISM V.3.00 (GraphPad Soft-

ware, San Diego, CA). Statistical significance among individual experimental groups of mice in hemopoietic parameters was calculated by One-way analysis of variance. The Newman-Keuls test for comparison of all pairs of columns and the Dunnett test for comparison of all columns with the control column were used in the analysis.

3. Results

3.1. An age dependence of the radioprotective effect of free and liposomal form of AdDP

Mice were divided into four groups according to their age: 6 weeks, 2 months, 3–5 months, and 12 months. Twenty-four hours prior to γ -irradiation with a dose of 5.5 Gy five animals of each experimental group were treated with free AdDP and the other 5 animals of the same age group with liposomal L-AdDP at the same doses of 3.65 mg AdDP/kg (200 nmol/mouse) and 500 mg phospholipid/kg (10 mg phospholipid/mouse). Another group consisted of control mice treated with PBS. Untreated and non-irradiated controls were used to compare radiosensitivity in the groups of various ages.

Concentration of GM-CFC/10⁵ in bone marrow of control irradiated animals increased on day 10 significantly with the age of animals. The lowest number of GM-CFC/10⁵ was found in mice aged 6 weeks while the highest one was observed in mice aged 12 months. These data suggest that radiation resistance of GM-CFC in the bone marrow increases with the age of animals. Both the total pool of GM-CFC and the concentration GM-CFC/10⁵ in femur increased simultaneously with the age of irradiated mice (Fig. 1). The total pool of GM-CFC progenitors in the bone marrow of non-irradiated untreated controls was age-dependent and increased with the age of mice (Fig. 1).

The hemopoietic effect of L-AdDP was significant only in the age groups 3–5 months and 2 months.

3.2. Protective effect of free or liposomal AdDP on the recovery of hemopoiesis in bone marrow of mice irradiated by various dosages

Similar protective effect at low radiation doses (3.5–4.5 Gy) was found for AdDP and L-AdDP; the protective/stimulatory effect of AdDP and L-AdDP on

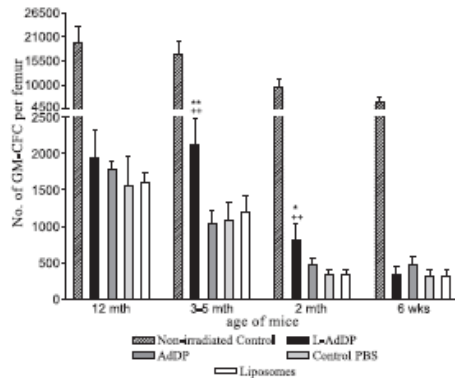


Fig. 1. Number of GM-CFC per femur on day 10 after sublethal γ -irradiation of mice treated with L-AdDP or free AdDP. Mice were divided into five groups according to their age; five animals per group. Preparations were applied by s.c. route 24 h prior to γ -irradiation (5.5 Gy). The numbers of GM-CFC per femur were counted on day 10 after irradiation (for details see Section 2.4.) Doses of free AdDP or liposomal AdDP were 3.65 mg/kg of body weight. ** $P < 0.01$, * $P < 0.05$ L-AdDP vs. PBS control. +* $P < 0.01$, L-AdDP vs. AdDP.

GM-progenitors in the bone marrow was significantly higher ($P < 0.01$) in comparison to PBS.

A significant difference between AdDP and L-AdDP with respect to their hemopoietic effect was found for higher irradiation doses (5.0, 5.5 and 6.0 Gy). However, following irradiation at the dose of 6.5 Gy, the counts of GM-CFC in the bone marrow were identical in both experimental and control groups.

A sharp decrease of GM-CFC counts that dropped down to the level of the control group was observed in mice treated with free AdDP. On the contrary, the counts of GM-CFC in the group treated with L-AdDP decreased much more slowly after irradiation with higher doses of γ -rays (Fig. 2).

3.3. Effect of AdDP and L-AdDP on the recovery of hemopoiesis in 2-year-old mice after irradiation (6.5 Gy)

More profound injury to the bone marrow of overaged mice was induced by radiation dose of 6.5 Gy. The ratio of GM-CFC per femur was around 14 for non-irradiated control related to the irradiated control (PBS treated). Only L-AdDP stimulated sig-

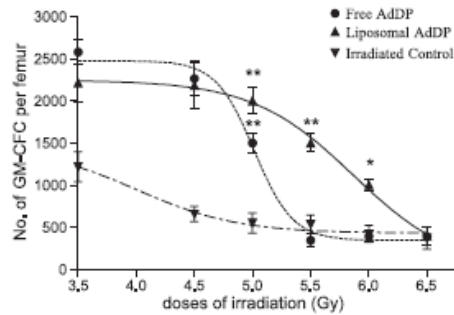


Fig. 2. Effect of various radiation doses on the number of GM-CFC in the bone femoral marrow on day 10 after γ -irradiation. Mice aged 3–5 months (five animals per group). The doses of AdDP or L-AdDP were 3.65 mg/kg/0.2 ml/mouse 24 h prior to γ -irradiation. Irradiated control groups were treated with PBS. AdDP or liposomal L-AdDP vs. irradiated control: ** $P < 0.01$, * $P < 0.05$.

nificantly hemopoiesis as expressed by the number of GM-CFC per femur (Fig. 3).

3.4. Kinetics of co-stimulating activity (CoSA) in sera from mice administered with AdDP, L-AdDP and empty liposomes

We have found that sera from mice treated with L-AdDP or AdDP showed no CSA, i.e. did not stimulate

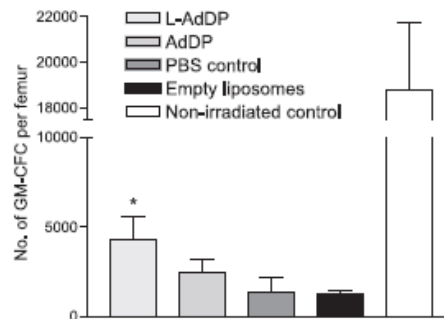


Fig. 3. Effect of L-AdDP and free AdDP on the number of GM-CFC per femur in γ -irradiated overaged mice. The doses of AdDP or L-AdDP administered s.c. were 3.65 mg/kg/0.2 ml/mouse 24 h prior to γ -irradiation (2 years old mice, five animals per group). Empty liposomes were administered at the dose of phospholipides 500 mg/kg corresponding to that for L-AdDP. Irradiated control groups were treated with PBS. * $P < 0.05$ L-AdDP vs. PBS control.

proliferation of hematopoietic progenitor cells for granulocyte and macrophage (GM-CFC) in vitro being presented in the culture as the only potential colony-stimulating factor (data not shown). However, sera from mice treated with AdDP or L-AdDP, as well as with empty liposomes, enhanced in vitro the number of colonies induced by a suboptimal concentration of mIL3 (Fig. 4), i.e. produced CoSA.

The time-dependence of the changes in CoSA of sera after AdDP administration showed statistically significant ($P < 0.01$) elevation 3 and 6 h after an injection and dropped down after 24 h. CoSAs of sera from mice treated with L-AdDP or empty liposomes were significantly higher and lasted longer than that of AdDP.

3.5. Number of femoral GM-CFC in mice treated with AdDP, L-AdDP and empty liposomes

Multiplication of GM-CFC in the bone marrow of non-irradiated mice was tested for AdDP, L-AdDP and empty liposomes 24 h after the application. We have found that AdDP and L-AdDP induced a signif-

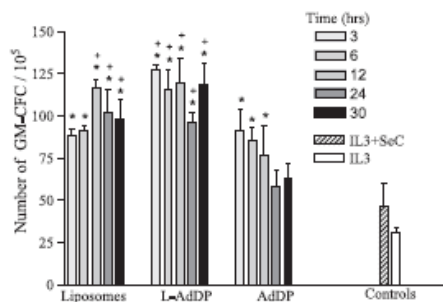


Fig. 4. Time-courses of the changes in CoSA of sera after administration of AdDP, L-AdDP and empty liposomes. Mice 3 months of age (four animals per group) were administered 0.2 ml of AdDP, L-AdDP or empty liposomes by s.c. injection. The doses of free and liposomal AdDP were 3.65 mg/kg of body weight. Sera of mice treated with AdDP or L-AdDP preparations were collected at indicated time intervals and evaluated for their CoSA expressed as a number of GM-CFC/ 10^5 cells. Bone marrow cell cultured in medium supplemented with IL-3 (IL3) or in a medium supplemented with IL-3 and control sera (IL3+SeC) were set as controls. *Statistically significant ($P < 0.01$) in comparison to the control (IL3+control serum). **Statistically significant ($P < 0.01$) in comparison to AdDP (corresponding time intervals were compared).

Table 1

Numbers of GM-CFC progenitors in the femur of mice (3 months of age) at 24 h after administration of AdDP, L-AdDP, and empty liposomes

Groups	GM-CFC/femur ($\times 10^3$) ^a
Control (PBS)	18.3 \pm 3.2
Liposomes	20.3 \pm 3.5
AdDP	31.5 \pm 1.8*
L-AdDP	52.8 \pm 2.6*

AdDP and L-AdDP were applied s.c. (3.65 mg/kg).

^a Mean values (four mice per group were used).

* The value is significantly ($P < 0.01$) higher in comparison with the control.

icant increase in the number of GM-CFC progenitors in the femur of intact non-irradiated mice, which means that both preparations guided the hemopoietic stem cells towards differentiation of granulocyte–macrophage progenitors. The effect of empty liposomes was not statistically significant (Table 1).

4. Discussion

Hemopoiesis is a very complex process, taking place in more than 200 areas in skeletal bones, which are synchronised to act as one organ. Central and peripheral nervous systems play a very important role in immune response, and the association with hemopoietic system of the bone marrow is well known [16]. Muramyl peptides and their different analogues including desmuramyl peptides (AdDP) have been shown to have beside the radio and chemoprotective activity also a number of other effects as closely linked together as the effect on immune and nervous systems [17]. Interactions between the neural and immune systems exist through humoral factors operating via the hypothalamic–pituitary–adrenal axis and cytokines acting over a relatively long distance. The intact innervation of bone marrow, lymphatic organs and other tissues has an important role in the regulation of production of blood cells and in the selective release of cells from the marrow into the circulation [18]. The observation that “the bone marrow” acts and reacts as “one organ” is due to the regulatory mechanisms: the humoral factors (such as erythropoietins, granulopoietins, thrombopoietins, etc.), the neural factors (central nervous regulation) and cellular factors (continuous migration of stem cells through the blood to assure a

sufficient stem cell pool size in each bone marrow “sub-unit”) [16]. The role of immunomodulatory molecules such as MDP and its analogues in this very complex neuro-immunological network is not fully understood since they act on both systems [17].

4.1. Radiosensitivity and age

Mice of various age, as well as other mammals including men, differ in their sensitivity to radiation injury of hemopoiesis. The rate of the recovery of hemopoiesis in bone marrow depends on the pool of survived hemopoietic stem cells. In aged mice more slow-dividing stem cells produce an equal number of peripheral blood cells, as do more actively cycling but less numerous stem cells in young mice. This fact contributes to higher sensitivity of young mice towards radiation injury. Data from Fig. 2 indicate that lower radiation doses should be applied if young animals are used as a model for testing radioprotective and hemopoietic effect. Both L-AdDP and AdDP preparations were not able to stimulate hemopoiesis in young mice whose pool of hemopoietic stem cells was drastically reduced by relatively high doses of γ -irradiation hence the spontaneous recovery was a long lasting event. The large numbers of surviving stromal cells in adult and old animals increase their proliferation activity during the recovery after sublethal γ -irradiation and can produce also cytokines supporting the recovery of the radiation-damaged hemopoiesis in bone marrow [19]. On the other hand, higher radiation doses should be used in old mice which are more resistant towards γ -irradiation and whose pool of hemopoietic stem cells remained relatively high after γ -irradiation. The L-AdDP administration was effective in overaged 2 years old mice irradiated with higher doses (6.5 Gy), which resulted in a deeper bone marrow injury in comparison to the dose of 5.5 Gy (see Fig. 3). On the other hand, the protective effect of L-AdDP in animals of 2 and 3–5 months old is evident (see Fig. 1). The mice of this age represent suitable model for testing a radioprotective activity of drugs and are generally used.

4.2. Liposomal preparation

Immunomodulatory agents that induce and control hemopoiesis via the monocyte macrophage system

can act radio- or chemoprotectively [20]. This is the case of muramyl dipeptide and its analogues [5–7,20]. Targeting of muramyl dipeptide analogues to monocyte–macrophage system by liposomes significantly improved their hemopoietic activity [6,7,20]. Liposomes as carriers of muramyl dipeptide analogues can play two roles. First, large liposomes can stay at the injection site after the subcutaneous administration and serve as a depot of the drug. Second, small liposomes, unlike the large ones, can penetrate through the extracellular matrix and reach the lymphatic tissues via the lymphatic capillaries thus delivering the encapsulated drug to the lymphatic tissue macrophages. After phagocytosis of the liposomal component by macrophages, the drug can be released into the cytoplasm and interact with intracellular receptors. Targeting of AdDP to macrophages can increase a production of cytokines enhancing the proliferation of hemopoietic stem cells and increasing the number of GM-CFC in the bone marrow above the level found in non-irradiated control group. Stimulation of macrophage functions can lead to the induction of secretion of IL-1, IL-6 and TNF known to have therapeutic effects on hemopoietic regeneration after irradiation [21,22]. Liposomes are not inert carrier, in this study they were able to induce costimulatory activity in sera but they were not active with respect to induction of elevation of the GM-CFC pool in the bone marrow of the femur (Fig. 4, Table 1). Entrapment of AdDP into liposomes reduced effective dose of AdDP [6,8] and improved significantly the ability of AdDP to stimulate hemopoiesis in mice irradiated by higher doses and this result is in a good accordance with the role of liposomes as drug carriers, as mentioned hereinbefore (Fig. 2).

4.3. Cytokines and costimulatory activity of sera

The effects of immunomodulators on the recovery of hemopoiesis after irradiation are partially attributed to the production of hemopoietic stimulators and the transition of stem cells into cycling in the irradiated mice [21–24].

Enhanced concentrations of endogenous cytokines, namely IL-3, G-CSF, GM-CSF [25–27] were reported in the irradiated mice. These cytokines are supposed to alleviate the injuries caused by irradiation both in

the bone marrow and the spleen, to activate hemopoietic cells and to increase granulopoiesis and megakaryopoiesis [28].

Our results suggests that AdDP as well as L-AdDP modulate hemopoietic cytokine network which was documented by the ability of sera from mice treated with this preparations to enhance the *in vitro* growth of GM-CFC colonies induced by a suboptimal amount of hemopoietic growth factor, namely rmlL3 (see Fig. 4) [5,15]. Notably, the sera of mice administered with L-AdDP enhanced the stimulatory effects of IL-3 on GM-CFC. Proliferation of GM-CFC *in vitro* corresponded with an *in vivo* effect of L-AdDP documented by the elevation of the GM-CFC pool in the bone marrow of the femur (see Table 1). The costimulatory effect of sera after L-AdDP injection persists longer than that after administration of AdDP alone. It is interesting that empty liposomes are not inert carriers.

In conclusion, administration of AdDP or L-AdDP induces CoSA activity of sera and may thus act together with elevated endogenous cytokines to enhance proliferation in critical pools stromal, hemopoietic stem and progenitor cells leading to increase of the pool of granulocyte-macrophage progenitors in the bone marrow. L-AdDP can represent a suitable effective drug formulation of AdDP for clinical application, since the compound in long-term toxicity studies on animals has shown no toxicity. This preparation is intended for use in the treatment of immunological and hemopoietic suppression induced by ionizing radiation or anticancer cytotoxic drugs. Subcutaneous application of L-AdDP represents a comfortable route of application.

Acknowledgements

This work was supported by the Ministry of Agriculture, Contract No.: MO-03-99-01 and MZE VZ-0002716201; NAZV, Contract No.: QF 3115; and grant PZ-Z2/25/97 from The Ministry of Industry and Trade of the Czech Republic. Our special acknowledgement is meant to Dr. Ivanka Závodná for her long-lasting support and coordination of the projects focused on development of new immunotherapeutics.

References

- [1] Mašek K, Seifert J, Flegel M, Krojidl M, Kolinský J. The immunomodulatory property of novel synthetic compound adamantylamide dipeptide. *Methods Find Exp Clin Pharmacol* 1984;6:667–9.
- [2] Masihi KN, Lange W, Rohde-Schulz B, Mašek K. Antiviral activity of immunomodulator adamantylamide dipeptide. *Int J Immunother* 1987;3:89–95.
- [3] Masihi KN, Mašek K. Effect of the synthetic immunomodulator adamantylamide dipeptide on replication of human immunodeficiency virus alone or in combination with azidothymidine. *Int J Immunother* 1993;9:143–50.
- [4] Franěk J, Malina J. Immunomodulatory capacity of drugs evaluated in a mouse model of *Klebsiella pneumoniae* infection. In: Masihi KN, Lange W, editors. *Immunotherapeutic prospects of infectious diseases*. Berlin: Springer-Verlag; 1990. p. 55–8.
- [5] Vacek A, Hofer M, Mašek K. Effect of *in vivo* administration of adamantylamide dipeptide on bone marrow granulocyte-macrophage hemopoietic progenitor cells (GM-CFC) and on ability of serum of the treated mice to stimulate GM-CFC colony formation *in vitro*: comparison with muramyl dipeptide and glucan. *Immunopharmacol Immunotoxicol* 1999; 21:1–14.
- [6] Turánek J, Záluská D, Vacek A, Borkovcová P, Thumvaldová J, et al. Stimulation of nonspecific immunity, haemopoiesis and protection of mice against radiation injury by 1-adamantylamide-L-alanyl-D-isoglutamine incorporated in liposomes. *Int Immunopharmacol* 2001;1:167–75.
- [7] Turánek J, Záluská D, Hofer M, Vacek A, Ledvína M, et al. Stimulation of hemopoiesis and protection of mice against radiation injury by synthetic analogues of muramyl dipeptide incorporated in liposomes. *Int J Immunopharmacol* 1997;19: 611–7.
- [8] Hofer M, Vacek A, Mašek K, Juchelková L, Pipalová L. Adamantylamide dipeptide stimulates haemopoiesis and increases survival in irradiated mice. *Int J Immunopharmacol* 2000;22: 91–7.
- [9] Mašek K. Immunopharmacological properties of synthetic muramyl peptides and their analogs. In: Masihi KN, Lange W, editors. *Immunomodulators and nonspecific host defence mechanisms against microbial infections*, vol. 68. *Advances in Biosciences*; 1988. p. 11.
- [10] Barratt G, Morin C. Liposomal immunomodulators. In: Puisieux F, Couvreur P, Delattre J, Devissaguet JP, editors. *Liposomes, New systems and new trends in their applications*. Paris: Scientific Publications; 1995. p. 461–506.
- [11] Hope MJ, Bally MB, Webb G, Cullis PR. Production of large unilamellar vesicles by a rapid extrusion procedure, characterization of size distribution, trapped volume and ability to maintain a membrane potential. *Biochim Biophys Acta* 1985;812: 55–65.
- [12] Turánek J, Záluská D, Neča J. Linkup of fast protein liquid chromatography system with a stirred thermostated cell for sterile preparation of liposomes by the proliposome-liposome method: application to encapsulation of antibiotics, synthetic

- peptide immunomodulators, and a photosensitizer. *Anal Biochem* 1997;249:131–9.
- [13] Vacek A, Rotkovská D, Bartoničková A. Radioprotection of hemopoiesis conferred by aqueous extract from chlorococcal algae (*Ivastimul*) administered to mice before irradiation. *Exp Hematol* 1990;18:234–7.
- [14] Karasuyama H, Melchers F. Establishment of mouse cell lines which constitutively secrete large quantities of interleukins 2, 3, 4, or 5 using modified cDNA expression vectors. *Eur J Immunol* 1988;18:97–104.
- [15] Vacek A, Hofer M, Weiterova L, Hoferova Z, Pipalova I, Masek K. Hemopoiesis-stimulating action of adamantylamide dipeptide: kinetics of increase of GM-CFC in femur and co-stimulating activity of serum, role of bone marrow stromal cells. *Immunopharmacol Immunotoxicol* 2001;23(4):505–17.
- [16] Fliedner TM, Graessle D, Paulsen C, Reimers K. Structure and function of bone marrow hemopoiesis: mechanisms of response to ionizing radiation exposure. *Cancer Biother Radiopharm* 2002;17:405–26.
- [17] Mašek K, Slánský J, Petrovický P, Hadden JW. Neuroendocrine immune interactions in health and disease. *Int Immunopharmacol* 2003;3:1235–46.
- [18] Miyan JA, Broome CS, Afan AM. Coordinated host defence through an integration of the neural, immune and haemopoietic systems. *Domest Anim Endocrinol* 1998;15(5):297–304.
- [19] Vacek A. Proliferation activity and number of stromal (CFU-f) and haemopoietic (CFUs) stem cells in bone marrow and spleen of rats of different ages. *Acta Vet Brno* 2000;69:25–31.
- [20] Fedoročko P. Liposomal muramyl tripeptide phosphatidylethanolamine (MTP-PE) promotes haemopoietic recovery in irradiated mouse. *Int J Radiat Biol* 1994;65:465–75.
- [21] Neta R, Vogel SN, Sipe JD, Wong GG, Nordan RP. Comparison of in vivo effects of human recombinant IL-1 and human recombinant IL-6 in mice. *Lymphokine Res* 1988;7:403–12.
- [22] Mac Patchen ML, Vitte TJ, Williams JL, Schwartz GN, Souza LM. Administration of interleukin-6 stimulates multilineage hematopoiesis and accelerates recovery from radiation-induced hemopoietic depression. *Blood* 1991;77:472–80.
- [23] Murray JL, Kleinerman ES, Cunningham JE, Tatom JR, Andrejcio K, et al. Phase I trial of liposomal muramyl tripeptide phosphatidylethanolamine in cancer patients. *J Clin Oncol* 1989;7:1915–25.
- [24] Slordal L, Warren DJ, Moore MA. Effect of recombinant murine tumor necrosis factor on hemopoietic reconstitution in sublethally irradiated mice. *J Immunol* 1989;142(3):833–5.
- [25] Peng R, Wang D, Xiong C, Gao Y, Li Y, Yang H, et al. Interleukin-3 gene expression in irradiated mouse bone marrow. *J Environ Pathol Toxicol Oncol* 1998;7:135–9.
- [26] Chang CM, Limanni A, Baker WH, Dobson ME, Kalinich JP, et al. Bone marrow and splenic granulocyte-macrophage colony-stimulating factor and transforming growth factor-beta mRNA levels in irradiated mice. *Blood* 1995;86:2130–6.
- [27] Kadar E, Sureda A, Manges MA, Ingles-Estave J, Valls A, Garcia J. Serum levels of G-CSF, IL-6, and GM-CSF after a single intraperitoneal dose of rhG-CSF in lethally irradiated B6D2F1 mice. *Acta Haematol* 1997;98:119–24.
- [28] Chang CM, Limanni A, Baker WH, Dobson ME, Kalinich JP, Patchen ML. Sublethal gamma irradiation increases IL-1-alpha, IL-6, and TNF-alpha mRNA levels in murine hemopoietic tissues. *J Interferon Cytokine Res* 1997;17:567–72.

Stimulation of innate immunity in newborn kids against *Cryptosporidium parvum* infection-challenge by intranasal/per-oral administration of liposomal formulation of N-L18-norAbu-GMDP adjuvant

J. TURÁNEK¹*, A. KAŠNÁ³, B. KOUDELA^{3,4}, M. LEDVINA⁴ and A. D. MILLER⁵

¹ Veterinary Research Institute, Hudcova 70, 62132 Brno, Czech Republic

² University of Veterinary and Pharmaceutical Sciences, Palackého 1-3, 61242 Brno, Czech Republic

³ Institute of Parasitology, Academy of Sciences of the Czech Republic, České Budějovice, Czech Republic

⁴ Institute of Organic Chemistry and Biochemistry, Academy of Sciences of the Czech Republic, Flemingovo náměstí 2, 16610 Prague, Czech Republic

⁵ Imperial College Genetic Therapies Centre, Department of Chemistry, Flowers Building, Armstrong Road, Imperial College London, London, SW7 2AZ, UK; IC-Vec Ltd, Flowers Building, Armstrong Road, London, SW7 2AZ, UK

(Received 21 October 2004; revised 21 December 2004; accepted 15 March 2005)

SUMMARY

The effects of a liposomal preparation of lipophilic immunomodulator β -D-GlcNstearoyl-(1-4)-norMurNAc-L-Abu-D-isoGln (N-L18-norAbu-GMDP) were investigated on resistance to *Cryptosporidium parvum* infection in neonatal kids. The liposomal preparation was administered subcutaneously or intranasally/orally (i.n./p.o.) twice at doses of 100 μ g, 200 μ g, or 1000 μ g per kid pre-infection challenge. The treatment schemes were (i) 72 and 24 h pre-infection challenge, (ii) 24 h pre-infection challenge and 24 h post-infection challenge (oral inoculation with 1×10^7 oocysts of *C. parvum* in 5 ml of PBS). Administration of liposomal N-L18-norAbu-GMDP by i.n./p.o. route at the cumulative dose of 2000 μ g per kid 72 and 24 h pre-infection challenge, lead to substantially increased clearance of coccidian parasites from various parts of the intestine. On the basis of histological examination, the distribution of cryptosporidia in the intestine and the severity of the infection, treated kids were classified on day 5 as having a strong reduction in infection in comparison to the control group ($P < 0.05$). No cryptosporidia were found on the mucosal surface of treated kids by day 10, while the intestines of the control kids were still infected. All doses and routes of administration were judged effective with respect to suppression of cryptosporidia infections.

Key words: *Cryptosporidium parvum*, immunomodulation, liposomes, muramyl dipeptide, muramyl dipeptide analogues, goat, β -D-GlcNstearoyl-(1-4)-norMurNAc-L-Abu-D-isoGln, N-L18-norAbu-GMDP.

INTRODUCTION

Cryptosporidium parvum, the causative agent of cryptosporidiosis, is classified with the phylum *Apicomplexa* and belongs to the various genera referred to as coccidia. The parasite primarily infects the microvillus border of the intestinal epithelium and to a lesser extent the extraintestinal epithelia. The infection is self-limiting except in immunodeficient hosts, in which case it may cause protracted and untreatable diarrhoea. Cryptosporidiosis is common in young farm animals (calves, lambs, kids) causing a debilitating disease that can lead to mortality. These infected animals may also play a key role in zoonotic transmission. Avian cryptosporidiosis is an emerging health problem in poultry, associated

with respiratory disease in chickens and other Galliformes, or with intestinal disease in turkeys and quails. Owing to an absence of effective drug treatments, the control of cryptosporidiosis relies mainly on the enforcement of hygiene provisions and other good management practice (O'Donoghue, 1995; De Graaf *et al.* 1999a). Host immune responses that induce protective immunity and contribute to pathogenesis are poorly understood. Recent studies with murine infection models suggest that interferon- γ (IFN- γ) plays a key role in mediating partial protective innate immunity against the infection identified in immuno-compromised mice, and also in mediating the elimination of the coccidia agent by CD4⁺ T-cells (McDonald, 1999, 2000).

There are 2 target groups for which the development of an immunomodulation strategy against cryptosporidiosis would be justifiable: children and AIDS sufferers in developing countries and newborn ruminants. In the former group, an immunomodulation strategy against cryptosporidiosis might contribute greatly to improvements in public health

* Corresponding author: Veterinary Research Institute, Department of Immunology, Hudcova 70, 621 32 Brno, Czech Republic. Tel: +420 5 3333 1311. Fax: +420 5 4121 1229. E-mail: turanek@vri.cz

when control by other preventive measures becomes impossible owing to poverty. Moreover, *Cryptosporidium* infection is one of the most devastating opportunistic complications of AIDS and should be controlled if for no other reason. In the latter group, the development of an immunomodulation strategy can be justified on the basis of economic losses due to the disease in neonatal ruminants deriving from coccidia present during livestock husbandry in less than sanitary conditions of the sort common in developing countries, and with limited availability of drugs. The development of a vaccine against cryptosporidiosis is a difficult task and many aspects of this problem were reviewed (De Graaf *et al.* 1999b). For this reason we elected to develop an alternative strategy using our own amphiphilic immunomodulator solubilized by liposome formulation.

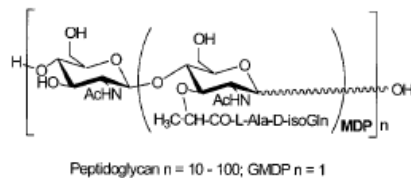
Muramyl dipeptide is the smallest active unit of the *Mycobacteria* cell wall, and has been found to possess a whole range of immunomodulation activities. Several hundred analogues have been synthesized over the years. They stimulate non-specific resistance to microbial infection and tumour cells, and have been shown to have an effect, *in vitro*, on all cell types of the immune system (Adam and Lederer, 1984). *In vivo* in experimental infections in mice, muramyl peptide derivatives have also been shown to induce an impressive antiparasitic immune response. This was demonstrated convincingly in models of protozoan infections caused by *Toxoplasma gondii* and *Leishmania donovani* (Krahnenuhl *et al.* 1981; Hockertz *et al.* 1991). Recently, we developed a lyophilized liposomal formulation of muramyl dipeptide analogue β -D-GlcNstearoyl-(1-4)-norMurNAc-L-Abu-D-isoGln (N-L18-norAbu-GMDP) building upon an extensive literature on the background of phospholipid liposome uses as versatile transport systems for immunomodulatory drugs and as biodegradable slow-release depots for administered drugs (Barratt and Morin, 1995). Here we report on how a liposomal formulation of N-L18-norAbu-GMDP is able to achieve effective immunomodulation of cryptosporidiosis infections in newborn kids that were challenged with *C. parvum* oocysts by intranasal/oral (i.n./p.o.) administration either pre- or post-administration of liposomal N-L18-norAbu-GMDP.

MATERIALS AND METHODS

N-L18-norAbu-GMDP

The structure of N-L18-norAbu-GMDP derives from peptidoglycan. N-L18-norAbu-GMDP was synthesized according to the procedure of Ledvina *et al.* (1998). The stearyl moiety was introduced into the structure to improve incorporation of the molecule into liposomes, which was presumed to represent a

A Peptidoglycan fragment



B N-L18-norAbu-GMDP

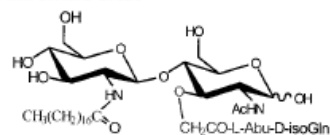


Fig. 1. Derivation of N-L18-norAbu-GMDP from peptidoglycan structure.

suitable carrier system for both subcutaneous and per-oral routes of administration of muramyl dipeptide-based immunomodulatory compounds. Structural formulae of peptidoglycan and N-L18-norAbu-GMDP are shown in Fig. 1.

Preparation of liposomes

Liposomes (frozen-and-thawed multilamellar vesicles, FTMLV) were prepared from egg-yolk phosphatidylcholine (EPC, purity $\geq 95\%$), negatively charged lipid 1-palmytoyl-2-oleoyl-sn-glycero-phosphatidylglycerol (POPG) (Avanti Polar Lipids, USA) and N-L18-norAbu-GMDP in molar ratio 4:16:1 by classical lipid film hydration in apyrogenic phosphate-buffered saline (PBS) (Turánek *et al.* 2003). For application, the liposomes were extruded through a 0.2 μ m isopore filter (Millipore) (Turánek *et al.* 1994). The size and zeta-potential (in PBS) of liposomes were determined by dynamic light scattering (Zetasizer 3000, Malvern Instruments, Malvern, UK).

Inoculum

The source of cryptosporidial oocysts was the faeces of a naturally infected scouring calf (12 days old). Morphologically the oocysts corresponded with the species *C. parvum*. The faecal material was suspended in 2.5% potassium dichromate and then passed through a series of graded sieves to remove large particles, giving a suspension that was kept at room temperature for 1 week. Oocysts were concentrated by flotation in Sheather's sugar solution and then washed with tap water to remove the flotation solution. To decontaminate the oocysts, the suspension was treated with bleach (SAVO, Bohemia, Bohumín, Czech Republic; 1.25%

Table 1. Tabular summary of the experimental groups

Experimental group	Infection (1×10^7 oocysts)	Single dose μg of N-L18- norAbu-GMDP	Route of application first; second	Schedule application (h post-infection challenge)
A – Untreated uninfected control	0	—	—	—
B – Untreated infected control – 6 animals	+	—	—	—
C 200 μg 6 animals	+	100	in/po; in/po	-72; -24
D 2000 μg 6 animals	+	1000	in/po; in/po	-72; -24
E 200 μg 6 animals	+	100	sc; sc	-72; -24
F 2000 μg 6 animals	+	1000	sc; sc	-72; -24
G 400 μg 6 animals	+	200	in/po; sc	-24; +24
H 400 μg 6 animals	+	200	sc; in/po	-24; +24

sodium hypochlorite) for 15 min. The purified oocysts were stored in 2.5% potassium dichromate at 4 °C for 27 days until used for the inoculation of kids in infection challenge experiments. Before inoculation, the suspension of the oocysts was washed 3 times by centrifugation in sterile phosphate-buffered saline (PBS, pH 7.2) and counted using a haemocytometer.

Experimental design

Forty-two 1-day-old kids (Saanen goat) of both sexes were obtained from a goat-cheese production unit of 110 spring kidding goats known to be free of cryptosporidia infection or other health problems typical of newborn kids. The kids were separated from their dams immediately after the birth. In the first 24 h, they were fed goat colostrum and then transported to an isolator room and fed commercial cow's milk replacer (SANO, Germany) 3 times daily. Before starting the experiment, 4 kids were separated from the herd, placed in a separate stable and served as a non-infective control. The presence of *Cryptosporidium* oocysts was tested in their excrements and was negative before and during the experiment. Experimental cryptosporidiosis in kids has been described in detail previously (Koudela and Vitovec, 1997).

Treatment and infection challenge

The forty-two neonatal kids were randomly separated into 7 groups (6 animals per group) and all were orally inoculated with 10^7 *C. parvum* oocysts at 6 days of age to initiate an infection challenge. In the case of experimental groups C-F, the liposomal formulation of N-L18-norAbu-GMDP was administered subcutaneously or intranasally/per-orally (i.n./p.o.) twice at doses of 100 μg or 1000 μg per kid (500 μl per nostril) at time-intervals of 72 h and 24 h pre-infection challenge. The term i.n./p.o. denotes a route of administration involving intranasal administration of liposomal formulation combined

with ingestion, hence both intranasal and intestinal mucosae were considered to have been exposed to the liposomal formulation. For the remaining groups G and H, kids were treated with liposomal formulation twice at doses of 200 μg per kid by a combination approach involving first subcutaneous (s.c.) administration (500 μl per kid) followed by i.n./p.o. administration (500 μl per nostril) (or *vice versa*), at time-intervals of 24 h pre- and 24 h post-infection challenge. Group B acted as an infection control that was not treated with any liposomal formulation. Three kids (group A) were kept in a separate stable and served as an untreated uninfected control. The experimental design is summarized in Table 1.

Assessment of infection

All kids were monitored twice a day for diarrhoea and other clinical signs by observing them. The severity of diarrhoea was scored as 0 for normal, 1 for loose and formless, 2 for semi-fluid, or 3 for watery.

Five days post-inoculation (p.i.) and 10 days, p.i. 3 kids from each experimental group were euthanized with an overdose of a barbiturate (Thiopental®, Spofa, Czech Republic). At necropsy, a complete examination of all organs and tissues was performed. Samples for histopathology were collected immediately after the animals were killed. The first specimen was taken from the ileum within 5 cm from the ileocaecal valve (ostium ileocaecale – OIC). More samples were removed 50 cm from the OIC and then every 50 cm cranially from the OIC so that the last jejunal specimen originated from the duodenum. In the large intestine specimens were collected from the apex caeci, colon near the ansa centralis, and rectum. Additional samples for histology were taken from the abomasum, liver, kidneys, spleen, lung, pancreas, and regional mesenteric lymph nodes. Material was fixed in 10% neutral formalin and processed by routine histological methods. Histological sections were stained with haematoxylin-eosin, and with Wolbach's modification of Giemsa staining. On the basis of such histological examination the distribution of cryptosporidia in the intestine and the

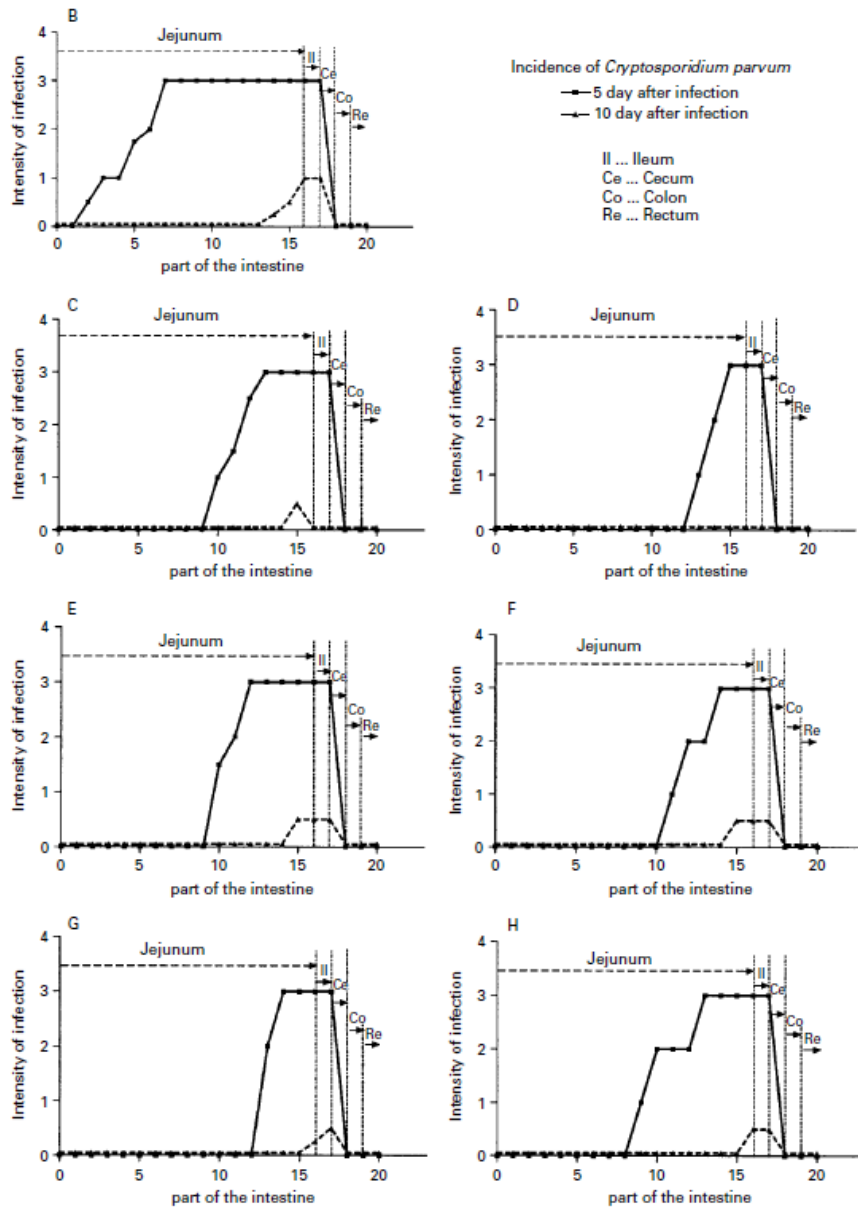


Fig. 2. Distribution and extent of *Cryptosporidium parvum* infection found in histological sections from the intestine of experimentally infected kids treated with liposomal N-L18-norAbu-GMDP. Detailed description of various experimental groups appears in Table 1. Sampling of the intestine for histological examination is described in the Materials and Methods section under *Assessment of infection*.

Table 2. Mean number of cryptosporidia per ileal villus in kids

Group (dose /route of application/ day p.i.)	5 Days p.i.	10 Days p.i.
B Untreated control	32.22 ± 19.36	4.70 ± 2.06
C (100 µg /i.n./p.o.: -72 h/-24 h)	37.52 ± 11.98	2.09 ± 2.01*
D (1000 µg /i.n./p.o.: -72 h/-24 h)	45.23 ± 15.08	0*
E (100 µg /s.c.: -72 h/-24 h)	28.96 ± 19.36	4.06 ± 2.95
F (1000 µg /s.c.: -72 h/-24 h)	36.23 ± 16.73	4.11 ± 2.55
G (200 µg /i.n./p.o. + s.c.: -24 h/-24 h)	34.23 ± 16.08	1.12 ± 2.96*
H (200 µg /s.c. + in/p.o.: -24 h/-24 h)	39.33 ± 19.56	3.65 ± 2.62

* Statistically significant in comparison with untreated control ($P < 0.05$).

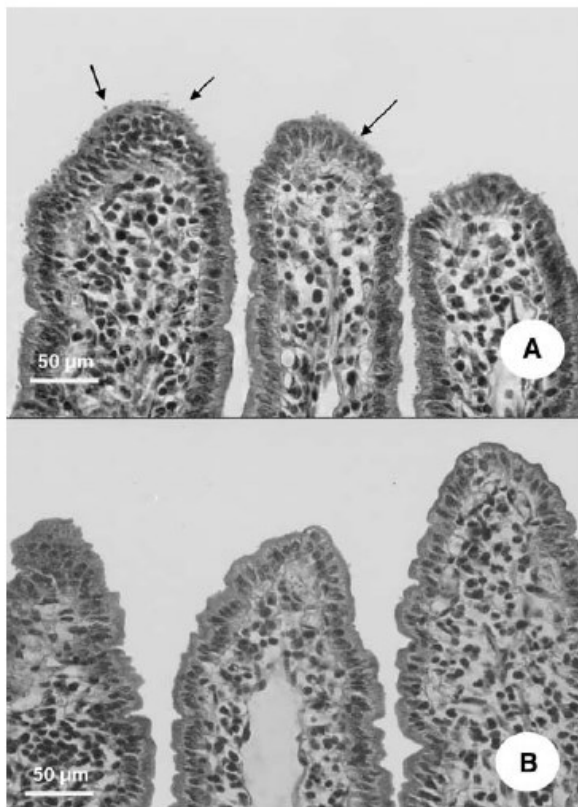


Fig. 3. Comparison of histological sections of the middle jejunum of an infected untreated kid (A) and a kid of group D (B); both were examined 10 days after infection. Cryptosporidial developmental stages on the intestinal surface are indicated by arrows.

degree of infection were classified as follows. Degree 0 – no cryptosporidia found on the mucosal surface; degree 1 – moderate infection, sporadic cryptosporidia distributed on the intestinal surface; degree 2 – medium infection, regularly disseminated cryptosporidia on the intestinal surface; degree

3 – massive infection, most of the epithelial surface covered by cryptosporidia. Microscopical examination of haematoxylin-eosin stained ileal sections was then carried out in order to enumerate cryptosporidia, in various stages of development, that were attached to the enterocytes of 10 villi from the

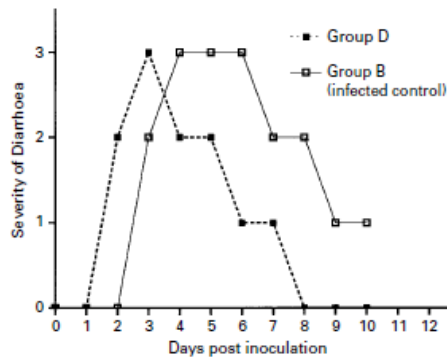


Fig. 4. The onset and duration of diarrhoea in the group D and infected control (group B). Classification of severity of diarrhoea is described in the Materials and Methods section.

ileum within 5 cm of the ileocaecal valve. The severity of ileal infection was then expressed as the mean number of cryptosporidia per villus.

Statistical analysis

Statistical analyses were carried out using the programme GraphPad PRISM V.3.03 (GraphPad Software Inc., San Diego, CA) where each graphical point represented a degree and distribution of *C. parvum* infection in the intestine. The severities of ileal infections were analysed by means of an analysis of variance (ANOVA) and comparisons of means (Newman-Keuls test).

RESULTS

Liposomal preparation of N-L18-norAbu-GMDP

Liposomal formulations with N-L18-norAbu-GMDP were prepared by lipid film hydration in PBS followed by extrusion through polycarbonate filters. Liposomes were characterized with a mean size of 178 nm (polydispersity 0.07) and a mean zeta-potential of -30.6 mV (PBS, 25°C). No side-effects (e.g. intumescence or hyperaemia of the nasal mucosa, oedema and soreness at the site of injection) were found after application of the liposomal preparation.

Histological examination and clinical signs

The distribution and extent of *C. parvum* infections found in histological sections from the intestine of experimentally inoculated kids is presented in Fig. 2. All doses and all routes of administration of liposomal N-L18-norAbu-GMDP appear to have been effective at suppression of infection, especially at

peak infection on day 5 ($P < 0.05$) (Fig. 2). Clearly, the most dramatic effects were observed when liposomal N-L18-norAbu-GMDP was administered i.n./p.o. 72 h and 24 h pre-infection challenge at a cumulative dose of $2000 \mu\text{g}$ per kid. In this instance, administration led to a considerably increased clearance of coccidian parasites from various parts of the intestine. On the basis of histological examination, the distribution of oocysts in the intestine and the severity of the infection (classified on day 5) were strongly reduced in comparison to the control group. Furthermore, no cryptosporidia were found on the mucosal surface of the treated kids on day 10, while the intestines of the control kids were still infected (Fig. 3). When a lower cumulative dose of $200 \mu\text{g}$ was employed, liposome administration was still effective, but residual infection was found on day 10. Dose-dependent responses were found for both i.n./p.o. and s.c. routes of administration. Pre- and post-infection applications of liposomal N-L18-norAbu-GMDP were more effective when liposomal preparation was applied first i.n./p.o. and then s.c. rather than *vice versa* (Table 2). According to histological examination of other organs (e.g. abomasum, liver, kidneys, spleen, lung, pancreas, and regional mesenteric lymph nodes), no spreading of *C. parvum* infection to other organs was found in both control and treated groups. Results from histological examinations correlated well with clinical observations made during the infectious period. The onset of diarrhoea after inoculation of oocytes was more rapid in kids treated with liposomal N-L18-norAbu-GMDP, but the duration of diarrhoea was considerably shorter compared to the control group. The curves reflecting the onset and duration of diarrhoea are presented in Fig. 4. Very similar curves were obtained for kids from different groups treated with liposomal N-L18-norAbu-GMDP, hence only the curve for liposome-treated group D is shown for the sake of clarity in comparison with that of control group B (Fig. 4).

DISCUSSION

The immunomodulatory effects of muramyl dipeptide, or its analogues, observed *in vivo* probably result from activation of intraepithelial lymphocytes, which are responsible for a resolution of intestinal infection. For instance, the treatment of mice with muramyl dipeptide appears to enhance resistance to challenge from the obligate intracellular protozoan *Toxoplasma gondii* (Krahenbuhl *et al.* 1981). In order to induce this effect, relatively high concentrations of this hydrophilic compound (80 mg/kg) were administered to mice to provoke sufficient immune response. This is probably due to poor penetration of hydrophilic muramyl dipeptide through cell membranes to reach intracellular macrophage receptors (Fogler and Fidler, 1986).

In addition, an immunomodulatory preparation based on oat β -glucan particles (1–3 μ m) has been found to induce an immune response against another coccidian parasite *Eimeria vermiformis*. Once again, relatively high doses of this preparation needed to be administered to mice by intragastrical or subcutaneous routes (150 mg/kg i.g., 25 mg/kg s.c.) before prophylactic effects could be seen (Yun *et al.* 1998).

Liposomes represent well-tolerated drug carriers for various routes of administration. In the case of s.c. administration, liposome particles (>120 nm) may stay at the injection site post-administration and can serve as a slow release drug depot, while smaller liposome particles (<120 nm) may penetrate through the extracellular matrix and reach the lymphatic tissues via the lymphatic capillaries thus delivering the encapsulated drug to the lymphatic tissue macrophages (Oussoren and Storm, 2001). Liposomal formulations of N-L18-norAbu-GMDP were approx. 200 nm in diameter with a few smaller liposome particles present (results not shown). Therefore, we presume in our case that liposomal formulations of N-L18-norAbu-GMDP post s.c.-administration were acting primarily as a slow release depot for N-L18-norAbu-GMDP.

Our data indicate that i.n./p.o.-administration gave the most effective immunomodulation with liposomal N-L18-norAbu-GMDP. The i.n./p.o. route of administration represents a non-invasive approach that is as a result attractive for both veterinary and human applications. However, the mechanism of immunomodulation is perhaps less obvious than for s.c.-administration. Post i.n./p.o. administration, liposomes can promote interactions with mucosal surfaces and thereby aid efficient per-mucosal absorption. Very few studies have been carried out on the mechanism of liposome uptake by mucosal Peyer's patches. Sections of Peyer's patches from experimental animals have been found with M cells harbouring endocytic vesicles containing liposomes. These results indicate that intact liposomes can be endocytosed by M cells and delivered to immune cells in Peyer's patches, so that direct activation of immune cells by the liposome formulation of an immunomodulator seems feasible (Childers *et al.* 1990). The fate of liposomes in the gastrointestinal tract depends on their stability towards low pH, physiological concentrations of bile salt and levels of pancreatic lipase. Both N-L18-norAbu-GMDP and other lipids used here for the preparation of FTMLV formulated with N-L18-norAbu-GMDP, are resistant to low pH but not the action of bile acids (unsaturated phospholipids are very bile acid sensitive). This problem could be serious where hydrophilic muramyl dipeptide or its analogues (including norAbu-GMDP) are entrapped in the central aqueous cavity of FTMLVs

since any defect in lipid membrane integrity must result in rapid release of liposome encapsulated contents into the surrounding medium.

Conclusions

A liposomal preparation of hydrophobic N-L18-norAbu-GMDP was able to stimulate innate immunity in newborn kids against *Cryptosporidium* delivering a prophylactic treatment regime. Non-invasive i.n./p.o. administration is most effective and is most favourable for use in both human and veterinary medicine. Further studies on the use of immunomodulatory liposomal formulations of N-L18-norAbu-GMDP for the therapeutic treatment of cryptosporidiosis in newborn ruminants and also for the treatment of immuno-compromised patients are tasks for future research.

This work was supported by a grant the Ministry of Agriculture of the Czech Republic (Grant no. MZE 0002716201 and NAZV, Contract no: QF 3115) and Academy of Sciences (IGA AV ČR No. Z4055905). We also thank IC-Vec Ltd, UK for support.

REFERENCES

- Adam, A. and Lederer, E.** (1984). Muramylpeptides, immunomodulators, sleep factors and vitamins. *Medicinal Research Reviews* **4**, 111–152.
- Barrat, G. and Morin, C.** (1995) Liposomal immunomodulators. In *Liposomes, New Systems and New Trends in their Applications* (ed. Puisieux, F., Couvreur, P., Delattre, J. and Devissaguet, J. P.), pp. 461–506. Scientific Publications, Paris.
- Childers, N. K., Denis, F. R., McGee, N. F. and Michalek, S. M.** (1990). Ultrastructural study of liposome uptake by M cells of rat Peyer's path, an oral vaccine system for delivery of purified antigen. *Regional Immunology* **3**, 8–16.
- De Graaf, D. C., Sspano, F., Petry, F., Sagodira, S. and Bonnin, A.** (1999b). Speculation on whether a vaccine against cryptosporidiosis is a reality or fantasy. *International Journal for Parasitology* **29**, 1289–1306.
- De Graaf, D. C., Vanopdenbosch, E., Ortega-Mora, L. M., Abbassi, H. and Peeters, J. E.** (1999a). A review of the importance of cryptosporidiosis in farm animals. *International Journal for Parasitology* **29**, 1269–1287.
- Fogler, W. E. and Fidler, I. J.** (1986). The activation of tumoricidal properties in human blood monocytes by muramyl peptides requires a specific intracellular interaction. *Journal of Immunology* **136**, 2311–7.
- Hockertz, S., Franke, G., Paulini, I. and Lohmann-Matthes, M. L.** (1991). Immunotherapy of murine visceral leishmaniasis with murine recombinant interferon- γ and MTPPE encapsulated in liposomes. *Journal of Interferon Research* **11**, 177–185.
- Koudela, B. and Vítvec, J.** (1997). Experimental cryptosporidiosis in kids. *Veterinary Parasitology* **71**, 273–281.

- Krahenbuhl, J. L., Sharma, S. D., Ferraresi, R. W. and Remington, J. S.** (1981). Effects of muramyl dipeptide treatment on resistance to infection with *Toxoplasma gondii* in mice. *Infection and Immunity* **31**, 716–722.
- Ledvina, M., Zýka, D., Ježek, J., Trnka, T. and Šaman, D.** (1998). New effective synthesis of (N-acetyl- and N-stearoyl-2-amino-2-deoxy-beta-D-glucopyranosyl)-(1->4)-muramoyl-L-2-aminobutanoyl-D-isoglutamine, analogs of GMDP with immunopotentiating activity. *Collection of Czechoslovak Chemical Communications* **63**, 577–589.
- McDonald, V.** (1999). Gut intraepithelial lymphocytes and immunity to coccidia. *Parasitology Today* **15**, 483–487.
- McDonald, V.** (2000). Host cell-mediated responses to infection with *Cryptosporidium*. *Parasite Immunology* **22**, 597–604.
- O'Donoghue, P.** (1995). *Cryptosporidium* and cryptosporidiosis in man and animals. *International Journal for Parasitology* **25**, 139–195.
- Oussoren, CH. and Storm, G.** (2001). Liposomes to target the lymphatics by subcutaneous administration. *Advanced Drug Delivery Reviews* **50**, 143–156.
- Turánek, J.** (1994). Fast-protein liquid chromatography system as a tool for liposome preparation by the extrusion procedure. *Analytical Biochemistry* **218**, 352–357.
- Turánek, J., Kašná, A., Záluská, D. and Neča, J.** (2003). Preparation of sterile liposomes by the proliposome – liposome method. *Methods in Enzymology* **367**, 111–129.
- Yun, Ch-H., Estrada, A., Van Kessel, A., Gajahar, A., Redmond, M. and Laarveld, B.** (1998). Immunomodulatory effects of oat β -glucan administered intragastrically or parenterally on mice infected with *Eimeria vermiformis*. *Microbiology and Immunology* **42**, 457–465.



Metallochelating liposomes with associated lipophilised norAbuMDP as biocompatible platform for construction of vaccines with recombinant His-tagged antigens: Preparation, structural study and immune response towards rHsp90

Josef Mašek^a, Eliška Bartheldyová^a, Pavlína Turánek-Knotigová^a, Michaela Škrabalová^a, Zina Korvasová^a, Jana Plocková^a, Štěpán Koudelka^a, Petra Škodová^a, Pavel Kulich^a, Michal Křupka^b, Kateřina Zachová^b, Lýdie Czerneková^b, Milada Horynová^b, Irena Kratochvílová^c, Andrew D. Miller^d, Daniel Zýka^e, Jaroslav Michálek^f, Jana Vrbková^g, Marek Šebela^h, Miroslav Ledvina^e, Milan Raška^{b,*}, Jaroslav Turánek^{a,**}

^a Veterinary Research Institute, Brno, Czech Republic

^b Palacky University, Faculty of Medicine and Dentistry, Department of Immunology, Olomouc, Czech Republic

^c Institute of Physics, Czech Academy of Sciences, Prague, Czech Republic

^d Imperial College London, Imperial College Genetic Therapies Centre, Department of Chemistry, London, UK; King's College London, Pharmaceutical Sciences Division, London, UK

^e Institute of Organic Chemistry and Biochemistry, Czech Academy of Sciences, Prague, Czech Republic

^f University Cell Immunotherapy Center, Masaryk University, Brno

^g Palacky University, Faculty of Science, Department of Mathematical Analysis and Applications of Mathematics, Olomouc, Czech Republic

^h Palacky University, Faculty of Science, Department of Biochemistry, Olomouc, Czech Republic

ARTICLE INFO

Article history:

Received 9 October 2010

Accepted 17 January 2011

Available online 21 January 2011

Keywords:

Recombinant vaccine

Liposome

Heat shock protein Hsp90

Muramyl dipeptide

Candida albicans

ABSTRACT

Hsp90-CA is present in cell wall of *Candida* pseudohyphae or hyphae – typical pathogenic morphotype for both systemic and mucosal *Candida* infections. Heat shock protein from *Candida albicans* (hsp90-CA) is an important target for protective antibodies during disseminated candidiasis of experimental mice and human. His-tagged protein rHsp90 was prepared and used as the antigen for preparation of experimental recombinant liposomal vaccine. Nickel-chelating liposomes (the size around 100 nm, PDI ≤ 0.1) were prepared from the mixture of egg phosphatidyl choline and nickel-chelating lipid DOGS-NTA-Ni (molar ratio 95:5%) by hydration of lipid film and extrusion methods. New non-pyrogenic hydrophobised derivative of MDP (C18-O-6-norAbuMDP) was incorporated into liposomes as adjuvans. rHsp90 was attached onto the surface of metallochelating liposomes by metallochelating bond and the structure of these proteoliposomes was studied by dynamic light scattering, AF microscopy, TEM and GPC. The liposomes with surface-exposed C18-O-6-norAbuMDP were well recognised and phagocytosed by human dendritic cells *in vitro*. *In vivo* the immune response towards this experimental vaccine applied in mice (*id.*) demonstrated both TH1 and TH2 response comparable to FCA, but without any side effects. Metallochelating liposomes with lipophilic derivatives of muramyl dipeptide represent a new biocompatible platform for construction of experimental recombinant vaccines and drug-targeting systems.

© 2011 Elsevier B.V. All rights reserved.

1. Introduction

Candidiasis, the infection caused by the *Candida* species, is considered an important medical problem in both developing and developed countries. The systemic or deep form of candidiasis occurs predominantly as a consequence of some high-risk medical proce-

dures, immunosuppressive therapy, and aging. It affects organs such as the brain, liver, spleen, lungs, eyes, heart, and kidneys leading to abscesses formation and organ failure associated with mortality in approx. 50% of all cases, irrespective of the administration of intensive antifungal therapy [1]. Humoral immunity provides substantial protection against *Candida* growth [2,3]. Protective antibodies have direct candidastatic activity with no direct need for cellular help. They can act by opsonisation, neutralisation of extracellular virulence factors (proteases, immunomodulating fungal products such as polysaccharides), inhibition of the *Candida* adherence to host tissue, inhibition of yeast-to-hyphae transition, and by direct fungicidal activity [4–6]. The switch from the yeast to a hyphal morphotype is one of the most important factors of *Candida* virulence and survival. Up to now, several *Candida* specific antigens have been identified that are considered to be a target for protective antibodies. Beside surface

* Correspondence to: M. Raška, Department of Immunology, Palacky University in Olomouc, Hnevotínska 3, 772 00 Olomouc, Czech Republic. Tel.: +420 585632752.

** Correspondence to: J. Turánek, Department of Toxicology, Pharmacology and Immunotherapy, Veterinary Research Institute, Hudecova 70, 621 32 Brno, Czech Republic. Tel.: +420 5 3333 1311; fax: +420 5 4121 1229.

E-mail addresses: raskam@uob.edu (M. Raška), turanek@vri.cz (J. Turánek).

exposed β -(1,2)-mannotriose or stress mannoproteins, inner cell wall β -(1,3)-glucans, and secreted aspartyl proteinases, heat shock protein 81 kDa (Hsp90) was identified as the protective antigen [3,4,6–8]. The *C. albicans* Hsp90 protein is localized only in the cell wall of budding yeasts and hyphae but not in the cell wall of non-proliferating yeasts [9]. It is essential for the *Candida* viability [10]. Hsp90 was structurally characterised in 1995 [10]. It is functionally involved in re-folding of mitogen-activated protein kinases, enzymes essential for the cell wall synthesis and *Candida* morphogenesis. A knock-out of *Candida* MAP kinase *mkc1* causes a) a lower growth rate, b) a loss of viability during cultivation at 42 °C, and c) a decreased thickness of the cell wall and higher vulnerability to lytic enzymes [9]. Hsp90 was suggested to be a protective antigen following the detection of high levels of Hsp90-specific antibodies in sera of patients that recovered from systemic candidiasis in contrast to those which succumb [11]. These antibodies recognised Hsp90-breakdown heat-stable C' terminal fragment of 47 kDa which is released from living *Candida* cells after hydrolytic digestion of Hsp90. Hsp90 was confirmed to be a protective antigen in an animal model of disseminated candidiasis [9,12]. Due to the strong evolutionary conservation of Hsp90 sequence there are speculations about the possibility that Hsp90 administration could elicit autoimmune reaction or tolerance. Nevertheless, until now there is no direct evidence of such effects [12–14].

The advent of recombinant vaccines based on both DNA and recombinant protein antigens has recently forced researchers to consider alternative vaccine designs and deal with the low immunogenicity of constructs with a corresponding need for strong and biologically acceptable adjuvants to accompany antigenic components. For the construction of prophylactic as well as therapeutic vaccines against *Candida* we have been considering the use of metallochelation liposomes for simple coupling of His-tagged recombinant Hsp90 (rHsp90). Liposomes are potentially very useful for the construction of vaccination systems given their ready biodegradability and versatility as carriers for varieties of molecules having different physico-chemical properties (such as size, hydrophilicity, hydrophobicity, or net electrical charge). Liposomes also offer the possibility for simultaneous association or entrapment of more than one type of molecule. Of particular interest to us has been the possibility the co-association of hydrophilic or lipophilic adjuvants (e.g. monophosphoryl lipid A [MPL A], CpG oligonucleotides, muramyl dipeptide (MDP) and/or MDP analogues) with soluble or membrane protein antigens, ligands for the targeting of specific receptors on antigen-presenting cells [15]. In this way, liposomes become transformed into multifunctional platforms for vaccination that represent real multifunctional vaccination particles.

This manuscript describes the preparation of rHsp90 proteoliposomes, the study of their structure by DLS, GPC, TEM and AFM as well as *in vivo* immune responses to rHsp90 proteoliposomes or prototype rHsp90 vaccination particles that also comprise a lipophilic derivative of muramyl dipeptide (MDP) known as C-18-O6-norAbuMDP (MT03). This is the first time that such a defined synthetic adjuvant has been used to construct a recombinant protein vaccination nanoparticle.

2. Materials and methods

DiO C18 (3,3'-dioctadecyloxacarbocyanine perchlorate) was purchased from Molecular Probes (Invitrogen, Carlsbad, CA). Lipids: egg phosphatidylcholine (EPC, purity of 99%), 1,2-Dioleoyl-sn-Glycero-3-[N-(5-Amino-1-Carboxypentyl)iminodiacetic Acid] Succinyl (Nickel Salt) (DOGS-NTA-Ni), lysamine-rhodamine phosphatidylethanolamine and fluorescein phosphatidylethanolamine were purchased from Avanti Polar Lipids (Birmingham, AL). 20 nm membrane filter Anotop 10 and 0.2 μ m Anotop 10 LC were purchased from Whatman (Maidstone, UK). All chemicals, unless otherwise specified, were from Sigma (St. Louis, MO).

2.1. Synthetic MDP derivative C-18-O6-norAbuMDP (MT03)

For the incorporation into the lipid structures such as liposomes, the normuramylglycopeptide was modified by stearoyl substituent on O-6 position of the sugar part of the molecule (Fig. 1). The syntheses and the confirmation of the structures are described by Ledvina and co-workers (Ledvina M., Turánek J., Miller A.D., Hipler K., Compound (Adjuvants): PCT appl., WO 2009/11582 A2, 2009, US 12/922,663).

2.2. Preparation, purification, and characterisation of rHsp90

Full length *Hsp90* cDNA was isolated from a clinical isolate of *C. albicans* verified at the Department of Microbiology, Faculty of Medicine and Dentistry, Palacky University in Olomouc, Czech Republic as reported before [12]. The cDNA was analyzed by sequencing and BLAST analysis, which confirmed the identity with *C. albicans Hsp90* (GenBank Accession No. X81025). The recombinant Hsp90 protein (rHsp90) was expressed as a fusion protein with both N' and C'-terminal His tag in *E. coli* [12] and further purified using Ni-NTA affinity agarose column under native conditions (Qiagen, Hilden, Germany) as reported elsewhere [16]. Endotoxin was removed by successive two-phase separation with Triton X-114 as described elsewhere [16]. The entire procedure was repeated until the endotoxin level was below 0.25 EU per 1 mg of protein.

2.3. SDS-PAGE, western blot, and MALDI-TOF analyses

Protein samples were separated on 10% SDS-PAGE and stained with Coomassie Blue R-250 or blotted to PVDF membrane (BioRad, Hercules, CA) and developed with HRP-conjugated Anti-T7 (Merck, Darmstadt, Germany) diluted 1:5,000 in SuperBlock plus 0.05% Tween 20 (SB-T) followed by detection with the SuperSignalWest Pico reagents (Pierce) and by exposition on an X-ray film (Kodak, Rochester, NY). Protein identity was confirmed by peptide mass fingerprinting of SDS-PAGE-resolved rHsp90 preparation using a Microflex LRF20 MALDI-TOF mass spectrometer (Bruker Daltonik, Bremen, Germany) as described before in detail [17,18]. Protein identification from the obtained mass spectra was achieved using the Mascot search engine (Matrix Science, London,

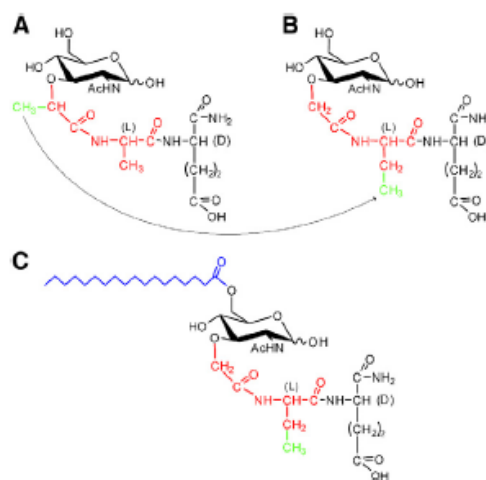


Fig. 1. Structural formula of C-18-O6-norAbuMDP (MT03) and MDP. Structural changes in the molecule of MT03 are marked in red and green. Hydrophobic accessory domain (stearoyl) is marked in blue. A) MDP; B) NorAbuMDP; C) C-18-O6-norAbuMDP.

UK; online version at <http://www.matrixscience.com>); searches were performed against UniProtKB/Swiss-Prot database (release 2010_09).

2.4. Preparation of rHsp90 proteoliposomes and their characterisation

Metallochelation liposomes were prepared by a method based on hydration of a lipid film followed by extrusion through 0.2 µm polycarbonate filters in an analogous way to that described previously by Turánek et al. [19,20]. The hand operated device Mini-Extruder (Avanti Polar lipids, USA) was used for the extrusion of small volumes of the liposome suspensions (up to 1 ml). Large volumes of the metallochelation liposome samples were extruded using a high-pressure cell (Millipore, USA) linked to an FPLC instrument (Pharmacia, Sweden) [19]. The solution of rHsp90 in PBS (rHsp90: DOGS-NTA-Ni molar ratio of 1:10; 1 mg Hsp90: 1.75 mg total lipid) was added to the prepared EPC/DOGS-NTA-Ni metallochelation liposomes. The mixture was stirred for 120 minutes. The hydrodynamic diameters of metallochelation liposomes and proteoliposomes were determined by dynamic light scattering instrument NanoSizer NS (Malvern, UK) at 25 °C using silica cuvette of 45-µl volume. The release of the bound rHsp90 from metallochelation liposomes was accomplished by the addition of EDTA to the final concentration of 1 mM. Fluorescence labelling of liposomes was accomplished by 0.5% (molar) of various fluorescence lipids (DiO C18, lysamine-rhodamine phosphatidylethanolamine or fluorescein phosphatidylethanolamine) added to lipid mixture used for preparation of liposomes.

2.5. Analyses of rHsp90 proteoliposomes by GPC and immunoblotting

The quantification of His-tagged rHsp90 attached to metallochelation liposomes was carried out by gel permeation chromatography. Non-bound protein was separated from liposome-bound using an FPLC system (Pharmacia, GE Healthcare). The separation conditions were as follows: column, Superose 6 (prep grade) filled in the Tricorn 5/200 column (Pharmacia, GE Healthcare); flowrate, 0.2 ml/min; mobile phase, PBS buffer; injected volumes, 25 µl; detection wavelength, 280 nm. Elution fractions of 0.25 ml were collected with fraction collector FRAC-100 (Pharmacia). Analyses of rHsp90 in the fractions eluted from Superose 6 column were carried out by the immunoblotting of the SDS-PAGE-separated fractions on the PVDF membrane Hybond-P (Amersham Biosciences, Buckinghamshire, UK).

2.6. Effect of protein–lipid ratio on the size of rHsp90 proteoliposomes and protein–lipid binding kinetics

rHsp90 and metallochelation liposomes were mixed at the recombinant protein to total lipid molar ratios as follows: 1:3, 1:5, 1:10, 1:20, 1:30, 1:50. After 2-h incubation, the size of proteoliposomes was measured using dynamic light scattering instrument NanoSizer NS (Malvern, UK) at 25 °C. The binding kinetics of His-tagged protein to metallochelation liposome surface were followed within 120 min immediately after mixing the metallochelation liposomes with recombinant protein at the protein to total lipid ratio of 1:10 (the ratio used for vaccination).

2.7. Characterisation of rHsp90 and rHsp90 proteoliposomes by differential scanning calorimetry

DSC measurement was performed using CSC 6100 Nano-Differential Scanning Calorimeter II (Setaram, France) with the cell volume of 0.3 ml. Prior to the injection, the samples (in PBS buffer, pH of 7.14) were extensively degassed. The protein concentration in the rHsp90 and rHsp90 proteoliposome sample was 2.1 and 0.37 mg/ml, respectively. The total lipid concentration in the liposome-bound sample was 5.19 mg/ml. Scans were run from 5 to 90 °C at the scan rate of 1 °C per minute. The reference baseline was obtained by buffer vs. buffer

scan and subtracted from the data measurement. The apparent molar heat capacity and excess molar heat capacity curves were obtained from the calorimetric profiles corrected by baseline subtraction and normalized with respect to the protein concentration.

2.8. Characterisation of rHsp90 and rHsp90 proteoliposomes by dynamic light scattering (DLS)

Thermal stabilities of the unbound and liposome-bound rHsp90 were determined over the temperature range of 4–80 °C using dynamic light scattering (DLS) technique. The stability of rHsp90 was determined at the concentration of 1 mg/ml, the stability of proteoliposomes at the protein to total lipid ratio of 1:10 in PBS buffer. The temperature gradient was set to 1 °C/2 min.

2.9. Transmission electron microscopy

The liposome structures were determined using Philips Morgagni transmission electron microscope (EM Philips 208 S, MORGAGNI software, FEI, CZ). All samples were negatively stained by 2% (w/w) ammonium molybdate (pH 6.8).

2.10. Immunogold labelling of rHsp90 proteoliposomes

Non-bound rHsp90 was separated from the proteoliposomes by gel permeation chromatography using Superose 6 column. The proteoliposome fractions were then concentrated in a centrifugation tube (cut off 30 kDa) and incubated with pooled sera from immunised mice (1:50 dilution) for 1 h at 37 °C. 10-nm colloidal gold–protein A conjugate was added. After 12-h incubation, the proteoliposomes were observed by electron microscope.

2.11. Atomic force microscopy

The topography of the metallochelation liposomes and proteoliposomes was investigated by atomic force microscopy (AFM). The AFM measurements were performed with NTEGRA Prima NT MDT system (Ireland) under ambient conditions. The tip–sample surface interaction monitored the van der Waals force between the tip and the surface; this may be either the short range repulsive force (in contact-mode) or the longer range attractive force (in non-contact mode–Tapping Mode). The AFM measurements on the metallochelation liposomes and proteoliposomes were performed using the Tapping Mode. Each sample was scanned under the soft CSG 10 type of probe. The tapping mode consisted of oscillating the cantilever at its resonance frequency (14–28 kHz) and lightly “tapping” the tip on the surface during scanning.

2.12. Interactions with human dendritic cells (DC)

2.12.1. DC cultivation

Incomplete, serum-free culture medium (CM) used for the cultivation of DC consisted of X-VIVO 10 (Cambrex, Belgium) supplemented with l-glutamine (Sigma, Germany). Cells were cultivated at 37 °C in a 5% CO₂ atmosphere. Immature monocyte-derived DCs were generated from buffy coats obtained from the Blood transfusion station in the Faculty Hospital Brno-Bohunice. At the day 0, the peripheral blood mononuclear cells (PBMC) were isolated by standard Histopaque 1077 (Sigma) gradient centrifugation. About 4.8×10^5 PBMC were suspended in 100 µl of CM and allowed to adhere to 96-well plates. After 2-h incubation at 37 °C, the nonadherent lymphocytes were removed and the adherent monocytes were grown for another 5 days in CM with 100 ng/ml of GM-CSF (Gentaur, France) and 100 ng/ml of IL-4 (Gentaur, France). The obtained immature DCs were used for further tests.

2.12.2. DC phagocytosis observed by confocal microscopy

On the day 6, Fluorescein-PE or Lissamine-rhodamine-PE-labelled metallochelation liposomes, metallochelation liposomes formulated with C-18-O6-norAbuMDP (MT03), rHsp90 proteoliposomes and rHsp90 vaccination particles formulated with MT03 at various mol% levels (final concentration of 10 µg/ml of total lipid) were added to the *in vitro*-derived DCs. After 3 h, the cells were washed once in PBS and stained with FITC or PE conjugated monoclonal antibodies (mAbs) against characteristic cell surface marker(s) CD86, CD83, HLA-DR (Immunotech, France) for 30 min at laboratory temperature, further washed in PBS and observed by the confocal scanning microscope Leica SP-2 (Leica) using the following parameters. The excitation laser was set at 488 nm (power of 20%) and the optoacoustic filter at the emission spectrum of Fluorescein-PE (505–530 nm); the excitation laser was set at 561 nm (power of 20%) and the filter at the emission spectrum of Lissamine-rhodamine-PE (575–620 nm); or the excitation laser was set at 488 nm (power of 20%), and the filter set at the emission spectrum of Phycoerythrin (605–620 nm).

2.12.3. Flow cytometry quantification of phagocytosis

DCs stained for the above described confocal microscopy analysis were phenotypically analyzed on FACS Calibur (Becton Dickinson) using CellQuest software. For the quantification of phagocytosis, DiO C18 fluorescence marker was used instead of Lissamine-rhodamine-PE and Phycoerythrin labelled monoclonal antibodies towards HLA-DR were used for DC identification.

2.12.4. Characterisation of immune responses to immunisation with rHsp90 vaccination nanoparticles prepared with C-18-O6-norAbuMDP in Mice

All experiments were performed on 6 to 8-week old female BALB/c mice (purchased from Biotest, Czech Republic). All animals were free of known pathogens at the time of the experiment. Standard pellet diet and water were given *ad libitum*. The research was conducted according to the principles enunciated in the Guide for the Care and Use of Laboratory Animals issued by the Czech Society for Laboratory Animal Science. The Ethics Committee of the Faculty of Medicine and Dentistry, Palacký University in Olomouc, Czech Republic, approved all vaccination experiments.

2.12.5. Immunisation and adjuvants

The mice were divided into 8 groups of 5 animals. The mice were immunised by *i.d.* application of two rHsp90 doses (20 µg per dose, vaccine formulated in appyrogenic PBS (phosphate buffered saline pH 7.2) in combination with different liposome and adjuvant C-18-O6-nor-AbuMDP derivative, metallochelation liposome) as indicated in Table 1 (total volume of 50 µl per dose). The interval between priming and booster was 14 days. Freund's complete and incomplete adjuvants (FCA, IFA) were used as adjuvant positive controls.

2.12.6. rHsp90-specific antibody response

Was quantified by ELISA. All assays were performed in triplicates for individual sera. Microplates (Nalge Nunc International, Rochester, NY) were coated with 1 µg/ml rHsp90. Antibodies from sera collected from tail vein blood samples were detected with horseradish peroxidase-labeled goat anti-mouse IgG + IgM + IgA (Ig*) (MP Bio-medicals, Solon, OH) and developed with O-phenylenediamine plus H₂O₂ substrate. The reaction was stopped with 1 M sulphuric acid and the absorbance was read at 490 nm. For antigen-specific ELISA, the results were expressed as the end point titer using Genesis Lite Software (Version 3.03, Life Sciences, Basingstoke, UK).

2.12.7. Cellular response

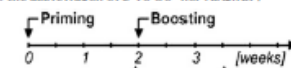
rHsp90-specific induction of INF-γ secretion was quantified by ELISPOT. The numbers of splenocytes secreting INF-γ were determined by commercially available ELISPOT kits (INFγ, IL-4, Development

Table 1

Immunisation scheme and composition of rHsp90 formulations tested.

Composition per one dose			
Vaccine designation	rHsp90	DOGS-NTA-Ni liposome	Adjuvant
rHsp90	20 µg	–	–
rHsp90 + FCA	20 µg	–	FCA 50%
rHsp90 + IFA	20 µg	–	IFA 50%
Lip-Ni-rHsp90	20 µg	35 µg	–
Lip-Ni-rHsp90 + MT03	20 µg	35 µg	MT03, 1.75 µg
rHsp90 + MT03 + IFA	20 µg	–	MT03, 1.75 µg IFA 50%
FCA	–	–	FCA 50%
IFA	–	–	IFA 50%
Lip-Ni + MT03	–	35 µg	MT03, 1.75 µg

MT03 is used as the abbreviation of C-18-O6-nor-AbuMDP.



Serum: Post prime serum sampling is indicated in gray, terminal (post boost) serum sampling together with splenocytes isolation is indicated in black.

Module, R&D Systems, Minneapolis, MN, USA) according to the manufacturer's protocols. 5×10^6 splenocytes from each mouse were seeded in separate wells (one for IFN-γ and one for IL-4 analysis). For the stimulation, depyrogenated rHsp90 was used at the final concentration of 15 µg per 1 ml RPMI 1640 supplemented with L-glutamine, 20% FCS, penicillin, and streptomycin. The numbers of cytokine-secreting cells were counted after three days of stimulation with the use of stereo microscope (Intraco Micro, Tachlovice, Czech Republic).

2.12.8. Statistics

The ELISA and ELISPOT results are expressed as arithmetic means \pm standard deviations (SD) for each group of mice. Statistical evaluation was performed using an "R project" package (<http://www.r-project.org>). The differences among end point titers were analyzed by Kruskal-Wallis nonparametric test. The differences among each group pair were statistically tested by Nemenyi test.

3. Results and discussion

3.1. Preparation, purification and characterisation of rHsp90

The molecular weight of rHsp90 protein including His tags was predicted to be 85.8 kDa by ProtParam tool (<http://www.expasy.ch>). The identity of the isolated recombinant Hsp90 was proved by SDS-PAGE and GPC. The purity determined by densitometry analysis is $\geq 95\%$. The identity of rHsp90 was confirmed by MALDI-TOF MS and subsequent database search. The band on the Coomassie Blue-stained gel was identified as *C. albicans* Hsp90 according to UniProtKB/Swiss-Prot database (accession no. P46598). Purified rHsp 90 was found to exist in monomeric and dimeric (noncovalent dimer) forms by DLS and GPC (Fig. 2) [main peak (V_r is 9.6 ml) correlates with rHsp90 monomer (MW 80.7 ± 15.4 kDa; 11.3 nm; R_h is 5.65 nm) and the smaller peak (V_r is 7.6 ml) with a dimer (MW 153.7 ± 17.6 kDa; 17.2 nm, R_h is 8.6 nm)] (Fig. 2, insert A,B), as described previously [21]. The application of GPC was used to further increase purity to $\geq 98\%$. The tendency of the purified monomeric rHsp90 to dimerise was observed regularly during protein storage in PBS buffer at 4 °C. Dimers were observed to form from monomer after 3 days of storage of monomeric rHsp90, as determined by DLS and GPC (data not shown). Moreover, we observed consistently that the presence of the His tag in rHsp90 did not abrogate the ability to form dimers and oligomers that are typically formed in response to heat shock [22,23].

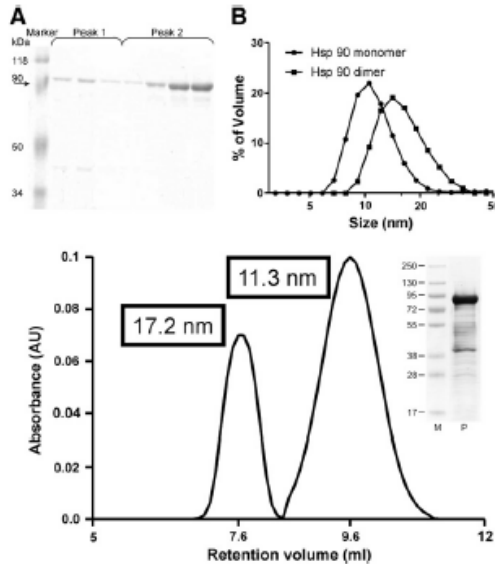


Fig. 2. DLS and GPC characterisation of rHsp90 protein. The GPC separation (Superose 12 column) of rHsp90 purified by metallochelating affinity chromatography. The monomer is baseline-separated from the dimer. Insert A – SDS-PAGE of the monomer (peak1) and the dimer (peak 2) separated by GPC. Insert B – the size of the monomer and the dimer analysed by DLS in the peaks 1 and 2. The purity of rHsp90 was $\geq 95\%$ (see SDS-PAGE insert C).

3.2. Preparation of proteoliposomes and their physical characterisation

Monodisperse metallochelation liposomes (size distribution shown in Fig. 3A) were prepared by lipid film hydration then extrusion through $0.1 \mu\text{m}$ polycarbonate filters. These liposomes (the size around 110–115 nm and polydispersity index $\text{PDI} \leq 0.1$) allowed for precise DLS measurements to be made following rHsp90 metallochelation, as demonstrated by progressive increases in R_h values. Changes in R_h values post metallochelation were found to be dependent on the His-tagged rHsp90 to total lipid mol ratio indicating formation of rHsp90 oligomers on the surface of liposomes (Fig. 3A, B). By observing R_h value changes as a function of time at fixed protein to lipid ratio (Fig. 3D), we observed that metallochelation was complete typically within 20 min. The physical association of rHsp90 with metallochelation liposomes was further confirmed independently by combination of GPC and SDS-PAGE followed by immunoblot (Fig. 3C).

Incubation of proteoliposomes in bovine serum (90% serum, 37°C , 3 h) revealed that 30% of rHsp90 in metallochelation with liposomes was retained at the end of incubation (Fig. 3C). The stability of the metallochelation bond depends on the character of particular protein or peptide as well as the local environmental conditions [24–26].

Further ultrastructural analysis of proteoliposomes was carried out by TEM. Plain metallochelation liposomes were characterised with sharp edges and no surface substructures (Fig. 4A). Monolayer of rHsp90 was observed clearly at a protein to lipid ratio of 0.025 (Fig. 4B). Immunogold staining was used to confirm that rHsp90 is present on the surface of metallochelation liposomes in a monolayer (Fig. 4D). At higher protein to lipid ratios, as illustrated (Fig. 4C, E), the existence of oligomeric rHsp90 structures was demonstrated on the surface of liposomes and these structures were also confirmed by AF microscopy (Fig. 4G). AFM technique is very sensitive to the surface

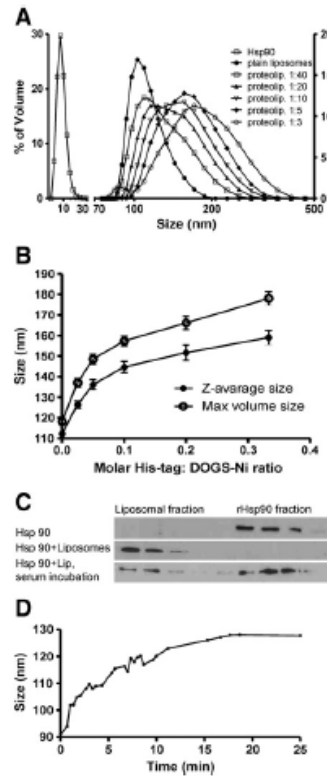


Fig. 3. Effect of rHsp90: metallochelation lipid ratio on size of rHsp90 proteoliposomes and confirmation of protein complexation by GPC. A) The effect of the protein: total lipid ratio on the size distribution of the proteoliposomes. B) The effect of the protein: liposome ratio on the size of the proteoliposomes. C) GPC and SDS-PAGE analyses of rHsp90 bound to metallochelation liposomes and the stability of resulting proteoliposomes in serum. D) Binding kinetics of rHsp90-proteoliposomes complex studied by DLS (the protein: total lipid ratio of 1:5).

structure and demonstrated extended oligomeric protein structures on the surfaces of proteoliposomes in line with our DLS observations (Fig. 3). The inclusion of non-pyrogenic muramyl dipeptide (MDP) adjuvant analogue, C-18-O6-nor-AbuMDP (MT03) (Fig. 1), into rHsp90 proteoliposomes was intended to generate prototype rHsp90 vaccination nanoparticles of the type alluded to in the introduction and illustrated (Fig. 4F).

3.3. Thermal stability of rHsp90

The DSC calorimetric profile of rHsp90 revealed two well separated irreversible sharp endothermic peaks with the maximum heat absorption at 50 and 62.9°C (Fig. 5B). The irreversibility of the first heat absorption maximum was proven by a separate experiment: at first, a heating run from 5 to 55°C revealed the first heat absorption maximum at 50°C . Then, no peak emerged at the cooling. The subsequent heating up to 90°C revealed only the second maximum at 62.9°C . rHsp90 bound onto the surface of the metallochelating liposomes showed analogical peaks whose heights were adequate to the lower concentration of the protein owing to the purification of the

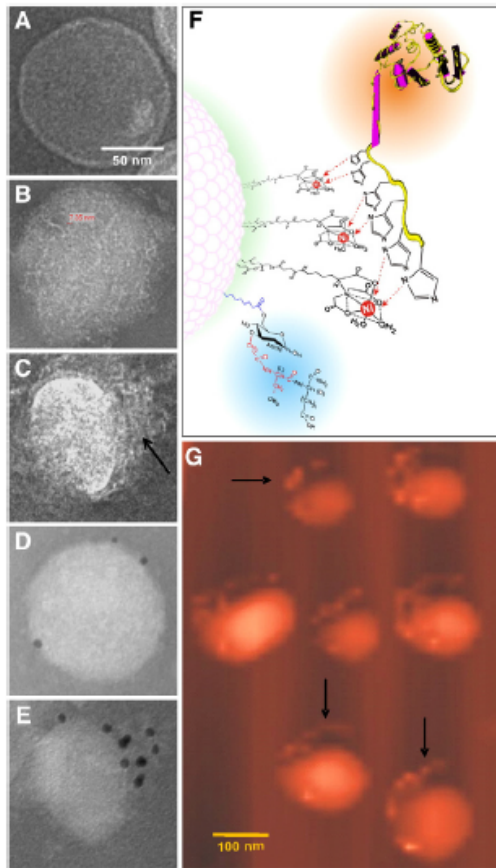


Fig. 4. Structure of metallochelation liposomes and rHsp90 proteoliposomes revealed by TEM, TEM immunogold staining and AF microscopy. A) TEM of the metallochelation liposomes; B) TEM of the rHsp90 proteoliposomes at the low protein: total lipid ratio of 1:40; C) TEM of rHsp90 proteoliposomes at the protein: total lipid ratio of 1:5, the arrow indicates rHsp90 oligomers extending from the proteoliposomal surface; D) Immunogold staining of rHsp90 bound onto the proteoliposomal surface at the protein: total lipid ratio of 1:40; E) Immunogold staining of rHsp90 bound onto the proteoliposomal surface at the protein: total lipid ratio of 1:5, the rHsp90 oligomers extending from the proteoliposome surface are clearly marked; F) schematic drawing of our prototypical recombinant protein vaccination nanoparticle based on His-Tag protein bound to a metallochelation liposome in the presence of C-18-O6-nor-AbuMDP (MT03) adjuvant; G) AF microscopy picture of the proteoliposomes at the protein: total lipid ratio of 1:5, the rHsp90 oligomers extending from the liposome surface are indicated (arrows). Barscale is valid for A–E.

proteoliposomes by GPC. The heat absorption maxima were at 48 and 62.6 °C.

The thermal transition seems to induce a rapid oligomerisation and we used the DLS method to confirm this effect of temperature. DLS revealed an increase of the size of the monomeric form during an increase of temperature, which confirmed the thermal transition between 50–60 °C accompanied by the formation of oligomeric structures (Fig. 5A). The effect of temperature on agglomeration of rHsp90-liposomes was also confirmed by DSC (Fig. 5B). We can assume that the metallochelating binding of rHsp90 did not change significantly the structure of the protein as reflected by nearly

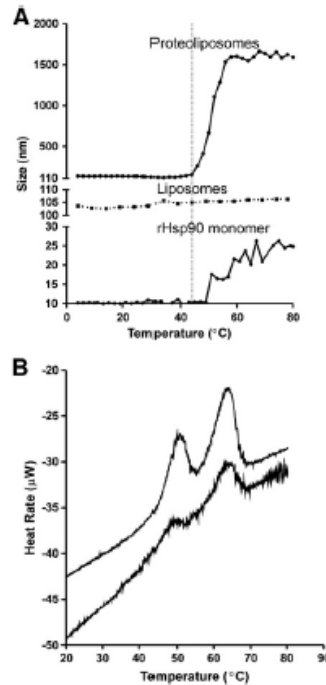


Fig. 5. DLS thermogram (A) and DSC thermogram (B) of free and liposome-bound rHsp90 A) Thermal stability of monomeric rHsp90 (low), plain metallochelating MT03 liposomes (middle), and rHsp90/MT03 proteoliposomes (upper). B) Upper curve: thermogram of free rHsp90 (the maxima of heat absorption at 50 and 62.9 °C); lower curve: thermogram of liposome bound rHsp90 (the maxima of heat absorption at 48 and 62.6 °C).

unchanged thermodynamic domains represented by two separated peaks (Fig. 5B). These data are in a good accordance with those found for mammalian Hsp90 obtained by the measurement of the effect of temperature on oligomerisation [22].

3.4. Interaction of C-18-O6-nor-AbuMDP liposomes with human dendritic cells

Metallochelation liposomes were prepared with and without 5 mol % of C-18-O6-nor-AbuMDP (MT03). In addition, rHsp90 proteoliposomes and rHsp90 vaccination nanoparticles were prepared with MT03. MT03-containing liposomes were recognised by DCs and internalized by phagocytosis about one order of magnitude more efficiently than metallochelation or proteoliposomes lacking MT03, according to flow cytometry studies (Fig. 6). The conclusions of these flow cytometry experiments were confirmed by confocal fluorescent microscopy (Fig. 6, insert).

Various markers (DIO C18, fluorescein-PE, lysamine-rhodamine-PE) were studied alone in metallochelation liposomes to exclude the possibility of any non-specific effects of fluorescent reporter ligands on phagocytosis. Thereafter, we observed that only 5 mol% MT03 liposomes were able to enter DCs purely by phagocytosis, ending up in giant lysosomes (see video in supplementary data). Similar pictures were obtained with any one out of the three possible fluorescence markers mentioned above (results not shown). Recently, the

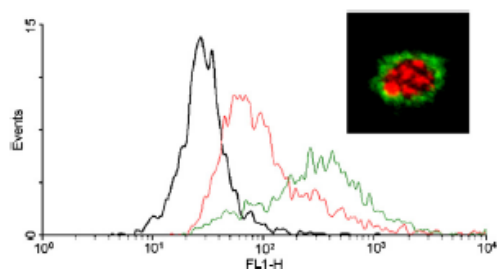


Fig. 6. Phagocytosis of rHsp90 vaccination nanoparticles studied by flow cytometry and confocal microscopy. DCs were incubated for 3 h with various liposomal preparations and the phagocytosis of DiO C18 labelled liposomes was quantified by flow cytometry. Black line – nonfluorescent metallochelation liposomes; red line – DiO C18 labelled metallochelation liposomes; green line – DiO C18 labelled metallochelation liposomes also formulated with C-18-O6-nor-AbuMDP (MT03). Inset: Confocal fluorescence microscopy picture of DC incubated with metallochelation liposomes formulated with MT03 and labelled with lissamine-rhodamine PE (E), the surface of DC was marked by monoclonal antibody against HLA-DR (fluorescein labelled – green). The giant lysosomes (red structures) containing the phagocytosed liposomes are clearly visible inside the cell.

molecular bases for MDP/MDP analogue recognition and subsequent stimulation of the host immune system have been uncovered. Myeloid immune cells (monocytes, granulocytes, neutrophils, and also DCs) possess two types of intracellular receptor for MDP/MDP analogues, namely NOD2 and Cryopyrin (inflammasome-NALP-3 complex)[27–29]. These two receptors recognise MDP/MDP analogues which represent a minimal recognition motif for bacterial cell wall peptidoglycans [28,29]. Clearly the recognition of MDP is crucial for the application of MDP analogues as adjuvants. Although the immuno-stimulatory effects of MDPs have been described for over three decades, the process of molecular recognition and binding of MDP/MDP analogues to NOD2 and cryopyrin receptors remains unclear. Within the cell, MDP/MDP analogues trigger intracellular signalling cascades that culminate in the transcriptional activation of inflammatory mediators such as the nuclear transcription factor NF- κ B. In the case of liposomal formulation of various MDP analogues, the relevant intracellular pharmacokinetics, molecular recognition and binding affinity towards NOD2 and Cryopyrin remain to be demonstrated. Such differences found for various MDP analogues are responsible for their various biological activities (e.g. pyrogenicity, ability to induce innate immune response etc.) and therefore could be utilised for precise tuning of intensity and character of immune response.

3.5. Experimental immunisation and immune response

Recombinant protein vaccination particles, such as rHsp90 vaccination particles are in our case constructed from rHsp90 binding to metallochelation liposomes that are also formulated with an adjuvant, namely MDP or lipophilised norAbu-MDP analogue. Such vaccination particles are designed to effect direct co-delivery of an adjuvant together with a selected recombinant antigen in order to induce a substantial and specific immune response. Here, we chose to test such an effect using experimental animals that were immunised with either rHsp90-vaccination particles or other rHsp90 formulations for comparison (Table 1), after which anti-Hsp90 immune responses were measured by ELISA and ELISPOT assays. The administration of rHsp90 alone was immunogenic as demonstrated by the mean value of rHsp90-specific Ig* end-point titers (IgG, IgM, and IgA isotypes) reached after the second vaccination 1:65,260 (Fig. 7A).

After administration of rHsp90 proteoliposomes that do not include adjuvant, final rHsp90 immunogenic effects were effectively doubled after the second immunisation (1:123,852). On the other hand, after administration of rHsp90-vaccination particles, final rHsp90 immunogenic effects were observed to increase by at least one order of magnitude after the second immunisation (1:904,179) compared with rHsp90 effects alone (Fig. 7A). In comparison, we observed that the immunogenic effects generated by combining rHsp90 with adjuvants such as FCA or IFA, or by combining rHsp90-proteoliposomes with IFA did not exceed the effects induced by rHsp90-vaccination particles (Fig. 7A), hence demonstrating the potency of MT03, our selected MDP analogue, as an adjuvant. In addition, where FCA was used, serious necrosis and inflammation was found typically in the skin at the site of FCA application (whether or not coupled with rHsp90 antigen protein). However, immunisations performed with the MT03 antigen induced neither necrosis nor pathologic inflammation.

Furthermore, cellular immune responses were also investigated post immunisation with a variety of rHsp90-vaccination particles (Fig. 7B). Immunisation with rHsp90 vaccination particles formulated with MDP analogue MT03 was notable for the clear induction of IFN- γ -production, although the simple combination of rHsp90 with FCA was more potent. Nevertheless, these data provide clear proof that MDP analogue MT03 is able to bias the specific cellular response toward Th1 type cytokine production. Parallel ELISPOT analyses of IL-4 secretion did not show significant differences among all groups tested (data not shown). These data are consistent in suggesting that MDP analogue MT03 is able to mount an effective adjuvant-mediated stimulation of both rHsp90-specific cellular response with Th1 cytokine secretion dominance and elicitation of rHsp90-specific antibody production. Previously, *Candida* Hsp90 has been confirmed to be a protective antigen in murine models of systemic candidiasis [9,12]. Recombinant antibody Mycograb, recognising the epitope overlapping with QQSKILKVIK peptide from *Candida* Hsp90, when combined with a lipid-formulation of amphotericin B, provided a significant clinical improvement in outcome for patients with invasive candidiasis [30]. The protective power of Hsp90-specific antibodies is probably associated with their binding to *Candida* cell wall-localized Hsp90 leading to alterations in changes in morphotype toward more resistant hyphal forms [9].

3.6. Safety of the adjuvants and metallochelating liposome vaccine

Our rHsp90 vaccination particle preparations prepared with MDP analogue MT03, and rHsp90 proteoliposomes did not exert any toxic effect in this study. This is in a good accordance with our previous experience with various animal species like mice, guinea pigs, goats, calves and pigs, which have been tested in our laboratory [31–34]. According to our experience, all synthetic lipophilic analogues of norAbuMDP as well as norAbuGMDP were non-pyrogenic in the rabbit test (Ledvina M., Turánek J., Miller A.D., Hipler K., Compound (Adjuvants): PCT appl., WO 2009/11582 A2, 2009, US 12/922,663). From a regulatory point of view induction of antibodies against HisTag epitope could raise obstacles for application of these antigens for construction of prophylactic vaccines. On the other hand antigenicity of HisTag peptide epitope is relatively weak as could be concluded from experimentally determined differences between HIV-1 p24-specific antibody titers detected in ELISA panels coated with recombinant proteins with His-tag and respective recombinant proteins devoid of His-tag whose were not higher than 15%. Here, for rHsp90 it remains to be experimentally determined.

4. Conclusion

Factors such as safety, efficiency, price, facility, and promptness of production of vaccines are the driving forces in the development of

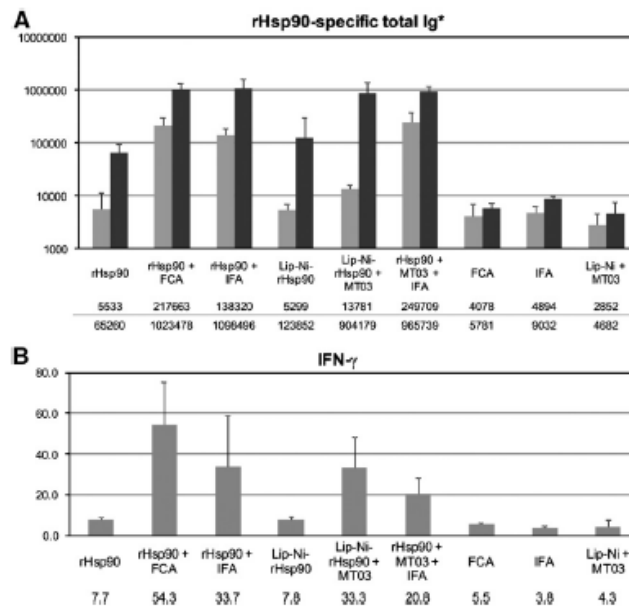


Fig. 7. Determination of rHsp90-specific antibody and cell responses elicited by rHsp90 vaccination nanoparticle immunisation. **A)** The mice were immunised by a combination of rHsp90 and adjuvants (MT03, FCA, or IFA) delivered in two i.d. doses in the form of: rHsp90 vaccination nanoparticles (prepared with MT03) (Lip-Ni-rHsp90+MT03), rHsp90 proteoliposomes (without MT03) (Lip-Ni-rHsp90) or as free soluble recombinant protein (rHsp90). Serum samples were used for the determination of rHsp90-specific antibodies titers. Means and standard deviations are shown. The end point titers measured in each group are statistically different at $p=0.05$, as determined by Kruskal-Wallis nonparametric test. **B)** Ten days after the second immunisation, splenocytes were isolated and *in vitro* stimulated by rHsp90. The production of IFN- γ was measured by ELISPOT. The numbers of IFN- γ -producing cells are statistically different at $p=0.05$, as determined by Kruskal-Wallis nonparametric test. The differences in numbers of IFN- γ -producing cells among each group pair were statistically tested by Nemenyi test which revealed statistically significant values ($p=0.05$) for group pairs: rHsp90 + FCA and Lip-Ni-rHsp90 as well as for Lip-Ni-rHsp90 + MT03 and Lip-Ni-rHsp90.

new adjuvants and delivery systems for the construction of well defined vaccines. Many studies have shown that liposomes are applicable as effective adjuvants to induce humoral and cellular immunity to a number of antigens. Metallochelation liposomes represent a new system for rapid and efficacious binding of recombinant proteins with His-tags onto their surfaces. In our opinion, the immunisation effects of prototype recombinant protein vaccination particles with MDP analogues could be further potentiated by the incorporation of various alternative synthetic immunomodulators like CpG oligonucleotides, MPL-A, or lipophilised analogues of MDP. Here, we have shown that an experimental recombinant vaccine system based on a proteoliposome core potentiated by a nonpyrogenic adjuvant such as C-18-O6-nor-AbuMDP (MT03) is able to induce the immune responses in the same order of magnitude as FCA in mice. Owing to the biodegradability and biocompatibility of liposomes and other components used for the construction of the above discussed experimental vaccine, no side effects were observed in various species. Furthermore, the advanced approaches to the investigation of the ultrastructures of metallochelation proteoliposomes can be considered of importance for the optimisation of the production and for the efficiency of such vaccines.

Supplementary materials related to this article can be found online at doi:10.1016/j.jconrel.2011.01.016.

Conflict of interest

The authors have declared that no conflict of interest exists.

Acknowledgement

This work was supported by grants: GAČR P304/10/1951; MSM 6198959223; MSMTP NPV12B06058; MZE 0002716202, KAN 200520703 AVČR and KAN 200100801.

References

- [1] M. Raska, J. Belakova, M. Krupka, E. Weigl, Candidiasis—do we need to fight or to tolerate the *Candida* fungus? *Folia Microbiol.* 52 (2007) 297–312.
- [2] A. Cassone, F. De Bernardis, A. Torosantucci, An outline of the role of anti-*Candida* antibodies within the context of passive immunization and protection from candidiasis. *Curr. Mol. Med.* 5 (2005) 377–382.
- [3] Y. Han, R.P. Morrison, J.E. Cutler, A vaccine and monoclonal antibodies that enhance mouse resistance to *Candida albicans* vaginal infection. *Infect. Immun.* 66 (1998) 5771–5776.
- [4] W. Magliani, S. Conti, S. Arseni, A. Salati, L. Ravanetti, D.I. Maffei, L. Giovanetti, L. Polonelli, Antibody-mediated protective immunity in fungal infections. *New Microbiol.* 28 (2005) 299–309.
- [5] W. Magliani, S. Conti, R. Frazzi, L. Ravanetti, D.I. Maffei, L. Polonelli, Protective antifungal yeast killer toxin-like antibodies. *Curr. Mol. Med.* 5 (2005) 443–452.
- [6] M.J. Ormaetxebarria, M.D. Moragues, N. Elguezal, A. Rodriguez-Alejandre, S. Brena, J. Schneider, L. Polonelli, J. Ponton, Antifungal and antitumor activities of a monoclonal antibody directed against a stress mannoprotein of *Candida albicans*. *Curr. Mol. Med.* 5 (2005) 393–401.
- [7] R.A. Calderone, W.A. Toná, Virulence factors of *Candida albicans*. *Trends Microbiol.* 9 (2001) 327–335.
- [8] F. De Bernardis, M. Boccacera, D. Adriani, E. Spreghini, G. Santoni, A. Cassone, Protective role of antimannan and anti-aspartyl proteinase antibodies in an experimental model of *Candida albicans* vaginitis in rats. *Infect. Immun.* 65 (1997) 3399–3405.
- [9] R.C. Matthews, J.P. Burnie, Human recombinant antibody to HSP90: a natural partner in combination therapy. *Curr. Mol. Med.* 5 (2005) 403–411.
- [10] R.K. Swoboda, G. Bertram, S. Budge, G.W. Gooday, N.A. Gow, A.J. Brown, Structure and regulation of the HSP90 gene from the pathogenic fungus *Candida albicans*. *Infect. Immun.* 63 (1995) 4506–4514.

- [11] R.C. Matthews, J.P. Burnie, Recombinant antibodies: a natural partner in combinatorial antifungal therapy, *Vaccine* 22 (2004) 865–871.
- [12] M. Raska, J. Belakova, N.K. Wudattu, L. Kafkova, K. Ruzickova, M. Sebestova, Z. Kolar, E. Weigl, Comparison of protective effect of protein and DNA vaccines hsp90 in murine model of systemic candidiasis, *Folia Microbiol.* 50 (2005) 77–82.
- [13] M. Raska, E. Weigl, Heat shock proteins in autoimmune diseases, *Biomed. Pap. Med. Fac. Univ. Palacky Olomouc Czech Repub.* 149 (2005) 243–249.
- [14] E. Weigl, P. Kopecek, M. Raska, S. Hradilova, Heat shock proteins in immune reactions, *Folia Microbiol.* 44 (1999) 561–566.
- [15] J.C. Altin, C.R. Parish, Liposomal vaccines-targeting the delivery of antigen, *Methods* 40 (2006) 39–52.
- [16] K. Zachova, M. Krupka, I. Chamrad, J. Belakova, M. Horynova, E. Weigl, M. Sebel, M. Raska, Novel modification of growth medium enables efficient *E. coli* expression and simple purification of an endotoxin-free recombinant murine hsp70 protein, *J. Microbiol. Biotechnol.* 19 (2009) 727–733.
- [17] M. Sebel, T. Stosova, J. Havlis, N. Wielsch, H. Thomas, Z. Zdrhal, A. Shevchenko, Thermostable trypsin conjugates for high-throughput proteomics: Synthesis and performance evaluation, *Proteomics* 6 (2006) 2959–2963.
- [18] T. Stosova, M. Sebel, P. Rehulka, O. Sedo, J. Havlis, Z. Zdrhal, Evaluation of the possible proteomic application of trypsin from *Streptomyces griseus*, *Anal. Biochem.* 376 (2008) 94–102.
- [19] J. Turanek, Fast-protein liquid chromatography system as a tool for liposome preparation by the extrusion procedure, *Anal. Biochem.* 218 (1994) 352–357.
- [20] J. Turanek, A. Kasna, D. Zaluska, J. Neza, Preparation of sterile liposomes by proplosome-liposome method, *Methods Enzymol.* 367 (2003) 111–125.
- [21] T. Nemoto, N. Sato, Oligomeric forms of the 90-kDa heat shock protein, *Biochem. J.* 330 (1998) 989–995.
- [22] A. Chadli, M.M. Ladjimi, E.E. Baulieu, M.G. Catelli, Heat-induced oligomerization of the molecular chaperone Hsp90. Inhibition by ATP and geldanamycin and activation by transition metal oxyanions, *J. Biol. Chem.* 274 (1999) 4133–4139.
- [23] R.S. Shapiro, P. Uppuluri, A.K. Zaas, C. Collins, H. Sern, J.R. Perfect, J. Heitman, L.F. Cowen, Hsp90 orchestrates temperature-dependent *Candida albicans* morphogenesis via Ras1-PKA signaling, *Curr. Biol.* 19 (2009) 621–629.
- [24] G.G. Chikh, W.M. Li, M.P. Schutze-Redelmeier, J.C. Meunier, M.B. Bally, Attaching histidine-tagged peptides and proteins to lipid-based carriers through use of metal-ion-chelating lipids, *Biochim. Biophys. Acta* 1567 (2002) 204–212.
- [25] R. Ruder, D. Muller, A. Fahr, R.E. Kontermann, In vitro characterization of binding and stability of single-chain Fv Ni-NTA-liposomes, *J. Drug Target.* 14 (2006) 576–582.
- [26] C.L. van Broekhoven, C.R. Parish, C. Demangel, W.J. Britton, J.G. Altin, Targeting dendritic cells with antigen-containing liposomes: a highly effective procedure for induction of antitumor immunity and for tumor immunotherapy, *Cancer Res.* 64 (2004) 4357–4365.
- [27] L. Agostini, F. Martinon, K. Burns, M.F. McDermott, P.N. Hawkins, J. Tschopp, NALP3 forms an IL-1 β -processing inflammasome with increased activity in Muckle-Wells autoinflammatory disorder, *Immunity* 20 (2004) 319–325.
- [28] S.E. Girardin, D.J. Philpott, Mini-review: the role of peptidoglycan recognition in innate immunity, *Eur. J. Immunol.* 34 (2004) 1777–1782.
- [29] C. McDonald, N. Inohara, G. Nunez, Peptidoglycan signaling in innate immunity and inflammatory disease, *J. Biol. Chem.* 280 (2005) 20177–20180.
- [30] J. Pachel, P. Svoboda, F. Jacobs, K. Vandewoude, B. van der Hoven, P. Spronk, G. Masterson, M. Malbrain, M. Acun, J. Garbino, J. Takala, L. Drgona, J. Burnie, R. Matthews, A randomized, blinded, multicenter trial of lipid-associated amphotericin B alone versus in combination with an antibody-based inhibitor of heat shock protein 90 in patients with invasive candidiasis, *Clin. Infect. Dis.* 42 (2006) 1404–1413.
- [31] P. Orsag, V. Kvardova, M. Raska, A.D. Miller, M. Ledvina, J. Turanek, Quantitative real-time PCR study on persistence of pDNA vaccine pVax-Hsp60 TMS14 in beef muscles, *Genet. Vaccin. Ther.* 6 (2008) 11.
- [32] J. Turanek, A. Kasna, B. Koudela, M. Ledvina, A.D. Miller, Stimulation of innate immunity in newborn kids against *Cryptosporidium parvum* infection-challenge by intranasal/per-oral administration of liposomal formulation of N-L18-norAbu-GMDP adjuvant, *Parasitology* 131 (2005) 601–608.
- [33] J. Turanek, M. Ledvina, A. Kasna, A. Vacek, V. Hribalova, J. Krejci, A.D. Miller, Liposomal preparations of muramyl glycopeptides as immunomodulators and adjuvants, *Vaccine* 24 (Suppl 2) (2006) 90–91.
- [34] J. Turanek, D. Zaluska, M. Hofer, A. Vacek, M. Ledvina, J. Jezek, Stimulation of haemopoiesis and protection of mice against radiation injury by synthetic analogues of muramyl dipeptide incorporated in liposomes, *Int. J. Immunopharmacol.* 19 (1997) 611–617.



Contents lists available at SciVerse ScienceDirect

Journal of Controlled Release

journal homepage: www.elsevier.com/locate/jconrel



Enhancement of immune response towards non-lipidized *Borrelia burgdorferi* recombinant OspC antigen by binding onto the surface of metallochelating nanoliposomes with entrapped lipophilic derivatives of norAbuMDP

Michal Křupka^{a,1}, Josef Mašek^{b,1}, Eliška Bartheldyová^{b,1}, Pavlína Turánek Knötigová^{b,1}, Jana Plocková^b, Zina Korvasová^b, Michaela Škrabalová^b, Štěpán Koudelka^b, Pavel Kulich^b, Kateřina Zachová^a, Lýdie Czerneková^a, Ondřej Strouhal^d, Milada Horynová^a, Marek Šebela^d, Andrew D. Miller^e, Miroslav Ledvina^c, Milan Raška^{a,*}, Jaroslav Turánek^{b,**}

^a Department of Immunology, Palacky University in Olomouc, Czech Republic

^b Department of Pharmacology, Toxicology and Immunotherapy, Veterinary Research Institute, Brno, Czech Republic

^c Institute of Organic Chemistry and Biochemistry, Czech Academy of Sciences, Prague, Czech Republic

^d Department of Biochemistry, Palacky University in Olomouc, Czech Republic

^e Imperial College Genetic Therapies Centre, Department of Chemistry, Imperial College London, London, UK; Institute of Pharmaceutical Science, King's College London, London, UK

ARTICLE INFO

Article history:

Received 5 September 2011

Accepted 18 February 2012

Available online 22 February 2012

Keywords:

Borrelia burgdorferi OspC
Metallochelating liposomes
MDP
Vaccine
nor-Abu-MDP

ABSTRACT

Lyme disease caused by spirochete *Borrelia burgdorferi sensu lato*, is a tick-borne illness. If the infection is not eliminated by the host immune system and/or antibiotics, it may further disseminate and cause severe chronic complications. The immune response to *Borrelia* is mediated by phagocytic cells and by *Borrelia*-specific complement-activating antibodies associated with Th1 cell activation. A new experimental vaccine was constructed using non-lipidized form of recombinant *B. burgdorferi* s.s. OspC protein was anchored by metallochelating bond onto the surface of nanoliposomes containing novel nonpyrogenic lipophilized norAbuMDP analogues denoted MT05 and MT06. After i.d. immunization, the experimental vaccines surpassed Alum with respect to OspC-specific titers of IgG2a, IgG2b isotypes when MT06 was used and IgG3, IgM isotypes when MT05 was used. Both adjuvants exerted a high adjuvant effect comparable or better than MDP and proved themselves as nonpyrogenic.

© 2012 Elsevier B.V. All rights reserved.

1. Introduction

Lyme disease is an infection caused by a spirochete *Borrelia burgdorferi sensu lato* vectored by the tick of the genus *Ixodes*. At least three species, namely *B. burgdorferi sensu stricto*, *B. afzelii*, and *B. garinii* are pathogenic for human [1]. The initial stage of Lyme disease characterized by non-specific flu-like symptoms is commonly associated with skin rash occurring within few weeks after the tick bites. If the infection is not eliminated by the host immune system and/or antibiotic treatment, it may further disseminate and affect the central nervous system and, rarely, heart. Symptoms of this secondary stage may vary and may disappear after days or months. The late, persistent infection may develop months to years after the initial infection and commonly affects nervous system,

skin, and joints. The antibiotic therapy of the late stage usually shows slow response with uncertain outcome. Relatively low effectiveness of available therapy emphasizes the need for alternative approaches such as preventive immunization, mainly in the endemic areas [1,2].

The immune response to *Borrelia* involves non-specific activity of complement, phagocytic cells, and *Borrelia*-specific Th1 lymphocytes-dependent response leading to production of complement-activating antibodies, in mouse presented mostly by IgG2a (IgG2b) [3]. During natural infection, nevertheless, *Borrelia* and tick saliva modulate the immune response toward non-protective Th2 type response, associated with production of neutralizing, poorly opsonizing *Borrelia*-specific antibodies [4]. *Borrelia* surface antigens OspA and OspC are among the most promising antigens tested for elicitation of opsonizing, phagocytosis-facilitating antibodies. OspC is expressed during the transfer and the initial stage of infection. In this case, the vaccine-induced immune memory has enough time to initiate a production of opsonizing antibodies preventing *Borrelia* spreading [5].

Recombinant naturally lipidized OspC antigen is difficult to express and isolate in the quantities and purity sufficient to immunize experimental animals. In contrast, non-lipidized recombinant OspC that is easy to produce and isolate exhibits poor immunogenicity

* Correspondence to: M. Raška, Department of Immunology, Palacky University Olomouc, Hnevotínská 3, 772 00 Olomouc, Czech Republic. Tel.: +420 585 63 27 52.

** Correspondence to: J. Turánek, Department of Toxicology, Pharmacology and Immunotherapy, Veterinary Research Institute, Hudcova 70, 620 00 Brno, Czech Republic. Tel.: +420 533 33 13 11.

E-mail addresses: raskam@uob.edu (M. Raška), turanek@vri.cz (J. Turánek).

¹ The first four authors equally contributed to this work.

and the elicitation of OspC-specific opsonizing antibodies requires co-application of Th1-response-inducing adjuvants including immunostimulators, microparticulate carriers, and emulsions or their combination.

Liposomes represent almost ideal carrier system for the preparation of synthetic vaccines due to their biodegradability and versatility for the incorporation of molecules exhibiting different physico-chemical properties such as the size of the molecule, hydrophilicity or hydrophobicity, or the electric charge. Due to the amphipathic character of liposomes, it is possible to encapsulate simultaneously different immunopotentiating compounds: hydrophilized/lipophilized adjuvants (e.g. monophosphoryl lipid A, CpG oligonucleotides, muramyl dipeptide and its analogues), soluble or membrane protein antigens, and ligands for the targeting of specific receptors on the antigen-presenting cells. Further, it is possible to coat the liposomes with mucoadhesive biopolymers and modify the liposome-surface with charged compounds (e.g., cationic lipids) [6]. Several papers report the implementation of metallochelating lipids that allow attaching recombinant proteins or synthetic peptides with His-Tag anchor (short peptide consisting of 4 to 6 molecules of histidine). Both the reversible character and the high affinity of the metallo-chelating bonds allow the formation of self-assembling supra-molecular structures that are the principal constituents of the experimental vaccines [7–9].

A successful development of a recombinant vaccine is based on the feasibility to produce a recombinant protein antigen in a large-scale. Also the availability of an efficient and safe adjuvant system for recombinant antigens is a very important factor because recombinant antigens are generally weak immunogens. In this paper we demonstrated an exceptionally high yield of the OspC antigen in its non-lipidized form derived from recombinant *B. burgdorferi* s.s. OspC protein (rOspC) expressed in *E. coli*. We also demonstrated that a novel adjuvant system based on metallochelating liposomes and lipophilic non-pyrogenic muramyl-dipeptide analogues, norAbuMDP, induced a high level of OspC-specific antibodies of IgG2a and IgG2b isotypes that are promising effectors of the protective immunity against *Borrelia* transmission to a host.

The preparation, characterization and *in vivo* effect of such a novel vaccine are reported in this study.

2. Materials and methods

2.1. General

Egg phosphatidylcholine (EPC, 99% purity), 1,2-dioleoyl-sn-glycero-3-phosphoethanolamine-N-(lissamine rhodamine B sulfonyl) (LysRho PE), and 1,2-dioleoyl-sn-glycero-3-[N-(5-amino-1-carboxypentyl)iminodiacetic acid]succinyl(nickel Salt) (DOGS-NTA-Ni) lipids were purchased from Avanti Polar Lipids (Birmingham, AL). 3,3'-diocetadecyloxycarbocyanine perchlorate (DiOC₁₈) was purchased from Molecular Probes (Invitrogen, Carlsbad, CA). 20 nm membrane filter Anotop 10 and 0.2 µm Anotop 10 LC were purchased from Whatman (Maidstone, UK). All other chemicals, unless specially specified, were from Sigma (St. Louis, MO).

2.2. Preparation and purification of non-lipidized recombinant OspC

Borrelia burgdorferi s.s. OspC cDNA (GenBank Acc. No. EF537426) lacking the first 54 nucleotides (coding for the first 18 amino acids serving as a lipidization signal) was amplified by the PCR using downstream primer (CACCATGTGTAATAATTCAGGGAAAGATGGG), upstream primer (AGGTTTTTTGGACTTCTGCC) and Phusion DNA polymerase (New England Biolabs, Ipswich, MA) and cloned into *E. coli* expression plasmid vector pET101 (Invitrogen) allowing expression of truncated OspC as a fusion protein containing C' terminal His tag, abbreviated further as rOspC. Protein was purified under native conditions using the Ni-NTA agarose according to the manufacturer's

instruction using the modifications of recommended buffers (Qiagen, Hilden, Germany) as follows: lysis buffer (50 mM Tris; 300 mM NaCl; 10 mM Imidazole; 0.5 mg/ml Hen egg white lysozyme; 0.1% Triton X-100; protease inhibitors: 0.2 mM PMSF; 0.4 µg/ml Leupeptin; 0.5 µg/ml Aprotinin; pH 8.0), wash buffer (50 mM Tris; 300 mM NaCl; 20 mM Imidazole; protease inhibitors as described above; pH 8.0), elution buffer (50 mM Tris; 300 mM NaCl; 500 mM Imidazole; pH 8.0). The purified protein was subsequently dialyzed against storage buffer (150 mM NaCl, 50 mM Tris, pH 7.5).

Endotoxin was removed by successive two-phase separation with Triton X-114 as described elsewhere [10]. The entire procedure was repeated until the endotoxin level was below 0.25 EU per 1 mg of protein, measured by the gel-dot assay using Limulus Amebocyte Lysate (Associates of Cape Cod, USA).

2.3. Characterization of rOspC by SDS-PAGE and MALDI-TOF MS

To determine a purity, rOspC preparation was separated on 10% SDS-PAGE and stained with Coomassie Brilliant Blue (CBB) R-250. Protein identity was confirmed by MALDI-TOF mass spectrometry as described elsewhere [11,12]. Protein identification from the obtained mass spectra was achieved using the program MascotServer 2.2 (Matrix Science, London, UK); searches were performed against a non-redundant protein database (NCBI nr; downloaded from ftp://ftp.ncbi.nih.gov/blast/db/FASTA in January 2010). As variables, oxidation of methionine and carbamidomethylation of cysteine plus one miscleavage were chosen for all searches performed without taxonomic restriction; a mass tolerance of 100 ppm was allowed.

2.4. Characterization of rOspC by differential scanning calorimetry (DSC)

DSC measurement was performed using a CSC 6100 Nano-Differential Scanning Calorimeter II (Setaram, France) with cell volume of 0.3 ml. Prior to injection, the protein sample (in PBS buffer, pH of 7.33, 0.53 mg/ml) was extensively degassed. The scan ran from 5 to 80 °C at the scan rate of 1 °C per min.

2.5. Preparation of proteoliposomes and their characterization by dynamic light scattering

Liposomes were prepared by a method based on a hydration of a lipid film followed by extrusion through 0.2 µm polycarbonate filters similarly to the procedure described previously [13,14]. A manually operated device Mini-Extruder (Avanti Polar Lipids) was used for the extrusion of small volumes of liposomes (up to 1 ml). Large volumes of liposomes were extruded by means of a high-pressure cell (Millipore, Billerica, MA) linked up to a FPLC instrument (Pharmacia, Uppsala, Sweden) [13]. The solution of rOspC in PBS was added to the prepared EPC/POPG/DOGS-NTA-Ni liposomes (EPC:POPG:DOGS-NTA-Ni of 76:19:5 mol%; DOGS-NTA-Ni lipid:rOspC molar ratio of 11:1; 7.4 mg total lipid:1 mg rOspC). The mixture was stirred for 20 min. The hydrodynamic diameters of the liposomes and proteoliposomes were determined by dynamic light scattering (DLS) on an instrument NanoSizer NS (Malvern, UK) at 25 °C. A silica cuvette of 45-µl volume (Hellma, Mullheim, Germany) was used. The release of the bound rOspC from the liposomes was accomplished by the addition of EDTA (in a final concentration of 1 mM).

2.6. Analyses of rOspC proteoliposomes by gel permeation chromatography and immunoblotting

Quantification of rOspC attached to the DOGS-NTA-Ni liposomes was carried out by gel permeation chromatography (GPC). The fraction of non-bound protein was separated from the liposomal one using the FPLC system. The separation conditions were as follows: column, Superose 6 (prep grade) filled in Tricorn 5/200 column

(Pharmacia, GE Healthcare); flow rate, 0.2 ml/min; mobile phase, PBS buffer; injected volumes, 25 µl; detection wavelength, 280 nm. Elution fractions of 0.25 ml were collected with a fraction collector FRAC-100 (Pharmacia). Analyses of rOspC in the fractions eluted from the Superose 6 column were carried out by the immunoblotting of SDS-PAGE separated fractions on the PVDF membrane Hybond-P (Amersham Biosciences, Buckinghamshire, UK).

2.7. Transmission electron microscopy (TEM)

The liposome structure was determined using FEI-Philips Morgagni 2085 transmission electron microscope (FEI Inc., Brno, Czech Republic). All samples were negatively stained by 2% (w/w) ammonium molybdate (pH 6.8).

2.8. Immunogold labeling of OspC proteoliposomes

Non-bound rOspC was separated from the proteoliposomes by gel permeation chromatography using Superose 6 column. The fraction of proteoliposomes was concentrated in a centrifugation tube (30 kDa cut off) and incubated with polyclonal rOspC antibody for 1 h, 37 °C. 10-nm colloidal gold protein A conjugate was added. After 12-h incubation, proteoliposomes were observed by electron microscope.

2.9. Synthetic nor-AbuMDP analogues

For the preparation of normuramyl glycopeptides that are modified on carboxy terminus of the peptide part of the molecule by bulky acyl substituents (Fig. 1), the solid phase synthesis was employed. The syntheses and confirmation of the structures are described by Ledvina and co-workers (Ledvina M., Turánek J., Miller A.D., Hipler K., Compound (Adjuvants): PCT appl, WO 2009/11582 A2, 2009). Based on preliminary experiments, the derivatives MT05 and MT06 were selected for this study from the series of lipophilic nor-AbuMDP derivatives modified by various lipophilic functions at sugar or peptide part of the molecule.

2.10. Experimental animals

All experiments were performed on 6 to 8-week old female BALB/c mice (purchased from Biotest, Czech Republic). All animals were free of known pathogens at the time of the experiment. Standard pellet diet and water were given *ad libitum*. The research was conducted according to the principles enunciated in the Guide for the Care and Use of Laboratory Animals issued by the Czech Society for Laboratory Animal Science. The vaccination experiments were approved by the Ethics Committee of the Faculty of Medicine and Dentistry, Palacky University Olomouc, Czech Republic.

2.11. Berlin test for toxicity of various vaccine formulations

The potential toxic effects of liposomal carrier and adjuvants were tested on the mice Balb/c (20–22 g). Doses containing 200, 100, 50, and 10 µg (10, 5, 2.5, and 0.5 mg/kg) of particular MDP analogues were administered s.c. The Berlin test was used as a method for the evaluation of toxic effects. Typical symptoms of toxicity were scored for the individual mouse immediately after the application of the drugs or within the following ten days. The site of application was monitored daily to notice any possible adverse effect like swelling, necrosis, ulceration or changes in hair quality.

2.12. Test of pyrogenicity

Standard pyrogenicity test on rabbits was used to prove safety of liposomal adjuvants. The test was carried out in the authorized

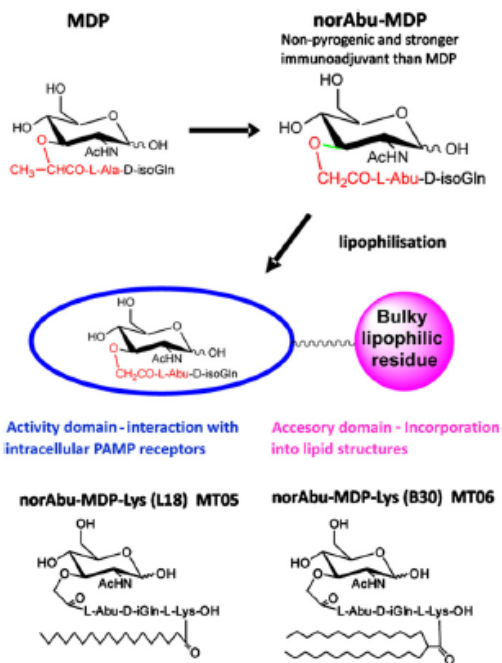


Fig. 1. Transformation of MDP structure into nor-AbuMDP and its lipophilic derivatives. The combination of structural modifications both in the saccharide and peptide moiety of MDP molecule leads to significant suppression or elimination of pyrogenicity and potentiation of immune-stimulatory activity. The substitution of muramic acid with normuramic acid and alanine with L-2-aminobutyric acid has led to suppression of pyrogenicity. Lipidization of norAbuMDP by hydrophobic ligands like stearyl or B30 improves incorporation into lipid membranes of liposomes.

laboratory ITTEST Plus s.r.o. (Bílá Vchýňnice 10, 533 13 Vápnou u Pířelouče, Czech Republic) according to the Czech Pharmacopoeia 2005 based on Ph.Eur. edition 4. Rabbits (New Zealand albino, 4–6 kg, 3 animals per group) were used for the testing. Liposomal preparations of a tested compound were applied by s.c. route (100 nmol/kg of an active compound). Empty liposomes were used as a negative control and a liposome as well as free form of muramyl dipeptide (MDP) (25 µg/kg and 50.7 nmol/kg, respectively) served as a positive control. The temperature was monitored after 1, 2, 3, 4, 6, and 24 h and a skin reaction at the application site was evaluated up to 14 days post application. A preparation was evaluated as nonpyrogenic, if the sum of + ΔT_{max} < 1.1 °C calculated for 3 rabbits per group. ΔT_{max} represents a maximum increase of measured temperature during the observation period for each animal.

2.13. Immunization of mice

All mice were immunized by *id.* application of the rOspC formulation by repeated (priming, one boosting) application of the same formulation per group as indicated in Table 1 and Fig. 2.

2.14. Adjuvants

Freund's Complete Adjuvant (FCA) and aluminium hydroxide (Biovet, Ivanovice na Hané, Czech Republic) were used as positive controls. The antigen formulation was prepared according to manufacturer's instructions. The FCA formulation was prepared by mixing

Table 1
Doses and vaccine formulations.

Groups of 5 mice	Composition per one dose (50 µl)		
	rOspC	AlOH	Liposome (total lipid µg)
rOspC	20 µg	–	–
Lip-Ni-rOspC	20 µg	–	148 µg
rOspC+ AlOH	20 µg	12.5 µl	–
rOspC+ FCA	20 µg	–	–
Lip-Ni-rOspC+ MDP	20 µg	–	148 µg
Lip-Ni-rOspC+ MT05	20 µg	–	148 µg
Lip-Ni-rOspC+ MT06	20 µg	–	148 µg
Control	–	–	–

the antigen with FCA (50/50 v/v), the Alum formulation was prepared by mixing the antigen with Alum (75/25 v/v), MDP, MT05 and MT 06 were added in equimolar amounts, 9.3 nmol per dose. The liposomal formulations contained EPC/POPG/DOGS-NTA-Ni (76/19/5 mol %) or EPC/POPG/DOGS-NTA-Ni/MDP or MT05/06 adjuvants (71/19/5/5 mol %). The doses of antigen are summarized in Table 1.

2.15. Antibody titres – estimation by ELISA

All assays were performed in triplicates. Microplates (Nalge Nunc International, Rochester, NY) were coated with 1 µg/ml rOspC. Antibodies in the sera collected from tail vein blood samples were detected with a horseradish peroxidase-labelled goat anti-mouse IgG+IgM+IgA (Ig total), goat anti-mouse IgG1 (MP Biomedicals, Solon, OH), goat anti-mouse IgG2a (Bethyl laboratories, Montgomery, TX), rabbit anti-mouse IgG2b (MP Biomedicals), or goat anti-mouse IgG3 (Bethyl Laboratories) and developed with O-phenylenediamine plus H₂O₂ substrate. The reaction was stopped by 1 M sulphuric acid and the absorbance was read at 490 nm. For antigen-specific ELISA, the results were expressed as the end point titre using Genesis Lite Software (Version 3.03, Life Sciences, Basingstoke, UK).

3. Results and discussion

3.1. Removal of the lipidization signal from OspC leads to a high yield and purity of rOspC preparation

OspC is one of the most promising protective antigens. Nevertheless, the full-length OspC is difficult to prepare in a high yield and purity as a recombinant protein. In our experiments, the removal of N' terminal lipidization signal was associated with an increase of the yield and purity of the recombinant protein. However, as demonstrated also for other *Borrelia* lipoproteins, it results in a decrease in immunogenicity [15–18]. The rOspC was expressed in *E. coli* and isolated under native conditions using Ni-NTA affinity chromatography. After 4 cycles of Triton X114 phase extraction of the endotoxin, its content was lower than 2.5 EU/mg rOspC. The yield of purified rOspC was determined to be 28 mg per 1 L of the bacterial culture. The purity of rOspC preparation was determined to be 93% by densitometry after SDS-PAGE (Fig. 3).

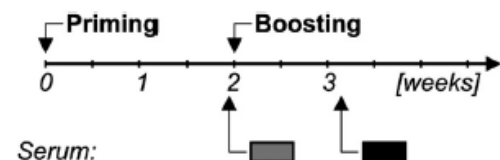


Fig. 2 Vaccination schedule. Time schedule used for vaccination of experimental mice. Serum samples were collected before the first immunization and subsequently at the indicated time points. Doses are shown in Table 1.

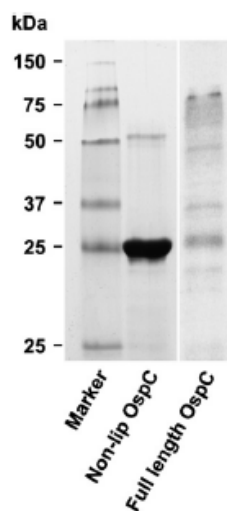


Fig. 3 SDS-PAGE analysis of recombinant OspC proteins. Non-lipidized His-Tagged OspC (rOspC) and full-length lipidized recombinant OspC (lipidized OspC) were separated by SDS-PAGE. The purity of the isolated rOspC was estimated by comparison of the band corresponding to rOspC protein with all bands in a respective separation line.

The identity of rOspC was confirmed by MALDI-TOF MS and subsequent database search. The band on the Coomassie-Blue-stained gel (Fig. 3) was identified as *B. burgdorferi* OspC. The sample could most likely be assigned to the accession number gi|21262258 in the NCBI nr database (Swiss-Prot accession number Q932W2). The parameters of the identification were as follows: 12 peptides identified, sequence coverage was 71% and probability-based MOWSE score was 146. The expectation number was $2.6e-08$ confirming unambiguous identification. As expected, no lipidization of the protein was registered. Further, we compared the purity and yield of the above described rOspC with full-length recombinant OspC (lipidized OspC) expressed under the same growing conditions as published before [19]. The yield of full-length recombinant OspC was 4 mg per 1 L of a culture and the purity reached 21% of total protein (Fig. 3). The removal of the lipidization signal substantially increases both the yield and purity of the isolated rOspC protein.

3.2. Characterization of rOspC by differential scanning calorimetry (DSC) and DLS

DSC measurement of the calorimetric profile revealed an irreversible sharp endothermic peak with the maximum heat absorption at 46.2 °C. The low T_c of rOspC indicates that the protein is relatively heat-labile. The size of the protein was determined to be 3.7 nm by DLS (hydrodynamic radius R_h of 1.85 nm) (Fig. 4). That value is in a good accordance with the projection of the protein observed by TEM (Fig. 5A).

3.3. Structure and stability of metallochelating proteoliposomes

Further, the rOspC was linked to metallochelating liposomes under condition described in Materials and methods. Binding of rOspC onto the surface of liposomes was proved by an increase of R_h as assayed by DLS. In comparison with plain liposomes, the R_h of rOspC metallochelating liposomes was about 2.75 nm higher (Fig. 4). This data is in

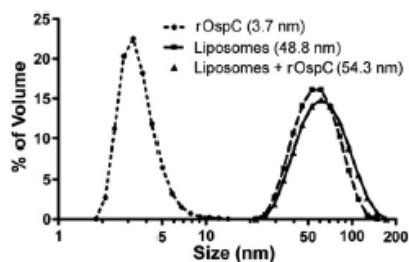


Fig. 4. Size distribution and hydrodynamic diameter of rOspC, plain metalochelating liposomes and rOspC proteoliposomes analyzed by DLS. The size distribution of parent monodispersed metalochelating liposomes (dashed line) was compared with that of rOspC proteoliposomes (full line). As a reference, the size distribution of rOspC (dotted line) is shown. Numbers in brackets represent mean hydrodynamic diameters of the particles.

a good agreement with $2R_0$ of OspC (3.7 nm). DLS proved itself a useful technique for the study of protein binding onto the metalochelating liposomes in the aqueous milieu, i.e. in the native state. Based on their size increase, the proteoliposomes were well distinguished from the plain liposomes, although the difference was only 5.5 nm. Considering the case of a homogenous coating of the liposomes by rOspC, the theoretical size increase would be about 7.4 nm. The lower increase observed (5.5 nm) indicates that the coating of the liposomal surface by the protein is incomplete and this is in a good accordance with the structure revealed by TEM (compare Figs. 4 and 5).

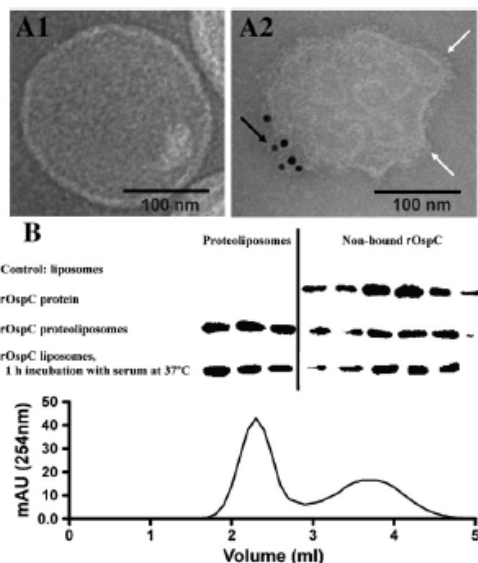


Fig. 5. Structure and stability of rOspC proteoliposomes. A1) Structure of a plain metalochelating liposome as obtained by TEM. A2) Structure of metalochelating liposome with rOspC bound onto the surface (white arrows – rOspC; black arrow – rOspC marked by 10-nm immunogold particles). B) Stability analysis of rOspC proteoliposomes by GPC. Non-bound rOspC was separated from the proteoliposomes by GPC using Superose 6 column. rOspC was detected in various fractions from GPC by immunoblotting. rOspC GPC elution profile is correlated with immunoblotting assay.

As determined by TEM, the binding of individual molecules of rOspC protein onto the liposomal surface is clearly visible on the rim of the liposome and the immunogold staining confirmed the identity of rOspC molecules as well as the preservation of the epitopes recognized by the polyclonal immuno-gold-labelled antibodies (Fig. 5A). Moreover, the TEM micrograph revealed an interesting organization of the bound rOspC into bead-like structures. This observation suggests that the conception of the proteoliposomal structures with randomly distributed protein molecules on the liposomal surface is just a simplification. It seems that different patterns of surface protein distribution could be observed, according to the nature of the protein and resulting protein–liposome and protein–protein interactions. In fact, using TEM and atomic force microscopy, we observed that some proteins can form higher structures like 2D crystal domains on the liposomal surface, as found for HIV-1 derived recombinant gp120, or hair-like structures formed by recombinant HSP90 [7,20].

OspC is an important factor of the virulence of *Borrelia burgdorferi*. It is expressed during and soon after invading the host, so it could be of interest to study whether these bead-like structures of OspC are also formed on bacteria surface during the invasion of the host and whether they are of biological relevance.

Binding of rOspC onto metalochelating liposomes was confirmed by GPC used as an independent method. The liposomal fraction was separated from free protein and rOspC was assayed using SDS PAGE followed by immunoblotting. The vast majority of rOspC was shown to be bound onto liposomes and was only slightly ripped from their surface by shearing forces taking place during passing through the GPC column (Fig. 5B). The tailing character of the rOspC elution profile supports this explanation. The stability of the metalochelating bond in biological fluids was determined by the exposition of rOspC liposomes to human serum. After a 1-h incubation at 37 °C, more than 60% of rOspC was associated with liposomes. Therefore, the half-life of rOspC proteoliposomes in serum was estimated to be at least 1 h. An increased stability of surface-exposed antigens on the liposomes can be achieved by chemical binding onto the outer liposomal surface that is appropriately functionalized. With respect to a potential application for the construction of vaccines, the question of *in vitro* and especially *in vivo* stability is of great importance. The stability of metalochelating bond depends on the character of the attached antigen, metal ions used, physico-chemical character of the metalochelating lipids, and their surface density on the particles. For example, it was shown that Ni-NTA3-DTDA liposomes with single-chain Fv fragments (anti CD11c) bound onto the liposomal surface were able to target dendritic cells *in vivo*. The application of the three-functional chelating lipid Ni-NTA3-DTDA probably endows the metalochelating bond with a higher *in vivo* stability [21] but this improved stability does not result in a higher immunogenicity [22]. There are only few references reporting the metalochelating bond implemented in the construction of supramolecular structures as vaccine carriers [7–9,23].

3.4. Immunization experiments

rOspC proteoliposomes were modified by addition of several adjuvants and used for immunization of experimental mice as detailed in Table 1 and Fig. 2. Immunization with rOspC itself did not elicit detectable OspC-specific antibodies of IgG, IgM, and IgA isotypes (Ig total) (Fig. 6A). Similarly, immunization with rOspC proteoliposomes (Lip-Ni-rOspC) induced only a negligible increase of OspC-specific total Ig after the second immunization (Fig. 6A). In contrast, immunization with rOspC plus adjuvants FCA or AIOH, or immunization with rOspC proteoliposomes (Lip-Ni-rOspC) plus MDP or norAbu-MDP-Lys derivatives MT05 or MT06 (see Fig. 1) elicited strong OspC-specific antibody responses (Fig. 6A). The contributions of particular IgG isotypes for the immune response showed differences among various adjuvants used (Fig. 6B) (FCA was not tested for the

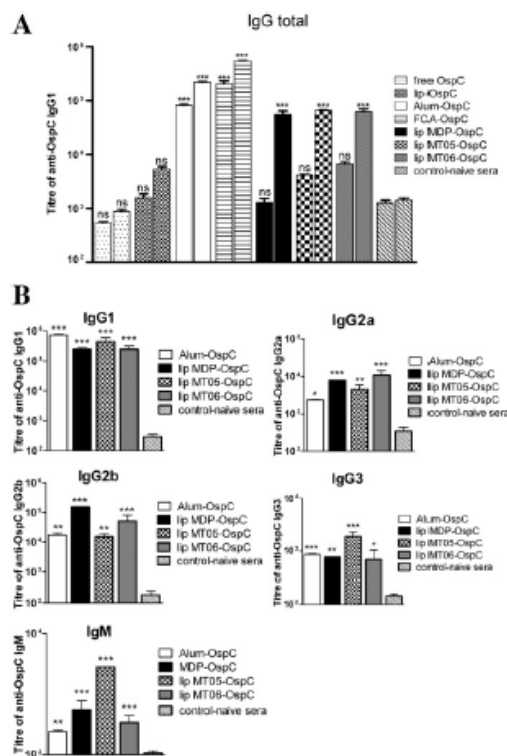


Fig. 6. ELISA analyses of specific antibody titres in sera of immunized mice. Mice (5 per group) were immunized by i.d. application of various liposome-adjvant formulations of rOspC according to the time schedule indicated in Fig. 1. Pooled sera from each group were used for ELISA analysis of the OspC-specific antibodies titres. Naive sera were obtained before immunization. ELISA plates were coated with 100 μ l of recombinant OspC (1 μ g/ml), incubated with serially diluted pooled sera obtained at the time of booster (left column in the pair) and 14 days later (right column in the pair) and developed with antimouse IgG + IgM + IgA (Ig total) **A**. To determine the OspC-specific Ig isotype titres, only the sera obtained 14 days after booster were used, and developed in ELISA under the same 12 conditions with secondary antibodies anti-mouse IgG2a, anti-mouse IgG2b, anti-mouse IgG3, or anti-mouse IgM B, and for both **A** and **B** after addition of OPD plus H_2O_2 , the absorbance was read at 490 nm on ELISA reader. The results are expressed as the end point titres using Genesis Lite Software (Version 3.03, Life Sciences, Basingstoke, UK) \pm SD. * $p > 0.05$; ** $p > 0.01$; *** $p > 0.001$.

IgG isotype response). Although AIOH adjuvant induced strong OspC-specific antibody responses in total immunoglobulin level (Ig total) and IgG1 isotype, the response in complement-activating IgG isotypes (IgG2a and IgG2b) was only modest. In comparison with AIOH, the synthetic adjuvant MT06 when combined with rOspC proteoliposomes induced a strong OspC-specific response in isotypes IgG2a and a lower one in IgG2b (Fig. 6B). The application of another synthetic adjuvant MT05 was associated with dominance of OspC-specific IgG3 and IgM isotypes (Fig. 6B). Furthermore, we compared responses to synthetic norAbuMDP adjuvants with the response to rOspC proteoliposomes plus MDP. The latter one elicits the strongest OspC-specific antibody response in IgG2b and a little bit lower one in IgG2a isotypes (Fig. 6B).

Borrelia-specific immunoglobulins act both in complement-dependent and complement-independent manner. In mice, complement-activating antibodies are of IgG2a and IgG2b isotypes. The availability of an immunization system which could simply change the isotype of the elicited antigen-specific immunoglobulin provides an advantage for further vaccine development. Here, we reported that the combination of rOspC proteoliposomes with MT05 or MT06 adjuvants induced dramatic changes in OspC-specific antibodies of isotypes – IgG2a and IgG2b dominating after MT06 adjuvant application whereas IgM dominated after MT05 application. The observed capacity of novel MT05 and MT06 adjuvants

in combination with rOspC proteoliposomes to change the isotype of OspC-specific antibodies is in contrast to the immunization experiments reported by other groups. They observed an induction of OspC-specific antibodies predominantly of IgM or IgG1 isotypes [21,23,24,26].

3.5. MDP analogues as adjuvants

Some lipophilic derivatives of MDP like B30-MDP and MDP-Lys (L18) were synthesized and tested as adjuvants for recombinant hepatitis B surface antigen [27] or influenza surface antigens hemagglutinin and neuraminidase [28]. We used new synthetic nonpyrogenic lipophilic analogues of norAbuMDP modified at a peptide part by two different hydrophobic ligands (Fig. 1). For the first time, these defined synthetic molecules were used in combination with metallochelating liposomes to construct an experimental recombinant vaccine. The important finding was that both MT06 and MT05 adjuvants exerted a high adjuvant effect comparable or better than MDP but proved itself as nonpyrogenic (rabbit pyrogenicity test) and safe. While alum induced a stronger antibody response in IgG1 subtype, both MT06 derivative and liposome-MDP induced a stronger immune response in both IgG2 subtypes. Interestingly, in comparison with MT06, the analogue MT05 induced a stronger response in IgG1 and IgG3 subclasses and IgM subtype. This interesting finding points out

the effect of lipophilic residues, which could not be supposed as the only accessory part of the molecule but can significantly affect the quality of the immune response. The position (peptide or sugar part) and the character (hydrophobicity and bulkiness) of the lipophilic function can affect the interaction with appropriate receptors as well as the metabolic degradation of the molecule. This aspect has not been described in the literature yet and is of interest for our understanding of the mechanism of action.

3.6. Boreliosis and OspC antigen

It was reported that the immunization of mice with non-lipidized OspC in strong adjuvants (FCA, TiterMax, or Alum) could induce intense OspC-specific antibody responses [24,25,29]. Here we demonstrated that a similarly strong response could be elicited by the immunization of experimental mice with rOspC proteoliposomes with entrapped lipophilic derivatives of norAbuMDP. Furthermore, MT06 induces OspC-specific antibodies isotypes associated with complement-dependent bactericidal activity (IgG2a, IgG2b) whereas MT05 induces preferentially OspC-specific IgM isotype, described earlier as borreliacidal mouse immunoglobulins [26]. Recently, immunizations of experimental mice with chimeric fusions consisting of surface-exposed variable A, B, D, and K or A, B, C, D, E, I, K, and N types of OspC fragments from 130 to 201 aa regions of *B. burgdorferi*, *B. garinii*, and *B. afzelii* plus conserved C' terminal region were published [24,25,29–31]. The selected epitopes represent highly divergent immunogenic OspC regions which are recognized during the infection with respective *Borrelia* types [25,32]. It would be interesting to test, whether the immunization with analogous chimeric antigens formulated in proteoliposomes with appropriate adjuvants could elicit OspC-specific isotypes as described in the present study.

3.7. Metallochelating liposomes as carriers for an antigen

Both hydrophobic and hydrophilic protein or peptide antigens can be associated with liposomes. Generally, antigens can be associated with liposomes in two ways and it is known that the encapsulated and the surface-linked liposomal antigens induce distinct humoral [33] and cell-mediated immunity [34]. The entrapment of an antigen into the aqueous space of a liposome protects the protein or peptide antigen against proteolytic degradation and decreases antigen clearance. On the other hand, liposomal membrane represents a barrier restricting the interaction of the antigen with and its recognition by B-cells. Especially, the stable multilamellar liposomes were found to be low immunogenic [35] and the antibody response reached is low or absent when the liposomes are made of lipids with a high transition temperature, in other words composed of saturated phospholipids [36]. These liposomes are very stable in body fluids as well as in digestive tract and prevent a release of the entrapped antigen. Also the interaction of the encapsulated antigens with B-cells is limited. The fluidity of liposomes was found to be an important parameter also for the immune response towards a surface-linked antigen. Again, more fluidic liposomes composed of unsaturated phospholipids were more efficiently phagocytosed by APC and induced a one-order-of-magnitude higher immune response than rigid liposomes composed of saturated phospholipids [37]. The development of an effective vaccine requires a preserved native conformation of OspC antigen. Therefore, the mild conditions for binding the protein onto liposomes by metallochelation are a suitable approach to fulfill this requirement. Further, it was shown that the protectivity of recombinant OspC isolated under native conditions differs from that one obtained when denaturing conditions are applied. The immunization with overheated or chemically denatured OspC elicited OspC-specific antibodies but the animals were not protected against tick-transmitted *Borrelia* infection. In the case of native recombinant OspC, both N' and C' termini were identified to be involved in the

induction of protective borreliacidal antibodies [29]. During the infection, human produces a high concentration of borreliacidal antibodies specific to the conserved C' terminal region of OspC [38].

3.8. Berlin test for toxicity of various vaccine formulations in mice

Balb/c mice untreated and treated with empty liposomes were used as controls. No typical signs of toxicity according to the Berlin test of general toxicity, i.e. motoric disorders, respiratory problems, apathy, horrent fur, behavioural changes, anorexia and loss of body mass, were observed immediately after the application or during the post-vaccination period on either mice. No morphological changes of inner organs were observed after dissection and microscopic examination. The safety data is in good accordance with the data published by us also for the experimental metallochelating liposome-based rHSP90 vaccine [7].

3.9. Pyrogenicity tests on rabbits

In contrast to MDP, both tested derivatives MT05 and MT06 passed the test and were proved to be non-pyrogenic (Table 2).

Recently, the molecular bases of MDP action on the immune system were uncovered slightly. Two intracellular receptors of MDP that belong to NOD family were determined. NOD2 is a general intracellular sensor of Gram-positive and Gram-negative bacteria and plays an essential role in intestinal mucosal immunity. [39,40]. This receptor recognizes MDP as the minimal motif in all peptidoglycans. NOD2 is expressed in myeloid lineage of immune cells like monocytes, granulocytes, neutrophils, and also in dendritic cells. The expression in dendritic cells is of importance with respect to the application of MDP analogues as adjuvants. Another recently reported sensor of MDP is cryopyrin (also known as CIAS1 and NALP3), which is a member of the NOD-LRR family [41]. Cryopyrin is a part of the inflammasome complex that is responsible for the processing of caspase-1 to its active form. Caspase-1 cleaves the precursors of interleukin IL-1 β and IL-18, thereby activating these proinflammatory cytokines and promoting their secretion. IL-1 β is known as a strong endogenous pyrogen induced by MDP. We showed that norAbuMDP analogues were not pyrogenic (Table 2), even if a high concentration, much higher than the concentrations used for vaccination, was applied. We supposed that the modification introduced into the structure of MDP to get norAbuMDP analogues had not changed their affinity to NOD2 but had substantially decreased the affinity to cryopyrin. This hypothesis is in accordance with our data on pyrogenicity (Table 2) and data published for murabutide as another nonpyrogenic derivative of MDP [42].

4. Conclusions

The development of a recombinant vaccine against Lyme disease is a difficult task. We have shown that the preparation of delipidized rOspC can significantly improve a yield of this antigen, which is a crucial step for the preparation in the industrial scale.

Recombinant rOspC with His-Tag is easy to purify by metallochelating chromatography and the His-Tag could be used also for a non-covalent coupling of rOspC antigen to the metallochelating liposomes. Again, this step is applicable to a large-scale preparation of the vaccine in the future.

Table 2
Pyrogenicity of MDP and norAbuMDP analogues.

	Tested compounds				
	Liposomes	Liposomal MDP	Free MDP	MT05	MT06
+ ΔT_{max} °C	0.2	2.7	2.9	0.5	0.4

In general, recombinant antigens are weak immunogens, hence, some adjuvant is necessary to induce a strong and directed immune response. In case of rOspC, the Th1 response provided by IgG2 antibodies is required. Nonpyrogenic lipophilic derivatives of norAbuMDP have been shown to be potent adjuvants for weak antigens like rOspC and are suitable adjuvant components for the construction of vaccines based on a liposomal platform. Adjuvant potency of these analogues is comparable to that of MDP but these analogues lack side effects like strong pyrogenicity and flu-like syndromes related to MDP or other MDP-based derivatives. The Th1 response induced by the tested derivatives is comparable to that of MDP, however, it is higher than that of AIOH adjuvants. The most important observation was that in all the vaccinated animals, the metallochelating liposome-based vaccines did not induce any side effects.

Altogether, the metallochelating liposomes in combination with lipophilic norAbuMDP derivatives represent a novel platform for the construction of synthetic recombinant vaccines.

Acknowledgements

This work was supported by grants: GAČR P304/10/1951 (to JT); TAČR TA01011165 (to JT); MSM 6198959223 (to MR); MZE 0002716202 (to JT); KAN 200520703 AVČR and KAN 200100801 (to JT and ML); Grant of the Faculty of Medicine and Dentistry, UP Olomouc, CR LF-2010-014 and LF-2011-002 (to MK).

References

- M. Krupka, K. Zachova, E. Weigl, M. Raska, Prevention of Lyme disease: promising research or Sisyphean task? Arch. Immunol. Ther. Exp. (Warsz.) 59 (2011) 261–275.
- K. Tilly, P.A. Rosa, P.E. Stewart, Biology of infection with *Borrelia burgdorferi*, Infect. Dis. Clin. North Am. 22 (2008) 217–234.
- G.G. Klaus, M.P. Pepps, K. Kitajima, B.A. Askonas, Activation of mouse complement by different classes of mouse antibody, Immunology 38 (1979) 687–695.
- D.L. Vesely, D. Fish, M.J. Shlomchik, D.H. Kaplan, L.K. Bockenstedt, Langerhans cell deficiency impairs *Ixodes scapularis* suppression of Th1 responses in mice, Infect. Immun. 77 (2009) 1881–1887.
- K. Tilly, J.C. Krum, A. Bestor, M.W. Jewett, D. Grimm, D. Bueschel, R. Byram, D. Dorward, M.J. VanRaden, P. Rosa, B. burgdorferi OspC protein required exclusively in a crucial early stage of mammalian infection, Infect. Immun. 74 (2006) 3554–3564.
- J.G. Altin, C.R. Parish, Liposomal vaccines—targeting the delivery of antigen, Methods 40 (2006) 39–52.
- J. Masek, E. Bartheldyova, P. Turanek-Knotigova, M. Skrabalova, Z. Korvasova, J. Plochova, S. Koudelka, P. Skodova, P. Kulich, M. Krupka, K. Zachova, L. Cernekova, M. Horynova, I. Kratochvilova, A.D. Miller, E. Zykva, J. Michalek, J. Vrbkova, M. Sebelka, M. Ledvina, M. Raska, J. Turanek, Metallochelating liposomes with associated lipophilised norAbuMDP as biocompatible platform for construction of vaccines with recombinant His-tagged antigens: preparation, structural study and immune response towards rHsp90, J. Control. Release 151 (2011) 193–201.
- G.C. Chikh, W.M. Li, M.P. Schutze-Redelmeier, J.C. Meunier, M.B. Bally, Attaching histidine-tagged peptides and proteins to lipid-based carriers through use of metal-ion-chelating lipids, Biochim. Biophys. Acta 1567 (2002) 204–212.
- J. Malliaros, C. Quinn, F.H. Arnold, M.J. Pearce, D.P. Drane, T.J. Stewart, R.J. Macfarlan, Association of antigens to ISCOMATRIX adjuvant using metal chelation leads to improved CTL responses, Vaccine 22 (2004) 3968–3975.
- S. Liu, R. Tobias, S. McClure, G. Styba, Q. Shi, G. Jackowski, Removal of endotoxin from recombinant protein preparations, Clin. Biochem. 30 (1997) 455–463.
- M. Sebelka, T. Stosova, J. Havlis, N. Wrielsch, H. Thomas, Z. Zdrhal, A. Shevchenko, Thermostable trypsin conjugates for high-throughput proteomics: synthesis and performance evaluation, Proteomics 6 (2006) 2959–2963.
- T. Stosova, M. Sebelka, P. Rehulka, O. Sedo, J. Havlis, Z. Zdrhal, Evaluation of the possible proteomic application of trypsin from *Streptomyces griseus*, Anal. Biochem. 376 (2008) 94–102.
- J. Turanek, Fast-protein liquid chromatography system as a tool for liposome preparation by the extrusion procedure, Anal. Biochem. 218 (1994) 352–357.
- J. Turanek, A. Kasna, D. Zaluska, J. Neca, Preparation of sterile liposomes by proliposome-liposome method, Methods Enzymol. 367 (2003) 111–125.
- L.F. Erdle, B. Guy, OspA lipoprotein of *Borrelia burgdorferi* is a mucosal immunogen and adjuvant, Vaccine 15 (1997) 988–996.
- J.J. Weis, Y. Ma, L.F. Erdle, Biological activities of native and recombinant *Borrelia burgdorferi* outer surface protein A: dependence on lipid modification, Infect. Immun. 62 (1994) 4632–4636.
- S.D. Lowrich, D.A. Jobe, R.F. Scheff, S.M. Callister, Borrelia burgdorferi antibodies specific for a highly conserved epitope are immunodominant in human Lyme disease and do not occur in mice or hamsters, Clin. Diagn. Lab. Immunol. 12 (2005) 746–751.
- R.D. Gilmore Jr., R.M. Bacon, A.M. Carpio, J. Piesman, M.C. Dolan, M.L. Mbow, Inability of outer-surface protein C (OspC)-primed mice to elicit a protective anamnestic immune response to a tick-transmitted challenge of *Borrelia burgdorferi*, J. Med. Microbiol. 52 (2003) 551–556.
- M. Krupka, J. Belakova, M. Sebestrova, J. Tuhackova, M. Raska, V. Vrzal, E. Weigl, Isolation and purification of recombinant outer surface protein C (rOspC) of *Borrelia burgdorferi sensu lato*, Biomed. Pap. Med. Fac. Univ. Palacky Olomouc 149 (2005) 261–264.
- J. Masek, E. Bartheldyova, Z. Korvasova, M. Skrabalova, S. Koudelka, P. Kulich, I. Kratochvilova, A.D. Miller, M. Ledvina, M. Raska, J. Turanek, Immobilization of histidine-tagged proteins on monodisperse metallochelation liposomes: preparation and study of their structure, Anal. Biochem. 408 (2011) 95–104.
- C.L. van Broekhoven, C.R. Parish, C. Demange, W.J. Britton, J.G. Altin, Targeting dendritic cells with antigen-containing liposomes: a highly effective procedure for induction of antitumor immunity and for tumor immunotherapy, Cancer Res. 64 (2004) 4357–4365.
- D.S. Watson, V.P. Platt, L. Cao, V.J. Venditto, E.C. Szonka Jr., Antibody response to polyhistidine-tagged peptide and protein antigens attached to liposomes via lipid-linked nitrotriactic acid in mice, Clin. Vaccine Immunol. 18 (2011) 289–297.
- J.D. Patel, R. O'Carra, J. Jones, J.G. Woodward, R.J. Mumper, Preparation and characterization of nickel nanoparticles for binding to His-Tag proteins and antigens, Pharm. Res. 24 (2007) 343–352.
- C.G. Earnhart, E.L. Buckles, R.T. Marconi, Development of an OspC-based tetavalent, recombinant, chimeric vaccine that elicits bactericidal antibody against diverse Lyme disease spirochete strains, Vaccine 25 (2007) 466–480.
- C.G. Earnhart, R.T. Marconi, An octavalent Lyme disease vaccine induces antibodies that recognize all incorporated OspC type-specific sequences, Hum. Vaccin. 3 (2007) 281–289.
- M. Kushima, K. Matsui, F. Yamada, S. Kawahashi, S.K. Nishikawa, Specific immune response to a synthetic peptide derived from outer surface protein C of *Borrelia burgdorferi* predicts protective borrelial antibodies, FEMS Immunol. Med. Microbiol. 29 (2000) 15–21.
- M. Tamura, Y.C. Yoo, K. Yoshimatsu, R. Yoshida, T. Oka, K. Ohkuma, J. Arikawa, I. Azuma, Effects of muramyl dipeptide derivatives as adjuvants on the induction of antibody response to recombinant hepatitis B surface antigen, Vaccine 13 (1995) 77–82.
- K. Nerome, Y. Yoshioka, M. Ishida, K. Okuma, T. Oka, T. Kataoka, A. Inoue, A. Oya, Development of a new type of influenza subunit vaccine made by muramyl dipeptide-liposome: enhancement of humoral and cellular immune responses, Vaccine 8 (1990) 503–509.
- R.D. Gilmore Jr., M.L. Mbow, Conformational nature of the *Borrelia burgdorferi* B31 outer surface protein C protective epitope, Infect. Immun. 67 (1999) 5463–5469.
- C.G. Earnhart, R.T. Marconi, OspC phylogenetic analyses support the feasibility of a broadly protective polyvalent chimeric Lyme disease vaccine, Clin. Vaccine Immunol. 14 (2007) 628–634.
- C.G. Earnhart, R.T. Marconi, Construction and analysis of variants of a polyvalent Lyme disease vaccine: approaches for improving the immune response to chimeric vaccines, Vaccine 25 (2007) 3419–3427.
- C.G. Earnhart, E.L. Buckles, J.S. Dunler, R.T. Marconi, Demonstration of OspC type diversity in invasive human Lyme disease isolates and identification of previously uncharacterized epitopes that define the specificity of the OspC murine antibody response, Infect. Immun. 73 (2005) 7869–7877.
- E. Shahum, H.M. Therien, Immunopotential of the humoral response by liposomes: encapsulation versus covalent linkage, Immunology 35 (1988) 315–317.
- A. Fortin, E. Shahum, K. Krzystyniak, H.M. Therien, Differential activation of cell-mediated immune functions by encapsulated and surface-linked liposomal antigens, Cell. Immunol. 169 (1996) 208–217.
- P.N. Shek, T.D. Heath, Immune response mediated by liposome-associated protein antigens. III. Immunogenicity of bovine serum albumin covalently coupled to vesicle surface, Immunology 50 (1983) 101–106.
- G. Gregoriadis, D. Davis, A. Davies, Liposomes as immunological adjuvants: antigen incorporation studies, Vaccine 5 (1987) 145–151.
- T. Uchida, M. Taneichi, Clinical application of surface-linked liposomal antigens, Mini Rev. Med. Chem. 8 (2008) 184–192.
- S.D. Lowrich, R.L. La Fleur, D.A. Jobe, J.C. Johnson, K.E. Asp, R.F. Scheff, S.M. Callister, Borrelial OspC antibody response of canines with Lyme disease differs significantly from that of humans with Lyme disease, Clin. Vaccine Immunol. 14 (2007) 635–637.
- S.E. Girardin, D.J. Philpott, Mini-review: the role of peptidoglycan recognition in innate immunity, Eur. J. Immunol. 34 (2004) 1777–1782.
- C. McDonald, N. Inohara, G. Nunez, Peptidoglycan signaling in innate immunity and inflammatory disease, J. Biol. Chem. 27 (2005) 20177–20180.
- L. Agostini, F. Martinon, K. Burns, M.F. McDermott, P.N. Hawkins, J. Tschopp, NALP3 forms an IL-1beta-processing inflammasome with increased activity in Muckle-Wells autoinflammatory disorder, Immunity 20 (2004) 319–325.
- E.C. Darcisow, V. Vidal, M. Guillaume, J.J. Theault, G.M. Bahr, Clinical tolerance and profile of cytokine induction in healthy volunteers following the simultaneous administration of IFN-alpha and the synthetic immunomodulator murabutide, J. Interferon Cytokine Res. 21 (2001) 655–661.

Molecular Adjuvants Based on Nonpyrogenic Lipophilic Derivatives of norAbuMDP/GMDP Formulated in Nanoliposomes: Stimulation of Innate and Adaptive Immunity

Pavlna Turánek Knotigová · Daniel Zyka · Josef Mašek · Anna Kovalová · Michal Křupka · Eliška Bartheldyová · Pavel Kulich · Štěpán Koudelka · Róbert Lukáč · Zuzana Kauerová · Antonín Vacek · Milada Stuchlová Horynová · Alois Kozubík · Andrew D. Miller · Ladislav Fekete · Irena Kratochvílová · Jan Ježek · Miroslav Ledvína · Milan Raška · Jaroslav Turánek

Received: 30 April 2014 / Accepted: 11 September 2014 / Published online: 30 January 2015
© Springer Science+Business Media New York 2015

ABSTRACT

Purpose The aim of this work was to demonstrate an immunostimulatory and adjuvant effect of new apyrogenic lipophilic derivatives of norAbuMDP and norAbuGMDP formulated in nanoliposomes.

Methods Nanoliposomes and metallochelating nanoliposomes were prepared by lipid film hydration and extrusion methods. The structure of the liposomal formulation was studied by electron microscopy, AF microscopy, and dynamic light scattering. Sublethal and lethal γ -irradiation mice models were used to demonstrate stimulation of innate immune system. Recombinant Hsp90 antigen (*Candida albicans*) bound onto metallochelating nanoliposomes was used for immunisation of mice to demonstrate adjuvant activities of tested compounds.

Results Safety and stimulation of innate and adaptive immunity were demonstrated on rabbits and mice. The liposomal formulation of norAbuMDP/GMDP was apyrogenic in rabbit test and lacking any side effect *in vivo*. Recovery of bone marrow after sublethal γ -

irradiation as well as increased survival of mice after lethal irradiation was demonstrated. Enhancement of specific immune response was demonstrated for some derivatives incorporated in metallochelating nanoliposomes with recombinant Hsp90 protein antigen.

Conclusions Liposomal formulations of new lipophilic derivatives of norAbuMDP/GMDP proved themselves as promising adjuvants for recombinant vaccines as well as immunomodulators for stimulation of innate immunity and bone-marrow recovery after chemo/radio therapy of cancer.

KEY WORDS Adjuvant · Bone-marrow radioprotection · Liposome · Muramyl dipeptide · Vaccine

ABBREVIATIONS

AFM	Atomic force microscopy
APC	Antigen presenting cell
CFA	Complete Freund's adjuvant
CMI	Cell-mediated immunity

Electronic supplementary material The online version of this article (doi:10.1007/s11095-014-1516-y) contains supplementary material, which is available to authorized users.

P. T. Knotigová · J. Mašek · E. Bartheldyová · P. Kulich · Š. Koudelka · R. Lukáč · Z. Kauerová · A. Vacek · J. Turánek (✉)
Department of Pharmacology and Immunotherapy
Veterinary Research Institute, Hudcova 70, 620 00 Brno, Czech Republic
e-mail: turanek@seznam.cz

D. Zyka · A. Kovalová · J. Ježek
Institute of Organic Chemistry and Biochemistry, Czech Academy of Sciences, Flemingovo náměstí 2, 160 00 Prague, Czech Republic

M. Křupka · M. S. Horynová · M. Raška (✉)
Faculty of Medicine and Dentistry, Department of Immunology
Palacky University Olomouc, Hnevotínska 3, 772 00 Olomouc, Czech Republic
e-mail: raskamil@uob.edu

A. Kozubík
Institute of Biophysics, Academy of Sciences of the Czech Republic, v.v.i
Brno, Czech Republic

A. D. Miller
Pharmaceutical Sciences Division, King's College London, London, UK

L. Fekete · I. Kratochvílová
Institute of Physics, Czech Academy of Sciences, Prague, Czech Republic

M. Ledvína (✉)
Department of Chemistry of Natural Compounds, Institute of Chemical
Technology, Prague 6, Czech Republic
e-mail: ledvina@uochb.cas.cz

Š. Koudelka
International Research Center, St. Anne's University Hospital Brno,
Brno, Czech Republic

DLS	Dynamic light scattering
DOGS-NTA-Ni	1,2-Dioleoyl-sn-Glycero-3-[[N (5-Amino-1-Carboxypentyl) iminodiAcetic Acid] Succinyl] (Nickel Salt)
EM	Electron microscopy
EPC	Egg phosphatidylcholine
GM-CFC	Granulocyte-monocyte colony-forming cells
iE-DAP	γ -D-glutamyl-meso-diaminopimelic acid
MDP	Muramyl dipeptide
MTP-PE	Muramyl tripeptide phosphatidylethanolamine
MT01 – MT08	Lipophilic derivatives based on norAbuMDP and norAbuGMDP
NALP3	NACHT LRR and PYD domains-containing protein 3
NOD	nucleotide-binding oligomerization domain
norAbuMDP	NorMurNAc-L-Abu-D-iGln
norAbuGMDP	NorAbu-glucosaminylmuramyl dipeptide
POPG	1-palmitoyl-2-oleoyl-sn-glycero-3-phospho-(1'-rac-glycerol) (sodium salt)
rHsp90	Recombinant Heat shock protein 90
SEC	Size exclusion chromatography
TLR	Toll-like receptor

INTRODUCTION

The immunostimulatory or adjuvant-like activity of the peptidoglycan component of bacterial cell walls has been known for a long time. The minimal structural element of peptidoglycan with adjuvant and immunomodulatory activity is muramyl dipeptide (MDP) [1]. Regrettably, a broader use of MDPs in medicine has been limited by some undesirable side reactions including fever, nausea, hyper- or hypotension, thrombocytolysis, local necrosis, and haemorrhages, development of granuloma at the injection site, and induction of autoimmune diseases [2, 3]. More than one thousand MDP derivatives have been synthesized in the search for powerful stimulants of innate immunity (against cancer, bacterial and viral infections [4–6]) and of adjuvants enhancing specific antibody responses plus specific cell-mediated immunity (CMI) [2, 7–9].

In spite of the enormous effort of many scientists and the pharmaceutical industry, only one derivative has recently reached the stage of clinical application. However, the side effects were not suppressed. Mifamurtide (liposomal muramyl tripeptide phosphatidylethanolamine, MTP-PE) is a non-specific immunomodulator, which can enhance the effects of the standard chemotherapy of osteosarcoma patients, but is not free of severe side effects [10, 11]. On the other hand, new lipophilic analogues based on norMurNAc-L-Abu-D-iGln (norAbuMDP) [12, 13] have been synthesized (Fig. 1), and

compared with MDP, these analogues appear to exhibit immunostimulatory activities with suppressed pyrogenicity. With respect to intended application of these analogues, we recently selected liposomes as a platform delivery technology for the construction of immunomodulatory preparations and liposome-based vaccines [14–16].

In this work, we now summarize our long-term effort to design and synthesise effective and safe synthetic lipophilic norAbu-MDP and norAbu-glucosaminylmuramyl dipeptide (GMDP) based immunomodulators for formulation into two types of liposomes for the construction of recombinant vaccines and preparations applicable to stimulate innate immunity.

MATERIALS AND METHODS

General

Egg phosphatidylcholine (purity of 99%), 1,2-Dioleoyl-sn-Glycero-3-[[N (5-Amino-1-Carboxypentyl) iminodiAcetic Acid] Succinyl] (Nickel Salt) (DOGS-NTA-Ni) lipids were purchased from Avanti Polar Lipids (Birmingham, AL). Membrane filter Anotop 10 (pore size of 20 nm) and Anotop 10 LC (pore size of 0.2 μ m) were purchased from Whatman (Maidstone, UK). All other chemicals were from Sigma (St. Louis, MO), unless else specified.

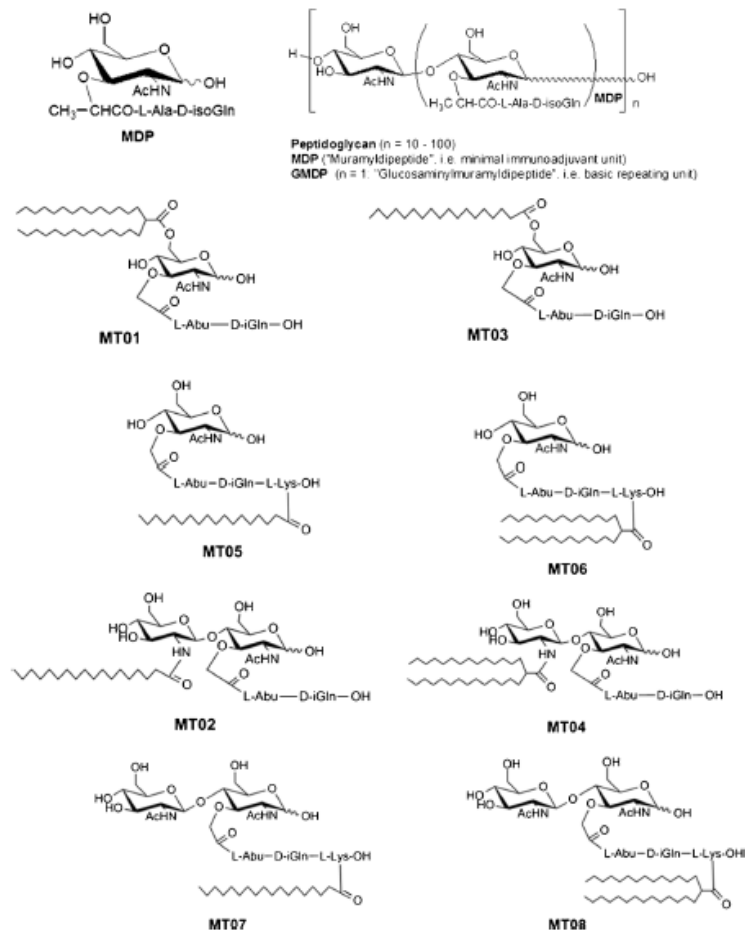
Characterization of Liposomes by Transmission and Scanning Electron Microscopy

The structure of the liposomes was determined using Philips Morgagni transmission electron microscope (EM Philips 208 S, MORGAGNI software, FEI, CZ). All samples were negatively stained with 2% (w/w) ammonium molybdate (pH 6.8). Scanning electron microscopy was performed on Hitachi SU 8010 (Hitachi, Japan). Samples were coated by Pt/Pd in the Cressington sputter coater 208HR (Cressington Scientific Instruments Ltd. UK) and observed at the magnification of 600 000, 15 kV.

Atomic Force Microscopy (AFM)

The topography of the liposomes and proteoliposomes was investigated by atomic force microscopy. The AFM measurements were performed with NTEGRA Prima NT MDT system (Ireland) under ambient conditions. The tip-sample surface interaction monitored the van der Waals force between the tip and the surface; this may be either the short-range repulsive force (in the contact mode) or the longer-range attractive force (in the non-contact tapping mode). The AFM measurements of the metallochelation liposomes and

Fig. 1 Structural formulae of peptidoglycan, MDP, GMDP, and norAbuMDP/GMDP derivatives.



proteoliposomes were performed using the tapping mode. Each sample was scanned under the soft CSG 10 type of probe. The tapping mode consisted of oscillating the cantilever at its resonance frequency (14–28 kHz) and light "tapping" the tip on the surface during scanning.

Syntheses and Characterization of MDP Analogues

The syntheses of lipophilic derivatives based on nor-AbuMDP and nor-AbuGMDP (coded as MT01 – MT08) and the confirmation of their structures are described in patent cooperation treaty (PCT) by Ledvina and co-workers (Ledvina M, Turánek J, Miller AD, Hipler K. US8653049 B2, EP

2271661 B3) (Supp. info section D). The structural formulae are presented in Fig. 1.

Recombinant Antigen rHsp90

Recombinant (r) Hsp90 antigen was prepared using cDNA from a clinical isolate of *C. albicans* as reported elsewhere [17]. cDNA was used for the construction of prokaryote expression vector allowing the expression of rHsp90 both C'- and N'-terminally fused with His-tag in *E. coli*. Endotoxin was removed by successive two-phase separation with Triton X-114 as described elsewhere [18]. The entire procedure was repeated until the endotoxin level was below 0.25 EU

per 1 mg of protein (measured by Limulus amoebocyte lysate according to FDA guidelines). Purity of the protein was above 95% (SDS PAGE).

Preparation and Characterization of Liposomes

Liposomes were prepared by the method based on hydration of a lipid film followed by extrusion through 0.2 and 0.1 μm polycarbonate filters in an analogous way to that described previously [19]. The hand-operated device Mini-Extruder (Avanti Polar Lipids) was used for the extrusion of small volumes of liposomes (up to 1 ml). Large volumes of the liposomes were extruded by means of a high-pressure cell (Millipore, Billerica, MA) linked with FPLC instrument (Pharmacia, Uppsala, Sweden). Liposomes with immunomodulators were composed of EPC/POPG/immunomodulator at the molar ratio of 76:19:5 mol%.

Metallochelating nanoliposome-based rHsp90 vaccine was prepared and characterized as recently described by our group [16, 20].

Characterization of Micelles and Liposomes by DLS, AFM and EM

The size distribution, zeta-potential and structures of various liposomal preparations were analysed by dynamic light scattering (DLS), Atomic force microscopy (AFM) and electron microscopy (EM) (supplementary material, section A, B).

Test of Pyrogenicity and Side Effects

Standard pyrogenicity test on rabbits was used to prove the safety of liposomal adjuvants. The test was carried out in the authorized laboratory TTEST Plus s.r.o. (Bílá Vchýnice 10, 533 13 Vápno u Přelouče, Czech Republic) according to the Czech Pharmacopoeia 2005. Details are described in the part C of supporting information.

Stimulation of Hemopoiesis *in Vivo* in Sublethally Irradiated Mice

Administration of Tested Compounds Prior to Sub-Lethal Irradiation

ICR mice (female, age of 3 months, 3–4 per group) were stimulated by *s.c.* administration of a tested preparations (volume of 200 μl , 100 nmol per dose) 24 h prior to sublethal γ -irradiation (6 Gy, ^{60}Co γ -ray source Chisostat (Chirana Ltd., Czech Republic) at the dose of 0.285 Gy/min). After 13 days, the mice were sacrificed and the recovery of granulocyte-monocyte colony-forming cells (GM-CFC) in femur was assayed by counting of colonies (CFC) grown up after cultivation in medium [21].

Administration of Tested Compounds after Sub-Lethal Irradiation

The tested preparations (volume of 200 μl , 100 nmol per dose) were administered 24 h after the sublethal γ -irradiation (6 Gy) and the effect was evaluated according to the same experimental protocol as described above. The statistical significance of the change of hemopoietic parameters was calculated by one-way analysis of variance. The Newman-Keuls test for the comparison of all pairs of columns and the Dunnett test for the comparison of all columns with the control column were used in the analysis.

Non-irradiated mice served as a control for normal GM-CFC count in femur. PBS and plain liposomes were used as controls for spontaneous recovery. Liposomal MDP was used as a reference standard.

Protection of Mice Against γ -Irradiation-Induced Death

Particular preparations (volume of 200 μl , 100 nmol per dose) were applied to ICR mice (female, the age of 3 months, 10 mice per group) by *s.c.* route 24 h prior to irradiation (radiation dose of 10 Gy). PBS and plain liposomes served as negative controls, free and liposomal muramyl dipeptide (MDP) served as positive controls. The methodological details of the model were published by Turanek and Kašná [21, 22].

Immunization and Adjuvants

Mice were divided into 8 groups, each of 5 animals, and immunized by two (priming, booster) *id.* applications of rHsp90 (20 μg per dose, vaccines formulated in apyrogenic PBS (phosphate buffered saline, pH 7.2) incorporated in metallochelation liposomes with different MT adjuvants) as indicated in Table I. The volume of each dose was 50 μl , the interval between priming and booster was 14 days. Complete Freund's adjuvant (CFA) and aluminium hydroxide (Bioveta, Ivanovice na Hané, Czech Republic) were used as adjuvant controls.

The animal experiments were approved by The Ethics Committees (Veterinary Research Institute, Brno and Palacky University, Olomouc) and were done according to the principles enunciated in the Guide for the Care and Use of Laboratory Animals (Czech Society for Laboratory Animal Science).

rHsp90-Specific Antibody Response

rHsp90-specific serum antibody levels were determined by ELISA. Sera were collected from the experimental mice 1 day before boosting (post prime) and 14 days after boosting (post boost) by tail-vein incision. For individual sera, all assays were performed in triplicates. 96-well microplates (Nalge Nunc International, Rochester, NY) were coated with 100 μl of 1 $\mu\text{g}/\text{ml}$ rHsp90. Bound antibodies were detected with

Table 1 Composition of rHsp90 Immunization Protocols Tested in this Experiment

Groups of 5 mice	Composition per one dose (50 μ l)				
	rHsp90 (μ g)	AlOH (μ l)	Liposome (total lipid, μ g)	CFA (μ l)	MDP derivate (μ g)
PBS (control)	–	–	–	–	–
rHsp90	20	–	–	–	–
Lip-Ni-rHsp90	20	–	35	–	–
rHsp90 AlOH	20	12.5	–	–	–
rHsp90 CFA	20	–	–	2.5	–
Lip-Ni-rHsp90 MT01	20	–	35	–	2.07
Lip-Ni-rHsp90 MT02	20	–	35	–	2.05
Lip-Ni-rHsp90 MT03	20	–	35	–	1.69
Lip-Ni-rHsp90 MT04	20	–	35	–	2.4
Lip-Ni-rHsp90 MT05	20	–	35	–	1.98
Lip-Ni-rHsp90 MT06	20	–	35	–	2.54
Lip-Ni-rHsp90 MT07	20	–	35	–	2.41
Lip-Ni-rHsp90 MDP	20	–	35	–	1.6

The dose of MDP derivatives is equivalent to 2.2 nmol per mouse

CFA and AlOH (Bioveta, Nanovice na Hané, Czech Republic) were used as positive controls. The antigen formulation was prepared according to manufacturer's instructions. The FCA formulation was prepared by mixing the antigen with CFA (50/50 v/v), the Alum formulation was prepared by mixing the antigen with Alum (75/25 v/v). MDP MT01 to MT07 were added in equimolar amounts, 9.3 nmol per dose. The liposomal formulations contained EPC/POPG/DOGS-NTA-Ni (76/19/5 mol%) or EPC/POPG/DOGS-NTA-Ni/MDP or MT01 to MT07 adjuvants (71/19/5/5 mol%).

horseradish peroxidase-labelled goat anti-mouse IgG + IgM + IgA (Ig total*) (MP Biomedicals, Solon, OH), goat anti-mouse IgG1 (MP Biomedicals, Solon, OH), goat anti-mouse IgG2a (Bethyl laboratories, Montgomery, TX), rabbit anti-mouse IgG2b (MP Biomedicals), or goat anti-mouse IgG3 (Bethyl laboratories), (MP Biomedicals, Solon, OH) and developed with O-phenylenediamine plus H₂O₂ substrate. The reaction was stopped with 1 M sulphuric acid and the absorbance was read at 490 nm. For antigen-specific ELISA, the results were expressed as mean end-point titre plus SD using Gen5 Software (release 2, BioTek Instruments, Vermont, USA).

RESULTS

Test of Pyrogenicity and Safety of norAbuMDP/GMDP and its Lipophilic Analogues

Intravenous Administration

The pyrogenicity of free analogues was tested. In comparison to MDP, norAbuMDP exerted a suppressed pyrogenicity owing to the structural changes in the molecule (Table II). However, at higher doses (200 and 1,000 nmol per kg), this compound

was proved to be pyrogenic similarly to MDP. Contrary to norAbuMDP, norAbuGMDP as well as the lipophilic analogues of both parent compounds were completely non-pyrogenic, even at higher doses (Table II).

Subcutaneous Administration

Pyrogenicity of liposomal formulations of MDP and lipophilic derivatives was tested. A standard pyrogenicity test (modified for *s.c.* application) was performed with rabbits. It showed that both free and liposomal MDP were pyrogenic. Sum + ΔT_{max} (3 rabbits per group) was 2.7°C and 2.9°C, respectively. Sum + ΔT_{max} for plain liposomes was 0.2°C. Both liposomal and free norAbuMDP, norAbuGMDP as well as their lipophilic derivatives MT were within the range of sum + ΔT_{max} of 0.4 – 0.6°C. Hence, these analogues were classified as non-pyrogenic (Table II). Pyrogenicity data obtained after *i.n.* and *s.c.* application of the tested compounds are in a good accordance. No adverse or toxic effects were observed for norAbuMDP, norAbuGMDP and their lipophilic derivatives MT in rabbits during a two-week period.

Recovery of Hemopoiesis (GM-CFS in femur) in Sublethally Irradiated Mice (6 Gy)

Lipophilic MDP Analogues Administered 24 h Prior to Irradiation

Compared with controls at the 13th day, all the tested compounds improved the recovery of hemopoiesis. MT02 improved the recovery process only slightly, MT04 resulted in nearly 75% of normal level and MT05, MT06, MT07, and MT08 induced recovery to normal level comparable to the level of non-irradiated control. The effect was comparable to liposomal MDP (Fig. 2a). In contrast, free MDP affected the recovery only negligibly (*results not shown*).

Lipophilic MDP Analogues Administered 24 h After Irradiation

Compared with controls at the 13th day, all the tested compounds improved the recovery of hemopoiesis. MT02 and MT07 surpassed liposomal MDP and induced recovery to normal level (comparable with non-irradiated controls, $C < 0.01$). MT04, MT05, MT06, and MT08 resulted in about 50 – 60% of normal level. The effect was comparable to liposomal MDP (Fig. 2b).

Survival Curves of Lethally Irradiated mice Stimulated by Various Liposomal Preparations of Lipophilic Analogues of MDP

As for sub-lethal irradiation applied after priming the mice with the test analogues or controls, the best performance was found with analogue MT05, followed by the performance of a

Table II Pyrogenicity Tests on Rabbits

subcutaneous application	Tested compounds										
	lip. MDP	Free MDP	lip. MT01	lip. MT02	lip. MT03	lip. MT04	lip. MT05	lip. MT06	lip. MT07	lip. MT08	
+ΔT _{max} [°C]	2.7	2.9	0.5	0.7	0.3	0.7	0.5	0.4	0.6	0.8	
Intravenous applicatio	free MDP; 40 nmol/kg	free MDP; 200 nmol/kg	free MDP; 1,000 nmol/kg	norAbu MDP; 40 nmol/kg	norAbu MDP; 200 nmol/kg	norAbu MDP; 1,000 nmol/kg	norAbu GMDP; 40 nmol/kg	norAbu GMDP; 200 nmol/kg	norAbu GMDP; 1,000 nmol/kg	norAbu GMDP; 1000 nmol/kg	
+ΔT _{max} [°C]	1.8	2.8	3.6	0.8	3.5	3.4	0.5	0.6	0.6	0.6	

A preparation was evaluated as nonpyrogenic, if the $\text{Sum} + \Delta T_{\text{max}} < 1.15^{\circ}\text{C}$ (3 rabbits/group).
liposomal molecular adjuvants MTT were applied at dose of 100 nmol/kg

“middle field” of other analogues. Overall protective effects were found in the case of MT01, MT02, MT05, MT06, MT07, and liposomal MDP (30–60% survivors). However, neither analogue MT04 nor free MDP showed any protective effects (Fig. 3).

Structure of rHsp90 Metallochelating Liposomes

Structures of metallochelating liposomes and proteoliposomes were studied by means of size exclusion chromatography (SEC), transmission electron microscopy (TEM) and AFM microscopy. All these methods clearly showed the molecules of rHsp90 bound onto the surface of liposomes (Fig. 4) leading to an increase in the hydrodynamic radii of the liposomes as confirmed by dynamic light scattering (*results not shown*).

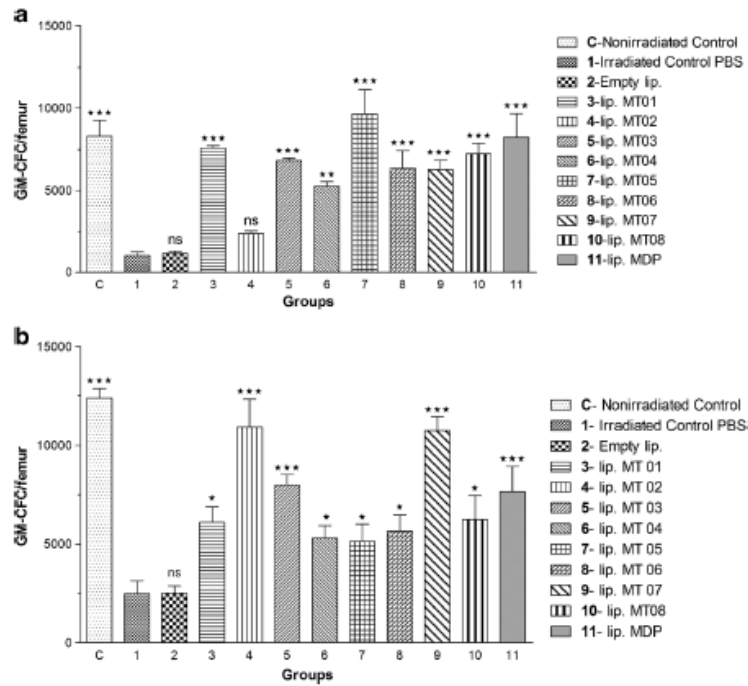
Induction of Adaptive Immunity

Immune Response

Candida rHsp90 with various lipophilic analogues of norAbuMDP and norAbuGMDP formulated into liposomes was tested for immunogenicity after intradermal administration in mice. End-point titers of Hsp90-specific antibodies (Ig total) were measured by ELISA (Fig. 5a). As a positive control, non-liposomal formulations of rHsp90 with Alum (aluminium hydroxide) or complete Freund's adjuvant (CFA) were tested in separate groups of mice. Also rHsp90 was tested without adjuvant present either as soluble protein or in the form of a proteoliposome (Lip-Ni-rHsp90). The highest Ig titres were obtained after the second immunization (post boost) with rHsp90 plus Alum or CFA. Both approaches elicited detectable antibodies even after the first immunization (post prime). Among the tested MDP analogues, the strongest Hsp90-specific antibody response was detected for MT03, and a rather lesser response for MT07, MT06, and MT05. The effect of other MDP analogues was comparable to rHsp90 or Lip-Ni-rHsp90. These compounds, especially MT02, MT04 and MT01, even showed some suppression of the elicited specific response. In the group of mice immunized with Lip-Ni-rHsp90 plus MDP, only moderate Hsp90-specific antibody responses were elicited. It should be emphasized that no side effects were recorded post administration of norAbuMDP, norAbuGMDP, or analogues (MT01 - MT07) formulated into rHsp90 proteoliposomes. In contrast, serious local inflammation, induration, ulceration and/or necrosis was found typically in animal skin at sites of CFA applications (whether or not co-administered with rHsp90 antigen protein, data not shown) while administration of rHsp90 plus MDP adjuvant led to local irritation in mice.

Furthermore, the effect of particular MDP analogues on the magnitude of rHsp90-specific IgG isotype titers (IgG1,

Fig. 2 Recovery of hemopoiesis (GM-CFC in femur) in sublethally irradiated mice (6 Gy). ICR mice (female, age of 3 months) were stimulated by s.c. application of the liposomal derivatives MTOX (200 μ l, 100 nmol per dose) 24 h before (Fig. 2A) or after (Fig. 2 B) sublethal γ -irradiation (6 Gy). The mice were sacrificed at the 13th day after the irradiation and the recovery of GM-CFC in femur was assayed by counting of colonies (CFC) formed after the cultivation in medium. Non-irradiated mice were used as a control for normal GM-CFC count in femur. PBS and empty liposomes were used as controls for spontaneous recovery. Liposomal MDP was the positive reference standard.



IgG2a, IgG2b and IgG3) was measured by ELISA to assess the Th1/Th2-type polarization (Fig. 5b). For each of the tested norAbuMDP and norAbuGMDP analogues, substantially different Hsp90-specific antibody titers in IgG2a and IgG2b (Th1) versus IgG1 (Th2) isotypes or IgG3 isotype were detected. Data illustrate that some MDP analogues were optimal in eliciting Th1-type rHsp90-specific immune responses and others in eliciting Th2-type responses. It should

be emphasized that Lip-Ni-rHsp90 formulated with MDP analogues MT03, MT07 and to a lesser extent MT06, MT05, and MT02 exhibited the capacity to elicit substantial rHsp90-specific titers in IgG2a and IgG2b isotypes indicating Th1 polarization of the specific immune response. CFA with rHsp90 elicited IgG2a and IgG2b antibodies even more effectively, however, due to its unacceptable adverse effects it was removed from comparison. On the other hand, Alum as

Fig. 3 Survival curves of irradiated mice stimulated by various liposomal preparations of lipophilic analogues of MDP. The mice of ICR strain, female, the age of 3 months. The preparations were applied s.c. 24 h before γ -irradiation (10 Gy).

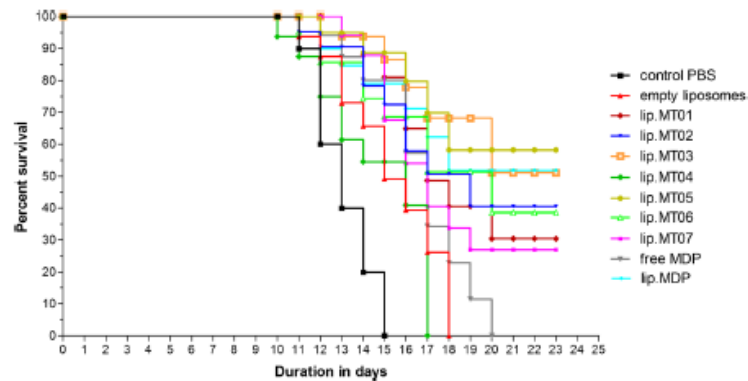
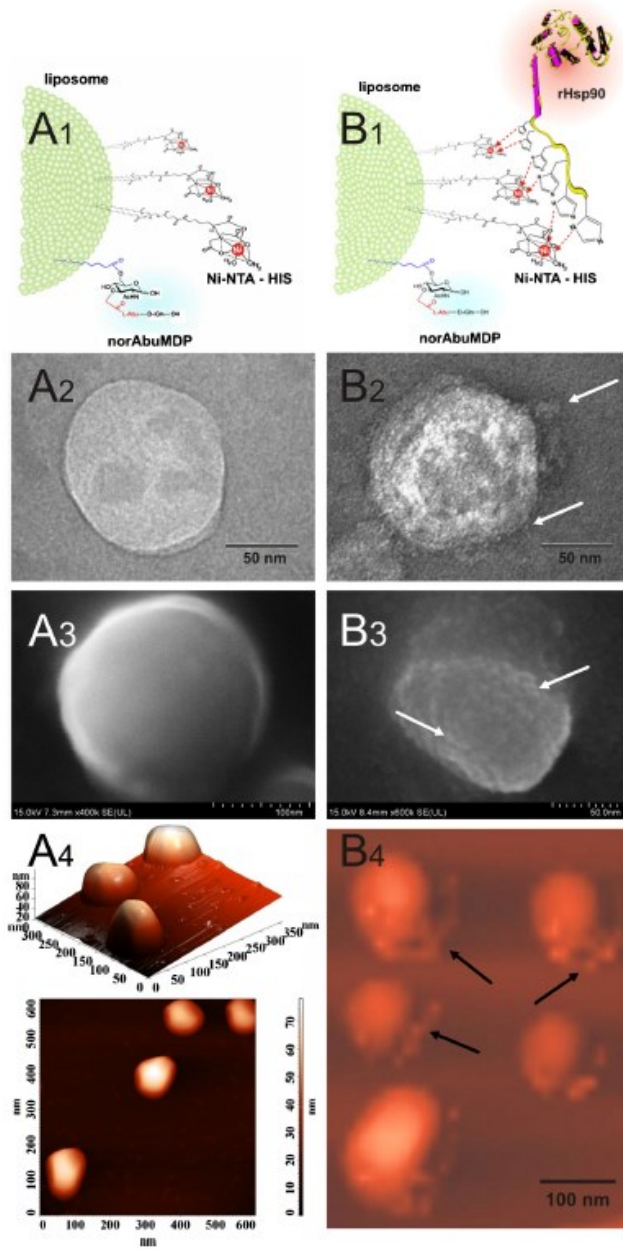


Fig. 4 Structure of metallochelating liposomes and proteoliposomes revealed by TEM, SEM and AFM. **(a1)** Schematic presentation of a metallochelating liposome with metallochelating lipids and incorporated lipidized norAbuMDP molecules. **(a2)** TEM photograph of a metallochelating liposome with metallochelating lipids and incorporated lipidized norAbuMDP molecules. **(a3)** SEM photograph of a metallochelating liposome with metallochelating lipids and incorporated lipidized norAbuMDP molecules. **(a4)** AFM photograph of a metallochelating liposome with metallochelating lipids and incorporated lipidized norAbuMDP molecules. **(b1)** Schematic presentation of a metallochelating liposome **(a1)** with rHsp90 bound via metallochelating bond. **(b2)** TEM photograph of a metallochelating liposome with rHsp90 bound via metallochelating bond. **(b3)** SEM photograph of a metallochelating liposome with rHsp90 bound via metallochelating bond. **(b4)** AFM photograph of a metallochelating liposome with rHsp90 bound via metallochelating bond. The arrows mark the molecules of liposomal surface-bound rHsp90.



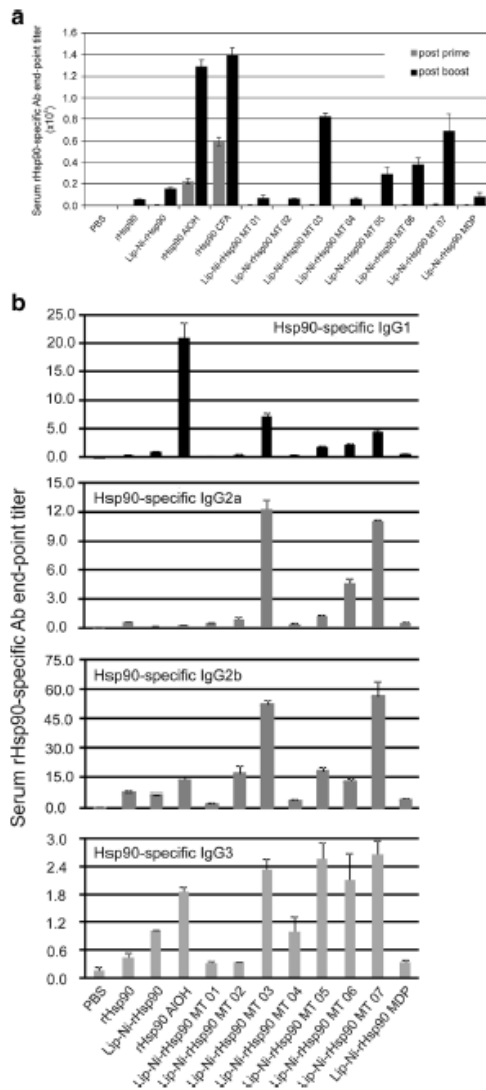


Fig. 5 Antibody response towards r-Hsp90 antigen formulated in various experimental vaccines. **(a)** ELISA titres of specific antibodies against r-Hsp90 induced by various MDP analogues. Experimental mice (5 per group) were immunized by intradermal administration of various formulations of r-Hsp90 as indicated in Table I. PBS was administered to the negative control group. The r-Hsp90 represents free soluble r-Hsp90; Lip-Ni-r-Hsp90 represents metallochelating liposomes with bound r-Hsp90; r-Hsp90 AOH represents free soluble r-Hsp90 with Alum; r-Hsp90 CFA represents free soluble r-Hsp90 in 50% Complete Freund's adjuvant; Lip-Ni-r-Hsp90 MT01, Lip-Ni-r-Hsp90 MT02, Lip-Ni-r-Hsp90 MT03, Lip-Ni-r-Hsp90 MT04, Lip-Ni-r-Hsp90 MT05, Lip-Ni-r-Hsp90 MT06, and Lip-Ni-r-Hsp90 MT07 represent metallochelating liposomes with r-Hsp90 and a respective lipophilic nor-AbuMDP or nor-AbuGMDP analogues of MDP; Lip-Ni-r-Hsp90 MDP represents metallochelating liposomes with r-Hsp90 and free MDP. Hsp90-specific IgG + IgM + IgA antibody (Ig total) titres were measured 1 day before the second immunization (post prime) and 14 days after the second immunization (post boost) by ELISA in triplicates. The results are expressed as the mean end-point titre and SD for each experimental group. **(b)** Effect of MDP analogues on Hsp90-specific mouse IgG isotypes after immunization. Experimental mice (5 per group) were immunized by intradermal administration of various formulations of r-Hsp90 as indicated in Table I. PBS was administered to the negative control group. The r-Hsp90 represents free soluble r-Hsp90; Lip-Ni-r-Hsp90 represents metallochelating liposomes with bound r-Hsp90; r-Hsp90 AOH represents free soluble r-Hsp90 with Alum; r-Hsp90 CFA represents free soluble r-Hsp90 in 50% Complete Freund's adjuvant; Lip-Ni-r-Hsp90 MT01, Lip-Ni-r-Hsp90 MT02, Lip-Ni-r-Hsp90 MT03, Lip-Ni-r-Hsp90 MT04, Lip-Ni-r-Hsp90 MT05, Lip-Ni-r-Hsp90 MT06, and Lip-Ni-r-Hsp90 MT07 represent metallochelating liposomes with r-Hsp90 and a respective lipophilic nor-AbuMDP or nor-AbuGMDP analogue of MDP. The Hsp90-specific IgG1, IgG2a, IgG2b, and IgG3 antibody titres were measured 14 days after the second immunization (post boosting) by ELISA. The results are expressed as the mean end-point titres and SD for each experimental group.

the only clinically applicable adjuvant was ineffective in eliciting both IgG2a and IgG2b isotypes. For eliciting IgG1, the most effective immunization was Lip-Ni-rHsp90 with MT03 and MT07 and to a lesser extent MT05 and MT06. Furthermore, IgG3 rHsp90-specific titres were effectively elicited by Lip-Ni-rHsp90 formulated with MT03, MT05, MT06, and MT07 and to a lesser extent with MT04. The IgG3 titres obtained were comparable with those detected for rHsp90 plus Alum.

Moreover, no toxic effects scored by the test of general toxicity (Berlin test: including motoric disorder, respiratory problems, apathy, horrent fur, behavioral changes and loss of body mass) were recorded in mice treated with the experimental vaccines containing norAbuMDP or norAbuGMDP lipophilic derivatives. The test was complemented by dissection of the euthanized animals and inspection of their organs (weighing, microscopic observation of morphological changes) (results not shown).

DISCUSSION

Several MDP analogues and related compounds such as stearoyl-MDP derivatives, MTP-PE, FK565, FK156, and RP40639, murabutide and MDP (thr) have been reported to stimulate the host innate immune system against bacterial infections in experimental models [23, 24].

MDP-Lys (L18) (Romurtide) appeared on the market in Japan, and was widely applied to cancer patients, previously treated by radiation therapy, in order to restore white blood cells. The most common side effect of Romurtide administration was fever that was controlled by antipyretics. Other side effects, such as local reactions at the injection site, were transient [25, 26].

Another MDP analogue (MTP-PE, Mifamurtide) was approved for combined chemotherapy and immunotherapy of osteosarcoma. As shown in clinical trials, administration of MTP-PE was associated with hypersensitivity reactions along with pleural and pericardial effusions, seizures, and muscle spasms. Severe hearing loss occurred in 12% of the Mifamurtide-treated patients *versus* 7% of other patients experiencing a pure chemotherapy regime [11]. The side effects mentioned above are tolerable for treatment of cancer but not for the application as adjuvants in prophylactic vaccines. This is the reason why no MDP analogue has been approved as an adjuvant yet.

Pharmaceutical Formulation of Lipophilic Analogues

The main goal in preparing various MDP-based therapeutic liposome formulations was to target adjuvants to enter relevant immune cells like dendritic cells or macrophages and combine with intracellular receptors. The lipophilic modification of MDP and its analogues represents a common approach for the improvement of their pharmacokinetics. On the other hand, the addition of a lipophilic moiety to hydrophilic glycopeptide core results in the creation of a surfactant-like molecular structure. Therefore, the formation of micelles and surfactant-related cytotoxicity must be taken into account.

All synthesized compounds of MT-series are able to form micelles (supplementary material Fig. 1S). Stearoyl derivatives form small well-defined micelles of the size of about 6–10 nm, while branched B30-modified fatty acid analogues formed larger structures with a bimodal size distribution. Owing to the large lipophilic moiety, no sign of *in vitro* toxicity or haemolytic activity (rabbit red blood cell haemolytic test) was observed when mouse and human dendritic cells or peripheral blood monocytes, T and B lymphocytes were tested (*data not shown*).

Lipid micelles are metastable structures and their interaction with biological milieu and cells can hardly be predicted. Therefore, we focused on the application of multifunctional liposomes, that represent a well established, much more stable platform for the formulation and inclusion of hydrophobic or hydrophilic drugs and for the construction of vaccines [20, 27, 28] which we further modified to reach adjuvant-antigen multifunctionality. No haemolytic activities of liposomal formulations were observed *in vitro* in absence or presence of rabbit sera.

Stimulation of Innate and Adaptive Immunity, Mechanism (s) of Action

The mechanism (s) of action of MDP and its analogues are not fully understood. Therefore, *in vivo* immunological models are the best endpoint for demonstration of immunostimulatory and adjuvant activities of tested complex preparations.

We tested series of lipophilic norAbu-MDP and norAbu-GMDP analogues formulated into liposomes for the restoration of haemopoiesis in sublethally and lethally γ -irradiated mice. These models address several aspects of stimulation of innate immunity at the level of haemopoiesis, stimulation of immune cells (e.g. macrophages) and tissue regeneration. Therefore this *in vivo* model represents perfect end point for testing of such a complex event as is stimulation of innate immunity. The capability of the tested analogues to stimulate regeneration of bone marrow was demonstrated by determination of GM-CFC regeneration 13 days after sublethal γ -irradiation of mice. Most of the tested derivatives stimulated GM-CFC regeneration to a level equivalent with non γ -irradiated control mice. The effect was comparable to or better than that obtained with liposome formulated MDP (Fig. 2). Control γ -irradiated non-treated mice exhibited signs of a deep bone-marrow haematopoietic depression. Interestingly, some analogues differed in their ability to stimulate the regeneration of bone marrow after γ -irradiation dependent on the time schedule of administration (pre- or post- γ -irradiation regime). In the post irradiation regime the highest efficacy was exhibited by formulations containing MT-02 and MT-07. This could be of interest with respect to possible combination with drugs causing leukopenia (e.g., cytostatics) or in the case of radiation therapy, or even post-irradiation therapy of accidentally irradiated persons.

The *in vivo* model of lethally γ -irradiated mice proves the potential of MDP analogues to induce complex protective and regenerative mechanisms including effective and long-lasting activation of macrophages that prevent spread of septicaemia from injured intestines in the early days post-irradiation. New findings about the expression of various peptidoglycan structural unit receptors like NOD-1 and NOD-2 in several cell types suggest that the activation of $\gamma\delta$ T-lymphocytes could be one of the mechanisms responsible for protection of intestinal mucosa [29]. Recruitment and differentiation of mesenchymal stem cells [30] and activation of hepatocytes [31] are other events leading to protection and regeneration of injured intestine mucosa and induction of innate immunity. Together with the restoration of haemopoiesis, these processes are responsible for the increased survival of lethally irradiated mice pretreated with immunomodulators in liposome formulations [21].

On the other hand, unlike liposomal formulations, free hydrophilic MDP molecules are not effective *in vivo* at tested doses (Fig. 3). This is because of several factors including pharmacokinetic effects such as short-half-life effects owing to rapid clearance, dilution, lack of significant occurrence at the site of interest, serum protein binding and enzymatic degradation. These unfavourable factors can be limited by appropriate means such as formulation with liposomes. After *s.c.* application, liposomes can penetrate through the extracellular matrix and can reach lymph nodes via lymphatic vessels [32].

Owing to the small size, liposomes are not completely retained in lymph nodes. Instead, they spread via the bloodstream and thereby reach the bone-marrow tissue. After passing through endothelial cell fenestrations, several cell populations could be targeted [32].

At the cellular and molecular level, the first evidence of the existence of a specific intracellular receptor for MDP was reported in 1989 by Tenu and colleagues [33]. Recent studies reveal NOD1, NOD2, and cryopyrin (NALP3) as possible intracellular receptors for peptidoglycan-(PGN-) derived units such as MDP (NOD2, NALP3) and D- γ -glutamyl-*meso*-DAP (iE-DAP), which can either be generated by a degradation of PGN in lysosomes or secreted by bacteria during replication [34, 35].

The mechanisms by which MDP or its analogues are able to cross the host's cell membrane to stimulate NOD1 and NOD2 remain incompletely understood. The same holds true for mechanisms responsible for the transport of peptidoglycan fragments like MDP from phagosome into the cytoplasm. Both NOD1 and NOD2 are highly expressed in antigen presenting cells (APCs) such as monocytes, macrophages, and dendritic cells [36, 37]. Several recent studies identified NOD2 expression also in other haematopoietic lines like B-lymphocytes [38] or T-cells [39]. In addition, NOD1 is expressed in many epithelial cell subsets, whereas NOD2 seems to be more restricted to specialized cell types such as Paneth cells in the small intestine. NOD2 expression is potently induced by TLR ligands including LPS and by inflammatory mediators such as TNF- α , IFN- γ , and IL-17 in other non-haematopoietic tissues. Nevertheless it is not known whether the intracellular receptors for MDP can directly interact also with lipophilic analogues or if the lipophilic moiety has to be cleaved-off first. In the latter case, the character of the lipophilic moiety and its chemical linkage to the glycopeptides affects the biological activity by changing the pharmacokinetics at the tissue and intracellular level (Fig. 6). Our data support these considerations and these aspects are of interest for future research.

Immunogenicity of rHsp90 Mounted by Metallochelation to Liposomes in the Presence and Absence of norAbuMDP/GMPD Analogues

It is supposed that the activation of inflammasome is the basis for the potent adjuvant effect of MDP and its analogues [40]. The mounting of recombinant antigen proteins (such as rHsp90) on liposomes by metallochelation represent an interesting new system for the formulation of weak recombinant antigens with a His-Tag anchor [15, 16]. In the present work we tested the adjuvant effect of lipophilic MDP derivatives during immunization with recombinant *Candida* Hsp90 antigen that is a target for specific antibodies during systemic candidiasis [17, 41]. The IgG2a and IgG2b antibody response associated with

Th1 dominance was elicited by the immunization with metallochelating rHsp90 liposomes containing MT03, MT07, or MT06 adjuvants. Such antibodies can act by opsonization, neutralization of extracellular virulence factors, inhibition of the *Candida* adherence to host tissues, inhibition of the yeast- to-mycelium transition, and by direct fungicidal activity [41].

Safety of norAbuMDP and norAbuGMDP Analogues

The main achievement of our approach based on structural changes in MDP (Fig. 1) was suppression of pyrogenicity (Table II) and suppression of related flu like syndromes. Moreover, no side effects on rabbits (including skin lesions at the site of application) were observed during a 1-month period after the application. NorAbuMDP and especially norAbuGMDP analogues were shown apyrogenic at doses far in excess of those appropriate for a clinical application (e.g. as adjuvants in vaccines).

In this study, none of the tested analogue exhibited any toxic effects. This is in a good accordance with our previous experience with various animal species like mice, guinea pigs, goats, calves and pigs, which have been tested in our laboratory [21, 42–44].

At present, in addition to the immunostimulatory effect of MT03, MT07 and to a lesser extent MT06, leading to dominance in Th1 responses specific to *C. albicans* rHsp90, liposomal formulations of MT05 and MT06 are in testing as adjuvants for veterinary recombinant vaccines. No side effects have so far been observed after *s.c.* or *i.m.* application of experimental recombinant vaccine against boreliosis in dog puppies or cats (unpublished data). These results are promising for the intended application in human vaccines.

Potential Toxicity of Nickel

Toxicity of nickel is broadly discussed topic. With respect to metallochelating liposomes, it should be stressed, that the problem is quite different from toxicity on inhaled nickel oxide nanoparticles, which are accumulated in lungs of workers in metall industry and this form of nickel is responsible for chronic inflammation and lung cancer.

For the general population, the predominant route of exposure to nickel is through food intake. Nickel intake in the United States ranges between 69 and 162 $\mu\text{g}/\text{day}$ for adults (>18 years of age) (http://rais.ornl.gov/tox/profiles/nickel_and_nickel_compounds_f_V1.html). The estimated dose of nickel in vaccine represents only 1–5% of daily intake.

In liposomes, Ni⁺² is complexed in the metallochelating ligand in metallochelating lipids. This complex is extremely stable, therefore leakage of Ni ions is very slow (basic characteristic generally known from metalloaffinity chromatography)

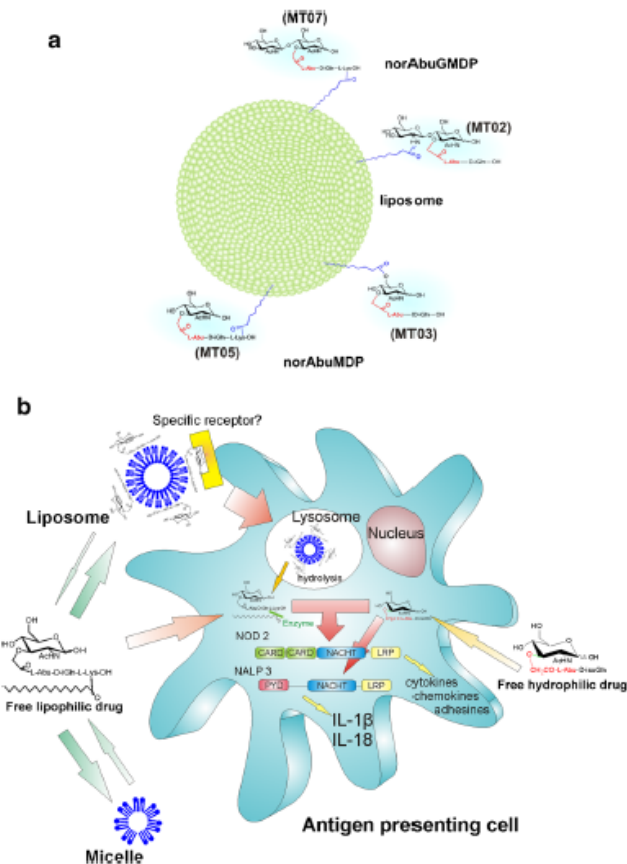


Fig. 6 Schematic structure of norAbuMDP/GMDP nanoliposomes and their pharmacokinetic pathways. **(a)** Schematic presentation of nanoliposome with various MT derivatives incorporated into bilayer. Various modifications of the norAbuMDP/GMDP molecule by lipidic residues affect the exposition of sugar- and peptide-moieties on the liposomal surface. Depending on the concentration of particular analogues or their mixture in the bilayer, new molecular patterns can be formed on the liposomal surface. These molecular patterns can be recognized by cell-membrane receptors. **(b)** Schematic presentation of pharmacokinetic pathways of liposomal and free MDP analogues at cellular and intracellular levels. A free hydrophilic drug (e.g., MDP) has difficulties to cross the cell membrane and thus, it is difficult to reach an efficient intracellular concentration *in vivo*. The hydrophobized analogues of MDP form micelles whose pathways are difficult to be predicted owing to the complexity of the interactions with the components of biological milieu. Direct interaction with the cell membrane and penetration into cytoplasm is supposed to occur. The liposomal formulation of both hydrophilic and lipophilic derivatives of MDP is relatively stable in biological milieu and endocytosed by dendritic cells. In comparison to the free drug, liposomal formulations significantly increase the intracellular concentration of MDP analogues. Lysosomal and cytoplasmic enzymes cleave the ester-bond-linking glycopeptide part to a hydrophobic residue. The importance of this pathway has not been recognized and fully understood yet. Nevertheless, it is reasonable to suppose that various derivatives will differ in their sensitivity to the enzymatic hydrolysis. Moreover, the mechanism of MDP-based activation of NOD and NALP3 receptors has not been precisely described and it is a hot issue. A question of a special relevance is, whether the hydrophobic residue of some derivatives has to be cleaved off to release the active glycopeptide molecule. The complexity of these processes is reflected in the variances in the effects of particular analogues having the same glycopeptide core but different position and structure of the hydrophobic residue.

and local long lasting increase of free Ni^{+2} is not the case. Moreover soluble nickel ions are not accumulated in the body, clearance is rapid and at least in animals nickel is essential element. We have not seen any adverse effect on metallochelating liposomes containing nickel applied

into several animal species. Our data are in very good accordance with the data from a Phase I Open-label Study of the Safety and Immunogenicity of Escalating Doses of Lipovaxin-MM (NCT01052142) (<http://clinicaltrials.gov/ct2/show/NCT01052142?term=>

NCT01052142&rank=1) regarding testing of anticancer vaccine based on metallochelating liposomal platform.

CONCLUSIONS

New lipophilic derivatives of norAbuMDP/GMDP proved themselves as promising molecular adjuvants for recombinant vaccines as well as immunomodulators for the stimulation of innate immunity and bone-marrow recovery after chemo/radio therapy of cancer. No side effects like pyrogenicity or local irritation (e.g. necrosis or ulceration) were observed in mice and rabbits. Liposome-based formulations were demonstrated to be an effective and safe application form for the tested lipophilic compounds.

At present clinical evaluation of a liposomal recombinant vaccine against Lyme boreliosis adjuvanted with lipophilic derivatives of norAbuMDP/GMDP is running in dogs and cats. Safety and induction of immune response has been demonstrated and data is in a good agreement with that published in this paper.

ACKNOWLEDGMENTS AND DISCLOSURES

By this paper we would like to revere the memory of deceased MUDr. Antonín Vacek, CSc., who pioneered the field of the effect of γ -rays on the immune system and haematopoiesis. His scientific work contributed to the cosmic flight of spaceships with human crew and was awarded by NASA and Russian space agency within the programme Intercosmos. Moreover, we would like to revere the memory of Prof. Antonín Holý, deceased in 2012, who pioneered the field of modern antiviral drugs. The development of new norAbuMDP/GMDP analogues would not have been possible without his long-lasting support to this project.

This Work was Supported by Grants GAP304/10/1951 to J.T, M.L, M.R; TAČR TA01011165 J.T, M.L, M.R ; GAP503/12/G147 to J.T; FNUSA-ICRC CZ.1.07/2.3.00/30.0043; The Ministry of Education, Youth and Sports of the Czech Republic (CZ.1.07/2.3.00/20.0164) to J.T. and M.R.; LF_2014_020 to M.K. and M.R., the projects MZE0002716202 of the Czech Ministry of Agriculture. Special thanks to the project AdmireVet (CZ.1.05/2.1.00/01.0006 - ED0006/01/01 from the Czech Ministry of Education) for permit the access to the scanning electron microscope.

Conflict of Interest The authors have declared that no conflict of interest exists. I certify that this manuscript, or any part of it, has not been published and will not be submitted elsewhere

 Springer

for publication while being considered by the journal Pharmaceutical Research.

REFERENCES

1. Elouz F, Adam A, Giorbaru R, Lederer E. Minimal structural requirements for adjuvant activity of bacterial peptidoglycan derivatives. *Biochem Biophys Res Commun.* 1974;59(4):1317–25.
2. Parant M. Biologic properties of a new synthetic adjuvant, muramyl dipeptide (MDP). *Springer Semin Immunopathol.* 1979;2(1):101–18.
3. Takada H, Kotani S. Immunopharmacological activities of synthetic muramyl-peptides. In: Stewart-Tull D, Davier M, editors. *Immunology of the bacterial cell envelope.* Chichester: Wiley; 1985. p. 119–52.
4. Adam A, Lederer E. Muramyl peptides - immunomodulators, sleep factors, and vitamins. *Med Res Rev.* 1984;4(2):111–52.
5. Parant M, Chedid I. Stimulation of non-specific resistance to infections by synthetic immunoregulatory agents. *Infection.* 1984;12(3):230–4.
6. Yoo YC, Saiki I, Sato K, Azuma I. MDP-lys (L18), a lipophilic derivative of muramyl dipeptide, inhibits the metastasis of hematogenous and non-hematogenous tumors in mice. *Vaccine.* 1994;12(2):175–80.
7. Lecrec C, Vogel RF. Synthetic immunomodulators and synthetic vaccines. *Crit Rev Ther Drug Carrier Syst.* 1986;2:353–406.
8. Matter A. Effects of muramyl dipeptide (MDP) in cell-mediated-immunity - comparison between in vitro and in vivo systems. *Cancer Immunol Immunother.* 1979;6(4):201–10.
9. Warren HS, Vogel FR, Chedid IA. Current status of immunological adjuvants. *Ann Rev Immunol.* 1986;4:369–88.
10. Ando K, Mori K, Corradini N, Redini F, Heymann D. Mifamurtide for the treatment of nonmetastatic osteosarcoma. *Expert Opin Pharmacother.* 2011;12(2):285–92.
11. No authors listed. Mifamurtide: osteosarcoma: ineffective and harmful. *Prescrire Int.* 2011;20:89
12. Lefrancier P, Lederer E. Muramyl-peptides. *Pure Appl Chem.* 1987;59(3):449–54.
13. McLaughlin CA, Schwartzman SM, Homer BI, Jones GH, Moffatt JG, Nestor JJ, et al. Regression of tumors in guinea-pigs after treatment with synthetic muramyl dipeptides and trehalose dimycolate. *Science.* 1980;208(4442):415–6.
14. Altin JG, Parish CR. Liposomal vaccines - targeting the delivery of antigen. *Methods.* 2006;40(1):39–52.
15. Krupka M, Masek J, Bartheldyova E, Turanek Knotigova P, Plockova J, Korvasova Z, et al. Enhancement of immune response towards non-lipidized *Borrelia burgdorferi* recombinant OspC antigen by binding onto the surface of metallochelating nanoliposomes with entrapped lipophilic derivatives of norAbuMDP. *J Control Release.* 2012;160(2):374–81.
16. Masek J, Bartheldyova E, Korvasova Z, Skrabalova M, Koudelka S, Kulich P, et al. Immobilization of histidine-tagged proteins on monodisperse metallochelation liposomes: preparation and study of their structure. *Anal Biochem.* 2011;408(1):95–104.
17. Raska M, Belakova J, Wudattu NK, Kaškova I, Ruzickova K, Sebestova M, et al. Comparison of protective effect of protein and DNA vaccines lsp90 in murine model of systemic candidiasis. *Folia Microbiol.* 2005;50(1):77–82.
18. Zachova K, Krupka M, Chamrad I, Belakova J, Horynova M, Weigl E, et al. Novel modification of growth medium enables efficient *E. coli* expression and simple purification of an endotoxin-free recombinant murine Hsp70 protein. *J Microbiol Biotechnol.* 2009;19(7):727–33.

19. Turanek J. Fast-protein liquid-chromatography system as a tool for liposome preparation by the extrusion procedure. *Anal Biochem.* 1994;218(2):352–7.
20. Masek J, Bartheldyova E, Turanek-Knotigova P, Skrabalova M, Korvasova Z, Plockova J, *et al.* Metallochelating liposomes with associated lipophilised norAbuMDP as biocompatible platform for construction of vaccines with recombinant His-tagged antigens: preparation, structural study and immune response towards rHsp90. *J Control Release.* 2011;151(2):193–201.
21. Turanek J, Zaluska D, Hofer M, Vacek A, Ledvina M, Jezek J. Stimulation of haemopoiesis and protection of mice against radiation injury by synthetic analogues of muramyl dipeptide incorporated in liposomes. *Int J Immunopharmacol.* 1997;19(9–10):611–7.
22. Kasna A, Turanek J, Vacek A, Zaluska D, Knotigova P, Masek K. Restoration of femoral GM-CFC progenitors in sublethally irradiated mice of various ages treated with liposomal adamantylamide dipeptide. *Int Immunopharmacol.* 2004;4(8):1099–106.
23. Dzierzbicka K, Wardowska A, Trzonkowski P. Recent developments in the synthesis and biological activity of muramyl peptides. *Curr Med Chem.* 2011;18(16):2438–51.
24. Traub S, von Aulock S, Hartung T, Hemann C. MDP and other muropeptides - direct and synergistic effects on the immune system. *J Endotoxin Res.* 2006;12(2):69–85.
25. Azuma I, Seya T. Development of immunoadjuvants for immunotherapy of cancer. *Int Immunopharmacol.* 2001;1(7):1249–59.
26. Sakamoto S, Okawa T, Ogawa N. Therapeutic effect of microtasin on cancer patients with leucopenia during radiation therapy. *J New Rem Clin.* 1989;39:1407–22.
27. Korvasova Z, Drasar I, Masek J, Knotigova PT, Kulich P, Matiasovic J, *et al.* Antiviral effect of HPMPC (Cidofovir (R)), entrapped in cationic liposomes: In vitro study on MDBK cell and BHV-1 virus. *J Control Release.* 2012;160(2):330–8.
28. Koudelka S, Turanek-Knotigova P, Masek J, Korvasova Z, Skrabalova M, Plockova J, *et al.* Liposomes with high encapsulation capacity for paclitaxel: preparation, characterisation and in vivo anticancer effect. *J Pharm Sci.* 2010;99(5):2309–19.
29. Marichen I, Wesch D, Oberg HH, Roenstiel P, Trad A, Shomali M, *et al.* Functional expression of NOD2 in freshly isolated human peripheral blood gamma delta T cells. *Scand J Immunol.* 2011;74(2):126–34.
30. Kim HS, Shin TH, Yang SR, Seo MS, Kim DJ, Kang SK, *et al.* Implication of NOD1 and NOD2 for the differentiation of multipotent mesenchymal stem cells derived from human umbilical cord blood. *PLoS One.* 2010;5(10):e15369.
31. Scott MJ, Chen C, Sun QA, Billiar TR. Hepatocytes express functional NOD1 and NOD2 receptors: a role for NOD1 in hepatocyte CC and CXC chemokine production. *J Hepatol.* 2010;53(4):693–701.
32. Oussoren C, Storm G. Liposomes to target the lymphatics by subcutaneous administration. *Adv Drug Deliv Rev.* 2001;50(1–2):143–56.
33. Tenu JP, Adam A, Souvannavong V, Yapo A, Petit JF, Douglas K. Photoaffinity-labeling of macrophages and lymphocyte-B using I-125-labeled aryl-azide derivatives of muramyl dipeptide. *Int J Immunopharmacol.* 1989;11(6):653–61.
34. Chamailard M, Hashimoto M, Horie Y, Masamoto J, Qiu S, Saab I, *et al.* An essential role for NOD1 in host recognition of bacterial peptidoglycan containing diaminopimelic acid. *Nat Immunol.* 2003;4(7):702–7.
35. Girardin SE, Travassos LH, Herve M, Blanot D, Boneca IG, Philpott DJ, *et al.* Peptidoglycan molecular requirements allowing detection by Nod1 and Nod2. *J Biol Chem.* 2003;278(43):41702–8.
36. Fritz JH, Ferreno RI, Philpott DJ, Girardin SE. NOD-like proteins in immunity, inflammation and disease. *Nat Immunol.* 2006;7(12):1250–7.
37. Kanneganti TD, Lamkanfi M, Nunez G. Intracellular NOD-like receptors in host defense and disease. *Immunity.* 2007;27(4):549–59.
38. Peterson T, Jendholm J, Marsson A, Bjartell A, Riesbeck K, Cardell LO. Effects of NOD-like receptors in human B lymphocytes and crosstalk between NOD1/NOD2 and toll-like receptors. *J Leukoc Biol.* 2011;89(2):177–87.
39. Shaw MH, Reimer T, Sanchez-Valdepenas C, Warner N, Kim YG, Fresno M, *et al.* T cell-intrinsic role of Nod2 in promoting type 1 immunity to *Taeniolasma gondii*. *Nat Immunol.* 2009;10(12):1267–74.
40. Martinon F, Agostini I, Meylan E, Tschopp J. Identification of bacterial muramyl dipeptide as activator of the NALP3/cryopyrin inflammasome. *Curr Biol.* 2004;14(21):1929–34.
41. Raska M, Belakova J, Krupka M, Weigl E. Candidiasis - do we need to fight or to tolerate the *Candida* fungus. *Folia Microbiol.* 2011;52:297–312.
42. Orsag P, Kvardova V, Raskova M, Miller AD, Ledvina M, Turanek J. Quantitative real-time PCR study on persistence of pDNA vaccine pVax-Hsp60 TM814 in beef muscles. *Genet Vaccines Ther.* 2008;6:1–11.
43. Turanek J, Kasna A, Koudela B, Ledvina M, Miller AD. Stimulation of innate immunity in newborn kids against *Cryptosporidium parvum* infection-challenge by intranasal/per-oral administration of liposomal formulation of N-L 18-norAbu-GDMP adjuvant. *Parasitology.* 2005;131:601–8.
44. Turanek J, Ledvina M, Kasna A, Vacek A, Hribalova V, Krejci J, *et al.* Liposomal preparations of muramyl glycopeptides as immunomodulators and adjuvants. *Vaccine.* 2006;24:90–1.

RESEARCH ARTICLE

The Position of His-Tag in Recombinant OspC and Application of Various Adjuvants Affects the Intensity and Quality of Specific Antibody Response after Immunization of Experimental Mice



CrossMark
click for updates

Michal Krupka¹, Josef Masek², Lucia Barkocziava¹, Pavlina Turanek Knotigova², Pavel Kulich², Jana Plockova², Robert Lukac², Eliska Bartheldyova², Stepan Koudelka^{2,3}, Radka Chaloupkova^{3,4}, Marek Sebel⁵, Daniel Zyka⁵, Ladislav Droz⁶, Roman Effenberg⁷, Miroslav Ledvina⁷, Andrew D. Miller⁸, Jaroslav Turanek^{2*}, Milan Raska^{1,2*}

1 Department of Immunology, Faculty of Medicine and Dentistry, Palacky University Olomouc, Olomouc, Czech Republic, **2** Department of Pharmacology and Immunotherapy, Veterinary Research Institute, Brno, Czech Republic, **3** International Clinical Research Center, St. Anne's University Hospital, Brno, Czech Republic, **4** Loschmidt Laboratories, Department of Experimental Biology and Research Centre for Toxic Compounds in the Environment RECETOX, Masaryk University, Brno, Czech Republic, **5** Centre of the Region Hana for Biotechnological and Agricultural Research, Faculty of Science, Palacky University Olomouc, Olomouc, Czech Republic, **6** Apigenex, Prague, Czech Republic, **7** Department of Chemistry of Natural Compounds University of Chemistry and Technology, Prague, Czech Republic, **8** King's College London, Institute of Pharmaceutical Science, London, United Kingdom, and GlobalAcorn Ltd, London, United Kingdom

* raskamil@uab.edu (MR); turanek@vuol.cz (JT)

OPEN ACCESS

Citation: Krupka M, Masek J, Barkocziava L, Turanek Knotigova P, Kulich P, Plockova J, et al. (2016) The Position of His-Tag in Recombinant OspC and Application of Various Adjuvants Affects the Intensity and Quality of Specific Antibody Response after Immunization of Experimental Mice. PLoS ONE 11(2): e0148497. doi:10.1371/journal.pone.0148497

Editor: Brian Stevenson, University of Kentucky College of Medicine, UNITED STATES

Received: November 6, 2015

Accepted: January 20, 2016

Published: February 5, 2016

Copyright: © 2016 Krupka et al. This is an open access article distributed under the terms of the [Creative Commons Attribution License](https://creativecommons.org/licenses/by/4.0/), which permits unrestricted use, distribution, and reproduction in any medium, provided the original author and source are credited.

Data Availability Statement: All relevant data are within the paper.

Funding: These studies were supported by LF_2014_020 and LF_2015_009 (Palacky University, Olomouc, Czech Republic) (MR, MK); project CENATOX; Grant of the European Union FP7 REGPOT – Human Bridge 316345 (RC); Grant Agency of Czech Republic, GAP503/12/G147 (JT); the Ministry of Education, Youth and Sports CZ.1.07/2.3.00/20.0/164 (MR, JT) and LO1304, LO1214 and LM2011028 (RC); MZE002716202 Czech Ministry

Abstract

Lyme disease, *Borrelia burgdorferi*-caused infection, if not recognized and appropriately treated by antibiotics, may lead to chronic complications, thus stressing the need for protective vaccine development. The immune protection is mediated by phagocytic cells and by *Borrelia*-specific complement-activating antibodies, associated with the Th1 immune response. Surface antigen OspC is involved in *Borrelia* spreading through the host body. Previously we reported that recombinant histidine tagged (His-tag) OspC (rOspC) could be attached onto liposome surfaces by metallochelation. Here we report that levels of OspC-specific antibodies vary substantially depending upon whether rOspC possesses an N' or C' terminal His-tag. This is the case in mice immunized: (a) with rOspC proteoliposomes containing adjuvants MPLA or non-pyrogenic MDP analogue MT06; (b) with free rOspC and Montanide PET GEL A; (c) with free rOspC and alum; or (d) with adjuvant-free rOspC. Stronger responses are noted with all N'-terminal His-tag rOspC formulations. OspC-specific Th1-type antibodies predominate post-immunization with rOspC proteoliposomes formulated with MPLA or MT06 adjuvants. Further analyses confirmed that the structural features of soluble N' and C' terminal His-tag rOspC and respective rOspC proteoliposomes are similar including their thermal stabilities at physiological temperatures. On the other hand, a change in the position of the rOspC His-tag from N' to C' terminal appears to affect

of Agriculture (JT); Technological Agency of Czech Republic TA01011105 – Multiepitopic vaccine against borreliosis (to JT, MR, ML); TA02010760 – Development of anticancer immunotherapeutics of new generation (ML, LD). SK was supported by the European Social Fund and the State Budget of the Czech Republic – Project FNUSA-ICRC, support for neurological research and development teams through postdoc position formations CZ.1.07/2.3.00/30.0043. The teams headed by Jaroslav Turánek, Milan Raška, and Andrew D. Miller are obligated to the Ministry of Education, Youth and Sports for supporting of the project "FIT" (Pharmacology, Immunotherapy, nanotoxicology). The funder provided support in the form of salaries for authors (DZ, LD), but did not have any additional role in the study design, data collection and analysis, decision to publish, or preparation of the manuscript. The specific roles of these authors are articulated in the 'author contributions' section.

Competing Interests: The authors declare no commercial or financial conflict of interest. The commercial affiliation of DZ, LD, and ADM does not alter the authors' adherence to PLOS ONE policies on sharing data and materials.

substantially the immunogenicity of rOspC arguably due to steric hindrance of OspC epitopes by the C' terminal His-tag itself and not due to differences in overall conformations induced by changes in the His-tag position in rOspC variants.

Introduction

Spirochete *Borrelia burgdorferi* s. l. is the causative agent of Lyme disease. Although at least nine *Borrelia* species are currently considered potentially pathogenic [1] *B. afzelii*, *B. garinii*, and *B. burgdorferi* s. s. still predominates in Europe and *B. burgdorferi* s. s. in the USA. If untreated by antibiotic therapy in time, Lyme disease can develop into a chronic phase of infection with long-lasting neural, cardiovascular, cutaneous, or orthopedic complications [2, 3]. In some patients, the chronic phase can develop in spite of intensive antibiotic treatment. This complication emphasizes the need for the development of protective vaccines to control either *Borrelia* transmission from tick to vertebrate host or subsequently from spreading through the mammalian host organism [4–6]. Currently, (Outer surface protein) OspA and OspC are considered as the most promising antigens for vaccination purposes [5].

OspC is a lipoprotein antigen of approximately 23 kDa and 210 amino acid residues localized on the *Borrelia* surface. The expression of OspC is required for *Borrelia* transmission from tick to vertebrate host and for the initial stage of vertebrate host infection. *Borrelia* lacking OspC and regulatory sigma factors RpoS, RpoN, or Rrp2 are severely impaired in their pathogenicity [7, 8]. The native conformation of OspC seems to be crucial for the induction of borreliacidal antibodies because if this antigen is denatured, the induction of the antibodies fails [9]. Epitopes recognized by protective antibodies were mapped to the C-terminal regions of OspC, specifically the regions loop 5, helix 5, and conserved last 20 amino acid residues [10, 11].

Nascent OspC contains a N-terminal lipidation signal sequence leading to the modification of OspC by addition of a the hydrophobic triacylglycerol moiety important for the subsequent integration of OspC into the outer membrane of *Borrelia* [12, 13]. Because full-length recombinant OspC is difficult to express in *E. coli*, a non-lipidated version of OspC was constructed by eliminating the signal sequence (amino acid residues 1–18) and a high yield of expression was achieved [13–15]. Nevertheless, non-lipidated OspC is only a weak immunogen, stressing the need for strong adjuvant co-administration [15, 16].

Liposomes can incorporate antigen and/or immunomodulatory molecules and can be employed as biocompatible particulate vaccine carriers [17]. Antigenic or adjuvant molecules can also be attached by non-covalent interactions such as metallochelation, a process in which recombinant antigenic proteins in particular with 4 to 6 histidine amino acid residue extensions (His-tags) are able to chelate with divalent metal ions that are complexed to liposome membrane surfaces via metal complexes anchored to those same liposomes surfaces by lipidic tails (e.g., DOGS-NTA-Ni). Proteoliposomes may be further modified to carry adjuvants such as monophosphoryl lipid A, muramyl dipeptide (MDP) and other non-pyrogenic analogues such as Nor-AbuMDP or Nor-AbuGMDP [18–21]. Although the His-tag is a short and poorly immunogenic sequence, its attachment to a recombinant protein might mask immunologically important epitopes and reduce the potential immune response towards the target antigen, a potential impact that requires experimental evaluation [22].

In this study, we compared the immune response of experimental mice after intradermal immunization with rOspC proteoliposomes formulated with synthetic lipophilic molecular adjuvants MPLA or MT06, with rOspC formulated with a Montanide PET GEL A dispersion, with rOspC formulated with alum, or with free rOspC variants formulated without adjuvant and differing only in the N' or C' terminal attachment of a His-tag.

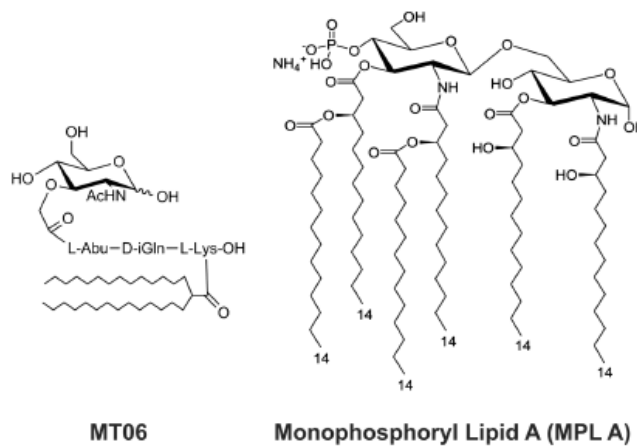


Fig 1. Synthetic molecular adjuvants MT06 and MPLA. Left panel shows MT06, a non-pyrogenic lipophilic derivative of muramyl dipeptide (MDP) analogue—Nor-AbuMDP. The right panel shows monophosphoryl lipid A, a derivative of lipopolysaccharide from *S. minnesota*.

doi:10.1371/journal.pone.0148497.g001

Material and Methods

General

Egg phosphatidylcholine (purity of 99%), 1,2-Dioleoyl-sn-Glycero-3-Phosphoethanolamine-N-(Lissamine Rhodamine B Sulfonyl) (LisR), 1,2-Dioleoyl-sn-Glycero-3-([N(5-Amino-1-Carboxypentyl)iminodiAcetic Acid]Succinyl)(Nickel Salt) (DOGS-NTA-Ni), lipid were purchased from Avanti Polar Lipids (Birmingham, AL). DIO18 was purchased from Molecular Probes (Invitrogen, Carlsbad, CA). 20 nm membrane filter Anotop 10 and 0.2 μm Anotop 10 LC were purchased from Whatman (Maidstone, UK). All other chemicals, unless specially specified, were from Sigma (St. Louis, MO).

Synthetic nor-AbuMDP analogue

The synthetic nor-AbuMDP analogue adjuvant, MT06, was prepared as described by Ledvina and coworkers [23] (Fig 1). This non-pyrogenic analogue adjuvant was selected for this study from a series of such nor-AbuMDP analogues. Monophosphoryl lipid A (MPLA) was purchased from Sigma (St. Louis, MO) (Fig 1). Both Montanide PET GEL A (Seppic, Paris, France) and Alum (InvivoGene, San Diego, CA) were used as standard adjuvants for comparison.

Preparation and purification of rOspC

B. burgdorferi s. s. OspC cDNA (corresponding to GenBank Acc. No. EF537426), lacking the first 54 nucleotides, coding for a lipidation signal, was isolated originally from *Borrelia burgdorferi* s. s. B31 plasmid DNA preparation, obtained using a Qiagen plasmid purification kit (Qiagen, Hilden, Germany) according to the manufacturer's recommended modification for *Borrelia* plasmid DNA, by RT-PCR.

The PCR product of the reaction performed with downstream adapter primer (CACCATG TGTAATAATTCAGGGAAGATGGG) and upstream primer (AGGTTTTTTTGGACTTT CTGCC) and Phusion DNA polymerase (New England BioLabs, Ipswich, MA) was cloned into *E. coli* expression plasmids pET101 and pET200 (Invitrogen) in order enable the expression of non-lipidated rOspC fusion proteins with a V5-tag and a C' terminal His-tag or an Xpress-tag with N' terminal His-tag. N' and C' terminal His-tag rOspC variants were purified under native conditions using the Ni-NTA agarose (Qiagen) as described earlier [15] with modified lysis buffer: (50 mM Tris; 300 mM NaCl; 10 mM Imidazole; 1 mg/ml hen egg white lysozyme; 0,1% Triton X-100; protease inhibitors: 0.2 mM PMSF; 0.4 µg/ml Leupeptin; 0.5 µg/ml Aprotinin; pH8.0). Subsequently, the proteins were dialyzed against Tris-HCl storage buffer (50 mM Tris, 150 mM NaCl, pH7.5).

Endotoxin removal

Lipopolysaccharide (endotoxin, LPS) was removed by repeated phase extraction procedure using detergent Triton X-114 as described earlier [15], until the endotoxin level in every rOspC samples was below 2.5 EU/mg. The endotoxin concentration was measured by the gel-clot assay using Limulus Amebocyte Lysate (Associates of Cape Cod, USA).

Characterization of rOspC by SDS-PAGE and MALDI-TOF MS

The purity of rOspC variants was analyzed using 12% T/3% C SDS-PAGE followed by staining with Coomassie Brilliant Blue (CBB) G-250. Protein identity was confirmed by peptide mass fingerprinting of SDS-PAGE-resolved samples on a Microflex LRF20 MALDI-TOF (matrix-assisted laser desorption/ionization time-of-flight) mass spectrometer (Bruker Daltonik, Bremen, Germany) as described previously [24]. In addition, the digests of the rOspC proteins were subjected to nanoflow liquid chromatography coupled with MALDI-TOF/TOF mass spectrometry (MS) and tandem mass spectrometry (MS/MS) analyses performed using an ultraflexXtreme mass spectrometer by Bruker Daltonik [25]. Proteins were then identified by peptide sequence comparisons with experimental peptide mass lists or MS/MS data, respectively, found in the NCBI nr protein sequence database (September 2015) using program Mascot, version 2.2.07 (Matrix Science, London, UK).

Preparation of rOspC-based immunization formulations

Each vaccine dose contained 20 µg of non-lipidated C' or N' terminal His-tag rOspC. Proteoliposome formulations were prepared by adding 20 µg of rOspC antigen to 300 µg of preformed EPC/POPG/DOGS-NTA-Ni/adjuvant metallochelation liposomes (71/19/5/5 mol%) (per one immunization dose), prepared by the "hydration of a lipid film" method followed by extrusion through 200 nm polycarbonate filters (Mini-Extruder, Avanti Polar Lipids, Alabaster, AL) [18, 19]. The rOspC was added to the preformed metallochelation liposomes formulated with either MT06 or MPLA as adjuvant. In addition, other soluble rOspC/adjuvant samples were prepared by mixing rOspC with alum or with Montanide PET GEL A. The composition of particular formulations is specified (Table 1). As a naïve control, we used sera from mice immunized with recombinant His-tag p24-Hsp70 protein [26].

Immunization of experimental mice

All experiments were performed on 6- to 8-week old female BALB/c mice purchased from Biotest (Konarovice, Czech Republic). All animals were free of known pathogens and were kept in a climate-controlled environment with 12 h light-dark-cycle, and were provided with

Table 1. Doses and vaccine formulations.

Groups of 5 mice	Composition per one dose (50 µl)					
	rOspC[µg]	Liposome[µg]	AIOH[%]	PET GEL[%]	MPLA[µg]	MT06[µg]
N' or C' rOspC	20	-	-	-	-	-
N' or C' rOspC + alum	20	-	25	-	-	-
N' or C' rOspC + PET GEL A	20	-	-	5	-	-
N' or C' rOspC + MT06 proteoliposome	20	300	-	-	-	21.4
N' or C' rOspC + MPLA proteoliposome	20	300	-	-	32.6	-
Control hsp70-p24	-	-	-	-	-	-

doi:10.1371/journal.pone.0148497.t001

pellet food and water *ad libitum*. The vaccination experiments were approved by the Ethics Committee of the Faculty of Medicine and Dentistry (Palacky University in Olomouc), and the Ministry of Education, Youth and Sport, Czech Republic. The animals were monitored daily by a veterinarian for their behavior, psychic activity, discharge from natural body forams, nutrition and hydration status, skin status and eventual lesions. The protocol for early/humane endpoints in cases where animals became severely or irreversibly ill prior to the experimental endpoint was implemented according to the animal facility rules, for recognition and assessment of pain, distress, and suffering, stating that the animals that are moribund or in a state of impending death should be immediately euthanized. The composition of doses is shown (Table 1). Because all tested adjuvants were earlier confirmed as safe and not inducing severe adverse side effects [15, 19] we opted for an intradermal (i.d.) route of vaccines administration in order to obtain intense immune responses. All mice were immunized twice with particular rOspC formulations (priming followed by boosting 14 days) by *i.d.* administration using a G29 needle into fur clipped and 70% ethanol disinfected skin of the ventral abdomen. The needle was inserted, bevel up, nearly parallel to the plane of the skin for at least 8 mm. The solution was slowly injected. The formation of a hard bleb was taken as a sign of successful administration of the vaccine. Blood samples (130 µl per mouse) were obtained using tail vein sample collection approach. During the experiment, none mouse died nor exhibited clinical signs of pain, distress, or suffering. After termination of the experiment, the animals were euthanized under Katemine/Xylazine anesthesia by cervical dislocation.

OspC-specific serum antibody levels determination by ELISA

All assays were performed in duplicates. For all ELISA, rOspC was devoid of all tags using recombinant enterokinase as described recently [26]. ELISA assays were performed as described [26]. In brief, ELISA wells were coated with 100 ng/well of non-tag rOspC. OspC-specific IgG+IgM+IgA (IgP), IgG1, IgG2a levels were then measured. The results were expressed as the specific antibodies O.D. determined at linear proportion of sera dilution determined in preliminary experiment using Genesis Lite Software (Version 3.03, Life Sciences, Basingstoke, UK).

Transmission electron microscopy and immunogold labeling of N' and C' terminal His-tag rOspC proteoliposomes

The liposome structures were determined using transmission electron microscope (EM Philips 208 S, MORGAGNI software, FEI, CZ). Non-liposome bound rOspC was separated from the proteoliposomes by Superose 6 gel permeation chromatography. The proteoliposome fractions were then concentrated using ultrafiltration centrifugation tube (cut off 30 kDa) and incubated

with murine OspC-positive or -naïve sera diluted 1:50 for 1 h at 37°C. 10-nm colloidal gold-protein A conjugate was added. After 12 h incubation, the proteoliposomes were negatively stained by 2% (w/w) ammonium molybdate (pH 6.8).

Determination of secondary structure and thermal stability of His-tag rOspC proteins by circular dichroism

Circular dichroism (CD) spectra were obtained at room temperature (22°C) using a Chirascan CD spectrometer (Applied Photophysics, United Kingdom). Data were collected from 185 to 260 nm at 100 nm/min, 1 s response time, and 2 nm bandwidth using a 0.1 cm quartz cuvette containing the rOspC in 50 mM potassium phosphate buffer, pH 7.5. Each spectrum shown is the average of five individual scans and was corrected for absorbance of the buffer. CD data were expressed as the mean residue ellipticity. The proportion of certain secondary structure was calculated from the measured spectra using CDSSTR, Selcon3, and CONTIN methods using DichroWeb server. Thermal unfolding of rOspC was followed by monitoring the ellipticity at 195 and 222 nm over the temperature range of 20 to 80°C, resolution of 0.1°C, at a heating rate of 1°C/min. Recorded thermal denaturation curves were roughly normalized to represent signal changes between approximately 1 and 0 and fitted to sigmoidal curves using software Origin 6.1 (OriginLab, Massachusetts, USA). The melting temperature (T_m) was evaluated as a midpoint of the normalized thermal transition.

Determination of secondary structure of His-tag rOspC proteins by Fourier transform infrared (FTIR) spectrometry

The infrared spectra of individual rOspC were obtained using a FTIR spectrometer TENSOR 27 (Bruker Optics, Germany) with an AquaSpec flow-through transmission cell and operating at 4 cm^{-1} spectral resolution. The protein concentration in 50 mM potassium phosphate buffer, pH 7.5, was 1 mg/ml. The same buffer was used for the background measurements. The secondary structure was determined by analyzing the amide-I band (1700–1600 cm^{-1}) via a multi-variant pattern recognition method based on a FTIR spectra library provided by the manufacturer.

Determination of thermal stability by DSC

Differential scanning calorimetry (DSC) measurements were performed using DSC 6100 Nano-Differential Scanning Calorimeter II (Setaram, Caluire, France) with a cell volume of 0.3 ml. Prior the injection, the samples in Dulbecco's PBS without calcium chloride and magnesium chloride were extensively degassed. The protein concentration of C' and N' terminal His-tag rOspC was 6.9 and 6.2 mg/ml, respectively. Scans ran from 10 to 85°C at a scan rate of 1°C per minute. The reference-baseline was obtained by buffer vs. buffer scan and subtracted from the data measurement. The apparent molar heat capacity and excess molar heat capacity curves were obtained from the calorimetric profiles corrected by baseline subtraction.

Determination of thermal stability by DLS

Thermal stability of C' and N' terminal His-tag rOspC proteins was determined also by dynamic light scattering (DLS). The hydrodynamic diameters of rOspC were monitored over the temperature range of 25–55°C at the temperature gradient of 1°C/min. The concentration of rOspC proteins in Dulbecco's PBS without calcium chloride and magnesium chloride was 1 mg/ml.

Statistical analyses

Statistical significance was determined by analysis of variance (ANOVA) followed by Dunnett's Multiple Comparison Test or Student-Newman-Keuls (SNK) Multiple Comparison Test. All statistical analyses were performed using GraphPad Prism 5 software (GraphPad Software Inc, CA, USA).

Results

Purification and identification rOspC antigens

Two rOspC variants were expressed in *E. coli*, reaching a yield of approximately 30 mg of rOspC per 1 L of culture. Due to different cloning strategies, both rOspC variants differed in theoretical molecular weight: 27.12 kDa for N' terminal His-tag rOspC and 23.96 kDa for C' terminal His-tag rOspC (ProtParam tool; www.expasy.ch). These molecular weights were confirmed experimentally by SDS-PAGE with CBB staining (Fig 2A). The purity of both rOspC variants was confirmed as higher than 93% by comparing the density of rOspC bands with all other visible bands on gel (using ImageJ 1.41a software).

The identities of both rOspC variants were further confirmed by peptide mass fingerprinting using MALDI-TOF MS, wherein the dominant protein bands (indicated by arrows Fig 2A) were sequence matched with the known OspC protein sequence (NCBI nr gi|374718430). Sequence coverage was 63% (13 peptides) for both N' and C' terminal His-tag rOspC. The corresponding probability-based MOWSE scores were 157 and 162, respectively. Examples of peptide MS spectra for both rOspC variants are provided in Fig 2B and 2C. In addition, nanoLC-MALDI-TOF/TOF MS and MS/MS were used for peptide-matching with respect to two other known OspC sequences: gi|68161620 for N' terminal His-tag rOspC (25 peptides, sequence coverage—75.7%, score—2743) and gi|1695212 for C' terminal His-tag rOspC (14 peptides, sequence coverage—77.6%, score—1825). The two recombinant proteins were distinguished by means of specific peptides found in respective peptide digests, such as *m/z* 2255.9 (DLYDDDDKDHFPFCNNSGK) for N' terminal His-tag rOspC.

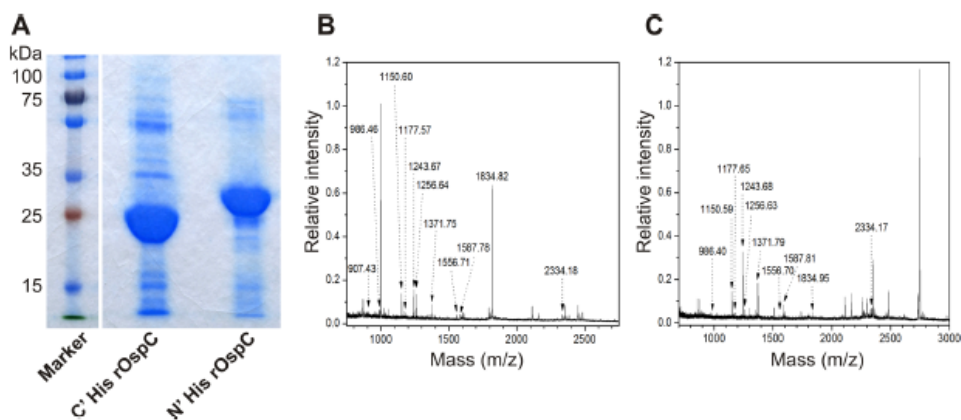


Fig 2. SDS-PAGE and MS analyses of recombinant N' and C' terminal His-tag rOspC. A) Recombinant N' and C' terminal His-tag rOspC proteins were separated using SDS-PAGE and stained by CBB G-250. The differences in mobility of both rOspC variants are caused by the length of labeling tags and spacers and correspond to theoretical prediction based on cDNA sequences: 23.96 kDa for C' and 27.12 for N' terminal His-tag rOspC. B, C) MALDI-TOF peptide mass fingerprinting of rOspC proteins. All spectra were acquired using CHCA matrix on Microflex LRF20 MALDI-TOF mass spectrometer. Panel B) refers to C' terminal His-tag rOspC and panel C) N' terminal His-tag rOspC.

doi:10.1371/journal.pone.0148497.g002

Immunization of mice with rOspC antigens

Using an ELISA approach, we identified that immunizations with soluble rOspC without any adjuvant elicited significant increases in the levels of OspC-specific antibodies response in total Ig isotypes (IgP), but only when N' terminal His-tag rOspC was used whereas C' terminal His-tag rOspC was significantly less effective (SNK test, $P < 0.001$) (Fig 3A). Similarly, even with adjuvants present, all groups of mice immunized with C' terminal His-tag rOspC exhibited substantially lower antibody responses in comparison to groups immunized with N' terminal His-tag rOspC (SNK test, $P < 0.001$) (Fig 3A). Otherwise, in terms of the antigen-adjuvant combinations tested, Montanide PET GEL A/His-tag rOspC combinations appeared the weakest antigen-adjuvant combinations tested (SNK test, $P < 0.001$), whilst the N' terminal His-tag rOspC proteoliposomes combination formulated with MPLA was the most effective antigen-adjuvant combination tested (SNK test, $P < 0.001$). The N' terminal His-tag rOspC proteoliposomes combination formulated with MT06 was able to induce equivalent levels of OspC-specific antibodies to the N' terminal His-tag rOspC/alum antigen-adjuvant combination (SNK test, $P < 0.001$) (Fig 3A). Furthermore, alum was found to be the most effective adjuvant to help induce antibody responses with C' terminal His-tag rOspC immunization (SNK test, $P < 0.001$).

In further experiments, we compared the stimulated levels of two specific IgG isotype antibodies following immunization with N' terminal His-tag rOspC/adjuvant combinations. The IgG isotype antibodies analyzed were IgG1 representing the Th2 type and IgG2a representing the Th1 type of immune response. Quite clearly, the presence of alum elicited the highest levels of OspC-specific IgG1 antibody production but only very weak corresponding IgG2a antibody production levels (SNK test, $P < 0.001$) (Fig 3B and 3C). Similarly, the presence of Montanide PET GEL A also resulted in respectable levels of OspC-specific IgG1 antibody production but also only weak corresponding IgG2a antibody production. Conversely, N' terminal His-tag rOspC proteoliposomal formulations, using either MPLA or MT06 as adjuvants, induced strong immune responses involving IgG1 and IgG2a isotypes (Fig 3B and 3C) and the IgG2a responses were substantially greater than the corresponding IgG2a responses seen when alum or Montanide PET GEL A were used as adjuvants, or when free N' terminal His-tag rOspC was administered without adjuvant (SNK test, $P < 0.001$) (Fig 3C). Otherwise, when C' terminal His-tag rOspC was tested, only proteoliposomes with added MPLA induced detectable increases in OspC-specific IgG2a antibodies (SNK test, $P < 0.001$), while alum helped promote a surprisingly effective C' terminal His-tag rOspC mediated induction of IgG1 responses (Fig 3B) (SNK test, $P < 0.001$). Of note, administration of rOspC proteoliposomes was associated with lowest, practically undetectable irritation at the application site (data not shown).

Immunogold TEM analyses of rOspC proteoliposomes

As the N' terminal His-tag rOspC proteoliposomes with MT06 or MPLA exhibited highest efficacy in inducing the OspC-specific IgG2a antibodies, these proteoliposomes were characterized in more detail using TEM (Fig 4). Gold nanoparticles labeling of rOspC gave rise to the appearance of short rOspC chains distributed on the liposome surface. Similar pattern was noted for C' terminal His-tag rOspC (data not shown). When OspC-naïve mouse sera were used for labeling, no positivity of immunogold was observed (data not shown).

Analyses of the secondary structure of rOspC proteins

Both rOspC proteins exhibited CD spectra with two sharp negative maxima at 222 and 208 nm and one highly intense positive maximum at 195 nm characteristic of α -helical structure, suggesting that the position of His tag has no detectable effect on the secondary structure

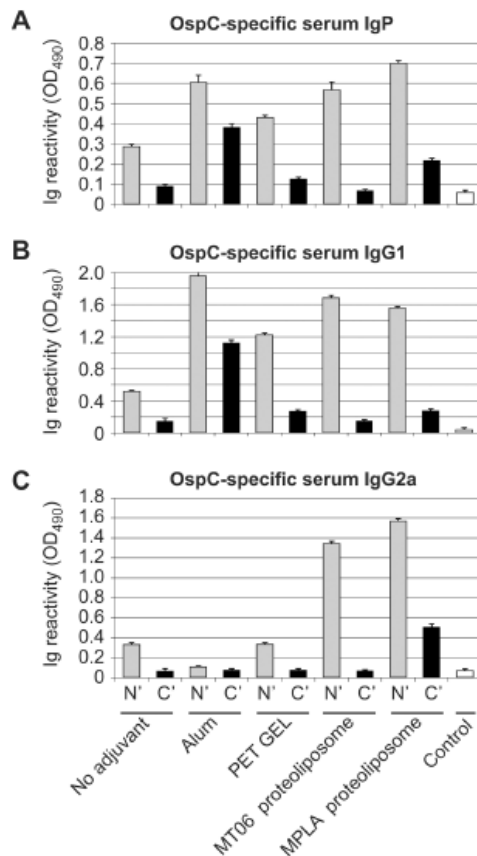


Fig 3. Determination of rOspC-specific antibodies in sera of immunized mice by ELISA. Mice (5 per group) were immunized twice in 14 days interval by i.d. administration of various N' and C' His-tagged rOspC formulations as specified in Table 1. Pooled sera from mice in each group were used for ELISA analysis of OspC-specific antibodies. Control sera were obtained from mice immunized by recombinant His-tagged p24-Hsp70 without adjuvants [26]. ELISA plates were coated with 0.1 µg of non-tagged rOspC, incubated with serially diluted pooled sera obtained 14 days after second immunization and developed with HRP-conjugated anti-mouse A) IgG+IgM+IgA (IgP), B) IgG1, and C) IgG2a, developed with orthophenylene diamine. The absorbance was read at 490 nm. The response of mice immunized by N' His-tagged rOspC are in gray, and C' His-tagged rOspC are in black. The results are expressed as mean absorbance (O.D.) at optimal sera dilutions (1:4000 for IgP and IgG2a; 1:8000 for IgG1) corresponding to linear portion of titration curve ± SD. The expressed values correspond to means from three independent immunization experiments.

doi:10.1371/journal.pone.0148497.g003

(Fig 5A). The analysis of the spectra revealed that the secondary structure is predominantly helical. The predicted α-helical content of both measured rOspC proteins was about 62% (Fig 5B) whereas the β-sheet content was only about 5%. The secondary structure determined by

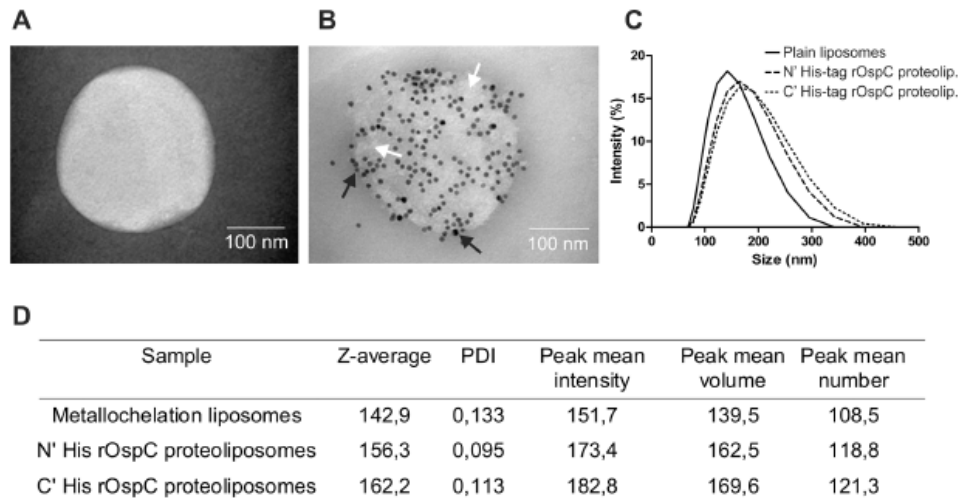


Fig 4. Characterization of metallochelating N' and C' terminal His-tag rOspC proteoliposomes by immunoEM and DLS. The EM picture of **A**) plain nanoliposome, **B**) metallochelation nanoliposome with surface bound N' terminal His-tag rOspC proteins. Metallochelation liposomes were incubated with N' and C' terminal His-tag rOspC proteins followed by incubation with pooled sera from rOspC-immunized mice (1:50 dilution) followed by addition of protein A-labeled 10-nm colloidal gold particles. After 12-h, the proteoliposomes were negatively stained by ammonium molybdate and observed using Philips Morgagni transmission EM. Black dots represent immunogold particles on rOspC proteins bound to the liposome surface (black arrows). rOspC protein molecules (white dots) forms chains on proteoliposome surfaces (white arrows). **C**) The increase of hydrodynamic radius after binding of rOspC proteins was measured by DLS. **D**) Tabular data characterizing the size of plain and rOspC proteoliposomes in detail.

doi:10.1371/journal.pone.0148497.g004

FTIR was in good correlation with the CD prediction (Fig 5B). Both techniques confirmed that the position of the His-ag at either terminus did not result in significantly alteration to rOspC protein secondary structure.

Assessment of thermostability of rOspC proteins

Thermally induced denaturation of rOspC proteins was followed to explore their structural stability and the reversibility of their refolding behavior (Fig 6). Thermal unfolding of both rOspC proteins was monitored by CD spectroscopy (Fig 6A and 6B), DSC (Fig 5C) and DLS (Fig 6D) as a function of temperature. Changes in CD signal induced by increased temperature increases were very similar for both rOspC proteins, and melting temperatures of 49.0 and 52.8 were calculated for C' and N' terminal His-tag rOspC respectively (Fig 6E). In order to determine the extent of reversibility of post thermally induced unfolding, CD spectra were measured prior to heating (22°C), at the temperature of denaturation (80°C) and again after cooling (22°C) (Fig 6A and 6B). Both rOspC proteins exhibited similarly irreversible thermal denaturation. The CD spectra of rOspC proteins after heating and cooling suggested that of α -helical character was retained but that this was still less than comparable levels seen in native proteins. Similar behavior was observed also when both rOspC proteins were heated to their transition midpoint at a heating rate of 1°C/min and then consequently cooled back to 22°C. The CD data were in a good agreement with data obtained by DSC and DLS. The transition midpoints of C' and N' terminal His-tag rOspC as determined by DSC were 49.7 and 51.9°C, respectively

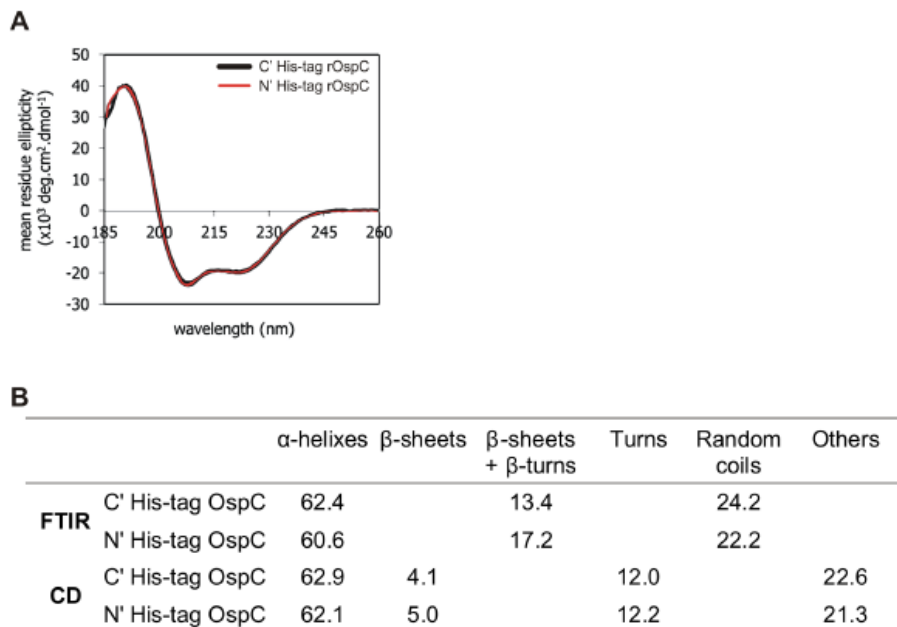


Fig 5. CD spectra of rOspC proteins. Secondary structure of N' and C' terminal His-tag rOspC proteins determined by CD and FTIR. **A)** CD and FTIR spectra were obtained at room temperature (22°C) using a Chirascan CD spectrometer and Tensor 27 FTIR, respectively. **B)** Comparison of secondary structures of rOspC proteins obtained by calculations based on FTIR and CD measurements.

doi:10.1371/journal.pone.0148497.g005

(Fig 6C). The cooling curves confirmed the irreversible unfolding of both rOspC proteins. Also the unfolding curves obtained by DLS demonstrated a dramatic Z-average increase at 48.2 and 52.3°C for C' and N' terminal His-tag rOspC, respectively (Fig 6D). Hence the results obtained by the three techniques were in a good agreement as regards protein melting points and the irreversibility of thermal protein unfolding. They show that N' terminal His-tag rOspC is more thermally stable than C' terminal His-tag rOspC.

Discussion

OspC antigen represents one of the most promising candidate antigens for Lyme disease-preventing vaccine since it is expressed by *Borrelia* during transmission from tick to vertebrate host and during an early phase of vertebrate infection, thus providing the window for targeting the *Borrelia* by OspC-specific antibody-mediated opsonization or complement-activation.

In this study we compared immunogenicity of two rOspC variants that differed in possessing a His-tag at either N' or C' terminus. Such His-tag used both to assist purification and to assist the anchoring of rOspC proteins onto the surface of metallochelation liposome. Given this, the necessity of comparing and contrasting these two protein variants arose from published reports showing that the N' versus C' position of His-tag can adversely affect conformation [27], and/or impair protein immunogenicity for a variety of potential reasons [28].

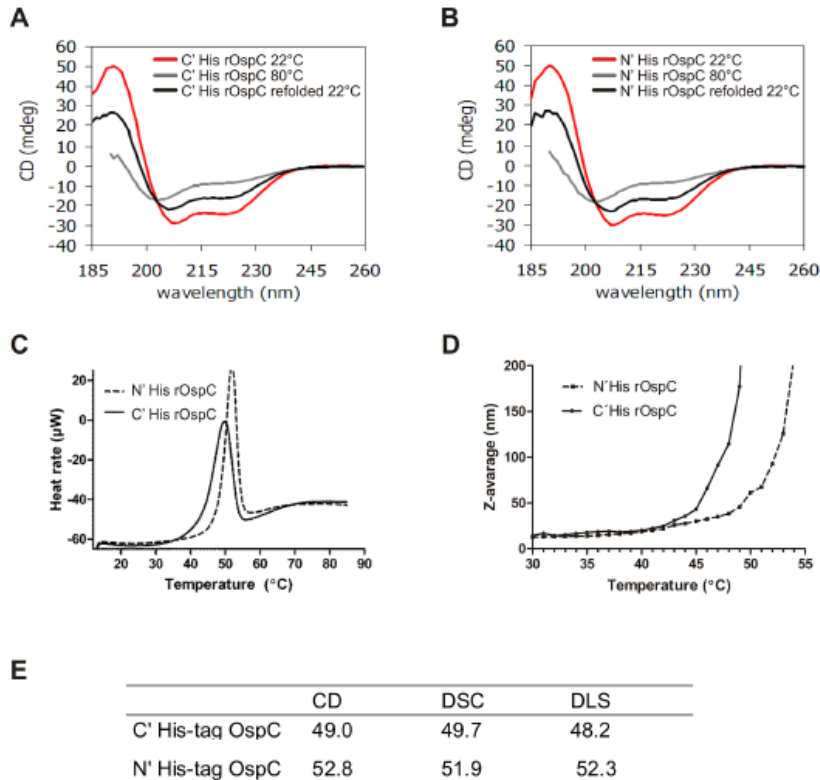


Fig 6. Determination of thermal stability of His-tag rOspC proteins by DLS, DSC and circular dichroism. A, B) rOspC ellipticity induced by temperature changes monitored by circular dichroism. CD spectra were obtained at room temperature (22°C) using a Chirascan CD spectrometer. Data were collected from 185 to 260 nm at 100 nm/min, 1 s response time, and 2 nm bandwidth using a 0.1 cm quartz cuvette. Thermal unfolding of rOspC proteins was followed by monitoring the ellipticity at 195 and 222 nm over the temperature range of 20 to 80°C, with a resolution of 0.1°C, at a heating rate of 1°C/min. C) Determination of thermal stability by measurement transition midpoints of rOspC proteins using DSC. Scans ran from 10 to 85°C at the scan rate of 1°C per minute. D) Thermal stability of rOspC determined by DLS. The hydrodynamic diameter of the proteins was monitored over the temperature range of 25–55°C. The lines are created from hydrodynamic radius measurements at the temperature gradient of 1°C/min. E) Transition temperatures (°C) of N' and C' terminal His-tag rOspC calculated from DLS, DSC, and FTIR measurements.

doi:10.1371/journal.pone.0148497.g006

On our case, in comparing N' versus C' terminal His-tag rOspC administered as soluble proteins with or without adjuvant, all N' terminal His-tag rOspC formulations exhibited substantially higher immunogenicity compared with all C' terminal His-tag rOspC variant formulations. Therefore, when protein secondary structures of both rOspC variants were compared using CD and FTIR spectroscopy, no substantial differences were observed in the content of α helix, β sheet/ β turn and random coil structures. On the other hand, thermal stability analyses performed by CD, DSC, and DLS did suggest that N' terminal His-tag rOspC was slightly more thermally stable which could contribute at least partially to preserving rOspC

epitopes *in vivo* after rOspC administration to mice. Still, in our case, changes in conformation as well as in thermal stability would only seem to play a minor role in modifying N' terminal His-tag rOspC and C' terminal His-tag rOspC epitope structures and their availability for immune recognition. Rather the best explanation for the distinctly different immunogenicities of both rOspC variants is that C' terminal His-tag sterically occludes access to critical adjacent C' terminal epitopes in a way that the N' terminal His-tag does not. This suggestion is corroborated by observations made using human early Lyme disease sera wherein dominant immunoprotective OspC epitopes were found to be located close to the conserved C' terminus [10, 11, 29]. On the other hand, the proximity of the N' and C' termini of OspC in crystallographic data [30], might suggest that an N' terminal His-tag could also have a steric impact on access to C' terminal epitopes as well although the immunostimulatory data presented here would suggest that this potential effect is much less of a problem than might be expected. Also our data (Fig 3) do give some grounds for suggesting that the inhibitory effect of a C' terminal His-tag can be overcome at least in part with a well selected adjuvant such as alum and to some extent MPLA, both of which appear able to boost immune responses otherwise interfered with by steric occlusion, as described above. Such differential immunostimulatory behavior between rOspC variants may be a general problem in different species with their different immune systems [29]. Still, further experimental work would clearly be needed to verify such a suggestion.

Other alternative *Borrelia* antigens for vaccination purposes are OspA, OspB, DbpA and BBk32 proteins. In 1998, the US FDA approved a recombinant OspA (rOspA)-based vaccine known as Lymerix that acts to prevent *Borrelia* transmission. Nevertheless, due to media-evoked concerns about potential autoimmune reactions of OspA, linked to its partial homology with the human integrin LFA-1 (CD11a/CD18), this recombinant vaccine has been withdrawn from the market since 2002. Various recombinant proteins derived from identified protective *Borrelia* antigens have also been expressed as fusion proteins together with various tags such as the glutathione S-transferase (GST) tag [31], the maltose-binding protein tag [32], or His-tag [33]. Interestingly, Bockenstedt et al., 1996 reported that the addition of a His-tag to a C' terminal fragment of OspA substantially enhanced immunogenicity in comparison to the situation with a GST-tag [34], suggesting that inclusion of the GST tag had induced significant conformational changes in the associated OspA antigen to impair immunogenicity [33]. When Koide et al, 2005 introduced an N' terminal His-tag to an OspA C' terminal fragment, the resulting recombinant protein became stabilized by residues promoting hydrophobic interactions and hence the vaccination efficacy of the redesigned OspA fragment was found to be equivalent to full-length OspA protein [35]. OspA is not necessarily an ideal antigen for anti-*Borrelia* vaccination given the diversity of known OspA serotypes. Still Comstedt et al, 2014 has reported that OspA dimers can be used for immunization of mice following the protein engineering of disulfide bridges to stabilize the C'-terminal region of various His-tag OspA fragments [36]. On the other hand, Earnhart et al, has reported on various N'-terminal His-tag chimeric OspC polyepitopes comprising the OspC C'-terminal region composed of loop 5 and α -helix 5 from invasive *Borrelia* isolates. Studies with these polyepitopes demonstrated that the immunogenicity of individual epitopes depends on individual epitope positions in sequence as well as the inclusion of the highly conserved C'-terminal OspC fragment [37].

In terms of commercialization potential and reduction to practice, large-scale production of rOspC is hindered by the low yield of lipidized rOsp antigens. Therefore we opted to use rOspC without a lipidation signal (expressing at ~ 28 mg per 1 L of bacterial culture) [15] but with a reduced level of immunogenicity compared to other *Borrelia* Osp antigens [15, 38]. OspC-specific antibody responses were then elicited in mice with either soluble rOspC or in the presence of various adjuvants such as Montanide PET GEL A and MPLA, a TLR4 ligand derived from the LPS of the Gram negative *Sabmonella minnesota* R595 bacteria. In contrast to

alum, that is known to promote Th2 responses, MPLA has been shown to induce preferentially Th1-biased immune responses in mice [39]. Accordingly, in our case we observed a potent immunostimulatory activity shifted towards the Th2 type of antibodies (IgG1) in response to the administration of soluble rOspC variants in conjunction with alum, in line with previous reports concerning to use of rOspC or rOspA [15, 40]. In contrast, rOspC proteoliposomes formulated with MPLA, followed by MT06, induced strongest OspC-specific Th1 antibody responses determined by the dominance of antibody IgG2a isotype [4, 5, 15, 40, 41]. The Montanide PET GEL A was generally the weakest adjuvant that was evaluated although OspC-specific Th1 antibody responses were also observed. Finally, in order to exclude the possibility that the observed differences in OspC-specific antibody responses were linked to particular rOspC sequence variants used in ELISA, we determined the reactivities of sera using the Lineblot OspC assay and found that the Lineblot OspC exhibited similar trends (data not shown).

Obviously the design of rOspC antigen used in the experiments described here does not appreciate the substantial variability of OspC confirmed from clinical isolates of *Borrelia* which would need to be taken in account in developing an actual vaccination system. Furthermore, experimental animals and humans have different pattern of epitope recognition too [5, 42–46]. Nevertheless, given the extensive use of His-tags and their potential use for efficacious affinity purification and oriented anchoring of antigenic proteins such as rOspC onto surface such as liposomes for vaccination purposes [14, 18, 19, 47] then there is a clear need to demonstrate the potentially pivotal significance to protein immunogenicity should the His-tag be located at N' or C' termini.

In conclusion, we have compared the immunogenicity of N' and C' terminal His-tag rOspC antigens in mice and identified that N' terminal His-tag rOspC induced strong OspC-specific antibody response whereas the C' terminal His-tag rOspC was found to be a much poorer immunogen. Both rOspC variants exhibited similar α -helix and β -sheet composition and were closely similar in terms of their thermal stability (until 42°C). Likewise, EM analyses of rOspC proteoliposomes identified no differences between both rOspC variants. Thus the observed differences in OspC-specific antibody responses are probably linked predominantly to direct steric hindrance of C' terminal rOspC epitopes brought about with a neighboring C' terminal His-tag. Based on our data we can conclude that a N' terminal His-tag rOspC attached by metal-chelation to liposomes formulation with MPLA or MT06 adjuvant are a promising starting point for the development of Lyme disease-preventing vaccines with both veterinary and human applications.

Acknowledgments

The teams headed by Jaroslav Turánek, Milan Raška, and Andrew D. Miller are obligated to the Ministry of Education, Youth and Sports for supporting of the project "FIT" (Pharmacology, Immunotherapy, nanoToxicology).

The funder provided support in the form of salaries for authors (DZ, LD), but did not have any additional role in the study design, data collection and analysis, decision to publish, or preparation of the manuscript. The specific roles of these authors are articulated in the author contributions' section.

Author Contributions

Conceived and designed the experiments: MR JT. Performed the experiments: MK LB JM PTK PK. Analyzed the data: JP RL EB SK RC MS MR. Contributed reagents/materials/analysis tools: DZ LD RE ML. Wrote the paper: MR JT ML MK JM ADM MS.

References

1. Ruderko N, Golovchenko M, Grubhoffer L, Oliver JH Jr. Updates on *Borrelia burgdorferi* sensu lato complex with respect to public health. *Ticks Tick Borne Dis*. 2011; 2(3): 123–128. doi: [10.1016/j.tbd.2011.04.002](https://doi.org/10.1016/j.tbd.2011.04.002) PMID: [21890064](https://pubmed.ncbi.nlm.nih.gov/21890064/)
2. Lantos PM. Chronic Lyme disease. *Infect Dis Clin North Am*. 2015; 29(2): 325–340. doi: [10.1016/j.idc.2015.02.006](https://doi.org/10.1016/j.idc.2015.02.006) PMID: [25999227](https://pubmed.ncbi.nlm.nih.gov/25999227/)
3. Halperin JJ. Chronic Lyme disease: misconceptions and challenges for patient management. *Infect Drug Resist*. 2015; 8: 119–128. doi: [10.2147/IDR.S66739](https://doi.org/10.2147/IDR.S66739) PMID: [26028977](https://pubmed.ncbi.nlm.nih.gov/26028977/)
4. Krupka M, Raska M, Belakova J, Horynova M, Novotny R, Weigl E. Biological aspects of Lyme disease spirochetes: unique bacteria of the *Borrelia burgdorferi* species group. *Biomed Pap Med Fac Univ Palacky Olomouc Czech Repub*. 2007; 151(2): 175–186. PMID: [18345249](https://pubmed.ncbi.nlm.nih.gov/18345249/)
5. Krupka M, Zachova K, Weigl E, Raska M. Prevention of Lyme disease: promising research or Sisyphean task? *Arch Immunol Ther Exp (Warsz)*. 2011; 59(4): 261–275.
6. Tilly K, Rosa PA, Stewart PE. Biology of infection with *Borrelia burgdorferi*. *Infect Dis Clin North Am*. 2008; 22(2): 217–234. v. doi: [10.1016/j.idc.2007.12.013](https://doi.org/10.1016/j.idc.2007.12.013) PMID: [18452798](https://pubmed.ncbi.nlm.nih.gov/18452798/)
7. Boardman BK, He M, Ouyang Z, Xu H, Pang X, Yang XF. Essential role of the response regulator Rrp2 in the infectious cycle of *Borrelia burgdorferi*. *Infect Immun*. 2008; 76(9): 3844–3853. doi: [10.1128/IAI.00467-08](https://doi.org/10.1128/IAI.00467-08) PMID: [18573895](https://pubmed.ncbi.nlm.nih.gov/18573895/)
8. Srivastava SY, de Silva AM. Reciprocal expression of ospA and ospC in single cells of *Borrelia burgdorferi*. *J Bacteriol*. 2008; 190(10): 3429–3433. doi: [10.1128/JB.00085-08](https://doi.org/10.1128/JB.00085-08) PMID: [18359818](https://pubmed.ncbi.nlm.nih.gov/18359818/)
9. Gilmore RD Jr., Mbow ML. Conformational nature of the *Borrelia burgdorferi* B31 outer surface protein C protective epitope. *Infect Immun*. 1999; 67(10): 5463–5469. PMID: [10496930](https://pubmed.ncbi.nlm.nih.gov/10496930/)
10. Jobe DA, Lovrich SD, Schell RF, Callister SM. C-terminal region of outer surface protein C binds borrelial antibodies in sera from patients with Lyme disease. *Clin Diagn Lab Immunol*. 2003; 10(4): 573–578. PMID: [12853388](https://pubmed.ncbi.nlm.nih.gov/12853388/)
11. Buckles EL, Earnhart CG, Marconi RT. Analysis of antibody response in humans to the type A OspC loop 5 domain and assessment of the potential utility of the loop 5 epitope in Lyme disease vaccine development. *Clin Vaccine Immunol*. 2006; 13(10): 1162–1165. PMID: [17028218](https://pubmed.ncbi.nlm.nih.gov/17028218/)
12. Wilske B, Preac-Mursic V, Jauris S, Hofmann A, Pradel I, Soutschek E, et al. Immunological and molecular polymorphisms of OspC, an immunodominant major outer surface protein of *Borrelia burgdorferi*. *Infect Immun*. 1993; 61(5): 2182–2191. PMID: [8478108](https://pubmed.ncbi.nlm.nih.gov/8478108/)
13. Fuchs R, Jauris S, Lottspeich F, Preac-Mursic V, Wilske B, Soutschek E. Molecular analysis and expression of a *Borrelia burgdorferi* gene encoding a 22 kDa protein (pC) in *Escherichia coli*. *Mol Microbiol*. 1992; 6(4): 503–509. PMID: [1560779](https://pubmed.ncbi.nlm.nih.gov/1560779/)
14. Krupka M, Belakova J, Sebestova M, Tuhackova J, Raska M, Vrzal V, et al. Isolation and purification of recombinant outer surface protein C (rOspC) of *Borrelia burgdorferi* sensu lato. *Biomed Pap Med Fac Univ Palacky Olomouc Czech Repub*. 2005; 149(2): 261–264. PMID: [16601766](https://pubmed.ncbi.nlm.nih.gov/16601766/)
15. Krupka M, Masek J, Bartheldyova E, Turanek-Knotigova P, Plockova J, Korvasova Z, et al. Enhancement of immune response towards non-lipidized *Borrelia burgdorferi* recombinant OspC antigen by binding onto the surface of metallochelating nanoliposomes with entrapped lipophilic derivatives of nor-AbuMDP. *J Control Release*. 2012; 160(2): 374–381. doi: [10.1016/j.jconrel.2012.02.017](https://doi.org/10.1016/j.jconrel.2012.02.017) PMID: [22387453](https://pubmed.ncbi.nlm.nih.gov/22387453/)
16. Knotigova PT, Zyka D, Masek J, Kovalova A, Krupka M, Bartheldyova E, et al. Molecular adjuvants based on nonpyrogenic lipophilic derivatives of norAbuMDP/GMDP formulated in nanoliposomes: stimulation of innate and adaptive immunity. *Pharm Res*. 2015; 32(4): 1186–1199. doi: [10.1007/s11095-014-1516-y](https://doi.org/10.1007/s11095-014-1516-y) PMID: [25630814](https://pubmed.ncbi.nlm.nih.gov/25630814/)
17. Altin JG, Parish CR. Liposomal vaccines—targeting the delivery of antigen. *Methods*. 2006; 40(1): 39–52. PMID: [16997712](https://pubmed.ncbi.nlm.nih.gov/16997712/)
18. Masek J, Bartheldyova E, Korvasova Z, Skrabalova M, Koudelka S, Kulich P, et al. Immobilization of histidine-tagged proteins on monodisperse metallochelation liposomes: Preparation and study of their structure. *Anal Biochem*. 2011; 408(1): 95–104. doi: [10.1016/j.ab.2010.08.023](https://doi.org/10.1016/j.ab.2010.08.023) PMID: [20732292](https://pubmed.ncbi.nlm.nih.gov/20732292/)
19. Masek J, Bartheldyova E, Turanek-Knotigova P, Skrabalova M, Korvasova Z, Plockova J, et al. Metallochelating liposomes with associated lipophilised norAbuMDP as biocompatible platform for construction of vaccines with recombinant His-tagged antigens: preparation, structural study and immune response towards rHsp90. *J Control Release*. 2011; 151(2): 193–201. doi: [10.1016/j.jconrel.2011.01.016](https://doi.org/10.1016/j.jconrel.2011.01.016) PMID: [21256901](https://pubmed.ncbi.nlm.nih.gov/21256901/)
20. Turanek J, Masek J, Krupka M, Raska M. Functionalised nanoliposomes for construction of recombinant vaccines: Lyme disease as an example. In: Giese M, editor. *Molecular Vaccines: From Prophylaxis to Therapy*. 2. London, UK: Springer-Verlag; 2014. p. 561–577.

21. Turanek J, Masek J, Raska M, Ledvina M. Application of Liposomes for Construction of Vaccines. In: Ghista DN, editor. Biomedical Science, Engineering and Technology. Rijeka, Croatia: In Tech; 2012. p. 653–678.
22. Mayer A, Sharma SK, Tolner B, Minton NP, Purdy D, Amlot P, et al. Modifying an immunogenic epitope on a therapeutic protein: a step towards an improved system for antibody-directed enzyme prodrug therapy (ADEPT). *Br J Cancer*. 2004; 90(12):2402–2410. PMID: [15162148](#)
23. Hippler K, Miller A, Turanek J, Ledvina M, inventors. Compounds derived from normuramylidpeptide2013.
24. Kowalska M, Galuszka P, Frebortova J, Sebela M, Beres T, Hluska T, et al. Vacuolar and cytosolic cytokinin dehydrogenases of *Arabidopsis thaliana*: heterologous expression, purification and properties. *Phytochemistry*. 2010; 71(17–18): 1970–1978. doi: [10.1016/j.phytochem.2010.08.013](#) PMID: [20825956](#)
25. Petrovska B, Jerabkova H, Chamrad I, Vrana J, Lenobel R, Urinovska J, et al. Proteomic analysis of barley cell nuclei purified by flow sorting. *Cytogenet Genome Res*. 2014; 143(1–3): 78–86. doi: [10.1159/000365311](#) PMID: [25059295](#)
26. Krupka M, Zachova K, Cahlikova R, Vrbkova J, Novak Z, Sebela M, et al. Endotoxin-minimized HIV-1 p24 fused to murine hsp70 activates dendritic cells, facilitates endocytosis and p24-specific Th1 response in mice. *Immunol Lett*. 2015; 166(1): 36–44. doi: [10.1016/j.imlet.2015.05.010](#) PMID: [26021827](#)
27. Figueroa CM, Iglesias AA. Aldose-6-phosphate reductase from apple leaves: Importance of the quaternary structure for enzyme activity. *Biochimie*. 2010; 92(1): 81–88. doi: [10.1016/j.biochi.2009.09.013](#) PMID: [19799961](#)
28. Bielecka MK, Devos N, Gilbert M, Hung MC, Weynants V, Heckels JE, et al. Recombinant protein truncation strategy for inducing bactericidal antibodies to the macrophage infectivity potentiator protein of *Neisseria meningitidis* and circumventing potential cross-reactivity with human Fcγ2b-binding proteins. *Infect Immun*. 2015; 83(2): 730–742. doi: [10.1128/IAI.01815-14](#) PMID: [25452551](#)
29. Lovrich SD, Jobe DA, Schell RF, Callister SM. Borrelia-specific OspC antibodies specific for a highly conserved epitope are immunodominant in human Lyme disease and do not occur in mice or hamsters. *Clin Diagn Lab Immunol*. 2005; 12(6): 746–751. PMID: [15939749](#)
30. Kumaran D, Eswaramoorthy S, Luft BJ, Koide S, Dunn JJ, Lawson CL, et al. Crystal structure of outer surface protein C (OspC) from the Lyme disease spirochete, *Borrelia burgdorferi*. *EMBO J*. 2001; 20(5): 971–978. PMID: [11230121](#)
31. Fikrig E, Barthold SW, Kantor FS, Flavell RA. Protection of mice against the Lyme disease agent by immunizing with recombinant OspA. *Science*. 1990; 250(4980): 553–556. PMID: [2237407](#)
32. Probert WS, LeFebvre RB. Protection of C3H/HeN mice from challenge with *Borrelia burgdorferi* through active immunization with OspA, OspB, or OspC, but not with OspD or the 83-kilodalton antigen. *Infect Immun*. 1994; 62(5): 1920–1926. PMID: [8168958](#)
33. Bockenstedt LK, Fikrig E, Barthold SW, Flavell RA, Kantor FS. Identification of a *Borrelia burgdorferi* OspA T cell epitope that promotes anti-OspA IgG in mice. *J Immunol*. 1996; 157(12): 5496–5502. PMID: [8955199](#)
34. Bockenstedt LK, Fikrig E, Barthold SW, Kantor FS, Flavell RA. Inability of truncated recombinant OspA proteins to elicit protective immunity to *Borrelia burgdorferi* in mice. *J Immunol*. 1993; 151(2): 900–906. PMID: [8335917](#)
35. Koide S, Yang X, Huang X, Dunn JJ, Luft BJ. Structure-based design of a second-generation Lyme disease vaccine based on a C-terminal fragment of *Borrelia burgdorferi* OspA. *J Mol Biol*. 2005; 350(2): 290–299. PMID: [15935380](#)
36. Comstedt P, Hanner M, Schuler W, Meinke A, Lundberg U. Design and development of a novel vaccine for protection against Lyme borreliosis. *PLoS One*. 2014; 9(11): e113294. doi: [10.1371/journal.pone.0113294](#) PMID: [25409015](#)
37. Eamhart CG, Marconi RT. Construction and analysis of variants of a polyvalent Lyme disease vaccine: approaches for improving the immune response to chimeric vaccinogens. *Vaccine*. 2007; 25(17): 3419–3427. PMID: [17239505](#)
38. Erdile LF, Brandt MA, Warakomski DJ, Westrask GJ, Sadziene A, Barbour AG, et al. Role of attached lipid in immunogenicity of *Borrelia burgdorferi* OspA. *Infect Immun*. 1993; 61(1): 81–90. PMID: [8418068](#)
39. Casella CR, Mitchell TC. Putting endotoxin to work for us: monophosphoryl lipid A as a safe and effective vaccine adjuvant. *Cell Mol Life Sci*. 2008; 65(20): 3231–3240. doi: [10.1007/s00018-008-8228-6](#) PMID: [18668203](#)

40. Ma J, Bulger PA, Davis DR, Perilli-Palmer B, Bedore DA, Kensil CR, et al. Impact of the saponin adjuvant QS-21 and aluminium hydroxide on the immunogenicity of recombinant OspA and OspB of *Borrelia burgdorferi*. *Vaccine*. 1994; 12(10): 925–932. PMID: [7975834](#)
41. Munson EL, Du Chateau BK, Jobe DA, Lovrich SD, Callister SM, Schell RF. Production of borrelial antibody to outer surface protein A in vitro and modulation by interleukin-4. *Infect Immun*. 2000; 68(10): 5496–5501. PMID: [10992445](#)
42. Eamhart CG, Buckles EL, Marconi RT. Development of an OspC-based tetravalent, recombinant, chimeric vaccinogen that elicits bactericidal antibody against diverse Lyme disease spirochete strains. *Vaccine*. 2007; 25(3): 466–480. PMID: [16996663](#)
43. Eamhart CG, Marconi RT. OspC phylogenetic analyses support the feasibility of a broadly protective polyvalent chimeric Lyme disease vaccine. *Clin Vaccine Immunol*. 2007; 14(5): 628–634. PMID: [17360854](#)
44. Eamhart CG, Marconi RT. An octavalent Lyme disease vaccine induces antibodies that recognize all incorporated OspC type-specific sequences. *Hum Vaccin*. 2007; 3(6): 281–289. PMID: [17921702](#)
45. Schulte-Spechtel U, Fingerle V, Goettner G, Rogge S, Wilske B. Molecular analysis of decorin-binding protein A (DbpA) reveals five major groups among European *Borrelia burgdorferi* sensu lato strains with impact for the development of serological assays and indicates lateral gene transfer of the dbpA gene. *Int J Med Microbiol*. 2006; 296 Suppl 40: 250–266. PMID: [16530482](#)
46. Wang G, van Dam AP, Dankert J. Evidence for frequent OspC gene transfer between *Borrelia valaisiana* sp. nov. and other Lyme disease spirochetes. *FEMS Microbiol Lett*. 1999; 177(2): 289–296. PMID: [10474195](#)
47. Malliaros J, Quinn C, Arnold FH, Pearse MJ, Drane DP, Stewart TJ, et al. Association of antigens to ISCOMATRIX adjuvant using metal chelation leads to improved CTL responses. *Vaccine*. 2004; 22(29–30): 3968–3975. PMID: [15364446](#)

4. SOUHRN LIPOSOMÁLNÍ TÉMATIKY

Liposomy představují nejstarší a nejvíce prozkoumaný nanosystém z hlediska použití v medicíně. Slouží jako model pro studium membrána a distribuce nanočástic v organismu. Příprava liposomů je zvládnuta jak v laboratorním, tak v průmyslovém měřítku a liposomální preparáty jsou povoleny FDA pro léčbu infekčních a nádorových nemocí. Na trhu již existují dermatologické preparáty s liposomy a liposomální diagnostika.

Biokompatibilní nosiče a nová bezpečná adjuvans jsou nutným předpokladem pro rozvoj moderní vakcinologie směřující k rekombinantním vakcínám. Výzkum vakcín založených na liposomech má již třicetiletou historii a na trh jsou uváděny nové moderní rekombinantní vakcíny.

Publikovali jsme práce v oblasti technologie přípravy liposomů, vývoje cílených protinádorových léčiv, bezpečných adjuvans, konstrukce rekombinantních vakcín a studia nových aplikačních postupů. Některé výsledky jsou také ve stádiu přípravy na realizaci v českých firmách. Na tomto moderním výzkumu se podílela celá řada studentů a mladých vědeckých pracovníků v rámci postgraduálního studia. Věřím, že tato práce přispěla k jejich odbornému růstu a obohatila také o nové poznatky oblast moderní farmakologie, imunoterapie a nanotechnologie.